Virchows Arch (2009) 454:1–16
DOI 10.1007/s00428-008-0707-5

REVIEW AND PERSPECTIVE

Precursor lesions to prostatic adenocarcinoma

Jonathan I. Epstein

Received: 30 October 2008 / Accepted: 17 November 2008 / Published online: 2 December 2008

Abstract High-grade prostatic intraepithelial neoplasia (PIN) is the one well-documented precursor to adenocarcinoma of the prostate. This review article defines both low- and high-grade PIN. Unusual variants of high-grade PIN are illustrated. Benign lesions that may be confused with high-grade PIN, including central zone histology, clear cell cribriform hyperplasia, and basal cell hyperplasia are described and illustrated. High-grade PIN is also differentiated from invasive acinar (usual) and ductal adenocarcinoma. The incidence of high-grade PIN, its relationship to carcinoma (including molecular findings), and risk of cancer on rebiopsy are covered in detail. Finally, intraductal carcinoma of the prostate, a controversial entity, is discussed and differentiated from high-grade PIN.

Keywords Prostatic intraepithelial neoplasia · Intraductal carcinoma of the prostate

Introduction

Over time, several lesions have been proposed as putative precursor lesions to adenocarcinoma of the prostate. Adenosis, also known as atypical adenomatous hyperplasia, had been considered by some authorities to be a precursor to low-grade transition zone adenocarcinomas given some morphological similarities between the two entities. Although, there is some conflicting molecular evidence concerning the relation of adenosis to adenocarcinoma, the cumulative results suggest that genetic alterations in adenosis are infrequent [1–4]. More importantly, morphological and follow-up data fail to link adenosis as a precursor to adenocarcinoma of the prostate. With rare exception, foci of adenocarcinoma are not seen in close association with adenocarcinoma. Most importantly, men with adenosis on follow-up are not at increased risk of developing adenocarcinoma [5]. Adenosis, although a mimicker of prostate cancer, should not be considered a precursor of prostatic adenocarcinoma.

Another lesion that has been proposed as a precursor to adenocarcinoma of the prostate is proliferative inflammatory atrophy (PIA). There is molecular and epidemiological and less so morphological evidence that long-standing PIA may predispose to prostate adenocarcinoma [6]. However, it is rare to see adenocarcinoma directly evolving from PIA. Furthermore, the finding of PIA on biopsy material is very frequent in the absence of carcinoma and does not increase the risk of cancer on repeat biopsy [7]. Consequently, from the practical standpoint, PIA should not be classified as a direct precursor to prostate adenocarcinoma.

Removing adenosis and PIA from the list of precursor lesions of prostate adenocarcinoma, one is left with only one well-established precursor to prostatic adenocarcinoma and that is prostatic intraepithelial neoplasia which will form the basis of this review.

Prostatic intraepithelial neoplasia

Prostatic intraepithelial neoplasia (PIN) as a precursor to some prostatic carcinomas was first described in the 1960s by McNeal under the name of "intraductal dysplasia," and more precisely characterized in 1986 by McNeal and Bostwick [8–11]. PIN consists of architecturally benign prostatic acini lined by cytologically atypical cells and is dichotomized into low- and high-grade PIN. In its original description, PIN was subcategorized into grades 1–3, with grade 1 equating to low-grade PIN and grades 2–3 combined into high-grade PIN.

J. I. Epstein (✉)
Departments of Pathology, Urology and Oncology,
The Johns Hopkins Hospital,
401 N. Broadway St., Rm 2242,
Baltimore, MD 21231, USA
e-mail: jepstein@jhmi.edu

Histology

At low magnification, PIN manifests as basophilic glands that are separated by a modest amount of stroma. PIN glands architecturally resemble benign glands in that they are large, branch, and typically have papillary and undulating luminal surfaces (Fig. 1). Their basophilic appearance is due to a combination of nuclear crowding, enlargement, and hyperchromasia, along with amphophilic cytoplasm. High-grade PIN is distinguished from low-grade PIN by the presence of prominent nucleoli (Fig. 2). However, there are no criteria as to how prominent or how frequent the nucleoli must be to diagnose high-grade PIN. My approach to maintain intraobserver reproducibility as well as not to overdiagnose cases with small nucleoli is to diagnose high-grade PIN when nucleoli are visible at ×20 magnification. Alternative diagnostic criteria are discussed later in the manuscript.

Low-grade PIN has minimal nuclear enlargement and stratification, yet an absence of prominent nucleoli (Fig. 3). If one has to look at high magnification for the rare cell with prominent nucleoli, then the gland should not be diagnosed as high-grade PIN. Occasionally, there are cases borderline between low and high-grade PIN; it is the recommendation of this author that the patient not be labeled as having high-grade PIN.

There are four architectural patterns of PIN [12]. The flat pattern consists of a single layer of cells with atypical nuclei (Fig. 4). The tufted pattern, which is the most common, results from alternating areas of stratification and piling up of cells adjacent to less hyperplastic areas (Fig. 5). When there is elongation of tufts to form tall columns of epithelium typically lacking fibrovascular cores, it is termed the micropapillary pattern (Fig. 6). Cribriform PIN is the final pattern (Fig. 7). It is distinctly uncommon for low-grade PIN to have a micropapillary or cribriform pattern. With tufting, micropapillary, and cribriform patterns of high-grade PIN, nuclei toward the center of the gland tend to have more bland cytology (Fig. 7). The grade of PIN is assigned based on the more atypical nuclei peripherally located up against the basement membrane.

Unusual variants include high-grade PIN with signet-ring features (Fig. 8), with small cell neuroendocrine features, with mucin cell metaplasia (Fig. 9), with mucinous features (Fig. 10), with foamy features (Fig. 11), with inverted nuclei (Fig. 12), with squamous differentiation (Fig. 13), and with paneth cell-like neuroendocrine differentiation (Fig. 14) [13–16].

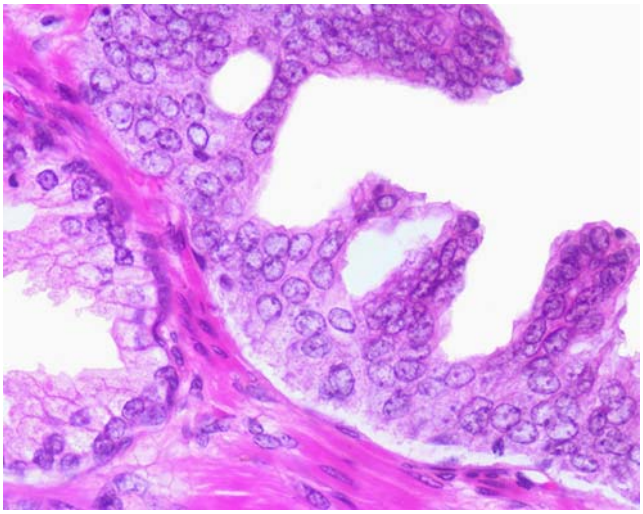

Fig. 2 High-grade PIN glands appearing basophilic as a result of enlarged nuclei, high nuclear to cytoplasmic ratio, and epithelial hyperplasia. Note paler benign gland in *lower left corner*

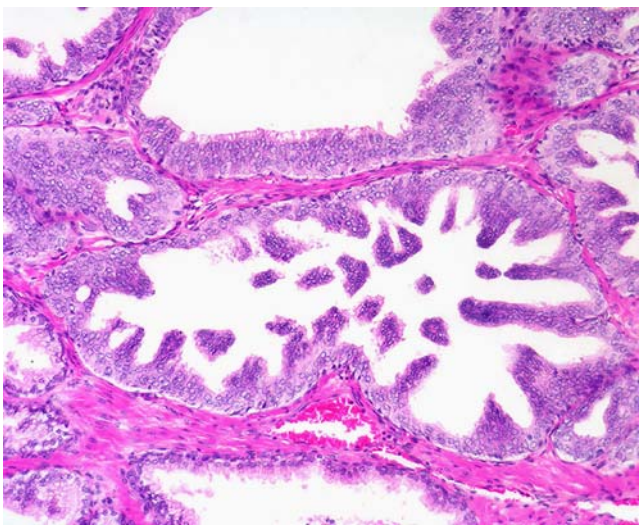

Fig. 1 **a** Glands involved by high-grade PIN architecturally resemble normal glands in their size, shape, and spatial relation to other glands

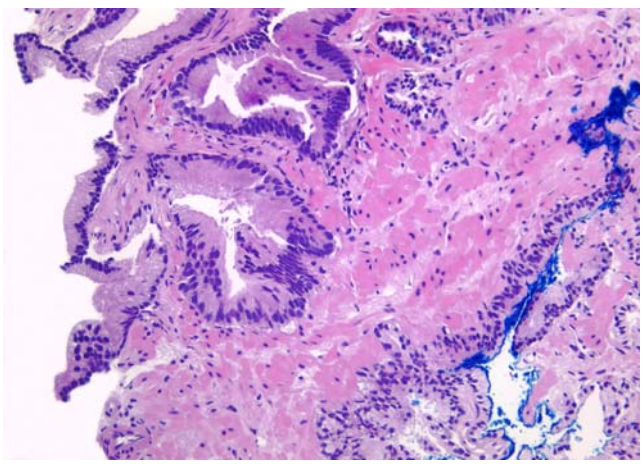

Fig. 3 Low-grade PIN (*upper left*) composed of architecturally benign glands composed of cells with nuclear stratification and hyperchromasia, yet a lack of prominent nucleoli

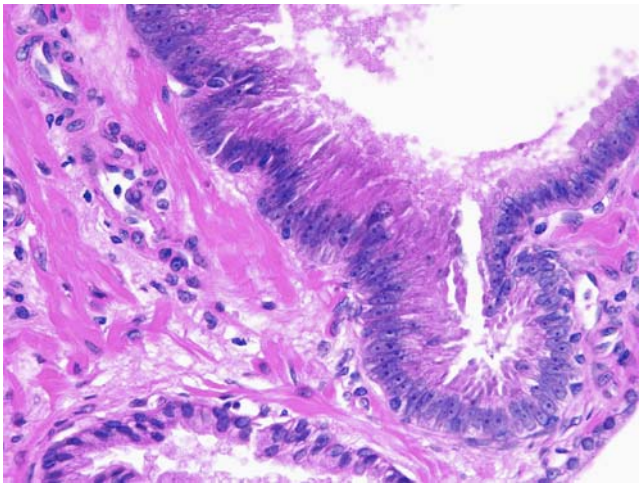

Fig. 4 Flat high-grade PIN

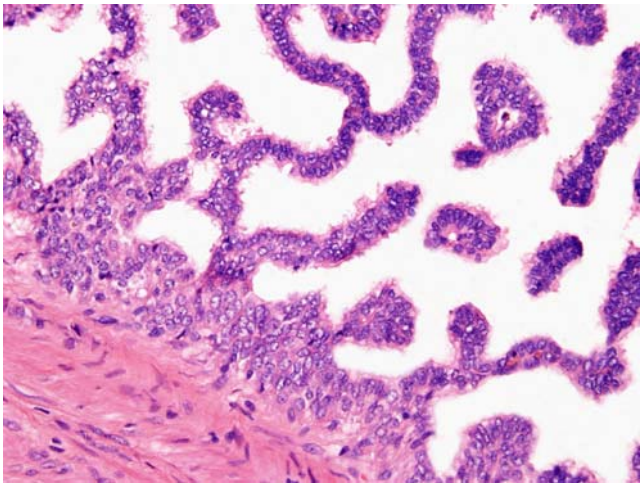

Fig. 6 Micropapillary high-grade PIN

Following complete androgen deprivation therapy there is a marked decrease in the prevalence and extent of high-grade PIN. In contrast, there does not seem to be large changes in the morphology of high-grade PIN after blockade with 5 alpha-reductase inhibitors (i.e., Finasteride) or following radiotherapy.

Differential diagnosis

Benign mimickers There are several benign lesions that may be confused with high-grade PIN. These include variations of normal histology and variants of hyperplasia.

Central zone histology

The central zone is an ill-defined region up at the base of the prostate around the ejaculatory ducts and adjacent to the seminal vesicle. Central zone glands are lined by tall pseudostratified epithelium which may be arranged in Roman bridge and cribriform glandular patterns, mimicking PIN (Fig. 15) [17]. In contrast to high-grade PIN, central zone glands lack cytological atypia, and some have a prominent basal cell layer.

Clear cell cribriform hyperplasia

It is not certain whether clear cell cribriform hyperplasia, also referred to as cribriform hyperplasia, is a variant of benign prostatic hyperplasia or a specific disease entity. Clear cell cribriform hyperplasia is typically located in the transition zone and typically although not always sampled on TURP, whereas high-grade PIN predominates in the peripheral zone. Clear cell cribriform hyperplasia consists of crowded cribriform glands with pale cytoplasm some-

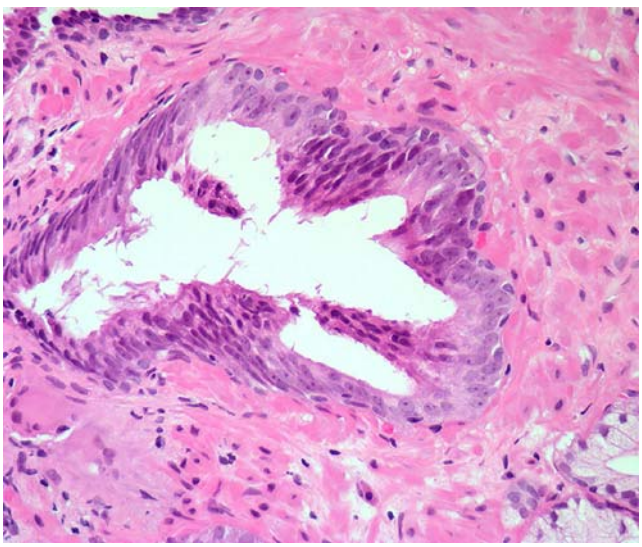

Fig. 5 Tufted high-grade PIN

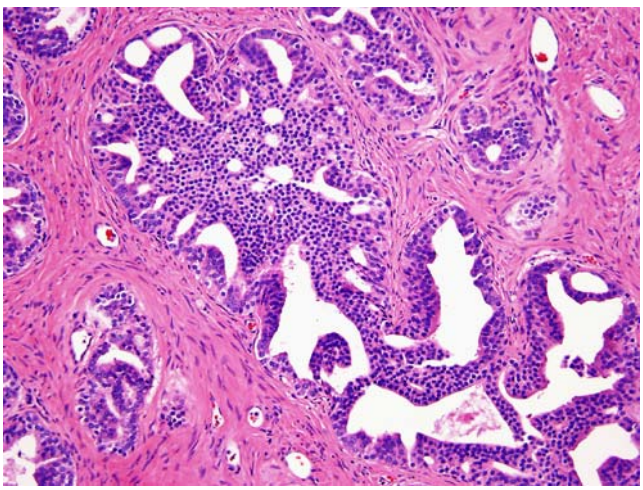

Fig. 7 Cribriform high-grade PIN. Note more benign appearing nuclei toward the center of the cribriform gland. Basal cell stains were positive around all of the glands (not shown)

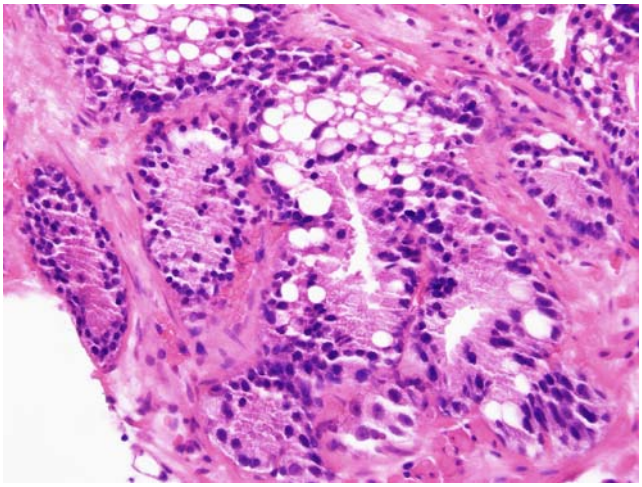

Fig. 8 High-grade PIN with clear cytoplasmic vacuoles

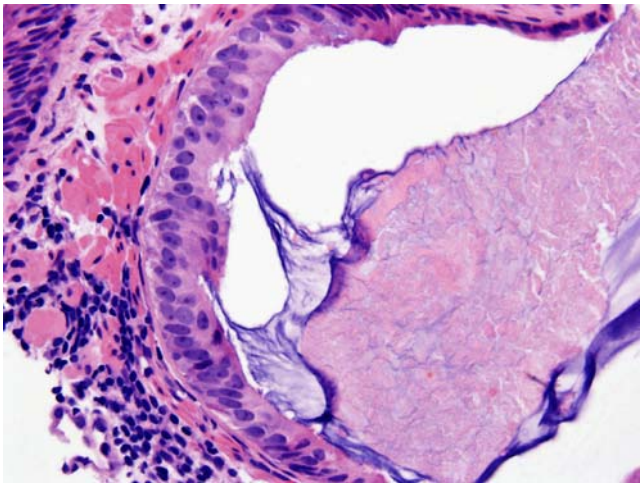

Fig. 10 High-grade PIN with mucinous features

times growing as a nodule and, in other instances, more diffusely (Fig. 16) [18]. The key feature distinguishing clear cell cribriform hyperplasia from high-grade PIN is the lack of nuclear atypia. Furthermore, within a nodule of clear cell cribriform hyperplasia, at least some of the cribriform glands show an obvious basal cell layer.

Basal cell hyperplasia

Basal cell hyperplasia and usual basal cells may be mistaken for high-grade PIN as they both can share prominent nucleoli and mitotic activity [19, 20] (Table 1). This worrisome cytology may be seen in several architectural patterns of basal cell hyperplasia including: (1) proliferation of small round crowded basaloid glands with atrophic cytoplasm or even solid nests; (2) proliferation of basal cells in preexisting larger open benign glands; and (3) cribriform and pseudocribriform basal cell hyperplasia. In contrast to basal cell hyperplasia with small crowded glands, high-grade PIN resembles usual prostate glands in their larger size, open lumina, abundant cytoplasm, and distribution (Fig. 17). Basal cell hyperplasia in larger benign glands stream parallel to the basement membrane and undermine overlying benign-appearing secretory cells. High-grade PIN has inconspicuous flattened often discontinuous basal cells with the overlying secretory cells having atypical nuclei oriented perpendicular to the basement membrane. Whereas cribriform high-grade PIN glands represent a single sheet of cells with punched out lumina, many of the glands within a focus of cribriform basal cell hyperplasia appeared as fused individual basal cell hyperplasia glands (pseudocribriform; Fig. 18) [21]. Cytologically, basal cell nuclei tend to be round and have a blue-gray appearance, in contrast to high-grade PIN which has more

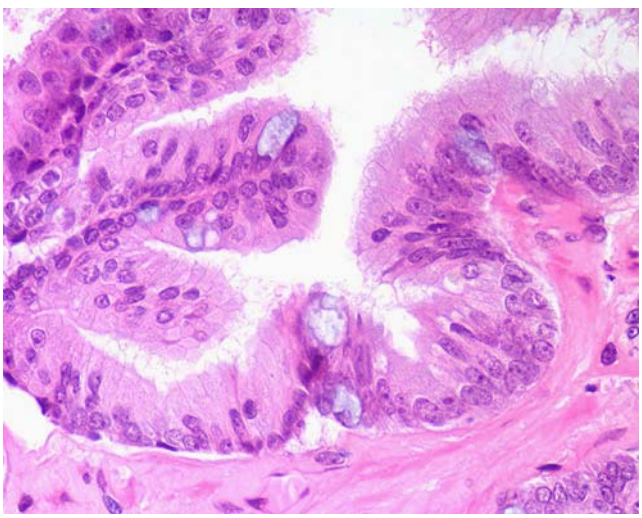

Fig. 9 High-grade PIN with mucin cell metaplasia

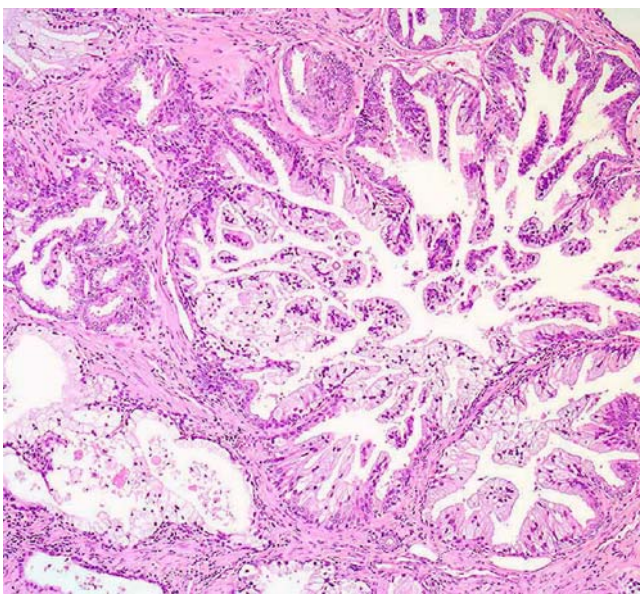

Fig. 11 Foamy high-grade PIN

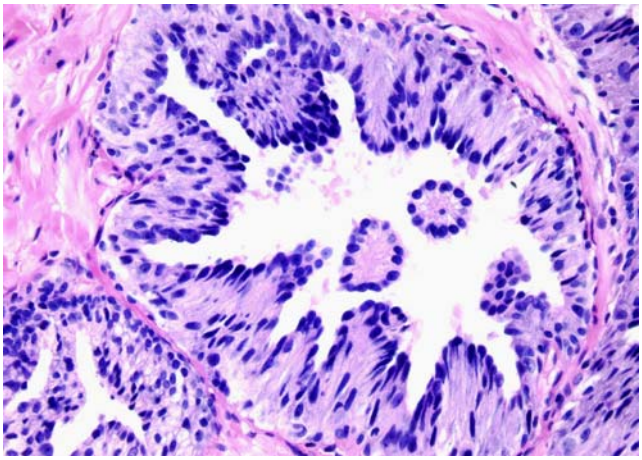

Fig. 12 High-grade PIN with inverted features, where the nuclei show reverse polarity and are situated at the luminal surface

pseudostratified and columnar nuclei with a red-violet hue. Basal cell hyperplasia reveals high molecular weight cytokeratin or p63 positivity in multilayered nuclei, although in some cases, the more centrally located cells are not immunoreactive (Fig. 19) [22]. In high-grade PIN, basal cell markers label only flattened cytologically benign basal cells beneath negatively stained atypical PIN cells (Fig. 20). Finally, most cases of basal cell hyperplasia are found in TURP specimens, indicating growth in the transition zone, in contrast to high-grade PIN's preferential location in the periphery of the prostate.

Malignant mimickers High-grade PIN must be differentiated from invasive prostate carcinoma. Acinar (usual) adenocarcinoma and even more so ductal adenocarcinoma can in some instances closely resemble high-grade PIN.

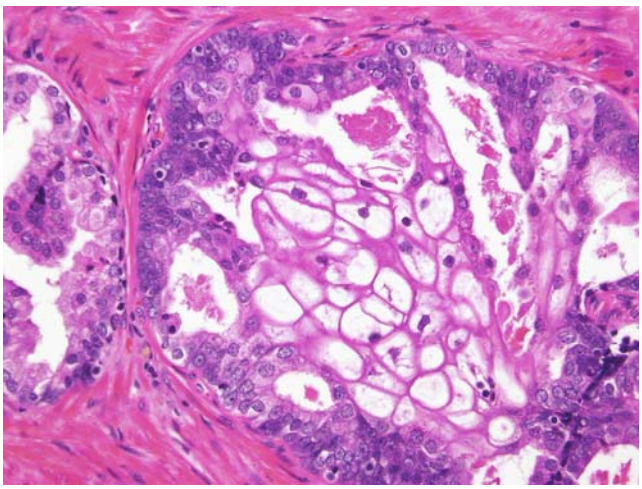

Fig. 13 High-grade PIN with squamous features (courtesy of Dr. Rodolfo Montironi)

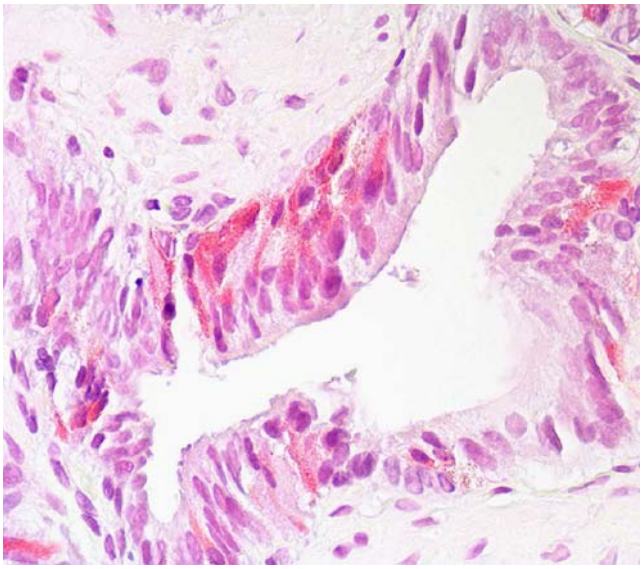

Fig. 14 High-grade PIN with paneth cell-like neuroendocrine differentiation

Acinar (usual) adenocarcinoma

In some cases, it is difficult to distinguish cribriform high-grade PIN from cribriform adenocarcinoma [23]. However, almost always, when there is cribriform carcinoma, it is accompanied by small glands of carcinoma. Only when cytologically atypical cribriform glands are so large, irregular, back-to-back, outside of the prostate, or show perineural invasion such that they are inconsistent with cribriform PIN should infiltrating cribriform carcinoma be diagnosed on H&E stained sections in the absence of small atypical infiltrating glands (Fig. 21). In the setting of numerous atypical cribriform glands, a negative immuno-

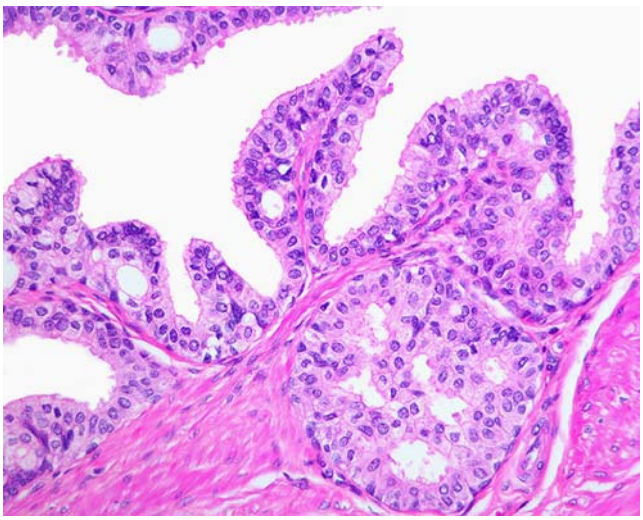

Fig. 15 Roman bridge and cribriform formation in central zone glands

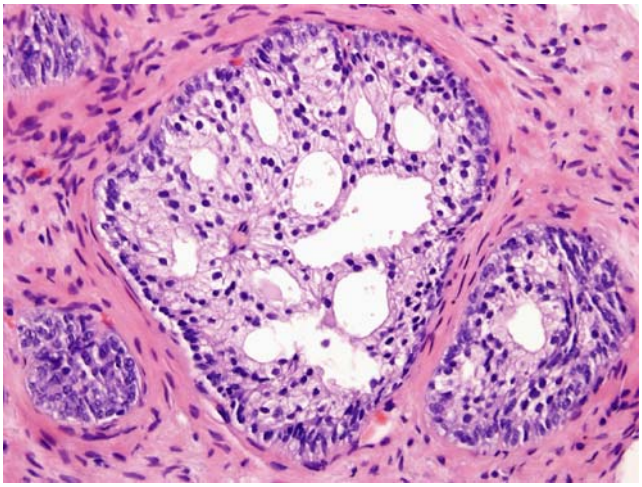

Fig. 16 Clear cell cribriform hyperplasia

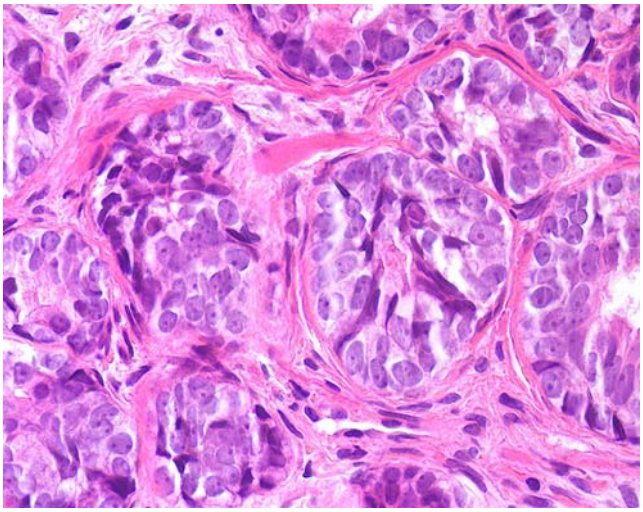

Fig. 17 Nests of basal cell hyperplasia with prominent nucleoli

reaction for basal cells in all of the glands is diagnostic of carcinoma; positive staining, even if patchy, verifies the lesion as cribriform PIN or intraductal carcinoma. If there are only a few cribriform glands, negative immunoreactivity for basal cell markers is not diagnostic of carcinoma [22]. In cases where there are only one or a few small cribriform glands on needle biopsy without small glands of infiltrating carcinoma, the diagnosis is typically "Focus of atypical cribriform glands" with a comment that "The distinction between cribriform high-grade PIN and cribriform carcinoma cannot be made with certainty, and repeat biopsy is recommended" [24].

A common differential diagnosis is when there are a few atypical glands immediately adjacent to high-grade PIN, and the issue is whether these small glands represent tangential sectioning or outpouching off of the high-grade PIN glands or a small focus of carcinoma adjacent to the high-grade PIN (Fig. 22) [23, 25]. We refer to these foci at PINATYP. A diagnosis of carcinoma can be rendered only if the small atypical glands are too numerous or too far away from the high-grade PIN glands to represent outpouching or tangential sectioning from the PIN glands (Fig. 23). In cases of PINATYP, the lack of basal cells in the small atypical glands can be construed as evidence that these glands represent infiltrating cancer only if there are more than a few such glands. One may also see classic high-grade PIN where some of the glands show the expected patchy basal cell layer and other identical glands are negative for the basal cell markers; these cases we would still diagnose as high-grade PIN (Fig. 24).

Table 1 Differential diagnosis: high-grade PIN and basal cell hyperplasia with nucleoli

Basal cell hyperplasia with nucleoli	High-grade PIN
Proliferation of small glands	Architecturally benign (large glands without crowding)
Occasional solid nests	Glands with well-formed lumina
Basal cells with atypical nuclei (blue) undermine secretory cells with benign nuclei (red/violet)	No two distinct cell population
Basal cell nuclei stream parallel to basement membrane	Atypical cells oriented perpendicular to basement membrane
Atypical nuclei positive for HMWCK with underlying flattened benign-appearing cells positive	Atypical nuclei negative for HMWCK

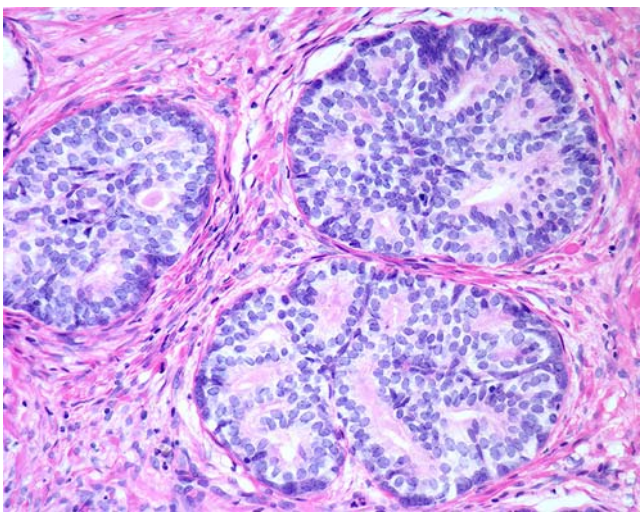

Fig. 18 Pseudocribriform basal cell hyperplasia

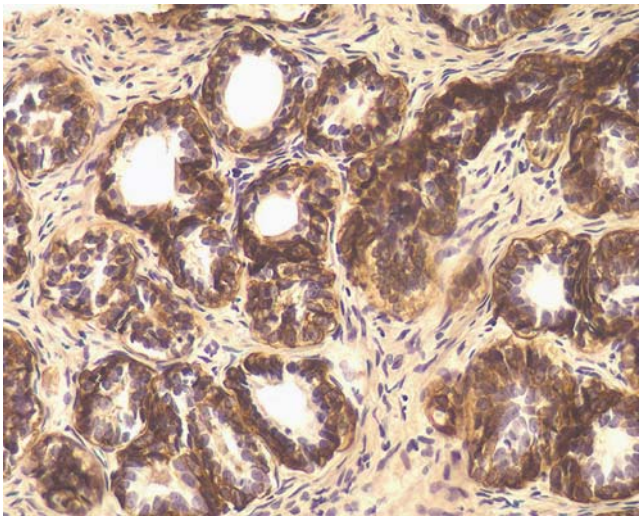

Fig. 19 Basal cell hyperplasia showing multiple cell layers labeled with high molecular weight cytokeratin

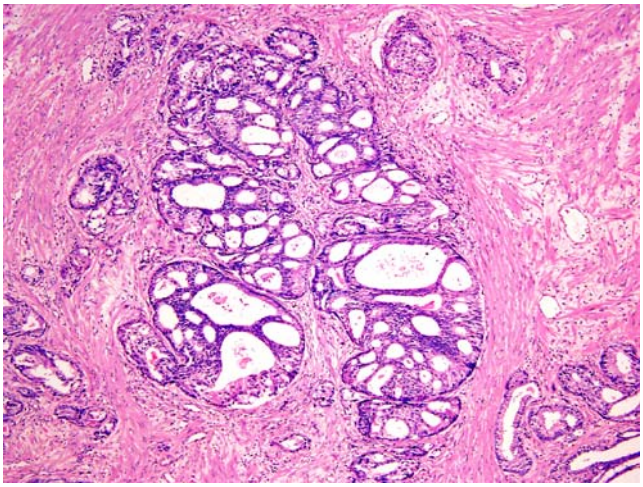

Fig. 21 Infiltrating cribriform carcinoma. Cribriform glands are too crowded to represent high-grade PIN. Also note small individual glands of carcinoma surrounding cribriform carcinoma

Ductal adenocarcinoma

A difficult distinction is between cribriform high-grade PIN and ductal adenocarcinoma of the prostate [26–28]. Ductal adenocarcinomas are often centrally located in the periurethral region and sampled on TURP. PIN is uncommonly found within the periurethral region and infrequently seen on TURP. Ductal adenocarcinomas often contain true papillary fronds with well-established fibrovascular cores, whereas high-grade PIN more frequently reveals micropapillary fronds with tall columns of epithelium without fibrovascular stalks (Fig. 25). Ductal adenocarcinomas frequently show solid cylinders or nests, which can contain comedonecrosis, which may be extensive, which is absent in PIN. Finally, ductal adenocarcinomas may consist of very large and/or back-to-back glands, whereas glands involved by PIN are of the size and

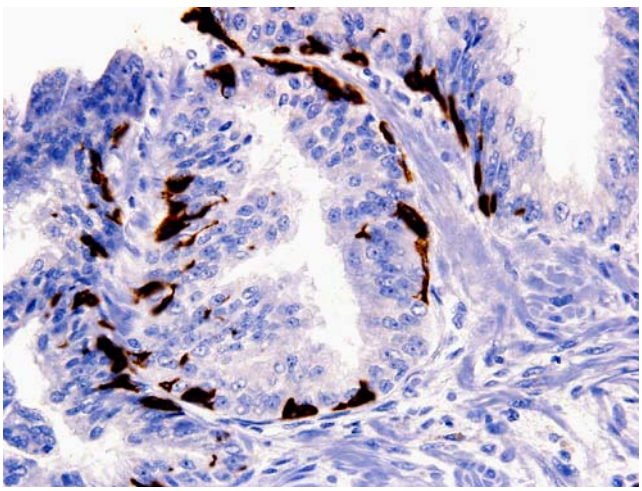

Fig. 20 High-grade PIN with a patchy basal cell layer

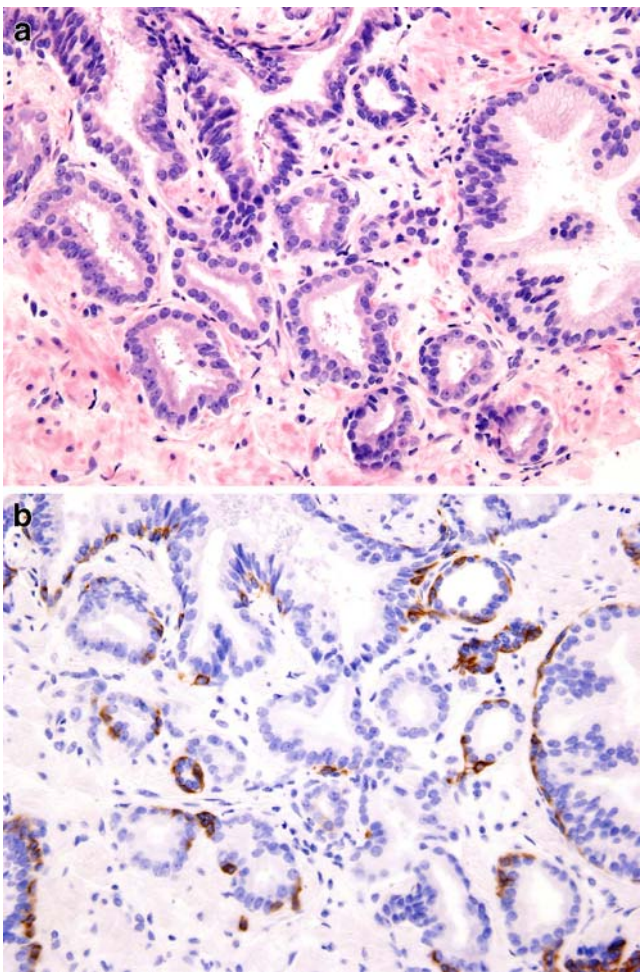

Fig. 22 **a** High-grade PIN with adjacent small atypical glands where the differential diagnosis is high-grade PIN with carcinoma versus outpouching or tangential sectioning of adjacent high-grade PIN (PINATYP). **b** High molecular weight cytokeratin stains show some glands with a patchy basal cell layer and others that are negative

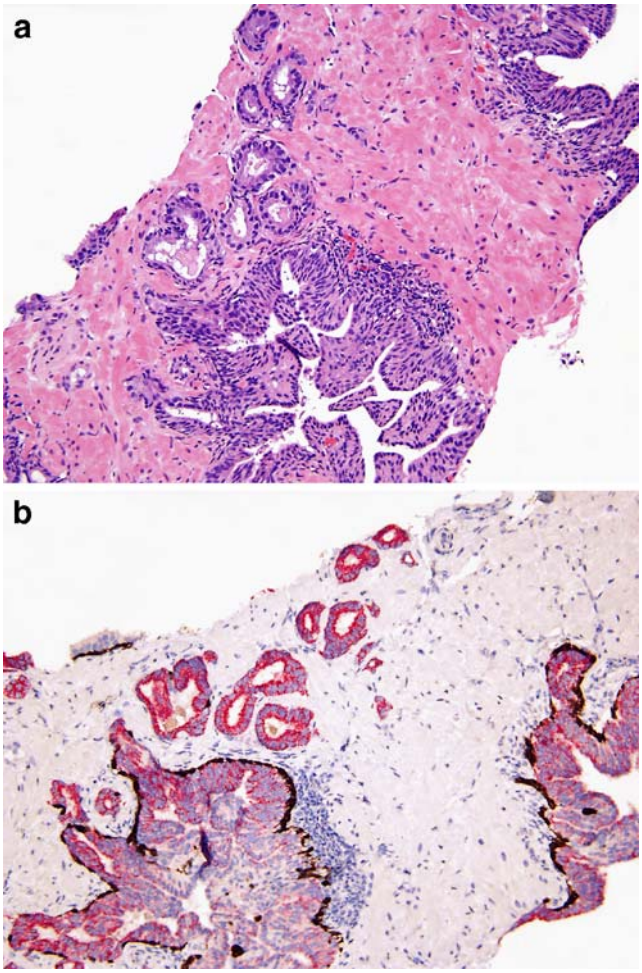

Fig. 23 **a** High-grade pin with small focus of adjacent carcinoma. The small glands of cancer trail away from the high-grade PIN. **b** Small glands of cancer are negative for high molecular weight cytokeratin and p63 (brown chromogen) and are positive for AMACR (red chromogen)

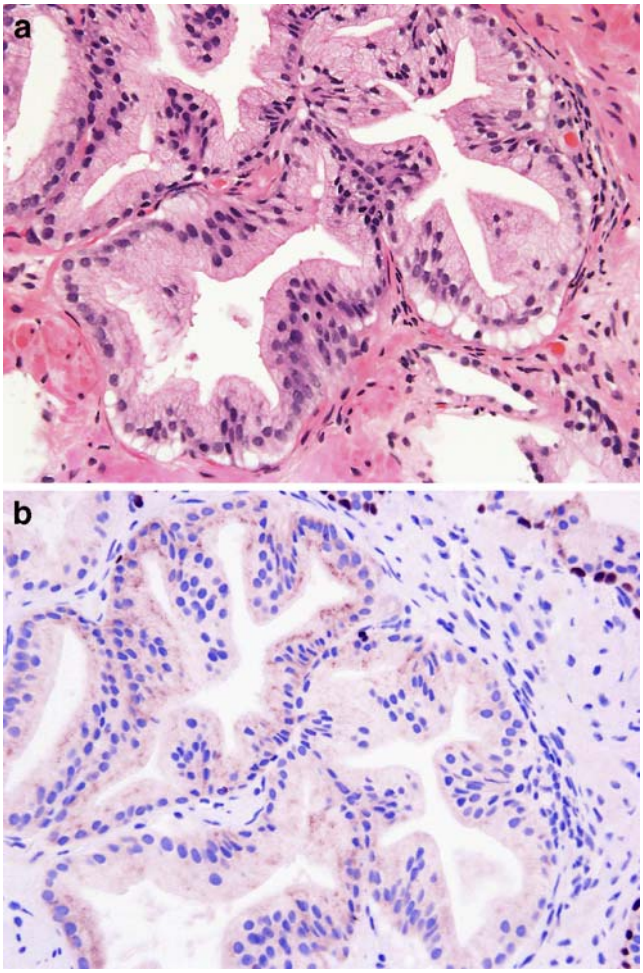

Fig. 24 **a** High-grade PIN. **b** High-grade PIN with rare basal cells labeled for p63. Depending on the plane of section, some glands of high-grade PIN many not demonstrate basal cell staining

distribution of benign glands. The use of basal cell markers in this differential diagnosis may be problematical, as both high-grade PIN and ductal adenocarcinoma may display a patchy basal cell layer. However, absence of a basal cell layer in numerous glands rules out PIN [29].

While the most common forms of ductal adenocarcinoma mimic micropapillary and cribriform high-grade PIN, ductal adenocarcinoma may be composed of simple glands lined by stratified columnar epithelium with cytological and architectural features of flat and tufting high-grade PIN. These PIN-like ductal cancers are distinguished from high-grade PIN either because the atypical glands are too crowded to represent high-grade PIN, or there are too many atypical glands that are negative for basal cell markers to be consistent with high-grade PIN (Fig. 26) [30, 31]. In some cases, there are only a few atypical glands with papillary fronds that are negative for basal cell markers that are highly suspicious for ductal adenocarcinoma, yet due to the limited number of atypical

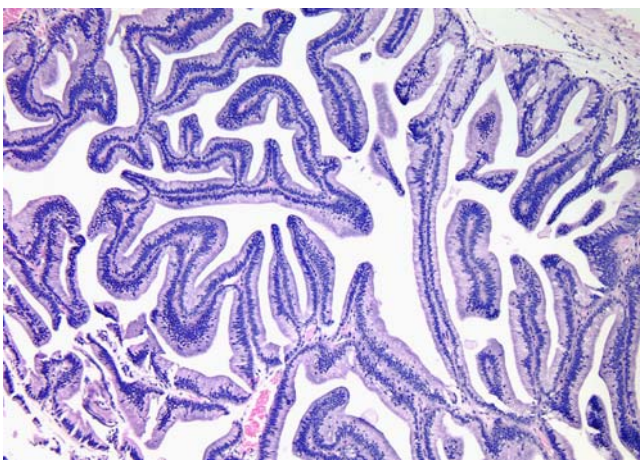

Fig. 25 Prostatic duct adenocarcinoma. Glands are too complex and show well-formed papillary fronds, ruling out high-grade PIN

glands, high-grade PIN cannot be ruled out with certainty. Repeat biopsy is recommended in these cases.

Immunohistochemistry

High-grade PIN typically demonstrates an interrupted immunoreactive single cell layer of basal cells when labeled with antibodies to either p63 or high molecular weight cytokeratin (Fig. 20). As high-grade PIN glands can have very discontinuous basal cells, one can envision tangential sections of PIN glands in which all cells would appear negative for basal cell markers, such that a few negative glands with the overall morphology of high-grade PIN is not diagnostic of cancer (Fig. 24). AMACR is upregulated in both carcinoma and high-grade PIN, such that it cannot be used to differentiate between the two entities [32].

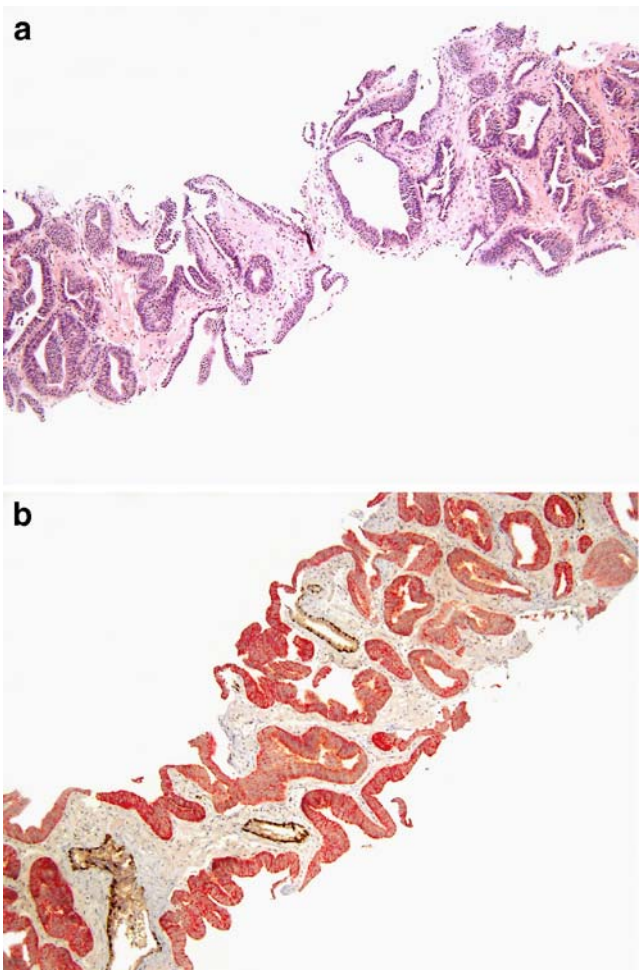

Fig. 26 **a** PIN-like ductal adenocarcinoma with numerous glands resembling high-grade PIN. **b** Triple cocktail demonstrates that all of the atypical glands are negative for basal cells (p63/HMWCK) and positive for AMACR diagnostic of carcinoma

Overall incidence of PIN

Based on data from a contemporary autopsy study, high-grade PIN is present in 8%, 23%, 29%, 49%, 53%, and 67% of Caucasian men from the third to eighth decades, respectively. Most of the cancers in the youngest groups are small and focal. Although these autopsies were optimally handled to select cases with less postmortem autolysis, these figures still most likely represent an underestimation of the true incidence as cases with focal high-grade PIN may have been under-recognized. In cystoprostatectomy specimens, the incidence of high-grade PIN ranges from 71% to and 83% [33]. African American men have higher incidences with corresponding values of high-grade PIN at autopsy of 7%, 26%, 46%, 72%, 75%, and 91%. This racial disparity has been noted in other countries as well, with African Brazilian men reported to have higher incidences of high-grade PIN at autopsy compared to white Brazilian men. Although they still have an increased risk of cancer following diagnosis of HGPIN on needle biopsy, Japanese men living in Japan have a much lower incidence of HGPIN compared to all men in the United States [34–36]. More recently, Han et al. demonstrated that the prevalence of HGPIN in Korean men with clinical prostate cancer was as great as that of Western men, with a lower prevalence of high-grade PIN in Asian men who underwent cystoprostatectomy [37]. Tan et al. also demonstrated that the current incidence of isolated high-grade PIN on prostate needle core biopsies in Asian men appears comparable to the rates reported for Western populations [38]. These data suggests that there has been an increase in either the detection or prevalence of high-grade PIN among certain Asian populations in recent times.

Relationship of PIN to carcinoma

There is epidemiological, morphological, and molecular evidence that high-grade PIN is a precursor lesion to some carcinomas of the prostate. PIN is first seen in men in their 20s and 30s and precedes the onset of prostate cancer by 10 years. Comparing prostates with and without carcinoma, there is an increase in the incidence, size, and number of high-grade PIN foci [39, 40]. Also, with increasing amounts of high-grade PIN, there are a greater number of multifocal carcinomas.

Morphologically, one can occasionally identify glands of carcinoma budding off from high-grade PIN as further histologic evidence that high-grade PIN is a precursor to some prostate carcinomas (Fig. 27) [41]. Several studies have also noted an increase of high-grade PIN in the peripheral zone of the prostate, corresponding to the site of origin for most adenocarcinomas of the prostate [42]. High-grade PIN is more closely related to peripheral, intermedi-

ate-, or high-grade cancers as opposed to low-grade transition zone cancers. Another feature shared with high-grade PIN and carcinoma is that with high-grade PIN, there is often a partial or, in some glands, a total lack of a basal cell layer when studied with basal cell markers (high molecular weight cytokeratin, p63).

Frequent changes in both prostate cancer and high-grade PIN are losses of chromosome 8p and gains of 8q. Chromosomal losses in high-grade PIN and cancer are also seen with some frequency in 10q, 16q, and 18q with gains of chromosomes 7, 10, 12, and Y. Overall, high-grade PIN has greater aneuploidy than benign prostate tissue, although somewhat less than seen in some invasive carcinomas. Telomere shortening and increased telomerase activity are both seen in high-grade PIN and invasive carcinoma. Glutathionine S-transferase P1 is hypermethylated in many high-grade PIN glands, paralleling the process seen with carcinoma. Overexpression in some cases of both high-grade PIN and carcinoma are seen in p16, p53, Bcl-2, MYC, alpha-methylacyl-coA racemase (AMACR), as well as many other genes. Decreased expression of genes are also identified in some cases of both high-grade PIN and carcinoma including NKX3.1 and p27 [39, 42, 43]. About 20% of high-grade PIN lesions harbor a *TMPRSS2-ERG* fusion gene, which is a common molecular abnormality detectable in about 50% of prostate cancers [44, 45]. Proliferative and apoptotic rates are increased in high-grade PIN analogous to that seen in carcinoma compared to benign glands.

With the prostate, there is currently no capability of monitoring a PIN focus to determine whether (a) there is no already infiltrating carcinoma at that site or (b) when infiltrating carcinoma evolves has it done so in the immediate vicinity of the PIN focus. Consequently, the one piece of evidence that we have for premalignant lesions in other organs, which is lacking in the prostate, is the natural history of high-grade PIN. The term "carcinoma in situ" of the prostate is not recommended as it has implications that these lesions will develop into infiltrating carcinoma at a sufficiently high frequency that may lead some clinicians to treat these lesions in a radical fashion.

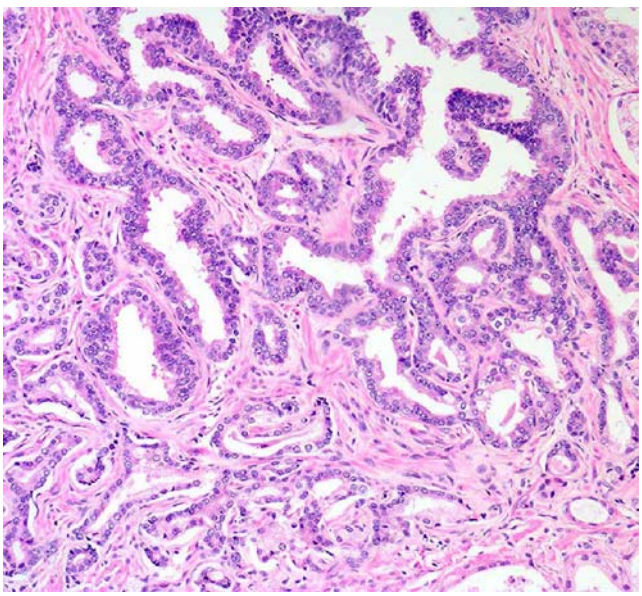

Fig. 27 Small glands of infiltrating carcinoma budding off of adjacent high-grade PIN

There is evidence that not all prostate cancers arise from high-grade PIN. The majority of prostates with early carcinomas lack any high-grade PIN within the entirely embedded prostate glands. In addition, even in prostate glands where there exists both early cancer and high-grade PIN, in only one third of the cases is high-grade PIN adjacent to the cancer [46, 47]. Low-grade carcinomas, especially those present within the transition zone are not closely related to high-grade PIN. In summary, it appears that high-grade PIN is a precursor lesion to many but not all peripheral intermediate to high-grade adenocarcinomas of the prostate.

Low-grade PIN on biopsy: risk of cancer on rebiopsy

Low-grade PIN on biopsy should not be listed in pathology reports as: (1) there is a lack of reproducibility in its diagnosis even by uropathologists; and (2) it is not associated with a higher risk of cancer on rebiopsy compared to that following a benign diagnosis on initial biopsy [48].

High-grade PIN on biopsy: incidence

There is marked variation within the literature on the incidence of high-grade PIN on needle biopsy, ranging from 0% to 24.6% [48]. The mean reported incidence of high-grade PIN on needle biopsy is 7.6% with a median value of 4.7%. Contrary to what might be expected, there is no consistent relationship between the number of cores sampled and the incidence of high-grade PIN on needle biopsy. The incidence of high-grade PIN on 24 core saturation biopsy was 22% according to one study [49].

The most likely explanation for the observed variation in the incidence of high-grade PIN relates to the vague definition of high-grade PIN. There are no criteria as to how prominent or how frequent the nucleoli must be to diagnose high-grade PIN. Different thresholds to diagnose high-grade PIN include: (1) any visible nucleoli; (2) nucleoli visible in at least 10% of the cells in the gland; (3) complete involvement of a gland with cells having nucleoli; and (4) nucleoli visible at ×20 magnification [50, 51]. In one study, 75% of cases diagnosed as high-grade PIN by outside pathologists sent to a genitourinary

pathology expert at the request of either the patient or urologist were confirmed as high-grade PIN [52].

Technical factors relating to the processing of needle biopsy specimens can also contribute to the reported variability in the incidence of high-grade PIN on biopsy. Fixatives that enhance nuclear detail and nucleolar prominence can increase the diagnosis of high-grade PIN, whereas thick sections and increased uptake of dyes can obscure fine nuclear detail. Although one study has reported that African American men have a higher incidence of high-grade PIN than Caucasian men, this by itself is unlikely an explanation for the marked variation seen in the literature [53].

High-grade PIN on biopsy: risk of cancer on rebiopsy

Studies from the early 1990s on relatively few cases reported a 50% risk of cancer following the diagnosis of high-grade PIN [48]. These earlier studies utilized sextant biopsies on the initial biopsy which missed associated cancers resulting in only high-grade PIN on the initial biopsy. On rebiopsy, some of these initially missed cancers were detected, yielding a high rebiopsy risk of cancer. More contemporary data report that the median risk of cancer following a diagnosis of high-grade PIN on biopsy is only 22% [48]. This compares to the median risk of finding cancer in a repeat biopsy following a benign diagnosis of 15–19% [48]. Of 12 publications that have examined in the same study the risk of cancer on rebiopsy following a needle biopsy diagnosis of high-grade PIN to that following a benign diagnosis, nine showed no statistically significant difference [48]. In these contemporary studies, sampling more extensively on the initial biopsy detects many associated cancers, such that, when only high-grade PIN is found, they often truly represent isolated high-grade PIN; therefore, re-biopsy even with good sampling does not detect many additional cancers [54]. The importance of sampling can be seen in the study by Eskicorapci et al. where the risk of cancer after an initial sextant biopsy showing HGPIN was 56.5% and was significantly more than following a benign diagnosis [55]. In contrast, Eskicorapci found that the risk of cancer after an extended biopsy (ten cores) showing HGPIN was only 22.9% and was not statistically different than that seen following a benign diagnosis.

Clinical parameters (various serum PSA measurements, digital rectal exam, imaging studies) do not identify which men with high-grade PIN on needle biopsy are more likely to have cancer on re-biopsy [48]. The morphology of high-grade PIN (flat vs. tufting vs. micropapillary vs. cribriform) also does not discriminate which high-grade PIN lesions are at greater risk of being associated with carcinoma on repeat biopsy, although it can be difficult to differentiate cribriform high-grade PIN from cribriform carcinoma from intraductal carcinoma [56–59]. The number of cores involved by high-grade PIN is the one pathological parameter that predicts a higher risk of subsequent carcinoma on rebiopsy. High-grade PIN on >3 cores is associated with a sufficiently high risk of subsequent cancer that rebiopsy within a year of the initial PIN diagnosis is warranted [60–62].

Recently, several studies have suggested that molecular findings associated with a high-grade prostatic intraepithelial neoplasia lesion might be able to predict which men are more likely to have cancer on rebiopsy. In one study utilizing radical prostatectomy specimens, high-grade PIN lesions adjacent to carcinoma had more AMACR overexpression (56%) than high-grade PIN lesions away from cancer (14%) [63]. In a recent study using needle biopsy cores, patients with at least one AMACR-positive high-grade PIN gland were 5.2 times more likely to have a subsequent diagnosis of prostate cancer on repeat biopsy than those without any AMACR-positive high-grade PIN glands [64]. Further studies are needed to determine whether quantitative AMACR expression of high-grade PIN lesions on needle biopsy could help predict which patients are more likely to have cancer. Other markers detected by immunohistochemistry, such as PTOV1, may be useful in the future to determine which PIN patients are more likely be diagnosed with cancer on re-biopsy, but all these markers are currently experimental and are not in routine use [65].

For cases with 1 or 2 cores of high-grade PIN on needle biopsy, it is recommended that men do not need a routine repeat needle biopsy within the first year following the diagnosis of high-grade PIN in the absence of other clinical indicators of cancer [48, 66]. In cases with high-grade PIN and adjacent small atypical glands, where the differential diagnosis of the small glands is adjacent cancer or outpouchings off the high-grade PIN (PINATYP), the risk of cancer is equivalent to that following a diagnosis of "atypical glands suspicious for carcinoma"; all these men need rebiopsy within 3–6 months of their PINATYP diagnosis [67].

There is scant data on the long-term risk of cancer following a diagnosis of high-grade PIN. Lefkowitz et al. reported in a small series that following an initial diagnosis of high-grade PIN on 12-core biopsy, the rate of cancer on repeat 12-core biopsy at 3 years was higher than if the rebiopsy was performed within 1 year of the high-grade PIN diagnosis [68, 69]. They hypothesized that the 3 year interval either allowed unsampled small cancers that were associated with the high-grade PIN at the time of initial biopsy to grow to a size where repeat biopsy could detect them, or alternatively some of the high-grade PIN lesions progressed to cancer over this 3 year interval. In an unpublished update from this group, they performed a 3-year-delayed interval biopsy in 101 men with isolated high-grade PIN and a 6-year delayed interval biopsy,

demonstrating cancer detection rates of 23.2% and 28.6%, respectively. Izawa et al. followed for an average of 72.2 months 21 men with isolated high-grade PIN. A total of seven men were diagnosed with cancer. Although these few studies lack a control population to assess the risk in men without high-grade PIN, because of the potential medico-legal consequences of not following up on a high-grade PIN diagnosis, a reasonable approach is to perform repeat biopsy 2–3 years following a high-grade PIN diagnosis on needle biopsy until more data is gathered. Rebiopsy should be proportionally more in the region of the original high-grade PIN site and in adjacent sites, although the entire prostate should be sampled [70–73].

High-grade PIN on TURP

There have been fewer studies on high-grade PIN on TURP. The reported incidence of high-grade PIN on TURP has varied widely from 2.8%, 3.2%, 17.8%, to 33% in the four studies reporting on this issue [66]. Three studies have found that high-grade PIN on TURP places an individual at higher risk for the subsequent detection of cancer, yet a long-term study from Norway demonstrated no association between the presence of high-grade PIN on TURP and the incidence of subsequent cancer [74–77]. In a younger man with high-grade PIN on TURP, we recommend that needle biopsies be performed to rule out a peripheral zone cancer. In an older man without elevated serum PSA levels, clinical follow-up is probably sufficient. When high-grade PIN is found on TURP, some pathologists recommend sectioning deeper into the corresponding block, and most pathologists recommend processing the entire specimen [75].

Intraductal carcinoma of the prostate

Intraductal carcinoma of the prostate (IDC-P) has in several studies been described in radical prostatectomy specimens [78–82]. Rarely, IDC-P may be identified on biopsy material in the absence of infiltrating carcinoma [83]. The definition of IDC-P on needle biopsy identifies objective morphological criteria that either architecturally or cytologically clearly exceed those seen in high-grade PIN (Figs. 28 and 29) (Table 2). Although dense cribriform (more solid than luminal areas) and solid patterns are not architectural patterns associated with high-grade PIN, loose cribriform and micropapillary patterns overlap between the two entities. To establish the diagnosis of IDC-P in the latter two patterns, markedly enlarged nuclei (six times larger than those in adjacent non-neoplastic cells) and nonfocal comedonecrosis are required. Cases which do not satisfy the strict criteria for IDC-P on needle biopsy yet appear more atypical either architecturally or cytologically than usual high-grade PIN can be diagnosed as borderline between IDC-P and high-grade PIN with a recommendation for immediate repeat biopsy.

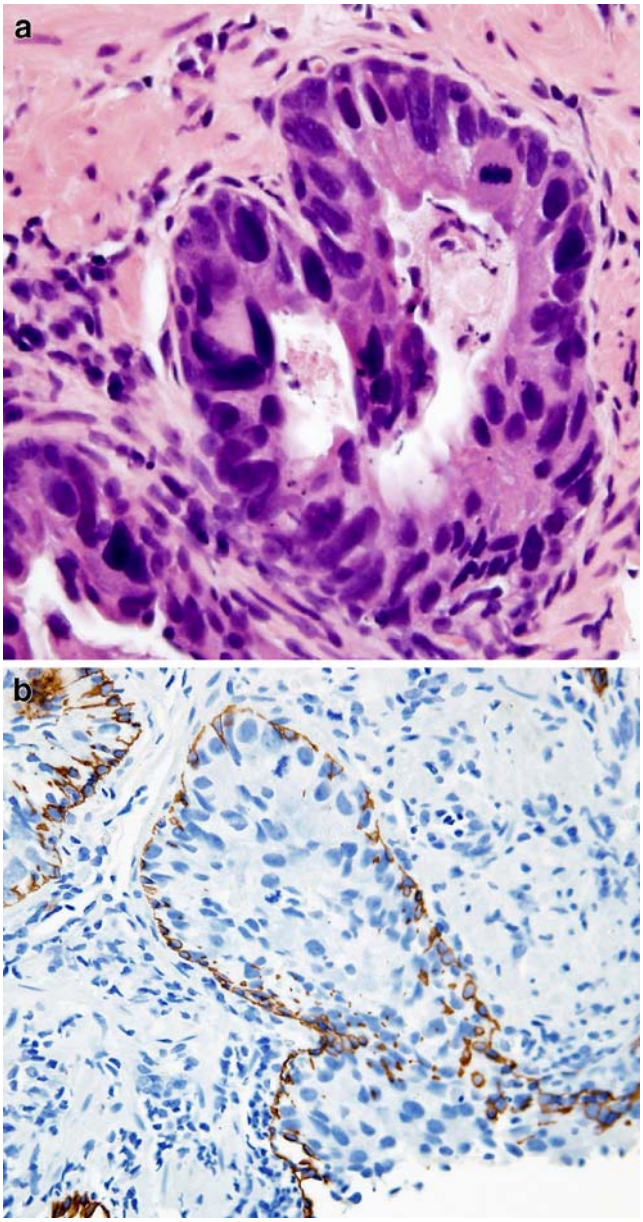

Fig. 28 **a** Intraductal carcinoma with marked nuclear pleomorphism beyond that seen with high-grade PIN. **b** High molecular weight cytokeratin outlines a preserved basal cell layer

Infiltrating cribriform acinar adenocarcinoma (Gleason pattern 4 or Gleason pattern 5 with comedonecrosis) closely mimics cribriform IDC-P. Most cases of IDC-P would be diagnosed as cribriform carcinoma if immunohistochemistry demonstrating basal cells had not been performed. In some cases, the contour and branching pattern of normal duct architecture distinguishes IDC-P from infiltrating carcinoma. Ultimately, the presence of a basal cell layer either identified on routine hematoxylin and eosin prepared slides or with

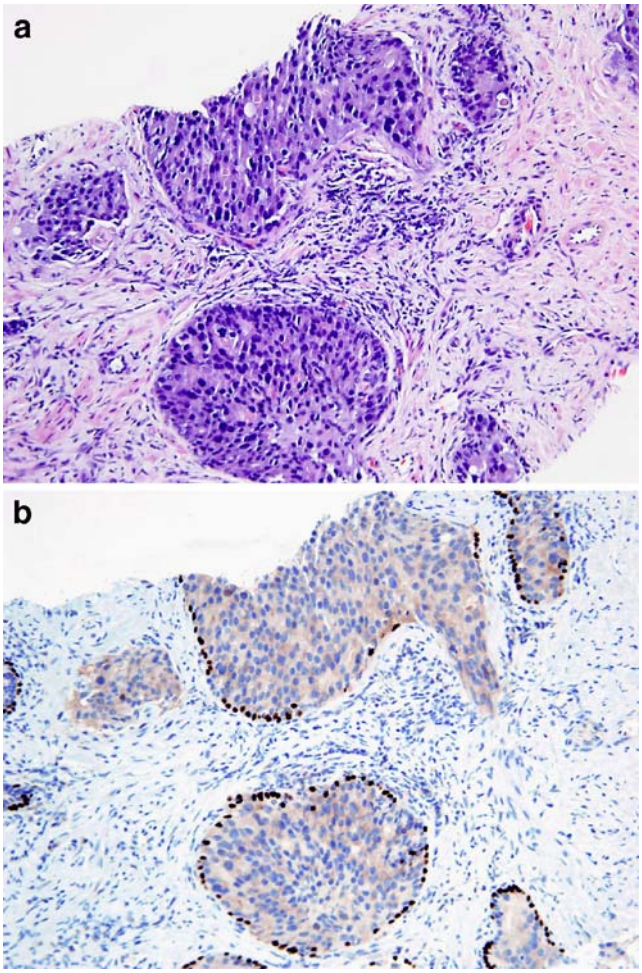

Fig. 29 **a** Intraductal carcinoma with solid nests and dense cribriform structures. **b** The nests are surrounded by basal cells visible on p63 immunohistochemistry

immunohistochemistry rules out infiltrating acinar prostate adenocarcinoma.

There is significant morphological overlap between ductal adenocarcinoma of the prostate and IDC-P. Distinguishing features seen in ductal adenocarcinoma include tall pseudostratified columnar epithelium usually with amphophilic cytoplasm, classically arranged in cribriform patterns with slit-like spaces and/or true papillary fronds. In contrast, IDC-P has cuboidal cells, cribriform patterns with rounded lumina, and micropapillary tufts without fibrovascular cores. In addition, basal cells are generally absent in ductal adenocarcinoma, although occasionally, there may be partial retention of basal cells as ductal adenocarcinoma can also spread within prostatic ducts.

Solid patterns of IDC-P may mimic intraductal spread of urothelial carcinoma in the prostate, as both demonstrate solid intraductal–acinar involvement [84]. Other overlapping morphological features include marked nuclear pleomorphism, frequent mitotic activity, and comedo-necrosis. However, solid patterns of IDC-P are often associated with cribriform or glandular patterns. When it is difficult to distinguish IDC-P from urothelial carcinoma, immunohistochemical studies generally resolve the problem, as IDC-P is usually positive for PSA, but negative for high molecular weight cytokeratin, p63, and thrombomodulin, opposite to what is typically seen with urothelial carcinoma.

Despite its morphology resembling high-grade PIN, IDC-P is not likely to be a preinvasive neoplastic condition. While high-grade PIN is often present in prostate glands that have not yet developed invasive carcinoma, IDC-P is almost always associated with invasive cancer. IDC-P on prostate biopsies is frequently associated with high-grade cancer and poor prognostic parameters at radical prostatectomy as well as advanced disease following other therapies [83]. Dawkins et al. found that 29% of Gleason pattern 4 cancers and 60% of IDC-P demonstrated loss of heterozygosity (LOH), while LOH was rarely observed in PIN and Gleason pattern 3 adenocarcinoma [85]. Their results indicate that IDC-P is a distinct lesion from high-grade PIN and represents a late event in prostate cancer evolution. Prostate cancers associated with IDC-P also have a higher Gleason score and larger tumor volume and are more likely to show seminal vesicle involvement and disease progression than those without IDC-P [82]. These findings support that IDC-P represents intraductal spread of carcinoma within preexisting ducts and acini and should not be categorized as a preinvasive neoplastic condition. Consideration should be given to treat patients with IDC-P on biopsy with definitive therapy even in the absence of documented infiltrating cancer.

Conclusions

High-grade PIN remains the one well-recognized precursor lesion to prostate cancer, although not all prostate cancers arise from high-grade PIN. The distinction of high-grade PIN from its many benign and malignant mimickers is now well characterized, although the distinction of low-grade PIN from high-grade PIN remains a problem due to the subjective and vague definition of high-grade PIN. The most significant change in our understanding and management of high-grade PIN has been that there is a decreased

Table 2 Definition of intraductal carcinoma

Malignant epithelial cells filling large acini and prostatic ducts, with preservation of basal cells and:
Solid or dense cribriform pattern or
Loose cribriform or micropapillary pattern with either:
Marked nuclear atypia: nuclear size 6× normal
Nonfocal comedonecrosis

risk of cancer following a biopsy showing high-grade PIN in the current era of extended prostate biopsy. Additional studies are needed to determine whether routine repeat biopsy should be performed several years following a high-grade PIN diagnosis on needle biopsy and, if so, how often and when. Molecular characterization of high-grade PIN on needle biopsy holds promise in helping to predict which PIN lesions are more likely associated with cancer. However, at the current time, the key role of the pathologist is to accurately diagnose high-grade PIN and its extent, along with educating urologists as to the decreased short-term and indeterminate long-term risk of cancer following its diagnosis on needle biopsy.

Conflict of Interest Statement I declare that I have no conflict of interest.

References

1. Cheng L, Shan A, Cheville JC, Qian J, Bostwick DG (1998) Atypical adenomatous hyperplasia of the prostate: a premalignant lesion? Cancer Res 58:389–391
2. Doll JA, Zhu X, Furman J et al (1999) Genetic analysis of prostatic atypical adenomatous hyperplasia (adenosis). Am J Pathol 155:967–971
3. Bettendorf O, Schmidt H, Eltze E et al (2005) Cytogenetic changes and loss of heterozygosity in atypical adenomatous hyperplasia, in carcinoma of the prostate and in non-neoplastic prostate tissue using comparative genomic hybridization and multiplex-PCR. Int J Oncol 26:267–274
4. Qian J, Jenkins RB, Bostwick DG (1995) Chromosomal anomalies in atypical adenomatous hyperplasia and carcinoma of the prostate using fluorescence in situ hybridization. Urology 46: 837–842
5. Meyer F, Tetu B, Bairati I, Lacombe L, Fradet Y (2006) Prostatic intraepithelial neoplasia in TURP specimens and subsequent prostate cancer. Can J Urol 13:3255–3260
6. Palapattu GS, Sutcliffe S, Bastian PJ et al (2005) Prostate carcinogenesis and inflammation: emerging insights. Carcinogenesis 26:1170–1181
7. Postma R, Schroder FH, van der Kwast TH (2005) Atrophy in prostate needle biopsy cores and its relationship to prostate cancer incidence in screened men. Urology 65:745–749
8. Bostwick DG, Brawer MK (1987) Prostatic intra-epithelial neoplasia and early invasion in prostate cancer. Cancer 59:788–794
9. Drago JR, Mostofi FK, Lee F (1989) Introductory remarks and workshop summary. Urol (suppl) 34:2–3
10. McNeal JE (1969) Origin and development of carcinoma in the prostate. Cancer 23:24–34
11. McNeal JE, Bostwick DG (1986) Intraductal dysplasia: a premalignant lesion of the prostate. Hum Pathol 17:64–71
12. Bostwick DG, Amin MB, Dundore P, Marsh W, Schultz DS (1993) Architectural patterns of high-grade prostatic intraepithelial neoplasia. Hum Pathol 24:298–310
13. Argani P, Epstein JI (2001) Inverted (hobnail) high-grade prostatic intraepithelial neoplasia (PIN): report of 15 cases of a previously undescribed pattern of high-grade PIN. Am J Surg Pathol 25:1534–1539
14. Berman DM, Yang J, Epstein JI (2000) Foamy gland high-grade prostatic intraepithelial neoplasia. Am J Surg Pathol 24:140–144
15. Reyes AO, Swanson PE, Carbone JM, Humphrey PA (1997) Unusual histologic types of high-grade prostatic intraepithelial neoplasia. Am J Surg Pathol 21:1215–1222
16. Melissari M, Lopez Beltran A, Mazzucchelli R, Froio E, Bostwick DG, Montironi R (2006) High grade prostatic intraepithelial neoplasia with squamous differentiation. J Clin Pathol 59:437–439
17. Srodon M, Epstein JI (2002) Central zone histology of the prostate: a mimicker of high-grade prostatic intraepithelial neoplasia. Hum Pathol 33:518–523
18. Ayala AG, Srigley JR, Ro JY, Abdul-Karim FW, Johnson DE (1986) Clear cell cribriform hyperplasia of prostate. Report of 10 cases. Am J Surg Pathol 10:665–671
19. Devaraj LT, Bostwick DG (1993) Atypical basal cell hyperplasia of the prostate. immunophenotypic profile and proposed classification of basal cell proliferations. Am J Surg Pathol 17:645–659
20. Epstein JI, Armas OA (1992) Atypical basal cell hyperplasia of the prostate. Am J Surg Pathol 16:1205–1214
21. Hosler GA, Epstein JI (2005) Basal cell hyperplasia: an unusual diagnostic dilemma on prostate needle biopsies. Hum Pathol 36:480–485
22. Hedrick L, Epstein JI (1989) Use of keratin 903 as an adjunct in the diagnosis of prostate carcinoma. Am J Surg Pathol 13:389–396
23. Epstein JI, Grignon DJ, Humphrey PA et al (1995) Interobserver reproducibility in the diagnosis of prostatic intraepithelial neoplasia. Am J Surg Pathol 19:873–886
24. Kronz JD, Shaikh AA, Epstein JI (2001) Atypical cribriform lesions on prostate biopsy. Am J Surg Pathol 25:147–155
25. Kronz JD, Shaikh AA, Epstein JI (2001) High-grade prostatic intraepithelial neoplasia with adjacent small atypical glands on prostate biopsy. Hum Pathol 32:389–395
26. Christensen WN, Steinberg G, Walsh PC, Epstein JI (1991) Prostatic duct adenocarcinoma. findings at radical prostatectomy. Cancer 67:2118–2124
27. Bostwick DG, Kindrachuk RW, Rouse RV (1985) Prostatic adenocarcinoma with endometrioid features. clinical, pathologic, and ultrastructural findings. Am J Surg Pathol 9:595–609
28. Epstein JI, Woodruff JM (1986) Adenocarcinoma of the prostate with endometrioid features. A light microscopic and immunohistochemical study of ten cases. Cancer 57:111–119
29. Samaratunga H, Singh M (1997) Distribution pattern of basal cells detected by cytokeratin 34 beta E12 in primary prostatic duct adenocarcinoma. Am J Surg Pathol 21:435–440
30. Hameed O, Humphrey PA (2006) Stratified epithelium in prostatic adenocarcinoma: a mimic of high-grade prostatic intraepithelial neoplasia. Mod Pathol 19:899–906
31. Tavora F, Epstein JI (2008) High-grade prostatic intraepithelial neoplasia-like ductal adenocarcinoma of the prostate: a clinicopathologic study of 28 cases. Am J Surg Pathol 32:1060–1067
32. Jiang Z, Woda BA, Wu CL, Yang XJ (2004) Discovery and clinical application of a novel prostate cancer marker: alpha-methylacyl CoA racemase (P504S). Am J Clin Pathol 122:275–289
33. Godoy G, Taneja SS (2008) Contemporary clinical management of isolated high-grade prostatic intraepithelial neoplasia. Prostate Cancer Prostatic Dis 11:20–31
34. Fujita MQ, Shin M, Yasunaga Y et al (1997) Incidence of prostatic intra-epithelial neoplasia in Osaka, Japan. Int J Cancer 73: 808–811
35. Watanabe M, Fukutome K, Kato H et al (1999) Progression-linked overexpression of c-met in prostatic intraepithelial neoplasia and latent as well as clinical prostate cancers. Cancer Lett 141: 173–178
36. Sakr WA (1999) Prostatic intraepithelial neoplasia: a marker for high-risk groups and a potential target for chemoprevention. Eur Urol 35:474–478

37. Han KS, Jeong IG, Joung JY et al (2007) Prevalence of high-grade prostatic intraepithelial neoplasia in prostate gland of Korean men: comparisons between radical prostatectomy and cystoprostatectomy. Urology 70:1100–1103
38. Tan PH, Tan HW, Tan Y, Lim CN, Cheng C, Epstein JI (2006) Is high-grade prostatic intraepithelial neoplasia on needle biopsy different in an Asian population: a clinicopathologic study performed in Singapore. Urology 68:800–803
39. Bostwick DG, Qian J (2004) High-grade prostatic intraepithelial neoplasia. Mod Pathol 17:360–379
40. Joniau S, Goeman L, Pennings J, Van Poppel H (2005) Prostatic intraepithelial neoplasia (PIN): importance and clinical management. Eur Urol 48:379–385
41. McNeal JE, Villers A, Redwine EA, Freiha FS, Stamey TA (1991) Microcarcinoma in the prostate: its association with duct-acinar dysplasia. Hum Pathol 22:644–652
42. Haggman MJ, Macoska JA, Wojno KJ, Oesterling JE (1997) The relationship between prostatic intraepithelial neoplasia and prostate cancer: critical issues. J Urol 158:12–22
43. Bostwick DG, Pacelli A, Lopez-Beltran A (1996) Molecular biology of prostatic intraepithelial neoplasia. Prostate 29:117–134
44. Cerveira N, Ribeiro FR, Peixoto A et al (2006) TMPRSS2-ERG gene fusion causing ERG overexpression precedes chromosome copy number changes in prostate carcinomas and paired HGPIN lesions. Neoplasia 8:826–832
45. Perner S, Mosquera JM, Demichelis F et al (2007) TMPRSS2-ERG fusion prostate cancer: an early molecular event associated with invasion. Am J Surg Pathol 31:882–888
46. Sakr WA, Grignon DJ, Crissman JD et al (1994) High grade prostatic intraepithelial neoplasia (HGPIN) and prostatic adenocarcinoma between the ages of 20–69: an autopsy study of 249 cases. In Vivo 8:439–443
47. Sakr WA, Haas GP, Cassin BF, Pontes JE, Crissman JD (1993) The frequency of carcinoma and intraepithelial neoplasia of the prostate in young male patients. J Urol 150:379–385
48. Epstein JI, Herawi M (2006) Prostate needle biopsies containing prostatic intraepithelial neoplasia or atypical foci suspicious for carcinoma: implications for patient care. J Urol 175:820–834
49. Schoenfield L, Jones JS, Zippe CD et al (2007) The incidence of high-grade prostatic intraepithelial neoplasia and atypical glands suspicious for carcinoma on first-time saturation needle biopsy, and the subsequent risk of cancer. BJU Int 99:770–774
50. Egevad L, Allsbrook WC Jr, Epstein JI (2006) Current practice of diagnosis and reporting of prostate cancer on needle biopsy among genitourinary pathologists. Hum Pathol 37:292–297
51. Allam CK, Bostwick DG, Hayes JA et al (1996) Interobserver variability in the diagnosis of high-grade prostatic intraepithelial neoplasia and adenocarcinoma. Mod Pathol 9:742–751
52. Chan TY, Epstein JI (2005) Patient and urologist driven second opinion of prostate needle biopsies. J Urol 174:1390–1394
53. Fowler JE Jr, Bigler SA, Lynch C, Wilson SS, Farabaugh PB (2001) Prospective study of correlations between biopsy-detected high grade prostatic intraepithelial neoplasia, serum prostate specific antigen concentration, and race. Cancer 91:1291–1296
54. Herawi M, Kahane H, Cavallo C, Epstein JI (2006) Risk of prostate cancer on first re-biopsy within 1 year following a diagnosis of high grade prostatic intraepithelial neoplasia is related to the number of cores sampled. J Urol 175:121–124
55. Eskicorapci SY, Guliyev F, Islamoglu E, Ergen A, Ozen H (2007) The effect of prior biopsy scheme on prostate cancer detection for repeat biopsy population: results of the 14-core prostate biopsy technique. Int Urol Nephrol 39:189–195
56. Bishara T, Ramnani DM, Epstein JI (2004) High-grade prostatic intraepithelial neoplasia on needle biopsy: risk of cancer on repeat biopsy related to number of involved cores and morphologic pattern. Am J Surg Pathol 28:629–633
57. Davidson D, Bostwick DG, Qian J et al (1995) Prostatic intraepithelial neoplasia is a risk factor for adenocarcinoma: predictive accuracy in needle biopsies. J Urol 154:1295–1299
58. Kronz JD, Allan CH, Shaikh AA, Epstein JI (2001) Predicting cancer following a diagnosis of high-grade prostatic intraepithelial neoplasia on needle biopsy: data on men with more than one follow-up biopsy. Am J Surg Pathol 25:1079–1085
59. San Francisco IF, Olumi AF, Kao J, Rosen S, DeWolf WC (2003) Clinical management of prostatic intraepithelial neoplasia as diagnosed by extended needle biopsies. BJU Int 91:350–354
60. Abdel-Khalek M, El-Baz M, Ibrahiem E (2004) Predictors of prostate cancer on extended biopsy in patients with high-grade prostatic intraepithelial neoplasia: a multivariate analysis model. BJU Int 94:528–533
61. Netto GJ, Epstein JI (2006) Widespread high-grade prostatic intraepithelial neoplasia on prostatic needle biopsy: a significant likelihood of subsequently diagnosed adenocarcinoma. Am J Surg Pathol 30:1184–1188
62. Akhavan A, Keith JD, Bastacky SI, Cai C, Wang Y, Nelson JB (2007) The proportion of cores with high-grade prostatic intraepithelial neoplasia on extended-pattern needle biopsy is significantly associated with prostate cancer on site-directed repeat biopsy. BJU Int 99:765–769
63. Wu CL, Yang XJ, Tretiakova M et al (2004) Analysis of alpha-methylacyl-CoA racemase (P504S) expression in high-grade prostatic intraepithelial neoplasia. Hum Pathol 35:1008–1013
64. Stewart J, Fleshner N, Cole H, Toi A, Sweet J (2008) Prognostic significance of alpha-methylacyl-coA racemase among men with high grade prostatic intraepithelial neoplasia in prostate biopsies. J Urol 179:1751–1755
65. Morote J, Fernandez S, Alana L et al (2008) PTOV1 expression predicts prostate cancer in men with isolated high-grade prostatic intraepithelial neoplasia in needle biopsy. Clin Cancer Res 14: 2617–2622
66. Godoy G, Taneja SS (2008) Contemporary clinical management of isolated high-grade prostatic intraepithelial neoplasia. Prostate Cancer Prostatic Dis 11:20–31
67. Kronz JD, Shaikh AA, Epstein JI (2001) High-grade prostatic intraepithelial neoplasia with adjacent small atypical glands on prostate biopsy. Hum Pathol 32:389–395
68. Lefkowitz GK, Sidhu GS, Torre P, Lepor H, Taneja SS (2001) Is repeat prostate biopsy for high-grade prostatic intraepithelial neoplasia necessary after routine 12-core sampling? Urology 58: 999–1003
69. Lefkowitz GK, Taneja SS, Brown J, Melamed J, Lepor H (2002) Follow-up interval prostate biopsy 3 years after diagnosis of high grade prostatic intraepithelial neoplasia is associated with high likelihood of prostate cancer, independent of change in prostate specific antigen levels. J Urol 168:1415–1418
70. Kamoi K, Troncoso P, Babaian RJ (2000) Strategy for repeat biopsy in patients with high grade prostatic intraepithelial neoplasia. J Urol 163:819–823
71. Naya Y, Ayala AG, Tamboli P, Babaian RJ (2004) Can the number of cores with high-grade prostate intraepithelial neoplasia predict cancer in men who undergo repeat biopsy? Urology 63: 503–508
72. Park S, Shinohara K, Grossfeld GD, Carroll PR (2001) Prostate cancer detection in men with prior high grade prostatic intraepithelial neoplasia or atypical prostate biopsy. J Urol 165:1409–1414
73. Girasole CR, Cookson MS, Putzi MJ et al (2006) Significance of atypical and suspicious small acinar proliferations, and high grade prostatic intraepithelial neoplasia on prostate biopsy: implications for cancer detection and biopsy strategy. J Urol 175:929–933
74. Pacelli A, Bostwick DG (1997) Clinical significance of high-grade prostatic intraepithelial neoplasia in transurethral resection specimens. Urology 50:355–359

75. Gaudin PB, Sesterhenn IA, Wojno KJ, Mostofi FK, Epstein JI (1997) Incidence and clinical significance of high-grade prostatic intraepithelial neoplasia in TURP specimens. Urology 49:558–563
76. Harvei S, Sander S, Tretli S, Langmark F (1993) Survival after transurethral and transvesical surgery in localized cancer of the prostate, Norway 1957–1981. Cancer 71:3966–3971
77. Meyer F, Tetu B, Bairati I, Lacombe L, Fradet Y (2006) Prostatic intraepithelial neoplasia in TURP specimens and subsequent prostate cancer. Can J Urol 13:3255–3260
78. Cohen RJ, McNeal JE, Baillie T (2000) Patterns of differentiation and proliferation in intraductal carcinoma of the prostate: significance for cancer progression. Prostate 43:11–19
79. McNeal JE, Reese JH, Redwine EA, Freiha FS, Stamey TA (1986) Cribriform adenocarcinoma of the prostate. Cancer 58:1714–1719
80. McNeal JE, Yemoto CE (1996) Spread of adenocarcinoma within prostatic ducts and acini. morphologic and clinical correlations. Am J Surg Pathol 20:802–814
81. Rubin MA, de La Taille A, Bagiella E, Olsson CA, O'Toole KM (1998) Cribriform carcinoma of the prostate and cribriform prostatic intraepithelial neoplasia: incidence and clinical implications. Am J Surg Pathol 22:840–848
82. Wilcox G, Soh S, Chakraborty S, Scardino PT, Wheeler TM (1998) Patterns of high-grade prostatic intraepithelial neoplasia associated with clinically aggressive prostate cancer. Hum Pathol 29:1119–1123
83. Guo CC, Epstein JI (2006) Intraductal carcinoma of the prostate on needle biopsy: histologic features and clinical significance. Mod Pathol 19:1528–1535
84. Oliai BR, Kahane H, Epstein JI (2001) A clinicopathologic analysis of urothelial carcinomas diagnosed on prostate needle biopsy. Am J Surg Pathol 25:794–801
85. Dawkins HJ, Sellner LN, Turbett GR et al (2000) Distinction between intraductal carcinoma of the prostate (IDC-P), high-grade dysplasia (PIN), and invasive prostatic adenocarcinoma, using molecular markers of cancer progression. Prostate 44: 265–270

Virchows Arch (2009) 454:17–23
DOI 10.1007/s00428-008-0706-6

ORIGINAL ARTICLE

Genomic hypomethylation and CpG island hypermethylation in prostatic intraepithelial neoplasm

Nam-Yun Cho · Jung Ho Kim · Kyung Chul Moon · Gyeong Hoon Kang

Received: 5 August 2008 / Revised: 10 October 2008 / Accepted: 16 November 2008 / Published online: 2 December 2008

Abstract Altered DNA methylation in cancer cells is characterized by focal CpG island hypermethylation and diffuse genomic hypomethylation. Both types of aberrant methylation are frequently found in human prostate adenocarcinoma (PCa). Prostatic intraepithelial neoplasm (PIN), a precursor lesion of PCa, has been demonstrated to contain CpG island hypermethylation, but little is known about the role of DNA hypomethylation. We analyzed the methylation status at 12 CpG island loci and at two repetitive DNA elements (*LINE-1* and *SAT2*) from normal prostate (n=20), PIN (n=25), and PCa (n=35) tissues using MethyLight assay or combined bisulfite restriction analysis. The methylation levels in *LINE-1* and *SAT2* decreased with progression of lesion types from normal prostate to PIN to PCa (P<0.05), whereas promoter CpG island loci displayed increased methylation. Ten genes were found to be hypermethylated in a cancer-specific manner and were further analyzed in another set of PCa tissues (n=64). The number of methylated genes was closely associated with TNM stage, Gleason sum, and preoperative serum PSA levels (P=0.020, 0.073, 0.033, respectively). These results suggest that genomic hypomethylation and CpG island hypermethylation, common among PCas, are early events in prostate carcinogenesis and may be implicated in the development of PIN.

Keywords CpG island · DNA methylation · Prostate adenocarcinoma · Prostate intraepithelial neoplasm

Introduction

Aberrant DNA methylation in cancer cells is characterized by focal CpG island hypermethylation and diffuse genomic hypomethylation. Promoter CpG island hypermethylation is associated with silencing of tumor suppressor genes or tumor-related genes, whereas diffuse genomic hypomethylation contributes to tumorigenesis by inducing chromosomal instability [12, 17]. The latter was demonstrated in a recent study in which structural or numerical chromosomal aberrations were induced by knocking out *DNMT1* and/or *DNMT3b*, which encode DNA methylases, in HCT116 cell lines [17]. Both types of aberrant DNA methylation have been observed in single tumors but have been shown to be not mechanically linked [5, 9, 10].

Prostate adenocarcinoma (PCa) is one of the tissue types of human cancer in which aberrant methylation changes are frequently found. To date, more than 50 genes have been shown to be inactivated by promoter CpG island hypermethylation in PCas [3]. Methylation of many of these genes has been demonstrated to be cancer-related and to correlate with clinicopathological parameters that predict poor prognosis, including high preoperative serum prostate specific antigen (PSA) levels, high Gleason scores, and high pathological tumor stage [2, 11, 16, 21]. Similarly, decreased genomic DNA methylation levels, assessed by

Electronic supplementary material The online version of this article (doi:10.1007/s00428-008-0706-6) contains supplementary material, which is available to authorized users.

N.-Y. Cho · G. H. Kang
Laboratory of Epigenetics, Cancer Research Institute,
Seoul National University College of Medicine,
Seoul, South Korea

J. H. Kim · K. C. Moon · G. H. Kang (✉)
Department of Pathology,
Seoul National University College of Medicine,
28 Yongon-dong, Chongno-gu,
Seoul 110-744, South Korea
e-mail: ghkang@snu.ac.kr

PCR analysis of surrogate repetitive DNA elements, have been shown to be tightly associated with these same PCa prognostic markers [5, 26].

Prostatic intraepithelial neoplasm (PIN) is recognized as a precursor lesion of PCa, evidenced by its common occurrence in the peripheral zone of the prostate, by higher incidence in tissue adjacent to PCas than in prostate tissue from non-cancer patients, and by molecular alterations similar to those in PCas [4, 25]. Promoter CpG island hypermethylation, which occurs commonly in PCas, has also been found in PINs, although with a decreased frequency compared to PCas [13, 16, 31]. However, genomic DNA hypomethylation, frequently observed in prostatic cancer cells, has been scarcely studied in PIN cells [22].

LINE-1 and *SAT2* are repetitive DNA elements and are located throughout the euchromatic regions of the genome and pericentromeric heterochromatin, respectively. These elements are heavily methylated in normal cells, and their methylation levels, as measured by PCR-based methods, correlate well with genomic 5-methylcytosine content [28]. In the present study, we examined the methylation status in 12 CpG island loci and in *LINE-1* and *SAT2* in PCa, PIN, and normal prostate tissues using real-time PCR-based methylation-specific PCR (MethyLight assay) or using combined bisulfite restriction analysis (COBRA). Our aim was to determine the chronological order of DNA hypo- and hypermethylation in the multistep carcinogenesis of PCa and to correlate DNA hypermethylation changes with clinicopathological factors of PCa patients.

Materials and methods

Patients and tissues

A total of 99 prostate samples were collected from patients treated at the Seoul National University Hospital, Seoul, Korea between 2002 and 2004. The samples were formalin-fixed, paraffin-embedded tissues from PCa patients that underwent radical prostatectomy (median age, 67 years; range 45–77 years). Twenty-five high-grade PIN samples were obtained from the prostatectomy specimens harboring PCa (median age, 68 years; range 57–75 years). Low-grade PINs were excluded from the study because of the ambiguity of histologic criteria for defining low-grade PINs from hyperplastic lesions. We selected high-grade PINs with micropapillary projections and excluded cribriform high-grade PINs because we could not rule out a possibility of infiltrating cribriform carcinoma. Twenty normal prostate tissue samples were obtained from patients who underwent radical cystoprostatectomy for urothelial carcinoma (median age, 68 years; range, 58–75 years); microscopic examination confirmed the absence of tumor cells. Two pathologists reviewed all histological slides from prostatectomy specimens and graded each PCa and PIN according to the Gleason grading system and the World Health Organization histologic criteria [8]. The distribution of the Gleason scores in the study samples was as follows: 2 + 3 tumors (n=3), 3 + 2 tumors (n=2), 3 + 3 tumors (n=9), 3 + 4 tumors (n=39), 4 + 3 tumors (n=32), 4 + 4 tumors (n=3), 4 + 5 tumors (n=9), 5 + 4 tumors (n=1), 5 + 5 tumors (n=1). Disease stage was assessed according to the clinical TNM classification of the American Joint Committee on Cancer. The study protocol was approved by the Institutional Review Board of Seoul National University Hospital.

DNA extraction and bisulfite modification

Ten serial sections (10 μm each) from each paraffin-embedded tissue sample were stained with hematoxylin and eosin and were examined microscopically. Cells with characteristics of PCa, PIN, or epithelial cell components of normal prostate were marked on tissue glass slides with red pens. Foci of high-grade PINs, separated from PCa by normal prostate acini, were selected. The marked areas were manually microdissected into microtubes, and collected samples were digested in lysis buffer (100 mM Tris–HCl (pH 8.0), 10 mM EDTA (pH 8.0), 1 mg/ml proteinase K, and 0.05 mg/ml tRNA) and incubated at 50°C overnight. Bisulfite modification of the digested tissue samples was performed using the EZ DNA methylation kit according to the manufacturer's specifications (Zymo Research, Orange, CA, USA).

DNA hypermethylation analysis

Utilizing the MethyLight assay, we quantified methylation in 12 CpG island loci [*ABCB1* (*MDR1*), *APC*, *BCL2*, *GSTP1*, *PTGS2* (*COX2*), *PYCARD* (*ASC*), *RARB*, *RARRES1*, *RASSF1*, *RBP1*, *TNFRSF10C*, and *THBS1*], all of which were selected based on a previous study in which cancer-specific hypermethylation was observed in these 12 CpG island loci and in which methylation frequencies were ≥25% in prostate cancer specimens [5]. Primer and probe sequences were as described [29]. In addition to primer and probe sets designed for amplification of specific CpG islands, an internal reference primer and probe set designed to amplify *ALU* repeats were utilized to normalize for input DNA [28]. The percentage of fully methylated alleles (percentage of methylated reference (PMR)) at each locus was calculated by dividing the *GENE*/*ALU* methylation ratio for each sample by the *GENE*/*ALU* methylation ratio from *M.SssI*-treated human white blood cell DNA and multiplying by 100 [28]. A PMR cut-off value of 4 was used to define methylation positive (>4) vs. negative (≤4) samples and was based on validated data [23].

DNA hypomethylation analysis

Using the COBRA technique, we determined the methylation level of *LINE-1* using bisulfite-modified genomic DNA as described [5]. In brief, *LINE-1* was amplified by PCR using oligonucleotide primers designed to anneal to short segments of genomic DNA lacking CpG sites for equal amplification of both methylated and unmethylated alleles. PCR amplification products were then treated with *Taq*I and *Tas*I to digest methylated alleles and unmethylated alleles, respectively. The digested PCR products were subjected to 12% polyacrylamide gel electrophoresis and stained with ethidium bromide. The intensities of the digested and undigested bands were assessed using Image J software (http://rsb.info.nih.gov/ij). The *LINE-1* methylation level was calculated by dividing the intensity of *Taq*I-digested band by the sum of the intensities of *Taq*I-digested band and the *Tas*I-digested band and multiplying by 100.

MethyLight analysis of *SAT2* was performed as described [28].

Statistical analysis

To compare means between groups, analysis of variance (ANOVA) or Student's *t* test was used. SPSS software was used for all analyses (SPSS for Windows, Release version 11.0, Chicago, IL, USA). *P* values less than 0.05 were considered statistically significant.

Results

Methylation profiles of 12 CpG island loci in normal, PIN, and PCa tissue samples

We performed MethyLight analysis of 12 CpG island loci on 80 DNA samples from normal prostate (n=20), PIN (n=25), and PCa (n=35) tissues. PMR values for each sample were calculated using MethyLight reaction data (Fig. 1). We also calculated the DNA methylation frequencies (PMR >4) at each CpG island locus in normal prostate, PIN, and PCa tissue samples. These 12 CpG island loci were analyzed in our previous study using methylation-specific PCR and found to be methylated in PCa in a cancer-specific manner [5]. In the present study, *TNFRSF10C* hypermethylation (PMR>4) was not detected in any of the prostate tissue samples. Three different groups of genes were recognizable according to their methylation behaviors along multistep carcinogenesis (Fig. 2): (1) Genes methylated in a non-neoplastic stage, including *ABCB1*, *RARRES1*, and *RASSF1* (>60% methylation frequency in normal prostate samples); (2) genes methylated in an early neoplastic stage, including *APC*, *GSTP1*, *PTGS2*, and

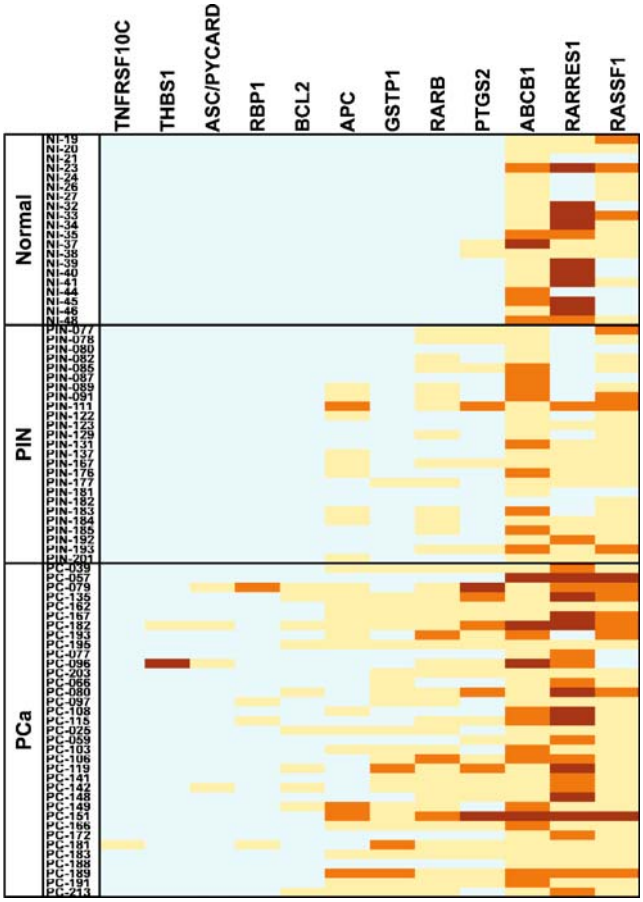

Fig. 1 Map of gene methylation in normal, pre-cancerous, and cancerous epithelial tissues. PMR values were obtained for the genes indicated at right from normal prostate tissues (n=20), prostatic intraepithelial neoplasias (1; n=25), and prostatic carcinomas (PCa; n=35). *Box color* represents the degree of allele methylation (*light blue*, 0<PMR<4; *yellow*, 4≤PMR<20; *orange*, 20≤PMR<50; *brown*, PMR≥50)

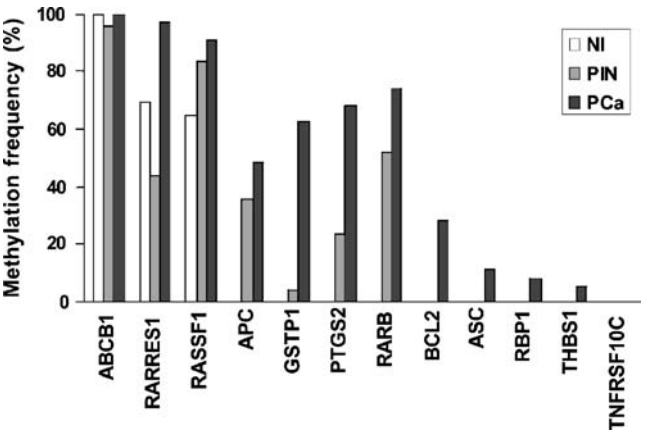

Fig. 2 Promoter CpG island methylation frequencies of 12 individual genes (PMR>4) from normal prostate (NI; n=20), prostatic intraepithelial neoplasia (1; n=25), and prostatic carcinoma (PCa; n=35) tissue samples

RARB (no methylation in normal prostate samples but the presence of methylation in PIN and PCa samples); (3) genes methylated in a late neoplastic stage, including *ASC*, *BCL2*, *RBP1*, and *THBS1* (occurrence of methylation in the PCa stage only). The number of methylated genes was 2.4, 3.3, and 6.5 in normal prostate, PIN, and PCa, respectively ($P<0.001$, ANOVA test).

Hypomethylation of repetitive DNA elements in normal prostate, PIN, and PCa tissue samples

LINE-1 and *SAT2* were used as surrogates for measurement of genomic DNA methylation content. We performed the COBRA assay to determine *LINE-1* methylation level and the MethyLight analysis to determine methylation level in the satellite DNA region *SAT2* using 80 DNA samples from normal prostate ($n=20$), PIN ($n=25$), and PCa ($n=35$) tissues. Methylation levels of *LINE-1* and *SAT2* decreased with the progression of carcinogenesis in samples from normal prostate to PIN to PCa: Methylation levels of *LINE-1* and *SAT2* were significantly lower in PIN than in normal prostate tissues but significantly higher in PIN than in PCa tissues ($P<0.001$, ANOVA test; Fig. 3).

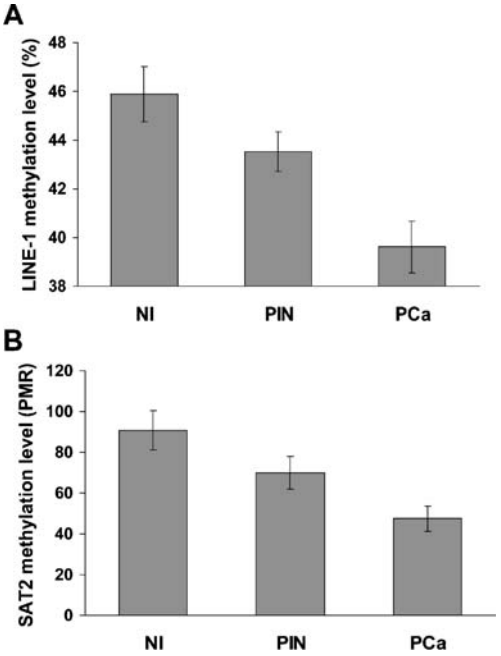

Fig. 3 Comparison of *LINE-1* (**a**) and *SAT2* (**b**) methylation levels from normal prostate (*NI*; $n=20$), prostatic intraepithelial neoplasia (1; $n=25$), and prostatic carcinoma (*PCa*; $n=35$) tissue samples. *LINE-1* methylation data were generated using COBRA analysis of bisulfite-modified genomic DNA. *SAT2* methylation data were generated using MethyLight analysis of genomic DNA. Data represent the means ± SE (error bars). *PMR*, percentage of methylated reference

Methylation levels in ten CpG island loci correlate with clinicopathological parameters

Ten CpG island loci were considered cancer-specific DNA methylation markers because they were more frequently methylated in PCa samples than in PIN and normal prostate samples ($P<0.05$) or were methylated in PCa samples only (*ABCB1* and *TNFRSF10C* not considered cancer-specific). These ten CpG island loci were further analyzed in an additional 64 PCa tissue samples using the MethyLight assay. PMR values for each CpG island locus were calculated from the MethyLight data. The methylation frequencies of those loci with a PMR>4 were also calculated. The number of methylated genes per case was closely associated with TNM stage and Gleason score sum: The number was significantly elevated in high-stage tumors compared to low-stage tumors (6.4 in stages III or IV vs. 5.0 in stages I or II, $P=0.020$; Fig. 4) and was elevated in tumors with a high Gleason score sum compared with tumors with a low score sum (5.6 in those with a score ≥3 + 4 vs. 4.2 in those with a score ≤3 + 3, $P=0.073$). A significant association was also found between the number of methylated genes and the preoperative serum PSA level (5.8 methylated genes in samples from patients with PSA> 8 ng/ml vs. 5.0 in samples from patients with PSA<8 ng/ml, $P=0.033$). When the methylation levels of individual genes were analyzed according to the above clinicopathological parameters, close associations were found between *BCL2* hypermethylation and high tumor stage ($P=0.012$), between *PTGS2* hypermethylation and high Gleason score sum ($P=0.043$), and between *ASC* hypermethylation and high PSA level ($P=0.013$). Although we did not find any significant difference in the methylation levels of individual

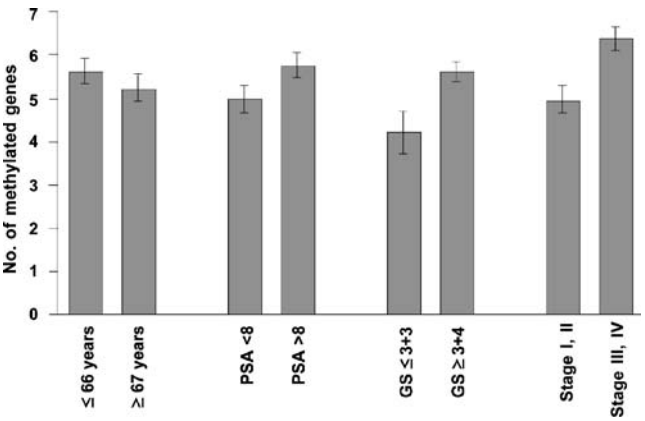

Fig. 4 Gene hypermethylation with respect to clinicopathological parameters. Comparison of the number of hypermethylated genes in tissue samples from patients ≤66 years of age ($n=44$), patients ≥67 years of age ($n=45$), patients with low PSA levels (<8, $n=44$), patients with high PSA levels (>8, $n=55$), patients with low Gleason score (*GS*) sums (≤3 + 3, $n=14$), and patients with high GS sums (≥3 + 4, $n=85$). Likewise, the number of hypermethylated genes in low-TNM stage tumors (I or II, $n=55$) and high-TNM stage tumors (III or IV, $n=44$) are compared. Data represent means ± SEM (error bars)

genes between PCas with a Gleason sum score ≤3 + 3 and those with a score ≥3 + 4, we found significant differences in the methylation levels of five genes (*PTGS2*, *RBP1*, *RARB*, *GSTP1*, and *APC*) when we trichotomized PCa cases into PCas with a score ≤3 + 3, those with 3 + 4 or 4 + 3, and those with ≥4 + 4 (Supplementary Figure). These genes showed higher methylation levels in tumors with a score ≥4 + 4 than in tumors with a score ≤3 + 3 and tumors with 3 + 4 or 4 + 3.

Discussion

Aberrant DNA methylation in cancer cells is characterized by both focal CpG island hypermethylation and generalized genomic hypomethylation. In epithelial malignancies, which develop through multistep carcinogenesis, CpG island loci that are hypermethylated in a cancer-specific manner have also been demonstrated to be hypermethylated in premalignant neoplastic lesions of the same tissue type, including gastric adenomas [15], colon adenomas [19], PINs [31], ovarian cystadenomas [9], and uterine cervical dysplasias [27], although the methylation frequencies at each locus are generally lower in premalignant neoplastic lesions than in malignant lesions from the same tissue type. These results suggest that promoter CpG island hypermethylation occurs in an early stage of multistep carcinogenesis and likely contributes to the progression from intraepithelial neoplasia to malignancy. A recent study showed that reduced DNA methyltransferase 1 (Dnmt1) activity enhanced microadenoma formation but suppressed tumor progression into macroadenoma in the colon of $APC^{Min/+}$ mice [30]. Another study in which APC^{Min+} mice with an inducible Dnmt3b1 transgene were generated demonstrated that upregulation of *DNMT3b1* expression caused DNA hypermethylation of specific tumor suppressor genes and increased the size of colonic microadenomas [20]. These data suggest that DNA hypo- and hypermethylation contribute to the initiation and progression, respectively, of colon tumors. In the present study, *APC*, *GSTP1*, *PTGS2*, and *RARB* were methylated in PIN and PCa tissue samples but not in normal prostate samples, and the methylation levels or frequencies in these genes were higher in PCa samples than in PIN samples, suggesting that hypermethylation of these genes is involved in the progression of PINs to PCas.

The number of methylated genes per case was closely associated with the clinicopathological features that herald poor prognosis for PCa patients. Higher numbers of methylated genes were observed in high-stage PCa tumors than in low-stage tumors, in PCa samples with high PSA serum levels than in PCa samples with low PSA levels, and in PCa samples with high Gleason score sums than in PCa samples with low Gleason score sums. These associations suggest a close relationship between acquisition of DNA hypermethylation and tumor progression. The acquisition of DNA hypermethylation as tumors become more aggressive is consistent with findings in several methylation studies of PCa samples [2, 5, 11, 16, 21], but such a relationship has rarely been observed in human cancers from other tissue types.

In contrast to DNA hypermethylation, the occurrence of DNA hypomethylation during multistep carcinogenesis varies depending on the tissue type. DNA hypomethylation has been shown in ovarian cystadenomas [9], gastric adenomas [6], and uterine cervical dysplasias [18], with more increased DNA hypomethylation occurring in the respective malignancies. However, increased hypomethylation was not observed in colorectal cancers compared with colorectal adenomas [1]. Only one study has reported DNA hypomethylation in PINs [22]; these investigators utilized quantitative image analysis of 5-methylcytosine immunohistochemistry and demonstrated higher methylcytosine staining in PCa tissues and lower methylcytosine staining in high-grade PIN tissues when compared with benign prostatic hypertrophy tissues. These findings contradict our data that methylation levels of *LINE-1* and *SAT2* were significantly lower in PCas than in PINs. Regional CpG island hypermethylation, which is more marked in PCas than in PINs, is unlikely to cause such higher staining in PCa than in PIN because repetitive DNA elements comprise approximately 45% of the human genome and the decreased methylation of repetitive elements in PCas compared to PINs would likely mask any gene-specific CpG island hypermethylation observed using 5-methylcytosine staining. This discrepancy seems to indicate that immunohistochemistry-based imaging analysis does not accurately reflect overall genomic DNA methylation levels. Our study, using COBRA analysis of *LINE-1* and MethyLight analysis of *SAT2* to determine genomic methylation levels, demonstrated that genomic hypomethylation occurs in premalignant prostate tumors and progressively increases during multistep carcinogenesis.

The majority of information regarding CpG island hypermethylation in PCas has come from studies using methylation-specific PCR (MSP). Although MSP is a highly sensitive tool for the detection of CpG island hypermethylation (it can detect methylation in one of 10,000 alleles) [14], MSP is prone to false-positive results due to inadequate primer design or to incomplete bisulfite modification of DNA samples [24]. Additionally, MSP cannot reliably distinguish low levels of methylation from high levels of methylation and may produce variable results depending on the amount of input template DNA and on the number of PCR cycles during amplification. Real-time PCR-based MethyLight technology can overcome the

drawbacks inherent to MSP and can quantitatively determine the number of methylated alleles among total alleles. MethyLight technology has been evaluated and validated for its precision and performance using DNA samples extracted from either fresh tissues or from formalin-fixed and paraffin-embedded tissues [7, 23]. Ogino et al. [23] have demonstrated that MethyLight technology is reproducible and precise and can be effectively utilized to assess methylation levels of CpG island loci in formalin-fixed, paraffin-embedded tissue samples.

In conclusion, we have compared methylation levels in regional CpG island loci and in repetitive DNA elements from normal prostate, PIN, and PCa tissues. Focal CpG island hypermethylation and generalized genomic hypomethylation, common findings in PCa tissues, were also observed in premalignant prostate tissues, namely PINs. Aberrant methylation, including both localized hypermethylation and diffuse hypomethylation, tended to be more advanced with progression of the lesions from PIN to PCa.

Acknowledgments This study was supported by the 21C Frontier Functional Human Genome Project from the Ministry of Science & Technology in Korea (FG06-11-02 to G.H.K.) by a grant from the National R&D Program for Cancer Control, Ministry of Health & Welfare, Republic of Korea (0720540) and by the second stage Brain Korea 21 project.

Conflict of interest The authors declare that they have no conflict of interest.

References

1. Bariol C, Suter C, Cheong K, Ku SL, Meagher A, Hawkins N, Ward R (2003) The relationship between hypomethylation and CpG island methylation in colorectal neoplasia. Am J Pathol 162:1361–1371
2. Bastian PJ, Ellinger J, Wellmann A, Wernert N, Heukamp LC, Muller SC, von Ruecker A (2005) Diagnostic and prognostic information in prostate cancer with the help of a small set of hypermethylated gene loci. Clin Cancer Res 11:4097–4106
3. Bastian PJ, Yegnasubramanian S, Palapattu GS, Rogers CG, Lin X, De Marzo AM, Nelson WG (2004) Molecular biomarker in prostate cancer: the role of CpG island hypermethylation. Eur Urol 46:698–708
4. Bostwick DG, Qian J (2004) High-grade prostatic intraepithelial neoplasia. Mod Pathol 17:360–379
5. Cho NY, Kim BH, Choi M, Yoo EJ, Moon KC, Cho YM, Kim D, Kang GH (2007) Hypermethylation of CpG island loci and hypomethylation of LINE-1 and Alu repeats in prostate adenocarcinoma and their relationship to clinicopathological features. J Pathol 211:269–277
6. Cravo M, Pinto R, Fidalgo P, Chaves P, Gloria L, Nobre-Leitao C, Costa Mira F (1996) Global DNA hypomethylation occurs in the early stages of intestinal type gastric carcinoma. Gut 39:434–438
7. Eads CA, Danenberg KD, Kawakami K, Saltz LB, Blake C, Shibata D, Danenberg PV, Laird PW (2000) MethyLight: a high-throughput assay to measure DNA methylation. Nucleic Acids Res 28:E32
8. Eble JN, Sauter G, Epstein JI, Sesterhenn IA (2004) Pathology and genetics of tumors of the urinary system and male genital organs. IARC, Lyon
9. Ehrlich M, Woods CB, Yu MC, Dubeau L, Yang F, Campan M, Weisenberger DJ, Long T, Youn B, Fiala ES, Laird PW (2006) Quantitative analysis of associations between DNA hypermethylation, hypomethylation, and DNMT RNA levels in ovarian tumors. Oncogene 25:2636–2645
10. Ehrlich M (2002) DNA methylation in cancer: too much, but also too little. Oncogene 21:5400–5413
11. Enokida H, Shiina H, Urakami S, Igawa M, Ogishima T, Li LC, Kawahara M, Nakagawa M, Kane CJ, Carroll PR, Dahiya R (2005) Multigene methylation analysis for detection and staging of prostate cancer. Clin Cancer Res 11:6582–6588
12. Gaudet F, Hodgson JG, Eden A, Jackson-Grusby L, Dausman J, Gray JW, Leonhardt H, Jaenisch R (2003) Induction of tumors in mice by genomic hypomethylation. Science 300:489–492
13. Henrique R, Jeronimo C, Teixeira MR, Hoque MO, Carvalho AL, Pais I, Ribeiro FR, Oliveira J, Lopes C, Sidransky D (2006) Epigenetic heterogeneity of high-grade prostatic intraepithelial neoplasia: clues for clonal progression in prostate carcinogenesis. Mol Cancer Res 4:1–8
14. Herman JG, Graff JR, Myohanen S, Nelkin BD, Baylin SB (1996) Methylation-specific PCR: a novel PCR assay for methylation status of CpG islands. Proc Natl Acad Sci USA 93:9821–9826
15. Kang GH, Lee S, Kim JS, Jung HY (2003) Profile of aberrant CpG island methylation along multistep gastric carcinogenesis. Lab Invest 83:519–526
16. Kang GH, Lee S, Lee HJ, Hwang KS (2004) Aberrant CpG island hypermethylation of multiple genes in prostate cancer and prostatic intraepithelial neoplasia. J Pathol 202:233–240
17. Karpf AR, Matsui S (2005) Genetic disruption of cytosine DNA methyltransferase enzymes induces chromosomal instability in human cancer cells. Cancer Res 65:8635–8639
18. Kim YI, Giuliano A, Hatch KD, Schneider A, Nour MA, Dallal GE, Selhub J, Mason JB (1994) Global DNA hypomethylation increases progressively in cervical dysplasia and carcinoma. Cancer 74:893–899
19. Lee S, Hwang KS, Lee HJ, Kim JS, Kang GH (2004) Aberrant CpG island hypermethylation of multiple genes in colorectal neoplasia. Lab Invest 84:884–893
20. Linhart HG, Lin H, Yamada Y, Moran E, Steine EJ, Gokhale S, Lo G, Cantu E, Ehrich M, He T, Meissner A, Jaenisch R (2007) Dnmt3b promotes tumorigenesis in vivo by gene-specific de novo methylation and transcriptional silencing. Genes Dev 21:3110–3122
21. Maruyama R, Toyooka S, Toyooka KO, Virmani AK, Zochbauer-Muller S, Farinas AJ, Minna JD, McConnell J, Frenkel EP, Gazdar AF (2002) Aberrant promoter methylation profile of prostate cancers and its relationship to clinicopathological features. Clin Cancer Res 8:514–519
22. Mohamed MA, Greif PA, Diamond J, Sharaf O, Maxwell P, Montironi R, Young RA, Hamilton PW (2007) Epigenetic events, remodelling enzymes and their relationship to chromatin organization in prostatic intraepithelial neoplasia and prostatic adenocarcinoma. BJU Int 99:908–915
23. Ogino S, Kawasaki T, Brahmandam M, Cantor M, Kirkner GJ, Spiegelman D, Makrigiorgos GM, Weisenberger DJ, Laird PW, Loda M, Fuchs CS (2006) Precision and performance characteristics of bisulfite conversion and real-time PCR (MethyLight) for quantitative DNA methylation analysis. J Mol Diagn 8:209–217
24. Rand K, Qu W, Ho T, Clark SJ, Molloy P (2002) Conversion-specific detection of DNA methylation using real-time polymerase chain reaction (ConLight-MSP) to avoid false positives. Methods 27:114–120

25. Sakr WA, Partin AW (2001) Histological markers of risk and the role of high-grade prostatic intraepithelial neoplasia. Urology 57(4 Suppl 1):115–120
26. Schulz WA, Elo JP, Florl AR, Pennanen S, Santourlidis S, Engers R, Buchardt M, Seifert HH, Visakorpi T (2002) Genomewide DNA hypomethylation is associated with alterations on chromosome 8 in prostate carcinoma. Gene Chromosome Canc 35:58–65
27. Virmani AK, Muller C, Rathi A, Zoechbauer-Mueller S, Mathis M, Gazdar AF (2001) Aberrant methylation during cervical carcinogenesis. Clin Cancer Res 7:584–589
28. Weisenberger DJ, Campan M, Long TI, Kim M, Woods C, Fiala E, Ehrlich M, Laird PW (2005) Analysis of repetitive element DNA methylation by MethyLight. Nucleic Acids Res 33:6823–6836
29. Weisenberger DJ, Siegmund KD, Campan M, Young J, Long TI, Faasse MA, Kang GH, Widschwendter M, Weener D, Buchanan D, Koh H, Simms L, Barker M, Leggett B, Levine J, Kim M, French AJ, Thibodeau SN, Jass J, Haile R, Laird PW (2006) CpG island methylator phenotype underlies sporadic microsatellite instability and is tightly associated with BRAF mutation in colorectal cancer. Nat Genet 38:787–793
30. Yamada Y, Jackson-Grusby L, Linhart H, Meissner A, Eden A, Lin H, Jaenisch R (2005) Opposing effects of DNA hypomethylation on intestinal and liver carcinogenesis. Proc Natl Acad Sci USA 102:13580–13585
31. Yamanaka M, Watanabe M, Yamada Y, Takagi A, Murata T, Takahashi H, Suzuki H, Ito H, Tsukino H, Katoh T, Sugimura Y, Shiraishi T (2003) Altered methylation of multiple genes in carcinogenesis of the prostate. Int J Cancer 106:382–387

Virchows Arch (2009) 454:25–29
DOI 10.1007/s00428-008-0701-y

ORIGINAL ARTICLE

Immunohistochemistry is not an accurate first step towards the molecular diagnosis of *MUTYH*-associated polyposis

Rachel S. van der Post · Carolien M. Kets · Marjolijn J. L. Ligtenberg · Joannes H. J. M. van Krieken · Nicoline Hoogerbrugge

Received: 9 September 2008 / Revised: 3 November 2008 / Accepted: 5 November 2008 / Published online: 25 November 2008

Abstract Identifying patients with germline *MUTYH* mutation-associated polyposis is presently difficult. The aim of this study is to investigate the possibilities of IHC as a screening test to select patients for *MUTYH* mutation analysis. The expression of MUTYH protein in colorectal adenomas or cancer was studied by IHC using three different (1 polyclonal and 2 monoclonal) antibodies in six samples from patients with biallelic *MUTYH* mutations, in three samples from patients with a single *MUTYH* mutation, and in 11 samples from patients without *MUTYH* mutations. With the polyclonal antibody, adenomas and carcinomas from patients with biallelic *MUTYH* mutations showed a strong supranuclear cytoplasmic staining without epithelial nuclear staining. The strong supranuclear staining was also observed in the three samples from patients with a single *MUTYH* mutation and in nine out of 11 samples from patients without *MUTYH* mutations, with or without nuclear staining. Samples incubated with the monoclonal antibodies showed a non-specific pattern. Our results demonstrate that, in contrast with previous data, the cytoplasmic staining in neoplastic cells does not discriminate *MUTYH* mutated from unmutated cases. At present, IHC cannot be used in clinical practice to differentiate between colorectal tissue with and without germline *MUTYH* mutations.

Keywords *MUTYH* · Polyposis · Colorectal carcinoma · Immunohistochemistry

Abbreviations

CRC	Colorectal cancer
MUTYH	MUTY homolog
MAP	*MUTYH*-associated polyposis
BER	Base excision repair
IHC	Immunohistochemistry
MSS	Microsatellite stable

Introduction

MUTYH-associated polyposis (MAP) is an autosomal-recessive disease characterized by multiple colorectal adenomas and cancer [1]. Approximately 30% of patients with more than15 adenomas that do not carry pathogenic *APC* mutations are biallelic *MUTYH* mutation carriers [2]. MAP was first reported in a British family, in which three affected siblings were compound heterozygote for *MUTYH* mutations [1]. *MUTYH* acts together with *OGG1* and *MTH1* in the base excision repair (BER) system, a repair system to defend cellular DNA against the mutagenic effects of 7,8-dihydro-8-oxoguanine (8-oxoG) [2, 3]. 8-OxoG easily mispairs with adenine residues leading to G:C→T:A transversion mutations in the daughter strand [1, 4]. Normally, MUTYH is expressed in mitochondria and in the nuclei of human cells [5].

R. S. van der Post · C. M. Kets · M. J. L. Ligtenberg · N. Hoogerbrugge (✉)
Department of Human Genetics 849,
Radboud University Nijmegen Medical Center,
P.O. Box 9101, 6500 HB Nijmegen, The Netherlands
e-mail: N.Hoogerbrugge@antrg.umcn.nl

M. J. L. Ligtenberg · J. H. J. M. van Krieken
Department of Pathology,
Radboud University Nijmegen Medical Center,
Nijmegen, The Netherlands

N. Hoogerbrugge
Department of Medical Oncology,
Radboud University Nijmegen Medical Center,
Nijmegen, The Netherlands

Identification of patients with biallelic *MUTYH* mutation-associated polyposis is important to target effective preventive measures for patients and their families, which may lead to reduction in CRC-related mortality. DNA mutation analysis can determine the possible genetic cause of polyposis. To avoid expensive, unnecessary, and time-consuming DNA mutation analyses, there is a need for a screening test to select individuals eligible for DNA mutation analysis.

Immunohistochemical analysis is a rapid and inexpensive method, useful for a wide range of diseases. In a recent study by Di Gregorio et al., immunohistochemical staining of MUTYH protein was performed to identify patients with MAP [6]. A specific pattern of staining for the MUTYH protein was seen; unlike in patients without *MUTYH* mutations, patients with biallelic *MUTYH* mutations showed absence of nuclear staining and segregation of immune reactivity in the cytoplasm (supranuclear staining), both in neoplastic and surrounding healthy mucosa [6]. Therefore, tissues from patients with and without mutations might be distinguished from each other. Consequently, IHC could be used to identify patients with *MUTYH*-associated polyposis. The aim of this study is to further investigate the possibilities of immunohistochemistry as a pre-screening test to select patients for *MUTYH* mutation analysis.

Materials and methods

The study included 20 samples from 19 patients, divided into three groups. Samples were collected in five different pathology laboratories in different hospitals in the Netherlands (Radboud University Nijmegen Medical Center; Rijnstaete Hospital, Arnhem; Amphia Medical Center, Breda; Jeroen Bosch Hospital, Den Bosch; MedischSpectrum Twente, Enschede).

Group 1 consists of five patients carrying biallelic *MUTYH* mutations (six samples from colorectal carcinoma or adenoma); an overview of the clinical features and mutations of these patients is given in Table 1. All patients were compound heterozygous for pathogenic mutations in *MUTYH*. Mutation analysis of *MUTYH* was performed, in the Leiden University Medical Center, as described by Nielsen et al. [7], with sequence analysis of exon 1 till 16. Group 2 consists of 11 patients with polyposis or CRC without detectable mutations in *MUTYH* (11 samples from adenoma or CRC). Group 3 consists of three patients carrying a monoallelic *MUTYH* mutation (with three samples from adenomas and normal mucosa).

Immunohistochemical staining was performed on 4-μm-thick, formalin-fixed, paraffin-embedded tissue sections that were prepared on coated slides and dried for 30 min

Table 1 Clinical features of patients with *MUTYH*-associated polyposis, the type biallelic mutations, and the immunoreactivity pattern of MUTYH protein, using the Abcam antibody

Patient	Number of adenomas	Sex	Age	Analyzed samples	Grading/ differentiation[a]	Site	Mutation *MUTYH*	Type of mutation	Supranuclear staining[b]	Epithelial nuclear staining[c]
1	>100	M	48	Adenoma cancer (T4N0)	Low grade G2	Asc. colon sigmoid	c.697C>T, p. Arg233X c.1172C>T, p.Pro391Leu	Nonsense Missense	1	0
2	>50	F	47	Adenoma	Low grade	Rectum	c.494A>G, p. Tyr165Cys c.1172C>T, p.Pro391Leu	Missense Missense	1	0
3	50	M	48	Cancer (T3N0)	G2	Cecum	c.494A>G, p. Tyr165Cys c.1145G>A, p.Gly382Asp	Missense Missense	1	0
4	40–50	M	46	Cancer (T3N0)	G2	Cecum	c.697C>T p. Arg233X c.1145G>A p.Gly382Asp	Nonsense Missense	1	0
5	>10	M	48	Adenoma	Low grade	Desc. colon	c.1145G>A, p.Gly382Asp c.1172C>T, p.Pro391Leu	Missense Missense	1	0

[a] Differentiation for carcinomas: *G1* well differentiated, *G2* moderately differentiated, *G3* poorly differentiated, *G4* undifferentiated
[b] 0=absent, 1=present
[c] 0=no staining, 1=minimal to mild staining (<10–50% section MUTYH positive), 2=strong staining (>50% section MUTYH positive)

at 55°C. Tissue sections were deparaffinized in xylene and rehydrated with alcohol. Antigen retrieval was done by boiling in 10 mM citrate buffer (PH 6) for 10 min at 95°C. Endogenous peroxidase activity was blocked by exposing the slides to 3% H_2O_2 in methanol for 10 min. Then, sections were incubated with primary MUTYH antibody overnight at 4°C. Polyclonal MUTYH antibody (residues 531–546, Abcam, Cambridge, UK) at 1:300, primary polyclonal MUTYH antibody (residues 33–51, Calbiochem) at 1:1,600, and primary monoclonal MutYH antibody (clone 4D10, Abnova Corporation) at 1:200 were used. These dilutions were determined after examining several dilution series, to obtain the best results. Next, sections were incubated with Poly-HRP-GAM/R/R IgG for 30 min. Visualizing was done with DAB for 5 min. Nuclei were counterstained with hematoxylin. Slides were dehydrated, cleared in xylene, and mounted with micromount.

Normal immunoreactivity of the MUTYH protein was defined as the presence of nuclear and light cytoplasmic staining. Altered expression was considered when the cells showed disappearance of staining from the nucleus and instead showed supranuclear staining. Staining for MUTYH in the nucleus was evaluated by the scoring system Gao et al. reported: 0=no staining; 1=minimal to mild staining (10–50% section positive); 2=strong staining (>50% section positive) [8]. Cytoplasmic staining was classified as present or absent.

Results

With the polyclonal antibody, adenomas and carcinomas of all patients with *MUTYH* biallelic mutations showed strong supranuclear cytoplasmic staining, without nuclear expression of protein (Table 1). Adjacent normal mucosa, in patients with biallelic *MUTYH* mutations, showed the same pattern of expression found in adenomas and carcinomas. As shown in Fig. 1, supranuclear cytoplasmic staining was localized at the apex of the colonocytes (a) or neoplastic cells (b). The 11 samples of colorectal tissue of patients without *MUTYH* mutations, incubated with the polyclonal antibody, showed several patterns (Table 2 and Fig. 2). Nine samples showed the supranuclear cytoplasmic staining described above of which five had weak and four no epithelial nuclear staining. Two samples did not show the supranuclear cytoplasmic staining; they showed weak nuclear and weak cytoplasmic staining. All three samples of colon tissue of patients with one *MUTYH* mutation showed supranuclear staining; additionally, two showed also nuclear staining.

Diffuse cytoplasmic staining was observed in some samples either with or without *MUTYH* mutations; the intensity was always weak. From these results, we conclude that we could not differentiate between tissue with or without *MUTYH* mutations, while using the polyclonal antibody.

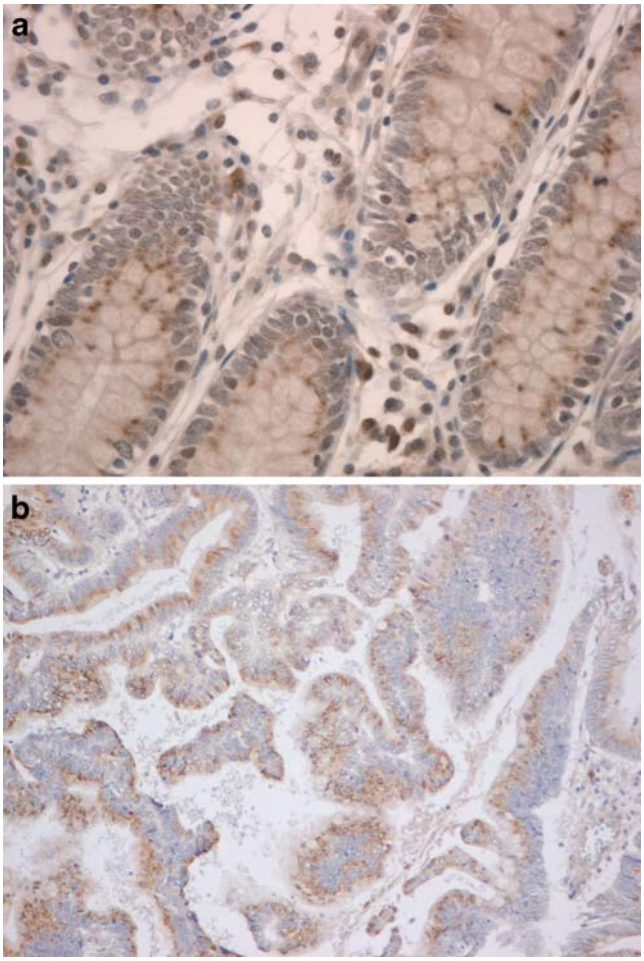

Fig. 1 Strong epithelial supranuclear cytoplasmic immunoreactivity and absence of nuclear expression of MUTYH protein in **a** normal mucosa (original magnification, ×500) and **b** carcinoma (original magnification, ×100) of patients with biallelic *MUTYH* mutations. Note nuclear staining in some stromal fibroblasts

Two monoclonal antibodies were used to evaluate the MUTYH protein staining pattern as well. Samples incubated with the Calbiochem antibody showed strong nuclear and cytoplasmic staining for all tissue regardless whether *MUTYH* mutations were present. Samples incubated with the Abnova antibody showed no epithelial nuclear or cytoplasmic staining at all; however, nuclear staining was observed in stroma cells. This pattern was the same for tissue with and without *MUTYH* mutations.

Discussion

Using the commercially available polyclonal antibody for *MUTYH*, cytoplasmic staining in neoplastic cells does not discriminate *MUTYH*-mutated samples from unmutated

Table 2 Clinical features of patients without *MUTYH*-associated polyposis, the mutations tested, and the immunoreactivity pattern, using the Abcam antibody

Patient	Number of adenomas	Sex	Age	Analyzed samples	*MUTYH* mutations	*APC* mutations	Mis-match repair deficiency	PTEN	Supranuclear staining[a]	Epithelial nuclear staining[b]
Polyposis										
6	>50	M	79	Cancer	Neg	Neg[c]	ND[d]	ND	1	0
7	>20	M	58	Adenoma	Neg	Neg	ND	ND	0	1
8	>10	M	62	Adenoma	Neg	Neg	ND	ND	1	1
9	>10	M	45	Adenoma	Neg	Neg	MSS[e]	ND	1	0
10	>10	M	60	Adenoma	Neg	Neg	MSS	ND	0	1
11	>10	F	44	Adenoma	Neg	Neg	MSS	ND	1	0
12	>10	F	56	Adenoma	Neg	Neg	MSS	ND	1	1
Non-polyposis										
13	10	M	61	Adenoma	Neg	ND	ND	ND	1	1
14	<10	F	41	Adenoma	Neg	ND	ND	ND	1	1
15	2	F	49	Adenoma	Neg	Neg	MSS	Neg	1	0
16	0	M	43	Normal tissue	Neg	Neg	MSS	Neg	1	1

[a] 0=absent, 1=present
[b] 0 =no staining, 1=minimal to mild staining (<10–50% section MUTYH positive), 2=strong staining (>50% section MUTYH positive)
[c] *Neg* tested negative
[d] *ND* not determined
[e] *MSS* microsatellite stable

cases; presence of nuclear staining excludes the *MUTYH* mutation, but is of limited specificity. Samples incubated with the Calbiochem or Abnova antibody showed a non-specific pattern since no differentiation was possible between tissue with and without *MUTYH* mutations. Consequently, the two other antibodies did not seem to work on formalin-fixed, paraffin-embedded tissue after using different pretreatments and dilutions. There are no indications that, with the present mutation analysis of *MUTYH*, mutations are being missed (reported by C.M.J. Tops, Center for Human and Clinical Genetics, Leiden University Medical Center).

There are just a few immunohistochemical studies of the MUTYH protein described. Di Gregorio et al. described that tissue of patients with biallelic *MUTYH* mutations showed absence of nuclear staining and segregation of immunoreactivity (supranuclear) in the cytoplasm [6]. Their hypothesis for this pattern was that the protein produced by the mutated gene could lack the capacity to transfer into the nucleus and remain trapped in the cytoplasm [6]. Our results confirm this finding, but importantly we show that this pattern of staining does not distinguish between tissue of patients with and without *MUTYH* mutations. Recently, O'Shea et al. published results more consistent with our own, showing MUTYH immunohistochemistry not discriminating controls, biallelic, and heterozygote *MUTYH* mutation carriers [9].

Koketsu et al. showed that loss of expression of the BER proteins, MUTYH, MTH1, and NTH1 occurs in sporadic colorectal cancer [10]. Nuclear MUTYH immunoreactivity was detected in only 57% of cases (46/81) [10]. They described that the presence of nuclear MUTYH expression showed a significant correlation with the T-stage of the tumor (p=0.04) [10].

Further, it is not clear whether MUTYH protein is always expressed in the nucleus. Boldogh et al. showed that the majority of MUTYH protein was distributed in the cytoplasm, which is in agreement with a mitochondrial association of MUTYH, and that in only a small percentage (3–5%) of the cells MUTYH-specific fluorescence was also localized to the nuclei [11]. These findings are in contrast with the data of Tsai-Wu et al. which suggest that the MUTYH protein is mainly nuclear specific, based on their own polyclonal rabbit antibodies [12]. Recently, it was shown by Van Puijenbroek et al. that somatic *KRAS2* mutation testing of carcinomas can successfully be used as a pre-screening test for germline *MUTYH* mutation analysis [13].

In conclusion, our results demonstrate that, in contrast with the findings of Di Gregorio et al., while using the same methods and two additional antibodies, cytoplasmic expression of the MUTYH protein is not specific for germline *MUTYH* mutation. At present, immunohistochemistry cannot be used in clinical practice to differentiate between colorectal tissue with and without *MUTYH* mutations.

Acknowledgement We would like to thank C.M.J. Tops (Center for Human and Clinical Genetics, Leiden University Medical Center).

Conflict of interest statement We declare that we have no conflict of interest.

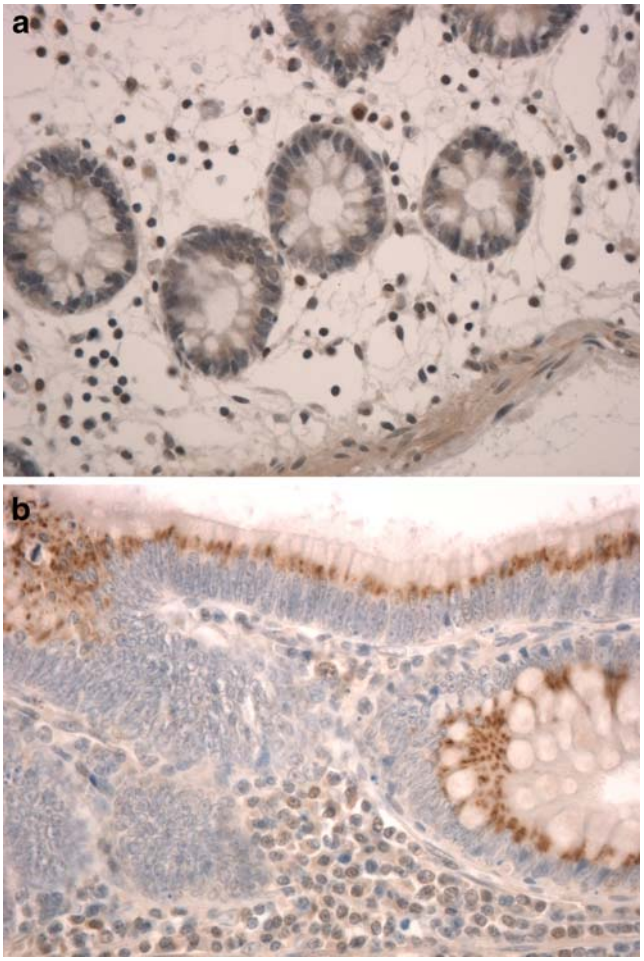

Fig. 2 Limited epithelial supranuclear cytoplasmic immunoreactivity and occasional nuclear expression of MUTYH protein in **a** normal mucosa but strong supranuclear and absent nuclear staining in **b** adenoma of patients without biallelic *MUTYH* mutations. Occasional nuclear staining in stromal cells (original magnification, ×500)

References

1. Al-Tassan N, Chmiel NH, Maynard J et al (2002) Inherited variants of *MYH* associated with somatic G:C→T:A mutations in colorectal tumors. Nat Genet 30:227–232
2. Sieber OM, Lipton L, Crabtree M et al (2003) Multiple colorectal adenomas, classic adenomatous polyposis, and germ-line mutations in *MYH*. N Engl J Med 348:791–799
3. Parker AR, Sieber OM, Shi C et al (2005) Cells with pathogenic biallelic mutations in the human MutYH gene are defective in DNA damage binding and repair. Carcinogenesis 26:2010–2018
4. Lipton L, Tomlinson I (2006) The genetics of FAP and FAP-like syndromes. Familial Cancer 5:221–226
5. Parker AR, Eshleman JR (2003) Human *MutY*: gene structure, protein functions and interactions, and role in carcinogenesis. Cell Mol Life Sci 60:2064–2083
6. Di Gregorio C, Frattini M, Maffei S et al (2006) Immunohistochemical expression of MYH protein can be used to identify patients with MYH-associated polyposis. Gastroenterology 131:439–444
7. Nielsen M, Franken PF, Reinards THCM et al (2005) Multiplicity in polyps count and extracolonic manifestations in 40 Dutch patients with MYH associated polyposis coli (MAP). J Med Genet 42:e54
8. Gao D, Wei C, Chen L et al (2004) Oxidative DNA damage and DNA repair enzyme expression are inversely related in murine models of fatty liver disease. Am J Physiol 287:1070–1077
9. O'Shea AM, Cleary SP, Croitoru MA et al (2008) Pathological features of colorectal carcinomas in MYH-associated polyposis. Histopathology 53:184–194
10. Koketsu S, Watanabe T, Nagawa H (2004) Expression of DNA repair protein: MYH, NTH1, and MTH1 in colorectal cancer. Hepatogastroenterology 51:638–642
11. Boldogh I, Milligan D, Soog Lee M et al (2001) hMYH cell cycle-dependent expression, subcellular localization and association with replication foci: evidence suggesting replication-coupled repair of adenine: 8-oxoguanine mispairs. Nucleic Acids Res 29 (13):2802–2809
12. Tsai-Wu JJ, Su HT, Wu YL et al (2000) Nuclear localization of the human mutY homologue hMYH. J Cell Biochem 77:666–677
13. Van Puijenbroek M, Nielsen M, Tops CMJ et al (2008) Identification of patients with (atypical) MUTYH-associated polyposis by KRAS2 c.34G>T prescreening followed by MUTYH hotspot analysis in formalin-fixed paraffin-embedded tissue. Clin Cancer Res 14(1):139–142

Virchows Arch (2009) 454:31–39
DOI 10.1007/s00428-008-0704-8

ORIGINAL ARTICLE

Microscopic esophagitis in gastro-esophageal reflux disease: individual lesions, biopsy sampling, and clinical correlations

Luca Mastracci · Paola Spaggiari · Federica Grillo · Patrizia Zentilin · Pietro Dulbecco · Paola Ceppa · Paola Baccini · Carlo Mansi · Vincenzo Savarino · Roberto Fiocca

Received: 24 September 2008 / Revised: 12 November 2008 / Accepted: 13 November 2008 / Published online: 2 December 2008

Abstract Patients with non-erosive reflux disease may show microscopic damage. This study is aimed to describe distribution, sensitivity, and specificity of histological lesions (i.e., basal cell hyperplasia—BH, papillae elongation—PE, dilatation of intercellular spaces—DIS, intraepithelial eosinophils—IE, neutrophils, and erosions) and sampling criteria. Four groups were identified on the basis of symptoms, endoscopy, and pH monitoring: (1) erosive esophagitis (n=48), (2) non-erosive esophagitis with abnormal pH (n=59), (3) non-erosive esophagitis with normal pH (n=12), and (4) controls (n=20). Biopsies were taken at the Z-line and 2 and 4 cm above it. BH, PE, DIS, IE, neutrophils, and erosions were assessed. A global severity score was calculated on the basis of the above parameters and allowed the distinction of patients from controls with 80% sensitivity and 85% specificity. Lesions were more severe at Z-line than proximally and more expressed in erosive than in non-erosive disease, although more than 70% of latter patients still showed histological damage. Esophageal biopsy seems very attractive in non-erosive disease where it may contribute to diagnosis and play a role in the comparative evaluation of different therapies.

Keywords Gastro-esophageal reflux disease · Microscopic esophagitis · NERD

L. Mastracci · P. Spaggiari · F. Grillo · P. Ceppa · P. Baccini · R. Fiocca
Department of Anatomic Pathology, University of Genova, Genova, Italy

P. Zentilin · P. Dulbecco · C. Mansi · V. Savarino
Department of Internal Medicine, University of Genova, Genova, Italy

R. Fiocca (✉)
Dipartimento di Discipline Chirurgiche, Morfologiche e Metodologie Integrate (DICMI), Università degli Studi di Genova, Via De Toni 14, 16132 Genova, Italy
e-mail: fiocca@unige.it

Introduction

The prevalence of gastro-esophageal reflux disease (GERD) is continuously increasing in western countries [1]. The term "esophagitis" currently refers to endoscopic alterations (mucosal breaks) [2] that are classified on the basis of their extent [3]; however, besides patients with endoscopic lesions (erosive reflux disease, ERD), the scenario of GERD includes more than half of patients that show no endoscopic abnormality whatsoever [4]. Patients who have normal endoscopy include those with abnormal acid exposure at prolonged pH-metry in the absence of endoscopic lesions (non-erosive reflux disease pH+, NERD pH+) and others showing typical symptoms but normal endoscopy and pH-metry (non-erosive reflux disease pH−, NERD pH−); both these categories are generally believed to be "functional" diseases [5, 6]. The accurate assessment of NERD has proved difficult, as endoscopy does not provide any useful information, symptoms may be variable or atypical, and even prolonged monitoring of esophageal pH shows no abnormality in about one-third of patients with otherwise typical symptoms [7]. Also, the evaluation of anti-reflux therapies is based on resolution of symptoms in NERD patients, and this suffers greatly from subjectivity. Therefore, an objective diagnostic tool with acceptable sensitivity and specificity remains an unmet need for clinicians facing the task of diagnosing and treating GERD patients.

From the 1960s, various histological lesions have been described, namely basal cell hyperplasia (BH) [8], papillae elongation (PE) [8], intraepithelial eosinophils (IE) [9], and neutrophils [10], which are able to identify GERD patients, with varying specificity and sensitivity. Despite this, histology has generally not been considered an important tool in the diagnostic work-up of GERD once metaplastic and neoplastic complications are excluded [11, 12]. More recently, dilatation of intercellular spaces (DIS) has been proposed as a sensitive marker of acid-induced damage in the squamous epithelium. The description of this individual lesion, identifiable both by electron [13–15] and light microscopy [16, 17], has provided a stimulus for clinicians to reconsider histology in the diagnosis of GERD.

Moreover, while some studies underlined the high sensitivity and specificity of some of the aforementioned elementary lesions, others suggested that these changes are rather unspecific and may also be found in control subjects. This seems largely due to methodological problems in patient definition and grouping. The definition of patients in most of the previous studies dealing with esophageal histology was based on symptoms and endoscopic lesions, while they lacked functional investigation by prolonged monitoring of esophageal pH and/or of an appropriate control group. The last point is especially important as it explains the variable and generally poor level of specificity of histology found in some studies [12, 18, 19]. Most of the abovementioned studies included in the control group either asymptomatic individuals or those with non-reflux symptoms and normal endoscopy in the absence of the assessment of esophageal acid exposure. The use of histology as a tool in GERD diagnosis is hampered by the questionable specificity of some lesions such as BH and PE coupled with the poor sensitivity of IE, neutrophils, necrosis, and erosions. Another source of inconsistency comes from the site of biopsy sampling. Some authors suggested that very distal (close to Z-line) esophageal biopsies could show lesions even in control subjects, a condition that decreases specificity and thus prompted sampling of the esophagus at least 4–5 cm away from the Z-line [18]. On the other hand, proximal biopsies are histologicaly normal in more than 50% of GERD patients [20] making this approach unreliable. The patchiness of microscopic changes is another factor which greatly influences the diagnostic reliability of histology [8]. Collins et al. [21] showed that increasing the number of bioptic samples significantly increased the efficacy of detection of histological lesions in GERD patients.

Finally, the reproducibility of lesions is also debated. Numerous studies either did not provide any data at all on the reproducibility of pathologists' readings or when they did this was limited to only some of the histological lesions [16, 21, 22].

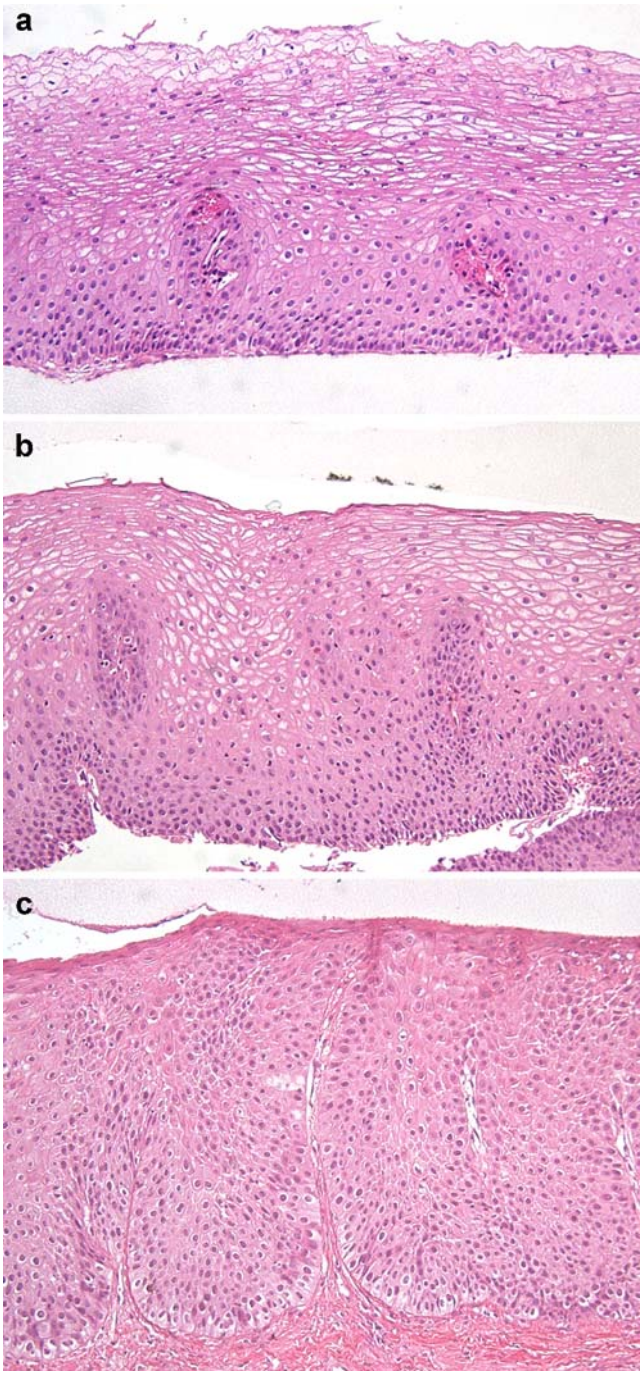

Fig. 1 Increasing grades of severity in basal cell hyperplasia: in normal epithelium basal layer thickness is lower than 15% (**a**); score 1 ranges between 15% and 30% (**b**), while in severe hyperplasia (score 2), basal cells make more than 30% of whole epithelial thickness (**c**)

The present study is based on the systematic investigation of a large series of GERD patients compared with an appropriate control group. All patients and controls underwent clinical investigation for symptoms, endoscopy, and 24-h pH monitoring coupled with a careful, systematic histological analysis aimed to define whether GERD is

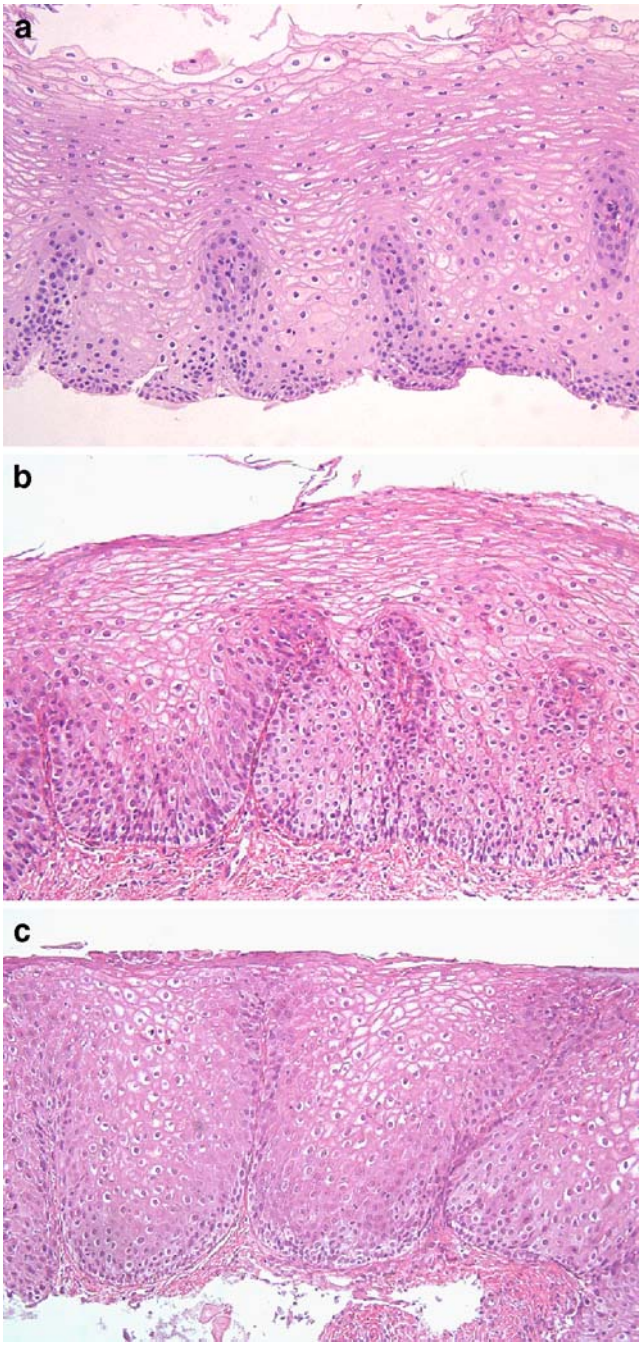

Fig. 2 Increasing grades of severity in papillary elongation: normally papillae measure less than 50% of epithelial thickness (**a**); mild elongation (score 1) does not exceed 75% (**b**), while in severe lesion (score 2), the upper limit of papillae approaches the epithelial surface (**c**)

associated with microscopic esophagitis, what lesions are mostly expressed, and which is the most appropriate sampling protocol. The clinical features and the main pathological findings of this series of patients have been published previously [23]; however, the previous study did not analyze systematically all the individual histological lesions and their distribution. The present study details the histological and sampling criteria used in that study [23] and describes analytically all the individual histological features in terms of distribution, sensitivity, and specificity.

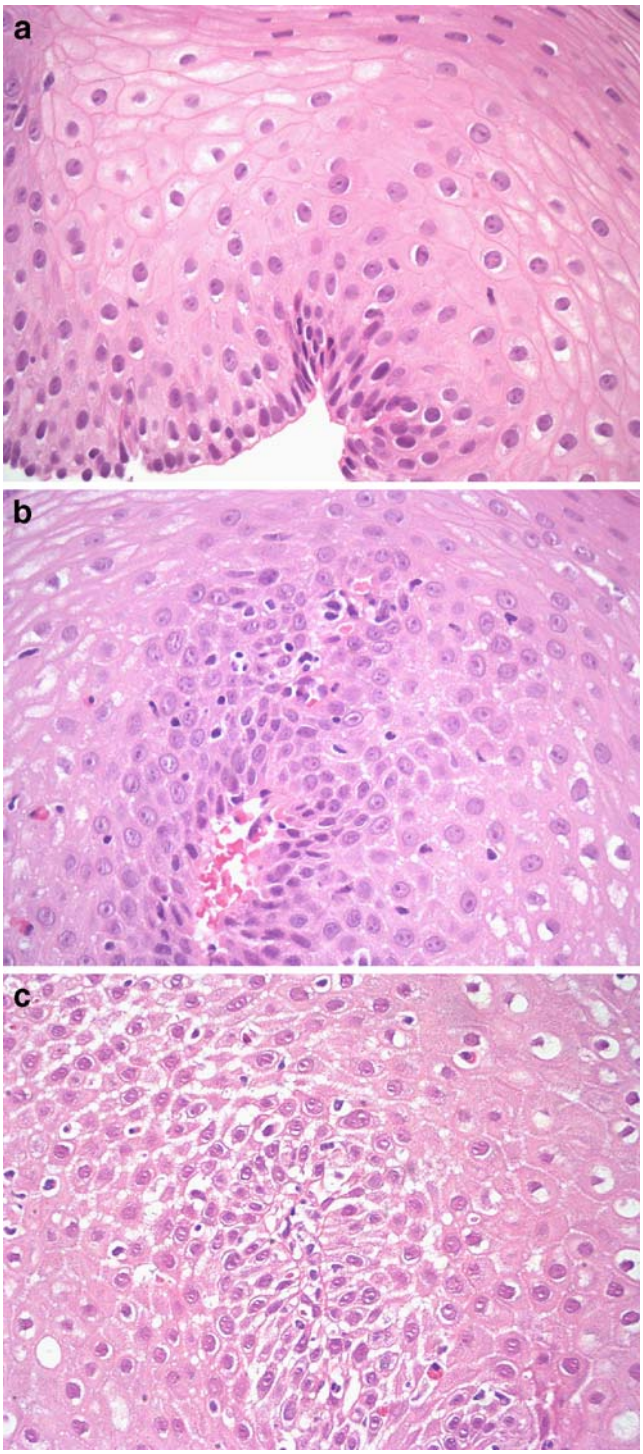

Fig. 3 Increasing grades of severity in DIS: normally epithelial cell are well sealed each other (**a**); small, irregular dilations (score 1) are shown close to a papilla in the right part of (**b**); severe DIS (score 2) produce a clear, empty halo around squamous cells (**c**). Few intraepithelial eosinophils are present in (**b**) and (**c**)

Table 1 Prevalence of basal cell hyperplasia (score 1 and 2) in patients and controls

Group	No. of cases	Cases with lesion	Lesions %	Lesions at 4 cm[a]	4 cm %	Lesions at 2 cm[a]	2 cm %	Lesions at Z-line[a]	Z-line %
ERD	48	47	98%	28/44	64%	38/46	83%	41/42	98%
NERD pH+	59	54	92%	30/54	56%	38/58	66%	50/59	85%
NERD pH−	12	10	83%	4/10	40%	8/12	67%	9/12	75%
All patients	119	111	93%	62/108	57%	84/116	72%	100/113	88%
Controls	20	11	55%	3/20	15%	3/19	16%	10/20	50%

The overall sensitivity (presence in patients %) was 93%, whereas specificity (absence in controls %) was 45%
ERD erosive reflux disease, *NERD pH+* non-erosive reflux disease with abnormal pH-metry, *NERD pH−* non-erosive reflux disease with normal pH-metry
[a] Number of cases with lesion/assessable cases

Patients and methods

Patients

One hundred and nineteen patients (68 M and 51 F, mean age 52 years, range 22–76) with typical or atypical symptoms of GERD were prospectively recruited in our open-access endoscopy service at the University of Genova between January 2001 and April 2003, as previously described [23]. Typical symptoms included the presence of heartburn and/or regurgitation and were present in 99 patients. Atypical symptoms (i.e., recurrent chest pain or respiratory symptoms) were found in 20 patients as detailed previously [23]; a positive PPI test was required before enrolling these patients. The frequency and intensity of symptoms and their impact on the patient's quality of life were registered using a structured and validated questionnaire for the diagnosis of GERD [24].

Patients taking antisecretory or prokinetic drugs were asked to stop any medication at least 30 and 15 days before endoscopy, respectively. On the basis of symptoms, endoscopy, and pH-monitoring results, three subgroups of patients were identified: (1) patients with erosive esophagitis (ERD); (2) patients with symptoms, negative endoscopy, and abnormal pH testing (NERD pH+); and (3) patients who had symptoms and negative results at both endoscopy and pH monitoring (NERD pH−).

Twenty subjects (12 M and 8 F, mean age 50.7 years, range 20–84) without esophageal symptoms were used as controls; they agreed to undergo upper GI endoscopy and 24-h esophageal pH monitoring and showed no abnormality in both exams.

The study was conducted in accordance with the Declaration of Helsinki and its revisions and was approved by our local Ethics Committee. Each subject gave informed consent to participate in the study.

Endoscopy and bioptic samples

All patients and controls underwent upper GI endoscopy. The endoscopic examinations were always performed by two operators (CM and PD) and the Los Angeles classification was used to grade esophagitis [3]. In each subject, multiple specimens were taken with standard biopsy forceps over the distal 4 cm of the esophagus: two across the squamo-columnar junction (SCJ or Z-line), two at 2 cm, and two at 4 cm above it. Most of the biopsy specimens were oriented on cellulose acetate supports (Endofilters, Bioptica Milano, Italy), fixed in 10% buffered formalin, and embedded in paraffin. On average, four sections were examined for each biopsy site. Histological assessment was performed by two

Table 2 Prevalence of intercellular space dilatation (score 1 and 2) in patients and controls

Group	No. of cases	Cases with lesion	Lesions %	Lesions at 4 cm[a]	4 cm %	Lesions at 2 cm[a]	2 cm %	Lesions at Z-line[a]	Z-line %
ERD	48	45	94%	27/44	61%	37/46	80%	36/43	84%
NERD pH+	59	49	83%	27/54	50%	34/59	58%	40/59	68%
NERD pH−	12	8	67%	4/10	40%	8/12	67%	6/12	50%
All patients	119	102	86%	58/108	54%	79/117	68%	82/114	72%
Controls	20	6	30%	1/20	5%	3/19	16%	5/20	25%

The overall sensitivity (presence in patients %) was 86%, whereas specificity (absence in controls %) was 70%
ERD erosive reflux disease, *NERD pH+* non-erosive reflux disease with abnormal pH-metry, *NERD pH−* non-erosive reflux disease with normal pH-metry
[a] Number of cases with lesion/assessable cases

Table 3 Prevalence of papillae elongation (score 1 and 2) in patients and controls

Group	No. of cases	Cases with lesion	Lesions %	Lesions at 4 cm[a]	4 cm %	Lesions at 2 cm[a]	2 cm %	Lesions at Z-line[a]	Z-line %
ERD	46	38	83%	9/40	23%	21/41	51%	29/35	83%
NERD pH+	57	30	53%	4/48	8%	10/51	20%	25/51	49%
NERD pH−	12	3	25%	0/8	0%	2/12	17%	1/9	11%
All patients	115	71	62%	13/96	14%	33/104	32%	55/95	58%
Controls	20	4	20%	0/19	0%	0/17	0%	4/17	24%

The overall sensitivity (presence in patients %) was 62%, whereas specificity (absence in controls %) was 80%
ERD erosive reflux disease, *NERD pH+* non-erosive reflux disease with abnormal pH-metry, *NERD pH−* non-erosive reflux disease with normal pH-metry
[a] Number of cases with lesion/assessable cases

expert pathologists (RF and LM) independently and in a blinded manner. Basal cell hyperplasia (BH), papillae elongation (PE), and dilatation of intercellular spaces (DIS) were semiquantitatively scored as 0 (absent), 1 (mild), and 2 (marked) on hematoxylin–eosin stained slides obtained from each biopsy site. Basal cell thickness (normal values=<15% at 2 and 4 cm and <20% at the Z-line) and length of papillae (normal values=<50% at 2 and 4 cm and <66% at the Z-line) were recorded as a percentage of the total epithelial thickness. The cytological features of basal and intermediate layer nuclei helped in defining basal cell hyperplasia in poorly oriented samples [25]. DIS were scored on the basis of their size. Before starting blind assessment, some reference pictures of the different grades of basal cell hyperplasia, papillary elongation, and DIS were selected and formed a sort of visual analogic scale ranging from 0 to 2 (Figs. 1, 2, and 3); a similar approach has been previously used in the updated Sydney system for assessing gastritis [26]. In addition, the presence of intraepithelial infiltration of eosinophils (IE) (score 0=absent, 1=1 eosinophil, 2=>1 eosinophil per HPF 40×), neutrophils (0=absent, 2=present), and necrosis/erosions (0=absent, 2=present) were recorded. When lesions were not homogeneously distributed in a given sample, the most severe change was considered.

The assessment of interobserver variation between two observers (RF and LM) was limited to BH, PE, and DIS, and included a first round where the lesions were graded independently and a second round where any discrepancy was solved by consensus. The data from the first round were used for the evaluation of interobserver variation whereas the consensus data were used for all the other analysis.

Global severity score

The overall severity of all the lesions was described by means of a global score (GS). The most informative elementary histological lesions (namely BH, PE, DIS, and IE) were considered when constructing this score. Calculation of the score was obtained by summing up all the scores for BH, PE, ISD, and IE (range 0–2) and dividing by the number of assessable lesions. The GS spanned from 0 to 2. In the presence of either intraepithelial neutrophils or necrosis/erosion (found almost exclusively in erosive disease), the assigned score was automatically 2 because such lesions represent the most severe end of the spectrum. The GS was calculated for each biopsy site and for more biopsy sites together (i.e., 4 cm+2 cm+Z-line and 2 cm+Z-line).

Twenty-four-hour ambulatory pH monitoring

Every patient and control underwent 24-h esophageal pH-metry according to a previously published methodology

Table 4 Prevalence of eosinophils (score 1 and 2) in patients and controls

Group	No. of cases	Cases with lesion	Lesions %	Lesions at 4 cm[a]	4 cm %	Lesions at 2 cm[a]	2 cm %	Lesions at Z-line[a]	Z-line %
ERD	48	33	69%	16/45	36%	15/46	33%	24/44	55%
NERD pH+	59	20	34%	3/56	5%	8/59	14%	16/59	27%
NERD pH−	12	5	42%	1/10	10%	5/12	42%	3/12	25%
All patients	119	58	49%	20/111	18%	28/117	24%	43/115	37%
Controls	20	2	10%	1/20	5%	1/20	5%	2/20	10%

The overall sensitivity (presence in patients %) was 49%, whereas specificity (absence in controls %) was 90%
ERD erosive reflux disease, *NERD pH+* non-erosive reflux disease with abnormal pH-metry, *NERD pH−* non-erosive reflux disease with normal pH-metry
[a] Number of cases with lesion/assessable cases

Table 5 Prevalence of neutrophils in patients and controls

Group	No. of cases	Cases with lesion	Lesions %	Lesions at 4 cm[a]	4 cm %	Lesions at 2 cm[a]	2 cm %	Lesions at Z-line[a]	Z-line %
ERD	48	6	13%	2/45	4%	1/47	2%	4/44	9%
NERD pH+	59	2	3%	0/56	0%	1/59	2%	2/59	3%
NERD pH−	12	0	0%	0/10	0%	0/12	0%	0/12	0%
All patients	119	8	7%	2/111	2%	2/118	2%	6/115	5%
Controls	20	0	0%	0/20	0%	0/20	0%	0/20	0%

The overall sensitivity (presence in patients %) was 7%, whereas specificity (absence in controls %) was 100%
ERD erosive reflux disease, *NERD pH+* non-erosive reflux disease with abnormal pH-metry, *NERD pH−* non-erosive reflux disease with normal pH-metry
[a] Number of cases with lesion/assessable cases

[23, 27]. The percentage of total time spent at pH<4.0 units during the whole 24-h period was evaluated [28]. pH testing was considered abnormal if pH<4.0 units was present for more than 5.5% of the total 24-h time [23, 27].

Statistical analysis

Sensitivity, specificity, and positive and negative predictive value (PPV and NPV) of histology were analyzed in relation to the different subgroups into which the patients were subdivided on the basis of symptoms, endoscopy, and pH-monitoring results, i.e., ERD vs. NERD pH+ vs. NERD pH−. ROC analysis was used to find out the optimal cut-off value for differentiating GERD and NERD patients from controls. Percentages were compared by means of chi-square test. Values of $p < 0.05$ were considered statistically significant. The level of interobserver agreement in grading histological lesions was assessed by kappa statistic with linear weighting.

Results

One hundred and nineteen GERD patients and 20 symptom-free, endoscopy-, and pH-metry-negative controls were recruited for this study. Patients were divided in accordance with the abovementioned categories: 48 showed endoscopic esophagitis (ERD), 59 showed altered pH-metry in the absence of endoscopic lesions (NERD pH+), and 12 suffered from typical symptoms but lacked both endoscopic and pH-metry alterations (NERD pH−).

The rates of occurrence of BH, DIS, PE, IE, intra-epithelial neutrophils, and necrosis/erosion in patients and controls are detailed in Tables 1, 2, 3, 4, 5, and 6; these tables describe analytically the distribution of lesions in different biopsy sites. Comparing the sensitivity of each lesion at different biopsy sites, it seems clear that their expression greatly increased moving from 4 cm to the Z-line. BH was seen both in ERD patients (98%) and in the majority of NERD pH+ and NERD pH− patients (92% and 83%, respectively). However, BH was also present in more than 50% of controls, especially as mild lesion in Z-line biopsies (Table 1). Similarly, DIS was largely expressed in ERD, NERD pH+, and NERD pH− patients (94%, 83%, and 67%, respectively). However, mild DIS was also found in 30% of controls, above all at the Z-line (Table 2).

As a whole, BH and DIS proved to be the most informative lesions (93% and 86% sensitivity, respectively), followed by PE and IE (62% and 49% sensitivity, respectively; Tables 3 and 4). In contrast, the sensitivity

Table 6 Prevalence of erosion and/or necrosis in patients and controls

Group	No. of cases	Cases with lesion	Lesions %	Lesions at 4 cm[a]	4 cm %	Lesions at 2 cm[a]	2 cm %	Lesions at Z-line[a]	Z-line %
ERD	48	9	19%	3/45	7%	5/47	11%	4/44	9%
NERD pH+	59	1	2%	1/56	2%	0/59	0%	0/59	0%
NERD pH−	12	0	0%	0/10	0%	0/12	0%	0/12	0%
All patients	119	10	8%	4/111	4%	5/118	4%	4/115	4%
Controls	20	0	0%	0/20	0%	0/20	0%	0/20	0%

The overall sensitivity (presence in patients %) was 8%, whereas specificity (absence in controls %) was 100%
ERD erosive reflux disease, *NERD pH+* non-erosive reflux disease with abnormal pH-metry, *NERD pH−* non-erosive reflux disease with normal pH-metry
[a] Number of cases with lesion/assessable cases

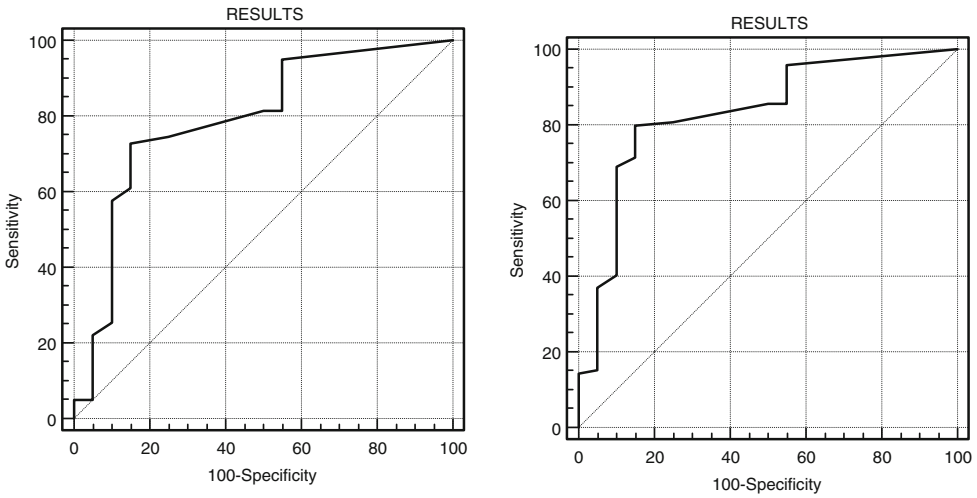

Fig. 4 Application of ROC curve analysis to the Global Severity Score for distinction of NERD patients from controls (**a**) and GERD patients from controls (**b**). Biopsy samples were taken at Z-line+2 cm above it

Sensitivity 73
Specificity 85
Criterion > 0.35
Area under the ROC curve = 0,792
Standard error = 0,052
95% Confidence interval = 0,69 to 0,88

Sensitivity 80
Specificity 85
Criterion > 0.35
Area under the ROC curve = 0,833
Standard error = 0,039
95% Confidence interval = 0,76 to 0,89

of intraepithelial neutrophils and necrosis/erosion was very low (7% and 8%, respectively) and they were almost limited to ERD patients (Tables 5 and 6).

The global severity score (GS) was calculated for biopsies taken at either 4 cm+2 cm+Z-line or 2 cm+Z-line; its mean value was 0.25 in controls and 0.87 in patients (1.23 in ERD and 0.63 in NERD, respectively). On the basis of values observed in patients and controls, the ROC curve analysis (Fig. 4) showed that 0.35 was the most efficient cut-off for distinguishing patients (either GERD or NERD) from controls. No difference in the ROC curves was observed when 4 cm+2 cm+Z-line and 2 cm+Z-line were compared showing that 4-cm biopsies did not provide any additional contribution. Therefore, Table 7 refers only to the GS obtained with 2 cm+Z-line samples. The 0.35 cut-off permitted the distinction of GERD patients from controls with 80% sensitivity and 85% specificity. The positive and negative predictive values of GS were 97% and 42%, respectively, for all GERD patients (94% and 85% for ERD, 94% and 45% for NERD) and the positive likelihood ratio was 5.33.

After defining the most efficient cut-off for distinguishing patients from controls (≥0.35), we applied the same criterion to the individual biopsy sites in order to weigh their respective contribution to the diagnosis. Table 8 details the different levels of sensitivity and specificity observed at 4 cm, 2 cm, and Z-line; as previously observed

Table 7 Overall assessment by using the global severity score (2 cm+Z-line) and a cut-off (0.35)

Group	No. of cases	Score ≥0.35	%	PPV	NPV
ERD	48	45	94	94%	85%
NERD pH+	59	43	73	94%	45%
NERD pH−	12	7	58		
All patients	119	95	80	97%	42%
Controls	20	3	15		

ERD erosive reflux disease, *NERD pH+* non-erosive reflux disease with abnormal pH-metry, *NERD pH−* non-erosive reflux disease with normal pH-metry, *PPV* positive predictive value, *NPV* negative predictive value

Table 8 Capability of the different biopsy sites to recognize patients (with microscopic esophagitis %) and to distinguish controls (without microscopic esophagitis %)

Group	4 cm	2 cm	Z-line
Sensitivity			
ERD	64%[a]	80%	89%
NERD pH+	41%	53%	73%
NERD pH−	40%	67%	50%
All patients	51%	64%	77%
Specificity			
Controls	90%[b]	90%	65%

The global severity score (cut-off value=0.35) was applied at each biopsy site

ERD erosive reflux disease, *NERD pH+* non-erosive reflux disease with abnormal pH-metry, *NERD pH−* non-erosive reflux disease with normal pH-metry

[a] Percent of cases with score >0.35 (sensitivity)

[b] Percent of controls with score <0.35 (specificity)

for individual lesions, Z-line biopsies increased sensitivity but decreased specificity also in this model.

Interobserver variability was calculated for BH, PE, and DIS since these lesions are more susceptible to subjective interpretation than inflammatory cell counting. As a whole, 1,142 paired assessments were performed and analyzed by *K* statistics. The rates of agreement and *K* values were 89% and 0.86 for BH, 92% and 0.87 for PE, and 92% and 0.91 for DIS.

Discussion

A recent study from our group [23] showed that esophageal histology can distinguish controls from patients with reflux disease and may represent a tool in NERD diagnosis. That study focused mainly on the clinico-pathological correlations of microscopic esophagitis; however, it did not report the impact of individual histological lesions and their distribution. The present study refers to the same series of patients and is aimed at detailing the histological and sampling criteria. All the individual histological features have been analytically described in terms of prevalence and distribution, and a simple score (GS) has been introduced for reporting the overall severity.

Among the lesions considered in the study, BH and DIS showed high levels of sensitivity and positive predictive value (PPV). They, however, suffered from poor specificity and low negative predictive value (NPV) because they occurred rather frequently also in normal controls as mild lesions, above all in Z-line biopsies. In contrast, intraepithelial neutrophils and erosion/necrosis were observed occasionally and limited to patients with erosive disease. Since the potential contribution of histology to the diagnosis of reflux disease is limited to NERD patients, the lesions that provided useful information in this context were BH, DIS, PE, and IE.

On the other hand, the frequent occurrence of either mild BH or DIS in controls and the inconsistent finding of PE and/or IE in GERD cases did not enable us to identify a single pathognomonic change provided with acceptable sensitivity and specificity. The high PPV of BH and DIS make them highly informative despite their low specificity and suggest they should be retained in a diagnostic panel. The occurrence of lesions with different levels of sensitivity and specificity and the need to include the most sensitive changes led to the introduction of a global score (GS) that expressed the overall severity of microscopic esophagitis in a simple and immediate way. This multiparameter approach and the use of ROC curve statistic permitted the identification of a cut-off that separates controls from patients efficiently. The GS is conceptually similar to the "refux score" previously described [23]; however, it is more precise because the mean value (as described in "Patients and methods" section) takes in account only the assessable lesions. We also assessed the rate of interobserver variation to address the objection concerning reproducibility. The assessment was limited to lesions potentially more affected by subjectivity and/or sample orientation (i.e., BH, DIS, and PE) and it showed a very acceptable agreement, at least among pathologists with a common training.

The information provided by different biopsy sites is likely to have a significant impact on the efficacy of histological diagnosis and it was not extensively covered in previous studies. Hereby, we showed that Z-line biopsies markedly increase sensitivity of histology although they decrease specificity. Since the gain in sensitivity overcomes greatly the loss in specificity, the overall information increases when Z-line biopsies were included. On the other hand, 4-cm biopsies did not provide additional information that could not be obtained by Z-line and 2-cm samples; as a consequence, they were considered redundant. As expected, microscopic esophagitis was more prevalent in ERD patients while it was less frequently found in patients with non-erosive disease, above all in those with normal esophageal acid exposure [23].

While the use of esophageal histology is not worthwhile in patients with ERD, where endoscopy is informative per se, the lack of a gold standard diagnostic test for patients without macroscopic lesions (NERD) makes histology very attractive in this group of subjects as focused in a recent review on this subject [29]. The finding that most NERD subjects do have microscopic alterations contributes to the general knowledge of disease because it demonstrates that the majority of these patients belong to a condition with an organic counterpart. The recognition of microscopic changes in NERD has also practical implications: histopathology might contribute to the assessment of some subgroups of patients (i.e., those with atypical symptoms) and play a role in the comparative evaluation of different therapies or drug regimens for NERD treatment.

The authors declare that they have no conflict of interest.

References

1. El-Serag HB, Sonnenberg A (1998) Opposing time trends of peptic ulcer and reflux disease. Gut 43:327–333
2. Armstrong D (1999) Endoscopic evaluation of gastro-esophageal reflux disease. Yale J Biol Med 72:93–100
3. Armstrong D, Bennet JR, Blum AL et al (1996) The endoscopic assessment of esophagitis: a progress report on observer agreement. Gastroenterology 111:85–92
4. Schindlbeck NE, Klauser AG, Berghammer G et al (1992) Three year follow-up of patients with gastroesophageal reflux disease. Gut 33:1016–1019

5. Vakil N, van Zanten SV, Kahrilas P et al (2006) The Montreal definition and classification of gastroesophageal reflux disease: a global evidence-based consensus. Am J Gastroenterol 101:1900–1920
6. Galmiche JP, Clouse RE, Bálint A et al (2006) Functional esophageal disorders. Gastroenterology 130:1459–1465
7. Quigley EM (1992) 24-h pH monitoring for gastroesophageal reflux disease: already standard but not yet gold. Am J Gastroenterol 87:1071–1075
8. Ismail-Beigi F, Horton PF, Pope CE (1970) Histological consequences of gastroesophageal reflux in man. Gastroenterology 58:163–174
9. Brown LF, Goldman H, Antonioli DA (1984) Intraepithelial eosinophils in endoscopic biopsies of adults with reflux esophagitis. Am J Surg Pathol 8:899–905
10. Ballem CM, Fletcher HW, Mc Kenna RD (1960) The diagnosis of oesophagitis. Am J Dig Dis 5:88–93
11. Dent J, Brun J, Fendrick AM et al (1999) An evidence-based appraisal of reflux disease management—the Genval Workshop Report. Gut 44:S1–S16
12. Nandurkar S, Talley NJ, Martin CJ et al (2000) Esophageal histology does not provide additional useful information over clinical assessment in identifying reflux patients presenting for esophagogastroduodenoscopy. Dig Dis Sci 45:217–224
13. Tobey NA, Carson JL, Alkiek RA et al (1996) Dilated intercellular spaces: a morphological feature of acid reflux–damaged human esophageal epithelium. Gastroenterology 111:1200–1205
14. Calabrese C, Fabbri A, Bortolotti M et al (2003) Dilated intercellular spaces as a marker of oesophageal damage: comparative results in gastro-oesophageal reflux disease with and without bile reflux. Aliment Pharmacol Ther 8:525–532
15. Caviglia R, Ribolsi M, Maggiano N et al (2005) Dilated intercellular spaces of esophageal epithelium in nonerosive reflux disease patients with physiological esophageal acid exposure. Am J Gastroenterol 100:543–548
16. Solcia E, Villani L, Luinetti O et al (2000) Altered intercellular glycoconjugates and dilated intercellular spaces of esophageal epithelium in reflux disease. Virchows Arch. 436:207–216
17. Villanacci V, Grigolato PG, Cestari R et al (2001) Dilated intercellular spaces as markers of reflux disease: histology, semiquantitative score and morphometry upon light microscopy. Digestion 64:1–8
18. Weinstein WM, Bogoch ER, Bowes KL (1975) The normal human esophageal mucosa: a histological reappraisal. Gastroenterology 68:40–44
19. Narayani RI, Burton MP, Young GS (2003) Utility of esophageal biopsy in the diagnosis of nonerosive reflux disease. Dis Esophagus 16:187–192
20. Schindlbeck NE, Wiebecke B, Klauser AG et al (1996) Diagnostic value of histology in non-erosive reflux disease. Gut 39:151–154
21. Collins BJ, Elliott H, Sloan JM et al (1985) Oesophageal histology in reflux oesophagitis. J Clin Pathol 38:1265–1272
22. Vieth M, Fiocca R, Haringsma J et al (2004) Radial distribution of dilated intercellular spaces of the esophageal squamous epithelium in patients with reflux disease exhibiting discrete endoscopic lesions. Dig Dis 22:208–212
23. Zentilin P, Savarino V, Mastracci L et al (2005) Reassessment of the diagnostic value of histology in patients with GERD, using multiple biopsy sites and an appropriate control group. Am J Gastroenterol 100:2299–2306
24. Carlsson R, Dent J, Bolling-Sternevald E et al (1998) The usefulness of a structured questionnaire in the assessment of symptomatic gastroesophageal reflux disease. Scand J Gastroenterol 33:1023–1029
25. Jarvis LR, Dent J, Whitehead R (1985) Morphometric assessment of reflux oesophagitis in fibreoptic biopsy specimens. J Clin Pathol 38:44–48
26. Dixon MF, Genta RM, Yardley JH et al (1996) Classification and grading of gastritis. The updated Sydney System. International Workshop on the Histopathology of Gastritis, Houston 1994. Am J Surg Pathol 20:1161–1181
27. Zentilin P, Conio M, Mele MR et al (2002) Comparison of the main oesophageal pathophysiological characteristics between short- and long-segment Barrett's oesophagus. Aliment Pharmacol Ther 16:893–898
28. Kahrilas PJ, Quigley EM (1996) Clinical esophageal pH recording: a technical review for practice guideline development. Gastroenterology 110:1982–1996
29. Dent J (2007) Microscopic esophageal mucosal injury in nonerosive reflux disease. Clin Gastroenterol Hepatol 5:4–16

Virchows Arch (2009) 454:41–53
DOI 10.1007/s00428-008-0708-4

ORIGINAL ARTICLE

Expression of estrogen receptor co-regulators NCoR and PELP1 in epithelial cells and myofibroblasts of colorectal carcinomas: cytoplasmic translocation of NCoR in epithelial cells correlates with worse prognosis

Vassiliki Tzelepi · Petros Grivas · Zinovia Kefalopoulou · Haralabos Kalofonos · John N. Varakis · Georgia Sotiropoulou-Bonikou

Received: 12 October 2008 / Revised: 16 November 2008 / Accepted: 18 November 2008 / Published online: 2 December 2008

Abstract Proline-, glutamic acid-, and leukine-rich protein (PELP1) is a novel co-regulatory protein that modulates genomic and non genomic actions of estrogen receptors. Nuclear receptor co-repressor (NCoR) represses estrogen-receptor-dependent transcription. PELP1 and NCoR expression was evaluated in tissue sections from 107 formalin-fixed, paraffin-embedded colectomy specimens. Normal mucosa and adenomas were also evaluated in 77 and 29 cases, respectively. PELP1 was expressed in a dot-like pattern in the nuclei of epithelial and stromal cells. Statistical analysis revealed an increase in PELP1 expression in myofibroblasts from normal mucosa through adenomas to carcinomas. NCoR was expressed in the nuclei and the cytoplasm of epithelial cells. Nuclear expression was more common in normal mucosa, whereas cytoplasmic expression was higher in malignant epithelial cells. Additionally, NCoR was expressed in the cytoplasm of cancer-associated myofibroblasts, but was rarely noted in myofibroblasts of normal mucosa or adenomas. Cytoplasmic expression of NCoR in epithelial cells correlated with better disease-free and overall survival on univariate analysis and was an independent prognostic marker for disease-free survival on multivariate analysis. These findings suggest that deregulation of co-regulators expression in both epithelial cells and myofibroblasts may contribute to the initiation and progression of colorectal carcinoma.

Keywords ERβ · PELP1 · NCoR · Colorectal carcinoma · Myofibroblasts

V. Tzelepi · Z. Kefalopoulou · J. N. Varakis · G. Sotiropoulou-Bonikou (✉)
Department of Anatomy and Histology–Embryology, University of Patras, 26500 Rion, Greece
e-mail: sotiropouloug@yahoo.com

V. Tzelepi · Z. Kefalopoulou
Department of Pathology, University of Patras, 26500 Rion, Greece

P. Grivas · H. Kalofonos
Division of Oncology, Department of Internal Medicine, Medical School, University of Patras, 26500 Rion, Greece

P. Grivas
Department of Internal Medicine, Hahnemann University Hospital/Drexel University College of Medicine, Philadelphia, PA 19102, USA

Introduction

Colon cancer represents the fourth more common malignancy and cause of cancer-related mortality worldwide [1]. Estrogen signaling has been implicated in colorectal carcinogenesis [2–4]. However, data regarding its precise role have been conflicting [2–5].

Estrogen signaling is complex and is mediated through hormone binding to estrogen receptors (ERs), engaging both genomic and non-genomic mechanisms [6]. ERs belong to the nuclear receptor family and represent ligand-dependent transcription factors involved in a variety of normal and pathologic conditions. Two types of estrogen receptors, ERα and ERβ, have been recognized, each of them demonstrating various splicing isoforms [6]. The diverse actions of nuclear receptors stem from the differential recruitment of various co-regulators (co-activators

and co-repressors) and the various modifications applied on these molecules by intracellular signaling cascades [7]. Co-regulators comprise multiple-protein regulatory machineries that modulate chromatin structure, thus determining the polarity of the transcriptional response [8]. In this context, co-activators are molecules that generally enhance transcription due to promoting the recruitment of molecules with intrinsic histone acetyltransferase activity, which mediate nucleosome disruption and chromatin relaxation [9]. On the other hand, co-repressors lower transcription rate since they either block access of activators and/or basal transcription factors to gene promoters or they recruit factors that enhance nucleosome formation [10]. Apart from regulating genomic actions, co-regulators facilitate the non-genomic actions of estrogens [11]. Additionally, their activity is enhanced and selectivity modulated after various posttranslational modifications [12, 13]. Thus, co-regulators serve as master regulators of cell function and differentiation and integrate a variety of signal transduction pathways with transcription [7].

Nuclear receptor co-repressor (NCoR) belongs to the nuclear co-repressor family and is thought to passively recruit histone deacetylases to the promoter of hormone responsive genes after binding to either unliganded or antagonist-bound nuclear receptors [14]. Recent data suggest that NCoR binds to ERβ via a nuclear receptor box-like motif that is also present in p160 co-activators and competes with p160 co-activators for the same AF-2 surface of ERβ [15]. Even though co-repressors are mainly distributed in the nuclei, there is increasing evidence that these proteins can translocate to the cytoplasm in response to various stimuli, including growth factors and cytokines [16–18]. Cytoplasmic dislocation of NCoR results in upregulation of NCoR-repressed promoters [17].

PELP1 (proline-, glutamic acid-, and leukine-rich protein) is a recently discovered ER-co-activator also known as modulator of non-genomic actions of estrogen receptor (MNAR). The primary structure of PELP1 contains several conserved protein–protein interaction motifs that mediate interaction of PELP1 with numerous proteins, including ERs, transcription factors, cell cycle regulators, growth factor receptors, and kinases, allowing for interaction with various intracellular pathways [19]. Additionally, PELP1 modulates both genomic and non-genomic actions of ER [11, 20]. Taken together, these data suggest that PELP1 functions as a scaffolding protein to couple various signaling pathways with ER signaling [19].

The non-malignant cells of tumor microenvironment are active participants of tumor development and progression and are now considered as promising targets of anticancer therapeutic modalities [21]. Additionally, differential gene expression patterns of stromal cells determine differences in the biology of tumors and are associated with diverse clinical outcomes in various human cancers [22, 23]. Myofibroblasts are the predominant cell type of cancer microenvironment and orchestrate stromal response [24]. Colorectal carcinomas are characterized by an intense stromal reaction [25]. Myofibroblasts increase early in the multistep process of colorectal carcinogenesis [26] and have multiple roles in tumor growth [27–30]. Additionally, deregulation of signaling in stromal cells is an important feature of colorectal carcinogenesis [31].

Myofibroblasts are present in various normal tissues, including normal colon, and have distinct functions [32]. Myofibroblasts of normal colonic mucosa reside in the pericryptal and subepithelial area and provide a permissive niche for stem cell self-renewal and proliferation, driving the development and differentiation of colonic epithelium [31].

Increasing evidence suggests that estrogens may mediate their effects on epithelial cells through indirect actions [33–36]. We have recently found that expression of ERβ1, AIB-1, and TIF-2 in myofibroblasts increased from normal mucosa through adenomas to colorectal carcinomas. Additionally, increased ERβ1 and AIB-1 expression was more frequently noted in advanced stage carcinomas (Tzelepi et al., submitted manuscript). Since these molecules are parts of multimolecular transcriptional complexes, the evaluation of additional co-regulators in cancer microenvironment was mandatory in order to elucidate the differential contribution of epithelia and stroma in colorectal carcinogenesis in the context of aberrant estrogen signaling.

Materials and methods

Tissue sections from 107 colorectal carcinoma specimens obtained from an equal number of patients were immunostained for PELP1 and NCoR expression. Patients were suffering from colorectal carcinoma and had undergone colectomy for therapeutic purposes. Tissue sections from non-neoplastic mucosa and from concurrent or metachronous adenomas were also evaluated in 77 and 29 patients, respectively.

The clinicopathologic characteristics of the patients are shown in Table 1. Patients' age ranged from 30 to 83 years (mean 64±10). All women were in the perimenopausal and postmenopausal age (mean age±SD for women 63±7 years, range 50–83). None of the patients had received chemo/radiotherapy prior to surgery. Follow-up data were available for all patients. Follow-up period ranged from 17 to 106 months (mean 67, SD 21). During the follow-up period, 42 relapses and 32 cancer-related deaths were noted.

Regarding non-neoplastic mucosa, 24 samples were located away from the tumor mass (corresponding to the healthy lateral margins of the colectomy specimen), whereas in the remaining 53 cases, mucosa adjacent the neoplastic

Table 1 Clinicopathologic characteristics of patients

Cinico-pathologic parameters	*N* (%)
Gender	
Male	68 (63.6%)
Female	39 (36.4%)
Stage (modified Astler Coller)	
B (B1-B2-B3)	41 (38.3%)
C (C1-C2-C3)	60 (56.1%)
D	6 (5.6%)
TNM stage	
Primary tumor (T)	
T2	15 (14%)
T3	82 (76.6%)
T4	10 (9.4%)
Lymph node (N)	
N0	41 (38.3%)
N1	40 (37.4%)
N2	26 (24.3%)
Metastasis (M)	
M0	101 (94.4%)
M1	6 (5.6%)
Grade	
I	22 (20.6%)
II	74 (69.1%)
III	11 (10.3%)
Histologic type	
Adenocarcinoma common type	95 (88.8%)
Mucinous adenocarcinoma	12 (11.2%)
Primary site	
Right colon	30 (28%)
Left colon	41 (38.3%)
Rectum	36 (33.7%)

mass (corresponding to normal mucosa present in the same paraffin block as the tumor) was evaluated. Regarding adenomas, 20 specimens displayed low-grade dysplasia and nine specimens displayed high-grade dysplasia.

This study received ethical approval from the Local Research Ethics Committee at University Hospital of Patras according to the principles laid down by Declaration of Helsinki.

Immunohistochemistry

Serial 4-μm formalin-fixed, paraffin-embedded tissue sections were subjected into immunohistochemical reaction using rabbit polyclonal antibodies against NCoR (H-303, 1:70, Santa Cruz, CA, USA), PELP1 (PELP1/MNAR, 1:700, Novus Biologicals, CO, USA) and ERβ (pre-diluted, AR385-5R, Biogenex, CA, USA) and mouse monoclonal antibodies against ERα (1:30, NCL-L-6F11, Novocastra, UK) and a-SMA (RTU-SMA, pre-diluted, Novocastra, UK). After deparaffination in xylene and rehydration in a series of graded ethanol solutions, endogenous peroxidase activity was blocked with 0.3% hydrogen peroxide for 15 min. For NCoR staining, antigen retrieval was performed by heating the sections in 1 mM EDTA–NAOH, pH 6, for 15 min in a microwave oven, whereas for ERβ and ERα, staining sections were heated in 10 mM citrate buffer, pH 6, for 15 min in a microwave oven. No antigen retrieval was performed for a-SMA. According to PELP1 manufacturer's instructions, antigen retrieval may hinder staining and decrease the sensitivity of the method; thus, it is not recommended. However, during the standardization of the immunohistohemical protocol for PELP1 antibody, antigen retrieval was tested. Indeed, heating the sections in 10 mM citrate buffer, pH 6, lessened nuclear staining, whereas heating with either 10 mM citrate buffer, pH 6, or 1 mM EDTA–NAOH buffer did not reveal any cytoplasmic staining. Thus, in our protocol, antigen retrieval was not performed for PELP1 immunostaining. Sections were then cooled to room temperature and incubated with blocking serum (1% bovine serum albumin Fraction V, Serva Electrophoresis, Germany) for 30 min and with the primary antibody for 1 h at room temperature. Slides were next incubated with Dako EnVision Labeled Polymer (Dako, CA, USA) for 45 min. Diaminobenzidine (Dako) was used as the chromogen. Nuclei were counterstained with hematoxylin. Known immunostaining positive specimens were used as a positive control. In negative control slides, the same method was performed and the primary antibody was substituted with 1% TBS.

Evaluation of immunostaining

Each slide was individually reviewed and scored in a blind fashion by two independent observers. Both epithelial cells and myofibroblasts were evaluated. Myofibroblasts of normal mucosa specimens and adenomas were recognized due to their typical morphology [37] and characteristic subepithelial (normal mucosa) or subepithelial and interstitial (adenomas) apposition [26]. Serial sections stained with a-SMA were also valuable in determining the myofibroblastic nature of the cells [25, 26]. Carcinoma-associated myofibroblasts were evaluated at areas of intense desmoplastic response, as identified by light microscopy and a-SMA immunostaining. Myofibroblasts of the granulation tissue formed at the base of areas of ulceration were ignored. Additionally, since PELP1 regulates both genomic and non-genomic actions of ER [11] and NCoR cytoplasmic dislocation has been associated with activation of the ER pathway [17], nuclear and cytoplasmic expression were separately assessed.

In each case, the percentage of cells exhibiting positive nuclear and positive cytoplasmic staining was determined. Representative areas were selected at low (×100) magnification. Cell counts were performed at a 400× magnification. At least 1,000 cells were counted in tissue sections

obtained from carcinomas. In tissue sections obtained from adenomas and normal mucosa, 200–300 cells were counted. Expression of the proteins was categorized in a five-scale system as follows 0: negative staining, 1+: 1–24%, 2+: 25–49%, 3+: 50–74%, 4+: ≥75%. For statistical purposes, 4+ expression was considered high expression. In myofibroblasts, 4+ expression of NCoR was very rare, and thus, 3+ and 4+ were regarded high expression.

Statistical analysis

Non-parametric Wilcoxon test was used to compare continuous data from paired samples of normal mucosa, adenomas, and carcinomas and Spearman's correlation test to detect any potential correlation between the markers. Mann–Whitney *U* test was used to compare expression of the proteins between normal mucosa specimens located adjacent and those located away from the tumor mass. For categorical data, chi-square test was used to record any differences between staining results and tumor features. The analysis of overall survival and disease-free survival was calculated with the Kaplan–Meier method, and the differences between the groups were recorded using the log-rank test. Multivariate analysis taking into account clinicopathologic factors and the expression of the proteins studied was performed using Cox proportional hazards method. All data were analyzed with the SPSS program (SPSS® release 16.0, Chicago, IL, USA). Any p value less than 0.05 was considered significant.

Results

NCoR

NCoR was expressed in both epithelial and stromal cells and was mainly localized in the cytoplasm but was variably seen in the nuclei of cells (Fig. 1).

NCoR expression in epithelial cells

NCoR expression was seen in the nuclei and the cytoplasm of epithelial cells (Fig. 1a–g). Mean levels of cytoplasmic expression of NCoR were 65±28% of the cells in normal mucosa, 87±28% in adenomas, and 93±22% in carcinomas. Nuclear expression was rare and was noted in 12±17% of epithelial cells of normal mucosa, 8±15% of epithelial cells of adenomas, and 0.6±1.7% of malignant epithelial cells. Number of cases with 0, 1+, 2+, 3+, and 4+ expression is depicted in Table 2. Statistical analysis revealed that nuclear NCoR expression was more frequently noted in epithelial cells of normal mucosa compared to malignant epithelial cells (Wilcoxon test, $p=0.001$, Fig. 1h). No difference in nuclear expression was noted between adenomas and either normal mucosa or carcinomas. On the other hand, cytoplasmic expression of NCoR was more frequently noted in carcinomas and adenomas compared to normal mucosa (Wilcoxon test, $p<0.001$ and $p=0.028$, Fig. 1h). There was no statistically significant difference between adenomas and carcinomas. Interestingly, normal mucosa adjacent to carcinomas displayed higher levels of cytoplasmic NCoR (80±25% positive epithelial cells) compared to mucosa tissue located away from the tumor mass (58±16.5% positive epithelial cells), and the difference was statistically significant (Mann–Whitney test, $p=0.019$). There was no difference in nuclear NCoR expression between samples adjacent and those located remote from the tumor mass. No correlation was noted between NCoR expression (cytoplasmic or nuclear) in epithelial cells and clinicopathologic parameters, including degree of dysplasia of adenomas and stage, grade, primary site, and histologic type of carcinomas (Table 3).

NCoR expression in myofibroblasts

NCoR was expressed in various cells other than epithelial, including endothelial cells, myofibroblasts and smooth muscle cells of vessels, muscularis mucosa, and muscularis propria. Expression in myofibroblasts was exclusively cytoplasmic (Fig. 1). Distinct nuclear expression was not recognized. Expression of NCoR was rare in myofibroblasts of normal mucosa and was noted only in one case of normal mucosa that was remotely located from the tumor mass. Additionally, adenoma-associated myofibroblasts did not display NCoR expression. In contrast, NCoR expression was frequently noted in carcinoma-associated myofibroblasts with a mean value of 16±26% of the cells (Wilcoxon test, $p=0.001$). Number of cases with 0, 1+, 2+, 3+, and 4+ expression are depicted in Table 2, and correlation of NCoR expression in cancer-associated myofibroblasts with clinicopathologic parameters is shown in Table 3. Notably, high NCoR expression in cancer-associated myofibroblasts was more frequently noted in N1/N2 carcinomas compared to carcinomas without lymph node involvement (chi-square test, $p=0.025$)

PELP1

Epithelial and stromal cells of normal mucosa, adenomas, and carcinomas displayed moderate to intense PELP1 immunostaining. PELP1 was expressed in the nuclei of cells in a punctuated/speckled fashion. Distinct cytoplasmic staining was not noted (Fig. 2).

PELP1 expression in epithelial cells

PELP1 was expressed in 96±4% of epithelial cells of normal mucosa, 94±7% of epithelial cells of adenomas,

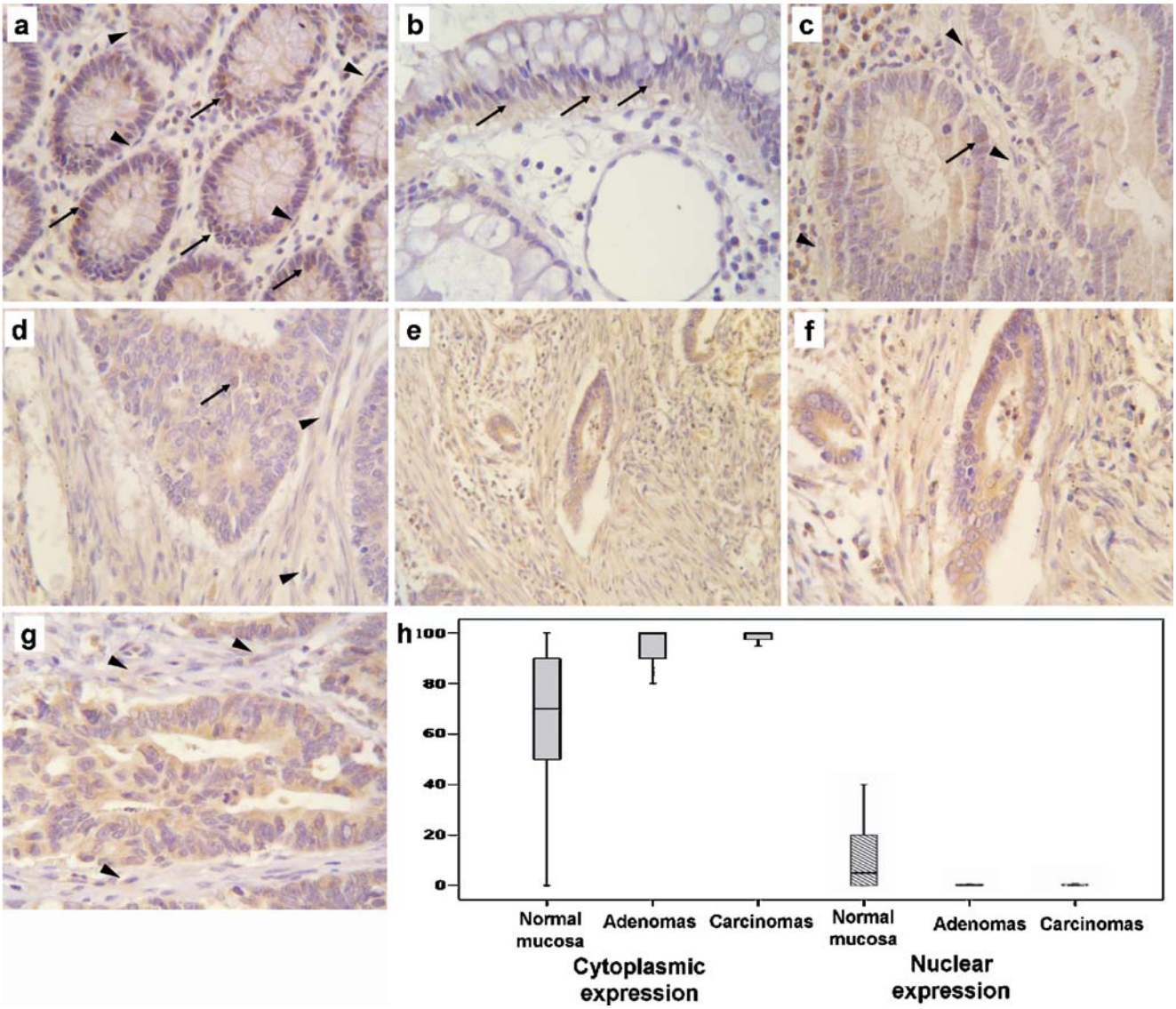

Fig. 1 NCoR expression in colorectal tissue. **a**, **b** NCoR is expressed in the nuclei (*arrows*) and the cytoplasm of epithelial cells of colonic mucosa. No expression is noted in pericryptal myofibroblasts (*arrowheads*). **c** Cytoplasmic and rare nuclear (*arrow*) expression is noted in epithelial cells of adenomas, whereas myofibroblasts (*arrowheads*) are negative for NCoR expression. **d**–**f** Moderate to intense cytoplasmic expression of NCoR in epithelial cells and myofibroblasts (*arrowheads*) of carcinomas. Rare epithelial cells exhibit nuclear immunostaining (*arrow*). **g** NCoR is abundantly expressed in epithelial cells and rarely in myofibroblasts (*arrowheads*) in this case of colorectal carcinoma (**a**, **e** original magnification ×200, **b**–**d**, **f**, **g** original magnification ×400). **h** Cytoplasmic expression of NCoR was higher in epithelial cells of carcinomas and adenomas compared to normal mucosa ($p<0.001$ and $p=0.028$, respectively), whereas nuclear expression of NCoR was higher in epithelial cells of normal mucosa compared to carcinomas ($p<0.001$)

and 90±19% of epithelial cells of carcinomas. Table 4 displays the expression levels of PELP1 in normal mucosa, adenomas, and carcinomas. No statistically significant difference was noted regarding the percentage of positive epithelial cells between paired samples of normal mucosa, adenomas, and carcinomas. Additionally, PELP1 expression did not correlate with any clinicopathologic parameter. However, low expression levels were more frequently noted in carcinomas from the right colon compared to those originating from the left colon ($p=0.015$). Representative images of PELP1 expression in normal mucosa, adenomas, and carcinomas are shown in Fig. 2a–h.

PELP1 expression in myofibroblasts

Expression levels of PELP1 in myofibroblasts are shown in Table 4. Statistical analysis revealed that PELP1 expression was less frequently noted in myofibroblasts of normal

Table 2 NCoR expression levels in normal mucosa, adenomas, and carcinomas

	Cell type	Subcellular localization	Expression level				
			0	1+	2+	3+	4+
Normal mucosa (*N*=77)	Myofibroblasts	Cytoplasmic	76[a] (99%)	1 (1%)	0 (0%)	0 (0%)	0 (0%)
		Nuclear	77 (100%)	0 (0%)	0 (0%)	0(0%)	0 (0%)
	Epithelium	Cytoplasmic	1 (1%)	2 (3%)	24 (31%)	28 (36%)	22 (29%)
		Nuclear	37 (48%)	35 (46%)	4 (5%)	1 (1%)	0 (0%)
Adenoma (*N*=29)	Myofibroblasts	Cytoplasmic	29 (100%)	0 (0%)	0 (0%)	0 (0%)	0 (0%)
		Nuclear	29 (100%)	0 (0%)	0 (0%)	0 (0%)	0 (0%)
	Epithelium	Cytoplasmic	1 (3%)	0 (0%)	0 (0%)	2 (7%)	26 (90%)
		Nuclear	23 (80%)	3 (10%)	3 (10%)	0 (0%)	0 (0%)
Carcinoma (*N*=107)	Myofibroblasts	Cytoplasmic	61 (57%)	24 (22%)	6 (6%)	13 (12%)	3 (3%)
		Nuclear	107 (100%)	0 (0%)	0 (0%)	0 (0%)	0 (0%)
	Epithelium	Cytoplasmic	4 (4%)	1 (1%)	0 (0%)	4 (4%)	98 (91%)
		Nuclear	97 (91%)	10 (9%)	0 (0%)	0 (0%)	0 (0%)

[a] No. of cases

mucosa (58±22%) and adenomas (58±25%) compared to cancer-associated myofibroblasts (89±22%; Wilcoxon test, $p<0.001$, Fig. 2i). PELP1 expression did not correlate with any clinicopathologic parameter, including degree of dysplasia of adenomas and stage, grade, primary site, and histologic type of carcinomas (Table 5).

ERα and ERβ expression and correlation of PELP1 and NCoR with ERβ and co-activators expression

ERα expression was rare in colorectal tissue of our cohort and was noted in two cases of colorectal carcinoma. In these cases, staining was observed in <1% of epithelial

Table 3 Correlation of cytoplasmic NCoR expression in epithelial cells and cancer-associated myofibroblasts with various clinicopathologic parameters

		Myofibroblasts		*p*	Epithelium		*p*
		Low (0–2+)	High (3–4+)		Low (0–3+)	High (4+)	
Gender	Male	56[a]	12	0.403	7	61	0.482
	Female	35	4		2	37	
T stage	T2	13	2	0.375	1	14	0.954
	T3	71	11		7	75	
	T4	7	3		1	9	
N stage	N0	39	2	0.025	2	39	0.477
	N1–N2	52	14		7	59	
Metastasis	M0	86	15	1.000	7	94	0.079
	M1	5	1		2	4	
Grade	I	18	4	0.332	3	19	0.222
	II	62	12		4	70	
	III	11	0		2	9	
Histologic type	Adenocarcinoma common type	80	15	1.000	7	88	0.265
	Mucinous adenocarcinoma	11	1		2	10	
Primary site	Right colon	28	2	0.199	3	27	0.183
	Left colon	32	9		1	40	
	Rectum	31	5		5	31	
Relapse	No relapse	57	8	0.409	3	62	0.150
	Relapse	34	8		6	36	
Event	No death	67	8	0.078	3	72	0.021
	Death	24	8		6	26	

[a] No of cases

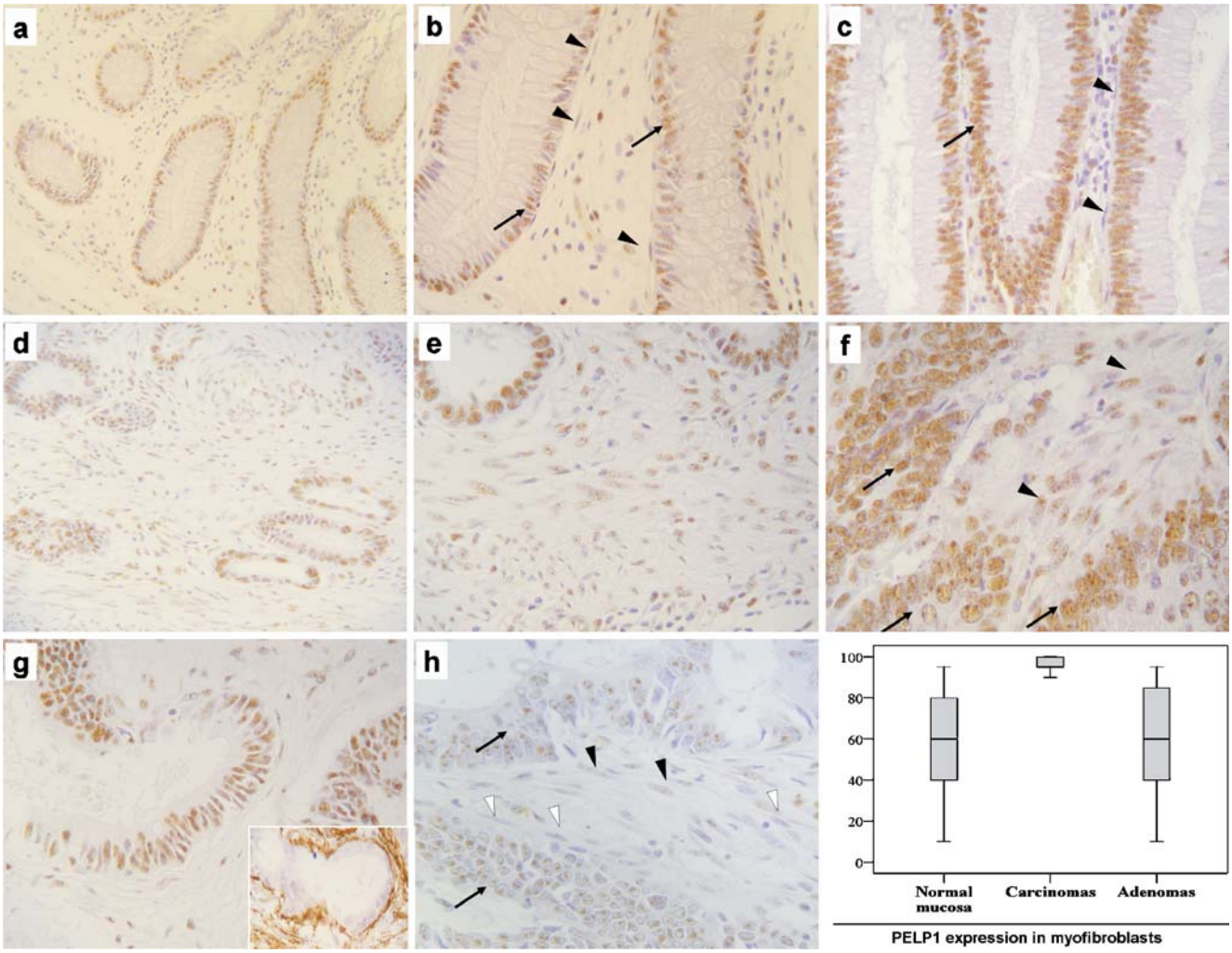

Fig. 2 PELP1 immunostaining in colonic tissue. **a**, **b** PELP1 is expressed in epithelial cells of normal mucosa but not in myofibroblasts (*arrowheads*). A punctuate pattern of immunostaining is noted (*arrows*). **c** Expression of PELP1 in epithelial cells of adenomas is strong and displays a punctuate pattern (*arrow*). Myofibroblasts are negative for PELP1 expression (*arrowheads*). **d**–**h** PELP1 expression in colorectal carcinomas. A punctuate/dot-like pattern of staining is evident in both epithelial cells (*arrows*) and myofibroblasts (*arrowheads*). a-SMA immunostaining in a serial section confirms the myofibroblastic nature of the cells (inset in **g**). A case with low PELP1 expression in cancer-associated myofibroblasts is depicted in **h** (*white arrowheads*: myofibroblasts with negative immunostaining; **a**, **d** original magnification ×200; **b**, **c**, **e**–**h** original magnification ×400). **i** Cancer-associated myofibroblasts display higher levels of PELP1 expression compared to myofibroblasts of normal mucosa and adenomas ($p<0.001$)

Table 4 Expression of PELP1 in normal mucosa, adenomas, and carcinomas

Expression level					
Myofibroblasts	0	1+	2+	3+	4+
Normal mucosa (*N*=77)	0[a] (0%)	6 (7%)	22 (29%)	27 (35%)	22 (29%)
Adenoma (*N*=29)	0 (0%)	2 (7%)	14 (48%)	6 (21%)	7 (24%)
Carcinoma (*N*=107)	0 (0%)	7 (7%)	1 (1%)	3 (3%)	96 (89%)
Epithelial cells					
Normal mucosa (*N*=77)	0 (0%)	0 (0%)	0 (0%)	0 (0%)	77 (100%)
Adenoma (*N*=29)	0 (0%)	0 (0%)	0 (0%)	0 (0%)	27 (100%)
Carcinoma (*N*=107)	0 (0%)	3 (3%)	4 (4%)	4 (4%)	96 (89%)

[a] No. of cases

Table 5 Correlation of PELP1 expression in epithelial cells and cancer-associated myofibroblasts with various clinicopathologic parameters

		Myofibroblasts		*p*	Epithelial cells		*p*
		Low (0–3+)	High (4+)		Low (0–3+)	High (4+)	
Gender	Male	5[a]	63	0.203	7	61	1.000
	Female	6	33		4	35	
T stage	T2	1	14	0.532	2	13	0.512
	T3	8	74		9	73	
	T4	2	8		0	10	
N stage	N0	5	36	0.745	2	39	0.198
	N1–N2	6	60		9	57	
Metastasis	M0	10	91	0.487	10	91	0.487
	M1	1	5		1	5	
Grade	I	0	22	0.170	1	21	0.118
	II	9	65		7	67	
	III	2	9		3	8	
Histologic type	Adenocarcinoma common type	11	84	0.609	10	85	1.000
	Mucinous adenocarcinoma	0	12		1	11	
Primary site	Right colon	5	25	0.394	7	23	0.015
	Left colon	3	38		1	40	
	Rectum	3	33		3	33	
Relapse	No relapse	8	57	0.522	7	58	1.000
	Relapse	3	39		4	38	
Event	No death	8	66	1.000	8	67	0.648
	Death	3	29		3	29	

[a] No. of cases

cells, but was not noted in myofibroblasts. Expression of ERβ was noted in 92±16% of epithelial cells of normal mucosa specimens, 95±45% of epithelial cells of adenomas, and 88±23% of epithelial cells of carcinomas. Mean expression levels of ERβ1 in myofibroblasts were 30±17% in normal mucosa specimens, 52±20% in adenomas, and 82±24% in carcinomas.

PELP1 and NCoR expression was correlated with ERβ1 and two ER co-activators (AIB-1, TIF-2) expression which have been previously evaluated in the same cohort of patients (Grivas et al, submitted manuscript; Tzelepi et al, submitted manuscript). Spearman's correlation test revealed that PELP1 expression in myofibroblasts of cancer microenvironment correlated with ERβ1 (p=0.001, r=0.326), AIB-1 (p<0.001, r=0.345), and TIF-2 (p=0.002, r=0.294) expression. Additionally, nuclear expression of NCoR in normal epithelial cells was inversely correlated to AIB-1 expression (p=0.038, r=−0.444) and nuclear expression of NCoR in malignant epithelial cells inversely correlated with nuclear ERβ1 expression (p=0.041, p=−0.199).

Survival analysis

Younger age (<50 years; p=0.007), advanced stage (p< 0.001), presence of metastases (p<0.001), and lymph node involvement (p=0.024) were associated with shorter disease-

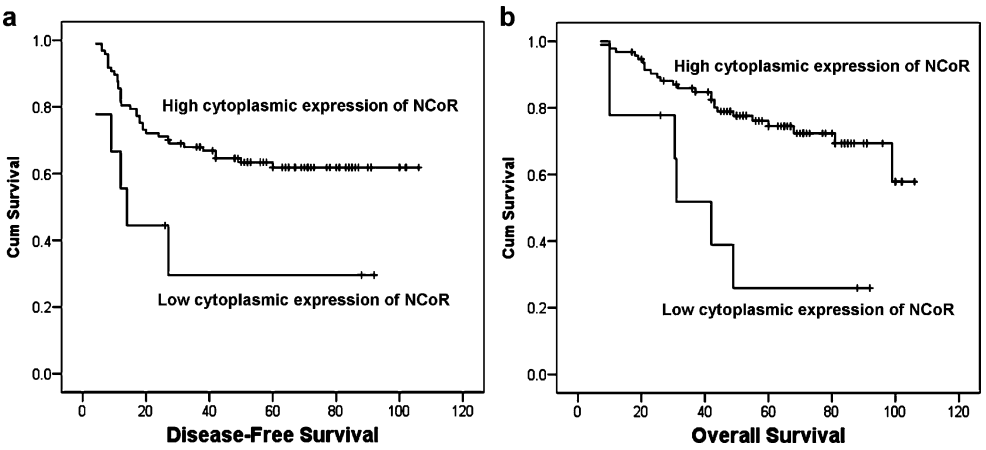

Fig. 3 Decreased cytoplasmic NCoR expression in malignant cells correlates with shorter disease-free (p=0.018) (**a**) and overall survival (p=0.002) (**b**)

Table 6 Cox regression analysis for disease-free survival

Clinicopathologic parameter	*p*	Exp(*B*)	95.0% CI for Exp(*B*)	
			Lower	Upper
Astler–Coller	0.000			
Astler–Coller (BvsD)	0.000	0.026	0.007	0.091
Astler–Coller (CvsD)	0.000	0.051	0.017	0.157
Grade	0.098			
Grade (I vs III)	0.085	0.291	0.071	1.185
Grade (II vs III)	0.868	1.093	0.383	3.122
Histologic type	0.145	0.420	0.131	1.350
Gender	0.643	1.179	0.588	2.362
Age	0.006	3.409	1.425	8.154
Primary site	0.949			
Primary site (right colon vs rectum)	0.748	1.149	0.492	2.680
Primary site (left colon vs rectum)	0.857	1.074	0.493	2.340
NCoR expression in epithelial cells	0.010	3.491	1.356	8.989

free survival on univariate analysis. Additionally, decreased expression of NCoR in the cytoplasm of cancer cells correlated with worse disease-free survival on univariate analysis (p=0.018, Fig. 3a). Cox regression analysis revealed that cytoplasmic expression of NCoR along with age and stage was an independent predictor of disease-free survival (Table 6).

Regarding overall survival, univariate analysis revealed that younger age (<50 years; p=0.046), advanced stage (p< 0.001), presence of metastasis (p<0.001), lymph node involvement (p=0.006), and poor differentiation (p= 0.001) were associated with decreased survival. Additionally, decreased cytoplasmic expression of NCoR was associated with decreased survival on univariate analysis (Fig. 3b); however, it was not an independent prognostic factor on multivariate analysis (Table 7).

Discussion

Nuclear receptor signaling is regulated by a finely tuned balance between co-activators and co-repressors [8, 10]. NCoR is a protein involved in repression of transcription mediated by various transcription factors including estrogen receptors [14]. It has been recently shown that phosphorylation of NCoR in colon cancer cells mediates its interaction with 14-3-3 adaptor proteins that regulate its subcellular localization and that cytoplasmic localization of NCoR is a common trait in colorectal carcinomas [16]. In line with these findings, in our study, cytoplasmic NCoR expression was more common in carcinomas and adenomas compared to normal mucosa, whereas nuclear expression of NCoR was more frequently noted in epithelial cells of normal mucosa compared to carcinomas. Increased cytoplasmic expression

Table 7 Cox regression analysis for overall survival

Clinicopathologic parameter	*p*	Exp(*B*)	95.0% CI for Exp(*B*)	
			Lower	Upper
Astler–Coller	0.906			
Astler–Coller (BvsD)	0.892	1002.618	0.000	2.2E+046
Astler-Coller (CvsD)	0.890	1120.344	0.000	2.5E+046
Grade	0.205			
Grade (I vs III)	0.089	0.365	0.114	1.167
Grade (II vs III)	0.263	0.535	0.178	1.602
Histologic type	0.071	0.263	2.435	1.136
Gender	0.385	1.256	0.752	2.098
Age	0.125	0.388	0.116	1.299
Primary site	0.557			
Primary site (right colon vs rectum)	0.382	1.326	0.704	2.499
Primary site (left colon vs rectum)	0.321	1.343	0.750	2.407
NCoR expression in epithelial cells	0.939	1.050	0.303	3.637

of NCoR was evident in normal mucosa adjacent to the neoplastic mass compared to normal mucosa remote from the tumor mass. Thus, a translocation of NCoR from the nucleus to the cytoplasm appears to be associated with colorectal carcinogenesis.

Cytoplasmic translocation of NCoR results in withdrawal of transcriptional repression [17] and can be mediated by various stimuli, including growth factors and cytokines [16–18]. Our findings might imply that nuclear NCoR in normal cells represses transcription mediated by ER or other transcription factors, whereas cytoplasmic translocation during malignant transformation renders the cells sensitive in the growth promoting effects of NCoR-repressed transcription factors. Thus, in epithelial cells of colonic mucosa, the balance between co-activators and co-repressors may result in transcriptional repression, whereas cytoplasmic translocation of NCoR in carcinomas may change the polarity of transcriptional response towards transcriptional activation. Additionally, it has been shown that estrogens target NCoR for proteosomal degradation in an ER-dependent manner and reduce its levels resulting in derepression of NCoR-regulated genes, including estrogen-responsive genes [38]. Concordantly, in our study, an inverse correlation of nuclear NCoR expression to nuclear ERβ1 expression was noted in epithelial cells.

Despite its role in the initiation of colorectal carcinomas, cytoplasmic sequestration of NCoR was associated with better disease-free and overall survival on univariate analysis and was independently associated with disease-free survival on multivariate analysis. Even though these findings merit verification in a larger cohort of patients, there are a number of possible explanations. NCoR is implicated in the repression of transcription mediated by a number of transcription factors [14]. In breast cancer, it has been proposed than loss of NCoR determines the selection of a more aggressive and hormone-unresponsive cancer, possibly due to withdrawal of its repressive role in the promoter of ER-dependent genes [39]. In astrocytomas, cytoplasmic translocation of NCoR results in induction of astrocytic differentiation and inhibits tumor growth, possibly due to removal of its repressive activity on RAR/RXR (retinoic acid receptor/retinoid X receptor) complex [40]. In colon cancer, NCoR expression inhibits the antiproliferative effects mediated by retinoic acid due to transcriptional repression of RA dependent genes [41]. Thus, the diversity of transcription factors associated with NCoR might explain its dual role in colorectal carcinogenesis. Besides, current anticancer approaches argue that signaling does not occur through parallel signaling cascades but rather through a complex network of interacting signaling pathways [42]. In line with the systemic model of carcinogenesis is the existence of complex interactions between NCoR and various transcription factors. Last but not least, posttranslational modifications may alter the protein structure and localization, thus influencing its biologic activity [43].

In our study, nuclear expression of NCoR was noted in rare malignant cells, whereas the vast majority of malignant epithelial cells displayed cytoplasmic expression. It has been proposed that nuclear NCoR expression may function as a marker of neural stem cells and undifferentiated glioblastoma multiforme cells [40, 44] and is crucial for blocking the differentiation of lymphoma cells [45]. Based on these findings, our observations might indicate that the rare cells with nuclear NCoR expression in colorectal carcinomas represent cancer stem cells. Diverse gene networks regulate the stemness of different stem cell types [46]. Epigenetic mechanisms, especially DNA methylation and histone modifications, result in alternating transcriptional repression and derepression that regulate embryonic and possibly adult stem cell properties [47]. NCoR participates in multiprotein histone modification complexes [14] and thus might be involved in stem cell regulation. Further studies will be needed to explore this possibility.

PELP1 activates both genomic and non-genomic actions of estrogen receptors. It binds to ERα and ERβ in a ligand-dependent manner and promotes modulation of local chromatin structure by recruiting co-regulators that have intrinsic acetytransferase activity, thereby increasing transcription of ER-responsive genes [48]. Additionally, PELP1 promotes non-genomic actions of ERs since it stabilizes the ER/Src kinase complex, thereby activating MAPK pathway [11, 49]. PELP1 exhibits both nuclear and cytoplasmic localization in various cells. Nuclear localization is consistent with its role in genomic actions of ERs, whereas cytoplasmic PELP1 mediates the non-genomic actions of estrogens [50]. In our study, PELP1 was localized in the nuclei in both epithelial cells and myofibroblasts, implying that PELP1 may not be that crucial for modulating the non-genomic actions of estrogens in our cohort of colorectal cancer patients. Antigen selection and the protocol followed might account for the lack of cytoplasmic staining in our study. However, using essentially the same protocol, cytoplasmic staining has been observed in glioma specimens (Kefalopoulou Z, manuscript in preparation). Additionally, antigen retrieval of the sections with either 10 mM citrate buffer, pH 6, or 1 mM EDTA–NAOH buffer did not reveal any cytoplasmic staining. A punctuate/speckle-like pattern of staining was noted in all cell types both in normal and malignant tissue, in line with previous observations [51], and might suggest that PELP1 co-localizes with structural components within the nucleus that create focal concentrations of the regulatory machinery of ER-dependent transcription. Additionally, PELP1 contains several protein–protein interaction motifs and functions as a landing platform for several other chromatin remodeling complexes that might result in a punctuate distribution in the cell nuclei [51].

Regarding myofibroblasts, NCoR displayed cytoplasmic expression in cancer-associated myofibroblasts, whereas PELP1 expression in myofibroblasts increased from normal mucosa through adenomas to carcinomas. Myofibroblasts are the predominant cell type in cancer microenvironment and orchestrate stromal response, thereby promoting the initiation and progression of carcinogenesis [37]. Estrogens may mediate their effects on epithelial cells through indirect mechanisms. The presence of estrogen receptors in stromal cells is crucial for estrogen-dependent growth of epithelial cells in the uterus, mammary gland, and prostate gland [33–35]. Additionally, estrogens enhance angiogenesis and recruit stromal cells from bone marrow in ER-negative tumors [36]. Furthermore, estrogens stimulate the proliferation of normal epithelial cells when co-cultured with stromal cells, but have no effect on epithelial cells when cultured in isolation even though epithelial cells express estrogen receptors [52].

We have recently showed, in the same cohort of patients, that ERβ1 expression increased in myofibroblasts from normal mucosa through adenomas to colorectal carcinomas along with two ER co-regulators, AIB-1 and TIF-2 (Tzelepi et al., submitted manuscript). The present study expands these findings, showing that another ER co-activator, PELP1, was more frequently expressed in cancer-associated myofibroblasts compared to normal mucosa and adenomas. Additionally, PELP1 expression in myofibroblasts correlated with ERβ1, AIB-1, and TIF-2 expression. Overexpression of PELP1 has oncogenic potential [53] and has been noted in various neoplasms [54]. However, to the best of our knowledge, its expression in cancer-associated myofibroblasts has not been assessed before. Taken together, our findings might imply that genomic actions of estrogens are increased in cancer-associated myofibroblasts, paralleling the normal mucosa–adenoma–carcinoma sequence of colorectal carcinogenesis.

Concordantly, NCoR expression in cancer-associated myofibroblasts was exclusively cytoplasmic, whereas it was rather sparse in adenoma- and normal mucosa-associated myofibroblasts. Cytoplasmic localization of NCoR and increased nuclear expression of ERβ1, AIB-1, and TIF-2 in cancer-associated myofibroblasts is in concordance with recent data suggesting that NCoR competes with p160 co-activators for the same AF-2 surface of ERβ [15]. Thus, since co-activators expression is increased whereas co-repressor is translocated in the cytoplasm, we speculate that ER signaling is activated in cancer-associated myofibroblasts mediating paracrine actions of estrogens, thus creating a supportive tumor microenvironment. This is also supported by the finding that cytoplasmic expression of NCoR in cancer-associated myofibroblasts correlates with lymph node involvement. These findings might suggest an important role of ERβ1-mediated transcriptional activation in the tumor promoting actions of cancer-associated myofibroblasts. However, the exact role of cytoplasmic translocation of NCoR and increased expression of co-activators in cancer-associated myofibroblasts merits further investigation.

In conclusion, our findings imply that increased expression of PELP1 in cancer-associated myofibroblasts and cytoplasmic translocation of NCoR in malignant epithelial cells and myofibroblasts might contribute to the initiation of colorectal carcinogenesis. Additionally, decreased cytoplasmic expression of NCoR in epithelial cells might be an indicator of worse prognosis. Further studies are needed to elucidate the functional role of ERβ1 signaling and its modulation by co-regulators in malignant cells and cancer-associated myofibroblasts of colorectal carcinomas. Additionally, co-regulators participate in complex molecular networks that include cytoplasmic signaling cascades and modulation of transcriptional activity of various transcription factors [7, 8]. Estrogen receptor-related receptors (ERR) comprise a family of nuclear receptors that are structurally connected to the ERs, bind to similar DNA sequences, and whose action is influenced by many of the ERs co-regulators [55]. Additionally, ERRa levels seem to be correlated with loss of differentiation and advanced stage of colorectal carcinomas [56]. Thus, each biomarker should be evaluated in the context of the cell type and molecular microenvironment where it is expressed and the signaling networks where it is involved in order to pave the way for a systemic approach in cancer therapy.

Conflict of interest statement We declare that we have no conflict of interest.

References

1. Parkin DM, Bray F, Ferlay J et al (2005) Global cancer statistics, 2002 CA. Cancer J Clin 55:74–108
2. Kampman E, Potter JD, Slattery ML et al (1997) Hormone replacement therapy, reproductive history, and colon cancer: a multicenter, case-control study in the United States. Cancer Causes Control 8:146–158
3. Lechner D, Kallay E, Cross HS (2005) Phytoestrogens and colorectal cancer prevention. Vitam Horm 70:169–198
4. Gunter MJ, Hoover DR, Yu H et al (2008) Insulin, insulin-like growth factor-I, endogenous estradiol, and risk of colorectal cancer in postmenopausal women. Cancer Res 68:329–337
5. Di Domenico M, Castoria G, Bilancio A et al (1996) Estradiol activation of human colon carcinoma-derived Caco-2 cell growth. Cancer Res 56:4516–4521
6. Deroo B, Korach KS (2006) Estrogen receptors and human disease. J Clin Invest 116:561–570
7. Lonard DM, O'Malley BW (2007) Nuclear receptor coregulators: judges, juries and executioners of cellular regulation. Mol Cell 27:691–700
8. McKenna NJ, O'Malley BW (2002) Combinatorial control of gene expression by nuclear receptors and coregulators. Cell 108:465–474

9. O'Malley BW (2006) Little molecules with big goals. Science 313:1749–1750
10. McKenna NJ, Lanz RB, O'Malley BW (1999) Nuclear receptor coregulators: cellular and molecular biology. Endocr Rev 20:321–344
11. Wong C-W, McNally C, Nickbarg E et al (2002) Estrogen receptor-interacting protein that modulates its nongenomic activity-crosstalk with Src Erk phosphorylation cascade. Proc Natl Acad Sci USA 99:14783–14788
12. Wu RC, Qin J, Yi P et al (2004) Selective phosphorylations of the SRC-3/AIB1 coactivator integrate genomic responses to multiple cellular signalling pathways. Mol Cell 15:937–949
13. Greger JG, Fursov N, Cooch N (2007) Phosphorylation of MNAR promotes estrogen activation of phosphatidylinositol 3-kinase. Mol Cel Biol 27:1904–1913
14. Smith CL, O'Malley BW (2004) Coregulator function: a key to understanding tissue specificity of selective receptor modulators. Endocr Rev 25:45–71
15. Webb P, Valentine C, Nguyen P et al (2003) ERβ binds N-CoR in the presence of estrogens via an LXXLL-like motif in the N-CoR C-terminus. Nucl Recept 1:4
16. Fernadez-Majada V, Pujadas J, Vilardell F et al (2007) Aberrant cytoplasmic localization of N-CoR in colorectal tumors. Cell cycle 6:1748–1752
17. Espinosa L, Santos S, Ingles-Esteve J et al (2002) p65-NFkappaB synergizes with Notch to activate transcription by triggering cytoplasmic translocation of the nuclear receptor corepressor N-CoR. J Cell Sci 115:1295–1303
18. Jonas BA, Privalsky ML (2004) SMRT and N-CoR corepressors are regulated by distinct kinase signalling pathways. J Biol Chem 279:54676–54686
19. Rajhans R, Vadlamudi RK (2006) Comprehensive analysis of recent biochemical and biologic findings regarding a newly discovered protein-PELP1/MNAR. Clin Exp Metastasis 23:1–7
20. Vadlamudi RK, Wang RA, Mazumdar A et al (2001) Molecular cloning and characterization of PELP1, a novel human coregulator of estrogen receptor α. J Biol Chem 276:38272–38279
21. Witz IP (2008) Yin–yang activities and vicious cycles in the tumor microenvironment. Cancer Res 68:9–13
22. Chang HY, Sneddon JB, Alizadeh AA et al (2004) Gene expression signature of fibroblast serum response predicts cancer progression: similarities between tumors and wounds. PLOS Biol 2:e7
23. West RB, Nuyten DSA, Subramanian S et al (2005) Determination of stroma signatures in breast carcinoma. PLOS Biol 3:e187
24. Desmoulliere A, Guyot C, Gabbiani G (2004) The stroma reaction myofibroblast: key player in the control of tumor cell behavior. Int J Dev Biol 48:509–517
25. Nakayama H, Enzan H, Miyazaki E et al (2000) Differential expression of CD34 in normal colorectal tissue, peritumoral inflammatory tissue, and tumor stroma. J Clin Pathol 53:626–629
26. Adegboyega PA, Mifflin RC, DiMari JF et al (2002) Immunohistochemical study of myofibroblasts in normal colonic mucosa, hyperplastic polyps and adenomatous colorectal polyps. Arch Pathol Lab Med 126:829–836
27. Chen AL, Soman KV, Rychahou PG et al (2005) Proteomic analysis of colonic myofibroblasts and effect on colon cancer cell proliferation. Surgery 138:382–390
28. De Wever O, Nguyen OD, Van Hoorde L et al (2004) Tenascin C and SF/HGF produced by myofibroblasts can provide convergent pro-invasive signals to human colon cancer cells through RhoA and Rac. FASEB J 18:1016–1028
29. Sivridis E, Giatromanolaki A, Koukourakis MI (2005) Proliferating fibroblasts at the invading tumour edge of colorectal adenocarcinomas are associated with endogenous markers of hypoxia, acidity, and oxidative stress. J Clin Pathol 58:1033–1038
30. Liebeau B, Heymann M-F, Henry F et al (1999) Immunomodulatory effects of tumor associated fibroblasts in colorectal tumor development. Int J Cancer 81:629–636
31. Scoville DH, Sato T, He XC et al (2008) Current view: intestinal stem cells and signaling. Gastroenterology 134:849–864
32. Powell DW, Mifflin RC, Valentich JD et al (1999) Mofibroblast I. Paracrine cells important in health and disease. Am J Physiol 277 (1 Pt 1):C1–C9
33. Cooke PS, Buchanan DL, Young P et al (1997) Stromal estrogen receptors mediate mitogenic effects of estradiol on uterine epithelium. Proc Natl Acad Sci USA 94:6535–6540
34. Cunha GR, Young P, Hom YK et al (1997) Elucidation of a role for stromal steroid hormone receptors in mammary gland growth and development using tissue recombinants. J Mammary Gland Biol Neoplasia 2:393–402
35. Prins GS, Birch L, Couse JF et al (2001) Estrogen imprinting of the developing prostate gland is mediated through stromal estrogen receptor alpha: studies with alphaERKO and betaERKO mice. Cancer Res 61:6089–6097
36. Gupta PB, Proia D, Cingoz O et al (2007) Systemic stromal effects of estrogens promote the growth of estrogen receptor-negative tumors. Cancer Res 67:2062–2071
37. Schurch W, Seemayer TA, Gabbiani G (1998) The myofibroblast. Am J Surg Pathol 22:141–147
38. Frasor J, Danes JM, Funk CC et al (2005) Estrogen down-regulation of the corepressor N-CoR: mechanism and implications for estrogen derepression of N-CoR-regulated genes. PNAS 102:13153–13157
39. Dobrzycka KM, Townson SM, Jiang S et al (2003) Estrogen receptor corepressors—a role in human breast cancer. Endocr Relat Cancer 10:517–536
40. Park DM, Li J, Okamoto H, Akeju O et al (2007) N-CoR pathway targeting induces glioblastoma derived cancer stem cell differentiation. Cell Cycle 6:467–470
41. Lee M-O, Kang H-J (2002) Role of coactivators and corepressors in the induction of the RARβ gene in human colon cancer cells. Biol Pharm Bull 25:1298–1302
42. Hornberg JJ, Bruggeman FJ, Westerhoff HV et al (2006) Cancer: a system biology disease. Biosystems 83:81–90
43. Jepsen K, Hermanson OM, Onami TM et al (2000) Combinatorial roles of the nuclear receptor corepressor in transcription and development. Cell 102:753–763
44. Hermanson O, Jepsen K, Rosenfeld MG (2002) N-CoR controls differentiation of neural stem cells into astrocytes. Nature 419:934–939
45. Grignani F, De Matteis S, Nervi C et al (1998) Fusion proteins of the retinoic acid receptor-a recruit histone deacetylase in promyelocytic leukaemia. Nature 391:815–818
46. Fortunel NO, Otu HH, Ng HH et al (2000) Comment on "'stemness': transcriptional profiling of embryonic and adult stem cells" and "a stem cell molecular signature". Science 302:393
47. Spirakov M, Fisher AG (2007) Epigenetic signatures of stem-cell identity. Nat Rev Genet 8:263–271
48. Vadlamudi RK, Kumar R (2007) Functional and biological properties of the nuclear receptor coregulator PELP1/MNAR. Nuclear Receptor Signaling 5:e004
49. Barleta F, Wong C-W, McNally C et al (2004) Characterization of the interactions of estrogen receptor and MNAR in the activation of cSrc. Mol Endocrinol 18:1096–1108
50. Vadlamudi RK, Manavathi B, Balasenthil S et al (2005) Functional implications of altered subcellular localization of PELP1 in breast cancer cells. Cancer Res 65:7724–7732
51. Nair SS, Mishra SK, Yang Z et al (2004) Potential role of a novel transcriptional coactivators PELP1 in histone H1 displacement in cancer cells. Cancer Res 64:6416–6423
52. King KJ, Nicholson HD, Assinder SJ (2006) Effect of increasing ratio of estrogen:androgen on proliferation of normal human

prostate stromal and epithelial cells, and the malignant cell line LNCaP. Prostate 66:105–114
53. Rajhans R, Nair S, Holden AH et al (2007) Oncogenic potential of the nuclear receptor coregulator proline-, glutamic acid-, leucine-rich protein 1/modulator of the nongenomic actions of the estrogen receptor. Cancer Res 67:5505–5512
54. Nair S, Vadlamudi RK (2007) Emerging significance of ER-coregulator PELP1/MNAR in cancer. Histol Histopathol 22:91–96
55. Horard B, Vanacker J-M (2003) Estrogen receptor-related receptors: orphan receptors desperately seeking a ligand. J Mol Endocrinol 31:349–357
56. Cavallini A, Notarnicola M, Giannini P et al (2005) Oestrogen receptor-related receptor alpha (ERRa) and oestrogen receptors (ERa and ERb) exhibit different gene expression in human colorectal tumour progression. Eur J Cancer 41:1487–1494

Virchows Arch (2009) 454:55–60
DOI 10.1007/s00428-008-0699-1

ORIGINAL ARTICLE

Mucinous adenocarcinoma of minor salivary glands: a high-grade malignancy prone to lymph node metastasis

Fumio Ide · Kenji Mishima · Akio Tanaka · Ichiro Saito · Kaoru Kusama

Received: 26 June 2008 / Revised: 30 October 2008 / Accepted: 4 November 2008 / Published online: 27 November 2008

Abstract Salivary gland mucinous adenocarcinoma (MAC) is a rarely encountered and poorly understood tumor. We describe two additional cases presenting as a lip lesion of older women. The prognosis was dismal with one death and one patient with recurrent/metastatic disease. Combining these with 19 cases in the literature unveiled that intraoral MAC occurred primarily in the palate (43%) of elderly individuals (average 65 years) with slight male preponderance (59%). Tumor evolved slowly (>2 years) and most (60%) were diagnosed at an advanced stage. Local recurrences were common (33%) and cervical lymph node and distant metastases were frequent (63% and 29%, respectively). About half the patients (47%) died of tumor within 6 years. Both histologically and immunohistochemically, MAC lacked acinar, myoepithelial, and neuroendocrine phenotypes. Cytokeratins 7 and 20 and estrogen and progesterone receptors, in some combination, may assist to distinguish primary versus metastatic mucinous carcinoma. Minor salivary gland MAC belongs to a high-grade category with a significant risk of local recurrence, lymph node metastasis, and fatal outcome.

Keywords Mucinous adenocarcinoma · Minor salivary gland · Immunophenotype · Clinicopathologic correlation

F. Ide (✉) · K. Mishima · I. Saito
Department of Pathology, Tsurumi University School of Dental Medicine, 2-1-3 Tsurumi, Tsurumi-ku, Yokohama 230-8501, Japan
e-mail: ide-f@tsurumi-u.ac.jp

F. Ide · A. Tanaka · K. Kusama
Division of Pathology, Department of Diagnostic and Therapeutic Sciences, Meikai University School of Dentistry, Saitama, Japan

Introduction

Mucinous adenocarcinoma (MAC) is an elusive and controversial tumor of the salivary glands; elusive because of its rarity and controversial because of its diagnostic uncertainty. There has been no long-term consensus on the definition and the term MAC has been applied to the broader and heterogeneous "mucin-producing adenocarcinoma" category in a descriptive manner [1–4]. For example, two photomicrographs of MAC sanctioned by the 1992 World Health Organization classification [5] are more suggestive of cystadenocarinomas [2]. A unifying pathologic description of MAC in the current standard textbooks is that of "small clusters and single carcinoma cells floating in large pools of extracellular mucin compartmentalized by fibrous septa" [3, 6, 7]. This defying feature is nearly identical to mucinous eccrine carcinoma of the skin, mucinous carcinoma of the breast, and colloid carcinoma of the intestine [1–3, 6]. Alternatively, definitive diagnosis of MAC as a primary salivary gland tumor is achieved by exclusion of metastatic disease [3].

A true MAC is distinctly uncommon [3, 7]. There were only five cases in the 1996 Armed Forces Institute of Pathology (AFIP) monograph [2]; all were found in the major glands (three submandibular, two parotid). Although the detailed data was not provided, MAC in the 2008 AFIP files were nearly equally divided between major and minor salivary glands [3]. The first series of MAC with minor salivary gland involvement (total four cases) was published in German by Gunzel et al. [8] in 1993, leading to bias toward intraoral tumors. Minor salivary gland MAC have been reported as individual examples (four cases; one of two reports published in Japanese [9] and two only in abstract form [10, 11]), in small series (10 cases; one series published in Chinese [12]) or collectively with other types

of carcinoma (five cases [13–15]). This specific situation served as the impetus for the present work.

We describe the clinicopathologic and immunohistochemical findings in two cases of MAC, both occurring in the lip. Our goal is to compare these data with those of 19 cases from the literature to comprehend the profile of MAC in the intraoral minor salivary glands.

Case reports

The clinical summary is listed in Table 1. Because of innocuous appearance, lip lesion in our patients was preoperatively diagnosed as a benign tumor (Fig. 1). Both cases were managed by surgery alone and a postoperative workup in search of occult primary malignancy of other sites contributed no abnormal findings. Case 1 subsequently requested that no additional treatment be performed, but remained under review until her death at another hospital, from widespread metastases (further information was not available), 6 years later. In case 2, the surgical margins were involved. Three years after re-excision, the patient developed local recurrence and underwent wide resection. A neck dissection was done for metastasis to submandibular lymph nodes 6 months later. This case remained free of tumor for a further 16 months.

Materials and methods

Formalin-fixed, paraffin-embedded sections were stained with hematoxylin and eosin, periodic acid-Schiff, mucicarmine and Alcian blue at pH 2.5. Indirect immunohistochemical staining was performed by the avidin–biotin peroxidase complex method with microwave pretreatment, using specific antibodies against cytokeratin (CK) AE1/AE3, CK7 (OV-TL 12/30), CK20 (Ks 20.8), epithelial membrane antigen (E29), S-100 protein (polyclonal), α-smooth muscle actin (1A4), neuron-specific enolase (BBS/NC/VI-H14), chromogranin A (DAK-A3), carcinoembryonic antigen (CEA; II-7), estrogen receptor (ER; 1D5), progesterone receptor (PR; PgR 636), and Ki-67 (MIB-1). All antibodies were purchased from Dakocytomation (Carpinteria, CA). Our institutional review boards approved this study (A 0313).

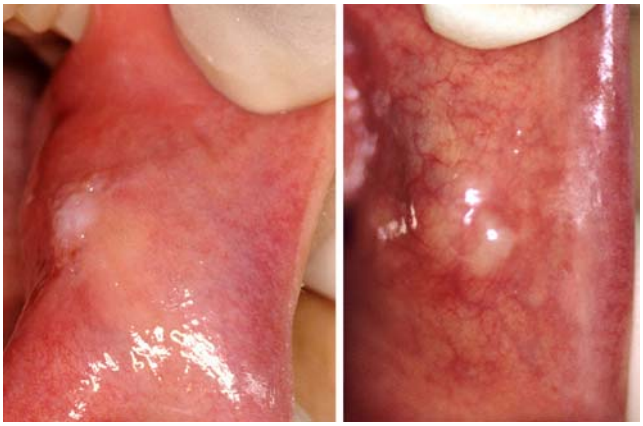

Fig. 1 Clinical appearance of lip tumor in case 1 (*left*) and case 2 (*right*)

Results

Two cases displayed a nearly identical histology. As shown in Fig. 2a, unencapsulated and invasive tumor was located on the mucosal side of the orbicularis oris muscle. Variably sized mucin lakes were loculated by fibrotic stroma and accounted for more than 90% of the total tumor area. Within mucin pools, detached tumor cells floated individually and in small clumps, either solid or clustering around microlumina (Fig. 2b). Some single cells manifested a signet-ring cytomorphology but never dominance. Case 2 tended to grow in slender cords and also exhibited proliferation of small single layered duct-like structures. Both tumors showed no solid, cribriform, targetoid, papillary-cystic, or acinar growth pattern. Diffuse infiltration into adipose, muscular, and neural periglandular tissues was evident (Fig. 2c, d). Neither tumor necrosis nor vascular invasion was apparent. Mitotic figures were infrequent. In case 1, focal permeation of the surface mucosal epithelium by tumor nests was observed (Fig. 2e). According to the cytologic grades of mucinous carcinoma of the skin [16], case 1 was Grade 3 (see Fig. 3c) and case 2 Grade 2. Two of 12 lymph nodes contained metastases with no extracapsular spread (Fig. 2f). The mucinous substance stained positively with periodic acid-Schiff, mucicarmine, and Alcian blue.

Table 1 Clinical features of the present patients

Case	Age/sex	Site	Clinical presentation	Treatment	Follow-up
1	76/female	Lower lip	1-cm Asymptomatic swelling for 3 years	Excisional biopsy	Death of disease at 6 years with multiple metastases
2	82/female	Upper lip	1.4-cm Painless mass for 8 months	Excisional biopsy, re-excision, wide resection, neck dissection	Local recurrence and cervical lymph node metastasis 3 years later

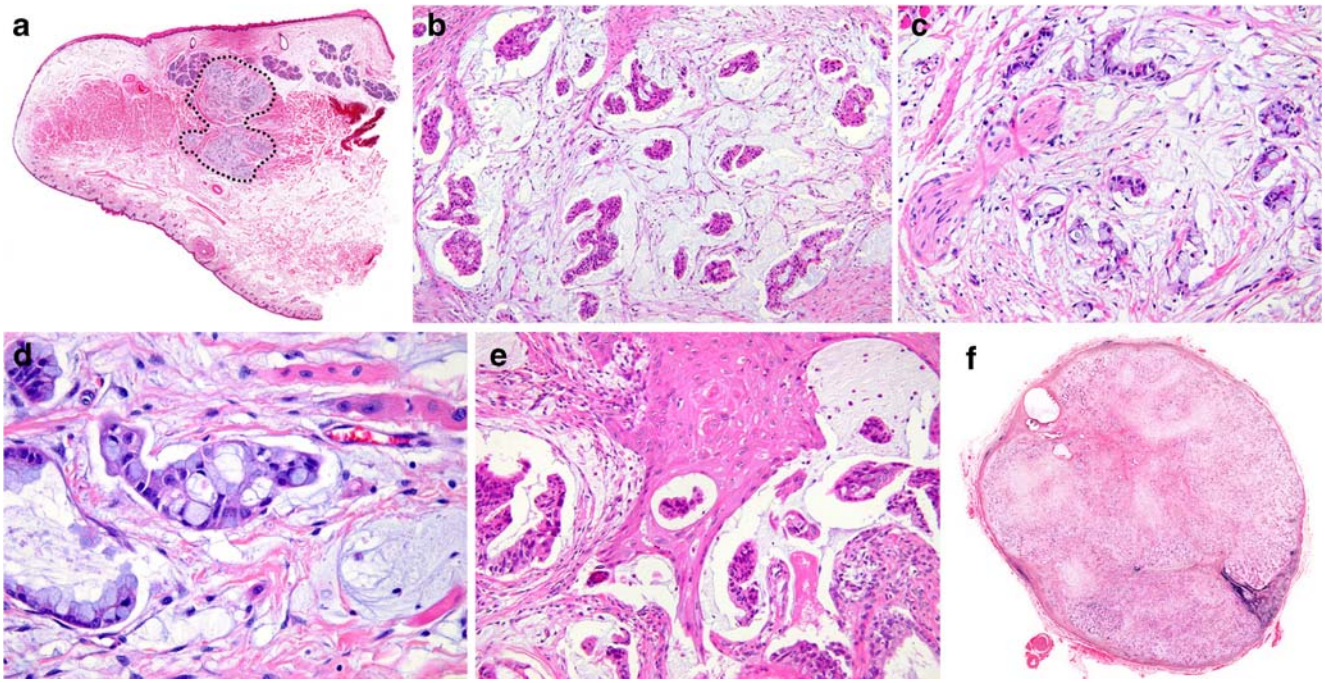

Fig. 2 Hematoxylin and eosin histology. **a** Whole-mounted view showing tumor location (*dotted line*) on the submucosal side of orbicularis oris muscle (case 2), ×2. **b** Clumps of carcinoma cells surrounded by a sea of mucin (case 1), ×100. **c** Perineural invasion (case 2), ×200. **d** Infiltration into skeletal muscle (case 2), ×400. **e** Carcinoma growing into the surface epithelium (case 1), ×200. **f** Total replacement of lymph node by metastatic carcinoma (case 2), ×2.5

All or almost all tumor cells showed strong immunoreactivity for AE1/AE3 (Fig. 3a) and CK7 (Fig. 3b), but not for CK20 (Fig. 3c). They were also variably positive for epithelial membrane antigen (Fig. 3d) and CEA (Fig. 3e). Smooth muscle actin, S-100 protein (Fig. 3f), neuron-specific enolase and chromogranin A were negative for tumor cells. None of them expressed for ER and PR. The Ki-67 index was 35% in case 1 and 32% in case 2.

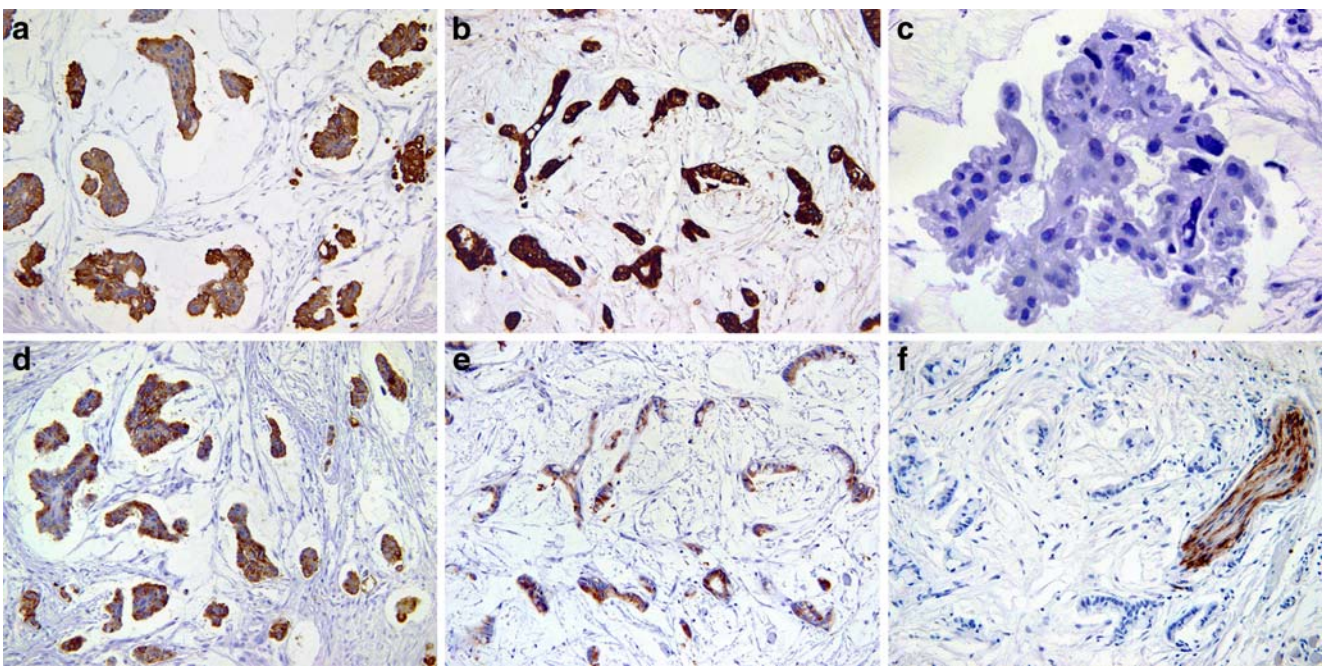

Fig. 3 Immunoprofile. AE1/AE3 (**a**) and cytokeratin 7 (**b**) highlighting carcinoma cells in case 1 (**a**) and case 2 (**b**), ×200. **c** Negative staining for cytokeratin 20 (case 1). Note substantial nuclear pleomorphism, ×400. **d** Positivity for epithelial membrane antigen (case 1), ×200. **e** Carcinoembryonic antigen expression (case 2), ×200. **f** Negativity for S-100 protein in carcinoma cells (case 2), ×200

Literature review

The real frequency of MAC remains unknown; it comprises less than 0.1% of epithelial salivary gland tumors in the AFIP files [3]. In Chinese population, MAC represented 0.1% (seven of 5,416) of all salivary gland tumors and 0.4% (seven of 1,994) of carcinomas [13]. Its incidence was also estimated to be 0.07% (1 of 1,392) of malignant salivary tumors in West China [14]. Recent study of minor salivary gland tumors from the United States indicated that MAC accounted for 0.2% (1 of 546) of all tumors and 0.4% (1 of 241) of malignancies [17].

Reports on MAC of minor salivary gland origin described by name have slowly accrued. Six brief reports including three abstracts provided combined analysis of the major and minor salivary tumors [2, 3, 6, 18–20] and accordingly were excluded from this analysis. There are other three sporadic case reports that were unacceptable, because their histopathology was different from MAC [21–23]. The clinical parameter of 21 cases (19 from the literature [8–15, 24] and two from our files) is summarized in Table 2.

Intraoral MAC is a tumor of older adults (average 64.6 years). No lesion has been observed in children and adolescents; the youngest patient was 42 years. There was a slight male predominance with a male-to-female ratio was 1.4:1. The palate was the typical site of involvement (43%). Tumor duration ranged from 2 months to 8 years and averaged 23 months. Most (60%) showed extraglandular extension at presentation, i.e., bone destruction at palatine sites. Unfortunately, information about the size of the lesions was incomplete. Local recurrence, cervical lymph node metastasis, and distant spread were recorded in 33%, 63%, and 29% of cases, respectively. Within 6 years, 47% of patients died of disease and of these, 57% had the clinically positive neck before diagnosis. The recommended treatment is complete surgical excision and the benefit of chemoradiotherapy as an adjunct remains empiric [3].

Table 2 Clinical summary of 21 cases of minor salivary gland mucinous adenocarcinoma

Age (years) (n=17)	
Average	64.6
Range	42–86
Sex (n=17)	
Male	10 (59%)
Female	7
Site (n=21)	
Palate	9 (43%)
Buccal mucosa	4
Oral floor	3
Lip	3
Tongue	2
Tumor duration (months) (n=10)	
Average	23
Range	2–96
Tumor extension (n=10)	
Mucosa only	4
Adjacent tissues	6 (60%)
Cervical lymph node metastasis (n=16)	
Yes	10 (63%)
No	6
Distant metastasis (n=14)	
Yes	4 (29%)
No	10
Local recurrence (n=9)	
Yes	3 (33%)
No	6
Follow-up (n=15)[a]	
Alive no disease	5
Alive with disease	2
Death of disease	7 (47%)
Death of unrelated cause	1

[a] Mean 30 months with range 6–72 months

Discussion

Mucinous appearance itself is not pathognomonic of MAC and many salivary gland carcinomas may exhibit this trait [1–3, 6, 7]. In this sense, the diagnosis of MAC by unaided histologic assessment is one of exclusion [3]. The differential diagnostic considerations in the realm of MAC are cystadenocarcinoma [25], mucoepidermoid carcinoma [22], mucin-rich salivary duct carcinoma [26] and signet-ring cell adenocarcinoma [4]. Requisitely absent from pure MAC are an additional non-mucinous component that characterizes these four named carcinomas [3]. Quantities of mucinous component in the above simulants, of course, are not as extensive as in MAC. Surgical specimens should always be sampled well to avoid missing a non-mucinous invasive component. It is interesting that a statistically significant difference in nuclear shape and chromatin texture between MAC and cystadenocarcinomas was observed with the aid of computerized histomorphometric analysis [20]. Moreover, nuclear size in MAC was significantly smaller as opposed to mucin-rich salivary duct carcinomas [20]. In our particular cases, the origin from intradermal sweat glands of the lip, namely a direct mucosal extension of mucinous eccrine carcinoma, must be considered [3, 27]. However, the exact intramucosal location of the tumor, as depicted above, convinced a labial salivary gland origin. As far as we know, lip has been free from primary mucinous carcinoma of the skin [3, 16, 28].

Because of their homologies, distinction of primary MAC from metastatic mucinous carcinoma is impossible on histologic grounds alone [1–3, 6]. The immunotyping of CK7/CK20 may aid in substantiating a tumor origin. In sum, the CK7(+)/CK20(–) phenotype may be a rationale for

a salivary primary [8, 9, 11, 18, 29], whereas a conjointly CK7(–) and CK20(+) profile may serve as a clue to an intestinal origin [16]. Interestingly, newer markers of gastrointestinal epithelial differentiation, CDX2 and villin, were reportedly negative in a case of MAC [11]. It is known, however, that CK pattern of MAC and its cutaneous and mammary counterparts are comparable [16], making a discrimination between them untenable. On the other hand, the reactivity for ER and PR strongly points to a skin/breast primary [16, 28], as opposed to its consistent absence in MAC (n=6 including our tumors [18, 29]). The remaining immunomarkers assessed showed differential, but proved to be less discriminating. The staining for CEA was found positive in MAC (n=4 including our cases [9, 10]), as are all intestinal carcinomas, while skin and breast tumors considerably vary [16]. Last, neuron-specific enolase and chromogranin A were not observed in any of the present MAC, as well as most, but not all, mucinous carcinomas of the skin, breast, and intestine [16]. In practice, reliance on clinical findings is crucial before rendering a final decision. A full evaluation failed to identify any concomitant malignancy in our patients. Furthermore, lip is an unlikely site for metastasis and there is no description in the literature concerning a solitary lip metastasis of pure mucinous carcinoma [30, 31].

The initial impression of a low-grade, indolent biologic behavior in MAC of the major salivary glands [1, 2] stands in sharp contrast to the recent notion [3, 6, 7, 11, 12, 19]. This discrepancy may be reflective of increased reporting of intraoral tumors. As is evident in this study, one of the most worrisome clinical features of minor salivary MAC is the high propensity for lymph node metastases (>60%). Given the fact that only a few cases of major salivary MAC have appeared in the literature (total 13 cases; eight parotid, four submandibluar, one sublingual [2, 6, 7, 13, 19, 20, 29]) and some of them were probably duplicated [2, 6, 19, 20], it is currently unclear whether there is any difference in the biologic behavior of MAC between major and minor salivary glands. The average percentiles of Ki-67 and proliferating cell nuclear antigen expressions in MAC (n=17 including our cases [8, 9, 12, 18]) were 38% (range, 32% to 46%) and 34% (range, 28% to 44%), respectively. A high Ki-67 index (>30%) has been found to correlate well with poor overall survival in salivary carcinomas [32]. Of additional note is DNA ploidy analysis that one metastasizing MAC was aneuploid [15]. In the future, this parameter could also be useful for predictive purposes.

In conclusion, MAC is more common in the intraoral minor salivary glands, with an approximately 2:1 predilection for the minor over major glands. Although available data is too limited to be statistically significant, our literature-based analysis reaffirms: (1) that MAC is one of the most aggressive types of salivary gland carcinoma plagued by early lymph node metastases, suggesting a possible role for elective neck management; (2) that on clinical grounds, MAC contrasts greatly with its cutaneous and mammary analogues which share an overall favorable prognosis; (3) that at this time, clinical stage is the most significant adverse prognosticator for MAC; and (4) that with a large series, immunohistochemistry including mucin profile (MUC antigen) and oncogene status is fundamental to our understanding of MAC biology and also prerequisite to resolve differential diagnostic problems surrounding MAC.

Conflict of interest statement We declare that we have no conflict of interest.

References

1. Ellis GL, Auclair PL, Gnepp DR (1991) Surgical pathology of the salivary glands. WB Saunders, Philadelphia, pp 480–482
2. Ellis GL, Auclair PL (1996) Tumors of the salivary glands, 3rd edn. Armed Forces Institute of Pathology, Washington DC, pp 349–352
3. Ellis GL, Auclair PL (2008) Tumors of the salivary glands, 4th edn. American Registry of Pathology and Armed Forces Institute of Pathology, Washington DC, pp 383–386
4. Ghannoum JE, Freedman PD (2004) Signet-ring cell (mucin-producing) adenocarcinomas of minor salivary glands. Am J Surg Pathol 28:89–93
5. Seifert G (1991) Histological typing of salivary gland tumours, 2nd edn. Springer, Berlin, p 27
6. Gnepp DR, Brandwein MS, Henley JD (2001) Colloid carcinoma. In: Gneppp DR (ed) Diagnostic surgical pathology of the head and neck. WB Saunders, Philadelphia, pp 402–403
7. Sun KH, Gao Y, Li TJ (2005) Mucinous adenocarcinoma. In: Barnes L, Eveson JW, Reichart P, Sidransky D (eds) Pathology and genetics of head and neck tumours. IARC, Lyon, pp 234–235
8. Gunzl H-J, Donath K, Schmelzle R (1993) Klinik und Pathohistologie muzinoser Adenokarzinome der kleinen Speicheldrusen. Pathologe 14:210–215
9. Mano T, Uchida K, Okafuji M et al (2006) A case of mucinous adenocarcinoma of the palate [in Japanese with English abstract]. Jpn J Oral Maxillofac Surg 52:507–510
10. Chen SY, Pringle GA (2002) Mucinous adenocarcinoma of buccal mucosa [abstract]. Oral Surg Oral Med Oral Pathol 94:207
11. Shumway A, Kalmar J, Steiner R, Allen C (2007) Mucinous adenocarcinoma of the palate: report of a case and review of the literature [abstract]. Oral Surg Oral Med Oral Pathol 103:e23–e24
12. Gao Y, Di P, Peng X, Yu G, Sun K (2002) Mucinous adenocarcinoma of salivary glands [in Chinese with English abstract]. Chin J Stomatol 37:356–358
13. Li J, Wang BY, Nelson M et al (2004) Salivary adenocarinoma, not otherwise specified. A collection of orphans. Arch Pathol Lab Med 128:1385–1394
14. Li L-J, Li Y, Wen Y-M, Liu H, Zhao H-W (2008) Clinical analysis of salivary gland tumor cases in West China in past 50 years. Oral Oncol 44:187–192

15. Vargas PA, Torres-Rendon A, Speight PM (2007) DNA ploidy analysis in salivary gland tumours by image cytometry. J Oral Pathol Med 36:371–376
16. Kazakov DV, Suster S, LeBoit PE et al (2005) Mucinous carcinoma of the skin, primary, and secondary. A clinicopathologic study of 63 cases with emphasis on the morphologic spectrum of primary cutaenous forms: homologies with mucinous lesions in the breast. Am J Surg Pathol 29:764–782
17. Pires FR, Pringle GA, de Almeida OP, Chen S-Y (2007) Intra-oral minor salivary gland tumors: a clinicopathological study of 546 cases. Oral Oncol 43:463–470
18. Alos L, Castillo M, Perez N et al (2002) Salivary gland mucinous adenocarcinoma: a clinicopathological, immunohistochemical and flow-cytometric study of three cases [abstract]. Histopathology 41:104
19. Gnepp D, Estalilla O, Henley J, Ellis G (1997) Primary colloid (mucinous) carcinoma of the salivary glands [abstract]. Oral Surg Oral Med Oral Pathol 84:188
20. Yakirevich E, Gnepp DR, Alos L, Cardesa A, Ellis G, Sabo E (2006) Primary mucin producing tumors of the salivary glands; a clinicopathologic and morphometric study [abstract]. Mod Pathol 19(Suppl 1):213A–214A
21. Hashitani S, Sakurai K, Noguchi K, Natori J, Urade M (2004) Mucinous adenocarcinoma with neuroendocrine differentiation of the mandibular ramus: report of a case. J Oral Pathol Med 33: 59–63
22. Kubo H, Ohnishi Y, Takekita A et al (2005) A case of mucinous adenocarcinoma arising in the palate [in Japanese with English abstract]. Jpn J Oral Maxillofac Surg 51:555–558
23. Honda K, Natsumi Y, Sakurai K, Ishikura R, Urade M (2006) Mucinous adenocarcinoma of the temporal region initially diagnosed as temporomandibular disorders: a case report. J Oral Pathol Med 35:582–585
24. Notani K, Iizuka T, Yamazaki Y et al (2002) Mucinous adenocarcinoma of probable minor salivary gland origin. Oral Surg Oral Med Oral Pathol 94:738–740
25. Foss RD, Ellis GL, Auclair PL (1996) Salivary gland cystadenocarcinomas. A clinicopathologic study of 57 cases. Am J Surg Pathol 20:1440–1447
26. Henley J, Summerlin D-J, Potter D, Tomich C (2005) Intraoral mucin-rich salivary duct carcinoma. Histopathology 47:436–437
27. Stavrianos SD, Wilson GR, McLean NR, Soames JV (1996) Adnexal adenocarcinoma of the upper lip. Int J Oral Maxillofac Surg 25:196–198
28. Breiting L, Dahlstrom K, Christensen L, Winther JF, Breiting V (2007) Primary mucinous carcinoma of the skin. Am J Dermatopathol 29:595–596
29. Krogdahl AS, Schou C (1997) Mucinous adenocarcinoma of the sublingual gland. J Oral Pathol Med 26:198–200
30. Cotton DWK, Fairris GM (1985) Metastatic breast carcinoma on the lip: case report. Dermatologica 171:362–365
31. Smith SP, Grossman K, Rao BK, Koh HK, Cooley TD (1991) Solitary papule of the lip in recurrent gastroesophageal carcinoma: an unusual presentation of cutaneous metastasis. Arch Dermatol 127:588–589
32. Ettl T, Schwarz S, Kuhnel T, Stockmann P, Reichert TE, Driemel O (2008) Immunhistochemie als Prognoseindikator bei Speicheldrusenkarzinomen. HNO 56:231–238

Virchows Arch (2009) 454:61–70
DOI 10.1007/s00428-008-0695-5

ORIGINAL ARTICLE

Small cluster invasion: a possible link between micropapillary pattern and lymph node metastasis in pT1 lung adenocarcinomas

Takehito Kawakami · Kazuki Nabeshima · Makoto Hamasaki · Akinori Iwasaki · Takayuki Shirakusa · Hiroshi Iwasaki

Received: 15 July 2008 / Revised: 20 September 2008 / Accepted: 21 October 2008 / Published online: 11 November 2008

Abstract Lung adenocarcinomas with micropapillary pattern (MPP) are associated with frequent nodal metastasis. However, little is known about the mechanisms that underlie MPP-associated nodal metastasis. In this study, we investigated how small micropapillary clusters of carcinoma cells present in tumoral alveolar spaces lead to increased lymph node metastasis. We analyzed 146 cases of pT1 lung adenocarcinomas with reference to the presence of MPP, small cluster invasion (SCI), and lymphatic involvement. SCI was defined as markedly resolved acinar–papillary tumor structures with single or small clusters of carcinoma cells invading stroma within fibrotic foci. The MPP-positive group (88/146 cases) was associated with significantly more frequent nodal metastasis and significantly worse survival. Moreover, SCI was significantly more frequent in the MPP-positive group (71/88 cases) than MPP-negative group (10/58 cases) and was significantly associated with lymphatic involvement ($p<0.0001$) and nodal metastasis ($p=0.0073$). The SCI-positive group showed significantly worse survival (5-year survival, 70%) than the SCI-negative group (91%, $p=0.0017$). Carcinoma cells undergoing SCI demonstrated the same characteristic MUC-1 expression on the outer surface of cell clusters as those undergoing MPP. Thus, SCI could link MPP to nodal metastasis; carcinoma cells with MPP tend to undergo SCI in scars and invade lymphatics in pT1 lung adenocarcinomas.

Keywords Lung adenocarcinoma · pT1 · Micropapillary pattern · Tumor invasion · Metastasis · Prognosis

T. Kawakami · K. Nabeshima (✉) · M. Hamasaki · H. Iwasaki
Department of Pathology, Fukuoka University Hospital,
7-45-1 Nanakuma, Jonan-ku,
Fukuoka 814-0180, Japan
e-mail: kaznabes@fukuoka-u.ac.jp

T. Kawakami · A. Iwasaki · T. Shirakusa
Department of Surgery Division of Thoracic, Endocrine, and Pediatric Surgery,
Fukuoka University Hospital and School of Medicine,
Fukuoka, Japan

Introduction

Among the major histological types of lung tumors, the incidence of adenocarcinoma is showing the most increase worldwide [1, 2]. Even in patients with stage I lung adenocarcinoma, the 5-year survival rate is still as low as 60–70% [3]. Some patients with pT1 adenocarcinoma may develop distant metastasis in a short period after complete surgical resection [4–6].

The micropapillary pattern is characterized by the presence of papillary structures with tufts lacking a central fibrovascular core [7]. Patients with micropapillary-pattern-positive lung adenocarcinomas have poor prognosis and tend to present with extensive lymph node involvement and metastatic disease [7–14], similar to those with micropapillary carcinomas of the breast [15], urinary bladder [16, 17], ureter [18, 19], colorectum [20, 21], and parotid gland [22, 23]. However, little is known about the mechanisms involved in micropapillary-pattern-associated lymph node metastasis. It is still unclear how small micropapillary clusters of carcinoma cells present in tumoral alveolar spaces invade lymphatics and lead to increased lymph node metastasis.

We have previously subclassified the stromal invasion grading system proposed as a prognostic marker by Sakurai et al. [24] according to the presence or absence of micropapillary pattern [8]. This subclassification provided

an advantage to their system because the largest group of patients with variable prognoses was subclassified into two smaller groups with different prognoses. Moreover, our study was the first to point to the possible association of micropapillary-pattern-positive carcinomas and small cluster invasion, which was defined as invasion of the fibrotic focus as isolated single or small clusters of carcinoma cells. Thus, we hypothesized that micropapillary-pattern-positive carcinomas may lead to lymph node metastasis via small cluster invasion and lymphatic involvement in the fibrotic focus. In the present study, we tested this hypothesis by analyzing the relationship between micropapillary pattern and lymph node metastasis with special reference to small cluster invasion.

Materials and methods

Patients

We reviewed 153 cases of pT1 lung adenocarcinoma that had been surgically resected at the Second Department of Surgery, Fukuoka University Hospital, between April 1993 and December 2003. Anonymous use of redundant tissue is part of the standard treatment agreement with patients in our hospital when no objection is expressed. The pathological stage was determined according to the tumor–node–metastasis classification of malignant tumors (International Union Against Caner) [25]. pT1 tumors were defined as "tumors of 3 cm or less in the greatest dimension, being surrounded by lung tissue or visceral pleura, and not involve the main bronchus [25]." Of the 153 cases, seven cases lost in the follow-up were excluded from the survival analysis. The remaining 146 cases were studied to explore the relationship among small cluster invasion, micropapillary pattern, and prognosis. All patients underwent complete resection of the tumors. The mean follow-up period was 75 months (range 2–132 months).

Pathologic evaluation

The surgically resected specimens were fixed routinely in 10% formalin, and the whole tumor nodules were processed into paraffin blocks for histopathological examination. Tissue sections were cut 4-μm thick, including the largest cut surface of the tumor, and stained with hematoxylin and eosin (H&E) and elastica-van-Gieson stain. For immunohistochemistry, 4-μm sections were mounted on Matsunami-Adhesive-Silane-coated glass slides, deparaffinized, and heated in a microwave oven (700 W) for 10 min to expose antigens in 10 mM Na-citrate buffer (pH 6.0). The antibodies used in this study are listed in Table 1. Immunohistochemical staining was performed by the labeled streptavidin–biotin method (Dako, Glostrup, Denmark). Alkaline phosphatase or horseradish peroxidase activity was visualized by naphthol-AS-BI-phosphate (Sigma, St. Louis, MO, USA) or metal-3,3′-diaminobenzidine (Pierce, Rockford, IL, USA) as a substrate, respectively. The immunohistochemical specificity of the antibodies was confirmed by two types of negative controls: substituting mouse nonimmune IgG for the primary antibodies and omitting the primary antibodies from the staining protocol.

Table 1 Antibodies used for immunohistochemistry

Antibody specificity	Antibody clone	Optimal dilution	Source retrieval	Antigen retrieval method
D2-40	D2-40	1:100	Dako Cytomation	Microwave
CD31	JC/70A	1:200	Dako Cytomation	Microwave
MUC1	Ma695	1:100	Novocastra Laboratories Ltd	Microwave

The histopathological type was determined according to the 2004 World Health Organization classification [26]. Lung adenocarcinomas exhibit a micropapillary pattern or true papillary structures. The true papillary structure is defined as consisting of one-layered glandular epithelium surrounding a fibrovascular core [27], whereas micropapillary pattern is characterized by papillary structures with tufts lacking a central fibrovascular core (Fig. 1a) [7]. Expression of cell surface glycoprotein MUC1 is observed along the entire outer surface of the micropapillary cell clusters (Fig. 1b). The extent of micropapillary pattern was determined as none (0% of the tumor), 1+ (<10%), 2+ (10–50%), or 3+ (>50%) based on the areas of micropapillary pattern in tumors. Furthermore, cases of none and 1+ were classified as micropapillary pattern negative, while those of 2+ and 3+ as micropapillary pattern positive, as described previously [11]. Lymphatic and vascular involvements were immunohistochemically confirmed using D2-40 and anti-CD31 antibodies, which detect lymph endothelial (Fig. 1c) and vascular endothelial (Fig. 1d) cells, respectively. Furthermore, we focused on the presence of single or small clusters of carcinoma cells at the invasive margin of the tumor within the fibrotic focus (Fig. 2a, inset). The small clusters appear to have separated from the acinar or papillary structures of tumors due to dedifferentiation. We named this mode of invasion small cluster invasion. This process is very similar to tumor budding in colorectal carcinomas [28]. These micropapillary pattern scoring and judgment of small cluster invasion and lymphatic and vascular involvement were performed independently by two pathologists (T. K. and K. N.), and a high level of

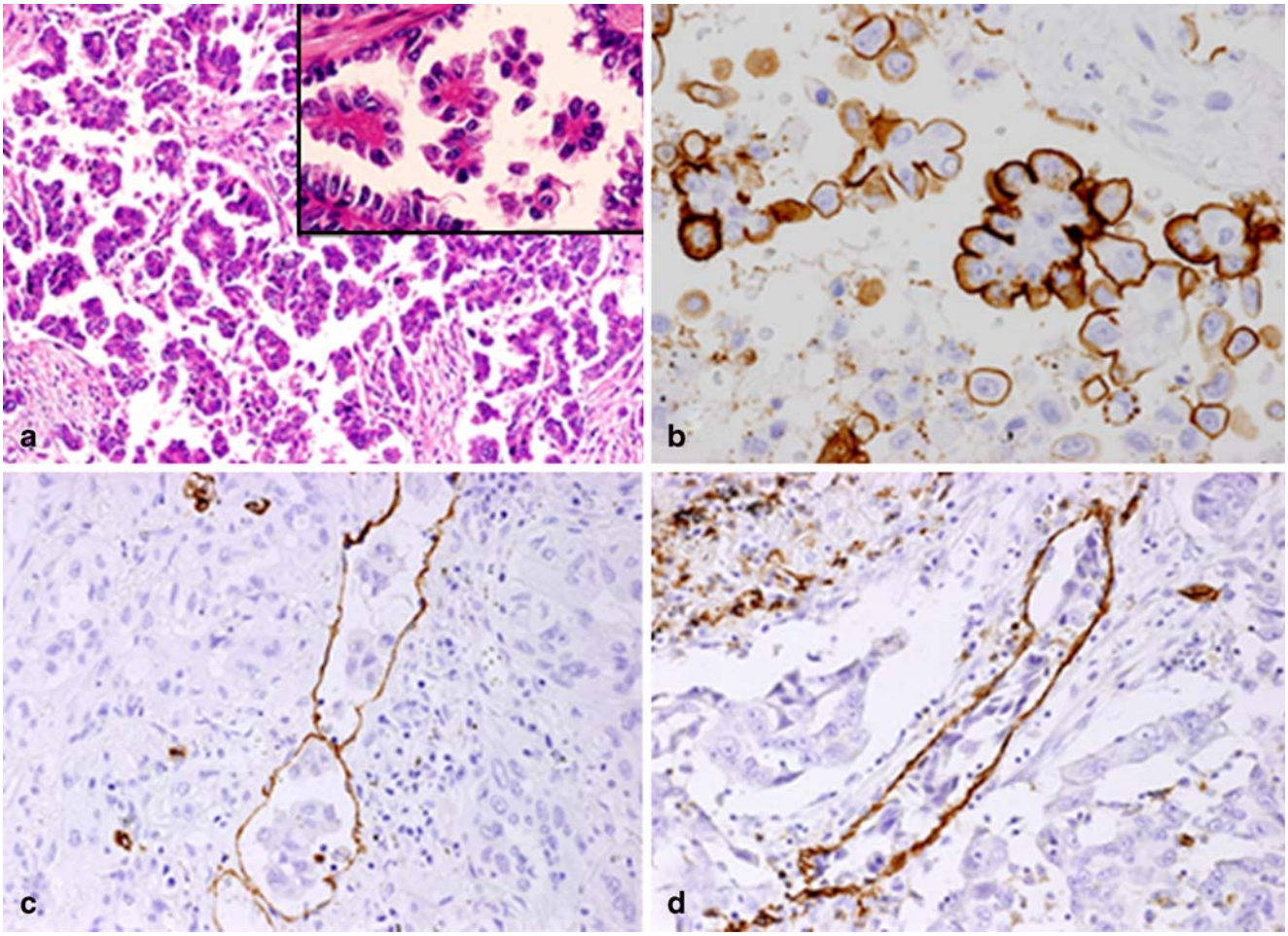

Fig. 1 **a** Micropapillary component observed in invasive lung adenocarcinoma. The *inset* shows micropapillary tufts lacking a central fibrovascular core. **b** MUC1 expression on the outer surface of micropapillary tufts. **c** Immunohistochemical demonstration of lymphatic involvement by carcinoma cells. Carcinoma cell clusters are seen in vessels lined by D2-40-reactive lymphatic endothelium. **d** Immunohistochemical demonstration of vascular involvement by carcinoma cells. Vessels lined by CD31-positive vascular endothelium contain carcinoma cell clusters. **a** H&E staining; **b** MUC-1 immunohistochemistry; **c** D2-40 immunohistochemistry; **d** CD31 immunohistochemistry

concordance (>90%) was achieved. In case of disagreement, the slides were reviewed again to obtain a consensus view.

The clinicopathological parameters considered in this study included age, gender, operative mode, histological subtype, pathological stage, tumor size, lymph node metastasis, pleural invasion, and small cluster invasion.

Statistical analysis

Summary statistics were obtained using standard methods and statistical analysis software StatView for Windows version 5.0 (SAS Institute Inc., Cary, NC). The relationships between several clinicopathological parameters and histopathological subgroups were evaluated using the χ^2 test and Fisher's exact test. Survival curves were plotted using Kaplan–Meier method, and p values were calculated using the log rank test. Multivariate analysis was performed by Cox regression. A p value of <0.05 was considered statistically significant.

Results

Clinical findings

Table 2 summarizes the clinicopathological characteristics of the 146 patients (60 males, 86 females; age range, 28–85 [mean=64.8] years). Lobectomy and limited surgery (segmentectomy or partial resection) were performed in 101 (69%) and 45 (31%) patients, respectively. Pathologically, 124 patients (85%) were classified as p-stage IA, eight patients (5%) as p-stage IIA, and 14 (10%) as p-stage

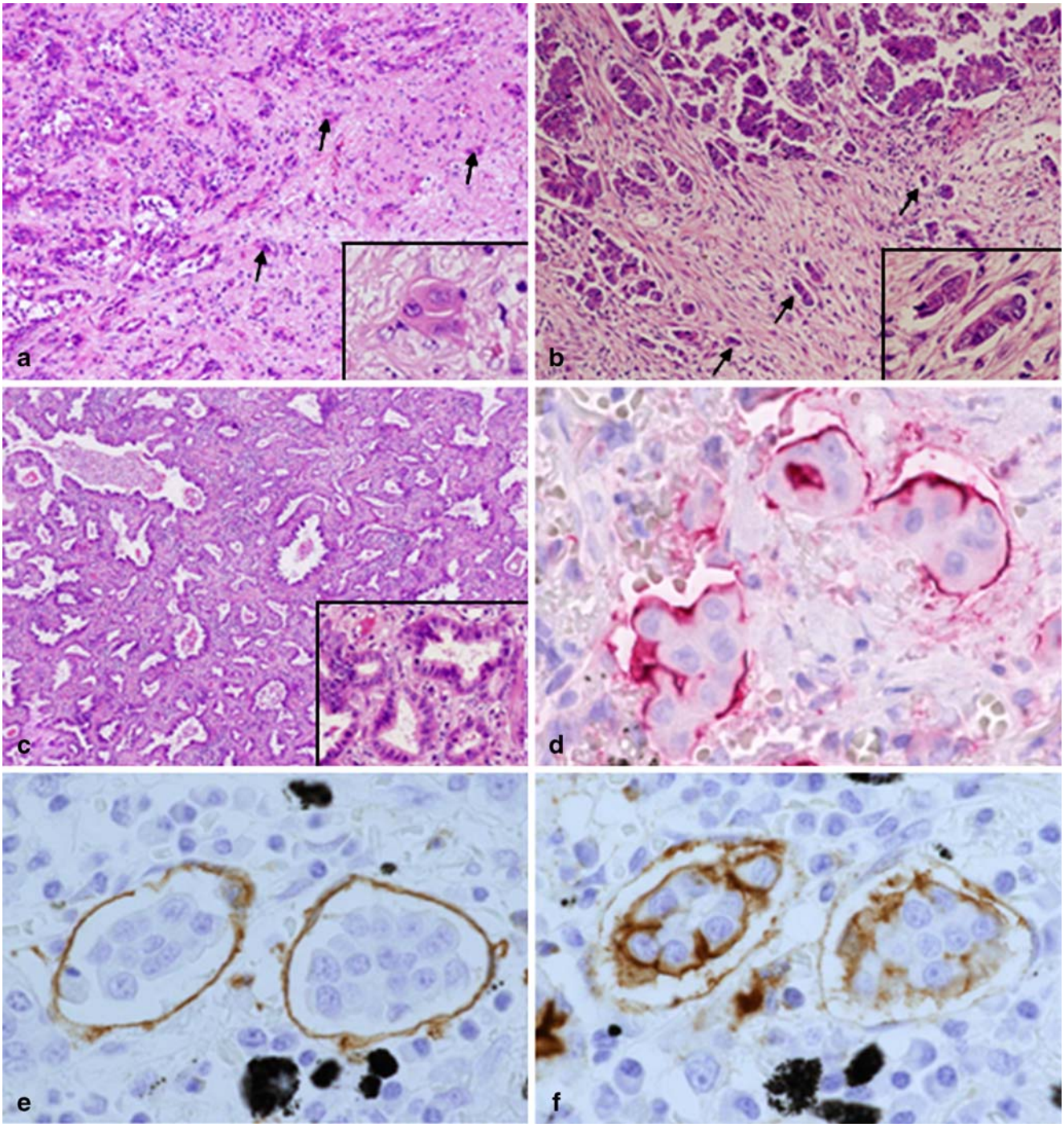

Fig. 2 **a** Lung adenocarcinoma with mixed papillary and acinar patterns of growth. At the invasive margin, the papillary and acinar structures were markedly resolved to induce small clusters of invading carcinoma cells (small cluster invasion). **b** Lung adenocarcinoma with mixed papillary and micropapillary patterns of growth undergoing small cluster invasion. *Insets* in **a** and **b** show isolated small clusters of invading carcinoma cells in the fibrotic focus. **c** Lung adenocarcinoma with mixed papillary and acinar patterns of growth without small cluster invasion. The *inset* shows invasion by compact papillary or acinar structures of carcinoma cells. **d** MUC1 expression on the outer surface of isolated small clusters of invading carcinoma cells. **e**, **f** Serial sections demonstrating carcinoma cell clusters involving lymphatics. Lymphatic endothelium is shown with D2-40 antibody (**e**), and MUC1 is expressed on the outer surface of small clusters of carcinoma cells (**f**). **a**–**c** H&E staining; **d**, **f** MUC-1 immunohistochemistry; **e** D2-40 immunohistochemistry

Table 2 Characteristics of patients with pTl adenocarcinoma

Characteristics	All cases	MPP		SCI	
		(+)	(−)	(+)	(−)
No. of patients	146	88	58	81	65
Age (year)					
Mean	64.8	64.6	65.3	64.5	65.4
Range	28–85	29–85	28–85	29–83	28–85
Gender					
Male	60 (43%)	39 (65%)	21 (35%)	37 (62%)	23 (38%)
Female	86 (57%)	49 (57%)	37 (43%)	44 (51%)	42 (49%)
Operative mode					
Lobectomy	101 (69%)	65 (64%)	36 (36%)	60 (59%)	41 (41%)
Limited surgery	45 (31%)	23 (51%)	22 (49%)	21 (47%)	24 (53%)
Histologic subtypes					
BAC	8 (5%)	0 (0%)	8 (100%)	0 (0%)	8 (100%)
Acinar	2 (1%)	0 (0%)	2 (100%)	2 (100%)	0 (0%)
Papillary	7 (4%)	3 (43%)	4 (57%)	2 (29%)	5 (71%)
Mixed subtypes	129 (90%)	85 (66%)	44 (34%)	77 (60%)	52 (40%)
Pathological stage					
IA	124 (85%)	70 (56%)	54 (44%)	63 (51%)	61 (49%)
IIA	8 (5%)	5 (63%)	3 (37%)	6 (75%)	2 (25%)
IIIA	14 (10%)	13 (93%)	1 (7%)	12 (86%)	2 (14%)

BAC bronchioloalveolar carcinoma, *MPP* micropapillary pattern, *SCI* small cluster invasion

IIIA. Most of p-stage IIIA cases were micropapillary pattern positive (13/14 cases, 93%) and small cluster invasion positive (12/14 cases, 86%).

Histopathological findings

The histopathological types included eight (5%) cases of bronchioloalveolar carcinoma (BAC), two (1%) acinar, seven (4%) papillary, and 129 (90%) mixed subtypes (Table 2). Micropapillary pattern was not observed in cases with BAC. Small cluster invasion was observed in 81/146 (55%) cases. There was no significant association between small cluster invasion and any specific histological subtypes of invasive carcinomas. At the site of small cluster invasion in the fibrotic focus, small clusters of invading carcinoma cells were induced and separated from acinar, papillary, or micropapillary structures of tumors due to focal dedifferentiation (Fig. 2a, b, insets). In about 39% of cases (57/146), carcinoma invaded the fibrotic focus as nonresolved papillary or acinar structures without small clusters of invading cells (Fig. 2c, inset). The invading small cell clusters expressed MUC1 along the outer cell surface (Fig. 2d), similar to the MUC1 expression pattern on micropapillary clusters (Fig. 1b). Small clusters of carcinoma cells that invaded lymphatics also showed MUC1 expression on their outer surface (Fig. 2e,f).

Table 3 summarizes the relationship between micropapillary pattern or small cluster invasion and pathological features. The overall micropapillary-pattern-positive and small-cluster-invasion-positive cases were 60% (88/146 cases) and 55% (81/146 cases), respectively. Micropapillary-pattern-positive and small-cluster-invasion-positive cases showed several statistically significant differences compared with negative cases; tumor size tended to be larger than 1 cm in diameter, and pathological findings related to tumor invasion–metastasis, such as lymph node metastasis, pleural invasion, and lymphatic involvement, were more frequently observed. Vascular involvement was also more frequent than in negative cases, although the difference was not statistically significant between micropapillary-pattern-positive and micropapillary-pattern-negative cases. Moreover, the presence of micropapillary pattern also correlated significantly with the presence of small cluster invasion. When focusing on lymphatic metastasis, the presence of micropapillary pattern, small cluster invasion, or lymphatic involvement each correlated significantly with more frequent lymph node metastasis (Table 4). Furthermore, as the extent of micropapillary pattern increased, all of small cluster invasion, lymphatic involvement, and lymph node metastasis tended to occur more frequently (Table 5). Small-cluster-invasion-, lymphatic-involvement-, and nodal-metastasis-positive cases were only 17% (10/58), 7% (4/58), and 7% (4/58) for micropapillary-pattern-negative (0 and 1+) carcinomas, respectively, whereas 85% (23/27), 52% (14/27), and 48% (13/27) were positive for small cluster invasion, lymphatic

Table 3 Micropapillary pattern (MPP), small cluster invasion (SCI), and pathological characteristics

	MPP		*p* value	SCI		*p* value
	(+), *n*=88	(−), *n*=58		(+), *n*=81	(−), *n*=65	
Tumor size (*n*=146)						
≦1 cm (*n*=18)	6 (33%)	12 (67%)	0.0192	4 (22%)	14 (78%)	0.0042
>l cm (*n*=128)	82 (64%)	46 (36%)		77 (60%)	51 (40%)	
Lymph node metastasis (*n*=146)						
Positive (*n*=22)	18 (82%)	4 (18%)	0.0324	16 (73%)	6 (27%)	0.0073
Negative (*n*=124)	70 (56%)	54 (44%)		65 (52%)	59 (48%)	
Pleural invasion (n=146)						
Positive (*n*=54)	40 (74%)	14 (26%)	0.0138	37 (69%)	17 (31%)	0.0151
Negative (*n*=92)	48 (52%)	44 (48%)		44 (48%)	48 (52%)	
Small cluster invasion (*n*=146)						
Positive (*n*=81)	71 (88%)	10 (12%)	<0.0001	–	–	–
Negative (n=65)	17 (26%)	48 (74%)				
Lymphatic involvement (*n*=146)						
Positive (*n*=39)	35 (90%)	4 (10%)	<0.0001	37 (95%)	2 (5%)	<0.0001
Negative (*n*=107)	53 (50%)	54 (50%)		44 (41%)	63 (59%)	
Vascular involvement (*n*=146)						
Positive (*n*=20)	16 (80%)	4 (20%)	0.0831	19 (95%)	1 (5%)	<0.0001
Negative (*n*=126)	72 (57%)	54 (43%)		62 (41%)	64 (59%)	

involvement, and lymph node metastasis, respectively, for micropapillary pattern graded as 3+. Micropapillary pattern is a significant and independent predictor for a shorter overall survival in p-stage IA cases [8, 9], suggesting its association with metastatic recurrence after surgical removal. For this purpose, we investigated the correlation between small cluster invasion and lymphatic involvement in micropapillary-pattern-positive p-stage IA cases. The presence of small cluster invasion in micropapillary-pattern-positive cases was significantly associated with more frequent lymphatic involvement (p=0.0282; Table 6).

Survival rates

As we reported previously [8, 11], also in this study, the micropapillary-pattern-positive group showed significantly worse survival compared with the micropapillary-pattern-negative group (5-year survival, 68.0% vs. 88.3%, respectively, p=0.0046, data not shown). The overall 5-year survival rates for patients with or without small cluster invasion were 70.0% and 90.8%, respectively, and the difference was also statistically significant (p=0.0017, Fig. 3).

Univariate analysis

Since the correlation of small cluster invasion with worse prognosis was suggested, univariate and multivariate analyses were performed including stratification for stage. For metastasis-related clinicopathological parameters of 124 cases of p-stage IA carcinoma, univariate analysis identified significant associations of micropapillary pattern (positive), lymphatic involvement (positive), small cluster invasion (positive), pleural invasion (positive), and vascular involvement (positive) with poor prognosis (Table 7, micropapillary pattern, p=0.0012; lymphatic involvement, p<0.0001; small cluster invasion, p=0.0017; pleural invasion, p=0.0182; vascular involvement, p<0.0001). No significant parameters were identified in p-stages IIA and IIIA carcinomas.

Table 4 Correlation of micropapillary pattern, small cluster invasion, and lymphatic involvement with lymph node metastasis

	MPP		*p* value	SCI		*p* value	LI		*p* value
	(+) (*n*=88)	(−) (*n*=58)		(+) (*n*=81)	(−) (*n*=65)		(+) (*n*=39)	(−) (*n*=107)	
Lymph node metastasis (*n*=146)									
Positive (*n*=22)	18	4	0.0324	16	6	0.0073	16	6	0.0004
Negative (*n*=l24)	70	54		65	59		23	101	

MPP micropapillary pattern, *SCI* small cluster invasion, *LI* lymphatic involvement

Table 5 Small cluster invasion, lymphatic involvement, and lymph node metastasis with different percentage of micropapillary pattern

MPP	Cases	Small cluster invasion (positive)	Lymphatic involvement (positive)	Lymph node metastasis (positive)
0 (0%)	29	1 (3%)	0 (0%)	1 (3%)
1+ (<10%)	29	9 (31%)	4 (14%)	3 (11%)
2+ (10–50%)	61	48 (79%)	21 (34%)	5 (8%)
3+ (>50%)	27	23 (85%)	14 (52%)	13 (48%)

MPP micropapillary pattern

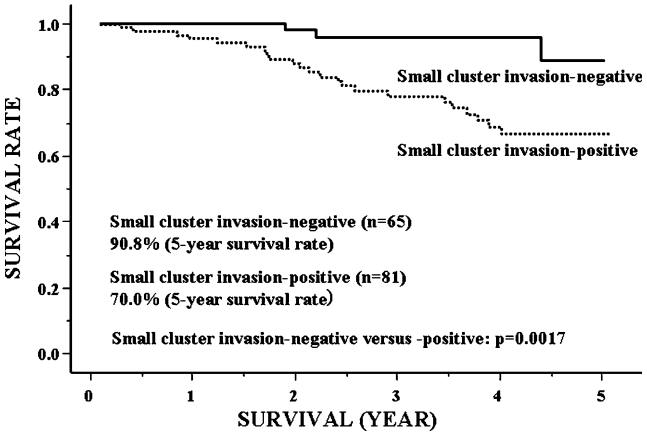

Fig. 3 Survival curves according to the status of small cluster invasion. The 5-year survival rate of patients without small cluster invasion was significantly higher than that of patients with small cluster invasion (log rank test, $p=0.0017$)

Multivariate analysis

All the aforementioned factors identified as significant by univariate analyses were entered into Cox multivariate regression analysis. This analysis identified lymphatic involvement (positive) as a significant and independent predictor of a shorter overall survival of patients with p-stage IA adenocarcinoma of the lung (Table 8, lymphatic involvement, $p<0.0001$).

Discussion

The presence of micropapillary pattern in lung adenocarcinomas is associated with higher incidence of lymph node metastasis and therefore with poorer prognosis [7–14, 29]. However, little is known about the mechanisms that underlie MPP-associated nodal metastasis. It is important to clarify how small papillary clusters of carcinoma cells present in tumoral alveolar spaces lead to increased lymph node metastasis. Our previous study demonstrated the significant association of micropapillary pattern with small cluster invasion in tumoral scar tissue [8]. Thus, we hypothesized that small cluster invasion may be an important link between micropapillary pattern and nodal metastasis. In the present study, both micropapillary pattern and small cluster invasion correlated with more frequent occurrence of lymphatic involvement and lymph node metastasis. Higher extents of micropapillary pattern are associated with a more frequent small cluster invasion, lymphatic involvement, and lymph node metastasis. Furthermore, in patients with micropapillary-pattern-positive pT1 lung adenocarcinomas, the presence of small cluster invasion significantly correlated with higher incidence of lymphatic involvement. Lymphatic involvement was the most statistically powerful and independent prognostic factor in patients with pT1 lung adenocarcinoma. These statistical analyses indicate the possible sequence from micropapillary pattern to lymph node metastasis via small cluster invasion and lymphatic involvement in tumoral scar.

It is important to recognize the micropapillary growth pattern especially in early-stage lung adenocarcinomas [8, 9, 11, 13, 14, 29]. In stage IA cases, the presence of micropapillary pattern is associated with early and more frequent metastatic disease. This information may be useful for clinicians to tailor the follow-up of patients to accommodate the likelihood of more aggressive disease that may

Table 6 Correlation of small cluster invasion and lymphatic involvement in p-stage IA micropapillary-pattern-positive carcinomas

	MPP positive ($n=70$)		p value
	SCI (+)	SCI (−)	
No. of patients	54 (77%)	16 (23%)	
Lymphatic involvement			
Positive ($n=20$)	19 (95%)	1 (5%)	
Negative ($n=50$)	35 (70%)	15 (30%)	0.0282

MPP micropapillary pattern, *SCI* small cluster invasion

Table 7 Correlation of MPP, lymphatic involvement, vascular involvement small cluster invasion, and pleural invasion with overall survival by univariate analysis in p-stage IA cases

Variable	Correlation with survival (p^a)
MPP (positive)	0.0012
Lymphatic involvement (positive)	<0.0001
Small cluster invasion (positive)	0.0017
Pleural invasion (positive)	0.0182
Vascular involvement (positive)	<0.0001

[a] Log-rank test

Table 8 Correlation of MPP and lymphatic involvement with overall survival by multivariate analysis in p-stage IA cases

Variable	Risk ratio	95% CI	*P* value
Lymphatic involvement (positive)	2.873	0.136–0.888	<0.0001
MPP(positive)	2.352	0.104–1.730	0.0957
Small cluster invasion (positive)	1.854	0.949–2.130	0.1741
Pleural invasion (positive)	1.397	0.241–2.962	0.3529
Vascular involvement (positive)	2.149	0.068–1.617	0.1769

CI confidence interval

require intensive management. However, histologic subtypes of micropapillary pattern with different prognoses were recently proposed [30]. The micropapillary pattern was subclassified into two subtypes based on breast-type and alveolar-type histology, and a breast-type micropapillary pattern was associated with poorer prognosis [30]. By their definition, the breast type resembles the morphology of invasive micropapillary carcinoma of the breast, accompanied by relatively thick fibrous stroma. This may correspond to cases with extensive small cluster invasion in our study. It may be important to investigate the subtypes of micropapillary pattern in a large-scale study to clarify their clinicopathological significance.

Alteration of expression of cell surface molecules has been shown to be associated with micropapillary pattern. For example, it is reported that MUC1 expression was predominantly demonstrated in the stroma-facing surface of the micropapillary cell clusters in micropapillary-pattern-positive breast, urinary bladder, and colon carcinomas and that this expression pattern indicates inversion of cell polarization since MUC1 is a glycoprotein normally located in the apical cell surface of normal glandular epithelium [31–33]. In this way, this expression pattern of MUC1 is characteristic for and common in micropapillary-pattern-positive carcinoma cells in other organs and recently also demonstrated in lungs [8, 12]. Thus, we investigated MUC1 expression as a marker for micropapillary pattern. In the present study, small groups of invading carcinoma cells recognized as small cluster invasion expressed MUC1 on their outer surface, similar to the expression pattern observed in intra-alveolar micropapillary tufts of carcinoma cells. The same expression pattern was also seen in carcinoma cell clusters within the lymphatics. Thus, we speculate that adenocarcinoma cells that show micropapillary pattern in alveolar spaces tend to behave as small cluster invasion when involved in invasion-related scar-forming processes, leading to lymphatic involvement and then lymph node metastasis. Small cluster invasion is also an important prognostic indicator: its presence was significantly associated with worse 5-year survival compared with its absence. Moreover, easy detection of small cluster invasion in H&E sections makes it useful, similar to micropapillary pattern.

Small cluster invasion in lung adenocarcinomas is very similar to tumor budding in colorectal adenocarcinomas. Tumor budding is defined as small clusters of carcinoma cells lying ahead of the invasive front of the lesion in colorectal adenocarcinomas [28]. The feature has been pointed out as a mode of carcinoma invasion by pathologists for decades [34, 35]. Aberrant intranuclear expression of β-catenin was shown in the budding carcinoma cells [36]. Nuclear β-catenin complexes with the T cell factor family of DNA-binding proteins and activates transcription of urokinase-like plasminogen activating receptor, matrilysin, CD44, and laminin-5 γ2, which are known to be critical in the process of tissue remodeling and cell migration [37–40]. Similar mechanisms may operate to induce small cluster invasion by micropapillary-pattern-positive lung adenocarcinoma cells. Additionally, in a micropapillary-pattern-positive lung adenocarcinoma case, IQGAP1 was detected in the micropapillary, but not in the nonmicropapillary, area [41]. IQGAP1 regulates cadherin-mediated cell–cell adhesion by interacting with β-catenin, dissociating α-catenin from the cadherin–catenin complex [42]. Expression of nonsuppressed IQGAP1 results in diminished cell–cell adhesion and is essential for cell migration and invasion [42]. IQGAP1 may be involved in the release of micropapillary clusters of cells. Moreover, the presence of MUC1 in the stroma-facing surface of micropapillary cell clusters may also lead to easy detachment of cells from the stroma since MUC1 inhibits the interaction between cell and stroma [31–33]. Tsutsumida et al. [12] showed high and low expressions of MUC1 and MUC4 on the surface of the micropapillary structure of lung adenocarcinoma, respectively, and suggested that this high expression of MUC1 in the micropapillary structure might correlate with lymph node metastasis since the authors showed in a study with pancreatic cancer cells that MUC1 downregulation by RNAi led to decreased proliferation and lymphatic metastasis [12, 43].

In conclusion, the present study indicated a possible link between micropapillary pattern and lymph node metastasis via small cluster invasion. Characterization and understanding of the mechanisms that underlie the small cluster invasion could be of help in the development of novel therapeutic interventions.

Conflict of interest statement We declare that we have no conflict of interest.

References

1. Kakizoe T, Sugiura S, Segami K (1999) Cancer statistics in Japan 1999. Foundation of Promotion of Cancer Research, Tokyo
2. Travis WD, Travis LB, Devesa SS (1995) Lung cancer. Cancer 75:191–202
3. Ginsberg RJ, Port JL (2000) Surgical therapy of stage I and nonT3N0 stage II non small cell lung cancer. In: Harvay IP, James BM, Johnson DH (eds) Lung cancer: principles and practice, 2nd edn. Lippincott Williams & Wilkins, Philadelphia, pp 682–693
4. Kurokawa T, Matsuno Y, Noguchi M et al (1994) Surgically curable "early" adenocarcinoma in the periphery of the lung. Am J Surg Pathol 18:431–438
5. Noguchi M, Morikawa A, Kawasaki M et al (1995) Small adenocarcinoma of the lung. Histologic characteristics and prognosis. Cancer 75:2844–2852
6. Higashiyama M, Kodama K, Yokouchi H et al (1999) Prognostic value of bronchioloalveolar carcinoma component of small lung adenocarcinoma. Ann Thorac Surg 68:2069–2073
7. Amin MB, Tamboli P, Merchant SH et al (2002) Micropapillary component in lung adenocarcinoma: a distinctive histologic feature with possible prognostic significance. Am J Surg Pathol 26:358–364
8. Kawakami T, Nabeshima K, Makimoto Y et al (2007) Micropapillary pattern and grade of stromal invasion in pT1 adenocarcinoma of the lung: usefulness as prognostic factors. Mod Pathol 20:514–521
9. Miyoshi T, Satoh Y, Okumura S et al (2003) Early-stage lung adenocarcinomas with a micropapillary pattern, a distinct pathologic marker for a significantly poor prognosis. Am J Surg Pathol 27:101–109
10. Roh MS, Lee JI, Choi PJ et al (2004) Relationship between micropapillary component and micrometastasis in the regional lymph nodes of patients with stage I lung adenocarcinoma. Histopathology 45:580–586
11. Makimoto Y, Nabeshima K, Iwasaki H et al (2005) Micropapillary pattern: a distinct pathological marker to subclassify tumours with a significantly poor prognosis within small peripheral lung adenocarcinoma (</=20 mm) with mixed bronchioloalveolar and invasive subtypes (Noguchi's type C tumours). Histopathology 46:677–684
12. Tsutsumida H, Nomoto M, Goto M et al (2007) A micropapillary pattern is predictive of a poor prognosis in lung adenocarcinoma, and reduced surfactant apoprotein A expression in the micropapillary pattern is an excellent indicator of a poor prognosis. Mod Pathol 20:638–647
13. Kamiya K, Hayashi Y, Douguchi J et al (2008) Histopathological features and prognostic significance of the micropapillary pattern in lung adenocarcinoma. Mod Pathol 21:992–1001
14. Sanchez-Mora N, Presmanes MC, Monroy V et al (2008) Micropapillary lung adenocarcinoma: a distinctive histologic subtype with prognostic significance. Case series. Hum Pathol 39:324–330
15. Nassar H, Wallis T, Andea A et al (2001) Clinicopathologic analysis of invasive micropapillary differentiation in breast carcinoma. Mod Pathol 14:836–841
16. Johansson SL, Borghede G, Holmang S (1999) Micropapillary bladder carcinoma: a clinicopathological study of 20 cases. J Urol 161:1798–1802
17. Amin MB, Ro JY, el-Sharkawy T et al (1994) Micropapillary variant of transitional cell carcinoma of the urinary bladder. Histologic pattern resembling ovarian papillary serous carcinoma. Am J Surg Pathol 18:1224–1232
18. Oh YL, Kim KR (2000) Micropapillary variant of transitional cell carcinoma of the ureter. Pathol Int 50:52–56
19. Vang R, Abrams J (2000) A micropapillary variant of transitional cell carcinoma arising in the ureter. Arch Pathol Lab Med 124:1347–1348
20. Haupt B, Ro JY, Schwartz MR et al (2007) Colorectal adenocarcinoma with micropapillary pattern and its association with lymph node metastasis. Mod Pathol 20:729–733
21. Kim MJ, Hong SM, Jang SJ et al (2006) Invasive colorectal micropapillary carcinoma: an aggressive variant of adenocarcinoma. Hum Pathol 37:809–815
22. Michal M, Skalova A, Mukensnabl P (2000) Micropapillary carcinoma of the parotid gland arising in mucinous cystadenoma. Virchows Arch 437:465–468
23. Nagao T, Gaffey TA, Visscher DW et al (2004) Invasive micropapillary salivary duct carcinoma: a distinct histologic variant with biologic significance. Am J Surg Pathol 28:319–326
24. Sakurai H, Maeshima A, Watanabe S et al (2004) Grade of stromal invasion in small adenocarcinoma of the lung: histopathological minimal invasion and prognosis. Am J Surg Pathol 28:198–206
25. Sobin L, Wittekind L (1997) TNM classification of malignant tumors. Wiley, New York
26. Travis WD, Brambilla E, Muller-Hermelink HK et al (2004) World health organization classification of tumors. Pathology and genetics of tumors of the lung, pleura, thymus and heart. International Agency for Research on Cancer Press, Lyon
27. Silver SA, Askin FB (1997) True papillary carcinoma of the lung: a distinct clinicopathologic entity. Am J Surg Pathol 21:43–51
28. Hase K, Shatney C, Johnson D et al (1993) Prognostic value of tumor "budding" in patients with colorectal cancer. Dis Colon Rectum 36:627–635
29. Hoshi R, Tsuzuku M, Horai T et al (2004) Micropapillary clusters in early-stage lung adenocarcinomas: a distinct cytologic sign of significantly poor prognosis. Cancer 102:81–86
30. Kuroda N, Hamaguchi N, Takeuchi E et al (2006) Lung adenocarcinoma with a micropapillary pattern: a clinicopathological study of 25 cases. Apmis 114:381–385
31. Pettinato G, Manivel CJ, Panico L et al (2004) Invasive micropapillary carcinoma of the breast: clinicopathologic study of 62 cases of a poorly recognized variant with highly aggressive behavior. Am J Clin Pathol 121:857–866
32. Nassar H, Pansare V, Zhang H et al (2004) Pathogenesis of invasive micropapillary carcinoma: role of MUC1 glycoprotein. Mod Pathol 17:1045–1050
33. Sakamoto K, Watanabe M, De La Cruz C et al (2005) Primary invasive micropapillary carcinoma of the colon. Histopathology 47:479–484
34. Imai T (1960) Growth patterns in human carcinoma. Their classification and relation to prognosis. Obstet Gynecol 16:296–308
35. Nabeshima K, Inoue T, Shimao Y et al (1999) Cohort migration of carcinoma cells: differentiated colorectal carcinoma cells move as coherent cell clusters or sheets. Histol Histopathol 14:1183–1197
36. Kirchner T, Brabletz T (2000) Patterning and nuclear beta-catenin expression in the colonic adenoma-carcinoma sequence. Analogies with embryonic gastrulation. Am J Pathol 157:1113–1121
37. Mann B, Gelos M, Siedow A et al (1999) Target genes of beta-catenin-T cell-factor/lymphoid-enhancer-factor signaling in human colorectal carcinomas. Proc Natl Acad Sci USA 96:1603–1608
38. Crawford HC, Fingleton BM, Rudolph-Owen LA et al (1999) The metalloproteinase matrilysin is a target of beta-catenin transactivation in intestinal tumors. Oncogene 18:2883–2891
39. Wielenga VJ, Smits R, Korinek V et al (1999) Expression of CD44 in Apc and Tcf mutant mice implies regulation by the WNT pathway. Am J Pathol 154:515–523

40. Hlubek F, Jung A, Kotzor N et al (2001) Expression of the invasion factor laminin gamma2 in colorectal carcinomas is regulated by beta-catenin. Cancer Res 61:8089–8093
41. Miyoshi T, Shirakusa T, Ishikawa Y et al (2005) Possible mechanism of metastasis in lung adenocarcinomas with a micropapillary pattern. Pathol Int 55:419–424
42. Fukata M, Nakagawa M, Kuroda S et al (1999) Cell adhesion and Rho small GTPases. J Cell Sci 112(Pt 24):4491–4500
43. Tsutsumida H, Swanson BJ, Singh PK et al (2006) RNA interference suppression of MUC1 reduces the growth rate and metastatic phenotype of human pancreatic cancer cells. Clin Cancer Res 12:2976–2987

Virchows Arch (2009) 454:71–79
DOI 10.1007/s00428-008-0694-6

ORIGINAL ARTICLE

Lysyl oxidase-like 4 is alternatively spliced in an anatomic site-specific manner in tumors involving the serosal cavities

Shulamit Sebban · Ben Davidson · Reuven Reich

Received: 6 June 2008 / Revised: 4 October 2008 / Accepted: 20 October 2008 / Published online: 18 November 2008

Abstract Lysyl oxidase-like enzymes (LOXL) are expressed in various cancers. We analyzed the expression of LOXL2, LOXL3, and LOXL4 in cancers involving the serosal cavities—breast carcinoma, ovarian carcinoma, and malignant mesothelioma using reverse-transcriptase polymerase chain reaction. We discovered two new alternative splice variants of LOXL4. The spliced segments were exon 9 (splice variant 1) or both exons 8 and 9 (splice variant 2). In ovarian carcinoma, splice variant 1 was significantly elevated in effusions compared to solid lesions ($p<0.001$). Splice variant 2 appeared only in effusions. In breast carcinoma, LOXL4 was expressed only in the effusion samples. In malignant mesothelioma, LOXL4 and its splice variants were expressed at all sites. Breast carcinoma effusions showed significantly higher LOXL2 ($p=0.003$) and lower LOXL3 ($p<0.001$) expression compared to primary carcinomas. Our data show differences in LOXL messenger RNA expression as a function of anatomic site and tumor type in cancers affecting the serosal cavities.

Keywords Lysyl oxidase-like enzymes · Ovarian carcinoma · Breast carcinoma · Malignant mesothelioma · Alternative splicing · Metastasis · Tumor progression

S. Sebban
Department of Pharmacology and Experimental Therapeutics, School of Pharmacy, Faculty of Medicine, The Hebrew University of Jerusalem, Jerusalem 91120, Israel

B. Davidson
Division of Pathology, Norwegian Radium Hospital, Rikshospitalet Medical Center, Oslo 0310, Norway

B. Davidson
Faculty Division Radiumhospitalet and The Medical Faculty, University of Oslo, Oslo 0310, Norway

R. Reich (✉)
Department of Pharmacology and Experimental Therapeutics, School of Pharmacy, Faculty of Medicine and the David R. Bloom Center for Pharmacy, The Hebrew University of Jerusalem, Jerusalem 91120, Israel
e-mail: reich@cc.huji.ac.il

Introduction

Lysyl oxidase (LOX) is an amine oxidase that is usually synthesized and secreted by fibrogenic cells. It catalyzes the final enzymatic step required for lysine-derived crosslinks, essential for the formation of collagen fibrils and insoluble elastic fibers in the extracellular matrix [1]. Publications of the last decade report LOX to have additional important functions in oncogenic and chemotactic behavior of cells [2–6]. Four LOX-like (LOXL) genes have been identified so far in mammalian genomes encoding four different LOX-like proteins: LOXL1, LOXL2, LOXL3, and LOXL4 [7]. All members of the LOX family show a highly conserved C terminus region that contains the catalytic domain. The N terminus of the LOX isoforms is less conserved among the different members and is thought to determine the individual role and tissue distribution of each isoenzyme [8]. It has been shown that LOXL1 is required for proper elastic fiber homeostasis [9]. The individual function of the remaining members of the family remains unclear, although recent evidence suggests involvement of LOX, LOXL2, and LOXL4 in the progression of breast,

head and neck, bladder, and colon carcinoma [10–12]. In addition, it was recently shown that LOXL2 and LOXL3 collaborate in vivo with the Snail transcription factor to repress E-cadherin expression, and evidence for a role of LOXL2 in tumor growth and progression was demonstrated [13], as well as involvement of LOXL1 and LOXL4 in the Ras/extracellular signal-regulated kinase (ERK) signaling pathway in human bladder cancer [14].

Ovarian carcinoma (OC) is the most lethal gynecologic cancer and currently ranks as the fifth in causing cancer-related deaths among women [15]. The major difficulty in achieving cure of OC is the fact that the majority of patients are diagnosed with advanced-stage (FIGO III–IV) disease, thereby impeding efforts directed at surgical removal of all tumor burden [16]. Another significant problem is the effort invested in studying the molecular characteristics of primary tumors, lesions that are amenable to surgical removal in the majority of cases, rather than metastatic cells in the peritoneal and pleural cavities, the most common site of dissemination and recurrence in OC [17].

Two additional cancers that enter the differential diagnosis of malignancy within the serosal cavities are malignant mesothelioma (MM) and breast carcinoma. MM is a tumor derived from mesothelial cells, the native cells of the body cavities. The pleural cavity is the most common site, with a present ratio of 9:1 with peritoneal tumors [18]. MM classically presents with plaques on the serosal surfaces with a concomitant malignant effusion, a clinical picture that is indistinguishable from OC when disease is localized to the peritoneum. MM is an aggressive and rapidly fatal disease, with a median survival of 8 months if untreated, although selected patients achieve longer survival in recent years when surgery is combined with adjuvant chemotherapy, especially in peritoneal disease [19–21].

Metastatic spread of breast carcinoma to the pleural cavity is responsible for 25% of malignant pleural effusions [22–24]. The pericardial and peritoneal cavities may also be involved, though less frequently. Breast cancer metastasis to the pleural space can occur at any point of time in the clinical course and may be the sole manifestation of metastasis [25]. It is associated with extremely poor prognosis, with a median survival of 5–11 months [25, 26].

The expression of LOX and LOX-like enzymes has not been investigated in OC or in MM to date. In breast carcinoma, no data are available regarding LOXL expression in effusions. The objective of the present study was to determine whether LOXL family members are differently expressed in cancers involving the serosal cavities and in benign reactive mesothelium (RM). In addition, we wished to analyze whether LOXL members are expressed in an anatomic site-dependent manner in OC and breast carcinoma. Finally, we wished to establish whether LOXL expression is related to clinicopathologic parameters in OC.

Materials and methods

Tumors and patients

The material analyzed in the present study consisted of 211 specimens (137 effusions, 78 solid tumors; Table 1). All specimens with the exception of 12 MM effusions were submitted for routine diagnostic purposes to the Division of Pathology, Norwegian Radium Hospital, in the period 1985–2005. Twelve MM effusions were submitted to the Department of Pathology in Aalborg Hospital, Aalborg, Denmark, during 1999, and were studied with kind permission (see Acknowledgment). Informed consent was obtained according to national and institutional guidelines.

The 70 OC effusions were from 56 patients diagnosed with epithelial (predominantly serous) OC (61 effusions), two patients with serous carcinoma of the fallopian tube (two effusions), and six patients who were diagnosed with primary peritoneal carcinoma (seven effusions), total=64 patients. Due to their closely linked histogenesis and phenotype, all of these tumors are referred to as OC effusions in the following sections. Table 2 presents the clinicopathologic data for the effusion patient cohort. The 55 solid OC had comparable histological type to that of the OC effusions (43 serous, three clear cell, three endometrioid, three undifferentiated, and three adenocarcinomas of mixed type). The majority of solid tumors were not patient-matched with respect to OC effusions.

The 31 breast carcinoma effusions and 23 primary tumors were from 54 patients, i.e., not patient-matched. Slides from the primary tumor were available for review for 27 of the 31 patients with effusions. These consisted of 25 infiltrating duct and two infiltrating lobular carcinomas. Tumor grade was as follows: one grade 1, 19 grade 2, and

Table 1 Specimens analyzed for LOXL mRNA expression

Tumor	Specimen type	Anatomic site	Number of specimens
Ovarian carcinoma	Effusion	Peritoneum	50
		Pleura	20
	Primary	Ovary	40
	Metastasis	Various[a]	15
Breast carcinoma	Effusions	Peritoneum	1
		Pleura	29
		Pericardium	1
	Primary	Breast	23
Malignant mesothelioma	Effusion	Peritoneum	5
		Pleura	20
Reactive mesothelium	Effusion	Peritoneum	2
		Pleura	5

[a] Metastases resected from the omentum (n=10), fallopian tube (n=2), vagina (n=2) and peritoneum (n=1)

Table 2 Clinicopathologic data of the ovarian carcinoma effusion cohort (64 patients)

Parameter		Number of specimens
Age	Range, 35–79	Mean=61
FIGO stage	II	1
	III	35
	IV	28
Grade	I	4
	II	20
	III	27[a]
	NA[b]	13
Residual disease	≤2 cm	20
	>2 cm	34
	NA[c]	10
Histology	Serous	52
	Clear cell	4
	Mixed epithelial	4
	Undifferentiated	3
	NA[d]	1
Chemotherapy[e]	No	30
	Yes	34

[a] Including four patients with clear cell carcinomas
[b] *NA* Non-available, including specimens from inoperable patients (7) and patients operated in hospitals in which tumor grade was not scored and primary tumor could not be accessed for assessment of grade (6)
[c] Including specimens from inoperable patients (7) and patients operated in hospitals in which tumor grade was not scored (3)
[d] One patient who was inoperable and underwent limited biopsy in order to establish a diagnosis of malignancy
[e] For the first specimen for patients with >1 effusion

seven grade 3 specimens. Primary breast carcinomas consisted of 19 infiltrating duct carcinomas, two infiltrating lobular carcinomas, and two infiltrating carcinomas of mixed lobular and duct type. Tumor grade was 1 in two cases, two in 14 cases, and three in seven cases.

MM effusions were from patients diagnosed with tumor of the epithelioid or biphasic type in biopsy specimens.

RM effusions were from patients who were suspected of having cancer or who were previously diagnosed with cancers of various types.

Effusions were all received in the fresh non-fixed state immediately after tapping. Specimens were centrifuged and pellets were fresh-frozen at −70°C in RPMI 1640 medium supplemented with 50% fetal calf serum and 20% dimethyl sulfoxide at a ratio of 1:1, immediately after tapping. Smears and H&E-stained cell block sections were reviewed by a surgical pathologist experienced in cytopathology (BD). Diagnoses were established using morphology and immunohistochemistry, as previously detailed [27]. The primary tumors were reviewed for all three cancer categories.

Frozen OC and breast carcinoma biopsies were evaluated for the presence of a >50% tumor component and absence of necrosis by frozen sections. H&E-stained sections from these tumors were reviewed to establish tumor type and histological grade.

RT-PCR analysis

LOXL2, LOXL3 and LOXL4 messenger RNA (mRNA) expression was analyzed in all 211 specimens. Total RNA was extracted using a commercial kit (Tri Reagent; Sigma-Aldrich, St. Louis, MO), and 0.5 μg of total RNA were reverse-transcribed using M-MLV Reverse Transcriptase (Promega, Madison, WI) with incubation for 2 h at 37°C, followed by 5 min at 95°C, and diluted to 1:5 with RNase-free water. Reverse-transcriptase polymerase chain reaction (RT-PCR) analysis was performed on complementary DNA (cDNA) samples with a DNA thermal cycler (Eppendorf Mastercycler gradient; Eppendorf, Hamburg, Germany) using primer sets for LOXL2, LOXL3, LOXL4, and 28S ribosomal RNA. Primer sequences were as follows: LOXL2, sense, 5′-CTGTGACAGTCGTGCCAGAT-3′; antisense, 5′-GAGTTGCCTGCTCAGAAACC-3′ (product size, 270 bp); LOXL3, sense, 5′-AGCAACACTCCTTTG GTCTGCATGGG-3′; antisense, 5′-CCTCCCCCTGAGGC TTCGACTGTTGTTG -3′ (product size, 206 bp); LOXL4, sense, 5′-TGTGTGGAGAAGCGCAATAG -3′; antisense, 5′-TCCCTAACATGGGCTTTCAG-3′ (product sizes, 247, 396, and 558 bp); 28S, sense 5′-GTTCACCCACTAATAG GG AACGTGA-3′, antisense 5′-GGATTCTGACTTAGA GGCG TTCAGT-3′ (product size, 212 bp).

The cycle parameters were as follows: *LOXL2*, denaturation at 95°C for 15 s, annealing at 63°C for 30 s, and extension at 72°C for 20 s for 26 cycles; *LOXL3*, denaturation at 95°C for 15 s, annealing at 67°C for 30 s, and extension at 72°C for 20 s for 34 cycles; *LOXL4*, denaturation at 95°C for 15 s, annealing at 60°C for 30 s, and extension at 72°C for 20 s for 34 cycles; and 28S, denaturation at 94°C for 15 s, annealing at 63°C for 20 s, and extension at 72°C for 10 s for 16 cycles. Products were separated on 1.5% agarose gels, isolated using the Invisorb Spin DNA extraction kit (Invitek GmbH, Berlin, Germany), and sequenced.

The HT-1080 fibrosarcoma cell line served as control in all LOXL2, LOXL3, and 28S reactions, and the MRC-5 human lung fibroblast cell line served as control in all LOXL4 reactions. Gels were photographed by the Kodak digital camera DC 290 system (Eastman Kodak, Rochester, NY). Densitometer analysis of films was performed using a computerized image analysis program (NIH Image 1.62, 1999 version). LOXL2, LOXL3, and LOXL4 mRNA levels were established by calculating the target molecule/28S ratio. All measurements in clinical specimens were carried out at the exponential phase of the reaction, as verified before sample analysis. This was verified for each gene separately. Results are shown as the average of two independent measurements of the RT-PCR reaction for each gene.

All PCR products were extracted from gel by MEGA-spin Agarose Gel DNA Extraction Kit (Talron Biotech, Israel) and sequence verified (Hy-Laboratories, Israel).

Immunoprecipitation

Twenty-five OC specimens were thawed and washed twice in phosphate-buffered saline (PBS). Samples were subsequently lysed in 1% NP-40, 20 mM Tris–HCl pH 7.5, 137 mM NaCl, 0.5 mM ethylenediaminetetraacetic acid (EDTA), 10% glycerol, protease inhibitor cocktail (Sigma-Aldrich), and 0.1% sodium dodecyl sulfate (SDS). After centrifugation, the supernatant was collected, and protein content was evaluated by the Bradford assay. Five hundred micrograms from each sample were taken for immunoprecipitation. Samples were diluted in lysis buffer (50 mM Tris, pH 8, 200 mM NaCl, 20 mM MgCl, 2% NP-40). Non-specific binding proteins were removed from the cell lysates by the addition of 50 μl of CL-4B pre-washed twice with washing buffer (0.5% NP-40 in 50 mM Tris, pH 7.4, 150 mM NaCl, and 5 mM EDTA). Samples were incubated overnight with 1 μl of LOXL4 polyclonal antibody (Abnova, Taipei, Taiwan), following the addition of 30 μl of Protein G PLUS-agarose (Santa Cruz Biotechnology, Santa Cruz, CA), previously washed with washing buffer, for 1 h. The pellet was washed three times with wash buffer plus 0.1% SDS and then re-suspended in Laemli sample buffer (Bio-Rad, Hercules, CA) containing 5% β-mercaptoethanol. The released materials were subjected to 8% SDS polyacrylamide gel electrophoresis and transferred to polyvinylidene difluoride membranes (Millipore, Billerica, MA). Nonspecific binding sites were blocked by incubating the membrane in PBS containing 5% skim milk. Blots were incubated with anti-LOXL4 polyclonal antibody (Abnova). Antibody was detected using anti-mouse secondary antibody (Jackson Immunoresearch, West Grove, PA) and enhanced chemiluminescence Western blotting detection reagents (Thermo Fisher Scientific, Waltham, MA).

Statistical analysis

Statistical analysis was performed applying the SPSS-PC package (Version 13, Chicago, IL). Probability of <0.05 was considered statistically significant. Comparative analyses of LOXL expression with respect to tumor type and anatomic site were performed both for quantitative measurement results and for absolute expression. Quantitative comparison of LOXL levels at different anatomic sites in OC and breast carcinoma was undertaken using the Mann–Whitney *U* test. The same test was applied to the analysis of association between LOXL expression in OC effusions and clinicopathologic parameters, including effusion site (peritoneum vs. pleura), patient age (≤60 vs. >60 years), histological grade (1–2 vs. 3), FIGO stage (III vs. IV), the volume of residual disease (≤1 vs. >1 cm), and chemotherapy status (pre- vs. post-chemotherapy specimens, previous treatment with platinum agents or paclitaxel). The Kruskal–Wallis *H* test was used for the comparative quantitative analysis of LOXL expression in effusions of different tumor types. Analyses of the association between absolute LOXL expression (yes vs. no) and anatomic site were performed using the two-sided chi-square test.

Results

LOXL enzymes are differentially expressed at various anatomic sites in OC and breast carcinoma

Previous studies have shown a role for LOXL2 in breast cancer invasion [11] and the involvement of LOXL2 and LOXL3 in induction of EMT in epithelial cells, further supporting their implication in tumor progression [12]. Our objective was to investigate whether LOXL2, LOXL3, and LOXL4 are expressed in OC, breast carcinoma, and MM and to analyze potential anatomic site-related differences in their expression level.

LOXL2, LOXL3, and full-length LOXL4 mRNA were detected in the majority of OC specimens at all anatomic sites (Table 3, Fig. 1a,b). Comparative analyses of expression levels obtained in quantitative analysis of band size and intensity for LOXL2, LOXL3, and LOXL4 did not show significant anatomic site-related differences in their expression ($p>0.05$, Kruskal–Wallis *H* Test). However, analysis of absolute expression (positive vs. negative cases) showed significantly more frequent LOXL3 mRNA expression in primary tumors and solid metastases compared to effusions ($p=0.001$, chi-square test; Fig. 1c).

As in OC, LOXL2 and LOXL3 were frequently expressed in breast carcinoma specimens at both the primary site and effusion. However, full-length LOXL4 mRNA was expressed only in effusions (Fig. 1d,f, Table 3). Comparative quantitative analysis showed significantly higher LOXL2 ($p=0.003$) and lower LOXL3 ($p<0.001$) expression in effusions compared to primary carcinomas.

LOXL4 mRNA undergoes alternative splicing

When performing RT-PCR for LOXL4 mRNA expression, three different products were generated, in the lengths of 558, 396, and 247 bp. Sequencing of these products revealed the two shorter products to be the products of alternative splicing, while the longest one represented the full-length LOXL4 mRNA. Analysis of the LOXL4 mRNA sequence for exon distribution revealed the spliced seg-

Table 3 Anatomic site-related LOXL mRNA expression

Tumor	Gene	Anatomic site			*p* value
		Effusion	Primary	Metastasis	
Ovarian carcinoma	LOXL2	65/70 (93%)	40/40 (100%)	15/15 (100%)	>0.05
	LOXL3	55/70 (79%)	40/40 (100%)	15/15 (100%)	0.001[a,b]
	LOXL4 FL	47/70 (67%)	29/40 (72%)	12/15 (80%)	>0.05
	LOXL4 Splv-1	41/70 (59%)	15/40 (37%)	7/15 (47%)	0.005[b,c]
	LOXL4 Svpl-2	26/70 (37%)	0/40 (0%)	0/15 (0%)	<0.001[b,c]
Breast carcinoma	LOXL2	30/31 (97%)	17/23 (74%)	NA	0.003[c,d]
	LOXL3	30/31 (97%)	23/23 (100%)	NA	<0.001[a,d]
	LOXL4 FL	22/31 (71%)	0/23 (0%)	NA	<0.001[b,c,d]
	LOXL4 Splv-1	12/31 (39%)	0/23 (0%)	NA	<0.001[b,c,d]
	LOXL4 Svpl-2	6/31 (19%)	0/23 (0%)	NA	<0.001[b,c,d]

FL full-length, *NA* not analyzed
[a] Solids>Effusions
[b] for absolute expression (yes vs. no)
[c] Effusions>solids
[d] For quantitative expression

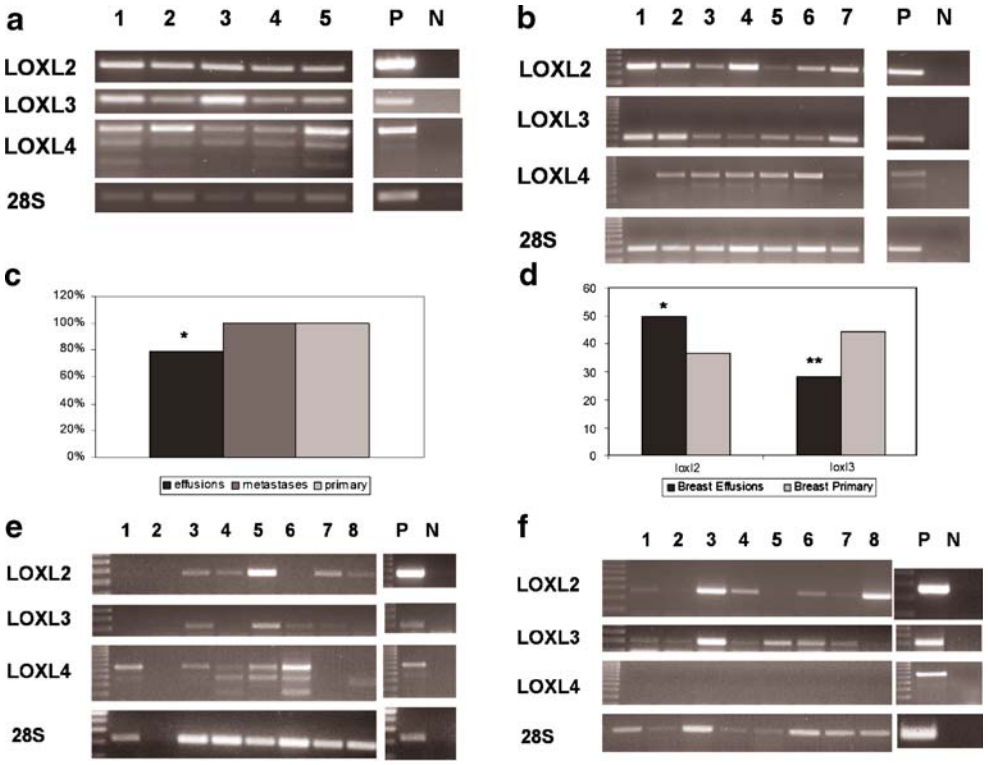

Fig. 1 LOXL enzymes are differentially expressed at various anatomic sites in ovarian and breast carcinoma. **a** RT-PCR analysis of LOXL2, LOXL3, LOXL4 mRNA, and 28S rRNA expression in five ovarian carcinoma (OC) effusions. All specimens express the enzymes. *P* positive control, *N* negative control. **b** RT-PCR analysis of LOXL2, LOXL3, LOXL4 mRNA, and 28S rRNA expression in seven primary OC. LOXL2 and LOXL3 are expressed in all cases, LOXL4 in six of seven tumors. *P* positive control, *N* negative control. **c** LOXL3 absolute expression is significantly lower in effusions compared with primary tumors and metastases. *Y-axis* Absolute expression (positive vs. negative cases). *$p=0.001$. **d** Comparative analysis shows significantly higher LOXL2 and lower LOXL3 expression in breast carcinoma effusions compared to primary breast carcinomas. *Y-axis* Mean ranks. *$p=0.003$, **$p<0.001$. **e** RT-PCR analysis of LOXL2, LOXL3, LOXL4 mRNA, and 28S rRNA expression in eight breast carcinoma effusions showing variable expression of the three enzymes. *P* positive control, *N* negative control. **f** RT-PCR analysis of LOXL2, LOXL3, LOXL4 mRNA, and 28S rRNA expression in eight primary breast carcinomas. Variable expression of LOXL2 and LOXL3 is seen, while LOXL4 is not expressed in any of the cases. *P* positive control, *N* negative control

ments to be exon 9 (splv-1) or both 8 and 9 (splv-2) (Fig. 2a). Within the encoded protein, exons 8 and 9 together are translated to a functional unit and form scavenger receptor cysteine rich 4 (SRCR4). In the 396-bp product, a 162-bp segment is cut out (splv-1), which comprises the second half of SRCR4. In the 247 bp product, the entire SRCR4 is cut out (splv-2).

Whereas full-length LOXL4 mRNA was detected in the majority of OC, the splv-1 and splv-2 variants were less frequently expressed at all anatomic sites (Table 3, Fig. 2b). The splv-1 variant was more highly expressed in effusions (p=0.005), while splv-2 was present only in effusions. Consequently, only effusion samples expressed all three mRNA variants, whereas primary tumors and metastases expressed only one or two isoforms. Another notable characteristic of LOXL4 expression was that the full-length variant was the most frequently apparent, either on its own or along with one or two splice variants. There were no specimens in which only splice variants were expressed.

As for full-length LOXL4 mRNA, splv-1 and splv-2 were expressed in breast carcinoma effusions but were uniformly absent in primary carcinomas (Table 3). As in OC, LOXL4 was expressed in breast carcinoma effusions in a complex manner, where the presence of one, two, or three isoforms was seen. Unlike in OC, 1/31 (3%) effusions expressed only the splv-2 variant.

LOXL2 and LOXL3 were found in all MM and RM effusions. LOXL4 full-length was found in 31% of MM and 25% of RM effusions (Fig. 3a). Splv-1 was found in 19% of MM and in 25% of RM effusions. Splv-2 was found in 31% of MM and in 37% of RM effusions (Fig. 3c). As in OC and breast carcinoma, one, two, or three LOXL4 isoforms were seen in MM effusions. Expression of only the shortest variant was seen in 3/25 (12%) MM effusions.

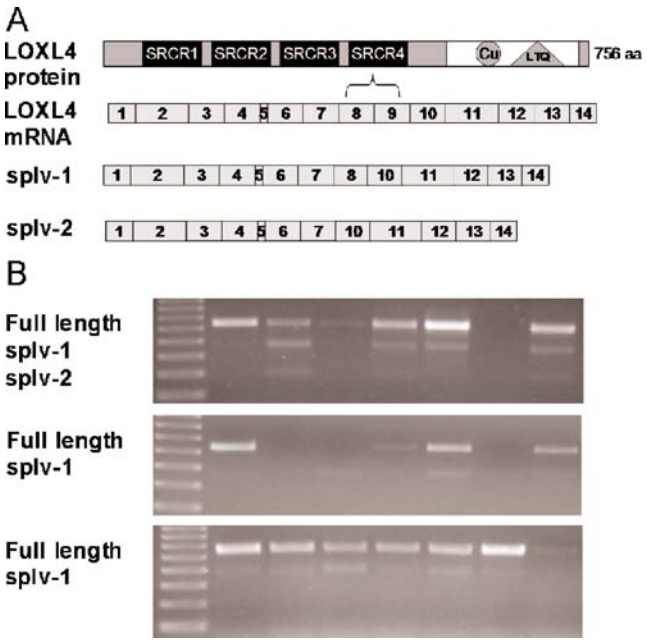

Fig. 2 LOXL4 splice variants. **a** Schematic diagram of LOXL4 full-length mRNA and protein and its splice variants. Exons are shown as *gray boxes*. In the protein diagram, SRCR domains are shown as *black boxes*, the copper-binding domain as a *gray circle* and LTQ residues as a *gray triangle*. **b** Variability in LOXL4 mRNA expression pattern at different anatomic sites in OC. All three variants are detectable in some effusions (*upper gel*), while solid metastases (*middle gel*) and primary carcinomas (*lower gel*) express only the full length and splv-1 forms

LOXL mRNA expression in effusions differs as function of tumor type

In an attempt to better characterize the expression of LOXLs in effusions, we compared the expression of LOXL2, LOXL3, and LOXL4 in OC, breast carcinoma, MM, and RM. Comparative analysis showed significantly higher expression of both LOXL2 and LOXL3 in MM compared to the other three specimen groups (p<0.001 for both). LOXL4 expression level was higher in OC and breast carcinomas compared to MM and RM effusions. The difference in LOXL4 expression was retained in analysis of the full-length and splv-1 variant (p<0.001 and p=0.001, respectively), with no statistically significant difference for the splv-2 variant (Fig. 3b).

LOXL mRNA expression in OC effusions is higher in post-chemotherapy effusions

The association between LOXL expression and clinicopathologic parameters was analyzed for 64 patients with OC effusions. A trend for higher LOXL4 levels was found in post-chemotherapy (disease recurrence) effusions compared to pre-chemotherapy (primary diagnosis) effusions (mean rank=36 vs. 28; p=0.06). This difference became significant when previous administration of platinum (mean rank=37 vs. 27; p=0.03) or paclitaxel (mean rank=38 vs. 26; p=0.011) was analyzed. Previous treatment using paclitaxel was also associated with more frequent presence of the splv-1 LOXL4 isoform (mean rank=28 vs. 36; p=0.046). Higher LOXL4 levels were additionally found in effusions from patients with smaller residual disease volume (≤1 cm; mean rank=33 vs. 24; p=0.03). No association with the mRNA level of any of the enzymes or the presence of LOXL4 isoforms and effusion site (peritoneum vs. pleura), patient age (≤60 vs. >60 years), histological grade (1–2 vs. 3), and FIGO stage (III vs. IV) was demonstrated (p>0.05, data not shown).

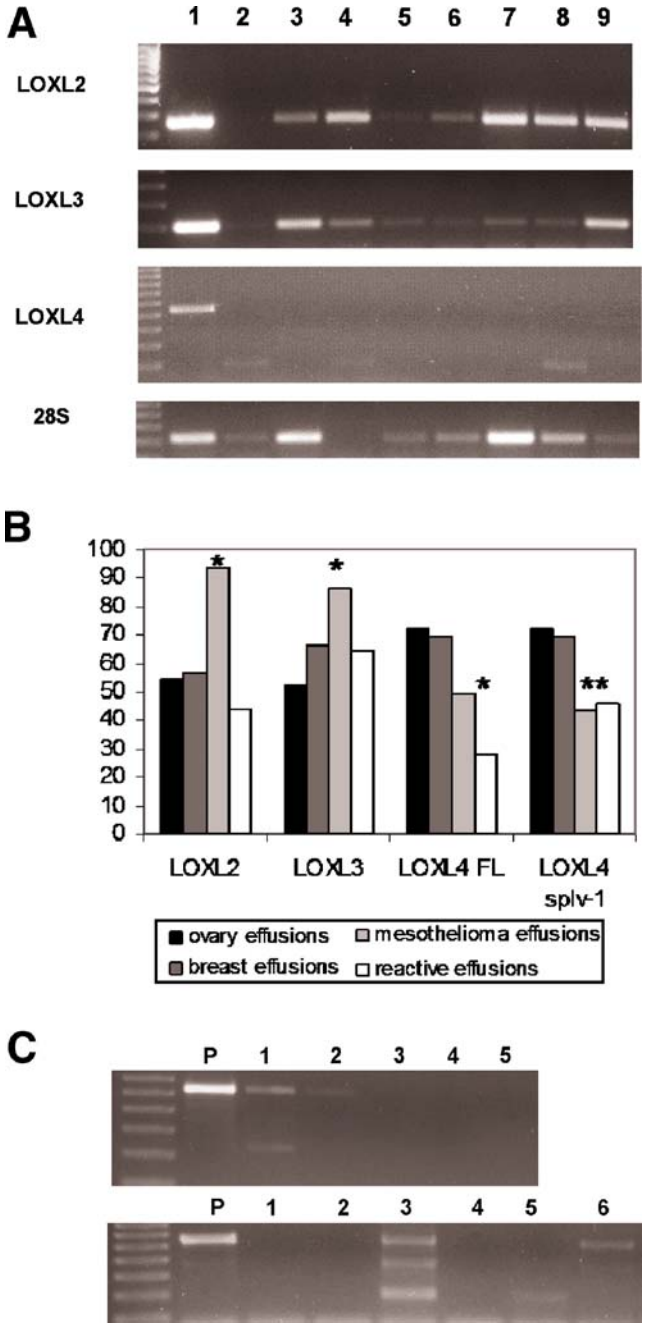

Fig. 3 LOXL expression in effusions differs as function of tumor type. **a** RT-PCR analysis of LOXL2, LOXL3, LOXL4 mRNA, and 28S rRNA expression in eight malignant mesothelioma (MM) samples. LOXL2 and LOXL3 are expressed in all specimens with varying intensity, with fewer cases expressing LOXL4. *Lane 1* Positive control. **b** LOXL2 and LOXL3 expression is significantly higher in MM effusions compared with OC, breast carcinoma, and reactive mesothelial (RM) effusions. LOXL4 full-length and splv-1 are significantly lower in MM and RM effusions compared with OC and breast carcinoma effusions. *Y-axis* Mean ranks. *$p<0.001$ **$p=0.001$. **c** LOXL4 expression pattern in reactive mesothelium (RM) vs. MM. LOXL4 is expressed in two of five RM specimens (*upper row*, *lanes 1–2*) and in three of six MM specimens (*lower row*, *lanes 3*, *5*, and *6*). Expression of the three LOXL4 variants is seen only in MM (*lane 3*). *P* positive control

LOXL4 protein is expressed in OC

Following our finding of LOXL4 alternative splicing, we were interested in learning whether these splice variants are translated into protein. Using immunblotting, we were unable to detect LOXL4 protein in our tumor samples. This was true using both existing commercial LOXL4 antibodies (Abnova) and an independently raised anti-LOXL4 antibody. We then decided to perform an immunoprecipitation assay on 25 representative OC specimens and were able to detect various amounts of LOXL4 protein. However, only the full-length protein was apparent, in the expected size of 98 kDa (Fig. 4).

Discussion

The two best-characterized members of the lysyl oxidase family, LOX and LOXL, have been known as extracellular enzymes responsible for crosslink formation in fibrillar collagen and elastin [28, 29]. Recent molecular cloning has revealed the existence of a human LOX family consisting of three additional paralogues, LOXL2, LOXL3, and LOXL4. Recently, members of the LOX family have been localized both intracellularly and intranuclearly [30] and implicated in various biological functions, including processes important to cancer development and progression, such as cell growth control [31], adhesion, motility, and invasion [10,32]. Previous studies have shown a pro-invasive role for LOXL2 in breast cancer cells [11] and involvement of LOXL2 and LOXL3 in tumor progression [13]. In the present study, we studied the expression of LOXL members with the aim of establishing whether they can differentiate between OC, breast carcinoma, MM, and RM in the diagnostic setting. We additionally compared LOXL mRNA expression in solid tumors vs. effusions in OC and breast carcinoma, with the objective of defining their potential role in tumor progression in these tumors, and analyzed the association between LOXL levels and clinicopathologic parameters in OC.

OC expressed LOXL2, LOXL3, and the full-length LOXL4 with no apparent site differences. However, analysis of absolute expression (positive vs. negative cases) showed significantly higher LOXL3 mRNA expression in

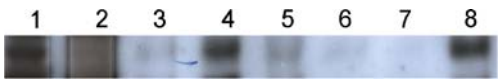

Fig. 4 Only the full-length LOXL4 protein is expressed in OC. IP analysis followed by immunoblotting of OC effusions and solid tumors. *Lane 1* Positive control (ES-2 cell line transfected with full-length LOXL4). *Lane 2* Negative control (ES-2 cell line transfected with a control vector). *Lanes 3–5* OC effusions. *Lanes 6–8* OC solid tumors

primary tumors and solid metastases compared to effusion samples.

Breast carcinomas showed a completely different expression profile. LOXL2 was significantly higher in effusions compared to primary tumors, while LOXL3 was significantly lower in effusions. LOXL4 was expressed only in effusion samples. These results indicate that LOXL3 down-regulation may be a common event in effusions of different origin, while differential regulation exists for LOXL2 and LOXL4 in OC and breast carcinoma, in spite of their common tendency to metastasize to the serosal cavities.

In order to obtain a broader view on LOXL expression in effusions, we also analyzed LOXL expression in two additional specimen types, MM and RM effusions. LOXL2 and LOXL3 were expressed both in MM and RM effusions. To our surprise, LOXL2 and LOXL3 were significantly higher in MM as compared to the other three effusion types, whereas LOXL4 expression was higher in OC and breast carcinoma effusions compared to MM or RM specimens. This suggests that high LOX4 expression is characteristic of adenocarcinomas in effusions, possibly taking over the role of LOX3, which is downregulated at this anatomic site.

While analyzing the expression of LOXL4, it became evident that this enzyme is expressed in at least three splice variants: a full-length variant, a variant lacking exon 9, and a variant lacking exons 8 and 9. Domain analysis of LOXL4 variants indicates deletion of a SRCR domain from the protein. These domains are known to mediate the protein–protein interactions for cell adhesion and cell signaling and are found either on the cell surface proteins or secreted proteins [33, 34]. The fact that LOXL4 and its splice variants are expressed more frequently in effusions may indicate on their involvement in the transition from the solid to the effusion state, while changing their cell–cell adhesion properties and their cell-matrix interactions.

The full-length variant showed no anatomic site preference in OC. Splv1 was significantly higher in OC effusions compared to solid tumors, while splv2 appeared only in OC effusions. Of special interest is our finding, though infrequent, of transformation in the expression of LOXL4 from full-length to variant in breast carcinoma and MM, a feature none of the OC samples showed.

LOXL4 protein was not easily detected in our tumor samples. This could be due to small amount of translation of this protein in the tumors or, more likely, due to poor performance of the available antibodies. LOXL4 splice variants were not shown to be translated into proteins in OC. This is of interest, as it may indicate a regulatory function these variants have at the RNA level.

Analysis of the association between LOXL levels and clinicopathologic parameters for patients with OC effusions revealed higher LOXL4 mRNA expression following treatment by both platinum compounds and paclitaxel. In our cohort, post-chemotherapy specimens were obtained at disease recurrence and are therefore more advanced in terms of tumor progression. The expression differences in full-length LOXL4 and the slpv-1 isoform may therefore suggest either induction of this enzyme by these agents or selection of LOXL4-producing tumor cell populations along tumor progression in OC effusions.

To our best knowledge, this is the first study to show anatomic site-related LOXL2, LOXL3, and LOXL4 expression in OC and breast carcinomas or to analyze the expression of these enzymes in MM or RM effusions. The differences in the LOXL expression profile between tumor cells in effusions and solid tumors in both OC and breast carcinoma support the significance of this enzyme family in the progression of cancer. Specifically, the unique splice variant distribution for LOXL4, with universal absence of this enzyme in primary breast carcinoma, lack of splv-2 variant in solid OC, and low LOXL4 expression in RM suggest a specific role in the late and generally rapidly fatal stage of tumor progression to effusion.

Acknowledgments This work was supported by the Norwegian and Israeli Cancer Societies and by the Research Foundation at the Radiumhospitalet. We wish to thank Mr. Søren Nielsen for the kind permission to use the malignant mesothelioma effusions from Aalborg Hospital in this study.

Conflict of interest statement We declare that we have no conflict of interest.

References

1. Kagan HM, Li W (2003) Lysyl oxidase: properties, specificity, and biological roles inside and outside of the cell. J Cell Biochem 88:660–672
2. Holtmeier C, Görögh T, Beier U et al (2003) Overexpression of a novel lysyl oxidase-like gene in human head and neck squamous cell carcinomas. Anticancer Res 23:2585–2591
3. Giampuzzi M, Botti G, Cilli M et al (2001) Down-regulation of lysyl oxidase-induced tumorigenic transformation in NRK-49F cells characterized by constitutive activation of ras proto-oncogene. J Biol Chem 276:29226–29232
4. Contente S, Kenyon K, Sriraman P et al (1999) Epigenetic inhibition of lysyl oxidase transcription after transformation by ras oncogene. Mol Cell Biochem 194:79–91
5. Lazarus HM, Cruikshank WW, Narasimhan N et al (1995) Induction of human monocyte motility by lysyl oxidase. Matrix Biol 14:727–731
6. Li W, Nellaiappan K, Strassmaier T et al (1997) Localization and activity of lysyl oxidase within nuclei of fibrogenic cells. Proc Natl Acad Sci U S A 94:12817–12822
7. Molnar J, Fong KS, He QP et al (2003) Structural and functional diversity of lysyl oxidase and the LOX-like proteins. Biochim Biophys Acta 1647:220–224
8. Maki JM, Kivirikko KI (2001) Cloning and characterization of a fourth human lysyl oxidase isoenzyme. Biochem J 355:381–387

9. Liu X, Zhao Y, Gao J et al (2004) Elastic fiber homeostasis requires lysyl oxidase-like 1 protein. Nat Genet 36:178–182
10. Kirschmann DA, Seftor EA, Fong SF et al (2002) A molecular role for lysyl oxidase in breast cancer invasion. Cancer Res 62:4478–4483
11. Akiri G, Sabo E, Dafni H et al (2003) Lysyl oxidase-related protein-1 promotes tumor fibrosis and tumor progression in vivo. Cancer Res 63:1657–1666
12. Fong SF, Dietzsch E, Fong KS et al (2007) Lysyl oxidase-like 2 expression is increased in colon and esophageal tumors and associated with less differentiated colon tumors. Genes Chromosomes Cancer 46:644–655
13. Peinado H, Del Carmen Iglesias-de la Cruz M, Olmeda D et al (2005) A molecular role for lysyl oxidase-like 2 enzyme in snail regulation and tumor progression. Embo J 24:3446–3458
14. Wu G, Guo Z, Chang X et al (2007) LOXL1 and LOXL4 are epigenetically silenced and can inhibit Ras/extracellular signal-regulated kinase signaling pathway in human bladder cancer. Cancer Res 67:4123–4129
15. Jemal A, Siegel R, Ward E et al (2008) Cancer statistics, 2008. CA Cancer J Clin 58:71–96
16. Goff BA, Mandel L, Muntz HG et al (2000) Ovarian carcinoma diagnosis. Cancer 89:2068–2075
17. Davidson B, Risberg B, Reich R et al (2003) Effusion cytology in ovarian cancer: new molecular methods as aids to diagnosis and prognosis. Clin Lab Med 23:729–754
18. Britton M (2002) The epidemiology of mesothelioma. Semin Oncol 29:18–25
19. Van Ruth S, Baas P, Zoetmulder FAN (2003) Surgical treatment of malignant pleural mesothelioma. Chest 123:551–561
20. Sugarbaker PH, Welch LS, Mohamed F et al (2003) A review of peritoneal mesothelioma at the Washington Cancer Institute. Surg Oncol Clin N Am 12:605–621
21. Feldman AL, Libutti SK, Pingpank JF et al (2003) Analysis of factors associated with outcome in patients with malignant peritoneal mesothelioma undergoing surgical debulking and intraperitoneal chemotherapy. J Clin Oncol 21:4560–4567
22. Hausheer FH, Yarbro JW (1985) Diagnosis and treatment of malignant pleural effusion. Semin Oncol 12:54–75
23. Martinez-Moragon E, Aparicio J, Sanchis J et al (1998) Malignant pleural effusion: prognostic factors for survival and response to chemical pleurodesis in a series of 120 cases. Respiration 65:108–113
24. Wilkes JD, Fidias P, Vaickus L et al (1995) Malignancy-related pericardial effusion. 127 cases from the Roswell Park Center Institute. Cancer 76:1377–1387
25. Dieterich M, Goodman SN, Rojas-Corona RR et al (1994) Multivariate analysis of prognostic features in malignant pleural effusions from breast cancer patients. Acta Cytol 38: 945–952
26. Banerjee AK, Willetts I, Robertson JF et al (1994) Pleural effusion in breast cancer: a review of the Nottingham experience. Eur J Surg Oncol 20:33–36
27. Davidson B, Nielsen S, Christensen J et al (2001) The role of Desmin and N-cadherin in effusion cytology. A comparative study using established markers of mesothelial and epithelial cells. Am J Surg Pathol 25:1405–1412
28. Borel A, Eichenberger D, Farjanel J et al (2001) Lysyl oxidase-like protein from bovine aorta: Isolation and maturation to an active form by bone morphogenetic protein-1. J Biol Chem 276:48944–48949
29. Csiszar K (2001) Lysyl oxidases: A novel multifunctional amine oxidase family. Prog Nucleic Acid Res Mol Biol 70:1–32
30. Hayashi K, Fong KS, Mercier F et al (2004) Comparative immunocytochemical localization of lysyl oxidase (LOX) and the lysyl oxidase-like (LOXL) proteins: Changes in the expression of LOXL during development and growth of mouse tissues. J Mol Histol 35:845–855
31. Butler E, Hardin J, Benson S (1987) The role of lysyl oxidase and collagen crosslinking during sea urchin development. Exp Cell Res 173:174–182
32. Payne SL, Fogelgren B, Hess AR et al (2005) Lysyl oxidase regulates breast cancer cell migration and adhesion through a hydrogen peroxide-mediated mechanism. Cancer Res 65:11429–11436
33. Hohenester E, Sasaki T, Timpl R (1999) Crystal structure of a scavenger receptor cysteine-rich domain sheds light on an ancient superfamily. Nat Struct Biol 6:228–232
34. Sasaki T, Brakebusch C, Engel J et al (1998) Mac-2 binding protein is a cell-adhesive protein of the extracellular matrix which self-assembles into ring-like structures and binds beta1 integrins, collagens and fibronectin. EMBO J 17:1606–1613

Virchows Arch (2009) 454:81–87
DOI 10.1007/s00428-008-0692-8

ORIGINAL ARTICLE

Ezrin immunohistochemical expression in cartilaginous tumours: a useful tool for differential diagnosis between chondroblastic osteosarcoma and chondrosarcoma

Sébastien Salas · Gonzague de Pinieux · Anne Gomez-Brouchet · Frédérique Larrousserie · Xavier Leroy · Sébastien Aubert · Anne-Valérie Decouvelaere · Roch Giorgi · Carla Fernandez · Corinne Bouvier

Received: 25 June 2008 / Revised: 22 September 2008 / Accepted: 16 October 2008 / Published online: 3 December 2008

Abstract Ezrin is a cytoskeleton linker protein that is actively involved in the metastatic process of cancer cells. We have recently reported that ezrin expression in conventional osteosarcoma was an independent prognostic factor for event-free survival and overall survival. In this work, ezrin expression was found in all histological subtypes. Especially cartilaginous areas in chondroblastic osteosarcomas were immunopositive for ezrin. We wanted to know if ezrin could be a useful diagnostic marker in bone pathology. We have searched for ezrin expression in 208 cartilaginous tumours by immunohistochemistry and in 16 chondroblastic osteosarcomas. All conventional

S. Salas · C. Fernandez · C. Bouvier
Service d'Anatomie Pathologique,
Hôpital la Timone,
Assistance Publique-Hôpitaux de Marseille,
264 rue Saint Pierre,
13385 Marseille cedex 5, France

S. Salas
Service d'Oncologie Médicale Adulte,
Hôpital la Timone,
Assistance Publique-Hôpitaux de Marseille,
264 rue Saint Pierre,
13385 Marseille cedex 5, France

G. de Pinieux
Service d'Anatomie Pathologique,
Hôpital Trousseau,
CHRU,
37044 Tours cedex 9, France

A. Gomez-Brouchet
Service d'Anatomie Pathologique,
Hôpital Rangueil,
av du Pr Poulhès,
31403 Toulouse, France

F. Larrousserie
Service d'Anatomie Pathologique,
Hôpital Cochin,
27 rue du Faubourg Saint Jacques,
75679 Paris cedex 14, France

X. Leroy · S. Aubert
Pôle Pathologie, CHRU,
av Oscar lambret,
59037 Lille, France

A.-V. Decouvelaere
Département d'Anatomie et de Cytologie Pathologique,
centre Léon Bérard,
28 rue Laennec,
69373 Lyon Cedex 8, France

R. Giorgi
Service de Santé Publique et d'Information médicale,
Hôpital la Timone,
Assistance Publique-Hôpitaux de Marseille,
rue Saint Pierre,
13385 Marseille cedex 5, France

R. Giorgi
LERTIM, EA 3283, Aix-Marseille Université,
Faculté de Médecine,
27 Bd Jean Moulin,
13385 Marseille Cedex, France

C. Bouvier (✉)
UMR 911, Equipe IV : Angiogénèse,
invasion et microenvironnement tumoral,
Faculté de Médecine Timone,
27, Bd Jean Moulin,
13005 Marseilles, France
e-mail: corinne.bouvier@univmed.fr

chondrosarcomas, whatever their grade, were negative, while ten of 16 chondroblastic osteosarcomas were positive. In contrast, dedifferentiated (five of 14) and mesenchymal chondrosarcomas (five of ten) showed ezrin positivity. Some chondroblastomas and more rarely chondromyxoid fibromas also exhibited ezrin expression. These data suggest that ezrin is a useful immunohistochemical marker for differential diagnosis between chondroblastic osteosarcomas and conventional chondrosarcomas with a specificity of 100%. Ezrin expression in dedifferentiated and mesenchymal chondrosarcomas which are aggressive neoplasms resistant to conventional treatment means that ezrin could be a therapeutic target. Ezrin expression in chondroblastomas is more intriguing and requires further study to assess prognostic value.

Keywords Ezrin · Cartilaginous tumours · Chondroblastic osteosarcomas · Conventional chondrosarcoma · Mesenchymal chondrosarcoma · Dedifferentiated chondrosarcoma · Chondroblastoma · Immunohistochemistry

Introduction

In bone pathology, diagnosis mainly relies on microscopic features with knowledge of imaging data since specific immunohistochemical markers of osteoblastic or chondrogenic lineage or markers of malignancy are lacking. Recently, overexpression of ezrin protein has been correlated with the metastatic potential of several cancers especially conventional osteosarcoma [1–3]. Ezrin belongs to the ezrin/radixin/moesin (ERM) protein family which act as membrane organizers and linkers between plasma membrane and cytoskeleton [4]. ERM proteins occur in the cytoplasm in an inactive closed conformation with N-terminal to C-terminal associations within the protein or with the other ERM members. Upon threonine and tyrosine phosphorylation, ezrin assumes an active open conformation, moves to the cell membrane and tethers F-actin directly or indirectly to the cell membrane [5]. Ezrin, also known as cytovillin or villin2, is a component of cell-surface structures which are involved in cell adhesion to the extracellular matrix as well as in cell–cell interactions, receptor tyrosine-kinase signalling (cmet/hepatocyte growth factor pathway), signal transduction through Rho GTPase and interactions with the Akt-mediated cellular apoptotic machinery. Khanna et al., using sets of cell line variants of osteosarcomas with low or high metastatic properties, found that *vil2* gene mapped to chromosome 6q25-26, was consistently overexpressed in the metastatically capable clones [1]. More recently, they also showed that stable transfection with full length anti-sense ezrin diminished experimental and spontaneous metastases of osteosarcoma in mice. High expression of ezrin in dog osteosarcomas was also associated with early pulmonary metastases, and a significant association with high ezrin expression and poor outcome was also found in a small cohort of pediatric osteosarcomas [6]. Additional studies have confirmed ezrin expression in vivo in a larger cohort of conventional central high-grade osteosarcomas, while low-grade osteosarcomas were negative [7]. More recently, we have shown that ezrin expression by immunohistochemistry (IHC) on biopsy prior to chemotherapy was an independent prognostic factor for event-free and overall survival in multivariate analysis in a series of 37 osteosarcomas [8]. In this work, ezrin expression was found in all histological subtypes of osteosarcomas. Especially cartilaginous areas in chondroblastic osteosarcomas (CBOS) were immunopositive for ezrin. As it is sometimes difficult to distinguish chondroblastic osteosarcoma from conventional chondrosarcoma (C-CHS) in a small biopsy, we have performed an immunohistochemistry study with anti-ezrin antibody in a large panel of benign and malignant cartilaginous tumours and in 16 chondroblastic osteosarcomas, in search of diagnostic value. We especially wanted to know if ezrin expression by IHC could help to differentiate chondrosarcomas from osteosarcomas.

Materials and methods

Tumour specimens

Sixteen biopsies at the time of diagnosis from chondroblastic osteosarcomas were available for immunohistochemical study. Osteosarcomas were selected if more than 50% of the matrix was cartilaginous. All tumours were high-grade conventional osteosarcomas. All patients were from the Timone hospital, and diagnosis was done between 1997 and 2007. Eight cases had been previously reported in a study dealing with prognostic value of ezrin expression in osteosarcomas [8]. Eight other cases have been added. All were children except two cases.

Malignant cartilaginous tumours encompassed : 101 central conventional chondrosarcomas (C-CHS; 18 grade I, 65 grade II and 18 grade III), three peripheral secondary grade I chondrosarcomas developed on a pre-existing osteochondroma, ten mesenchymal chondrosarcomas, 14 dedifferentiated chondrosarcomas (D-CHS), ten clear-cell chondrosarcomas. Seventy benign cartilaginous tumours were studied and included 20 enchondromas, 20 osteochondromas, eight chondromyxoid fibromas (CMF) and 22 chondroblastomas (CB). The cartilaginous tumour specimens were retrieved from the archives of the Timone, Cochin, Rangueil, Trousseau,

Leon Bérard and Lille hospitals. The work was carried out collaboratively by the French Group of Bone Pathologists. For all tumours, histological diagnosis was performed on haematoxylin phloxin saffron staining according to the World Health Organization (WHO) classification of bone tumours by two pathologists: the pathologist of the center of origin of the patients and Dr C. Bouvier, who performed the IHC study.

Immunohistochemistry

All specimens were fixed in formalin. Decalcification was used if necessary and was heterogeneous between the different institutions. Sections of 4 μm thickness were prepared from one representative paraffin block of formalin-fixed benign cartilaginous tumours, clear cell, mesenchymal, dedifferentiated chondrosarcomas and chondroblastic osteosarcomas. For conventional central chondrosarcomas, we studied 30 cases (ten grade I, 15 grade II and five grade III) with a selected whole block of paraffin retrieved from the pathology archives of the Timone Hospital. We also performed ezrin IHC in an independent cohort of C-CHS using tissue-microarray (TMA) blocks constructed with tumour specimens from the Cochin hospital to increase the number of tumours studied. They encompassed eight grade I, 50 grade II and 13 grade III C-CHS. For each tumour, cores of 1 mm diameter were punched to build the TMA blocks. Automated immunohistochemistry was performed with avidin–biotin–peroxidase complex on a Ventana 320 Device (Tucson, AZ, USA) with Ventana kits (Strasbourg, France) including 3-amino-9-ethylcarbazole reagent. Sections were counterstained with haematoxylin and mounted in glycergel (Dakocytomation, USA). Ezrin antibody (Sigma, clone 3C12) was diluted to 1:250. Heat antigen retrieval was used with citrate buffer (pH=6). Paraffin sections from placenta collected after birth were used as external positive control. Slides incubated without antibodies were performed for negative control. Immunohistochemistry was recorded as positive for ezrin when membranous and/or cytoplasmic staining was observed. For positive cases, a semiquantitative assessment was done. A percentage of stained cells was calculated. One hundred cells were counted in the most stained areas when whole paraffin sections were used. A percentage of staining among all the cells present on the three cores was calculated for each tumour present on TMA blocks. More than 5% of the cells stained was the arbitrary cut-off to accept positivity. Then three classes of ezrin positivity were defined: 5–10%, 11–25% or >25% of stained cells.

Statistical analysis

To evaluate the performances of ezrin for the differential diagnosis between chondroblastic osteosarcomas and chondrosarcomas, we assessed the sensitivity, specificity and positive and negative predictive values of ezrin. The 95% confidence interval (95%) of these indicators was computed using binomial probabilities (R free software, version 2.6.1).

Results

Malignant tumours

Ten of 16 (62.5%) CBOS showed ezrin cytoplasmic positivity (Fig. 1a,b; Tables 1 and 2) in the cartilaginous lobules and in the spindle cells at the periphery of the lobules. Three cases had no more than 10% of stained cells, four cases had 11–25% of stained cells, and three cases had more than 25% of stained cells. There was no ezrin expression in C-CHS whatever their grade (Fig. 1c,d). Secondary peripheral chondrosarcomas were also negative. Tumour cells did not express ezrin in clear cell chondrosarcomas (CCC), while osteoblasts were positive in the areas of osteogenesis (Fig. 2a,b). In contrast, ezrin cytoplasmic positivity was present (in less than 25% of the cells) in five of 14 dedifferentiated chondrosarcomas and in five of ten mesenchymal chondrosarcomas. In both subtypes of chondrosarcomas, ezrin expression was only observed in the high-grade cellular areas, while hyalin cartilage islands were negative (Fig. 2c–f). No osteosarcomatous contingent was observed in areas of dedifferentiation in D-CHS. Ezrin positivity was observed in areas of pleimorphic sarcoma in these tumours.

For differential diagnosis between chondroblastic osteosarcomas and all types of chondrosarcomas, the sensitivity was 62.5% (95% CI=0.38–0.81), and the specificity was 91% (95% CI=0.85–0.95). Positive predictive value was 50% (95% CI=0.30–0.70) and negative predictive value 94.7% (95% CI=0.89–0.97). When comparing chondroblastic osteosarcomas with conventional chondrosarcomas, sensitivity was 62.5% (95% CI=0.38–0.81), while specificity was 100% (95% CI=0.95–1.00). The positive predictive value was 100% (95% CI=0.72–1.00), and the negative predictive value 93.1% (95% CI=0.85–0.96).

Benign tumours

Only chondroblastomas and chondromyxoid fibromas showed some positivity. Seven from 22 (32%) CB had either cytoplasmic and membranous expression of ezrin (four cases; Fig. 1e) or cytoplasmic immunotaining only (three cases; Fig. 1f). In four cases of CB, more than 25% of the cells were stained.

In two cases of CMF, ezrin positivity was observed very focally at the periphery of the lobules in cells that look like

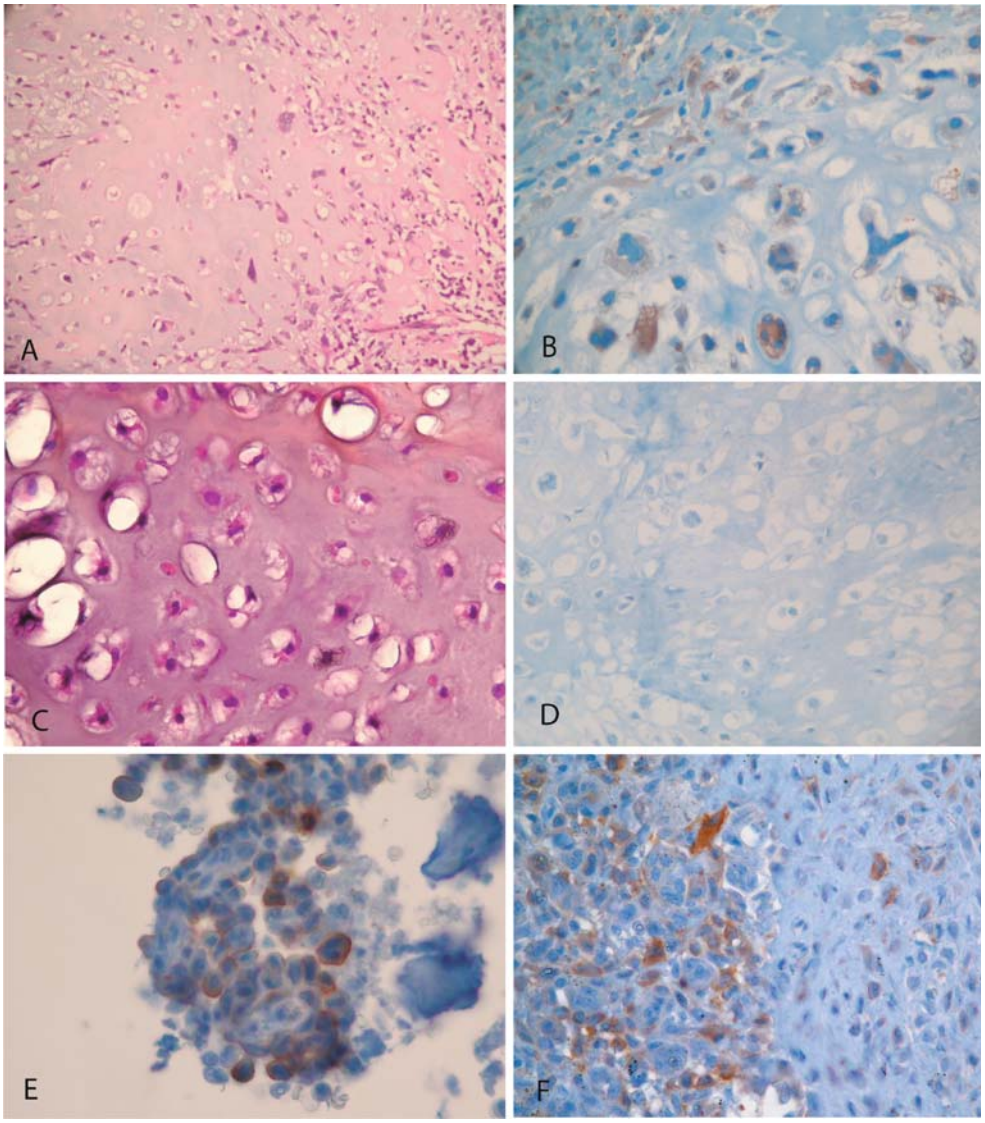

Fig. 1 **a**, **b** Chondroblastic osteosarcoma (haematoxylin phloxin saffron (HPS), **a** ×40) ezrin expression by IHC (**b**, ×100): spindle peripheral cells and cells in lacunae are positive in cartilaginous areas. **c**, **d** Conventional grade II chondrosarcoma (HPS, **c** ×100) lack of ezrin expression by IHC (**d** ×100). **e**, **f** Ezrin immunostaining in chondroblastoma: membranous and cytoplasmic staining (**e** ×40) or cytoplasmic staining only (**f** ×40)

chondroblasts. All enchondromas and osteochondromas were negative (data not shown).

Discussion

The cytoskeleton linker protein ezrin is involved in tumour development and progression in several types of cancers such as gliomas, melanomas, soft tissue sarcomas and more recently osteosarcomas [1–3, 9]. We [8] and others [6, 10] have previously reported the prognostic value of ezrin expression in central conventional osteosarcomas. We wanted to investigate the diagnosis value of ezrin expression in bone tumours, especially in order to distinguish osteosarcoma from chondrosarcoma. In our previous series [8], 62% of paraffin-embedded samples of central high-grade osteosarcomas were positive for ezrin by IHC, and ezrin expression was observed in all the histological subtypes including chondroblastic osteosarcomas [8]. Ferrari et al. also reported ezrin expression in chondroblastic osteosarcomas (nine of nine cases). Interestingly, in the present series, no case of central conventional chondrosarcoma, even of high grade (II and III), showed ezrin expression by IHC. Specificity and positive predictive values for ezrin IHC were 100%, though sensitivity is lower. These data may be useful to distinguish chondroblastic osteosarcoma from chondrosarcoma on a small biopsy. About 25% of osteosarcomas showed prominent cartilage differentiation and are called chondroblastic. They are made of lobules of cartilage with cells in the lacunae having the cytologic features of high-grade malignancy. They also show a condensation of spindle cells at the periphery of the lobules with a gradual transition from the chondroid areas to the spindle cell areas. Interestingly, ezrin immunodetection highlights these spindle cells. Lace-like osteoid is usually seen between the spindle cells, but when sometimes lacking, its absence is assumed to result

Table 1 Ezrin expression by immunohistochemistry in cartilaginous tumours and chondroblastic osteosarcomas

Histologic diagnosis	Total number of tumours	Ezrin positive cases
C-CHS grade I	18	0
C-CHS grade II	65	0
C-CHS grade III	18	0
Peripheral secondary grade I	3	0
Chondrosarcomas		
Clear cell chondrosarcomas	10	0
Mesenchymal chondrosarcomas	10	5
Dedifferentiated chondrosarcomas	14	5
Enchondromas	20	0
Osteochondromas	20	0
Chondroblastomas	22	7
Chondromyxoid fibromas	8	2
Chondroblastic osteosarcomas	16	10

C-CHS conventional chondrosarcomas

from a sampling problem. While lack of ezrin expression is not contributive, positivity for ezrin in a high-grade cartilage tumour with spindle cells but without clear-cut osteoid production allows the tumour to be classified as an osteosarcoma rather than a chondrosarcoma. Of course, clinical and radiological data are also of utmost importance to distinguish osteosarcoma from chondrosarcoma.

Among histological subtypes of chondrosarcomas, dedifferentiated chondrosarcomas could rarely be misdiagnosed as osteosarcoma especially when areas of osteogenesis are observed. Ezrin IHC in those cases would not be discriminant since dedifferentiated chondrosarcomas showed variable positivity in the anaplastic component, and diagnosis will rely on microscopic distinctive features. In CBOS, the cartilage component is very malignant-looking and merges into the spindle cell component, unlike the abrupt change from a low-grade to high-grade spindle cell sarcoma in dedifferentiated chondrosarcoma. In contrast to mesenchymal and dedifferentiated chondrosarcomas, clear cell chondrosarcomas were always negative. These data are in line with the more indolent behaviour of the CCC which are usually of a low grade of malignancy giving mainly local recurrence but rarely metastases, while mesenchymal or dedifferentiated chondrosarcomas are highly malignant tumours with high metastatic rates and dismal prognosis [11, 12]. This is the first report of ezrin expression in these neoplasms. However, activation of the mTOR pathway has been previously reported in mesenchymal chondrosarcomas [13]. In Ewing sarcoma [2] and in osteosarcoma [14], the metastatic action of ezrin is dependent on the AKT/mTOR signal transduction cascade. Further studies are required on mesenchymal chondrosarcomas to clarify the relationship between ezrin and the mTOR signalling pathway. As these neoplasms are resistant to conventional chemotherapy, rapamycine would be an alternative treatment.

Table 2 Semi quantitative ezrin expression by IHC

Number of positive cases		5–10%	11–25%	>25%
10	Chondroblastic osteosarcomas	3	4	3
5	Mesenchymal chondrosarcomas	1	4	0
5	Dedifferentiated chondrosarcomas	2	3	0
7	Chondroblastomas	2	1	4
2	Chondromyxoid fibromas	2	0	0

Exceptional cases of "chondroblastoma-like" or "chondromyxoid fibroma-like" osteosarcomas have been reported [15–17]. Again, in these cases, ezrin IHC could not be used to distinguish them from CB or CMF since these tumours showed consistent positivity.

However, positivity for ezrin in CB is an interesting finding to help to distinguish them from clear cell chondrosarcomas which sometimes have radiological and histological overlapping features with CB [18]. Except for collagen II which is present in the extracellular matrix of CCC only, no other immunohistochemical marker is helpful for this differential diagnosis [18]. Even if CB belongs to cartilaginous tumours in the WHO classification, its histogenesis is controversial. Some authors have previously shown that CB shared some antigens such as collagene type I with osteogenic tumours [19]. In line with these data, ezrin which is mainly expressed by osteogenic tumours could be an additional marker of CB.

The pattern of ezrin expression in CB cytoplasmic or membranous and cytoplasmic is also intriguing. Recently, in conventional high-grade osteosarcomas, Ferrari et al. showed that only membranous and cytoplasmic ezrin expression was pejorative for prognosis [10]. As after threonine and tyrosine phosphorylation, ezrin which is in the cytoplasm achieves an active conformation and moves to the cell membrane, it is possible that membranous ezrin expression corresponds to the "active" form of ezrin, and this might explain why this pattern of expression is correlated to more aggressive behaviour in osteosarcoma. In contrast, the majority of chondroblastomas have a benign course. However, local recurrence or metastases can occasionally occur. The quality of surgery remains the main prognostic factor for recurrence in these tumours [20]. Further studies are required to show whether ezrin expression could be predictive of recurrence or metastasis and also to elucidate the value of the membranous immunostaining in these tumours.

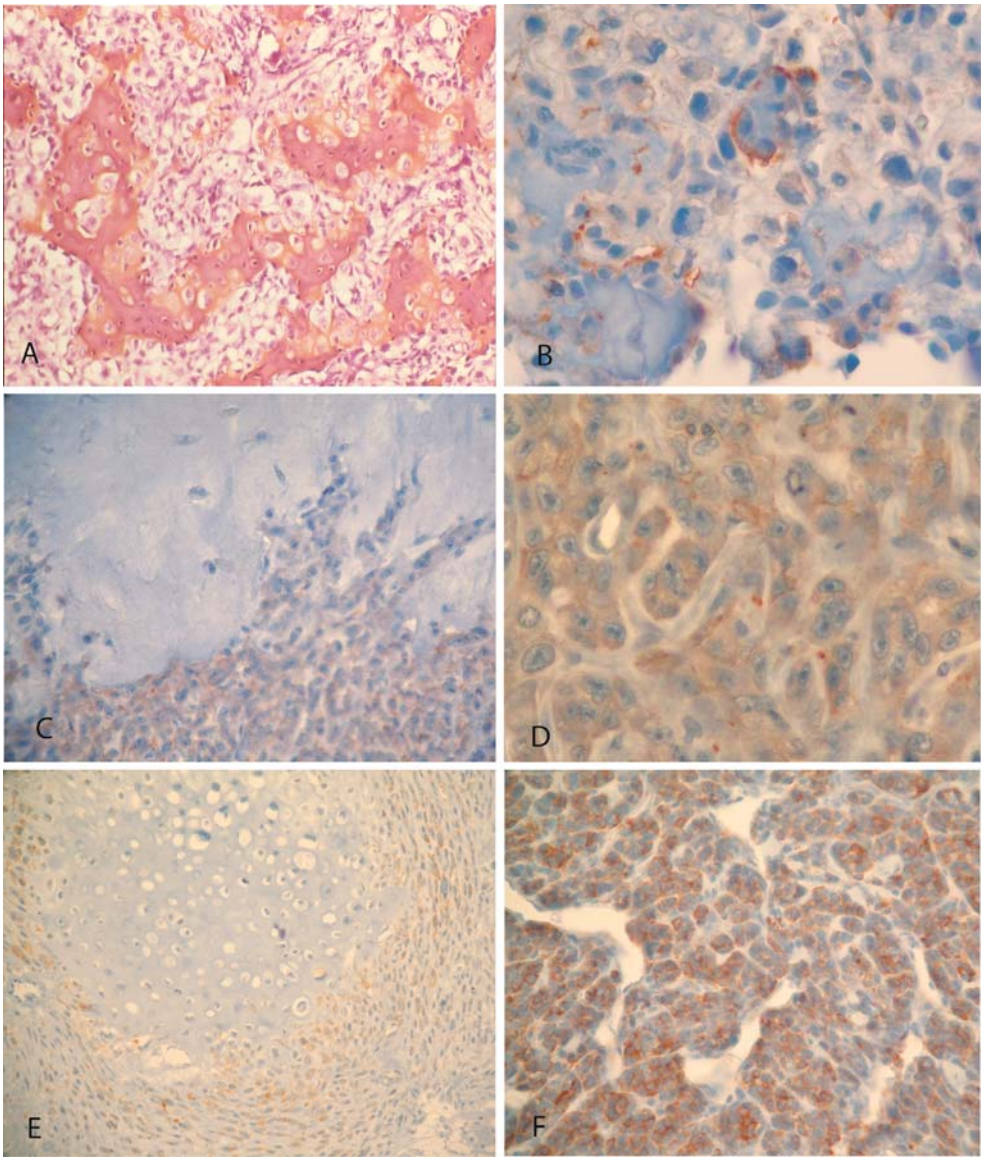

Fig. 2 **a**, **b** Clear cell chondrosarcoma (HES, **a** ×40), ezrin expression in osteoblasts but not in cartilaginous tumoral cells (**b** ×100). **c–f** In dedifferentiated and mesenchymal chondrosarcomas areas, containing hyalin cartilage were negative (**c** ×40 and **e** ×100), while high-grade cellular areas were ezrin positive (respectively, **d** ×40 and **f** ×40)

This study has some limitations. Firstly, ezrin is a marker involved in the metastatic process in osteosarcomas with variable expression. Ezrin positivity was reported in 43% to 62.5% of osteosarcomas [7, 8, 10]. It might be argued that, for a diagnosis marker, the sensitivity is low. In contrast, the specificity is high since no C-CHS expressed ezrin. So, used in special circumstances with knowledge of clinical and radiological data, ezrin expression is in favour of CBOS rather than C-CHS. Secondly, it is a retrospective study comparing IHC data achieved either on biopsies (CBOS and C-CHS) or on resection specimens (C-CHS). However, patients with a C-CHS did not have any treatment before surgery that could have modified ezrin expression at the time of surgery. Ezrin expression should not differ on biopsies or on resection. Nevertheless, more powerful data would be provided by a prospective study on biopsy specimens on the basis of these preliminary interesting results.

Thirdly, decalcification which could alter antigenicity always makes it difficult to perform immunohistochemical studies in bone pathology. However, retrieval antigen techniques and new-generation IHC automates now make it possible to work more reliably on decalcified specimens. Ideally, a homogenous decalcification process adopted in different pathology departments would improve IHC reproducibility.

Fourthly, the use of TMA in the IHC study raised the question of their reliability since small cores might not adequately represent the whole section because of heterogeneous protein expression. Concordance between results achieved with TMA or whole sections appears to be marker- and tissue-specific [21]. However, TMA representativeness is improved if the number and size of cores is increased, as was done in the present study.

In conclusion, we have shown in this study that, among malignant cartilaginous tumours, only aggressive histological

subtypes of CS: dedifferentiated and mesenchymal CS expressed ezrin by IHC, suggesting that ezrin could be a molecular therapeutic target in these tumours. Ezrin expression in CB is more intriguing, and further series are required to determine its prognostic value in large series. The lack of ezrin expression by conventional chondrosarcoma is an interesting finding that is helpful to distinguish them from chondroblastic osteosarcoma. A prospective study on biopsies is mandatory to confirm these data.

Acknowledgments We are grateful to P. Morando and Arlette Calisti for technical assistance. This work was supported by Institutional grants, by the "Appel d'offre APHM 2005" and by the Philippe Daher foundation.

Disclosure of conflict of interest We declare that we have no conflict of interest.

References

1. Khanna C, Khan J, Nguyen P et al (2001) Metastasis-associated differences in gene expression in a murine model of osteosarcoma. Cancer Res 61:3750–3759
2. Krishnan K, Bruce B, Hewitt S et al (2006) Ezrin mediates growth and survival in Ewing's sarcoma through the AKT/mTOR, but not the MAPK, signaling pathway. Clin Exp Metastasis 23:227–236
3. Weng WH, Ahlen J, Astrom K et al (2005) Prognostic impact of immunohistochemical expression of ezrin in highly malignant soft tissue sarcomas. Clin Cancer Res 11:6198–6204
4. Mangeat P, Roy C, Martin M (1999) ERM proteins in cell adhesion and membrane dynamics. Trends Cell Biol 9:187–192
5. Vaheri A, Carpen O, Heiska L et al (1997) The ezrin protein family: membrane–cytoskeleton interactions and disease associations. Curr Opin Cell Biol 9:659–666
6. Khanna C, Wan X, Bose S et al (2004) The membrane–cytoskeleton linker ezrin is necessary for osteosarcoma metastasis. Nat Med 10:182–186
7. Park HR, Jung WW, Bacchini P et al (2006) Ezrin in osteosarcoma: comparison between conventional high-grade and central low-grade osteosarcoma. Pathol Res Pract 202:509–515
8. Salas S, Bartoli C, Deville JL et al (2007) Ezrin and alpha-smooth muscle actin are immunohistochemical prognostic markers in conventional osteosarcomas. Virchows Arch 451:999–1007
9. Ogino W, Takeshima Y, Mori T et al (2007) High level of ezrin mRNA expression in an osteosarcoma biopsy sample with lung metastasis. J Pediatr Hematol Oncol 29:435–439
10. Ferrari S, Zanella L, Alberghini M et al (2008) Prognostic significance of immunohistochemical expression of ezrin in non-metastatic high-grade osteosarcoma. Pediatr Blood Cancer 50:752–756
11. Dickey ID, Rose PS, Fuchs B et al (2004) Dedifferentiated chondrosarcoma: the role of chemotherapy with updated outcomes. J Bone Jt Surg 86-A:2412–2418
12. Staals EL, Bacchini P, Bertoni F (2006) Dedifferentiated central chondrosarcoma. Cancer 106:2682–2691
13. Brown RE (2004) Morphoproteomic portrait of the mTOR pathway in mesenchymal chondrosarcoma. Ann Clin Lab Sci 34:397–399
14. Wan X, Mendoza A, Khanna C et al (2005) Rapamycin inhibits ezrin-mediated metastatic behavior in a murine model of osteosarcoma. Cancer Res 65:2406–2411
15. Chow LTC, Lin J, Kumta SM et al (1996) Chondromyxoid fibroma-like osteosarcoma: a distinct variant of low-grade osteosarcoma. Histopathology 29:429–436
16. Klein MJ, Siegal GP (2006) Osteosarcoma. Anatomic and histologic variants. Am J Clin Pathol 125:555–581
17. Schajowicz F, de Prospero JD, Cosentino E (1990) Case report 641: chondroblastoma-like osteosarcoma. Skelet Radiol 19:603–603
18. Soder S, Oliveira AM, Inwards CY et al (2006) Type II collagen, but not aggrecan expression, distinguishes clear cell chondrosarcoma and chondroblastoma. Pathology 38:35–38
19. Aigner T, Loos S, Inwards C et al (1999) Chondroblastoma is an osteoid-forming, but not cartilage-forming neoplasm. J Pathol 189:463–469
20. van der Geest IC, van Noort MP, Schreuder HW et al (2007) The cryosurgical treatment of chondroblastoma of bone: long-term oncologic and functional results. J Surg Oncol 96:230–234
21. Hassan S, Ferrario C, Mamo A et al (2008) Tissue microarrays: emerging standard for biomarker validation. Curr Opin Biotechnol 19:19–25

Virchows Arch (2009) 454:89–99
DOI 10.1007/s00428-008-0697-3

ORIGINAL ARTICLE

Renal angiomyoadenomatous tumor: morphologic, immunohistochemical, and molecular genetic study of a distinct entity

M. Michal · O. Hes · J. Nemcova · R. Sima · N. Kuroda · S. Bulimbasic · M. Franco · N. Sakaida · D. Danis · D. V. Kazakov · C. Ohe · M. Hora

Received: 11 May 2008 / Revised: 26 September 2008 / Accepted: 29 October 2008 / Published online: 20 November 2008

Abstract We present a series of a distinct tumorous entity named renal angiomyoadenomatous tumor (RAT). Five cases were retrieved from the consultation files of the authors. Histologic and immunohistochemical features were evaluated. Sequencing analysis of coding region of the VHL gene was carried out in all cases. The tumors were composed of admixture of an epithelial clear cell component and prominent leiomyomatous stroma. Epithelial cells formed adenomatous tubular formations endowed with blister-like apical snouts. All tubular/glandular structures were lined by a fine capillary network. The epithelial component was positive for epithelial membrane antigen, CK7, CK20, AE1-AE3, CAM5.2, and vimentin in all cases. In all analyzed samples, no mutation of the VHL gene was found. RAT is a distinct morphologic entity, being different morphologically, immunohistochemically, and genetically from all renal tumors including conventional clear cell carcinoma and mixed epithelial and stromal tumor of kidney.

Keywords Renal angiomyoadenomatous tumor · Mixed epithelial and stromal tumor · Leiomyomatous stroma · Kidney

Introduction

Renal angiomyoadenomatous tumor (RAT) is a recently described neoplasm microscopically characterized by leiomyomatous stroma often forming abortive vascular structures surrounding and encasing a distinctive epithelial component [18]. Since the time we published a case of RAT, we have been receiving in consultation putative cases of RAT with the request to confirm or exclude the

M. Michal · O. Hes · J. Nemcova · R. Sima · D. V. Kazakov
Department of Pathology,
Charles University, Faculty Hospital,
Plzen, Czech Republic

M. Hora
Department of Urology,
Charles University, Faculty Hospital,
Plzen, Czech Republic

N. Kuroda
Red Cross Hospital Kochi,
Kochi, Japan

N. Sakaida · C. Ohe
Department of Pathology,
Kansai Medical University Hirakata Hospital,
Osaka, Japan

S. Bulimbasic
University Hospital Dubrava,
Zagreb, Croatia

M. Franco
EPM/UNIFESP,
Sao Paulo, Brazil

D. Danis
Cytopathos s.r.o.,
Bratislava, Slovakia

M. Michal (✉)
Sikl's Department of Pathology,
Laboratore Spec. Diagnostiky Medical Faculty Hospital,
Charles University,
Alej Svobody 80,
304 60 Plzen, Czech Republic
e-mail: michal@medima.cz

diagnosis. This resulted in identification of five new cases of RAT, which clinicopathologic and genetic features are presented herein.

Materials and methods

The five cases of RAT were collected from the files of the Charles University Hospital Plzen in the Czech Republic, the Red Cross Hospital Kochi (originated from Kansai Medical School Hirakata Hospital) in Japan, the University Hospital Dubrava in Zagreb in Croatia, the EPM/UNIFESP Sao Paulo in Brazil, and Cytopathos s.r.o. Bratislava in the Slovak Republic.

Histologic sections of formalin-fixed, paraffin-embedded tissue were stained with hematoxylin and eosin. Primary antibodies to the following antigens were employed: cytokeratins CK7 and 8 (clone CAM5.2, at 1:50, Becton-Dickinson, San Jose, CA, USA), Pancytokeratin (clone AE1-AE3, at 1:500, Boehringer, Mannheim, Germany), CK7 (clone OV-TL 12/30, at 1:200, DakoCytomation, Glostrup, Denmark), CK20 (clone K20.8, at 1:1,000, Neomarkers, Fremont, CA, USA), epithelial membrane antigen (EMA; clone E29, at 1:1,000, DakoCytomation), carbonic anhydrase IX (R&D Systems, Minneapolis, MN, USA; clone 303123, at 1:500), Ki-67 (clone MIB1, at 1:200, DakoCytomation), HMB45 (clone HMB45, at 1:300, DakoCytomation), S100 protein (polyclonal, at 1:200, Novocastra, Newcastle, UK), TFE3 (polyclonal, at 1:500, Santa Cruz Biotechnology, Santa Cruz CA, USA), CD34 (clone QBEnd10 at 1:800, Neo-Markers), CD117 (polyclonal, at 1:150, NeoMarkers), vimentin (clone V9, at 1:1,000, Neomarkers), racemase (clone P504S, at 1:3,500, Assay Design, Ann Arbor, MI, USA), smooth muscle actin (clone 1A4, at 1:1,000, DakoCytomation), desmin (clone D33, at 1:3,000, DakoCytomation), caldesmon (clone h-CD, at 1:50, DakoCytomation), calponin (clone CALP, at 1:1,000, DakoCytomation) and factor VIII (polyclonal, at 1:4,000, DakoCytomation), tyrosinase (clone T311, at 1:400, DakoCytomation), and Melan A (clone A103, at 1:400, DakoCytomation). The primary antibodies were visualized using the supersensitive streptavidin–biotin–peroxidase complex (BioGenex, San Ramon, CA, USA).

Analysis of VHL gene mutation and 3p loss of heterozygosity

Five 10-μm thick sections of tumor tissue were cut from formalin-fixed, paraffin-embedded blocks. Epithelial and smooth muscle components were manually microdissected. DNA was extracted separately from each component by the NucleoSpin Tissue Kit (Macherey Nagel, Duren, Germany) according to manufacturer's protocol. Polymerase chain reaction (PCR) for the VHL gene analysis was carried out using primers displayed in Table 1. PCR for loss of heterozygosity (LOH) analysis of chromosome 3p was performed using short tandem repeat (STR) markers and primers shown in Table 2. Normal tissues of the same patients were used as a reference. The reaction conditions were as follows: 12.5 μl of HotStart Taq PCR Master Mix (QIAgen, Hilden, Germany), 10 pmol of each primer, 100 ng of template DNA, and distilled water up to 25 μl. Amplification program for all fragments, except the marker D3S666, consisted of denaturation at 95°C for 15 min, then 40 cycles of denaturation at 95°C for 1 min, annealing at 55°C for 1 min, and extension at 72°C for 1 min. The program was finished by 72°C incubation for 7 min. Annealing temperature for fragment D3S666 was 58°C.

Successfully amplified PCR products of the VHL gene were purified with a Montage PCR Centrifugal Filter Devices (Millipore, Billerica, MA, USA) and sequenced using a Big Dye Terminator Sequencing kit (PE/Applied Biosystems, Foster City, CA, USA). Samples were then run on an automated sequencer ABI Prism 310 (PE/Applied Biosystems) at a constant voltage of 11.3 kV for 20 min. Successfully amplified PCR products of STR markers were mixed with a size marker and run on an automated sequencer ABI Prism 310 (PE/Applied Biosystems) at a constant voltage of 15 kV for 28 min.

Ultrastructure

Formalin-fixed wet material from one case was available for ultrastructural analysis. The formalin-fixed sample was postfixed in 2% glutaraldehyde, contrasted in 1% osmium tetroxide, and embedded in epoxy resin (Durcupan-Epon). Semithin sections were cut, stained with toluidine blue, and examined by light microscopy. Thin sections from representative areas were then cut, stained with uranyl acetate and lead citrate, and examined with a Philips (Eindhoven, Holland) EM208S transmission electronic microscope.

Small pieces of paraffin-embedded tissues were obtained from additional two cases. Tissues were deparaffinized according protocol of Widéhn and Kindblom and reprocessed for ultrastructure examination [22].

Results

Clinical features

The basic clinicopathologic data of the patients are summarized in Table 3.

Four out of the five patients with RAT were men, and one patient was a woman. The age of the patients ranged

Table 1 Primers for amplification and sequencing of the VHL gene

Exon	Name	Sequence 5′ → 3′	Reference
Exon 1	VHL e1–1	CGCGAAGACTACGGAGGT	New primers
	VHL e1–2	GTCTTCTTCAGGGCCGTA	
	VHL e1–3	GAGGCAGGCGTCGAAGAG	
	VHL e1–4	GCGATTGCAGAAGATGACCT	
	VHL e1–5	GCCGAGGAGGAGATGGAG	
	VHL e1–6	CCCGTACCTCGGTAGCTGT	
	VHL e1–7	CCGTATGGCTCAACTTCGAC	
	VHL e1–8	GCTTCAGACCGTGCTATCGT	
Exon 2	VHL e2–1	ACCGGTGTGGCTCTTTAACA	New primers
	VHL e2–2	TCCTGTACTTACCACAACAACCTT	
Exon 3	VHL e3–1	GATTTGGTTTTTGCCCTTCC	Michal et al. [17]
	VHL e3–2	ACATTTGGGTGGTCTTCCAG	
	VHL e3–3	CGTCAGGTCGCTCTACGAA	
	VHL e3–4c	CCATCAAAAGCTGAGATGAAAC	

from 49 to 93 years (mean 64.6 years). None of the patients had signs of tuberous sclerosis. The female patient had adenocarcinoma of sigmoid colon diagnosed 1 year before nephrectomy for the RAT. The kidney tumor was discovered during a regular check-up oncologic examination; it remained unknown whether the renal tumor was present already at the time of abdominal surgery for the adenocarcinoma of the colon. The adenocarcinoma of the colon recurred 1 year after the nephrectomy, and the recurrence was surgically excised. Twenty-nine months after the nephrectomy, the patient died of metastatic colonic adenocarcinoma without recurrence of RAT. Of the remaining four patients, three were alive and well at 8, 9, and 12 months, and one patient was lost to follow-up.

Gross findings

The largest dimensions of RATs ranged from 2.3 to 8.5 cm (mean 4.1 cm). The renal pelvis, renal veins, and sinus were not involved by any of the tumors. Grossly, RATs were grayish or tan to light brown in color (Fig. 1a). The tumors were sharply circumscribed with a variously thick capsule.

Table 2 Primers for amplification of STR markers for LOH 3p analysis

STR marker	Sequence 5′ → 3′
D3S1317	TACAAGTTCAGTGGAGAACC
	CCTCCAGGCCATACACAGTCA
D3S1300	AGCTCACATTCTAGTCAGCCT
	GCCAATTCCCCAGATG
D3S666	CAAGGCATTAAAGTGGCCACGC
	GTTTGAACCAGTTTCCTACTGAG
D3S1768	GGTTGCTGCCAAAGATTAGA
	CACTGTGATTTGCTGTTGGA

Microcystic change was apparent in all cases. One case revealed marked cystic changes (Fig. 1b). There were no grossly apparent necroses; however, patchy hemorrhagic areas were frequent.

Microscopic findings

Histologically, all tumors had a variously thick capsule formed by a layer of bands of smooth muscle (Fig. 2). All tumors were characterized by the intimate intermixture of an epithelial component and smooth muscle tissue. The latter formed a predominant component of the tumor mass in case 3; it was prominent but not dominant in three cases and rather inconspicuous but still well developed in the remaining case 5. The epithelial tissue was represented by adenomatous structures composed of cells with small deeply basophilic nuclei, often in a linear arrangement reminding of small beads on a string (Fig. 3). The nuclei of the neoplastic cells were of equal size and small; only in case 3, there were rare cells with somewhat enlarged nuclei. Some glandular structures were more distended and contained deeply eosinophilic colloid with "moth-eaten" peripheral areas (Fig. 4). Cytologically, the nuclei of the epithelial cells in these glandular structures were irregular and manifested one to several inconspicuous nucleoli; there were many cells with variously cleaved nuclei. In a majority of the well-formed tubular or branching structures, the nuclei were in a basal position close to the basal membrane. The cytoplasm of the cells was covered by typical clear snouts, which looked like optically clear blisters and appeared as though being grafted on the luminal surface of the cells. The equal size of the secretory cells with basophilic nuclei caused by dense nuclear chromatin alienated along the basal membrane combined with the prominent apical clear snouts resulted in a focal

Table 3 Clinical features

	Sex/age	Side	Size	Follow-up
Case 1	M/58	Right	2.3×2.3×1.8 cm	9 months AW
Case 2	M/49	Left	Diameter 4.6 cm	1 year AW
Case 3	M/93	Right	8.5×8×3 cm	8 months AW, then LOF
Case 4	F/73	Left	Diameter 2.5 cm	29 months DWT[a]
Case 5	M/50	Right	Diameter 2.5 cm	LOF

F female, *M* male, *AW* alive and well, *LOF* loss on follow-up, *DWT* died without tumor
[a] Patient died of metastatic disease of colonic adenocarcinoma

but characteristic appearance of some adenomatous structures reminiscent of a "shark's smile" (Fig. 5). Focally, the lumina of the tubules were collapsed, which resulted in a solid growth pattern in these areas (Fig. 6). In other places, the tumors showed gradual (Fig. 7a) or sharp (Fig. 7b) transitions to areas with a clear cell change. Focally, these clear cell adenomatous structures grew interspersed among the adenomatous areas with basophilic nuclei (Fig. 7c).

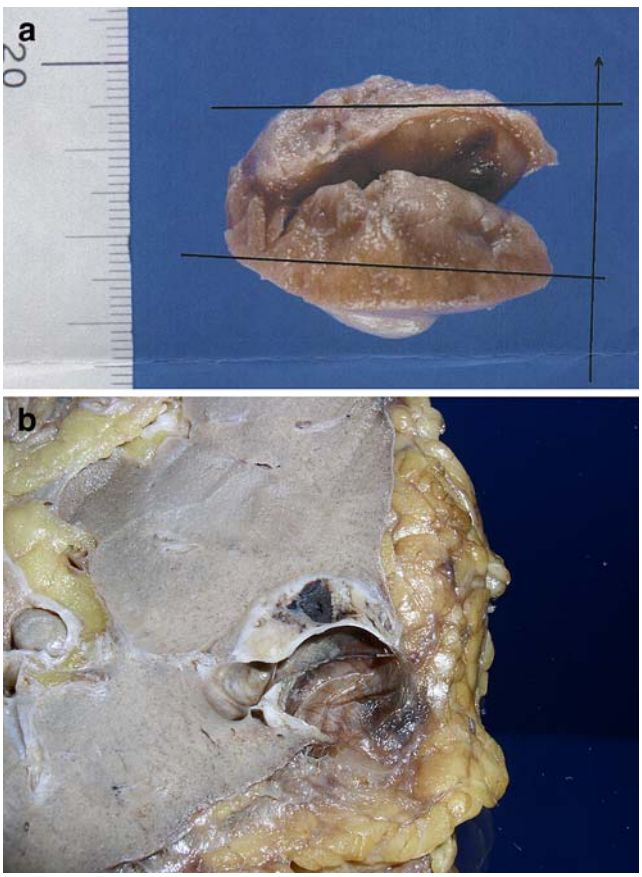

Fig. 1 The tumor is grayish or tan to light brown in color (**a**). Marked cystic changes as evident here were detected in one case (**b**)

These clear cell areas bore some resemblance to conventional clear cell carcinomas, grade 1 according to Fuhrman. In these clear cell areas, the nuclei of the neoplastic cells often lost their basal positions, and the clear snouts were much less conspicuous or entirely absent (Fig. 7d).

There was a remarkable relationship between a capillary network and the epithelial component in the sense that every single adenomatous structure of RAT, whether in the solid, tubular, or clear cell areas, was associated with a capillary network, with the capillaries intimately surrounding the circumference of the basal membrane of all adenomatous structures (Fig. 8). In those areas, in which the adenomatous structures branched and formed micropapillary projections, these capillaries formed their only supportive stroma. This capillary vasculature was often poorly recognizable in hematoxylin and eosin stained slides but was apparent with immunohistochemical stains for endothelial markers or pericytes (see below). No such capillary network was observed in ten randomly selected cases of the clear cell renal carcinoma and one case of clear cell renal carcinoma associated with leiomyomatous stroma from our files.

There were no atypias or mitoses apparent in the tumors. The stromal muscular component formed eosinophilic bundles and strands of leiomyomatous tissue composed of elongated cells with cigar-shaped nuclei when cut along the long axis. The leiomyomatous stroma grew inside the tumors among the epithelial component, and in addition, variously thick bands of leiomyomatous tissue encircled the whole tumors, forming thus a continuous capsule (Fig. 1). Focally, the leiomyomatous tissue formed abortive vessels with formations of incomplete walls with lumina, which usually lacked elastic layer, or the elastic stains showed a small amount of thin disorganized elastic fibers. The leiomyomatous tissue often entirely encased patches of adenomatous structures (Fig. 9a, b), or it formed only small leiomyomatous islands within the epithelial component (Fig. 9c). The leiomyomatous

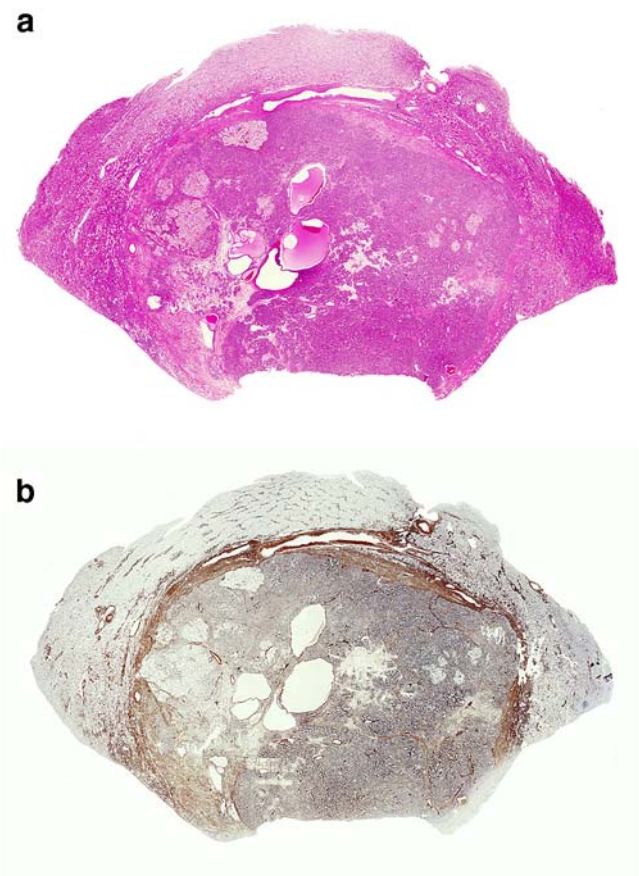

Fig. 2 **a** The tumor is surrounded by a variously thick capsule formed by a layer of bands of smooth muscle incorporating abortive angiomatous structures (hematoxylin and eosin stain). The same slide with smooth muscle actin antibody staining (**b**)

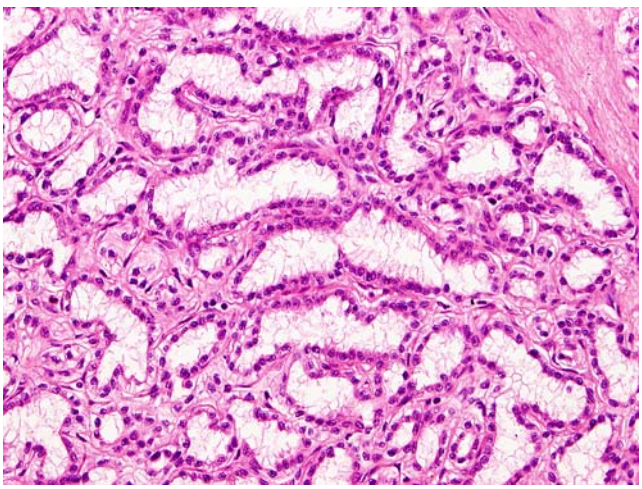

Fig. 3 The epithelial component is represented by adenomatous structures composed of cells with small deeply basophilic nuclei often in a linear arrangement reminding small beads on a string. The cytoplasm of the cells manifest clear snouts appearing like optically clear blisters at the apical surface (hematoxylin and eosin stain)

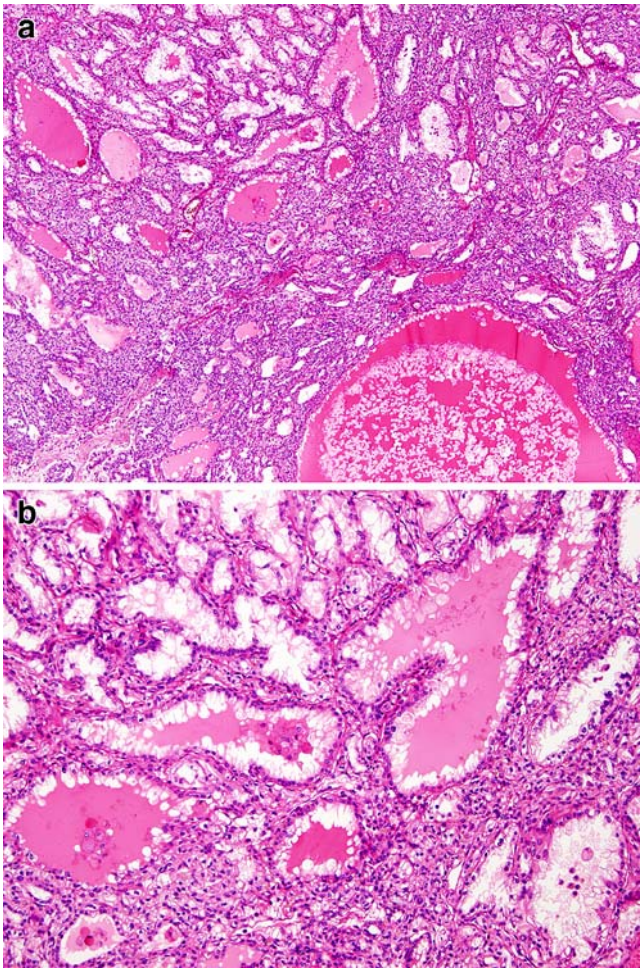

Fig. 4 Some glandular structures are distended and contain deeply eosinophilic colloid, which has a "moth-eaten" appearance at the periphery (**a**, **b**) (hematoxylin and eosin stain)

stroma frequently underwent a myxoid or hyaline change. Metaplastic ossification was noted in case 3. Adipose tissue and other tissues such as, for example, thick blood vessels devoid of elastic layer with the typical arrangement of the myoid stromal cells perpendicularly to the lumina of these vessels, that may be seen in renal angiomyolipoma (PECOMA), were not detected in our cases of RAT. Multinucleated cell granulomas or hyaline globules, which are sometimes seen in conventional clear renal cell carcinomas [8–10], were not observed in any of the tumors in our series.

Histochemical findings

Mucicarmine stain was negative throughout the tumors. Glycogen and periodic acid–Schiff (PAS) stainings showed various amounts of glycogen (digested with PAS-diastase) in the adenomatous structures including the clear snouts (Fig. 10), as the amount of glycogen in tissues depends on the time of fixation in formol.

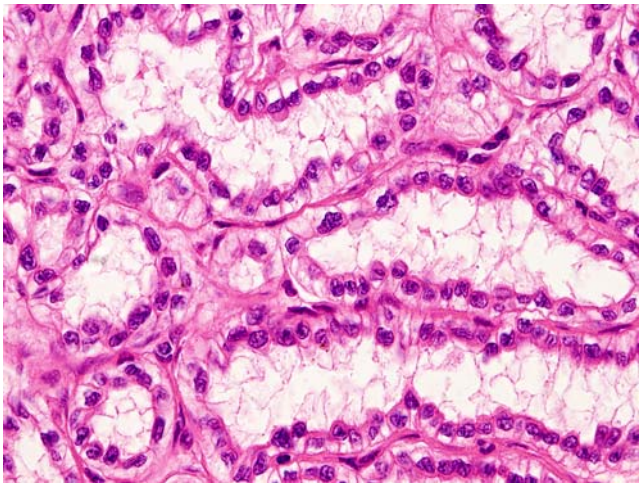

Fig. 5 The equal size of the secretory cells with basophilic nuclei alienated along the basal membrane together with prominent apical clear snouts producing a similarity to a "shark's smile" (hematoxylin and eosin stain)

Immunohistochemical findings

Immunohistochemically, the epithelial component of tumors was positive with all antibodies to cytokeratins AE1-AE3, CAM 5.2, CK 7, and CK 20. While CK7 always strongly stained all epithelial tissues, the reaction with CK20 was only weak and often focal. In addition to cytokeratin positivity, the epithelial component was strongly positive for EMA and vimentin in all cases and, unexpectedly, for tyrosinase in one case. CD10 reacted negatively in four tumors, while in the remaining case, there were rare epithelial cells that stained weakly for this marker. The epithelial component was negative with all the rest of the tested antibodies including HMB45 and Melan A. Carbonic anhydrase IX antibody reacted in the epithelial component positively and negatively in the leiomyomatous component in all five cases.

The stromal leiomyomatous component reacted positively and strongly with antibodies to caldesmon, calponin, vimentin, and smooth muscle actin in all cases, whereas immunostaining for desmin was patchy and weak. The leiomyomatous stromal component was negative with all the rest of the tested antibodies, including the melanocytic markers (HMB45, Melan A, and tyrosinase).

The endothelial cells of the capillary network were positive for FVIII and CD34 in all cases. Conspicuous positivity of the pericytic network was apparent with CD31 or smooth muscle actin stains, highlighting the intimate relationship of the capillary network with the glandular structures (Fig. 11). The proliferative index (MIB1) was generally very low, and always less than 1% of the cells reacted positively.

Electron microscopic findings

Ultrastructurally, the epithelial cells had a well-formed cytoplasmic membrane and were attached by desmosomes. The cytoplasm was rich in organelles (Golgi apparatus, lysosomes, mitochondria, and smooth endoplasmic reticulum). Nuclei were round with irregular clefts and inconspicuous nucleoli. The cytoplasm of the tumor cells formed edematous organelle-poor clear cytoplasmic snouts corresponding with the structures visible at the light microscopic level. Microvilli were present between snouts on the apical surface of epithelial cells.

The leiomyomatous cells had convoluted and intended nuclei and inconspicuous nucleoli; the cytoplasm contained well-developed endoplasmic reticulum and intermediate filaments. The ultrastructural features of the leiomyomatous component were thus identical to other benign leiomyomas.

No melanosomes (or similar structures) were detected in both cellular populations. There were no neurosecretory granules seen in the cytoplasm of the cells.

Analysis of the VHL gene mutation and 3p LOH

Molecular genetic findings are summarized in Table 4. Case no. 5 was excluded from the further analysis because of low quality of DNA. In the remaining four cases, no mutation of coding sequence of the VHL gene was found in epithelial and smooth muscle cell components of the tumors. PCR for LOH analysis of chromosome region 3p did not reveal any copy number changes in all successfully analyzed samples.

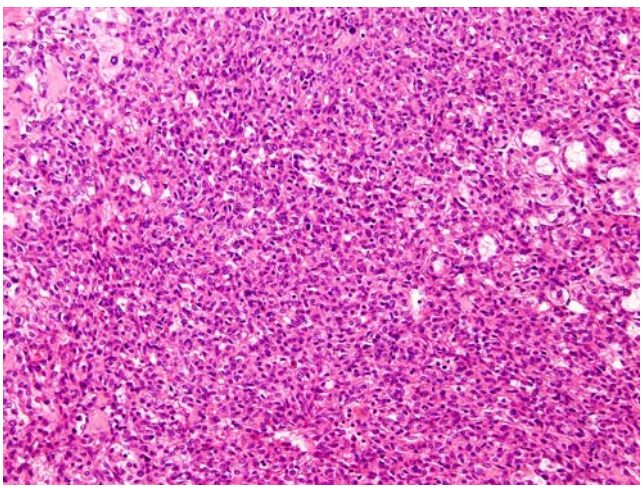

Fig. 6 Focal collapse of the lumina of the tubules resulting in a solid growth pattern in these areas (hematoxylin and eosin stain)

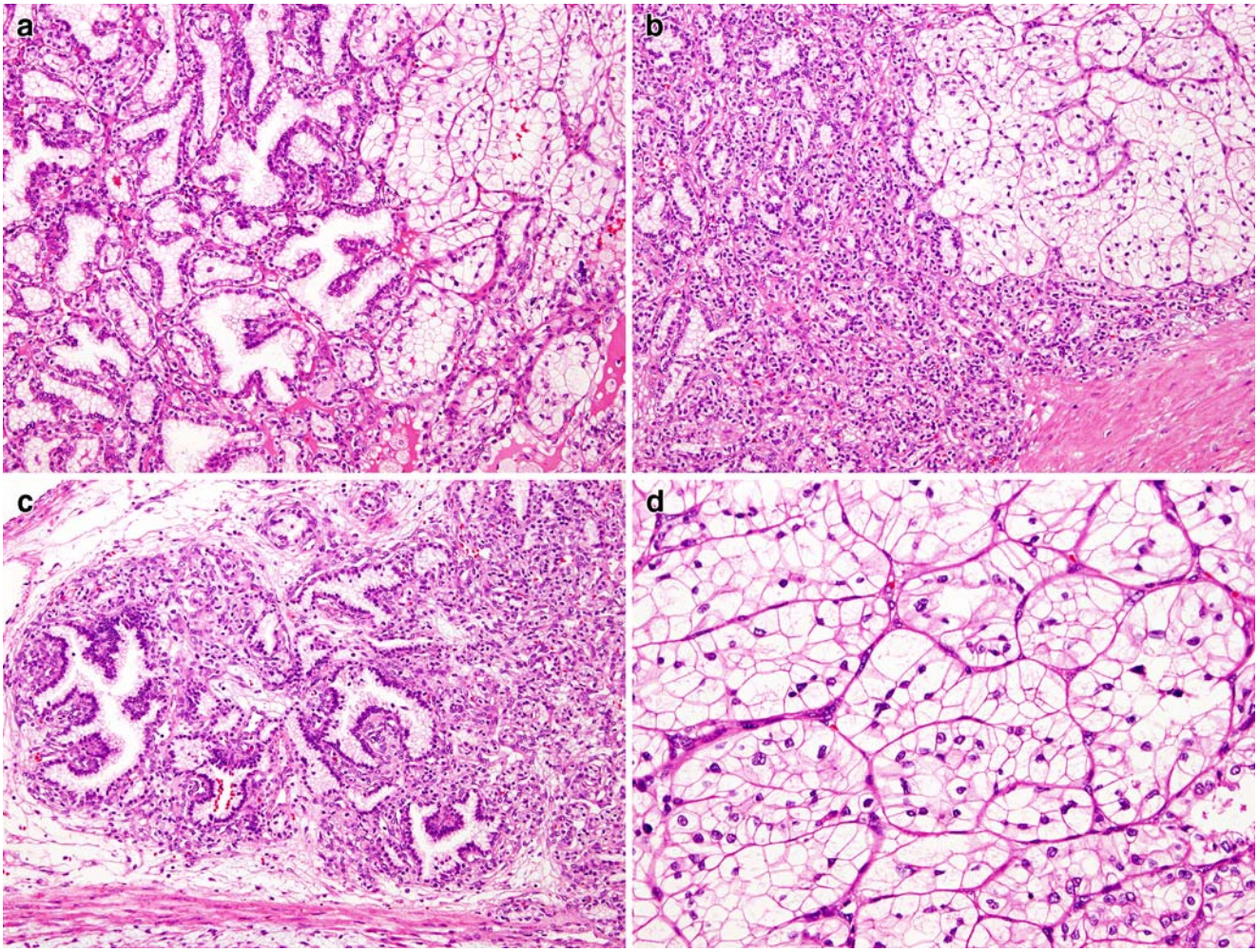

Fig. 7 Areas with a clear cell change. These transitions to clear cell areas were either gradual (**a**) or sharp (**b**). In this area, clear cell adenomatous structures are interspersed among adenomatous areas with basophilic nuclei (**c**). In the clear cell areas, the nuclei of the neoplastic cells often lost their basal positions and the clear snouts were absent (**d**) (hematoxylin and eosin stain)

Discussion

There are two types of renal tumors that manifest the characteristic epithelial and stromal components that are mixed epithelial and stromal tumors of the kidney (MESTK) and RAT. One of these two tumors, MESTK, is a recently defined entity [1, 14–16, 20, 23] which, together with cystic partially differentiated nephroblastomas and mesoblastic nephromas, used to be lumped in the past under the diagnostic term "cystic nephroma" [13]. RAT, first described by Michal et al. in 2000, is characterized by tubular to branching adenomatous structures endowed with apical clear snouts and surrounded by a capillary network and variously copious, HMB45-negative, leiomyomatous stroma focally forming abortive vascular structures [18]. We consider tyrosinase immunohistochemical positivity in the epithelial component of one case of RAT in this series to be an aberrant, however, interesting feature of the lesion.

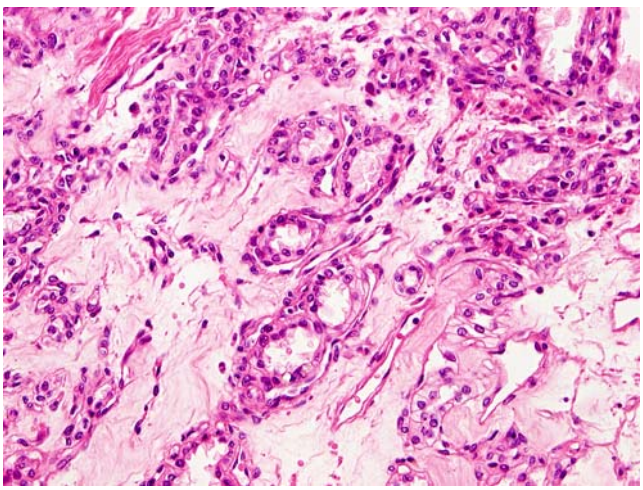

Fig. 8 Capillaries intimately surrounding the circumference of the basal membranes of adenomatous structures (hematoxylin and eosin stain)

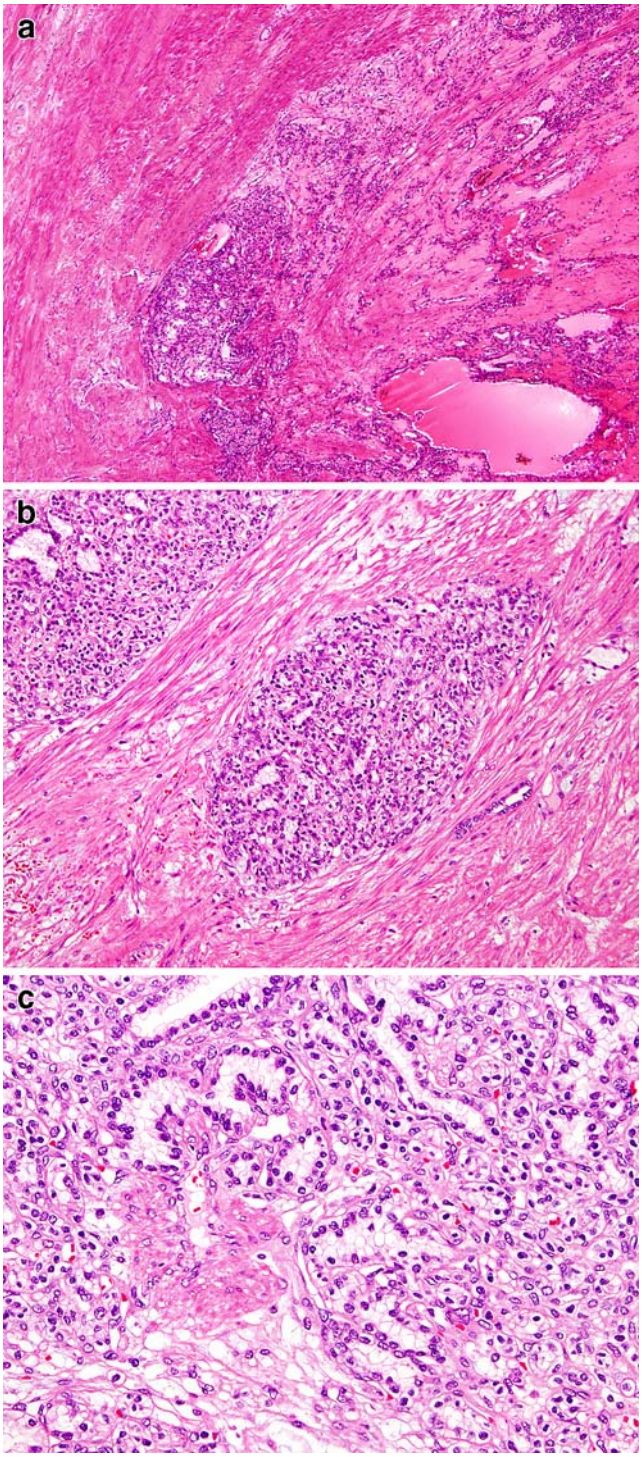

Fig. 9 Leiomyomatous stroma encasing patches of adenomatous structures (**a**, **b**) or forming only small leiomyomatous islands within the epithelial component (**c**) (hematoxylin and eosin stain)

The amount of leiomyomatous stroma in RAT is highly variable. It may range from 10% to 70% of the whole tumor mass, it forms abortive vascular structures, and notably, it lacks a lipomatous component. In our experience and according to the publication by Kuhn et al. [12], this

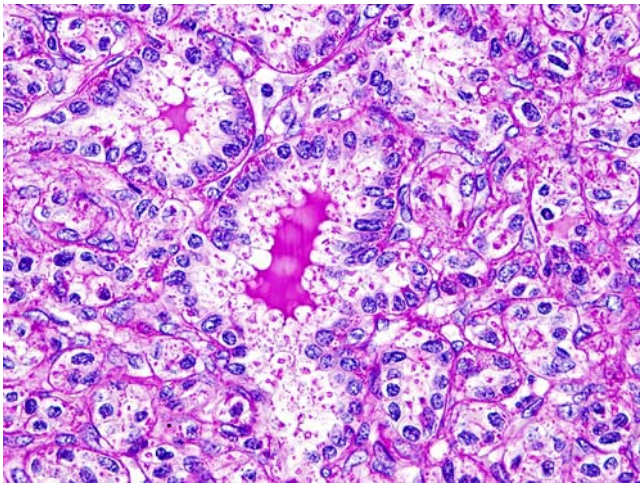

Fig. 10 PAS staining: note glycogen in glandular structures including clear snouts (PAS staining)

angioleiomyomatous stroma is not entirely specific for RAT, as it can rarely be seen in conventional renal clear cell carcinomas.

The epithelial component of RAT is unique to this tumor. The equal size of the secretory cells with basophilic nuclei lined in the basal positions and the apical clear snouts are responsible for the typical appearance of the glandular structures reminiscent of a "shark smile." The other typical feature is the fine and delicate network of capillaries surrounding every single neoplastic tubule best visible on immunohistochemical slides stained, for example, with CD31 or smooth muscle actin (Fig. 11). In our experience, the degree of this capillary networking in RAT surpasses vasculature of the renal clear cell carcinomas.

The association of the above-described epithelial component of RAT with the capillary network is also unique and can serve as a diagnostic clue. This can be illustrated

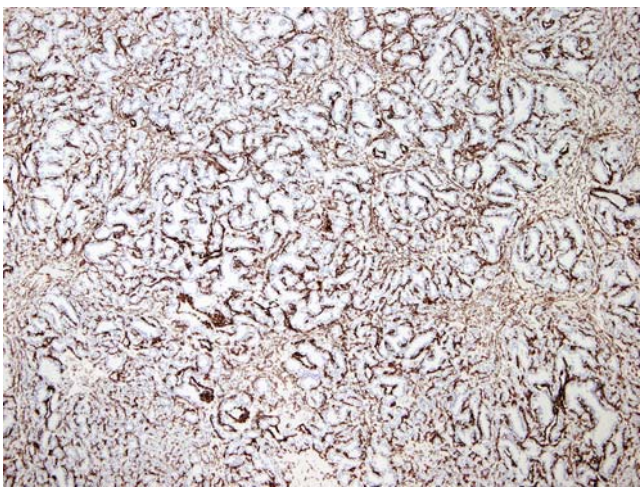

Fig. 11 Conspicuous positivity of a pericytic network (immunohistochemistry with smooth muscle actin antibody)

Table 4 Molecular genetic findings

Number of specimen	D3S1317	D3S1300	D3S666	D3S1768	VHL mutation status
No 1	Negative	NI	Negative	NA	wt/wt
No 2	Negative	Negative	Negative	Negative	wt/wt
No 3	Negative	NA	NA	NA	wt/wt
No 4	Negative	Negative	NI	Negative	wt/wt
No 5	NA	NA	NA	NA	NA

NA non-analyzable, *NI* non-informative, *wt* wild type

by case 5 of this series, from which we originally received only one tissue block, wherein there were present only glandular structures with apical snouts forming the "shark's smile" and the garland-like capillaries endowing every single tubule typical of RAT, with nearly no angioleiomyomatous stroma. Being sure that the tumor represented RAT, we asked the referring pathologist for additional tissue blocks, and tissue sections from three of the four additional blocks evidenced the typical angioleiomyomatous stroma, although in this particular case, it represented a minor component of the neoplasm, forming approximately 10% of the whole tumor mass.

There are several cases of renal cell tumors having glandular component and leiomyomatous stroma published in the literature. Honey et al. published a case of a bilateral metachronous renal cell carcinoma in an 18-year-old female patient with clinical evidence of tuberous sclerosis [11]. Beside the renal cell carcinoma, they described "an abnormally large quantity of smooth muscle, not apparently related to the pelvis or calyces, nor to blood vessels". Unfortunately, the authors provided neither description nor illustration of the relationship between these bundles and the renal cell carcinoma. Their patient was alive and well 4 years later [11]. Govaerts et al. reported a case of a 54-year-old woman with no evidence of tuberous sclerosis, which had a conventional renal cell carcinoma embedded within a mesenchymal lesion thought to be of a hamartomatous nature and called by the authors as angiofibroma [7]. No follow-up information was provided. Canzonieri et al. reported a case of a 54-year-old woman patient without signs of tuberous sclerosis with three anatomically separated tumors in the same kidney. One was a typical angiomyolipoma, whereas the other two were renal cell carcinomas with a "fibroleiomuscular" component. The patient was alive and well 6 months later [5]. The largest series of these tumors was described by Kuhn et al., who described five cases of renal cell carcinomas with an angioleiomyoma-like proliferation [12]. Their patients included four women and one man aged 37–75 years. One patient died 3 years later with bone metastases, and no follow-up was provided for the remaining four patients [12]. Having reviewed figures of all above cited papers, we think that none of them described a tumor similar to the RAT. Specifically, no reported case reveals the typical snouts in the apical parts of the glandular structures, and none of the paper shows the basophilic nuclei alienated along the basal membrane producing the typical "shark' smile" arrangement. In addition, by the generosity of the authors, we were able to review a slide of the case published by Canzonieri et al. [5]. The stroma in their case seems to be unique, as it was much more fibrous with a "desmoplastic quality," much different from the "angioleiomyomatous" stroma in our cases or those published by Kuhn et al. [12].

RAT further differs in one clinical aspect from the renal cell tumors associated with angioleiomyomatous stroma published so far [5, 7, 11, 12]. While published cases of the latter shows a female predominance (seven out of eight patients) [5, 7, 11, 12], four out of the five patients with RAT in our series were males.

We are, however, aware of one possible case of RAT published recently. On the page 187, the authors of AFIP Fascicle 1 of "The Atlas of Tumor Pathology of Tumors of the Kidney, Bladder and Related Structures" show a putative mixed epithelial and stromal tumor of the kidney. Their Fig. 2-175 illustrates a lesion with branching adenomatous structures composed of basophilic nuclei alienated close to the basal membrane and having focally the same apical snouts as those in RAT. In addition, the rich capillary network rimming the adenomatous structures in their case seems to be identical to that seen in RAT [19]. We have never seen such an epithelial component in more than 40 cases of MESTKs in our files. Although no stroma is illustrated in the above figure of "MESTK" [19], we suppose that the stroma of the tumor must have been most probably angioleiomyomatous, being thus typical of RAT, rather than ovarian type stroma characteristic of MESTK [1, 16].

In the differential diagnosis, RAT should be distinguished from MESTK, angiomyolipomas, and clear renal cell carcinomas with angioleiomyomatous stroma. MESTK, in contrast to RAT, has a stroma, which is identical to ovarian stroma. In our experience with more than 40 cases of MESTK [14–16, 20, 23], pure leiomyomatous differen-

tiation in the ovarian stroma of MESTK is a rare finding, and if present, it looks as a focal metaplasia usually arising on the background of spindle cell ovarian stroma. MESTK further differs from RAT by the frequent occurrence of various Müllerian epithelial type differentiations including those of Fallopian tubal, endometrial, squamous ones [16] and even a variety with intestinal mucinous glandular epithelium revealing typical Paneth cells [23]. This mixture of various types of these Müllerian epithelia can often be seen within a single tumor mass in MESTK [16]. In addition, the ovarian stroma of MESTK can infrequently reveal fibrous areas indistinguishable from corpora albicantia [15], and rarely, there may even be lutein stromal cells identical to those seen in the ovaries [4]. Such epithelial and stromal features are never seen in RATs.

Angiomyolipomas differ from RAT by the presence of fat tissue and thick blood vessels devoid of elastic layer with the typical arrangement of the myoid stromal cells running perpendicularly to the lumina of these vessels. Most angiomyolipomas are associated with tuberous sclerosis complex, an association not observed with RATs. In addition, angiomyolipomas are usually devoid of glandular epithelial component, the exception being occasional renal cysts occurring especially in tuberous sclerosis patients. Immunohistochemically, angioleiomyomas react with melanocytic markers, especially with HMB45 practically in all cases. None of the melanocytic markers tested positive in the angioleiomyomatous stroma of RATs.

We further think that RAT differs from conventional clear cell carcinomas, which can rarely be associated with an identical leiomyomatous stroma occasionally forming abortive vascular structures. However, the epithelial component of RAT is entirely different from that in conventional clear cell carcinomas and is very distinctive, with basophilic nuclei arranged in typical rows and apical clear snouts resulting in the typical focal appearance of glandular structures to a "shark's smile." We have not encountered such an epithelial component in any of the 14,000 renal cell tumors in the Pilsen registry for kidney tumors. In addition, the VHL gene mutations, so common of conventional clear cell carcinomas, have not been found in any of the five cases of RAT. Immunohistochemically, CD10, which is a reliable marker of conventional clear cell carcinomas [3], was entirely negative in RAT, with the exception of one case wherein a small percentage of the neoplastic cells showed positive immunoreaction. Carbonic anhydrase IX cannot help in distinguishing RAT from clear cell renal carcinomas as both are positive. This antibody is, in our experience, rather nonspecific. Besides being reported to be present in many extrarenal neoplasms [2], it is seen in occasional cases of the papillary renal carcinoma [21]. In addition, it was reported to be positive in all cases recently reported clear cell papillary renal cell carcinomas, which the authors considered to be a distinct histopathologic and molecular genetic entity [6]. The immunopositivity of carbonic anhydrase IX of clear cell renal carcinoma, clear cell papillary renal cell carcinoma [21], and RAT is, however, interesting, because all these three tumor types reveal abundant clear cell cytoplasm within the epithelial component.

The last issue to discuss is the biological significance of RAT. In the original paper describing the tumor in 2000, we called it "benign renal angiomyoadenomatous tumor" [18]. In all four patients with RAT of the current series for whom the follow-up was available, the tumor behaved in a benign fashion. Histologically, all tumors looked benign. In spite of these facts, we contemporary removed the adjective "benign" from the name of the neoplasm until more cases with a long follow-up are available to meaningfully estimate their clinical behavior.

In summary, we describe five cases of a distinctive entity which we named as renal angiomyoadenomatous tumor. RAT was composed of typical epithelial component never seen in other tumors in our registry and angioleiomyomatous HMB45 negative stroma, which formed focally abortive vascular structures. Most cases of RATs in our series occurred in adult to old men (four of five), behaved in a benign fashion, and were not associated with tuberous sclerosis complex.

Acknowledgment The authors are grateful to Dr. Petr Mukensnabl for preparing excellent microscopical figures. This study was supported by grant IGA 9722-4

References

1. Adsay NV, Eble JN, Srigley JR, Jones EC, Grignon DJ (2000) Mixed epithelial and stromal tumor of the kidney. Am J Surg Pathol 24:958–970
2. Al-Ahmadie HA, Alden D, Qin L-X, Olgac S, Fine SW, Gopalan A, Russo P, Motzer RJ, Reuter VE, Tickoo ST (2008) Carbonic anhydrase IX expression in clear cel renal cell carcinoma. An immunohistochemical study comparing 2 antibodies. Am J Surg Pathol 32:377–382
3. Avery AK, Beckstead J, Renshaw AA, Corless CL (2000) Use of antibodies to RCC and CD10 in the differential diagnosis of renal neoplasms. Am J Surg Pathol 24:203–210
4. Buritica C, Serrano M, Zuluaga A, Arrabal M, Regauer S, Nogales FF (2007) Mixed epithelial and stromal tumour of the kidney with luteinised ovarian stroma. J Clin Pathol 60:98–100
5. Canzonieri V, Volpe R, Gloghini A, Carbone A, Merlo A (1993) Mixed renal tumor with carcinomatous and fibroleiomyomatous components, associated with angiomyolipoma in the same kidney. Pathol Res Pract 189:951–956
6. Gobbo S, Eble JN, Grignon DJ, Martignoni G, MacLennan GT, Shah RB, Zhang S, Brunelli M, Ceng L (2008) Clear cell papillary renal cell carcinoma. A distinct histopathologic and molecular genetic entity. Am J Surg Pathol 32:1239–1245
7. Govaerts JJL, van Gooswilligen JC, Vooys GP, Ramaekers FC, Herman CJ, Debruyne FM (1987) Renal hamartoma associated with renal cell (Grawitz) tumor. Eur Urol 13:276–280

8. Hes O, Michal M, Šulc M, Kočová L, Hora M, Rousarová M (1998) Glassy hyaline globules in granular cell carcinoma, chromophobe cell carcinoma and oncocytoma renal tumors. Anna Diagn Pathol 2:12–18
9. Hes O, Benákova K, Vaněček T, Šíma R, Michal M (2005) Clear cell type of renal cell carcinoma with numerous hyaline globules: A diagnostic pitfall. Pathol Intern 55:150–154
10. Hes O, Hora M, Vaněček T, Šulc M, Havlíček F, Michal M (2003) Conventional renal cell carcinoma with granulomatous reaction. A report of three cases. Virchows Archiv 443:220–221
11. Honey RJ, Honey RM (1977) Tuberous sclerosis and bilateral renal carcinoma. Br J Urol 49:441–446
12. Kuhn E, De Anda J, Manoni S, Netto G, Rosai J (2006) Renal cell carcinoma associated with prominent angioleiomyoma-like proliferation. Report of 5 cases and review of the literature. Am J Surg Pathol 30:1372–1381
13. Madewell JE, Goldman SM, Davis CJ, Hartman DS, Feigin DS, Lichtenstein JE (1983) Multilocular cystic nephroma. A radiographic-pathologic correlation of 58 patients. Radiology 146:309–321
14. Michal M, Syrůček M (1998) Benign mixed epithelial and stromal tumour of the kidney. Pathol Res Pract 194:445–448
15. Michal M (2000) Benign mixed epithelial and stromal tumor of the kidney. Pathol Res Pract 196:275–276
16. Michal M, Hes O, Bisceglia M, Simpson RW, Spagnolo DV, Parma A, Boudová L, Zachoval R, Suster S (2004) Mixed epithelial and stromal tumors of the kidney. A report of 22 cases. Virchows Archiv 445:359–367
17. Michal M, Vaněček T, Šíma R, Mukenšnabl P, Boudová L, Broučková M (2004) Primary capillary hemangioblastoma of peripheral soft tissues. Am J Surg Pathol 28:962–966
18. Michal M, Hes O, Havlíček F (2000) Benign renal angiomyoadenomatous tumor: A previously unreported renal tumor. Annals Diagn Pathol 4:311–315
19. Murphy WM, Grignon DJ, Perlman EJ (2004) AFIP atlas of tumor pathology (fourth series). Tumors of the kidney, bladder, and related urinary structures. American Registry of Pathology, Washington DC (Figure 2–175, 187 pp)
20. Švec A, Hes O, Michal M, Zachoval R (2001) Malignant mixed epithelial and stromal tumor of the kidney. Virchows Arch 439:700–702
21. Tu JJ, Chen Y-T, Hyjek E, Tickoo SK (2005) Carbonic anhydrase IX as a highly sensitive and specific marker of clear cell renal cell carcinoma: a comparative immunohistochemical study using a panel of commonly utilized antibodies in the differential diagnosis of renal cell tumors. Modern Pathol 18(suppl 1):169A
22. Widéhn S, Kindblom LG (1988) A rapid and simple method for electron microscopy of paraffin-embedded tissue. Ultrastruct Pathol 12:131–136
23. Yang Y, Hes O, Lanjing Z, Min L, Jian L, Min L, Hua W, Jie Z, Michal M (2005) Mixed epithelial and stromal tumor of the kidney with intestinal differentiation. A case report. Virchows Archiv 447:669–671

Virchows Arch (2009) 454:101–105
DOI 10.1007/s00428-008-0698-2

ORIGINAL ARTICLE

Can CD10 be used as a diagnostic marker in thyroid pathology?

Gülçin Yegen · Mehmet Akif Demir · Yeşim Ertan · Olcay Ak Nalbant · Müge Tunçyürek

Received: 19 February 2008 / Revised: 4 October 2008 / Accepted: 29 October 2008 / Published online: 25 November 2008

Abstract CD10–common acute lymphoblastic leukemia antigen is a membrane-bound zinc metalloproteinase that is expressed by different hematopoietic cell types at unique stages of lymphoid and myeloid differentiation. It was reported to be expressed in various nonlymphoid cells and tissue, as well as in various types of neoplasms. Recently, it has been found to be useful in the differential diagnosis of benign and malignant follicular-patterned lesions of the thyroid. In the present study, we evaluated the staining pattern of CD10 in various thyroid lesions, including 14 benign and 61 malignant cases, as well as in adjacent thyroid tissue. CD10 was negative in normal thyroid tissue, adenomatous nodules, minimally invasive follicular carcinoma, and well-differentiated carcinoma. It was expressed in nine of 14 (64.2%) conventional papillary carcinomas, four of 24 (16.6%) follicular variant of papillary carcinomas, three of six (50%) papillary microcarcinomas, one of nine (11.1%) widely invasive follicular carcinomas, and three of ten (30%) follicular adenomas. In contrast to results of previous studies, CD10 is not useful in the classification of thyroid follicular lesions as benign or malignant, but it shows strong positivity in conventional papillary carcinoma.

Keywords Thyroid · Differential diagnosis · CD10–CALLA

G. Yegen
Department of Pathology, Celal Bayar University,
Manisa, Turkey

M. A. Demir
Pathology Department,
Celal Bayar University School of Medicine,
Manisa, Turkey

Y. Ertan · M. Tunçyürek
Department of Pathology, Ege University,
İzmir, Turkey

O. A. Nalbant
Department of Pathology,
The Ministry of Health Manisa State Hospital,
Manisa, Turkey

Present address:
M. A. Demir (✉)
Pathology and Cytology Department,
Sahlgrenska University Hospital,
Gula Straket 8,
41345 Gothenburg, Sweden
e-mail: makifdemirtr@yahoo.com

Introduction

Follicular-patterned lesions of the thyroid encompassing four entities—follicular adenoma, follicular carcinoma, follicular variant of papillary carcinoma, and even nonneoplastic nodules of goiters (adenomatous nodules)—may pose a diagnostic challenge even to the most experienced pathologists [1–6]. There are two different problems in the diagnosis of follicular-patterned lesions: the distinction of minimally invasive follicular carcinoma from follicular adenoma or adenomatous nodule and the confident identification of follicular carcinoma [6–8]. The standard basis for the former differential is the presence of capsular and/or vascular invasion in follicular carcinoma, while nuclear features such as nuclear overlapping, intranuclear pseudoinclusions, optically clear nuclei, and grooves have been emphasized as the major distinguishing features of the follicular variant of papillary carcinoma [6, 8, 9]. Nuclear features encountered in follicular nodules often show some, but not all, of the nuclear features of papillary carcinoma, making a clear-cut diagnosis difficult. Furthermore, decision of vascular or capsular invasion is often difficult even by serial sections, when the invasion is minimal [7, 10]. In an

effort to overcome this problem, several markers of malignancy have been investigated in both surgical and fine-needle aspiration (FNA) cytology specimens, but they all present some advantages and some limitations [6, 11, 12].

CD10 is a membrane-bound zinc metalloproteinase that was originally used as a marker for common acute lymphoblastic leukemia antigen (CALLA) [13, 14]. Recently, it has been found to be reactive in various nonlymphoid cells and tissue and in various types of neoplasms [13, 14, 17]. In thyroid pathology, it was identified in thyroid marginal zone non-Hodgkin lymphoma [18]. It was also recently reported to be valuable in the classification of thyroid follicular lesions into benign and malignant groups [17].

In the present study, we aimed to assess whether CD10 can be used as a malignancy marker in thyroid pathology.

Materials and methods

Tissue specimens

Hematoxylin and eosin sections of 75 cases from the Pathology Departments of Celal Bayar University, Ege University, and the Ministry of Health Manisa State Hospital, from 1997 to 2005, were evaluated. All tumors were classified on the basis of World Health Organization histological classification by two independent investigators [9]. For confident diagnosis, immunohistochemistry with CD34 and thyroglobulin was performed. Cases included 10 follicular adenomas, 7 minimally invasive follicular carcinomas, 9 widely invasive follicular carcinomas, 24 follicular variant of papillary carcinomas, 14 conventional papillary carcinomas, 6 papillary microcarcinomas (two with follicular pattern and the remainder with classical papillary pattern), 1 well-differentiated carcinoma, and 4 adenomatous nodules. Eighteen cases had accompanying lymphocytic thyroiditis. One paraffin block with the most representative tumoral area and including adjacent thyroid tissue wherever possible was selected for immunohistochemical study.

Immunohistochemistry

Immunohistochemistry was performed on formalin-fixed 5-μm-thick paraffin-embedded tissue sections using the streptavidin–biotin complex method (Lab Vision Corp.) with monoclonal mouse antibody against human CD10/CALLA Ab-2 (Neomarkers, MS-728-R7/60-min incubation). Prior to primary antibody, sections were pretreated in a microwave for 6×5 min in 10 mmol/L citrate buffer solution (pH 6.0). Immune complexes were visualized by diaminobenzidine precipitation. Slides were counterstained with Mayer's hematoxylin and mounted.

Tonsil was used as the positive control and negative controls were obtained by omitting the primary antibody.

Immunohistochemical evaluation

All slides were evaluated by two independent investigators who were blinded with respect to the histological diagnosis. The cells were regarded as positive when immunoreactivity was clearly observed in the cytoplasm and cell membrane. Immunoreactivity was graded as 0 (negative) when less than 10% of the lesion was positive, 1 (weak) when the positivity was restricted to 10–49% of the lesion, and 2 (strong) for staining in more than 50% of the lesion, as previously reported [12].

Statistical analysis

Sensitivity, specificity, and diagnostic accuracy were assessed. Sensitivity was defined as true positive/(true positive+false negative) and specificity as true negative/(true negative+false positive). Diagnostic accuracy was defined as (frequency×sensitivity)+(1−frequency×specificity). The frequency was determined by calculating the ratio of malignant cases to all cases.

Results

The results of immunohistochemical examination are summarized in Table 1. No reactivity with CD10 was determined in adjacent thyroid tissue (n=75), adenomatous nodules (n=4), minimally invasive follicular carcinomas (n=7), or well-differentiated carcinomas (n=1). Cases with accompanying lymphocytic thyroiditis showed positivity in germinal centers of lymphoid follicles but not in follicular cell cytoplasm or cell membrane of thyroid

Table 1 Immunoreactivity of CD10 in each diagnostic category

Diagnosis	Total case number	CD10 immunostaining *n* (%)		
		Weak	Strong	Negative
Conventional PC	14	1 (7.1)	8 (57.1)	5 (35.7)
Follicular variant of PC	24	2 (8.3)	2 (8.3)	20 (83.3)
Papillary microcarcinoma	6	0	3 (50)	3 (50)
Minimally invasive FC	7	0	0	7 (100)
Widely invasive FC	9	0	1 (11.1)	8 (88.8)
Well-differentiated carcinoma	1	0	0	1 (100)
Follicular adenoma	10	2 (20)	1 (10)	7 (70)
Adenomatous nodule	4	0	0	4 (100)

PC papillary carcinoma, *FC* follicular carcinoma

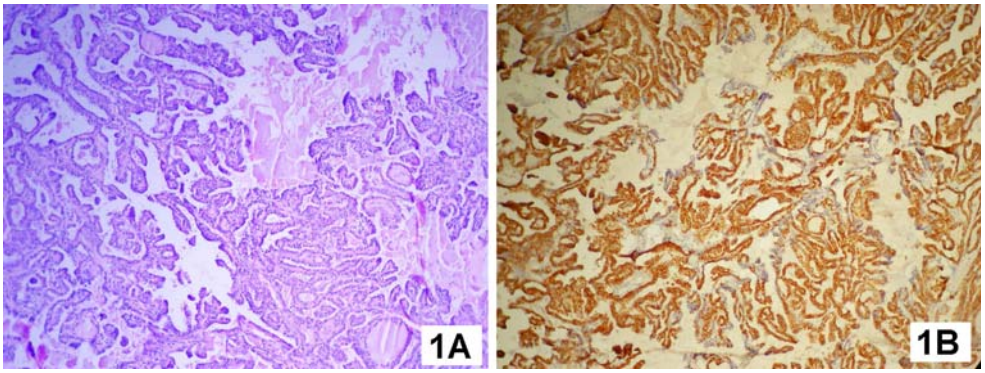

Fig. 1 **a** Conventional papillary carcinoma with papillary pattern and typical nuclear features. **b** Strong positivity of CD10 in conventional papillary carcinoma

follicles. On the other hand, CD10 staining was identified in nine of 14 (64.2%) conventional papillary carcinomas, four of 24 (16.6%) follicular variant of papillary carcinomas, one of nine (11.1%) widely invasive follicular carcinomas, three of six (50%) papillary microcarcinomas, and three of ten (30%) follicular adenomas. Papillary microcarcinomas that were positive with CD10 all showed classical papillary pattern while two of the three negative cases showed follicular pattern. CD10 was expressed strongly in eight of nine positive-stained conventional papillary carcinomas (Fig. 1a, b). Percentage of positive-stained cases and staining intensity were greater in conventional papillary carcinomas than in follicular variant of papillary carcinomas, widely invasive follicular carcinomas (Fig. 2a, b), and follicular adenomas (Fig. 3a, b).

Sensitivity, specificity, and diagnostic accuracy of CD10 in the diagnosis of malignancy in follicular-patterned thyroid lesions were 12%, 78%, and 29.2%, respectively.

Discussion

CD10/NEP is a membrane-bound zinc metalloproteinase that functions by reducing cellular responses to peptide hormones. Recent studies suggest that CD10/NEP also regulates peptide-mediated cellular proliferation [13]. It was originally used as tumor-associated cell surface antigen expressed by the majority of acute lymphoblastic leukemias [13, 15]. CD10 was also expressed on a variety of nonhematopoietic cell types including bronchial epithelial cells, cultured fibroblasts, bone marrow stromal cells, renal proximal tubular epithelial cells, breast myoepithelium, biliary canaliculi, fetal intestine, and certain solid tumor cell lines [13, 14, 17].

CD10 was recently studied in the thyroid gland by Tomoda et al. [17] and found to be valuable in the classification of thyroid follicular lesions into benign and malignant groups and in the diagnosis of follicular variant of papillary thyroid carcinoma.

Perhaps the most difficult problem in thyroid pathology is the distinction of follicular carcinoma from follicular adenoma and the clear-cut diagnosis of follicular variant of papillary carcinoma. In a study that evaluated the observer variation in the diagnosis of follicular variant of papillary carcinoma, all ten experienced thyroid pathologists showed agreement in the diagnosis in only 39% of cases [16]. Another study by Franc et al. that evaluated interobserver and intraobserver reproducibility in the histopathology of follicular carcinoma found the diagnosis of vascular and

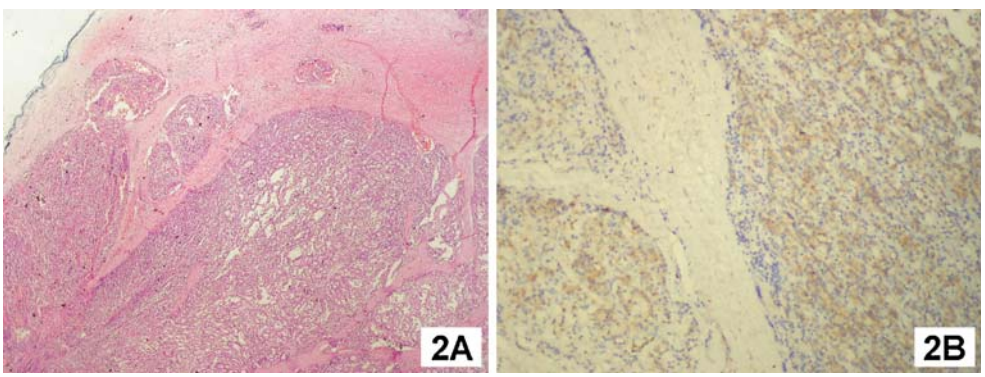

Fig. 2 **a** Follicular carcinoma with extensive capsular and vascular invasion. **b** Weak positivity of CD10 in widely invasive follicular carcinoma

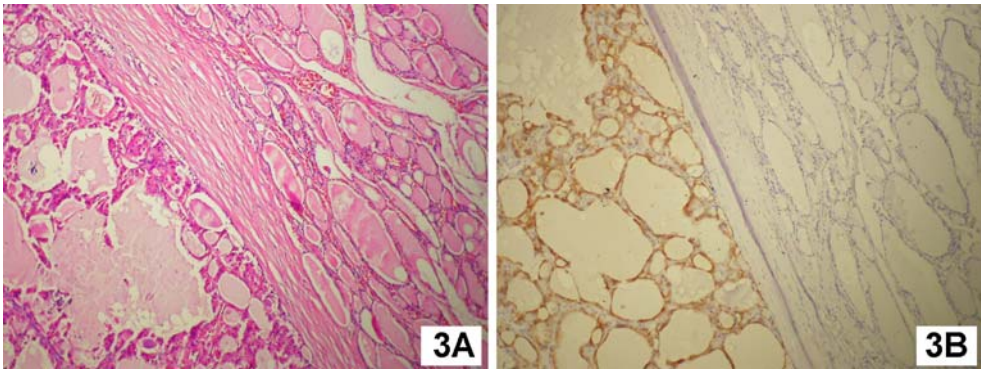

Fig. 3 **a** Follicular adenoma (*left corner*), separated from neighboring thyroid tissue by a thick fibrous capsule. **b** Strong positivity of CD10 in follicular adenoma and negativity in adjacent normal thyroid tissue

capsular invasion and the analysis of nuclear features to be unreliable criteria for establishing malignancy in difficult cases of encapsulated follicular thyroid tumors [10]. In order to overcome the limitations in the histological diagnosis of follicular-patterned thyroid lesions, several markers of malignancy—such as Galectin-3, HMBE-1, cytokeratin 19, CD44v6, thyroid peroxidase, S100, and CD57—have been studied in both surgical and FNA cytology specimens [6, 11, 12]. However, to date, none of them has been found to be a specific malignancy marker for follicular-patterned lesions.

CD10 was reported to be negative in normal thyroid tissue, adenomatous nodules, follicular adenomas, and conventional papillary carcinomas and positive in 80% of follicular carcinomas and 77% of follicular variant papillary carcinomas by Tomoda et al. [17]. Thus, it was suggested as a useful marker for distinguishing follicular carcinoma from follicular adenoma and benign hyperplastic nodules and in the diagnosis of follicular variant of papillary carcinoma. In the present study, consistent with the results of Tomoda et al., CD10 was not detected in adenomatous nodules and normal thyroid tissue adjacent to the lesions. In contrast, we observed strong positivity in 64.2% of conventional papillary carcinomas, while it was positive in 16.6% of follicular variant of papillary carcinomas and in 11.1% of widely invasive follicular carcinomas and negative in all minimally invasive follicular carcinomas. We also observed positivity in 30% of follicular adenomas. Papillary microcarcinomas with papillary architecture showed strong reactivity with CD10 while those with follicular pattern were negative. There was a significant difference in positivity of CD10 in conventional papillary carcinoma and follicular variant. This might support the conclusion that follicular variant of papillary carcinoma shows genetic differences from conventional papillary carcinoma and suggests that at least a subset of follicular variant of papillary carcinoma shares some features of follicular carcinomas.

In conclusion, CD10 shows strong positivity in conventional papillary carcinoma. It does not seem to be useful in the classification of thyroid follicular lesions as benign and malignant.

References

1. Vasko V, Ferrand M, Di Cristofaro J, Carayon P, Henry JF, de Micco C (2003) Specific pattern of RAS oncogene mutations in follicular thyroid tumors. J Clin Endocrinol Metab 88(6):2745–2752
2. Miller B, Burkey S, Lindberg G, Snyder WH 3rd, Nwariaku FE (2004) Prevalence of malignancy within cytologically indeterminate thyroid nodules. Am J Surg 188(5):459–462
3. Baloch ZW, Livolsi VA (2002) Follicular-patterned lesions of the thyroid: the bane of the pathologist. Am J Clin Pathol 117(1):143–150
4. Gasbarri A, Martegani MP, Del Prete F, Lucante T, Natali PG, Bartolazzi A (1999) Galectin-3 and CD44v6 isoforms in the preoperative evaluation of thyroid nodules. J Clin Oncol 17 (11):3494–3502
5. Oestreicher-Kedem Y, Halpern M, Roizman P, Hardy B, Sulkes J, Feinmesser R, Stern Y (2004) Diagnostic value of galectin-3 as a marker for malignancy in follicular patterned thyroid lesions. Head Neck 26(11):960–966
6. Beesley MF, McLaren KM (2002) Cytokeratin 19 and galectin-3 immunohistochemistry in the differential diagnosis of solitary thyroid nodules. Histopathology 41(3):236–243
7. Williams ED (2000) Guest editorial: two proposals regarding the terminology of thyroid tumors. Int J Surg Pathol 8(3):181–183
8. Evans HL (1984) Follicular neoplasms of the thyroid. A study of 44 cases followed for a minimum of 10 years, with emphasis on differential diagnosis. Cancer 54(3):535–540
9. DeLellis RA, Lloyd RV, Heitz PU, Eng C (2004) Thyroid and parathyroid tumours. World Health Organization Classification of Tumours. Pathology and genetics of tumours of endocrine organs. IARC, Lyon, pp 51–123
10. Franc B, de la Salmonière P, Lange F, Hoang C, Louvel A, de Roquancourt A, Vildé F, Hejblum G, Chevret S, Chastang C (2003) Interobserver and intraobserver reproducibility in the histopathology of follicular thyroid carcinoma. Hum Pathol 34 (11):1092–2001
11. Volante M, Bozzalla-Cassione F, DePompa R, Saggiorato E, Bartolazzi A, Orlandi F, Papotti M (2004) Galectin-3 and HBME-1 expression in oncocytic cell tumors of the thyroid. Virchows Arch 445(2):183–188

12. Nasir A, Catalano E, Calafati S, Cantor A, Kaiser HE, Coppola D (2004) Role of p53, CD44V6 and CD57 in differentiating between benign and malignant follicular neoplasms of the thyroid. In Vivo 18(2):189–195
13. Shipp MA, Look AT (1993) Hematopoietic differentiation antigens that are membrane-associated enzymes: cutting is the key. Blood 82(4):1052–1070
14. Mechtersheimer G, Möller P (1989) Expression of the common acute lymphoblastic leukemia antigen (CD10) in mesenchymal tumors. Am J Pathol 134(5):961–965 May
15. Ritz J, Pesando JM, Notis-McConarty J, Lazarus H, Schlossman SF (1980) A monoclonal antibody to human acute lymphoblastic leukaemia antigen. Nature 283(5747):583–585
16. Lloyd RV, Erickson LA, Casey MB, Lam KY, Lohse CM, Asa SL, Chan JK, DeLellis RA, Harach HR, Kakudo K, LiVolsi VA, Rosai J, Sebo TJ, Sobrinho-Simoes M, Wenig BM, Lae ME (2004) Observer variation in the diagnosis of follicular variant of papillary thyroid carcinoma. Am J Surg Pathol 28(10):1336–1340
17. Tomoda C, Kushima R, Takeuti E, Mukaisho K, Hattori T, Kitano H (2003) CD10 expression is useful in the diagnosis of follicular carcinoma and follicular variant of papillary thyroid carcinoma. Thyroid 13(3):291–295
18. Millar EK, Waldron S, Spencer A, Braye S (1999) CD10 positive thyroid marginal zone non-Hodgkin lymphoma. J Clin Pathol 52 (11):849–850

Virchows Arch (2009) 454:107–114
DOI 10.1007/s00428-008-0700-z

ORIGINAL ARTICLE

Molecular and morphological analysis of adenoid cystic carcinoma of the breast with synchronous tubular adenosis

Leonard Da Silva · Lyndall Buck · Peter T. Simpson · Lynne Reid · Naomi McCallum · Barry J. Madigan · Sunil R. Lakhani

Received: 3 September 2008 / Accepted: 5 November 2008 / Published online: 25 November 2008

Abstract Adenoid cystic carcinoma (ACC) of the breast is a rare tumour. Its recognition as a special type of breast carcinoma is very important because its prognosis is better than the not-otherwise-specified invasive ductal carcinoma and its treatment may not include axillary dissection. Tubular adenosis (TA) is a very rare condition of the breast that is histologically benign; however, it has been described in association with invasive ductal carcinoma. There are scant data regarding the molecular genomic alterations in ACC of the breast and no data has been presented on TA. Herein, we provide a morphological characterisation of TA arising synchronically with ACC in the breast. To characterise these lesions, we performed ultrastructural analysis, three-dimensional reconstruction and molecular analysis using immunohistochemistry and comparative genomic hybridisation. The copy number alterations found in ACC were restricted to small deletions on 16p and 17q only, whereas the TA harboured gains on 1q, 5p, 8q, 10q, 11p and 11q and losses on 1p, 10q, 11q, 12q, 14q, 15q and 16q. These molecular data highlight the genomic instability of TA, a benign florid proliferation intermingled with ACC, and do not provide evidence of molecular evolution from TA to ACC.

L. Da Silva (✉) · P. T. Simpson · L. Reid · S. R. Lakhani
University of Queensland Centre for Clinical Research,
The Royal Brisbane & Women's Hospital,
Level 6, Building 71/918, Herston,
Brisbane 4029, Australia
e-mail: l.dasilva@uq.edu.au

L. Da Silva · P. T. Simpson · L. Reid · S. R. Lakhani
Molecular & Cellular Pathology, School of Medicine,
University of Queensland,
Brisbane 4006, Australia

L. Buck · N. McCallum · B. J. Madigan · S. R. Lakhani
Pathology Queensland: The Royal Brisbane & Women's Hospital,
Brisbane 4029, Australia

Keywords Adenoid cystic carcinoma · Tubular adenosis · Microglandular adenosis · Breast cancer · Comparative genomic hybridisation

Introduction

The breast and salivary glands are both comprised of tubuloacinar exocrine glands. Not surprisingly, classifications of tumours of breast and salivary glands show the histological types of tumours in both sites. For instance, adenoid cystic carcinoma (ACC), mucoepidermoid carcinoma and pleomorphic adenomas are a few of such examples of tumours which can be found in both breast and salivary glands [1–3].

In sharp contrast to ACC of the breast, which represents about 0.1% of all breast carcinomas [4], adenoid cystic carcinoma accounts for about 10% to 15% of all parotid malignancies [1]. Contrary to what is found in the salivary gland, ACC of the breast is considered a much less aggressive disease. The likelihood of an overt malignant clinical progression is low and the growth of the tumour is indolent [5]. ACC of the breast usually does not show the classical appearance of invasive ductal carcinoma on either mammography or ultrasound, perhaps owing to its relatively well-defined borders [6]. Regional lymph node involvement is rare [7]. Distant metastatic dissemination is rarely seen at the time of the diagnosis, although local recurrence and metastatic disease several years after initial presentation can occur. Nonetheless, survival after the metastatic event is good and death from mammary ACC is believed to be a rare event [3, 8–12]. Hence, treatment consisting of local conservative management [13–15] or mastectomy without axillary dissection has been proposed [4]. Thus, the correct classification of a tumour as being an ACC is of relevance in clinical practice, and misclassification as

an invasive ductal carcinoma may lead to mismanagement of patients.

ACCs of the breast may exhibit cribriform, trabecular–tubular and/or solid patterns of growth. The solid pattern comprised rounded or lobulated aggregates of tumour cell nests with different sizes, and these nests may demonstrate cyst-like spaces. The cribriform pattern exhibits a sieve-like appearance, and islands of neoplastic epithelial cells may group as multiple small and round, so-called pseudocystic structures since continuity of the pseudolumens with the connective tissue stroma is observed in some instances. The tubular–trabecular variant has cells arranged in small nests. Such cells can also circumscribe individual cyst-like spaces. It is noteworthy that a mixture of such elements is the usual picture of ACCs. Ultrastructural studies have shown a bidirectional differentiation of ACC with luminal (ductal) and abluminal (myoepithelial/basaloid) cells. Basaloid cells are positive for vimentin and cytokeratin 14 (CK14) and focally for myoepithelial markers, including smooth muscle actin (SMA), calponin, p63 and maspin. The luminal cell type is usually positive for cytokeratin 7 (CK7). Positivity for oestrogen receptor is rarely seen [8, 13, 16, 17]

There are limited cytogenetic and molecular data on ACCs of the breast, restricted to cytogenetic analyses of a few cases: 46,XX,t(4;4)(q21;q35),t(5;11)(q13;q21), 46,XX, +1,der(1;16)(q10;p10) [18] and 46,XX,inv(9) [19]. Therefore, ACC of the breast has been regarded as an important and potential field of further investigation [20]. CD117 (c-kit), a tyrosine kinase receptor and a target for Gleevec® (Novartis AG, NJ, USA), has been shown to be expressed in 100% of ACCs of the breast, which emphasises the importance of recognising this entity in routine practice [17]. ACCs in sites other than breast have been shown to harbour deletions of 6q, 12q and 13q and gains of chromosome 19 as well as rearrangements involving chromosomes 6q and 9p [19]. Recently, high-resolution array comparative genomic hybridisation analysis showed that bronchial and salivary ACC harbour low levels of genetic instability with few copy number alterations or high level amplifications. Recurrent gains included 7p15.2, 17q21-25 and 22q11-13, and recurrent losses included 1p35, 6q22-25, 8q12-13, 9p21, 12q12-13 and 17p11-13 [21].

"Tubular adenosis" (TA) of the breast, a term that is believed to have been firstly coined by Oberman [22, 23], is a rare benign lesion. It comprised elongated tubules which are lined by an inner bland-looking layer of cells and surrounded by an intact myoepithelial outer layer, growing in a haphazard and apparently branching fashion. The morphology of this entity is rarely described. The importance of its recognition relies on the likelihood of being misclassified as invasive ductal carcinoma, especially at intraoperative frozen section or when the lesion is colonised by DCIS [24]. Adenomyoepithelioma with apocrine adenosis as described by Eusebi et al. [25, 26] is a lesion with a similar morphology and probably in the same spectrum as tubular adenosis; however, this lesion has a prominent myoepithelial cell layer and less elongated tubules. Another differential diagnoses under the umbrella of adenosis-type lesions is microglandular adenosis (MGA) [27–29]. MGA is a benign and rare mammary lesion in which the initial form of presentation may be as an incidental microscopic lesion or as a palpable tumour. Morphological evidence of transition from MGA to ACC or invasive ductal carcinoma has been suggested [16, 30–33]; however, there are no experimental data to link tubular adenosis with progression to malignancy. Herein, we present the first report of ACC of the breast associated with tubular adenosis, including the first molecular report of tubular adenosis. We have performed immunohistochemistry (IHC), electronic microscopy, comparative genomic hybriditisation (CGH) and three-dimensional reconstruction (3D-r) on the tissue to better understand the relationship between these lesions.

Methodology

Clinical and pathological examination

A 50-year-old female patient from the Solomon Islands presented with a 8.0×6.0×5.5 cm mass in her left breast without evidence of axillary involvement. Mammography showed a lesion with ill-defined borders, and the patient underwent simple mastectomy without axillary dissection. Formalin-fixed, paraffin-embedded (FFPE) tumour sections were stained with haematoxylin and eosin (H&E), periodic acid-Schiff-diastase (PAS-D) and a panel of immunohistochemical markers to confirm the diagnosis. The slides were reviewed by three pathologists (LDS, LB and SRL). The patient provided consent, and the study was approved by the local research ethics committees.

Immunohistochemistry

Sections from representative areas were cut at 4 μm and mounted on silane-coated slides. Immunohistochemistry was performed using the Envision® dual link system (Dakocytomation, Denmark) according to the manufacturer's recommendations. Table 1 shows all antibodies used along with the antibody clone and dilution. Antigenic retrieval for all antibodies (except SMA) and epithelial membrane antigen (EMA) which did not require any antigen retrieval required 2-min pressure cooking (105°C) in EDTA (pH 8.0) buffer. Positive and negative controls were included in all runs, and all slides were analysed by two pathologists (LDS, SRL) under a double-headed optical light microscope. Cellular localisation and percentage of cells stained for each antibody

Table 1 Details of antibodies used in immunohistochemistry

Antibody	Company	Clone–Dilution
PR	Novocastra	1A6–1:500
ER	Novocastra	6F11–1:100
HER2	DAKO	Herceptest
p63	DAKO	4AL–1:400
SMA	DAKO	1A4–1:100
Calponin	DAKO	CALP–1:100
Colagen IV	DAKO	CIV22–1:100
EMA	DAKO	E29–1:200
S100	DAKO	Polyclonal–1:5000
CK5/6	DAKO	D5/16B4–1:50
CK14	Neomarkers	LL002–1:50
c-kit	DAKO	Polyclonal–1:200
E-cadherin	Zymed	HECD–1 1:20
GCDFP15	Signet	D6–1:600
CK19	DAKO	RCK108–1:25
CK7	DAKO	OV-TL12/30–1:500
Cyclin D1	Neomarkers	SP4–1:50

were recorded on both ACC and tubular adenosis. Intensity was based on a four-tier system (negative, weak, moderate and strong).

Ultrastructural analysis

Paraffin-embedded tissue was subjected to xylene treatment. Subsequently, 1.0-mm-thick tissue blocks were rehydrated and refixed in 5% buffered glutaraldehyde overnight and followed by post-fixation in osmium tetroxide and re-embedding in Epon. Viewing of the structures was performed in a JEOL transmission electron microscopes (100/120 kV) JEM-1011 (Washington, USA).

Comparative genomic hybridisation

Five-micron-thick FFPE sections were cut and stained with nuclear fast red. ACC and TA were separately microdissected using the PixCell laser capture microdissection system (Arcturus, Mountain View, CA, USA). DNA was extracted using proteinase K digestion [34]. High-resolution CGH (HR-CGH) [34, 35] was used to assess whole genome copy number changes. DNA amplification and fluorescent labelling of DNA was carried out by degenerate oligonucleotide-primed polymerase chain reaction in two rounds, and CGH was performed according to a previously described protocol [34]. CGH on both components was repeated to validate the findings.

Three-dimensional reconstruction

Serial H&E-stained sections were cut at 4 μm. A total of 50 sections were analysed. For 3D-r, the series of slides were scanned sequentially using a scanscope® (Aperio Technologies, Vista, CA, USA). Then, digital images of areas of containing both TA and ACC were chosen and saved as tagged image format files using ImageScope® (Aperio Technologies). For each image, three fiducial points (cores of liver inserted within the paraffin block containing the lesion) present in two consecutive sections were chosen to allow the alignment of the serial sections. Reconstruct is a free editor developed for 3D-r [36] and is freely available at http://synapses.bu.edu/ or http://synapses.mcg.edu/. Thus, it was used for the montage, alignment, analysis and visualisation of the serial sections. Traces were applied to areas of the TA and ACC. After tracing and alignment, a 3D-r representation with the relations between the TA and ACC was generated. The tracing and choosing of the images were performed by one pathologist (LDS).

Results

Morphological analysis

The ACC was characterised by a predominance of the solid component. At least 70% of the tumour mass comprised solid nests and sheets of neoplastic cells, including areas of the recently described basaloid type, accounting for around 20% of the tumour [40]. The cribriform and trabecular–tubular elements were also present, however in a lesser extent (Fig. 1a,b). No lymphatic or perineural invasion was seen. Mitoses were easily identified with an average count of 20/10 fields (Olympus Microscope, model BX51, 40× objective, 0.55-mm field diameter). Strikingly, the tumour was totally infiltrated within and beyond its borders by a lesion which was composed of elongated tubules which were lined by an inner bland-looking layer of cells that displayed, in some instances, accumulation of mucin in the cytoplasm revealed by PAS-D positivity and oncocytiod morphology characterised by eosinophilic granular cytoplasm. Nuclei were bland and mitoses scant. The luminal cells were surrounded by an intact myoepithelial layer and basement membrane. The glands grew in a haphazard fashion with an apparent branching pattern, evidenced by single glands with several transversal lumen as well as glands with dumbbell shapes (Fig. 1c,d). Furthermore, a small adenomyoepithelioma was identified, measuring 0.5 cm in maximum dimension and present adjacent to the ACC. The adenomyoepithelioma comprised tubular glands that displayed two cell populations, an outer multilayered myoepithelial type and an inner single layer epithelial type. The myoepithelial component was composed of cuboidal to spindle-shaped cells with round to elongated nuclei with very small nucleoli. The epithelial component was composed of columnar cells with eosinophilic cytoplasm. No mitosis or evidence of atypia was identified in this tumour.

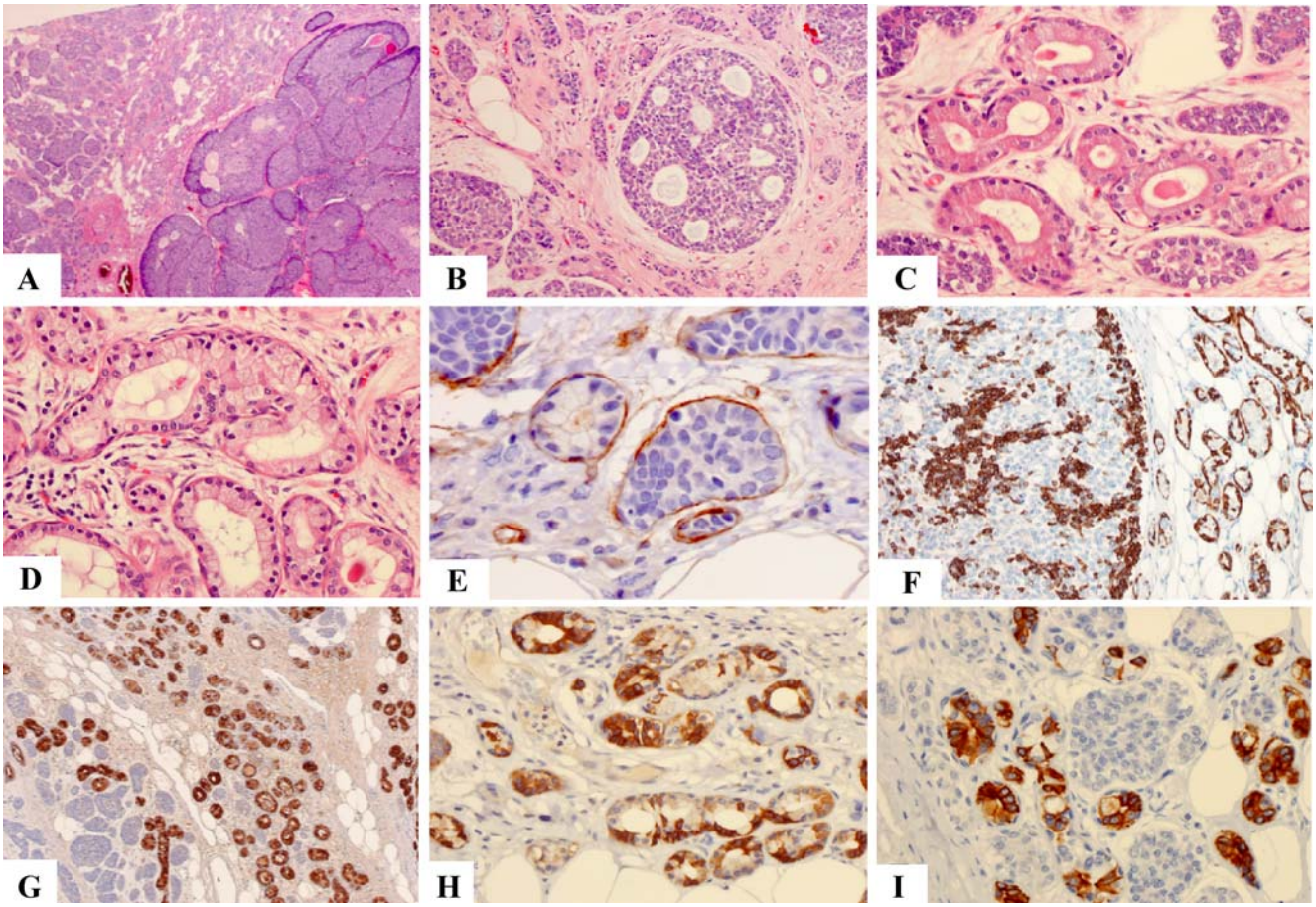

Fig. 1 Morphological and immunohistochemical analysis of adenoid cystic carcinoma (*ACC*) and tubular adenosis (*TA*) components. **a** Low-power magnification (40×) of solid-basaloid areas of ACC. **b** Classical cribriform areas of ACC. **c** TA glands showing 'dumbbell' shapes, depicting the branching architecture, pale and eosinophilic cytoplasm and luminal secretion. The glands are side by side and admixed with small nests of ACC. **d** TA glands with pale cytoplasm and budding. **e** Islands of ACC and TA surrounded by collagen type IV. **f** Cytoketarin 14 staining highlighting the myoepithelial layer of TA (*right-hand side*) and cells in the basaloid island of ACC (*left-hand side*). **g** GCDFP-15 immunohistochemical positivity highlights TA glands amongst nests of ACC which are negative. **h** TA showing positivity for c-kit. **i** Cytokeratin 19 staining of luminal cells in the TA glands, whereas ACC nests are negative

Immunohistochemistry

The detailed results of the immunohistochemistry analysis performed on the sections are displayed in Table 2. Briefly, ACC showed areas of positivity for CK14, CK5/6, CK19, CK7, S100, SMA, calponin and p63 and negativity for EMA. In contrast, only the luminal cells of the TA were positive for EMA, CK19 (Fig. 1i) and CK7, and only the outer layer of myoepithelial cells were positive for S100, CK14 (Fig. 1f), CK5/6, SMA, calponin and p63. GCDFP-15 (gross cystic diseases fluid protein) highlighted the infiltrative character of TA among negative nests of ACC (Fig. 1g). Collagen type IV highlighted the basal membrane-type material produced by the ACC and also the basal membrane surrounding the TA glands (Fig. 1e). C-kit was positive in both lesions, however to a much lesser extent in the TA glands (Fig. 1h). The ACC was negative for ER and PgR; however, a few glands in the TA showed positivity for ER. CyclinD1 was positive 50% of cells in the TA and in 20% cells positive in the ACC. E-cadherin was positive in both lesions. HER2 was negative. The adenomyoepithelioma had the same pattern of expression as for the ACC. The luminal cells were positive for CK7 and CK19, whilst the myoepithelial cells were positive for S100, SMA, CK14 and CK5/6, calponin and p63, assuring its myoepithelial phenotype.

Comparative genomic hybridisation

The adenomyoepithelioma, ACC and TA were separately microdissected and analysed for copy number alterations by HR-CGH. The adenomyoepithelioma had no detectable genomic alterations. The ACC harboured deletion of small regions on 16p and 17q only. The TA harboured several gross copy number changes which involved gains on 1q, 5p, 8q, 10q, 11p and 11q and losses on 1p, 10q, 11q, 12q, 14q, 15q and 16q.

Table 2 Results of immunohistochemistry in the different morphological components

Antibody	Tubular adenosis	Adenoid cystic carcinoma	Adenomyoepithelioma
PR	Negative	Negative	Negative
ER	Weak positive, N, 5% luminal cells	Negative	Negative
HER2	Negative	Negative	Negative
p63	Strong positive, N, 90% myoepithelial cells	Strong positive, N, 50% of cells	Strong positive, N, 90% myoepithelial cells
SMA	Strong positive, C, 90% myoepithelial cells	Strong positive, C, 50% of cells	Strong positive, C, 90%myoepithelial cells
Calponin	Strong positive, C, 90% myoepithelial cells	Strong positive, C, 20% of cells	Strong positive, C, 80% myoepithelial cells
Collagen IV	Strong positive, BM, 90%, around TA glands	Strong positive, around nests of tumour cells	Strong positive, around nests of tumour cells
EMA	Strong positive, C, 90% luminal cells	Negative	Not performed
S100	Strong positive, N & C, 90% myoepithelial cells	Strong positive, N & C, 50% cells	Strong positive, N & C, 80% myoepithelial cells
CK5/6	Strong positive, C, 90% myoepithelial cells	Strong positive, C, 50% of cells	Strong positive, C, 90% myoepithelial cells
CK14	Strong positive, C, 90% myoepithelial cells	Strong positive, C, 50% of cells	Strong positive, C, 90% myoepithelial cells
c-kit	Strong positive, C & M, 30% of cells	Strong positive, C & M, 60% of cells	Not performed
E-cadherin	Strong positive, M, 90% of cells	Strong positive, M, 90% of cells	Strong positive, M, 90% cells
GCDFP15	Strong positive, C, 90% luminal cells	Negative	Negative
CK19	Strong positive, C, 50% luminal cells	Weak positive, C, 10% of cells	Strong positive, C, 50%. luminal cells
CK7	Strong positive, C, 90%. luminal cells	Strong positive, C, 50% of cells	Strong positive, C, 90%. luminal cells
Cyclin D1	Strong positive, N, 50% myoepithelial cells	Strong, N, 20% cells	Not performed

When positive, the staining intensity, localisation and percentage of positive cells are given. In addition, the epithelial cell type (luminal or myoepithelial) of positive staining is also given for tubular adenosis and adenomyoepithelioma
N nuclear, *M* plasma membrane, *C* cytoplasm, *BM* basal membrane

Three-dimensional reconstruction

The 3-D-r highlighted and confirmed the features that were displayed in the H&E sections. The TA glands form a network of branches that are interconnected between themselves and spread across different directions in the breast parenchyma. Figure 2c,d shows different aspects of this system, highlighting the branching of the tubules and their interconnections. The interconnection and budding of the tubules is not a feature of classical MGA when analysed in H&E slides.

Ultrastructural analysis

Ultrastructural analysis confirmed the bidirectional differentiation of adenoid cystic carcinoma with luminal and abluminal (myoepithelial) cells. The luminal cells had microvilli on the luminal aspect and were joined by desmosomes. They also

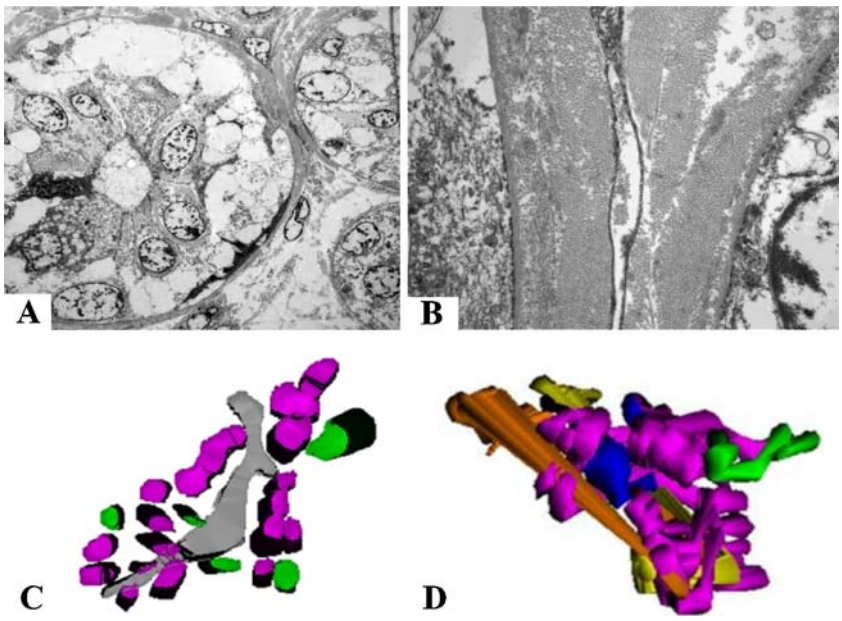

Fig. 2 Ultrastructural morphology of a tubular adenosis gland showing a double-layered tubule surrounded by a basal membrane (**a**) and high power detail of the basal membranes of two TA glands side by side (**b**). Two-dimensional view (**c**) of tubules chosen for three-dimensional reconstruction (**d**) showing several tubules in different colors interconnecting between each other and forming a complex branching network

displayed tonofilaments and rough endoplasmic reticulum. The myoepithelial cells had irregular nuclei, narrow cytoplasmic processes and prominent amounts of fine filaments with focal dense bodies in their cytoplasm. The TA glands had their double layer of luminal and myoepithelial cells confirmed as well as the presence of a basal membrane surrounding the tubules (Fig. 2a,b). The luminal cells had, in some instances, cytoplasm vacuoles, and the myoepithelial cells had very scant cytoplasm.

Discussion

ACCs of the breast are very rare lesions with a very good prognosis when compared to their counterpartners of other sites [5]. The case that we describe comprised approximately 70% solid variant of ACC. There is evidence in the literature that histological growth pattern correlates with prognosis in ACC of breast and that tumours with a solid growth pattern are believed to show a more aggressive clinical course [37]. Ro et al. categorised [37] ACC in three groups according to the percentage of solid growth (I = no solid elements; II <30% of solid elements; III >30% solid elements). Tumors with more solid elements displayed larger size and these patients were more likely to develop recurrences. In their series, the one patient who developed metastases had a grade III tumour. Some solid variants of breast ACC have a striking basaloid appearance. These tumours are believed to be a source of axillary nodal metastases, but yet carry a better prognosis than an invasive poorly differentiated duct carcinoma of similar size [15]. Therefore, the correct diagnosis of ACC is warranted, since misdiagnosis may lead to mismanagement of patients. The patient described here did not undergo sentinel node examination, as the procedure was not available in the hospital where she had her surgery.

The immunohistochemical staining is in keeping with the bidirectional differentiation of ACC which showed positivity for luminal and myoepithelial markers such as CK19 and CK14, respectively. This is also consistent with the current view that ACCs are part of the basal-like molecular subset of breast carcinomas, a subgroup of tumour which shares expression of genes generally expressed by myoepithelial cells [38, 39]. Basal-like tumours are an increasingly heterogenous group of tumours with an apparent poor prognosis in some studies, but in other studies with detailed analysis and long-term follow-up, there is evidence of a group of basal tumours which have a relatively good long-term prognosis [40, 41]. ACCs, like medullary carcinomas of the breast, are part of the basal-like tumour spectrum which have a much better prognosis and low trend for lymph node metastasis when compared to other ductal carcinomas of not-otherwise-specified [42–45].

The TA showed a haphazard arrangement with its classical branching. The 3D-r provided nice visualisation of the complex network of branching tubules and thus helped in differentiating this entity from MGA from a morphological point of view, since the MGA tubules seem to be individually separated. The immunohistochemistry also highlighted the striking myoepithelial layer of the TA which is an important feature when one tries to make a distinction from MGA and, even more importantly, from ductal carcinoma. The classical myoepithelial markers like p63 and S100 were strongly positive in the outer layer of the TA tubules, in sharp contrast to what is observed in MGA. There are data in the literature linking adenomyoepithelioma with adenoid cystic carcinoma, and the report by Eusebi et al. [26] describes an ‘infiltrating’ variant with similar morphology to this case. However, we believe that this case represents a TA rather than an adenomyoepithelioma, as the myoepithelial cell layer around the tubules is not prominent. Further, the CGH data from the adenomyoepthelioma are different from the component labelled TA (see below).

The different components of this case were examined by immunohistochemistry and CGH. TA and ACC showed positivity for CK14, CK7, c-kit and Cyclin D1. The ACC had very low levels of genetic instability with only losses at 16p and 17q, reflecting that reported in the literature for ACC at other sites and the possible role of additional epigenetic mechanisms in the tumour progression as suggested previously [21, 46]. Interestingly, the loss on 17q was in the region of BRCA1 which, although speculative, suggests a possible involvement in the development of basal features in this tumour. ACC of the breast has been described in association with adenomyoepithelioma, thus suggesting the existence of a spectrum of benign epithelial-myoepithelial neoplasms towards malignancy [47]. Loss of 16p has been shown in myoepithelial carcinomas [48]. The small foci of adenomyoepithelioma had no copy number changes yet an overlapping IHC profile to the ACC. It is therefore tempting to speculate that the adenomyoepithelioma represents a precursor lesion to the ACC in this case, given also the very small number of genomic changes in the ACC, although unfortunately, we do not have direct molecular evidence to confirm this.

Surprisingly, the TA demonstrated a range of gross genomic alterations demonstrating its genomic instability. These changes involved gains on 1q, 5p, 8q, 10q, 11p and 11q and losses on 1p, 10q, 11q, 12q, 14q, 15q and 16q. Interestingly, the gain on chromosome 11q was in the region of the gene for cyclin D1 (*CCND1*), and this reflects the strong immunohistochemical positivity in this component and may be related to the high proliferative character of such a lesion. The molecular data suggest that a progression from TA to ACC is unlikely in this case. The

myriad of genetic changes found in the TA is noteworthy and may also represent a potential for non-obligatory malignant progression to invasive carcinoma, but this cannot be proven in this report. However, this would not be a surprise, since there is clinical association reported between TA and invasive ducal carcinoma [24] as well as between MGA and ACC and invasive ductal carcinoma [16, 30–33].

The study of a single case of TA in association with ACC is the main limitation of this study. Molecular analysis of a series of tubular adenosis associated with malignancy would broaden our understanding whether there is a possible malignant progression of such lesions.

In summary, we have described the first molecular characterisation of tubular adenosis intermingled with ACC in a form of a florid proliferation. In addition, the differential diagnosis of ACC is crucial since inaccuracies may lead to mismanagement of patients, and further molecular biology analysis of TA and MGA is warranted in order to establish possible evidence of neoplastic progression at the genomic level.

Acknowledgements LDS is the recipient of a PhD Fellowship from the Ludwig Institute of Cancer Research. The authors thank the Genetics Department at QML Pathology for technical resources and support.

Conflict of interest statement The authors declare that there is no conflict of interest regarding this manuscript.

References

1. Barnes L, Eveson J, Reichart P, Sidransky D (2005) Pathology and genetics of head and neck tumours. In: Kleihues R, Sobin LH (eds) World Health Organization classification of tumours. IARC, Lyon, France
2. Ellis IO, Schnitt SJ, Sastre-Garau X et al (2003) Invasive breast carcinomas. In: Tavassoli FA, Devilee P (eds) Pathology and genetics of tumours of the breast and female genital organs. IARC, Lyon, pp 13–59
3. Galloway JR, Woolner LB, Clagett OT (1966) Adenoid cystic carcinoma of the breast. Surg Gynecol Obstet 122:1289–1294
4. Muslimani AA, Ahluwalia MS, Clark CT, Daw HA (2006) Primary adenoid cystic carcinoma of the breast: case report and review of the literature. Int Semin Surg Oncol 3:17
5. Page DL (2005) Adenoid cystic carcinoma of breast, a special histopathologic type with excellent prognosis. Breast Cancer Res Treat 93:189–190
6. Shen SS, Sahin AA (2004) Invasive ductal carcinoma of the breast with a microglandular adenosis pattern. Ann Diagn Pathol 8:39–42
7. Nicholson BP, Pisters KM, Page DL, Johnson DH (1999) Adenoid cystic carcinoma of the breast. In: Raghavan D, Brecher ML, Johnson D (eds) Textbook of uncommon cancer. Wiley, Chichester, pp 719–724
8. Anthony PP, James PD (1975) Adenoid cystic carcinoma of the breast: prevalence, diagnostic criteria, and histogenesis. J Clin Pathol 28:647–655
9. Cavanzo FJ, Taylor HB (1969) Adenoid cystic carcinoma of the breast. An analysis of 21 cases. Cancer 24:740–745
10. Fisher ER, Gregorio RM, Fisher B et al (1975) The pathology of invasive breast cancer. A syllabus derived from findings of the National Surgical Adjuvant Breast Project (protocol no. 4). Cancer 36:1–85
11. Qizilbash AH, Patterson MC, Oliveira KF (1977) Adenoid cystic carcinoma of the breast. Light and electron microscopy and a brief review of the literature. Arch Pathol Lab Med 101:302–306
12. Verani RR, Van der Bel-Kahn J (1973) Mammary adenoid cystic carcinoma with unusual features. Am J Clin Pathol 59:653–658
13. Arpino G, Clark GM, Mohsin S et al (2002) Adenoid cystic carcinoma of the breast: molecular markers, treatment, and clinical outcome. Cancer 94:2119–2127
14. Millar BA, Kerba M, Youngson B et al (2004) The potential role of breast conservation surgery and adjuvant breast radiation for adenoid cystic carcinoma of the breast. Breast Cancer Res Treat 87:225–232
15. Shin SJ, Rosen PP (2002) Solid variant of mammary adenoid cystic carcinoma with basaloid features: a study of nine cases. Am J Surg Pathol 26:413–420
16. Acs G, Simpson JF, Bleiweiss IJ et al (2003) Microglandular adenosis with transition into adenoid cystic carcinoma of the breast. Am J Surg Pathol 27:1052–1060
17. Azoulay S, Lae M, Freneaux P et al (2005) KIT is highly expressed in adenoid cystic carcinoma of the breast, a basal-like carcinoma associated with a favorable outcome. Mod Pathol 18:1623–1631
18. Pandis N, Teixeira MR, Gerdes AM et al (1995) Chromosome abnormalities in bilateral breast carcinomas. Cytogenetic evaluation of the clonal origin of multiple primary tumors. Cancer 76:250–258
19. Mark HF, Hanna I, Gnepp DR (1996) Cytogenetic analysis of salivary gland type tumors. Oral Surg Oral Med Oral Pathol Oral Radiol Endod 82:187–192
20. Bennett AK, Mills SE, Wick MR (2003) Salivary-type neoplasms of the breast and lung. Semin Diagn Pathol 20:279–304
21. Bernheim A, Toujani S, Saulnier P et al (2008) High-resolution array comparative genomic hybridization analysis of human bronchial and salivary adenoid cystic carcinoma. Lab Invest 88:464–473
22. Oberman HA (1984) Benign breast lesions confused with carcinoma. In: McDivitt RW, Oberman HA, Ozzello L, Kaufman N (eds) The breast—United States–Canadian Academy of Pathology monographs in pathology. Williams and Wilkins, Baltimore, pp 1–33
23. Rosen PP, Oberman HA (1993) Tumors of the mammary gland. In: Rosai J (ed) Atlas of tumor pathology. Armed Forces Institute of Pathology, Washington, DC, pp 54–56
24. Lee KC, Chan JK, Gwi E (1996) Tubular adenosis of the breast. A distinctive benign lesion mimicking invasive carcinoma. Am J Surg Pathol 20:46–54
25. Eusebi V, Foschini MP, Betts CM et al (1993) Microglandular adenosis, apocrine adenosis, and tubular carcinoma of the breast. An immunohistochemical comparison. Am J Surg Pathol 17:99–109
26. Eusebi V, Casadei GP, Bussolati G, Azzopardi JG (1987) Adenomyoepithelioma of the breast with a distinctive type of apocrine adenosis. Histopathology 11:305–315
27. Clement PB, Azzopardi JG (1983) Microglandular adenosis of the breast—a lesion simulating tubular carcinoma. Histopathology 7:169–180
28. Rosen PP (1983) Microglandular adenosis. A benign lesion simulating invasive mammary carcinoma. Am J Surg Pathol 7:137–144
29. Tavassoli FA, Norris HJ (1983) Microglandular adenosis of the breast. A clinicopathologic study of 11 cases with ultrastructural observations. Am J Surg Pathol 7:731–737

30. James BA, Cranor ML, Rosen PP (1993) Carcinoma of the breast arising in microglandular adenosis. Am J Clin Pathol 100:507–513
31. Khalifeh IM, Albarracin C, Diaz LK et al (2008) Clinical, histopathologic, and immunohistochemical features of microglandular adenosis and transition into in situ and invasive carcinoma. Am J Surg Pathol 32:544–552
32. Koenig C, Dadmanesh F, Bratthauer GL, Tavassoli FA (2000) Carcinoma arising in microglandular adenosis: an immunohistochemical analysis of 20 intraepithelial and invasive neoplasms. Int J Surg Pathol 8:303–315
33. Rosenblum MK, Purrazzella R, Rosen PP (1986) Is microglandular adenosis a precancerous disease? A study of carcinoma arising therein. Am J Surg Pathol 10:237–245
34. Simpson PT, Gale T, Reis-Filho JS, Jones C, Parry S, Sloane JP, Hanby A, Pinder SE, Lee AH, Humphreys S, Ellis IO, Lakhani SR (2005) Columnar cell lesions of the breast: the missing link in breast cancer progression? A morphological and molecular analysis. Am J Surg Pathol 29:734–746
35. Kirchhoff M, Gerdes T, Rose H, Maahr J, Ottesen AM, Lundsteen C (1998) Detection of chromosomal gains and losses in comparative genomic hybridization analysis based on standard reference intervals. Cytometry 31:163–173
36. Fiala JC (2005) Reconstruct: a free editor for serial section microscopy. J Microsc 218:52–61
37. Ro JY, Silva EG, Gallager HS (1987) Adenoid cystic carcinoma of the breast. Hum Pathol 18:1276–1281
38. Kreike B, van Kouwenhove M, Horlings H et al (2007) Gene expression profiling and histopathological characterization of triple-negative/basal-like breast carcinomas. Breast Cancer Res 9:R65
39. Sorlie T, Perou CM, Tibshirani R et al (2001) Gene expression patterns of breast carcinomas distinguish tumor subclasses with clinical implications. Proc Natl Acad Sci USA 98:10869–10874
40. Fulford LG, Reis-Filho JS, Ryder K et al (2007) Basal-like grade III invasive ductal carcinoma of the breast: patterns of metastasis and long-term survival. Breast Cancer Res 9:R4
41. Laakso M, Tanner M, Nilsson J et al (2006) Basoluminal carcinoma: a new biologically and prognostically distinct entity between basal and luminal breast cancer. Clin Cancer Res 12:4185–4191
42. Jacquemier J, Padovani L, Rabayrol L et al (2005) Typical medullary breast carcinomas have a basal/myoepithelial phenotype. J Pathol 207:260–268
43. Lakhani SR, Gusterson BA, Jacquemier J et al (2000) The pathology of familial breast cancer: histological features of cancers in families not attributable to mutations in BRCA1 or BRCA2. Clin Cancer Res 6:782–789
44. Pedersen L, Zedeler K, Holck S et al (1995) Medullary carcinoma of the breast. Prevalence and prognostic importance of classical risk factors in breast cancer. Eur J Cancer 31A:2289–2295
45. Weigelt B, Horlings H, Kreike B et al (2008) Refinement of breast cancer classification by molecular characterization of histological special types. J Pathol 216:141–150
46. Yu Y, Baras AS, Shirasuna K et al (2007) Concurrent loss of heterozygosity and copy number analysis in adenoid cystic carcinoma by SNP genotyping arrays. Lab Invest 87:430–439
47. Van Dorpe J, De Pauw A, Moerman P (1998) Adenoid cystic carcinoma arising in an adenomyoepithelioma of the breast. Virchows Arch 432:119–122
48. Jones C, Foschini MP, Chaggar R et al (2000) Comparative genomic hybridization analysis of myoepithelial carcinoma of the breast. Lab Invest 80:831–836

Virchows Arch (2009) 454:115–124
DOI 10.1007/s00428-008-0691-9

CASE REPORT

HNPCC-associated synchronous early-stage signet-ring cell carcinomas of colonic origin. A comparative morphological and immunohistochemical study of an intramucosal and a submucosal example

Louise Klarskov · Inge Bernstein · Susanne Holck

Received: 1 August 2008 / Revised: 11 October 2008 / Accepted: 14 October 2008 / Published online: 11 November 2008

Abstract Signet-ring cell carcinoma (SRCC) developing in the colorectum (CR) is infrequently identified at an early stage (no deeper than submucosa). Most such examples involve the submucosa. Merely 13 cases of intramucosal CR SRCC are at hand. We recently had the opportunity to study a specimen with two synchronous early-stage SRCC, developed in a 65-year-old hereditary nonpolyposis colorectal cancer male patient with a known disease-causing mutation in MLH1. A right hemicolectomy specimen comprised a 15-mm intramucosal cecal lesion, featuring zones of conventional tubular adenoma and intraepithelial SRCC as well as tumor cells multifocally permeating the lamina propria and a 12-mm submucosally expanding SRCC of the ascending colon. The intramucosal and intraepithelial as well as stromal lesional cells displayed a normal membranous expression of β-catenin and E-cadherin; submucosally infiltrating cells featured alterations in this complex with loss of membranous expression of both proteins and a shift with nuclear accumulation of β-catenin, suggesting a disruption of the Wingless signaling pathway taking place at the transition from the intramucosal to the submucosal level.

Keywords Early-stage signet-ring cell colorectal carcinoma · β-catenin–E-cadherin complex · HNPCC

L. Klarskov · S. Holck (✉)
Department of Pathology, HNPCC-register, Hvidovre Hospital, Faculty of Health Sciences, University of Copenhagen, Copenhagen, Denmark
e-mail: Susanne.holck@hvh.regionh.dk

I. Bernstein
Department of Gastroenterology, HNPCC-register, Hvidovre Hospital, Faculty of Health Sciences, University of Copenhagen, Copenhagen, Denmark

Introduction

Signet-ring cell carcinoma (SRCC) developing in the colon and rectum (CR) constitutes from 0.01% to 2.6% of all colorectal carcinomas (CRC) [1–8]. The prevalence depends, however, on the criteria applied [9, 10], as well as on the clinical scenario and molecular status. Thus, association with microsatellite-instability high (MSI-H) status, hereditary or sporadic [11, 12], as well as with chronic inflammatory bowel disease has been noticed [1, 13]. As opposed to the decreasing incidence of the conventional CRC, a tendency to a rising occurrence and/or detection of SRCC has been entertained [14, 15]. The vast majority of SRCC arising in CR or in other anatomic sites presents in an advanced stage [1, 9, 15] and the outlook is generally dismal [9]. The significance of the stage vs. the histological subtype on the course has, however, been debated [5, 9] and the biological potential of SRCC is diverse with exceptional cases pursuing a more favorable course [3]. The possibility that indolent-behaving carcinomas, interpreted as SRCC, may be misdiagnosed and rather represent composite carcinomas including a goblet cell component has previously been alluded to [16].

SRCC is rarely identified at an early stage (carcinoma growing no deeper than the submucosa) [17]. In fact, the experience by Tung et al. [8] led to the conclusion that detection of CR SRCC always seems associated with a late stage. Nevertheless, cases of early-stage CR SRCC are on record [18–23].

A thorough histological analysis of early-stage carcinoma may provide important pieces of information that contribute to our understanding of the morphogenesis of CRC [17]. The general morphology of early-stage SRCC is not well delineated [24] and the immunohistochemical expression of important proteins, such as β-catenin and

E-cadherin, as well as adenomatous polyposis coli (APC), key markers of the Wingless–Wnt signaling pathway, has not yet been explored in this rarely detected tumor. We recently had the unique opportunity to expand current knowledge on histological and immunophenotypical attributes of early-stage SRCC, based on two such synchronous tumors, making comparative morphological analysis of intramucosal and submucosal SRCC feasible, including brief comments on the carcinogenesis. Additionally, data extracted from previous studies, addressing such topics, are provided. Where appropriate, parallels to SRCC of other anatomic sites are drawn.

Case report

A 65-year-old hereditary nonpolyposis colorectal cancer (HNPCC) male patient with a known disease-causing mutation in MLH1 has since 1999 been monitored biannually by colonoscopic surveillance. At the endoscopy performed in 2007, superficial biopsies of a polypoid lesion in the cecum were obtained. The histological examination was interpreted as adenoma with possible transition in carcinoma. Subsequently, the patient was subjected to a right hemicolectomy, which comprised a 15-mm soft lesion of the cecum, slightly elevated from the adjacent mucosa, observed and sampled at the recent endoscopy, as well as a 12-mm discrete concave, plaque-like lesion of the ascending colon, localized approximately 11 cm from the ileocecal valve. This linitis-plastica-like lesion was not visualized on colonoscopy. There were no morphological signs of regional spread and no clinical evidence of systemic dissemination. One year postoperatively, there were no signs of recurrence. The patient's family history included 11 members operated for CRC. Eight of these were coded as mucinous carcinoma. Informed consent from the patient to publish this material was obtained.

Material and methods

Five-micrometer-thick, formalin-fixed, and paraffin-embedded sections of the specimens were stained with hematoxylin–eosin (HE), periodic acid Schiff with diastase (PASD), and van-Gieson-alcian blue (AB at pH 2.6). Immunohistochemical studies were performed using standard immunoperoxidase procedures with diaminobenzidine as substrate. The primary antibody panel included the cytokeratins (CK) 7 and 20, the proliferating marker Ki-67, the components of the Wnt signaling pathway β-catenin, E-cadherin, and APC proteins, the mismatch repair proteins (MMRP) MLH1, MSH2, MSH6, and PMS2, and the endocrine markers synaptophysin and chromogranin A. Details regarding sources and dilutions are given in Table 1.

The expression characteristics of the markers CK7, CK20, and APC for stained cytoplasm, Ki-67 and MMRP for stained nuclei, and β-catenin and E-cadherin for stained cell membranes, cytoplasm, and nuclei, respectively, were carried out separately for the individual neoplastic components in the cecal lesion and in the submucosal compartment of the tumor of the ascending colon, respectively. For CK7, CK20, APC, and Ki-67, as well as β-catenin and E-cadherin (membranous and nuclear), the following semiquantitative scoring system was used: 0 all tumor cells negative; 1 >0–10% positive cells; 2 >10–50% positive cells; 3 >50% positive cells. The staining intensity was not scored. Cytoplasmic β-catenin and E-cadherin were recorded but not included in the scoring process. The distribution pattern of cells with aberrant β-catenin and E-cadherin expression was noticed. Expression for the endocrine markers was recorded as present or absent. The MMRP staining was characterized as retained, provided nuclear expression was identified, regardless the number of stained nuclei, as lack of expression in cases of no staining.

Appropriate positive and negative controls were run concurrently for all antibodies tested.

Table 1 Primary antibodies used in this study, their dilutions and commercial sources

Target antigen	Clone	Ig class	Dilution	Source
CK7	OV-TL 12/30	IgG1, k	1:2,000	DAKO A/S
CK20	Ks20.8	IgG2a, k	1:25	DAKO A/S
APC	Poly	IgG	1:100	Neomarkers
Ki-67	MIB-1	IgG1, k	1:50	DAKO A/S
β-catenin	β-catenin-1	IgG1, k	1: 400	DAKO A/S
E-cadherin	NCH-38	IgG1, k	1: 20	DAKO A/S
Chromogranin A	Poly	IgG	1:500	DAKO A/S
Synaptophysin	Poly	IgG	1:50	DAKO A/S
MLH1	G168-15	IgG1, k	1:40	BD PharMingen, California, USA
MSH2	25D12	IgG1, k	1:200	Novocastra Laboratories Ltd, Newcastle, Great Britain
MSH6	44	IgG1	1:200	BD Transduction Laboratories, Lexington, Kentucky, USA
PMS2	A16-4	IgG1, k	1:200	BD PharMingen, California, USA

Results

Histology of the tumor of the ascending colon

Histologically, the lesion of the ascending colon (Fig. 1a,b) featured a biphasic population of tumor cells (Fig. 1a) comprising typical SRC intermingled with similarly sized rounded cells with ovoid vesicular nuclei, often with one central prominent nucleolus, failing to reach the cytomorphological threshold of classical SRC. A small amount of mucin, usually neutral, less commonly acidic, occupied limited areas of the cytoplasm of some of the latter cells, resulting in minimal or no changes of the nuclear morphology (Fig. 1a, inset). Other tumor cells were void of identifiable mucin. For simplicity, we hereafter label tumor cells lacking overt SRC traits on HE sections poorly differentiated cells (PDC). The tumor cells infiltrated the superficial third of the submucosa, including vascular involvement. The invasive front was pushing in type, yet tumor budding cells invested by a dense hyalinized fibrous stroma were noticed (Fig. 1b).

Histology of the cecal lesion

The cecal neoplasm (Fig. 1c,d) comprised a similar constellation of SRC and PDC tumor cells, generally occupying limited areas, focally extending from the most superficial to the deepest compartments. This neoplastic proliferation entailed a distortion of the normal architecture with displacement of nonneoplastic crypts laterally, focally abutting the muscularis mucosa (Fig. 1c). Splaying of its fibers was, however, not a feature. Though areas of predominant SRC alternating with PDC-predominant zones were noticed, a layered pattern as previously described and depicted in intramucosal gastric SRCC [25, 26] was not convincingly demonstrated.

Further details on the general histology of the two lesions are given in Table 2.

Immunoprofile of the two synchronous lesions

The scores of the markers CK7, CK20, APC, Ki-67, β-catenin, and E-cadherin are summarized in Table 3. All neoplastic elements were immunonegative for CK7 (not shown) and extensively positive for Ki-67 (not shown). The immunoprofiles for CK20 and APC (Fig. 2a–f) were comparable, with high scores of SRC and low scores of PDC, whether intramucosal (Fig. 2c,d) or submucosal (Fig. 2e,f). For conventional tubular adenoma (CTA; Fig. 2a,b), intermediate scores of these two markers were obtained.

β-catenin and E-cadherin staining of the intramucosal lesional cells consistently displayed a membranous expression and absence of aberrant cytoplasmic or nuclear staining (Fig. 3a,c); (whereas intraepithelial SRC were readily apparent, SRC in the lamina propria were not convincingly demonstrated in the sections immunostained for β-catenin and E-cadherin, despite the production of several additional sections). Conversely, tumor cells infiltrating the submucosa consistently displayed loss of membranous staining of both markers as well as nuclear staining of β-catenin, corresponding to a score 2 for the SRC and 3 for the PDC (Fig. 3b). This aberration was demonstrated throughout this tumor. Cytoplasmic expression of β-catenin, usually noticed in association with nuclear reactivity, was consistently of a lesser staining intensity compared with that of the nuclei. There was no cytoplasmic or nuclear expression of E-cadherin (Fig. 3d).

Both the lesion of the ascending colon and the cecal lesions, including the intraepithelial components, disclosed loss of MLH1 and PMS2 (not shown) expression and retained nuclear expression for MSH2 and MSH6 (not shown).

Additionally, the distal lesion comprised a minor scattering of endocrine cells, visualized immunohistochemically for synaptophysin and chromogranin A (not shown). These cells did not manifest SRC attributes. Such cells were unapparent in the cecal growth.

Discussion

Carcinomas detected during screening occasionally afford us the opportunity to study their very early stages, as demonstrated herein. The present case is particularly notable for four reasons: (1) the synchronous presence of two early-stage SRCC (to our knowledge not previously reported), one of which was confined to the mucosa, the other invading the superficial third of the submucosal space, providing us the rare opportunity to perform comparative morphological studies of early-stage SRCC relating to its level of growth, (2) the coexistence of diverse precursor proliferations in the cecal mucosa, including conventional tubular adenomatous tissue and SRC–PDC in an intraepithelial and stromal location, (3) loss of normal membranous expression of β-catenin and E-cadherin and abundant nuclear expression of β-catenin throughout the submucosal growth and a normal membranous staining pattern of the intramucosal neoplastic elements of these proteins, contrasting a universal silencing of MLH1–PMS2 of all neoplastic elements, (4) the endoscopic detection of an elevated intramucosal lesion, whereas the carcinoma of the ascending colon, involving the submucosa, escaped detection by the endoscopist.

The present example of SRCC, grossly featuring a linitis-plastica-like growth pattern [27], is a rarely observed subtype of CRC, as opposed to that of the gastric counterpart [28], and its identification at an early stage is distinctly

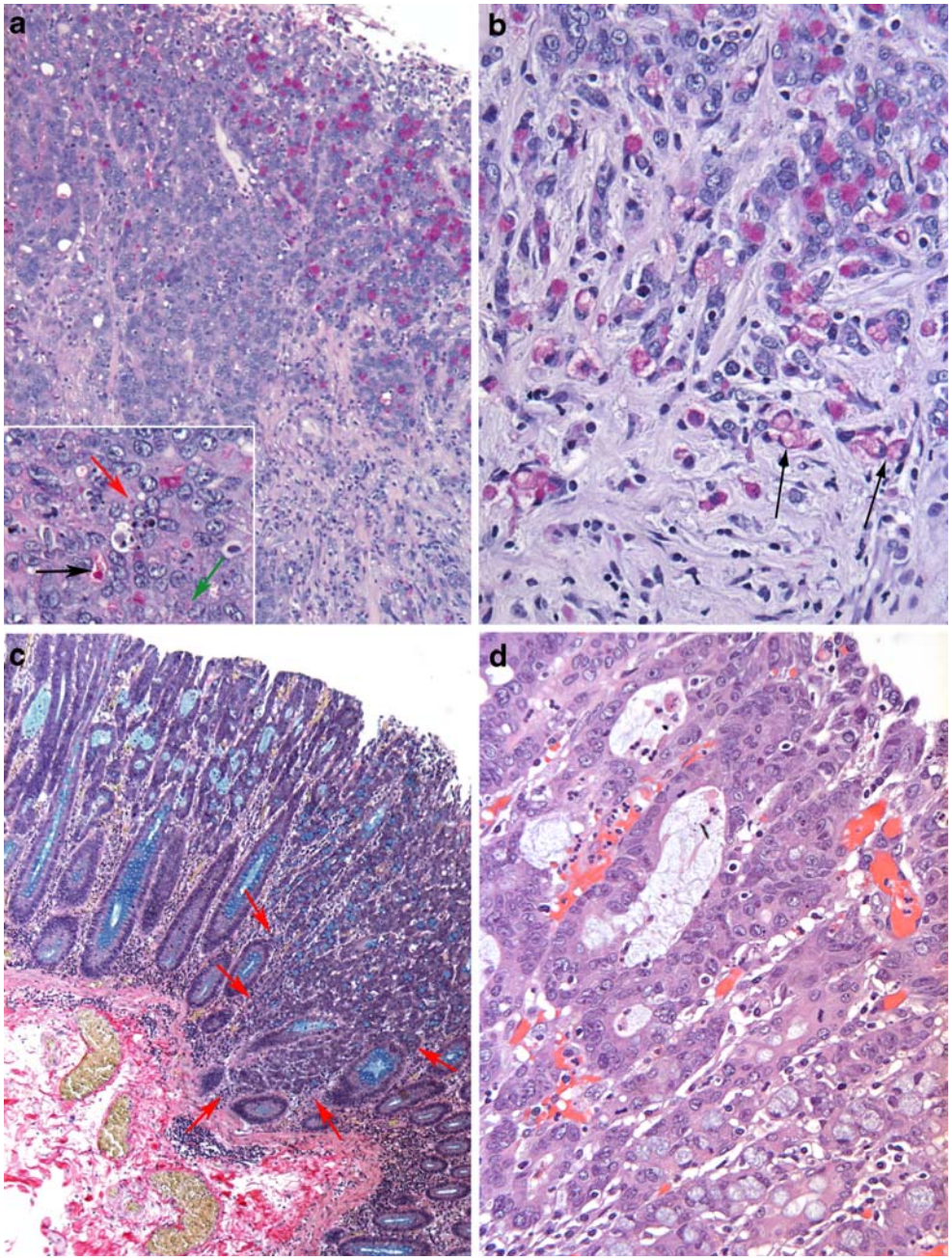

Fig. 1 Histology of the carcinoma of the ascending colon, demonstrating transition from confluences of cells void of overt signet-ring cell morphology (*left*) to an area dominated by signet-ring cells (*right*) PASD (**a**). A close-up view of a cell population with a non-signet-ring cell morphology features cells with centralized nuclei and occasional miniscule cytoplasmic mucin droplets (*colored arrows*), unapparent on hematoxylin–eosin-stained sections, though a subtle nuclear indentation appear in relation to one of these minute droplets (at *green arrow*). Additionally, a small round mucin-filled space is marked by a *black arrow*, PASD (*inset* in **a**). The invasive front of an area dominated by signet-ring cells set in a dense fibrous stroma as well as a reticulated quality of the intracellular PASD-positive material (*arrowed*) is demonstrated in **b**. Histology of the cecal lesion featuring transition from intraepithelial carcinoma involving the superficial half of the mucosa to zones of neoplastic cells focally infiltrating the lamina propria (zone between *arrows*) displacing the nonneoplastic crypts laterally and abutting the muscularis mucosa. The lesional cells comprise a mixture of SRC and PDC (van-Gieson alcian blue; **c**). A closer view of the superficial compartment demonstrated in **c** pinpoints a prevalence of cells with cytomorphological traits of PDC, lining the irregularly shaped and mucin-filled glands (*left*). Conversely, SRC is the predominating cell, lining the narrow, closely apposed tubules, right, hematoxylin–eosin (**d**)

Table 2 Histopathological details of the lesions in the cecum and the ascending colon

	Cecum (pTis)	Ascending colon (pT1)
Predominate cell type	PDC > SRC	PDC > SRC
Arrangement of tumor cells	Small aggregates, multifocally in lamina propria	Rows, confluent solid sheets, rare abortive glands
Mitotic activity	High	High
Necrosis	None	Focally present
Stromal mucin	Absent	Absent
Lymphocytic component	Present, moderate	Present, moderate
Transition in intraepithelial precursor proliferation	Present (conventional tubular adenoma and intraepithelial SRCC) (Fig. 1d)	Absent

PDC poorly differentiated cell, *SRC* signet-ring cell, *SRCC* signet-ring cell carcinoma

uncommon, as it appears from Table 4, with merely six previous publications in English-language literature [18–23].

Though not meeting the strict quantitative criteria for SRCC, frequently quoted [29] histological features of the present lesions are shared with variants of SRCC [26, 30–34]. Thus, in concert with the description of diverse cell types noticed within the realm of gastric SRCC [31, 35], the present lesions featured in addition to a component of classical SRC, constituting less than 50% of the examined tumor cell population, a predominance of lesional cells, sized and shaped as SRC but void of its classical cytomorphology. This predominant, "aberrant" cell, best corresponding to the anaplastic subtype of the gastric counterpart [36], occasionally featured minute cytoplasmic mucin droplets that failed to significantly displace the nucleus or otherwise modify its morphology and thereby readily passed unnoticed on HE-stained sections. Such cells may provide a morphological link between the classical SRC and its nonmucinous counterpart, which is here perceived as a poorly differentiated variant of SRC. The immunopattern of the β-catenin and E-cadherin of the submucosal growing tumor could support the latter contention. Such cell type seems insufficiently emphasized in the context of the CR lesions, presumably due to a true infrequency combined with lack of awareness of the cytomorphological variants of CR SRCC.

The immunoreaction for the markers APC, CK7, CK20, Ki-67, and MMRP recorded in the cecal lesion was maintained in the submucosally expanding growth of the ascending colon. Of note is the retained low expression of APC, as well as of CK20 and the high Ki-67 score of the PDC in both sites, regardless the level of involvement as well as the conspicuous expression for these three markers of the SRC intramucosally and submucosally.

The immunoprofile of β-catenin and E-cadherin proved, on the other hand, primarily a function of the depth of involvement. Thus, normal membranous expression characterized the intramucosal lesion. Conversely, alterations in the expression pattern of the two proteins characterized the submucosal growth with universal loss of membranous expression as well as aberrant nuclear reaction of β-catenin.

In addition to the central role in the carcinogenesis of defective DNA replication error repair of this HNPCC patient, a dysregulation of the Wnt signaling pathway

Table 3 Scores of immunoexpression in relation to type of neoplastic cells of the lesions in the cecum and the ascending colon

Markers	Cecal lesion (pTis)			Lesion of ascending colon (pT1)	
	CTA	PDC^m	SRC^m	PDC^s	SRC^s
CK7[a]	0	0	0	0	0
CK20[a]	2	1	3	1	3
APC[a]	2	1	3	1	3
Ki-67[a]	3	3	3	3	3
β-catenin, membranous[a]	3	3	?	0	0
β-catenin, nuclear[a]	0	0	?	3	2
E-cadherin membranous[a]	3	3	?	0	0
E-cadherin nuclear[a]	0	0	?	0	0

CTA conventional tubular adenoma, PDC^m poorly differentiated, non-signet-ring cells of mucosa, intraepithelial or stromal, SRC^m signet-ring cells of the mucosa, intraepithelial or stromal, PDC^S poorly differentiated, non-signet-ring cells of the submucosa, SRC^S signet-ring cells of the submucosa

[a] Scores: 0, all tumor cells negative; 1, >0–10% positive tumor cells; 2, >10–50% positive tumor cells; 3, >50% positive tumor cells. ?, SRC were not convincingly present in the lamina propria of the sections immunostained for β-catenin or E-cadherin

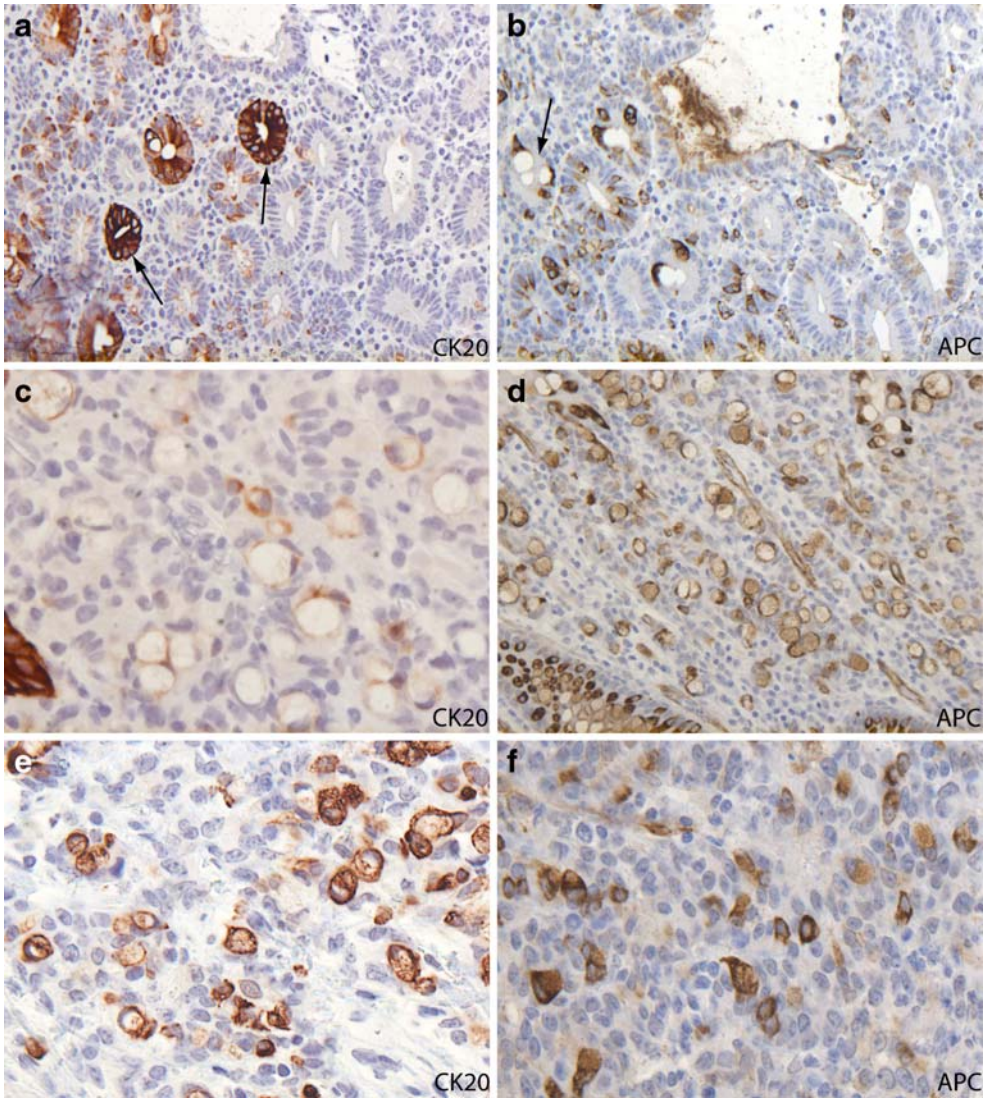

Fig. 2 Corresponding areas of conventional tubular adenoma of the cecum, immunostained for CK20 (**a**) and APC (**b**). The immunopattern is variegated with positively and negatively reacting neoplastic cells. Few remnants of native crypts surrounded by the adenoma are *arrowed*. The goblet cells are intensely stained, especially for APC. Tumor cells infiltrating the lamina propria feature CK20- and APC-positive SRC, admixed with sparsely decorated to nonreactive PDC (**c**, **d**). A similar immunoprofile characterizes tumor cells of the submucosa (CK 20 (**e**), APC (**f**))

seems to contribute to the tumor progression at the pT1 stage, i.e., neither as an initiating nor as a late event. Additionally, dysregulation of CK20 may be a contributory factor.

Whereas the intramucosal β-catenin and E-cadherin profile of CR SRCC, as presented herein, to our knowledge, has not previously been addressed, few comparative analysis of intramucosal gastric SRCC are at hand. In one such study, lesional cells were recorded as β-catenin negative, whereas immunostaining for E-cadherin was retained, albeit reduced in intensity [35]. Tsukashita et al. [37] demonstrated an absence of nuclear staining of β-catenin in concert with our studies, pinpointing that the β-catenin expression pattern does not always reflect malignant transformation in early-stage carcinogenesis, thus in line with our observations. Of further note is the dynamic alteration of the E-cadherin immunoprofile, reported by Nakamura et al. [38], implying its downregulation of the intramucosal gastric SRCC in contrast to the reappearance of E-cadherin staining in the submucosally growing lesion. Conversely, complete loss of E-cadherin characterized the submucosal component of SRCC in the present patient. The use of diverse antibodies may in part explain this observation.

The immunoexpression of β-catenin and E-cadherin in CR SRCC growing beyond the mucosa has, to our knowledge, been explored in two communications [39, 40]. Moon et al. [39] recorded nuclear shifting of β-catenin

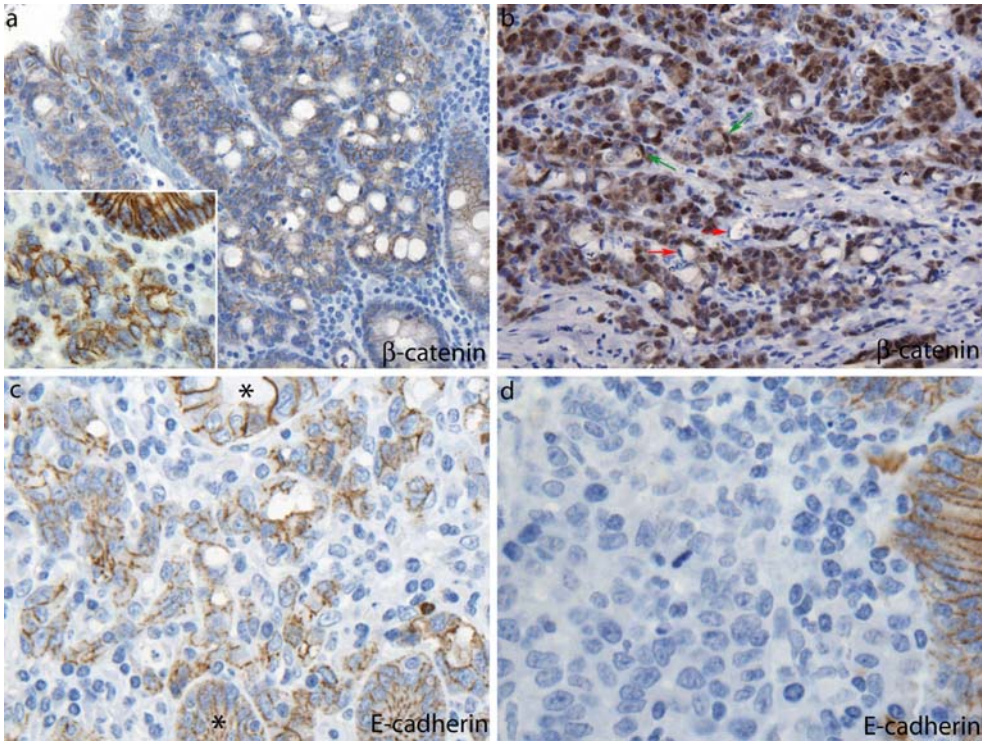

Fig. 3 β-catenin expression of the intramucosal (**a**) and submucosal (**b**) growths. In **a** illustrating an intraepithelial neoplastic component, including SRC, in *inset* **a** featuring PDC in the lamina propria, membranous expression is a consistent attribute, similar to that of the native crypts, having a chicken-wire appearance. A comparable immunoprofile characterizes conventional tubular adenoma (not shown). In the submucosa, membranous expression is universally lost. Whereas a nuclear translocation is a predominant feature of PDC, the score of such aberrant expression is lower for SRC. Some SRC displaying nuclear shifting are indicated by *green arrows*; other SRC displaying a lack of expression are marked by *red arrows* (**b**). E-cadherin expression of the intramucosal (**c**) and submucosal (**d**) growths. In **c**, membranous reaction characterizes PDC in the lamina propria as well as the epithelium of the native crypts (two of which are marked by *asterisks*). Expression of E-cadherin is uniformly lost in the submucosal growth, in **d** illustrating infiltrating PDC (*lower left quadrant*). Nor did SRC express this protein (not shown). Base of a crypt, *far right*, displays normal membranous reaction

Table 4 Available examples labeled early-stage colorectal signet-ring cell carcinoma (SRCC), based on English-language literature

Authors	pTis, *n*	pT1, *n*	Age/sex	Presenting symptoms/mode of detection	Size/site	Transition in precursor proliferation	Additional comments by authors
Nakamura et al. [21]	0	1	67/M	Bleeding per rectum	26 mm/rectum	TVA	Four separate foci of SRCC + four foci of CRC, NOS
Tandon et al. [23]	0	1	59/M	FOBT+	15 mm/sigmoid	TA	
Mai et al. [20]	2	0	NS	NS	NS	TA and IESRCC	One of the cases p53+
Shimaoka et al. [22][a]	0	1	72/F	Abdominal fullness	7 mm/desc. colon	Not present	Ascites with SRC
Fu et al. [18][b]	0	1	67/M	Surveillance colonoscopy	7 mm/transv. colon	Not present	MLH1−, MSH2+
Lewin et al. [19]	3	0	NS	Colonoscopy	NS	Present	
Klarskov et al., present case	1[c]	1[c]	65/M	Surveillance colonoscopy	15 mm/cecum (pTis) 12 mm/asc. colon (pT1)	TA + IESRCC Not present	MLH1−, PMS2−, MSH2+, MSH6+

TVA tubulovillous adenoma, *CRC* colorectal carcinoma, *NOS* not otherwise specified, *FOBT* feces for occult blood test, *TA* tubular adenoma, *NS* not stated, *IESRCC* intraepithelial signet-ring cell carcinoma, *SRC* signet-ring cell

[a] The authors collected additional 14 cases "with appearance of early-stage SRCC" from the literature, all Japanese contributions. Their definition of early-stage SRCC did, however, deviate from that generally used, making interpretation difficult. Judging from their Table 1, two cases of intramucosal and three cases of submucosa SRCC were identified

[b] The authors collected additional l9 pT1 cases (one of which was also included by Shimaoka et al. [22]) and six pTis cases from the literature, all Japanese contributions

[c] Two synchronous cases

and E-cadherin in nine out of ten and in seven out of ten cases, respectively. Conversely, Wong et al. [40] found aberrant β-catenin location in merely two of their 18 examples, leading to the conclusion that dysregulation in the Wnt signaling pathway played no prominent role in the oncogenesis in most CR SRCC. These divergent results may relate to the predominate cytomorphology of the tumor, its pTNM stage, and/or to the HNPCC status. Such specific characteristics of the study populations were, however, not given in these two communications. It is possible that the β-catenin and E-cadherin expressions visualized in the present case are modified by the HNPCC status. Thus, mutations in the regulatory domain of β-catenin are not uncommon in that setting, however, particularly in cases of advanced stages (pN1–2 and pM1) [41]. Such aberrating expression usually appears in a heterogenous distribution, particularly at the invasive front of the tumor [42, 43]. Despite the low stage (pT1, N0) of the present lesion of the ascending colon, nuclear β-catenin was a prominent finding throughout the tumor, including the superficial regions, possibly in part, related to the small size of this tumor.

Wong at al. [40] called attention to the aggressive behavior of SRCC with aberrant expression of β-catenin. In concert, studies of other types of neoplasms have demonstrated correlation between increased invasiveness and altered expression of the E-cadherin–β-catenin complex [44]. Caution in translating such data to HNPCC-associated SRCC should, however, be exercised. In the same vein, Jass [11] has recently commented on our lack of knowledge as to the course of patients with SRCC in the context of MSI-H status. Indeed, nuclear β-catenin and E-cadherin in this clinical setting have been previously shown to play no role for survival [45]. It remains to be determined whether the same applies to (1) the high Ki-67 index, approaching 100% of the neoplastic cells in our patient, as well as to (2) the decrease in CK20 expression of the predominate PDC. The latter staining profile probably denotes immaturity [46] and poor differentiation of the lesional cells. Again, extrapolation from MMR-proficient CRC to CRC complicating the HNPCC syndrome may, however, not be appropriate.

The present case was a recent one, but, as of this writing, some 12 months postoperatively, no evidence of recurrence has appeared. The low stage of the present lesions coupled with histological features of the submucosal growing tumor, such as the pushing-type deep margin and the morphological presence of a host immune response, evidenced by a lymphocytic component, may favorably influence the course; the budding quality of the tumor cells as well as the altered immunoprofile of the E-cadherin–β-catenin complex may, however, exert the opposite effect.

As recently alluded to [24], the morphology of early stages of SRCC is not well established and demonstration of association with intraepithelial precursor neoplasms, as observed in the present case, is uncommon [6]. This has led to the claim of a de novo carcinogenesis [12, 14, 47]. Examples of spatial and probably functional relation between early-stage SRCC and conventional adenoma are, however, on record [19, 21, 23]. The identification of intraepithelial signet-ring cell carcinoma (IESRCC) in combination with CTA, characterizing the present cecal lesion, has been previously described in only one communication [20]. The uncommonly observed IESRCC may be a result of the rapidly growing quality of SRCC, obscuring in situ components. Our case, featuring IESRCC, a most likely precursor proliferation, in addition to CTA, robustly argues against a de novo pathway as well as against the possibility that the intramucosal cecal lesion represented a metastasis from the submucosal SRCC of the ascending colon.

Conclusion

In this study, prompted by an HNPCC-associated case of two synchronous early-stage SRCC, a submucosal and an intramucosal, an attempt has been made to contribute morphological observations on early-stage SRCC of colonic origin, including the histological spectrum and the immunoprofile. Cytomorphologically, a spectrum of attributes ranging from cells with overt SRC traits to similarly sized and shaped cells with centralized nuclei, labeled PDC, resulted in a biphasic pattern. The intramucosal tumor featured transition from tumor cells in the lamina propria to precursor proliferations (conventional tubular adenoma and intraepithelial SRC). The immunoprofile of the E-cadherin–β-catenin complex suggested that disruption of the Wnt signaling pathway was neither an initiating nor a late event, becoming immunohistochemically apparent at the pT1-stage, thus being preceded by inactivation of mismatch repair genes, apparent already intramucosally. Additionally, dysregulation of CK20 may play a role in the early morphogenesis.

Conflict of interest statement We declare that we have no conflict of interest.

References

1. Anthony T, Georg R, Rodriguez-Bigas M et al (1996) Primary signet-ring cell carcinoma of the colon and rectum. Ann Surg Oncol 3:344–348

2. Börger ME, Gosens MJEM, Jeuken JWM et al (2007) Signet ring cell differentiation in mucinous colorectal carcinoma. J Pathol 212:278–286
3. Connelly JH, Robey-Cafferty SS, El-Naggar AK et al (1991) Exophytic signet-ring cell carcinoma of the colorectum. Arch Pathol Lab Med 115:134–136
4. Messerini L, Palomba A, Zampi G (1995) Primary signet-ring cell carcinoma of the colon and rectum. Dis Colon Rectum 38:1189–1192
5. Nissan A, Guillem JG, Paty PB et al (1999) Signet-ring cell carcinoma of the colon and rectum. A matched control study. Dis Colon Rectum 42:1176–1180
6. Ooi BS, Ho YH, Eu KW et al (2001) Primary colorectal signet-ring cell carcinoma in Singapore. ANZ J Surg 71:703–706
7. Secco GB, Fardelli R, Campora E et al (1994) Primary mucinous adenocarcinomas and signet-ring cell carcinomas of colon and rectum. Oncol 51:30–34
8. Tung S-Y, Wu C-S, Chen P-C (1996) Primary signet ring cell carcinoma of colorectum: an age- and sex-matched controlled study. Am J Gastroenterol 91:2195–2199
9. Sasaki O, Atkin WSA, Jass JR (1987) Mucinous carcinoma of the rectum. Histopathol 11:259–272
10. Svrcek M, Cosnes J, Beaugerie L et al (2007) Colorectal neoplasia in Crohn's disease: a retrospective comparative study with ulcerative colitis. Histopathol 50:574–583
11. Jass JR (2007) Classification of colorectal cancer based on correlation of clinical, morphological and molecular features. Histopathol 50:113–130
12. Kawabata Y, Tomita N, Monden T et al (1999) Molecular characteristics of poorly differentiated adenocarcinoma and signet-ring-cell carcinoma of colorectum. Int J Cancer 84:33–38
13. Psathakis D, Schiedeck THK, Krug F et al (1999) Ordinary colorectal adenocarcinoma *vs*. primary colorectal signet-ring cell carcinoma - study matched for age, gender, grade, and stage. Dis Colon Rectum 42:1618–1625
14. Jass JR (1989) Do all colorectal carcinomas arise in preexisting adenomas? World J Surg 13:45–51
15. Kang H, O'Connell JB, Maggard MA et al (2005) A 10-year outcomes evaluation of mucinous and signet-ring cell carcinoma of the colon and rectum. Dis Colon Rectum 48:1161–1168
16. Fujiyoshi Y, Kuhara H, Eimoto T (2005) Composite glandular-endocrine cell carcinoma of the stomach. Report of two cases with goblet cell carcinoid component. Pathol Res Pract 200:823–829
17. Shimoda T, Ikegami M, Fujisaki J et al (1989) Early colorectal carcinoma with special reference to its development de Novo. Cancer 64:1138–1146
18. Fu K-I, Sano Y, Kato S et al (2006) Primary signet-ring cell carcinoma of the colon at early stage: a case report and a review of the literature. World J Gastroenterol 12:3446–3449
19. Lewin MR, Fenton H, Burkart AL et al (2007) Poorly differentiated colorectal carcinoma with invasion restricted to lamina propria (intramucosal carcinoma): a follow-up study of 15 cases. Am J Surg Pathol 31:1882–1886
20. Mai KT, Isotalo PA, Guindi M et al (2002) Intestinal epithelial lesions associated with signet ring cell carcinoma of the colon and small intestine. Pathology 34:51–56
21. Nakamura T, Nakano G-I, Sakamoto K (1983) Adenoma of the rectum with multiple foci of signet-ring cell carcinoma. Report of a case. Dis Colon Rectum 26:529–532
22. Shimaoka S, Niihara T, Tashiro K et al (2002) Signet-ring cell carcinoma of the colon 7 mm in size with peritonitis carcinomatosa. J Gastroenterol 37:550–555
23. Tandon M, Sostek M, Klein MA (1999) Focus of signet ring cell carcinoma in an adenoma of the sigmoid colon. Arch Pathol lab Med 123:957–959
24. Makino T, Tsujinaka T, Mishima H et al (2006) Primary signet-ring cell carcinoma of the colon and rectum: report of eight cases and review of 154 Japanese cases. Hepato-Gastroenterol 53:845–849
25. Sugihara H, Hattori T, Fujita S et al (1989) Distribution of fibronectin and laminin in early and advanced signet-ring-cell carcinomas of the stomach. Int J Cancer 43:263–269
26. Xuan ZX, Ueyama T, Ambe K et al (1992) Signet-ring cell carcinoma of the stomach. A quantitative analysis on its submucosal invasion using a computer image analyzer. Path Res Pract 188:1060–1066
27. Ojeda VJ, Mitchell KM, Walters MN-I et al (1982) Primary colorectal linitis plastica type of carcinoma: report of two cases and review of the literature. Pathology 14:181–189
28. Odze RD, Goldblum JR, Crawford JM (2004) Surgical pathology of the GI tract, liver, biliary tract, and pancreas. Elsevier, Philadelphia
29. Hamilton SR, Vogelstein B, Kudo S et al (2000) Carcinoma of the colon and rectum. In: Hamilton SR, Aaltonen LA (eds) World Health Organization classification of tumours. Pathology and genetics. Tumours of the digestive system. IARC, Lyon, pp 105–119
30. Fenoglio-Preiser CM, Noffsinger AE, Stemmermann GN et al (2007) Gastrointestinal pathology, 3rd edn. Lippincott, Williams & Wilkins, Philadelphia
31. Fujiyoshi Y, Eimoto T (2008) Chromogranin A expression correlates with tumour cell type and prognosis in signet ring cell carcinoma of the stomach. Histopathol 52:305–313
32. Kiyokawa T, Young RH, Sculla RE (2006) Krukenberg tumors of the ovary. A clinicopathologic analysis of 120 cases with emphasis on their variable pathologic manifestations. Am J Surg Pathol 30:277–299
33. Laufman H, Saphir O (1951) Primary linitis plastica type carcinoma of the colon. Arch Surg 62:79–91
34. Shirouzu K, Isomoto H, Morodomi T et al (1994) Primary linitis plastica carcinoma of the colon and rectum. Cancer 74:1863–1868
35. Kumarasinghe MP, Lim TKH, Ooi C-J et al (2006) Tubule neck dysplasia: precursor lesion of signet ring cell carcinoma and the immunohistochemical profile. Pathology 38:468–471
36. Fenoglio-Preiser C, Carneiro F, Correa P et al (2000) Gastric carcinoma. In: Hamilton SR, Aaltonen LA (eds) World Health Organization classification of tumours. Pathology and genetics. Tumours of the digestive system. IARC, Lyon, pp 39–52
37. Tsukashita S, Kushima R, Bamba M et al (2003) Beta-catenin expression in intramucosal neoplastic lesions of the stomach. Comparative analysis of adenoma/dysplasia, adenocarcinoma and signet-ring cell carcinoma. Oncology 64:251–258
38. Nakamura E, Sugihara H, Bamba M et al (2005) Dynamic alteration of the E-cadherin/catenin complex during cell differentiation and invasion of undifferentiated-type gastric carcinomas. J Pathol 205:349–358
39. Moon KC, Cho SY, Lee HS et al (2006) Distinct expression patterns of E-cadherin and β-catenin in signet ring cell carcinoma components of primary pulmonary adenocarcinoma. Arch Pathol Lab Med 130:1320–1325
40. Wong SCC, Chan ATC, Lo ESF et al (2005) Nuclear β-catenin expression is rare and its potential association with short survival in colorectal signet-ring cell carcinoma. Appl Immunohistochem Mol Morphol 13:248–251
41. Johnson V, Volikos E, Halford SE et al (2005) Exon 3 β-*catenin* mutations are specifically associated with colorectal carcinomas in hereditary non-polyposis colorectal cancer syndrome. Gut 54:264–267
42. Brabletz T, Jung A, Hermann K et al (1998) Nuclear over-expression of the oncoprotein β-catenin in colorectal cancer is

localized predominantly at the invasion front. Pathol Res Pract 194:701–704
43. Gavert N, Ben-Zeév A (2007) β-catenin signaling in biological control and cancer. J Cell Biochem 102:820–828
44. Chetty R, Serra S, Asa SL (2008) Loss of membrane localization and aberrant nuclear E-cadherin expression correlates with invasion in pancreatic endocrine tumors. Am J Surg Pathol 32:413–419
45. Lugli A, Zlobec I, Minoo P et al (2007) Prognostic significance of the wnt signalling pathway molecules APC, β-catenin and E-cadherin in colorectal cancer—a tissue microarray-based analysis. Histopathol 50:453–464
46. Davenport A, Hale RJ, Hunt CR et al (2003) Expression of Ki-67 and cytokeratin 20 in hyperplastic polyps of the colorectum. J Clin Pathol 56:200–204
47. Stolte M, Bethke B (1995) Colorectal mini-de Novo carcinoma: a reality in Germany too. Endoscopy 27:286–290

Miscellaneous

Part of this study has been previously presented at the annual meeting of the Danish Society of Pathological Anatomy and Cytology, 2008.

Virchows Arch (2009) 454:125–131
DOI 10.1007/s00428-008-0711-9

REVIEW AND PERSPECTIVE

Retroperitoneal margin of the pancreaticoduodenectomy specimen: anatomic mapping for the surgical pathologist

Mahmoud A. Khalifa · Vlad Maksymov · Corwyn Rowsell

Received: 2 September 2008 / Revised: 16 November 2008 / Accepted: 19 November 2008 / Published online: 6 December 2008

Abstract Surgical margin status of the pancreaticoduodenectomy specimen is an independent predictor of survival in patients with pancreatic head cancer. Although most surgical pathologists are familiar with the protocols for grossing and evaluation of the various margins of the specimen, the currently prevailing definitions of the retroperitoneal surgical margin minimize the fact that this margin is actually a combination of surfaces of different anatomical structures. The unfamiliarity with its detailed anatomy often creates communication gaps when the pathologic findings are presented to other members of the multidisciplinary team. The following discussion is the collective opinion of hepato-pancreato-biliary pathologists in two tertiary care Canadian medical centers in this field. It describes the authors' proposed nomenclature and landmarks for anatomic mapping of the retroperitoneal margin of the pancreaticoduodenectomy resected specimen. Increasing familiarity with the subtleties of the retroperitoneal margin is expected to improve communication and sets the stage for future quality improvement initiatives and translational research in the multidisciplinary setting.

Keywords Surgical margins · Whipple's specimen · Pancreaticoduodenectomy · Anatomy · Pancreas

M. A. Khalifa (✉) · C. Rowsell
Department of Pathology, Sunnybrook Health Sciences Center,
2075 Bayview Avenue, Room E-400,
Toronto, ON M4N 3M5, Canada
e-mail: Mahmoud.Khalifa@sunnybrook.ca

V. Maksymov
Department of Pathology, Memorial University of Newfoundland,
St. John's, Canada

Introduction

Positive surgical margin or incomplete resection of pancreatic cancer by the pancreaticoduodenectomy (PD) procedure is associated with early tumor recurrence and no survival benefit compared to palliative therapy [1–4]. Surgical margin status has been identified as an independent predictor of survival [1, 5]. Typically surgical margins of the PD specimen are luminal (proximal gastric and distal duodenal/jejunal), pancreatic (also known as distal pancreatic or pancreatic transection margin and it results from transecting the pancreatic neck) [5], bile duct, and what is commonly referred to as retroperitoneal (also known as posterior, radial, or circumferential margin). Assessment of the bile duct and pancreatic surgical margins is a well-established routine practice. It is usually a part of the intraoperative consultation (IOC) and grossing protocols of the PD specimen. Luminal margins of the specimen are routinely submitted and examined on permanent sections. Standardized protocols regarding the pathologic assessment of the retroperitoneal margin of the PD specimen, however, are not routinely applied, partly because of its unfamiliar anatomy [6]. This endeavor may have also been hindered by the notion that assessment of the retroperitoneal surgical margin intraoperatively is irrelevant since the surgeon cannot do much about it due to its anatomic barriers, namely the superior mesenteric artery (SMA) and superior mesenteric vein/portal vein (SMV/PV). However, the extended radical operation for pancreatic head cancer which includes the en block resection of the posteriorly located great vessels is now becoming more common for advanced disease [2, 7, 8]. As a result, pathologists are increasingly involved in the more detailed assessment of the retroperitoneal margin intraoperatively as well as during their routine grossing of the PD specimen. This article intends

to review the literature and to elaborate on our approach in defining and describing the retroperitoneal margin based on the experience gathered in two high-volume, tertiary care Canadian medical centers. It also aims at stimulating the discussion of this topic among members of the hepato-pancreato-biliary multidisciplinary community. It was not written to propose a standardized approach to the handling or assessment of this margin since we believe that an agreement on the definition of its basic components is needed first.

The pancreas is a retroperitoneal organ. At one point in the PD procedure, in order to mobilize the pancreas, the surgeon has to cut the posterior wall of the lesser sac along the superior and the inferior borders of the pancreas. Accordingly, the anterior aspect of the pancreatic head in the PD specimen forms the posterior wall of the lesser sac. As it sits in the abdominal cavity, this surface is partly covered by the gastric body and pylorus. Since the surgeon does not have to resect or dissect it from any other structure, it is not considered as a surgical margin, although assessment and documentation of its involvement have been advocated [9]. By contrast, the retroperitoneal margin is a true surgical margin as it results from the surgeon's resection (using a sharp knife or blade) and dissection (using the hand and scissors) of the pancreas from the posterior abdominal wall.

Definition of the retroperitoneal margin

The retroperitoneal surgical margin of the PD specimen was defined by some authors as "the soft tissue margin directly adjacent to the proximal 3 to 4 cm of SMA" [2, 9–11]. Almost similarly, Varadhachary et al. [4] defined it as "the tissue to the right of the proximal 3 to 4 cm of the SMA" while Zamboni et al. [12] defined it as "the peripancreatic adipose tissue behind the head of the pancreas that is located dorsally and laterally to the SMA". These definitions, although all are accurate, do minimize the fact that this margin is actually a combination of surfaces of different anatomical structures. They do, however, emphasize certain aspects about this margin such as it being in the vicinity of SMA, dorsal (posterior), and often consisting of an adipose tissue layer that covers the pancreatic parenchyma. Since pathologists handle the PD specimen in vitro, defining the retroperitoneal margin by its topographic relation to the SMA, which is typically left in the body, is not particularly informative. It has been noted in our practice that some surgeons even use the terms "retroperitoneal margin", "posterior margin", "radial margin", and "uncinate margin" interchangeably.

Verbeke [9] has recently offered a thorough discussion of the concept of the circumferential resection margin (CRM) of the pancreaticoduodenectomy specimen, which is divided into three components: the anterior, posterior, and medial surfaces. He further proposes a protocol for the gross and microscopic evaluation of the CRM using multicolor inking. A similar multicolor protocol has been described by Esposito et al. [5] distinguishing the medial margin (referred to in our proposed approach as "uncinate process") from the remains of the posterior margin. The purpose of our proposed mapping is to further highlight the anatomy of the posterior and medial surfaces, which have been collectively referred to as the "retroperitoneal margin" (Table 1). It is also hoped that the proposed mapping will inspire practicing pathologists to work-up the entire retroperitoneal margin clearly identifying each of its components. Malignant cells present at this margin will categorize it as "positive". However, when the margin is free of malignancy, it could be designated as "negative" while its distance from the closest malignant cells is reported in millimeters (Fig. 1).

The uncinate process and margin

The College of American Pathologists, in their pancreatic cancer protocol and checklist, recommends reporting the posterior retroperitoneal margin and the uncinate margin separately [13]. The uncinate process is the elongation of the head of the pancreas that wraps posterior to the SMV/PV and extends as a tongue-like projection to touch the right lateral aspect of the SMA. To pathologists, it is seen in the PD specimen posteriorly as an elevation of the pancreatic head, usually with a thin overlay of adipose tissue that could be prominently vascular and it represents a surgical dissection margin (Fig. 2). In some cases, this surface could be covered by considerable adhesions which could trigger for an intraoperative assessment. The posterior surface of the uncinate process sits in the body directly

Table 1 Components of the retroperitoneal surgical margin

Component	Nature	Assessment	Related structures
Uncinate process	Dissection	Permanent only	Posterior wall fat
Uncinate margin	Resection	IOC and permanent	SMA
Groove	Dissection	Permanent only	SMV/PV
Medial aspect (when present)	Dissection	Permanent only	Posterior wall fat
Superior and inferior	Dissection	Permanent only	Abdominal fibroadipose tissue

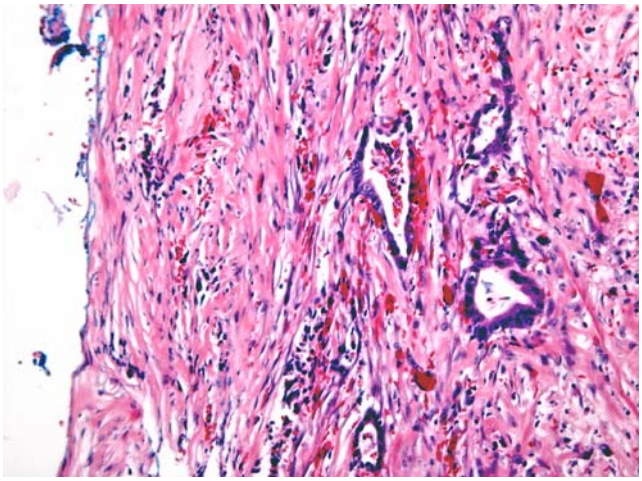

Fig. 1 A photomicrograph depicting malignant, gland-forming cells present within less than 1 mm from the inked retroperitoneal margin (H&E×100)

attached to the posterior abdominal wall and the surgeon separates it from its underlying adipose tissue by gentle dissection.

In order to deliver the specimen, the surgeon needs to divide the soft tissue adjacent to the uncinate process as close to the SMA as possible, creating what is known as the uncinate resection margin. It is the only element of the entire retroperitoneal margin that is truly a resection margin (Fig. 2). This anatomic relationship to the SMA has led some authors to rename the uncinate margin as the "SMA margin" [14]. We define the uncinate resection margin as the cut surface produced by the surgeon's knife while dissecting the uncinate process from the SMA, which tends to be granular and irregular and is usually comprised of adipose tissue, often densely innervated. This is different from the remaining smooth and regular retroperitoneal surface of the pancreatic head that is produced by dissection. As indicated earlier, this surgical resection margin is referred to as the "medial" margin by other authors [5, 9].

The surgeon's goal is to resect the uncinate process from SMA without damaging it or the autonomic nerve plexus surrounding it. It is our experience that denuding the peri-arterial nerve plexus often results in a prolonged postoperative gastric ileus. Technically, this is a very challenging step in the PD procedure since the uncinate process is very well vascularized and tends to bleed. Also, the SMA is quite adherent to the most distal aspect of the uncinate process. As a result, there is a natural tendency on the part of the surgeon to leave behind, in the patient, the bit of uncinate tissue closest to the SMA. In cases of carcinoma involving the uncinate process, as the surgeon dissects away from the SMA (closer to the pancreatic tissue) he/she may run the risk of producing a positive margin, leaving behind extra-pancreatic malignant cells in the adipose tissue around the SMA or even intra-pancreatic malignancy if a portion of the uncinate process was left adherent to the SMA. It is, therefore, important to assess the uncinate resection margin intraoperatively [15]. We have described our technique that enables the pathologist to provide an accurate IOC on the uncinate resection margin [16, 17]. In cases where excision of additional tissue from the immediate vicinity of the SMA is still technically feasible, the intraoperative reporting of a positive uncinate resection margin may prompt its revision to ensure complete excision of all cancerous tissue by complete removal of any adipose tissue directly adjacent to the SMA.

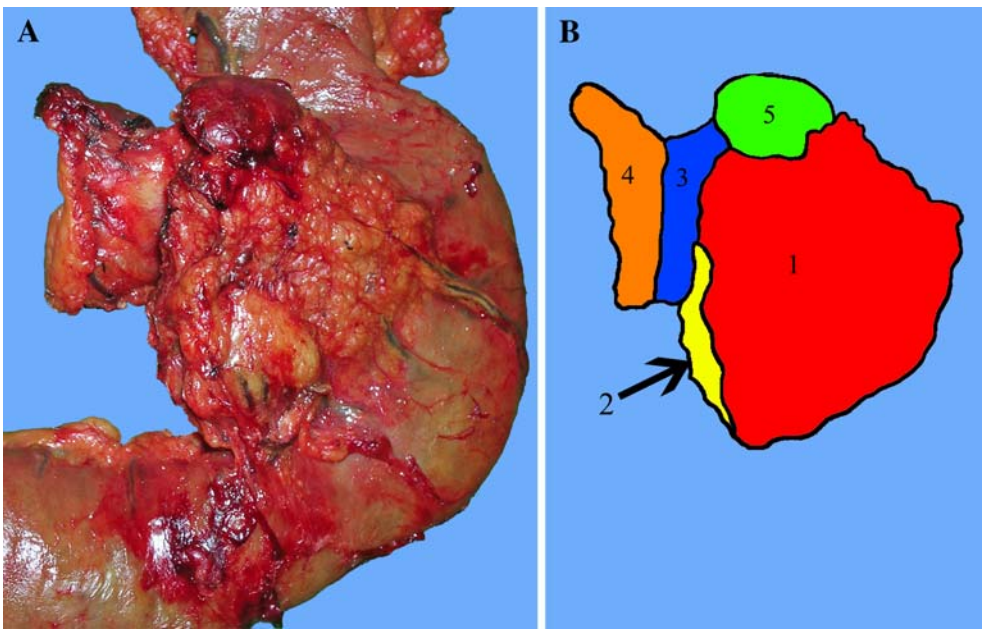

Fig. 2 Pancreaticoduodenectomy specimen. **a** The retroperitoneal surgical margin. **b** A diagrammatic mapping of the same specimen highlighting its various elements; *1* posterior surface of uncinate process, *2* uncinate margin, *3* the medial part of the vascular groove (the more lateral part is obscured by the uncinate process tip), *4* the medial aspect (only in cases with extended pancreatic resection), *5* a superior mesenteric lymph node that is not part of the retroperitoneal margin but happened to be excessively enlarged in this particular case

The groove (vascular bed)

The vascular groove is the anatomical term describing the concavity where the SMV/PV comes in contact with retroperitoneal surface of the pancreas (Fig. 3). It is also used as a landmark which defines the uncinate process from the rest of the pancreatic head. In the majority of cases, pathologists recognize it as a concave depression with a smooth, glistening surface immediately to the left of the uncinate process. The vascular groove is another surgical margin that the surgeon produces by gentle dissection of the pancreas from the SMV/PV (dissection margin). As the tumor of the pancreatic head increases in size and gets closer to the vascular groove, the groove becomes more prominent. On the other hand, when the tumor overlaps the pancreatic head and uncinate process, it may flatten the vascular groove making the vascular bed less recognizable. The fact that the prominence of the vascular groove varies from one case to the next depending on the exact location of the tumor within the pancreatic head and its size accounts, for the most part, for the perceived unfamiliarity of pathologists with this landmark.

The medial aspect (not in every case)

It is important in this context to remember that the pancreatic body is the part of the pancreas from the left edge of the SMV/PV to the left border of the aorta. In most cases, when the tumor is limited to the pancreatic head or its uncinate process, the surgeon cuts the pancreas at its neck (i.e. immediately after the vascular groove, at the left edge of the SMV/PV) to separate the head from the body. In these PD specimens, the posterior surface of the pancreatic head will end immediately at the medial edge of the vascular groove. However, in cases where a tumor in the head overrides the pancreatic neck or even extends in the body, the surgeon's cut will be located more medially. In these cases, the posterior surface of the pancreas will have an additional area that could extend for a few centimeters medial to the vascular groove to the level of the pancreatic body resection margin (Fig. 2). Inside the human body, this part of the pancreas is sitting directly on the posterior abdominal wall, between the SMV/PV and the aorta and is adherent to its adipose tissue. The surgeon gently dissects the posterior aspect of the pancreatic head and neck creating this margin, in order to free the PD specimen from the posterior abdominal wall (dissection margin). Again, this part of the retroperitoneal margin might not be present in every PD specimen.

The superior and inferior surfaces

These two surfaces may need some gentle dissection in order to free the specimen. Since in the strictly sagittal section of the body these two surfaces exist posterior to the visceral peritoneum and are not covered by mesothelium, they can appropriately be considered as components of the retroperitoneal margin of the PD specimen.

Benefits of mapping the retroperitoneal margin

Table 2 summarizes the terms used in our proposed mapping as they relate to the descriptions used by other authorities in the field. The suggested mapping of the retroperitoneal margin is beneficial since involvement of its different components by tumor may have different implications. We believe that its clinical relevance has not been fully understood yet, mostly because the current collective reporting of the "posterior" or "radial" margin has impeded clinical–radiologic–pathologic correlative studies in this regard. When the tumor is present at the uncinate process surface (dissection margin) or in the medial aspect of the retroperitoneal margin (when included in the specimen), it is reasonable to assume that residual tumor would likely to involve the posterior abdominal wall adipose tissue. To the

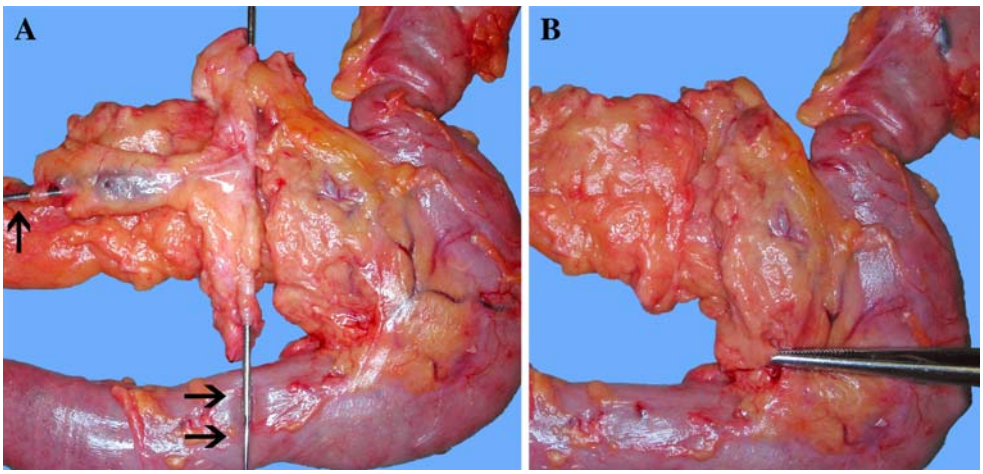

Fig. 3 A pancreatic postmortem dissection specimen. **a** The probed SMV/PV complex (*double arrows*) is still in the groove while uniting with the probed splenic vein (*single arrow*). **b** All the veins are removed exposing the empty vascular groove

Table 2 Summary of the terms used in our proposed mapping

Terms used in our proposed mapping	Corresponding terms used by others
Retroperitoneal margin	• Soft tissue margin directly adjacent to the proximal 3–4 cm of SMA [2, 4, 10, 11] • Circumferential resection margin: posterior [9] • Peripancreatic adipose tissue behind the head of the pancreas located dorsally and laterally to the SMA [12]
Uncinate process margin	• Medial margin [5] • Circumferential resection margin: medial [9]
Uncinate margin	• SMA margin [14]
The groove (vascular bed)	•Generally included in the "posterior/dorsal" margin
Medial aspect of the retroperitoneal margin (not in every case)	• Generally included in the "posterior/dorsal" margin

best of our knowledge, this assumption has not yet been systematically validated by comparative sampling studies. These two components of the retroperitoneal margin are assessed on permanent sections only and we are not aware of any protocol for their intraoperative evaluation.

The uncinate resection margin, as defined and described earlier, is different, and in several institutions including ours, is assessed intraoperatively. A positive uncinate margin on IOC could be revised whenever feasible. A final positive margin is a likely indicator of involvement of the SMA. The vascular groove is not typically assessed intraoperatively and when it is found positive for malignancy on permanent sectioning, it may suggest, given the anatomic proximity, that residual tumor is in the vicinity of the SMV/PV complex. Vascular en block radical resection is becoming more acceptable as a relatively safe procedure since involvement of the SMV/PV or SMA doesn't necessarily indicate a more aggressive behavior or an association with histologic poor prognosticators [2, 12, 18]. Involvement of the SMV/PV is believed to be a function of tumor location rather than an indicator of aggressive tumor biology [2]. Tumor adherence to the posterolateral wall of the SMV/PV is often the only barrier to complete tumor resection at the time of the PD [2]. Properly selected patients with pancreatic head cancer who undergo en block vascular resection have a median survival of approximately 2 years, which does not significantly differ from that of patients who undergo standard PD, but is superior to non-operative management, which is the traditional approach in this setting [2, 8].

Decisions about en block resection are usually made preoperatively by the surgeon, in consultation with radiologists based on documenting the involvement of SMV/PV by MRI or CT. Alternatively, the decision could be made intraoperatively based on the in situ gross inspection, usually in cases where preoperative imaging was non-conclusive. In the latter case, the surgeon relies entirely on the macroscopic impression during surgery and the feasibility of separating the retroperitoneal surface of the pancreatic head from the SMA and SMV/PV. Postoperative histological analysis of en block resection cases with inconclusive preoperative images showed that 37% of patients did not have true invasion of the SMV [19, 20]. It is interesting that pathologists are not typically involved in the decision making in this situation; probably due to the common belief that the intraoperative microscopic assessment is inaccurate in defining the relationship between a pancreatic head cancer and the adjacent vascular structures. We have witnessed in our own institution an increasing trend for requesting IOC on the uncinate resection margin in cases where surgeons believed they could go back and excise additional perivascular tissue in the pursuit of a negative margin and we have been successful in answering this question as it relates to the SMA [16, 17]. Again, we are not aware of any literature describing protocols for the intraoperative pathologic assessment of the status of the vascular groove. Certainly, assessment of the vascular groove margin is unlikely to become part of routine IOC for pancreaticoduodenectomy specimens, but one could imagine a limited role in situations where preoperative imaging has suggested very close proximity of the tumor to the SMV/PV.

IOC and grossing protocols

It is relevant in this context to briefly address some hints regarding the IOC and grossing of the retroperitoneal surgical margin. The key to accurate assessment is a proper orientation by careful inspection on mapping of its components. A surgeon's help to orient the specimen might be needed, especially in cases with unusual operative scenarios or unfamiliar anatomic variants. Our protocol for the intraoperative assessment of the uncinate resection margin was discussed in detail in earlier publications [15–17]. Following the submission of the uncinate process margin as indicated, the retroperitoneal margin could be inked in three different colors, one for each of its components; the remaining surface of the uncinate process, the vascular groove, and the medial aspect (when present). Inking extends to cover the superior and inferior surfaces. It has been suggested to

serially section (bread-loaf) the PD specimen at 3-mm intervals, perpendicular to its retroperitoneal margin [21]. Sections of the retroperitoneal margin are submitted entirely, including the superior and inferior surfaces. It is believed that extensive sampling of the retroperitoneal margin increases the frequency of its positivity [9, 22]. The College of American Pathologists recommends reporting of the status of the retroperitoneal and the uncinate margins separately [13]. We are taking this concept even further to open the door for future investigation regarding the prognostic significance of tumor involvement of each of the components discussed. Similar to what is already implemented in other institutions, our final report indicates the status of the uncinate process dissection margin, the uncinate resection margin, the vascular groove, and the remaining medial aspect of the retroperitoneal margin separately. We are hoping that this detailed mapping and reporting will provide the surgeon and the oncologist with more specific information regarding the tissues or structures that could potentially harbor residual malignancy. Correlation between the detailed pathologic findings and the preoperative images, especially when the latter were inconclusive, is hoped to help the surgeons improve on their selection criteria for patients needing en block resections. The detailed anatomic mapping of the various components of the retroperitoneal margin could also serve as a quality indicator for imaging and its results will be available for research projects and quality improvement initiatives. We would like to leave the door open at this time for the future consideration of the value and feasibility of the intraoperative assessment of the vascular groove in order to help surgeons who currently rely solely on their intraoperative macroscopic inspection in borderline cases. At the present time, IOC of the vascular groove is not advocated routinely. One would have to weigh the potential benefit of identification of a positive margin intraoperatively versus the additional resources needed to properly sample the margin and the surgeon's ability to do further resection in light of the confines of the procedure and individual patient factors. In selected cases, however, knowledge of the anatomy of this aspect of the retroperitoneal margin may allow for its meaningful intraoperative assessment and thus factor in an intraoperative decision regarding vascular resection.

Conclusion

The pancreaticoduodenectomy surgery is an operator-dependent surgery and the same applies to the handling of its resected specimen. It is our viewpoint that mapping the retroperitoneal surgical margin and reporting its various components separately has the potential to improve the assessment of residual tumor status in resected pancreatic cancer. We believe this is a good practice since it provides more correlative parameters to the multidisciplinary care of pancreatic head cancer patients. It is also hoped that this article can initiate multidisciplinary discussion around better defining the "radial" margin of the PD specimen.

Conflict of interest statement We declare that we have no conflict of interest.

References

1. Allema JH, Reinders ME, vanGulik TM et al (1995) Prognostic factors for suvival after pancreaticoduodenectomy for patients with carcinoma of the pancreatic region. Cancer 75:2069–2076
2. Fuhrman GM, Leach SD, Staley CA et al (1996) Rationale for en bloc resection in the treatment of pancreatic adenocarcinoma adherent to the superior mesenteric-portal vein confluence. Pancreatic Tumor Study Group. Ann Surg 223(2):154–162
3. Li D, Xie K, Wolff RA, Abbruzzese JL (2004) Pancreatic cancer. Lancet 363:1049–1057
4. Varadhachary GR, Tamm EP, Abbruzzese JL et al (2006) Borderline resectable pancreatic cancer: definitions, management, and role of preoperative therapy. Ann Surg Oncol 13:1035–1046
5. Esposito I, Kleeff J, Bergmann F et al (2008) Most pancreatic cancer resections are R1 resections. Ann Surg Oncol 15:1651–1660
6. Verbeke CS, Menon KV (2008) Variability in reporting resection margin status in pancreatic cancer. Ann Surg 247:716–717
7. Poon RT, Fan ST, Lo CM et al (2004) Pancreaticoduodenectomy with en block portal vein resection for pancreatic carcinoma with suspected portal vein involvement. World J Surg 28(6):602–608
8. Tseng JF, Raut CP, Lee JE et al (2004) Pancreatoduodenectomy with vascular resection; margin status and survival duration. J Gastrointest Surg 8(8):935–949
9. Verbeke CS (2007) Resection margins and R1 rates in pancreatic cancer—are we there yet. Histopathology 52(7):787–796
10. Fuhrman GM, Charnsangavej C, Abbruzzese JL et al (1994) Thin-section contrast-enhanced computer tomography accurately predicts the resectability of malignant pancreatic neoplasms. Am J Surg 167:104–113
11. Staley CA, Cleary KR, Abbruzzese JL et al (1996) The need for standardized pathologic staging of pancreaticoduodenectomy specimens. Pancreas 12:373–380
12. Zamboni G, Capelli P, Pesci A et al (2000) Pancreatic head mass; what can be done? Classification: the pathological point of view. JOP.J Pancreas (on line) 1(3suppl):77–84
13. Compton CC (2007) Exocrine pancreas: protocol applied to all carcinomas of the exocrine pancreas. Available from College of American Pathologists web site. http://www.cap.org/apps/docs/cancer_protocols/2005/pancreasexo05_pw.doc
14. Raut CP, Tseng JF, Sun CC et al (2007) Impact of resection status on pattern of failure and survival after pancreaticoduodenectomy for pancreatic adenocarcinoma. Ann Surg 246(1):52–60
15. Khalifa MA (2007) Intraoperative assessment of the Whipple's resection specimen. J Clin Pathol 60:975–980
16. Khalifa MA, Maksymov V, Rowsell CH et al (2007) A novel approach to the intraoperative assessment of the uncinate margin of the pancreaticoduodenectomy specimen. Hepato Pancreato Biliary (HPB) 9:146–149
17. Rowsell CH, Hanna S, Hsieh E et al (2007) Improved lymph node retrieval in Whipple specimens as a result of implementation of a

new uncinate margin protocol. Hepato Pancreato Biliary (HPB) 9:388–391
18. Nato M, Miwa K, Kitagawa H et al (2005) Pancreas head carcinoma: frequency of invasion to soft tissue adherent to the superior mesenteric artery. Am J Surg Pathol 29:1056–1061
19. Zhou GW, Wu WD, Xiao WD et al (2005) Pancreatectomy combined with superior mesenteric-portal vein resection: report of 32 cases. Hepatobiliary Pancreat Dis Int 4:130–134
20. Aramaki M, Matsumoto T, Etoh T et al (2003) Clinical significance of combined pancreas and portal vein resection in surgery for pancreatic adenocarcinoma. Hepatogastroenterology 50(49):263–266
21. Luttges J, Vogel I, Menke M et al (1998) The retroperitoneal resection margin and vessel involvement are important factors determining survival after pancreaticoduodenectomy for ductal adenocarcinoma of the head of the pancreas. Virchows Arch 433:237–242
22. Verbeke CS, Leitch D, Menon KV et al (2006) Redefining the R1 resection in pancreatic cancer. Br J Surg 93:1232–1237

Virchows Arch (2009) 454:133–142
DOI 10.1007/s00428-008-0710-x

ORIGINAL ARTICLE

The monoclonal anti-BCL10 antibody (clone 331.1) is a sensitive and specific marker of pancreatic acinar cell carcinoma and pancreatic metaplasia

Stefano La Rosa · Francesca Franzi · Silvia Marchet · Giovanna Finzi · Moira Clerici · Davide Vigetti · Anna Maria Chiaravalli · Fausto Sessa · Carlo Capella

Received: 22 September 2008 / Revised: 15 November 2008 / Accepted: 19 November 2008 / Published online: 9 December 2008

Abstract Acinar cell carcinoma (ACC) is a rare pancreatic cancer which may be difficult to distinguish from other solid nonadenocarcinoma tumors. The diagnosis depends on the demonstration of acinar differentiation, obtained with antibodies recognizing various pancreatic enzymes that, although specific, show different sensitivity. The C-terminal portion of the BCL10 protein shows homology with carboxyl ester hydrolase (CEH), an enzyme produced by pancreatic acinar cells. We investigated the usefulness of a C-terminal BCL10 monoclonal antibody in the diagnosis of ACCs. We examined normal pancreases and different pancreatic tumors including ACCs, mixed acinar–endocrine carcinomas, ductal adenocarcinomas, mucinous, serous, solid pseudopapillary, and endocrine neoplasms. In addition, various normal tissues and cases of pancreatic metaplasia of the gastroesophageal mucosa, cases of ectopic pancreas, gastrointestinal endocrine tumors, salivary and breast acinic cell carcinomas, gastric adenocarcinomas with and without acinar differentiation, and hepatocellular carcinomas were studied. BCL10 immunoreactivity paralleled that of CEH and was restricted to acinar cells of normal and ectopic pancreas, of pancreatic metaplasia, and of ACCs. The anti-BCL10 antibody was more sensitive in detecting ACCs and pancreatic metaplasia than antibodies directed against other pancreatic enzymes. We suggest using BCL10 antibody for diagnosing pancreatic tumors and whenever an acinar differentiation is suspected in gastrointestinal neoplastic and metaplastic lesions.

Keywords Pancreas · BCL10 · Acinar cell · Acinar cell carcinoma

S. La Rosa (✉) · G. Finzi · A. M. Chiaravalli
Department of Pathology, Ospedale di Circolo,
Viale Borri 57,
21100 Varese, Italy
e-mail: anapat@ospedale.varese.it

F. Franzi · S. Marchet · F. Sessa · C. Capella
Anatomic Pathology Unit, Department of Human Morphology,
University of Insubria,
Varese, Italy

M. Clerici · D. Vigetti
Department of Biomedical, Experimental and Clinical Sciences,
University of Insubria,
Varese, Italy

F. Sessa
Department of Pathology, Fondazione IRCCS Multimedica,
Milan, Italy

Introduction

Acinar cell carcinoma (ACC) is a rare pancreatic cancer accounting for about 1–2% of all pancreatic neoplasms in adults [1, 2]. Morphologically, ACC may be difficult to distinguish from other pancreatic solid nonadenocarcinoma neoplasms. Differential diagnostic difficulties are more often encountered with pancreatic endocrine tumors (PETs), solid pseudopapillary neoplasms, and pancreatoblastomas than with common ductal adenocarcinomas. Tumors with mixed morphological features may be especially problematic, including mixed acinar–endocrine carcinomas [3–5]. It is important to differentiate ACCs from well-differentiated PETs because of the different prognosis of patients, which is certainly better for PET patients [6]. Symptoms of ACCs are generally nonspecific, related to tumor growth, and include abdominal pain, anorexia, weight loss, nausea, and vomiting. Only in rare cases lipase production by tumor cells may cause polyarthralgia–polyarthritis and dissemi-

nated subcutaneous fat necrosis [1, 2]. ACC may occur anywhere in the pancreas and macroscopic aspects are not typical. Histologically, ACCs are characterized by a proliferation of cells producing zymogen granules which contain pancreatic enzymes. Tumors generally show marked cellularity with four main patterns of growth (acinar, solid, glandular, and trabecular), sometimes combined in the same tumor. The diagnosis of ACCs relies on the detection of acinar differentiation, which includes histopathologic, histochemical, immunohistochemical, and ultrastructural features; among these, immunohistochemistry now has a relevant role in the diagnosis and helps in identifying pancreatic enzymes such as lipase, trypsin, chymotrypsin, and amylase [7]. However, the rarity of this cancer, which implies only an occasional use of these specific antibodies in most laboratories, may lead to misdiagnosis of the tumor, which is mainly confused with a well-differentiated PET [1, 8].

Carboxyl ester hydrolase (CEH) is an enzyme secreted by acinar cells starting from the 16th week of pregnancy [9], which is involved in digestive processes and which represents about 4% of pancreatic juice proteins [10]. This enzyme has been isolated from pancreases of different species and has been differently named according to the substrates used for the determination of its activity. For this reason, different synonyms can be found in the literature including carboxyl ester lipase, lysophospholipase (phospholipase A1), nonspecific lipase, cholesterol ester hydrolase, and sterol ester hydrolase [11]. This enzyme is a glycoprotein of 105-kDa molecular weight [12] which, unlike lipase, hydrolyzes a wide variety of lipid substrates. As well as in the pancreas, this protein enzyme has been identified in other organs, where it has been differently named. For example, the lactating mammary gland synthesizes and secretes an enzyme named human milk bile salt-stimulated lipase which is identical to pancreatic CEH [12–14]. The mammary human milk bile salt-stimulated lipase, after specific activation by primary bile salts, contributes to the breast-fed infant's endogenous capacity for intestinal fat digestion [15]. In addition, an enzyme identical to CEH has also been found in endothelial cells lining the vessel wall where it is thought to be involved in mechanisms leading to the accumulation of atherogenic lipoproteins [16, 17].

The C-terminal portion of CEH (blast accession number: NP_001798.2), a region rich in proline, displays high homology with the carboxyl-terminal part of the BCL10 molecule (blast accession number: NP_003912.1). BCL10 is a proapoptotic 233 amino acid protein expressed in lymphoid tissues. BCL10 is detected in some extranodal marginal zone B-cell lymphomas of mucosa-associated lymphoid tissue (MALT), in which specific translocations result in BCL10 overexpression with the loss of its proapoptotic activity and an increase in functional activation of nuclear factor-kB, with enhancement of malignant transformation [18]. There are several commercially available antibodies recognizing the C-terminal portion of BCL10 which, in view of its homology with the C-terminal portion of the CEH, could hypothetically be used as a marker of acinar cells. The aim of the present study was to investigate the immunohistochemical expression of the C-terminal portion of the BCL10 protein in a series of different pancreatic tumors and in cases of pancreatic (acinar) metaplasia of gastric and esophageal mucosa to verify its usefulness as an acinar cell marker.

Materials and methods

Cases

Twenty normal human pancreases from adult subjects and a series of 114 pancreatic tumors including 14 ductal adenocarcinomas, two intraductal papillary mucinous neoplasms, three mucinous cystic neoplasms (two mucinous cystadenomas and one mucinous cystadenocarcinoma), three serous microcystic adenomas, seven ACCs, one acinar cell cystadenocarcinoma, two intraductal ACCs [19], two mixed acinar–endocrine carcinomas, 77 PETs, and three solid pseudopapillary tumors were collected from the files of the Department of Pathology of the Ospedale di Circolo in Varese. In addition, a series of normal human tissues (including lymph node, stomach, intestine, liver, salivary gland, thyroid, parathyroid, adrenal gland, breast, lactating breast, brain, prostate, placenta, heart, and aorta), four cases of pancreatic acinar cell metaplasia of the gastric mucosa (three of them associated with chronic atrophic autoimmune gastritis), three case of pancreatic acinar cell metaplasia of the esophageal mucosa (one associated with Barrett's esophagus), five cases of ectopic pancreatic tissue localized in the duodenal wall, 44 gastrointestinal endocrine tumors, five salivary and four breast acinic carcinomas, 17 gastric adenocarcinomas, four of which showed acinar differentiation, and six hepatocellular carcinomas were included in the study. All tissues were fixed in buffered formalin (formaldehyde 4% *w*/*v* and acetate buffer 0.05 M) and routinely processed to paraffin wax. Five-micrometer-thick sections were stained with hematoxylin–eosin and Alcian-blue/periodic acid-Schiff for morphological evaluations.

Tissue microarray preparation

Tissue microarrays of 104 well-characterized gastroenteropancreatic (GEP) endocrine tumors (44 gastrointestinal and 60 pancreatic) were prepared from formalin-fixed, paraffin-embedded donor blocks. Representative areas of each tumor were identified on hematoxylin–eosin stained

Table 1 Antibodies and antisera used

Antibodies/antisera	P/M (clone)	Dilution	Source
BCL10 (C-terminal)	M (331.3)	1:200	Santa Cruz Biotechnology Inc., Santa Cruz, CA, USA
BCL10 (N-terminal)	P	1:100	Santa Cruz Biotechnology Inc.
Carboxyl ester hydrolase[a]	P	1:50	Santa Cruz Biotechnology Inc.
Pancreatic type amylase	M (6103)	1:2,500	Biogenex Laboratories, San Ramon, CA, USA
Salivary type amylase[b]	P	1:2,000	Biogenesis, Bournemouth, UK
Trypsin	P	1:1,500	Biodesign International, Saco, ME, USA
Lipase	M (MAB1453)	1:1,000	Chemicon International inc, Temecula, CA, USA
Insulin	M (AE9D6)	1:200	Biogenex Laboratories
Glucagon	P	1:1,250	Milab, Malmo, Sweden
Pancreatic polypeptide	M (CA08327)	1:4,000	Cambridge Research Biochemicals, Cambridge, UK
Somatostatin	P	1:500	Dako, Carpinteria, CA, USA
Chromogranin A	M (Phe5)	1:50	Enzo Diagnostics, New York, USA

[a] In the Santa Cruz catalog, the protein is named with the synonym carboxyl ester lipase
[b] This antibody was used to diagnose acinic carcinomas of the salivary glands and breast

slides. At least two core tissue biopsy samples with a diameter of 0.6 mm were taken from tissue blocks and placed in a tissue microarray using a semiautomated tissue array device. Four-micrometer-thick sections were cut after incubating the constructed blocks for 10 h at 37°C.

Immunohistochemistry

For immunohistochemistry, paraffin sections were collected on Superfrost Plus slides and completely processed automatically with a BenchMark XT immunostainer (Ventana) using the ultraView universal DAB detection kit (Ventana). In particular, antigen retrieval was performed for 30 min and the primary antibody was applied for 20 min at 42°C.

The monoclonal anti-BCL10 antibody (clone 331.3) was raised against the 168–233 amino acid sequence of the COOH terminal portion of the BCL10 protein. In addition, an anti-BCL10 antibody (N-20) recognizing the terminal N-portion of the BCL10 molecule was also used. The anti-CEH antibody was raised against a peptide mapping within the internal region of human CEH. The technical characteristics of the other antibodies employed are listed in Table 1.

Specificity controls consisted of absorption of each antiserum with 10–20 nM of its homologous antigen per milliliter of diluted antiserum, omission of the first layer, and use of control tissues with or without the pertinent antigen. Unfortunately, Santa Cruz Company does not provide the specific blocking peptide for the antibody

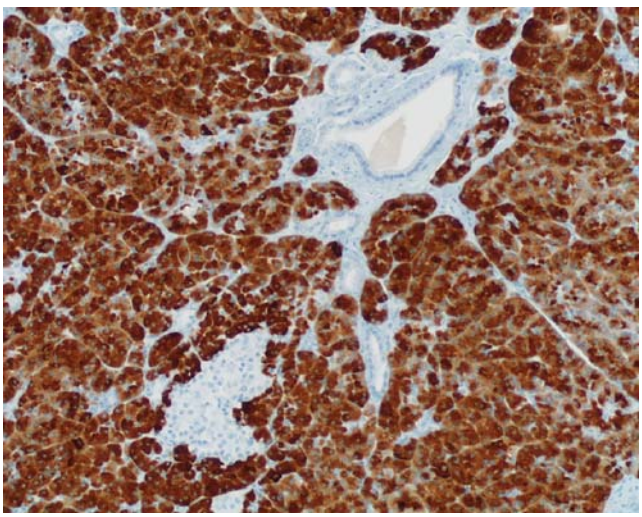

Fig. 1 BCL10 immunoreactivity in normal pancreas. The stain is intense and confined to the cytoplasm of acinar cells, while endocrine islet cells and duct cells are completely negative

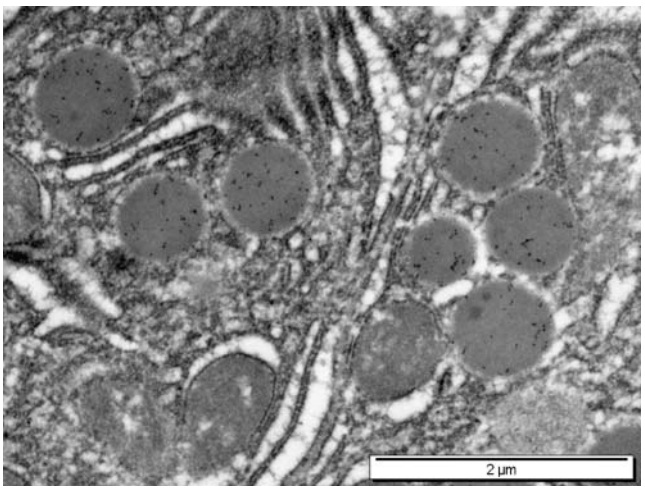

Fig. 2 Electron microscopy immunocytochemistry shows that the staining for BCL10 is localized in zymogen granules of a pancreatic acinar cell

Table 2 BCL10 expression in normal tissues and in heterotopic pancreatic tissue

Tissues	BCL10 C-terminal	CEH	BCL10 N-terminal
Pancreas	+[a]	+[a]	–
Heterotopic pancreas	+[a]	+[a]	–
Lymph node	+	–	+
Stomach	–	+[c]	–
Intestine	–	–	–
Liver	–	–	–
Salivary gland	–	–	–
Thyroid	–	–	–
Parathyroid	–	–	–
Adrenal	–	–	–
Breast	–	–	–
Lactating breast	+ (focal)[b]	+ (focal)[b]	–
Brain	–	–	–
Prostate	–	–	–
Placenta	–	–	–
Heart	–	–	–
Aorta	–	–	–

[a] Immunoreactivity was confined to acinar cells, while ductal and endocrine cells were negative
[b] Milk was also strongly positive
[c] Immunoreactivity was confined to chief cells of the fundic mucosa

directed against the C-terminal portion of BCL10 employed; for this reason, we performed a Western blotting analysis (see below).

The intensity of immunoreactivity was scored as follows: weak (1+) when the intensity of the reaction was weak in the cytoplasm and frequently observed in less than 50% of tumor cells; intense (3+) when it was strong, frequently with diffusion of the reaction, and generally present in the majority of cells; and moderate (2+) when it showed features between scores 1+ and 3+. The specificity and sensitivity of BCL10, CEH, amylase, lipase, and trypsin immunostainings in detecting pancreatic ACCs was calculated as follows: specificity = true negatives/(true negatives + false positives) and sensitivity = true positives/(true positives + false negatives) [20]. False positives were defined as pancreatic non-ACCs showing enzyme immunoreactivity while false negatives were pancreatic ACCs lacking it. True positives were defined as ACCs positive for enzyme immunohistochemistry while true negative pancreatic tumors, unlike ACCs, were negative for enzymes.

Electron microscopy immunocytochemistry

For ultrastructural immunocytochemistry, samples of normal pancreas were fixed for 2 h at 4°C in a mixture of 2% paraformaldehyde and 0.5% glutaraldehyde in 0.05 M pH 7.3 cacodylate buffer and embedded in London White Resin. Thin sections, after pretreatment with ovoalbumin 1% in Tris-buffered saline 0.05 M pH 7.4 for 5 min at room temperature, were incubated for 24 h at 4°C with the primary monoclonal anti-BCL10 antibody (Santa Cruz), then with a gold-tagged goat antimouse antibody (EY Laboratories, San Mateo, CA, USA) for 1 h at room temperature and finally counterstained with uranyl acetate and lead citrate. Specificity controls consisted of omission of the first layer and use of tissues with or without pertinent antigens. Thin sections were examined with a Philips (Morgagni 268 D) electron microscope.

Western blotting

For Western blotting analysis, normal pancreatic and lymph node frozen tissues and human milk were used. A total protein extract from tissues was prepared by homogenizing ~0.5 g of tissue in 1 ml of ice-cold phosphate buffered saline with 0.2 mM dithiothreitol and a protease inhibitor cocktail (Roche). After centrifugation at 12,000×*g* for 15 min at 4°C, the supernatant was recovered and the protein concentration was quantified by using the Bradford (Biorad) method. Human milk was centrifuged to remove fats and cells that could alter protein electrophoresis [21]. Thirty micrograms of tissue and human milk proteins were separated by sodium dodecyl sulfate polyacrylamide gel electrophoresis and blotted onto a nitrocellulose membrane using a semidry apparatus (BioRad). After transfer, the blots were stained with Ponceau S (Sigma Chemical Co.) to verify the transfer. Protein band immunodetection was performed with monoclonal anti-BCL10 (dilution 1:1,000, Santa Cruz) as the primary antibody and horseradish peroxidase-conjugated bovine antimouse IgG as the secondary antibody (dilution 1:15,000). Bands were visualized by using enhanced chemiluminescence (ECL Advance Western Blotting Detection Kit, GE) as specified by the manufacturer.

Statistical analysis

The different percentages of BCL10-, CEH-, and trypsin-positive cells in ACCs were statistically evaluated using the Wilcoxon test.

Results

Using the anti-BCL10 antibody recognizing the C-terminal part of the molecule (clone 331.3), we observed an intense BCL10 immunoreactivity (IR) in acinar cells of normal pancreases, while ductal and islet cells were completely negative (Fig. 1). The pattern of IR was cytoplasmic and granular and paralleled the distribution of zymogen granules. At the ultrastructural level, the gold immunolabeling

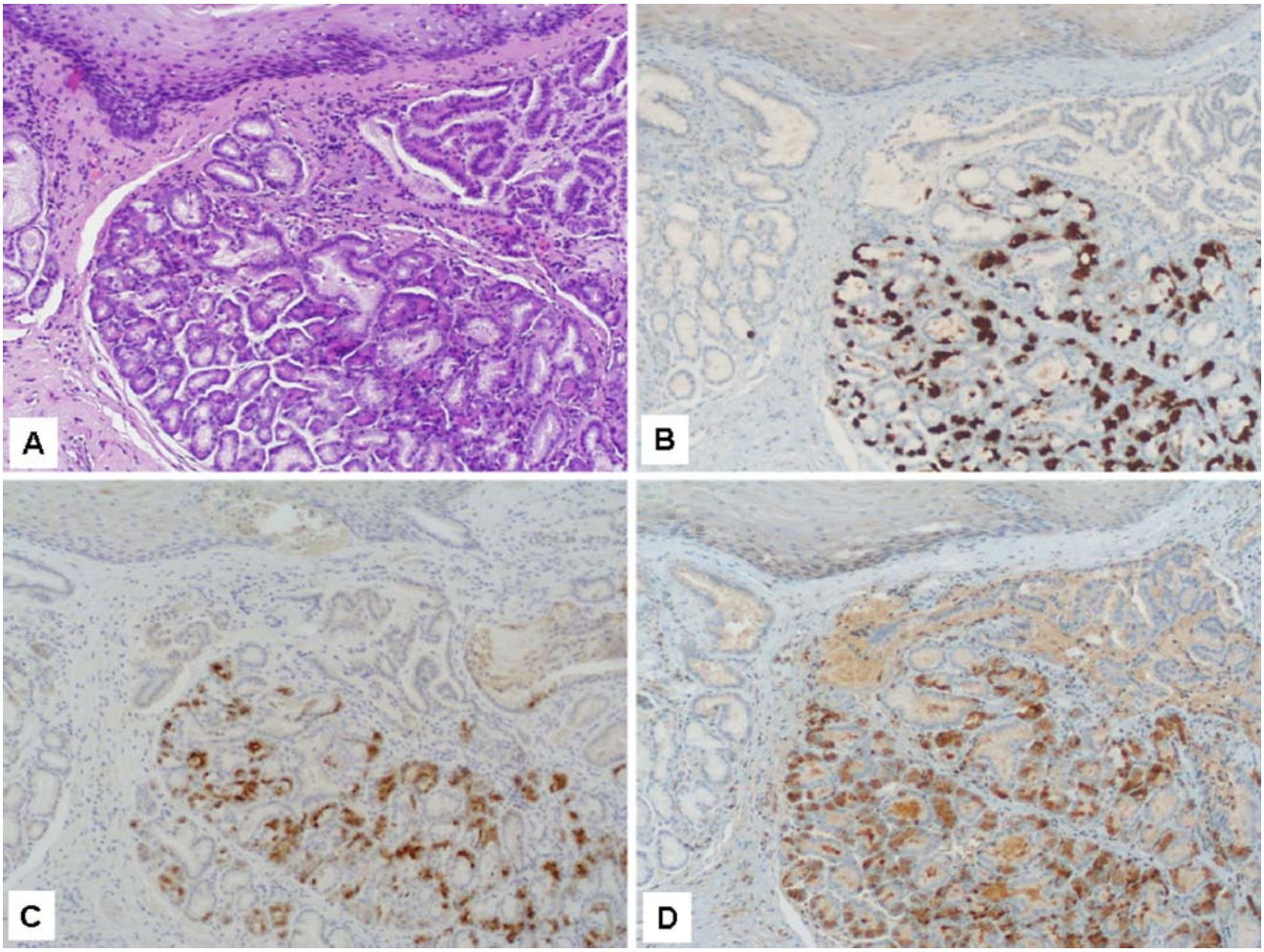

Fig. 3 Acinar cells in this focus of pancreatic metaplasia of the esophageal mucosa (**a**) are strongly positive for BCL10 (**b**). They are also immunoreactive for CEH (**c**) and trypsin (**d**). The intensity of BCL10 immunoreaction is stronger than that obtained using the other antibodies

was confined to spherical electron dense zymogen granules (Fig. 2), while the other cytoplasmic organelles did not show any labeling. This pattern of ultrastructural localization suggested that the antibody identified at least one of the pancreatic enzymes, which are typically stored in zymogen granules. The other normal tissues investigated did not show any BCL10-IR, with the exception of lymph nodes and scattered cells in the lactating mammary gland (Table 2). The seven foci pancreatic acinar cell metaplasia of the gastric and esophageal mucosa were also intensely BCL10 immunoreactive (Fig. 3), as were the acinar cells of the five ectopic pancreatic tissues investigated. In all tissues, normal lymphocytes were BCL10 positive although the reaction was less intense than that observed in acinar cells. The immunohistochemical expression of BCL10 overlapped that of CEH (Table 2), identified using a specific anti-CEH antibody, but the intensity of the BCL10 staining was stronger.

Western blotting analysis showed that in normal human pancreatic and milk protein extracts, the monoclonal anti-BCL10 antibody (clone 331.3), which recognizes the C-terminal portion of the molecule homologous with the CEH, detected a protein with a molecular weight of 105 kDa, which corresponds to the molecular weight of CEH. By contrast, in the lymph node extract, the antibody detected a protein with the molecular weight of BCL10 (Fig. 4). This result confirmed that the anti-BCL10 antibody used in this study, in addition to recognizing the BCL10 protein typically expressed in lymphocytes, recognized CEH. Moreover, as expected, a band of the molecular weight of BCL10 was also observed in the lines of both milk and pancreatic protein extracts.

Among pancreatic neoplasms, all ACCs (Fig. 5) as well as mixed acinar–endocrine carcinomas were intensely BCL10-IR, while the other tumor types including ductal adenocarcinomas, serous, mucinous, solid pseudopapillary,

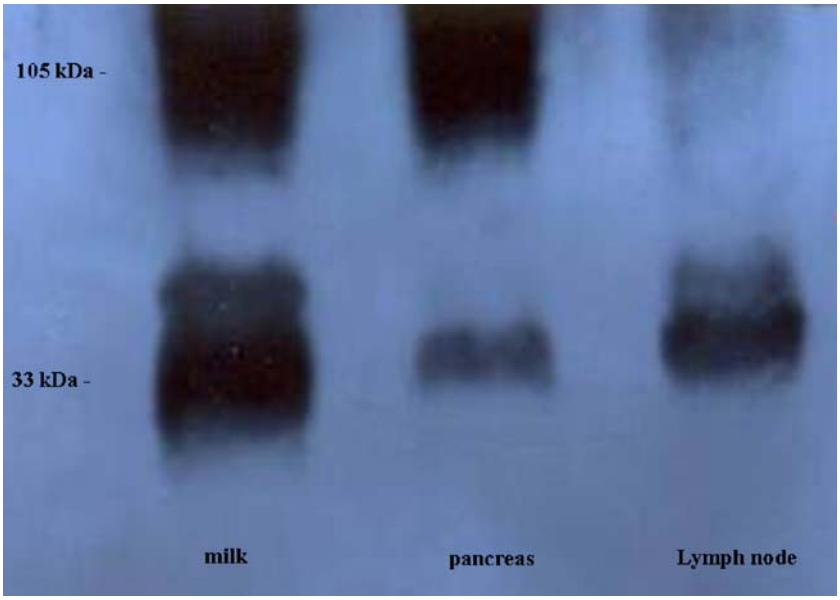

Fig. 4 Western blotting analysis of protein extracts from normal pancreas, human milk, and lymph node using the 331.3 anti-BCL10 antibody. Normal pancreas and milk, but not lymph node, showed the band at 105 kDa, which corresponds to the molecular weight of CEH. The band at about 33 kDa, which corresponds to BCL10, was evident in all the *lines*. The result was expected because lymphocytes of the lymph node express BCL10 and both milk and pancreas are known to express BCL10 as suggested by expression profile databases (i.e., UNIGENE expression profile http://www.ncbi.nlm.nih.gov/UniGene/ESTProfileViewer.cgi?uglist=Hs.193516)

and endocrine tumors were all negative (Table 3). The BCL10-IR was diffuse in the cytoplasm but in several cases, a reinforcement at the apical portion of the cytoplasm, in correspondence to the minute lumens frequently present in acinar and glandular architectural patterns, was observed. BCL10-IR was more sensitive in detecting acinar differentiation than amylase, lipase, and CEH (Table 4). We indeed observed BCL10-IR in all cases of pancreatic ACCs, while amylase, lipase, and CEH positivity was found in one of eight, five of 11, and nine of ten cases, respectively. In addition, in lipase-, CEH-, and amylase-positive tumors, BCL10-IR cells were more numerous than lipase-, CEH-, and amylase-positive cells ($p<0.01$). Trypsin-IR was identified in all cases of ACCs but the number of positive cells was statistically ($p<0.01$) lower than that of BCL10. In addition, the intensity of BCL10 immunoreaction was stronger than that of trypsin (Table 5).

Among the five salivary gland acinic cell carcinomas, we found an intense BCL10-IR in only one case displaying dedifferentiated features like cytologic pleomorphism, high proliferative rate, and necrosis [22]. The other four well to moderately differentiated acinic cell carcinomas of the salivary glands were BCL10 negative. All breast acinic cell carcinomas were negative for BCL10, which was conversely found in groups of cells of gastric adenocarcinomas with acinar differentiation. The other gastric adenocarcinomas and all the hepatocellular carcinomas were BCL10 negative. Among the 44 gastrointestinal endocrine tumors investigated, only one gastric type 1 ECL-cell carcinoid resulted BCL10 positive (Table 6). As in normal tissues, in all positive neoplasms, BCL10-IR overlapped that of CEH with the only difference that CEH (but not BCL10) expression was observed in rare sparse cells of two hepatocellular carcinomas (Table 3). Using the polyclonal anti-BCL10 antibody (N-20), which identifies the N-terminal part of the protein, we did not find any immunoreactivity in the pancreas or pancreatic tumors, nor in the other normal and neoplastic tissues investigated, with the exception of lymph nodes (Table 2).

Discussion

As far as we are able to ascertain, the present study is the first report indicating that normal pancreatic acinar cells, metaplastic acinar cells, and pancreatic ACCs are immunoreactive with an anti-BCL10 antibody, suggesting that this antibody can be used as a marker of acinar differentiation. ACC is one of the rarest tumors of the pancreas, and for this reason, most surgical pathology laboratories rarely have at their disposal a panel of antibodies directed against various pancreatic enzymes. Consequently, slides of suspected ACCs are frequently sent to referral centers for specific immunostainings. The anti-BCL10 antibody is frequently included in the panel of antibodies used for the diagnosis of

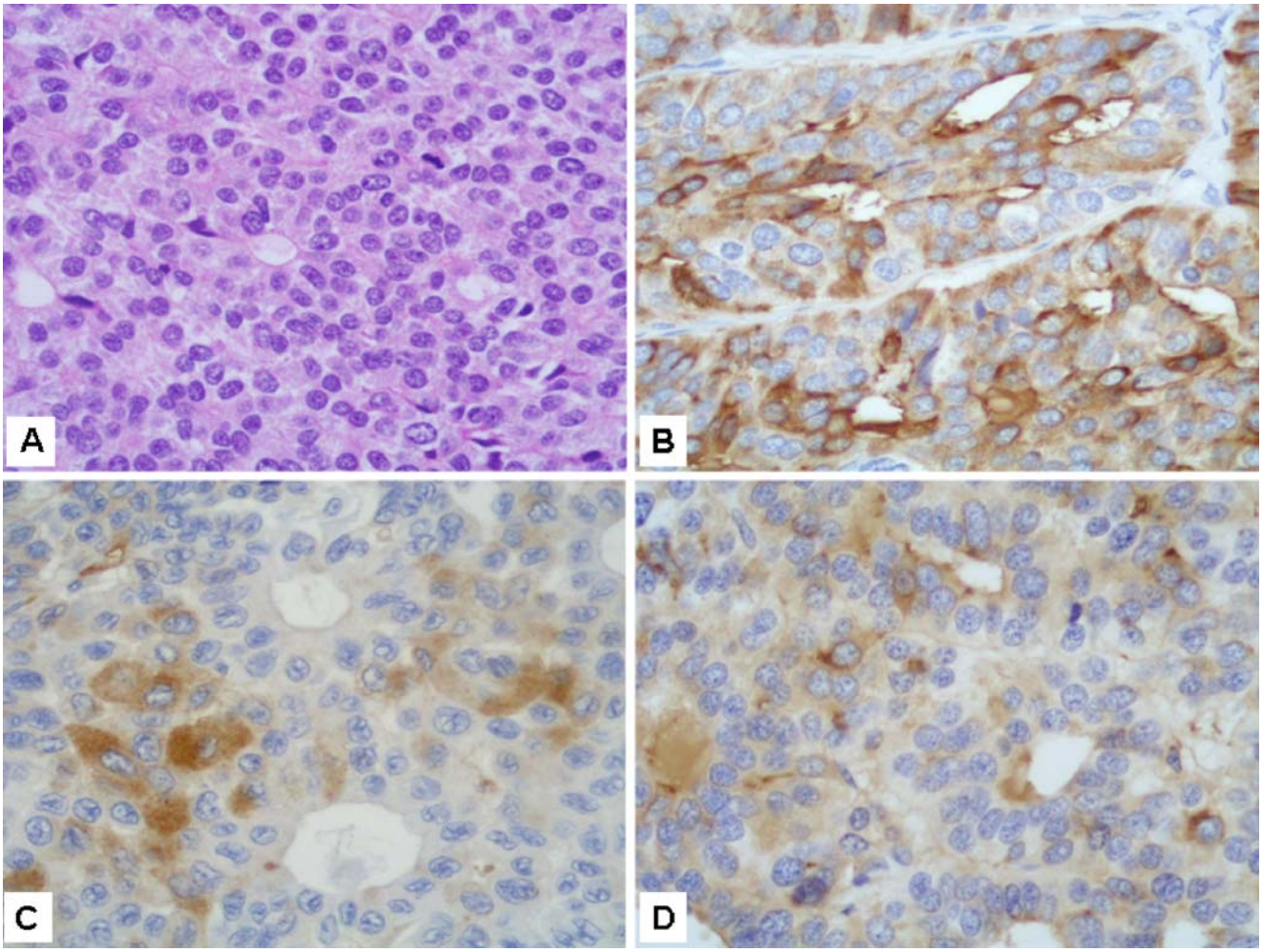

Fig. 5 Pancreatic acinar cell carcinoma characterized by proliferation of neoplastic cells forming minute luminal spaces (**a**). The immunoreactivity for BCL10 was cytoplasmic, intense, and diffuse with a reinforcement at the apical portion of the cytoplasm in correspondence to the minute lumens (**b**). Tumor cells were also immunoreactive for CEH (**c**) and trypsin (**d**), although the intensity of reactions and the number of positive cells were less than that of BCL10

MALT lymphoma, a disease which is certainly more frequent than ACC. As a consequence, the opportunity to use BCL10 as a marker of both ACCs and MALT lymphomas has the advantage that a single antibody can be employed for diagnosing two different neoplasms.

In addition to these practical and economic considerations, the results of our study have demonstrated that the BCL10 immunostaining is better than immunostains performed using antibodies directed against various pancreatic enzymes in recognizing ACCs. In our series, BCL10 immunohistochemistry seemed to be more sensitive than amylase and lipase immunohistochemistry in detecting ACCs. In addition, it also appeared to be more sensitive than CEH immunostaining, although antibodies directed against this particular pancreatic enzyme, with some exceptions [23], are not generally included in the panel for diagnosing ACC. Although both trypsin and BCL10 immunoreactivities were found in all ACCs and in mixed acinar–endocrine carcinomas, the BCL10 immunoreaction was stronger than that of trypsin. Similarly, the intensity of BCL10 immunoreaction was stronger than that observed when the other antibodies directed against various pancreatic enzymes (CEH, amylase, and lipase) were employed. The different sensitivity of such antibodies in identifying ACC is well known. Among them, trypsin and chymotrypsin have been found to have the highest degree of sensitivity [1, 24], although the latter one has been also reported to be less sensitive than trypsin [25]. Lipase has been found positive in about 80% of ACCs [24] while amylase has been rarely identified, despite its strong immunoreactivity in normal acinar cells [7, 26]. The sensitivity of trypsin, lipase, and amylase in our series is in line with the data reported in the literature (Table 4). Our results suggest that BCL10 is highly sensitive, since it was

Table 3 BCL10 expression in tumors of the pancreas and of other sites

Tumor type	BCL10 C-terminal	Trypsin	CEH	Amylase	Lipase
Pancreas					
Ductal carcinomas	0/14	0/14	0/14	0/14	0/14
Acinar cell carcinomas[a]	10/10	10/10	8/9	1/8[f]	5/10
Mixed acinar–endocrine cancers	2/2	2/2	1/1	ne	0/1
Mucinous tumors[b]	0/5	0/5	0/5	0/5	0/5
Serous tumors	0/3	0/3	0/3	0/3	0/3
Solid pseudopapillary tumors	0/3	0/3	0/3	0/3	0/3
Endocrine tumors[c]	0/77	0/77	0/77	0/77	0/77
Salivary gland					
Acinic cell carcinomas	1/5[e]	0/5	1/5	0/5[g]	0/5
Stomach					
Adc with acinar differentiation	4/4[f]	3/4	2/4	0/3	1/3
Adenocarcinomas[d]	0/13	0/13	0/13	0/13	0/13
Liver					
Hepatocellular carcinomas	0/6	0/6	2/6[f]	0/6	0/6
Breast					
Acinic carcinomas	0/4	0/4	0/4	0/4[g]	0/4

CEH carboxyl ester hydrolase, *Adc* adenocarcinoma, *ne* not evaluated
[a] Seven ACCs, one acinar cell cystadenocarcinoma, and two intraductal ACCs
[b] Two intraductal papillary mucinous neoplasms and three mucinous cystic neoplasms (two mucinous cystadenomas and one mucinous cystadenocarcinoma)
[c] This series included 76 well-differentiated tumors (nonfunctioning, insulinomas, gastrinomas, and vipomas) and one poorly differentiated carcinoma. Sixty cases were included in the microarray slide
[d] Diffuse and glandular types of gastric adenocarcinomas were included
[e] The positive cancer was poorly differentiated
[f] The immunoreactivity was focal
[g] Tumors were negative for pancreatic amylase, while positive for salivary gland type amylase

immunohistochemically detected in 100% of our cases. In addition, the fact that we did not find BCL10-IR in other pancreatic tumors confirms that BCL10 immunohistochemistry is highly specific in detecting pancreatic acinar cell differentiation. Moreover, the lack of CEH expression in pancreatic tumors other than ACCs is in agreement with the findings reported by Reuss et al. [27].

In addition to the diagnosis of pancreatic ACCs, our results indicate the practical usefulness of BCL10 immunohistochemistry in detecting pancreatic acinar cell metaplasia, which is relatively frequently found in gastric and esophageal mucosa. Although morphology can suggest the presence of metaplastic tissue, the immunohistochemical detection of a specific pancreatic enzyme helps for the correct diagnosis. The expression of BCL10 is highly sensitive and specific for this purpose and we suggest using it in any case of a suspected focus of pancreatic metaplasia.

Table 4 Specificity and sensitivity of antibodies directed against various pancreatic enzymes in detecting pancreatic ACCs

Antibody	Specificity (%)	Sensitivity (%)
BCL10	100	100
Trypsin	100	100
CEH	100	90
Lipase	100	45
Amylase	100	12

CEH carboxyl ester hydrolase

Unlike the pancreas, where acinar cells were strongly BCL10-positive, the majority of normal tissues investigated were BCL10 negative, with the exception of the lactating breast and human milk. Obviously, lymph nodes were also BCL10 positive, a result which was expected since it is well known that normal lymphocytes express BCL10. Excluding lymph nodes, the distribution of BCL10 immunostaining, identified with the monoclonal (331.3) antibody, among normal and ectopic pancreas, acinar metaplasia, and ACCs well reflected that of CEH. Our results on CEH distribution (Table 2) are in line with those previously published, since CEH was found in the pancreas and lactating breast, while neither CEH protein nor mRNA were observed in other normal tissues, with the exception of the gastric mucosa [9, 10, 12–14, 27–29].

The overlap between BCL10 and CEH immunohistochemistry, together with the ultrastructural localization of

Table 5 BCL10, trypsin, CEH, amylase, and lipase immunoreactivity in different types of pancreatic acinar cell carcinomas

No.	Type	BCL10		Trypsin		CEH		Amylase		Lipase	
		Intensity	% of IR cells	Intensity	% of IR cells	Intensity	% of IR cells	Intensity	% of IR cells	Intensity	% of IR cells
1	Acinar cell carcinoma	3+	70	2+	50	3+	40	1+	5	1+	3
2	Acinar cell carcinoma	3+	80	3+	80	3+	60		0		0
3	Acinar cell carcinoma	3+	90	2+	90	3+	70		0	2+	60
4	Acinar cell carcinoma	3+	80	2+	80	3+	80		0	2+	3
5	Acinar cell carcinoma	3+	80	3+	50		0		0		0
6	Acinar cell carcinoma	3+	70	2+	60	1+	30		0		0
7	Acinar cell carcinoma	3+	80	3+	60	1+	20		0		0
8	Acinar cystadenocarcinoma	2+	80	1+	30		ne		ne	2+	5
9	Intraductal acinar cell carcinoma	3+	80	3+	60	1+	10		ne	1+	10
10	Intraductal acinar cell carcinoma	3+	80	3+	80	1+	10		0		0
11	Mixed acinar–endocrine carcinoma	3+	70	2+	60	3+	10		ne		0
12	Mixed acinar–endocrine carcinoma	2+	80	2+	60		ne	ne	ne		ne
	Mean value	2.8+	78.3*	2.3+	63.3*	2.1+	36.6*	1+	5	1.6+	16.2

For details, see "Materials and methods"
CEH carboxyl ester hydrolase, *% of IR cells* percentage of immunoreactive cells in positive cases, *Intensity* intensity of immunoreaction, *ne* not evaluated
*$p<0.01$

Table 6 BCL10 expression in gastrointestinal endocrine tumors of different sites

Type	BCL10 C-terminal
Stomach	
ECL-cell	1/7
PDEC	0/5
Duodenum	
G-cell	0/2
D-cell	0/4
EC-cell	0/1
PDEC	0/2
Gangliocytic paraganglioma	0/1
Ileum	
EC-cell	0/12
Appendix	
EC-cell	0/11
Goblet cell carcinoid	0/1
Colon–rectum	
L-cell	0/4
EC-cell	0/2
PDEC	0/9

PDEC poorly differentiated endocrine carcinoma

BCL10 in zymogen granules of acinar cells and the Western blotting results, has demonstrated that the anti-BCL10 monoclonal (331.3) antibody also recognizes pancreatic CEH. This fact is not surprising since the sequence between amino acid 156 and 205 of the BCL10 protein (blast accession number: NP_003912.1) shows high homology with the sequence between amino acid 564 and 608 of CEH (blast accession number: NP_001798.2).

Interestingly, using the anti-BCL10 polyclonal antibody (N-20), which recognizes the N-terminal portion of the BCL10 protein, we did not observe any immunoreactivity in the normal pancreas, pancreatic tumors nor in the other neoplasms and normal tissues investigated, with the exception of lymph nodes and lymphocytes present in various tissues. This finding supports the hypothesis that the BCL10 expression found in acinar cells using the 331.3 antibody is due to the homology in sequence between CEH and BCL10 and not to the expression of the BCL10 peptide.

In conclusion, we have demonstrated that the antibody directed against the C-terminal portion of the BCL10 is useful in the diagnosis of pancreatic ACC. This finding depends on the homology between the C-terminal portion of BCL10 and CEH. Based on our experiments and our experience, we suggest that this antibody should be included in the panel used for diagnosing pancreatic neoplasms, because it is highly specific and it is more sensitive than antibodies directed against other pancreatic enzymes in detecting acinar cell differentiation. In addition, the opportunity to also use the anti-BCL10 antibody in the

diagnosis of lymphoid tumors has a practical and economic advantage, especially for those laboratories in which pancreatic surgical pathology is less frequent.

Acknowledgments This study was supported by a grant from the University of Insubria, Varese. Silvia Marchet is the recipient of a fellowship from the "Varese per l'Oncologia" Association. The authors thank Anna and baby Riccardo La Rosa for providing samples of human milk and Dr. Luigi Terracciano (Institute of Pathology, University Hospital of Basel, Switzerland) for preparing the microarray slides.

Conflict of interest statement We declare that we have no conflict of interest.

References

1. Hruban RH, Pitman MB, Klimstra DS (2007) Acinar neoplasms. In: Silverberg SG, Sobin LH (eds) Atlas of tumor pathology, series 4. Tumors of the pancreas. American Registry of Pathology, Washington, DC, pp 191–218
2. Lack EE (2003) Acinar cell carcinoma. In: Lack EE (ed) Pathology of the pancreas, gallbladder, extrahepatic biliary tract, and ampullary region. Oxford University Press, New York, pp 307–317
3. Klöppel G (2000) Mixed exocrine–endocrine tumors of the pancreas. Semin Diagn Pathol 17:104–108
4. Ohike N, Kosmahl M, Klöppel G (2004) Mixed acinar–endocrine carcinoma of the pancreas: a clinico-pathological study and comparison with acinar cell carcinoma. Virchows Arch 445:231–235
5. Volante M, Righi L, Asioli S et al (2007) Goblet cell carcinoids and other mixed neuroendocrine/nonneuroendocrine neoplasms. Virchows Arch 451(suppl 1):S61–S69
6. Holen KD, Klimstra DS, Hummer A et al (2002) Clinical characteristics and outcomes from an institutional series of acinar cell carcinoma of the pancreas and related tumors. J Clin Oncol 20:4673–4678
7. Morohoshi T, Kanda M, Horie A et al (1987) Immunocytochemical markers of uncommon pancreatic tumors. Acinar cell carcinoma, pancreatoblastoma, and solid cystic (papillary-cystic) tumor. Cancer 59:739–747
8. Solcia E, Capella C, Klöppel G (1997) Acinar cell carcinoma. In: Rosai J, Sobin LH (eds) Atlas of tumor pathology: tumors of the pancreas. Armed Forces Institute of Pathology, Washington, DC, pp 103–112
9. Carrère J, Figarella-Branger D, Senegas-Balas F et al (1992) Immunohistochemical study of secretory proteins in the developing human exocrine pancreas. Differentiation 51:55–60
10. Lombardo D, Guy O, Figarella C (1978) Purification and characterization of carboxyl ester hydrolase from human pancreatic juice. Biochim Biophys Acta 527:142–149
11. Rinderknecht H (1993) Pancreatic secretory enzymes. In: Go VLW, DiMagno EP, Gardner JD et al (eds) The pancreas: biology, pathobiology, and disease, 2nd edn. Raven, New York, pp 219–251
12. Nilsson J Blackberg L, Carlsson P et al (1990) cDNA cloning of human-milk bile-salt-stimulated lipase and evidence for its identity to pancreatic carboxylic ester hydrolase. Eur J Biochem 192:543–550
13. Christie DL, Cleverly DR, O'Connor CJ (1991) Human milk bile-salt stimulated lipase. Sequence similarity with rat lysophospholipase and homology with the active site region of cholinesterases. FEBS Lett 278:190–194
14. Wang CS (1988) Purification of carboxyl ester lipase from human pancreas and the amino acid sequence of the N-terminal region. Biochem Biophys Res Commun 155:950–955
15. Bernback S, Blackberg L, Hernell O (1990) The complete digestion of human milk triacylglycerol in vitro requires gastric lipase, pancreatic colipase-dependent lipase, and bile salt-stimulated lipase. J Clin Invest 85:1221–1226
16. Brodt-Eppley J, White P, Jenkins S et al (1995) Plasma cholesterol esterase level is a determinant for an atherogenic lipoprotein profile in normolipidemic human subjects. Biochem Biophys Acta 1272:69–72
17. Li F, Hui DY (1998) Synthesis and secretion of the pancreatic-type carboxyl ester lipase by human endothelial cells. Biochem J 329:675–679
18. Willis TG, Jadayel DM, Du MQ et al (1999) BCL10 is involved in t(1;14)(p22;q32) of MALT B cell lymphoma and mutated in multiple tumor types. Cell 96:35–45
19. Basturk O, Zamboni G, Klimstra DS et al (2007) Intraductal and papillary variants of acinar cell carcinomas. A new addition to the challenging differential diagnosis of intraductal neoplasms. Am J Surg Pathol 31:363–370
20. La Rosa S, Rigoli E, Uccella S et al (2004) CDX2 as a marker of intestinal EC-cells and related well-differentiated endocrine tumors. Virchows Arch 445:248–254
21. Qiu J, Hendrixson DR, Baker EN et al (1998) Human milk lactoferrin inactivates two putative colonization factors expressed by *Haemophilus influenzae*. Proc Natl Acad Sci U S A 95:12641–12646
22. Henley JD, Geary WA, Jackson CL et al (1997) Dedifferentiated acinic cell carcinoma of the parotid gland: a distinct rarely described entity. Hum Pathol 28:869–873
23. Kuopio T, Ekfors TO, NIkkanen V et al (1995) Acinar cell carcinoma of the pancreas. Report of three cases. APMIS 103:69–78
24. Ordonez NG (2001) Pancreatic acinar cell carcinoma. Adv Anat Pathol 8:144–159
25. Klimstra DS, Heffess CS, Oertel JE et al (1992) Acinar cell carcinoma of the pancreas. A clinico-pathologic study of 28 cases. Am J Pathol 16:815–837
26. Hoorens A, Lemoine NR, McLellan E et al (1993) Pancreatic acinar cell carcinoma. An analysis of cell lineage markers, p53 expression, and Ki-ras mutation. Am J Pathol 143:685–698
27. Reuss R, Aberle S, Klingel K et al (2006) The expression of the carboxyl ester lipase gene in pancreas and pancreatic adenocarcinomas. Int J Oncol 29:649–654
28. Aho HJ, Sternby B, Kallajoki M et al (1989) Carboxyl ester lipase in human tissues and acute pancreatitis. Int J Pancreatol 5:123–134
29. Nilsson J, Hellquist M, Bjursell G (1993) The human carboxyl ester lipase-like (CELL) gene is ubiquitously expressed and contains a hypervariable region. Genomics 17:416–422

Virchows Arch (2009) 454:143–151
DOI 10.1007/s00428-008-0717-3

ORIGINAL ARTICLE

Histopathological predictor for regional lymph node metastasis in gastric cancer

Hiroshi Morita · Yukio Ishikawa · Yuri Akishima-Fukasawa · Kinji Ito · Yoshikiyo Akasaka · Chiaki Nishimura · Yoshinori Igarashi · Kazumasa Miki · Toshiharu Ishii

Received: 25 June 2008 / Revised: 1 December 2008 / Accepted: 6 December 2008 / Published online: 23 December 2008

Abstract Regional lymph node metastasis in gastric cancer is a definitive indicator of the patient's prognosis. The goal of this study was to identify the predictors for lymph node metastasis among all the possible histopathological parameters, especially by conducting an objective discrimination of the lymphatic and blood vessels. A total of 210 resected primary gastric cancers with or without lymph node metastasis were evaluated based on the conventional histopathological parameters together with immunohistochemistry using antisera-recognizing lymphatic endothelial hyaluronan receptor-1 (LYVE-1), von Willebrand factor, and lymphangiogenesis promoter vascular endothelial growth factor-C (VEGF-C) antibodies. A multivariate regression analyses of the results indicated that only lymphatic invasion was a significant independent predictor of lymph node metastasis at any stage of cancer invasion. VEGF-C expression was partially related to lymph node metastasis in early gastric cancer. The identification of lymphatic invasion by LYVE-1 antibody is therefore useful to predict regional lymph node metastasis in gastric cancer.

Keywords Gastric cancer · Lymph node metastasis · Lymphatic vessel endothelial hyaluronan receptor-1 (LYVE-1) antibody · Lymphatic invasion · Vascular endothelial growth factor-C (VEGF-C)

H. Morita · Y. Ishikawa · K. Ito · Y. Akasaka · T. Ishii
Department of Pathology, School of Medicine, Toho University, Tokyo, Japan

H. Morita (✉) · Y. Igarashi · K. Miki
Division of Gastroenterology and Hepatology, Department of Internal Medicine (Omori), School of Medicine, Toho University,
6-11-1 Omorinishi, Ota-ku,
Tokyo 143-8541, Japan
e-mail: morita-hiroshi@med.toho-u.ac.jp

Y. Akishima-Fukasawa
Pathology Division, National Cancer Center Research Institute, Tokyo, Japan

C. Nishimura
Department of Medical Informatics, School of Medicine, Toho University,
Tokyo, Japan

Introduction

Regional lymph node metastasis is an independent prognostic factor in patients with gastric cancer [1]. Among the routes by which cancer cells metastasize to the regional lymph nodes, metastasis through the lymphatics at the primary site is a major candidate. Conventional histopathological examinations reveal many small lymphatics and blood capillaries at the primary site of gastric cancer; however, the objective discrimination of these two types of vessels is often difficult when using only hematoxylin and eosin (HE) and Victoria blue staining. Recently, several immunohistochemical markers that recognize the endothelium of a lymphatic vessel have been successively developed, including LYVE-1 [2], D2-40 [3], podoplanin [4], and prox-1 [5]. These markers are practically useful to demonstrate the relationship between cancer invasion and metastasis in early gastric cancer [6]. In addition, an immunochemical analysis with the lymphatic endothelial hyaluronan receptor-1 (LYVE-1) antibody in early gastric cancer reveals that lymphatic invasion by cancer cells predicts regional lymph node metastasis [7]. However, the relationship between the lymphatic invasion and lymph node metastasis should be universally explored at any stage of gastric cancer invasion because the characteristics of the local anatomical structure

of the gastric wall may influence the route of gastric cancer metastasis.

Although angiogenesis as well as the dissemination of malignant cells through blood vessels play major roles in tumor growth [8, 9], lymphangiogenesis and the development of lymphatic vessels are directly responsible for the lymphatic spread of tumors [10, 11]. Various molecules belonging to the vascular endothelial growth factor (VEGF) family are thought to regulate the lymphatic vessel development [12, 13]. Some studies have demonstrated that VEGF factor C (VEGF-C) expression is closely associated with the prognosis of breast [14], lung [15], stomach [16], and colorectal [17] cancers. VEGF mediates angiogenesis and vascular permeability [18]. On the other hand, similar up-regulation of VEGF-C can lead to lymphangiogenesis, intralymphatic tumor growth, and lymph node metastasis [19]. However, in gastric cancer, there is no evidence confirming the relationship between VEGF-C expression and lymphatic invasion using immunohistochemistry.

The present study attempted to explore the relationship between lymphatic invasion and regional lymph node metastasis in conjunction with several histopathological parameters at any stage of gastric cancer invasion, focusing on the discrimination of the lymphatics and blood vessels, using immunohistochemistry. In addition, the possible role of VEGF-C-mediated lymphangiogenesis and the spread of gastric cancer were investigated.

Materials and methods

Materials

The surgically resected specimens of gastric cancer with the regional lymph nodes were obtained from a total of 210 patients. The patients were diagnosed and treated with a curative gastrectomy at Toho University Omori Medical Center, Saiseikai Kanagawa-Ken Hospital and Hiratsuka Municipal Hospital, Japan, between 1989 and 2005.

Curative surgery was defined as the removal of all gross cancer and the microscopic evaluation of the tumor-negative surgical margin. The patients underwent a lymph node dissection of group 1 and group 2 according to the Japanese Classification of Gastric Carcinoma [20], which were located at the nearest and the second nearest area of the primary cancer site. Lymph node metastasis was considered to be present when at least one lymph node invaded by cancer cells was observed. The patients were free from other types or degrees of invasion, distant visceral metastases, and complications due to other conditions. None of the patients underwent either preoperative chemotherapy or radiotherapy. Written informed consent to use the tissue specimens was provided by all patients at each medical institute.

In this study, as we considered that the route of gastric cancer metastasis may be influenced by the characteristics of the local anatomical structure of the gastric wall, we aimed to explore the relationship between the lymphatic invasion and lymph node metastasis. The patients were divided into six groups, including the following: cancer invasion confined to within the mucosa or submucosa (SM), with or without metastasis; tumor invasion up to the external rim of the propriate muscle layer (MP), with or without metastasis; and tumor invasion reaching subserosal layers (SS) with or without metastasis. We assigned the latest 35 consecutive cases that met the definition for each group from that surgically resected specimens previously described. We combined the cancer invasion confined within the mucosa or submucosa invasion as a single group according to the World Health Organization (WHO) classification with the Japanese modification [21]. The number of mucosal invasion cancers in the group with lymph node metastasis was 5 out of 35, while for the group without it, the number was 20 out of 35.

All of surgically resected stomachs were opened along the greater curvature, pinned on a cork board, and fixed in 10% formalin. After a careful gross inspection of the location of the primary cancer, the tumor size was measured on the length of its major axis. Each tumor was cut into 4-mm slices parallel to the major axis of the specimen and to the minor axis crossing the halfway point of the long axis. The slices were embedded in paraffin, cut into 3-μm-thick sections, and treated by double staining with Victoria blue and HE dyes to aid the identification of elastic fibers in the blood vessel structures, especially with regard to the veins.

Immunohistochemistry

The primary antibodies for immunohistochemistry used in this study were anti-LYVE-1, which was previously raised against a LYVE-1 polypeptide fragment [2], anti-human von Willebrand factor (vWF) antibody (Dako, Carpinteria, CA, USA), and anti-VEGF-C (Zymed Lab. Inc., South San Francisco, CA, USA). Immunohistochemistry with LYVE-1, vWF, and VEGF-C antibodies were carried out after deparaffinizing and dehydration of the thin-sectioned specimens. For LYVE-1 and VEGF-C, the sections were pretreated with 10 mM citrate buffer solution (pH 6.0) for 15 min at 95°C. They were then treated with 40 μg/ml proteinase K (Dako) for 3 min at room temperature.

After washing in distilled water, the sections were incubated with LYVE-1 (1:200 dilution) and VEGF-C (1:200 dilution) antibody for 1.5 h at room temperature, washed in Tris-buffered saline (TBS) containing Tween 20

and treated with the Catalyzed Signal Amplification II kit (Dako) according to the manufacturer's instructions. For vWF immunohistochemistry, the sections were pretreated with 10 mM citrate buffer solution (pH 6.0) for 15 min at 95°C. After washing in TBS, they were treated with 3% hydrogen peroxide for 10 min and then with 3% non-fat dried milk in TBS containing Tween 20 for 30 min. The sections were then incubated with vWF antibody (1:25 dilution) for 2 h at room temperature. A further wash in TBS was followed by treatment with peroxidase-labeled polymer conjugated to goat and anti-rabbit or anti-mouse immunoglobulins (Envision+kit; Dako) for 30 min at room temperature. The immunostaining was visualized with diaminobenzidine tetrahydrochloride, followed by counter-staining with hematoxylin.

Histopathological variables

Each case was evaluated for the histopathological classification of primary cancer, the presence of vessel invasion, vessel density, and VEGF-C expression in cancer cells. The tumor type was assessed by examining sections that were stained with H&E and VB. The histopathological classification was determined according to the WHO classification with the Japanese modification. To determine the grade of differentiation, the major histopathological type showing at the primary site was categorized as papillary adenocarcinoma, well differentiated, moderately differentiated, poorly differentiated adenocarcinoma, or signet ring cell carcinoma. For the statistical analysis, the former three types were combined as a low-grade malignancy group and the latter two types as a high-grade malignancy group, according to the conventionally accepted relationship between cancer typing and biological behavior. All the histopathological specimens were separately reviewed by the three pathologists (HM, YI, and IF), and the results were finally determined after consensus readings when they were different among them.

The location and number of vessel invasion was examined under the view field at a magnification of ×200. For this analysis, vascular invasion was defined as invasion and adherence of cancer cells to the inner surface of the lymphatic vessels determined by anti-LYVE-1 antibody or blood vessels determined by anti-vWF antibody with the use of Victoria blue-staining for the detection of the venous structure. Lymphatic and blood vessel invasion was considered to be present when at least one vessel invaded by cancer cells was observed in a given case. The location of the lymphatic and blood vessel invasion was also noted throughout the observation of the primary tumor.

To examine the lymphatic vessel density (LVD) by light microscopy, the immunostained sections were scanned along the tumor front margin at a low magnification of ×40, and the highly distinctive areas for lymphatic vessels with LYVE-1 antibody were selected. The number of lymphatic vessels lumens in these areas was counted in five view fields under a magnification of ×200. The average number of lymphatic vessels at each area was designated as the LVD. Blood vessel density (BVD) was determined with anti-vWF antibody, and their density was determined by the same procedures used for the LVD.

VEGF-C was evaluated according to the extent of staining as described by Siironen et al. [22]. Briefly, under the light microscope, when more than 10% of the primary cancer cells expressed VEGF-C in the cytoplasm of the cancer cells, they were recorded as positive.

Statistical analysis

Statistical analyses were performed using the chi-square test, Fisher's exact test, and the Mann–Whitney's *U* test to assess the significance of the impact of each subset of histopathological parameters on the lymph node status. Multivariate logistic regression analyses including these variables selected by backward elimination were also carried out to identify the independent predictors for lymph node metastasis. Any differences in the *P* value of less than 0.05 were considered to be statistically significant. All of the statistical analyses were examined using the StatView software program (SAS Institute, Raleigh, NC, USA).

Results

Comparison of each parameter between the node-negative and node-positive groups

A summary of the clinicopathologic characteristics of the patients in this study is shown in Table 1. The differences in the histopathological parameters between the node-negative and node-positive groups were indicated by the invasion depth in the gastric wall (Tables 2, 3, and 4). In all 15 cases on the SM invasion group with lymphatic invasion, cancer invasion reached the submucosa. The variables of age, sex, and the location of tumor were not always significant in conjunction with the lymph node status by the depth of cancer invasion in the following statistical treatments (data not shown). Therefore, those variables were omitted in the tables of the present study.

A significant difference was recognized between tumor size and regional lymph node metastasis in all the subsets by invasion depth using Mann–Whitney's *U* test. The two varieties of vessel invasion were readily distinguished by LYVE-1 (Fig. 1) and vWF (Fig. 2) immunostaining. The frequency of lymphatic vessel invasion was significantly greater in the node-positive groups than the node-negative groups at any invasion depth, based on Fisher's exact test.

Table 1 Clinicopathologic characteristics of patients in this study (n=210)

	Node-negative group	Node-positive group
Mean age	67.0	65.0
Sex		
Men	82 (78.1%)	79 (75.2%)
Women	23 (21.9%)	26 (24.8%)
Mean size	33.0	44.9
Tumor location		
U	28 (26.7%)	36 (34.3%)
M	52 (19.5%)	31 (29.5%)
L	25 (23.8%)	38 (36.2%)
Grade of cancer differentiation		
Low-grade malignancy	61 (58.1%)	58 (55.2%)
High-grade malignancy	44 (41.9%)	47 (44.8%)
Lymphatic invasion		
Negative	82 (78.1%)	50 (47.6%)
Positive	23 (21.9%)	55 (52.4%)
Mean LVD	11.7	10.7
Blood vessel invasion		
Negative	66 (62.9%)	62 (59.0%)
Positive	39 (37.1%)	43 (41.0%)
Mean BVD	14.7	13.6
VEGF-C expression		
Negative	72 (68.6%)	60 (57.1%)
Positive	33 (31.4%)	45 (42.9%)

M middle, *U* upper, *L* lower third of the gastric surface area

On the other hand, there was no significant relationship between blood vessel invasion and regional lymph node metastasis.

In all of the subsets of invasion depth, the low-grade malignancy group was predominant in the node-negative group, but there was no significant difference in cancer differentiation between the node-positive and node-negative groups as assessed by Fisher's exact test. In addition, there was no significant difference in LVD and BVD between the node-positive and node-negative groups as assessed by Mann–Whitney's *U* test. Although the frequency of VEGF-C expression in the node-positive groups tended to be greater than the node-negative groups, there was no significant difference for any invasion depth as assessed by Fisher's exact test.

Logistic regression analyses of histopathological parameters for lymph node metastasis

The results of the multivariate analyses of the histopathological parameters for lymph node metastasis are shown in Table 5. In the SM invasion group, the size of tumor (odds ratio, 1.043; P=0.0192), lymphatic invasion, and positive VEGF-C expression (odds ratio, 5.184;P=0.0225) were significant independent predictors of lymph node metastasis by the multivariable analyses. In the MP invasion group, the size of the tumor and lymphatic invasion (odds ratio, 6.174; p=0.0032) were significant independent predictors of lymph node metastasis by the multivariable analyses. In the SS invasion group, lymphatic invasion (odds ratio, 3.036; p=0.0344) and LVD (odds ratio, 0.977; p=0.0429) were significant independent predictors for lymph node metastasis by the multivariable analyses. In all the cases, the size of tumor (odds ratio, 1.044; p=0.0038) and lymphatic invasion (odds ratio, 4.328; p=0.0092) were significant independent predictors for lymph node metastasis based on multivariable analyses. Only lymphatic invasion was the consistent significant predictor for lymph node metastasis in any depth of tumor invasion based on the multivariate analysis.

Table 2 Comparison of the histopathological parameters by the lymph node status in SM invasion group (n=70)

Parameter	Node-negative Group	Node-positive Group	P-value
Size (mean), mm	22.0	31.5	0.0057[a]
Grade of cancer differentiation			NS[b]
Low-grade malignancy	23 (66.0%)	19 (54.0%)	
High-grade malignancy	12 (34.0%)	16 (46.0%)	
Lymphatic invasion			0.0088[b]
Negative	32 (91.0%)	23 (66.0%)	
Positive	3 (9.0%)	12 (34.0%)	
LVD (mean)	13.7	14.7	NS[a]
Blood vessel invasion			NS[b]
Negative	32 (91.0%)	31 (89.0%)	
Positive	3 (9.0%)	4 (11.0%)	
BVD (mean)	14.0	11.9	NS[a]
VEGF-C expression			NS[b]
Negative	28 (80.0%)	22 (63.0%)	
Positive	7 (20.0%)	13 (37.0%)	

[a] Mann–Whitney's *U* test
[b] Fisher's exact test

Table 3 Comparison of the histopathological parameters by the lymph node status in MP invasion group (n=70)

Parameter	Node-negative Group	Node-positive Group	P value
Size (mean), mm	31.0	44.7	0.0025[a]
Grade of cancer differentiation			NS[b]
Low-grade malignancy	20 (57.0%)	17 (49.0%)	
High-grade malignancy	15 (43.0%)	18 (51.0%)	
Lymphatic invasion			0.0004[b]
Negative	30 (86.0%)	16 (46.0%)	
Positive	5 (14.0%)	19 (54.0%)	
LVD (mean)	9.2	8.6	NS[a]
Blood vessel invasion			NS[b]
Negative	21 (60.0%)	22 (63.0%)	
Positive	14 (40.0%)	13 (37.0%)	
BVD (mean)	16.8	14.4	NS[a]
VEGF-C expression			NS[b]
Negative	21 (60.0%)	20 (57.0%)	
Positive	14 (40.0%)	15 (43.0%)	

[a] Mann–Whitney's U test
[b] Fisher's exact test

Sites of lymphatic vessel invasion within the gastric wall by the invasion depth of cancer

Although the lymphatic and blood vessels were readily distinguished by LYVE-1 and vWF immunostaining in the normal part of the resected stomach, they frequently appeared to be affected and destroyed within the tumors. The spatial distribution of lymphatic vessel invasion within the gastric wall by the invasion depth of all the 78 lymphatic invasion-positive cases is indicated in Table 6. For this analysis, the submucosal layer was arbitrarily subdivided into two groups: SM1, in which cancer invaded up to the upper half of the submucosa, and SM2, in which cancer invaded the whole layer of the submucosa. In the SM invasion group, lymphatic invasion was detected in the mucosa (6.7%, 1/15), the SM1 (93.3%, 14/15), and the SM2 (26.7%, 4/15). In the MP invasion group, lymphatic invasion was detected in the SM1 (79.1%, 19/24), the SM2 (16.7%, 4/24), and the muscularis propria (8.3%, 2/24). In the SS invasion group, lymphatic invasion was detected in the mucosa (5.1%, 2/39), SM1 (66.7%, 26/39), SM2 (17.9%, 7/39), and the muscularis propria (41.0%, 16/39). Accordingly, in any depth of cancer invasion, lymphatic invasion was most frequently detected in the SM1 layer.

Table 4 Comparison of the histopathological parameters by the lymph node status in SS invasion group (n=70)

Parameter	Node-negative Group	Node-positive Group	P value
Size (mean), mm	46.0	58.5	0.0053[a]
Grade of cancer differentiation			NS[b]
Low-grade malignancy	18 (60.0%)	22 (63.0%)	
High-grade malignancy	17 (40.0%)	13 (37.0%)	
Lymphatic invasion			0.0303[b]
Negative	20 (57.0%)	11 (31.0%)	
Positive	15 (43.0%)	24 (69.0%)	
LVD (mean)	12.2	8.9	NS[a]
Blood vessel invasion			NS[b]
Negative	13 (37.0%)	9 (26.0%)	
Positive	22 (63.0%)	26 (74.0%)	
BVD (mean)	13.3	14.6	NS[a]
VEGF-C expression			NS[b]
Negative	23 (66.0%)	18 (51.0%)	
Positive	12 (34.0%)	17 (49.0%)	

[a] Mann–Whitney's U test
[b] Fisher's exact test

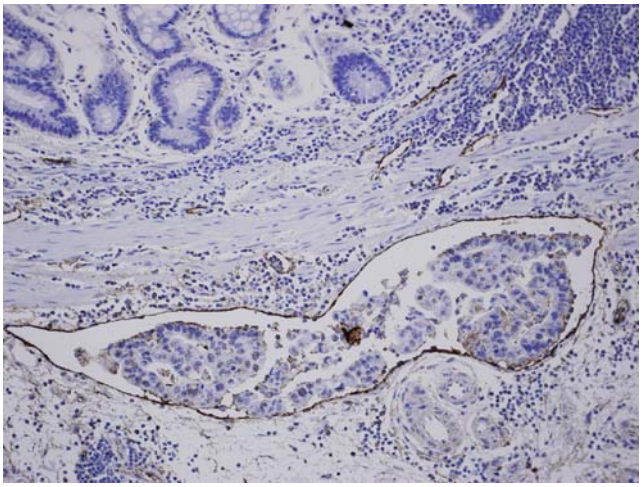

Fig. 1 A mass of a poorly differentiated adenocarcinoma invading the lymphatic vessels, which is lined with LYVE-1-positive endothelial cells just beneath the lamina muscularis mucosae (×400)

Comparison of each parameter with the expression of VEGF-C

In the stomach, VEGF-C expression was mainly present at the tumor front (Fig. 3) and usually detected as small heterogeneous nodules in the cytoplasm of the cancer cells. In addition, it was also weakly present in the cytoplasm of some normal ductal cells. In the SM invasion group, the VEGF-C expression was positive in 20 cases (28.6%, 20/70). As for the PM invasion group, VEGF-C expression was detected in 29 cases (41.4%, 29/70). In the SS invasion group, it was detected in 29 cases (41.4%, 29/70). Although the frequency of the positive expression of VEGF-C in the node-positive cases was higher than in node-negative groups in any group of invasion depth, there was no statistical significance between them.

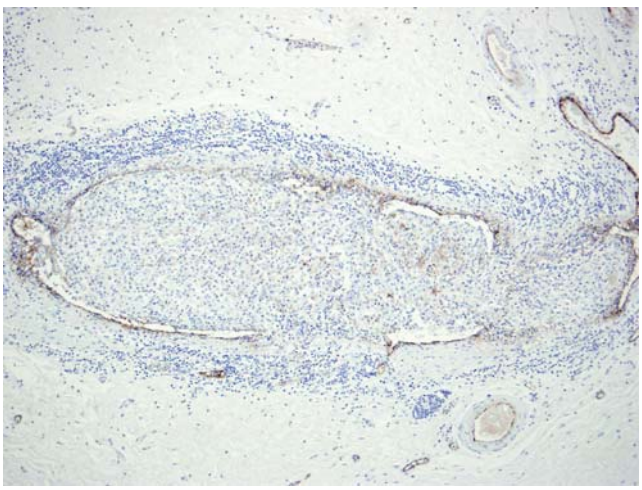

Fig. 2 The blood capillary lumen positively stained with the vWF antibody in the submucosal layer is almost completely occluded with a large mass of a poorly-differentiated adenocarcinoma (×400)

Table 5 Result of the histopathological parameters for node-positive cancer by multivariate logistic analyses

Parameter	Odds ratio	95%CI	*P* value
All the cases (n=210)			
Size	1.044	1.014–1.075	0.0038
Lymphatic invasion	4.328	1.436–13.043	0.0092
SM invasion group (n=70)			
Size	1.043	1.010–1.084	0.0192
Lymphatic invasion	5.222	1.839–20.736	0.0242
VEGF-C expression	3.312	1.002–10.950	0.0497
MP invasion group (n=70)			
Size	1.046	1.010–1.084	0.0118
Lymphatic invasion	6.174	1.839–20.736	0.0032
SS invasion group (n=70)			
Lymphatic invasion	3.036	1.085–8.499	0.0344
LVD	0.977	0.955–0.999	0.0429

95%CI 95% confidence interval

A further comparison of histopathological variables, such as the location of the primary cancer, the tumor size, grade of cancer differentiation, blood vessel invasion, LVD, and BVD, was made with the expression of VEGF-C. However, none of the variables defined were significant. In addition, the depth of cancer invasion was also not significantly related to the frequency of VEGF-C expression.

Discussion

The present study demonstrated the significance of lymphatic vessel invasion on regional lymph node metastasis in gastric cancer using LYVE-1 and vWF antibodies for the objective discrimination of the lymphatic and blood vessels. The results of a multivariate analysis indicated that only the lymphatic invasion by cancer cells was consistently recognized as an independent histopathological predictor of regional lymph node metastasis at any depth of tumor invasion. The macroscopic issue of tumor size and microscopic VEGF-C expression in cancer cells were also significant; however, their roles seemed to differ with regard to the stage of cancer invasion. Since the lymphatic vessels are a route to lymph node, it would be reasonable to

Table 6 Site of lymphatic vessel invasion by invasion depth of cancer

Site of lymphatic invasion	Invasion depth of cancer (%)		
	SM	MP	SS
Mucosa	1/15 (6.7)	0/24 (0.0)	2/39 (5.1)
SM1	14/15 (93.3)	19/24 (79.1)	26/39 (66.7)
SM2	4/15 (26.7)	4/24 (16.7)	7/39 (17.9)
MP	–	2/24 (8.3)	16/39 (41.0)
SS	–	–	0/39 (0.0)

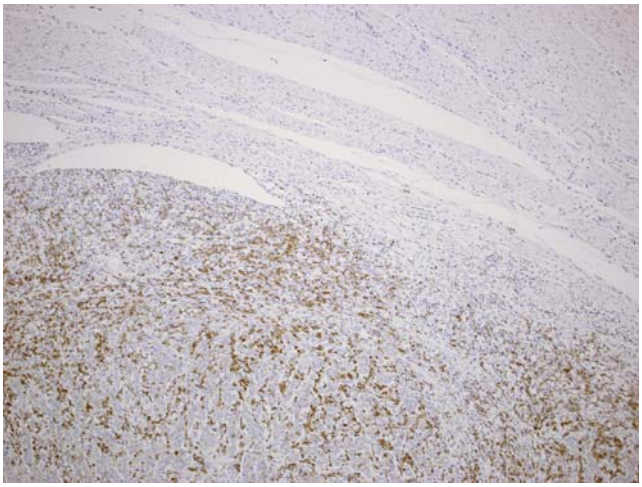

Fig. 3 VEGF-C expression is positive in gastric cancer. VEGF-C is mainly present in the cytoplasm of cancer cells in the peripheral part of the tumor (×200)

conclude that only lymphatic invasion is a notable predictor for lymph node metastasis. In the tumor, node, metastasis system, the extent of lymph node metastasis is one of the essential factors for assessing the extent of disease, determining prognosis, and establishing the therapy strategies in gastric cancer patients.

Recently, several immunohistochemical markers recognizing the lymphatic vessel endothelium have been successively identified, including LYVE-l [2], D2-40 [3], podoplanin [4], prox-1[5], desmoplakin [23], and D6 [24]. In addition, a more specific LYVE-1 antibody has been raised from the epitope that is a part of the polypeptide-fragment of the original LYVE-1 [2]. This antibody has enabled the objective detection of lymphatics in studies of the normal prostate [25], atherosclerosis [26], early-stage gastric cancer [7], and early-stage colorectal cancer [27]. In this study, it also enabled the distinctive discrimination of the lymphatic vessels from the blood vessels at any stage of gastric cancer.

The lymphatic spread of cancer is assumed to occur through the permeating of cancer cells into the peritumorous lymphatics, eventually reaching the regional lymph nodes. The close contact between tumor cells and lymphatics is thought to be an initial step in lymphatic metastasis. It is reasonable that cancer cells invading the submucosal layer easily penetrate the lymphatic lumen because most of the lymphatics are present just beneath the lamina muscularis mucosae in the normal stomach. The depth and total volume of submucosal invasion by the gastric cancer are closely correlated with lymph node metastasis [28–30]. In the current study, lymphatic invasion by cancer cells was most frequently found in the submucosal layer, and its frequency was highest in gastric cancer invading within the submucosal layer. The current results suggest that lymphatic vessels in the submucosal layer provide the main entry source for lymph node metastasis through lymphatic invasion even in advanced gastric cancers.

The lymphatic vessels at the tumor margin probably play a functional role in the drainage to the lymph nodes [31]. Therefore, in this study, the number of lumens in the lymphatic vessels was counted at the peripheral part of the tumor. The results, however, indicated no significant difference in the LVD between the node-positive and node-negative groups in the SM and MP invasion groups. On the other hand, in the SS invasion group, the results of a multivariate analysis demonstrated the LVD to be a significant independent predictor for lymph node metastasis. One reason why there are some differences between the current results and those in the previous studies [32–34] is due to the fact that the number of lymphatic vessels tend to decrease in the central portion of the primary cancer. The cancer cells may invade or destroy vessels in the central portion, while newly proliferating lymphatic vessel may provide the entry to cancer invasion at the peripheral area of the tumor, especially in the submucosal layer. Such differences in the decrease or increase of the number of the lymphatic vessels at each site may collectively result in the determination of the value.

In conjunction with the LVD, vascular or lymphatic metastasis may also be regulated through angiogenesis and lymphangiogenesis mediated by the growth factors expressed by the cancer cells. Among these, VEGF-C has been recently examined with regard to the relationship of the lymphatic vessels with cancer cell invasion. VEGF-C expression from cancer cells promotes lymphangiogenesis [35], which may provide the route for cancer invasion. Despite a significant correlation between lymph node metastasis and VEGF-C expression in esophageal [36], gastric, and colorectal cancers [37], such a relationship was not evident in the present study under the objective definitions of the location and estimation for VEGF-C expression. This indicates that VEGF-C expression from cancer cells does not seem to always promote lymphangiogenesis in the stroma, while cancer cells actively invade and damage the stroma.

Apart from the potentiality of lymphatic invasion through lymphangiogenesis, VEGF-C expression from cancer cells has been directly considered in conjunction with positive lymph node metastasis in cancers of the breast [38], thyroid [39], lung [40], and prostate [41]. In gastric cancer, based on a similar correlation of VEGF-C with lymph node metastasis, patients with high expression of VEGF-C show a poor prognosis [42, 43]. The present results indicated that significant up-regulation of VEGF-C from cancer cells was recognized in the patients with regional lymph node metastasis, but only in early gastric cancer. This finding is in agreement in part with that described in a previous report [44], thus suggesting the

possibility that VEGF-C up-regulation may promote lymph node metastasis via lymphatic vessels in patients with gastric cancer.

In the present study, as lymphatic invasion is usually found in the submucosal layer at any stage of gastric cancer, such detection therefore considered to be essential to predict regional lymph node metastasis in gastric cancer. It is especially important for the detection of lymphatic invasion to observe the submucosa around the primary tumor in patients with gastric cancer. The application of an endoscopic resection for early gastric cancer has been extended to the larger and more deeply invaded cases on the basis of guideline criteria [45]. Even in such cases, we cannot rule out the possibility of regional lymph node metastasis when we encounter the lymphatic invasion in the gastric mucosa or submucosa. Apart form these situations, when lymphatic invasion by gastric cancer is demonstrated in the gastrectomied cases of PM and SS invasions without any regional lymph node metastasis, we will carefully follow the possibility of any regional lymph node metastasis in those patients. If we can predict metastasis to the lymph node from a lymphatic vessel invasion in the primary site, it may be an important tool for choosing the optimal treatment protocol for cancer recurrence. Furthermore, the early identification of patients who is such at high risk and the appropriate treatment may significantly improve the survival rate.

In this study, LYVE-1 immunohistochemistry is therefore considered to be useful in predicting lymph node metastasis from gastric cancer with various depths of invasion.

Acknowledgment The authors are grateful to Ms. E. Ohnishi and Ms. T. Sato for their skillful technical assistance throughout the study. This work was partly supported by the Grants-in-Aid for Scientific Research (no. 19590368) from the Ministry of Education, Culture, Sports, Science, and Technology of Japan.

Conflict of interest statement We declare that we have no conflict of interest.

References

1. Bando E, Yonemura Y, Taniguchi K et al (2002) Outcome of ratio of lymph node metastasis in gastric carcinoma. Ann Surg Oncol 9:775–784
2. Akishima Y, Ito K, Zhang L et al (2004) Immunohistochemical detection of human small lymphatic vessels under normal and pathological conditions using the LYVE-1 antibody. Virchows Arch 444:153–157
3. Kahn HJ, Marks A (2002) A new monoclonal antibody, D2-40, for detection of lymphatic invasion in primary tumors. Lab Invest 82:1255–1257
4. Wigle JT, Oliver G (1999) Prox1 function is required for the development of the murine lymphatic system. Cell 98:769–778
5. Ebata N, Nodasaka Y, Sawa Y et al (2001) Desmoplakin as a specific marker of lymphatic vessels. Microvasc Res 61:40–48
6. Sako A, Kitayama J, Ishikawa M et al (2006) Impact of immunohistochemically identified lymphatic invasion on nodal metastasis in early gastric cancer. Gastric Cancer 9:295–302
7. Fujimoto A, Ishikawa Y, Akishima-Fukasawa Y et al (2007) Significance of lymphatic invasion on regional lymph node metastasis in early gastric cancer using LYVE-1 immunohistochemical analysis. Am J Clin Pathol 27:82–88
8. Shore VH, Wang TH, Wang CL et al (1997) Vascular endothelial growth factor, placenta growth factor and their receptors in isolated human trophoblast. Placenta 18:657–665
9. Cao Y, Linden P, Shima D et al (1996) In vivo angiogenic activity and hypoxia induction of heterodimers of placenta growth factor/vascular endothelial growth factor. J Clin Invest 98:2507–2511
10. Duff SE, Li C, Jeziorska M et al (2003) Vascular endothelial growth factors C and D and lymphangiogenesis in gastrointestinal tract malignancy. Br J Cancer 89:426–430
11. Pepper MS, Tille JC, Nisato R et al (2003) Lymphangiogenesis and tumor metastasis. Cell Tissue Res 314:167–177
12. Joukov V, Pajusola K, Kaipainen A et al (1996) A novel vascular endothelial growth factor, VEGF-C, is a ligand for the Flt4 (VEGFR-3) and KDR (VEGFR-2) receptor tyrosine kinases. EMBO J 15:290–298
13. Jeltsch M, Kaipainen A, Joukov V et al (1997) Hyperplasia of lymphatic vessels in VEGF-C transgenic mice. Science 276:1423–1425
14. Jin Q, Hemminki K, Enquist K et al (2005) Vascular endothelial growth factor polymorphisms in relation to breast cancer development and prognosis. Clin Cancer Res 11:3647–3653
15. Koukourakis MI, Papazoglou D, Giatromanolaki A et al (2004) VEGF gene sequence variation defines VEGF gene expression status and angiogenic activity in non-small cell lung cancer. Lung Cancer 46:293–298
16. Liu DH, Zhang XY, Fan DM et al (2001) Expression of vascular endothelial growth factor and its role in oncogenesis of human gastric carcinoma. World J Gastroent 7:500–505
17. Yamamori M, Sakaeda T, Nakamura T et al (2004) Association of VEGF genotype with mRNA level in colorectal adenocarcinomas. Biochem Biophys Res Commun 325:144–150
18. Koukourakis MI, Papazoglou D, Giatromanolaki A et al (2004) VEGF gene sequence variation defines VEGF gene expression status and angiogenic activity in non-small cell lung cancer. Lung Cancer 46:293–298
19. Ferrara N (2002) VEGF and the quest for tumour angiogenesis factors. Nat Rev Cancer 2:795–803
20. Japanese Research Society for Gastric (1995) Japanese classification of gastric carcinoma, 1st edn. Kanehara, Tokyo
21. Sugano H, Nakamura K, Kato Y (1982) Pathological studies of gastric carcinoma. Acta Pathol Jpn 32(suppl 2):329–347
22. Siironen P, Ristimäki A, Narko K et al (2006) VEGF-C and COX-2 expression in papillary thyroid cancer. Endocr Relat Cancer 13:465–473
23. Nibbs RJ, Kriehuber E, Ponath PD et al (2001) The beta-chemokine receptor D6 is expressed by lymphatic endothelium and a subset of vascular tumors. Am J Pathol 158:867–877
24. Irjala H, Johansson EL, Grenman R et al (2001) Mannose receptor is a novel ligand for L-selectin and mediates lymphocyte binding to lymphatic endothelium. J Exp Med 194:1033–1042
25. Soh S, Ishii T, Sato E et al (2005) Topographic distribution of lymphatic vessels in the normal human prostate. Prostate 63:330–335
26. Nakano T, Nakashima Y, Yonemitsu Y et al (2005) Angiogenesis and lymphangiogenesis and expression of lymphangiogenic factors in the atherosclerotic intima of human coronary arteries. Hum Pathol 36:330–340
27. Ishikawa Y, Akishima-Fukasawa Y, Ito K et al (2008) Histopathologic determinants of regional lymph node metastasis in early colorectal cancer. Cancer 112:924–933

28. Cai J, Ikeguchi M, Maeta M et al (2000) Micrometastasis in lymph nodes and microinvasion of the muscularis propria in primary lesions of submucosal gastric cancer. Surgery 127:32–39
29. Kurihara N, Kubota T, Otani Y et al (1998) Lymph node metastasis of early gastric cancer with submucosal invasion. Br J Surg 85:835–839
30. Matsuzaki H, Kikuchi S, Kakita A (2003) Evaluation of the morphology of submucosal tumor invasion and its volume in early gastric cancer. In Vivo 17:41–44
31. Padera TP, Kadambi A, di Tomaso E et al (2002) Lymphatic metastasis in the absence of functional intratumor lymphatics. Science 296:1883–1886
32. Wang TB, Deng MH, Qiu WS et al (2007) Association of serum vascular endothelial growth factor-C and lymphatic vessel density with lymph node metastasis and prognosis of patients with gastric cancer. World J Gastroenterol 28:1794–1797
33. Yuanming L, Feng G, Lei T et al (2007) Quantitative analysis of lymphangiogenic markers in human gastroenteric tumor. Arch Med Res 38:106–112
34. Nakamura Y, Yasuoka H, Tsujimoto M et al (2006) Importance of lymph vessels in gastric cancer: a prognostic indicator in general and a predictor for lymph node metastasis in early stage cancer. J Clin Pathol 59:77–82
35. Hachisuka T, Narikiyo M, Yamada Y et al (2005) High lymphatic vessel density correlates with overexpression of VEGF-C in gastric cancer. Oncol Rep 13:733–737
36. Kitadai Y, Amioka T, Haruma K et al (2001) Clinicopathological significance of vascular endothelial growth factor (VEGF)-C in human esophageal squamous cell carcinomas. Int J Cancer 93:662–666
37. Parr C, Jiang WG (2003) Quantitative analysis of lymphangiogenic markers in human colorectal cancer. Int J Oncol 23:533–539
38. Kurebayashi J, Otsuki T, Kunisue H et al (1999) Expression of vascular endothelial growth factor (VEGF) family members in breast cancer. Jpn J Cancer Res 90:977–981
39. Fellmer PT, Sato K, Tanaka R et al (1999) Vascular endothelial growth factor-C gene expression in papillary and follicular thyroid carcinomas. Surgery 126:1056–1062
40. Ohta Y, Nozawa H, Tanaka Y et al (2000) Increased vascular endothelial growth factor and vascular endothelial growth factor-c and decreased nm23 expression associated with microdissemination in the lymph nodes in stage I non-small cell lung cancer. J Thorac Cardiovasc Surg 119:804–813
41. Tsurusaki T, Kanda S, Sakai H et al (1999) Vascular endothelial growth factor-C expression in human prostatic carcinoma and its relationship to lymph node metastasis. Br J Cancer 80:309–313
42. Yonemura Y, Endo Y, Fujita H et al (1999) Role of vascular endothelial growth factor C expression in the development of lymph node metastasis in gastric cancer. Clin Cancer Res 5:1823–1829
43. Takahashi A, Kono K, Itakura J et al (2002) Correlation of vascular endothelial growth factor-C expression with tumor-infiltrating dendritic cells in gastric cancer. Oncology 62:121–127
44. Kitadai Y, Kodama M, Cho S et al (2005) Quantitative analysis of lymphangiogenic markers for predicting metastasis of human gastric carcinoma to lymph nodes. Int J Cancer 115:388–392
45. Gotoda T (2007) Endoscopic resection of early gastric cancer. Gastric Cancer 10:1–11

Virchows Arch (2009) 454:153–160
DOI 10.1007/s00428-008-0713-7

ORIGINAL ARTICLE

Prevalence of *Helicobacter pylori* infection, chronic gastritis, and intestinal metaplasia in Mozambican dyspeptic patients

Carla Carrilho · Prassad Modcoicar · Lina Cunha · Mamudo Ismail · Acucena Guisseve · Cesaltina Lorenzoni · Fabiola Fernandes · Bárbara Peleteiro · Raquel Almeida · Céu Figueiredo · Leonor David · Nuno Lunet

Received: 8 July 2008 / Revised: 20 November 2008 / Accepted: 1 December 2008 / Published online: 20 December 2008

Abstract We estimated the prevalence of *Helicobacter pylori* infection, chronic gastritis, atrophy, and intestinal metaplasia in dyspeptic patients from Maputo Central Hospital, Mozambique and evaluated the relationship between infection and histopathological features of chronic gastritis. Biopsies from 109 consecutive patients observed in 2005–2006 were collected from antrum, incisura angularis, and corpus for histopathological study according to the Modified Sydney system. *H. pylori* infection was assessed by histology and polymerase chain reaction. *H. pylori* prevalence was 94.5%. Chronic gastritis was the most frequent diagnosis (90.8%). Degenerative surface epithelial damage was associated with higher *H. pylori* density. Glandular atrophy (8.3%) and intestinal metaplasia (8.3%) were infrequent. Our results confirm previous observations in African countries with high prevalence of *H. pylori* infection and low rates of gastric cancer: high frequency of chronic *H. pylori*-associated gastritis with very low frequency of gastric atrophy and intestinal metaplasia.

Keywords *Helicobacter pylori* infection · Chronic gastritis · Intestinal metaplasia · Mozambique · African enigma

Introduction

Helicobacter pylori infection affects more than 50% of the world adult population, with two thirds of all cases of stomach cancer being attributed to it [1], but many countries with high prevalence of *H. pylori* infection have low rates of gastric cancer [2], which is known as the "African enigma" [3]. The lack of correspondence between the prevalence of infection and the gastric cancer frequency, however, is surely overestimated due to the scarcity of high

C. Carrilho · M. Ismail · A. Guisseve · C. Lorenzoni · F. Fernandes
Department of Pathology, Medical Faculty, Eduardo Mondlane University, Maputo, Mozambique

C. Carrilho · M. Ismail · C. Lorenzoni · F. Fernandes
Department of Anatomical Pathology, Maputo Central Hospital, Maputo, Mozambique

P. Modcoicar · L. Cunha
Department of Gastroenterology, Maputo Central Hospital, Maputo, Mozambique

B. Peleteiro · N. Lunet
Department of Hygiene and Epidemiology, Medical Faculty, University of Porto, Porto, Portugal

B. Peleteiro · N. Lunet
Institute of Public Health (ISPUP), University of Porto, Porto, Portugal

R. Almeida · C. Figueiredo · L. David
Institute of Molecular Pathology and Immunology (IPATIMUP), University of Porto, Porto, Portugal

R. Almeida · C. Figueiredo · L. David
Department of Pathology, Medical Faculty, University of Porto, Porto, Portugal

C. Carrilho (✉)
Serviço de Anatomia Patologica, Hospital Central de Maputo, P. O. Box 1164, Maputo, Mozambique
e-mail: carrilhocarla@hotmail.com

quality data on cancer incidence and mortality for most African countries and has been labeled as a myth [4].

H. pylori has also been implicated in the development of other gastric diseases such as chronic gastritis, peptic ulcer, and gastric MALT lymphoma [5–7]. The diversity of clinicopathological presentation of *Helicobacter*-associated diseases is related to the interaction of many factors, namely host genetic susceptibility [8], bacterial virulence [9], and environmental factors, mainly smoking [10] and diet [11–13]. Ecological [2, 14] and individual level [15] studies support the hypothesis of a synergistic effect of *H. pylori* and smoking, suggesting that the low cigarette consumption found in most countries in Africa contributes to the low gastric cancer frequency in the region, despite the high prevalence of infection. Similar evidence has been produced for precancerous lesions [16, 17], but data from African countries are scarce.

Several studies regarding histopathological changes of gastric mucosa and *H. pylori* infection have been published in Africa [18–21]. However, the publication of these investigations spanned over many years and relied in different methods and criteria for classification of gastric lesions. Moreover, caution is required when comparing results from independent studies conducted in different parts of the world due to less than optimal inter-observer agreement [22]. Robust data from the African setting, particularly in sub-Saharan Africa, may contribute to clarify the role of *H. pylori* in the web of gastric cancer causation, from gastritis to cancer, and to understand the so-called African enigma.

Data from Mozambique are practically inexistent. The first estimates of cancer frequency, based on a cancer survey conducted in Lourenço Marques (now Maputo) more than three decades ago [23], showed a low gastric cancer incidence (0.9/100,000 inhabitants in women and 1.1/100,000 inhabitants in men). The only population-based cancer registry in the country was recently set up in Beira city, in the center of the country, but no gastric cancer cases were observed among the 377 cases of cancer registered in 2006 (Ferro et al., unpublished data). Among 4,934 cancer cases diagnosed at Maputo Central Hospital between 1992 and 1999, 18 were gastric cancers, representing 0.4% of all malignancies registered (Ferro et al., unpublished data). Maputo Central Hospital is the only hospital in the south of the country that has anatomical pathology facilities. All gastric endoscopies in the south of the country are done in three places: Maputo Central Hospital (approximately 95% of all endoscopies) and in other two private clinics. All samples are sent to the Department of Pathology of Maputo Central Hospital.

Regarding *H. pylori* infection, a previous study on *H. pylori* in dyspeptic patients at Maputo Central Hospital with a very small series (n=69 dyspeptic patients) showed the presence of this bacteria, in histological sections, in 61% of the cases (Prassad et al., unpublished data).

The aim of this study is to estimate the prevalence of chronic gastritis, atrophy, and intestinal metaplasia among dyspeptic patients from Maputo Central Hospital using the Modified Sydney system and to evaluate the relationship between different histopathological features of chronic gastritis and *H. pylori* infection.

Materials and methods

Study area

This prospective descriptive study was conducted at the Maputo Central Hospital (MCH) between August 2005 and May 2006. The MCH is a public hospital with tertiary level care, which serves as the referral center for other hospitals in Southern Mozambique.

Study population and evaluation of participants

Among the patients observed in the Outpatient Department of Gastroenterology at MCH, those having dyspeptic symptoms and clinical criteria for upper digestive endoscopy were consecutively invited for this study. The present series includes 109 patients (median age, 37 years; percentile 25–percentile 75, 28–46 years; 67.9% female; 93.5% black). The protocol included the collection of four biopsy specimens—one from the greater curvature of the antrum, two from the incisura angularis, and one from the anterior wall of the corpus—for the histopathological study in the Department of Pathology at the MCH. From the 109 patients involved in the study, only the biopsies with adequate size were considered for histopathological study, which corresponded to 107 samples collected from the incisura angularis, 106 from the antrum, and 67 from the corpus. The lower number of biopsies from the corpus is due to a high frequency of erroneous labeling as corpus of samples collected from antrum or incisura.

Histopathological study

Biopsy specimens were fixed in 10% formalin, embedded in paraffin, and cut into 4-μm sections. Hematoxylin–eosin and modified Giemsa-stained sections were used to classify the lesions and to identify the presence/absence of *H. pylori*, respectively. Alcian blue/PAS stain was performed to demonstrate intestinal metaplasia.

Histological evaluation was performed according to the Modified Sydney system [24] by two experienced pathologists (CC and LD) using a semi-quantitative scoring (0 = absent; 1 = mild; 2 = moderate; 3 = marked) for chronic inflammation, polimorphonuclear neutrophil activity, glandular atrophy, and density of *H. pylori*. Moreover, we also

evaluated surface epithelial damage, lymphoid follicles, and intestinal metaplasia as present or absent. Intestinal metaplasia was classified as complete or incomplete, using mucin (MUC1, MUC2, and MUC5AC) immunohistochemistry as previously described [25]. Complete intestinal metaplasia was defined by expression of MUC2 (intestinal mucin) and absence of expression of MUC1 and MUC5AC (gastric mucins), and incomplete intestinal metaplasia was characterized by co-expression of MUC2, MUC1, and MUC5AC [25]. Dysplasia and gastric cancer was also recorded if present.

The global histopathological diagnosis was characterized as: normal mucosa, chronic gastritis, gastric dysplasia, and gastric cancer. In the gastritis group, we considered antral gastritis, gastritis of antrum and incisura, gastritis of corpus, pangastritis, pangastritis predominantly from the antrum, and pangastritis predominantly from the corpus.

Assessment of *H. pylori* infection by polymerase chain reaction (PCR)

Total DNA was extracted from antral biopsy specimens after digestion with Proteinase K for at least 12 h at 55°C. Proteinase K was inactivated by incubation at 95°C for 10 min. Ten microliters of the lysate was used for PCR for detection of *H. pylori* with primers previously described [26], amplifying the s and m regions of the *vacA* gene. Amplified products were visualized after electrophoresis in 2% agarose gels.

Statistical analysis

Statistical analysis was performed using the Chi-square test with Yates correction or the Fisher's exact test, as appropriate. A significance level of 5% was used in all analyses.

Ethics

The study protocol was approved by the National Mozambican Ethics Committee, and written informed consent was obtained from all participants.

Results

H. pylori colonization and histopathological diagnosis

H. pylori was identified in 68 out of 109 cases (62.4%) based on histological assessment and in 100 out of 108 cases (92.6%) when assessed by PCR. PCR was not performed in one *H. pylori*-positive case by histology due to insufficient material remaining in the paraffin block. In three cases, *H. pylori* was positive by histology and negative by PCR. Infection was considered present when the results where positive for at least one of the two detection methods. The overall prevalence of infection was 94.5%. Ten cases had normal mucosa. Chronic gastritis, irrespective of topography, was the most frequent diagnosis, accounting for 99 cases (90.8%). Pangastritis was observed in 54 cases (Table 1). One case (0.9%) with chronic gastritis had a concomitant gastric adenocarcinoma.

Histopathological scoring of lesions and of *H. pylori* colonization

The results from the histopathological scoring of the lesions are shown in Table 2 and Fig. 1. Chronic inflammation, presence of lymphoid follicles, and neutrophilic activity were more frequent in the antrum and incisura than in the corpus. Chronic inflammation in the antrum and incisura was more frequently moderate to abundant, whereas in the corpus, a mild infiltrate was predominant. Neutrophilic activity was mostly in the mild/moderate range in all gastric locations. Glandular atrophy was accessed in 81 samples of the antrum, 97 of incisura angularis, and in 67 of corpus.

Glandular atrophy was identified in two cases (2.5%), six cases (6.2%), and one case (1.5%), respectively, in the antrum, incisura angularis, and corpus, all with intestinal metaplasia. Intestinal metaplasia was detected in nine cases, six of the complete and three of the incomplete type (Fig. 2). From those nine cases, two had intestinal metaplasia in more than one location, namely in antrum and incisura angularis, totalizing 11 samples and corresponding to 3.8% of the samples (four of 106) in antrum and 6.5% (seven of 107) in incisura angularis. Samples from the cases with two intestinal metaplasia foci in different locations had the same sub-type of intestinal metaplasia in the two foci (one of the complete and one of the incomplete types).

To compute an overall prevalence estimate, both glandular atrophy and intestinal metaplasia were considered to be present if there was detection in any of the biopsy specimens (antrum, corpus, or incisura), even if participants had only biopsies from one location, resulting in a prevalence of 8.3% for atrophy and 8.3% for intestinal metaplasia, though not in overlaping cases: Six cases had

Table 1 Histopathological diagnosis in gastric biopsies ($n=109$)

Histology	No. of cases	Percentage
Normal mucosa	10	9.2
Pangastritis, NOS	45	41.3
Pangastritis, antral predominant	9	8.3
Chronic gastritis of antrum and incisura angularis	43	39.4
Antral chronic gastritis	2	1.8
Total	109	100

NOS Not otherwise specified

Table 2 Histopathological scoring of lesions in the antrum (n=106), incisura angularis (n=107), and corpus (n=67) according to the modified Sydney system and scoring of *H. pylori* colonization detected by histology

	Antrum[a], *n* (%)	Incisura angularis[a], *n* (%)	Corpus[a], *n* (%)
Chronic inflammation score			
0 (absent)	6 (5.6)	8 (7.5)	10 (14.9)
1 (mild)	43 (40.6)	33 (30.8)	41 (61.2)
2 (moderate)	46 (43.4)	51 (47.7)	14 (20.9)
3 (marked)	11 (10.4)	15 (14.0)	2 (3.0)
Lymphoid follicles			
Absent	57 (53.8)	46 (43.0)	49 (73.1)
Present	49 (46.2)	61 (57.0)	18 (26.9)
Neutrophil activity score			
0 (absent)	49 (46.2)	49 (45.8)	46 (68.7)
1 (mild)	22 (20.8)	32 (29.9)	12 (17.9)
2 (moderate)	27 (25.5)	17 (15.9)	8 (11.9)
3 (marked)	8 (7.5)	9 (8.4)	1 (1.5)
Glandular atrophy score[b]			
0 (absent)	79 (97.5)	91 (93.8)	66 (98.5)
1 (mild)	2 (2.5)	3 (3.1)	0 (0.0)
2 (moderate)	0 (0.0)	2 (2.1)	1 (1.5)
3 (marked)	0 (0.0)	1 (1.0)	0 (0.0)
Intestinal metaplasia			
Absent	102 (96.2)	100 (93.5)	67 (100.0)
Present	4 (3.8)	7 (6.5)	0 (0.0)
H. pylori presence/density score			
0 (absent)	43 (40.6)	45 (42.0)	28 (41.8)
1 (mild)	15 (14.1)	20 (18.7)	19 (28.4)
2 (moderate)	27 (25.5)	20 (18.7)	15 (22.4)
3 (marked)	21 (19.8)	22 (20.6)	5 (7.4)

[a] From the 109 participants, there were no biopsy samples available from the antrum, incisura angularis, and corpus, respectively, for three, two, and 42 subjects

[b] From the 109 participants, the available biopsies did not allow a reliable evaluation of atrophy in the samples from the antrum and incisura angularis, respectively, for 25 and ten subjects

intestinal metaplasia without atrophy, and six cases had atrophy without intestinal metaplasia.

The frequency of *H. pylori* colonization was similar in all gastric locations, with a lower frequency of marked colonization in the corpus than in the antrum and incisura.

Relationship between *H. pylori* colonization and chronic inflammation, presence of lymphoid follicles, and neutrophilic activity

The presence of *H. pylori* was significantly more frequent when chronic inflammatory infiltrate and neutrophilic activity were observed, regardless of the anatomic localization. A similar association was observed for the presence of lymphoid follicles, but significant differences were observed only in the incisura angularis (Table 3).

Relationship between *H. pylori* density and degenerative surface epithelial damage

The presence of degenerative surface epithelial damage was significantly associated with higher density of *H. pylori*, both in antrum, incisura angularis, and corpus (Table 4).

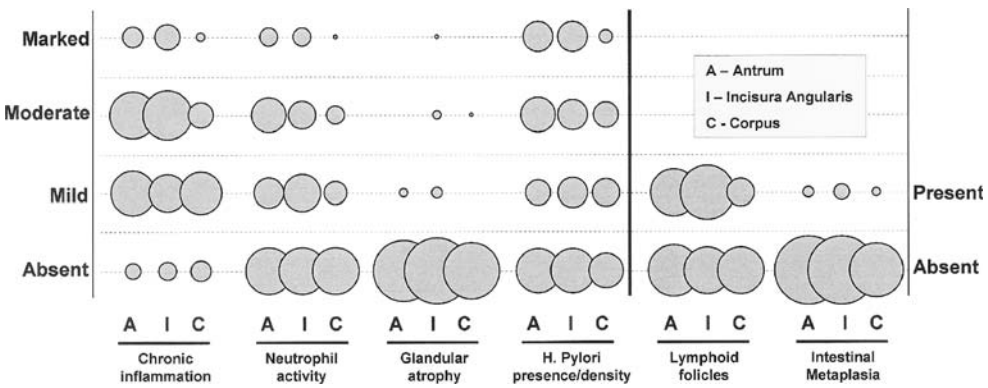

Fig. 1 Plot representing the number of cases—size of the circles—according to the scoring of gastric lesions and *H. pylori* presence/density in the different gastric locations

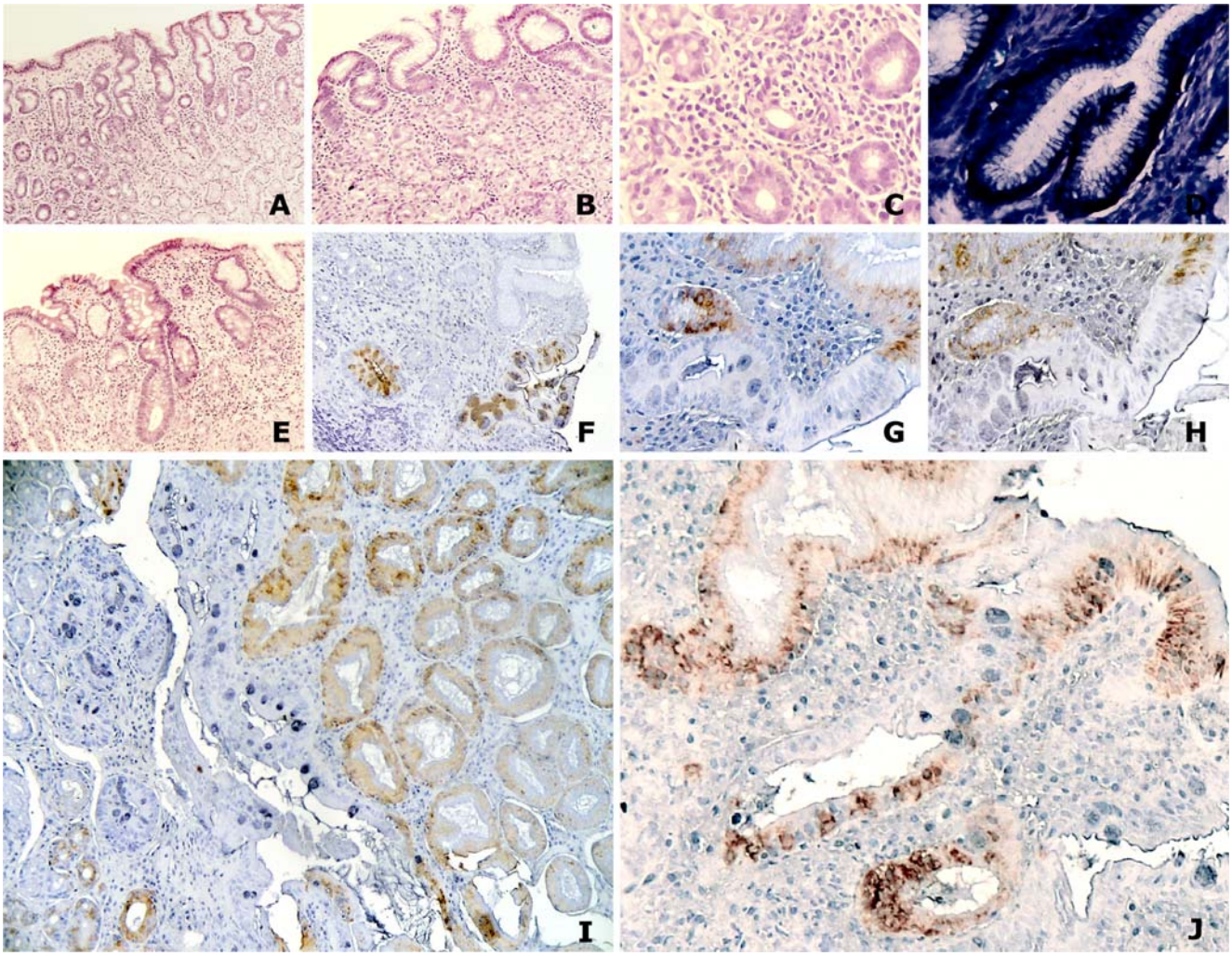

Fig. 2 Lesions of chronic atrophic gastritis and intestinal metaplasia (IM). H&E-stained sections from a case with pangastritis in the antrum (**a**), corpus (**b**), and incisura (**c**); in the incisura, neutrophilic activity was identified. In the same case, Giemsa-stained sections showed numerous *H. pylori* (**d**). Complete IM (H&E—**e**), expressing MUC2 (PMH1—**f**) and without expression of MUC5AC (CLH2—**g**) or MUC1 (HMFG2—**h**); adjacent non-metaplastic mucosa expressing MUC5AC (**g**) and MUC1 (**h**). MUC5AC very clearly separates complete IM, without expression in the metaplastic foci (**i**), and incomplete IM, with MUC5AC expression in the metaplastic foci (**j**)

Table 3 Relationship between *H. pylori* detected by histology and inflammatory indicators in the different gastric localizations

	Antrum (n=106)			Incisura angularis (n=107)			Corpus (n=67)		
	H. pylori, *n* (%)			*H. pylori*, *n* (%)			*H. pylori*, *n* (%)		
	Absent	Present	*p*	Absent	Present	*p*	Absent	Present	*p*
Chronic inflammation[a]									
Absent	5 (83.3)	1 (16.6)	0.013	8 (100.0)	0 (0.0)	<0.001	10 (100.0)	0 (0.0)	<0.001
Present	33 (33.0)	67 (67.0)		32 (32.3)	67 (67.7)		16 (28.1)	41 (71.9)	
Lymphoid follicles[a]									
Absent	25 (43.9)	32 (56.1)	0.064	30 (65.2)	16 (34.8)	<0.001	21 (42.9)	28 (57.1)	0.262
Present	13 (29.5)	36 (73.5)		10 (16.4)	51 (83.6)		5 (27.8)	13 (72.2)	
Neutrophilic activity[a]									
Absent	33 (67.4)	16 (32.6)	<0.001	34 (69.4)	15 (30.6)	<0.001	24 (52.2)	22 (47.8)	0.001
Present	5 (8.8)	52 (91.2)		6 (10.3)	52 (89.7)		2 (9.5)	19 (90.5)	

[a] The histopathological parameters were classified as absent (grade 0) or present (grades 1–3), according to the modified Sydney system

Table 4 Relationship between density of *H. pylori* detected by histology and presence or absence of degenerative surface epithelial damage in antrum and incisura angularis

	Antrum (n=106)				Incisura angularis (n=107)				Corpus (n=67)			
	H. pylori presence/density—n (%)				*H. pylori* presence/density—n (%)				*H. pylori* presence/density—n (%)			
Degenerative surface epithelial damage	0 (absent)	1 (mild)	2 (moderate)	3 (marked)	p	0 (absent)	1 (mild)	2 (moderate)	3 (marked)	p	0 (absent)	1 (mild)	2 (moderate)	3 (marked)	p
Absent	43 (48.9)	15 (17.0)	22 (25.0)	8 (9.1)	<0.001	44 (47.3)	19 (20.4)	18 (19.4)	12 (12.9)	<0.001	28 (44.4)	19 (30.2)	14 (22.2)	2 (3.2)	<0.001
Present	0 (0.0)	0 (0.0)	5 (27.8)	13 (72.2)		1 (7.1)	1 (7.1)	2 (14.3)	10 (71.4)		0 (0.0)	0 (0.0)	1 (25.0)	3 (75.0)	

Relationship between *H. pylori* infection and glandular atrophy and intestinal metaplasia

No statistically significant differences were observed for the presence of intestinal metaplasia and glandular atrophy according to *H. pylori* colonization. *H. pylori* infection (histologically assessed) was present in 50.0% of the cases with intestinal metaplasia or glandular atrophy and in 64.1% of the subjects without any of these lesions (p= 0.282). *H. pylori* infection (assessed by PCR) was present in 87.5% of the cases with intestinal metaplasia or glandular atrophy and in 93.4% of the subjects without any of these lesions (p=0.407), but all the subjects with intestinal metaplasia were infected.

Discussion

This study was conducted in dyspeptic patients attending the outpatient clinic of the Gastroenterology Department of the MCH, which performs 95% of the endoscopies performed in the south of the country. In this Mozambican population, 8.3% of the patients had chronic atrophic gastritis, and 8.3% had intestinal metaplasia, despite the high prevalence of *H. pylori* infection (94.5%) and chronic gastritis (90.8%).

The prevalence of *H. pylori*, reported in studies conducted in dyspeptic patients from different African populations, was approximately 72%, in a review by Kidd et al. [18], varying from 25% in Uganda and 97% in Ghana. More recent reports also show a wide range of infection rates, with a seroprevalence of anti-*H. pylori* IgG antibodies of 85.6% in 215 dyspeptic individuals from Ethiopia [27] and an unexpectedly low prevalence—17.5%—in pregnant women from Zanzibar [28, 29]. In our series, the prevalence of *H. pylori* infection was in the upper range of previous reports, and, noteworthy, the proportion of infected subjects changed from 65% to nearly 100% when PCR was used for assessment of infection status. Also, in most infected subjects, the density of colonization was mild or moderate, as defined by histological evaluation. These results contribute to explain the heterogeneity in prevalence estimates across African countries, for which a high prevalence of infection is expected given the strong association between infection and low socioeconomic status.

Detection of *H. pylori* was higher by PCR than by histology, which indicates low sensitivity of histology for *H. pylori* detection in routine sections, mostly in cases with low scores for *H. pylori*. On the other hand, three cases of our series were *H. pylori* positive by histology and negative by PCR. All these three cases had very few identifiable bacteria in the sections, and possibly, the serial sections

used for DNA extraction did not have *H. pylori*. Taken together, our data reinforce the usefulness of using more than one methodology for *H. pylori* detection. The low level of histological detection in this population may be due to the frequent use of antibiotics, as documented in a survey conducted in Mozambican university students [30] and may contribute to the presence of very low numbers of bacteria, which for that reason escape detection under microscopic screening and also by PCR. Another possible explanation could be a high socioeconomic status of the subjects from this series. However, this does not seem to be the case, as a large proportion of subjects (20.6%) had less than 5 years education, and 53.7% had no electricity or running water at home. Furthermore, gastric atrophy and intestinal metaplasia lead to a pH increase in the stomach, which can create an unfavorable environment for *H. pylori* survival, thus contributing to lower prevalence of the bacteria in these settings [20]. However, in our study, approximately 14% of the patients had chronic atrophic gastritis or intestinal metaplasia, and therefore, it could not be the main reason for the low prevalence of infection, detected by histology. Regarding the frequency of precancerous lesions, our results are in accordance with the observations in other African populations [18, 19, 21, 31].

Chronic inflammatory infiltrate, presence of lymphoid follicles, neutrophilic activity, presence and high density of *H. pylori* colonization, atrophy, and intestinal metaplasia were more frequently observed in the antrum and incisura. These observations are in agreement with the profile of *H. pylori*-associated gastritis in other countries [18, 21, 31]. The same holds true for the association we observed between the density of *H. pylori* colonization and the presence of degenerative alterations in the surface epithelium [32–34].

Pangastritis was the most frequent diagnosis in our series, corresponding to 49.6% of the cases. The relatively low percentage of pangastritis can be partly attributed to the small number of corpus samples available for histopathology analysis. Isolated corpus gastritis was not identified in our series of 67 cases with samples from the corpus.

Noteworthy, the frequency of pangastritis (49.6%) as well as the high frequency of detection of *H. pylori* in the corpus (58.2%) follows the profile described for countries with a high rate of *H. pylori* infection, that usually also have a high frequency of atrophy, intestinal metaplasia, and carcinoma [6]. What is exceptional in our series, in the aforementioned context of a high rate of *H. pylori* infection and gastritis (including pangastritis), is the low frequency of atrophy and intestinal metaplasia. Looking at the profile of infection and of associated gastric lesions, we are tempted to assume that there is, in Mozambique, an interruption of the natural history of gastric carcinogenesis that does not proceed from inflammatory lesions to atrophy and intestinal metaplasia. Regarding this issue, concomitant intestinal infection with helmints, which is virtually always present from early life in Mozambique, can contribute for low prevalence of atrophic gastritis. Helmintic infection has been suggested to reduce gastric *H. pylori*-associated atrophy by down-regulation of host immunologic response [35], although such infections tend to be also frequent in South American countries with high prevalence of infection.

The lack of a significant association between atrophy and intestinal metaplasia and *H. pylori* infection observed in our study reflects the high prevalence of infection and probably the lack of exposure to factors that may modulate the progression to the severest lesions. Furthermore, we also identified cases with intestinal metaplasia and no atrophy, corresponding to focal metaplastic change in the foveolar epithelium, not involving the glands, suggesting the presence of minor lesions with low potential for progression.

Data from the literature indirectly supports the aforementioned hypothesis. In fact, a review of African studies [18] shows that atrophic gastritis was observed in 28%, whereas intestinal metaplasia was identified in only 14% of the patients, with *H. pylori* infection present in 78% of them in both cases. The authors of this review recognize that neither gastritis nor intestinal metaplasia were adequately graded in the studies reviewed but it would indicate, in this case and if atrophy was correctly evaluated, a lack of progression to intestinal metaplasia, as we observed. More recently, a study [19] in Gambian adults and children found that gastric atrophy and intestinal metaplasia were uncommon in this population—each was observed respectively, in two and four of 45 adults; furthermore, intestinal metaplasia was observed in 18.6% of 102 infected subjects in the Ivory Coast [36].

In a follow-up endoscopic series of 51 *H. pylori*-positive patients in Kenya [37], 61% had atrophic gastritis, and 24% had both atrophic gastritis and intestinal metaplasia, following the profile identified in high-risk populations of Western, South American world and Japan. After a 1-year follow-up, the progression from moderate to severe atrophy was 1.8% (95%CI, −0.9% to 4.4%), suggesting that progression of *H. pylori* gastritis in this African setting is similar to what is observed in other parts of the world, with environmental and genetic factors being important in the progression of *H. pylori*-initiated gastritis to more serious outcomes [38].

In conclusion, our results are similar to the ones obtained in countries with high prevalence of *H. pylori* and low rates of gastric cancer: high frequency of chronic gastritis, antral predominant, with very low prevalence of gastric atrophy, and intestinal metaplasia. Further studies are needed to identify determinants of gastric precancerous lesions, such as genetic host factors or environmental factors that could

contribute to the interruption of progression or even lead to regression of intestinal metaplasia in chronic *H. pylori*-associated gastritis in African settings.

Acknowledgments We thank Prof. Fátima Carneiro for many helpful suggestions and for reviewing slides from cases that raised discrepant observations between the two observers (CC and LD), Jorge Thembo for helping in the technical part of the study, and Nuno Mendes for expert technical support. This work was supported by the Fundação Calouste Gulbenkian (project no. FC-54918).

Conflict of interest statement We declare that we have no conflict of interest.

References

1. Parkin DM (2006) The global health burden of infection-associated cancers in the year 2002. Int J Cancer 118:3030–3044
2. Lunet N, Barros H (2003) *Helicobacter pylori* infection and gastric cancer: facing the enigmas. Int J Cancer 106:953–960
3. Holcombe C (1992) *Helicobacter pylori*: the African enigma. Gut 33:429–431
4. Agha A, Graham DY (2005) Evidence-based examination of the African enigma in relation to *Helicobacter pylori* infection. Scand J Gastroenterol 40:523–529
5. Wyatt JI (1995) Histopathology of gastroduodenal inflammation: the impact of *H. pylori*. Histopathology 26:1–15
6. Correa P (1996) *Helicobacter pylori* and gastric cancer. Cancer Epidemiol Biomarkers Prev 5:477–481
7. Blaser MJ (1997) Ecology of *Helicobacter pylori*. Clin Microbiol Rev 100:720–741
8. Kamangar F, Cheng C, Abnet CC et al (2006) Inlerleukin-1B polymorphisms and gastric cancer risk—a meta-analysis. Cancer Epidemiol Biomarkers Prev 15:1920–1928
9. Atherton JC (1998) *Helicobacter pylori* virulence factors. Br Med Bull 54:105–120
10. Ladeiras-Lopes R, Pereira AK, Nogueira A et al (2008) Smoking and gastric cancer: a systematic review and meta-analysis of cohort studies. Cancer Causes Control 19:689–701
11. Tsugane S, Sasazuki S (2007) Diet and the risk of gastric cancer: review of epidemiological evidence. Gastric Cancer 10:75–83
12. Lunet N, Lacerda-Vieira A, Barros H (2005) Fruit and vegetables consumption and gastric cancer: a systematic review and meta-analysis of cohort studies. Nutr Cancer 53:1–10
13. Lunet N, Valbuena C, Vieira AL et al (2007) Fruit and vegetables consumption and gastric cancer by location and histological type: case–control and meta-analysis. Eur J Cancer Prev 16:312–327
14. Lunet N, Barros H (2004) *Helicobacter pylori* infection and gastric cancer: facing the enigmas (part II). Int J Cancer 112:168–169
15. Brenner H, Arndt V, Bode G et al (2002) Risk of gastric cancer among smokers infected with *Helicobacter pylori*. Int J Cancer 98:446–449
16. Peleteiro B, Lunet N, Figueiredo C et al (2007) Smoking, *Helicobacter pylori* virulence, and type of intestinal metaplasia in Portuguese males. Cancer Epidemiol Biomarkers Prev 16:322–326
17. Peleteiro B, Bastos J, Barros H et al (2008) Systematic review of gastric intestinal metaplasia prevalence and its area level association with smoking. Gac Sanit 22:236–247
18. Kidd M, Louw JA, Marks IN (1999) *Helicobacter pylori* in Africa: observations on an "enigma within an enigma". J Gastroenterol Hepatol 14:851–858
19. Campbell DI, Warren BF, Thomas JE et al (2001) The African enigma: low prevalence of gastric atrophy, high prevalence of chronic inflammation in West African adults and children. Helicobacter 6:263–267
20. Wabinga H (2005) *Helicobacter pylori* and histopathological changes of gastric mucosa in Uganda population with varying prevalence of stomach cancer. Afr Health Sci 5:234–237
21. Kalebi A, Rana F, Mwanda W et al (2007) Histopathological profile of gastritis in adult patients seen at a referral hospital in Kenya. World J Gastroenterol 13:4117–4121
22. Chen XY, van der Hulst RW, Bruno MJ et al (1999) Interobserver variation in the histopathological scoring of *Helicobacter pylori* related gastritis. J Clin Pathol 52:612–615
23. Prates MD, Torres FO (1965) A cancer survey in Lourenço Marques. J Natl Cancer Inst 35:729–757
24. Dixon MF, Genta RM, Yardley JH et al (1996) Classification and grading of gastritis. The updated Sydney system. Am J Surg Pathol 20:1161–1181
25. Reis CA, David L, Correa P et al (1999) Intestinal Metaplasia of human stomach displays distinct patterns of mucins (MUC1, MUC2, MUC5AC, and MUC6) expression. Cancer Res 59:1003–1007
26. van Doorn LJ, Figueiredo C, Sanna R et al (1998) Expanding allelic diversity of *Helicobacter pylori vacA*. J Clin Microbiol 36:2597–2603
27. Mogges F, Kassu A, Mengistu G et al (2006) Seroprevalence of Helicobacter pylori in dyspeptic patients and its relationship with HIV infection, ABO blood groups and life style in a university hospital Northwest Ethiopia. World J Gastroenterol 12:1957–1961
28. Farag TH, Stolzfus RY, Khalfan SS et al (2007) Unexpectedly low prevalence of Helicobacter pylori infection among pregnant women on Pemba Island, Zanzibar. Trans R Soc Trop Med Hyg 101:915–922
29. Graham DY, Yamaoka Y, Malaty HM (2007) Thoughts about populations with unexpected low prevalences of Helicobacter pylori infection. Trans R Soc Trop Med Hyg 101:849–851
30. Lucas R, Lunet N, Carvalho R et al (2007) Pattern of medication use by students in a University from Maputo, Mozambique. Cad Saude Publica 23:2845–2852
31. Oluwasola AO, Ogunbiyi JO (2004) Chronic gastritis and *Helicobacter pylori* infection in University College Hospital Ibadan, Nigeria—a study of 85 fibre optic gastric biopsies. Niger J Med 13:372–378
32. Nogueira C, Figueiredo C, Carneiro F et al (2000) Associação entre os genotipos de *Helicobacter pylori* e o desenvolvimento de gastrite cronica atrofica e metaplasia intestinal. Primeiros resultados de uma acção de rastreio. GE 7:137–146
33. Chan WY, Hui PK, Leung KM et al (1992) Modes of *Helicobacter pylori* colonisation and gastric epithelial damage. Histopathology 21:521–528
34. Carneiro F, Fonseca E, Sobrinho-Simões M (1992) Epithelial degeneration induced by *Helicobacter pylori*. Human Pathol 23:1314–1315
35. Fox JG, Beck P, Dangler CA et al (2000) Concurrent enteric helminth infection modulates inflammation and gastric immune responses and reduces helicobacter-induced gastric atrophy. Nat Med 6:536–542
36. Attia KA, N'dri Yoman T, Diomande MI et al (2001) Clinical, endoscopic and histologic aspects of chronic *Helicobacter pylori* gastritis in Cote d'Ivoire: study of 102 patients. Bull Soc Pathol Exot 94:5–7
37. McFarlane GA, Wyatt J, Forman D et al (2000) Trends over time in Helicobacter pylori gastritis in Kenya. Eur J Gastroelterol Hepatol 12:617–621
38. Kuipers EJ, Meijer GA (2000) *Helicobacter pylori* in Africa. Eur J Gastroenterol Hepatol 12:601–603

Virchows Arch (2009) 454:161–179
DOI 10.1007/s00428-008-0709-3

ORIGINAL ARTICLE

Vascular lesions of bone in children, adolescents, and young adults. A clinicopathologic reappraisal and application of the ISSVA classification

Elisabeth Bruder · Antonio R. Perez-Atayde · Gernot Jundt · Ahmad I. Alomari · Johannes Rischewski · Steven J. Fishman · John B. Mulliken · Harry P. W. Kozakewich

Received: 11 February 2008 / Revised: 10 November 2008 / Accepted: 19 November 2008 / Published online: 24 December 2008

Abstract Vascular lesions of bone are rare and their terminology is not standardized. Herein, we report 77 patients with such lesions in order to characterize their morphologic spectrum and the applicability of the International Society for the Study of Vascular Anomalies (ISSVA) classification. In this system, malformations are structural anomalies distinguishable from tumors, which are proliferative. The radiologic images/reports and pathologic materials from all patients were reviewed. All lesions were either restricted to bone or had minimal contiguous soft tissue involvement with the exception of some multifocal lymphatic lesions that extensively affected soft tissue and/or viscera. We found that certain lesions of bone often regarded as tumors should be classified as malformations. Malformations (n=46) were more common than tumors (n=31); lymphatic and venous malformations were equally frequent. In the tumor category, hemangioendothelioma and epithelioid hemangioma were the most common. We also describe new vascular entities that arise in or involve bone. Utilizing the ISSVA approach, the diverse and often contradictory terminology of vascular lesions of bone can be largely eliminated. Standardized nomenclature is critical for scientific communication and patient management, and we hereby recommend the ISSVA classification be applied to vascular lesions of bone, just as for skin, soft tissue, and viscera.

E. Bruder · G. Jundt
Institute for Pathology, University Hospital Basel,
Basel, Switzerland

E. Bruder
Institute of Surgical Pathology, Paediatric Pathology Section,
University Hospital Zurich, Zurich University,
Zurich, Switzerland

G. Jundt
Bone Tumor Reference Center University Hospital Basel,
Basel, Switzerland

J. Rischewski
Department of Oncology, Children's University Hospital Basel,
Basel, Switzerland

A. R. Perez-Atayde · H. P. W. Kozakewich (✉)
Department of Pathology, Children's Hospital Boston,
Harvard Medical School,
300 Longwood Avenue,
Boston, MA 02115, USA
e-mail: harry.kozakewich@childrens.harvard.edu

A. I. Alomari
Department of Radiology,
Children's Hospital Boston,
Harvard Medical School,
Boston, MA 02115, USA

S. J. Fishman
Department of Surgery,
Children's Hospital Boston,
Harvard Medical School,
Boston, MA 02115, USA

J. B. Mulliken
Department of Plastic Surgery,
Children's Hospital Boston,
Harvard Medical School,
Boston, MA 02115, USA

A. I. Alomari · S. J. Fishman · J. B. Mulliken ·
H. P. W. Kozakewich
Vascular Anomalies Center, Children's Hospital Boston
and Harvard Medical School,
Boston, MA 02115, USA

Keywords Bone · Vascular malformation · Vascular tumor · Hemangioma · Lymphatic · Pathology · Pediatric · Kaposiform · Hemangioendothelioma · Lymphangiomatosis

Introduction

Primary vascular lesions of bone are rare in surgical pathology [1, 2]. Their uncommon occurrence is exemplified by the Mayo Clinic experience with 11,087 bony lesions of which only 201 (1.8%) were vascular and, of these, only 32 (14.5%) occurred during the first two decades of life [3]. However, the most common vascular lesion of bone, the vertebral "hemangioma," was incidentally found in 10.7% of individuals in a careful study of the spine at autopsy [4]. The histopathology of vascular lesions of bone in young individuals has not been as thoroughly described and categorized as it has been in adults.

Vascular lesions, in general, have been notoriously difficult for pathologists to diagnose and classify because of the large number of entities and their variants, the frequently overlapping clinical and histopathologic features, and, until recently, the lack of markers distinguishing blood vascular from lymphatic endothelium. This problem has been compounded by imprecise terminology with various names referring to the same lesion or, conversely, a particular term denoting different entities. For example, "hemangioma" has often been used in a generic and indiscriminate manner resulting in the inclusion of lesions with different biology under one rubric. In this regard, we have encountered patients with malformative lesions that had been previously diagnosed at other institutions as "hemangioma" or "lymphangioma" or some other designations ending in "oma" and regarded as being neoplastic lesions, and therefore treated inappropriately with anti-angiogenic agents, sometimes resulting in morbidity and rarely fatality. Our experience is that precise terminology of vascular lesions is essential for their proper treatment.

For these reasons, the International Society for the Study of Vascular Anomalies (ISSVA), an organization comprised of specialists in various disciplines interested in vascular anomalies, approved a classification of vascular lesions that distinguishes malformations from tumors and provides an easily understood and concise nomenclature [5]. This classification has proven invaluable in improving scientific communication and the management of patients with vascular anomalies involving skin, soft tissue, viscera, and bone. The ISSVA nomenclature has not been widely applied to the categorization of osseous vascular lesions. A brief introduction to this concept was recently published by us in the German literature [6].

We present, herein, our experience with osseous vascular lesions applying the ISSVA classification, from two institutions—the Bone Tumor Reference Center at the University Hospital in Basel, Switzerland, serving as a registry for osseous tumors in Switzerland and major parts of Germany and Austria, and the Vascular Anomalies Center and Department of Pathology at Children's Hospital Boston that regularly evaluates a large number of patients with vascular lesions, particularly those that are difficult to diagnose or manage. This work is primarily a histopathological study of vascular lesions of bone and the application of the ISSVA classification system. Treatment and follow-up are beyond the scope of this study. The natural history of the classical entities we describe is well documented in the literature.

Materials and methods

All vascular lesions of bone were retrieved from the files of the Basel Bone Tumor Reference Center (from 1978 to 2007) and the Department of Pathology at Children's Hospital Boston (from 1975 to 2006) that included patients evaluated at its Vascular Anomalies Center. The lesions selected for the study were either restricted to bone or had minimal contiguous soft tissue involvement, with the exception of some multifocal lymphatic malformations (LMs) and kaposiform lymphangiomatosis that also extensively affected soft tissue and/or viscera. All patients had biopsy or resection of the osseous lesion except for four with multifocal lymphatic and one with arteriovenous malformation (AVM) who had only the soft tissue component biopsied.

This study includes only patients 25 years or younger since termination of skeletal maturation with closure of all epiphyseal growth plates and apophyses occurs by this age [7, 8]. Patients with predominantly soft tissue lesions and only minor cortical bony involvement, such as those that can occur with venous or lymphatic malformations, kaposiform hemangioendothelioma, Klippel-Trenaunay syndrome, and PTEN-associated vascular anomaly were excluded from the study.

A total of 77 patients (44 from Children's Hospital Boston and 33 from the Basel Bone Tumor Reference Center) constitute this report. The clinical and imaging data as well as the pathological material including reports, slides, and photographs were reviewed. Immunohistochemistry was performed in 33 selected cases, largely determined by the availability of paraffin blocks. These cases included eight venous malformations, four lymphatic malformations, four epithelioid hemangiomas, seven epithelioid hemangioendotheliomas, three kaposiform hemangioendotheliomas, four kaposiform lymphangiomatoses, five angiosarcomas, and three unclassifiable tumors. Antibodies utilized were those against CD31 (DAKOCytomation, Glostrup, Denmark), CD34 (DAKOCytomation, Glostrup, Denmark), and factor-VIII-related antigen (Medite, Nunningen, Switzerland) for identifying hemovascular endothelium,

D2-40 (DAKOCytomation, Glostrup, Denmark) and LYVE-1 (Reliatech, Braunschweig, Germany) for lymphatic endothelium, smooth muscle actin (DAKOCytomation, Zug, Switzerland) and caldesmon (DAKOCytomation, Zug, Switzerland) for smooth muscle, GLUT-1 (NeoMarkers, Fremont, CA, USA) for infantile hemangioma, CD68 (DAKOCytomation, Zug, Switzerland) for histiocytes, MIB1 (DAKOCytomation, Zug, Switzerland) for cellular proliferation, and WT1 (used in seven venous malformations, two epithelioid hemangiomas, two hemangioendotheliomas, one angiosarcoma; DAKOCytomation, Zug, Switzerland) a transcription factor expressed in endothelium of hemangiomas and absent in malformations [9].

This study was approved by the Children's Hospital Boston Committee on Clinical Investigation and the Basel Ethics Committee.

Results

We used the ISSVA classification [5] (Table 1) to categorize 77 vascular lesions of bone as shown in Table 2. The age of the patients ranged from 3 months to 25 years (median 15 years, average 13.1 years). The sex ratio was nearly equal with 41 males and 36 females.

To help differentiate between malformations and tumors, the following were taken into consideration: clinical history, imaging, histopathology, and proliferative activity including immunohistochemistry applying a proliferation marker. Malformations often presented at or shortly after birth, did not usually show disproportionate expansion in relation to child's growth, and morphologically were lined by flattened endothelium without mitoses and had a negligible proliferative index.

Forty-six lesions were classified as malformations and 31 as tumors. Lymphatic and venous malformations were equally common (22 of each type). Lymphatic malformations were localized (monostotic) in nine patients and multifocal (polyostotic) in 13. Only three venous malformations were multifocal (polyostotic). In the tumor category, there were seven epithelioid hemangiomas, eight hemangioendotheliomas (seven epithelioid and one NOS), three kaposiform hemangioendotheliomas (*vide infra*), four provisionally designated as kaposiform lymphangiomatoses, five angiosarcomas, and three were unclassifiable.

Malformations

Venous malformations

VMs were most often located in craniofacial bones, followed by vertebra, appendicular skeleton, and pelvis. The radiographic features varied according to the skeletal region. The cranial lesions typically showed expansion of the bone with extensive sunburst-like new bone formation (Fig. 1). In contrast, those in the vertebral body, for example, usually showed preservation of bony contours, osteolysis, and coarse vertical striations. In the long bones, there was minor expansion and osteolysis with peripheral sclerosis.

Histopathology showed thin-walled, irregularly round or elongated, sometimes focally anastomosing channels, ranging from approximately 20 μm to 4 mm in diameter and lined by flat or occasionally slightly plump endothelium (Fig. 2). In some lesions, there was a minor small vessel component (vessel diameter around 20 μm). No atypia or mitoses were present. The stroma was loosely collagenous and usually scant, but areas with back-to-back channels were sometimes present, and some lesions had solid foci with slit-like lumens. Pericytes were present, but smooth muscle investiture was absent except in occasional large channels. The channels contained blood and occasionally organizing thrombi or were empty. Organizing thrombi with Masson papillary endothelial hyperplasia were occasionally observed. In most calvarial lesions, bone formation was prominent, in contrast to vertebral VM, where bone resorption predominated. Endothelial positivity was strong for

Table 1 Classification of vascular anomalies according to the International Society for the Study of Vascular Anomalies (ISSVA)

Vascular anomalies
Tumors
Hemangioma[a]
Infantile hemangioma
Epithelioid hemangioma
Spindle cell hemangioma
Other
Hemangioendothelioma
Hemangioendothelioma NOS
Epithelioid hemangioendothelioma
Angiosarcoma
Other tumors
Malformations
Simple
Capillary
Lymphatic
Venous
Arterial
Combined
Arteriovenous malformation
Capillary–venous malformation
Capillary–lymphatic–venous malformation
Lymphatic–venous malformation
Capillary–arteriovenous malformation
Capillary–lymphatic–arteriovenous malformation

Modified from Enjolras and Mulliken [5]

[a] "Hemangioma" refers to a benign neoplastic endothelial proliferation; the term should include an appropriate qualifier, e.g., "infantile," "spindle cell," "epithelioid"

Table 2 Classification of 77 vascular lesions of bone

Malformation	Number of patients	Age range	Sex	Sites (*n*=frequency of involvement)	Localized (L), multifocal (M)	Extraosseous involvement (skin, soft tissue, viscera)
Venous	22 *n*=4: calvaria, mandible *n*=3: maxilla *n*=2: pelvis, tibia, phalanx *n*=1: humerus, metacarpal, femur	4–24 years, mean 16.0 years	11M,11F	*n*=7: vertebra *n*=1: tongue, skin	L 15, M 6	*n*=2: cheek muscle
Lymphatic	22	3 months–24 y, mean 9.9 years	15M, 7F	*n*=9: rib, vertebra *n*=7: femur *n*=5: calvaria *n*=4: clavicle, humerus, pelvis *n*=3: sternum *n*=2: mandible, scapula, tibia *n*=1: cranial base, maxilla, radius, sacrum, fibula	L 9, M 7 Gorham 6	*n*=3: skin, chest wall, pleura, spleen *n*=2: soft tissue (periocular, mediastinum, retroperitoneum) *n*=1: soft tissue (forehead, tongue, shoulder, axilla, subclavicular, suprasternal, thoracic duct, diaphragm, mesentery, peritoneum, arm, buttock, thigh), liver, pancreas
Arteriovenous	3	2–15 years, mean 9.3 years	3F	*n*=1: maxilla, mandible, humerus, ulna, radius, carpus	2 L, 1 M	*n*=1: soft tissue upper limb
Tumor						
Epithelioid hemangioma	7	8–23 years, mean 15.7. years	3 M, 4 F	*n*=3: phalanx, tibia *n*=2: mandible, metatarsal *n*=1: cranial base, orbit, navicular, cuboid, cuneiform, tarsus (NOS)	L 3, M 4	*n*=1: soft tissue (infratemporal fossa, cheek/buccal mucosa, foot)
Hemangioendothelioma	8	7–19 years, mean 14.9 years	M 3, F 5	*n*=3: calvaria, clavicle *n*=1: vertebra, ulna, tibia, fibula *n*=1: sternum, scapula, pelvis, radius, navicular, cuneiform, metatarsal	L 4, M 5,	*n*=3: lung *n*=1: soft tissue finger, liver
Kaposiform hemangioendothelioma	3	3–15 years, mean 8.4 years	M1, F2	*n*=1: humerus, ulna, femur, tibia	L 2, M 1	*n*=1: soft tissue (thigh, upper limb)
Kaposiform lymphangiomatosis[a]	4	3–14 years, mean 8 years	M 3, F 1	*n*=3: vertebra *n*=2: pelvis *n*=1: skull, mandible, clavicle, scapula, rib, humerus, radius, ulna, carpus, femur, tibia	L 1, M 3	*n*=3: spleen *n*=2: mediastinum *n*=1: soft tissue neck, skin, thyroid, esophagus, lung, retroperitoneum
Angiosarcoma	5	3–25 years, mean 15 years	M 3, F 2	*n*=2: humerus, ulna, tibia *n*=1: mastoid, vertebra, radius, ulna, femur	L 1, M 4	*n*=1 soft tissue thigh, lung, liver
Unclassified	3	Birth–18 years, mean 9.7 years	M 2, F 1	*n*=1: maxilla, mandible, tibia	L 2, M 1	*n*=1: liver

[a] This is a designation for a proposed entity that requires further investigation to be validated.

CD34 and moderate to strong for CD31 and FVIII whereas immunoreactivity for GLUT1 or D2-40 was consistently absent. Smooth muscle actin immunoreactivity was present in pericytes and smooth muscle. Immunoreactivity for WT1 was either absent or present in rare endothelial cells. The MIB1 proliferative index was low (far less than 1%).

Lymphatic malformations

LMs affected most commonly the craniofacial bones, followed by the appendicular skeleton (Table 2). Radiographs demonstrated confluent geographic osteolysis with faint marginal sclerosis (Figs. 3 and 4). Histopathology showed elongated, anastomosing tubular, and stag-horned or grape-like thin-walled vessels, generally ranging from approximately 20 μm to 2 mm in caliber without an obvious smooth muscle coat and lined usually by flattened endothelial cells. Rarely, the lesions appeared as solitary spaces up to 2 cm in diameter. Lumina were empty or contained lacy proteinaceous material, lymphocytes, or a few macrophages, some containing hemosiderin. The lining cells expressed D2-40, but reactivity in the larger channels tended to be focal and faint. A discontinuous thin periendothelial layer of pericyte-like cells was immunoreactive for smooth muscle actin. There was no discernible endothelial labeling for MIB1.

Multifocal LMs affected one or more skeletal regions with variable involvement of individual osseous elements. The bones of the spine, thorax, and shoulder girdle were most often involved, followed by femur and pelvis (Table 2). Radiographs showed poorly circumscribed confluent osteolysis of cortical and cancellous bone with moderately coarse striations and focal minor expansion. Massive bone loss (Gorham-Stout disease) was seen in six patients with subtotal or total destruction of individual or contiguous skeletal elements. Both cortex and medulla were affected with loss of bony contours and slight sclerosis of residual cancellous bone resulting in a coarsely striated trabeculated pattern. Remaining skeletal elements showed tapering ends. Soft tissue and visceral involvement were almost always present (Table 2). Histopathology was similar to the localized form, but the lesions tended to be more permeative with smaller channels and a more prominent anastomotic pattern. Areas of massive osteolysis showed prominent osteoclast-mediated bony resorption and fibrous replacement. Endothelial cells were either negative or showed rare immunopositivity for MIB1.

Arteriovenous malformations

One arteriovenous malformation (AVM) involved the maxilla, another the mandible, and the third affected multiple bones of an upper extremity (Table 2). Radiographs showed multiple osteolytic foci with cortical thinning and disruption, minimal perilesional sclerosis, variable bone expansion, and coarse trabeculation of residual bone. Angiographically, the lesions were fast-flow with large tortuous arteries entering convoluted vascular aggregates and early venous filling. Histopathologically, AVM consisted of an assortment of variably sized arteries and veins and some vessels of indeterminate morphology separated by loose stroma (Fig. 5). Some channels showed thick muscular walls and/or intimal myofibroblastic proliferation. Focal organizing thrombi were observed. Adjacent bone showed osteoclast-mediated osteolysis and minimal sclerosis.

Tumors

Epithelioid hemangioma

The predominant site for epithelioid hemangioma was the distal lower extremity followed by the craniofacial skeleton (Table 2). Radiographs showed solitary or multifocal excentric geographic osteolysis with minimal marginal sclerosis, cortical erosion, and expansion (Fig. 6). Three lesions extended into adjacent soft tissue. Histopathology typically showed lobular architecture; solid sheets and cords were also present (Fig. 7). Small or inconspicuous lumens were lined by large epithelioid cells resulting in a cobblestoned or brick-like appearance. The cells had abundant eosinophilic to amphophilic cytoplasm with an occasional large vacuole. The nuclei were small without significant pleomorphism. Mitoses were inconspicuous and necrosis was absent. The intervening loose to moderately dense fibrous stroma contained occasional eosinophils. Basophilic cartilage-like matrix and stromal hyalinization were not observed.

Four tumors also had a spindled cell component, which comprised up to half of the tumor, and were regarded as epithelioid and spindle cell hemangioma, a variant of epithelioid hemangioma (Andrew Rosenberg, personal communication). Spindled cells were bland and monomorphous with moderately prominent nucleoli and occasional mitoses. Small foci of necrosis were accompanied by hemosiderin and neutrophils.

The surrounding medullary and cortical bone showed moderate osteoclastic resorption and minimal new bone. Immunohistochemistry revealed expression of CD31, CD34, and factor VIII in tumoral endothelium but not GLUT1, D2-40, caldesmon, or CD68. WT1 was strongly positive in lesional endothelial cells. MIB1 was positive in approximately 3% of lesional cells. Endothelial aggregates and channels were surrounded by smooth-muscle-actin-positive cells.

Hemangioendothelioma

Multiple skeletal elements and/or viscera were involved in more than half of the patients (Table 2). Radiographically,

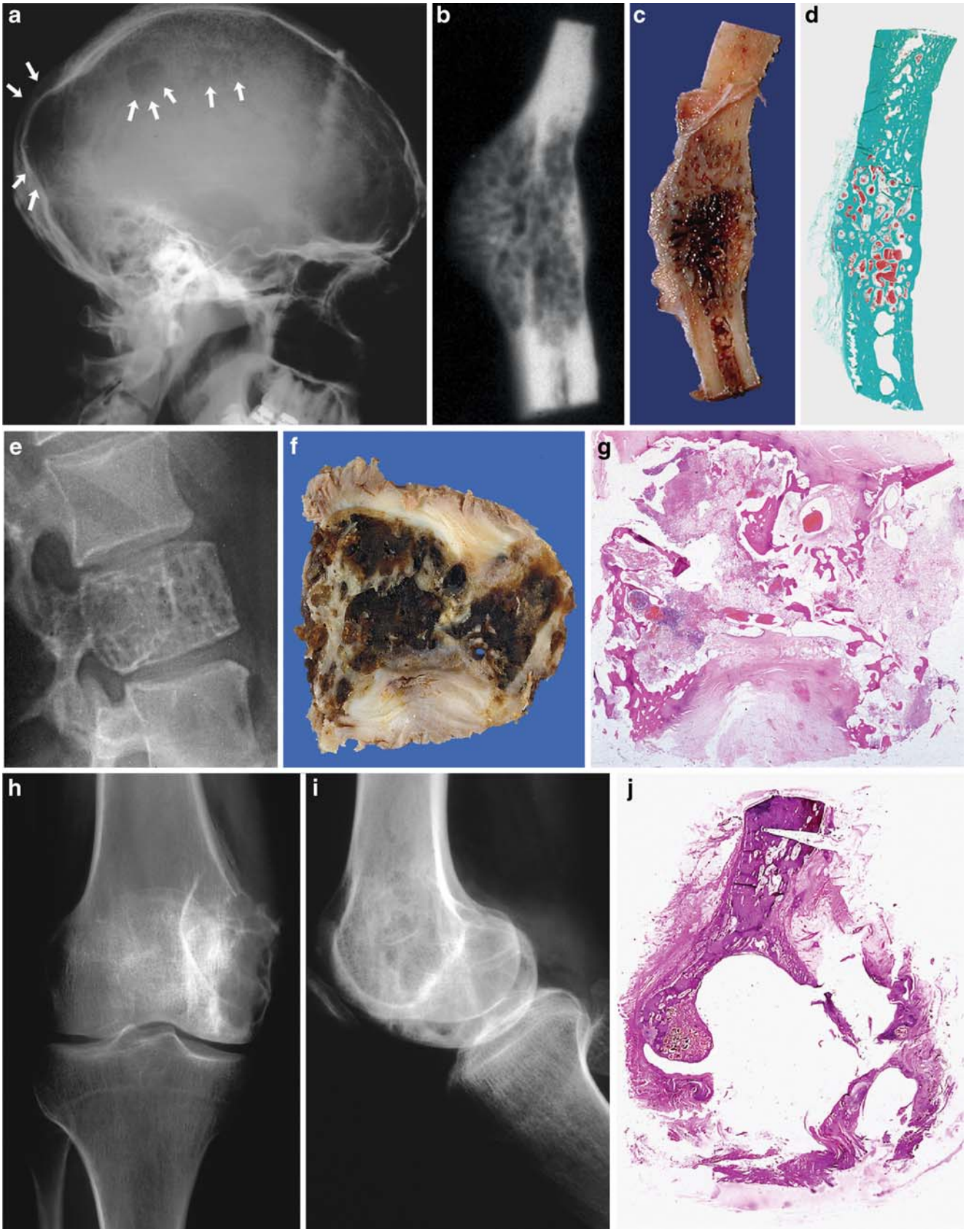
a
b
c
d
e
f
g
h
i
j

◀ **Fig. 1** Venous malformation. **a** Cranial geographic osteolysis on lateral plain film (*arrows*; 17-year-old male). **b–d** Specimen radiograph, gross and whole mount section showing spongy appearance and expansion of the skull. Large abnormal channels contain blood (same patient as in **a**). **e–g** Coarsely trabeculated osteolytic lesion of the third lumbar vertebra (22-year-old female). The hemisected vertebral body and whole mount section show central collapse, loss of bone and abnormal channels of varying size. The vertebra was removed because of compression fracture following sclerotherapy. **h–j** Multiple lucent areas with coarse trabeculations involving distal femur on radiographs and spongy appearance with massive channels on whole mount section (22-year-old male)

they typically exhibited partly permeative osteolysis with variable peripheral sclerosis, cortical destruction, and periosteal new bone.

Seven tumors had characteristics typical of epithelioid hemangioendothelioma with densely cellular sheets lacking a lobular architecture or obvious lumen formation (Fig. 8). The tumor cells were epithelioid with abundant eosinophilic or amphophilic cytoplasm, often with a solitary vacuole which sometimes contained erythrocytes. Nuclei were moderately pleomorphic with prominent nucleoli and mitoses were few without atypical forms. Focal necrosis was present. Tumor cells were dispersed in a pale or myxoid matrix that was focally calcified when adjacent to residual bone. Perilesional bone showed active osteoclastic resorption and seams of woven bone. WT1 immunoreactivity was strongly and diffusely positive and MIB1 proliferative index up to 50%.

One hemangioendothelioma consisted of small monotonous mildly pleomorphic epithelioid cells with prominent lumen formation but also with solid zones. Cytoplasmic vacuoles were absent and areas of pale myxoid/chondroid

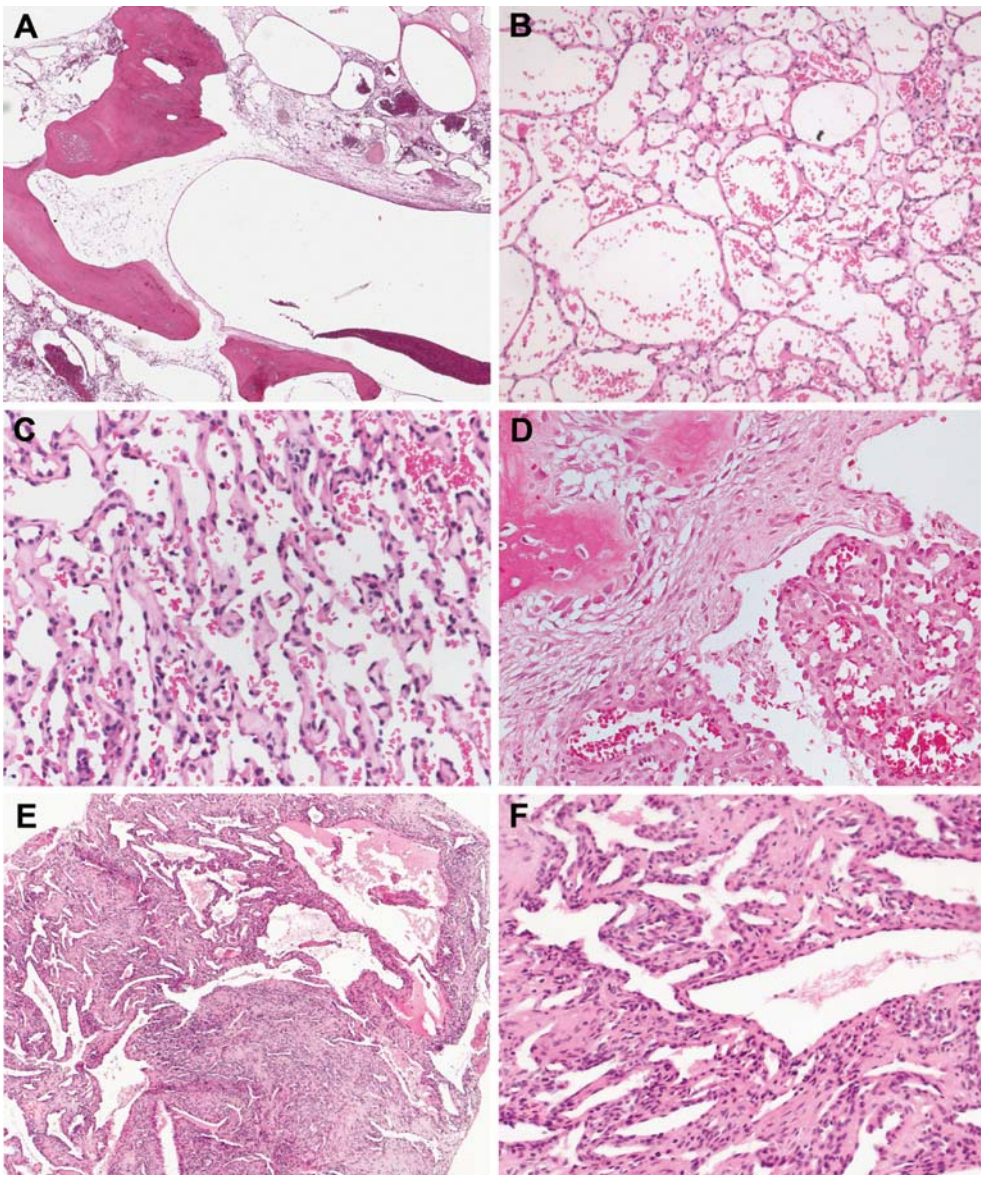

Fig. 2 Venous malformation. **a** Mostly large thin-walled channels, some containing blood (22-year-old female). **b** Back-to-back, small-to-large, irregularly round channels have flat endothelium and are devoid of muscle (same patient as in **a**). **c** Anastomosing elongated channels have bland endothelium (same patient as in **a**). **d** Focus of small round channels with a more prominent endothelium protrudes into large channel (13-year-old female). **e–f** Interspersed with large channels are more solid areas with stromal collagen (4-year-old male)

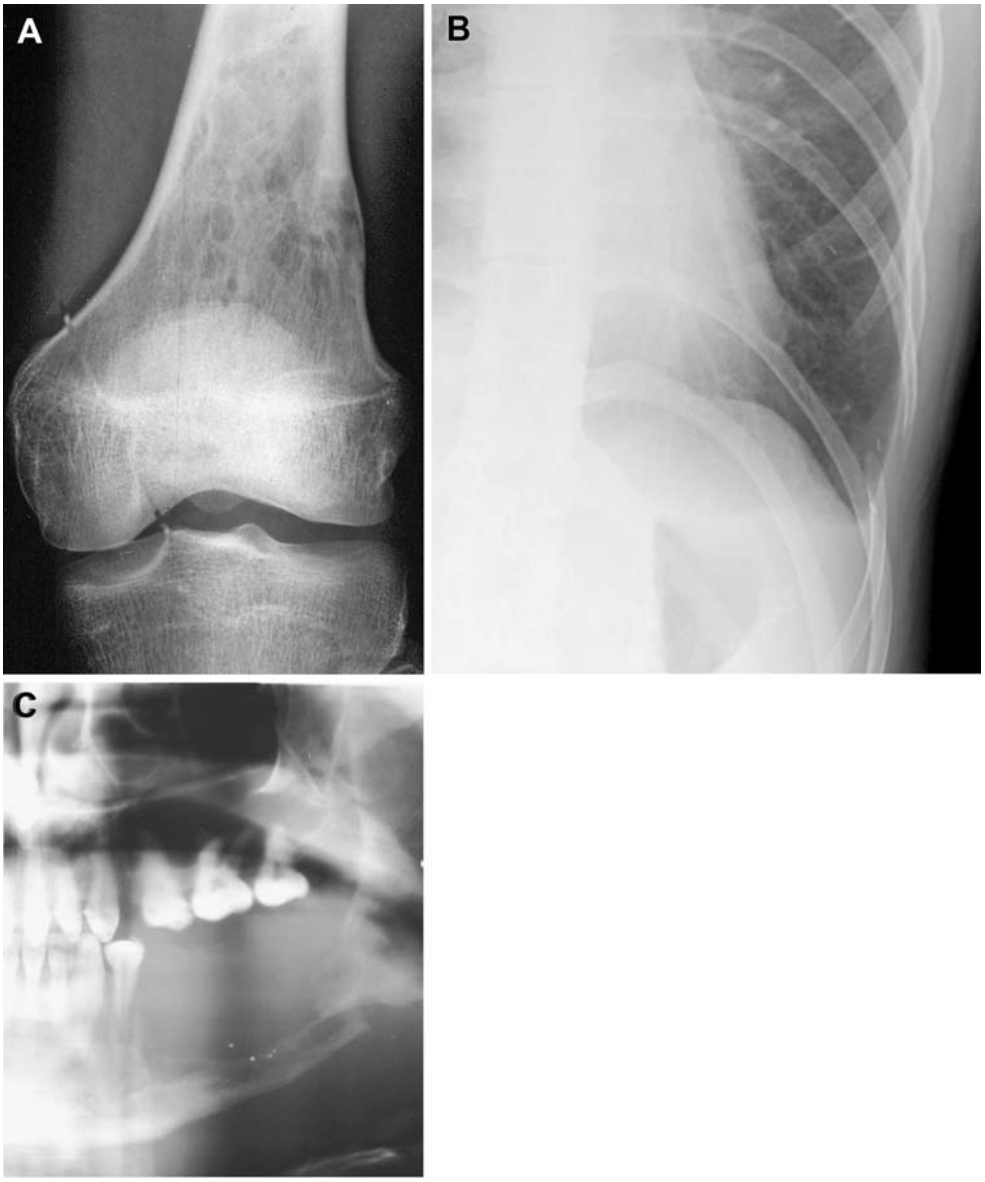

Fig. 3 Lymphatic malformation. **a** Frontal plain film of the knee shows multiple coalescing radiolucent foci in the metaphysis of the distal femur. There is incomplete sclerosis of the margins and cortical thinning and elevation (18-year-old male). **b** Lymphatic malformation with massive osteolysis of left ninth rib (Gorham-Stout disease; 16-year-old female). **c** Large mandibular osteolytic lesion without marginal sclerosis; there is loss of alveolar bone and teeth (24-year-old male)

matrix were minimal. The biopsy was small and although epithelioid hemangioendothelioma was a distinct possibility, because of the lack of some of the typical features, we chose to designate this lesion hemangioendothelioma NOS.

Kaposiform hemangioendothelioma

These tumors showed a histopathologic resemblance to kaposiform hemangioendothelioma of soft tissue (Fig. 9). They were in the humerus, ulna, femur, and tibia and radiographically showed irregular osteolysis with minor soft tissue extension in two patients. One patient had involvement of two bones. Histopathology showed ill-defined coalescing nodules of spindled moderately plump cells forming strands and fascicles with slit-like lumina containing erythrocytes. Foci of round cells with larger nuclei and clear cytoplasm were also seen. Cytoplasmic hemosiderin and cytoplasmic hyaline globules were present and one lesion had microthrombi. Dilated lymphatic channels were not conspicuous. Immunohistochemistry showed the lesional cells to be positive for CD31 and CD34, focally positive for D2-40, and negative for GLUT1.

Kaposiform lymphangiomatosis (provisional term)

These lesions were multifocal and involved soft tissue, viscera, and bone in all patients. The affected bones were rib, clavicle, scapula, vertebra, sacrum, ilium, femur, radius, ulna, and those of the wrist. Radiographs showed osteolysis as in multifocal LM. Histopathologically, the soft tissue and visceral lesions were that of multifocal LM, but were also accompanied by isolated areas that mimicked kaposiform

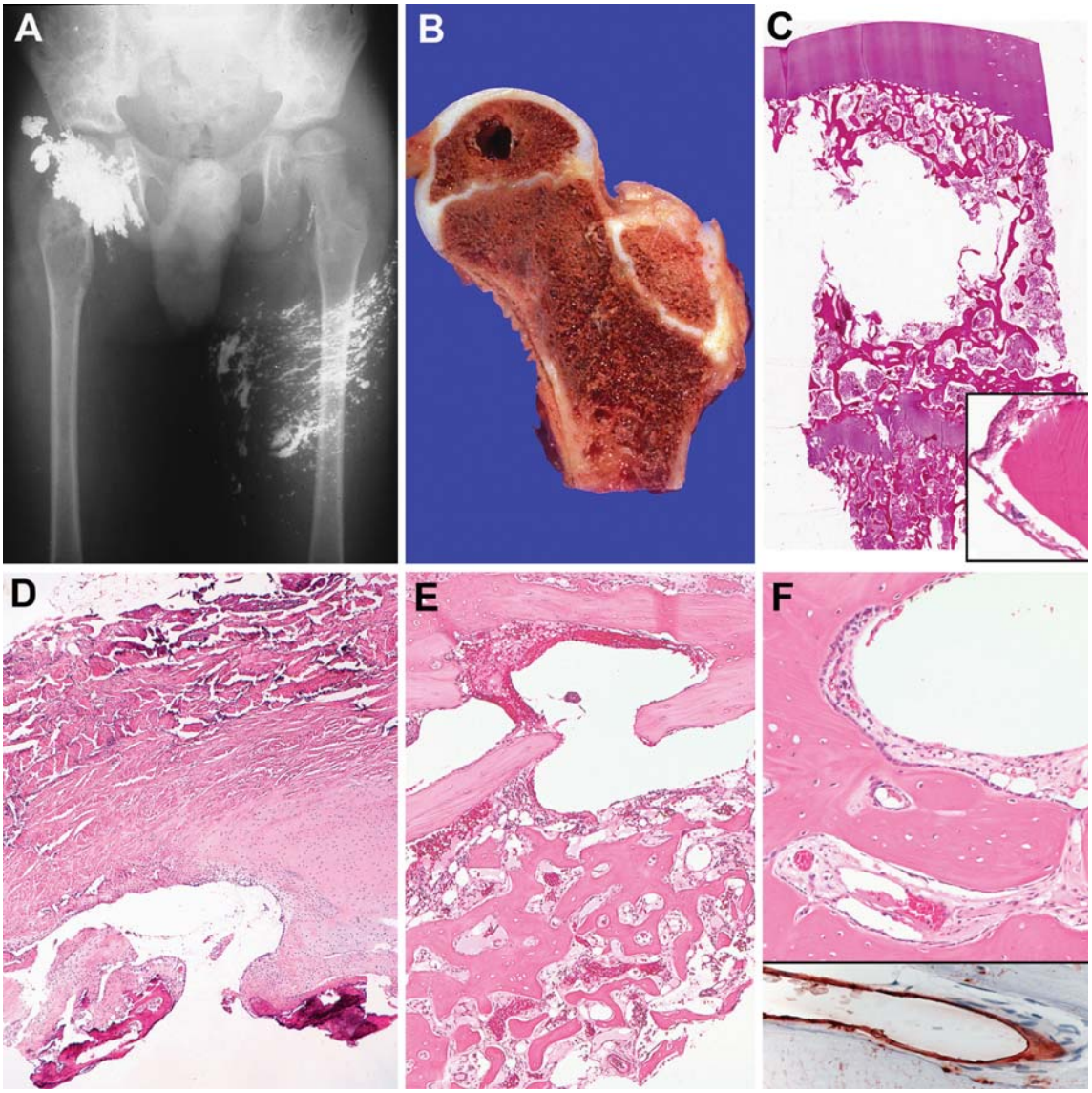

Fig. 4 Lymphatic malformation. **a** Multiple geographic osteolyses of pelvic bones, femoral metaphyses and left femoral head. Lymphangiogram shows ectatic channels in skin and soft tissue (11-year-old male). **b** Hemisectioned proximal femur at autopsy shows single epiphyseal cavity and multiple spaces in the metaphysis and diaphysis (*arrows*; same patient as in **a**). **c** Whole mount section of femoral head of same specimen depicted in **b** shows a large irregular space rimmed by trabecular bone and lined by a flat endothelium (*inset*; same patient as in **b**). **d** Cortical resorption and extension of thin-walled channels into periosteum. Contiguous soft tissue also shows lymphatic malformation (4-year-old male). **e**–**f** Anastomosing network of lymphatic channels permeating medulla and cortex. Extensive reactive medullary bone is present (17-year-old female). **g** Lymphatic channels have thin walls and flattened endothelium immunoreactive to D2-40 (*inset*; 18-year-old male)

hemangioendothelioma with densely cellular small sheets of irregularly ovoid to spindled cells with slit-like lumina containing erythrocytes. These areas had minimal or absent nuclear pleomorphism and rare mitoses, and the cytoplasm was frequently hemosiderotic. The biopsied skeletal lesions had the histopathology of multifocal LM, but in three patients the kaposiform component was also present (Fig. 10). The lesional cells were immunopositive for CD31 and CD34 and focally for D2-40. The surrounding bone showed osteoclastic resorption.

Angiosarcoma

These tumors were localized (monostotic) in three patients and multifocal (polyostotic) in two. The affected bones were mastoid, humerus, radius, ulna, femur, and tibia. Multicentric tumor involving a single skeletal element was present in two patients, one with monostotic (tibia) and another with polyostotic disease (radius). Radiographs showed areas of irregular osteolysis involving cortex and medulla, absent perilesional sclerosis, and minimal periosteal reaction.

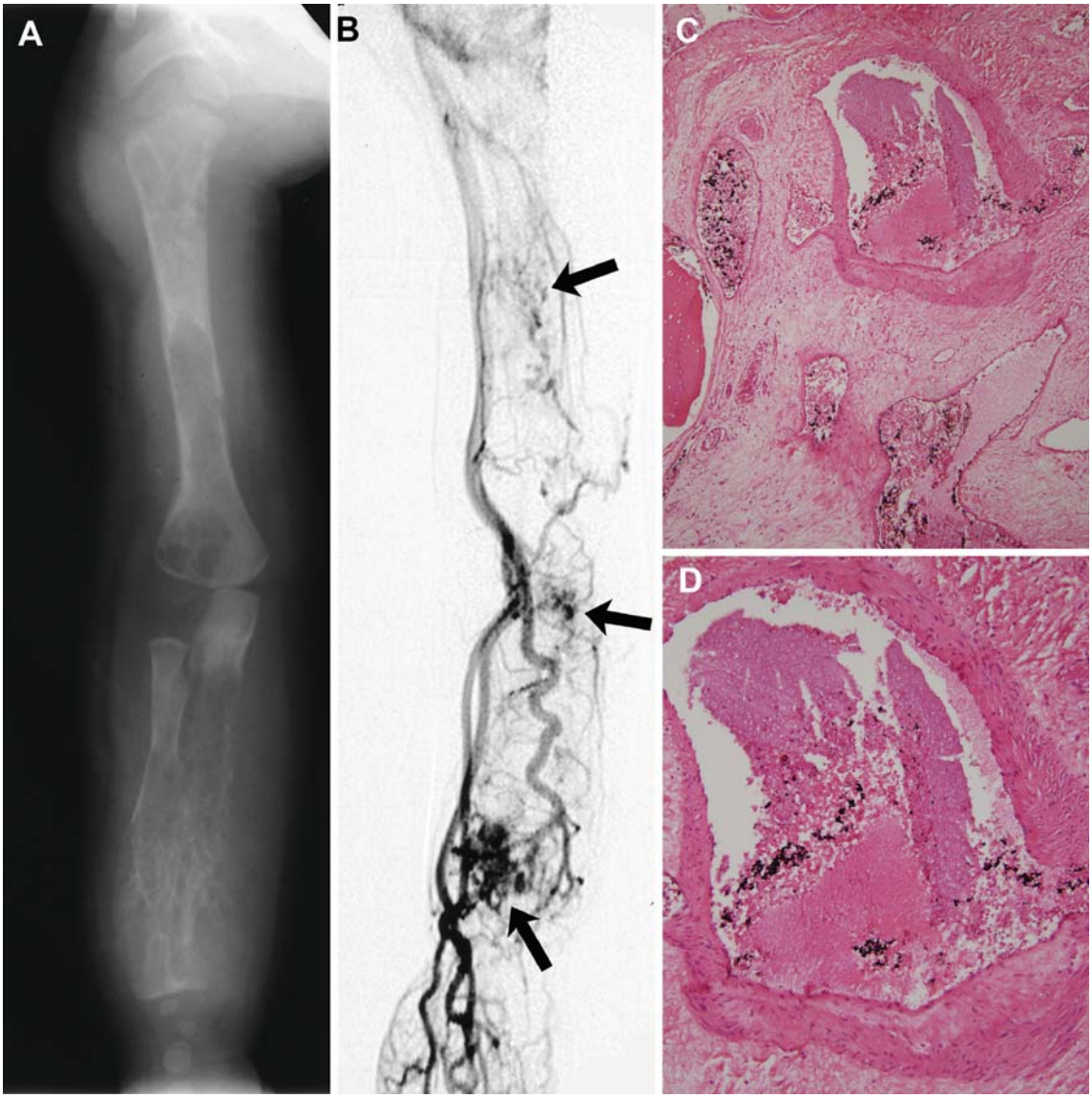

Fig. 5 Arteriovenous malformation. **a** Extensive lytic changes in humerus, ulna, and radius with cortical thinning and disruption and minimal reactive bone (1-year-old female). **b** Venous phase of an arteriographic study demonstrates filling of ectatic and tortuous veins communicating with the osseous malformations (*arrows*; same patient as in **a**). **c**–**d** Arteriovenous malformation involving maxilla with thin-walled venous structures and a large vessel of indeterminate type with irregular muscular wall and intimal hyperplasia (6-year-old female; in this patient, the maxillectomy specimen was extensively involved, but because of a dominant soft tissue component, she was excluded from the study)

Histopathology varied among the tumors as well as within individual tumors (Fig. 11). Tumor cells were arranged in cords, strands, and sheets with infiltrative margins. Vasoformation was variable and cytoplasmic vacuoles were rare. The channels were generally small, round, elongated, or irregular with complex anastomotic patterns. Significant cellular atypia with nuclear pleomorphism, hyperchromasia, and mitoses were present in all lesions. In two cases, there was a prominent epithelioid component with cells having abundant eosinophilic cytoplasm and large nucleoli. Cellular spindled cell areas were observed in one tumor. The surrounding bone showed osteoclastic resorption with minimal new bone; there was invasion of the soft tissue in all. WT1 was strongly and diffusely expressed in tumor cells and MIB1 proliferative index was high.

Unclassifiable

Three vascular tumors had unusual histopathologic features and could not be classified. A large congenital tumor of the maxilla had variably sized and shaped thin-walled vascular channels lined by bland flat-to-cuboidal endothelium within

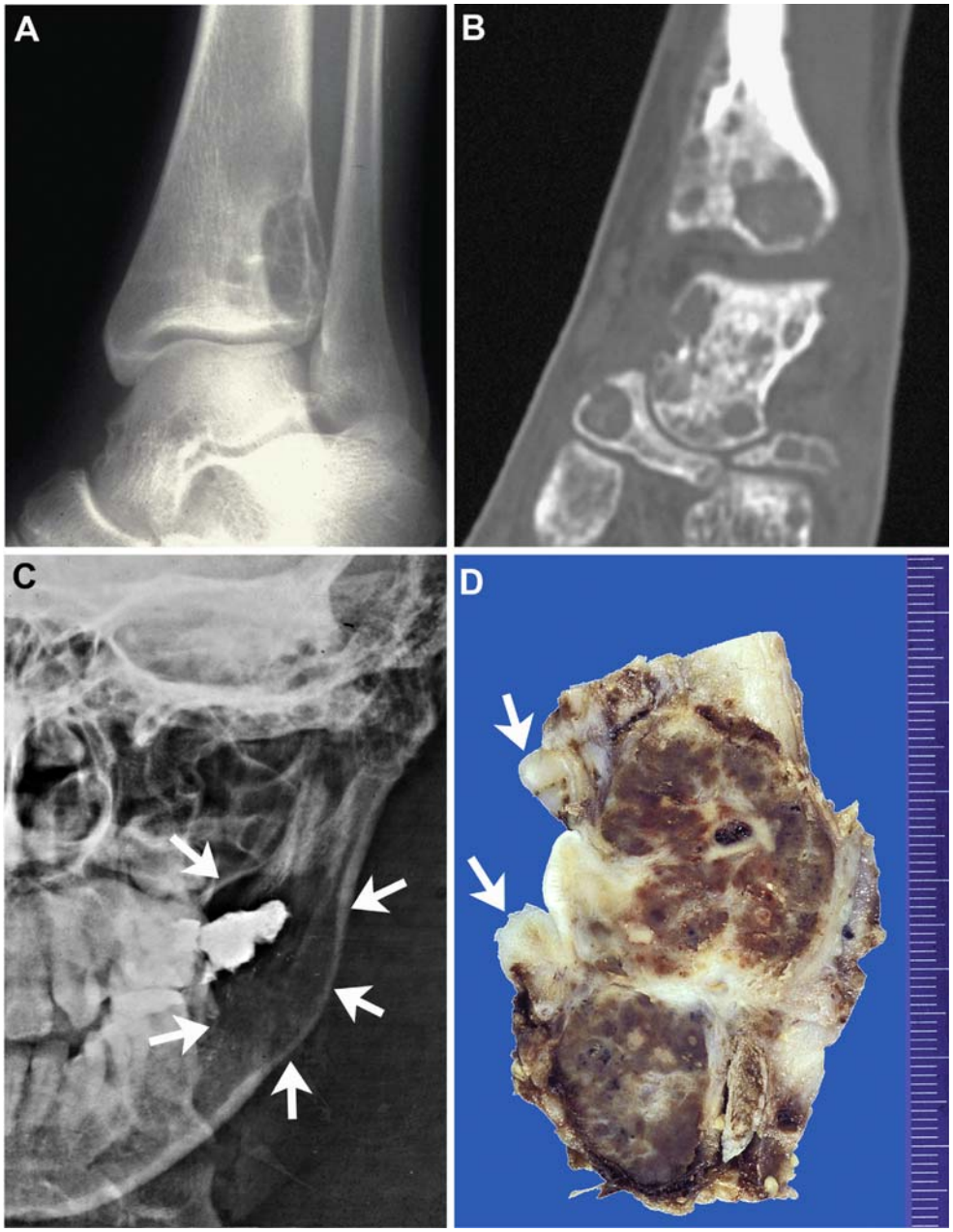

Fig. 6 Epithelioid hemangioma. **a** Excentric, well-defined lucencies in distal tibia with thinning of cortex (17-year-old female). **b** CT shows multifocal osteolyses and rarefaction of distal tibia and tarsal bones with focal cortical loss (17-year-old male). **c** Expansile osteolytic lesion of the angulus and ramus mandibulae (16-year-old female). **d** Partial mandibulectomy, hemisectioned specimen after fixation from patient depicted in **c**, shows dark-brown solid tumor destroying bone and extending into adjacent soft tissue. Two teeth are displaced (*arrows*)

a densely fibrous stroma. A morphologically similar small mass was identified within the liver. They had some resemblance to polymorphous hemangioendothelioma of soft tissue [10]. A mandibular lesion in an 18-year-old consisted of clusters of large thin-walled vascular structures with grape-like and glomeruloid tufts and an endothelium that was focally hobnailed. The tumor had some similarities to non-involuting congenital hemangioma [11]. A tibial tumor in an 11-year-old was comprised of an irregular network of small vessels with plump and focally epithelioid endothelium and bore some resemblance to epithelioid hemangioma; however, cytoplasmic vacuoles were not present and a loose fibrous stroma was prominent.

Discussion

The nomenclature of vascular anomalies has been confusing, hindering communication and contributing to errors in diagnosis, treatment, and research. Therefore, in 1996, the ISSVA issued a multidisciplinary consensus on a binary classification of vascular lesions: *tumors* that arise by endothelial proliferation and *malformations* that are structural abnormalities exhibiting slow (normal) endothelial turnover [5]. They stated that the suffix "oma" should refer only to neoplastic growths. Therefore, terms such as "lymphangioma," "venous hemangioma," or "arteriovenous hemangioma" are inappropriate since these are malforma-

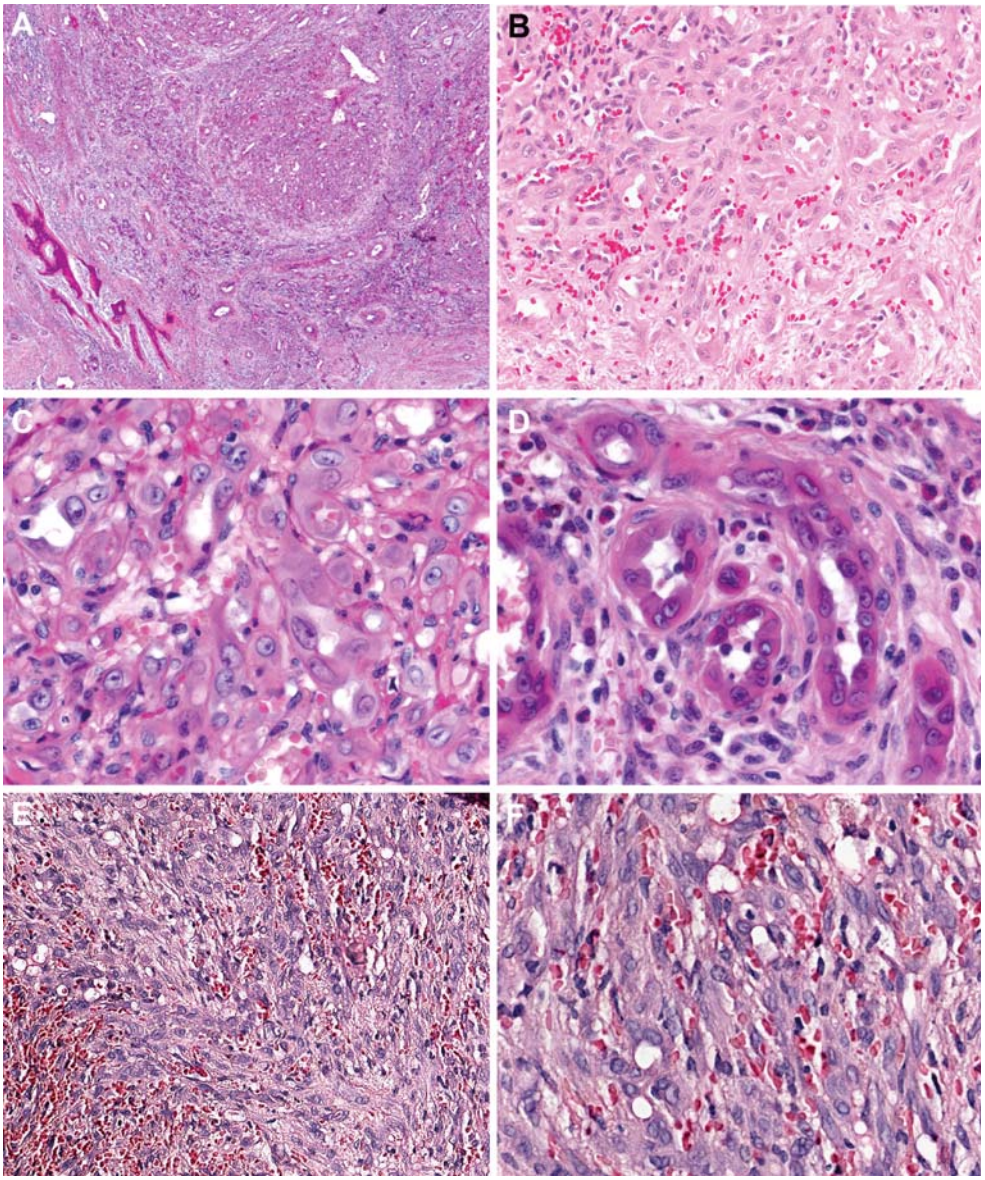

Fig. 7 Epithelioid hemangioma. **a** Nodular masses of tumor have destroyed cortex and extend into soft tissue (16-year-old female). **b** Vascular channels lined by large epithelioid cells with eosinophilic cytoplasm (16-year-old female). **c** Epithelioid cells have large rounded nuclei with minor variation in size and shape, open chromatin, and small distinct nucleoli. The eosinophilic cytoplasm has occasional vacuoles (same patient as in **a**). **d** Well-formed vascular channels in a background containing lymphocytes and eosinophils (same patient as in **a**). **e**–**f** Spindled cell component with numerous interspersed red blood cells, nascent canalization, occasional cytoplasmic vacuoles, and absence of hemosiderin (same patient as in **a**)

tions that do not exhibit disproportionate growth in relation to the child. Furthermore, they indicated that the term "hemangioma" has been used indiscriminately to designate various tumors and malformations. It was recommended that hemangioma refer only to a benign lesion that arises by endothelial proliferation and that it should be accompanied by the appropriate qualifier, e.g., "infantile," "spindle cell," and "epithelioid,"

Besides ISSVA, others are in agreement with our concept that certain lesions often regarded as tumors are in fact malformations. For example, in the *WHO Classification of Tumours of Soft Tissue and Bone* [12] the following statements are made: "The clinical evolution and clinicopathological features (of 'venous haemangioma') suggest that these lesions represent vascular malformations"; "Arteriovenous haemangioma (AVH) is a non-neoplastic vascular lesion…"; "Early or even congenital appearance in life and lesional architecture (of 'lymphangioma') are in favour of developmental malformations, with genetic abnormalities playing an additional role"; and finally, "angiomatosis probably represents congenital malformations (rather than neoplasms) which make their appearance during childhood". Consequently, none of the lesions that we consider malformative are regarded by the WHO as tumors.

We were able to apply the ISSVA nomenclature to the categorization of osseous vascular lesions in our study. All bony vascular lesions, except the unclassifiable ones, had histopathologic features that are similar to their counterparts in skin, soft tissue, and viscera. Therefore, just as in extraskeletal sites, it was possible to classify the bony lesions as malformations or tumors. Table 3 depicts the

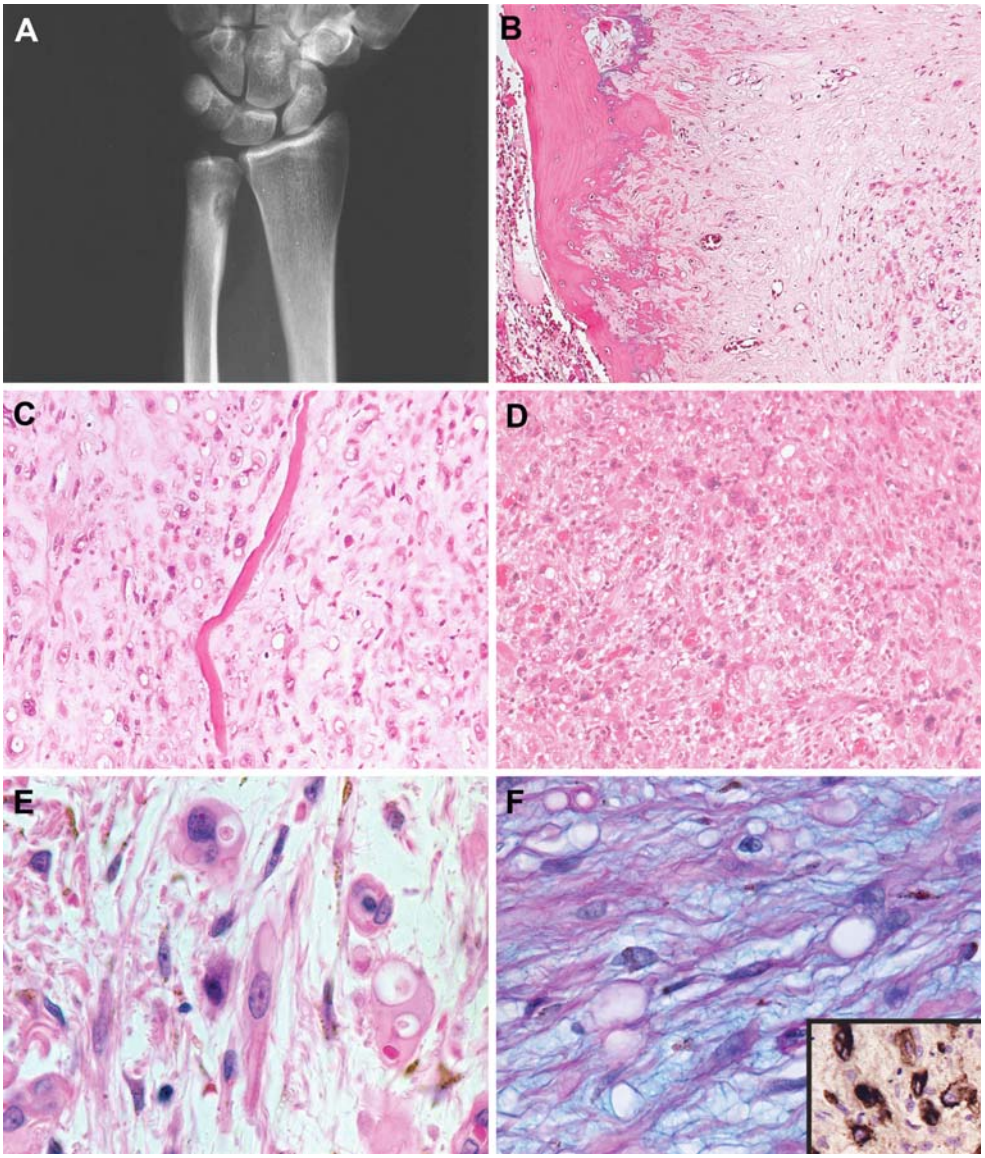

Fig. 8 Epithelioid hemangioendothelioma. **a** Well-circumscribed excentric osteolysis of the distal ulna with cortical destruction (19-year-old female). **b** Tumor cells are dispersed in ample extracellular matrix. Cortical destruction is present (10-year-old female). **c** Mostly single epithelioid and spindled tumor cells with variable nuclear pleomorphism and cytoplasmic vacuoles are immersed in pale extracellular matrix. A thinned bony trabecula is surrounded by tumor (same patient as in **b**). **d** Cellular area with focal anaplasia. Nascent canalization is present (same patient as in **b**. **e** Cytoplasmic vacuoles containing erythrocytes and other hematogenous cells (same patient as in **a**). **f** Mucopolysaccharide-rich matrix is stained with alcian blue (19-year-old female). Tumor cells are immunoreactive for factor-VIII-related antigen (*inset*; same patient as in A)

equivalent terminology for the various entities listed in the WHO classification of vascular tumors of bone [12] and those in the ISSVA schema as applied to our series.

Localized osseous VM in the literature is generally called "hemangioma of bone," whereas multiple VM is variously termed "hemangiomatosis" or "angiomatosis" when regional and "cystic angiomatosis" when generalized [2, 13]. These designations with the suffixes "oma" or "omatosis" imply neoplasia; however, the clinical and histopathological features are more those of a vascular malformation. Clinically, in soft tissue and visceral VM, there is usually no disproportionate growth, except some expansion during puberty or over time, a phenomenon attributed to hormonal or rheologic factors, respectively [14]. Also, in osseous VM, there is no disproportionate growth except occasionally in some lesions, particularly calvarial. Histopathologically, the lesions are composed mostly of large, thin-walled channels lined by flattened cells without mitoses, indicating a relatively inert endothelium. As in extraskeletal VM, there can be foci of small channels, cuboidal endothelium, or organizing thrombi, which mimic a proliferative lesion. Evidence of proliferative activity reflected by MIB1 expression has been observed in some cutaneous, soft tissue, and cerebral vascular malformations [15–17]. We have also found evidence of proliferative activity in some venous malformations, but the proliferative index was low. Several explanations for this finding are possible including growth of the lesion (commensurate with that of the child), slow expansion because of rheologic mechanisms facilitated by the diminished muscle in the malformed veins (LaPlace's law), and reparative changes due to organizing thrombi or hemorrhage, which may be subtle or resolved and therefore not always evident in the sections. Furthermore,

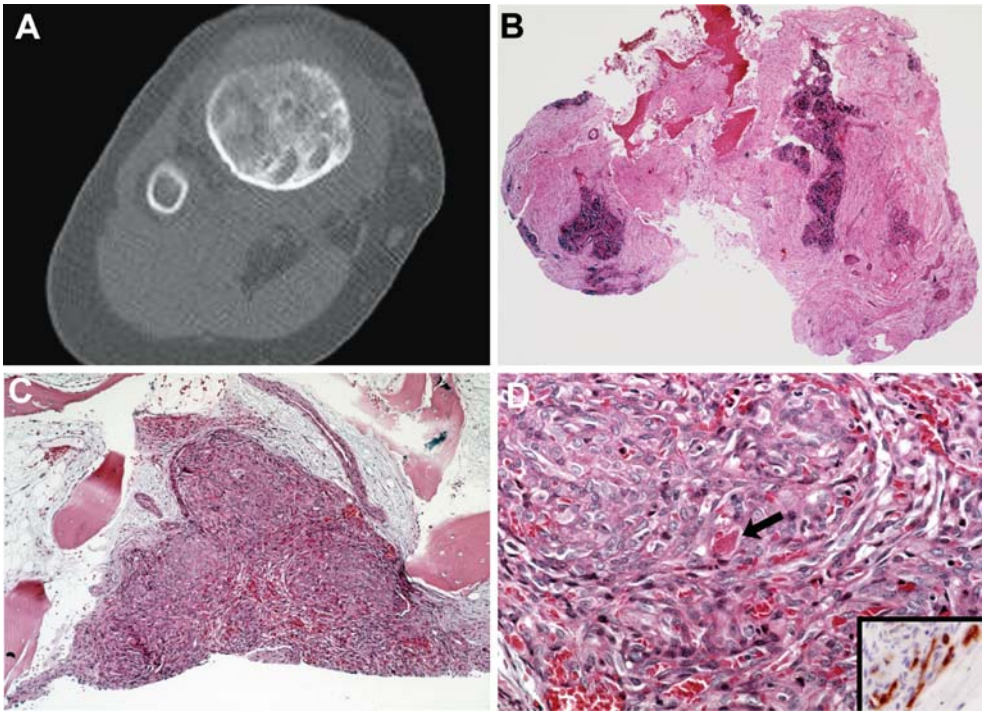

Fig. 9 Kaposiform hemangioendothelioma. **a** Axial CT image of proximal tibia demonstrates confluent heterogeneous osteolysis, cortical thinning and destruction, and faint reactive sclerosis (7-year-old female). **b** Irregular islands of tumor with sclerotic stroma infiltrating and destroying bone (7-year-old female). **c** Coalescent nodules of tumor with spindling at their periphery (same patient as in **b**). **d** Nodule of plump tumor cells with peripheral spindling, variable canalization and thrombus (*arrow*; same patient as in **c**). Some channels are immunoreactive for D2-40 (*inset*; 7-year-old female)

WT1 immunoreactivity, which is observed in tumors but not in malformations, in our study, was absent or rare in the VMs [9].

The concept of so-called vertebral "hemangioma" as a malformation was proposed by Jaffe nearly 50 years ago; he observed that "these asymptomatic vertebral vascular lesions probably represent, for the most part, mere focal varicosities rather than true hemangiomas" [18]. In addition to the WHO, others have also stated that most or all "hemangiomas of bone" are developmental or hamartoma-

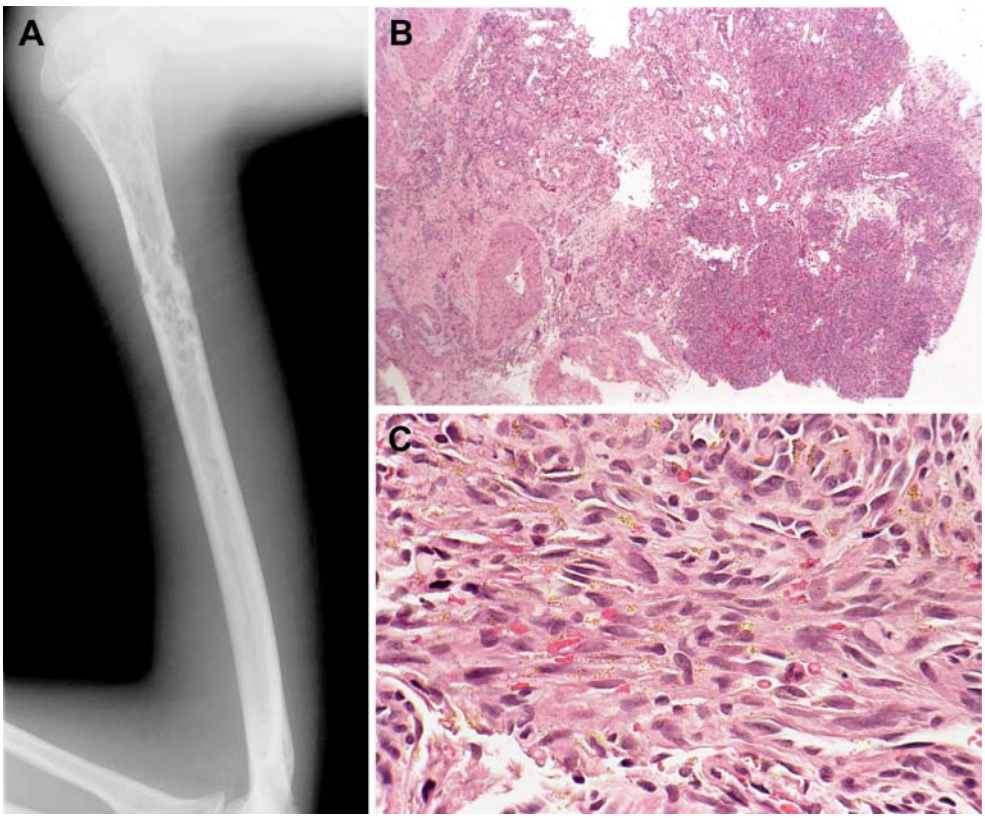

Fig. 10 Kaposiform lymphangiomatosis (provisional term). **a** Multiple confluent lucencies of cortex and medulla of proximal humeral metadiaphysis (14-year-old male). **b** Biopsy of fifth metacarpal lesion showing coalescent cellular nodules and aggregates of abnormal vessels (same patient as in **a**). **c** Hemosiderotic spindled cells with interspersed erythrocytes (same patient as in **a**)

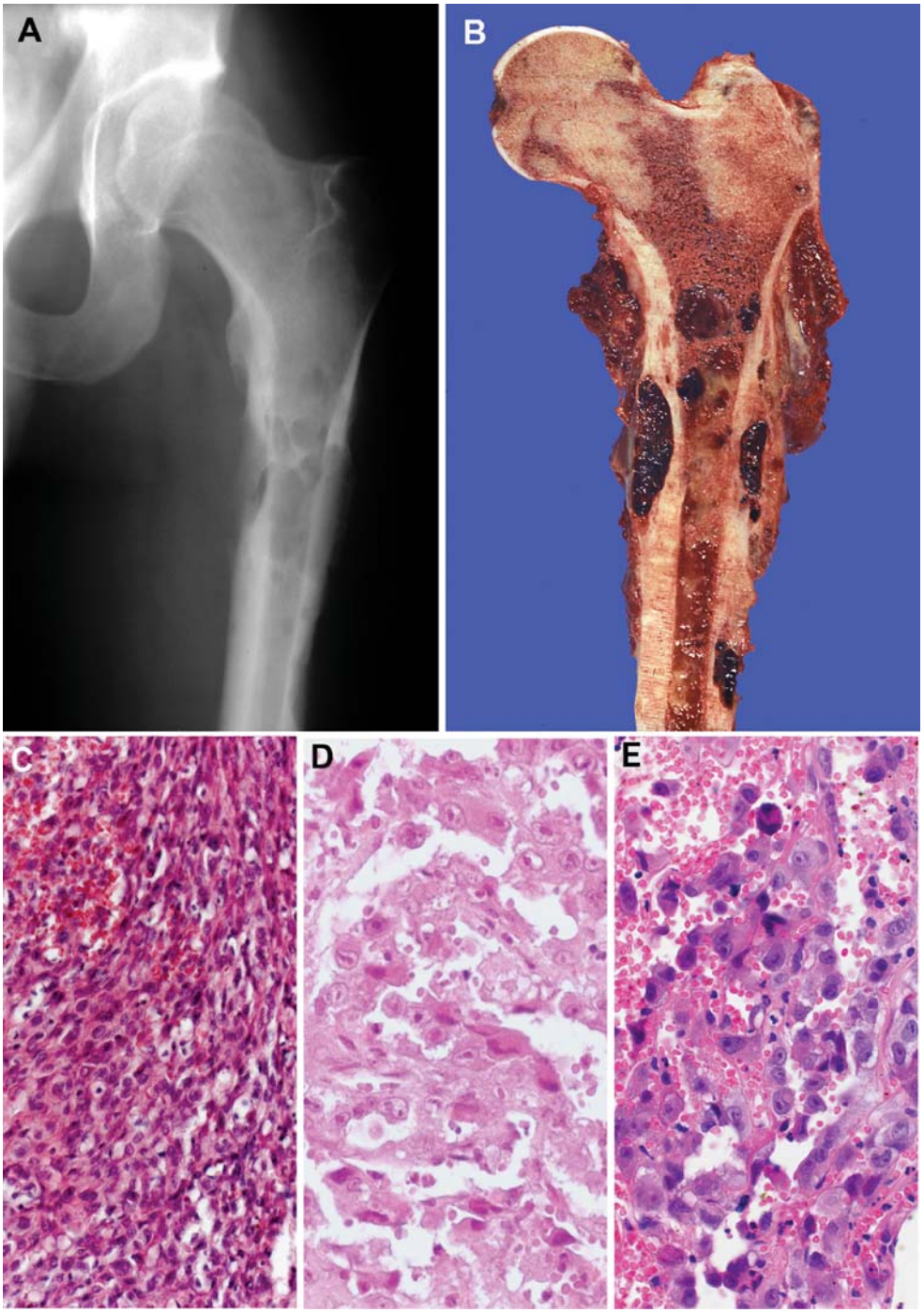

Fig. 11 Angiosarcoma. **a** Plain film of the proximal femur demonstrates osteolytic areas in the metadiaphysis with cortical destruction and lack of sclerosis (25-year-old male). **b** Hemisected femur shows multiple dark-red–brown osteolytic foci in the diaphyseal cortex and medulla. Periosteal elevation is present laterally and there is extensive soft tissue infiltration (the pale yellow areas in the femoral head, metaphysis, and greater trochanter are fatty marrow; same patient as in **a**). **c** Soft tissue component showing highly cellular area of spindled endothelial cells with moderate nuclear pleomorphism and slit-like lumina containing red blood cells (same patient as in **a**). **d** Epithelioid angiosarcoma. Moderately anaplastic tumor cells have abundant pink cytoplasm and prominent eosinophilic nucleoli (25-year-old male). **e** Discohesive growth of epithelioid anaplastic cells forming irregular channels (same patient as in **d**)

tous rather than true neoplasms [2, 3, 13, 19, 20]. With the increasing appreciation that these lesions are malformative rather than neoplastic, sclerotherapy is growing in popularity, thereby avoiding the morbidity of an operation, antiangiogenic therapy, or radiation.[21–25]. In one study, the authors describe their experience in treating a series of vascular malformations of the mandible and advocate that terms such as "intraosseous central or peripheral angioma" and "tumoral angioma" should not be used so as to avoid tumor therapies such as radiation [23].

Localized VMs were more common than multiple VMs. No patient had cutaneous involvement as has been reported in patients with multiple mucocutaneous VMs and Maffucci, or blue rubber bleb nevus syndromes [26, 27]. The majority of VMs, particularly those in the vertebrae, are discovered incidentally, have characteristic imaging, and do not require biopsy. Histopathologically, VM often suggests a differential diagnosis that includes, in particular, LM. LMs generally have thinner walls without pericytes or smooth muscle and their lumens may be empty or contain a

Table 3 Comparison of the WHO classification with the ISSVA classification (as applied to our series)

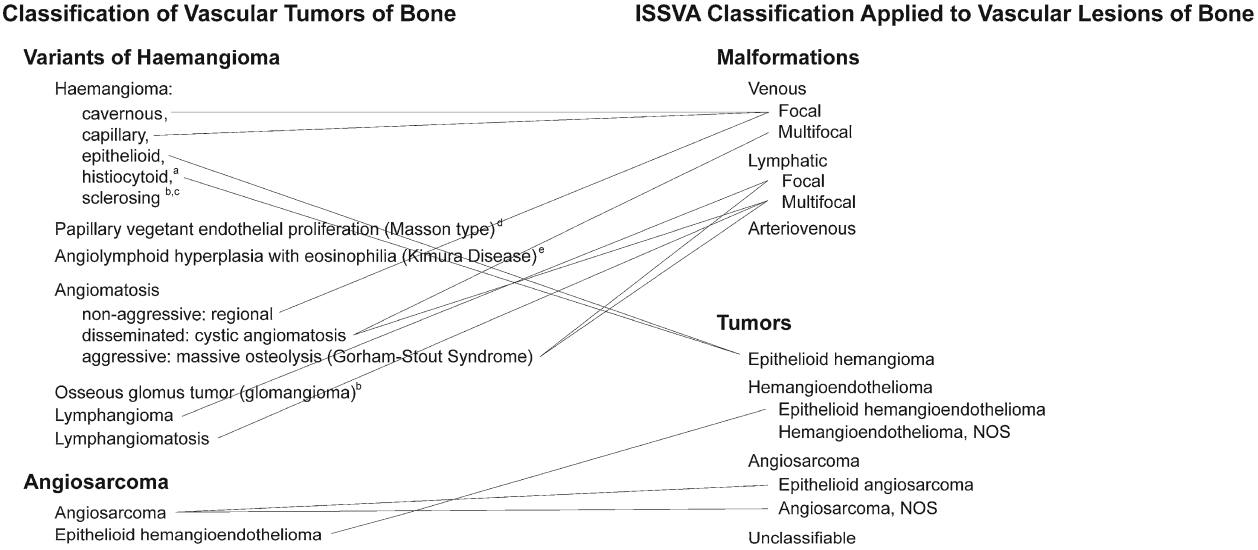

NOS not otherwise specified

[a] Currently considered synonymous with epithelioid hemangioma

[b] Not encountered in our series

[c] Sclerosing hemangioma is not discussed in standard textbooks describing vascular tumors of bone

[d] Currently considered a secondary process in organizing thrombi or hematomas

[e] Angiolymphoid hyperplasia with eosinophilia is currently considered a synonym for epithelioid hemangioma and unrelated to Kimura disease

proteinaceous lacy network, macrophages, and lymphocytes. Luminal blood may be present but is usually related to surgical trauma. Immunoreactivity of the endothelial cells for D2-40 is characteristic of LM and discriminates between these two lesions. The somewhat polymorphic appearance of VM and its small vessel component may mimic a neoplasm, but the proliferative index is low except in areas of organizing thrombi. Some venous malformations have organizing thrombi or organizing hemorrhage further mimicking a neoplastic proliferation. In small biopsies, AVM may also mimic VM when only dilated venous channels are seen and channels of indeterminate type or with thick muscular walls and/or intimal myofibroblastic proliferation have not been sampled. While some aspects of VM may suggest infantile hemangioma, diagnostic features are absent, including Glut-1 immunoreactivity [28]. It is intriguing that, to the best of our knowledge, infantile hemangioma, the most common vascular tumor in children, has not been convincingly shown to originate in bone. A congenital cranial hemangioma that regressed with time has been reported but the histopathology was not illustrated [29].

Mutations in the genes for *TIE1* and *TIE2*, *Glomulin*, and *KRIT1* have been described in various extraskeletal VMs [30]. It is unknown if the molecular mechanisms underlying osseous VMs are similar.

In the literature, LM is most often designated "lymphangioma" when localized and "lymphangiomatosis" or "cystic angiomatosis" when multifocal. These terms with the suffixes "oma" or "omatosis" imply neoplasia. We believe that LMs are malformations; there is no disproportionate growth except if they are expanded by lymph, become infected, or bleed. The diagnosis of osseous LM is usually possible by imaging, as with VM. In contrast to VM, multifocal lesions were more common than localized lesions. In multifocal LM, extraskeletal extensive involvement of skin, soft tissue, and viscera is almost always present.

The most common histopathological mimicker of LM is VM. Although there are histopathological differences (*vide supra*), the distinction is greatly facilitated by endothelial immunopositivity for D2-40 and LYVE-1 in LM [31]. Although, in our experience, decalcification impairs LYVE-1 immunoreactivity, that of D2-40 is preserved. The histopathology of multifocal LM is similar to that of localized LM, except that, in the former, there is a tendency for the channels to be smaller, more numerous, and to have more complex anastomoses.

LM can be associated with chromosomal abnormalities such as Down, Turner, and Noonan syndromes and mutations in *FLT4*, *FOXC2*, and *SOX18* have been reported in various types of congenital lymphedema [32]. Nevertheless, genetic alterations in primary osseous lymphatic malformations have not been described.

The terms massive osteolysis, disappearing bone disease, phantom bone disease, or Gorham-Stout disease refer to a gradual and often complete resorption of one or multiple skeletal elements with the vertebrae, scapulae, clavicles,

ribs, proximal humeri, ilia, and proximal femora being the sites of predilection [33–35]. Gorham and colleagues [34, 35] used the term "angiomatosis" (or "hemangiomatosis") of blood vessels and rarely of lymphatic vessels to describe the histopathology. It has been stated that "the vascular changes in Gorham disease represent hemangiomas, lymphangiomas, or a combination" [2]. Our experience is that massive osteolysis is associated only with LM.

Although the pathogenesis of Gorham-Stout disease is not entirely elucidated, it is thought that the monocyte-derived precursors of osteoclasts play a crucial role [36]. Circulating osteoclastic precursors with increased sensitivity to interleukin (IL)-6, IL-1β, and tumor necrosis factor alpha and elevated serum levels of IL-6 have been reported [37].

AVM was the least common malformation encountered in our series and, as in the literature, the craniofacial bones were most commonly affected. The involvement of the skeletal element(s) is usually extensive and there may be an adjacent soft tissue component. Hypertrophy of the skeletal element(s) may ensue. Lesional change in size associated with microvascular proliferation, attributed to rheologic factors, may occur, particularly in areas with substantial shunting [15]. The molecular basis for AVMs is an area of active investigation. Mutations in the *RASA1* gene cause the capillary malformation–arteriovenous malformation phenotype, but primary osseous involvement in this condition has not been reported [30]. The lesions in hereditary hemorrhagic telangiectasia caused by mutations in activin and endoglin may include large AVMs of lung, liver, and brain but not bone.

In the tumor category, benign neoplasms outnumbered malignant ones. The most commonly encountered benign tumor was epithelioid hemangioma. This tumor has been delineated from other epithelioid vascular tumors such as epithelioid hemangioendothelioma and epithelioid angiosarcoma [38]. Nevertheless, some investigators have questioned the ability to distinguish epithelioid hemangioma from epithelioid hemangioendothelioma [39]. Although epithelioid hemangioendothelioma is often multicentric or polyostotic, in our series, 25% of epithelioid hemangiomas were similarly so, indicating that these features do not necessarily imply malignancy. The histopathology of epithelioid hemangioma is usually characteristic, but, when solid growth predominates and/or nuclear pleomorphism is present, epithelioid hemangioendothelioma and epithelioid angiosarcoma should be considered in the differential diagnosis. Cytologic atypia in epithelioid hemangioma, if present, is minor and solid growth is always accompanied by more typical areas. The stromal hyalinization or basophilic chondroid ground substance characteristic of epithelioid hemangioendothelioma and necrosis are not present [40]. Absence of significant cellular atypia and frequent mitoses, including abnormal forms, helps to exclude epithelioid angiosarcoma.

Epithelioid and spindle cell hemangioma, originally delineated as a separate entity [41], is now regarded as a variant of epithelioid hemangioma (Andrew Rosenberg, personal communication). Our experience with four patients is in accordance with published data that this lesion is benign and a variant of epithelioid hemangioma.

The term hemangioendothelioma has been applied to tumors of indeterminate behavior, with the prototype being epithelioid hemangioendothelioma. Currently, in the WHO soft tissue section, it is stated that "the behaviour of epithelioid hemangioendothelioma is intermediate between haemangiomas and conventional (high grade) angiosarcomas…" whereas, in the bone section, it is classified as an angiosarcoma [12]. With one exception, epithelioid hemangioendothelioma was the only type of hemangioendothelioma encountered in our series. It has a tendency to be multicentric within an individual osseous element or multifocal (polyostotic), particularly in the same skeletal region. Synchronous involvement of paired bones is common, further confounding the issue of multifocality versus metastasis. Visceral involvement, particularly hepatic and/or pulmonary, may also be present, as noted in our study. Radiographically, they are lytic lesions which may include cortical destruction and extension into soft tissue and joints, but the features are not specific. We observed a hemangioendothelioma that was difficult to characterize, which we designated hemangioendothelioma NOS. The major differential diagnosis is epithelioid hemangioma and epithelioid angiosarcoma. The histopathological features helpful in distinguishing it from epithelioid hemangioma are described above. Epithelioid angiosarcoma has more nuclear pleomorphism, hyperchromasia, and a higher mitotic rate.

The molecular pathogenesis of epithelioid hemangioendothelioma is gradually being unraveled. A t(1;3)(p36.3; q25) translocation has been reported in two epithelioid hemangioendotheliomas [42]. Overexpression of TP53, murine double minute protein, and vascular endothelial growth factor and decrease of caveolin 1 have been observed in one patient with a progressive tumor [43].

Pediatric angiosarcoma of bone has only rarely been reported [44]. It is typically a localized lesion, but, in our series, more than half of the lesions were multicentric within an individual osseous element and/or multifocal (polyostotic). Radiographically, they are destructive lytic lesions with poorly defined borders and may extend into soft tissue. The diagnosis can be challenging given the great variability in their histopathology. The malignant nature of the tumor is usually evident with disorganized architecture, marked cytologic atypia, and frequent mitoses. While vasoformation is usually present, immunopositivity for endothelial markers is helpful or sometimes essential to reach a diagnosis. Angiosarcoma often expresses immuno-

phenotypic markers associated with both blood vascular and lymphatic endothelium [45].

The prognosis of pediatric angiosarcoma is poor, as it is in adults. Our limited follow-up does not permit a definitive statement in this regard: only one patient, who had an intermediate-grade angiosarcoma treated with chemotherapy and radical resection, is a long-term survivor.

Kaposiform lymphangiomatosis has been recently described in an abstract as a provisional entity that mostly affects older children and frequently involves bone, retroperitoneum, mediastinum, lungs, and spleen [46]. Recurrent pleural effusions, progressive multifocal osteolytic lesions, and minor thrombocytopenia dominate the clinical course. Mediastinal, pleural, pericardial, or abdominal hemorrhage can occur and be fatal. Imaging shows a multifocal LM (lymphangiomatosis). The histopathology is also that of multifocal LM with a minor component of small sheets of closely apposed spindled cells with poorly formed or slit-like lumina containing erythrocytes and occasional microthrombi, prominent cytoplasmic and interstitial hemosiderosis, and focal cytoplasmic eosinophilic globules. Kaposiform lymphangiomatosis has a superficial similarity to kaposiform hemangioendothelioma. However, unlike kaposiform hemangioendothelioma, kaposiform lymphangiomatosis is not a single mass; the dominant component is a multifocal LM; the kaposiform component is minimal, is intimately admixed with the lymphatic component, and generally lacks solid growth, lobular architecture, glomeruloid structures, and intersecting fascicles [46]. Additionally, in contrast to kaposiform hemangioendothelioma, older children or adolescents are affected; thrombocytopenia is absent or minor, and a diffuse splenic sinusoidal involvement is characteristic.

Our understanding of kaposiform lymphangiomatosis is incomplete, but the lesion could be provisionally viewed as either an "*ab initio*" disorder or as a multifocal LM that has undergone focal transformation to low-grade neoplasia. It should be emphasized that this is simply a provisional descriptive term for a lesion that needs to be further investigated.

Kaposiform hemangioendothelioma arising in bone has not been reported, although it can secondarily involve bone [47]. A 39-year-old woman with a recently diagnosed cutaneous KHE had a long history of osteolytic lesions in the humerus and radius, but the original diagnosis of the osseous lesions was not stated and the pathology slides were not retrievable for review [48]. Three tumors in our series had histopathologic features similar to kaposiform hemangioendothelioma. Unlike the typical child with kaposiform hemangioendothelioma, these patients were older and only one had thrombocytopenia, albeit minor. Histopathologically, the lobularity in these tumors was minimal and there were no vicinal dilated or malformed lymphatics. It is possible that these morphologic differences are related to the particular milieu of the site of origin. The lesions had features that prompted one to consider spindle cell hemangioma, epithelioid and spindle cell hemangioma, Kaposi sarcoma, and kaposiform lymphangiomatosis in the differential diagnosis. Nevertheless, the clinical findings and the constellation of the histopathological features, including focal immunopositivity for D2-40, are those that characterize kaposiform hemangioendothelioma. Additional studies of similar tumors should help resolve whether these lesions are *bona fide* kaposiform hemangioendothelioma.

Although most osseous lesions in this study were similar to their extraskeletal counterparts, there remained a small heterogeneous group which could not be classified. Some may be known entities with a modified appearance because of the site of origin, while others may be lesions yet to be described.

In summation, a multidisciplinary approach to diagnosis and management of vascular anomalies of bone is crucial, as it is in all bony lesions. Particularly important is radiologic imaging, and, in most malformations, it is characteristic if interpreted by radiologists with experience in this area. Biopsy is usually not required. If there is uncertainty about the nature of the lesion, biopsy might be necessary. Malformations outnumbered tumors with LM and VM being the most common. In the tumor category, hemangioendothelioma and epithelioid hemangioma were the most frequent. We describe kaposiform hemangioendothelioma which has not been reported arising in bone, and expand upon our experience with a lesion that we provisionally termed kaposiform lymphangiomatosis. We also conclude that the standardization of the nomenclature of vascular lesions of bone could be achieved by employing the ISSVA system and its use will facilitate scientific communication and patient management.

Acknowledgments We are indebted to the technical staff of the Department of Pathology of Children's Hospital Boston and the Institute of Pathology, University Hospital Basel for performance of immunohistochemistry and coordinators of the Vascular Anomalies Center of the Children's Hospital Boston. We thank Thomas Schuerch and Jan Schwegler for scanning radiographs and whole mount sections and for help with the digital imaging. Above all, we are grateful to Petra Huber of the Basel Bone Tumor Reference Center for her invaluable assistance in retrieval of slides, clinical charts, and radiographic documentation.
We declare that we have no conflict of interest

References

1. Fechner RE, Mills SE (1993) Tumors of the bones and joints. Atlas of tumor pathology. Armed Forces Institute of Pathology Washington DC 1993
2. Dorfman HD, Czerniac B (1998) Bone tumors. Mosby, St. Louis 1998
3. Unni KK (1996) Dahlin's bone tumors. General aspects and data on 11,087 cases. Lippincott Raven, Philadelphia 1996

4. Schmorl G, Junghanns H (1959) The human spine in health and disease. Grune & Stratton, New York 1959
5. Enjolras O, Mulliken JB (1997) Vascular tumors and vascular malformations (new issues). Adv Dermatol 13:375–423
6. Bruder E, Kozakewich H (2004) Skeletal vascular lesions in childhood and adolescence. Pathologe 25:311–316
7. Frick H, Leonhardt H, Starck D (1992) Allgemeine anatomie, spezielle anatomy I. Extremitaeten-Rumpfwand. Thieme, Stuttgart 1992
8. Standring S, Ellis H, Healey JC et al (2005) Gray's anatomy. Elsevier Churchill Livingstone, Edinburgh
9. Lawley LP, Cerimele F, Weiss SW et al (2005) Expression of Wilms tumor 1 gene distinguishes vascular malformations from proliferative endothelial lesions. Arch Dermatol 141:1297–1300
10. Nascimento AG, Keeney GL, Sciot R et al (1997) Polymorphous hemangioendothelioma: a report of two cases, one affecting extranodal soft tissues, and review of the literature. Am J Surg Pathol 21:1083–1089
11. Enjolras O, Mulliken JB, Boon LM et al (2001) Noninvoluting congenital hemangioma: a rare cutaneous vascular anomaly. Plast Reconstr Surg 107:1647–1654
12. Fletcher CD, Unni KK, Mertens F (2002) World Health Organization classification of tumours. Pathology and genetics of tumours of soft tissue and bone. IARC Press, Lyon 2002
13. Mirra JM, Picci B, Gold RH (1989) Bone tumors. Clinical, radiologic and pathologic correlations. Lea & Febiger, Philadelphia 1989
14. Mulliken JB, Fishman SJ, Burrows PE (2000) Vascular anomalies. Curr Probl Surg 37:517–584
15. Meijer-Jorna LB, van der Loos CM, de Boer OJ et al (2007) Microvascular proliferation in congenital vascular malformations of skin and soft tissue. J Clin Pathol 60:798–803
16. Sure U, Butz N, Schlegel J et al (2001) Endothelial proliferation, neoangiogenesis, and potential de novo generation of cerebrovascular malformations. J Neurosurg 94:972–977
17. Sure U, Freman S, Bozinov O et al (2005) Biological activity of adult cavernous malformations: a study of 56 patients. J Neurosurg 102:342–347
18. Jaffe HL (1958) Tumors and tumorous conditions of bones and joints. Lea & Febiger, Philadelphia 1958
19. Huvos AG (1991) Bone tumors: diagnosis, treatment and prognosis. Saunders, Philadelphia 1991
20. Greene AK, Rogers GF, Mulliken JB (2007) Intraosseous "hemangiomas" are malformations and not tumors. Plast Reconstr Surg 119:1949–1950
21. Chen L, Zhang CL, Tang TS (2007) Cement vertebroplasty combined with ethanol injection in the treatment of vertebral hemangioma. Chin Med J (Engl) 120:1136–1139
22. Doppman JL, Oldfield EH, Heiss JD (2000) Symptomatic vertebral hemangiomas: treatment by means of direct intralesional injection of ethanol. Radiology 214:341–348
23. Giaoui L, Princ G, Chiras J et al (2003) Treatment of vascular malformations of the mandible: a description of 12 cases. Int J Oral Maxillofac Surg 32:132–136
24. Goyal M, Mishra NK, Sharma A et al (1999) Alcohol ablation of symptomatic vertebral hemangiomas. AJNR Am J Neuroradiol 20:1091–1096
25. Persky MS, Yoo HJ, Berenstein A (2003) Management of vascular malformations of the mandible and maxilla. Laryngoscope 113:1885–1892
26. Casanova D, Boon LM, Vikkula M (2006) Venous malformations: clinical characteristics and differential diagnosis. Ann Chir Plast Esthet 51:373–387
27. Maffucci AM (1881) Di un caso di encondroma ed angioma multiplo. Contribuzione alla genesi embrionale dei tumori. Mov Med Chir Napoli 13:399–412
28. North PE, Waner M, Mizeracki A et al (2000) GLUT1: a newly discovered immunohistochemical marker for juvenile hemangiomas. Hum Pathol 31:11–22
29. Koulouris G, Rao P (2005) Multiple congenital cranial hemangiomas. Skeletal Radiol 34:485–489
30. Vikkula M, Boon LM, Mulliken JB (2001) Molecular genetics of vascular malformations. Matrix Biol 20:327–335
31. Flores-Vargas A, Vargas SO, Debelenko LV et al (2008) Comparative analysis of D2-40 and LYVE-1 immunostaining in lymphatic malformations. Lymphology 41:103–110
32. Hirakawa S, Detmar M (2004) New insights into the biology and pathology of the cutaneous lymphatic system. J Dermatol Sci 35:1–8
33. Coley BL (1949) Neoplasms of bone and related conditions. Their etiology, pathogenesis, diagnosis and treatment. Paul B. Hoeber, New York 1949
34. Gorham LW, Stout AP (1955) Massive osteolysis (acute spontaneous absorption of bone, phantom bone, disappearing bone); its relation to hemangiomatosis. J Bone Joint Surg Am 37-A:985–1004
35. Gorham LW, Wright AW, Shultz HH et al (1954) Disappearing bones: a rare form of massive osteolysis; report of two cases, one with autopsy findings. Am J Med 17:674–682
36. Colucci S, Taraboletti G, Primo L et al (2006) Gorham-Stout syndrome: a monocyte-mediated cytokine propelled disease. J Bone Miner Res 21:207–218
37. Hirayama T, Sabokbar A, Itonaga I et al (2001) Cellular and humoral mechanisms of osteoclast formation and bone resorption in Gorham-Stout disease. J Pathol 195:624–630
38. O'Connell JX, Kattapuram SV, Mankin HJ et al (1993) Epithelioid hemangioma of bone. A tumor often mistaken for low-grade angiosarcoma or malignant hemangioendothelioma. Am J Surg Pathol 17:610–617
39. Evans HL, Raymond AK, Ayala AG (2003) Vascular tumors of bone: a study of 17 cases other than ordinary hemangioma, with an evaluation of the relationship of hemangioendothelioma of bone to epithelioid hemangioma, epithelioid hemangioendothelioma, and high-grade angiosarcoma. Hum Pathol 34:680–689
40. O'Connell JX, Nielsen GP, Rosenberg AE (2001) Epithelioid vascular tumors of bone: a review and proposal of a classification scheme. Adv Anat Pathol 8:74–82
41. Keel SB, Rosenberg AE (1999) Hemorrhagic epithelioid and spindle cell hemangioma: a newly recognized, unique vascular tumor of bone. Cancer 85:1966–1972
42. Mendlick MR, Nelson M, Pickering D et al (2001) Translocation t (1;3)(p36.3;q25) is a nonrandom aberration in epithelioid hemangioendothelioma. Am J Surg Pathol 25:684–687
43. Theurillat JP, Vavricka SR, Went P et al (2003) Morphologic changes and altered gene expression in an epithelioid hemangioendothelioma during a ten-year course of disease. Pathol Res Pract 199:165–170
44. Lezama-del Valle P, Gerald WL, Tsai J et al (1998) Malignant vascular tumors in young patients. Cancer 83:1634–1639
45. Folpe AL, Veikkola T, Valtola R et al (2000) Vascular endothelial growth factor receptor-3 (VEGFR-3): a marker of vascular tumors with presumed lymphatic differentiation, including Kaposi's sarcoma, kaposiform and Dabska-type hemangioendotheliomas, and a subset of angiosarcomas. Mod Pathol 13:180–185
46. Debelenko LV, Marler JJ, Perez-Atayde AR et al (Abstract) (2004) Kaposiform lymphangiomatosis: an aggressive variant of lymphangiomatosis. Mod Pathol 17:267
47. Zukerberg LR, Nickoloff BJ, Weiss SW (1993) Kaposiform hemangioendothelioma of infancy and childhood. An aggressive neoplasm associated with Kasabach-Merritt syndrome and lymphangiomatosis. Am J Surg Pathol 17:321–328
48. Mac-Moune Lai F, To KF, Choi PC et al (2001) Kaposiform hemangioendothelioma: five patients with cutaneous lesion and long follow-up. Mod Pathol 14:1087–1092

Virchows Arch (2009) 454:181–188
DOI 10.1007/s00428-008-0722-6

ORIGINAL ARTICLE

Active neovascularization and possible vascular-centric development of gastric and periscapular elastofibromas

Keita Kai · Kenichiro Kusano · Masashi Sakai · Masanobu Tabuchi · Seiji Yunotani · Kohji Miyazaki · Osamu Tokunaga

Received: 3 September 2008 / Revised: 9 November 2008 / Accepted: 16 December 2008 / Published online: 9 January 2009

Abstract An elastofibroma is a benign and rare fibrous lesion that most commonly occurs in the periscapular region. A gastrointestinal elastofibroma is extremely rare. In the present study, six cases of elastofibromas including a case in the stomach were evaluated. The gastric case revealed widely distributed lesions in the submucosal layer with perivascular fibrotic lesions (PVFLs) and some PVFLs were distributed to the skip lesions of elastofibroma. These PVFLs were also observed in all five periscapular cases and invariably contained elastic fibers which showed various degree of maturation. CD34-positive stromal cells were observed not only in elastofibromas but also in PVFLs in each case. These findings suggested the possibility of the PVFLs were the primary lesions of elastofibroma and their vascular-centric development. The percentage of the CD105-positive vessels in elastofibroma group was significantly higher than in the control group. This result indicates active neovascularization in elastofibromas.

K. Kai (✉) · K. Kusano · O. Tokunaga
Department of Pathology and Biodefense,
Saga University Faculty of Medicine,
Nabesima 5-1-1,
Saga city, Saga 849-8501, Japan
e-mail: kaikeit@cc.saga-u.ac.jp

M. Sakai · M. Tabuchi · S. Yunotani
Department of Surgery, Karatsu Red Cross Hospital,
Saga, Japan

K. Kai · K. Miyazaki
Department of Surgery, Saga University Faculty of Medicine,
Nabesima 5-1-1,
Saga city, Saga 849-8501, Japan

Keywords Elastofibroma · Stomach · Amyloidosis · CD34 · CD105 · Quantitative double-fluorescence immunohistochemistry (qDFIHC)

Introduction

An elastofibroma is a benign and rare lesion first described by Järvi and Saxén [1] as "Elastofibroma dorsi" in 1961. The abnormal elastic fibers display a beaded, globular, or serrated appearance with a large amount of collagen and usually arise in the periscapular region of elderly individuals [2]. These elastinophilic fibers are immunohistochemically [3] and biochemically different from normal elastic fibers [4]. This lesion was thought to arise from the elastotic degeneration of collagen fibers or a degenerative change of elastic fibers themselves in the past [5, 6]. However, there is the evidence, such as familial history [7], multiple cases [8], clonal chromosomal aberrations, and chromosome instability [9–11], suggesting a neoplastic process. Ultrastructural studies show that stromal spindle cells appear to synthesize the collagen and elastic fibers [12–14] and these cells are frequently CD34 positive [3, 10, 15]. No conclusive evidence has been presented to define the histogenesis of this lesion.

A gastrointestinal elastofibroma is extremely rare. Only two stomach cases [16, 17] and several colorectal cases [18–20] have been reported. Interestingly, some of these lesions were associated with perivascular pseudo-amyloidosis [17, 18, 20]. Bilateral subscapular elastofibromas were lately found in one gastric case [16].

In the present study, an extremely rare case of gastric elastofibroma with perivascular fibrotic lesions (PVFLs) was documented. To pursue the histogenesis of elastofibromas,

an additional five cases of periscapular elastofibroma and control cases were analyzed pathologically.

Transforming growth factor beta 1 (TGFβ-1) activates the mitogen-activated protein kinase kinase 3 (MKK3)-p38 mitogen-activated protein kinase signaling cascade, thus leading to the induction of type I collagen synthesis [21, 22]. To elucidate the fibrotic process of elastofibromas, the expression of TGFβ-1 and transforming growth factor beta receptor 2 (TGFβR-2) in stromal cells were assessed by quantitative double-fluorescence immunohistochemistry (qDFIHC) [23].

Endoglin (CD105) is a receptor for TGFβ-1 which modulates TGFβ signaling by interacting with TGFβR-2. CD105 is predominantly expressed on cellular lineages within the vascular system and is overexpressed on proliferating endothelial cells. Therefore, CD105 is considered to be a powerful marker of neovascularization [24–27]. To examine the neovascularization status in elastofibromas, the ratio of CD105-positive vessels was assessed by immunohistochemistry and the expression of CD105 in stromal cells was also assessed by qDFIHC.

Material and methods

Sample collection and preparation

Five cases of subscapular elastofibroma, including three bilateral cases, surgically treated and pathologically diagnosed at the Saga University and one case of gastric elastofibromas surgically treated at Karatsu Red Cross Hospital and pathologically diagnosed at Saga University were included in this study. The control skin specimens were obtained from three cases of resected breast cancer samples without skin invasion. Formalin-fixed and paraffin-embedded specimens were prepared and 4-μm sections were cut for hematoxylin and eosin (HE) staining, Weigert's elastic stain counterstained with van Giessen technique (EVG), Congo red stain, and immunohistochemical staining.

Immunohistochemical staining

The primary antibodies used and antigen retrieval conditions are summarized in Table 1. The Envision+® System (Dako Cytomation) was used as the second antibody. The slides were visualized by diaminobenzidine tetrahydrochloride and the nuclei were counterstained with hematoxylin. To contrast the elastic fibers, some slides were double-counterstained with hematoxylin and Victoria blue.

The results were judged by the rate of positively stained stromal cells. When the rate of positive cells were less than 10%, more than 10%, more than 50%, and more than 80%, the result was judged as negative (−), weak (+), moderate (++), and strong (+++), respectively. If the immunoreactivity was too weak to evaluate, then the sample was judged to be faintly positive (+/−). The CD105-positive vessel rate was evaluated by judging 100 vessels in each stained sample.

Electron microscopy

An ultrastructural study was performed only in the stomach case. The elastic fiber was stained by tannic acid. For electron microscopy, samples were fixed with 2.5% glutaraldehyde in phosphate-buffered saline. Samples were postfixed in 1% osmium tetroxide in cacodylate buffer (pH 7.4) for 2 h at 4°C and embedded in Epon 812. Ultrathin sections were stained with uranyl acetate and tannic acid and then stained by lead citrate. The samples were examined by transmission electron microscopy (JEM 1210, Japan Electron Optics Laboratory, Tokyo, Japan).

Table 1 The primary antibodies and antigen retrieval conditions

Antibody	Dilution	Clone	Pretreatment	Company
Vimentin	1:30	Mono	MW-CB	Dako Cytomation
S-100	Prediluted	Poly	None	Dako Cytomation
α-SMA	1:200	Mono	MW-EDTA	Dako Cytomation
Desmin	1:50	Mono	MW-EDTA	Dako Cytomation
Ki-67	1:50	Mono	MW-EDTA	Beckman coulter
CD34	1:50	Mono	MW-EDTA	Novocastra
c-KIT	1:30	Poly	None	Dako Cytomation
TGFβ-1	1:50	Poly	MW-EDTA	Santa Cruz
TGFβR-2	1:100	Poly	MW-EDTA	Santa Cruz
CD105	1:50	Mono	MW-EDTA	Novocastra
CD31	1:30	Mono	Proteinase K	Dako Cytomation

MW-EDTA microwave in ethylenediaminetetraacetic acid, *MW-CB* microwave in citrate buffer

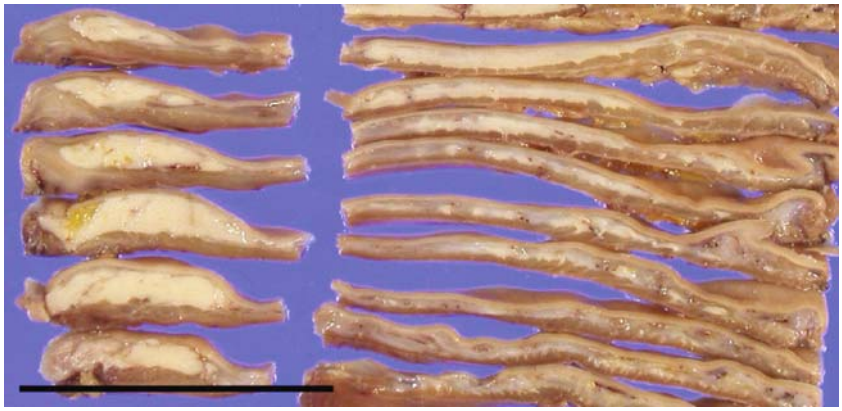

Fig. 1 The serial sections of the gastric lesion. The submucosa is widely thickened with yellowish and rubbery changes. *Bar*=5 cm

Quantitative double-fluorescence Immunohistochemistry

Each sample was triple-stained for target proteins (TGFβ-1, TGFβR-2, and CD105), β-actin, and vimentin. The staining of vimentin was added to recognize the stromal cells. The primary antibodies and staining conditions against TGFβ-1, TGFβR-2, CD105, and vimentin were the same of immunohistochemistry staining. The secondary antibodies used were fluorescein isothiocyanate isomer 1 (FITC)-conjugated anti-rabbit IgG (Dako Cytomation,

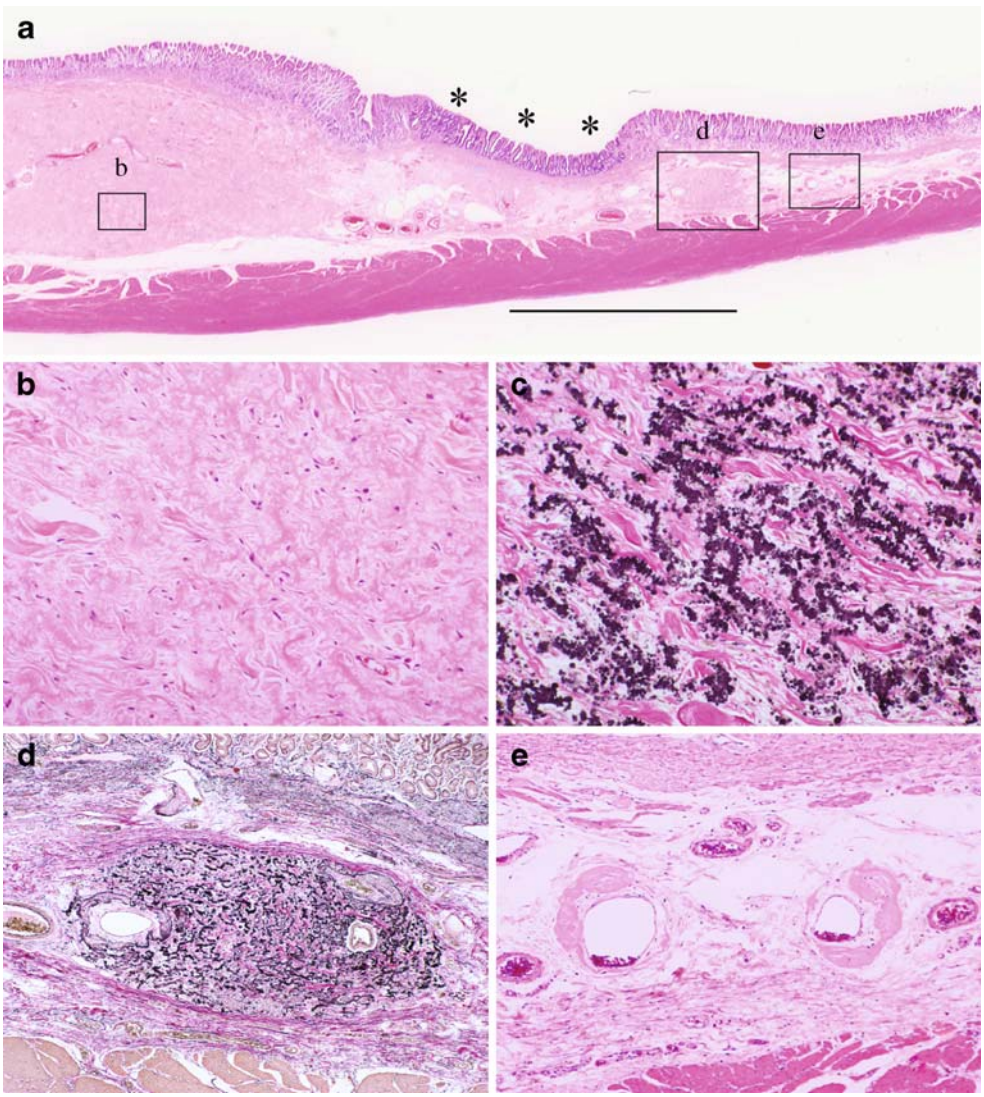

Fig. 2 **a** Low magnification shows a dense fibrotic lesion in the submucosal layer of the antrum and this lesion skipped discontinuously. The *letters above* each *panel* correspond to the following figures. The depressed area is a cancerous lesion (*asterisks*). *Bar*=5 mm. **b** The thickened submucosa consisted of connective tissue with scattered spindle cells, collagen bundles, and numerous eosinophilic serpiginous fibers (HE, original magnification ×100). **c** EVG staining of **b**. Numerous mature elastic fibers with dense cores and serrated edges or linearly arranged globules are observed (original magnification × 100). **d** The characteristic structures of an elastofibroma are also observed in the skipped lesions (EVG staining, original magnification ×40). **e** The PVFLs with hyalinization are observed on the surrounding vessels (HE, original magnification ×40)

dilution 1:100) for TGFβ-1 and TGFβR-2, the FITC-conjugated anti-mouse IgG (ZYMED, dilution 1:100) for CD105, and the Cy5-conjugated anti-mouse IgG (CHEMICON, dilution 1:100) for vimentin.

The Cy3-conjugated anti-mouse IgG (CHEMICON, dilution 1:100) and the Cy3-conjugated anti-rabbit IgG (CHEMICON, dilution 1:100) were used as the second antibodies for mouse monoclonal anti-β-actin antibody (SIGMA, dilution 1:500) for TGFβ-1 and TGFβR-2 and rabbit polyclonal anti-β-actin antibody (Gene Tex, prediluted) for CD105, respectively. Each primary and second antibody reaction was carried out at room temperature for 2 h and for 30 min, respectively.

The digital images were acquired on a confocal Laser Scanning Microscope LSM5 Pascal (Carl Zeiss Micro-imaging, Jena Germany) at ×600 magnification. To quantify the stromal-cell-specific expression, original image was cut to contain only the stromal cells. The fluorescent signals of cut images were analyzed with "LSM Image Examiner" attached software in the LSM system as previously described [23]. The ratio of the total fluorescence intensity of the target proteins to β-actin (target protein/β-actin) was determined. The 30 stromal cells in each sample were analyzed and the average score of target protein/β-actin was determined to quantify the expression.

Statistical analysis

A statistical analysis was performed using the JMP software program version 5.1 (SAS Institute, Cary, NC, USA). The Kruskal–Wallis test was used to compare the elastofibroma and control groups. A p value of less than 0.05 indicated a statistically significant difference.

Results

Clinical summary of the gastric elastofibroma

A 77-year-old Japanese female was admitted to the Karatsu Red Cross Hospital for the treatment of early gastric cancer found by screening gastroscopy. She had no symptoms and a biopsy specimen showed tubular adenocarcinoma. The physical examination on admission revealed no subcutaneous mass lesion including the periscapular area. A partial gastrectomy with lymph node dissection was performed.

Macroscopic findings of the gastric elastofibroma

An irregular-edged depressed lesion that measured 8×8 mm in diameter was found in the lesser curvature of the antrum. A thickening of the submucosa with yellowish and rubbery changes was widely found in the serial tissue sections (Fig. 1).

Microscopic findings of the gastric elastofibroma

At low magnification, the specimen appeared to contain a dense fibrotic lesion in the submucosal layer of the antrum with skipped lesions (Fig. 2a). A tubular adenocarcinoma was found in the mucosa. The thickened submucosa contained scattered spindle cells, collagen bundles, and numerous eosinophilic, deeply stained, serpiginous fibers (Fig. 2b). EVG outlined these fibers to have a dense core and the margins were serrated or linearly arranged globules, resembling beads on a string (Fig. 2c) and these findings led the diagnosis of a gastric elastofibroma. Elastofibroma-like structures were also observed in the skipped lesions (Fig. 2d). Amyloid-like fibrotic lesions were observed on surrounding vessels (Fig. 2e), but these lesions were not stained by Congo red. These unique lesions were termed

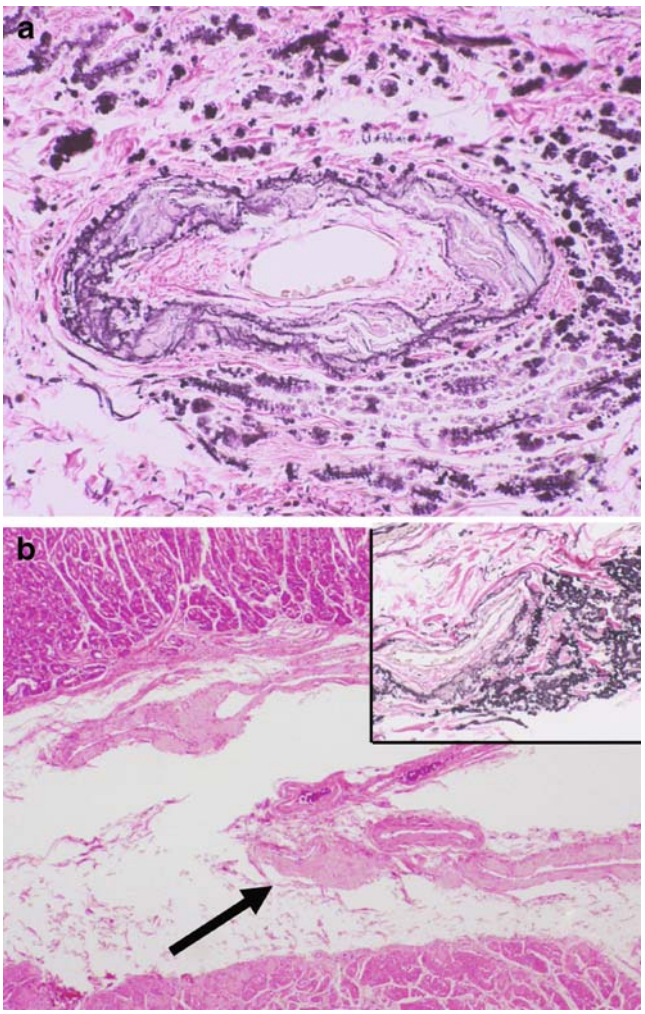

Fig. 3 **a** The PVFLs were distributed to the skip lesions of an elastofibroma. Immature and mature elastic fibers are observed (EVG staining, original magnification ×100). **b** The tiny PVFLs which are isolated from the main lesion of elastofibroma (*arrow*; original magnification ×40). *Inset* is EVG staining (original magnification ×100)

PVFLs. The PVFLs sometimes showed hyalinization. The PVFLs were observed at vessel walls and they were more dominant in veins than in arteries. Some PVFLs were distributed to the skip lesions of the elastofibroma and showed a composite of immature and mature elastic fibers (Fig. 3a), thus suggesting the skipped elastofibromatous lesions to have arisen from PVFLs. The abnormal elastic fibers were observed by EVG staining even in the tiny PVFLs which were completely isolated from the elastofibroma and could not be recognized macroscopically (Fig. 3b).

The evaluation of CD34-positive stromal cells and the ultrastructural findings of gastric elastofibroma

The elastofibroma lesion contained many CD34-positive stromal cells. These CD34-positive cells sometimes exhibited elastic-fiber-mediated synapse-like structures with other cells (Fig. 4a). CD34-positive cells were also observed in the PVFLs (Fig. 4b).

Transmission electron microscopy revealed that both the elastin and collagen fibers were closely associated with the spindle-shaped stromal cells (Fig. 4c). The small clusters of elastin and globules of collagen fibers were closely attached to the plasma membrane. The stromal spindle cells had a long tail and sometimes formed elastic-fiber-mediated synapse-like structure with other cells (Fig. 4d).

The microscopic findings and the evaluation of CD34-positive stromal cells of the periscapular elastofibromas

The other five specimens were from subscapular lesions including three bilateral lesions. The abnormal granular elastic fibers characteristic of elastofibromas were observed in each specimen by HE and EVG. Interestingly, PVFLs and perivascular hyalinization were observed either continuously or discontinuously to the elastofibromas in all cases. Abnormal elastic fibers showing various degrees of maturation were observed in each PVFL (Fig. 5a). Interspread spindle or stellate-shaped CD34-positive stromal cells were observed in all cases. These CD34-positive cells and synapse-like structures were also observed in PVFLs of the periscapular elastofibromas (Fig. 5b).

Immunohistochemical comparison between the elastofibromas and controls

The immunohistochemical analysis of the stromal cells included vimentin, S-100, alpha smooth muscle actin, desmin, Ki-67, CD34, c-KIT, TGFβ-1, TGFβR-2, CD105, and CD31. Elastofibromas were compared to controls. These data are summarized in Table 2. There was no remarkable difference between the two groups except for a slight difference in the S-100 expression. The TGFβ-1 and

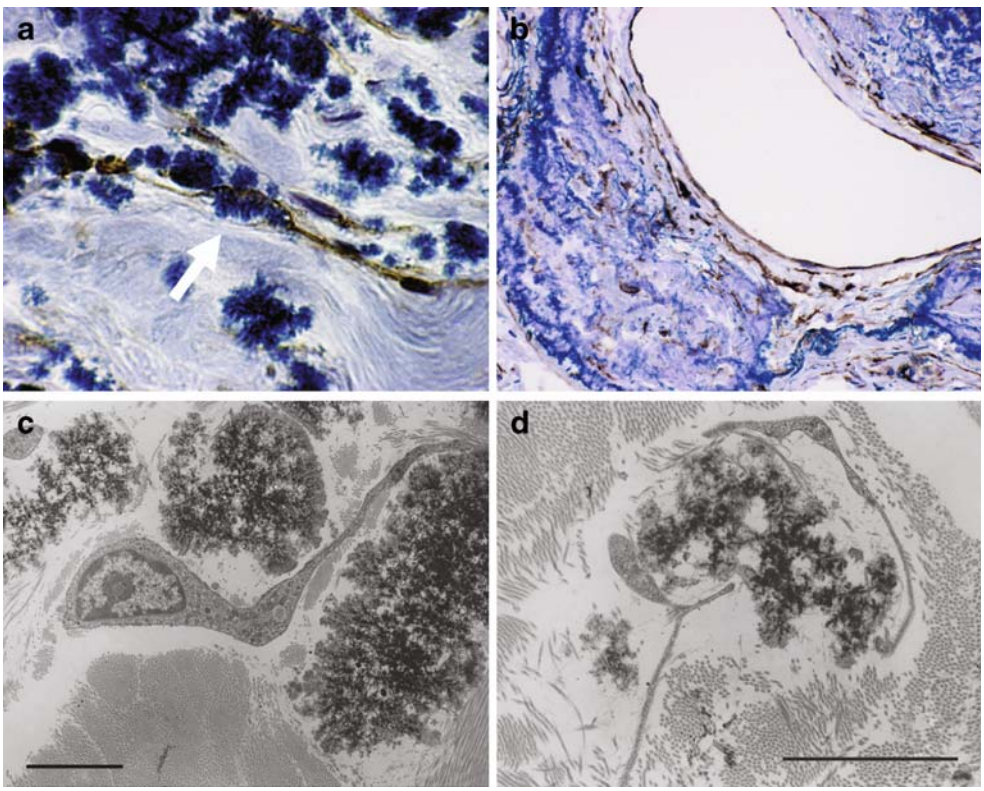

Fig. 4 **a** Immunohistochemistry of CD34, double-counterstained with hematoxylin and Victoria blue (**a**, **b**). CD34-positive cells sometimes reveal elastic-fiber-mediated synapse-like structures with other cells (original magnification ×1,000). **b** The PVFLs containing relatively mature elastic fibers. CD34-positive spindle cells are also observed (original magnification × 200). **c** Transmission electron microscopy (**c**, **d**). Both the elastin and collagen fibers were closely associated with the spindle-shaped stromal cells (original magnification ×4,000, *bar*=10 μm). **d** The tail end of some spindle cells formed elastic-fiber-mediated synapse-like structures with other cells (original magnification ×10,000, *bar*=5 μm)

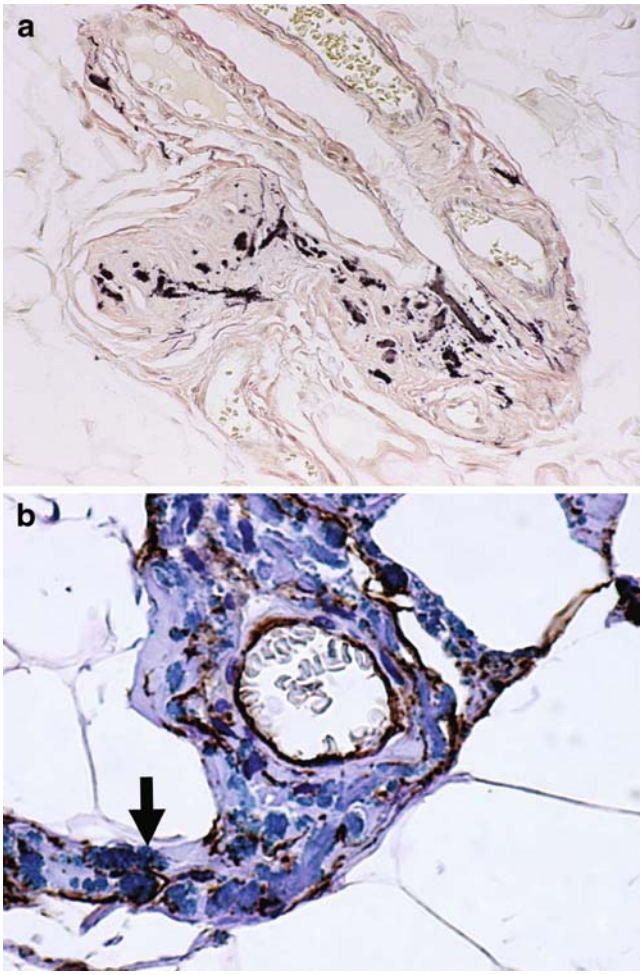

Fig. 5 **a** The PVFLs in case 2 of Table 2. Abnormal elastic fibers without organized structure are observed (EVG staining, original magnification ×200). **b** Immunohistochemistry of CD34, double-counterstained with hematoxylin and Victoria blue of the case 6 on Table 2. The PVFLs contain both the CD34-positive stromal cells and abnormal elastic fibers and a synapse-like structure (*arrow*) can be observed (original magnification ×200)

TGFβR-2 expression in the elastofibroma group appeared to be higher than in the control group, but the difference was not significant.

The TGFβ-1, TGFβR-2, and CD105 expression evaluated by qDFIHC between elastofibromas and controls

To make a definite comparison of TGFβ-1, TGFβR-2, and CD105 between the elastofibromas and the controls, a qDFIHC analysis was performed. The triple-stained picture, the cut picture by vimentin-positive spindle cell, and the analyzing status are demonstrated in Fig. 6a, b, respectively. The evaluated mean ± standard deviation (SD) of TGFβ-1/β-actin was 1.09±0.14 in elastofibromas and 1.02±0.09 in controls. The TGFβR-2/β-actin was 1.57±0.15 in elastofibromas and 1.58±0.04 in controls. There was no difference in the mean values for TGFβ-1 and TGFβR-2 between elastofibromas and controls (P=0.605 and P=0.518, respectively). The CD105/β-actin ratios were 1.82±0.27 in elastofibromas and 1.46±0.04 in controls. The mean value of the elastofibroma group was higher than the control group, but there was no statistically significant difference (P=0.12).

The proportion of CD105-positive vessels in elastofibromas and controls

CD105-positive vessels were predominant in elastofibromas (Fig. 7a) whereas they were a minority in control cases. The proportion of positive (mean ± SD) vessels was 78.7±6.6% in the elastofibroma group and 13.3±6.8% in control group (Fig. 7b). There was a significant difference between the two groups (P=0.02). The positive proportion of positive vessels of the control skin was almost the same as previously described by Minhajat et al. [25].

Discussion

The gastric elastofibroma revealed a widely distributed lesion in the submucosal layer. The notable features of this case were the presence of skip lesions and PVFLs. Most of the elastic fibers in main lesion were mature showing an organized structure whereas the elastic fibers in PVFLs showed various degrees of maturation. Some PVFLs were distributed to the skip lesions of the elastofibroma and showed a composite of immature and mature elastic fibers. The PVFLs were also found in all the cases of periscapular elastofibroma. Some of them were isolated from the main lesion and the elastic fibers also revealed various degree of maturation. These findings suggest the possibility that the PVFLs are the primary lesions of elastofibromas and that possibility is supported by the vascular-centric development of elastofibromas.

The stromal spindle cells seem to synthesize both the elastic and collagen fibers as described in several previous reports [10, 12–15]. Some of the stromal cells showed a synapse-like structure as if they communicate using the elastic material as a mediator. This is the characteristic morphology, but there is insufficient evidence to explain this phenomenon.

It therefore appears to be difficult to explain the existence of PVFLs and skip lesions based on the neoplastic development theory alone. In addition, neither mitosis nor Ki-67-positive stromal cells were observed in either the present study or previously reported investigations [15]. We therefore hypothesized that some types of elastofibroma-specific differentiation of the stromal cells

Table 2 The pathologic and immunohistochemical features of the elastofibromas and controls

	Case 1	Case 2	Case 3	Case 4	Case 5	Case 6	Cont. 1	Cont. 2	Cont. 3
Location	Stomach	Unilateral SSL	Bilateral SSL	Bilateral SSL	Bilateral SSL	Unilateral SSL	Lt. breast	Rt. breast	Rt. breast
Presence of PVFL	Yes	Yes	Yes	Yes	Yes	Yes	No	No	No
AEF in PVFL	Present	Present	Present	Present	Present	Present	NA	NA	NA
IHC									
Vimentin	+++	+++	+++	+++	+++	+++	+++	+++	+++
S-100	−	−	−	−	−	−	−	+	+
α-SMA	−	−	−	−	−	−	−	−	−
Desmin	+	+	+	+/−	+	+	+	+	+
Ki-67	−	−	−	−	−	−	−	−	−
CD34	++	+++	++	++	++	++	+++	+++	+++
c-KIT	−	+	+	+	++	+	+	+	+
TGFβ-1	+	++	+	+	++	++	+	+	+
TGFβR-2	+	+++	+	+	+++	++	+	+	+
CD105	+/−	+/−	+/−	+/−	+/−	+/−	+/−	+/−	+/−
CD31	−	−	−	−	−	−	−	−	−

PVFL perivascular fibrotic lesion, *SSL* subscapular lesion, *AEF* abnormal elastic fiber, *IHC* immunohistochemistry, *α-SMA* alpha smooth muscle actin, *NA* not available, − negative, +/− faint, + weak, ++ moderate, +++ strong

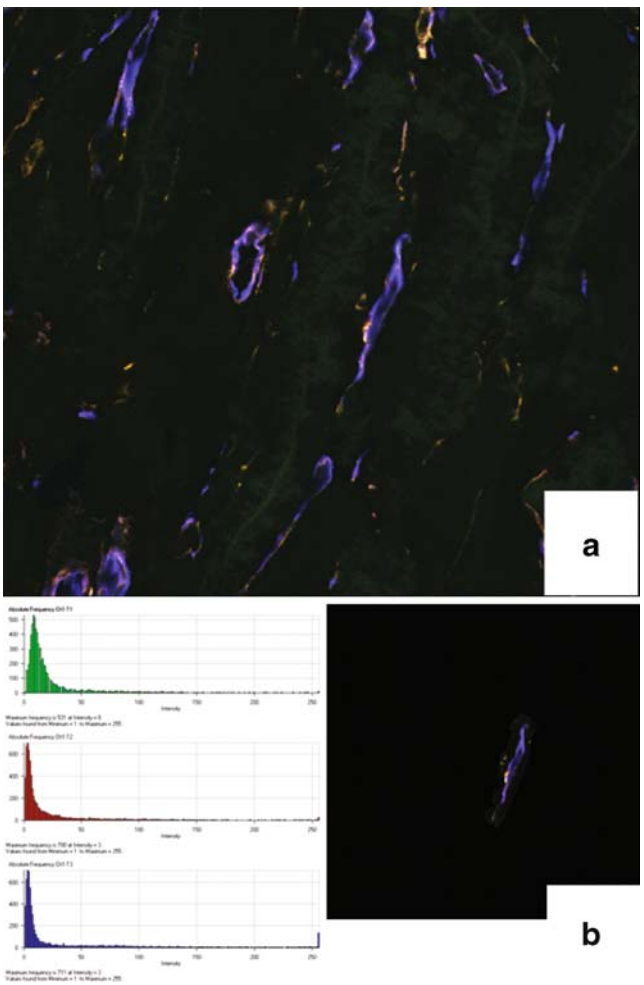

Fig. 6 **a** Merged image of triple staining with TGFβ-1 (*green*), β-actin (*red*), and vimentin (*blue*) for qDFIHC. **b** *Right side*; the cut picture (**a**) by vimentin-positive spindle-shaped stromal cell. *Left side*; analyzing status of the fluorescent signals. The ratio of the total fluorescence intensity of the target proteins to β-actin is the quantification value

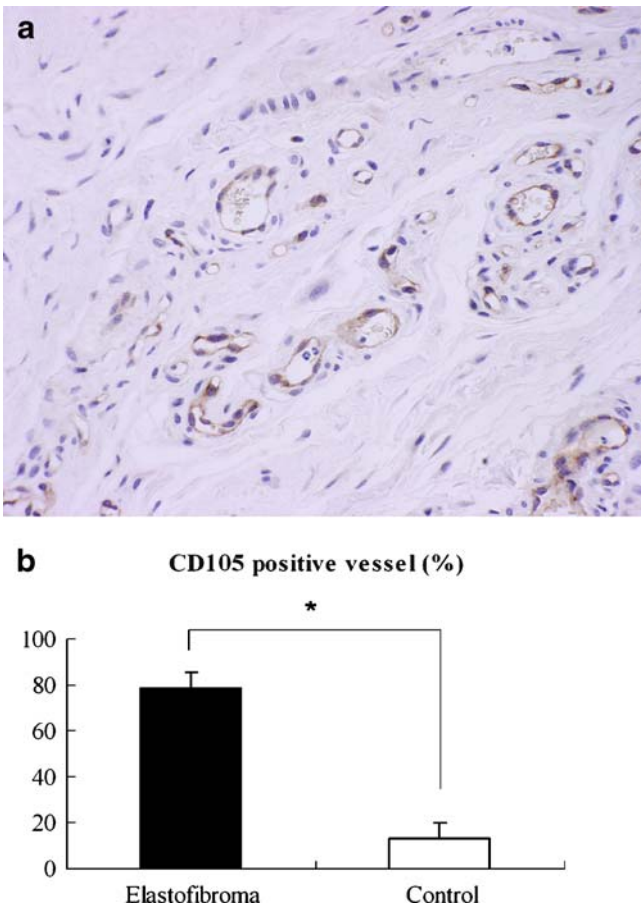

Fig. 7 **a** The immunohistochemical staining of CD105 in an elastofibroma (case2 of Table 2). The majority of vessels are positively stained by CD105. **b** The CD105-positive rate (mean ± SD) of the vessels. The positive rate is 78.7±6.6% in elastofibromas whereas 13.3±6.8% in controls (P=0.02)

might play an important role in the development of such elastofibromas.

To elucidate such elastofibroma-specific differentiation of the stromal cells, first, an immunohistochemical analysis of myogenic and neurogenic markers was performed, but there was no remarkable difference except for a slight difference in the S-100 expression, as observed in other reports [10, 18, 28]. Second, to assess the collagen production ability of stromal cells, TGFβ-1, TGFβR-2, and CD105 expression were analyzed by qDFIHC. Both the TGFβ-1 and TGFβR-2 expression level in the stromal cell were identical between the elastofibroma group and the control group. Although the CD105 expression in the stromal cells of the elastofibroma group was higher than that in the control group, there was no statistical significance. This result indicates that the fibrotic process of elastofibromas does not depend on the TGFβ signaling cascade. Third, to investigate the neovascularization status, the CD105 expression in the blood vessels was analyzed. The percentage of CD105-positive blood vessels in the elastofibroma group was significantly higher than that in the control group. This result indicates the presence of active neovascularization in elastofibromas.

In conclusion, a rare case of a gastric elastofibroma was observed. The results of this study suggest the vascular-centric development and active neovascularization of an elastofibroma.

Acknowledgements We would like to thank Mr. F. Mutoh and Mr. S. Nakahara for their valuable contributions to the immunohistochemical and ultrastructural studies.

Conflict of interest statement We declare that we have no conflict of interest.

References

1. Järvi OH, Saxén AE (1961) Elastofibroma dorse. Acta Pathol Microbiol Scand Suppl 51(Suppl 144):83–84
2. Kempson RL, Fletcher CD, Evans HL et al (2001) Atlas of tumor pathology tumors of the soft tissues. Armed forces Institute of Pathology, Washington, DC, pp 45–47
3. Fukuda Y, Miyake H, Masuda Y et al (1987) Histogenesis of unique elastinophilic fibers of elastofibroma: ultrastructural and immunohistochemical studies. Hum Pathol 18:424–429
4. Nakamura Y, Okamoto K, Tanimura A et al (1986) Elastase digestion and biochemical analysis of the elastin from an elastofibroma. Cancer 58:1070–1075
5. Järvi OH, Saxén AE, Hopsu-Havu VK, Wartiovaara JJ, Vaissalo VT (1969) Elastofibroma—a degenerative pseudotumor. Cancer 23:42–63
6. Stemmermann GN, Stout AP (1962) Elastofibroma dorsi. Am J Clin Pathol 37:499–506
7. Nagamine N, Nohara Y, Ito E (1982) Elastofibroma in Okinawa. A clinicopathologic study of 170 cases. Cancer 50:1794–1805
8. Machens HG, Mechtersheimer R, Göhring U et al (1992) Bilateral elastofibroma dorsi. Ann Thorac Surg 54:774–776
9. Batstone P, Forsyth L, Goodlad J (2001) Clonal chromosome aberrations secondary to chromosome instability in an elastofibroma. Cancer Genet Cytogenet 128:46–47
10. Hisaoka M, Hashimoto H (2006) Elastofibroma: clonal fibrous proliferation with predominant CD34-positive cells. Virchows Arch 448:195–199
11. McComb EN, Feely MG, Neff JR et al (2001) Cytogenetic instability, predominantly involving chromosome 1, is characteristic of elastofibroma. Cancer Genet Cytogenet 126:68–72
12. Dixon AY, Lee SH (1980) An ultrastructural study of elastofibromas. Hum Pathol 11:257–262
13. Kindblom LG, Spicer SS (1982) Elastofibroma. A correlated light and electron microscopic study. Virchows Arch 396:127–140
14. Winkelmann RK, Sams WM Jr (1969) Elastofibroma. Report of a case with special histochemical and electron-microscopic studies. Cancer 23:406–415
15. Yamazaki K (2007) An ultrastructural and immunohistochemical study of elastofibroma: CD 34, MEF-2, prominin 2 (CD133), and factor XIIIa-positive proliferating fibroblastic stromal cells connected by Cx43-type gap junctions. Ultrastruct Pathol 3:209–219
16. Enjoji M, Sumiyoshi K, Sueyoshi K (1985) Elastofibromatous lesion of the stomach in a patient with elastofibroma dorsi. Am J Surg Pathol 9:233–237
17. Saint-Paul MC, Musso S, Cardot-Leccia N et al (2003) Elastofibroma of the stomach. Pathol Res Pract 199:637–639
18. Goldblum JR, Beals T, Weiss SW (1992) Elastofibromatous change of the rectum. A lesion mimicking amyloidosis. Am J Surg Pathol 16:793–795
19. Sakatani T, Shomori K, Adachi H et al (2000) Elastofibroma of the sigmoid colon. Pathol Res Pract 196:205–207
20. Märkl B, Kerwel TG, Langer E et al (2008) Elastosis of the colon and the ileum as polyp causing lesions: a study of six cases and review of the literature. Pathol Res Pract 204:395–399
21. Kim SI, Kwak JH, Zachariah M et al (2007) TGF-beta-activated kinase 1 and TAK1-binding protein 1 cooperate to mediate TGF-beta1-induced MKK3-p38 MAPK activation and stimulation of type I collagen. Am J Physiol Renal Physiol 292:F1471–F1478
22. Wang L, Ma R, Flavell RA et al (2002) Requirement of mitogen-activated protein kinase kinase 3 (MKK3) for activation of p38alpha and p38delta MAPK isoforms by TGF-beta 1 in murine mesangial cells. J Biol Chem 277:47257–47262
23. Kai K, Kitajima Y, Hiraki M et al (2007) Quantitative double-fluorescence immunohistochemistry (qDFIHC), a novel technology to assess protein expression: a pilot study analyzing 5-FU sensitive markers thymidylate synthase, dihydropyrimidine dehydrogenase and orotate phosphoribosyl transferases in gastric cancer tissue specimens. Cancer Lett 258:45–54
24. Minhajat R, Mori D, Yamasaki F et al (2006) Endoglin (CD105) expression in angiogenesis of colon cancer: analysis using tissue microarrays and comparison with other endothelial markers. Virchows Arch 448:127–134
25. Minhajat R, Mori D, Yamasaki F et al (2006) Organ-specific endoglin (CD105) expression in the angiogenesis of human cancers. Pathol Int 56:717–723
26. Okada K, Satoh T, Fujimoto K et al (2004) Interaction between morphology and angiogenesis in human early colorectal cancers. Pathol Int 54:490–497
27. Piao M, Tokunaga O (2006) Significant expression of endoglin (CD105), TGFbeta-1 and TGFbeta R-2 in the atherosclerotic aorta: an immunohistological study. J Atheroscler Thromb 13 (2):82–89
28. Gun BD, Bahadir B, Behzatoglu K et al (2007) Elastofibroma: a clinicopathologic and immunohistochemical study of seven cases and literature review. APMIS 115:115–119

Virchows Arch (2009) 454:189–194
DOI 10.1007/s00428-008-0721-7

ORIGINAL ARTICLE

Myxoid solitary fibrous tumor: a clinicopathologic study of three cases

Sean K. Lau · Lawrence M. Weiss · Peiguo G. Chu

Received: 2 October 2008 / Revised: 10 November 2008 / Accepted: 12 December 2008 / Published online: 6 January 2009

Abstract While focal myxoid areas are occasionally observed in solitary fibrous tumors, neoplasms of this type exhibiting extensive myxoid change are considered exceedingly uncommon. Due to their rarity, the biologic behavior of myxoid solitary fibrous tumor has not been determined. Three cases of myxoid solitary fibrous tumor are described in order to better characterize the clinical and pathologic features of this uncommon variant of solitary fibrous tumor. The tumors occurred in one man and two women, with ages of 37, 47, and 58 years, respectively. Sites of involvement included the retroperitoneum, pelvis, and soft tissue of the neck. Histologically, all cases were characterized predominantly by the presence of myxoid stroma comprising 70% to 100% of the tumor. The tumor cells were predominantly spindled in all cases, and arranged randomly, in loose fascicles, or in anastomosing strands imparting a microcystic/reticular appearance. The lesional cells had a bland cytologic appearance and low mitotic count. All tumors lacked necrosis and areas of increased cellularity. By immunohistochemistry, all cases were positive for CD34, CD99, and bcl-2, and negative for keratin, epithelial membrane antigen, desmin, actin, smooth muscle actin, and S-100 protein. To date, all cases have followed a benign course without evidence of recurrence or metastasis with a follow-up duration ranging from 50 to 87 months. The data suggest that myxoid solitary fibrous tumors are associated with an indolent clinical course and favorable prognosis.

Keywords Myxoid · Solitary fibrous tumor · Soft tissue

S. K. Lau (✉) · L. M. Weiss · P. G. Chu
Department of Pathology, City of Hope National Medical Center,
1500 East Duarte Road,
Duarte, CA 91010, USA
e-mail: SLau@coh.org

Introduction

Solitary fibrous tumor is a relatively rare mesenchymal neoplasm comprised of spindle cells exhibiting fibroblastic differentiation. Although initially described as a pleura-based lesion, solitary fibrous tumor has been subsequently recognized as a ubiquitous neoplasm which may occur in a wide range of anatomic sites [1, 2]. Typical histologic features of solitary fibrous tumor include haphazardly arranged spindle cells, alternating hypocellular and hypercellular areas, collagenous stroma, and thin-walled branching blood vessels [1, 2]. While focal myxoid change is a not an uncommon finding in solitary fibrous tumor [3–5], solitary fibrous tumors characterized by a prominent myxoid stroma are quite rare. To date, less than 15 cases of myxoid solitary fibrous tumor have been reported in the literature [6–13].

The clinical course of morphologically typical solitary fibrous tumor is considered unpredictable; most demonstrate benign behavior, though approximately 10–15% exhibit recurrence or metastasis [2]. In contrast, the biologic behavior of myxoid solitary fibrous tumor has not been determined due to the limited number of reported cases of this entity and relatively short duration of follow-up [6–13]. In order to expand on the clinical, morphologic, and immunophenotypic characterization of this uncommon variant of solitary fibrous tumor, three additional cases of myxoid solitary fibrous tumor with long-term clinical follow-up are reported herein.

Materials and methods

Cases were identified from the files of the Department of Pathology, City of Hope National Medical Center, Duarte,

California. Sampling of each tumor consisted of a minimum of one section for each centimeter of greatest tumor dimension, with the exception of case 2 which had been entirely submitted for microscopic examination. In all cases, myxoid stroma comprised at least 50% of the total tumor in the sections examined histologically, as defined by de Saint Aubain Somerhausen et al. [6]. The resected specimens from each case were fixed in 10% neutral buffered formalin. Paraffin sections were stained with hematoxylin and eosin for routine histology. Immunohistochemical studies were performed on paraffin-embedded tissue sections using an automated immunostainer (Dako, Carpinteria, CA, USA), followed by antibody detection using the Dako EnVision+ System and 3,3′-diaminobenzidine as a chromogen. The primary antibodies, sources, and dilutions used in this study are listed in Table 1. Appropriate positive and negative tissue controls were used throughout.

Results

Clinical findings

The clinical features of the three cases are summarized in Table 2. The patients included two women and one man, with ages ranging from 37 to 58 years. One tumor arose in the soft tissue of the neck, one in the retroperitoneum, and one in the pelvis adjacent to the rectum. All lesions were treated by surgical resection alone, without adjuvant chemotherapy or radiation. Clinical follow-up data were available for all cases. None of the patients developed local recurrence or distant metastases, and all are currently alive with no evidence of disease.

Pathologic findings

Grossly, the tumors were described as solid masses with white to tan, firm, fibrous cut surfaces with softer areas of gelatinous appearing myxoid change. No areas of necrosis were noted. Microscopically, all three tumors showed similar histologic features. The tumors were characterized by a proliferation of cytologically bland spindle cells in a loose myxoid stroma. The neoplastic cells had oval to elongated nuclei, with evenly distributed chromatin, inconspicuous nucleoli, and scant amounts of pale eosinophilic cytoplasm. In general, the cells were arranged randomly (Fig. 1a) or in loose fascicles (Fig. 1b). In case 1, the tumor cells formed interconnecting strands, resulting in a microcystic/reticular appearance (Fig. 1c). Frequent small thin-walled vessels were present in the myxoid stroma (Fig. 1d). Cases 1 and 2 showed foci of morphologically typical solitary fibrous tumor with areas of alternating cellularity and haphazardly arranged spindle cells in a collagenized stroma (Fig. 1e). Mitotic activity was low in all tumors; one mitotic figure per ten high power fields was observed in case 1, two mitotic figures per ten high power fields were seen in case 2, and no mitotic figures were identified in case 3. Mitoses were present exclusively in non-myxoid areas of the tumors. No atypical mitotic figures or necrosis were seen in any of the cases.

Table 1 Immunohistochemical reagents

Antigen	Clone	Dilution	Source
Keratin	OSCAR	1:100	Covance, Berkley, CA
EMA	E29	1:800	DakoCytomation, Carpinteria, CA
Actin	HHF35	1:75	Accurate Chemical & Scientific Corporation, Westbury, NY
Desmin	D33	1:300	DakoCytomation
SMA	1A4	1:500	DakoCytomation
S-100	Polyclonal	1:3,000	DakoCytomation
CD34	QBEnd10	1:100	DakoCytomation
CD99	O13	1:100	Covance
Bcl-2	124	1:50	DakoCytomation

Immunohistochemical findings

The tumor cells in all cases showed strong and diffuse immunoreactivity for CD34 (Fig. 1f), CD99, and bcl-2 in both myxoid and non-myxoid areas. All tumors lacked expression of keratin, epithelial membrane antigen (EMA), desmin, actin, smooth muscle actin (SMA), and S-100 protein.

Discussion

Myxoid change is a common, though generally focal finding in solitary fibrous tumors. In contrast, solitary fibrous tumors exhibiting a predominantly myxoid stroma are rarely encountered. Since the initial series of myxoid solitary fibrous tumors described by de Saint Aubain Somerhausen et al. [6], only seven additional cases of this entity have been reported (Table 3) [7–13]. The histologic features of myxoid solitary fibrous tumor are relatively non-specific and include the presence of abundant, pale myxoid matrix, thin-walled stromal blood vessels, and haphazardly arranged, cytologically bland spindle cells. Focal areas of morphologically typical solitary fibrous tumor are present in some cases, and can aid in diagnosis [6, 11]. Similar to conventional solitary fibrous tumor, by immunohistochemistry, the myxoid variant commonly expresses CD34, CD99, and bcl-2, and is typically negative for keratin, EMA, S-100 protein, and muscle-associated antigens [3–5, 14, 19, 22, 25, 26].

Table 2 Clinicopathologic data in three cases of myxoid solitary fibrous tumor

Case no.	Gender	Age (years)	Clinical presentation	Tumor location	Size (cm)	% myxoid	Follow-up
1	F	58	Asymptomatic, mass palpated on bimanual pelvic exam	Retroperitoneum	15.0	70	NED, 87 months
2	F	47	Neck mass×7 years	Soft tissue, neck	1.3	90	NED, 84 months
3	M	37	Constipation, palpable pararectal mass	Pelvis	9.5	100	NED, 50 months

F female, *M* male, *NED* no evidence of disease

The differential diagnosis of myxoid solitary fibrous tumor is quite broad, as a variety of tumors may demonstrate a histologic appearance characterized by a predominant myxoid morphology [14]. Important entities to consider in the differential diagnosis include low grade fibromyxoid sarcoma, myxofibrosarcoma, and myxoid variants of synovial sarcoma, dermatofibrosarcoma protuberans, leiomyosarcoma, liposarcoma, and nerve sheath tumors.

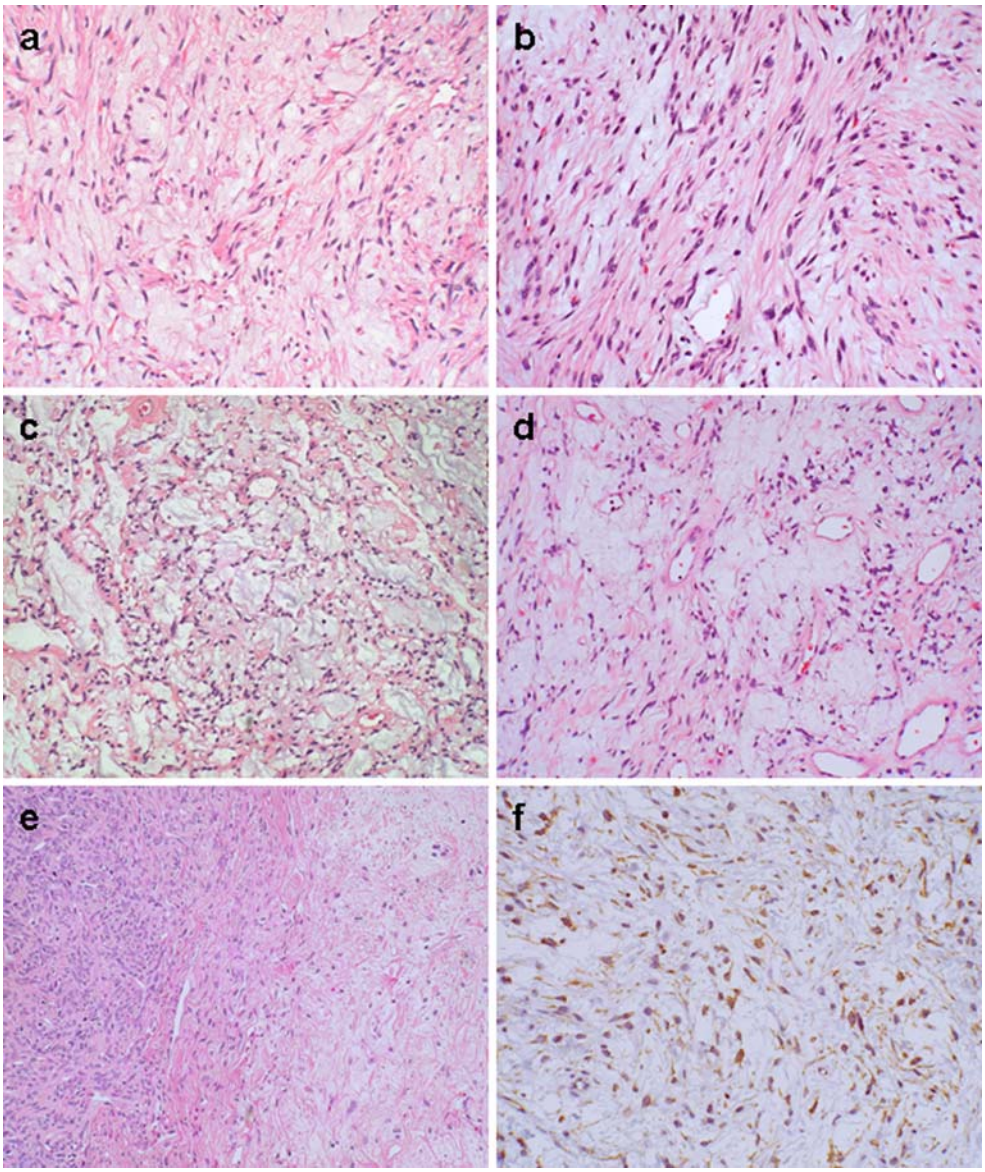

Fig. 1 Histologic features of myxoid solitary fibrous tumor. The tumors were characterized by a prominent myxoid stroma and cytologically bland spindle cells exhibiting haphazard (**a**) and loose fascicular (**b**) growth patterns. One case showed a microcystic/reticular morphology (**c**). The presence of thin-walled blood vessels was also a consistent finding (**d**). Focal areas of conventional, non-myxoid solitary fibrous tumor (*left*) were present in two cases (**e**). All tumor exhibited positive immunoreactivity for CD34 (**f**)

Table 3 Reported cases of myxoid solitary fibrous tumor

Reference	Gender	Age (years)	Tumor location	Tumor size (cm)	Follow-up
de Saint Aubain Somerhausen et al. [6]	F	45	Abdominal wall	14	NA
	M	50	Thigh	11	NED, 27 months
	M	42	Chest wall	4.9	NED, 25 months
	F	64	Pleura	3.5	NED, 13 months
	M	68	Orbit	3.0	NED, 10 months
	M	44	Parotid region	NA	None
	F	35	Abdominal wall	11.5	None
Chang et al. [7]	F	42	Skin, thigh	1.0	NED, 24 months
Yap et al. [8]	M	41	Ischiorectal fossa	6.0	None
Pakasa et al. (case 3) [9]	M	27	Spinal cord	2.5	Recurrence, 168 months
Cheng et al. [10]	M	42	Axilla	8.0	NED, 18 months
Wei et al. [11]	M	65	Seminal vesicle	9.0	NED, 14 months
Kosem et al. [12]	F	27	Meninges	3.8	None
Shin et al. [13]	M	56	Retroperitoneum	NA	None

F female, *M* male, *NA* not available, *NED* no evidence of disease

Low grade fibromyxoid sarcoma contains myxoid areas and cytologically bland spindle cells which may be confused with myxoid solitary fibrous tumor. The constituent spindle cells of the former tumor, however, typically adopt a characteristic whorled or swirling growth pattern not seen in myxoid solitary fibrous tumor [15]. By immunohistochemistry, low grade fibromyxoid sarcoma, unlike myxoid solitary fibrous tumor, is generally negative for CD34, and can express EMA in a subset of cases [16].

Myxofibrosarcomas of low histologic grade may superficially resemble myxoid solitary fibrous tumor, though the presence of multinodular growth with fibrous septa, cells with atypical hyperchromatic nuclei, and mucin containing pseudolipoblasts are features which are unique to myxofibrosarcoma [17]. Myxoid synovial sarcoma may exhibit reticular and loose fascicular growth patterns similar to myxoid solitary fibrous tumor, but can be distinguished from the latter by positive immunoreactivity for keratin or EMA [18].

Myxoid solitary fibrous tumor involving the subcutis may be particularly difficult to differentiate from myxoid dermatofibrosarcoma protuberans, as both are characterized by a proliferation of bland spindle cells in a richly vascular myxoid stroma and immunohistochemical expression of CD34 [19, 20]. As myxoid solitary fibrous tumors are generally well-circumscribed lesions, the presence of an infiltrative growth pattern with entrapment of fat in a honeycomb pattern would favor a diagnosis of myxoid dermatofibrosarcoma protuberans.

Myxoid leiomyosarcoma is a rare variant of leiomyosarcoma which can be distinguished from myxoid solitary fibrous tumor morphologically by the presence of spindle cells with comparatively more eosinophilic cytoplasm and cigar-shaped nuclei [21]. By immunohistochemistry, myxoid leiomyosarcomas are positive for desmin, actin, and SMA, which are generally not detected in myxoid solitary fibrous tumor [21]. Myxoid liposarcoma is separable from myxoid solitary fibrous tumor by the presence of lipoblasts, an arborizing capillary vasculature, and pools of stromal mucin [22].

Nerve sheath tumors, in particular neurofibroma and malignant peripheral nerve sheath tumor, may on occasion show extensive myxoid change, which may impart a histologic appearance similar to myxoid solitary fibrous tumor [14]. The presence of cells with wavy or buckled nuclei would favor a diagnosis of a myxoid nerve sheath tumor, though such cells may be seen focally in solitary fibrous tumor [6]. S-100 protein expression, when present, would support a diagnosis of a myxoid neurofibroma or malignant peripheral nerve sheath tumor, as myxoid solitary fibrous tumor is negative for this marker. A negative result is however non-contributory in the context of resolving this particular differential diagnosis, as only approximately half of cases of malignant peripheral nerve sheath tumor are S-100 protein positive.

Solitary fibrous tumors are generally considered indolent neoplasms with a low but definite potential for recurrence and metastasis. In the context of conventional non-myxoid solitary fibrous tumors, pathologic parameters associated with unfavorable clinical outcome have included the presence of areas of increased cellularity, nuclear pleomorphism, necrosis, greater than four mitoses per ten high power fields, and size exceeding 10 cm [4, 23, 24]. The relationship between these pathologic variables and biologic behavior is imperfect, however, as some solitary fibrous tumors exhibiting the aforementioned atypical features have pursued a benign course, while others lacking such features have behaved aggressively [4, 5, 23–26].

There is considerably less information available concerning the clinical behavior of the myxoid variant of solitary fibrous tumor, which is largely attributable to the rarity of this neoplasm, and the relative absence of extended clinical follow-up in reported cases of this entity [6–13]. Among three cases of myxoid solitary fibrous tumor comprising the present series, none were associated with local or distant relapse, with follow-up ranging from 50 to 87 months. All cases lacked atypical pathologic features associated with malignant behavior as described for conventional non-myxoid solitary fibrous tumors including nuclear pleomorphism, hypercellularity, necrosis, and mitotic figures exceeding four per ten high power fields, though in one case, the size of the tumor was greater than 10 cm.

Cases of myxoid solitary fibrous tumor described to date have been similarly largely devoid of features of biologic aggressiveness [7–13], with the exception of three tumors in one series which were more than 10 cm in size [6]. No follow-up information was available in two cases, while in the third, the patient showed no evidence of recurrent disease at 27 months follow-up. As has been demonstrated in conventional solitary fibrous tumors [24], large size alone in the absence of other atypical histologic features thus does not appear to necessarily portend an unfavorable clinical course in the context of myxoid solitary fibrous tumors.

Among the previously documented cases of myxoid solitary fibrous tumor, all have behaved in a benign fashion, with no reports of distant metastases or tumor-related deaths and only a single instance of tumor relapse (Table 3) [6–13]. This particular tumor involved the spinal cord of a 27-year-old male and measured 2.5 cm [9]. The tumor was characterized histologically by a myxoid component comprising 50–70% of the lesion, bland spindle cells, "occasional mitoses," and an absence of tumor necrosis. Following incomplete resection, the patient developed a histologically identical appearing lesion in the spinal cord distant from the site of the original tumor 14 years later [9]. In this particular case, it is difficult to determine whether tumor relapse was attributable to an inability to obtain a clear surgical margin or a function of the inherent biology of the tumor.

Observations in the current and previous reports of myxoid solitary fibrous tumor suggest that pathologic features predictive of malignant clinical behavior in conventional non-myxoid solitary fibrous tumors are generally lacking in the myxoid variant. Myxoid solitary fibrous tumor appears to carry a favorable prognosis with a very low potential for recurrence, though clearly more experience with additional cases is required to validate the biologic behavior of this variant of solitary fibrous tumor.

Conflict of interest statement The authors declare that they have no conflict of interest.

References

1. Chan JK (1997) Solitary fibrous tumour-everywhere, and a diagnosis in vogue. Histopathology 31:568–576
2. Gengler C, Guillou L (2006) Solitary fibrous tumour and haemangiopericytoma: evolution of a concept. Histopathology 48:63–74
3. Suster S, Nascimento AG, Miettinen M et al (1995) Solitary fibrous tumors of soft tissue. A clinicopathologic and immunohistochemical study of 12 cases. Am J Surg Pathol 19:1257–1266
4. Vallat-Decouvelaere AV, Dry SM, Fletcher CD (1998) Atypical and malignant solitary fibrous tumors in extrathoracic locations: evidence of their comparability to intra-thoracic tumors. Am J Surg Pathol 22:1501–1511
5. Hasegawa T, Matsuno Y, Shimoda T et al (1999) Extrathoracic solitary fibrous tumors: their histological variability and potentially aggressive behavior. Hum Pathol 30:1464–1473
6. de Saint Aubain Somerhausen N, Rubin BP, Fletcher CD (1999) Myxoid solitary fibrous tumor: a study of seven cases with emphasis on differential diagnosis. Mod Pathol 12:463–471
7. Chang SE, Bae GY, Choi JH et al (2002) Cutaneous solitary fibrous tumour with myxoid stroma. Br J Dermatol 147:1267–1269
8. Yap T, Hamzah L, Oshowo A, Taylor I (2003) Myxoid solitary fibrous tumour of the ischiorectal fossa. Eur J Surg Oncol 29:98–100
9. Pakasa NM, Pasquier B, Chambonnière ML et al (2005) Atypical presentations of solitary fibrous tumors of the central nervous system: an analysis of unusual clinicopathological and outcome patterns in three new cases with a review of the literature. Virchows Arch 447:81–86
10. Cheng NC, Tang YB, Liang CW et al (2005) Myxoid solitary fibrous tumour of the axilla. J Plast Reconstr Aesthet Surg 59:86–89
11. Wei YC, Li CF, Sung MT et al (2006) Primary myxoid solitary fibrous tumor involving the seminal vesicle. Pathol Int 56:642–644
12. Kösem M, Arslan M, Kontaş O et al (2006) Myxoid solitary fibrous tumour of the meninges: case report. Histopathology 49:443–445
13. Shin SS, Jeong YY, Kang HK (2008) Myxoid solitary fibrous tumor of the retroperitoneum: MRI findings with the pathologic correlation. Korean J Radiol 9:279–282
14. Graadt van Roggen JF, Hogendoorn PC, Fletcher CD (1999) Myxoid tumours of soft tissue. Histopathology 35:291–312
15. Evans HL (1993) Low-grade fibromyxoid sarcoma. A report of 12 cases. Am J Surg Pathol 17:595–600
16. Guillou L, Benhattar J, Gengler C et al (2007) Translocation-positive low-grade fibromyxoid sarcoma: clinicopathologic and molecular analysis of a series expanding the morphologic spectrum and suggesting potential relationship to sclerosing epithelioid fibrosarcoma: a study from the French Sarcoma Group. Am J Surg Pathol 31:1387–1402
17. Mentzel T, Calonje E, Wadden C et al (1996) Myxofibrosarcoma. Clinicopathologic analysis of 75 cases with emphasis on the low-grade variant. Am J Surg Pathol 20:391–405
18. Krane JF, Bertoni F, Fletcher CD (1999) Myxoid synovial sarcoma: an underappreciated morphologic subset. Mod Pathol 12:456–462
19. Reimann JD, Fletcher CD (2007) Myxoid dermatofibrosarcoma protuberans: a rare variant analyzed in a series of 23 cases. Am J Surg Pathol 31:1371–1377
20. Mentzel T, Schärer L, Kazakov DV et al (2007) Myxoid dermatofibrosarcoma protuberans: clinicopathologic, immunohistochemical, and molecular analysis of eight cases. Am J Dermatopathol 29:443–448

21. Rubin BP, Fletcher CD (2000) Myxoid leiomyosarcoma of soft tissue, an underrecognized variant. Am J Surg Pathol 24:927–936
22. Kilpatrick SE, Doyon J, Choong PF et al (1996) The clinicopathologic spectrum of myxoid and round cell liposarcoma. A study of 95 cases. Cancer 77:1450–1458
23. England DM, Hochholzer L, McCarthy MJ (1989) Localized benign and malignant fibrous tumors of the pleura. A clinicopathologic review of 223 cases. Am J Surg Pathol 13:640–658
24. Gold JS, Antonescu CR, Hajdu C et al (2002) Clinicopathologic correlates of solitary fibrous tumors. Cancer 94:1057–1068
25. Brunnemann RB, Ro JY, Ordonez NG et al (1999) Extrapleural solitary fibrous tumor: a clinicopathologic study of 24 cases. Mod Pathol 12:1034–1042
26. Morimitsu Y, Nakajima M, Hisaoka M et al (2000) Extrapleural solitary fibrous tumor: clinicopathologic study of 17 cases and molecular analysis of the p53 pathway. APMIS 108:617–625

Virchows Arch (2009) 454:195–201
DOI 10.1007/s00428-008-0705-7

ORIGINAL ARTICLE

Biomaterial-induced sarcomagenesis is not associated with microsatellite instability

Achim Weber · Annette Strehl · Erik Springer · Torsten Hansen · Arno Schad · C. James Kirkpatrick

Received: 18 June 2008 / Revised: 4 October 2008 / Accepted: 13 November 2008 / Published online: 19 December 2008

Abstract Sarcomagenesis, in contrast to carcinogenesis, is poorly understood. Microsatellite instability has been implicated in the development of many cancers, in particular those associated with chronic inflammatory conditions. In an experimental animal model, rats developed not only a peri-implantational chronic inflammatory reaction, but also malignant mesenchymal tumors in response to different biomaterials. Therefore, it was the aim of our study to test if the development of biomaterial-induced sarcomas is characterized by a mutator phenotype. A multiplex-PCR approach was designed to screen biomaterial-induced sarcomas for the presence of microsatellite instability. Seven different microsatellite loci were tested in ten tumors for microsatellite instability using a fluorochrome-labelled multiplex-PCR and subsequent fragment analysis. All tumors provided a microsatellite-stable phenotype at all loci tested. Our data suggest that microsatellite instability is rarely or not at all a feature of malignant transformation of biomaterial-induced soft tissue tumors. Thus, there is no evidence that a mutator phenotype is a hallmark of biomaterial-induced sarcomagenesis.

A. Weber · A. Strehl · E. Springer · T. Hansen · A. Schad · C. J. Kirkpatrick
Institute of Pathology, Johannes Gutenberg University of Mainz, Langenbeckstr. 1,
55101 Mainz, Germany

Present address:
A. Weber (✉)
Department of Pathology, Institute of Surgical Pathology, University Hospital of Zurich,
Schmelzbergstr. 12,
8091 Zurich, Switzerland
e-mail: achim.weber@usz.ch

Keywords Biomaterials · Sarcoma · Microsatellite instability · Mutator phenotype

Introduction

Tumorigenesis is now widely accepted as resulting from a stepwise accumulation of genetic instability [1]. The biological and molecular mechanisms involved in the development of carcinomas in humans and mammals have been extensively investigated. In contrast, the molecular steps in the development of sarcomas and other soft tissue tumors are less well understood. A progression from a benign precursor lesion to malignant tumor, characterisitic of many epithelial tumors, is exceptional for soft tissue tumors. However, a biological continuum of benign and malignant soft tissue tumors has been postulated for example in the case of lipomatous [2] and nerve sheath tumors [3, 4].

In a previous study, we had established an animal model for the tumorigenesis of soft tissue tumors [5]. Malignant mesenchymal tumors were induced around subcutaneously implanted biomaterial disks. In addition to fully developed tumors, implantation sites showed lymphocyte and macrophage infiltrates reflecting an inflammatory reaction, as a characteristic response to the implantation of foreign materials [6, 7] as well as hyper-proliferative lesions, reflecting precursor lesions. This animal model allowed a detailed investigation of sarcoma tumorigenesis, especially because a spectrum of preneoplastic lesions could be identified.

Several mechanisms are known to result in genetic instability and consequent malignant transformation of cells. One pathway is the development of chromosomal instability with numerical and structural chromosomal

changes and aneuploidy of tumor cells. Another pathway is the development of a "mutator phenotype" with changes at the nucleotide level. These alterations may result in the accumulation of multiple mutations in genes relevant to cell growth and homeostasis, eventually leading to growth advantage and transformation of cells. Multiple short tandem repetitive DNA-sequences, also known as microsatellites, are present throughout the genome of humans and other mammals [8]. A mutator phenotype is frequently reflected by widespread sequence length alterations of these microsatellites, designated as microsatellite instability [9, 10]. Besides inherited deficiencies of mismatch repair (MMR) genes and inactivation by methylation, an underlying impairment of repair enzymes in association with chronic inflammation [11, 12] has been demonstrated, most likely due to oxidative stress [13].

While there is a clear association of specific or typical chromosomal translocations or translocation of gene fusion products with many soft tissue tumors, microsatellite instability has also been reported for some entities [14–17]. Since a chronic inflammatory condition is associated with microstallite-associated carcinogenesis, we sought to investigate if the tumorigenesis of biomaterial-induced sarcomas is based on the development of a mutator phenotype. Using the above-mentioned rat model, biomaterial-induced sarcomas were screened for microsatellite instability.

Materials and methods

Animal model

Ten formalin-fixed, paraffin-embedded tumor samples (Table 1) were retrieved from the previously published rat sarcoma collective [5]. Briefly, in this study a total of 490 Fischer rats had been implanted with nine different standard medical grade biomaterials. In about one quarter of implantations, animals developed (mostly malignant) mesenchymal tumors of different histological type, including fibrosarcomas, leimyosarcomas, and rhabdomyosarcomas, around the implantation sites.

Laser capture microdissection

Sections of normal and transformed tissues (either tumors or precursor lesions) from the above mentioned paraffin blocks were prepared on membrane mounted-slides (PALM MembraneSlides, P.A.L.M., Bernried, Germany) and de-paraffinized. Microdissection was performed using a PALM MicroBeam system with a pulsed UV-A nitrogen laser (337 nm). The selected areas were marked, cut out, and pulsed into a 0.5-ml microfuge tube with adhesive filling (PALM AdhesiveCaps, P.A.L.M.), taking care to keep the normal and tumor tissues separate. "Normal tissue" was prepared so distant from the implantation site that it was morphologically not affected by the implants and corresponding tissue reactions.

Multiplex PCR and fragment analysis

Since (in contrast to human and mouse) no well-established and characterized panels of markers for the analysis of microsatellite instability was described in rat, sequence information of rat microsatellite loci was taken from several studies [18–20]. In order to compensate for a potentially low sensitivity of these markers in detecting MSI, seven markers instead of the more common panel of five markers was used (Table 2). DNA was isolated by proteinase K digestion, followed by phenol-chloroform extraction and ethanol/salt precipitation using standard protocols [21]. Two multiplex PCR-reactions were performed using two different primer mixtures with fluorochrome-labelled oligonucleotide primers. In each case, either the forward or the reverse primer was fluorochrome-labelled. Primermix A contained oligonucleotide primers of the loci GH, NGFR, SECR, and UCP; primermix B contained oligonucleotide primers of the loci ANF, PPY, and SMST (Table 2). Non-fluorescent oligonucleotide primers were purchased from

Table 1 Biomaterial-induced soft tissue tumors

Code	Implanted biomaterial	Tumor
46 PU 101	Aliphatic polyurethane	Pleomorphic rhabdomyosarcoma
11 PMMA 84	Polymethylmethacrylate	Osteosarcoma
1 PMMA 86	Polymethylmethacrylate	Sarcoma, NOS
16 Si 80	Silicone	Pre-neoplastic lesion
2 Si 90	Silicone	Sarcoma, NOS
4 PVC 105	Polyvinyl chloride	Fibrosarcoma
5 NiCr 107	Nickel chromium	Dedifferentiated liposarcoma
25 NiCr 107	Nickel chromium	Pleomorphic sarcoma
24 Alu 103	Aluminum	Spindle cell sarcoma
1 Si 87	Silicone	Sarcoma, NOS

The study included a total of ten different biomaterial-induced soft tissue tumors. Every rat was given an identification code describing the implanted material. The resulting tumor was histologically diagnosed

Table 2 Microsatellite loci and oligonuceotide primer sets

Locus	Acc. No.	Oligo nucleotide sequence	Size[a]	Dye	Ref.
Mix A					
GH	X12967	F 5′-ATGGGAGGGAACAAGTCTTC-3′ R 5′-GAGGGAGAGAGAAAGAGAGACAG-3′	135	D4	[18, 19]
NGFR	X05137	F 5′-ACCCCACAATCCAACACTATAC-3′ R 5′-GCAGGATCTAGTCTCAGCCC-3′	126	D3	[18, 19]
SECR	M64033	F 5′-ACCATGGAGCCTCTACTGC-3′ R 5′-GTCCCGTCCGAGTGTCTT-3′	194	D4	[18, 20]
UCP	X12925	F 5′-TGCCCGTCTCTGTTACTCAT-3′ R 5′-CAAGAACCCTGAGGCAATAA-3′	111	D4	[18, 19]
Mix B					
SMST	K02248	F 5′-TTTCCAGGTGCCAAATGTAG-3′ R 5′-TATATTGTGACAAAAGAAAGGCAC-3′	154	D4	[18, 20]
ANF	K02062	F 5′-TCCACAACCTTGATCTTTCG-3′ R 5′-GTTGAGGGCCATAGTGTGAC-3′	160	D2	[18, 20]
PPY	M27450	F 5′-CACACTGACCAGGCCTAGG-3′ R 5′-TGTCAGCTCAGCTGCTTTG-3′	153	D3	[18, 20]

Microsatellite loci and oligonucletide primer sequences information
GH growth hormone, *NGFR* nerve growth factor receptor, *SECR* secretin, *UCP* uncoupling protein, *SMST* somatostatin, *ANF* atrial natriuretic factor, *PPY* pancreatic polypeptide
[a] Sizes are indicated as expected according to NCBI database information and differed significantly from the fragment sizes observed in this study in case of the GH, UCP, and PPY loci, respectively

biomers.net, Ulm, Germany and the fluorescent oligonucleotide primers from Sigma-Aldrich, Germany.

The final 25-μl multiplex reaction mix consisted of the following: 12.5 μl Qiagen-Multiplex-Mastermix (Qiagen, Hilden, Germany), 2.5 μl 10× primer-mix, 7.5 μl H_2O, and 2.5 μl template. The 10× primer-mix was composed by mixing 50 μM fluorescent primers and 100 μM non-fluorescent primers at a concentration of 2 μM each in H_2O.

PCR was performed using a GeneAmp 9700 thermocycler (Applied Biosystems, Foster City, CA, USA) under the following conditions: initial denaturation at 95° for 15 min, followed by 45 cycles of: 30 s at 94°, 90 s at 54°, and 1 min at 72° with a final 30-min extension period at 60°. The resulting PCR-product was then analyzed by gel-electrophoresis on a 2% agarose gel and subsequent fragment analysis of the fluorescently labelled PCR products was performed using a Beckman Coulter CEQ 8000 Sequencer (Beckman Coulter, Krefeld, Germany) with the corresponding CEQ System software. The detected fragments of normal and malignant tissue were compared to determine the stability for each locus.

Results

Tissue selection and isolation of tumor and normal DNA

Histology of the samples was re-evaluated in order to define suitable areas of tumor and non-neoplastic tissue, respectively. In all cases studied, a clear identification of tumors and non-tumorous areas was possible, providing the basis for the laser-capture analysis and tissue preparation (Fig. 1). Following laser-capture (P.A.L.M.)-based tissue preparation and standard nucleic acid extraction, a sufficient amount and quality of DNA could be isolated from all samples analyzed.

Development of a multiplex-PCR assay for microsatellite instability testing

PCR conditions were first optimized, and all samples were initially tested in a single PCR setting. In the case of the GH and PPY locus, respectively, significantly lower amplification sizes were observed when compared to information from either the gene bank (see Table 2) and/or the literature [18]. In the case of the PPY locus, higher amplification sizes were observed. The SECR locus revealed rather a single peak instead of the characteristic stuttering pattern in all samples tested. However, all loci displayed a constant size comparing different animals (due to the same genetic background of animals).

After successfully testing each pair of oligonucleotide primers in a single-PCR, a multiplex-PCR-assay was designed by dividing the seven different primers into two groups of three or four primer pairs, respectively. Using this multiplex-PCR approach, all loci test were successfully amplified and analyzed by fluorescence-based fragment analysis. No difference between single PCR fragment analysis patterns and the multiplex approach was observed,

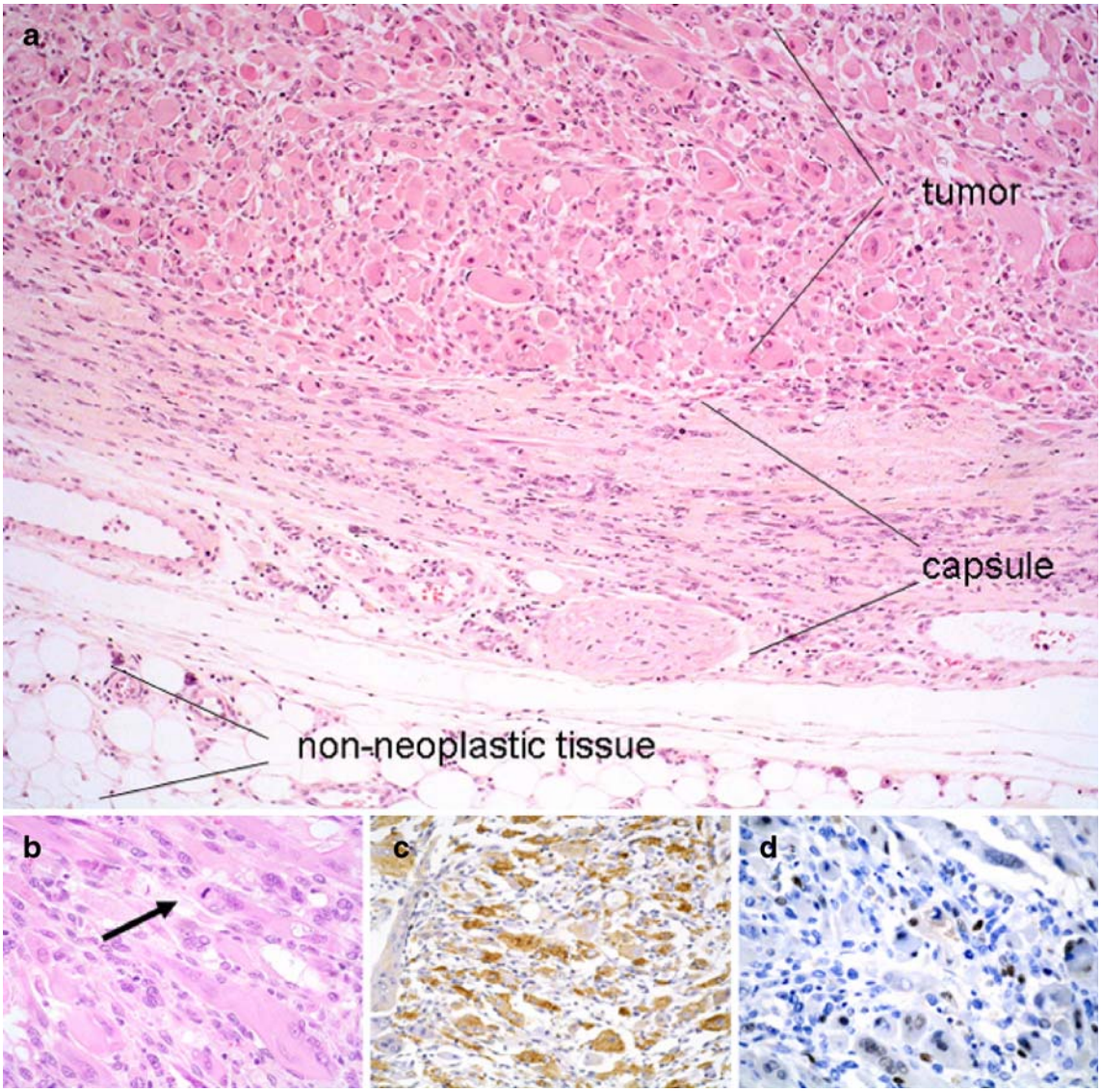

Fig. 1 Examples of a biomaterial-induced sarcoma (pleomorphic rhabdomyosarcoma from animal 46 PU 101). **a** Histology revealed a pleomorphic tumor with rhabdomyoblastic differentiation (*upper left*) and a rather well-defined border surrounded by a fibrous connective tissue capsule with proliferative lesions, possibly pre-neoplastic. (Tissue for DNA isolation was prepared by laser-microdissection from tumors, capsule tissue, and surrounding non-neoplastic tissue, respectively). **b** Higher magnification of the tumor shows atypical tumor cells with vacuoles similar to lipoblasts and a mitotic figure (*arrow*). **c** Tumor cells show a widespread positive cytoplasmic immunoreactivity for desmin, **d** as well as a strong nuclear positivity for myogenin

indicating that the multiplex assay used was a valid method for the simultaneous testing of several microsatellite loci (Fig. 2).

All microsatellite loci showed a stable phenotype

A total of 140 microsatellites was analyzed, with 70 microsatellites displaying microsatellites of neoplastic or preneoplastic tissue, and the other 70 reflecting the corresponding normal tissue, respectively. Nearly all microsatellites were informative with the exception of three cases (PND locus of animals: one PMMA 86, two Si90, and four PVC 105). In these cases, the fragment analysis revealed signals which were too low or unspecific to be readable, so that a definite statement about the stability of the microsatellite loci for these particular samples could not be made.

For all other microsatellite loci tested, no size or frame shifts were observed on comparing normal and the tumor/precursor lesion tissue (see examples in Fig. 3). Thus, even assuming that the PND locus in case of the three tumors, in which this particular locus was not amplified, had shown a change in microstatellite pattern, the overall diagnostic criteria for microsatellite instability would not have been fulfilled. Therefore, all loci provided stable microsatellites.

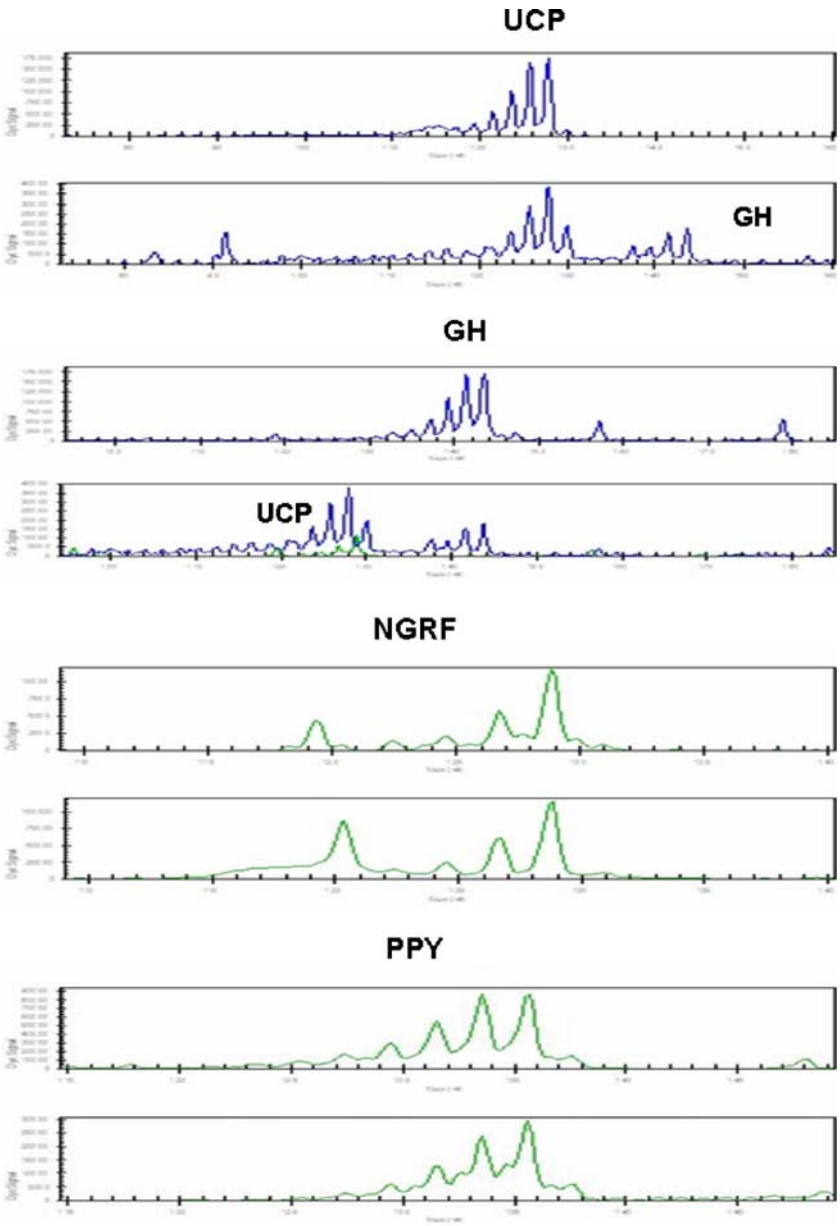

Fig. 2 Comparison of microsatellite profiles in single versus multiplex amplification show no changes in microsatellite patterns. In each pair, the microsatellite pattern from the single PCR amplification is shown in the *upper row* and the profile of the multiplex amplification is shown in the *lower row*. (In case of NGRF and PPY, respectively, only one locus is shown while the fluorochromes of further loci are not displayed). Amplificates result from tumor DNA of animal 5 NiCr 107 showing loci UCP and GH and NGFR loci (primer mix A) and locus PPY (primer mix B)

Discussion

The etiology of most benign and malignant soft tissue tumors is unknown. The vast majority of soft tissue tumors seem to arise without an apparent causative factor. Among suspected or proven causative factors are genetic and environmental factors, viral infections, immune deficiencies, local environmental factors like scars or implants as well as chronic inflammatory conditions. In contrast to many epithelial tumors, a clear multistage tumorigenesis or a clear precursor-sarcoma-sequence so far has rarely been identified in soft tissue tumors. However, the demonstration of common genetic alterations in the case of benign and malignant lipomatous tumors [2, 22] as well as benign and malignant nerve sheath tumors [3, 4] makes it reasonable that a stepwise development in soft tissues tumors is relevant for at least some entities.

In a previous study, an experimental animal model has been presented in which a high incidence of malignant soft tissue tumors arose around implanted biomaterials [5]. Sarcoma induction by biomaterials required direct contact with the respective substances. Remarkably, a broad spectrum of soft tissue tumors developed, obviously independent of the specific kind of agent implanted and lacking any consistent correlation between biomaterial groups and specific histological type of tumor. This observation suggested that it is not a specific genetic damage, interfering with a defined pathway, which is

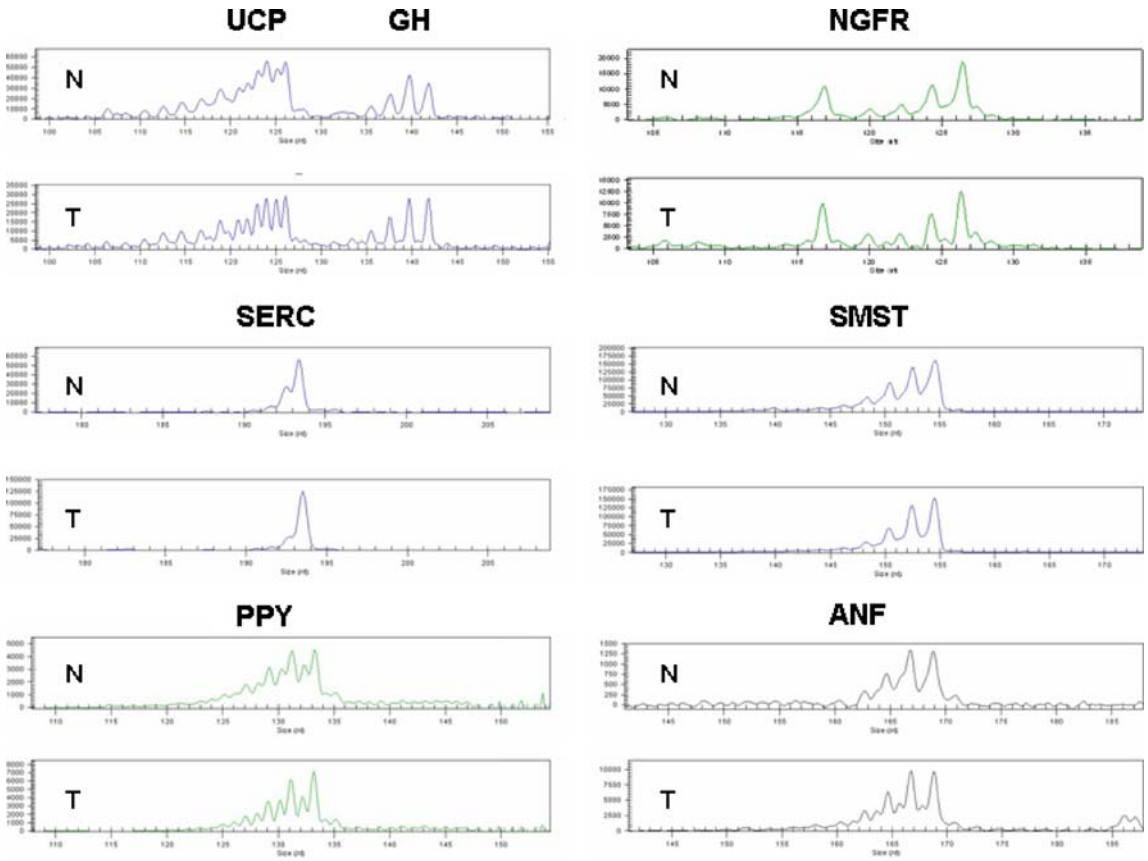

Fig. 3 No difference in microsatellite profiles comparing tumor and normal tissue in all tumor and all seven loci tested. In each pair, the microsatellite pattern from the normal tissue (*N*) is shown in the *upper row* and the pattern of the tumor (*T*) is shown in the *lower row*. Loci UCP, GH, NGFR, SECR, and PPY are shown from animal 11 PMMA 84, loci SMST, and ANF from animal 25 NiCr 107

induced. In this case, one would expect a less heterogenous spectrum of histologic entities, as are described for several specific carcinogenic substances resulting in defined tumor entities, e.g. mesotheliomas following asbestos exposure [23]. The heterogenous spectrum of lesions observed in this study rather argues for a (or several) more or less random insult(s). What might be the nature of this insult?

A characteristic hallmark of tumors developing in this model was the reaction of the peri-tumorous tissue, characterized by a chronic inflammation and hyperproliferative changes at peri-implantational sites, known as a typical response to foreign materials for a long time [6]. Chronic inflammation, characterized by free radical stress, can be a significant contributor to carcinogenesis [13, 24]. One could easily imagine that the microenvironment around the implants, probably through inflammation-mediated factors, might interfere with replication repair enzymes in this proliferation. Such a defect is expected to be reflected by microsatellite instability. There are several observations providing evidence that chronic inflammation indeed can result in an impaired mismatch-repair capacity, even in the absence of any genetic inactivation of the mismatch repair system [11–13]. Although rare, microsatellite instability has been observed in sarcomas of different histogenetic type [14, 16]. This prompted us to search for microsatellite instability in biomaterial-induced sarcomas. However, in the present study we have not observed a single microsatellite instability, neither in fully developed tumors nor in preneoplastic lesions. Based on this observation, we found no evidence that a replication-repair-associated defect is crucial for biomaterial-induced sarcomagenesis.

If this is not the case, what could be the responsible factor? As stated above, with respect to the heterogenous spectrum of tumor entities, it seems unlikely that a specific genetic insult underlies biomaterial-induced sarcomagenesis. Although the diversity of different physical compounds able to induce soft tissue tumors argues against a direct toxic effect of substances released, there is obviously the possibility of a genotoxic effect with subsequent genetic or epigenetic changes. Alternatively, sarcomagenesis is probably associated with genetic instabilty on the chromosomal (cytogenetic) level, for example induced by interference with cell check points. Carcinogen-induced sarcomagenesis in Trp53+/− mice suggests that loss of p53 function is, at least in part, an important mechanism in the development of

sarcomas at the implantation site [24, 25]. Since the hypothesis that a mutator phenotype could be responsible for the development of biomaterial-induced sarcomas is not supported by our data, further investigation should test the latter possibilities.

Acknowledgments We thank Mrs U. Hildebrand for her expert technical assistance and the state of Rhineland-Palatinate for financial support.

Conflict of interest The authors declare that they have no conflict of interest.

References

1. Hanahan D, Weinberg RA (2000) The hallmarks of cancer. Cell 100(1):57–70
2. DeiTos A, Doglioni C, Piccinin S et al (2000) Coordinated expression and amplification of the MDM2, CDK4, and HMGI-C genes in atypical lipomatous tumours. J Pathol 190(5):523–525
3. Woodruff JM, Selig AM, Crowley K et al (1994) Schwannoma (neurilemoma) with malignant transformation. A rare, distinctive peripheral nerve tumor. Am J Surg Pathol 18(9):882–895
4. Kindblom L, Ahlden M, Meis-Kindblom J et al (1995) Immunohistochemical and molecular analysis of p53, MDM2, proliferating cell nuclear antigen and Ki67 in benign and malignant peripheral nerve sheath tumours. Virchows Arch 427:19–26
5. Kirkpatrick CJ, Alves A, Kohler H et al (2000) Biomaterial-induced sarcoma: a novel model to study preneoplastic change. Am J Pathol 156(4):1455–1467
6. Brand KG, Buoen LC, Johnson KH et al (1975) Etiological factors, stages, and the role of the foreign body in foreign body tumorigenesis: a review. Cancer Res 35(2):279–286
7. Donaldson K, Tran CL (2002) Inflammation caused by particles and fibers. Inhal Toxicol 14(1):5–27
8. Ellegren H (2004) Microsatellites: simple sequences with complex evolution. Nat Rev Genet 5(6):435–445
9. Ionov Y, Peinado MA, Malkhosyan S et al (1993) Ubiquitous somatic mutations in simple repeated sequences reveal a new mechanism for colonic carcinogenesis. Nature 363(6429):558–561
10. Thibodeau SN, Bren G, Schaid D (1993) Microsatellite instability in cancer of the proximal colon. Science 260(5109):816–819
11. Hofseth LJ, Khan MA, Ambrose M et al (2003) The adaptive imbalance in base excision-repair enzymes generates microsatellite instability in chronic inflammation. J Clin Invest 112(12):1887–1894
12. Lee SH, Chang DK, Goel A et al (2003) Microsatellite instability and suppressed DNA repair enzyme expression in rheumatoid arthritis. J Immunol 170(4):2214–2220
13. Chang CL, Marra G, Chauhan DP et al (2002) Oxidative stress inactivates the human DNA mismatch repair system. Am J Physiol Cell Physiol 283(1):C148–C154
14. Ottini L, Esposito DL, Richetta A et al (1995) Alterations of microsatellites in neurofibromas of von Recklinghausen's disease. Cancer Res 55(23):5677–5680
15. Martin SS, Hurt WG, Hedges LK et al (1998) Microsatellite instability in sarcomas. Ann Surg Oncol 5(4):356–360
16. Sourvinos G, Parissis J, Sotsiou F et al (1999) Detection of microsatellite instability in sporadic cardiac myxomas. Cardiovasc Res 42(3):728–732
17. Kawaguchi K, Oda Y, Takahira T et al (2005) Microsatellite instability and hMLH1 and hMSH2 expression analysis in soft tissue sarcomas. Oncol Rep 13(2):241–246
18. Serikawa T, Kuramoto T, Hilbert P et al (1992) Rat gene mapping using PCR-analyzed microsatellites. Genetics 131(3):701–721
19. Mironov NM, Aguelon AM, Hollams E et al (1995) Microsatellite alterations in human and rat esophageal tumors at selective loci. Mol Carcinog 13(1):1–5
20. Walchle C, Diwan BA, Shiao YH et al (1999) Microsatellite instability is infrequent in azoxymethane-induced rat intestinal tumors: an assessment by capillary electrophoresis. Toxicol Appl Pharmacol 157(1):9–15
21. Sambrook J, Fritsch E, Maniatis T (1989) Molecular cloning: a laboratory manual. Cold Spring Harbor, New York
22. Mentzel T (2000) Biological continuum of benign, atypical, and malignant mesenchymal neoplasms—does it exist? J Pathol 190 (5):531–536
23. Spirtas R, Heineman EF, Bernstein L et al (1994) Malignant mesothelioma: attributable risk of asbestos exposure. Occup Environ Med 51(12):804–811
24. Tazawa H, Tatemichi M, Sawa T et al (2007) Oxidative and nitrative stress caused by subcutaneous implantation of a foreign body accelerates sarcoma development in Trp53+/− mice. Carcinogenesis 28(1):191–198
25. French JE, Lacks GD, Trempus C et al (2001) Loss of heterozygosity frequency at the Trp53 locus in p53-deficient (+/−) mouse tumors is carcinogen-and tissue-dependent. Carcinogenesis 22(1):99–106

Virchows Arch (2009) 454:203–210
DOI 10.1007/s00428-008-0703-9

ORIGINAL ARTICLE

One-step nucleic acid amplification—a molecular method for the detection of lymph node metastases in breast cancer patients; results of the German study group

Christian Schem · Nicolai Maass · Dirk O. Bauerschlag · Martin H. Carstensen · Thomas Löning · Christian Roder · Olivera Batic · Walter Jonat · Katharina Tiemann

Received: 6 August 2008 / Revised: 2 October 2008 / Accepted: 11 November 2008 / Published online: 20 December 2008

Abstract Sentinel lymph node (SN) biopsy is part of the staging procedure in breast cancer patients. In this study, we compared an intraoperative tool named one-step nucleic acid amplification (OSNA) to our routine histological investigation. OSNA consists of a short homogenization step followed by amplification of cytokeratin (CK) 19 mRNA directly from the lysate. To evaluate the performance of OSNA in comparison to histology, analysis of 343 axillary lymph nodes (ALN) from 93 breast cancer patients was performed with both methods. Discordant samples were subjected to other methods. If these tests supported the OSNA results, these samples were excluded from the study. The concordance rate was 91.8%, sensitivity 98.1%, and specificity 90.8% before and 95.5%, 100%, and 95.6%, respectively, after discordant case investigation. Our results show that OSNA is an excellent method for the detection of metastases in lymph nodes and can be applied as an intraoperative diagnostic approach.

Keywords OSNA · Breast cancer · Intraoperative diagnosis · CK19 · Sentinel lymph node

C. Schem (✉) · N. Maass · D. O. Bauerschlag · W. Jonat
Department of Obstetrics and Gynecology,
University Clinic of Schleswig-Holstein, Campus Kiel,
Michaelisstr. 16,
24105 Kiel, Germany
e-mail: schemc@email.uni-kiel.de

O. Batic · K. Tiemann
Department of Pathology,
University Clinic of Schleswig-Holstein, Campus Kiel,
Kiel, Germany

T. Löning · C. Roder
Department of Pathology, Albertinen-Hospital,
Hamburg, Germany

M. H. Carstensen
Department of Gynecology and Obstetrics, Albertinen-Hospital,
Hamburg, Germany

Introduction

The sentinel lymph node (SN) is the first lymph node to receive lymph drainage from the tumor area and is highly predictive for the status of the remaining axillary lymph nodes (ALN) [1]. Since SN biopsy is a minimally invasive technique, it spares the patient from the unpleasant side effects as well as morbidity associated with axillary clearance [2] and has readily evolved into the up-to-date standard staging procedure in clinically node-negative breast cancer patients [3–6].

Intraoperative detection of tumor deposits in SN is conventionally achieved by frozen sections, touch imprints, and cytological smears. In case tumor deposits are detected in the SN, adjuvant ALN dissection (ALND) is directly performed. Unfortunately, these techniques suffer from a rather low sensitivity, and the degree of tumor spread into the lymph nodes is often underestimated [7–10]. If postoperative in-depth histological examination [11] proves to be positive, the patient is subjected to ALND in a second surgery. Besides additional costs and discomfort for the patient associated with a second surgical intervention, the investigation of permanent sections is subject to a variety of protocols with regard to the degree of SN sectioning, staining procedure, and antibody used [12]. In addition, the

evaluation of tissue sections by the pathologist might be influenced by a subjective interpretation [13]. As a consequence, there is a need for a standardized and reproducible method with a high predictive value which can be applied intraoperatively.

Molecular methods based on reverse-transcriptase polymerase chain reaction (RT-PCR) were employed for the detection of metastatic deposits in lymph nodes of breast cancer patients [14–16] and indicated usefulness as a molecular staging tool [17] and prognostic factor [18]. Despite these promising investigations, on the condition that nucleic acids have to be isolated beforehand, these assays are too time-consuming for routine diagnosis within a defined time frame.

An intraoperative molecular test system for the detection of metastases in the SN of breast cancer patients was provided and showed a sensitivity of 87.6% and specificity of 94.2%. Discordant results were thought to be partly due to the fact that different tissue sections were used for this molecular assay and histology [19].

A different commercially available, molecular method for intraoperative diagnosis of lymph node metastases in breast cancer patients called one-step nucleic acid amplification (OSNA) was previously presented [20, 21]. The semiautomated OSNA assay (Sysmex, Kobe, Japan) consists of a short sample preparation step and real-time amplification of CK19 mRNA directly from the homogenate, without any RNA purification steps. The time to perform the assay takes 30–40 min for 3–4 LN. This quantitative molecular assessment allows the distinction of the size of the metastasis [20]. Also, in patients with colorectal cancer, the OSNA method with CK19 as a marker in tandem with frozen section histology increased intraoperative sensitivity when compared to frozen sections alone [22].

The aim of this study was to find out whether the performance of the OSNA assay was comparable to extensive histologic work-up: staining with hematoxylin and eosin (H&E) as well as a pan-cytokeratin antibody. Accordingly, 343 ALN from 93 German breast cancer patients were investigated with both approaches.

Material and methods

Patient samples

ALN samples, 343, from 93 breast cancer patients were included in this study. Patient characteristics are presented in Table 1. They were derived from complete axillary dissection which had been performed due to a previously positive SN or a clinically positive lymph node. The specimens were collected at the two participating German institutes in this study, University Clinic of Schleswig-Holstein in Kiel, and the Albertinen Hospital in Hamburg, Germany. The 93 patients were fully informed about the study and had given written consent before surgery in compliance with the regulations of the local ethical committees of the University of Kiel and Albertinen Hospital.

Table 1 Clinical characteristics of 93 breast cancer patients

	Number of patients
Primary tumor	
1a	6
1b	11
1c	29
2	36
3	4
4a	1
4b	6
Nodal status	
0	46
1a	27
2a	13
3a	7
Ductal invasive:	68
Lobular invasive:	21
Mixed (duct/lob.):	4

Study design

The 343 lymph node samples were longitudinally cut into four nearly equal slices (a, b, c, d) with a special cutting tool consisting of three blades being either 1 or 2 mm apart, as depicted elsewhere [20]. ALN were categorized into groups according to their size: ALN with a minor axis smaller than 0.4 cm were excluded from the study; lymph nodes with a minor axis between 0.4 and 0.6 cm (group 1) were centrally cut into four slices with the 1–mm cutting tool; ALN between 0.6 and 1.0 cm (group 2) were centrally cut into four slices with a 2-mm cutting tool. Lymph nodes with a minor axis larger than 1.0 cm (group 3) were either halved or cut into several pieces, and each piece, depending on its size, was treated in a similar fashion as described for groups 1 and 2. Alternate slices were allocated to the OSNA method (a&c) and to histological work-up (b&d) at five levels. The slices used for OSNA (a&c) were shock frozen in liquid nitrogen and stored at −80°C before the analysis. Histological analysis was performed for slices b&d as outlined in a different section. Concordance and sensitivity were determined based on the comparison of these two methods in 343 ALN samples. All histological investigations were done without knowing the results of the OSNA method and vice versa. The first 120 histologically

negative out of the 343 lymph node samples, as determined by five-level histology, were cut into further levels until no remnants remained. Specificity was calculated based on the extended investigation of these 120 samples in order to avoid sampling errors caused by uninvestigated material.

If discordant results between the OSNA assay and five-level histological examination occurred, the histological work-up of these cases was also extended until no tissue remained in the paraffin blocks. In addition, the homogenates of these discordant cases were also analysed by Western Blot and quantitative RT-PCR (QRT-PCR) as depicted in a different section. Provided that these supplemental analyses gave the same result as the OSNA assay, these samples were excluded from the study cohort because an uneven distribution of the metastases within pieces a, b, c, and d (tissue allocation bias) was likely to be the case.

One-step nucleic acid amplification

OSNA with CK19 mRNA as the marker was previously described in-depth [20]. In short, the lymph node slices a&c were homogenized together in 4 ml of homogenizing buffer Lynorhag, pH 3.5, (Sysmex, Kobe, Japan) on ice. Twenty microliters of this homogenate were further used for automated amplification of CK19 mRNA via reverse transcription loop-mediated isothermal amplification (RT-LAMP) [23]. Real-time amplification was accomplished with the Lynoamp Kit (Sysmex, Kobe, Japan) on the RD-100i (Sysmex, Kobe, Japan). Four lymph nodes can be analyzed in one run. The degree of amplification was detected via a by-product of the reaction, pyrophosphate [24]. The resulting change in turbidity, upon precipitation of magnesium pyrophosphate, was in turn correlated to CK19 mRNA copy number/μL of the original lysate via a standard curve which was established beforehand with three calibrators containing different CK19 mRNA copy numbers. Since no isolation or purification of RNA was required for OSNA, results were available after a total of 30–40 min. The lymph node lysates were stored at −80°C until further use.

If the CK19 mRNA copy number/μL lysate was less than 250 copies/μL, the result was regarded as (−); copy numbers between 250 and 5,000/μL were regarded as (+), and copy numbers larger than 5,000/μL as (++).

Histologic work-up

Lymph node slices b&d were fixed with neutral buffered formaldehyde and embedded in the same paraffin block. Each slice was identified by color coding.

Two initial H&E sections (representing frozen sections of SN), one initial level, and four additional levels with a 0.1-mm skip space were cut from the 343 blocks. Each level consisted of four 4 μm sections: one was used for H&E staining, one for immunohistochemistry (IHC) with the pan anticytokeratin antibody LU5 (T-1302, Dianova, Germany), one for CK19 IHC (M0888, clone RCK 108, DAKO, Germany), and one spare section. For the specificity study, the paraffin blocks of 120 histologically negative samples, as judged by five-level histological work-up, were cut into further levels until no remnants remained. IHC was performed according to a standard protocol. Shortly, deparaffinised sections were cooked in a pressure cooker in Tris–ethylenediaminetetraacetic acid–sodium citrate buffer, pH 7.8, for 4 min. After blocking, incubation with the primary antibody was performed for 40 min and with the secondary antibody for 30 min. Visualization was done with diaminobenzidine tetrahydrochloride (Vector, Burlingame, CA, USA). Staining with the LU5 antibody was done using the NEXES staining automat and the I-View-Kit (Ventana, Illkirch, France).

Metastatic deposits were recorded, according to the TNM classification of UICC 6th and AJCC 6th edition [25, 26] as isolated tumor cells (ITC) if their largest diameter was smaller than 0.2 mm, as micrometastases if they were larger than 0.2 mm but not larger than 2 mm in diameter, and as macrometastases if they were larger than 2 mm in diameter. In concordance with the TNM designation of ITC as pN0(i+), lymph node samples were only regarded as positive if at least one micrometastasis or macrometastasis was found. Consequently, lymph nodes with ITC were considered as negative in this study.

Western Blot as part of discordant case investigation

Twenty microliters of the homogenate of discordant specimens were analyzed by Western Blot for CK19. The procedure was recently described in detail [20]. In short, the lysate was mixed with 10 μL loading buffer containing 150 mM Tris–HCl, 300 mM dithiothreitol, 6% sodium dodecyl sulfate (SDS), 0.3% bromophenol blue, and 30% glycerol. The solution was boiled and subjected to electrophoresis on a 7% (*w*/*v*) polyacrylamide gel in the presence of SDS (PAG Mini; Daiichi Pure Chemicals, Tokyo, Japan). Proteins were transferred to an Immobilon-FL polyvinylidene fluoride (PVDF) membrane (Millipore, Billierica, MA, USA). After the blocking procedure, the blot was incubated with the primary anticytokeratin 19 antibody A53-B/A2 (Santa Cruz Biotechnology, Santa Cruz, CA, USA) and developed with the ECL-Advance detection kit (GE Healthcare, Chalfont St. Giles, UK). CK19 protein concentrations of the lysate, as expressed in nanograms per microliter of the original lysate, were determined on the basis of a previously performed standard curve created with four calibrators of known CK19 protein concentration (Biodesign, Saco, ME). The cutoff value for CK19 protein expression of 0.13 ng/μL (mean + 3 standard

deviations = SD) was assigned as previously presented [20].

QRT-PCR as part of DCI

Total RNA was extracted with the RNeasy Mini Kit (QIAGEN, Valencia, CA, USA) from 200 μL of each discordant sample lysate. The quality of the isolated RNA was controlled by performing QRT-PCR of the housekeeping gene beta-actin. QRT-PCR was carried out with CK19 and two breast cancer-specific markers, SPDEF (SAM pointed domain containing ETS transcription factor), and FOXA1 (forkhead box A1).

QRT-PCR was performed on the ABI Prism 7700 detector in duplicates (Applied Biosystems, Foster City, CA, USA). Two microliters of RNA was subjected to one-step QRT-PCR with QuantiTest SYBR Green (QIAGEN, Hilden, Germany) as described by the manufacturer. Primer sequences for CK19, SPDEF, FOXA1, and beta-actin amplification are listed elsewhere [20, 21].

The cutoff levels for each marker as expressed in threshold cycles (ct) were assigned in reference to data obtained with several histologically negative and positive lymph nodes, respectively. The cutoff levels were as follows: 24 for beta-actin, 31.5 for CK19, 33.8 for FOXA1, and 31.6 for SPDEF.

Results

OSNA versus histology

In this study, 343 ALN samples from 93 breast cancer patients were investigated by both OSNA and histological methods (Table 2). Two hundred eleven samples were negative with both methods, including two samples with ITC. One hundred four samples gave positive results with both assays. Samples, 97 out of 104, contained a macrometastasis, with 90 of them expressing more than 5,000 CK19 mRNA copies/μL (++) (Fig. 1) and seven between 250 and 5,000 CK19 mRNA copies/μL (+). Seven lymph node specimens with a histologically detectable micrometastasis displayed a (++) OSNA result; however, a direct correlation between metastasis size and copy number is not possible since different tissue slices were investigated by each method. H&E staining and immunostaining exhibited concordant results except in three cases which contained a H&E positive micrometastasis or a macrometastasis of 7 or 8 mm, and only weak or no LU5 /CK19 IHC. Remarkably, all these samples gave (++) results in OSNA.

In one sample containing a 2-mm micrometastasis and one sample with a micrometastasis present in only one level, negative values in the slices used for OSNA were observed. On the other hand, 26 histology negative samples, including one with ITC, yielded a positive result in the OSNA assay. Eleven of these 26 samples had rather low CK19 mRNA copy numbers/μL (250–750 copies/μL; Table 3).

These findings, without taking any data from additional discordant case investigation (DCI) into account, resulted in a concordance rate of 91.8% and sensitivity of 98.1%. The specificity rate of 91.7% was based on the investigation of 120 histologically negative samples, in which the usual five levels plus all additional levels available were analyzed by histology.

Table 2 Analyses results of 343 lymph nodes as indicated by OSNA and histological investigation

OSNA	Histological investigation			
	Macrometastases	Micrometastases	Isolated tumor cells	Negative
++	90	7	–	9
+	7	–	1[a]	16
–	0	2[b]	2[c,d]	209

[a] In level 1–3
[b] Only micrometastasis in level 4
[c] Only in level 2
[d] In levels 1 and 2

Discordant case investigation

RNA and proteins were extracted from the lysates of the 28 discordant cases, followed by QRT-PCR for beta-actin, CK19, FOXA1, and SPDEF as well as Western Blotting for CK19. If the data obtained by those additional analyses were consistent with the results obtained by OSNA, it was concluded that tumor deposits were either only present in slices b or d used for histology or in slices a or c used for OSNA. As a consequence, these samples were excluded from the sample cohort because, in all likelihood, a tissue allocation bias (TAB) had occurred (Table 3).

The two histology positive/OSNA negative samples gave negative results in both QRT-PCR and Western blot (Table 3). In 11 of the 26 histology negative/OSNA positive samples, the outcome of additional analyses indicated the presence of tumor deposits in the slices a or c used for OSNA. When these 13 samples with discordant results between histology and OSNA were not taken into account anymore, the concordance rate changed to 95.5% (315 out of 330) and sensitivity to 100% (104 out of 104). The specificity accounted for 96.5% (109 out of 114) because discordant samples 2, 8, 10, 15, 18, and 25 were part of the specificity study.

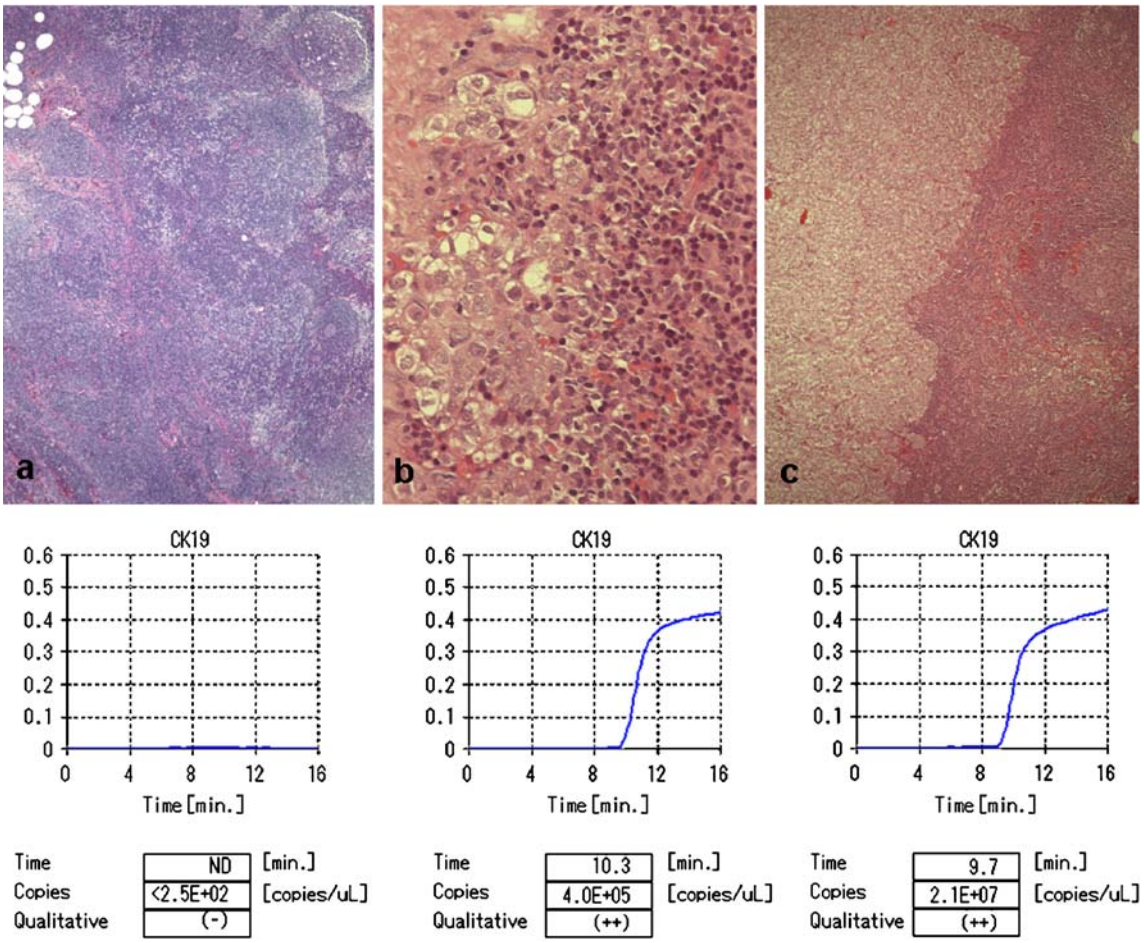

Fig. 1 Histologically negative samples (**a**), micrometastases (**b**), and macrometastases (**c**; *top*) are correlated to CK19 mRNA copy number/μL (*bottom*). The rise time, which is defined as the time point when the turbidity reached 0.1, is related to CK19 mRNA copy number via a standard curve which was performed beforehand with three calibrators

Interestingly, more than one OSNA positive/histology negative sample originated from the same patient: samples 1 and 15; samples 7, 13, and 17; samples 22–24; as well as samples 18 and 20 came from one patient, respectively, suggesting the presence of tumor cells in the lymph nodes of these patients.

Discussion

Recently, several studies have addressed the intraoperative use of molecular methods to detect metastatic deposits in SN of breast cancer patients, with varying degree of success. The GeneSearch breast lymph node (BLN) assay which uses CK19 in combination with mammaglobin as targets for RT-PCR gave concordance rates of 92.3% [19, 27] with an inferior performance at detecting micrometastases, as 57% sensitivity were reported. The concordance rates of the OSNA method as determined in two studies were 98.2% [20] and 94.8% [21]. Whereas the BLN assay gave negative or positive results based on ct, the results of OSNA were categorized into (++), (+), as well as (−), and further described by a display of CK19 mRNA copy number as a quantitative information.

In this study, the OSNA performance versus five-level histology (H&E staining, IHC with LU5) was evaluated in 343 ALN from 93 German breast cancer patients. The concordance rate was 91.7%, sensitivity 98.1%, and specificity 90.8%. Since alternate slices of the LN were used for OSNA and histology, it is self-evident that in some events, tumor deposits might be confined to the slices analyzed by OSNA or to the slices used for histology (TAB). In fact, it was recently shown that most discrepancies obtained from analysis of SN by histological and molecular approaches arise from the use of alternate slices for each method [28]. In order to clarify if some of the discordant results obtained in this study occurred as a consequence of this TAB, the homogenates of these lymph node samples were subjected to DCI by RT-PCR and Western blotting. In both of the OSNA negative/histology

Table 3 Discordant case investigation

No.	Histology	OSNA	QRT-PCR				Western Blot	Conclusion
		Copies/μL (++/+/−)	Beta-actin +/−	CK19 +/−	FOXA1 +/−	SPDEF+/−	CK19 +/−	
1	–	250 (+)	+	−	−	−	−	Discordant
2		280 (+)	+	+	+	+	+	Sampling bias
3	–	320 (+)	+	+	−	−	−	Sampling bias
4	–	320 (+)	+	−	−	−	−	Discordant
5	–	330 (+)	+	−	−	−	−	Discordant
6	–	470 (+)	Could not be performed					Discordant
7	–	540 (+)	+	−	−	−	−	Discordant
8	–	690 (+)	+	+	−	+	+	Sampling bias
9	–	730 (+)	+	−	−	−	−	Discordant
10	–	750 (+)	+	+	+	+	+	Sampling bias
11	–	820 (+)	+	−	+	−	−	Sampling bias
12	–	1,000 (+)	+	–[a]	−	−	−	discordant
13	–	1,300 (+)	+	−	−	−	−	Discordant
14	–	1,500 (+)	+	+	−	−	−	Sampling bias
15	ITC	1,800 (+)	+	+	+	+	+	Sampling bias
16	–	2,100 (+)	+	−	−	−	−	Discordant
17	–	1,900 (+)	+	−	−	−	−	Discordant
18	–	12,000 (++)	+	+	+	+	+	Sampling bias
19	–	16,000 (++)	+	−	−	−	−	Discordant
20	–	18,000 (++)	+	−	−	−	−	Discordant
21	–	20,000 (++)	+	−	−	−	−	Discordant
22	–	20,000 (++)	+	−	−	−	−	Discordant
23	–	45,000 (++)	+	+	−	−	+	Sampling bias
24	–	90,000 (++)	+	+	−	+	+	Sampling bias
25	–	360,000 (++)	+	+	+	+	+	Sampling bias
26	–	52,000 (++)	+	−	−	−	−	Discordant
27	Micrometastasis in level 4-	ND[a]	+	−	−	−	−	Sampling bias
28	Micrometastasis	ND	+	−	−	−	−	Sampling bias

[a] Gave some nonspecific bands upon electrophoresis
[b] ND not detected

positive and 11 out of 26 OSNA positive/histology negative samples, DCI revealed equivalent results to the ones seen in the OSNA assay. When these specimens were removed from the sample cohort, the concordance rate was 95.5%, sensitivity 100%, and specificity 95.6%. It cannot be fully excluded that even a higher proportion of discordant results were due to TAB because the homogenates were exposed to long storage and transport conditions which might have lowered the concentration and quality of RNA and proteins. This is especially true for OSNA samples with copy numbers close to the cutoff level as QRT-PCR, and Western blot investigation is then also likely to be close to the detection limit.

By taking the study design into consideration, it is quite apparent that in the OSNA assay, the whole of slices a&c was analyzed, whereas multiple 100 μm skip ribbons of the slices used for histology were left uninvestigated, a concept which is inherently indicative of OSNA positive/histology negative results. At the same time, since this protocol reflects the real situation in its best-case scenario with regard to routine histological investigation of sentinel nodes, the advantage of OSNA is at hand. Even more small metastases might have been missed if the lymph nodes had been cut in 500 μm intervals because the German guidelines recommend two to three sections between 100 and 500 μm [29]. Eleven out of the 26 OSNA positive/histology negative had CK19 mRNA copy numbers/μL below 1,000. With 250 copies/μL as the cutoff level, these positive OSNA results very likely indicate a low tumor burden in the lymph nodes which was probably absent in the tissue sections used for histological investigation.

It was reported that almost all (98.2%) breast cancer tumors express CK19 [30]. The results obtained in the present study support this notion, since OSNA based on CK19 mRNA expression detected all metastases which were reported by histology, after correcting the results for TAB. One must keep in mind that these numbers dealing with CK19 expression in breast cancer tumors are based on protein but not mRNA expression. In one OSNA-positive specimen, H&E staining revealed a macrometastases (8 mm

in diameter). This metastasis exhibited a very weak reaction with LU5 and no reaction with the CK19 antibody. This example shows that low CK19 protein expression is no compelling evidence for low CK19 mRNA expression. Except this one case, all H&E-positive samples were also positive with CK19 IHC.

In summary, the OSNA assay based on CK19 mRNA expression proved to be a reliable and standardized tool for the intraoperative detection of lymph node metastases in breast cancer patients. Since OSNA showed a similar performance to in-depth histological analyses routinely performed in SN of German breast cancer patients, its adoption as a clinical approach could lead to a benefit for the patients in that unnecessary second surgeries are avoided, and diagnosis is improved.

Acknowledgements The authors want to thank Sunna Frank, Anja Bredtmann, Maike Pacena, and Silvia Holz for their contribution in coordinating the study and their technical assistance.

This study was supported by Sysmex (Kobe, Japan).

Conflict of interest statement We declare that we have no conflict of interest.

References

1. Morton DL, Wen DR, Wong JH et al (1992) Technical details of intraoperative lymphatic mapping for early stage melanoma. Arch Surg 127:392–399
2. Golshan M, Martin WJ, Dowlatshahi K et al (2003) Sentinel lymph node biopsy lowers the rate of lymphedema when compared with standard axillary lymph node dissection. Am Surg 69:209–211
3. Veronesi U, Paganelli G, Viale G et al (1999) Sentinel lymph node biopsy and axillary dissection in breast cancer: results in a large series. J Natl Cancer Inst 91:368–373
4. Lyman GH, Giuliano AE, Somerfield MR et al (2005) American Society of Clinical Oncology guideline recommendations for sentinel lymph node biopsy in early-stage breast cancer. J Clin Oncol 23:7703–7720
5. Ferrari A, Rovera F, Dionigi P et al (2006) Sentinel lymph node biopsy as the new standard of care in the surgical treatment for breast cancer. Expert Rev Anticancer Ther 6:1503–1515
6. Mabry H, Giuliano AE (2007) Sentinel node mapping for breast cancer: progress to date and prospects for the future. Surg Oncol Clin N Am 16:55–70
7. Motomura K, Inaji H, Komoike Y et al (2000) Intraoperative sentinel lymph node examination by imprint cytology and frozen sectioning during breast surgery. Br J Surg 87:597–601
8. Creager AJ, Geisinger KR, Shiver SA et al (2002) Intraoperative evaluation of sentinel lymph nodes for metastatic breast carcinoma by imprint cytology. Mod Pathol 15:1140–1147
9. Leidenius MH, Krogerus LA, Toivonen TS et al (2003) The feasibility of intraoperative diagnosis of sentinel lymph node metastases in breast cancer. J Surg Oncol 84:68–73
10. Brogi E, Torres-Matundan E, Tan LK et al (2005) The results of frozen section, touch preparation, and cytological smear are comparable for intraoperative examination of sentinel lymph nodes: a study in 133 breast cancer patients. Ann Surg Oncol 12:173–180
11. Cserni G, Amendoeira I, Apostolikas N et al (2003) Pathological work-up of sentinel lymph nodes in breast cancer. Review of current data to be considered for the formulation of guidelines. Eur J Cancer 39:1654–1667
12. Cserni G, Amendoeira I, Apostolikas N et al (2004) Discrepancies in current practice of pathological evaluation of sentinel lymph nodes in breast cancer. Results of a questionnaire based survey by the European Working Group for Breast Screening Pathology. J Clin Pathol 57:695–701
13. Roberts CA, Beitsch PD, Litz CE et al (2003) Interpretive disparity among pathologists in breast sentinel lymph node evaluation. Am J Surg 186:324–329
14. Mitas M, Mikhitarian K, Walters C et al (2001) Quantitative real-time RT-PCR detection of breast cancer micrometastases using a multigene marker panel. Int J Cancer 93:162–171
15. Weigelt B, Verduijn P, Bosma AJ et al (2004) Detection of metastases in sentinel lymph nodes of breast cancer patients by multiple mRNA markers. Br J Cancer 90:1531–1537
16. Nissan A, Jager D, Roystacher M et al (2004) Multimarker RT-PCR assay for the detection of minimal residual disease in sentinel lymph nodes of breast cancer patients. Br J Cancer 94:681–685
17. Gimbergues P, Dauplat MM, Cayre A et al (2007) Correlation between molecular metastases in sentinel lymph nodes of breast cancer patients and St Gallen risk category. Eur J Surg Oncol 33:16–22
18. Gillanders WE, Mikhitarian K, Hebert R et al (2004) Molecular detection of micrometastatic breast cancer in histopathology-negative axillary lymph nodes correlates with traditional predictors of prognosis: an interim analysis of a prospective multi-institutional cohort study. Ann Sur 239:828–837, discussion 837–840
19. Julian TB, Blumencranz P, Deck K et al (2008) Novel intraoperative molecular test for sentinel lymph node metastases in patients with early-stage breast cancer. J Clin Oncol 26:3338–3345
20. Tsujimoto M, Nakabayashi K, Yoshidome K et al (2007) One-Step Nucleic Acid Amplification (OSNA) for intraoperative detection of lymph node metastasis in breast cancer patients. Clin Can Res 13:4807–4816
21. Visser M, Jiwa M, Horstman A et al (2008) Intra-operative rapid diagnostic method based on CK19 mRNA expression for the detection of lymph node metastases in breast cancer. Int J Cancer 122:2562–2567
22. Taniyama K, Motoshita J, Sakane J et al (2006) Combination analysis of a whole lymph node by one-step nucleic acid amplification and histology for intraoperative detection of micrometastasis. Pathobiology 73:183–191
23. Notomi T, Okayama H, Masubuchi H et al (2000) Loop-mediated isothermal amplification of DNA. Nucleic Acids Research 28:e63
24. Mori Y, Nagamine K, Tomita N et al (2001) Detection of loop-mediated isothermal amplification reaction by turbidity derived from magnesium pyrophosphate formation. Biochem Biophys Res Commun 289:150–154
25. Sobin LH, Wittekind C et al (2002) UICC TNM classification of malignant tumours, 6th edn. John Wiley & Sons, Inc., New York
26. Singletary SE, Greene FL (2003) Revision of breast cancer staging: the 6th edition of the TNM classification. Semin Surg Oncol 21:53–59
27. Blumencranz P, Whitworth PW, Deck K et al (2007) Sentinel node staging for breast cancer: intraoperative molecular pathology

overcomes conventional histologic sampling errors. Am J Surg 194:426–432

28. Daniele L, Annaratone L, Allia E et al (2008) Technical limits of comparison of step-sectioning, immunohistochemistry and RT-PCR on breast cancer sentinel nodes: a study on methacarn fixed tissue. J Cell Mol Med (in press)
29. Kreienberg R, Kopp I, Albert U et al (2008) Interdisciplinary S3-Guideline for breast cancer diagnostic procedures, therapy and follow-up. (article in German) W. Zuckschwerdt Verlag 1. Aktualisierung 02/2008, ISBN: 978-3-88603-934-0
30. Chu PG, Weiss LM (2002) Keratin expression in human tissues and neoplasms. Histopathology 40:403–439

Virchows Arch (2009) 454:211–215
DOI 10.1007/s00428-008-0702-x

ORIGINAL ARTICLE

Vascular invasion demonstrated by elastic stain—a common phenomenon in benign granular cell tumors

Gábor Cserni · Rita Bori · István Sejben

Received: 16 September 2008 / Revised: 7 November 2008 / Accepted: 11 November 2008 / Published online: 10 December 2008

Abstract Granular cell tumor is generally benign, but rare malignant cases have been documented. Features of malignancy include necrosis, cellular spindling, vesicular nuclei with large nucleoli, increased mitotic activity, high nuclear to cytoplasmic ratio, and pleomorphism, but not vascular invasion. Venous invasion was incidentally identified with the orcein elastic stain in an otherwise benign granular cell tumor (propositus case). Four further benign granular cell tumors were also analyzed; venous invasion was discovered in three. It is suggested that vascular invasion is not uncommon in granular cell tumors and should not lead to the classification of the tumor as malignant or atypical. It is likely that in most cases there is only invasion of the vascular wall. It is also suggested that some cases of vascular invasion identified by elastic stains in tumors such as colorectal carcinomas (where these stains are recommended for routine use) may also represent invasion of vascular structures without the propensity of metastasis.

Keywords Granular cell tumor · Vascular invasion · Venous invasion · Orcein · Elastic stain

Introduction

Granular cell tumor is a well-described tumor recognized as of probable Schwannian origin but distinct from Schwannomas [1]. It is typically a benign tumor, most commonly occurring in dermal, subcutaneous, or submucosal locations, but has been described in a multitude of other sites of the body. Very rare cases with metastases have also been reported, and malignant behavior has been approached on the basis of histological features too, namely the presence of necrosis, cellular spindling, vesicular nuclei with large nucleoli, increased mitotic activity (>2/10 ×200 magnification field), high nuclear to cytoplasmic ratio, and pleomorphism. Tumors with at least three out of the six listed morphologic characteristics have been classified as malignant, whereas those having only one or two of these features are termed as atypical [2, 3]. The rest, the vast majority of the tumors, remain in the benign category.

The incidental finding of vascular invasion in an otherwise conventional granular cell tumor that would have been categorized as benign on the basis of the Fanburg-Smith criteria [2] listed above resulted in a diagnostic challenge that could not be easily solved on the basis of published cases and major textbooks [3–5]. There seems to be no documentation of this feature in this type of tumor.

The identification of venous invasion in an otherwise benign granular cell tumor (the propositus case) made us look for this feature in a few other unselected cases of this specific tumor.

Materials and methods

Besides the propositus case, we collected two further cases of typical granular cell tumors from our prospective surgical excision specimens and two from our recent archives to check whether blood vessel invasion could be demonstrated in them.

Orcein, a simple monochromatic elastic stain, was employed to demonstrate the presence of an elastic lamina

G. Cserni (✉) · R. Bori · I. Sejben
Department of Pathology,
Bács-Kiskun County Teaching Hospital,
Nyiri ut 38.,
6000 Kecskemét, Hungary
e-mail: cserni@freemail.hu

of blood vessels, and this was also used to identify vascular invasion within the tumor, the same way as it is routinely used in our department for colorectal cancer specimens (Fig. 1). Briefly, following deparaffination, the staining is carried out overnight in a solution of 0.1 g of orcein (Reanal, Budapest, Hungary) in 100 ml 70% ethanol and 2 ml concentrated hydrochloric acid. This is followed by differentiation in 70% ethanol, dehydration, clearing in xylene, and mounting.

For immunohistochemistry, the following antibodies were used: S100 (DakoCytomation, Glostrup, Denmark, N1573—ready to use), CD31 (DakoCytomation, N1596—ready to use), and CD34 (DakoCytomation, N1632—ready to use).

Results

The relevant features of the five studied tumors are reported in Table 1. Tumors removed in toto were relatively circumscribed, nodular, firm, rubbery with homogeneous gray-white cut surface.

Microscopically, the tumors consisted of small groups and cords of cells with characteristic round to polygonal shape and obvious eosinophilic cytoplasmic granularity or similar individual cells. The nuclei lacked atypia and were generally uniform in size with a homogeneous chromatin pattern and occasional small nucleoli. Typical mitotic figures ranged from 0 to 1 per 10 ×400 high power fields. No necrosis was present. The neoplasms had infiltrative borders which at minute foci interfered with the inked resection margins (Table 1). The cells were typically S-100 and PAS positive. In the propositus case, intraneuronal growth was suspected in one slide, and an orcein stain was requested for differentiation from vascular invasion. Close to the focus of intraneuronal growth, this demonstrated a circular elastic lamina characteristic of small veins encircling granular cells of the tumor. Despite the fact that none of the Fanburg-Smith criteria for malignancy were met, vascular invasion was perceived as a worrying feature, and the tumor was labeled as atypical. As the inked margins contained minor expansions of the tumor, which was therefore considered to be incompletely excised, a careful clinical follow-up was recommended instead of reexcision after discussion with the patient, a surgeon himself. As shown in Table 1, vascular invasion, when searched for by means of the elastic stain, was present in three further cases. In case 4, one instance of vascular invasion could be detected, with granular cells within the boundaries of the elastic lamina, but the endothelium-lined lumen being free (Table 1; Fig. 2).

The identification of venous invasion by elastic stain prompted us to look for endothelial markers (CD31 and CD34) with immunohistochemistry, but neither of the areas identified with orcein and lacking a lumen on this stain demonstrated an endothelial lining; therefore, the intraluminal presence of tumor cells could not be documented. An exception to this was one vessel in case 3, where at the deeper level taken for immunohistochemistry an intact endothelial lining and a narrowed empty lumen could be seen, despite the invasion of the vascular wall (Fig. 3).

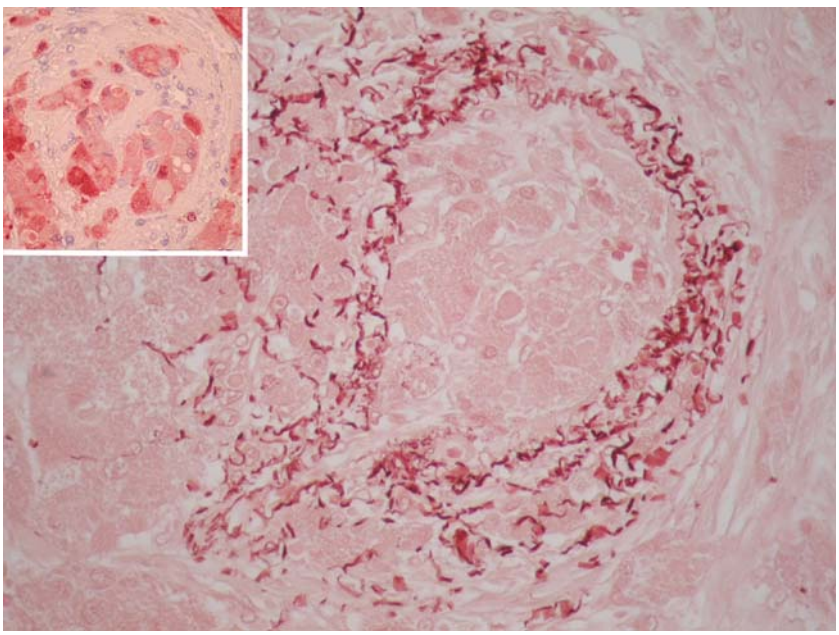

Fig. 1 Venous invasion noticed on orcein stain in case 1. The granular tumor cells destroy the structure of the vein, especially on the left side, but the circular arrangement of the elastic fibers makes it easy to recognize the vascular structure. *Inset* shows the same circumscribed area immunostained for S100 protein (orcein ×400, *inset* S100 ×400)

Table 1 Relevant features of the five studied tumors

Case	Age	Sex	Location	Size (mm)	Number of blocks/ instances of VI	Localization of VI (distance from tumor edge)	Excision margins	Follow-up (months)	Comment
1 (propositus)	40	M	Infraclavicular, behind the major pectoral muscle	25	4/1	Central (4 mm)	Positive	6 NED	Fig. 1
2	65	F	Tip of the tongue[a]	n.a. (8 mm clinically)	4/2	Central + peripheral (1 mm)	n.a.	6 NED	
3	23	F	Left shoulder, dermal/subcutaneous	14	2/4	Central (5 mm)	Focally positive	1 NED	Fig. 4
4	42	M	Stomach, submucous[b]	15	2/1	Central (3 mm)	Reaching	18 NED[c]	Fig. 2
5	42	F	Posterior axillary region, dermal/subcutaneous	10	2/0	n.a.	Negative	5 NED	

n.a. not applicable, *VI* vascular invasion
[a] The tumor was removed in multiple pieces
[b] Incidental finding during surgery for a bleeding ulcer
[c] Clinically, endoscopic control denied

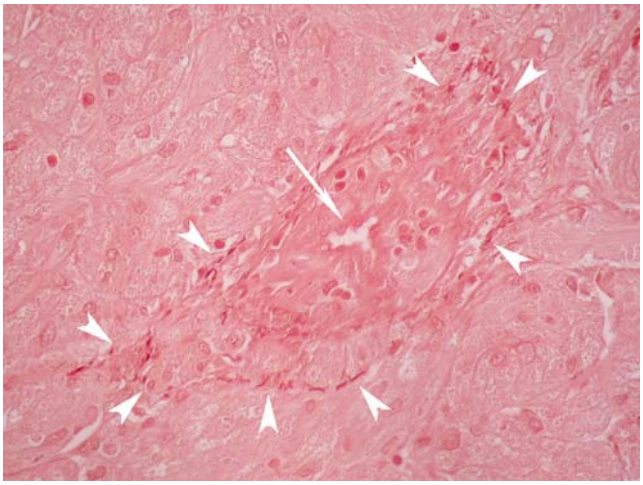

Fig. 2 Involvement of a venous wall in the fourth tumor. Granular tumor cells are seen at 7–8 o'clock position beyond the elastic lamina (*arrowheads*). The vascular lumen (*arrow*) remained patent and uninvolved

Discussion

Vascular invasion is generally a sign of malignancy and is associated with metastasis formation and disease recurrence. Lymphatic vessel invasion is associated with lymph node metastases and blood vessel invasion with systemic metastases. At the capillary level, conventional histological stains do not allow the differentiation between lymphatic and blood vessels, and immunostains for lymphatic endothelium-specific markers are not part of the standard assessment of tumors. As a consequence, some authorities have suggested to use the non-committed term of "(lympho-)vascular invasion" or simply vascular invasion instead of lymphatic or blood vessel invasion [6]. At the larger vessel level, the vascular channels which are invaded generally represent smaller veins. Elastic stains such as the elastic van-Gieson or orcein (used in the present work) have been employed to enhance the demonstration of venous invasion in colorectal carcinoma [7, 8], and we have successfully used orcein for this purpose in gastric carcinomas and carcinoids as well.

Although angioinvasion is identified by visualization of tumor cells in vessels, pathologists are well aware of artificial displacement of tumor cells into vascular channels, resulting in nearly identical morphology, but most probably a substantially different meaning. This phenomenon of cellular displacement occurring at different sites of the body is sometimes referred to as pseudo-invasion [9–13]. However, tumor cells breaking through the elastic lamina of a vessel are not artifactual and represent a worrisome feature, since blood vessel invasion is generally associated with malignant behavior and distant metastases [14].

Nevertheless, some benign conditions showing lymphatic or blood vessel invasion have been reported previously and

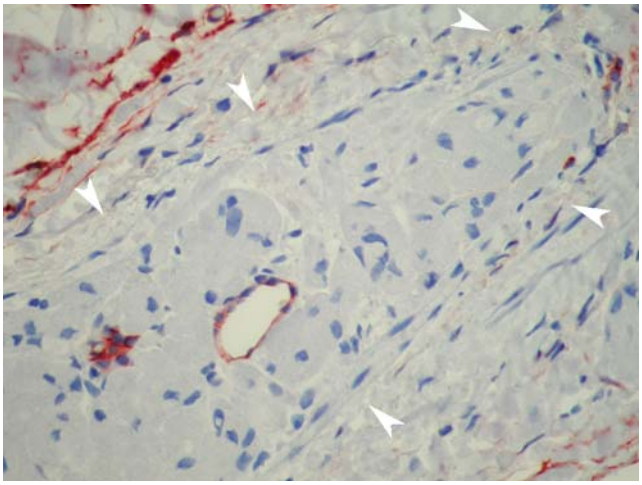

Fig. 3 Deeper level of the vessel seen in top left position of Fig. 4. The narrowed central lumen devoid of tumor cells is highlighted by the stained endothelial cells. The position of the elastic lamina is shown by *arrowheads* (CD34 ×400)

these include cutaneous nevi [15], sclerosing adenosis of the breast [16], and vasitis nodosa [17]. It might be supposed that looking for vascular invasion with elastic stains may not only increase the detection rate of vascular invasion but may highlight its presence in previously unsuspected conditions as suggested by Eusebi and Azzopardi [16].

A search in Pubmed showed no mention of "vascular invasion" in relation with granular cell tumors, and no guidance relating to this feature could be found in major textbooks either [3–5]. The largest available series dealing with the criteria of malignancy is that of Fanburg-Smith et al. [2], and vascular invasion is not listed as a criterion for malignancy. Furthermore, the cases deemed malignant on the basis of histological features lacked vascular invasion. Seeking for an external opinion in the first case was obvious, and this reinforced the view that, on the sole basis of vascular invasion, a tumor with the morphological features of a benign granular cell tumor should not be categorized as malignant, but because of the lack of reports on the importance of this worrying finding, a careful follow-up was advised for this "atypical" granular cell tumor.

We are aware of only one case of granular cell tumor located on the penis, where vascular invasion was documented on hematoxylin and eosin slides, and the tumor behaved in a benign fashion [18]. The small series of penile granular cell tumors including the case with invasion of a vessel (more precisely the vascular wall as depicted in Figure 1B of the publication) also suggested that minor involvement of the surgical margins did not obviously result in local recurrences, and, given the problematic nature of reexcision at that anatomic location, follow-up could also be a reasonable first choice as clinical decision [18].

Our few cases cannot give an estimate of the incidence of venous invasion that can be detected by using elastic stains, but suggest that the invasion of blood vessel walls is much more common in granular cell tumors than previously thought. It seems likely that the instances of vascular invasion are related to the invasive growth pattern of granular cell tumors. Similarly to small nerve invasion [3, 18, 19], the

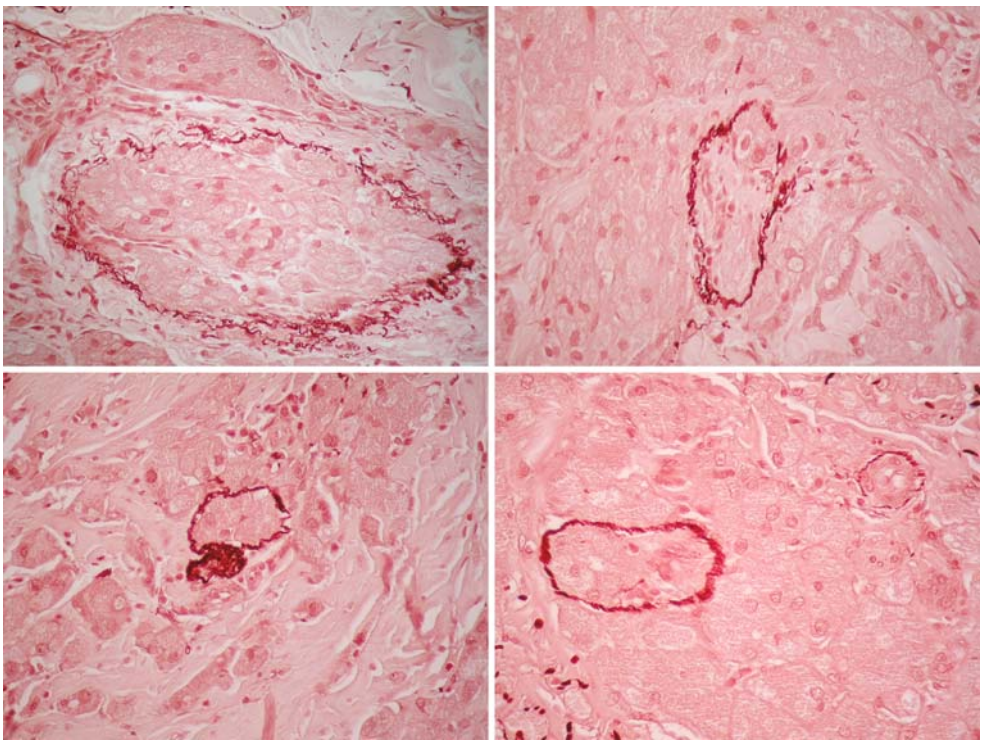

Fig. 4 Four different examples of vascular invasion seen in case 3. Granular tumor cells occupy most of the area inside the vascular elastic lamina, except the example on the right upper part, where only three adjacent cells are seen at 12–1 o'clock position (orcein ×400)

tumor cells may simply grow through the vessel wall as well, without a real propensity to metastasize.

In two instances of venous invasion from this small series, the intact endothelial lining of the involved vessel could be visualized either in the orcein stained slide (Fig. 2) or at a deeper level immunostained with endothelial markers; the lumen contained no tumor cells (Fig. 3). Therefore, it is likely that at least some (and probably most) examples of venous invasion demonstrated by elastic stains do not correspond to intravascular tumor cells with the ability to be taken away by the blood flow to distant metastatic sites but are merely the result of infiltration of the subendothelial layers of the vessels. The partial infiltration of the vascular wall depicted in Fig. 4 (upper right) also supports this notion. Our observation must be true for other anatomic sites (e.g., the colon and the rectum) too, where elastic stains have been recommended as a routine to identify venous invasion [7, 8]. Indeed, elastic stains have been found to be sensitive but of questionable specificity to detect real vascular invasion [20].

Serial sectioning of the blocks in search of a central lumen was not thought to be necessary in all instances of vascular invasion detected by elastic stains, as it was felt that areas such as the one shown in Figure 3 could have been localized in the part already cut away. It was also felt that tangential sectioning, as a random event, could not explain all instances of vascular invasion visualized, and at least some of them could represent the total destruction of the vessels by the ingrowth of benign granular tumor cells. Free-floating malignant tumor cells and tumor cells filling the veins have been reported to be more often associated with liver metastases in colorectal carcinomas than the so called obliterative type of venous invasion [14]. All the vascular invasions detected by the elastic stains would have belonged to this latter variant according to the classification by Ouchi et al. [14], so even if the cells would have been those of a malignant tumor, the association with metastatic potential would have been expected to be less than in the case of free-floating or filling types of venous invasion.

As granular cell tumors are generally benign and metastasizing or histologically malignant cases are extremely rare, the common demonstration of venous (wall) invasion by elastic stains should not be considered a sign of malignancy and probably should not even require the tumor to be labeled as atypical. The lack of recurrences or signs of metastasis supports the benign and typical overall appearance of the granular cells tumors, but the follow-up of our patients is short. Larger series with longer follow-up are needed to clarify the impact of identifying vascular invasion on the diagnosis and behavior of these tumors.

Acknowledgments The authors thank Prof. Thomas Krausz from the University of Chicago Department of Pathology for his opinion on our initial case and Drs. Csaba Olah, Kornel Vajda, Laszlo Marko, Karoly Szajki, and Ferenc Oberna for the clinical follow-up data.

Conflict of interest statement We declare that we have no conflict of interest.

References

1. Ordonez NG (1999) Granular cell tumor: a review and update. Adv Anat Pathol 6:186–203
2. Fanburg-Smith JC, Meis-Kindblom JM, Fante R et al (1998) Malignant granular cell tumor of soft tissue: diagnostic criteria and clinicopathologic correlation. Am J Surg Pathol 22:779–794
3. Weiss SW, Goldblum JR (2001) Benign tumors of peripheral nerves. In Weiss SW, Goldblum JR (eds) Enzinger and Weiss's soft tissue tumors, 4th edn. Mosby, St Louis, pp 1111–1207
4. Fletcher CDM (2007) Peripheral neuroectodermal tumors. In: Fletcher CDM (ed) Diagnostic histopathology of tumors, 3rd edn. Churchill-Livingstone-Elsevier, Philadelphia, pp 1731–1761
5. Rosai J (2004) Soft tissues. In: Rosai J (ed) Rosai and Ackerman's surgical pathology, 9th edn. Mosby, St Louis, pp 2237–2371
6. Ellis IO, Pinder SE, Bobrow L et al (2005) Pathology reporting of breast disease. Available via http://www.cancerscreening.nhs.uk/breastscreen/publications/nhsbsp58-low-resolution.pdf. Accessed 15 September 2008
7. Vass DG, Ainsworth R, Anderson JH et al (2004) The value of an elastic tissue stain in detecting venous invasion in colorectal cancer. J Clin Pathol 57:769–772
8. Abdulkader M, Abdulla K, Rakha E et al (2006) Routine elastic staining assists detection of vascular invasion in colorectal cancer. Histopathology 49:487–492
9. McLachlin CM, Devine P, Muto M et al (1994) Pseudoinvasion of vascular spaces: report of an artifact caused by cervical lidocaine injection prior to loop diathermy. Hum Pathol 25:208–211
10. Diaz LK, Wiley EL, Venta LA (1999) Are malignant cells displaced by large-gauge needle core biopsy of the breast. Am J Roentgenol 173:1303–1313
11. Nagi C, Bleiweiss I, Jaffer S (2005) Epithelial displacement in breast lesions: a papillary phenomenon. Arch Pathol Lab Med 129:1465–1469
12. Rosai J, Kuhn E, Carcangiu ML (2006) Pitfalls in thyroid tumour pathology. Histopathology 49:107–120
13. Logani S, Herdman AV, Little JV et al (2008) Vascular "pseudo invasion" in laparoscopic hysterectomy specimens: a diagnostic pitfall. Am J Surg Pathol 32:560–565
14. Ouchi K, Sugawara T, Ono H et al (1996) Histologic features and clinical significance of venous invasion in colorectal carcinoma with hepatic metastasis. Cancer 78:2313–2317
15. Howat AJ, Variend S (1985) Lymphatic invasion in Spitz nevi. Am J Surg Pathol 9:125–128
16. Eusebi V, Azzopardi JG (1976) Vascular invasion in benign breast disease. J Pathol 118:9–16
17. Balogh K, Travis WD (1985) Benign vascular invasion in vasitis nodosa. Am J Clin Pathol 83:426–430
18. Laskin WB, Fetsch JF, Davis CJ Jr et al (2005) Granular cell tumor of the penis: clinicopathologic evaluation of 9 cases. Hum Pathol 36:291–298
19. Angiero F, Crippa R, Stefani M (2006) Granular cells tumour in the oral cavity: report of eleven cases treated with laser surgery. Minerva Stomatol 55:423–430
20. Kingston EF, Goulding H, Bateman AC (2007) Vascular invasion is underrecognized in colorectal cancer using conventional hematoxylin and eosin staining. Dis Colon Rectum 50:1867–1872

Virchows Arch (2009) 454:217–222
DOI 10.1007/s00428-008-0696-4

ORIGINAL ARTICLE

Sphingosine-1-phosphate receptor 1 is a useful adjunct for distinguishing vascular neoplasms from morphological mimics

Takashi Akiyama · Shuji Hamazaki · Yasumasa Monobe · Hirotake Nishimura · Isao Irei · Yoshito Sadahira

Received: 15 August 2008 / Revised: 22 October 2008 / Accepted: 24 October 2008 / Published online: 13 November 2008

Abstract Sphingosine-1-phosphate receptor 1 ($S1P_1$) has been shown to play an important role in the migration, proliferation, and survival of endothelial cells. $S1P_1$ of vascular and lymphatic endothelial cells can be detected by immunostaining of paraffin-embedded sections using a rabbit anti-$S1P_1$ antibody. In this study, to distinguish vascular tumors from histologic mimics using immunohistochemical means, we evaluated the expression of $S1P_1$ in a range of vascular tumors. $S1P_1$ expression was observed in eight of eight hemangiomas, four of four lymphangiomas, four of four epithelioid hemangioendotheliomas, three of three Kaposi's sarcomas, and 15 of 15 angiosarcomas with vasoformative, spindle, epithelioid, and undifferentiated features. Conventional analysis and use of a tissue microarray of soft tissue tumors revealed three of 21 liposarcomas to have weak cytoplasmic staining and one of five squamous cell carcinomas to have membranous staining in a very limited area among 115 nonvascular tumors including histological mimics of angiosarcoma such as undifferentiated carcinoma, melanoma, and epithelioid sarcoma. The sensitivity with regards to the angiosarcoma cases was equal to, or even exceeded in undifferentiated angiosarcoma, that of CD31. Based on this study, $S1P_1$ may be a useful adjunct to CD31 in cases where a vascular neoplasm requires a differential diagnosis.

T. Akiyama · S. Hamazaki · H. Nishimura · I. Irei · Y. Sadahira (✉)
Department of Pathology, Kawasaki Medical School,
577 Matsushima,
Kurashiki 701-0192, Japan
e-mail: sadapath@med.kawasaki-m.ac.jp

Y. Monobe
Department of Pathology, Kawasaki Hospital,
Okayama, Japan

Keywords Sphingosine-1-phosphate receptor 1 · Endothelial cells · Angiosarcoma · Immunohistochemistry

Introduction

Surgical pathologists infrequently encounter difficult cases of vascular tumors that need to be distinguished from histological mimics. Immunohistochemical markers of endothelial differentiation such as von Willebrand factor (factor-VIII-related antigen) [1], CD31 [2], and CD34 [3] and more recently reported markers such as thrombomodulin [4], Fli-1 [5], podoplanin [6], and angiostatin receptor annexin II [7] are used for elucidating the endothelial nature of tumors. In the case of angiosarcoma, von Willebrand factor and CD31 are considered the most specific markers [8, 9]. No marker superior to CD31 has been reported which allows the sensitive detection of undifferentiated angiosarcomas [10].

Sphingosine-1-phosphate (S1P), a potent lipid mediator, is produced by the metabolism of sphingolipids in cells [11]. It transduces intracellular signals involved in diverse cellular effects through the activation of S1P receptors including S1P receptor 1 ($S1P_1$), $S1P_2$, $S1P_3$, $S1P_4$, and $S1P_5$ [12]. These S1P receptors are seven-truncated plasma membrane receptors expressed ubiquitously in different tissues and coupled to different intracellular second messenger systems, including adenylate cyclase, phospholipase C, phosphatidylinositol 3-kinase/protein kinase Akt, and mitogen-activated protein kinases, as well as Rho- and Ras-dependent pathways. As a consequence, S1P influences different biological processes depending on the relative expression of S1P receptors [12, 13].

$S1P_1$ is the major S1P receptor subtype in the cardiovascular system. The $S1P_1$ gene was initially isolated as

endothelial differentiation gene-1 (*Edg-1*) from human endothelial cells [14]. S1P binds to $S1P_1$, which induces endothelial cell migration, proliferation, survival, and morphogenesis into capillary-like structures [15]. $S1P_1$ knockout mice died in the uterus between embryonic days 13.5 and 14.5 due to impairment to the maturation of blood vessels [16]. $S1P_1$ was strongly expressed in tumor vessels and the injection of $S1P_1$ siRNA into tumors suppressed angiogenesis, which resulted in suppression of the tumors' growth [17]. However, little is not known about the *in vivo* expression and function of $S1P_1$ in human tissues.

We have recently characterized the tissue expression of $S1P_1$ in paraffin-embedded sections using a commercial rabbit anti-$S1P_1$ antibody against the C-terminal portion of human $S1P_1$. $S1P_1$ expression was restricted to normal vascular and lymphatic endothelial cells in all tissues examined and lymphocytes including thymic medullary lymphocytes and mantle cells in the secondary lymphoid follicles [18]. In this study, we have investigated the usefulness of $S1P_1$ as a diagnostic immunohistochemical marker for distinguishing vascular tumors, especially angiosarcomas, from their histological mimics.

Materials and methods

Antibodies

A rabbit polyclonal antibody against amino acids 322–381 of $S1P_1$ of human origin (Santa Cruz Biotechnology, Santa Cruz EDG-1 (H60): sc-25489) was used. This antibody can react with $S1P_1$ of human, mouse, and rat tissues and had been thoroughly checked for specificity by comparing immunostaining results of the vasculature in paraffin-embedded sections of $S1P_1^{-/-}$ and $S1P_1^{+/-}$ mouse embryos and an angiosarcoma cell line expressing a considerable quantity of $S1P_1$ mRNA [18]. Monoclonal antibodies to D2-40 (a relatively specific marker for lymphatic endothelium, Cosmo Bio, Tokyo, Japan) [19] and CD31 (Dako, Kyoto, Japan) were also used.

Tissue specimens

Case materials were obtained from the Kawasaki Medical School Hospital and Kawasaki Hospital. Specimens of one case of angiosarcoma with lung metastasis were sampled at autopsy. All autopsy samples were obtained within 3 h after death. Surgical specimens were from five cases of breast carcinoma, five cases of colon carcinoma, three cases of renal cell carcinoma, five cases of squamous cell carcinoma including acantholytic squamous cell carcinoma, one case of anaplastic carcinoma of thyroid, two cases of undifferentiated carcinoma (pancreas and stomach), two cases of carcinosarcoma (esophagus and lung), five cases of malignant melanoma, one case of clear cell sarcoma, four cases of lipoma, one case of glomus tumor, two cases of vascular leiomyoma, three cases of malignant fibrous histiocytoma (MFH), one case of hemangiopericytoma, eight cases of hemangioma, four cases of lymphangioma, four cases of epithelioid hemangioendothelioma, 15 cases of angiosarcoma from ten patients, three cases of Kaposi's sarcoma, one case of epithelioid sarcoma, two cases of chondrosarcoma, one case of alveolar soft part sarcoma, three cases of synovial sarcoma, five cases of liposarcoma, two cases of rhabdomyosarcoma, two cases of malignant peripheral nerve sheath tumor (MPNST), two cases of Ewing sarcoma–primitive neuroectodermal tumor (PNET), and five cases of gastrointestinal stromal tumor (GIST).

A tissue microarray was also studied, being composed of one case of hemangiopericytoma, one case of angiosarcoma, one case of osteosarcoma, two cases of alveolar soft part sarcoma, six cases of MPNST, four cases of synovial sarcoma, eight cases of leiomyosarcoma, four cases of rhabdomyosarcoma, 16 cases of liposarcoma, and ten cases of MFH.

Immunohistochemistry

For whole tissue section immunohistochemistry, tissues were fixed in 4% buffered formaldehyde, embedded in paraffin and sectioned at 4 μm. Whole-tissue and tissue microarray sections were stained with a fully automatic immunohistochemical system (Ventana XT system Discovery; Ventana Medical System, Tucson, AZ, USA) using the polyclonal rabbit anti-$S1P_1$ antibody (1/20 dilution) according to instructions. The immunostaining was performed with an avidin–biotin detection system. The incubation time for the first antibody was 15 min. A diaminobenzidine hydrochloride solution with hydrogen peroxide was the chromogen. The experiments had both a positive control and a negative control.

The expression of $S1P_1$ and CD31 in angiosarcoma cases was evaluated semiquantitatively using four scores, according to the percentage of positive cells in individual lesions: 0, less than 1% of tumor cells reactive; 1+, 1% to 30% of tumor cells reactive; 2+, 31–70% of tumor cells reactive; 3+, more than 70% of tumor cells reactive.

Results

Immunohistochemical expression of $S1P_1$ in vascular tumors

In surgical specimens, tumor cells of all vascular lesions including hemangiomas (Fig. 1a), lymphangiomas (Fig. 1b),

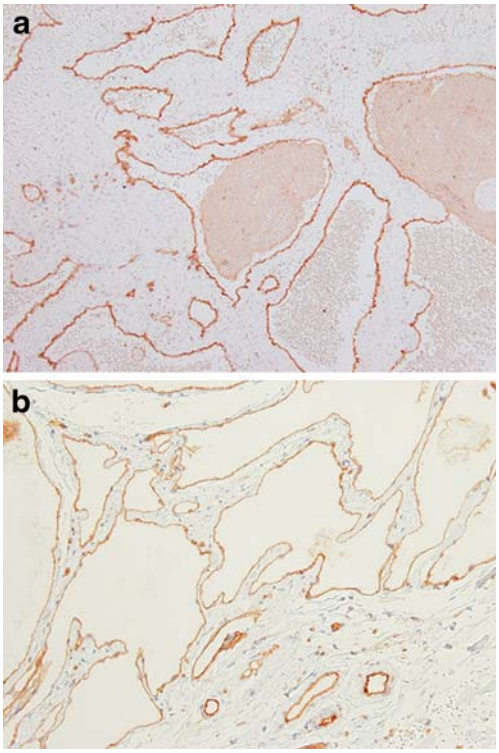

Fig. 1 Expression of $S1P_1$ in benign vascular tumors. Hemangioma of the intestine (77-year-old male, **a**). $S1P_1$ was expressed in the endothelium of dilated vessels. Lymphangioma of the intestine (63-year-old male, **b**). Dilated lymphatic vessels were stained with anti-$S1P_1$ antibody

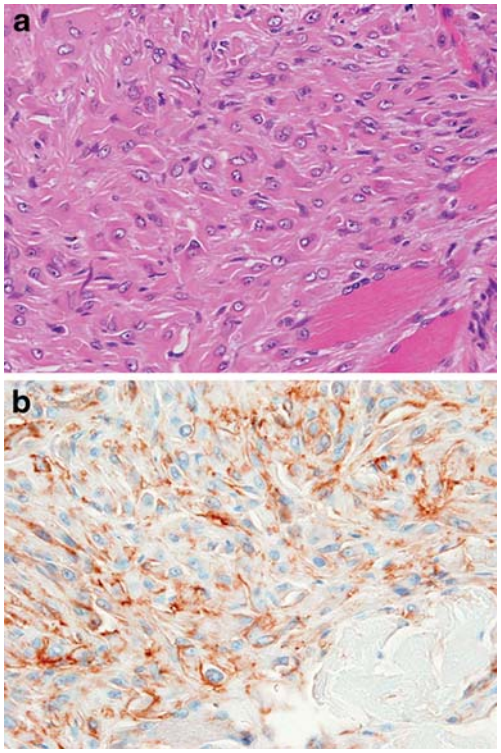

Fig. 2 Epithelioid hemangioendothelioma of the upper arm (42-year-old male). **a** H–E stain. **b** $S1P_1$ immunostaining displays membranous staining of neoplastic cells

Kaposi's sarcomas, epithelioid hemangioendotheliomas (Fig. 2a, b), and angiosarcomas were positive for $S1P_1$.

Lipomas, glomus tumors, vascular leiomyomas, clear cell sarcomas, MFHs, chondrosarcomas, alveolar soft part tumors, synovial sarcomas, MPNSTs, Ewing sarcoma–PNETs, and GISTs were negative for $S1P_1$ except the interstitial vascular and lymphatic elements. In liposarcoma cases, $S1P_1$ was expressed on many capillaries. In one case, lipoblasts and spindle cells showed weak cytoplasmic staining.

A tissue microarray composed of soft tissue tumors including hemangiopericytomas, osteosarcomas, alveolar soft part sarcomas, MPNSTs, synovial sarcomas, leiomyosarcomas, rhabdomyosarcomas, liposarcomas, and MFHs was screened for $S1P_1$ expression. As a result, no membranous staining was observed in any cases while two of 16 liposarcoma cases showed cytoplasmic staining for $S1P_1$.

Utility of $S1P_1$ as a diagnostic marker for angiosarcoma

Focusing on the diagnostic utility of anti-$S1P_1$ in cases of angiosarcoma, we next stained 15 sections from ten patients with angiosarcoma using the anti-$S1P_1$ antibody and compared the results with those obtained with anti-CD31 antibody (Table 1). Overall, all the angiosarcoma samples screened exhibited immunostaining for $S1P_1$ as well as CD31. The neoplastic cells showed strong $S1P_1$ immunoreactivity with membranous and, in some areas, cytoplasmic staining in angiosarcomas with vasoformative, spindle, and epithelioid features (Fig. 3a–c). The lung tumor of patient 8 had obvious vasoformative areas but focally exhibited a more solid and compact growth pattern. In the undifferentiated area where sheets and nests of spindle cells displaying cytologic atypia and faint CD31 expression were seen (Fig. 3d), $S1P_1$ was strongly expressed (Fig. 3e). The diagnosis of patient 9 was initially difficult because the tumor from the chest wall exhibited a poorly differentiated solid growth pattern and increased mitotic activity. While CD31 was hardly expressed in neoplastic cells (Fig. 3f), $S1P_1$ was visibly though weakly expressed in neoplastic cells (Fig. 3g). Autopsy revealed a tumor with a clear vasoformative pattern in the lung of this patient and a diagnosis of angiosarcoma was established. In a very rare case of ovarian angiosarcoma (patient 10), $S1P_1$ immunostaining was as helpful as CD31 in distinguishing the angiosar-

Table 1 Clinical and pathologic features of 15 cases of angiosarcoma

Patient's no.	Age (year)/ sex	Site of disease	Immunoreactivity[a]	
			CD31	$S1P_1$
1	77/F	Skin head	3+	3+
2	51/M	Skin	2+	2+
3	76/F	Skin upper arm	2+	3+
4	64/M	Skin	2+	3+
5	65/M	Skin	2+	2+
6	26/F	Breast	2+	2+
		Breast, recurrence	2+	2+
		Breast, 2nd recurrence	3+	3+
7	69/F	Liver	1+	2+
8	61/M	Pericardium	2+	3+
		Lung (autopsy)	3+	3+
9	65/M	Chest wall	0	1+
		Lung (autopsy)	1+	2+
10	38/F	Ovary	3+	3+
		Ascites	2+	3+

[a] 0, less than 1% of tumor cells reactive; 1+, 1% to 30% of tumor cells reactive; 2+, 31–70% of tumor cells reactive; 3+, more than 70% of tumor cells reactive

comatous component from ovarian stroma. In the case of the immunostaining of cell blocks prepared from peritoneal effusion of the ovarian angiosarcoma patient, $S1P_1$ was expressed on cohesive groups of atypical epithelioid cells but CD31 was expressed on not only the atypical cells but also reactive macrophages [20].

We also investigated a spectrum of non-mesenchymal-related entities, especially the morphological mimics that form sheets of epithelioid cells and enter the differential diagnosis of epithelioid angiosarcoma. Epithelioid sarcoma, malignant melanoma, anaplastic carcinoma of thyroid, and undifferentiated carcinoma showed no significant $S1P_1$ expression while tumor-associated blood vessels showed clear positive staining (Fig. 3h).

Breast carcinoma, colon carcinoma, and renal cell carcinoma were negative, but one of five squamous cell carcinomas showed weak membranous staining of atypical squamous cells in a very limited area.

Discussion

In this study, we have clearly demonstrated that $S1P_1$ is strongly expressed in neoplasms showing vascular and lymphatic endothelial differentiation. In cases of malignant vascular tumors where morphological endothelial differentiation is not apparent [21], it may be necessary to confirm the endothelial nature of the tumor by immunohistochemistry using antibodies against endothelial antigens such as von Willebrand factor (factor-VIII-related antigen), CD31, CD34, and Fli-1 [22]. Among these antigens, CD31 is generally regarded as the single best marker of endothelial cell differentiation because it is expressed in approximately 90% of vascular tumors but only very rarely in carcinomas, lymphomas, and mesotheliomas. In this regard, the most intriguing finding of this study was visible staining for $S1P_1$ in an undifferentiated angiosarcoma where immunostaining for CD31 was uninformative. In addition, $S1P_1$ was not expressed in putative morphological mimics of angiosarcoma such as epithelioid sarcoma [23], melanoma [24], spindle cell variant of anaplastic carcinoma of thyroid [25], and undifferentiated carcinoma [21], suggesting that the anti-$S1P_1$ antibody provides a robust means of distinguishing angiosarcoma from its morphological mimics when combined with standard antibodies against endothelial antigens.

The $S1P_1$ in hemangioma and lymphangioma was mainly located in the luminal surface membrane of the neoplastic vascular space. This subcellular distribution was the same as that seen in normal endothelial cells [18]. In the angiosarcoma cases, however, cytoplasmic staining was frequently observed as well. Because this pattern of staining was obtained even with an Envision kit (Dako), this cytoplasmic staining may not represent a false-positive result.

Three of 21 liposarcoma cases were positive for $S1P_1$. In such cases, however, the expression was weak and occurred in the cytoplasm of neoplastic cells. In contrast, strong expression was observed in the neovasculature of all tumors examined. It is of particular interest that the microcapillaries were very clearly stained with anti-$S1P_1$. This finding is consistent with the report that $S1P_1$ was required for tumor angiogenesis [17, 26].

In summary, $S1P_1$ can be used as an immunohistochemical marker for vascular neoplasms including angiosarcoma and this antigen may be particularly valuable as an adjunct to CD31 in cases where a vascular neoplasm requires a differential diagnosis.

Acknowledgments This study was supported by a Grant-in-aid for Scientific Research from the Ministry of Education, Science, Sports, and Culture of Japan and in part by a Research Project Grant from Kawasaki Medical School.

Conflict of interest statement We declare that we have no conflict of interest.

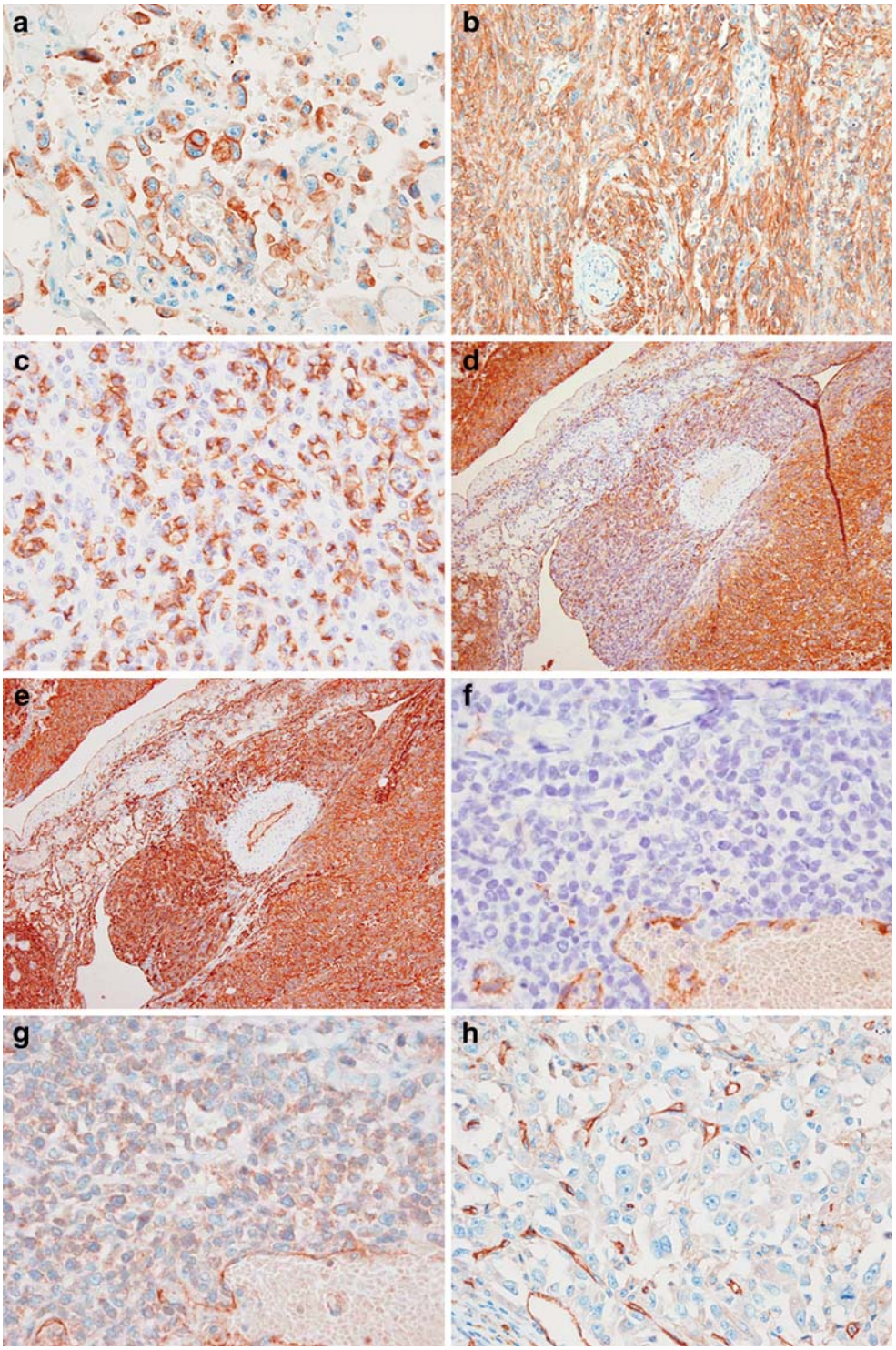

Fig. 3 Expression of $S1P_1$ in cases of angiosarcoma. **a** Expression of $S1P_1$ in an angiosarcoma showing obvious vasoformative growth with complex anastomosing channels (patient 3). **b** Expression of $S1P_1$ in an angiosarcoma showing a spindle growth pattern (patient 1). **c** Expression of $S1P_1$ in an angiosarcoma showing an epithelioid cytomorphology (patient 4). **d** An angiosarcoma showing an undifferentiated area around a medium-sized artery (patient 8). CD31 is faintly expressed in the undifferentiated area. **e** Sequential section of **d**. $S1P_1$ is strongly expressed in the undifferentiated area and in endothelial cells of the artery. **f** An undifferentiated angiosarcoma (patient 9). No definitive staining of CD31 is seen while staining is clearly evident in a nonneoplastic vein. **g** Sequential section of **f**. Neoplastic cells are positive for $S1P_1$ although the staining is weaker than that of nonneoplastic vessels. **h** Undifferentiated carcinoma. Large neoplastic cells are negative while intratumoral blood capillary vessels are clearly stained for $S1P_1$

References

1. Mukai K, Rosai J, Burgdorf WH (1980) Localization of factor VIII-related antigen in vascular endothelial cells using an immunoperoxidase method. Am J Surg Pathol 4:273–276
2. Parums DV, Cordell JL, Micklem K et al (1990) JC70: a new monoclonal antibody that detects vascular endothelium associated antigen on routinely processed tissue sections. J Clin Pathol 43:752–757
3. Ramani P, Bradley NJ, Fletcher CD (1990) QBEND/10, a new monoclonal antibody to endothelium: assessment of its diagnostic utility in paraffin sections. Histopathology 17:237–242
4. Appleton MAC, Attanoos RL, Jasani B (1996) Thrombomodulin as a marker of vascular and lymphatic tumours. Histopathology 29:153–157
5. Folpe AL, Chand EM, Goldblum JR et al (2001) Expression of Fli-1, a nuclear transcription factor, distinguishes vascular neoplasms from potential mimics. Am J Surg Pathol 25:1061–1066
6. Breiteneder-Geleff S, Soleiman A, Kowalski H et al (1999) Angiosarcomas express mixed endothelial phenotypes of blood and lymphatic capillaries: podoplanin as a specific marker for lymphatic endothelium. Am J Pathol 154:385–394
7. Sajjad P, Syed MD, Martin A et al (2007) Angiostatin receptor annexin II in vascular tumors including angiosarcoma. Hum Pathol 38:508–513
8. Miettenin M, Lindemayer AE, Chaubal A (1994) Endothelial cell markers CD31, CD34, and BNH9 antibody to H- and Y- antigens: evaluation of their specificity and sensitivity in the diagnosis of vascular tumors and comparison with von Willebrand factor. Mod Pathol 7:82–90
9. Ohsawa M, Naka N, Tomita et al (1995) Use of immunohistochemical procedures in diagnosing angiosarcoma. Cancer 75:2867–2874
10. Poblet E, Gonzalez-Palacios F, Jimenez FJ (1996) Different immunoreactivity of endothelial markers in well and poorly differentiated areas of angiosarcomas. Virchows Arch 428:217–221
11. Spiegel S, Milstien S (2002) Sphingosine-1-phosphate, a key cell signaling molecule. J Biol Chem 277:25851–25854
12. Sanchez T, Hla T (2004) Structural and functional characteristics of S1P receptors. J Cell Biochem 92:913–922
13. Peters SL, Alewijnse AE (2007) Sphingosine-1-phosphate signaling in the cardiovascular system. Curr Opin Pharmacol 7:186–192
14. Hla T, Maciag T (1990) An abundant transcript induced in differentiating human endothelial cells encodes a polypeptide with structural similarities to G-protein-coupled receptors. J Biol Chem 265:9308–9313
15. Wang F, Van Brocklyn JR, Hobson JP et al (1999) Sphingosine 1-phosphate stimulates cell migration through a G(i)-coupled cell surface receptor. Potential involvement in angiogenesis. J Biol Chem 274:35343–35350
16. Liu Y, Wada R, Yamashita T et al (2000) Edg-1, the G protein-coupled receptor for sphingosine-1-phosphate, is essential for vascular maturation. J Clin Invest 106:951–961
17. Chae SS, Paik J, Furneaux H et al (2004) Requirement for sphingosine 1-phosphate receptor-1 in tumor angiogenesis demonstrated by in vivo RNA interference. J Clin Invest 114:1082–1089
18. Akiyama T, Sadahira Y, Matsubara K, Mori M, Igarashi Y (2008) Immunohistochemical detection of sphingosine-1-phosphate receptor 1 in vascular and lymphatic endothelial cells. J Mol Histol 39:527–533
19. Kahn HJ, Bailey D, Marks A (2002) Monoclonal antibody D2-40, a new marker of lymphatic endothelium, reacts with Kaposi's sarcoma and a subset of angiosarcomas. Mod Pathol 15:434–440
20. Ruco LP, Pomponi D, Pigott R et al (1992) Expression and cell distribution of the intercellular adhesion molecule, vascular cell adhesion molecule, endothelial leukocyte adhesion molecule, and endothelial cell adhesion molecule (CD31) in reactive human lymph nodes and in Hodgkin's disease. Am J Pathol 140:1337–1344
21. Meis-Kindblom JM, Kindblom LG (1998) Angiosarcoma of soft tissue: a study of 80 cases. Am J Surg Pathol 22:683–697
22. Pusztaszeri MP, Seelentag W, Bosman FT (2006) Immunohistochemical expression of endothelial markers CD31, CD34, von Willebrand factor, and Fli-1 in normal human tissues. J Histochem Cytochem 54:385–395
23. Miettinen M, Fanburg-Smith JC, Virolainen M, Shmookler BM, Fetsch JF (1999) Epithelioid sarcoma: an immunohistochemical analysis of 112 classical and variant cases and a discussion of the differential diagnosis. Hum Pathol 30:934–942
24. Nakhleh RE, Wick MR, Rocamora A, Swanson PE, Dehner LP (1990) Morphologic diversity in malignant melanomas. Am J Clin Pathol 93:731–740
25. Mills SE, Gaffey MJ, Watts JC et al (1994) Angiomatoid carcinoma and 'angiosarcoma' of the thyroid gland: a spectrum of endothelial differentiation. Am J Clin Pathol 102:322–330
26. LaMontagne K, Littlewood-Evans A, Schnell C et al (2006) Antagonism of sphingosine-1-phosphate receptors by FTY720 inhibits angiogenesis and tumor vascularization. Cancer Res 66:221–231

Virchows Arch (2009) 454:223–227
DOI 10.1007/s00428-008-0693-7

CASE REPORT

Microcystic urothelial cell carcinoma with neuroendocrine differentiation arising in renal pelvis. Report of a case

Donatella Pacchioni · Martino Bosco · Elena Allia · Baudolino Mussa · Gregor Mikuz · Gianni Bussolati

Received: 27 August 2008 / Revised: 16 October 2008 / Accepted: 17 October 2008 / Published online: 11 November 2008

Abstract Microcystic urothelial cell carcinoma is a rare variant of urothelial cell carcinoma which occurs in the bladder and, rarely, in the renal pelvis. Neuroendocrine differentiation is uncommon in pure urothelial carcinoma and is more frequently found in neoplasms with glandular differentiation. We report a case of microcystic urothelial cell carcinoma arising in renal pelvis and showing focal neuroendocrine differentiation. A 55-year-old man with a history of non-small cell cancer of the lung presented with abdominal pain and hematuria. Imaging studies and gross examination revealed a partially cystic mass in the left kidney. Microscopic examination disclosed invasive carcinoma with prominent microcystic features, with microcysts lined by low columnar and flat cells. Immunohistochemical analysis confirmed the urothelial histotype (positive for thrombomodulin, p63 and high-molecular-weight cytokeratins) and disclosed focal neuroendocrine differentiation.

Keywords Urothelial cell carcinoma · Microcystic variant · Neuroendocrine differentiation

D. Pacchioni · M. Bosco (✉) · E. Allia · G. Bussolati
Department of Biomedical Sciences and Human Oncology,
University of Turin,
via Santena 7,
10126 Turin, Italy
e-mail: martino.bosco@unito.it

D. Pacchioni
e-mail: dpacchioni@molinette.piemonte.it

E. Allia
e-mail: elena.allia@unito.it

G. Bussolati
e-mail: gianni.bussolati@unito.it

B. Mussa
Department of Surgical and Oncological Sciences,
University of Turin,
C.so Dogliotti 14,
10126 Turin, Italy
e-mail: baudolino.mussa@unito.it

G. Mikuz
Institute of Pathology, Medical University Innsbruck,
Muellerstrasse 44,
A 6020 Innsbruck, Austria
e-mail: gregor.mikuz@i-med.ac.at

Introduction

High-grade urothelial neoplasm may present with unusual morphologic features which can cause diagnostic difficulties. These variants include micropapillary, lymphoepithelioma-like, sarcomatoid carcinoma, squamous, glandular or trophoblastic differentiation, or presence of cell of rhabdoid, clear, signet-ring, or plasmacytoid type [1]. In 1991, Young described an unusual form of urothelial carcinoma of the bladder characterized by microcystic architecture with cysts lined by multiple layers of low-grade cuboidal or flattened cells [2]. In the last two decades, other reports contributed to the clinical and pathological characterization of this urothelial neoplasm [3–5].

Neuroendocrine differentiation of bladder tumors other than small cell carcinoma has been rarely described in primary adenocarcinoma, urachal carcinoma and urothelial neoplasm with glandular differentiation [6] but not in urothelial cell carcinoma.

Here, we report a unique case of microcystic urothelial cell carcinoma arising in renal pelvis and showing focal neuroendocrine differentiation.

Clinical history

A 55-year-old man with a past diagnosis of lung adenocarcinoma surgically removed in 1998 presented at medical attention with macrohematuria and abdominal pain. Cystoscopy revealed no tumor in the bladder. Abdominal computed tomographic scan and ultrasound studies showed a 17×14 cm, partially cystic mass in the left kidney. Thoracic computed tomographic scan revealed multiple bilateral pulmonary nodules. A ureteronephrectomy and transthoracic fine-needle biopsy of the biggest pulmonary nodule were performed. Fifteen months after the nephrectomy, the patient developed local recurrence of the renal neoplasm.

Materials and methods

Immunohistochemical staining was performed using an automated immunostainer (Benchmark XT, Ventana). The following monoclonal antibodies were used: p63 (clone 4A4, Dako); p53 (clone D0-7, Ventana); ki-67 (clone MIB1, Dako); chromogranin A (clone LK2H10, Ventana); thrombomodulin (clone 1009, Dako); high-molecular-weight cytokeratins (HMW-CKs; clone AE3, Biogenex); neuron-specific enolase (NSE; clone E27, Ventana); synaptophisin (polyclonal, Ventana); thyroid transcription factor-1 (TTF1; clone 8G7G3/1, Ventana); neural-cell adhesion molecule (N-CAM, CD56; clone SCLC, Zymed); cytokeratin 20 (clone KS20.8, Dako).

The presence of chromogranin A (CG-A), chromogranin B (CG-B) and chromogranin C (CG-C) mRNA was investigated in formalin-fixed, paraffin-embedded material by means of reverse transcriptase polymerase chain reaction (RT-PCR; Applera, Foster City, Ca, USA) with the following targets and amplicon dimensions: CG-A: exon 4–5, 115 bp; CG-B: exon 1–2, 133 bp; CG-C: exon 1-2, 69 bp. To exclude contamination by peripheral nervous structures, areas exclusively occupied by neoplastic tissue were microscopically identified and sampled by means of tissue-array sampler.

Pathological findings

Renal mass Gross examination showed a gray-whitish mass, measuring 10 cm in the largest dimension and deforming almost the entire renal surface. On section, the lesion was predominantly cystic, with walls composed by whitish, friable tissue with papillary features and large necrotic areas which occupied the renal pyelocaliceal cavities and the proximal tract of the urethra and infiltrated renal parenchyma and peripelvic fat.

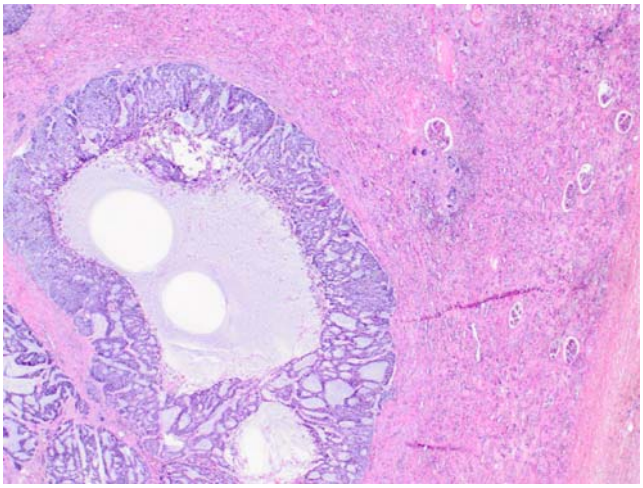

Fig. 1 The neoplasm displayed mainly a microcystic architecture with deep infiltration of renal parenchyma

Microscopic examination showed an invasive neoplasm mainly displaying a micro cystic arrangement which deeply infiltrated the wall of the renal pelvis, perinephric fat, and renal parenchyma (Fig. 1). Abundant necrosis was present. The microcystic structures were variable in size and shape and lined by small cuboidal or flattened cells arranged in one to several layers. Neoplastic cell had a high nucleo-cytoplasmic ratio, a lightly eosinophylic, non-granulated cytoplasm and round, hyperchromatic nuclei with small nucleoli (Fig. 2). Mitotic activity was low (four mitotic figures per ten high-power fields). Eosinophylic or blue secretions stainable with PAS were frequently seen in the lumen of the microcysts. Some cystic structures had a central squamous differentiation with comedonecrosis. Squamous metaplasia was also seen in the non-neoplastic

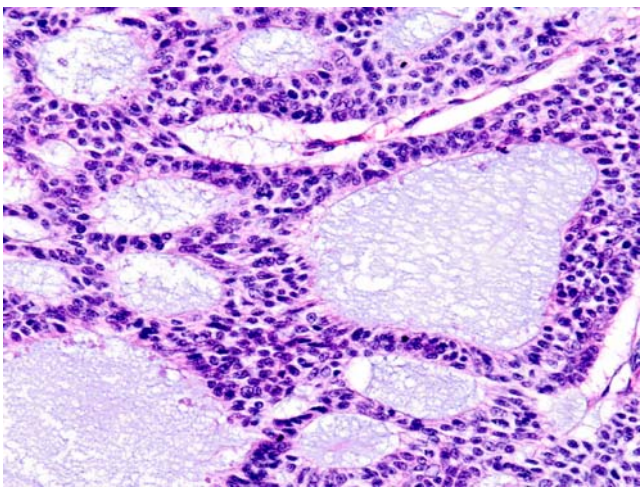

Fig. 2 The microcystic structures were variable in size and shape and lined by small cuboidal or flattened cells arranged in one to several layers. Neoplastic cell had an high nucleo-cytoplasmic ratio and round, hyperchromatic nuclei with small nucleoli

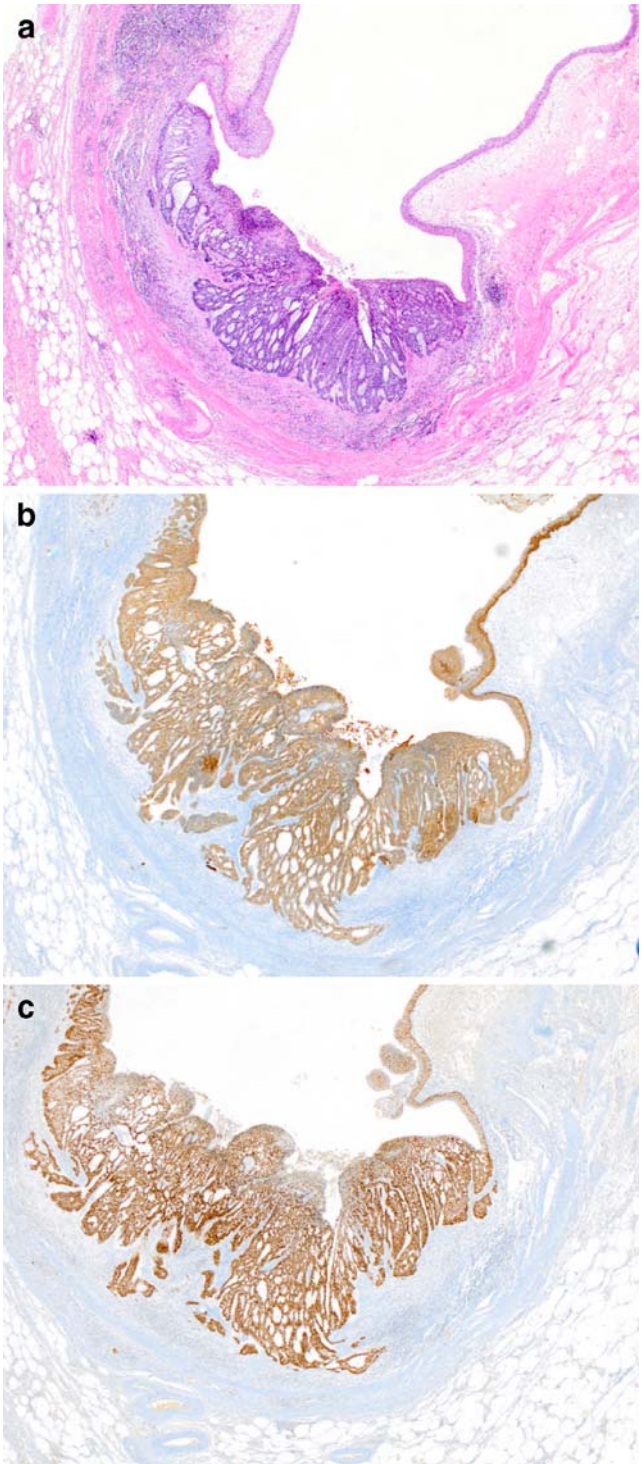

Fig. 3 An area of transition between in situ urothelial carcinoma and invasive microcystic neoplasm was evident in the proximal tract of the ureter (**a**). Diffuse expression of p63 (**b**) and HMW-CK (**c**) was evident in the neoplasm and in the surrounding normal urothelium

urothelium on the pelvis. Identification of better differentiated areas of urothelial carcinoma as well as demonstration of transition with in situ urothelial carcinoma was possible in the proximal tract of the ureter (Fig. 3a). The

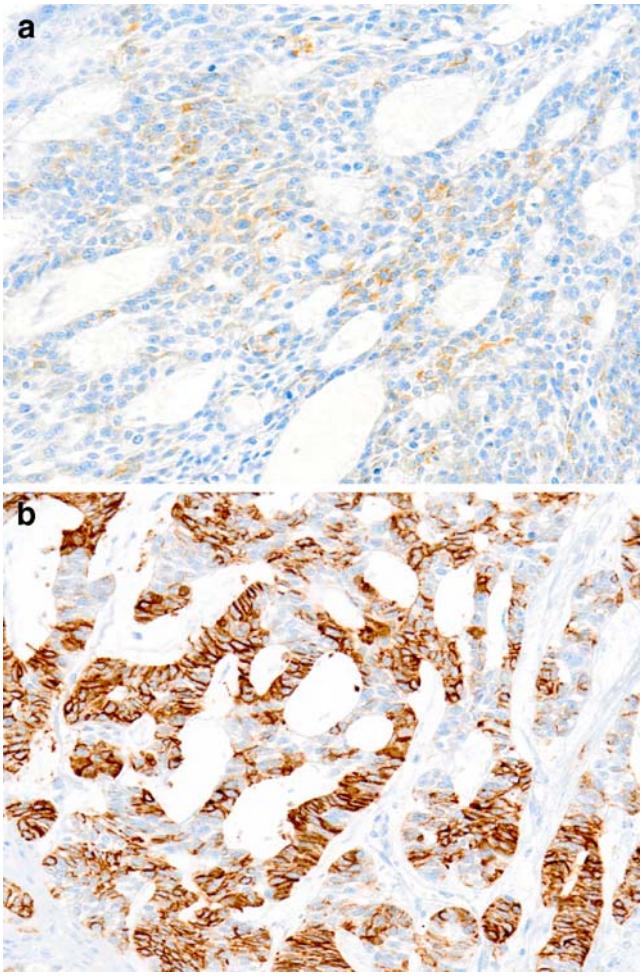

Fig. 4 The neoplasm displayed focal expression of CG-A (**a**) and CD56 (**b**)

diffuse expression by the neoplasm of thrombomodulin, HMW-CKs and p63 (Fig. 3b,c) supported the urothelial nature of the neoplasm [7, 8]. Immunohistochemical analysis also identified focal neuroendocrine differentiation: expression of CG-A and CD56 (N-CAM) was detected in 8% and 20% of the neoplastic cells, respectively, while synaptophysin was negative (Fig. 4a,b). This finding was

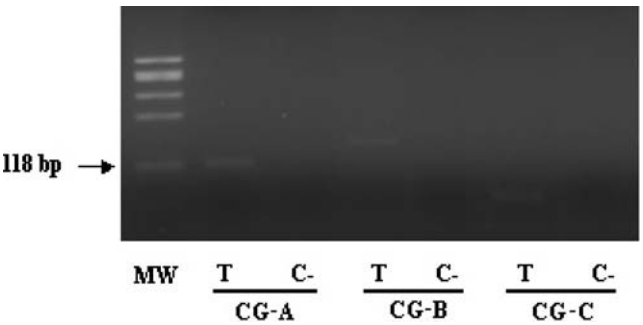

Fig. 5 Detection of CG-A, CG-B and CG-C mRNAs by means of RT-PCR. (*T*: tumor samples; *C*−: negative controls)

confirmed by identification of mRNA for CG-A, CG-B and CG-C by means of RT-PCR (Fig. 5).

Lung nodule Fine-needle aspiration biopsy under computed tomographic guide of the biggest pulmonary lung nodule showed few, small fragments of fibrous tissue containing small, atypical cells with eosinophylic cytoplasm, round, hyperchromatic nuclei with inconspicuous nucleoli arranged in small clusters and microcysts. The atypical cells were TTF-1 negative and thombomodulin-positive. Therefore, the pulmonary lesion resembled the renal neoplasm at both the morphological and immunohistochemical level.

Discussion

Urothelial carcinomas arising in the renal pelvis are relatively rare tumors accounting for approximately 7% of all renal neoplasm, are more frequently high-grade tumors and are often at higher stage than bladder urothelial cancer.

Morphologic variation due to aberrant differentiation is a well-recognized phenomenon in urothelial carcinoma of the bladder and includes focal squamous, glandular, or trophoblastic differentiation or micropapillary, lymphoepithelioma-like, nested, sarcomatoid, lymphoma-like, plamocytoid, clear cell, or rhabdoid features [9]. Divergent differentiation of urothelial cancer has also been described in the renal pelvis neoplasms and seems to be relatively common in high-grade neoplasms [1]. Recently, a variant of urothelial carcinoma characterized by microcystic pattern unrelated to primary bladder adenocarcinoma has been described. In this variant, the neoplastic cells are arranged in round or oval cysts ranging to microscopic to 2 mm in diameter. The cysts may contain necrotic material or secretions and are lined by urothelial, flattened, or cuboidal cells which can display mucinous differentiation [2]. The differential diagnosis of this variant of urothelial carcinoma includes cystitis/urethritis glandularis or cystica, nephrogenic metaplasia, and primitive adenocarcinoma of the urothelial tract. The most similar tumor is, however, the nested-type urothelial carcinoma [10] which has been only once described in the pelvis [11]. This type of urothelial carcinoma is a rather aggressive neoplasm with innocuous appearing histology.

The histopathological features displayed by our case are those of the microcystic variant of urothelial carcinoma. Although the invasive component of the neoplasm did not contain areas typical of urothelial carcinoma and the microcyst were not lined by cells with urothelial appearance, the urothelial nature of the neoplasm was supported by the presence of high-grade urothelial carcinoma at the boundaries between invasive carcinoma and normal urothelium and by its immunohistochemical features, which included focal positivity for thrombomodulin, HMW-CKs, cytokeratin 20, and p63 [7, 8].

An unusual feature of this neoplasm is its localization in the renal pelvis. Only two other cases of microcystic variant of urothelial carcinoma arising in the renal pelvis have been reported in literature so far [4]; in particular, no case of this variant is reported in the recent work by Perez-Montiel et al. about divergent differentiation in a large series of urothelial renal pelvis neoplasms [1].

The microcystic variant of urothelial carcinoma is associated with high-stage and high-grade bladder tumors and with other primary tumors [3]. Interestingly, this patient has a past history of a moderately differentiated lung adenocarcinoma.

An unusual feature displayed by this neoplasm is the presence of focal neuroendocrine differentiation, as showed by immunohistochemical and molecular analysis. This phenomenon, which is absent in urothelial carcinoma of conventional type, is relatively common in adenocarcinoma of the urothelial tract and in urothelial carcinoma with glandular differentiation [6] but it has not been reported for the microcystic variant of urothelial carcinoma so far. Since the microcystic variant of urothelial carcinoma commonly displays some grade of glandular differentiation of the cell lining of the cysts, presence of neuroendocrine differentiation in this neoplasm should not be a completely unexpected finding.

The previously unreported clinical and diagnostic significance of focal neuroendocrine differentiation in urothelial cancer remains to be defined.

Conflict of interest statement We declare that we have no conflict of interest

References

1. Perez-Montiel D, Wakely PE, Hes O (2006) High-grade urothelial carcinoma of the renal pelvis: clinicopathologic study of 108 cases with emphasis on unusual morphologic variants. Mod Pathol 19:494–503
2. Young RH, Zukerberg LR (1991) Microcystic transitional cell carcinomas of the urinary bladder. A report of four cases. Am J Clin Pathol 96:635–639
3. Paz A, Rath-Wolfson L, Lask D et al (1997) The clinical and histological features of transitional cell carcinoma of the bladder with microcysts: analysis of 12 cases. Br J Urol 79:722–725
4. Leroy X, Leteurtre E, De La Taille A et al (2002) Microcystic transitional cell carcinoma: a report of 2 cases arising in the renal pelvis. Arch Pathol Lab Med 126:859–861
5. Radopoulos D, Kalyvas K, Kotakidou R et al (2005) Case report: microcystic transitional cell carcinoma of the urinary bladder. Int Urol Nephrol 37:291–293
6. Bollito ER, Pacchioni D, Lopez-Beltran A et al (2005) Immunohistochemical study of neuroendocrine differentiation in primary

glandular lesions and tumors of the urinary bladder. Anal Quant Cytol Histol 27:218–224
7. Parker DC, Folpe AL, Bell J et al (2003) Potential utility of uroplakin III, thrombomodulin, high molecular weight cytokeratin, and cytokeratin 20 in noninvasive, invasive, and metastatic urothelial (transitional cell) carcinomas. Am J Surg Pathol 27:1–10
8. Langner C, Ratschek M, Tsybrovskyy O et al (2003) P63 immunoreactivity distinguishes upper urinary tract transitional-cell carcinoma and renal-cell carcinoma even in poorly differentiated tumors. J Histochem Cytochem 51:1097–1099
9. Lopez-Beltran A, Sauter G, Gasser T (2004) Infiltrating urothelial carcinoma. In: Eble JN, Sauter G, Epstein JI, et al (eds) Tumours of the urinary system and male genital organs. Lyon, World Health Organization Classification of Tumours, pp 93–109
10. Drew PA, Furman J, Civantos F et al (1996) The nested variant of transitional cell carcinoma: an aggressive neoplasm with innocuous histology. Mod Pathol 9:989–994
11. Pusztaszeri M, Hauser J, Iselin C et al (2007) Urothelial carcinoma "nested variant" of renal pelvis and ureter. Urology 69:778

Virchows Arch (2009) 454:229–232
DOI 10.1007/s00428-008-0714-6

CASE REPORT

Histoplasma-associated inflammatory pseudotumour of the kidney mimicking renal carcinoma

Michael A. den Bakker · Natascha N. T. Goemaere · Juliëtte A. Severin · J. L. Nouwen · Paul C. M. S. Verhagen

Received: 26 October 2008 / Revised: 19 November 2008 / Accepted: 3 December 2008 / Published online: 6 January 2009

Abstract A 56-year-old female, originally from Suriname, with an otherwise unremarkable previous medical history was found to have a renal mass highly suspicious for renal cancer for which a nephrectomy was performed. Within the kidney, a tumourous mass was found which, on histological examination, showed an inflammatory pseudotumour caused by *Histoplasma capsulatum*. Further investigations revealed an idiopathic $CD4^+$ lymphopenia. Mass lesions mimicking a malignant tumour caused by infection with *Histoplasma* have rarely been described. To the best of our knowledge, this is the first report of a *Histoplasma*-associated inflammatory pseudotumour mimicking cancer occurring in the kidney

M. A. den Bakker
Department of Pathology,
Erasmus MC–University Medical Center Rotterdam,
PO Box 2040, 3000 CA Rotterdam, The Netherlands

J. A. Severin · J. L. Nouwen
Department of Medical Microbiology and Infectious Diseases,
Erasmus MC–University Medical Center Rotterdam,
PO Box 2040, 3000 CA Rotterdam, The Netherlands

P. C. M. S. Verhagen
Department of Urology,
Erasmus MC–University Medical Center Rotterdam,
PO Box 2040, 3000 CA Rotterdam, The Netherlands

M. A. den Bakker (✉)
Josephine Nefkens Institute,
Room Be204a, Erasmus MC, P.O. Box 2040, 3000 CA
Rotterdam, The Netherlands
e-mail: m.denbakker@erasmusmc.nl

Present address:
N. N. T. Goemaere
Stichting PATHAN, St. Franciscus Hospital,
Kleiweg 500, 3045 PM,
Rotterdam, The Netherlands

Keywords *Histoplasma capsulatum* · Inflammatory pseudotumour · Immunodeficiency · Kidney neoplasms

Introduction

Infection by *Histoplasma capsulatum*, a dimorphic fungus endemic in North and South America, Africa and Asia, may go unnoticed in otherwise healthy individuals or may cause symptoms in a number of ways. Histoplasmosis diagnosed in patients outside of endemic areas invariably results from prior infection during stay or residence in an endemic area [1]. Although most infections with *H. capsulatum* remain subclinical or are self-limited, severe disease may occur in debilitated and immunodeficient individuals. In immunosuppressed individuals, primary infection or reactivation of an old infection may lead to disseminated histoplasmosis [1]. Mass lesions resulting from *Histoplasma* infection have rarely been described, usually involving the lungs, central nervous system, adrenal glands and rarely the colon. These mass lesions may, on occasion, simulate a malignant tumour. In this case report, we describe a renal fibro-inflammatory pseudotumour closely mimicking a malignant tumour caused by *H. capsulatum*. A diagnosis of idiopathic $CD4^+$ lymphopenia was established after laboratory investigation and the occurrence of additional lesions caused by *H. capsulatum*. To the best of our knowledge, *Histoplasma*-associated pseudotumour mimicking renal cancer has not been previously reported in the literature.

Clinical history

A 56-year-old female from the Dutch West Indies domiciled in The Netherlands for 35 years presented with

malaise and severe weight loss over a period of several months without fever or night sweats. She did not smoke or use alcohol. She had previously been diagnosed with type 2 diabetes and hypertension. Laboratory investigations revealed a mild normocytic anaemia. Further investigations revealed a mass in the left kidney clinically and radiologically consistent with a malignant tumour (Fig. 1). Because of the high index of suspicion, a biopsy was not obtained and a nephrectomy was performed. The nephrectomy specimen revealed a 7-cm pink homogenous mass in the upper pole, bulging out of the surface of the kidney but not extending through the capsule (Fig. 2).

Materials and methods

The resected specimen was processed routinely. HE sections and special stains [PAS and silver stains (Grocott)] were ordered for selected slides.

Results

Histology of the mass revealed a circumscribed non-encapsulated lesion composed of fibro-histiocytic inflammatory tissue composed of plump fibroblasts and histiocytes admixed with lymphocytes and plasma cells (Fig. 3a). On high magnification, microorganisms, measuring approximately 3–5 μm, were identified which were predominantly intracellular in location. The organisms were more easily identified in the PAS and silver (Grocott) stains (Fig. 3b, c). Based on the size of the organisms and the tinctorial properties, a diagnosis of *H. capsulatum*-associated inflammatory pseudotumour was established. An ulcerated oral lesion was found at repeated physical examination, in addition to several skin lesions. The oral lesion was biopsied

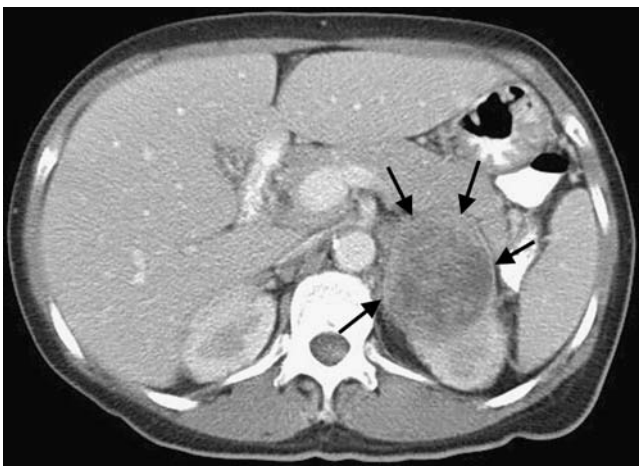

Fig. 1 CT image at the level of the kidneys showing a mass (*arrows*) bulging out of the upper pole of the left kidney

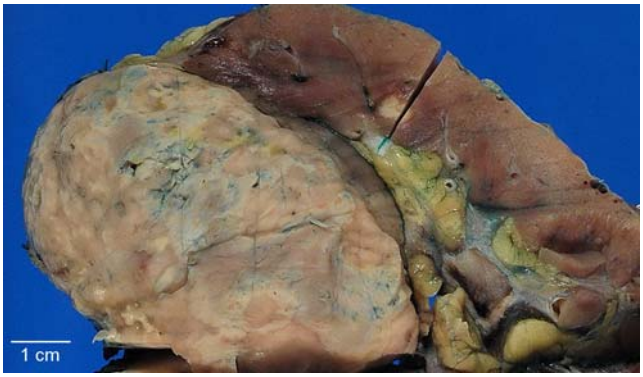

Fig. 2 Nephrectomy specimen. A pink circumscribed mass is seen bulging into, but not penetrating, the renal capsule

and histology again revealed *H. capsulatum*, which subsequently was confirmed by culture; the skin lesions showed granulomatous inflammation consistent with *Histoplasma* infection. Imaging revealed an adrenal lesion consistent with a *Histoplasma* abscess in the right adrenal gland. *H. capsulatum* polysaccharide antigen was detected in urine (1.23 ng/ml; positive, low). A diagnosis of disseminated histoplasmosis was established. Further tests aimed at establishing an underlying immunodeficiency syndrome revealed a low CD4 count (total T cell count 0.22×10^9/L, CD-4 count 0.06×10^9/L, CD-8 count 0.15×10^9/L). Results of serological tests for antibodies to HIV-1 and HIV-2 were negative. Idiopathic $CD4^+$ lymphopenia was considered the

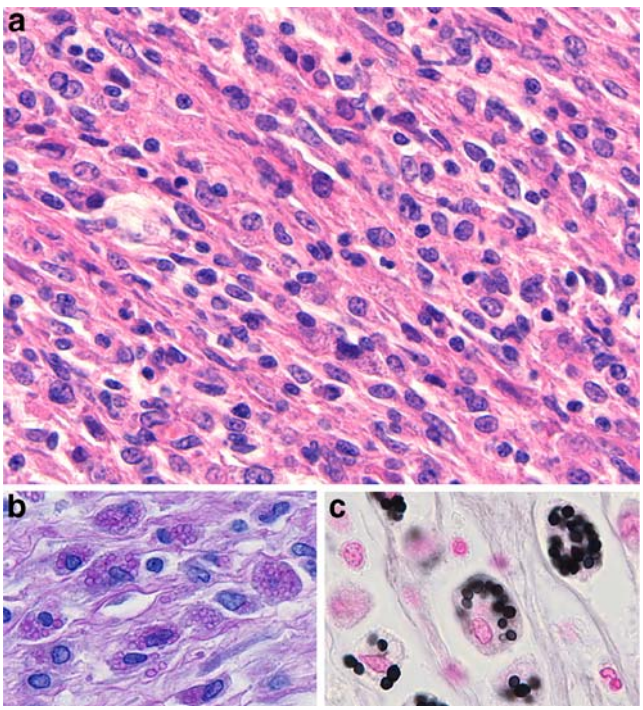

Fig. 3 Histology of the renal mass. **a** A cellular histiocytic infiltrate is seen, admixed with lymphocytes. The cytoplasm has a granular aspect caused by numerous intracellular *Histoplasma* organisms. PAS diastase (**b**) and Grocott (**c**) stains

cause of the immunodeficiency leading to disseminated histoplasmosis.

The patient was treated with itraconazole. Her condition improved and oral and skin lesions completely resolved. After 9 weeks, the patient was placed on maintenance therapy. Repeat laboratory analysis showed persistent low CD4 counts.

Discussion

H. capsulatum infection usually remains asymptomatic in the majority of people. If disease develops in immunocompetent individuals, it is commonly a self-limited flu-like illness. Heavy exposure may result in pneumonic disease and may be associated with rheumatic disease. Involved sites in *Histoplasma* infection may include lungs, lymph nodes, bone marrow, heart, spleen, liver, adrenal gland, central nervous system, gastrointestinal tract, genitourinary tract and the skin [2]. Occasionally, infection by *Histoplasma* may lead to the formation of mass lesions which may be confused with malignant disease. In the lung, *Histoplasma* nodules are known as "histoplasmomas" and are commonly found in a sub-pleural location. Radiologically, histoplasmomas are described as coin lesions, and similar lesions are caused by *Mycobacteria* (tuberculoma) and *Coccidioides immitis* (coccidioidoma). However, in areas where *Histoplasma* is endemic, these lesions are generally well recognised and are unlikely to be confused with malignancy, particularly when tell-tale calcifications are present [3]. Mass lesions caused by *Histoplasma* infection may also occur in the central nervous system, including the spinal cord, and here can radiologically simulate a neoplasm [4–7]. Diffuse enlargement of the adrenal glands without a definable mass is not uncommon in *Histoplasma* infection [8]. Mass lesions or strictures simulating cancer caused by *Histoplasma* infection have been described as one of four patterns of colonic disease and appear particularly common in AIDS [9, 10]. In these cases, the diagnosis is often delayed until surgical resection and pathological examination. The more common ulcerating lesions caused by *Histoplasma* may also lead to an erroneous diagnosis of malignancy as has been described in the larynx [11, 12]. The histology of *Histoplasma* infection, be it as ulcero-inflammatory lesions or as pseudotumours, is similar. A mixed inflammatory infiltrate develops, mainly composed of histiocytes and lymphocytes, admixed with neutrophils, eosinophils and lymphocytes. The microorganisms are predominantly observed intracellularly in macrophages [10, 13]. An exaggerated form of pseudotumour which may be caused by *Histoplasma* is mediastinal fibrosis. Although organisms are often not demonstrated in tissue, a relentless fibrosing reaction develops, encasing vital mediastinal structures ultimately with a fatal outcome [14–16].

Immunodeficiency predisposes to *Histoplasma* infection or reactivation, which, as evidenced in the case described, here may occur decades after residing in an endemic area. Although, low CD4 counts predisposing to symptomatic and disseminated histoplasmosis may result from HIV infection or may be idiopathic. It has also been demonstrated that CD4 depletion may result from *Histoplasma* infection; anti-fungal treatment of a patient with disseminated histoplasmosis resulted in restoration of CD4 counts [17].

Although renal involvement by *Histoplasma* is a recognised complication in renal transplant patients, as an interstitial nephritis or rarely as (necrotising) papillitis, renal mass lesions have not been previously described [18]. In the case described here, the preoperative suspicion of malignancy was sufficient to opt for nephrectomy. It is uncertain whether the renal mass would have resolved on antifungal treatment had the diagnosis been established by biopsy.

In conclusion, the case presented here of a renal fibrohistiocytic *Histoplasma*-associated pseudotumour expands the spectrum of mass lesions caused by this organism in immunosuppressed individuals.

Acknowledgements The authors wish to thank Prof. Sebastian Lucas, Dept. of Pathology, St Thomas' Hospital, London for expert review of the histology described in this report.

Conflict of interest The authors declare that they do not have a conflict of interest.

References

1. Wheat LJ (2006) Histoplasmosis: a review for clinicians from non-endemic areas. Mycoses 49:274–282
2. Kennedy CC, Limper AH (2007) Redefining the clinical spectrum of chronic pulmonary histoplasmosis: a retrospective case series of 46 patients. Medicine (Baltimore) 86:252–258
3. Goodwin RA Jr, Snell JD Jr (1969) The enlarging histoplasmoma. Concept of a tumor-like phenomenon encompassing the tuberculoma and coccidioidoma. Am Rev Respir Dis 100:1–12
4. Vakili ST, Eble JN, Richmond BD, Yount RA (1983) Cerebral histoplasmoma. Case report. J Neurosurg 59:332–336
5. Venger BH, Landon G, Rose JE (1987) Solitary histoplasmoma of the thalamus: case report and literature review. Neurosurgery 20:784–787
6. Wheat LJ, Batteiger BE, Sathapatayavongs B (1990) *Histoplasma capsulatum* infections of the central nervous system. A clinical review. Medicine (Baltimore) 69:244–260
7. Tan V, Wilkins P, Badve S, Coppen M, Lucas S, Hay R, Schon F (1992) Histoplasmosis of the central nervous system. J Neurol Neurosurg Psychiatry 55:619–622

8. Lerttumnongtum P, Muttarak M, Visrutaratna P, Ya-In C (2004) Imaging features of unusual adrenal masses. Australas Radiol 48:107–113
9. Lee JT, Dixon MR, Murrell Z, Konyalian V, Agbunag R, Rostami S, French S, Kumar RR (2004) Colonic histoplasmosis presenting as colon cancer in the nonimmunocompromised patient: report of a case and review of the literature. Am Surg 70:959–963
10. Suh KN, Anekthananon T, Mariuz PR (2001) Gastrointestinal histoplasmosis in patients with AIDS: case report and review. Clin Infect Dis 32:483–491
11. Mave V, Mushatt D (2008) A case of laryngeal histoplasmosis mimicking carcinoma with a review of the literature. J La State Med Soc 160:160–163
12. Phatak AM, Bhattacharya I, Misra V, Prabhu AM, Natraj U (2006) Disseminated histoplasmosis mimicking laryngeal carcinoma from central India—a case report. Indian J Pathol Microbiol 49:452–454
13. Kahi CJ, Wheat LJ, Allen SD, Sarosi GA (2005) Gastrointestinal histoplasmosis. Am J Gastroenterol 100:220–231
14. Goodwin RA, Loyd JE, Des Prez RM (1981) Histoplasmosis in normal hosts. Medicine (Baltimore) 60:231–266
15. Goodwin RA, Nickell JA, Des Prez RM (1972) Mediastinal fibrosis complicating healed primary histoplasmosis and tuberculosis. Medicine (Baltimore) 51:227–246
16. Schowengerdt CG, Suyemoto R, Main FB (1969) Granulomatous and fibrous mediastinitis. A review and analysis of 180 cases. J Thorac Cardiovasc Surg 57:365–379
17. Rhew DC, Goetz MB, Louie MH (1995) Reversible $CD4^{+}$ T lymphocyte depletion in a patient who had disseminated histoplasmosis and who was not infected with human immunodeficiency virus. Clin Infect Dis 21:702–703
18. Kedar SS, Eldar S, Abrahamson J, Boss J (1988) Histoplasmosis of kidneys presenting as chronic recurrent renal disease. Urology 31:490–494

Virchows Arch (2009) 454:233–235
DOI 10.1007/s00428-008-0712-8

ERRATUM

KRAS mutation testing for predicting response to anti-EGFR therapy for colorectal carcinoma: proposal for an European quality assurance program

J. H. J. M. van Krieken · A. Jung · T. Kirchner · F. Carneiro · R. Seruca · F. T. Bosman · P. Quirke · J. F. Fléjou · T. Plato Hansen · G. de Hertogh · P. Jares · C. Langner · G. Hoefler · M. Ligtenberg · D. Tiniakos · S. Tejpar · G. Bevilacqua · A. Ensari

Published online: 9 January 2009

Erratum to: Virchows Arch
DOI 10.1007/s00428-008-0665-y

In Fig. 2 of this article the DNA sequencing data were incorrect, and parts of Fig. 3 were illegible.

Corrected versions of these figures are given here.

The online version of the original article can be found at http://dx.doi.org/10.1007/s00428-008-0665-y.

J. H. J. M. van Krieken (✉) · M. Ligtenberg
Department of Pathology,
Radboud University Nijmegen Medical Centre,
P.O. Box 9101, Nijmegen 6500 HB, The Netherlands
e-mail: J.vanKrieken@pathol.umcn.nl

A. Jung · T. Kirchner
Department of Pathology, Ludwig-Maximilians Universität,
Munich, Germany

F. Carneiro · R. Seruca
Institute of Molecular Pathology and Immunology
of the University of Porto (IPATIMUP),
Porto, Portugal

F. Carneiro · R. Seruca
Medical Faculty of the of Porto,
Porto, Portugal

F. Carneiro
Department of Pathology, Hospital S. João,
Porto, Portugal

F. T. Bosman
University Institute of Pathology,
Lausanne, Switzerland

P. Quirke
Pathology and Tumour Biology, University of Leeds,
Leeds, England

J. F. Fléjou
Department of Pathology, Saint-Antoine Hospital,
University Paris 6, Paris, France

T. P. Hansen
Department of Pathology, Odense University Hospital,
Odense, Denmark

G. de Hertogh
Department of Pathology, University Hospitals KU Leuven,
Leuven, Belgium

P. Jares
Department of Pathology, Hospital Clinic, Barcelona, Spain

C. Langner · G. Hoefler
Institute of Pathology, Medical University Graz, Graz, Austria

M. Ligtenberg
Department of Human Genetics,
Radboud University Nijmegen Medical Centre,
Nijmegen, The Netherlands

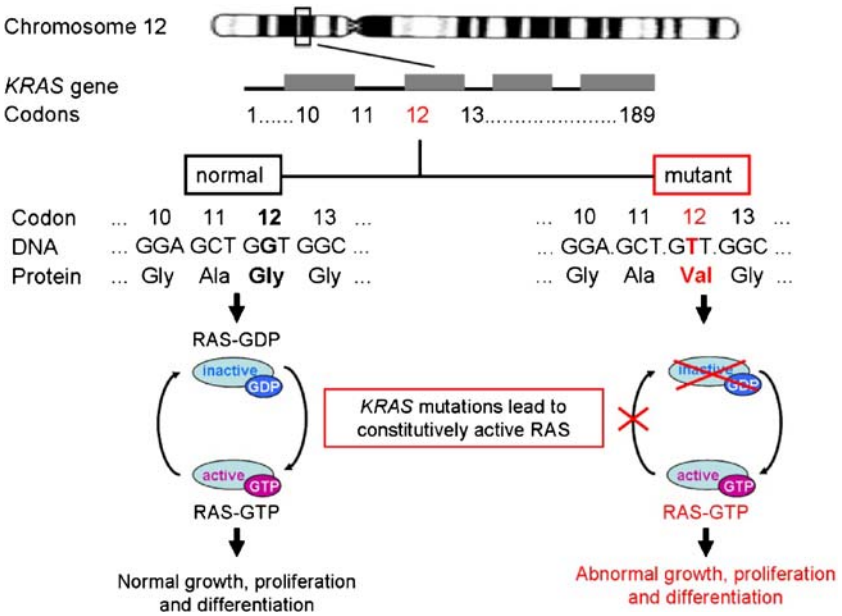

Fig. 2 Role of *KRAS* mutations in oncogenic activation of intracellular signaling. The human *KRAS* gene, located on chromosome 12, encodes a small G-protein that functions downstream of EGFR-induced cell signaling. This G-protein belongs to the family of RAS proteins involved in signal transduction pathways that regulate cell development and function. RAS proteins normally cycle between active (RAS-GTP) and inactive (RAS-GDP) conformations. Somatic missense mutations in codon 12 of the *KRAS* gene, leading to single amino acid substitutions such as p.Gly12Val, are the most common alterations found in colorectal tumors. These *KRAS* mutations result in RAS proteins that are constitutively in the active RAS-GTP conformation. Unlike wild-type RAS proteins which are deactivated after a short time, the mutated RAS proteins cause continuous activation of RAS signaling pathways in the absence of upstream stimulation of EGFR/HER receptors. This oncogenic activation of RAS signaling pathways leads to abnormal cell growth, proliferation and differentiation

D. Tiniakos
Laboratory of Histology and Embryology,
Medical School University of Athens,
Athens, Greece

G. Bevilacqua
Department of Oncology,
University of Pisa and Pisa University Hospital,
Pisa, Italy

S. Tejpar
Digestive Oncology Unit, University Hospital Gasthuisberg,
Leuven, Belgium

A. Ensari
Department of Pathology, Ankara University Medical School,
Ankara, Turkey

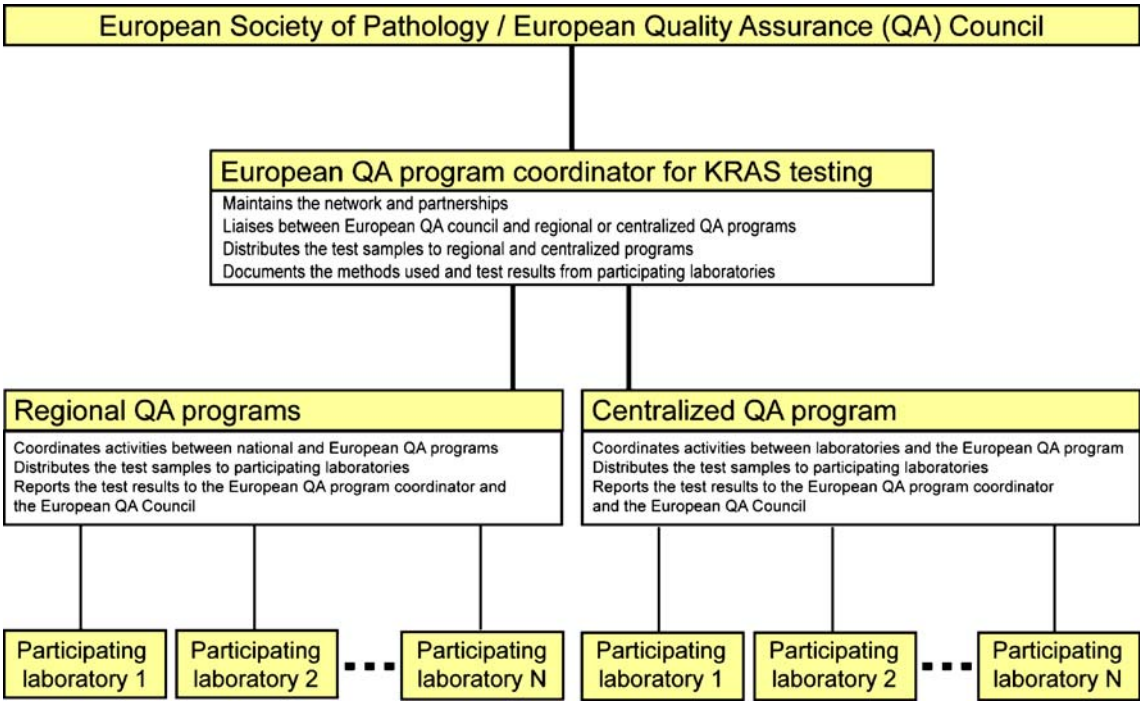

Fig. 3 Proposed framework for a European quality assurance (QA) program for *KRAS* mutation testing in colorectal cancer. The European QA program, under the direction of a QA council, will be organized by the European Society of Pathology in close collaboration with existing regional and/or national QA programs. The QA program, together with a designated coordinator, will be responsible for establishing QA guidelines and testing criteria, implementing the QA program and performing laboratory accreditation. Participating laboratories can attain accreditation at the regional or centralized level

Virchows Arch (2009) 454:237–238
DOI 10.1007/s00428-008-0718-2

ERRATUM

Systems pathology—or how to solve the complex problem of predictive pathology

Manfred Dietel · Reinhold Schäfer

Published online: 23 December 2008

Erratum to: Virchows Arch
DOI 10.1007/s00428-008-0656-z

Both Fig. 1b and the legend of Fig. 1 were incorrect.
The correct figure and legend are given here.

The online version of the original article can be found at http://dx.doi.org/10.1007/s00428-008-0656-z.

M. Dietel (✉) · R. Schäfer
Department of Pathology, Charité—University Medicine Berlin,
Charitéplatz 1,
10117 Berlin, Germany
e-mail: manfred.dietel@charite.de

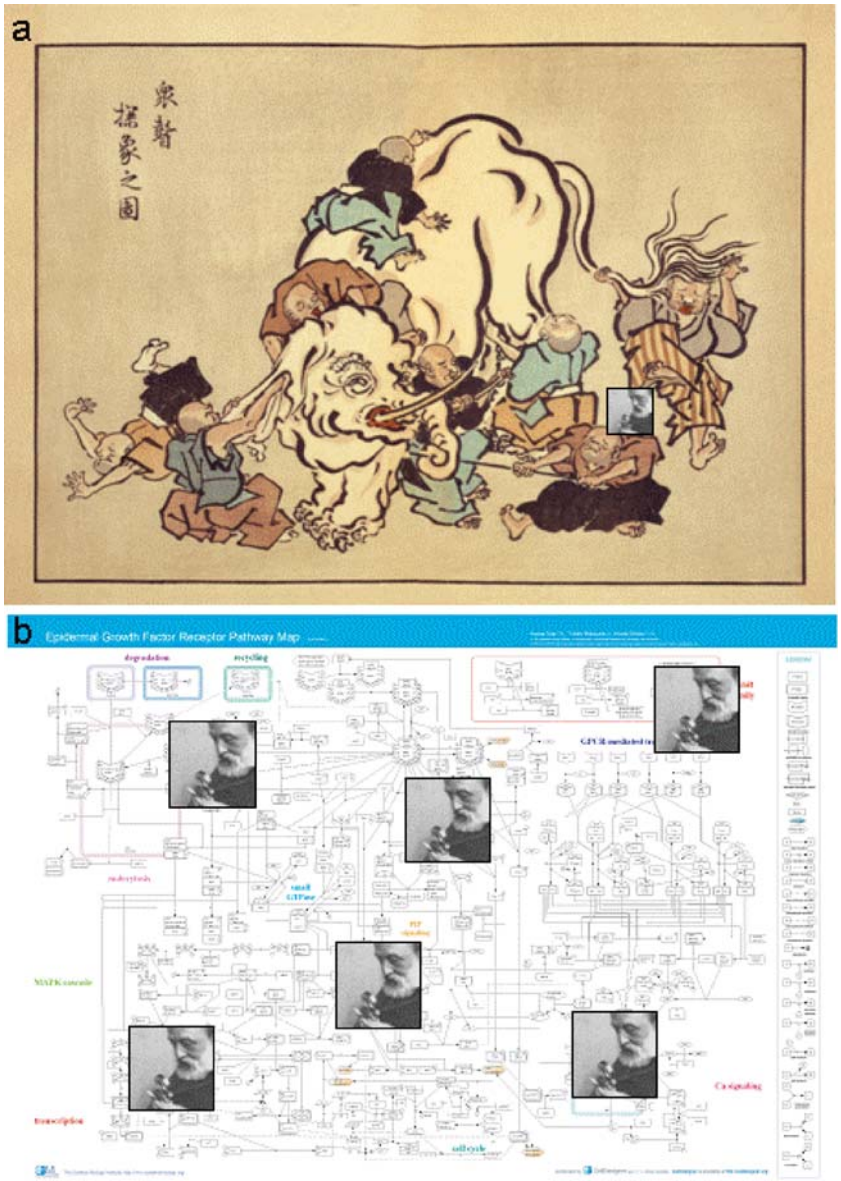

Fig. 1 **a** "Blind monks examining an elephant" by Itcho Hanabusa (1652-1724 [17]) and **b** a modern scientist's concept of the "Epidermal growth factor receptor pathway map" [18]. Is there really a fundamental difference between the (re-) searchers at the top and those at the bottom regarding the "objective truth" of the systems?

Virchows Arch (2009) 454:239
DOI 10.1007/s00428-008-0719-1

ERRATUM

Expression of estrogen receptor co-regulators NCoR and PELP1 in epithelial cells and myofibroblasts of colorectal carcinomas. Cytoplasmic translocation of NCoR in epithelial cells correlates with better prognosis

Vassiliki Tzelepi · Petros Grivas · Zinovia Kefalopoulou · Haralabos Kalofonos · John N. Varakis · Georgia Sotiropoulou-Bonikou

Published online: 23 December 2008

Erratum to: Virchows Arch
DOI 10.1007/s00428-008-0708-4

The title of the article was rendered incorrectly.
The correct title is as given above.

The online version of the original article can be found at http://dx.doi.org/10.1007/s00428-008-0708-4.

V. Tzelepi · Z. Kefalopoulou · J. N. Varakis · G. Sotiropoulou-Bonikou (✉)
Department of Anatomy and Histology-Embryology,
University of Patras,
26500 Rion, Greece
e-mail: sotiropouloug@yahoo.com

V. Tzelepi · Z. Kefalopoulou
Department of Pathology, University of Patras,
26500 Rion, Greece

P. Grivas · H. Kalofonos
Department of Internal Medicine-Division of Oncology,
Medical School, University of Patras,
26500 Rion, Greece

P. Grivas
Department of Internal Medicine, Hahnemann University Hospital/Drexel University College of Medicine,
Philadelphia, PA 19102, USA

Virchows Arch (2009) 454:241–248
DOI 10.1007/s00428-009-0728-8

ORIGINAL ARTICLE

Comprehensive immunohistochemical analysis of Her-2/neu oncoprotein overexpression in breast cancer: HercepTest™ (Dako) for manual testing and Her-2/neuTest 4B5 (Ventana) for Ventana BenchMark automatic staining system with correlation to results of fluorescence in situ hybridization (FISH)

Doris Mayr · Sibylle Heim · Cedric Werhan · Evelyn Zeindl-Eberhart · Thomas Kirchner

Received: 31 July 2008 / Revised: 23 December 2008 / Accepted: 5 January 2009 / Published online: 24 January 2009

Abstract Overexpression of Her-2/neu-oncoprotein is used as marker for Herceptin® therapy. To investigate the sensitivity and specificity of automatic immunohistochemistry (Benchmark, Ventana), we compared the results to the manual testing (Dako) in 130 breast carcinomas and validated the results by fluorescence in situ hybridization (FISH). Manual and automatic immunohistochemistry of Her-2/neu-oncoprotein using two different antibodies (HercepTest™, Her-2/neuTest 4B5) was analyzed. FISH was performed in all cases with uncertain or strong overexpression in either immunohistochemical stainings or with different immunohistochemical results. Same immunohistochemical results were seen in 73.8%. Two cases with overexpression, detected with Her-2/neuTest 4B5 and confirmed by FISH, showed no overexpression using HercepTest™. From 21 cases with 2+ by Her-2/neuTest 4B5, 15 cases had no gene amplification (two of them with 3+ HercepTest™); three cases showed a gene amplification (one of them with failing overexpression by HercepTest™); two other cases were polysomic; one could not be analyzed. Ventana immunohistochemistry seems to be of same reliability like Dako with a little better concordance to FISH in our study.

Keywords Breast cancer · Her-2/neu-immunohistochemistry · BenchMark · FISH

D. Mayr (✉) · S. Heim · E. Zeindl-Eberhart · T. Kirchner
Pathologisches Institut,
Ludwig Maximilians Universitaet München,
Thalkirchner Strasse 36,
80337 München, Germany
e-mail: doris.mayr@med.uni-muenchen.de

C. Werhan
Ventana,
Strasbourg, France

Introduction

Her-2/neu (c-*erb*-B2) oncogene encodes a transmembrane receptor protein which is structurally related to the epidermal growth factor receptor. Her-2/neu oncogene amplification/overexpression has been observed in several types of carcinomas [1–3] and can be demonstrated in about 20–30% of invasive carcinomas of the breast, in more than 90% caused by amplification. Protein overexpression without oncogene amplification occurs infrequently; in these cases, patients' outcome is similar to that without amplification. Her-2/neu amplification has been associated with poor prognosis with shorter disease-free and overall survival in lymph node-positive and lymph node-negative breast cancer and, moreover, has been a predictive factor for response to chemotherapy, antiestrogens, and Herceptin® [4–7]. Because of these therapeutical consequences, an accurate and reliable determination of Her-2/neu status is indispensable.

Previous molecular analyses indicate that oncogene amplification is closely associated with protein overexpression, but reports by clinical laboratories show a different

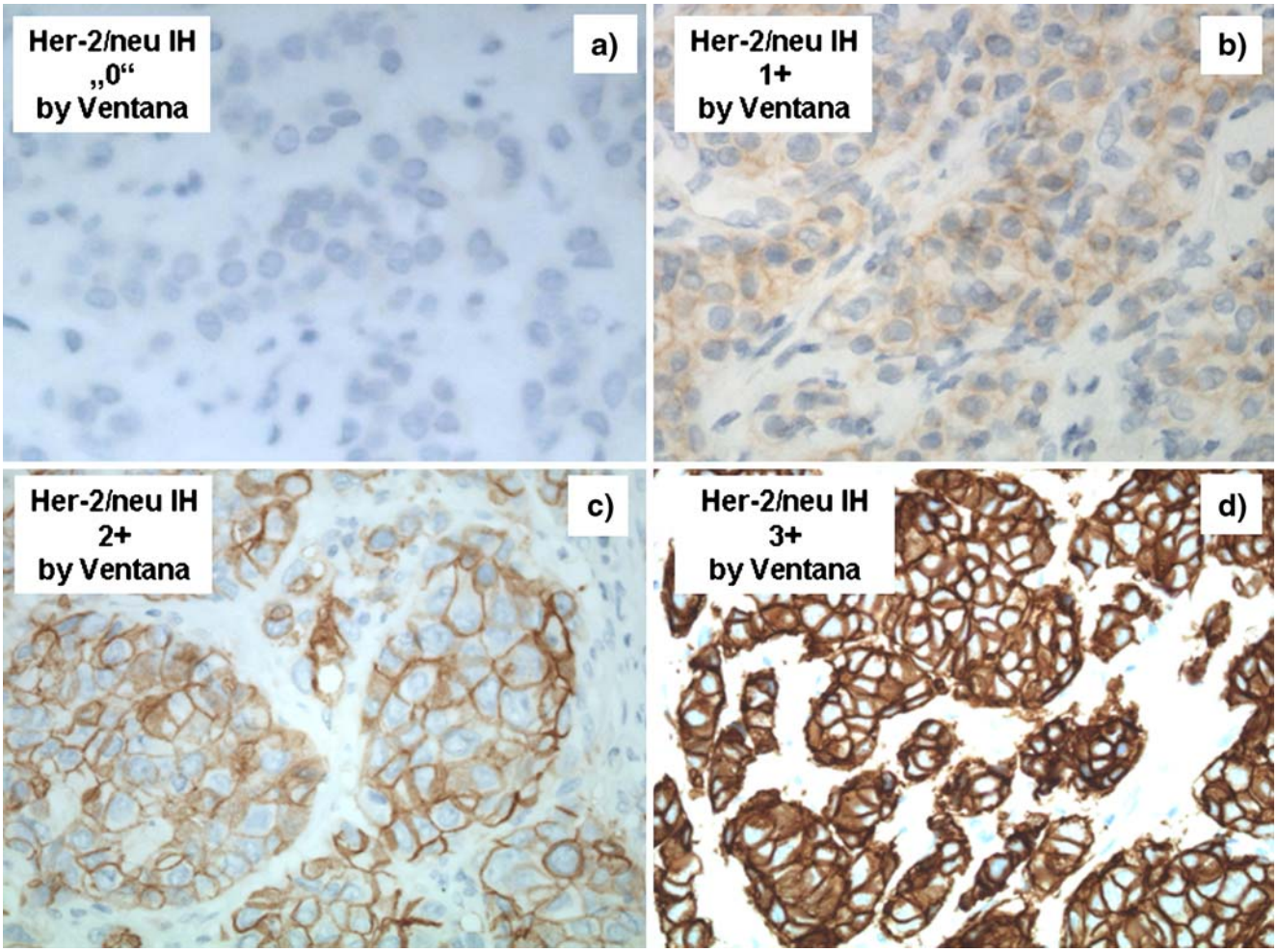

Fig. 1 **a** Score “0”: negative case, no staining. **b** Score 1+: weak staining of the incomplete membrane in more than 10% of the tumor cells. **c** Score 2+: weak to moderate staining of the entire membrane in more than 10% of the tumor cells. **d** Score 3+: strong staining of the entire membrane in more than 30% of the tumor cells

number of detected cases in their immunohistochemical (ICH) results. Most discrepancies are seen between local and central testing and because of using nonstandardized test kits [8–10].

The aim of this study was to compare the fully automatic staining system (Ventana BenchMark) and the manual testing system (Dako) for immunohistochemical detecting of Her-2/neu overexpression in 130 formalin-fixed and paraffin-embedded invasive breast carcinomas, using two different antibodies (HercepTest™ and Her-2/neuTest 4B5) and validated the results by applying fluorescence in situ hybridization (FISH).

Table 1 Frequencies of staining intensity for Her2-/neu expression with Dako and Ventana antibody

Staining	Dako	Ventana
Score 0	33 (25.4%)	20 (15.4%)
Score 1+	31 (23.8%)	28 (21.5%)
Score 2+	40 (30.8%)	50 (38.5%)
Score 3+	26 (20.0%)	32 (24.6%)
All	130	130

Table 2 Correlation between Dako and Ventana immunohistochemistry

	Ventana 0	Ventana 1+	Ventana 2+	Ventana 3+	All
All cases					
Dako 0	14	13	6	0	33
Dako 1+	6	12	11	2	31
Dako 2+	0	3	29	8	40
Dako 3+	0	0	4	22	26
All	20	28	50	32	130
Core biopsies cases					
Dako 0	6	6	4	0	16
Dako 1+	6	7	4	1	18
Dako 2+	0	2	14	1	17
Dako 3+	0	0	3	10	13
All	12	15	25	12	64

Table 3 FISH results of 85 cases

FISH result	Number of cases
Negative	38
Amplification	43
Polysomy	3
Not evaluable	1
All	85

Materials and methods

Paraffin-embedded material of 130 patients with breast cancer was available, including 111 invasive ductal, 13 invasive lobular, and four mucinous carcinomas and one case of tubular and one of papillary subtype. Tumor grade I was seen in seven cases, grade II in 63 cases, and grade III in 60 cases.

All 130 patients were treated at the Department of Obstetrics and Gynaecology, Ludwig Maximilians University of Munich and diagnosed at the Department of Pathology, Ludwig Maximilians University of Munich between 2006 and 2007. In 64 cases (49.2%), the material came from core biopsies, in 66 (50.8%) excision biopsies. All samples were fixed in 4% neutral buffered formalin and paraffin-embedded.

Immunohistochemistry

Immunohistochemical analyses of Her-2/neu oncoprotein were performed, using two different antibodies: the HercepTest™ (DakoCytomation, Glostrup, Denmark) and the Her-2/neuTest 4B5 (Ventana Medical Systems, S.A., Illkirch, France). For both immunohistochemistries, all paraffin-embedded specimens were cut at 2–3 μm, using conventional histological techniques and transferred to slides (Super Frost Plus, Menzel, Germany).

Dako

Immunohistochemical evaluation of HER-2 overexpression was done by standard methods using the Dako HercepTest™.

Ventana

The immunohistochemical staining was performed automatically with Ventanas Benchmark® XT, using the Her-2/neuTest 4B5.

Scoring system

For interpretation, only the membrane staining intensity and pattern was evaluated, using the Dako scoring system [11] in consideration of the new recommendations of the American Society of Clinical Oncology/College of American Pathologists [12]: No staining at all or membrane staining in less than 10% of the tumor cells resulted in a score of "0". A faint or barely perceptible incomplete membrane staining in more than 10% of the tumor cells was scored "1+". A weak to moderate staining of the entire membrane in more than 10% of the tumor cells was scored "2+" and a strong staining of the entire membrane in more than 30% of the tumor cells resulted a score of "3+". Strong staining only in areas of tissue borders was ignored. Prior to this, positive and a negative control slides had been examined. The evaluation of both immunohistochemical results was carried out blindly.

Fluorescence in situ hybridization

FISH was performed as described previously [13], using DNA-specific probes from PathVision™ (Abbott/Vysis: LSI® HER2 SpectrumOrange™ and CEP 17 SpectrumGreen™). This validation was performed in all cases with uncertain or strong overexpression (23+) and in all cases with different results by immunohistochemistry.

Hybridization signals were counted in 50 nuclei per sample. All overlapping nuclei were excluded; only nuclei with a distinct nuclear border were evaluated. The interpretation followed the criteria of Pauletti and coworkers [14] in consideration of the new recommendations of the American Society of Clinical Oncology/College of American Pathologists [12]. Negativity for Her-2/neu gene amplification is existing when FISH ratio is <1.8 or Her-2/neu gene copy is

Table 4 Correlation between IHC and FISH

FISH	IHC (Dako)					IHC (Ventana)				
	0	1	2	3	All	0	1	2	3	All
Negative	6	9	21	2	38	0	3	35	0	38
Amplification	0	3	16	24	43	0	0	11	32	43
Polysomy	0	0	3	0	3	0	0	3	0	3
Not evaluable	0	1	0	0	1	0	0	1	0	1
Not performed	27	18	0	0	45	21	24	0	0	45
All	33	31	40	26	130	20	28	50	32	130

Table 5 Correlation between amplified, nonamplified, and polysomic cases to IHC

FISH	IHC			
	0/1+	2+	3+	All
Amplification	3[a]	16[a]	24[a]	43
	0[b]	11[b]	32[b]	
Negative	15[a]	21[a]	2[a]	38
	3[b]	35[b]	0[b]	
Polysomy	0[a]	3[a]	0[a]	3
	0[b]	3[b]	0[b]	

[a] Dako
[b] Ventana

<4.0. Positivity for Her-2/neu gene amplification is existing when FISH ratio is >2.2 or Her-2/neu gene copy is >6. Cases with FISH ratio between 1.8 and 2.2 or Her-2/neu gene copy between 4.0 and 6.0 are evaluated as equivocal. As in our laboratory, a dual color fluorescence in situ hybridization for Her-2/neu gene amplification has been performed; in all cases, the ratio of Her-2/neu gene signal to centromere 17 signal was calculated and used as single criterion for amplification or nonamplification.

Statistical analysis

For all statistical calculations, Superior Performance Software System 16 (SPSS for Windows, Microsoft USA) was used. The various parameters were compared by using chi square tests. p values<0.05 were considered statistically significant.

Results

Immunohistochemistry

All 130 cases could be analyzed in both immunohistochemical procedures. The quality of automatic staining with Ventana was equivalent to the staining used so far (see Fig. 1). The frequencies of staining intensity are demonstrated in Table 1.

Correlation between Dako and Ventana immunohistochemistry was excellent (p<0.005), even when we analyzed only cases sampled by core biopsies as shown in Table 2. Same immunohistochemical results were seen in 96/130 (73.8%) cases (22 cases with strong expression=3+, 29 with uncertain overexpression=2+, and 45 with no overexpression=0 or 1+).

Table 6 p value for IHC Dako and IHC Ventana and for IHC and FISH

Correlation of	p value
IHC Dako to IHC Ventana	<0.005
IHC Dako to FISH	<0.005
IHC Ventana to FISH	<0.005

Table 7 Correlation between 2+ cases by Dako or by Ventana and FISH

IHC	FISH				
	Negative	Amplification	Polysomy	No evaluation	All
Dako 2+	21	16	3	0	40
Ventana 2+	35	11	3	1	50

Discrepant results were seen in 34/130 (26.2%) cases, including 12 cases (10.8%) with a difference between score 2+ and score 3+. Three cases (2.3%) were 1+ by Ventana and 2+ by Dako, 17 cases (13%) were assessed as 2+ by Ventana and as negative by Dako (0 or 1+), and two cases (1.5%) showed a strong reaction (3+), detected by Ventana, but no overexpression (1+) by Dako.

For core biopsies cases same immunohistochemical results were seen in 49/64 (76.6%) cases (ten cases with strong expression=3+, 14 with uncertain overexpression=2+, and 25 with no overexpression=0 or 1+). In 15 cases (23.4%), discrepant results were seen: four cases (26.6%) with score 2+ or 3+, eight cases (53.3%) with Dako 0/1+ and Ventana 2+, one case (6.6%) with a negative result (1+) by Dako and a strong reaction (3+) by Ventana, and two cases (13.3%) assessed as 2+ by Dako and negative (1+) by Ventana.

No differences could be demonstrated by using the previous scoring system standard (3+: strong staining of the entire membrane in more than 10% of the tumor cells). Neither the staining with Dako nor with Ventana demonstrated a case with strong reaction in only a small part (<30%) of the tumor cells.

Table 8 Correlation between Dako IHC and Ventana IHC to FISH for the 34 immunohistochemical discordant cases

Number of cases	Dako	Ventana	FISH
6	0	2+	All negative
11	1+	2+	9× negative
			1× amplified
			1× no evaluation
2	1+	3+	All amplified
4	3+	2+	2× negative
			2× amplified
3	2+	1+	All negative
8	2+	3+	All amplified
34			

FISH

FISH was performed in all cases with 2+ or 3+ by Dako and/or by Ventana immunohistochemistry (n=85). Results of all performed FISH analyses are demonstrated in Table 3. The correlation between IHC results (Dako and Ventana) and FISH and between amplified and nonamplified cases by FISH and IHC results (Dako versus Ventana) were each of high significance (see Tables 4, 5, and 6).

All cases (n=22) with an immunohistochemical equivocal result 3+ by Dako and by Ventana were amplified ($p<$ 0.005). From all cases (n=29) with an equivocal immunohistochemical result 2+ by Dako and by Ventana, 18 cases (62.1%) were negative by FISH, eight cases (27.5%) were amplified, and three cases (10.3%) were polysomic. From 40 cases with an immunohistochemical result 2+ by Dako, 21 cases (52.5%) showed no Her-2/neu oncogen amplification, 16 cases (40%) were amplified, and three cases (7.5%) were polysomic, all detected by FISH. From 50 cases with an immunohistochemical result 2+ by Ventana, 35 cases (70%) had no amplification, 11 cases (22%) were amplified, three cases (6%) were polysomic, and one case (2%) could not be evaluated by FISH (see Table 7). None of the polysomic cases by FISH showed a strong expression (3+) by immunohistochemistry (Dako or Ventana).

In 34 cases (26.2%), discordant results (0/1+ versus 2+ or 3+ and 2+ versus 3+) were seen (see Table 8). Examples are given in Fig. 2a–h.

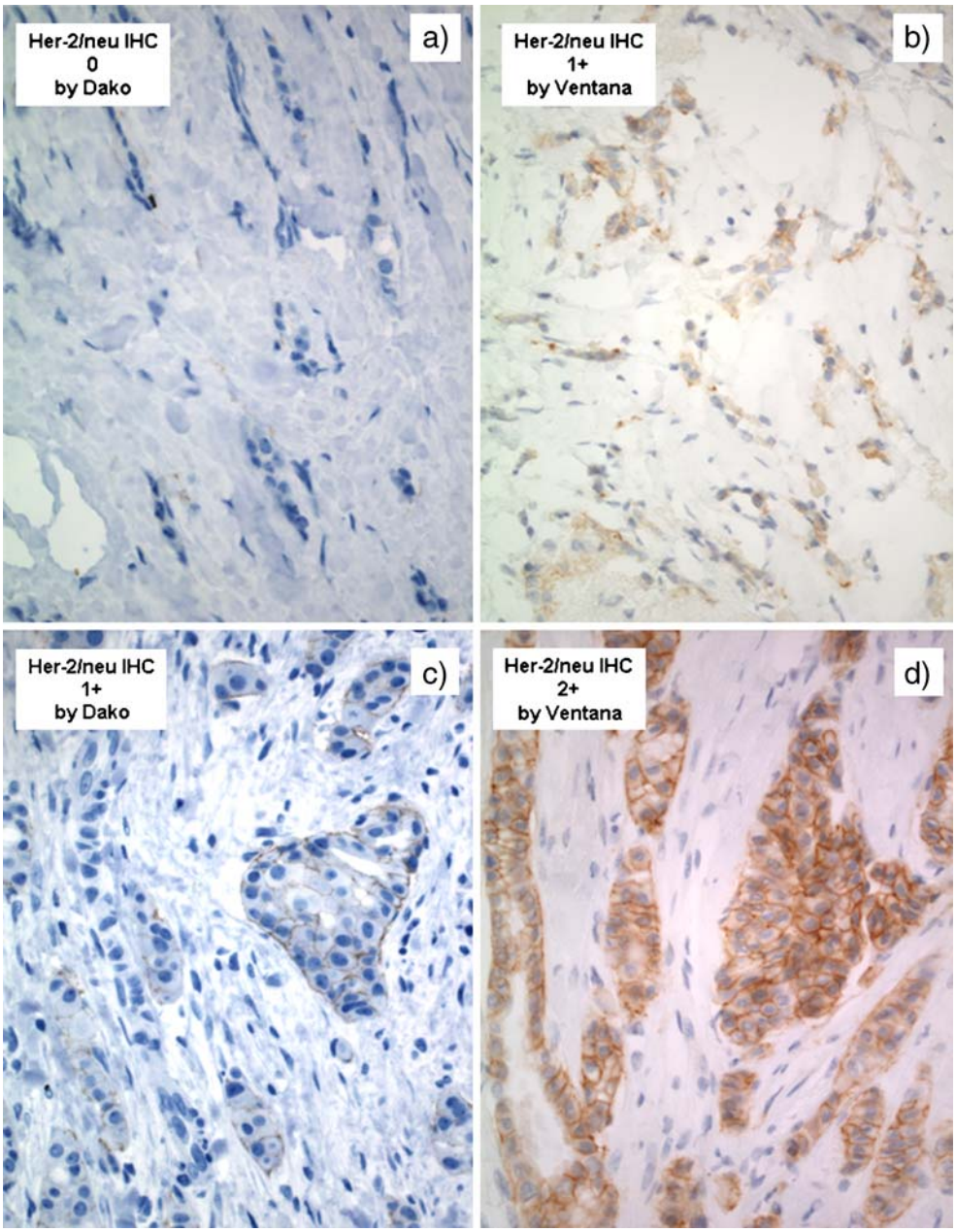

Fig. 2 Immunohistochemical discrepant cases. **a**, **b** Her-2/neu immunohistochemical staining, score 0 by Dako, 1+ by Ventana with weak staining of the incomplete membrane. **c**, **d** Her-2/neu immunohistochemical staining, score 1+ by Dako with weak staining of the incomplete membrane, 2+ by Ventana with moderate staining of the entire membrane. **e**, **f** Her-2/neu immunohistochemical staining, score 2+ by Dako with moderate staining of the entire membrane, 1+ by Ventana with weak staining of the incomplete membrane. **g**, **h** Her-2/neu immunohistochemical staining, score 3+ by Dako with strong staining of the entire membrane in more than 30%, 2+ by Ventana with moderate staining of the entire membrane

From 19 cases negative by Dako (0 or 1+) with moderate or strong expression by Ventana (2+ or 3+), three cases were amplified (10.5%). Four cases showed a high expression by Dako (3+) and moderate expression by Ventana (2+), two of them with amplification (FISH). All three cases with 2+ by Dako and 1+ by Ventana were negative by FISH, but all eight cases 2+ by Dako and 3+ by Ventana were amplified. To prove predictive values, sensitivity, and specificity of IHC for these 34 cases, a binary classification had to be established. In one case, the IHC 2+ cases had to be treated as positive, in the other case as negative. The starting points and different possibilities are summarized in Tables 9 and 10.

Discussion

Her-2/neu oncogene amplification and/or protein overexpression in breast carcinomas are of high importance, because of their correlation to prognosis and to prediction of responsiveness to treatment. Several different laboratory methods exist to identify women with a Her-2/neu amplification or overexpression. Some authors prefer the more reproducible in situ hybridizations with fluorescence, chromogen, or silver to prove the oncogene amplification [15–17]; others depend on immunohistochemistry to prove the protein overexpression [9, 18] and, if required, applying FISH in addition. As is known, there is a big spectrum of

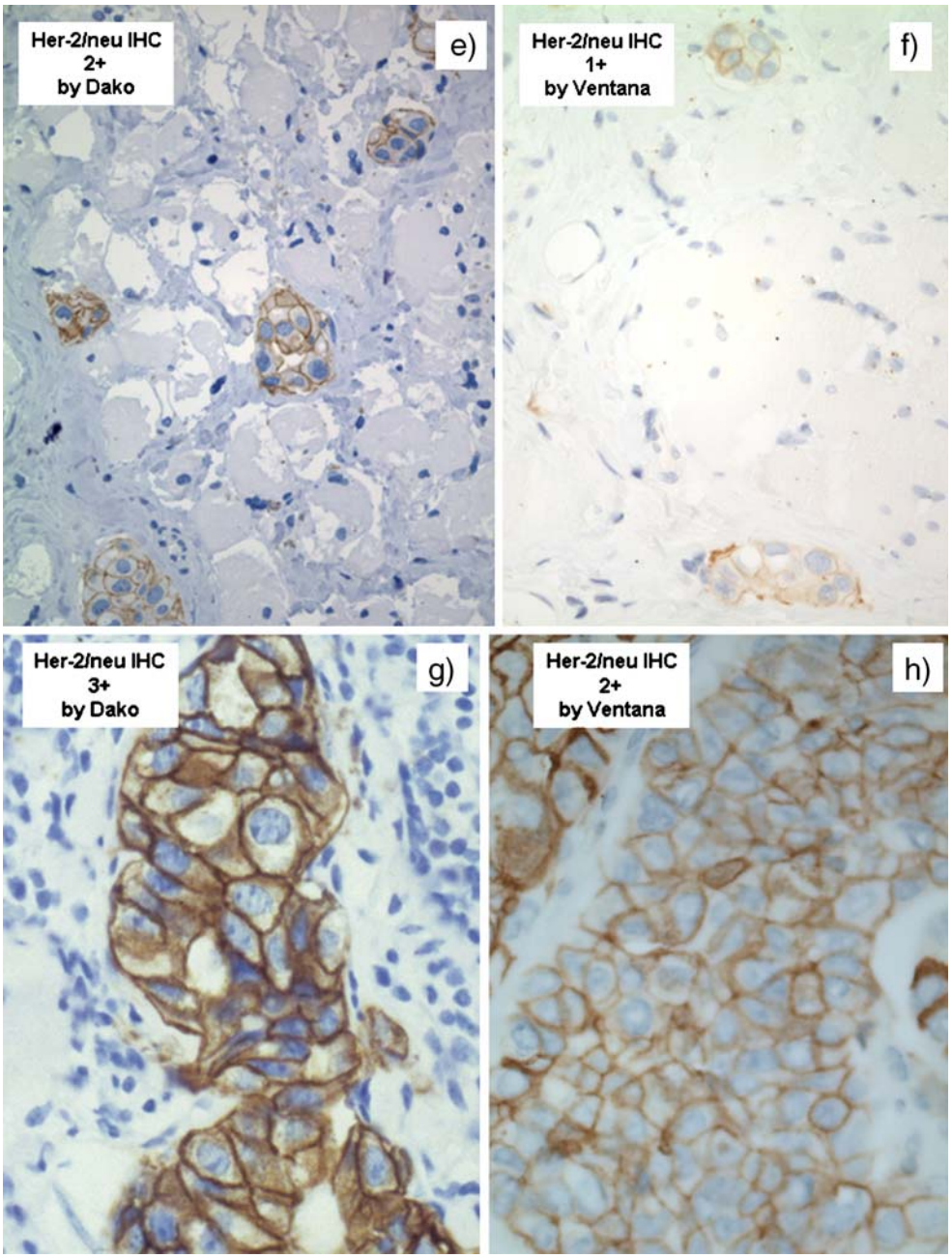

Fig. 2 (continued)

Table 9 Starting point for Dako and Ventana IHC

		FISH amplification	FISH negative	All
Dako	3+	2	2	4
	2+	8	3	11
	1+[a]	3	9	12
	0	0	6	6
	All	13	20	33
Ventana	3+	2	2	4
	2+[b]	8	3	11
	1+	3	9	12
	0	0	6	6
	All	13	20	33

[a] One time no evaluation possible
[b] One time no evaluation possible

used antibodies for immunohistochemistry which could direct to concordance of results and IHC is still discussed contrary for reproducibility, susceptibility, sensitivity, and specificity [19–21].

In Germany, most pathologists first examine the Her-2/neu protein overexpression, followed by FISH in failed or doubtful cases (immunohistochemical result 2+). This procedure is preferred in order to save time and money: time because immunohistochemistry is quicker to perform and money because common material for immunohistochemistry (antibody) is less costly than the DNA-specific probes for (F)-ISH. Moreover, immunohistochemistry can be performed as integral part of a routine diagnostic in nearly any laboratory, included as, however, in situ hybridization requires specific knowledge and specific devices.

We initiated this study testing two different antibodies: first HercepTest™ (Dako), which has to be performed manually and second Her-2/neuTest 4B5 (Ventana), which can be used automatically with Ventanas Benchmark® XT. We analyzed 130 cases of invasive breast carcinomas, using the new standard of 30% strong positivity (Wolff et al.) and correlated these results to the results of the FISH.

In nearly three of four cases (73.8%), an identical result could be obtained with immunohistochemistry ($p<0.005$). The remaining cases (26.2%) showed discrepant evaluations. Comparison to other studies, reasons for this relative high discrepancy could be laboratory variability, tumor heterogeneity, or artifacts and our focus on immunohistochemical unclear cases. However, in all our cases, the whole slide was evaluated and neither the staining with Dako nor with Ventana demonstrated a case with strong reaction in only a very small part (<30%) of the tumor cells. Differences in excision or core biopsies could not be noticed. Staining and evaluation was of similar quality; significance for correlation between Dako and Ventana immunohistochemistry in core biopsies cases was as high as for excision biopsies.

Retrospectively performed evaluation with the previous scoring system could not demonstrate any difference. These results are in contradictory to the results of Brunelli et al. [22], who noticed a shift from 3+ to 2+ by using the new scoring system with a better concordance to Her-2/neu amplification. In summary, we agree the findings of Moeder et al. [23] who suggest that a tumor with uniform positive staining pattern is driven by that pathway, unlike to a tumor with missing staining in a significant portion.

In 10.8% of the discordant cases, the deviation was seen between the score 2+ and 3+, all cases with 3+ by Ventana were amplified by FISH, but two of four cases (one excision biopsy, one core biopsy) with 3+ by Dako and 2+ by Ventana did not show any amplification. These patients had received Herceptin® therapy without an oncogene amplification. From 19 additional cases with a negative immunohistochemical result by Dako (0 or 1+), three cases were amplified (two excision biopsies, one core biopsy). These three patients did not receive Herceptin®, although a Her2-/neu oncogene amplification have been validated by FISH. The remaining case could not be examined by FISH. Two cases with an immunohistochemical score of 2+ by Ventana and negative by Dako did not show an oncogene amplification; same is true for three cases with 2+ by Dako and 1+ by Ventana.

In conclusion, the results of Her-2/neu testing by Ventana differ little from those by Dako (correlation $p<0.005$), no woman received Herceptin® without a Her-2/neu oncogene amplification, and no woman missed out the therapy with Herceptin® because of the immunohistochemical results by Ventana. Regrettably, the incorrect immunohistochemical results by Dako in five cases (3.8%)—two times false positive and three times false negative—validated with FISH, caused wrong therapies. As a consequence, two times patients were exposed to an

Table 10 Predictive values, including positive and negative values, sensitivity, and specificity of immunohistochemistry

Binary classification	Positive predictive value	Negative predictive value	Predictive value	Sensitivity	Specificity
Dako 0/1+ versus 2+/3+ and FISH +/−	0.67	0.83	0.76	0.77	0.75
Dako 0/1+/2+ versus 3+ and FISH +/−	0.50	0.62	0.60	0.15	0.90
Ventana 0/1+ versus 2+/3+ and FISH +/−	0.43	1	0.48	1	0.15
Ventana 0/1+/2+ versus 3+ and FISH +/−	1	0.86	0.91	0.91	0.76

expensive and pretty harmful therapy and three patients would have substantially benefited from Herceptin®, but did not get this therapy.

In summary, the automatically performed and hence time-efficient and standardized Her-2/neu immunohistochemistry by Ventana offers the same excellent quality and reliability like Dako and demonstrates a little better concordance to fluorescence in situ hybridization in our study.

Acknowledgments The authors thank Gabi Charell, Gabi Janssen, and Annegret Schäfer for their outstanding technical contribution, Simone Fenn for critically reading the manuscript, and Jutta Engel for statistical analysis.

Conflict of interest statement All authors declare that no conflict exists for devices or material used in the current study.

References

1. Berchuck A, Kamel A, Whitaker R et al (1990) Overexpression of HER-2/neu is associated with poor survival in advanced epithelial ovarian cancer. Cancer Res 50:4087–4091
2. Press MF, Pike MC, Hung G et al (1994) Amplification and overexpression of HER 2/neu in carcinomas of the salivary gland: correlation with poor prognosis. Cancer Res 54:5675–5682
3. Raspollini MR, Amunni G, Villanucci A et al (2006) HER-2/neu and bcl-2 in ovarian carcinoma: clinicopathologic, immunohistochemical, and molecular study in patients with shorter and longer survival. Appl Immunohistochem Mol Morphol 14:181–186
4. Formenti SC, Spicer D, Skinner K et al (2002) Low HER2/neu gene expression is associated with pathological response to concurrent paclitaxel and radiation therapy in locally advanced breast cancer. Int J Radiat Oncol Biol Phys 52:397–405
5. Gasparini G, Longo R, Torino F et al (2005) Therapy of breast cancer with molecular targeting agents. Ann Oncol 16(Suppl 4): iv28–iv36
6. Gusterson BA, Gelber RD, Goldhirsch A et al (1992) Prognostic importance of c erbB-2 expression in breast cancer. International (Ludwig) Breast Cancer Study Group. J Clin Oncol 10:1049–1056
7. Pegram MD, Pauletti G, Slamon DJ (1998) HER-2/neu as a predictive marker of response to breast cancer therapy. Breast Cancer Res Treat 52:65–77
8. Paik S, Bryant J, Tan-Chiu E et al (2002) Real-world performance of HER2 testing—National Surgical Adjuvant Breast and Bowel Project experience. J Natl Cancer Inst 94:852–854
9. Rhodes A, Jasani B, Anderson E et al (2002) Evaluation of HER-2/neu immunohistochemical assay sensitivity and scoring on formalin-fixed and paraffin-processed cell lines and breast tumors: a comparative study involving results from laboratories in 21 countries. Am J Clin Pathol 118:408–417
10. Rhodes A, Jasani B, Couturier J et al (2002) A formalin-fixed, paraffin-processed cell line standard for quality control of immunohistochemical assay of HER-2/neu expression in breast cancer. Am J Clin Pathol 117:81–89
11. . DAKO A/S, F. Hoffmann-La Roche Ltd (eds) (2002) Atlas of interpretation of HercepTestTM staining. (2000)
12. Wolff AC, Hammond ME, Schwartz JM et al (2007) American Society of Clinical Oncology/College of American Pathologists guideline recommendations for human epidermal growth factor receptor 2 testing in breast cancer. J Clin Oncol 25:118–145
13. Mayr D, Diebold J (2000) Grading of ovarian carcinomas. Int J Gynecol Pathol 19:348–353
14. Pauletti G, Godolphin W, Press MF et al (1996) Detection and quantitation of HER-2/neu gene amplification in human breast cancer archival material using fluorescence in situ hybridization. Oncogene 13:63–72
15. Bankfalvi A, Simon R, Brandt B et al (2000) Comparative methodological analysis of erbB-2/HER-2 gene dosage, chromosomal copy number and protein overexpression in breast carcinoma tissues for diagnostic use. Histopathology 37:411–419
16. Press MF, Slamon DJ, Flom KJ et al (2002) Evaluation of HER-2/neu gene amplification and overexpression: comparison of frequently used assay methods in a molecularly characterized cohort of breast cancer specimens. J Clin Oncol 20:3095–3105
17. Tubbs RR, Pettay JD, Roche PC et al (2001) Discrepancies in clinical laboratory testing of eligibility for trastuzumab therapy: apparent immunohistochemical false positives do not get the message. J Clin Oncol 19:2714–2721
18. Dowsett M, Hanby AM, Laing R et al (2007) HER2 testing in the UK: consensus from a national consultation. J Clin Pathol 60:685–689
19. Gouvea AP, Milanezi F, Olson SJ et al (2006) Selecting antibodies to detect Her2 overexpression by immunohistochemistry in invasive mammary carcinomas. Appl Immunohistochem Mol Morphol 14:103–108
20. Powell WC, Hicks DG, Prescott N et al (2007) A new rabbit monoclonal antibody (4B5) for immunohistochemical (IHC) determination of Her2 status in breast cancer: comparison with CB11, fluorescence in situ hybridization (FISH), and interlaboratory reproducibility. Appl Immunohistochem Mol Morphol 15:94–102
21. Ricardo SAV, Milanezi F, Carvalho ST et al (2008) Her2 evaluation using the novel rabbit monoclonal antibody SP3 and CISH in tissue microarrays of invasive breast. J Clin Path 60:1001–1005
22. Brunelli M, Manfrin E, Martignoni G et al (2008) Her-2/neu assessment in breast cancer using the original FDA and new ASCO/CAP guideline recommendations: impact on selecting patients for Herceptin therapy. Am J Clin Pathol 129:907–911
23. Moeder CB, Giltnane JM, Harigopal M et al (2007) Quantitative justification of the change from 10% to 30% for human epidermal growth factor receptor 2 scoring in the American Society of Clinical Oncology/College of American Pathologists guidelines: tumor heterogeneity in breast cancer and its implications for tissue microarray-based assessment of outcome. J Clin Oncol 25:5418–5425

Virchows Arch (2009) 454:249–256
DOI 10.1007/s00428-009-0725-y

ORIGINAL ARTICLE

Histological grading in a large series of advanced stage ovarian carcinomas by three widely used grading systems: consistent lack of prognostic significance. A translational research subprotocol of a prospective randomized phase III study (AGO-OVAR 3 protocol)

Stefan Kommoss · Dietmar Schmidt · Friedrich Kommoss · Juergen Hedderich · Philipp Harter · Jacobus Pfisterer · Andreas du Bois

Received: 14 August 2008 / Revised: 4 December 2008 / Accepted: 3 January 2009 / Published online: 27 January 2009

Abstract While there is no doubt that histologic grading is applicable in early stage ovarian carcinoma, it is still in controversial discussion concerning advanced stage ovarian carcinoma. It was the aim of this study to assess the three most widely used grading systems for ovarian carcinoma in terms of prognostic significance, concordance rates, and reproducibility in a large number of advanced stage ovarian carcinomas of all types after standardized chemotherapy. Representative hematoxylin and eosin slides from 334 cases of stage IIB–IV ovarian carcinoma (prospective randomized, multi-center, phase III study) were used. The first round was grading of all cases according to FIGO, GOG, and Silverberg by one author. The second round (after 1 year) was 30 randomly selected cases graded by three authors. None of the three grading systems was prognostically significant (FIGO p=0.38; GOG p=0.70; Silverberg p=0.92). The concordance rates between the three systems were as follows: FIGO/GOG 95.5%, κ=0.929; Silverberg/FIGO 69.9%, κ=0.533; Silverberg/GOG 66.8%, κ=0,481. Grading of advanced stage ovarian carcinomas was of no value for estimation of prognosis in this homogeneously treated patient group. Alternative methods should be defined, which might help to separate patients with high risk of tumor progression from others with low risk.

Keywords Grading · Ovarian carcinoma · Prognosis · FIGO · GOG · Silverberg

S. Kommoss (✉) · P. Harter · A. du Bois
Department of Gynecology & Gynecologic Oncology,
Dr.-Horst-Schmidt-Kliniken (HSK) Wiesbaden,
Ludwig-Erhard-Str. 100,
65199 Wiesbaden, Germany
e-mail: stefan.kommoss@gyn-patho.de

S. Kommoss · D. Schmidt · F. Kommoss
Institute of Pathology, A2, 2,
68159 Mannheim, Germany

J. Hedderich
Biometrie, University Hospital Schleswig-Holstein,
Kiel, Germany

J. Pfisterer
Ubbo-Emmius-Klinik, Gynäkologie und Geburtshilfe,
Aurich, Germany

Introduction

Histologic grading has been shown to be of prognostic significance in a variety of tumor entities. Grading is an integral and universally accepted part of clinical decision making in breast and endometrium cancer [1, 2]. While grading of tumor differentiation has been shown to be of prognostic significance in early stage ovarian carcinoma [3], it is still in controversial discussion concerning advanced stage ovarian carcinoma. One reason might be that there is as yet no universally accepted grading system such as have been established for breast and endometrial carcinoma [1, 2]. There are several grading systems that are used in different institutions all qualifying for prognostic significance in some tumor series [4–9], but lacking general acceptance and reproducibility among pathologists as described by several authors [10–13].

One of the most widely used grading systems is the FIGO grading system, mainly based on architectural features [6]. Another well-established grading system, at least in the United States, is that of the Gynecologic Oncology Group [4]. Recently, Silverberg et al. reported a new grading system, which is based on a modification of the Nottingham grading system for breast cancer and can be used for all types of ovarian carcinoma [9]. Several authors reported the Silverberg grading system to provide independent prognostic information with levels of significance comparable to [14–16] or even to be superior to the FIGO grading system [17].

It was the aim of the present retrospective study to assess the three most widely used grading systems for ovarian carcinoma in terms of prognostic significance, concordance rates, and reproducibility from a large homogeneous collection of patients with primary advanced stage ovarian carcinoma treated with platinum and paclitaxel-containing standardized chemotherapy [18].

Materials and methods

Study material After completion of a prospective randomized, multi-center, phase III study of a total of 798 patients with ovarian cancer, FIGO stages IIB–IV, comparing cisplatin 75 mg/m^2 plus paclitaxel 185 mg/m^2 (PT) with paclitaxel 185 mg/m^2 plus carboplatin (TC) [18], tissue blocks were requested from participating centers for scientific analysis. Between one and 53 paraffin blocks per case were received from a total of 334 study cases. Selection of these patients did not follow any rule but was mainly based on both availability of material and willingness to cooperate. An explorative comparison of patient characteristics between patients with or without available paraffin blocks was performed and did not show a selection bias. Paraffin sections were cut from all blocks and stained with hematoxylin and eosin. After review of all slides and exclusion of material, which contained no tumor tissues or was insufficient for adequate histopathological analysis (32 cases), between one and nine stained sections each from a total of 302 cases of primary invasive epithelial ovarian carcinomas were available for further study. All slides were reviewed by two gynecopathologists (FK, DS) who were blinded for the outside diagnoses. All ovarian carcinomas were typed according to the current WHO criteria and classified as either serous, mucinous, endometrioid, clear cell, transitional cell, or undifferentiated carcinoma [19–21]. A diagnostic consensus was reached in each case.

Grading All tumors were graded applying the criteria of the three grading systems by an experienced gynecopathologist (FK). The *FIGO grading* system is based on architectural features. Grade 1 is assigned to tumors showing <5% solid growth, grade 2 tumors show between 5% and 50% solid growth, and grade 3 tumors are characterized by <50% solid growth [6] (Fig. 1a–c). *GOG grading* depends on the histologic type of the tumor. Specific rules are proposed for the grading of each carcinoma type; however, clear cell carcinomas are not graded by this system [4] (Fig. 1d–f). The *Silverberg grading system* consists of three parameters: architectural pattern, nuclear grade, and mitotic activity. Each of these parameters is assigned a score from 1 to 3. Final grade is derived from summation of the latter scores [9] (Fig. 1g–i). The ocular diameter of the microscope was taken into account as previously described by Mayr and Diebold [15].

Intra-/interobserver variability To evaluate the initial results as well as to assess the reproducibility of the grading systems, 30 randomly chosen slides were reviewed by the same pathologist after 1 year as well as independently by two other observers. All reviewers were blinded for each other's results, as well as for initial diagnosis, including FIGO stage, clinical outcome, and initial grading or typing.

Statistical analysis The exploratory analysis of possible selection bias of the study population was performed by the Chi-square test [22]. Survival analyses were performed according to the method of Kaplan and Meier [23]; survival times were compared using the log rank test [24] applying SSPS13 software [25]. Agreement of grading by the same or other observer was expressed by the kappa coefficient [26].

Results

The analyzed patient cohort was treated within a randomized prospective trial comparing cisplatin or carboplatin plus paclitaxel as postoperative chemotherapy after radical surgery. Three hundred two cases of primary invasive epithelial ovarian carcinomas were selected without following any rule, other than being dependent on availability of material and willingness to cooperate. No significant selection bias was found after explorative analysis of patient characteristics (patient age, ECOG clinical performance, FIGO stage, preoperative extraovarian tumor, postoperative residual tumor) comparing patients with and without available paraffin blocks by Chi-square analysis (data not shown). The distribution of FIGO stage, age, postoperative residual tumor, and histological types of ovarian carcinomas according to current WHO criteria after central review of hematoxylin and

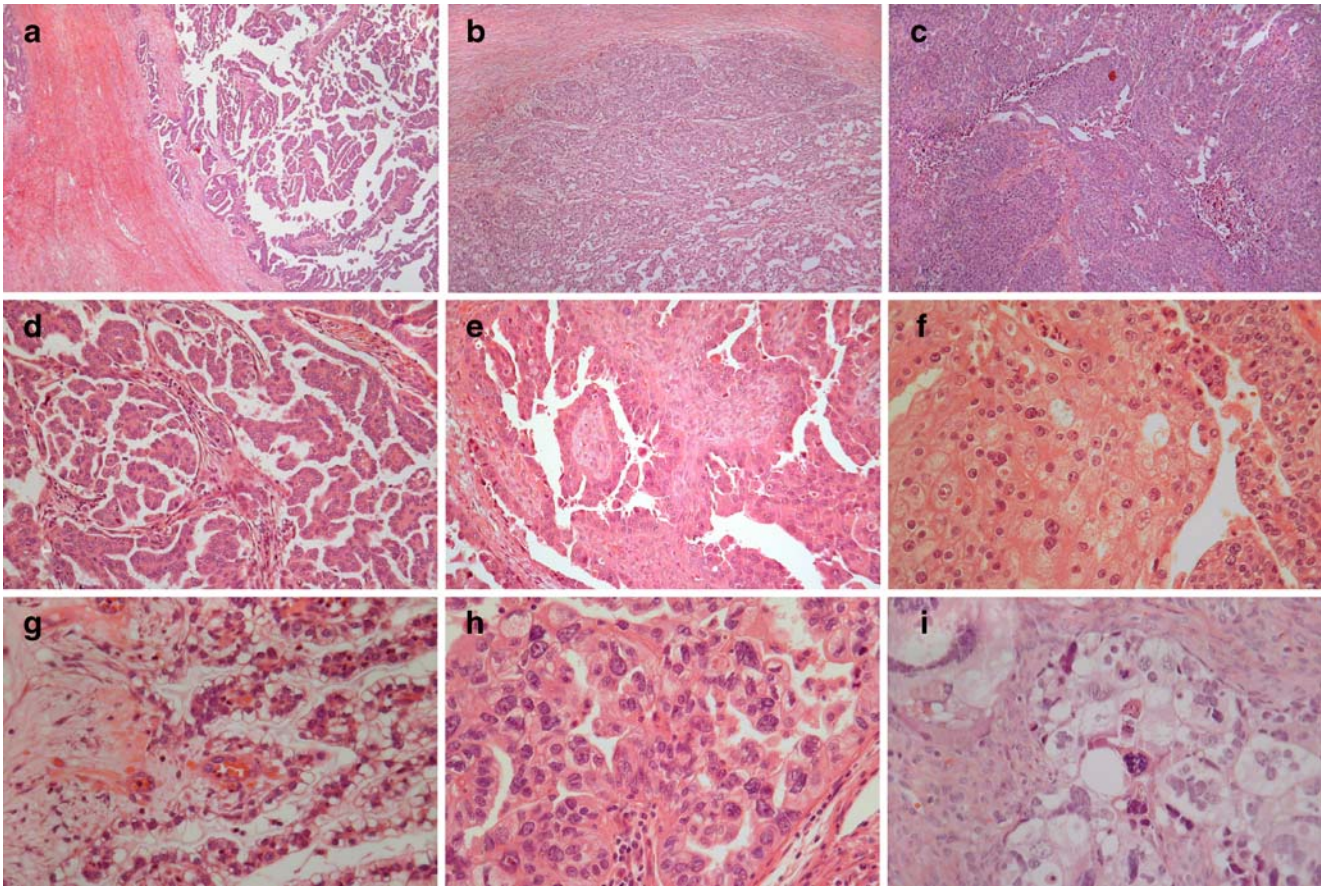

Fig. 1 FIGO grading system G1 (**a**), G2 (**b**), G3 (**c**); GOG grading system G1 (**d**), G2 (**e**), G3(**f**); Silverberg grading system G1 (**g**), G2 (**h**), G3 (**i**)

eosin stained recuts from all available paraffin blocks is shown in Table 1.

The results of tumor grading according to the several grading systems were as follows. G1: FIGO n=60/302 (19.9%), GOG n=53/265 (20.0%), Silverberg n=67/302 (22.2%); G2: FIGO n=114/302 (37.7%), GOG n=111/265 (41.9%), Silverberg n=127/302 (42.1%); G3: FIGO n=128/302 (42.4%), GOG n=101/265 (38.1%), Silverberg n=108/302 (35.7%; Table 2).

Table 1 Distribution of histological type, postoperative residual tumor, age, and FIGO stage

Histological type	Serous	135 (44.7%)	302 (100%)
	Mucinous	24 (7.9%)	
	Endometrioid	58 (19.2%)	
	Clear cell	37 (12.3%)	
	Transitional cell	16 (5.3%)	
	Undifferentiated	32 (10.6%)	
Postoperative residual tumor	0 mm	82 (27.2%)	302 (100%)
	1–10 mm	94 (31.2%)	
	11+ mm	126 (41.6%)	
Age	<65 years	219 (72.5%)	302 (100%)
	>65 years	83 (27.5%)	
FIGO stage	IIB	7 (2.3%)	302 (100%)
	IIC	12 (4.0%)	
	IIIA	16 (5.3%)	
	IIIB	35 (11.6%)	
	IIIC	186 (61.6%)	
	IV	46 (15.2%)	

Survival analyses were performed for all patients, as well as for cohorts separated by histological types and postoperative residual tumor being the most important clinical prognostic factor. Median follow-up time of all patients was 36.6 months; patients without event had a median follow-up time of 57.3 months. Established prognostic factors were proven to be of prognostic significance in this study (FIGO IIB–IIA vs. IIIB–IV: p=0.0006; postoperative residual tumor 0 mm vs. >0 mm: p<0.0001; ECOG performance status 0 vs. >0: p=0.002; Age <65 vs. >65 years: p=0.03). The 5-year survival rates and median survival time in relation to tumor grading were as follows: FIGO (p=0.38): G1 37.4% (35.5 months), G2 28.5% (39.0 months), G3 33.7% (45.5 months); GOG (p=0.70): G1 31.9% (35.5 months), G2 33.1% (39.1 months), G3 33.0% (45.5 months); Silverberg (p=0.92): G1 36.7% (39.0 months), G2 31.9% (40.2 months), G3 29.7% (41.2 months; Table 2). Life table curves are shown in Fig. 2a–c. Similarly, there was no prognostically significant correlation between tumor grading and relapse-free survival (data not shown). A therapy-

Table 2 Survival of patients: FIGO, GOG, and Silverberg grading systems

		G1			G2			G3		
		n	Survival		*n*	Survival		*n*	Survival	
			5 years (%)	Median (months)		5 years (%)	Median (months)		5 years (%)	Median (months)
All cases	FIGO (p=0.38) (p=0.48)[a] (p=0.86)[b] (p=0.39)[c]	60/302 (19.9%)	37.4	35.5	114/302 (37.7%)	28.5	39.0	128/302 (42.4%)	33.7	45.5
	GOG[d] (p=0.70) (p=0.63)[a] (p=0.50)[b] (p=0.74)[c]	35/265 (20.0%)	31.9	35.5	111/265 (41.9%)	33.1	39.1	101/265 (38.1%)	33.0	45.5
	Silver (p=0.92) (p=0.92)[a] (p=0.73)[b] (p=0.92)[c]	67/302 (22.2%)	36.7	39.0	127/302 (42.1%)	31.9	40.2	108/302 (35.7%)	29.7	41.2
No postop. tumor	FIGO (p=0.12)	20/82 (24.4%)	60.8	–[e]	32/82 (39.0%)	48.0	43.1	30/82 (36.6%)	62.5	–[e]
	GOG[d] (p=0.32)	18/72 (25.0%)	54.5	–[e]	33/72 (45.8%)	53.8	73.2	21/72 (29.2%)	62.0	–[e]
	Silver (p=0.27)	27/82 (32.9%)	47.3	40.7	33/82 (40.3%)	60.3	73.2	22/82 (26.8%)	58.5	–[e]
Serous	FIGO (p=0.62)	31/135 (23.0%)	31.6	35.9	67/135 (49.6%)	34.0	41.1	37/135 (27.4%)	35.9	45.6
	GOG (p=0.52)	30/135 (22.2%)	28.8	35.0	68/135 (50.4%)	35.1	41.1	37/135 (27.4%)	35.9	45.6
	Silver (p=0.97)	31/135 (23.0%)	37.6	35.9	72/135 (53.3%)	33.3	43.1	32/135 (23.7%)	32.6	35.4
Non serous	FIGO (p=0.28)	29/167 (17.4%)	42.8	38.6	47/167 (28.1%)	20.3	38.9	91/167 (54.5%)	32.7	45.2
	GOG[d] (p=0.97)	23/130 (17.7%)	34.8	38.6	43/130 (33.1%)	29.7	39.0	64/130 (49.2%)	30.9	45.5
	Silver (p=0.91)	36/167 (21.6%)	36.1	39.0	55/167 (32.9%)	29.6	39.1	76/167 (45.5%)	28.2	43.5

FIGO International Federation of Gynecology & Obstetrics, *GOG* Gynecologic Oncology Group, *Silver* grading system by Silverberg et al.

[a] Adjusted for FIGO stage (IIB–IIIA vs. IIIB–IV)

[b] Grouped grading data (G1 vs. G2–3)

[c] Stratification by therapy arm (cisplatin/paclitaxel vs. carboplatin/paclitaxel)

[d] Clear cell ovarian carcinomas are not graded by the GOG grading system; therefore, case numbers in this group are lower

[e] Median survival could not be calculated since <50% of patients were dead of disease at the time of analysis

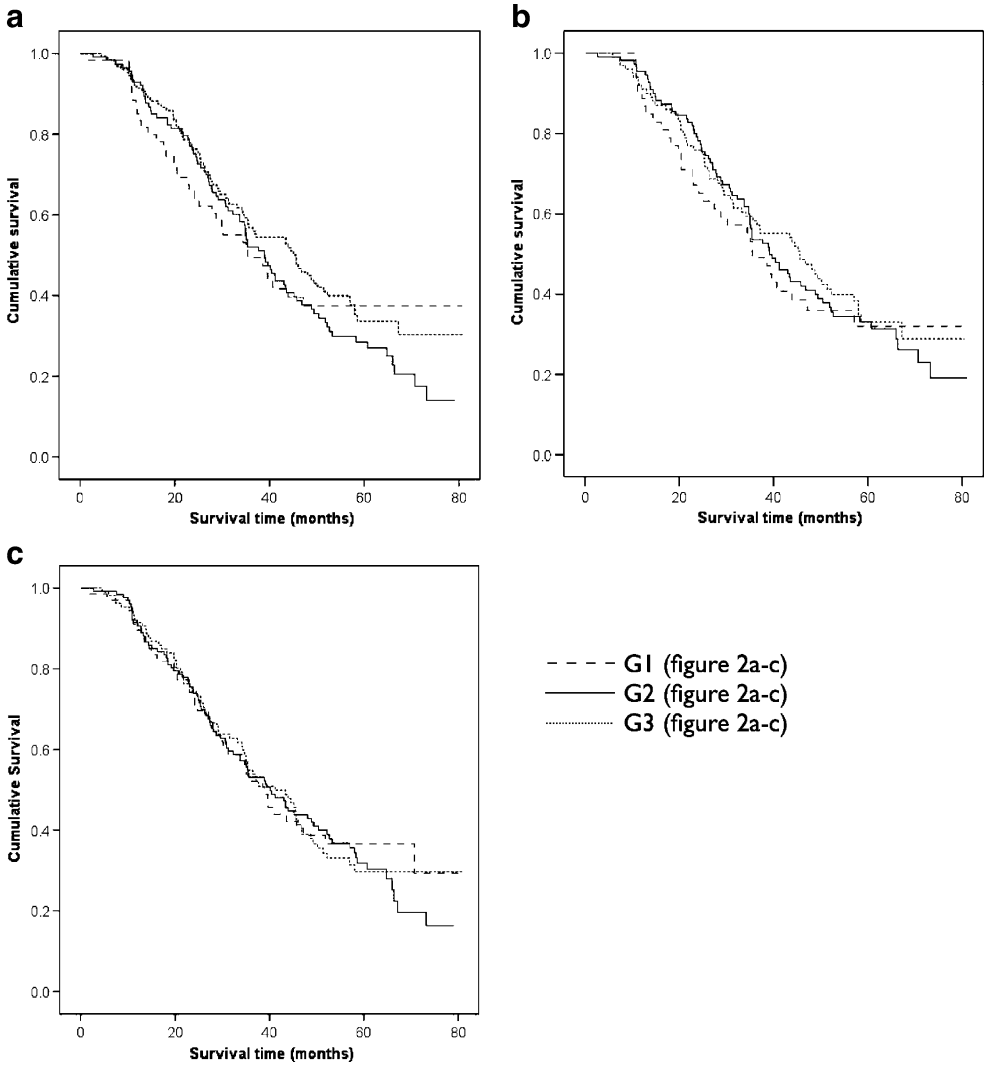

Fig. 2 Kaplan Meier survival estimates showed no prognostic significance after grading by **a** FIGO (p=0.38), **b** GOG (p=0.70), and **c** Silverberg grading system (p=0.92)

based bias was excluded by stratification by therapy arm. Survival analyses were adjusted for grouped grading data (G1 vs. G2-3) and FIGO stage (IIB–IIIa vs. IIIb–IV; Table 2).

There was a similar distribution of patient characteristics age, ECOG performance status, and postoperative residual tumor among all tumor grades irrespective of the grading system applied. Tumor grades determined by the FIGO grading system were significantly associated with tumor stage (p=0.039) and preoperative tumor size (p=0.017; Table 3). The same trend was shown by the GOG grading system for preoperative tumor size (p=0.013, data not shown). Tumor grades as defined by the Silverberg grading system showed no statistically significant associations with any of the above-mentioned patient or tumor characteristics.

Concordance rates between the three grading systems were as follows: FIGO/GOG 95.5% (κ=0.929), Silverberg/FIGO 69.9% (κ=0.553), Silverberg/GOG 66.8% (κ=0.481). Agreement in tumor grading by the same observer after 1 year varied between 80% and 100% (FIGO 100%, GOG 96.7%, Silverberg 80%). Interobserver reproducibility after grading by three independent investigators showed slightly lower agreement rates: FIGO 80%, GOG 80%, Silverberg 77.8% (Table 4).

Discussion

In this retrospective study, grading was of no prognostic significance in patients with advanced stage ovarian carcinomas after radical cytoreductive surgery and standardized chemotherapy with platinum and paclitaxel. Rather unexpectedly, a trend toward better survival in patients with high-grade carcinomas was observed. Our results may seem to contradict published studies in which histologic grade has been shown to be an important prognostic factor in advanced stage ovarian carcinoma [8, 9, 14–17, 27, 28].

Like in our present series (n=302), Ozols et al. (n=82) studied the correlation of histologic grade and survival in

Table 3 Patient characteristics in ovarian carcinomas graded by the FIGO grading system

Parameters		FIGO G1		FIGO G2		FIGO G3		Total		Chi-square test
		n	%	*n*	%	*n*	%	*n*	%	
Tumor postop	<1 cm	39	66.1	66	58.4	71	55.5	176	58.7	p=0.389
	>1 cm	20	33.9	47	41.6	57	44.5	124	41.3	
Tumor preop	<1 cm	16	27.1	11	10.1	21	16.7	48	16.3	p=0.017
	>1 cm	43	72.9	98	89.9	105	83.3	246	83.7	
Age	<65	46	76.7	88	77.2	85	66.4	219	72.5	p=0.124
	>65	14	23.3	26	22.8	43	33.6	83	27.5	
FIGO stage	IIb–IIIa	12	20.0	8	7.0	15	11.7	35	11.6	p=0.039
	IIIb–IV	48	80.0	106	93.0	113	88.3	267	88.4	
ECOG	0	27	45.0	48	42.1	58	45.3	133	44.0	p=0.869
	>0	33	55.0	66	57.9	70	54.7	169	56.0	

FIGO International Federation of Gynecology & Obstetrics, *ECOG* Eastern Cooperative Oncology Group

advanced stage ovarian carcinomas, but tumors of borderline malignancy (n=6) were also included in the study [27]. Since benign ovarian tumors and most borderline tumors usually do not significantly affect patient prognosis, it seems likely that the prognostic benefit of tumors with well-differentiated pattern grade in the latter study was influenced by the a priori better prognosis of borderline tumors; of note, no difference between grade 2 and 3 tumors was found in this series. Other authors reporting tumor differentiation grade to be of prognostic significance studied tumor series comprising ovarian carcinomas of all FIGO stages. Given the established prognostic significance of tumor grading in early stage ovarian carcinomas [3], it has to be taken into account that statistically significant results in a subgroup of tumors (early stage carcinomas) may influence significance of tumor grading in a series with both early and advanced stage tumors if the prognostic effect in that subgroup is strong enough. This statistical effect is exemplified in the subgroup of endometrioid carcinomas in a series of 461 epithelial ovarian cancers published by Shimizu et al. [8]. While grading was a significant prognosticator in FIGO stage I–II tumors (p=0.0042), the opposite was true for FIGO stage III–IV tumors (p=0.1148). Analysis of endometrioid carcinoma of all stages together resulted in a still significant impact of grading in endometrioid type of ovarian carcinoma irrespective of tumor stage (p<0.0001) [8]. Taking all these considerations together, we conclude from our findings that histopathologic tumor grading of ovarian carcinomas as well as the study of other biological parameters should be done separately for early and advanced stage disease.

From a clinical as well as biological point of view, early stage ovarian epithelial carcinoma may be a different entity as compared to advanced stage ovarian carcinoma. Early stage disease may start as a localized lesion, in many cases intracystic, among which only the less well-differentiated tumors may acquire the potential to spread leading to progressive disease. On the other hand, advanced stage ovarian carcinoma may represent a neoplasm with a potential for intraperitoneal spread from very early on, irrespective of histologic tumor grade. These clinical observations are reflected by a new model of ovarian tumorigenesis, which has been proposed recently and is based on morphology as well as molecular evidence [29]. In contrast to the established view assuming that ovarian carcinomas arise as lesions limited to the ovary then undergo progressive dedifferentiation associated with increasing intraperitoneal spread, the new model divides ovarian carcinomas into two different types of tumors. Type I tumors are slow-growing, indolent tumors that develop from precursor lesions in a stepwise fashion. In contrast, type II tumors are rapidly growing, aggressive tumors arising de novo. Current grading systems like the FIGO, GOG, or Silverberg grading systems imply a stepwise progression from a well to a poorly differentiated growth pattern. That concept obviously does no longer reflect the current understanding of the tumor biology of ovarian carcinoma [30].

Table 4 Intra-/ Interobserver agreement in histological grading of ovarian carcinomas

	Intraobserver	Interobserver
FIGO	100% (κ=1.000)	80% (κ=0.691)
GOG	96.67% (κ=0.953)	80% (κ=0.716)
Silverberg	80% (κ=0.692)	77.78% (κ=0.651)
Silverberg: nucleus	86.66% (κ=0.767)	66.55% (κ=0.381)
Silverberg: architecture	93.33% (κ=0.874)	82.22% (κ=0.690)
Silverberg: count of mitosis	76.66% (κ=0.624)	80% (κ=0.646)

Furthermore, according to current therapy guidelines, all advanced stage ovarian carcinomas are treated by combination chemotherapy. In a previously published study of the current tumor series, the authors have shown that high proliferative activity was significantly associated with better outcome [31]. In addition, there is a statistically significant correlation between high proliferative activity and high tumor grade. In the current study, a trend toward better survival of high-grade carcinomas was observed by grading with all three grading systems without reaching statistical significance. Median survival of G3 tumors as defined by FIGO and GOG grading was 45 months as compared to G1 carcinomas with only 35 months. If one assumes that G3 carcinomas may respond better to antiproliferative treatment because of their high proliferative activity, it is well conceivable that accurate chemotherapy may eliminate a potential prognostic disadvantage of chemonaive G3 cancers. Since postoperative chemotherapy is currently an integral part of treatment for patients with ovarian carcinoma, it must remain a matter of speculation if untreated high-grade ovarian carcinomas might indeed have a worse prognosis in comparison to others as the above assumption might imply.

In our study, the most complex system (Silverberg) proved to be the least reproducible. Among the parameters which have to be assessed in this grading system, assessment of the nuclear features, showing a kappa value of only 0.381, seemed to be extremely variable, highly dependent on the observers' individual judgment. While evaluation of mitotic activity and tumor growth pattern involves assessment of only one parameter, one of which can even be measured quantitatively, assessment of the cell nucleus comprises judgment of up to six parameters, which are measured subjectively to a much greater extent. This complexity may add up to a worse intra- and interobserver variability of nuclear grading. In view of the current findings in this homogeneously treated patient group and in consideration of the new model of ovarian carcinogenesis [29], it seems to be obvious that grading of advanced stage ovarian carcinomas by "conventional" grading systems can no longer be recommended for estimation of prognosis. New methods should be defined, which might provide meaningful prognostic information and could help to separate patients with high risk of tumor progression from others with low risk.

We suggest a switch from the traditional three-tier grading systems to a two-tier grading system of invasive ovarian carcinomas separating low-grade tumors from high-grade lesions only [7]. Superior reproducibility and prognostic value of the two-tier grading system have been reported [32]. The new two-tier system should ideally incorporate aspects of type-specific grading, which has recently been shown to be of importance in ovarian carcinomas [33].

Conflict of interest statement We declare that we have no conflict of interest.

References

1. Elston CW, Ellis IO (1991) Pathological prognostic factors in breast cancer. I. The value of histological grade in breast cancer: experience from a large study with long-term follow-up. Histopathology 19:403–410
2. Tavassoli FA, Devilee P (2003) Pathology and genetics of tumours of the breast and female genital organs. International Agency for Research on Cancer, Lyon
3. Vergote I, De Brabanter J, Fyles A et al (2001) Prognostic importance of degree of differentiation and cyst rupture in stage I invasive epithelial ovarian carcinoma. Lancet 357:176–182
4. Benda JA, Zaino R (1994) GOG pathology manual. Gynecologic Oncology Group, Buffalo, NY
5. Bichel P, Jakobsen A (1989) A new histologic grading index in ovarian carcinoma. Int J Gynecol Pathol 8:147–155
6. Classification and staging of malignant tumours in the female pelvis. (1971) Acta Obstet Gynecol Scand 50:1–7
7. Malpica A, Deavers MT, Lu K et al (2004) Grading ovarian serous carcinoma using a two-tier system. Am J Surg Pathol 28:496–504
8. Shimizu Y, Kamoi S, Amada S, Akiyama F, Silverberg SG (1998) Toward the development of a universal grading system for ovarian epithelial carcinoma: testing of a proposed system in a series of 461 patients with uniform treatment and follow-up. Cancer 82:893–901
9. Silverberg SG (2000) Histopathologic grading of ovarian carcinoma: a review and proposal. Int J Gynecol Pathol 19:7–15
10. Baak JP, Langley FA, Talerman A, Delemarre JF (1986) Interpathologist and intrapathologist disagreement in ovarian tumor grading and typing. Anal Quant Cytol Histol 8:354–357
11. Hernandez E, Bhagavan BS, Parmley TH, Rosenshein NB (1984) Interobserver variability in the interpretation of epithelial ovarian cancer. Gynecol Oncol 17:117–123
12. Lund B, Thomsen HK, Olsen J (1991) Reproducibility of histopathological evaluation in epithelial ovarian carcinoma. Clinical implications. APMIS 99:353–358
13. Singh N, Ayhan A, Menon U et al (2008) Grading of serous ovarian carcinoma: further evidence of a lack of agreement between conventional grading systems. Histopathology 52:393–395
14. Ishioka S, Sagae S, Sugimura M, Nishioka Y, Kobayashi K, Kudo R (2001) Clinical factors and biomarkers which affect a new universal grading system for ovarian epithelial carcinoma. J Obstet Gynaecol Res 27:313–318
15. Mayr D, Diebold J (2000) Grading of ovarian carcinomas. Int J Gynecol Pathol 19:348–353
16. Sato Y, Shimamoto T, Amada S, Asada Y, Hayashi T (2003) Prognostic value of histologic grading of ovarian carcinomas. Int J Gynecol Pathol 22:52–56
17. Ishioka S, Sagae S, Terasawa K et al (2003) Comparison of the usefulness between a new universal grading system for epithelial ovarian cancer and the FIGO grading system. Gynecol Oncol 89:447–452
18. du Bois A, Luck HJ, Meier W et al (2003) A randomized clinical trial of cisplatin/paclitaxel versus carboplatin/paclitaxel

as first-line treatment of ovarian cancer. J Natl Cancer Inst 95:1320–1329
19. Ordonez NG (2000) Transitional cell carcinomas of the ovary and bladder are immunophenotypically different. Histopathology 36:433–438
20. World Health Organisation International Classification of Tumours (1999) Histological typing of ovarian tumours, 2nd edn. Springer, Berlin
21. Young RH, Scully RE (1988) Urothelial and ovarian carcinomas of identical cell types: problems in interpretation. A report of three cases and review of the literature. . Int J Gynecol Pathol 7:197–211
22. Armitage P (1981) Statistical methods in medical research. Blackwell, New York
23. El K, Meier P (1958) Nonparametric estimation from incomplete observations. J Am Stat Assoc 53:458–481
24. Mantel N (1966) Evaluation of survival data and two new rank order statistics arising in its consideration. Cancer Chemother Rep 50:163–170
25. SPSS for Windows (2004) Rel 13.0.1. SPSS, Chicago
26. Landis JR, Koch GG (1977) The measurement of observer agreement for categorical data. Biometrics 33:159–174
27. Ozols RF, Garvin AJ, Costa J, Simon RM, Young RC (1980) Advanced ovarian cancer: correlation of histologic grade with response to therapy and survival. Cancer 45:572–581
28. Sorbe B, Frankendal B, Veress B (1982) Importance of histologic grading in the prognosis of epithelial ovarian carcinoma. Obstet Gynecol 59:576–582
29. Shih I, Kurman RJ (2004) Ovarian tumorigenesis: a proposed model based on morphological and molecular genetic analysis. Am J Pathol 164:1511–1518
30. Kurman RJ (2008) Surface epithelial neoplams of the ovary (short course). USCAP Annual Meeting. Denver, CO
31. Kommoss S, du Bois A, Schmidt D, Parwaresch R, Pfisterer J, Kommoss F (2006) Chemotherapy may be more effective in highly proliferative ovarian carcinomas—a translational research subprotocol of a prospective randomized phase III study (AGO-OVAR 3 protocol). Gynecol Oncol 103:67–71
32. Malpica A, Deavers MT, Tornos C et al (2007) Interobserver and intraobserver variability of a two-tier system for grading ovarian serous carcinoma. Am J Surg Pathol 31:1168–1174
33. Malpica A (2008) Grading of ovarian cancer: a histotype-specific approach. Int J Gynecol Pathol 27:175–181

Virchows Arch (2009) 454:257–261
DOI 10.1007/s00428-008-0723-5

ORIGINAL ARTICLE

Learning in the working place: the educational potential of a multihead microscope in pathology postgraduate training

Dominique Sandmeier · Fred Bosman · Maryse Fiche

Received: 14 July 2008 / Revised: 15 December 2008 / Accepted: 18 December 2008 / Published online: 14 January 2009

Abstract Training future pathologists is an important mission of many hospital anatomic pathology departments. Apprenticeship—a process in which learning and teaching tightly intertwine with daily work, is one of the main educational methods in use in postgraduate medical training. However, patient care, including pathological diagnosis, often comes first, diagnostic priorities prevailing over educational ones. Recognition of the unique educational opportunities is a prerequisite for enhancing the postgraduate learning experience. The aim of this paper is to draw attention of senior pathologists with a role as supervisor in postgraduate training on the potential educational value of a multihead microscope, a common setting in pathology departments. After reporting on an informal observation of senior and junior pathologists' meetings around the multihead microscope in our department, we review the literature on current theories of learning to provide support to the high potential educational value of these meetings for postgraduate training in pathology. We also draw from the literature on learner-centered teaching some recommendations to better support learning in this particular context. Finally, we propose clues for further studies and effective instruction during meetings around a multihead microscope.

D. Sandmeier · F. Bosman · M. Fiche
Institut Universitaire de Pathologie,
Centre Hospitalier Universitaire Vaudois (CHUV),
Université de Lausanne,
Lausanne, Switzerland

M. Fiche (✉)
Maryse Fiche Unité Pédagogique,
Faculté de Biologie et de Médecine,
Université de Lausanne,
Bugnon 21 1011 Lausanne, Switzerland
e-mail: maryse.fiche@chuv.ch

Keywords Pathology training · Postgraduate training · Microscope · Workplace learning · Apprenticeship · Socialization

Introduction

The quality of future pathologists training is paramount for quality of patient care. The competencies to be acquired include knowledge—a complex repertoire of images, concepts, and terminology, skills, and attitudes. Postgraduate training is part of the mission of hospital anatomic pathology departments. The educational approach in use in most programs includes, like for other medical specialties, "learning by doing," and specifically doing together with senior pathologists, an approach defined as *companionship.* As pointed out by Swanwick '(…) the bulk of learning is expected to take place at, through or from work' [1–3].

Though apprenticeship is highly valued as a method for various kinds of learning, the tight intrication of training and daily work in pathology departments may hamper an adequate recognition of the educational process embedded in diagnostic tasks [4]. Paying attention to quality of training in this context requires first to recognize educational opportunities and to understand how learning occurs and can be supported. A few reports have addressed this issue, so far, in the specific context of pathology postgraduate training [5, 6].

In our institution, the Lausanne University Pathology Institute, like in a multitude of similar institutes, a multihead microscope (MHM) is used for daily meetings to discuss and share problematic cases but also for other kinds of collaborative work involving also technicians, clinicians, and researchers [7]. This tool is used in complement of other practices, around individual or double-headed microscopes

and use of digital images on computers or projection screens. While observing pathologists' meetings around the MHM, numerous and an old tradition in our institution, we realized that this setting in which a small group of professionals with various levels of expertise, interactively discuss authentic cases, presented several of the characteristics of effective learning as defined in current medical education conceptions. This was the starting point of the observations and reflections presented in this paper. Our aim is to draw the attention of postgraduate training supervisors on the educational potential of the multihead microscope, which can be optimized once its educational potential is recognized.

Methods

Two authors (DS, MF) first shared the observations they had gathered as participants in meetings around the MHM at the Lausanne University Pathology Department, during, respectively, 15 and 6 years of daily attendance. This informal observation was pursued prospectively during one more year by one author (MF), with a focus on trainers and trainees' roles and interactions. The findings were confirmed by a third observer (FB), also a frequent attender of these meetings for more than 15 years. We then reviewed the literature on effective learning and teaching in order to explain why, and under which conditions, and requirements, the meetings around the MHM provide a high educational value for postgraduate pathology training.

The multihead microscope: a venue for learning and socialization

The MHM, for multihead microscope, is a central tool at the University Institute of Pathology of the Lausanne University, in Switzerland. A lot of people come around it, looking at microscopic preparations through its 13 appendiceal eyes which make it look like an octopus [Fig. 1]. All day long, different groups successively sit around the MHM, either for fixed appointments or for more spontaneous and informal ones [7]. From its permanent though silent and central position, the MHM witnesses the daily life of the Pathology Institute as a privileged observer of an important process going on in the institution: the perpetual renewal of newcomers and their progressive transformation into "old-timers" [4].

Four days a week, at 8:15 A.M., about 15 pathologists, senior, residents, and clerks, meet around the MHM for about 45 min—just like in a clinical morning round. Some junior or senior pathologists present current typical or challenging diagnostic cases from different subspecialty domains (gastrointestinal tract, pediatrics, soft tissues, and the like) to the whole medical staff. After a brief clinical history and a microscopic description, a differential diagnosis is exposed, and the clues for the diagnosis are debated. Most of the time, presented cases trigger questions, discussions, and different understandings are confronted. If present, a specialist of the domain will usually provide elements of evidence or new insights to clarify the debate, or someone will pick a textbook. Friday morning meetings are dedicated to reviewing systematically the frozen section diagnosis of the previous week, and two Thursday meetings per month to discussing ten challenging cases sent from one of the nine other institutes participating in the "Kansas" international seminar series initiated by Ivan Damjanov from Kansas City (Kansas, USA). Whatever the level of pathology knowledge, each participant can improve his diagnostic experience through these meetings. However, older voices are heard more often than younger ones. Some immediately venture a diagnosis, while others tend to seek opinions in asking questions. Many junior attendees are rather silent; though, they do come everyday and seem to appreciate these meetings.

The end of these morning meetings around the MHM offers a frequently used opportunity to make announcements and discuss domestic topics, organizational decisions, or various other issues. Resulting discussions

Fig. 1 Senior and junior pathologists working around the multihead microscope

represent an opportunity for socialization of trainees in all aspects of the life of a histopathology department.

Other types of meetings are also held on a regular basis. Weekly, one pathologist and two cytologists meet for 1 h to confront cytology and histology results for the same patients, for the purposes of the internal quality control process, often with the participation of one or more residents. Some diagnoses are revised, and the basis for revision is clarified. A common culture of learning from mistakes is progressively built. Once a week too, a formal teaching session for pathology trainees takes place. Within a program elaborated on a yearly basis by trainees and supervisors together, senior pathologists prepare, in turn, a set of didactic sections on a given theme. The residents try to elaborate a diagnosis before the meeting, using their prior knowledge as well as textbooks, articles, or established guidelines. Then, around the MHM and with the aid of faculty and peers, the cases are reviewed, diagnostic hypotheses and relevant ancillary techniques are debated.

Once a month, a clinicopathologic correlation meeting in general surgery is held around the MHM. Clinicians select difficult cases, while the responsible pathologist presents the related histopathology. These meetings aim at bringing light to the interpretation of the whole clinical history and emphasize the role pathology plays in clinical management. By joining around the microscope, clinicians and residents progressively understand the pitfalls and limitations of morphology, whereas a detailed clinical history helps the pathologist interpreting difficult lesions. The dialogue between clinicians and pathologists is enhanced, and the reciprocal trust grows. During these meetings too, the MHM observes different types of participation: older attendees tend to more often ask questions, raise objections, while younger participants are more silent. A similar clinicopathological meeting around patients' biopsies sections is also held weekly for renal transplants biopsies.

By these meetings, pathologists are repeatedly exposed to a variety of microscopic images presented in their clinical context, and to peer discussion in small groups and in an informal atmosphere, characteristics which meet several of the conditions for effective learning.

Learning around the MHM

What do trainees learn around the MHM?

As presenters, they will get experience in exposing a case in a clear and understandable voice and a logical sequence. They will read prior to the session to collect additional information on the disease they present. As nonpresenters, they will increase their repertoire of images and associated vocabulary. The set of competencies they will build through repeated attendance also includes professional skills like framing a diagnostic problem, reaching a consensus through peer discussion, searching information, acknowledging new data, or changing concepts. They will progressively acquire a relevant idea of areas of diagnostic uncertainty and of pitfalls and hopefully an attitude toward best diagnostic accuracy.

How does learning occur?

The MHM presents, as an educational tool and context, several characteristics expected, according to sociocognitive theories of learning, to support its efficiency for professional training.

First, learning around the MHM fulfils the conditions for *situated learning* in the meaning attributed to this term by Lave and Wenger in their work entitled "Situated learning and peripheral participation" [4]. Around the MHM, participants learn from real cases, discussed by physicians with the responsibility to reach a diagnosis and sign a report. Within Lave and Wenger's theory, this staff around the MHM represents a "community of practice" sharing common professional constraints, rules, and language. Included in this concept is *peripheral participation*: as in traditional forms of apprenticeship, newcomers first participate by observing the process—the type of cases shown, presenters' behaviors, how discussions are led [4]. Later on, as their knowledge and level of responsibility in the diagnostic workload grows, they progressively move to a more central participation, as presenters and active discussants. Learning under such conditions is considered as highly efficient [4].

The way residents learn around the MHM is expected to be efficient also according to the perspective of *cognitive psychology* [8–11]. Within cognitive psychology, learners actively build their knowledge, in a cumulative process, on the basis of what they already know. Memory is crucial to the process and divided into short-term and long-term parts, with limited and unlimited capacity, respectively [8–11]. The way knowledge is acquired and organized for storage in long-term memory is of highest importance for future recall and application. From this perspective, learning around the MHM offers at least three favorable conditions for efficient learning. First, and close to the concept of situated learning, knowledge is acquired in a relevant *context*, like current cases representative of future relevant professional problems. Thus, it is stored in the learner's memory in association with other pieces of the context, which enhances the chances of adequate retention and further recall in similar contexts. Second, *deliberation on knowledge*, as it takes place during discussions around images and concepts, is considered to favor deep learning, at higher levels [10]. This happens when, through questions

and comments, learners elucidate links between prior and new knowledge, and overcome partial or misunderstandings. *Deliberation on knowledge* contributes to the building of a robust basis of images, vocabulary, concepts, older and new insights, adequately structured around relevant problems, similar to the ones these trainees will face in their future practice. Finally, as demonstrated by sustained residents' attendance, trainees view meetings around the MHM as interesting moments that sustain their motivation, another essential element of efficient learning according to cognitive psychology [8–11].

Finally, and most importantly, the MHM is a venue for *reflective practice* and education of *reflective physicians*, according to the concept developed by Schön [12]. According to Schön, professional competence is a particular and complex type of knowledge which can be best developed through the process of *reflection*, including critical retrospective examination of one's practice, with its positive or negative outcomes, confrontation to some sort of reference framework, and peer discussion [12]. Around the MHM, trainees can observe how seniors model the skills and attitudes of reflection *in* and *on* action and thus learn an important dimension of professional practice. This process is especially at work during quality control sessions around the MHM, during which ancient cases are reviewed, sometimes in confrontation with further documentation such as additional specimen or clinical outcome.

Unique educational advantages of the multihead microscope
The multihead microscope allows trainees to learn from:
Broadened exposition to microscopic images with peer discussion
Accumulated experience in real-life daily cases
Active involvement in cases search and presentation
Observation of senior pathologists' practice in image analysis, diagnostic reasoning, and consensus building
Development of a reflective attitude and an awareness of pitfalls, risks of errors, and difficult diagnostic areas

Teachers around the MHM

What do senior pathologists do around the MHM?

They attend, present cases, or encourage residents to do so; some of them enrich the institution's caseload with their external consultation cases; they bring their experience and medical knowledge to the discussion, reorient a debate, redress misunderstandings and false diagnosis; by the manner they intervene in the discussion, they hopefully contribute to create a challenging and nonthreatening learning climate.

Is that teaching?

Though few senior physicians do consider that they teach in this context (personal observations), it is quite clear that they support residents' learning around the MHM, even in meetings which are not part of a structured instructional program. MHM meetings are generally viewed primarily as part of the *diagnostic* work and reaching the right diagnosis is a main concern for the group. Demonstration of content expertise, including image recognition, is the contribution expected from the more experienced participants in this perspective. On the basis of what we have described above, however, MHM sessions do also have an important *educational* potential, in line with the educational mission of pathology departments in academic hospitals within the *companionship* framework [1–4]. The common accomplishment, by trainees and supervisors, of daily tasks related to patient care represents the major teaching responsibility of pathology faculty, be it ill defined and insufficiently recognized, much more important than formal teaching sessions in terms of amount of time spent. The growing attention paid to the quality of postgraduate training should include recognition of the educational importance of physicians as postgraduate educators and the need for explicit training for and evaluation and rewarding of this role [13–15]. Recognizing potential learning and teaching moments within daily activities of a Pathology Institute, and fostering attitude and behavior for their optimal use is one of the challenges of companionship [1–3]. However, acknowledging MHM sessions as no longer diagnostic-only but also educational moments, certainly does not imply turning these sessions into lectures!

Improving teaching around the MHM

The following suggestions, derived from authors' informal observations as well as from the literature on effective learning and teaching in medical education, would have to be supported by further studies. We expect, however, that they could serve as a starting guide for faculty willing to improve their participation as educators around a MHM.

In a student-centered perspective, teachers should care about *what learners do* (16, 17). Trainees learn more and better when they are exposed to numerous cases, selected for their level of training, be they common—but archetypical, or more exceptional; when they actively engage in the diagnostic and bibliographic research, for a case in which they have a responsibility; when they take the opportunity to present a case and receive constructive feedback adapted to their level, in a nonthreatening climate and respectful manner [13, 18]. Trainees benefit from senior pathologists appropriately demonstrating well-structured, clinically rele-

vant and up-to-date pathology knowledge, as well as modeling rigorous and methodical reasoning, enthusiasm, curiosity, and constructive peer-discussion skills [13, 19]. Their knowledge basis is reinforced by interventions addressing the structure of knowledge, rather than the accumulation of isolated detailed facts, as well as those recalling important basic diagnostic processes, which they can re-use in their future practice. They benefit from seniors triggering a debate ("*why*?"), broadening the discussion, or closing it by a short synthesis in due time [13–16]. Teachers should also be aware of who they are and why they sit around the MHM.

Trainees get frustrated when discussions start from implicit diagnostic hypotheses, understood only by a few senior physicians, when the right diagnosis is given away without time for discussion. They do not necessarily learn from seniors exposing very specialized knowledge nor do they value inter-senior fights.

Teacher around the MHM

Dos	*Don'ts*
Provide cases	Neglect to come
Think of learners first	Forget novices in the audience
Select didactic cases	Go straight to the diagnosis
Respect the discovery process in novices	Jump into inter-experts discussion
Model explicit and systematic presentation	Assume everyone already knows
Encourage (and allow time for) reasoning	Forget the big picture
Favor structure, general rules	Overvalue details against the big picture
Ask or trigger relevant questions	Injure other participants
Reformulate and summarize difficult points	Despise not knowing (just not learning)
Care for the climate	
Be happy of everyone's learning	

Perspectives for further work

This paper presents an observation of the use of a MHM in a hospital pathology department, and a literature review supporting the analysis of its potential role as an educational format, with some resulting requirements for effective teaching in this context. In summary, the MHM is a venue for situated learning and reflective practice. Meetings around the MHM may represent fruitful learning and teaching moments within the context of apprenticeship, the dominant educational strategy for postgraduate pathology training. Clarifying the theoretical background of this approach is important to better understand, behind a traditional practice in the many institutions equipped with a MHM, an educational activity with specific requirements for effectiveness. Though knowledgeable senior pathologists are essential around the MHM, knowledge and seniority do not guarantee optimal educational approaches. These should be explicitly favored in managing MHM sessions. Further studies should address trainee perception of the actual contribution of meetings around the MHM to their training and explore how supervisors' effectiveness could be improved in this context.

Conflict of interest statement We declare that we have no conflict of interest.

References

1. Swanwick T (2005) Informal learning in postgraduate medical education: from cognitivism to 'culturism'. Med Educ 39: 859–865
2. Bleakley A (2002) Pre-registration house officers and ward based learning: a 'new apprenticeship' model. Med ed 36:9–15
3. Teunissen PW, Scheele F, Scherpbier AJ et al (2007) How residents learn: qualitative evidence for the pivotal role of clinical activities. Med Educ 41:763–770
4. Lave J, Wenger E (1991) Situated learning: Legitimate peripheral participation. Cambridge University Press, Cambridge, UK
5. West K (2005) Early training in Histopathology. Curr Diag Pathol 11:317–322
6. Syred KS (2005) Learning histopathology: a trainee's viewpoint. Current Diagnostic Pathology 11:323–328
7. Sandmeier D, Fiche M (2008) The educational benefits of a multihead microscope in an academic hospital. Med Teach 30:437–439
8. Shulman LS (1970) Cognitive learning and the educational process. J Med Educ 45:90–100
9. Shuell TJ (1986) Cognitive conceptions of learning. Rev Edu Res 56:411–436
10. Biggs JB (1991) Teaching for learning. The view from cognitive psychology. ACER, Victoria (Australia)
11. Regehr G, Norman GR (1996) Issues in cognitive psychology: implications for professional education. Acad Med 71:988–1001
12. Schön DA (1987) Educating the reflective practitioner: Toward a new design for teaching and learning in the professions. Jossey Bass, USA, San Francisco
13. Pratt DD, Arseneau R, Collins JB (2001) Reconsidering "good teaching" across the continuum of medical education. J Contin Educ Health Prof 21:70–81
14. Gordon J, Hazlett C, Cate OT et al (2000) Strategic planning in medical education: enhancing the learning environment for students in clinical settings. Med Educ 34:841–850
15. Kilminster S, Cottrell D, Grant J et al (2007) AMEE Guide N° 27: effective educational and clinical supervision. Med Teach 29:2–19
16. Mann KV (2001) Thinking about learning: implications for principle-based professional education. J Contin Educ Health Prof 21:90–96
17. Weimer M (2002) Learner-centered teaching. Five key changes to practice. Jossey-Bass San Francisco
18. Billet S (2002) Toward a workplace pedagogy: guidance, participation and engagement. Adult Educ Q 53:27–43
19. Kenny NP, Mann KV, MacLeod H (2003) Role modelling in physicians' professional formation: reconsidering an essential but untapped educational strategy. Acad Med 78:1203–1210

Virchows Arch (2009) 454:263–271
DOI 10.1007/s00428-008-0724-4

ORIGINAL ARTICLE

Immunohistochemical localization and mRNA expression of matrix Gla protein and fetuin-A in bone biopsies of hemodialysis patients

Giorgio Coen · Paola Ballanti · Giuliana Silvestrini · Daniela Mantella · Micaela Manni · Salvatore Di Giulio · Stefania Pisanò · Martina Leopizzi · Giuseppe Di Lullo · Ermanno Bonucci

Received: 31 October 2008 / Accepted: 21 December 2008 / Published online: 17 January 2009

Abstract Matrix Gla protein (MGP) and fetuin-A are inhibitors of arterial calcifications. In blood of rats, calcium–phosphate–fetuin–MGP complexes, produced in bone, have been identified. Indeed, an association between bone resorption, release of such complexes, and arterial calcifications has been reported. We have investigated the synthesis and localization of fetuin-A and MGP in bone of hemodialysis patients and the possible contribution of bone cells in arterial calcifications. Bone biopsies from 11 hemodialysis patients were used for histology, in situ hybridization of fetuin-A and MGP messenger RNA (mRNA), immunohistochemistry of fetuin-A, and total, carboxylated, and non-carboxylated MGP proteins. Patients showed various types of renal osteodystrophy, or normal bone. MGP was synthesized and expressed (total and carboxylated) by osteoblasts, osteocytes, and most osteoclasts, while fetuin-A by osteoblasts and osteocytes. Fetuin-A and carboxylated MGP proteins were positive in the calcified matrix, while total MGP was negative. Osteoid seams were negative to fetuin-A, lightly positive to carboxylated MGP, and occasionally positive to total MGP. Undercarboxylated MGP was mostly undetectable. In adult humans, fetuin-A is produced also by osteoblasts, and not only by hepatocytes, as previously believed. MGP, essentially carboxylated, is synthesized by osteoblasts and most osteoclasts. Increased bone turnover can be an important contributor to arterial calcifications.

Keywords Vascular calcification · Bone biopsy · Renal osteodystrophy · Matrix Gla protein · Fetuin-A

G. Coen (✉)
Nephrology and Hypertension Unit, Ospedale Israelitico,
Via Dandolo 75,
00153 Rome, Italy
e-mail: giorgio.coen@gmail.com

P. Ballanti · G. Silvestrini · S. Pisanò · M. Leopizzi · E. Bonucci
Department of Experimental Medicine,
Sapienza University of Rome,
Rome, Italy

D. Mantella · S. Di Giulio
Department of Nephrology, S. Camillo Hospital,
Rome, Italy

M. Manni
Department of Nephrology, S. Giovanni-Addolorata Hospital,
Rome, Italy

S. Pisanò · G. Di Lullo
Clinical Laboratory Unit, Ospedale Israelitico,
Rome, Italy

Introduction

Vascular calcifications are of frequent occurrence in uremic subjects, and it is assumed that they greatly contribute to the increased cardiovascular mortality both in conservative and hemodialysis (HD) stages of uremia [1, 2]. Several risk factors of vascular calcifications have been identified. Age and hemodialysis vintage are among the most important. Also serum calcium, phosphate, CaxP product [3], as well as the rates of hyperparathyroidism [4] and of bone turnover [5] are considered of great importance. In addition, inflammation and malnutrition may play a role, directly and/or through the reduction of fetuin-A, an important

calcium–phosphate solubilizing agent [6]. It has been shown that fetuin-A-deficient mice develop diffuse extraskeletal calcifications when administered a mineral and vitamin D-rich diet [7]. Cross-sectional analyses of patients with end-stage renal disease have shown that lower fetuin-A concentrations in serum are associated with more extensive vascular and heart valve calcifications, and with increased cardiovascular events and all-cause mortality in longitudinal studies [8]. Fetuin-A is known to be synthesized by the liver of adult humans, and it is found in high concentrations in serum and bone.

Another important protein capable of controlling extraskeletal calcifications in experimental animal models is the matrix Gla protein (MGP). MGP-deficient mice die in the first weeks of life due to extensive calcifications of the vascular tree, with consequent rigidity and rupture of the aorta [9]. MGP is a protein mainly found in bone, dentine, and cartilage, which contains five vitamin-K-dependent γ-carboxyglutamic acid (Gla) residues that confer it a high affinity for calcium and phosphate ions, and for hydroxyapatite crystals. The presence of Gla residues, therefore, is regarded as critical for the function of MGP, while undercarboxylated MGP, which may result from poor vitamin K status, is considered inactive [10, 11]. Therefore, fetuin-A and MGP can inhibit extraosseous and specifically arterial calcifications, as well as bone mineralization [2, 12].

However, the origin of these proteins is not entirely known. There are reasons to believe that the bone cells may give a contribution to the production of these substances. Biochemical studies have demonstrated that, in the serum of rats, fetuin and MGP form a complex with calcium and phosphate which maintains in solution these minerals, otherwise considered in a state of supersaturation, thus able to mineralize extraskeletal tissues [13]. This complex, very probably identical with the calciprotein particles detected by using electron microscopy and dynamic light scattering [14], is convincingly produced in the bone-remodeling compartment (BRC) [13]. In rats, however, the administration of bisphosphonates, inhibitors of osteoclast resorption, was found to prevent the arterial calcifications induced by warfarin or warfarin plus vitamin D, by reducing the release of the calcium–phosphate–fetuin–MGP complex from the BRC [10]. Further experimental studies have shown a direct association between increase of bone resorption, release of the calcium-phosphate–fetuin–MGP complex, and arterial calcifications [12]. Thus, the fetuin-A and MGP inhibition of extraosseous and, specifically, arterial calcifications is probably exerted locally in the soft tissues and can be somehow impaired in cases of high bone turnover and consequent increase of the mineral-containing complexes in the blood [2, 12].

The present study was carried out to evaluate the synthesis and localization of fetuin-A and MGP directly in bone tissue of uremic HD patients with a wide range of bone turnover by immunohistochemistry (IHC) and in situ hybridization (ISH). The total, carboxylated, and non-carboxylated forms of MGP were examined. The possible mechanism of how bone tissue, and specifically osteoclast resorption, could be implicated in the calcium–phosphate–fetuin–MGP complex formation is discussed.

Materials and methods

A total of 11 patients (seven men and four women; 49.45±12.26 years) with chronic renal failure in HD treatment were considered. Each patient underwent transiliac bone biopsy with a Bordier trocar following a double cycle of per os administration of tetracycline with 12 days interval. The biopsies were taken 4 to 5 days after the last dose administration. Biopsies were fixed in 4% paraformaldehyde in 0.1 M phosphate buffer at pH 7.2. They were then cut longitudinally into two halves with a razor blade and washed in buffer solution.

One half was dehydrated in acetone and processed for glycolmethacrylate embedding without decalcification. Sections, 1–2 μm thick, were stained with methylene blue-azure II for histology. Sections, about 5 μm thick, were prepared unstained for the analysis of tetracycline fluorescent labels under UV light. Other sections, about 3–4 μm thick, were stained with the aluminon method. Renal osteodystrophy was diagnosed on the basis of morphologic criteria [15, 16]. Moreover, histomorphometric descriptors were obtained in correspondence of the trabecular bone, by using an interactive color video-based image analysis system [15], and expressed in agreement with the American Society for Bone and Mineral Research [17]. The variable bone formation rate (BFR/BS, $\mu m^3/\mu m^2$/day; the volumetric amount of new mineralized bone per unit of trabecular bone surface per day) was considered for the evaluation of bone turnover [18]; mineralization was examined by osteoid volume (OV/BV, %; percent of trabecular bone volume consisting of osteoid), osteoid thickness (O.Th, μm; thickness of osteoid seams), and mineralization lag-time (Mlt, days; the mean time interval between deposition of osteoid matrix and its mineralization) results [19]; the volume of trabecular bone was given by the measure of bone volume (BV/TV, %; percent of whole trabecular bone volume occupied by calcified and uncalcified bone tissue). Then, the recently proposed turnover/mineralization/volume (TMV) classification system [16] was applied by considering the standard deviation scores (SDS) of the measured variables [20] in relation to our normal control values [15].

IHC and ISH

The other half of bone biopsy was decalcified in 10% disodium EDTA in 0.1 M phosphate buffer at pH 7.0 and processed for paraffin embedding. Serial sections (about 2 to 5 μm thick) were deparaffinized and treated for 10 min with 3% H_2O_2 in methanol.

Slides for IHC were washed for 20 min in phosphate-buffered saline (PBS) containing 0.1% Tween 20. For MGP detection, sections were incubated for 10 min in the blocking reagent of the Vectastain Universal Quick kit (Vector Laboratories, Inc; Burlingame, CA, USA). Serial sections were stained with monoclonal antibodies against total (amino acids 3–15; Biodesign International®, Saco, ME, USA; dilution 1:200), fully carboxylated (amino acids 35–54; ALEXIS® Biochemicals, Lausen, Switzerland; dilution 1:800), and non-carboxylated (amino acids 35–49; ALEXIS® Biochemicals, Lausen, Switzerland; dilution 1:250) MGP by overnight incubation at 4°C. Immunodetection with secondary biotinylated antibody and the streptavidin–peroxidase conjugate complex was performed by the Vectastain Universal Quick kit. The Liquid DAB+ Substrate Chromogen System (DakoCytomation, Inc.; Carpinteria, CA, USA) was then applied, followed by a counterstain with 1:15 diluted Mayer's hemalum solution.

For fetuin-A IHC, sections were treated with the Superblock reagent (Scytek Laboratories, Inc; Logan, UT, USA). Then, the goat anti-human fetuin-A/AHSG polyclonal antibody (R&D Systems, Inc; Minneapolis, MN, USA) was applied (1:500 dilution) for 1 h. Immunodetection was performed using the LSAB2 System-HRP kit (DakoCytomation, Inc., Carpinteria, CA, USA). The substrate-chromagen diaminobenzidine and counterstain with Mayer's hemalum were utilized, as already described for MGP IHC.

Negative controls were obtained by omitting the primary antibodies. Positive controls for MGP and fetuin-A were tested by using samples of arteries with atherosclerotic disease. Moreover, samples of fetal liver were tested for fetuin-A. For each antibody, the optimal working dilution was chosen after testing different concentrations.

For ISH, dewaxed sections were permeabilized for 15 min at 37°C with 75 μg/ml proteinase K (Sigma Chemical Co; St. Louis, MO, USA) and post-fixed in paraformaldehyde 4% in PBS-DEPC. The double FITC human MGP and the double FITC human fetuin-A HybriProbe™ kits provided by Biognostick® (Göttingen, Germany) were used in separate slides, respectively. The oligonucleotide sequences of MGP and fetuin-A HybriProbes were based on the NM_000900 and the NM_001622 GenBank Accession number, respectively. The specific probes were hybridized (1.5 μl HybriProbes in 25 μl HybriBuffer-ISH) overnight at 35°C. After washing in TRIS/HCl buffer at pH 7.55 containing 5% BSA and 0.1% Tween 20, immunodetection was performed with peroxidase anti-FITC goat antibody (whole molecule) diluted 1:750. Diaminobenzidine (Liquid DAB+) was used as chromogen. Sections were counterstained with 1:15 diluted Mayer's hemalum solution. Positive and negative control probes included in the HibriProbe kits were tested. Moreover, negative controls were achieved by omitting incubation with MGP or fetuin-A probes.

Results

The following diagnoses were assigned: four patients were affected by osteodystrophy with predominant hyperparathyroidism, showing a general increase in bone turnover, increased numbers of osteoclasts within wide Howship's lacunae, and many plump osteoblasts along numerous osteoid seams, together with areas of woven bone and endosteal fibrosis; three patients were affected by osteodystrophy with predominant osteomalacia, characterized by a decrease of bone turnover and a mineralization defect, in which the increased osteoid seams were mostly in contact with flat osteoblasts, while Howship's lacunae with osteoclasts were rarely found: two of these patients had fully developed osteomalacia, being all three osteoid indices (surface extent, volume, and thickness) increased, while one of them showed the so-called atypical osteomalacia, since osteoid seams were increased in surface and volume but not in thickness [19]; one patient was affected by mixed osteodystrophy, which includes signs of both hyperparathyroidism and osteomalacia; one patient had features of adynamic osteodystrophy, characterized by reduced bone turnover, thin osteoid seams almost completely lined by flat osteoblasts, and very few osteoclasts; two patients were free of pathologic bone lesions. The histomorphometric TMV classification of the patients is shown in Table 1. The aluminum staining was negative in all patients.

MGP

In all bioptical samples, the IHC for total MGP was negative in correspondence of the calcified bone matrix. Moreover, no staining was found in the osteoid seams, except for one case with advanced hyperparathyroidism and one with severe osteomalacia in which some occasional seams showed a lightly brownish staining. In all cases, some positive osteocytes were found. Immunolabeling consisted of brown aggregates inside the osteocyte cytoplasm. Positive cells were mainly found in correspondence and in proximity to the osteoid seams, or within the calcified matrix next to the quiescent endosteal surfaces. Less frequently, some positive osteocytes were found more

Table 1 Turnover/mineralization/volume (TMV) classification

Patient, sex/age (years)	Histopathologic diagnosis	Turnover	Mineralization				Volume
		Bone formation rate (BFR/BS, $\mu m^3/\mu m^2$/day)	Osteoid volume (OV/BV, %)	Osteoid thickness (O.Th, μm)	Mineralization lag-time (Mlt, days)	Mineralization	Bone volume (BV/TV, %)
M/32	Hyperparathyroidism	High	High	High	Normal	N-abnormal	Normal
M/40	Hyperparathyroidism	High	High	High	N-high	N-abnormal	N-high
F/48	Hyperparathyroidism	High	High	High	N-low	N-abnormal	High
F/49	Hyperparathyroidism	High	High	N-high	Normal	N-abnormal	High
M/47	Osteomalacia	N/A	High	High	N/A	Abnormal	N/A
F/58	Osteomalacia	Low	High	High	High	Abnormal	N-high
M/39	Atypical osteomalacia	Low	High	Normal	High	N-abnormal	Low
M/41	Mixed osteodystrophy	N-high	High	High	High	Abnormal	High
F/71	Adynamic osteodystrophy	Low	Normal	N-high	High	N-abnormal	Normal
M/50	Without pathologic alteration	Normal	Normal	Normal	N-low	Normal	Normal
M/69	Without pathologic alteration	Normal	Normal	Normal	N-low	Normal	Normal

High, >2 SDS from mean; Low, <2 SDS from mean; N-high, 1–2 SDS above mean; N-low, 1–2 SDS below mean
N-abnormal mildly abnormal, *N/A* not available

inside the calcified matrix. In adjacent sections, the ISH messenger RNA (mRNA) labeling was mainly localized in the cytoplasm of some osteocytes, with a similar pattern of distribution (Fig. 1).

Apart from the case with adynamic bone disease, in which plump osteoblasts could not be found, these cells resulted positive to the IHC reaction both along the trabeculae and in correspondence of cortical bone, and independently of the type of bone alteration. These same cells were intensely stained by ISH for mRNA (Fig. 1).

Cells of endosteal fibrosis, which could be detected in the bone biopsies of patients with high turnover bone disease (hyperparathyroidism and mixed type of renal osteodystrophy), were positive to both IHC and ISH reactions (Fig. 1).

Multinucleated osteoclasts could not be detected in one case with severe osteomalacia. In all the other cases, most of these cells were variably positive to total MGP IHC in trabecular and cortical bone; however, some negative osteoclasts were found, with no apparent difference in frequency between the types of bone alterations. In agreement with these findings, osteoclasts showed either variably diffused ISH mRNA labeling in the cytoplasm or no signal at all (Fig. 2).

In all samples, the results described above for total MGP IHC coincided with those found by the antibody specifically recognizing the carboxylated form of the protein, in osteocytes, osteoblasts, osteoclasts, and cells of endosteal fibrosis (Fig. 3). For both types of IHC reaction, cell positivity was clearly visible although the antibody concentrations for total MGP and for carboxylated MGP were 5 and 3.2 times lower than those suggested in the respective product data sheet. In contrast to total MGP, in all cases, a

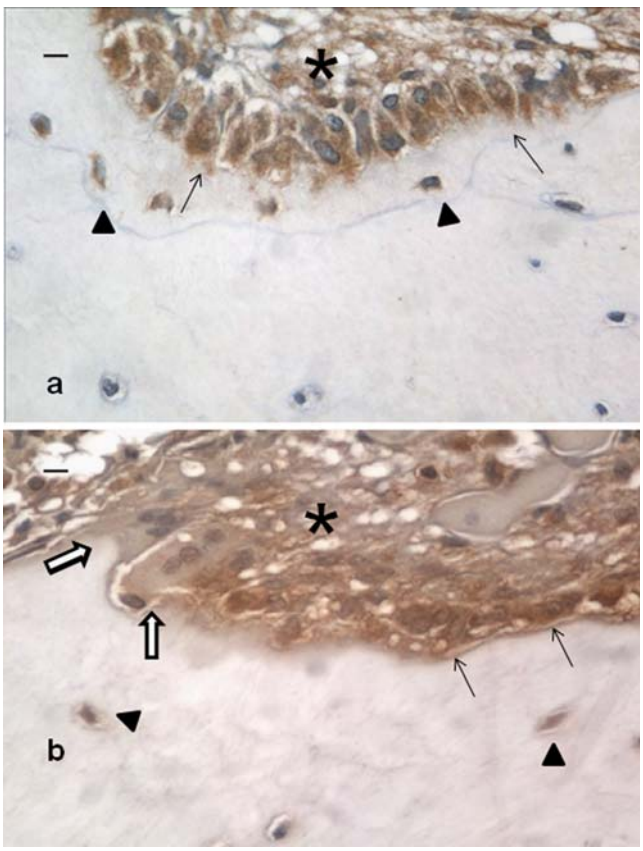

Fig. 1 Total MGP: **a** osteoblasts (*arrows*), endosteal fibrosis cells (*asterisk*), and some young osteocytes (*arrowheads*) are positive to IHC; **b** osteoblasts (*arrows*), endosteal fibrosis cells (*asterisk*), and some osteocytes (*arrowheads*) are positive to ISH, while two osteoclasts (*empty arrows*) are negative. Trabecular bone, hyperparathyroidism. Bars=10 μm

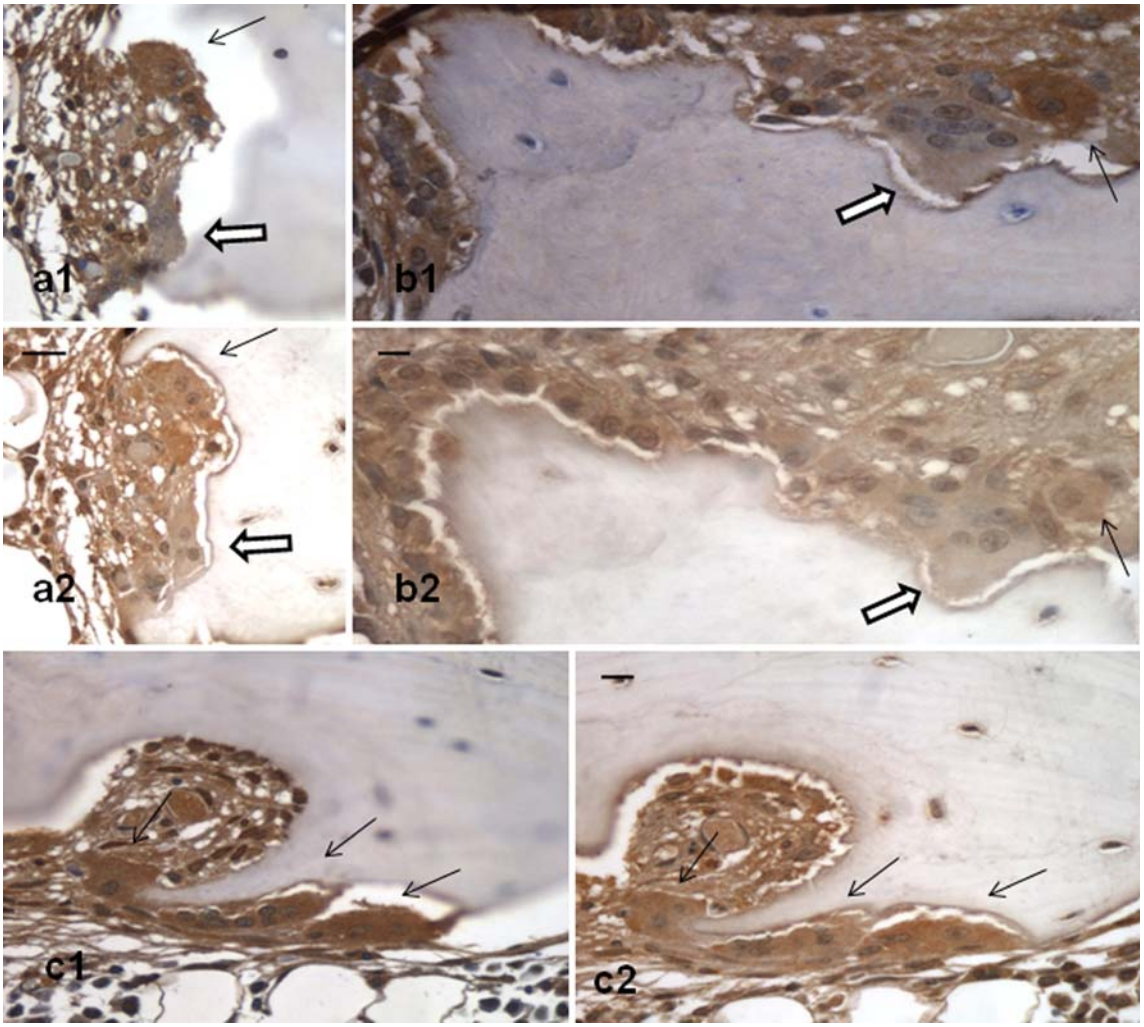

Fig. 2 Total MGP: (*a1*, *b1*, and *c1*) negative (*empty arrows*) and/or positive (*arrows*) osteoclasts to IHC are visible; (*a2*, *b2*, and *c2*) sections adjacent to *a1*, *b1*, and *c1*, respectively: the same osteoclasts positive to IHC in *a1*, *b1*, and *c1* are also positive to ISH (*arrow*). Trabecular bone, hyperparathyroidism. Bars=10 μm

light and diffuse carboxylated MGP immunostaining was found in the calcified bone matrix and in most osteoid seams, although the staining intensity in the latter was very faint (Fig. 3).

In some cases, independent of the type of bone condition, some of the flat, lining cells which border the quiescent bone surfaces were positive to the IHC reaction for total and carboxylated MGP, as well as to the ISH reaction for MGP mRNA. However, because their cytoplasm is characteristically reduced to a very thin rim, the recognition of the labeling of these cells was generally difficult.

Undercarboxylated MGP IHC, performed by using exactly the antibody concentration indicated by the product data sheet, was practically negative in all bioptical samples. Only a very weak immunostaining was present in the osteoid and/or calcified bone matrix of a minority of patients, without any reference to the types of bone lesions. In these cases, rare osteocytes, osteoblasts, and/or osteoclasts were very lightly stained.

Fetuin-A

The antibody dilution used for fetuin-A IHC was optimized at a concentration which was 10 times lower than the lower limit of the working dilution suggested by the data sheet. In both cortical and trabecular bone of all cases, the IHC reaction was strongly positive in correspondence of the calcified bone matrix. In contrast, the osteoid seams were not stained. Some positive osteocytes were found in all cases within the calcified bone matrix. Sometimes, positive osteocytes were also present in correspondence of the osteoid seams, mainly next to plump osteoblasts (Fig. 4). In agreement with these findings, ISH showed a positive signal within some osteocytes localized in both the calcified matrix and in the osteoid (Fig. 5).

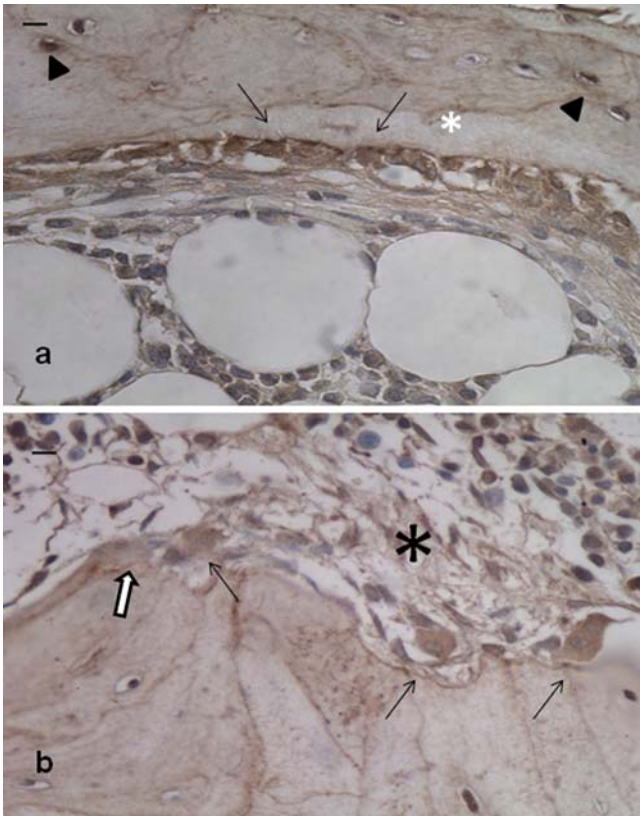

Fig. 3 Carboxylated MGP, IHC: **a** osteoblasts (*arrows*) and some osteocytes (*arrowheads*) are positive, the osteoid seam is barely stained (*white asterisk*); **b** one almost negative (*empty arrow*) and three positive (*arrows*) osteoclasts, together with positive endosteal fibrosis cells (*asterisk*) within the Howship's lacuna, are visible. In both **a** and **b**, a diffuse positivity of calcified bone matrix is present. Trabecular bone, hyperparathyroidism. Bars=10 μm

In all samples, with the only exception of the case with adynamic osteodystrophy in which active osteoblasts were not found, most of the plump osteoblasts were lightly or intensely stained by the fetuin-A IHC reaction (Fig. 4). Such IHC positivity was confirmed by ISH reactivity (Fig. 5). No differences were found between trabecular and cortical bone.

In bone samples characterized by increased turnover, cells of endosteal fibrosis were positive to both IHC and ISH reactions. Osteoclasts, in all cases in which these cells were found, were negative to both IHC and ISH (Figs. 4 and 5).

In a few cases, some endosteal lining cells appeared immunohistochemically positive and showed a ISH signal. However, as described for MGP, the reaction products of both IHC and ISH in these cells were sometimes hard to be detected due to their very thin cytoplasm.

Discussion

All patients but two were affected by the wide spectrum of bone cells and matrix alterations, ranging from high to low bone turnover diseases, which are proper of renal osteodystrophy [18].

For MGP IHC, antibodies against total, fully carboxylated, and non-carboxylated proteins were tested, to evaluate the carboxylation status of MGP. For each of the three forms of MGP, the amino acid sequences recognized by the respective monoclonal antibodies corresponded exactly to those of a recent study performed in human arteries [11]. In the vascular wall, the inhibition of γ-carboxylation of Glu residues yielded the undercarboxylation of MGP and the subsequent calcification of the tunica media [10]. Moreover, it has been shown in the bone tissue of transgenic mice, which produced two distinct mutated forms of MGP in osteoblasts, that the Gla residues are required for MGP antimineralization function [21].

In all patients, the calcified bone matrix was almost completely negative to the antibody directed against the total MGP. This result is similar to that obtained by Spronk et al. [22] in human fetal bone, by using two monoclonal antibodies, against the N- and C-terminus of MGP. In contrast, Carlson et al. [23] reported slight positive IHC staining for total MGP in widely scattered areas of calcified matrix in vertebrae of monkeys. Such variation in immuno-

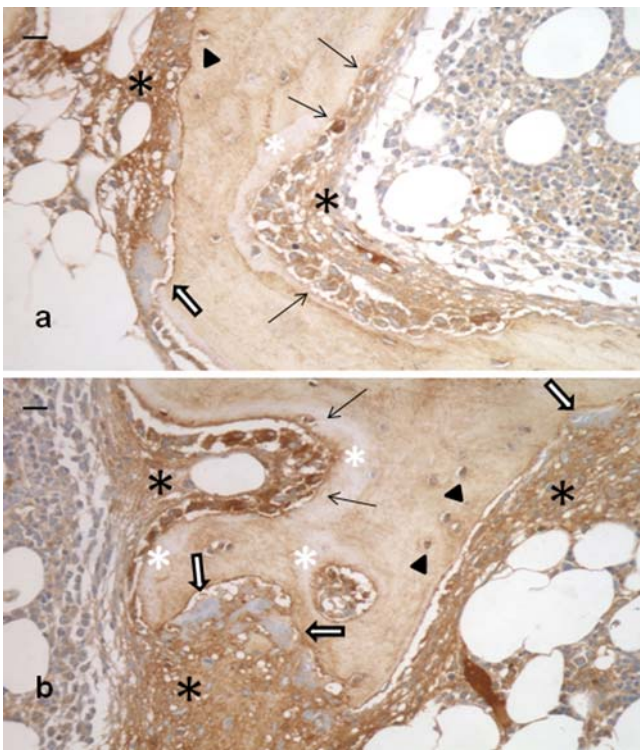

Fig. 4 Fetuin-A, IHC: **a** osteoblasts with variable intensity of positivity are present (*arrows*); **b** osteoblasts are highly positive (*arrows*). In both **a** and **b**, endosteal fibrosis cells (*asterisks*) and some osteocytes (*arrowheads*) are positive, while osteoclasts are negative (*empty arrows*); a clear positivity of calcified bone matrix is visible, while the osteoid seams are negative (*white asterisks*). Trabecular bone, hyperparathyroidism. Bars=20 μm

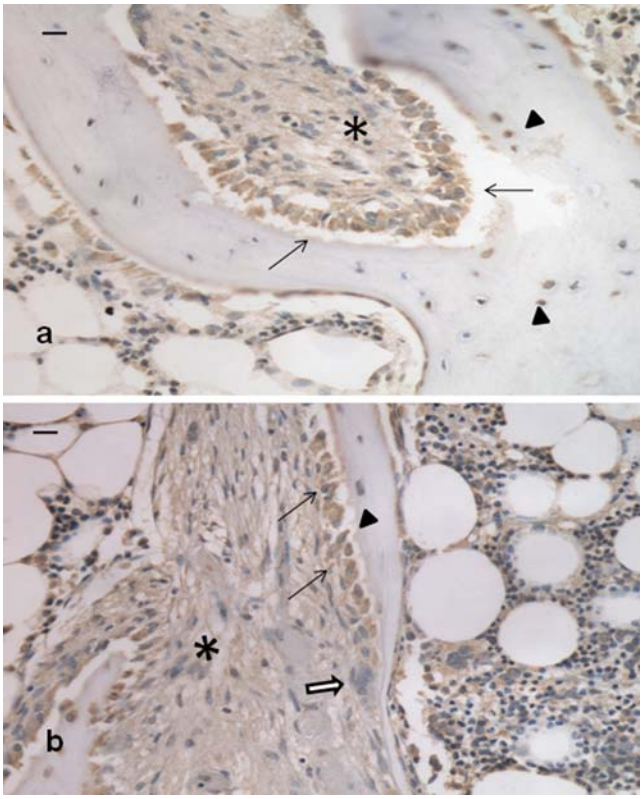

Fig. 5 Fetuin-A, ISH: **a**, **b** Osteoblasts (*arrows*) and some osteocytes (*arrowheads*) and endosteal fibrosis cells (*asterisks*) are positive. In **b**, a negative osteoclast is present (*empty arrow*). Trabecular bone, hyperparathyroidism. Bars=20 μm

reactivity might be due to the different animal species or, most probably, to differences in the sequences recognized by the various monoclonal antibodies. In any case, the calcified matrix in all bone biopsies of the present study was lightly and diffusely immunostained for carboxylated MGP.

Among bioptical samples, only some occasional osteoid seams were immunostained for total MGP in one case with hyperparathyroidism and one with osteomalacia. In human fetal bone, Spronk et al. [22] reported a weak total MGP signal that was associated with the extracellular matrix at sites of non-calcified bone. Moreover, Carlson et al. [23] found some areas of osteoid seams positive to total MGP. These authors suggested that the presence of MGP within the osteoid tissue might have a role in preventing its premature mineralization. In the present study, in contrast to total MGP, a very faint positivity to carboxylated MGP was found in most osteoid seams in all types of bone conditions.

In all bone biopsies, osteoblasts were invariably positive to total MGP. Some IHC positive osteoblasts were also found by Carlson et al. [23]. In our samples, these cells were also positive to the carboxylated form of MGP. Moreover, they expressed the MGP gene. This result appears especially significant on the basis of the contradictory reports available in the literature. Using ISH, Hirakawa et al. [24] could not detect MGP mRNA in rat osteoblasts, although the authors were aware that it had been detected in osteoblastic cell culture. Luo et al. [25] also did not find MGP mRNA by ISH in mouse osteoblasts; they hypothesized, therefore, that, like fetuin-A, the protein could accumulate in bone through blood circulation. In biopsies of human fracture callus, the signal for MGP mRNA was only found in osteoblasts of the woven bone in non-unions, and not in osteoblasts of the old bone [26].

In our bioptical samples, not only osteoblasts, but also some osteocytes, especially those that appeared to be the youngest, were positive to total MGP IHC. This is in contrast with the results of Carlson et al. [23] who found negative osteocytes. However, in our experience, osteocytes were also positive to the carboxylated form of MGP and expressed MGP mRNA. These results are in line with the osteoblastic origin of the osteocytes. Also the findings that some endosteal lining cells are immunostained for the total and carboxylated MGP protein and express the corresponding mRNA are in agreement with the origin of the lining cells from the osteoblasts. Similarly, the observation that the cells of endosteal fibrosis that accumulate in bone marrow in cases of hyperparathyroidism are positive to both total and carboxylated MGP and express the corresponding mRNA might depend on the fact that these cells are probably osteoblast precursors, secondary to parathormone-stimulated proliferation of bone marrow stromal cells [27].

The present study has shown that most osteoclasts are immunostained for total MGP in any type of bone condition, a result in agreement with the findings of Carlson et al. [23]. In our experience, the same cells are immunostained for the carboxylated MGP, too, and ISH has shown that they express the corresponding mRNA.

Undercarboxylated MGP immunostaining was almost negative in all bioptical samples, although some very light positivity was found in a minority of cases in calcified or uncalcified bone matrix and in bone cells. This indicates that the MGP protein present in bone, where calcification is a physiological event, is predominantly in its active form, and demonstrates that, at least locally, there is not a significant vitamin K deficiency. Interestingly, in the intima of atherosclerotic arteries and in Mönckeberg's sclerosis of the media, where pathological calcifications of different etiologies occur, undercarboxylated MGP was almost exclusively localized in sites of calcification, while total and carboxylated MGP were mostly found in the non-calcified areas of the tunica media [11].

The IHC localization of fetuin-A in the mineralized areas of bone matrix has been already described in normal adult humans [28] and other mammals [29, 30]. Our results show that the protein is highly represented in mineralized matrix of normal bone of uremic patients, as well as in any form of renal osteodystrophy, independent of the rate of bone

turnover and of the type (lamellar or woven) of bone structure. Osteoid seams were invariably negative: in this respect, no comparative data could be found in the literature.

It is a general opinion, ensued from old findings [28, 31] and confirmed by relatively recent studies [32, 33], that fetuin-A is synthesized in the liver and is incorporated, via the bloodstream, into the bone matrix during the mineralization process, as a result of its high affinity for hydroxyapatite [2, 12, 34, 35]. In the present study, most osteoblasts were immunostained for fetuin-A in all types of renal osteodystrophy, as well as in normal bone. Our IHC and ISH findings demonstrate that human osteoblasts do have fetuin-A in the cytoplasm and synthesize it. To our knowledge, these results were not previously described in humans, although some IHC positivity of the rat counterpart of human fetuin-A had been found in osteoblasts of adult rats [29]. Moreover, in a very recent paper, some fetuin-A uptake by osteoblast-like cells was reported [36].

On the basis of our results, the localization of fetuin-A in the mineralized bone matrix appears to be due to an active osteoblast participation, rather than to a mere accumulation of the protein from the blood. The previously reported osteoblast negative results could be probably explained, at least in part, by hypothesizing that the degree of synthesis of fetuin-A in bone of adult humans could be much lower than that in the liver, as it was found in mouse osteoblastic cells [37] and for the rat counterpart of the protein [38].

With reference to fetuin-A, no previous papers dealing with osteocytes in humans have been found. Our results show that some osteocytes are both IHC and ISH positive. Similarly, the IHC positivity of the rat counterpart of human fetuin-A was described in osteocytes of adult rats [29]. As commented above for MGP, these findings, as well as the positivity to both reactions in some endosteal lining cells and cells of endosteal fibrosis in hyperparathyroidism are in agreement with the osteoblastic relationship of these cells.

In vitro experiments have suggested that fetuin-A, and its rat counterpart, might stimulate bone resorption [39, 40]. Moreover, it has been hypothesized that osteoclasts may clear the calciprotein particles by phagocytosis [14], thus mediating the recycling of extracellular calcium and phosphate from basic calcium phosphate. However, in our study, osteoclasts were negative to both fetuin-A IHC and ISH, so that no information could be drawn on fetuin-A involvement in bone resorption.

In conclusion, we have examined, for the first time, the localization and the synthesis of fetuin-A and MGP, directly in the bone tissue of patients with chronic renal failure in HD treatment. In contrast with the general opinion that, in adult humans, the fetuin-A is synthesized in the liver, transported via the bloodstream to bone, and incorporated in the calcified matrix, we have shown that it is produced by osteoblasts, too. It is possible that the bone synthesis of the protein can contribute to the formation within the BRC of the calcium–phosphate–fetuin–MGP complex described in rats by Price et al. [13]. The MGP protein, synthesized by osteoblasts and accumulated in bone, is essentially of carboxylated type, thus in its active form. Also, osteoclasts synthesize MGP, which is contained in these cells in the carboxylated form. This new finding suggests that these cells, other than osteoblasts, can be an important source of the calcium–phosphate–fetuin–MGP complexes. In agreement with the findings in rats [12], these results point to the increased bone turnover and specifically to the osteoclastic resorption as important factors which can promote extraskeletal and arterial calcifications in uremia. However, further studies are necessary to confirm whether the calcium–phosphate–fetuin–MGP complexes, detected under some circumstances in rats, are also present in humans, and particularly in uremic patients with artery and soft tissue calcifications [12].

Conflict of interest statement The authors declare that they have no conflict of interest.

References

1. Foley RN, Parfrey PS, Sarnak MJ (1998) Epidemiology of cardiovascular disease in chronic renal disease. J Am Soc Nephrol 9(Suppl 12):S16–S23
2. Moe SM, Reslerova M, Ketteler M et al (2005) Role of calcification inhibitors in the pathogenesis of vascular calcification in chronic kidney disease (CKD). Kidney Int 67:2295–2304
3. Coen G, Manni M, Agnoli A et al (2006) Cardiac calcifications: fetuin-A and other risk factors in hemodialysis patients. ASAIO J 52:150–156
4. Ganesh SK, Stack AG, Levin NW et al (2001) Association of elevated serum PO_4, Ca × PO_4 product, and parathyroid hormone with cardiac mortality risk in chronic hemodialysis patients. J Am Soc Nephrol 12:2131–2138
5. London GM, Marty C, Marchais SJ et al (2004) Arterial calcifications and bone histomorphometry in end-stage renal disease. J Am Soc Nephrol 15:1943–1951
6. Wang AY, Woo J, Lam CW et al (2005) Associations of serum fetuin-A with malnutrition, inflammation, atherosclerosis and valvular calcification syndrome and outcome in peritoneal dialysis patients. Nephrol Dial Transplant 20:1676–1685
7. Schäfer C, Heiss A, Schwarz A et al (2003) The serum protein α_2-Heremans-Schmid glycoprotein/fetuin-A is a systemically acting inhibitor of ectopic calcification. J Clin Invest 112:357–366
8. Hermans MM, Brandenburg V, Ketteler M et al (2007) Association of serum fetuin-A levels with mortality in dialysis patients. Kidney Int 72:202–207

9. Luo G, Ducy P, McKee MD et al (1997) Spontaneous calcification of arteries and cartilage in mice lacking matrix GLA protein. Nature 386:78–81
10. Price PA, Faus SA, Williamson MK (2001) Bisphosphonates alendronate and ibandronate inhibit artery calcification at doses comparable to those that inhibit bone resorption. Arterioscler Thromb Vasc Biol 21:817–824
11. Schurgers LJ, Teunissen KJF, Knapen MHJ et al (2005) Novel conformation-specific antibodies against matrix γ-carboxyglutamic acid (Gla) protein—undercarboxylated matrix Gla protein as marker for vascular calcification. Arterioscler Thromb Vasc Biol 25:1629–1633
12. Price PA, Williamson MK, Nguyen TM et al (2004) Serum levels of the fetuin-mineral complex correlate with artery calcification in the rat. J Biol Chem 279:1594–1600
13. Price PA, Caputo JM, Williamson MK (2002) Bone origin of the serum complex of calcium, phosphate, fetuin, and matrix Gla protein: biochemical evidence for the cancellous bone-remodeling compartment. J Bone Miner Res 17:1171–1179
14. Heiss A, DuChesne A, Denecke B et al (2003) Structural basis of calcification inhibition by α_2-HS glycoprotein/fetuin-A. Formation of colloidal calciprotein particles. J Biol Chem 278:13333–13341
15. Coen G, Ballanti P, Bonucci E et al (1998) Bone markers in the diagnosis of low turnover osteodystrophy in haemodialysis patients. Nephrol Dial Transplant 13:2294–2302
16. Moe S, Drüeke T, Cunningham J et al (2006) Definition, evaluation, and classification of renal osteodystrophy: a position statement from Kidney Disease: Improving Global Outcomes (KDIGO). Kidney Int 69:1945–1953
17. Parfitt AM, Drezner MK, Glorieux FH et al (1987) Bone histomorphometry: standardization of nomenclature, symbols, and units. J Bone Miner Res 2:595–610
18. Ballanti P, Coen G, Mazzaferro S et al (2001) Histomorphometric assessment of bone turnover in uraemic patients: comparison between activation frequency and bone formation rate. Histopathology 38:571–583
19. Parfitt AM (2003) Renal bone disease: a new conceptual framework for the interpretation of bone histomorphometry. Curr Opin Nephrol Hypertens 12:387–403
20. Waller S, Shroff R, Freemont AJ et al (2008) Bone histomorphometry in children prior to commencing renal replacement therapy. Pediatr Nephrol 23:1523–1529
21. Murshed M, Schinke T, McKee MD et al (2004) Extracellular matrix mineralization is regulated locally; different roles of two Gla-containing proteins. J Cell Biol 165:625–630
22. Spronk HMH, Soute BAM, Schurgers LJ et al (2001) Matrix Gla protein accumulates at the border of regions of calcification and normal tissue in the media of the arterial vessel wall. Biochem Biophys Res Commun 289:485–490
23. Carlson CS, Tulli HM, Jayo MJ et al (1993) Immunolocalization of noncollagenous bone matrix proteins in lumbar vertebrae from intact and surgically menopausal cynomolgus monkeys. J Bone Miner Res 8:71–81
24. Hirakawa K, Hirota S, Ikeda T et al (1994) Localization of the mRNA for bone matrix proteins during fracture healing as determined by in situ hybridization. J Bone Miner Res 9:1551–1557
25. Luo G, D'Souza R, Houge D et al (1995) The matrix Gla protein is a marker of the chondrogenesis cell lineage during mouse development. J Bone Miner Res 10:325–334
26. Lawton DM, Andrew JG, Marsh DR et al (1999) Expression of the gene encoding the matrix Gla protein by mature osteoblasts in human fracture non-unions. J Clin Pathol: Mol Pathol 52:92–96
27. Bianco P, Bonucci E (1991) Endosteal surfaces of hyperparathyroidism: an enzyme cytochemical study on low-temperature-processed, glicol-methacrylate-embedded bone biopsies. Virchows Archiv A Pathol Anat 419:425–431
28. Dickson IR, Poole AR, Veis A (1975) Localization of plasma α_2HS-glycoprotein in mineralizing human bone. Nature 256:430–432
29. Ohnishi T, Arakaki N, Nakamura O et al (1991) Purification, characterization, and studies on biosynthesis of a 59-kDa bone sialic acid-containing protein (BSP) from rat mandible using a monoclonal antibody. J Biol Chem 266:14636–14645
30. Zweras M, Liu D, Partridge EA et al (2002) α_2-HS glycoprotein/fetuin, a transforming growth factor-β/bone morphogenetic protein antagonist, regulates postnatal bone growth and remodeling. J Biol Chem 277:19991–19997
31. Triffitt JT, Gebauer U, Ashton BA et al (1976) Origin of plasma α_2HS-glycoprotein and its accumulation in bone. Nature 262:226–227
32. Yang F, Schwartz Z, Swain LD et al (1991) α_2HS-glycoprotein: expression in chondrocytes and augmentation of alkaline phosphatase and phospholipase A_2 activity. Bone 12:7–15
33. Schinke T, Amendt C, Trindl A et al (1996) The serum protein α_2-HS glycoprotein/fetuin inhibits apatite formation in vitro and in mineralizing calvaria cells. J Biol Chem 271:20789–20796
34. Ketteler M, Wanner C, Metzger T et al (2003) Deficiencies of calcium-regulatory proteins in dialysis patients: a novel concept of cardiovascular calcification in uremia. Kidney Int 63(suppl. 84): S84–S87
35. Kazama JJ, Gejyo F, Ei I (2005) The immunohistochemical localization of α_2-Heremans-Schmid glycoprotein/fetuin-A (AHSG). Nephrol Dial Transplant 20:851–852
36. Chen NX, O'Neill KD, Chen X et al (2007) Fetuin-A uptake in bovine vascular smooth muscle cells (BVSMC) is calcium dependent and mediated by annexins. Am J Physiol Renal Physiol 292:F599–F606
37. Xie J, Baumann MJ, McCabe LR (2005) Adsorption of serum fetuin to hydroxylapatite does not contribute to osteoblast phenotype modifications. J Biomed Mater Res 73A:39–47
38. Ohnishi T, Nakamura O, Ozawa M et al (1993) Molecular cloning and sequence analysis of cDNA for a 59 kD bone sialoprotein of the rat: demonstration that it is a counterpart of human α_2-HS glycoprotein and bovine fetuin. J Bone Miner Res 8:367–377
39. Colclasure GC, Lloid WS, Lamkin M et al (1988) Human serum α_2HS-glycoprotein modulates in vitro bone resorption. J Clin Endocrinol Metab 66:187–192
40. Nakamura O, Kazi JA, Ohnishi T et al (1999) Effect of rat fetuin on stimulation of bone resorption in the presence of parathyroid hormone. Biosci Biotechnol Biochem 63:1383–1391

Virchows Arch (2009) 454:273–281
DOI 10.1007/s00428-009-0727-9

ORIGINAL ARTICLE

Adenosine receptors in COPD and asymptomatic smokers: effects of smoking cessation

Mieke Versluis · Nick ten Hacken · Dirkje Postma · Begona Barroso · Bea Rutgers · Marie Geerlings · Brigitte Willemse · Wim Timens · Machteld Hylkema

Received: 27 August 2008 / Revised: 5 December 2008 / Accepted: 5 January 2009 / Published online: 23 January 2009

Abstract Our group has shown that 1-year smoking cessation persisted or increased airway inflammation in chronic obstructive pulmonary disease (COPD). We compared adenosine and adenosine receptor (AR) expression in COPD and asymptomatic smokers (AS) before and after 1-year smoking cessation. Sputum cytospins and bronchial biopsies of (ex)smoking COPD patients and AS were studied for A_1R, $A_{2A}R$, $A_{2B}R$, and A_3R expression. Adenosine and inflammatory mediators were measured in sputum supernatants. At baseline, COPD patients had lower levels of adenosine and higher levels of vascular endothelial growth factor in sputum than AS. Smoking cessation induced significantly different effects in COPD than in AS, i.e. an increase in percentages of A_3R expressing neutrophils and A_1R expressing macrophages in COPD as increase in adenosine and monocyte chemoattractant protein-1 levels in sputum. Adenosine-related effector mechanisms may contribute to the persistence and progression of airway inflammation in COPD following 1-year smoking cessation.

M. Versluis · B. Rutgers · M. Geerlings · B. Willemse · W. Timens · M. Hylkema (✉)
Department of Pathology,
University Medical Center Groningen, University of Groningen,
P.O. Box 30.001, 9700 RB Groningen, The Netherlands
e-mail: m.n.hylkema@path.umcg.nl

M. Versluis · N. ten Hacken · D. Postma · B. Willemse
Department of Pulmonary Diseases,
University Medical Center Groningen, University of Groningen,
P.O. Box 30.001, 9700 RB Groningen, The Netherlands

B. Barroso
Department of Analytical Biochemistry,
University Center for Pharmacy, University of Groningen,
Antonie Deusinglaan 1,
9713 GZ Groningen, The Netherlands

Keywords Adenosine · Adenosine receptors · COPD · Smoking cessation

Introduction

Chronic obstructive pulmonary disease (COPD) is a disease caused mainly by smoking and it is characterized by chronic airflow limitation and a range of pathological changes in the lung [1]. It is known that smoking cessation stops the accelerated lung function decline present in COPD [2, 3]. We found that smoking cessation improves both direct (methacholine) and indirect (adenosine 5′-monophosphate, AMP) airway hyperresponsiveness (AHR) after 1-year smoking cessation [4]. Interestingly, improvement of AHR was not associated with changes in lung function or sputum inflammation. Our previous paper showed that COPD patients who successfully ceased smoking for 1-year, overall airway inflammation persisted in bronchial biopsies, while the number of neutrophils, lymphocytes, interleukin (IL)-8, and eosinophil-cationic-protein levels significantly increased in sputum. In addition, no significant changes in vascular adhesion molecules (i.e. P-selectin, E-selectin, intercellular antigen-1 (ICAM-1) or vascular cell adhesion molecule (VCAM)) were found with smoking cessation in COPD patients also suggesting an ongoing inflammatory process in the airways. In asymptomatic smokers who successfully quitted smoking, some inflammatory markers (e.g. sputum macrophages, eosinophils, and IL-8) significantly decreased while others did not change [5]. This indicates that factors other than inflammatory cells or measured mediators likely induced the observed improvement in AHR.

Adenosine has been suggested to play a role in COPD [6]. Patients with COPD are significantly more responsive

to AMP than healthy smoking volunteers [7, 8] and smokers have significantly increased concentrations of adenosine in the airway lining fluid [9]. Recently, a first report on the presence of adenosine receptors in lung parenchyma showed an enhanced density and decreased affinity of the adenosine receptors in subjects with COPD compared with control smokers [10]. Adenosine is a purine nucleoside that is released during tissue hypoxia and inflammation. It has both pro- and anti-inflammatory features, which are mediated by four different G-protein-coupled receptors, A_1 (G_i coupled), A_{2A} (G_s coupled), A_{2B} (G_s and G_{q11} coupled), and A_3 (G_s and G_{q11} coupled). Activation of adenosine receptors (AR) can have different effects, depending on the type of G protein that is involved and the cell type [6]. Activation of G_i-protein-coupled receptors decreases adenylyl cyclase activity and cAMP levels whereas activation of G_s coupled receptors increases cAMP levels [11]. With respect to the cell types involved, activation of A_1R on neutrophils promotes adherence to endothelial cells and chemotaxis, indicating a pro-inflammatory response [12], whereas activation of A_1R on cells from the monocytes/macrophage lineage inhibits the production of several pro-inflammatory cytokines (TNF, IL-8, and IL-6) and enhances the release of the anti-inflammatory cytokine IL-10, displaying an anti-inflammatory response [13, 14]. Therefore, each receptor can be either beneficially and/or detrimentally implicated in the inflammatory process of COPD.

In this study, our primary aim was to investigate whether adenosine-related effector mechanisms could be involved in the persistence and/or progression of the inflammatory response in COPD following 1-year smoking cessation. Therefore, adenosine content and receptor expression in sputum (macrophages and neutrophils) and bronchial biopsies of smokers with COPD and asymptomatic smokers were measured, both before and after 1-year smoking cessation. Since activation of adenosine receptors can influence the secretion of mediators from inflammatory cells, we related changes in adenosine and its receptors with changes in growth factors (VEGF) and chemokines (monocyte chemoattractant protein (MCP)-1) related to remodeling and inflammation that may underlie lung function loss in COPD.

Materials and methods

Subjects

Bronchial biopsy and sputum material of 11 COPD and 15 asymptomatic smoking subjects who successfully stopped smoking for at least 1 year from the study of Willemse et al. were studied (patient characteristics; Table 1) [5, 4, 15]. In short, the main important inclusion and exclusion criteria for both groups were: COPD (according to the American Thoracic Society (ATS)/ European Respiratory Society (ERS) guidelines [16]): forced expiratory volume $(FEV)_1$/ forced vital capacity post-bronchodilator <0.7, and chronic respiratory symptoms for at least 3 months for two successive years. Asymptomatic smokers: $FEV_1 \geq 85\%$, predicted, and no chronic respiratory symptoms or airway obstruction. Participants in both groups were between 45 and 65 years of age, had >10 packyears smoking, smoked ≥10 cigarettes/day, had reversibility to salbutamol <9% of the predicted FEV_1, did not use inhaled or oral corticosteroids in the previous 6 months, had no signs of atopy, and no respiratory tract infections 1 month prior to the study. During the study, COPD patients only used $beta_2$-agonists or ipratropium on a regular basis; inhaled corticosteroids were not used. Only in case of an exacerbation, a short course of oral corticosteroids was allowed. Before each measurement, subjects were asked not to use long- or short-acting β_2-agonists and/or ipratropium at least 12 h before the test. They did not suffer from a respiratory tract infection nor used oral corticosteroids in the month prior to any of the measurements.

The local medical ethics committee of our University Medical Center Groningen approved the study protocol and all subjects gave their written informed consent.

Study design and smoking cessation program

The study design and smoking cessation program have been described previously [5]. Sputum cells and supernatant as well as bronchial biopsies were only used if present both before and after 1-year smoking cessation.

Bronchoscopy and biopsy processing

Bronchial biopsies were taken from the subcarinae of the right, middle, or lower lobe and processed as described previously [17]. For immunostaining, sections (one per patient) were dried and fixed in acetone for 10 min and washed with phosphate-buffered saline (PBS). The following polyclonal antibodies were used: rabbit anti-rat adenosine A_1 receptor, rabbit anti-canine adenosine A_{2A} receptor, rabbit anti-human adenosine A_{2B} receptor (all from Alpha Diagnostic International, San Antonio, TX, USA), and rabbit anti-human adenosine A_3 receptor (Santa Cruz Biotechnology, Santa Cruz, CA, USA). Antibodies directed against adenosine A_1 and A_{2A} receptors cross-reacted with human A_1R and $A_{2a}R$. The secondary antibody used was goat anti-rabbit biotin conjugated (SBA, Birmingham, AL, USA) and the tertiary antibody StreptABComplex peroxidase conjugated (DAKO, Glostrup, Denmark). As chromogen, 3-amino-9-ethyl-carbazol substrate was used; tissue was counterstained with Mayers' Hematoxylin.

Table 1 Patient characteristics

	COPD		Asymptomatic smokers	
	Baseline	1-year SC	Baseline	1-year SC
Subjects, *n*	11		15	
Age, years	57 (46–63)		50 (45–57)*	
Sex (male/female)	7/4		7/8	
Packyears smoking	30 (15–66)		23 (13–32)*	
Cigarettes, *n*/day	20 (10–40)		20 (12–30)	
FEV_1 post BD, % pred	75.6 (44.4–100.4)	78.1 (49.4–106)**	109.6 (95.5–134.1)*	110.0 (90.0–133.1)
FEV_1/VC post BD, %	58.1 (30.1–69.5)	57.5 (36.8–76.2)	78.8 (71.8–88.7)*	79.7 (68.9–92.3)
PC_{20} Mch, mg/ml	1.02 (0.25–78.4)	13.4 (0.13–78.4)**	33.4 (4.3–78.4)*	78.4 (1.8–78.4)
PC_{20} AMP, mg/ml	46.2 (4.5–640)	640 (1.04–640)**	640 (73.9–640)*	640 (20–640)***

Data are presented as median (range)
1-year SC 1-year of smoking cessation, *FEV_1* forced expiratory volume in one second, *VC* vital capacity, *post BD* after 400 μg bronchodilator (salbutamol), *% pred* percentage of predicted value, *Mch* Methacholine, *AMP* adenosine 5′-monophospate
*$p<0.05$ vs. COPD; **$p<0.05$ vs. baseline; ***$p<0.05$ change in COPD versus change in asymptomatic smokers (delta's)

Intensity of adenosine receptor expression in biopsies were scored in a blinded way (all by the same observer) with a semiquantitative three-point scale, with sections scored as negative, positive, or strongly positive. In addition, the total number of positive single cells in the biopsy was counted. Since not all biopsies presented all tissue structures scored, numbers presented can vary between graphs.

Sputum induction and processing

Sputum was induced by inhalation of hypertonic saline and processed as described previously [18]. Sputum samples consisting for >80% of squamous cells were excluded from analysis. Cytospins were dried and fixed in acetone for 10 min and washed with PBS for immunostaining. The same antibodies and chromogen substrate were used as described in the biopsy staining. Three hundred neutrophilic granulocytes and 300 macrophages were counted in every cytospin and scored as negative or positive; the percentage of cells expressing adenosine receptors was calculated. Due to the small numbers of lymphocytes present in sputum, we could not reliably quantify adenosine receptor expression on this cell type.

Measurement of adenosine in sputum supernatant using HPLC

Adenosine was measured using a Waters 2690 Alliance Separation Module HPLC system (Waters, Milford, MA, USA) coupled on-line to a Finnigan TSQ Quantum Triple Quadruple Mass Spectrometer (Finnigan Thermo Fisher Scientific, Waltham, MA, USA). Chromatographic separation was performed with a C18, 3 μm, Atlantis column (Waters) 2.1 mm I.D.×100 mm length using a gradient of mobile phase A (ammonium acetate 20 mM, pH 7.0, in water) and B (ammonium acetate 20 mM, pH 7.0, in acetonitrile) at 0.2 mL/min flow rate. Before measurements samples were pre-treated as follows: 100 μl of sputum supernatant was acidified with 20 μl of HCl 120 mM, then 200 μl of chloroform was added to precipitate proteins and eliminate lipids. After vortexing and subsequent centrifugation, 80 μl of the aqueous supernatant was transferred to a glass injection vial and 5 μl of this solution was injected into the high-performance liquid chromatography (HPLC)-mass spectrometry (MS) system. MS detection was performed using ESI ionization in positive ion mode. Multiple-reaction monitoring mode was used to increase the sensitivity. Adenosine was quantified using the transition m/z 260>m/z 136 corresponding to the loss of the ribofuranose ring. Samples were measured in a randomized way, twice independently at two different days. Results were in good agreement within a maximum of 10% variation. The calibration line consisted of eight points in the range of 5 to 1,000 ng/ml adenosine in a mixture of PBS and water (pretreated in the same way as the study samples). Adenosine levels are presented as concentrations.

Chemokine and growth factor measurement in sputum supernatant using multiplex ELISA

Sputum supernatant contents (sensitivity level) of monocyte chemoattractant protein (MCP)-1 (10 pg/ml), "regulated upon activation of normal T cell expressed and secreted" (RANTES, 15 pg/ml), tumor necrosis factor (TNF, 10 pg/ml), epidermal growth factor (EGF, 15 pg/ml), fibroblast growth factor (FGF)-basic (also known as FGF2, 15 pg/ml), vascular endothelial growth factor (VEGF, 15 pg/ml), and platelet-derived growth factor (PDGF)-BB (<10 pg/ml) were measured using a human custom multiplex antibody bead

kit from Biosource International (Camarillo, CA, USA). Standard solutions were diluted with sputolysin reagent (Calbiochem®, Darmstadt, Germany) to copy the effect of it on sputum content during processing.

Statistical analysis

Statistics were performed using a Wilcoxon signed-rank test to assess differences between both measurements within the groups and a non-parametric Mann–Whitney *U* test to assess differences between both groups at baseline. A value of $p<0.05$ was considered significant. Correlations between parameters were investigated using a Pearson's Rho test. For some patients material at one time point was missing due to insufficient quality of the sample. At baseline the single measurements were used for baseline differences between both groups, but they were excluded from the paired test to obtain differences within the groups.

Results

Adenosine receptor expression in bronchial biopsies

The adenosine receptors A_{2A}, A_{2B}, and A_3 were expressed by airway epithelial, endothelial, and smooth muscle cells in airway wall biopsies and by cells (morphologically macrophages) in the submucosa in both COPD and asymptomatic smokers (Fig. 1). In contrast, the A_1 receptor was only expressed on a small number of cells (morphologically macrophages) in the tissue surrounding the airways. The pattern of expression of the four ARs was not different between COPD patients and their controls.

The intensity of AR expression (scored semiquantitatively with immunohistochemistry) is presented in Fig. 2. There was no significant difference in AR expression between both groups at baseline. The A_{2A} receptor expression on airway smooth muscle decreased significantly after 1-year smoking cessation ($p=0.025$) in asymptomatic smokers, but not in COPD. A_1R, A_{2B}R, and A_3R expression did not change with smoking cessation in both groups. In addition, no differences were found in the number of cells staining positive for all four ARs between the different groups. Total biopsy areas were similar for high and low numbers of positive cells.

Adenosine receptor expression by sputum cells

In sputum, all four ARs were expressed by neutrophils and macrophages of both COPD and asymptomatic smokers. There was no difference in AR expression between both groups at baseline. The percentage of A_3R positive neutrophils increased significantly in COPD patients after 1-year smoking cessation when compared to baseline ($p=0.038$). This change in A_3R expression was significantly different from the change occurring in asymptomatic smokers ($p=0.050$, Fig. 3a). No changes were detected in percentages of neutrophils expressing A_1R, A_{2A}R, and A_{2B}R. In COPD patients, the percentage of A_1R positive macrophages increased after 1-year smoking cessation when compared to baseline ($p=0.017$, Fig. 3b), an effect that was not observed in asymptomatic smokers. Smoking cessation had no effect on expression of the other ARs on macrophages. No significant differences were found in percentage expression of all ARs on macrophages between COPD and asymptomatic smokers.

Adenosine, growth factors, and cytokine levels in sputum supernatant

Adenosine levels in sputum supernatant were significantly lower in COPD at baseline ($p=0.017$, Fig. 4a) than in asymptomatic smokers, whereas VEGF levels were higher ($p=0.020$, Fig. 4b). In addition, the change in adenosine levels with smoking cessation was significantly different in COPD and asymptomatic smokers ($p=0.023$), as was the change in MCP-1 ($p=0.013$) (Fig. 4). No differences were detected in RANTES and other growth factors involved in tissue repair (EGF and PDGF-BB) (Fig. 4). Levels of FGF-b and TNF were below the sensitivity level and therefore not analyzed statistically.

Discussion

We investigated the effect of smoking cessation on adenosine content and adenosine receptor expression in sputum and biopsies taken from COPD patients and asymptomatic smokers. Our most important observations were that COPD patients responded significantly different to smoking cessation than asymptomatic smokers with respect to sputum adenosine content, MCP-1 levels, and percentage of neutrophils expressing A_3R and macrophages expressing A_1R. This resulted in an increased adenosine content (trend) and increased percentage of A_3R positive neutrophils and A_1R positive macrophages in sputum of COPD patients. In addition, smokers with COPD have a lower level of adenosine and a higher level of VEGF in sputum than asymptomatic smokers.

Previous observations in these patients have elucidated that smoking cessation improved AHR, whereas inflammation persisted or even increased in sputum of COPD patients [4, 5]. Since adenosine is implicated in the development and persistence of inflammation, we investigated in the current study whether the observed increase in (aspects of) inflammation in COPD could be explained by

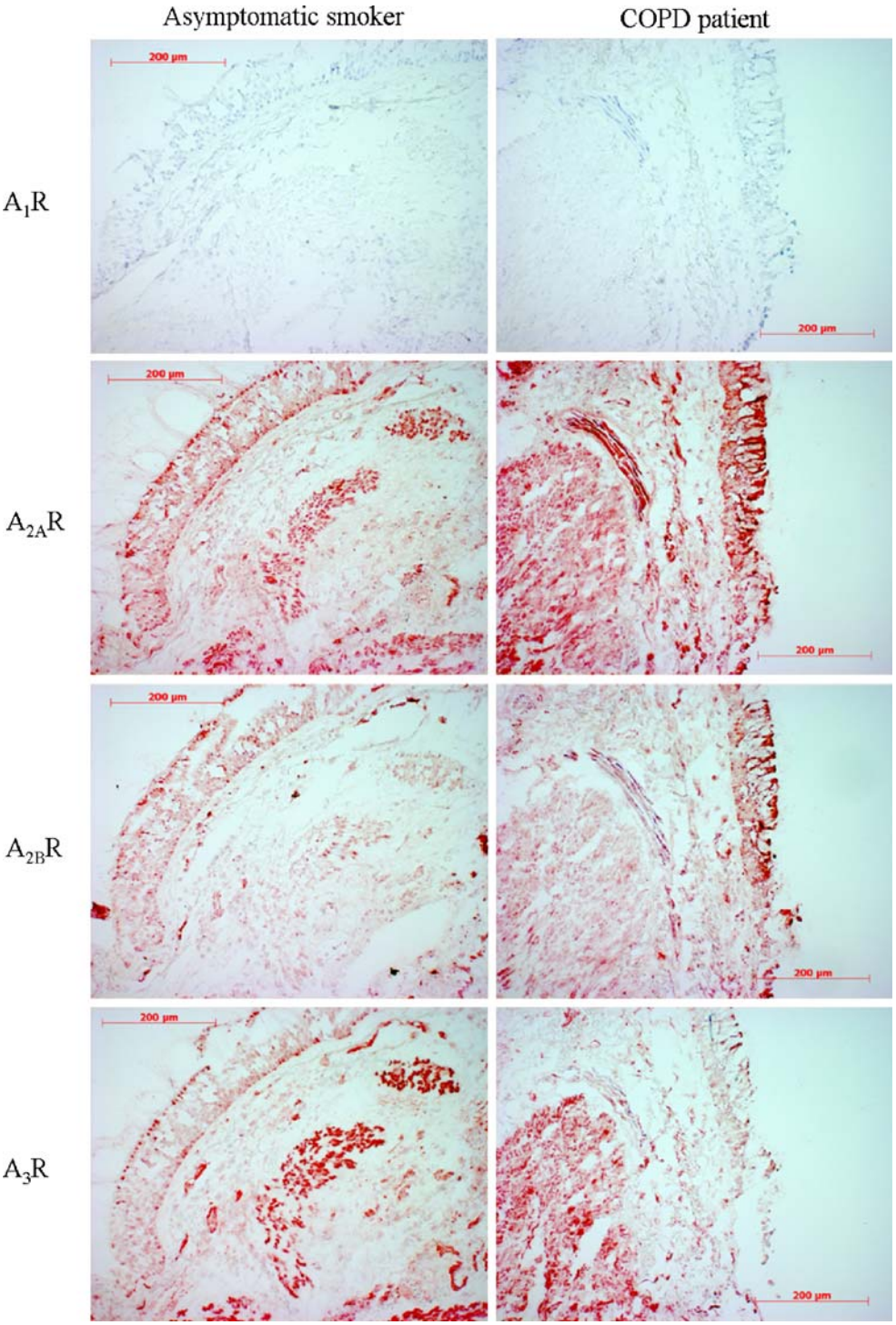

Fig. 1 Adenosine receptor expression on bronchial biopsies from smoking asymptomatic (*left panel*) and COPD (*right panel*) subjects

the presence of adenosine and the expression of adenosine receptors as measured in two different compartments of the airways, i.e. sputum and bronchial biopsies.

We confirmed the pattern of ARs expression that was recently described by Varani et al. [10]. Thus, the $A_{2A}R$ and A_3R were expressed on bronchial epithelium, smooth muscle cells, endothelial cells, and infiltrating cells (mostly macrophages), whereas A_1R was only expressed by a few cells (morphologically macrophages). For $A_{2B}R$, Varani and co-workers detected expression on mast cells and macrophages only, whereas we additionally detected expression on epithelium, smooth muscle and endothelial cells, using the same antibody. With respect to the intensity of AR expression, no differences were found between COPD and asymptomatic smokers in our study. Interestingly, Varani et al. detected an increased expression of $A_{2A}R$ and A_3R

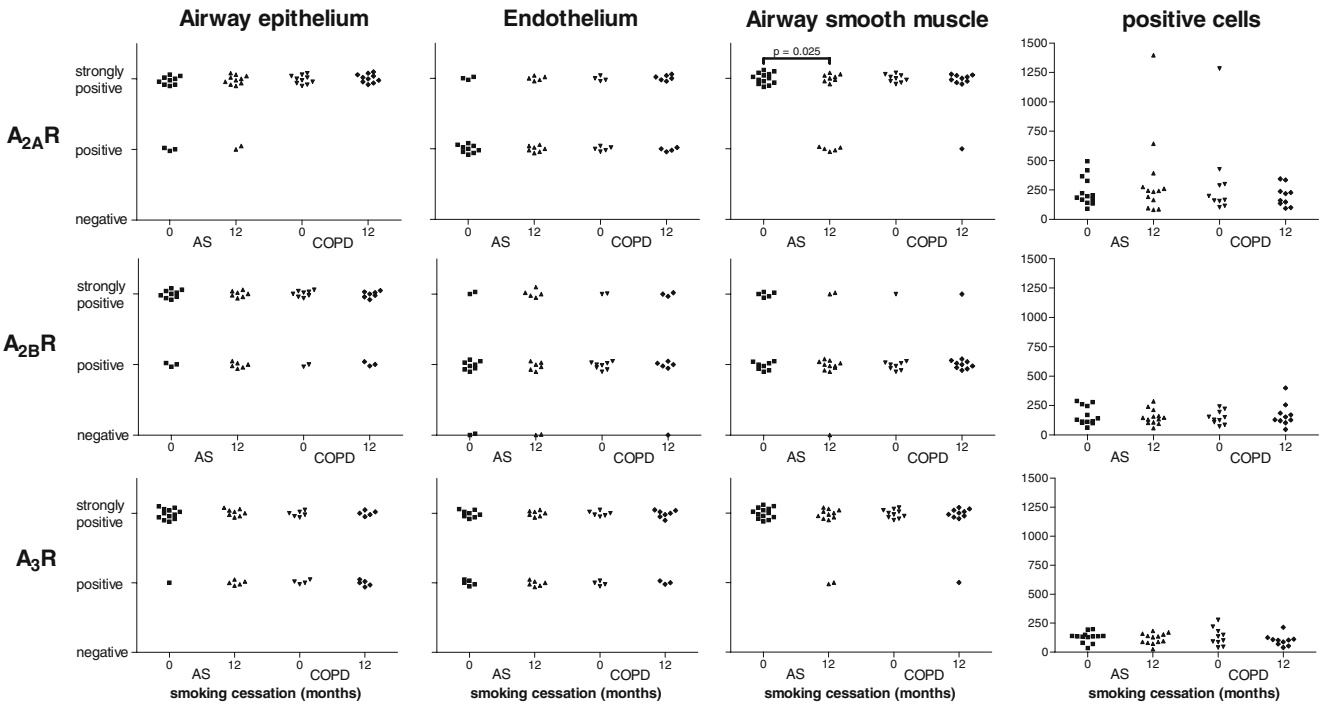

Fig. 2 Semi-quantitative scoring of the immunohistochemical staining of adenosine receptor expression on bronchial biopsies from smoking asymptomatic (AS) and COPD subjects, before and 1-year after smoking cessation. Structures present in bronchial biopsies were scored negative, positive, or strongly positive. Significant differences are depicted in the graphs. Paired data for 11 asymptomatic smokers and ten COPD patients

at the mRNA level, a decreased expression of $A_{2B}R$ and no differences for A_1R mRNA in airway wall tissue of COPD patients. We did not study mRNA expression of AR. Other differences between both studies may be explained by differences in the clinical characteristics of the investigated participants. At baseline, we investigated current smokers, whereas both the COPD and healthy smoking groups of Varani et al. consisted of a mixture of ex- and current smokers. Our data on the effects of 1-year smoking cessation show that this may have affected the results of the latter study. Also, some of the participants of Varani et al. were older and had higher packyears of smoking.

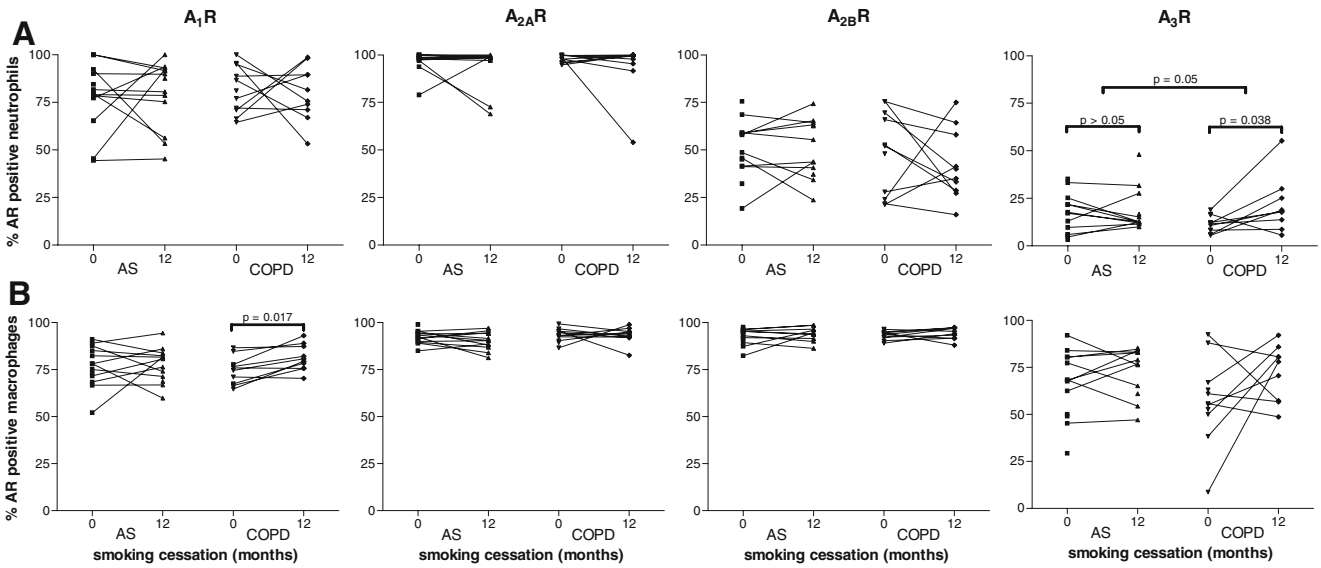

Fig. 3 Adenosine receptor expression on neutrophils (**a**) and macrophages (**b**) in sputum of COPD patients and asymptomatic smokers (AS), before and after 1-year smoking cessation. Significant differences are depicted in the graphs. Paired data for 11 asymptomatic smokers and ten COPD patients

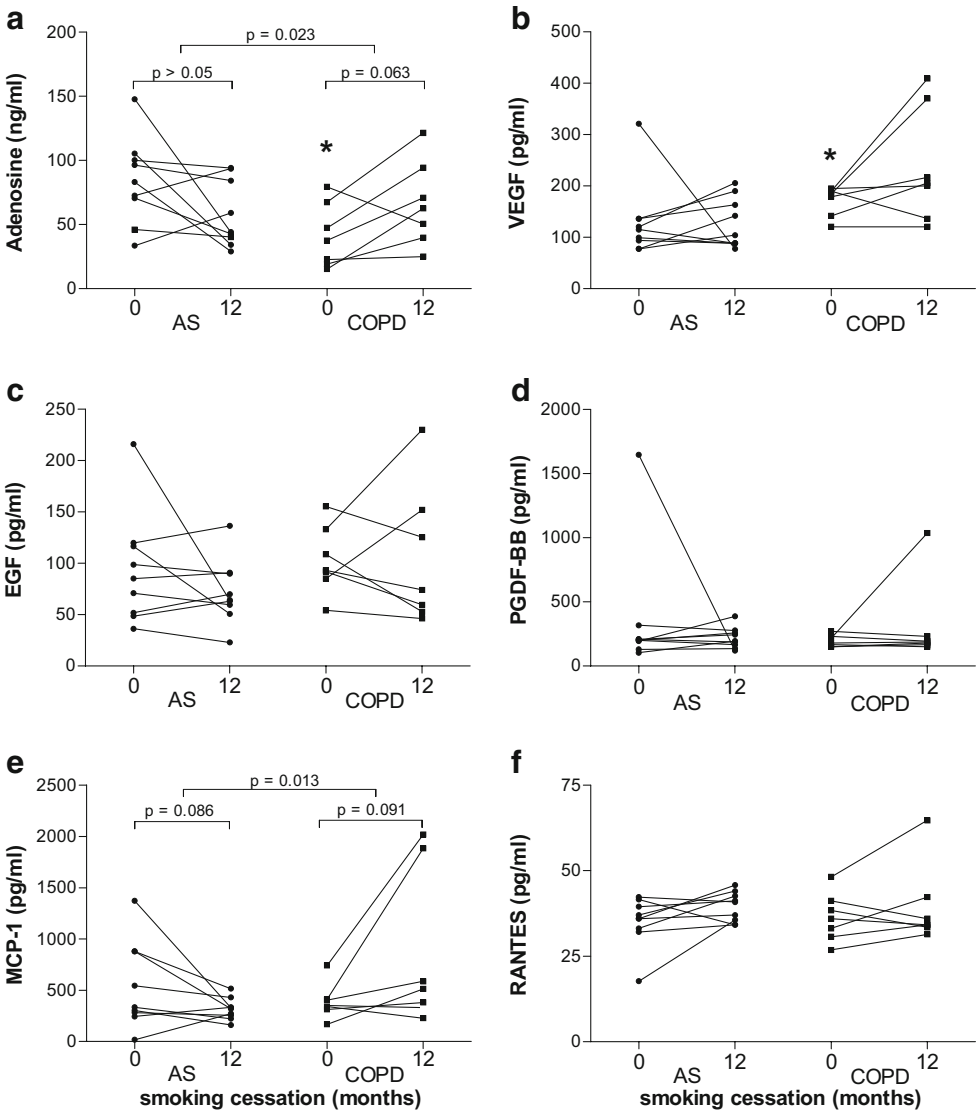

Fig. 4 Sputum adenosine (**a**), VEGF (**b**), EGF (**c**), PDGF-BB (**d**), MCP-1 (**e**), and RANTES (**f**) levels of CODP patients and asymptomatic smokers (AS), before and after 1-year smoking cessation. * Significant difference at baseline ($p<0.05$) between COPD and AS, other significant differences are depicted in the graphs. Paired data for nine asymptomatic smokers and seven COPD patients

We report for the first time the expression of all four adenosine receptors on neutrophils and macrophages in sputum of COPD and asymptomatic smokers. At baseline, no differences were found between asymptomatic smokers and COPD patients. With respect to neutrophils, smoking cessation resulted in a significantly higher percentage of sputum neutrophils expressing A_3R on their membrane in COPD, an effect not observed in asymptomatic smokers. The role of the human adenosine A_3 receptor is poorly understood. mRNA for the adenosine A_3 receptor is highest in the central nervous system, liver, and lung [19, 20]. A recent study showed that a ligand which combines adenosine A_{2A} receptor agonist and A_3 receptor antagonist activity inhibits the release of preformed granule proteins from neutrophils [21]. Another recent study showed that the A_3R on neutrophils is additionally involved in neutrophilic chemotaxis [22]. This is of interest since we previously showed that the number of sputum neutrophils significantly increased in COPD patients who successfully quitted smoking for 1 year. The role of these neutrophils is still not clear but theoretically they could contribute to the enhanced adenosine levels after smoking cessation in COPD. The exact contribution of adenosine in the persistence and progression of the inflammatory response is further dictated by the expression pattern of the four different adenosine receptors.

The percentage of macrophages expressing the A_1R was increased in COPD patients after 1-year of smoking cessation. Recently, a role for the A_1R on monocytes was described in modulation of angiogenesis [23]. The A_1R-selective agonist N^6-cyclopenthyladenosine increased VEGF production by human monocytes in vitro and increased angiogenesis in a chicken chorioallantoic membrane model. In the present study, levels of chemokines and various growth factors were measured in sputum supernatant, to explain the increase in inflammation as a repair

mechanism in the airways. Smoking cessation had a differential effect on MCP-1 production in sputum supernatant when comparing COPD with asymptomatic smokers. Since this chemokine is involved in recruitment of macrophages, the observed relative increase in MCP-1 in COPD with smoking cessation compared to asymptomatic individuals is in line with the previously published observation that the number of macrophages decreases upon smoking cessation in asymptomatic smokers, whereas it persists in COPD [5]. RANTES levels were similar in both groups and smoking cessation did not alter this. RANTES increases during COPD exacerbations [24] and is involved in chemotaxis of eosinophils. The percentage of eosinophils decreased in both COPD and asymptomatic patients after smoking cessation [5]. This thus could not be explained by RANTES. We found that COPD patients had higher levels of VEGF in sputum than asymptomatic smokers, compatible with findings described by Rovina et al. [25] and other research groups describing higher VEGF levels in sputum of patients suffering from chronic bronchitis and lower levels in patients with emphysema [25–27]. Cigarette smoking may upregulate VEGF, as suggested by an acute increase of VEGF plasma levels during smoking [28], yet we here show that smoking cessation did not reduce VEGF levels in both our groups.

Finally, we observed that smoking cessation decreased levels of adenosine in asymptomatic smokers, whereas it increased (trend) adenosine levels in COPD patients. This is of interest and in line with the observation that a number of inflammation markers significantly decreased in asymptomatic smokers who successfully quitted smoking while the number of sputum neutrophils, lymphocytes, interleukin-8, and eosinophil-cationic-protein levels significantly increased in COPD patients who successfully ceased smoking for 1 year [5].

Conclusions

We have shown that COPD patients respond significantly different to smoking cessation than asymptomatic smokers with respect to adenosine production and adenosine receptor expression. Our results may indicate that adenosine-related effector mechanisms are involved in the persistence and progression of the inflammatory response in COPD following 1-year smoking cessation.

Acknowledgement This study was financially supported by the Groningen University Graduate School for Drug Exploration (GUIDE).

Conflicts of interest statement We declare that we have no conflict of interest.

References

1. Rabe KF, Hurd S, Anzueto A et al (2007) Global strategy for the diagnosis, management, and prevention of chronic obstructive pulmonary disease: GOLD executive summary. Am J Respir Crit Care Med 176:532–555
2. Anthonisen NR, Connett JE, Kiley JP et al (1994) Effects of smoking intervention and the use of an inhaled anticholinergic bronchodilator on the rate of decline of FEV1. The Lung Health Study. JAMA 272:1497–1505
3. Kanner RE, Connett JE, Williams DE et al (1999) Effects of randomized assignment to a smoking cessation intervention and changes in smoking habits on respiratory symptoms in smokers with early chronic obstructive pulmonary disease: the Lung Health Study. Am J Med 106:410–416
4. Willemse BW, ten Hacken NH, Rutgers B et al (2004) Smoking cessation improves both direct and indirect airway hyperresponsiveness in COPD. Eur Respir J 24:391–396
5. Willemse BW, ten Hacken NH, Rutgers B et al (2005) Effect of 1-year smoking cessation on airway inflammation in COPD and asymptomatic smokers. Eur Respir J 26:835–845
6. Polosa R (2002) Adenosine-receptor subtypes: their relevance to adenosine-mediated responses in asthma and chronic obstructive pulmonary disease. Eur Respir J 20:488–496
7. Oosterhoff Y, de Jong JW, Jansen MA et al (1993) Airway responsiveness to adenosine 5′-monophosphate in chronic obstructive pulmonary disease is determined by smoking. Am Rev Respir Dis 147:553–558
8. Oosterhoff Y, Jansen MA, Postma DS et al (1993) Airway responsiveness to adenosine 5′-monophosphate in smokers and nonsmokers with atopic asthma. J Allergy Clin Immunol 92:773–776
9. Driver AG, Kukoly CA, Ali S et al (1993) Adenosine in bronchoalveolar lavage fluid in asthma. Am Rev Respir Dis 148:91–97
10. Varani K, Caramori G, Vincenzi F et al (2006) Alteration of adenosine receptors in patients with chronic obstructive pulmonary disease. Am J Respir Crit Care Med 173:398–406
11. Cronstein BN (1994) Adenosine, an endogenous anti-inflammatory agent. 76:5–13
12. Cronstein BN, Daguma L, Nichols D et al (1990) The adenosine/neutrophil paradox resolved: human neutrophils possess both A1 and A2 receptors that promote chemotaxis and inhibit O2 generation, respectively. J Clin Invest 85:1150–1157
13. Hasko G, Szabo C, Nemeth ZH et al (1996) Adenosine receptor agonists differentially regulate IL-10, TNF-alpha, and nitric oxide production in RAW 264.7 macrophages and in endotoxemic mice. J Immunol 157:4634–4640
14. Le Moine O, Stordeur P, Schandene L et al (1996) Adenosine enhances IL-10 secretion by human monocytes. J Immunol 156:4408–4414
15. Willemse BW, ten Hacken NH, Rutgers B et al (2005) Association of current smoking with airway inflammation in chronic obstructive pulmonary disease and asymptomatic smokers. Respir Res 6:38
16. Celli BR, MacNee W (2004) Standards for the diagnosis and treatment of patients with COPD: a summary of the ATS/ERS position paper. Eur Respir J 23:932–946

17. Aleva RM, Kraan J, Smith M et al (1998) Techniques in human airway inflammation: quantity and morphology of bronchial biopsy specimens taken by forceps of three sizes. Chest 113:182–185
18. Rutgers SR, Timens W, Kaufmann HF et al (2000) Comparison of induced sputum with bronchial wash, bronchoalveolar lavage and bronchial biopsies in COPD. Eur Respir J 15:109–115
19. Ralevic V, Burnstock G (1998) Receptors for purines and pyrimidines. Pharmacol Rev 50:413–492
20. Fredholm BB, Arslan G, Halldner L et al (2000) Structure and function of adenosine receptors and their genes. Naunyn Schmiedebergs Arch Pharmacol 362:364–374
21. Bevan N, Butchers PR, Cousins R et al (2007) Pharmacological characterisation and inhibitory effects of (2R,3R,4S,5R)-2-(6-amino-2-{[(1S)-2-hydroxy-1-(phenylmethyl)ethyl]amino}-9 H-purin-9-yl)-5-(2-ethyl-2H-tetrazol-5-yl)tetrahydro-3,4-furandiol, a novel ligand that demonstrates both adenosine A(2A) receptor agonist and adenosine A(3) receptor antagonist activity. Eur J Pharmacol 564:219–225
22. Chen Y, Corriden R, Inoue Y et al (2006) ATP release guides neutrophil chemotaxis via P2Y2 and A3 receptors. Science 314:1792–1795
23. Clark AN, Youkey R, Liu X et al (2007) A1 adenosine receptor activation promotes angiogenesis and release of VEGF from monocytes. Circ Res 101:1075–7077
24. Zhu J, Qiu YS, Majumdar S et al (2001) Exacerbations of Bronchitis: bronchial eosinophilia and gene expression for interleukin-4, interleukin-5, and eosinophil chemoattractants. Am J Respir Crit Care Med 164:109–116
25. Rovina N, Papapetropoulos A, Kollintza A et al (2007) Vascular endothelial growth factor: an angiogenic factor reflecting airway inflammation in healthy smokers and in patients with bronchitis type of chronic obstructive pulmonary disease? Respir Res 8:53
26. Kanazawa H, Asai K, Hirata K et al (2003) Possible effects of vascular endothelial growth factor in the pathogenesis of chronic obstructive pulmonary disease. Am J Med 114:354–358
27. Kanazawa H, Asai K, Nomura S (2007) Vascular endothelial growth factor as a non-invasive marker of pulmonary vascular remodeling in patients with bronchitis-type of COPD. Respir Res 8:22
28. Wasada T, Kawahara R, Katsumori K et al (1998) Plasma concentration of immunoreactive vascular endothelial growth factor and its relation to smoking. Metabolism 47:27–30

Virchows Arch (2009) 454:283–290
DOI 10.1007/s00428-009-0730-1

ORIGINAL ARTICLE

Complement C3a expression and tryptase degranulation as promising histopathological tests for diagnosing fatal amniotic fluid embolism

Vittorio Fineschi · Irene Riezzo · Santina Cantatore · Cristoforo Pomara · Emanuela Turillazzi · Margherita Neri

Received: 15 September 2008 / Revised: 18 November 2008 / Accepted: 6 January 2009 / Published online: 27 January 2009

Abstract To date, the most recent specific diagnostic investigations for amniotic fluid embolism have been unable to conclusively identify any mechanism of disease other than a physical block to the circulation. We selected eight fatal cases in previously healthy women with uneventful singleton term pregnancies who presented to tertiary care centers in Italy for delivery. Pathologic features were assessed immunohistochemically using anti-fibrinogen, anti-tryptase, anti-C_{3a}, and anti-cytokeratin antibodies. AE1/AE3 cytokeratin stains proved positive, and tryptase-positive material was documented outside pulmonary mast cells. In all studied cases, expression of complement C_{3a} was twofold lower than in the control group, suggesting a possible complement activation in AFE, initiated by fetal antigen leaking into the maternal circulation.

Keywords C3a · Complement activation · Tryptase · Cytokeratin · Amniotic fluid embolism

Introduction

Amniotic fluid embolism (AFE) is a rare and severe obstetric emergency with an incidence ranging roughly from 1/600 to 1/120,000, but the best estimate of 1/20,000 pregnancies comes from a population based study using hospital discharge diagnoses [1–3]. Traditionally thought to be 90% fatal, with maternal survival casting doubt upon the diagnosis, the population-based study found a mortality rate of 26% [3, 4]. The reported case fatality rate is between 22 and 86% [5–7]. Although its pathophysiology remains unclear, it has been postulated that amniotic fluid and fetal debris enter the maternal circulation causing pulmonary embolism and cardiorespiratory collapse [8]. This syndrome classically occurs acutely during or soon after labor with a wide array of clinical manifestations that resemble both embolism and anaphylaxis [8]. The diagnosis is essentially one of exclusion based on clinical presentation or traditionally made at autopsy in fatal cases upon identification of fetal squamous cells in the maternal pulmonary circulation [9]. Since the first descriptions of AFE, its post-mortem diagnosis had previously been based on the evidence of squamous cells or debris in the pulmonary artery vasculature [10]. The inadequacy of routine staining methods has improved with the use of histochemical [11] and immunohistochemical [12–17] techniques for a correct diagnosis [18, 19]. The high degree of variability in symptoms, the lack of characteristic findings from radiological examination, the absence of a dose-response effect on symptoms, and the occasional occurrence of coagulopathies are not entirely consistent with a physical block to the circulation as the main mechanism of disease. Alternatively, it might be the result of complement activation initiated by fetal antigen leaking into the maternal circulation.

To verify this hypothesis, we report eight fatal cases of AFE as confirmed by clinical course and post-mortem examination, particularly focusing on new pathophysiologic hypothesis testing immunohistochemical techniques such as anti-tryptase and anti-C_{3a}.

V. Fineschi (✉) · I. Riezzo · S. Cantatore · C. Pomara · E. Turillazzi · M. Neri
Department of Forensic Pathology, University of Foggia,
Ospedale Colonnello D'Avanzo,
Via degli Aviatori 1,
71100 Foggia, Italy
e-mail: vfinesc@tin.it

Material and methods

We selected eight fatal cases in previously healthy women with uneventful singleton term pregnancies who presented to tertiary care centers in Italy for delivery. The clinical course of all the women was complicated by the abrupt onset of very different clinical signs. In all cases prompt resuscitation and appropriate multidisciplinary treatment were unsuccessfully given. Autopsies were performed 36–48 h after death and bilateral samples of pulmonary tissue were collected according to standard criteria (a sample of each lobe and a perihilar sample). All specimens were fixed in formalin and embedded in paraffin. Pathologic features were assessed using histologic sections stained with hematoxylin–eosin, (H&E) and modified alcian green-phloxine tartrazine (Attwood's stain). Alcian blue stain (for acid mucosubstances and acetic mucins) was used to confirm the presence of amniotic fluid in pulmonary vessels. In addition, immunohistochemical investigation of samples was performed utilizing anti-fibrinogen, anti-tryptase, anti-C_{3a}, and anti-cytokeratin. We used 4-μm thick paraffin sections mounted on slides covered with 3-amminopropyl-triethoxysilane (Fluka, Buchs, Switzerland). Pretreatment was necessary to facilitate antigen retrieval and to increase membrane permeability to antibodies: for fibrinogen, enzymatic digestion with Proteinase K in 20 mM Tris-HCl, pH 8.0 for 15 min (temperature 20°C); for tryptase, enzymatic digestion with Proteolytic Enzyme (Dako, Copenhagen, Denmark), for 5 min (temperature 20° C); and for C_{3a} and cytokeratin, boiling in 0.25 mM EDTA buffer (Microwave 640 Watt, two 7-min cycles). The primary antibody was applied in a ratio of 1:3,000 for fibrinogen, 1:1,000 for tryptase, 1:500 for C_{3a}, and 1:50 for cytokeratin, and incubated for 120 min at 20°C. The detection system utilized was the LSAB + kit (Dako, Copenhagen, Denmark), a refined avidin–biotin technique in which a biotinylated secondary antibody reacts with several peroxidise conjugated streptavidin molecules. The

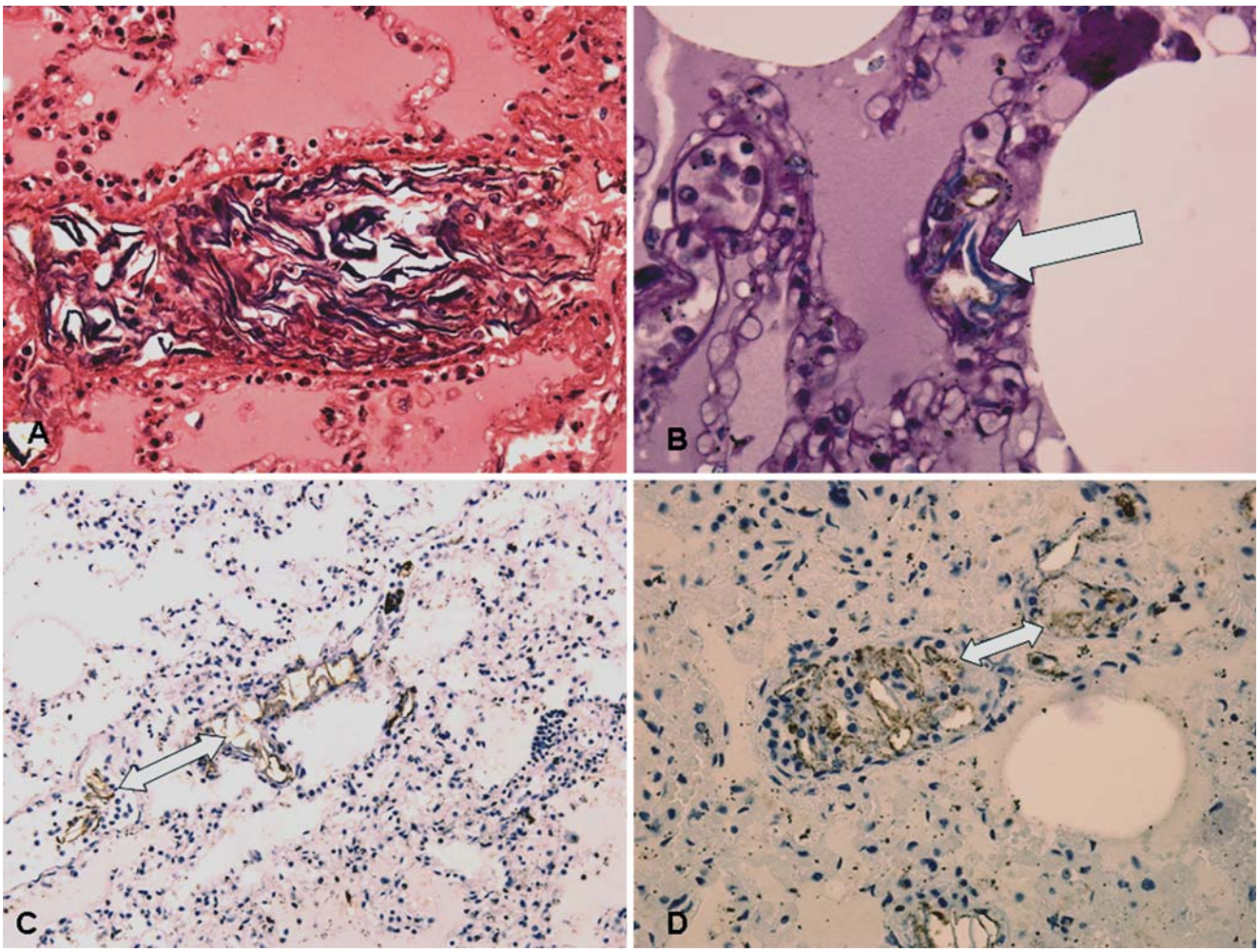

Fig. 1 a Evidence of fetal squamous cells, lanugo hairs, vernix caseosa, in the pulmonary artery vasculature (H&E, 200×). **b** Fetal squames (*arrows*) are in blue with Alcian blue stain (100×). **c**, **d** AE1/AE3 cytokeratin stains on the lungs showed intense intravascular positivity of fetal squamous cells (*arrows*)

positive reaction was visualized by 3,3-diaminobenzidine peroxidation, according to standard methods. The sections were counterstained with Mayer's hematoxylin, dehydrated, coverslipped and observed in a Leica DM4000B optical microscope (Leica, Cambridge, UK). The samples were also examined under a confocal laser scanning microscope (CLSM True Confocal Scanner, Leica TCS SPE).

The control group consisted of six women whose death was clearly caused by trauma during pregnancy.

Results

Information regarding previous pregnancies were not available in the FIVE multiparous women. Medical histories included only three women with a history of allergy and two women with a BMI>25 Kg/m^2. The most frequent peripartal symptoms were tachycardia and shock (62.5%), followed by bradycardia and coma (37.5%). The interval between onset of labor and symptoms ranged between 0.4 and 7.5 h (average time 3.75 h). All the women died within 7 h of onset of the symptoms.

External examination of the bodies gave no significant findings. Frequent findings at autopsy included pulmonary edema, congestion, and focal atelectasis. In six cases, cardiac and subpleural blood extravasation and extensive soft tissue blood accumulation were detected around operative and intravascular catheter insertion sites. In three cases, surgical incisions of the uterus were observed. Other organs were unremarkable upon gross examination, except for cerebral and pulmonary edema. In the six cases with clinical symptoms referred to DIC, subpleural and subepicardial hemorrhages and microthrombi in pulmonary septal capillaries and in small cerebral and renal vessels were observed. Microscopic examination of uterus samples was unremarkable. The other organs showed changes consistent with prolonged hypotension and anoxia. Routine histological examination of lung samples revealed the presence of fetal squames and debris in pulmonary vessels (Fig. 1a), acute emphysema, focal atelectasis, and pulmo-

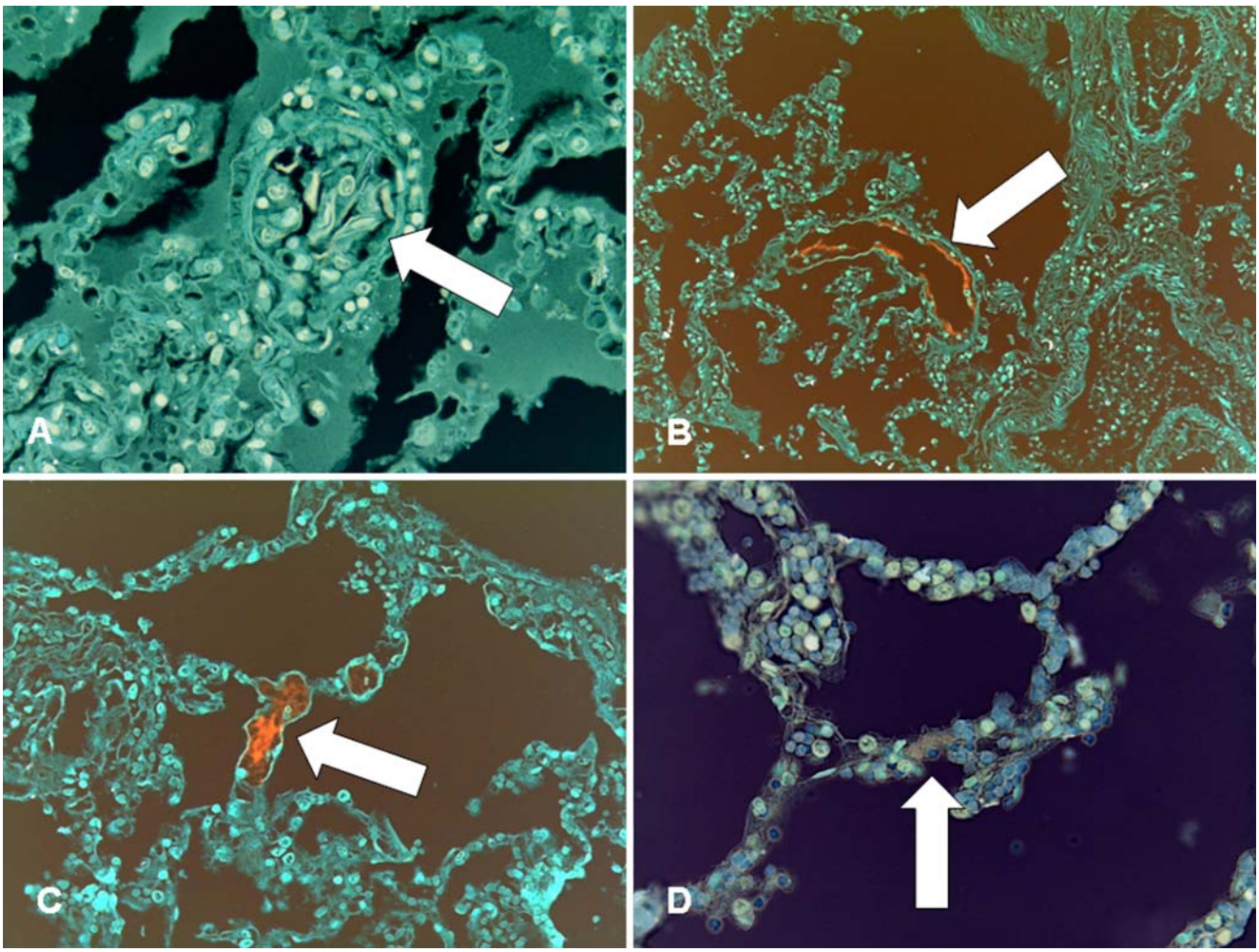

Fig. 2 Confocal laser scanning microscope: **a** Lanugo hairs and nuclei of fetal squamous cells are clearly visible (*arrows*). **b**, **c** Mucin fluoresced (*in red*) in the pulmonary artery vasculature and **d** in capillary septa (*arrows*)

nary edema. With special stains (Alcian blue and Attwood modified), squamous cells and mucin (Fig. 1b) were clearly evident. AE1/AE3 cytokeratin stains of the lung tissue showed intense intravascular positivity (Fig. 1c, d). Examination of the lung tissue samples under the confocal laser microscope showed fluorescence of mucin and lanugo hairs (Fig. 2a–d). An elevated number of pulmonary mast cells were identified by immunohistochemistry in the bronchial walls and capillary septa in all eight cases. A halo of tryptase positiveness around the mast cells (Fig. 3a–c) indicated mast cell degranulation and a great number of degranulating mast cells with tryptase-positive material was documented outside the cells using the CLSM technique (Fig. 4). The serum tryptase level was tested in one case with a result of 47.2 ng/ml (post-mortem normal value ≤40 ng/ml).

Levels of complement C_{3a} were twofold lower in these AFE cases than in control cases, suggesting a possible complement activation in AFE (Fig. 5). These results (Table 1) offer a convincing argument for obtaining acute plasma and serum samples in suspected AFE cases.

Toxicological analysis was performed in all cases and the results were negative for drugs of abuse; in six cases they showed the presence of substances consistent with iatrogenic administration for anesthesia and pain control and/or resuscitation efforts.

Discussion

Our study suggests a diagnostic immunohistochemical approach based on recent clinical hypotheses about AFE [4]. The clinical course with AFE is far more variable than that seen with pulmonary embolism, suggesting that the mechanism may not be limited to physical pulmonary vessel obstruction. It should be emphasized that an immune mediated constriction of the pulmonary arteries can produce many of the same physiologic effects as a physical

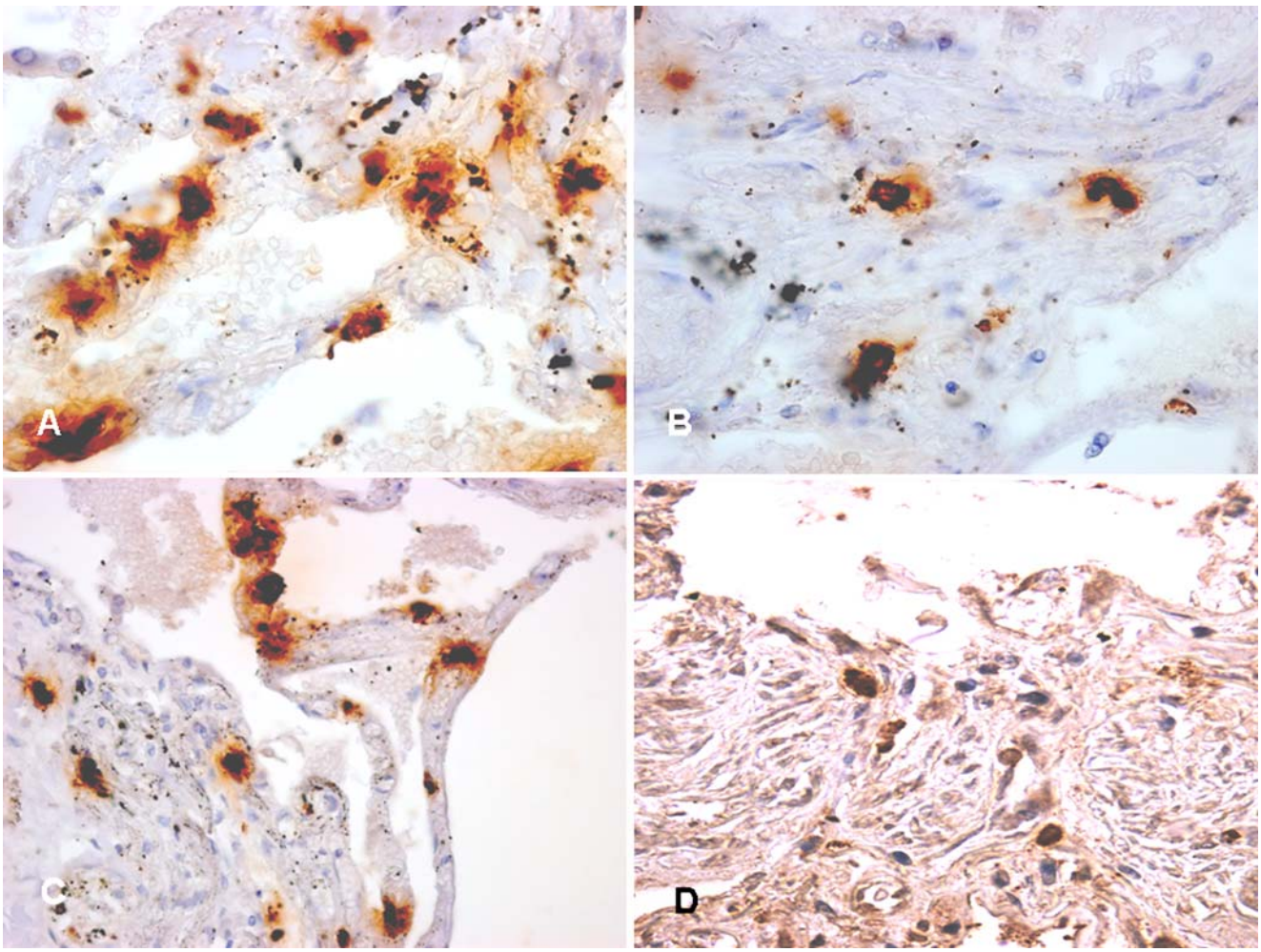

Fig. 3 **a–c** Degranulating mast cells (*starry effect*) with tryptase-positive material outside the cells. A halo (golden reaction) of tryptase positiveness around the mast cells reveals evidence of mast cell degranulation (Ab anti-tryptase). **d** Control case with negative reaction outside the cells (Ab anti-tryptase)

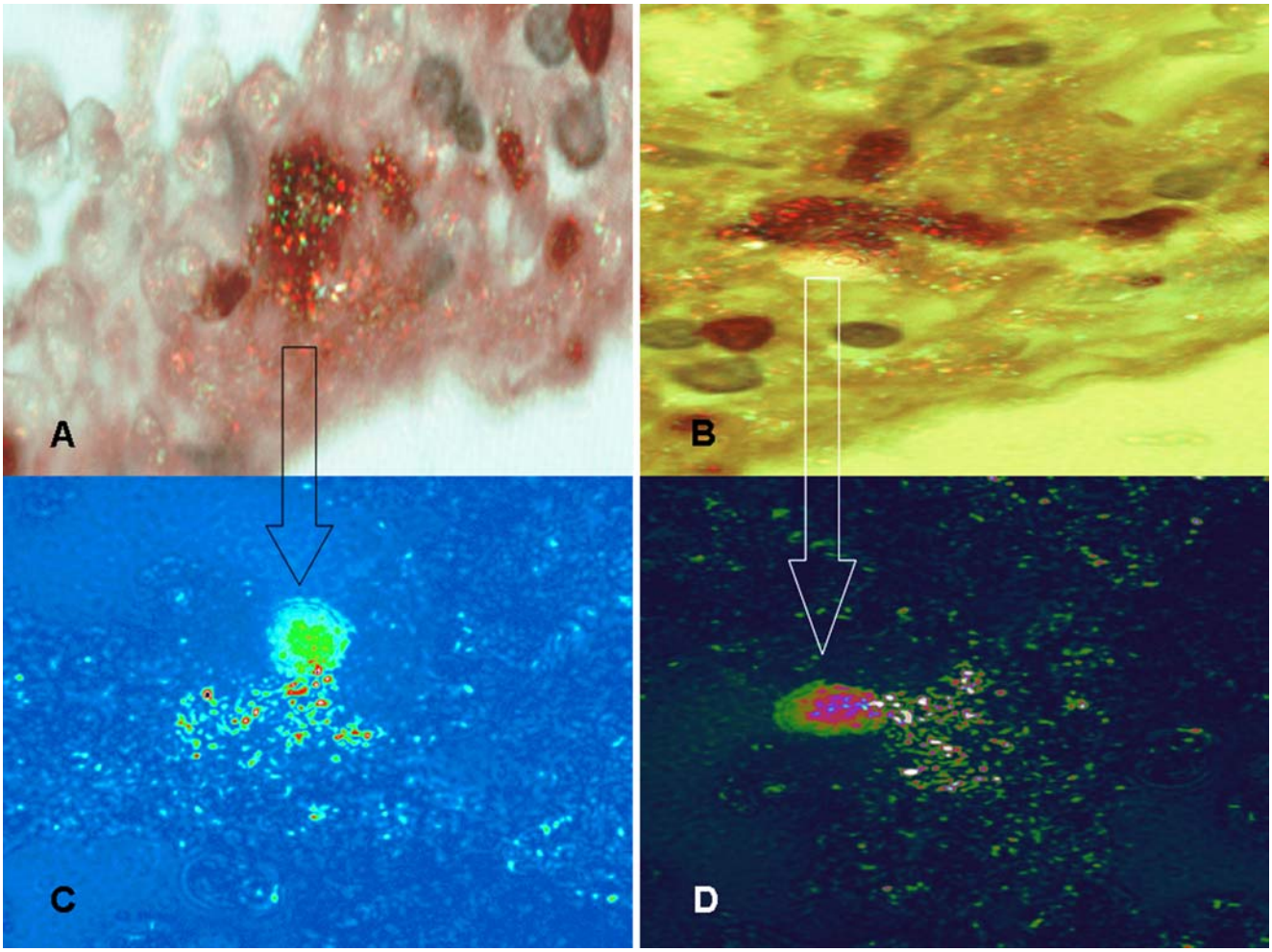

Fig. 4 **a**, **b** Capillary septa: evidence of degranulating mast cells (*starry effect*) with tryptase-positive material outside the cells. **c**, **d** Degranulating mast cells (same as in **a**, **b**) with tryptase-positive material (in *red* and in *white*, respectively) outside the cells documented by confocal laser scanning microscope technique

obstruction [20, 21]. Coagulopathy and neurologic symptoms can occur in isolation or in advance of cardiorespiratory symptoms. A physical obstruction of the pulmonary vasculature with fetal debris cannot explain these clinical observations. Physical obstruction of the pulmonary vasculature as seen in pulmonary embolism does not explain the complement activation or tryptase release that has been reported. These findings directly implicate an immune mechanism, not observed in pulmonary embolism [4].

Conventional wisdom describes the efflux of amniotic fluid components into maternal vasculature as driven by a pressure or electrochemical gradient through lacerations in the lower uterine segment, endocervical vessels, and placental site [22]. Plugging of the cervical vasculature by amniotic fluid elements has been described, although the mechanism by which this leads to AFE is unclear [23]. Amniotic fluid contains various concentrations of fetal squamous epithelial cells, lanugo hair, vernix, mucin, zinc coproporphyrin, prostaglandins, and platelet activating factor. One possible mechanism of disease includes the effect of direct procoagulant substances found in amniotic fluid on maternal systems. The presence of vasoactive substances, such as platelet activating factor, in the placenta and amniotic fluid has been shown to cause increased vascular permeability, bronchoconstriction, platelet aggregation, recruitment of leukotrienes, cytokines, and thromboxanes, and the cascade of prostaglandin production [23–26]. Review of all published data on the hemodynamics of the syndrome indicates early transient pulmonary hypertension [27]. The use of endothelin antagonists or nitric oxide in experimental models may shed some light on the pathophysiology of the condition and lead to therapeutic manipulations of the condition [21]. Currently, there is no suitable animal model for amniotic fluid embolus secondary to the limitations of autologous amniotic fluid [28]. Laboratory testing for the fetal antigen sialyl-Tn has shown some diagnostic value with AFE [20, 23, 29, 30]. Sialyl-Tn

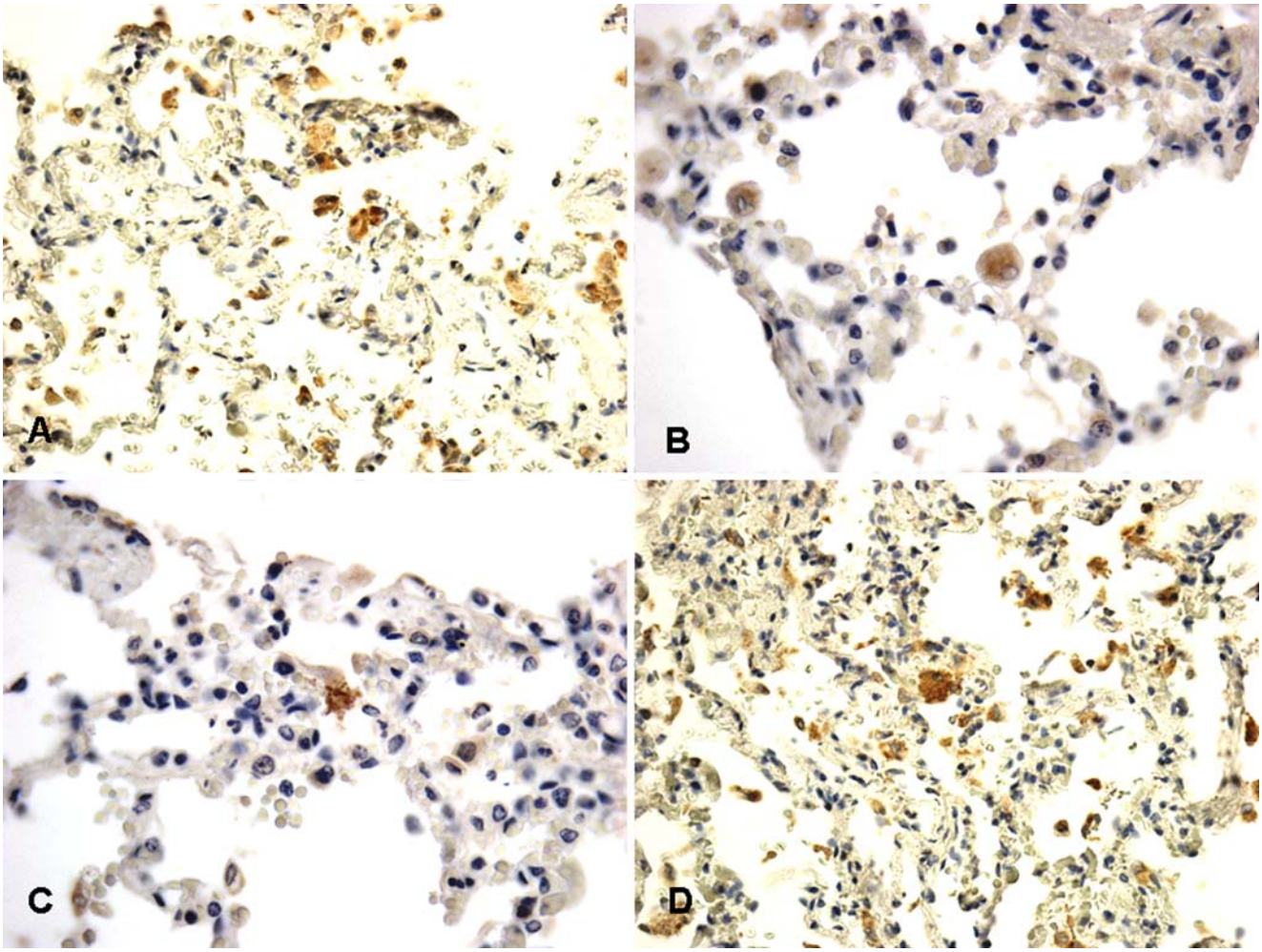

Fig. 5 **a**–**c** Weak expression of complement C_{3a} in all AFE cases; **d** moderate expression in control case

is a fetal antigen present in meconium and amniotic fluid detected most accurately with the TKH-2 monoclonal antibody [17, 20]. In addition, special immunohistochemical stains for the presence of fetal antigen in lung tissue were positive in women who had a history of AFE, and seven out of nine women diagnosed with AFE had elevated serum levels of fetal antigen compared with control subjects [30]. An anaphylactic or complement activation reaction to sialyl-Tn may explain the mechanism of the disease [23]. Complement activation was found along with high levels of sialyl-Tn; levels of complement C3 and C4 were twofold to three times lower than normal [29]. When these markers were used for evaluation of anaesthesia-induced allergic anaphylaxis, however, similar results were found [23, 29, 31]. An alternative immunologic mechanism for AFE involves the possibility of anaphylaxis with massive mast cell degranulation, independent of antigen antibody-mediated classic anaphylaxis. In early studies, immunohistochemical staining in post-mortem cases of AFE revealed high numbers of mast cells in the pulmonary vasculature [19]. Tryptase has been examined as a factor involved in anaphylaxis because it is specific to mast cells and has a longer half-life than histamine. Since tryptase is a mediator stored together with histamine and proteoglycan in the secretory granules of mast cells, the degranulation of mast cells is accompanied, either in immunological or non-immunological activation, by the release of this enzyme. Its localization in secretory granules is initially indicated by its release, together with histamine, from immunologically activated mast cells previously dispersed in human lung

Table 1 Complement C3a, tryptase release and cytokeratine responses in heart specimens

Antibody	AFE Group	Control group
Complement C3a	+	++
Tryptase release	++++	−
Cytokeratine	++++	−

Staining pattern is categorized as absent (−), weak (+), moderate (++), intense (+++), or strong (++++)

tissue [32]. In one study using serum tryptase and urinary histamine concentrations as markers for mast cell degranulation, no difference was found between women who had a history of AFE compared with control subjects [29]. Other investigators, however, found elevated tryptase levels in women who had AFE, but these values were compared with nonpregnant control subjects [33, 34]. Of note, in some cases where complement is involved in classic antibody-antigen anaphylaxis, mast cell degranulation can occur [4]. The studies evaluating serum tryptase levels in AFE cases did not simultaneously measure complement levels [23, 33, 34].

One report postulates that an attempt should also be made to quantify the size of the embolus since not all amniotic fluid embolisms are fatal [35], even though no relationship has been demonstrated between the severity of the clinical features and the amount of particulate material in the lungs and even less so with the actual volume of embolized fluid [36]. The presence of squamous cells in the maternal pulmonary artery circulation is no longer considered pathognomonic [37] and the introduction of amniotic fluid into the maternal circulation holds pathogenic characteristics of AFE only in certain situations tied to particular components of this fluid [26]. In a small percentage of women this exposure causes a pathological complex resulting, in many cases, in the death of the patient. The clinical variability of the onset of AFE can be compared with the antigenic variability of the amniotic fluid and with individual reactions similar to other anaphylactic or anaphylactoid reactions [1, 38]. A hypothesis has been put forward that AFE may have an underlying immunologic source involving the presentation of pregnancy-associated antigen in the maternal circulation. Amniotic fluid leakage into maternal circulation per se seems an unlikely cause given the absence of a satisfactory animal model, the variable timing of symptoms after the supposed 'leak' and the highly variable presentation of patients. A more feasible attractive hypothesis could be an immunologically mediated response to the same type of pregnancy-associated antigen leaking into the maternal circulation [1]. Thus, new laboratory tests are needed, such as the serum tryptase levels, which should provide scientific support for the presumed immunological mechanism of AFE [39]. Although the serum tryptase analysis is totally reliable when performed during a clinical course [40], a post-mortem comparison of tryptase values is discordant since the blood samples are collected at the autopsy many hours after death [41].

In our study, we searched for complement activation too. While complement activation appears to be a frequent occurrence in AFE, the question remains as to whether it is the primary mechanism of the disease. In addition to the need to evaluate more patients with AFE, a new control group of critically ill pregnant women needs to be assessed for complement activation [4]. Our retrospective study does not allow for final conclusions but C_{3a} appears involved in our cases. The semiquantitative differences between control groups and AFE must be further studied with a large cohort group in order to better understand the significance of the data. According to Benson, this hypothesis leads to predictions that can be tested in humans: (1) complement levels will be consistently depressed in AFE patients and not in parturients seriously ill from other conditions. It has already been established that significant complement activation is not a physiologic aspect of birth. (2) It might be possible to identify immune complexes in the circulation or tissues of patients with amniotic fluid embolism. Though difficult in practice, the inciting antigen might be identified through analysis of the immune complexes (if present). (3) There may be characteristic patterns in HLA typing seen in maternal–fetal pairs experiencing amniotic fluid embolism. Alternatively, there may be abnormalities in the amounts or type of HLA antibodies in the circulation of women with the disease [4].

In conclusion, to date no single laboratory or clinical findings can be used to diagnose or exclude AFE. There is still no routine specific diagnostic scheme that can be used to diagnose AFE, but some tests may support diagnosis [42]. The diagnosis of AFE is one of exclusion and mostly presumptive; it is made on the basis of the clinical presentation of a woman in labor or within 48 h of delivery. Post-mortem diagnosis was previously based on the presence of squamous cells or debris in the pulmonary artery vasculature; the inadequacy of routine staining methods has improved with the use of histochemical and immunohistochemical techniques for a correct diagnosis [18]. A validation of our proposed laboratory tests, allows the pathologist to obtain a more reliable diagnosis of AFE, confirming that the term amniotic fluid embolism appears to be a misnomer and should be discarded and the syndrome of acute peripartum hypoxia, hemodynamic collapse and coagulopathy should be hereafter described as anaphylactic or anaphylactoid pregnancy syndrome [38].

Conflict of interest statement We declare that we have no conflict of interest.

References

1. Benson MD (1993) Nonfatal amniotic fluid embolism: three possible cases and a new clinical definition. Arch Fam Med 2:989–994
2. Tuffnell DJ (2005) United Kingdom amniotic fluid embolism register. BJOG 112:1625–1629
3. Gilbert Wm, Danielsen B (1999) Amniotic fluid embolism: decreased mortality in a population-based study. Obstet Gynecol 93:973–977
4. Benson MD (2007) A hypothesis regarding complement activation and amniotic fluid embolism. Med Hypotheses 68:1019–1025

5. Burrows A, Khoo SK (1995) The amniotic fluid embolism syndrome: 10 years' experience at a major teaching hospital. Aust N Z J Obstet Gynaecol 35:245–250
6. Morgan M (1979) Amniotic fluid embolism. Anaesthesia 34:20–32
7. Fletcher SJ, Parr MJ (2000) Amniotic fluid embolism: a case report and review. Resuscitation 43:141–146
8. Moore J, Baldisseri MR (2005) Amniotic fluid embolism. Crit Care Med 33:S279–S285
9. Christiansen LR, Collins KA (2006) Pregnancy-associated deaths: a 15-year retrospective study and overall review of maternal pathophysiology. Am J Forensic Med Pathol 27:11–19
10. Steiner PE, Lushbaugh CC (1941) Maternal pulmonary embolism by amniotic fluid as a cause of obstetric shock and unexpected death in obstetrics. JAMA 117:1245–1254
11. Attwood HD (1958) The histological diagnosis of amniotic fluid embolism. J Pathol Bacteriol 76:211–215
12. Hanish FG, Hegge H, Katalinic JP, Uhlenbruck G (1993) Monoclonal antibody FW6 defines an epitope on 3–4 monofucosylated polylactosaminoglycans expressed by fetal and colon carcinoma-associated mucins. Cancer Res 53:4367–4375
13. Schwonzen M, Schmitz R, Baldus SE et al (1992) Monoclonal antibody FW6 generated against a mucin-carbohydrate of human amniotic fluid recognizes a colonic tumor-associated epitope. Br J Cancer 65:559–565
14. Kurosaka A, Kitagawa H, Fukui S et al (1988) A monoclonal antibody that recognizes a cluster of a disaccharide, Neu Ac 26 Gal Nac, in mucin-type glycoproteins. J Biol Chem 263:8724–8726
15. Garland IWC, Thompson WD (1983) Diagnosis of amniotic fluid embolism using an antiserum to human keratin. J Clin Pathol 36:625–627
16. Lunetta P, Penttilä A (1996) Immunohistochemical identification of syncytiotrophoblastic cells and megakaryocytes in pulmonary vessels in a fatal case of amniotic fluid embolism. Int J Legal Med 108:210–214
17. Kobayashi H, Ohi H, Terao T (1993) A simple, noninvasive, sensitive method for diagnosis of amniotic fluid embolism by monoclonal antibody TKH-2 that recognizes NeuAc 2–6 GalNac. Am J Obstet Gynecol 168:848–853
18. Hernandez M, Bajanowski T (1991) Tödliche Fruchtwasserembolie. Rechtsmedizin 2:35–38
19. Fineschi V, Gambassi R, Gherardi M, Turillazzi E (1998) The diagnosis of amniotic fluid embolism: an immunohistochemical study for the quantification of pulmonary mast cell tryptase. Int J Legal Med 111:238–243
20. Kobayashi H, Ooi H, Hayakawa H et al (1997) Histological diagnosis of amniotic fluid embolism by monoclonal antibody TKH-2 that recognizes NeudAC alpha 2-GalNAc epitope. Hum Pathol 28:428–433
21. Khong TY (1998) Expression of endothelin-1 in amniotic fluid embolism and possible pathophysiological mechanism. Br J Obstet Gynaecol 105:802–804
22. Resnik R, Swartz WH, Plumer MH, Benirschke K, Stratthaus ME (1976) Amniotic fluid embolism with survival. Obstet Gynecol 47:295–298
23. Stafford I, Sheffield J (2007) Amniotic fluid embolism. Obstet Gynecol Clin N Am 34:545–553
24. Karetsky M, Ramirez M (1998) Acute respiratory failure in pregnancy. An analysis of 19 cases. Medicine 77:41–49
25. Petroianu GA, Toomes LM, Maleck WM, Friedberg C, Bergler WF, Rüfer R (2000) Administration of autologous fetal membranes: effects on the coagulation in pregnant mini-pigs. Pediatric Crit Care Med 1:65–71
26. Clark SL (1990) New concepts of amniotic fluid embolism: a review. Obstet Gynecol Surv 45:360–368
27. el Maradny E, Kanayama N, Halim A, Maehara K, Terao T (1995) Endothelin has a role in early pathogenesis of amniotic fluid embolism. Gynecol Obstet Invest 40:14–18
28. Stolte L, van Kessel H, Seelen J, Eskes T, Wagatsuma T (1967) Failure to produce the syndrome of amniotic fluid embolism by infusion of amniotic fluid and meconium into monkeys. Am J Obstet Gynecol 98:694–697
29. Benson MD, Kobayashi H, Silver RK, Oi H, Greenberger PA, Terao T (2001) Immunologic studies in presumed amniotic fluid embolism. Obstet Gynecol 97:510–514
30. Oi H, Kobayashi H, Hirashima Y, Yamazaki T, Kobayashi T, Terao T (1998) Serological and immunohistochemical diagnosis of amniotic fluid embolism. Semin Thromb Hemost 24:479–484
31. Harboe T, Benson MD, Oi H, Softeland E, Bjorge L, Guttormsen AB (2006) Cardiopulmonary distress during obstetrical anaesthesia: attempts to diagnose amniotic fluid embolism in a case series of suspected allergic anaphylaxis. Acta Anaesthesiol Scand 50:324–330
32. Schwartz LB (1981) Acid hydrolases and tryptases from secretory granules of dispersed human lung mast cells. J Immunol 126:1290–1294
33. Nishio H, Matsui K, Miyazaki T, Tamura A, Iwata M, Suzuki K (2002) A fatal case of amniotic fluid embolism with elevation of serum mast cell tryptase. Forensic Sci Int 126:53–56
34. Farrar SC, Gherman RB (2001) Serum tryptase analysis in a woman with amniotic fluid embolism. A case report. J Reprod Med 46:926–928
35. Rushton DI, Dawson IMP (1982) The maternal autopsy. J Clin Pathol 35:909–921
36. Toner PG, Crane J (1994) Pathology of death in pregnancy. In: Anthony PP, MacSween RNM (eds) Recent advances in histopathology. Churchill Livingstone, London, pp 189–211
37. Clark SL, Pavlova Z, Greenspoon J, Horenstein J, Phelan JP (1986) Squamous cells in the maternal pulmonary circulation. Am J Obstet Gynecol 154:104–106
38. Clark SL, Hankins DVG, Dudley DA, Dildy GA, Porter FT (1995) Amniotic fluid embolism: analysis of the national registry. Am J Obstet Gynecol 172:1158–1169
39. Benson MD, Lindberg RE (1996) Amniotic fluid embolism, anaphylaxis, and tryptase. Am J Obstet Gynecol 175:737
40. Schwartz LB, Metcalfe DD, Miller JS, Earl H, Sullivan T (1987) Tryptase levels as an indicator of mast-cell activation in systemic anaphylaxis and mastocytosis. N Engl J Med 316:1622–1626
41. Randall B, Butts J, Halsey JF (1995) Elevated post-mortem tryptase in the absence of anaphylaxis. J Forensic Sci 2:208–211
42. Turillazzi E, Karch BS, Neri M, Pomara C, Riezzo I, Fineschi V (2008) Confocal laser scanning microscopy. Using new technology to answer old questions in forensic investigations. Int J Legal Med 122:173–177

Virchows Arch (2009) 454:291–302
DOI 10.1007/s00428-009-0731-0

ORIGINAL ARTICLE

Over-expression of cathepsin E and trefoil factor 1 in sessile serrated adenomas of the colorectum identified by gene expression analysis

Maria Caruso · James Moore · Gregory J. Goodall · Michelle Thomas · Stuart Phillis · Anna Tyskin · Glenice Cheetham · Nancy Lerda · Hiroyuki Takahashi · Andrew Ruszkiewicz

Received: 11 September 2008 / Revised: 25 November 2008 / Accepted: 8 January 2009 / Published online: 27 January 2009

Abstract Sessile serrated adenomas are now recognised as precursor lesions of a substantial subset of colorectal cancers arising via a so-called "serrated pathway". However, their biological markers remain to be defined. The aim of our study was to identify differentially expressed genes in sessile serrated adenomas and conventional adenomas. Gene expression analysis demonstrated molecular differences between polyp types. Further studies using quantitative real-time polymerase chain reaction on cathepsin E (CTSE) demonstrated a significantly ($p<0.05$) higher expression in sessile serrated adenomas as compared to hyperplastic polyp and tubular adenomas. Trefoil Factor 1 showed the same trend of expression for sessile serrated adenomas as compared to hyperplastic polyps and was significantly higher in both polyps compared to tubular adenomas. Immunohistochemistry for both proteins demonstrated strong cytoplasmic staining of abnormal crypts in all sessile serrated adenomas, while staining in tubular adenomas and hyperplastic polyps was absent or weak and focal. BRAF and KRAS mutation analysis were employed to further validate polyp discrimination. The findings demonstrated the positive association of the BRAF mutation, V600E, with sessile serrated adenomas and KRAS mutations with tubular adenomas ($p<0.05$). This study demonstrates the over-expression in CTSE, in particular, and TFF1 in sessile serrated adenomas compared to both hyperplastic polyps and tubular adenomas.

Keywords Sessile serrated adenoma · Gene expression · Colorectal cancer · Cathepsin E · Trefoil factor 1 · Serrated neoplasia pathway

M. Caruso · H. Takahashi · A. Ruszkiewicz (✉)
Gastroenterology Research Laboratory, Surgical Pathology,
SA Pathology, Adelaide 5000, Australia
e-mail: andrew.ruszkiewicz@imvs.sa.gov.au

M. Caruso
e-mail: maria.caruso@imvs.sa.gov.au

H. Takahashi
e-mail: Hiroyuki.Takahashi@imvs.sa.gov.au

J. Moore · M. Thomas
Colorectal Surgery Unit, Royal Adelaide Hospital,
Adelaide 5000, Australia

J. Moore
e-mail: mooreby4@internode.on.net

M. Thomas
e-mail: drmlthomas@optusnet.com.au

G. J. Goodall · A. Tyskin
Hanson Institute, SA Pathology, Adelaide 5000, Australia

G. J. Goodall
e-mail: greg.goodall@imvs.sa.gov.au

A. Tyskin
e-mail: Anna.Tsykin@imvs.sa.gov.au

S. Phillis · G. Cheetham · N. Lerda
Division of Molecular Pathology,
SA Pathology, Adelaide 5000, Australia

S. Phillis
e-mail: Stuart.Phillis@imvs.sa.gov.au

G. Cheetham
e-mail: glenice.cheetham@imvs.sa.gov.au

N. Lerda
e-mail: nancy.lerda@imvs.sa.gov.au

G. J. Goodall
Department of Medicine,
The University of Adelaide,
Adelaide 5000, Australia

Introduction

The traditional view that all colorectal cancers (CRC) arise via the adenoma–carcinoma sequence and that the conventional adenoma is the sole precursor of CRC is no longer valid. The existence of an aggressive variant of hyperplastic polyp (HP) emerged from studies of so-called "serrated polyps" of the colorectum and their relationship to microsatellite unstable CRC as well as DNA methylation in colorectal lesions [1–7]. In earlier studies from the Jass group, these polyps were called "sessile serrated polyps" with reference to their endoscopic configuration and microscopically observed serration of the surface epithelium [4, 8, 9]. The currently preferred term for this polyp, "sessile serrated adenoma" (SSA), signifies its neoplastic nature and was recently introduced by Torlakovic and colleagues [10]. While the malignant potential of traditional serrated adenomas (SA), a related polyp type, has been known for almost three decades, SSAs were grouped with hyperplastic polyps and regarded as innocuous, non-neoplastic lesions with no potential for malignant transformation [11].

SSAs belong to a group of serrated polyps including HPs, mixed hyperplastic/adenomatous polyps (MHAP) and traditional SAs. HPs are thought to be innocuous lesions; however SSAs, along with MHAPs and SAs, are now recognised as precursors of a substantial subset of colorectal cancers arising via the so-called "serrated pathway" [2, 4, 9, 12]. A small proportion of CRC arising through this pathway demonstrate glandular serration reminiscent of their precursor lesion and are designated "serrated adenocarcinomas" [13–15]. Interestingly, serrated adenocarcinomas show a distinct gene expression profile which provides molecular support for their separation from conventional colorectal adenocarcinoma into a separate CRC subtype [14, 15]. Mutation in the BRAF gene (V600E) has been suggested as a specific marker for a serrated polyp pathway [16, 17] and has been shown to be a potential discriminator of SSAs and other polyp types on a molecular level [18, 19].

Recognition of the malignant potential of SSAs underscores the necessity of accurate pathological diagnosis of these lesions, which may pose diagnostic difficulties [12, 20–22]. Usual HPs have no associated cancer risk, but their differentiation from SSAs may be problematic particularly with early, small lesions and with small, endoscopically obtained samples. Despite substantial progress being made in the study of SSAs, identification of objective morphological risk factors and biomarkers by their characterisation on a molecular level still remains to be explored.

The aim of our study was to identify differentially expressed genes in SSAs and tubular adenomas (TAs) using cDNA and oligonucleotide microarrays and to validate these results with quantitative real-time polymerase chain reaction (QRT-PCR) and immunohistochemistry (IHC). The validation component of our study also included a group of HPs.

Materials and methods

Expression microarray analysis

Patients and polyp samples

Polyp samples were obtained from surgical resection specimens, resections for cancer or endoscopically unresectable benign lesions. The fresh specimens were examined and sampled in theatre immediately after resection or in the pathology laboratory within 30 min of resection. Specimens were transported to the laboratory on ice.

Halves of the polyps were immediately snap frozen in liquid nitrogen. The other halves were formalin fixed and paraffin embedded, then routinely processed and stained with haematoxylin and eosin (H&E). Frozen halves of the polyps selected for the study were further verified histologically prior to RNA extraction. The polyp tissue was fixed in RNAlater-ICE (Ambion) at −20°C for 24 h. A small portion of tissue was then fixed in formalin, paraffin embedded and sections stained with H&E. The remaining polyp tissue was used for RNA extraction.

Normal colonic mucosa from four colorectal resections for non-neoplastic conditions were used for the preparation of a pooled, normal reference RNA. The samples were collected, processed and histologically verified in a similar manner to the polyp tissues.

Selection criteria for SSAs and TAs

The diagnostic criteria for SSAs were based on the recently published criteria relying mainly on polyp architecture [10, 23, 24]. The architectural features which were assessed included crypt branching, horizontal dilatation of basal crypts and presence of serration at the base of the crypts. Polyps were classified as SSAs when at least two of these features were present.

As small SSAs may have overlapping histological features with traditional HPs, only lesions with a sessile configuration and a diameter of 10 mm or more from the right colon (up to the splenic flexure) were included. Only non-dysplastic polyps were included.

Standard histological criteria for diagnosis of TAs were applied. Only polyps from the left colon and rectum with pedunculated configuration, tubular architecture and low-grade dysplasia were included.

Patients known or suspected to have familial adenomatous polyposis or hereditary non-polyposis colorectal cancer syndromes were excluded.

Microarray hybridisation and analysis

Total cellular RNA was harvested with Trizol (Invitrogen, Carlsbad, CA, USA) and further purified with the RNeasy RNA purification kit (Qiagen, Valencia, CA, USA). cDNA was generated using 25–40 μg total RNA as a template and primed with PolyT(V)N (4.0 μg) and random hexamers (1.0 μg, Amersham, UK). cDNA was labelled with Cy5 or Cy3 dyes using the Cy-Scribe post-labelling kit (Amersham) as per the instructions. Labelled cDNA was hybridised to microarray slides printed with the CompuGen Human OligoLibrary (Compugen Human Oligo Library (v1) containing 18861 60-mer oligonucleotides, representing approximately 16,000 unique genes) by the Adelaide Microarray Centre (Australia). Slides were scanned using a GenePix 3000B scanner (Axon Instruments, Sunnydale, CA, USA), and the Spot package (CSIRO, Australia) was used to identify spots and estimate fore- and background intensities (using a morphological opening background estimator) [25, 26]. Data analysis was performed in *R* (http://www.r-project.org) using the Limma package of Bioconductor [27, 28]. Loess print tip method was used to correct for dye-bias and intensity within each group of adjacent spots printed by one pin [29]. Linear modelling was performed with the Limma package of Bioconductor [28].

QRT-PCR

Patients and polyp samples

Polyps used in the QRT-PCR study were endoscopically removed and immediately placed in RNAlater at room temperature for at least 3 h. A small portion of the tissue was shaved from the lesional tissue and stored at-86°C prior to RNA extraction. The main bulk of polyps was placed in formalin, routinely processed, embedded in paraffin, and H&E sections were examined histologically. Diagnostic criteria for SSAs and TAs were the same as for the microarray study. An additional group of polyps with typical endoscopic and histologic appearance of traditional HPs was included into the study. Pooled RNA extracted from normal colonic mucosa obtained from six fresh surgical resection specimens of unrelated patients was used as a control.

Total RNA was prepared, including column DNase digestion using the QIAGEN RNeasy Plus Mini Kit (Qiagen) according to the manufacture's instructions. RNA integrity and concentration was assessed using the Agilent BioAnalyzer; any samples with integrity readings below 7 were excluded.

First-strand synthesis and QRT-PCR were carried out in a one-step reaction using the iScript™ One-Step RT-PCR kit with SYBR® Green (Bio-Rad), on the iQ5 Bio-rad real-time instrument. Briefly, a 25 μl reaction volume contained 1× SYBR® Green RT-PCR reaction Mix, 10 ng of template RNA, 70 nM of each forward and reverse primers and 0.12 U/μl of iScript Reverse Transcriptase. First-strand synthesis took place at 50°C for 10 min followed by a polymerase activation and denaturation step of 95°C for 5 min. After which, 40 cycles of 95°C for 10 s and 60°C annealing for 30 s was performed. All reactions were performed in triplicate.

Two of the most differentially expressed genes identified in the microarray study (trefoil factor 1 (TFF1) and cathepsin E (CTSE)) were selected for further analysis with QRT-PCR.

The following primer pairs were used: glyceraldehyde-3-phosphate dehydrogenase (GAPDH; as a control gene) forward primer 5′gagtcaacggatttggtcgt3′ and reverse primer 5′gacaagcttcccgttctcag3′, TFF1 forward primer 5′tttggagca gagaggagg3′ and reverse primer 5′ttgagtagtcaaagtcagag cag3′ and CTSE forward primer 5′gaggcactgttatgttctgc3′ and reverse primer 5′attcccacggtcaaagactg3′.

To avoid amplification of genomic DNA, primers were designed to span across two exons. Primers were optimized, and a melt curve analysis was performed to ensure specificity. The cycle threshold value was used to calculate the normalised expression of CTSE and TFF1 for each sample using software provided with the iQ5 Bio-Rad real-time machine.

Data analysis

Using a nonparametric approach, Kruskal–Wallis and Mann–Whitney *U* tests were employed to identify whether statistically significant differences exist between the three groups (SSA, HP and TA) with respect to CTSE and TFF1 expression. Results were significant for $p<0.05$.

Immunohistochemical analysis

Patients and polyp samples

Automated immunohistochemistry, using commercially available monoclonal antibodies for CTSE (R&D Systems, Minneapolis, cat. no. AF1294) and TFF1 (ZYMED, S. San Francisco, CA, USA, cat. no. 18-0162) was performed on the samples used in the initial QRT-PCR experiment and a further 56 samples of SSA, 70 HP and 80 TAs, to assess the protein expression of the two most up-regulated genes identified from the microarray analysis. The additional samples were obtained from colorectal resection specimens and polyps randomly selected during diagnostic service at our laboratory.

Sections (4 μm) of paraffin wax embedded tissue were cut, mounted on coated slides, de-waxed and rehydrated by

Table 1 Microarray gene list

Gene name (abbreviation)	Genbank accession no.	SSA/TA	TA/reference	SSA/reference
Trefoil factor 1 (breast cancer, estrogen-inducible sequence)	NM_003225	8.0862	0.8523	6.8915
Cathepsin E	NM_001910	6.58377	1.079	7.1037
Dehydrogenase/reductase (SDR family) member 9	NM_005771	4.21602	0.341	1.4377
Glucosaminyl (*N*-acetyl) transferase 3, mucin type	NM_004751	4.10193	0.3267	1.3402
Mucin 17	AK026404	3.82734	1.2367	4.7333
Alanyl (membrane) aminopeptidase (aminopeptidase N, aminopeptidase M, microsomal aminopeptidase, CD13, p150)	NM_001150	3.44025	0.2311	0.7949
SIB 276 intestinal mucin (MUC3)	AF007190	3.15686	0.576	1.8184
Carcinoembryonic antigen-related cell adhesion molecule 6 (non-specific cross-reacting antigen)	NM_002483	3.01516	0.9512	2.8679
Meprin A, alpha (PABA peptide hydrolase)	NM_005588	2.99876	0.2544	0.7628
Keratin 19 pseudogene	AB041269	2.81968	0.4519	1.2743
Mucin 3A, intestinal	M55406	2.65625	0.6015	1.5977
Keratin 19	NM_002276	2.50372	0.6531	1.6352
BENE protein	U17077	2.44577	0.4155	1.0163
Pregnancy-specific beta-1-glycoprotein 3	M23575	2.4352	0.4173	1.0162
Sulfotransferase family, cytosolic, 1C, member 1	NM_001056	2.41344	1.2228	2.9511
Mucin (MUC3)	AF007193	2.35851	0.7968	1.8792
Hydroxysteroid (17-beta) dehydrogenase 2	NM_002153	2.35208	0.4379	1.03
Hypothetical gene supported by AK026328	AK026328	2.10019	0.5485	1.1519
Basic helix–loop–helix domain containing, class B, 3	AJ270695	2.04739	0.8079	1.6541
Malic enzyme 1, NADP(+)-dependent, cytosolic	NM_002395	2.00635	1.2406	2.4892
Syndecan binding protein (syntenin) 2	NM_015685	1.94829	0.486	0.9468
2′,5′-Oligoadenylate synthetase 1, 40/46 kDa	NM_016816	1.93248	0.7436	1.437
Retinoic acid receptor responder (tazarotene induced) 3	NM_004585	1.899	0.7205	1.3683
Annexin A1	NM_000700	1.87712	1.1888	2.2315
Homo sapiens clone 24659 mRNA	AF070569	1.83507	0.51	0.9359
Carboxylesterase 2 (intestine, liver)	NM_003869	1.81334	0.358	0.6491
Solute carrier family 6 (neurotransmitter transporter, creatine), member 8	NM_005629	1.81253	0.6228	1.1289
Solute carrier family 9 (sodium/hydrogen exchanger), isoform 3 regulator 1	NM_004252	1.77325	0.5543	0.9829
Transmembrane 4 superfamily member 1	X75684	1.76336	1.4805	2.6106
MAX dimerization protein 1	NM_002357	1.7493	0.5571	0.9746
Lupus brain antigen 1	AB002340	1.7462	0.5144	0.8983
Amiloride binding protein 1 (amine oxidase (copper-containing))	NM_001091	1.73996	0.5232	0.9103
Collagen, type XVII, alpha 1	NM_000494	1.73622	0.7918	1.3747
Xanthine dehydrogenase	NM_000379	1.73589	0.6759	1.1732
Mucin and cadherin-like	NM_017717	1.69113	0.4702	0.7951
Solute carrier family 22 (organic cation transporter), member 18	NM_002555	1.67613	0.7613	1.276
Cathepsin G	NM_001911	1.66915	1.0134	1.6915
Transmembrane protease, serine 2	NM_005656	1.65278	0.5928	0.9797
LIM domain only 4	NM_006769	1.65052	0.9388	1.5495
Interleukin 2 receptor, gamma (severe combined immunodeficiency)	NM_000206	1.64826	0.6583	1.0851
Sphingomyelin phosphodiesterase 1, acid lysosomal (acid sphingomyelinase)	NM_000543	1.64106	0.6306	1.0349
Polymerase (DNA-directed), delta 4	AF179890	1.64078	0.6742	1.1062
Aminoacylase 1	NM_000666	1.63734	1.0587	1.7335
Tissue inhibitor of metalloproteinase 2	NM_003255	1.63344	0.7029	1.1482
Monoglyceride lipase	NM_007283	1.62443	0.555	0.9016
SH3 domain binding glutamic acid-rich protein like 3	AF304163	1.61052	0.977	1.5735
LIM domain 7	AF174600	1.60782	0.8544	1.3738

Table 1 (continued)

Gene name (abbreviation)	Genbank accession no.	SSA/TA	TA/reference	SSA/reference
Insulin receptor substrate 2	NM_003749	1.58909	0.9517	1.5123
Protease, serine, 3 (mesotrypsin)	NM_002771	1.57572	0.7223	1.1381
Clathrin, light polypeptide (Lcb)	NM_007097	1.5634	0.7902	1.2354
ERO1-like (S. cerevisiae)	NM_014584	1.56069	1.1604	1.811
DKFZP564O123 protein	NM_014043	1.54253	0.9399	1.4498
Dual specificity phosphatase 6	NM_001946	1.52714	0.9599	1.4659
Solute carrier organic anion transporter family, member 2A1	NM_005630	1.52197	0.6084	0.9259
Abhydrolase domain containing 2	AK000554	1.51958	1.173	1.7825
Calcium and integrin binding 1 (calmyrin)	NM_006384	1.50921	0.7664	1.1567
Similar to aspartate beta hydroxylase (ASPH)	NM_020437	1.50078	0.9398	1.4105
Basigin (OK blood group)	NM_001728	1.49584	0.4161	0.6224
Arylsulfatase A	NM_000487	1.48131	0.8368	1.2396
Protein tyrosine phosphatase, receptor type, H	NM_002842	1.47661	0.6163	0.9101

Most differentially expressed genes in SSAs (n=13) compared to TAs (n=13). Genes are given in the order of highest expression

routine techniques. Microwave antigen retrieval was performed in 10 mM citrate buffer (pH 6) for 15 min. After cooling to 30°C, the sections were incubated for 60 min at room temperature with primary monoclonal antibodies (dilutions: CTSE 1:100, TFF1 1:200). The polymer systems MACH4 (TFF1) or ADVANCE™HRP (CTSE) (DakoCytomation PTY LTD.) which employ diaminobenzidine were used as detection systems. Counterstaining was performed using Meyer's haematoxylin.

CTSE and TFF1 immunostaining was scored as negative, weakly positive (focal staining limited to the surface epithelium and upper portion of crypts) and strongly positive (strong staining extending to the base of crypts). Positive staining of colonocytes in lymphoglandular bodies served as internal control. Appropriate negative controls were performed for each batch of slides.

KRAS and BRAF mutation screening

DNA was prepared from tumour tissue macrodissected from formalin-fixed and paraffin-embedded (FFPE) slides using the QIAamp DNA FFPE Tissue kit (Qiagen). Screening for mutations in codons 12 and 13 of the KRAS gene was performed using a multiplex assay as described by Di Fiore et al. [30]. The V600E mutation in the BRAF gene was detected using a single-nucleotide primer extension assay comparable to the KRAS assay. Portion of exon 15 of the BRAF gene encompassing the V600E mutation was amplified, and the V600E mutation was detected using a SNaPshot multiplex kit (Applied Biosystems) and a specific primer (C_5TGATTTTGGTCTAGCTACAG). All reactions were run on a 3730 capillary sequencer (Applied Biosystems), and results were analysed using GeneMapper software version 4.0 (Applied Biosystems).

Results

Microarray

Microarray analysis was performed on 13 SSAs and 11 TAs. SSAs were from four men and nine women (mean age of 75), and TAs were from five men and six women (mean age of 72). Samples were directly hybridised to each other (SSA versus TA; matched, where possible, for sex and age) or to a pooled normal control (SSA versus control, TA versus control). A linear model [28] was fitted to the data bringing together the three contrasts: SSA versus control, TA versus control and SSA versus TA. Genes that were differentially expressed between SSAs and TAs were ranked on moderated t statistics [27]. As there is no consensus on appropriate adjustment of p values in the context of microarrays, this cutoff was chosen on a combination of statistical and biological indicators, and a list of the 65 genes with absolute values of t above 5.4 and expression ratios in SSAs to TAs either below 0.8 or above 1.37 is shown in Table 1. Figure 1 graphically demonstrates the most differentially expressed genes for each microarray sample set.

QRT-PCR

QRT-PCR was used to investigate expression changes in TFF1 and CTSE in 19 TAs, 16 SSAs and 15 HPs with values normalised with the level of GAPDH. Using Spearman's rank order correlations, a moderate to strong positive correlation between expression of CTSE and TFF1 in SSAs ($p<0.01$), HPs ($p<0.01$) and TAs ($p<0.05$) was found (Fig. 2).

CTSE expression was significantly up-regulated in SSAs compared to both HPs and TAs. Also, the expression of

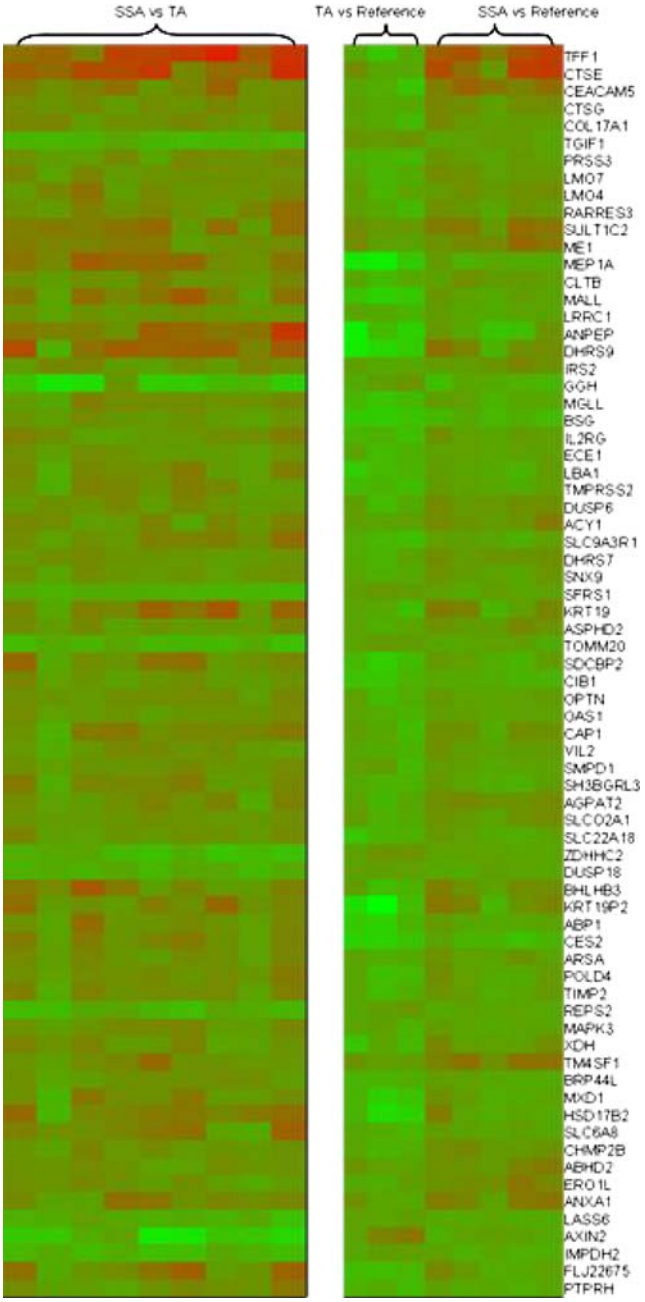

Fig. 1 Heat map showing the most differentially expressed genes for each microarray sample set, of polyp type-versus-normal (reference) expression. Genes are given in order of highest expression on the *vertical axis*. Sample set types are given on the *horizontal axis*. The expression values after normalization have been colour-coded (*green* down in expression; *red* increased expression.)

CTSE in HPs was significantly up-regulated compared with that of TAs. CTSE expression was found to be significantly up-regulated in SSAs compared to normal mucosa ($p<0.0001$), with 50% of samples showing a 25- to 96-fold increase in CTSE expression. CTSE expression in SSAs was significantly higher than in HPs ($p=0.003$) with 50% of samples having a 2.5- to 33-fold increased expression compared to normal mucosa and TAs ($p=0.002$). CTSE expression in TAs was not up-regulated compared to normal mucosa (Fig. 3a).

The expression of TFF1 was significantly up-regulated in SSAs and HPs compared with TAs ($p<0.005$ and $p=0.002$ respectively) and normal mucosa ($p<0.0001$ for both). The QRT-PCR analysis demonstrated TFF1 expression in SSAs with the middle 50% of values lying between 7.33- and 43.68-fold increases, for HP between 1.08 and 13.00 and for TA between 0.11 and 1.38. TFF1 expression was significantly higher in both SSA and HP compared to TA. Although TFF1 expression in SSAs did not reach a significantly higher expression than in HPs, the same trend as for CTSE was observed (Fig. 3b).

Immunohistochemistry

The expression microarray results were also validated by IHC staining for CTSE and TFF1 proteins, as these two genes were validated by QRT-PCR as being significantly up-regulated in SSAs compared to HPs and TAs (CTSE) and in SSAs and HPs compared to TAs (TFF1).

SSAs show strong, cytoplasmic expression of CTSE and TFF1 within the abnormal crypts in all 72 polyps examined (Fig. 4b, c). The staining abruptly ended in adjacent normal non-serrated crypts, with no transition phase between serrated and non-serrated crypts (Fig. 4c). CTSE staining was also present within single cells and groups of

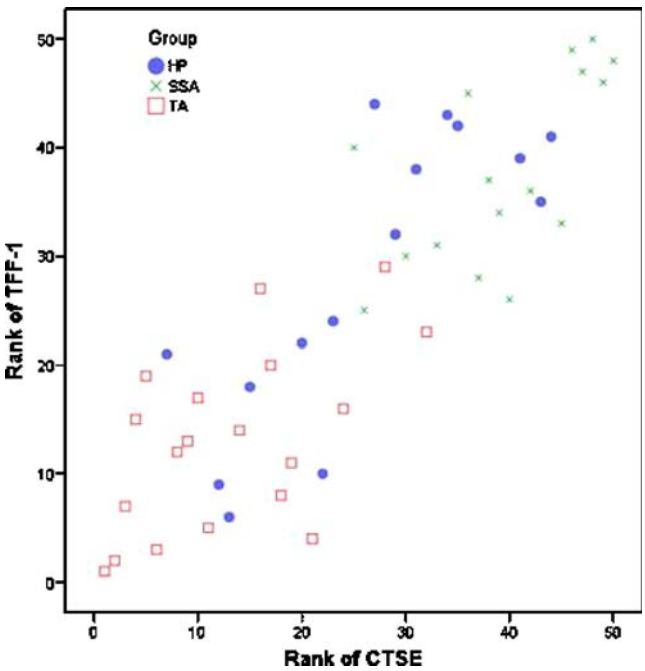

Fig. 2 CTSE and TFF1 expression had a moderate to strong and positive correlation for all three polyps types (SSA $p<0.01$, HP $p<0.01$ and TAs $p<0.05$). As CTSE expression increased, so too did TFF1

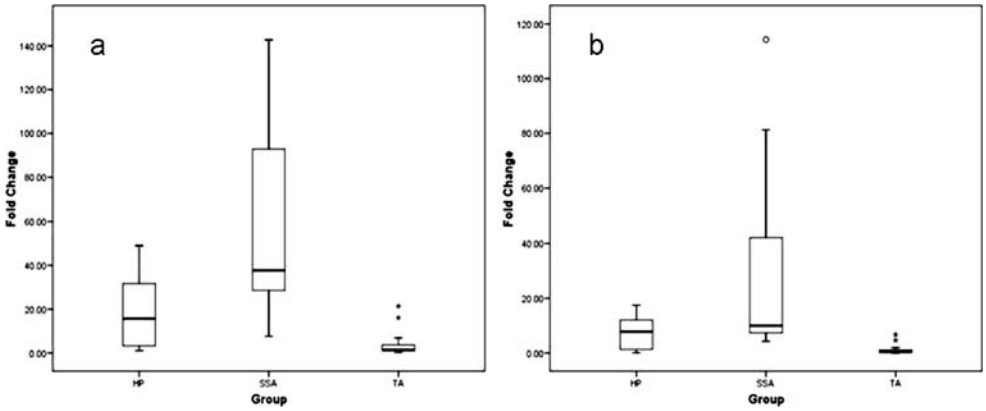

Fig. 3 Expression levels of CTSE (**a**) and TFF1 (**b**) by QRT-PCR in SSAs, HPs and TAs, compared to normal tissue (with a mean value of 1). *Box whisker plot* shows the 25th, 50th (median) and 75th percentiles for each group, the "whiskers" represent the minimum and maximum values. Expression levels for CTSE was significantly up-regulated in SSAs ($n=16$) compared to both TAs ($n=19$) ($p<0.005$), HPs ($n=15$) ($p=0.003$) and normal ($p<0.0001$) and also in HPs compared to TAs ($p=0.002$) and normal ($p<0.0001$). TFF1 was significantly up-regulated in SSAs and HPs compared to TAs ($p<0.005$ and $p=0.002$, respectively) and normal ($p<0.0001$ for both), and showed the same trend of expression in SSAs compared to HPs, although not reaching significance

colonocytes of the lymphoglandular complexes providing a useful internal positive control for this antibody.

All TAs (99 cases) were negative for CTSE and TFF1 staining (Fig. 4h–j). Of 85 HPs tested, 82 showed weak and focal CTSE (Fig. 4f) and TFF1 (Fig. 4g) staining of surface epithelium and superficial portions of abnormal crypts. IHC for the remaining three HPs showed significant background staining. These cases were considered technical failures and could not be critically assessed.

KRAS and BRAF mutation screening

Of the polyps used for IHC and QRT-PCR experiments, 62 had sufficient tissue available and were deemed suitable for the assessment of KRAS and BRAF mutations. The incidence of KRAS and BRAF mutations and their relationship to pathological diagnosis is shown in Table 2.

Discussion

We performed gene expression profiling of SSAs, TAs and normal colonic mucosa and validated these results with QRT-PCR and immunohistochemistry. Our results demonstrate over-expression of CTSE and TFF1 in SSAs compared to HPs and TAs.

CTSE is an intracellular aspartic protease which is predominantly present in dendritic cells of the immune system and is implicated in antigen processing and presentation [31]. Interestingly, CTSE has also been demonstrated in the neoplastic proliferation of dendritic derived cells (Langerhans' cell histiocytosis) and related atypical histiocytic proliferation (sinus histiocytosis with massive lymphadenopathy) [32]. The role of CTSE in the antigen processing function within the MHCII class pathway has been supported not only by the presence of this protein in human myeloid dendritic cells but also by the demonstration of disruption of antigen processing by the selective inhibition of aspartic proteinase in an animal model [33]. The predicted sequence of human CTSE was determined using gastric adenocarcinoma cell lines, and the CTSE gene was subsequently localised on human chromosome 1 [34].

CTSE is expressed in 75% of gastric adenocarcinomas; however, its prevalence depends on the histological type of tumour. It is most frequent in diffuse gastric carcinomas while in mucinous type is observed only in 32% [35]. CTSE has been suggested as a potential marker of human pancreatic cancer as it was found to be present in pancreatic ductal adenocarcinoma cells and pancreatic juice and absent in normal pancreatic ductal epithelium [36–38]. Expression of CTSE in uterine cervical adenocarcinomas was interpreted as differentiation towards gastrointestinal and pancreatobiliary epithelium, but CTSE was also found in the squamous epithelium of cervical intra-epithelial neoplasia lesions [39, 40].

The role and expression of CTSE in normal human colorectal mucosa and epithelial tumours has not been comprehensively investigated. CTSE positive cells have been reported in the epithelial cells of lymphoglandular complexes (intestinal follicle-associated epithelium) with a majority of positive cells having M-cell morphology [41, 42]. These observations are concordant with our findings of strong cytoplasmic expression of CTSE in scattered epithelial cells of the lymphoglandular complexes, which conveniently served as internal control for immunohistochemistry. Protein expression of CTSE was examined by IHC in a study primarily investigating the characteristics of

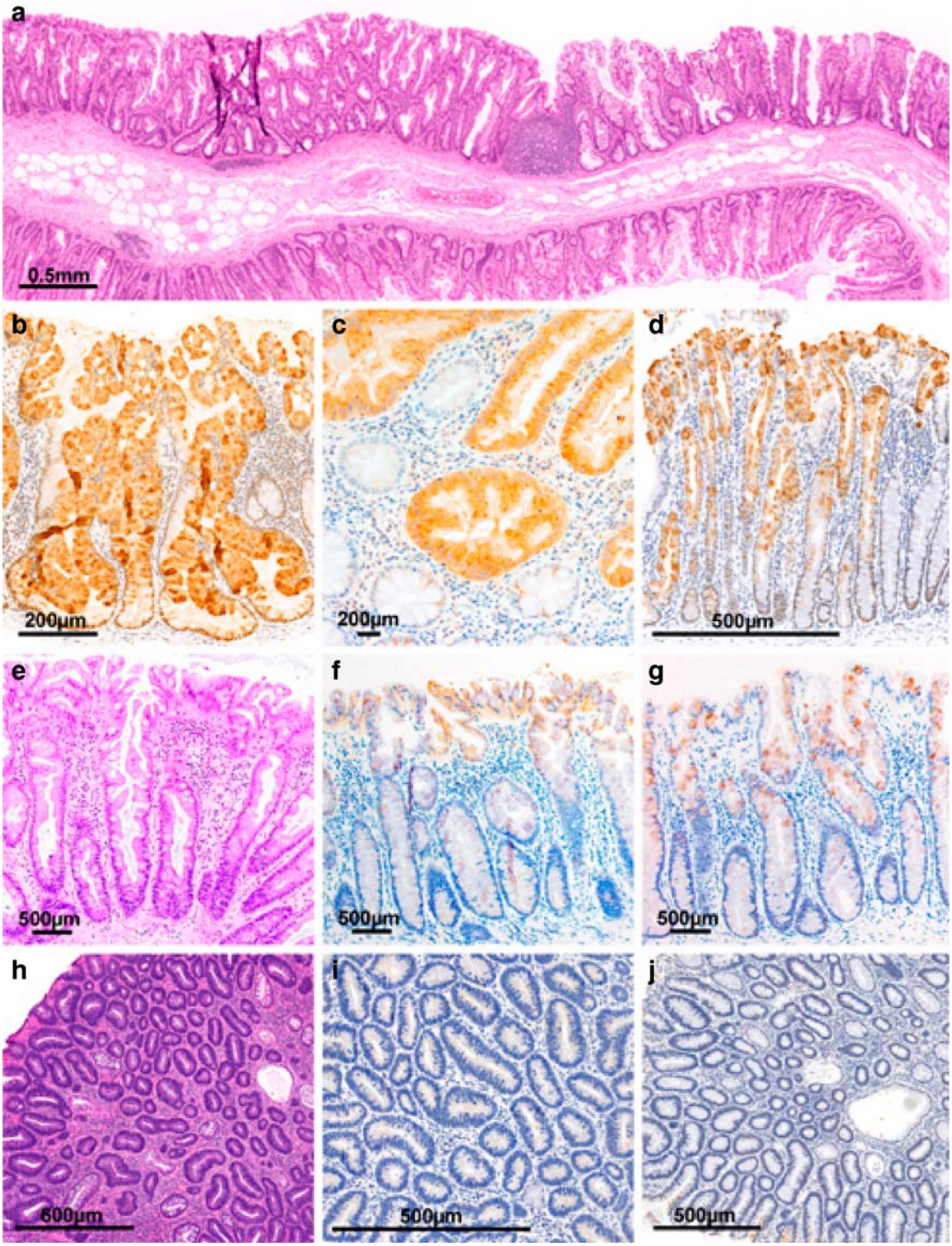

Fig. 4 Sessile serrated adenoma morphology, with configuration resembling wide mucosal fold. There is basal dilatation, branching and horizontal orientation of abnormal crypts with excessive serration extending to the crypt base (H&E stain) (**a**). CTSE in SSAs (**b**, c) showed strong cyotplasmic expression which extended through the entirety of all abnormal crypts. The absence of staining in normal crypts contrasted strongly with adjacent positively staining serrated crypts (**c**). TFF1 expression (**d**) was strong and extended toward the base of abnormal crypts in all SSAs examined. Hyperplastic polyp morphology shows straight, unbranched and elongated crypts (H&E stain) (**e**). Absent or weak CTSE staining was seen in the superficial portions of abnormal crypts in HPs (**f**). Similar weak superficial staining was noted for TFF1 (**g**). Tubular adenomas, composed of tubular formation crypts (H&E stain) (**h**), were negative for CTSE (**i**) and TFF1 (**j**) protein

Table 2 The incidence of BRAF and KRAS mutations and their relationship to pathological diagnosis

	Total	KRAS (%)	BRAF (%)
All samples	62	23 (36.5)	27 (42.9)
SSA	23	1 (4.3)	21 (91)[a]
HP	19	12 (63.2)	6 (31.6)
TA	20	10 (50)[b]	0 (0)

[a] Fisher's exact test, SSA versus HP, $p<0.001$; SSA versus TA, $p<0.001$
[b] Fisher's exact test, TA versus HP, $p=0.049$; TA versus SSA, $p<0.001$

M cells on a limited number of colorectal adenomas and hyperplastic polyps, showing positivity in scattered and superficial cells in seven of eight colorectal adenomas and widespread cytoplasmic staining in four of five hyperplastic/metaplastic polyps [42]. While there is a minor difference with our negative results of CTSE in TAs, this may represent methodological differences related to staining interpretation and use of polyclonal versus monoclonal antibodies. QRT-PCR results in our study demonstrated no change in the expression of CTSE in TAs comparing to normal mucosa, which supports our negative result for protein expression of CTSE in TA tissue on immunostaining.

A more important discordance is between results of CTSE expression in hyperplastic polyps in both studies. The reported "widespread" cytoplasmic staining in hyperplastic polyps contrasts with our results but may not be totally dissimilar. We found expression in HPs was weak and limited mainly to the surface epithelium and upper portions of serrated crypts, which may have been interpreted as "widespread" by the authors. Also, it is important to note that, at the time of publication of that study, the "sessile serrated adenoma" concept was evolving, and as such, this variant of hyperplastic polyps was not generally reported by pathologists. Significantly, the authors did not discriminate between various subtypes of serrated or hyperplastic polyps, and the provided photograph of "hyperplastic" polyp included a superficial portion of crypts and surface epithelium where expression of CTSE protein was demonstrated in our study. More importantly, our results of CTSE protein expression in TAs, SSAs and HPs were concordant with results of CTSE gene expression in RT-PCR experiments where CTSE expression was significantly up-regulated in SSAs compared to both HPs and TAs.

In a recent animal study, semi-quantitative RT-PCR of colonic adenomas in $APC^{Min/+}$ mice found CTSE to be up-regulated compared to normal mucosa. Furthermore, IHC analysis showed strong CTSE staining in the mice adenomas, whereas normal tissues showed no expression [43]. The disparity with our results, with TAs found to have negative CTSE expression, and those in the study by Busquets et al. [43], may be attributed to the use of the $APC^{Min/+}$ mouse model. This specific genetic defect accounts for all the cancers developed by this animal tumour model, whereas, in humans there may be many genetic reasons, environmental triggers or other predispositions which lead to the development of colorectal lesions and/or cancer.

As was predicted by the microarray results, QRT-PCR demonstrated the expression of TFF1 is significantly up-regulated in SSAs and HPs compared with TAs. Although TFF1 expression in SSAs did not reach a significantly higher expression than in HP, the same trend as CTSE expression was observed. IHC analysis of SSAs showed strong, cytoplasmic expression within the abnormal crypts of all polyps examined, with no staining in normal non-serrated crypts. While in HPs weak focal staining was only observed in the upper portions of serrated crypts, all TAs were negative for TFF1.

TFF1 (pS2) belongs to the trefoil factor family and was originally identified as an estrogen-induced protein in the MCF-7 breast cancer cell line [44, 45]. TFF1 protein is expressed in the mucus-secreting mucosal lining of the gastrointestinal tract and is primarily expressed in the stomach and colon [46, 47]. The main function of trefoil factors including TFF1 is mucosal protection through mucus stabilisation and stimulation of epithelial restitution after injury [48, 49].

Up-regulation of mucosal TFF1 expression and elevated serum levels of TFF1 in patients with inflammatory bowel disease including ulcerative colitis and Crohn's disease is suggestive of TFF1 being a potential marker of disease activity [48, 50, 51]. There is also extensive evidence of the increased expression of TFF1 in different types of tumours. TFF1 has been found to be over-expressed in gastric cancer [52], colon cancer, lung adenocarcinoma and pancreatic cancer [53–56].

The secretion of neutral mucin in hyperplastic polyps and in chronic inflammatory bowel conditions such as Crohn's disease prompted the investigation of TFF1 (pS2) in a series of 17 hyperplastic polyps [57]. This study showed TFF1 immunostaining in the upper three quarters of the crypts and mRNA for TFF1 signal in the upper portions of crypts in hyperplastic polyps. While these results are not dissimilar to our findings, it should be noted that this study was performed when SSAs were not recognised as a pathological entity, and some of these polyps may, in fact, be SSAs. SSAs have evaded pathologists over the decades, and differentiation of HPs and SSAs is still a diagnostic dilemma in daily practice; therefore, finding a reliable marker would be highly desirable from a practical point of view. In a recent study of SSAs, HPs and traditional SAs, expression of TFF1 was not discriminatory for SSAs and HPs nor was expression of

MUC6 as demonstrated by immunohistochemistry [58]. However, other authors have claimed the MUC6 protein as being exclusively expressed in SSAs and not in HPs [59].

In an early study, TFF1 was shown to have significantly higher expression in right-sided colorectal tumours than in left. Also, TFF1 was found to be significantly more expressed in mucinous tumours which were mostly located in the right colon [60]. The current classification of SSA and serrated pathway CRCs were not in practice in 1993. It may be assumed that the mucinous right-sided cancers from this study are in fact CRCs arising via the serrated pathway from SSA precursor lesions. This correlates with our data trend showing TFF1 expression is higher in SSAs, which are mostly found in the right colon, than in HP found mostly in the left, and implicates TFF1 as having a role in the progression from SSA to CRC. This is further supported by studies which show TFF1 expression progresses from absent in normal colon tissue to strong expression in premalignant cells and present but varied expression in adenocarcinomas of the colon [53, 61]. In a recent study, premalignant cells transduced to force the expression of TFF1 were injected into mice. These cells obtained tumourogenic potential and increased the speed of tumour onset, growth rate and invasiveness of the tumours compared to cells which were not transduced, indicating TFF1 over-expression is a step in the early transition from premalignant cells to neoplastic [61]. Our findings may also indicate the increased expression of TFF1 in SSAs as a potential marker for the transition to neoplasia.

BRAF is associated with the RAS–RAF–MEK–ERK–MAP pathway, which is responsible for the mediation of cellular responses to proliferation signals. The V600E BRAF mutation (previously reported as V599E) in the kinase domain [62, 63] mimics regulatory phosphorylation and leads to the constitutive activation of the MAP kinase pathway, independent of KRAS activation [64]. The occurrence of the BRAF mutation V600E has previously been reported as a potential discriminator of SSAs from other polyp types [19, 65]. We have found the BRAF mutation in 42.9% of polyps examined and 91% of SSAs studied, which concurs with a previous finding of 43% and 81%, respectively [19]. Similarly, Chan et al. found 36% of non-dysplastic hyperplastic polyps exhibited the V600E BRAF mutation [66]. In addition, there were no cases of BRAF and KRAS mutations occurring concurrently in any of the polyps analysed, and this is supported by studies showing that BRAF and KRAS mutations are mutually exclusive in colorectal polyps [19, 62, 63]. We believe our data, showing the high incidence of BRAF mutations in SSAs (91%) and HPs (31.6%; notably, some HPs may be small SSAs) compared to no BRAF mutations found in TAs lends substantial weight to our morphological classification of polyps.

In the present study, the expression of CTSE has been shown to be significantly higher in SSAs than in HP or TAs, and the expression of TFF1 was shown to follow the same trend. BRAF mutations were also found to be associated with SSAs compared to the other two groups. We have shown CTSE and TFF1 expression to be correlated in SSAs, HPs and TAs. While our data suggest that expression of these proteins, CTSE in particular, and the incidence of the V600E mutation differs amongst the common colorectal polyp types, their discriminatory potential in a diagnostic setting remains to be further validated and tested. Our study has demonstrated SSAs as having molecular features which are distinct from conventional adenomas and hyperplastic polyps.

Ethics

The study was approved by the Ethics Committees of participating institutions.

Informed, written consent was obtained from all patients who were enrolled into the study. The study complied with the appropriate institutional guidelines.

Acknowledgements The authors thank Kay Taylor, Gastroenterology Research Laboratory, SA Pathology, for her technical assistance with the immunohistochemistry and Nancy Brigs for her assistance with the statistical analysis. This study was supported by Cancer and Bowel Research Trust, SA, Australia.

Conflict of interest The authors declare that they have no conflict of interest.

References

1. Iino H, Simms L, Young J et al (2000) DNA microsatellite instability and mismatch repair protein loss in adenomas presenting in hereditary non-polyposis colorectal cancer. Gut 47:37–42
2. Jass JR, Iino H, Ruszkiewicz A et al (2000) Neoplastic progression occurs through mutator pathways in hyperplastic polyposis of the colorectum. Gut 47:43–49
3. Hawkins NJ, Ward RL (2001) Sporadic colorectal cancers with microsatellite instability and their possible origin in hyperplastic polyps and serrated adenomas. J Natl Cancer Inst 93:1307–1313
4. Jass JR (2001) Serrated route to colorectal cancer: back street or super highway? J Pathol 193:283–285
5. Young J, Biden KG, Simms LA et al (2001) HPP1: a transmembrane protein-encoding gene commonly methylated in colorectal polyps and cancers. Proc Natl Acad Sci U S A 98:265–270
6. Chan AO, Issa JP, Morris JS et al (2002) Concordant CpG island methylation in hyperplastic polyposis. Am J Pathol 160:529–536
7. Park SJ, Rashid A, Lee JH et al (2003) Frequent CpG island methylation in serrated adenomas of the colorectum. Am J Pathol 162:815–822
8. Jass JR (1999) Serrated adenoma and colorectal cancer. J Pathol 187:499–502

9. Jass JR (2003) Serrated adenoma of the colorectum: a lesion with teeth. Am J Pathol 162:705–708
10. Torlakovic E, Skovlund E, Snover DC et al (2003) Morphologic reappraisal of serrated colorectal polyps. Am J Surg Pathol 27:65–81
11. Longacre TA, Fenoglio-Preiser CM (1990) Mixed hyperplastic adenomatous polyps/serrated adenomas. A distinct form of colorectal neoplasia. Am J Surg Pathol 14:524–537
12. Sandmeier D, Seelentag W, Bouzourene H (2007) Serrated polyps of the colorectum: is sessile serrated adenoma distinguishable from hyperplastic polyp in a daily practice? Virchows Arch 450:613–618
13. Tuppurainen K, Makinen JM, Junttila O et al (2005) Morphology and microsatellite instability in sporadic serrated and non-serrated colorectal cancer. J Pathol 207:285–294
14. Laiho P, Kokko A, Vanharanta S et al (2007) Serrated carcinomas form a subclass of colorectal cancer with distinct molecular basis. Oncogene 26:312–320
15. Makinen MJ (2007) Colorectal serrated adenocarcinoma. Histopathology 50:131–150
16. O'Brien MJ, Yang S, Mack C et al (2006) Comparison of microsatellite instability, CpG island methylation phenotype, BRAF and KRAS status in serrated polyps and traditional adenomas indicates separate pathways to distinct colorectal carcinoma end points. Am J Surg Pathol 30:1491–1501
17. Kambara T, Simms LA, Whitehall VL et al (2004) BRAF mutation is associated with DNA methylation in serrated polyps and cancers of the colorectum. Gut 53:1137–1144
18. Jass JR (2004) Hyperplastic polyps and colorectal cancer: is there a link? Clin Gastroenterol Hepatol 2:1–8
19. Jass JR, Baker K, Zlobec I et al (2006) Advanced colorectal polyps with the molecular and morphological features of serrated polyps and adenomas: concept of a 'fusion' pathway to colorectal cancer. Histopathology 49:121–131
20. Farris AB, Misdraji J, Srivastava A et al (2008) Sessile serrated adenoma: challenging discrimination from other serrated colonic polyps. Am J Surg Pathol 32:30–35
21. Smith FB, Aksenov S (2007) Potential role of nuclear appearance in pathologic recognition and delimitation of sessile serrated polyps of the colon: a karyometric study. Anal Quant Cytol Histol 29:326–332
22. Torlakovic EE, Gomez JD, Driman DK et al (2008) Sessile serrated adenoma (SSA) vs. traditional serrated adenoma (TSA). Am J Surg Pathol 32:21–29
23. Goldstein NS, Bhanot P, Odish E et al (2003) Hyperplastic-like colon polyps that preceded microsatellite-unstable adenocarcinomas. Am J Clin Pathol 119:778–796
24. Snover DC, Jass JR, Fenoglio-Preiser C et al (2005) Serrated polyps of the large intestine: a morphologic and molecular review of an evolving concept. Am J Clin Pathol 124:380–391
25. Yang YH, Buckley MJ, Speed TP (2001) Analysis of cDNA microarray images. Brief Bioinform 2:341–349
26. Ritchie ME (2004) Quantitative quality control and background correction for two-color microarray data. Melbourne, University of Melbourne. Ph.D. thesis:1–139
27. Gentleman RC, Carey VJ, Bates DM et al (2004) Bioconductor: open software development for computational biology and bioinformatics. Genome Biol 5:R80
28. Smyth GK (2004) Linear models and empirical bayes methods for assessing differential expression in microarray experiments. Stat Appl Genet Mol Biol 3:Article3
29. Yang YH, Dudoit S, Luu P et al (2002) Normalization for cDNA microarray data: a robust composite method addressing single and multiple slide systematic variation. Nucleic Acids Res 30:e15
30. Di Fiore F, Blanchard F, Charbonnier F et al (2007) Clinical relevance of KRAS mutation detection in metastatic colorectal cancer treated by Cetuximab plus chemotherapy. Br J Cancer 96:1166–1169
31. Zaidi N, Kalbacher H (2008) Cathepsin E: a mini review. Biochem Biophys Res Commun 367:517–522
32. Paulli M, Feller AC, Boveri E et al (1994) Cathepsin D and E co-expression in sinus histiocytosis with massive lymphadenopathy (Rosai-Dorfman disease) and Langerhans' cell histiocytosis: further evidences of a phenotypic overlap between these histiocytic disorders. Virchows Arch 424:601–606
33. Chain BM, Free P, Medd P et al (2005) The expression and function of cathepsin E in dendritic cells. J Immunol 174:1791–1800
34. Azuma T, Pals G, Mohandas TK et al (1989) Human gastric cathepsin E. Predicted sequence, localization to chromosome 1, and sequence homology with other aspartic proteinases. J Biol Chem 264:16748–16753
35. Fiocca R, Villani L, Tenti P et al (1990) The foveolar cell component of gastric cancer. Hum Pathol 21:260–270
36. Sessa F, Bonato M, Frigerio B et al (1990) Ductal cancers of the pancreas frequently express markers of gastrointestinal epithelial cells. Gastroenterology 98:1655–1665
37. Azuma T, Hirai M, Ito S et al (1996) Expression of cathepsin E in pancreas: a possible tumor marker for pancreas, a preliminary report. Int J Cancer 67:492–497
38. Uno K, Azuma T, Nakajima M et al (2000) Clinical significance of cathepsin E in pancreatic juice in the diagnosis of pancreatic ductal adenocarcinoma. J Gastroenterol Hepatol 15:1333–1338
39. Tenti P, Romagnoli S, Silini E et al (1994) Cervical adenocarcinomas express markers common to gastric, intestinal, and pancreatobiliary epithelial cells. Pathol Res Pract 190:342–349
40. Mota F, Kanan JH, Rayment N et al (1997) Cathepsin E expression by normal and premalignant cervical epithelium. Am J Pathol 150:1223–1229
41. Finzi G, Cornaggia M, Capella C et al (1993) Cathepsin E in follicle associated epithelium of intestine and tonsils: localization to M cells and possible role in antigen processing. Histochemistry 99:201–11
42. Wong NA, Herriot M, Rae F (2003) An immunohistochemical study and review of potential markers of human intestinal M cells. Eur J Histochem 47:143–150
43. Busquets L, Guillen H, DeFord ME et al (2006) Cathepsin E is a specific marker of dysplasia in APC mouse intestine. Tumour Biol 27:36–42
44. Jakowlew SB, Breathnach R, Jeltsch JM et al (1984) Sequence of the pS2 mRNA induced by estrogen in the human breast cancer cell line MCF-7. Nucleic Acids Res 12:2861–2878
45. Nunez AM, Jakowlev S, Briand JP et al (1987) Characterization of the estrogen-induced pS2 protein secreted by the human breast cancer cell line MCF-7. Endocrinology 121:1759–1765
46. Madsen J, Nielsen O, Tornoe I et al (2007) Tissue localization of human trefoil factors 1, 2, and 3. J Histochem Cytochem 55:505–513
47. Perry JK, Kannan N, Grandison PM et al (2008) Are trefoil factors oncogenic? Trends Endocrinol Metab 19:74–81
48. Rio MC, Chenard MP, Wolf C et al (1991) Induction of pS2 and hSP genes as markers of mucosal ulceration of the digestive tract. Gastroenterology 100:375–379
49. Playford RJ (1997) Trefoil peptides: what are they and what do they do? J R Coll Physicians Lond 31:37–41
50. Gronbaek H, Vestergaard EM, Hey H et al (2006) Serum trefoil factors in patients with inflammatory bowel disease. Digestion 74:33–39
51. Longman RJ, Poulsom R, Corfield AP et al (2006) Alterations in the composition of the supramucosal defense barrier in relation to disease severity of ulcerative colitis. J Histochem Cytochem 54:1335–1348

52. Ren JL, Luo JY, Lu YP et al (2006) Molecular forms of trefoil factor 1 in normal gastric mucosa and its expression in normal and abnormal gastric tissues. World J Gastroenterol 12:7361–7364
53. Welter C, Theisinger B, Rio MC et al (1994) Expression pattern of breast-cancer-associated protein pS2/BCEI in colorectal tumors. Int J Cancer 56:52–55
54. Tuna B, Sokmen S, Sarioglu S et al (2006) PS2 and HSP70 expression in rectal adenocarcinomas: an immunohistochemical investigation of 45 cases. Appl Immunohistochem Mol Morphol 14:31–36
55. Higashiyama M, Doi O, Kodama K et al (1996) Estimation of serum level of pS2 protein in patients with lung adenocarcinoma. Anticancer Res 16:2351–2355
56. Prasad NB, Biankin AV, Fukushima N et al (2005) Gene expression profiles in pancreatic intraepithelial neoplasia reflect the effects of Hedgehog signaling on pancreatic ductal epithelial cells. Cancer Res 65:1619–1626
57. Hanby AM, Poulsom R, Singh S et al (1993) Hyperplastic polyps: a cell lineage which both synthesizes and secretes trefoil-peptides and has phenotypic similarity with the ulcer-associated cell lineage. Am J Pathol 142:663–668
58. Mochizuka A, Uehara T, Nakamura T et al (2007) Hyperplastic polyps and sessile serrated 'adenomas' of the colon and rectum display gastric pyloric differentiation. Histochem Cell Biol 128:445–455
59. Owens SR, Chiosea SI, Kuan SF (2008) Selective expression of gastric mucin MUC6 in colonic sessile serrated adenoma but not in hyperplastic polyp aids in morphological diagnosis of serrated polyps. Mod Pathol 21:660–669
60. Shousha S, Luqmani YA, Sannino P et al (1993) pS2 immunostaining of colorectal carcinoma. Mod Pathol 6:446–448
61. Rodrigues S, Rodrigue CM, Attoub S et al (2006) Induction of the adenoma-carcinoma progression and Cdc25A-B phosphatases by the trefoil factor TFF1 in human colon epithelial cells. Oncogene 25:6628–6636
62. Rajagopalan H, Bardelli A, Lengauer C et al (2002) Tumorigenesis: RAF/RAS oncogenes and mismatch-repair status. Nature 418:934
63. Yuen ST, Davies H, Chan TL et al (2002) Similarity of the phenotypic patterns associated with BRAF and KRAS mutations in colorectal neoplasia. Cancer Res 62:6451–6455
64. Davies H, Bignell GR, Cox C et al (2002) Mutations of the BRAF gene in human cancer. Nature 417:949–954
65. Yang S, Farraye FA, Mack C et al (2004) BRAF and KRAS Mutations in hyperplastic polyps and serrated adenomas of the colorectum: relationship to histology and CpG island methylation status. Am J Surg Pathol 28:1452–1459
66. Chan TL, Zhao W, Leung SY et al (2003) BRAF and KRAS mutations in colorectal hyperplastic polyps and serrated adenomas. Cancer Res 63:4878–4881

Virchows Arch (2009) 454:303–310
DOI 10.1007/s00428-009-0733-y

ORIGINAL ARTICLE

Congenital granular cell epulis presents an immunohistochemical profile that distinguishes it from the granular cell tumor of the adult

Marilena Vered · Alex Dobriyan · Amos Buchner

Received: 26 November 2008 / Accepted: 8 January 2009 / Published online: 11 February 2009

Abstract Congenital granular cell epulis (CGCE), a rare benign lesion arising from the mucosa of the alveolar ridges of the jaws in newborns, has a clinical course characterized by lack of further growth after birth. Histomorphologically, it resembles a granular cell tumor (GCT) of the adult. The histogenesis of this lesion is unclear. We submitted a series of five CGCEs to a large panel of antibodies in order to trace the origin of the constituent granular cells. The resultant immunohistochemical profile showed positivity of these cells to vimentin, NKI/C3, and PGP9.5. This does not confirm any particular cell type for the histogenetic origin of CGCE but may rather reflect a local metabolic or reactive change, providing supporting evidence that the lesion is of a non-neoplastic nature. In addition, the granular cells were non-reactive for S-100, NGFR/p75, and inhibin-α, which further contributes to the distinction between a CGCE and the adult GCT.

Keywords Congenital granular cell epulis · Granular cell tumor · Immunohistochemistry · Origin

M. Vered (✉) · A. Buchner
Department of Oral Pathology and Oral Medicine,
Goldschleger School of Dental Medicine, Tel Aviv University,
Tel Aviv, Israel
e-mail: mvered@post.tau.ac.il

M. Vered
Institute of Pathology, The Chaim Sheba Medical Center,
Tel Hashomer, Israel, affiliated to the Sackler Faculty of Medicine,
Tel Aviv University,
Tel Aviv, Israel

A. Dobriyan · A. Buchner
Department of Oral and Maxillofacial Surgery,
The Chaim Sheba Medical Center, Tel Hashomer, Israel,
affiliated to the Sackler Faculty of Medicine, Tel Aviv University,
Tel Aviv, Israel

Introduction

A congenital granular cell epulis (CGCE) is a unique and rare benign lesion arising from the mucosa of the alveolar ridges of the jaws in newborns. This terminology was suggested by the newest histological classification of the World Health Organization [1], but the lesion is also known in recent literature under a variety of names, including congenital epulis, congenital epulis of the newborn, congenital granular cell tumor, congenital granular cell lesion, and gingival granular cell tumor of the newborn.

CGCE is found almost exclusively on the alveolar mucosa of newborns, and it occurs three times as often in the maxilla as in the mandible. Most lesions are located in the anterior region of the jaws. CGCE is predominantly a lesion of females, with a male-to-female ratio of 1:10 [2]. Clinically, it usually presents as a pedunculated nodule of less than 2 cm in size [3, 4], although larger lesions have been reported, some even large enough to protrude from the mouth [5–7]. Most lesions are single, but multiple lesions may also occur on the same or different alveolar ridges [2, 4]. Rarely, a congenital granular cell lesion may occur in the anterior ventral surface of the tongue, either alone or with simultaneous lesions on the alveolar ridge [8, 9].

Histologically, a CGCE is similar to a granular cell tumor (GCT) of adults and is composed of large, slightly eosinophilic cells with granular cytoplasm. Pseudoepitheliomatous hyperplasia of the overlying mucosa, which is common in GCTs, does not, however, occur in CGCEs.

The histogenesis of CGCEs has, thus far, remained enigmatic in spite of a vast number of immunohistochemical and ultrastructural studies. Several theories have been proposed, including origins from odontogenic epithelium, fibroblasts, histiocytes, smooth muscle, nerve-related cells, endothelial cells, pericytes, myofibroblasts, and

undifferentiated mesenchymal cells (Table 1) [6, 10–25]. In search of the origin of the granular cells, numerous epithelial, myogenous, neurogenous, neuroendocrine, vascular, fibroblastic, histiocytic, and hormonal immunostains have been tested. With the exception of vimentin, they were all found to be negative in most of the studies, including the S-100 protein that is positive in GCT. Neuron-specific enolase (NSE) was found to be positive in some studies of CGCE [20, 22, 25–28] and negative in others [3, 21, 24, 29].

One of the main deficiencies of immunohistochemical studies on CGCEs is due to its rarity, with most studies having been performed on one or two lesions and only a few on 3–5 lesions. Reaching a meaningful conclusion from a single lesion or a very small series is invariably difficult.

The aim of this study is twofold: to expand the present knowledge on CGCE by reassessing the immunohistochemical profile of the lesional cells in five unreported lesions by means of new immunohistochemical markers that have been recently used in studies of adult GCTs and to compare the findings of CGCEs with those of adult oral GCTs.

Material and methods

The study consisted of a series of five heretofore unreported cases of CGCE. All the patients were females: four cases were from the anterior maxillary alveolar ridge (Fig. 1) and one was from the anterior mandibular ridge. The lesions were excised between postpartum days 1–14.

The immunoreactivity of the granular cells was examined by a panel of ten commercially available primary antibodies, both traditional and new ones (Table 2). This extensive panel of immunostains was chosen to determine the immunoprofile of CGCE lesions and, in addition, to enable us to compare it to a large series of oral GCTs, which we recently examined using a similar panel of immunostains. Immunostaining was detected by using a SuperPicTure™ polymer kit (Zymed–Invitrogen, Carlsbad, CA, USA) according to the manufacturer's recommendations. For negative controls, the slides were treated with the same procedures, including antigen retrieval, except for the application of the primary antibodies.

Immunohistochemical stain assessment of the granular cells

Immunoreactivity was semiquantitatively scored according to the method of Laskin et al. [30]: 0 = no detectable immunoreactivity, 1 = 1–10% of the tumor cells are reactive, 2 = 11–25% of the tumor cells are reactive, 3 = 26–50% of the tumor cells are reactive, and 4 = >50% of the tumor cells are reactive. In addition, immunoreactivity was graded according to the staining intensity as performed by Williams and Williams [31] and Fine and Li [32]: '–' = negative, '+' = weak; '++' = moderate, and '+++' = strong.

Table 1 Suggested cell of origin for congenital granular cell epulis according to the chronologic order of studies and means of investigation

Cell of origin	Authors, year [reference]	Means of investigation
Epithelial cells	Kay et al., 1971 [10]	EM
Undifferentiated mesenchymal cells that undergo cytoplasmic autophagocytosis	Regezi et al., 1979 [11]	EM
Pericytes	Rohrer and Young, 1982 [12]	EM
Histiocytes and fibroblasts	Lack et al., 1982 [13]	EM
Primitive mesenchymal cells with smooth muscle/ myofibroblastic differentiation	Zarbo et al., 1983 [14]	EM + IHC
Fibroblasts	Kameyama et al., 1993 [15]	EM + IHC
Mesenchymal cells	Slootweg et al., 1983 [16]	IHC
Mesenchymal cells	Lifshitz et al., 1984 [17]	EM + IHC
Neural-related mesenchymal cells	Nanthrath and Remberger 1986 [18]	IHC
Myofibroblasts and fibroblasts	Dastur and Manghani, 1988 [19]	EM
Nerve-related mesenchymal cells	Takahashi et al., 1990 [20]	IHC
Myofibroblasts	Tucker et al., 1990 [21]	EM + IHC
Early mesodermal cells that express pericytic and myofibroblastic features that undergo autophagocytosis	Damm et al., 1993 [22]	EM + IHC
Mesenchymal cells	Hoshi et al., 1995 [23]	IHC
Uncommitted mesenchymal cells	Filie et al., 1996 [24]	IHC
Uncommitted nerve-related mesenchymal cells	Ugras et al., 1997 [25]	IHC
Histiocytes and fibroblasts	Lapid et al., 2001 [6]	EM + IHC

EM electron microscopy, *IHC* immunohistochemistry

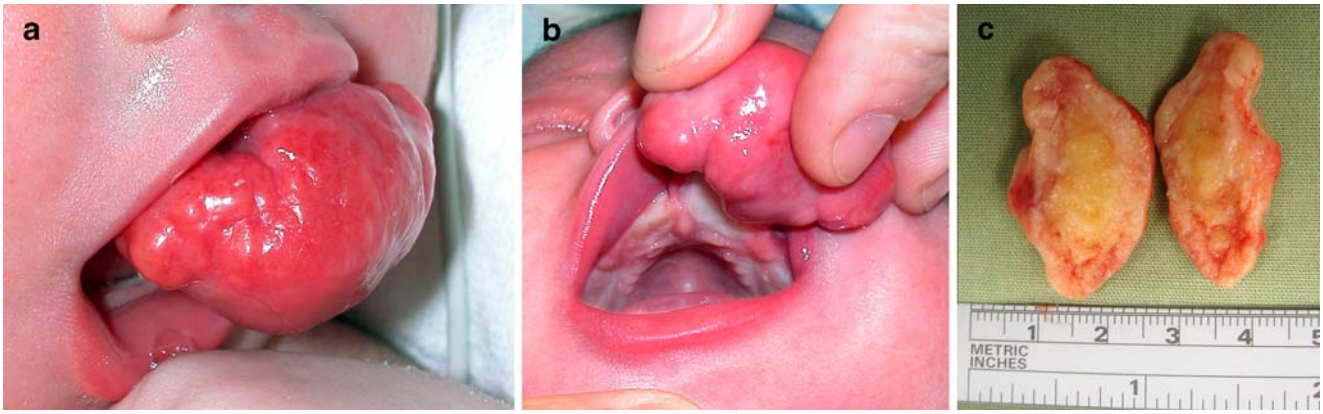

Fig. 1 **a** A congenital granular cell epulis in the anterior maxillary alveolar ridge preventing normal closure of the mouth of a newborn; **b** the lesion is pedunculated; **c** the excised lesion measured about 3 cm in its greatest diameter

Results

Histopathological findings

The histomorphology of the five lesions was similar. The mucosal mass was composed of closely packed, large, rounded, and polyhedral cells with slightly eosinophilic granular cytoplasm (Fig. 2). Non-granular, medium-sized polyhedral cells and elongated forms were occasionally seen (interstitial cells). The cell membranes were prominent in most areas, while they were delicate and indistinct in others, thereby creating an impression of syncytium. The granular cells extended to the overlying epithelium in two lesions and a narrow band of fibrovascular connective tissue separated the granular cells from the surface epithelium in three lesions. The nuclei of the cells were usually small, dark, round-to-oval in shape, and placed somewhat eccentrically. Some nuclei appeared to be vesicular with a well-defined nucleolus.

A prominent and complex network of vascular channels, ranging from small capillaries to dilated vessels, was regularly dispersed between the granular cells. Some vessels had well-developed walls, but the majority—even those of fairly large caliber—were composed of a single layer of endothelium. Two lesions exhibited perivascular lymphocytic and histiocytic infiltration, and some of the vessels of these two lesions displayed reactive hyperplasia of their endothelial lining cells. Fibrous stroma was minimally present and appeared to be completely lacking for the most part. Vascular channels were abundant in the pedicles.

The overlying epithelium was focally ulcerated in three lesions. In the remaining areas and in the two non-ulcerated lesions, the epithelium had uniform thickness, it was flat with no rete ridges, and it was atrophic in one of them. No

Table 2 Source of antibodies and laboratory procedures

Antibody	Manufacturer	Type of antibody	Antigen retrieval procedure	Concentration	Control tissue
Vimentin	Dako A/S, Glostrup, Denmark	Mouse, V-9	Citrate buffer pH=6	1:500	Malignant melanoma
S-100	Dako A/S, Glostrup, Denmark	Rabbit polyclonal	Protease K 0.1%	1:500	Malignant melanoma
NSE	DakoCytomation, Carpinteria, CA, USA	Mouse, BBS/NC/ VI-H14	Pressure cooker, citrate buffer pH=6	Ready to use	Pancreas
CD-68	DakoCytomation, Carpinteria, CA, USA	Mouse, clone KP-1	Protease K 0.1%	1:100	Lymph node
CD-68	Dako A/S, Denmark	Mouse, clone PG-M1	Protease K 0.1%	1:100	Lymph node
Calretinin	Zymed, San Francisco, CA, USA	Rabbit polyclonal, ready to use	Pressure cooker, Nuclear Decloaker*, pH=9.5	Ready to use	Mesothelioma
PGP9.5	Diagnostic BioSystems, Pleasanton, CA, USA	Rabbit polyclonal	Pressure cooker, Nuclear Decloaker pH=9.5	1:60	Adenocarcinoma of pancreas
p75/ NGFR	Diagnostic BioSystems, Pleasanton, CA, USA	Mouse, clone ME 20.4	Protease K 0.1%	1:50	Malignant melanoma
NKI/C3	Biogenex, San Ramon, CA, USA	Mouse, clone AM077	Not required	Ready to use	Malignant melanoma
Inhibin-α	ABD Serotec, Oxfordshire, UK	Mouse, clone R1	Pressure cooker, Nuclear Decloaker pH=9.5	1:50	Normal human testis

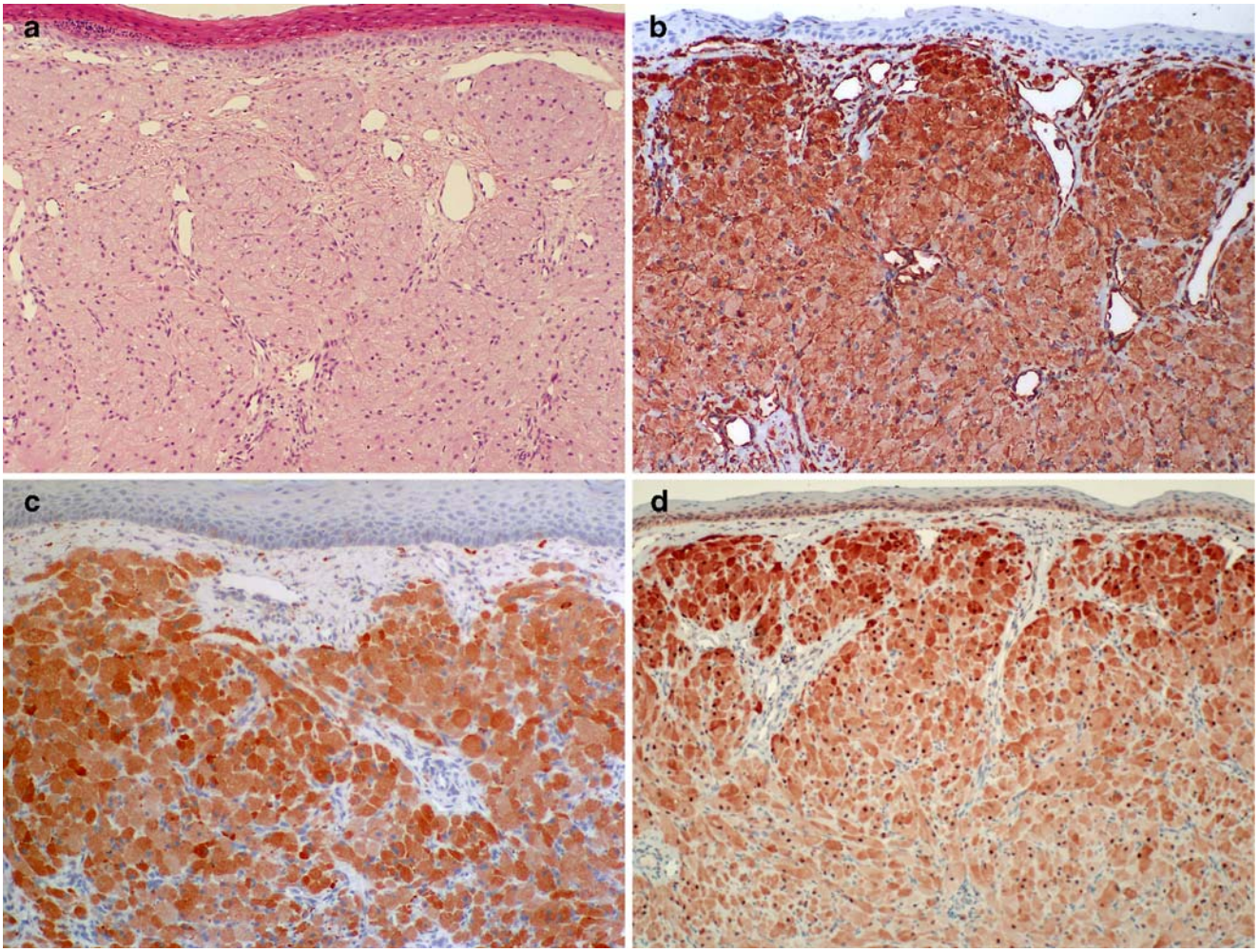

Fig. 2 **a** The lesion is lined by stratified squamous epithelium devoid of rete ridges, and numerous blood vessels are seen throughout. The granular cells are seen to be tightly packed, with abundant pale granular cytoplasm (hematoxylin and eosin, original magnification ×100). The granular cells are diffusely positive for **b** vimentin, **c** NKI/C3, and **d** PGP9.5 (AEC method, original magnification ×100)

lesion exhibited pseudoepitheliomatous hyperplasia or odontogenic rests.

Immunohistochemical findings

The results obtained with the immunohistochemical markers we used in this study are summarized in Table 3. The granular cells were immunoreactive in a diffuse pattern with a moderate-to-strong staining intensity for vimentin, NKI/C3, and PGP9.5 in the specimens of all five cases (Fig. 2). The granular cells were negative for S-100, KP-1, PG-M1, NGFR/p75, and inhibin-α. Immunoreactivity for NSE was observed in two cases: it was of moderate intensity and involved most of the granular cells in one case and fewer

Table 3 Staining pattern (score and intensity) of the granular cells for the various immunohistochemical stains

Specimen #	Vimentin	S-100[a,b]	NSE	CD-68 (KP-1)[a]	CD-68 (PG-1)[a]	Calretinin[a,b]	PGP9.5	NGFR/p75[b]	NKI/C3	Inhibin-α
1	4, +++	–	–	–	–	–	4, ++	–	4, ++	–
2	4, ++	–	3, ++	–	–	–	4, ++	–	4, +++	–
3	4, ++	–	4, ++	–	–	3, ++	4, ++	–	4, ++	–
4	4, ++	–	–	–	–	–	4, ++	–	3, ++	–
5	4, ++	–	–	–	–	–	2, ++	–	4, +++	–

[a] Positive interstitial cells
[b] Positive nerve bundles within the lesion

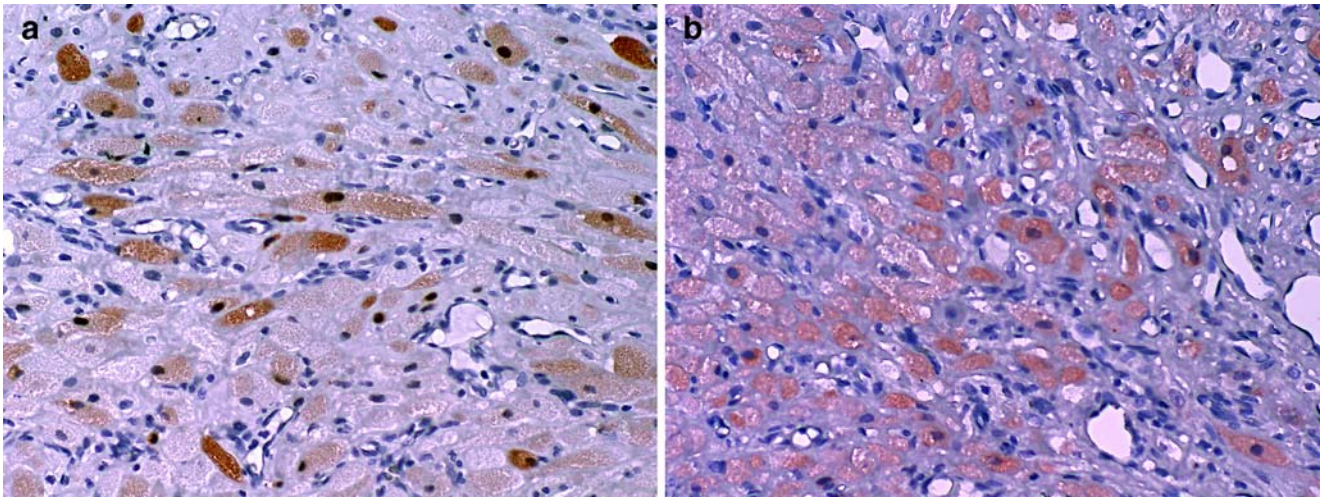

Fig. 3 Granular cells in some CGCEs are also positive for **a** calretinin and **b** NSE (AEC method, original magnification ×100)

than 50% in the other (Fig. 3). Calretinin was positive in only one case (about 50% of the granular cells; Fig. 3).

Interstitial cells were found to be immunoreactive for S-100, PG-M1, and KP-1, and a few of them also stained for calretinin (Fig. 4). Sparse nerve bundles within the lesions were usually immunoreactive for S-100, NGFR/p75, and calretinin.

Discussion

In the past, some pathologists related to CGCEs and GCTs as one lesion because of the similarity of the two lesions under light microscopy [10, 11]. Further investigations with electron microscopy and immunohistochemistry, however, revealed new observations that support their being two distinct lesions. As such, CGCEs and GCTs are now considered to represent separate entities based on their clinical manifestation and behavior, certain histopathologic features, and immunophenotype markers.

Clinically, a CGCE can be detected on prenatal sonography [33]. It has been diagnosed as early as the 26th week of gestation [34] and was found to exhibit accelerated growth during the third trimester [35]. The lesion grows only during the intrauterine period and ceases to grow at birth [34, 35]. There are no reports in the literature to suggest that CGCEs increase in size after birth [2, 36]. Furthermore, there is reported evidence that small lesions regressed during the first year of life [36–39]. Another point of interest is that there are no reports of recurrence of a CGCE in spite of an incomplete excision [4, 36]. This latter observation has also been reported in cases of GCTs [40, 41].

Histopathologically, the granular cells of a CGCE are more tightly and homogeneously packed than those of a GCT. The lesional margins of CGCEs are more circumscribed than those of most GCTs, and there is no pattern of

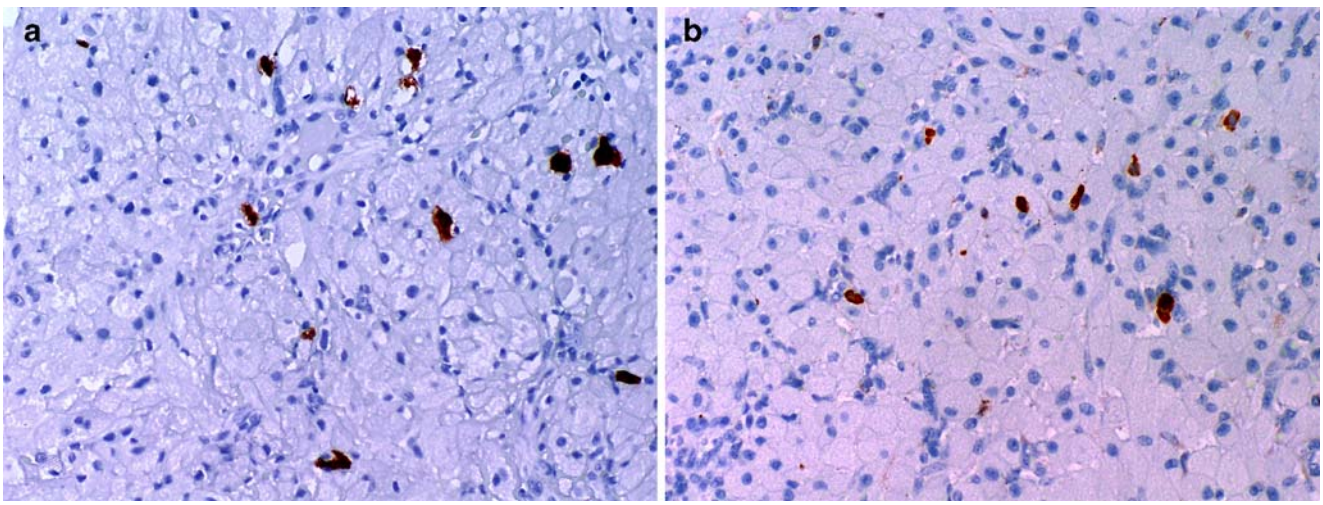

Fig. 4 Interstitial cells are positive for **a** S-100 and **b** KP-1 (AEC method, original magnification ×100)

infiltration or "invasion" into the surrounding tissue, as is often seen in GCTs [40]. The overlying epithelium of a CGCE demonstrates stratified squamous epithelium that lacks rete ridges and that is sometimes slightly thinned, as opposed to the epithelium of a GCT that often shows epithelial hyperplasia or even pseudoepitheliomatous hyperplasia. This phenomenon is never seen in CGCEs. A CGCE is significantly more vascular than a GCT and exhibits a prominent complex network of vascular channels that are often dilated [12, 24, 26]. In addition, marked blood flow could be detected by Doppler ultrasound examination within a CGCE [34].

A vast array of immunohistochemical studies has been undertaken in an effort to determine the profile of the granular cells in the CGCE. These encompassed markers from all known lines of differentiation. Table 4 summarizes the results derived from the English-language literature of the most common markers that have been used for this purpose. The table includes only studies that have been performed since 1990 as it coincides with the standardization of the laboratory techniques of immunohistochemistry [2, 6, 8, 20–29]. There are a total of 13 previous studies on 28 lesions and the five additional lesions from the present study. Among the traditional markers, positive vimentin immunoreactivity was the most frequently reported (93% of the cases), followed by NSE (48% of the cases). Positivity of the granular cells for macrophage markers, such as KP-1, PG-M1, Ki-M1P (representing different CD-68 epitopes), α1-antichemotrypsin, α1-antitrypsin, and HLA-DR, was reported in 12–37% of the cases [24, 28]. These results, however, were based on only a small number of lesions and were sometimes obtained only after modification of the working methods [28]. One anecdotal case was found to be weakly positive for S-100 after microwave treatment [28]. The nature of the immunoreactivity of our five cases was generally in accordance with the descriptions in the literature: 100% of the lesions were vimentin positive, 40% were NSE positive, and 100% were S-100 negative. Calretinin, an S-100-related marker, has not been previously examined in CGCE, and we found it to be moderately positive in only one case (20%).

In addition to the traditional markers, we submitted our specimens to newer and less common markers, such as PGP9.5, NGFR/p75, NKI/C3, and inhibin-α. PGP9.5 and NGFR/p75 had been previously studied in only two lesions [23], with results similar to ours, i.e., the granular cells were found to be PGP9.5 positive and NGFR/p75 negative. NKI/C3 and inhibin-α had not been investigated before in CGCE: our results revealed that the granular cells were positive for NKI/C3 but negative for inhibin-α.

A comparison of the CGCE immunoprofile to that of a large series of GCTs that were submitted to the same panel of markers revealed a similar pattern of positive staining to

Table 4 Immunohistochemical panel of markers of congenital granular cell epulis studies (1990–2008) according to the line of differentiation [2, 6, 8, 20–29]

	Epithelial/ myoepithelial	Neurogenic	Neuroendocrine	Myogenous	Histiocytic	Mesenchymal/ non-specific	Vascular	Immune-related	Hormone receptors/ hormone-related
Markers	Cytokeratin	S-100	NSE	Desmin	A1-AT	Vimentin	Factor 8	OKT-6	ER
	EMA	Calretinin	Leu-7	Myoglobin	A1-ACT	NKI/C3		LCA	PR
	CEA	Myelin	Chromogranin	SMA	Lysozyme			CD 49e	Inhibin-α
	E-cadherin	NF	PGP9.5	MSA	HLA-DR				
	GFAP	NGFR/p75			KP-1				
					Ki-M1P				
					PG-M1				
					MAC3873A5				
Positive immunoreactivity/ total stained cases (%)	Negative to all markers	S-100 1/33 (3%)[a]	NSE 14/29 (48%)	Negative to all markers	Ki-M1P 2/12 (16%)[a]	Vimentin 26/28 (93%)	Negative	Negative to all markers	Negative to all markers
					KP-1 5/15 (33%)[b]				
		Calretinin 1/5 (20%)[b]	PGP9.5 7/7 (100%)		HLA-DR 1/3 (33%)[c]	NKI/C3 5/5 (100%)[a]			
					A1-ACT 3/8 (37.5%)				
					A1-AT 2/16 (12.5%)				
Remarks		[a]After MW			[a]After MW	[a]Only in present study			
		[b]Only in present study			[b]After MW in 2 cases				
					[c]5% of cells				

EMA epithelial membrane antigen, *CEA* carcino-embryonic antigen, *GFAP* glial fibrilar acidic protein, *NF* neurofilaments, *NGFR/p75* nerve growth factor receptor, *NSE* neuron-specific enolase, *SMA* smooth muscle actin, *MSA* muscle-specific actin, *A1-AT* α1-antitrypsin, *A1-ACT* α1-antichemotrypsin, *LCA* leukocyte common antigen, *ER* estrogen receptor, *PR* progesterone receptor, *MW* microwave

PGP9.5 and NKI/C3 for both lesions [40]. Notably, the granular cells of GCTs reacted positively to NGFR/p75 and inhibin-α, but the granular cells of CGCEs did not. These results expand the immunophenotypic distinction between the two lesions, which until now has largely relied solely on the negativity of S-100 in CGCEs.

The positive immunoreactivity of CGCE to NKI/C3 and PGP9.5 does not imply any specific line of differentiation [42, 43]. Although these markers were originally thought to be specific for melanocytic and neurogenic or neuroendocrine lines of differentiation, respectively, their expression has been found in a large array of tissues, both benign and malignant. Moreover, PGP9.5 is currently believed to reflect metabolic cellular activity, irrespective of cell origin [43]. Likewise, the positivity of CGCEs to NSE does not support a neuroendocrine differentiation. NSE is not neuron or neuroendocrine cell-specific, as had originally been assumed [42]. It can be useful in combination with other more specific antibodies, such as chromogranin and synaptophysin, for identification of neuroendocrine cells. Since chromogranin was found to be consistently negative in CGCEs [26], however, its contribution to the understanding of the origin of the granular cell is limited.

We examined the immunostaining pattern of the interstitial cells as well. Some authors found them to be S-100 positive [17, 44], and one study reported that they are also positive for NSE [20]. The nature of these isolated non-granular cells is not clear, and so several authors suggested that the interstitial cells may represent developing neural tissue [17], Langerhans cells [44], or some sort of neuroendocrine differentiation [20]. In the present study, the interstitial cells were found to be positive for S-100 and macrophage markers (KP-1 and PG-M1), and a few of them were also positive for calretinin, while being negative for NSE. S-100 protein serves as a marker for schwannian/neural cell origin, but its reaction was also identified in cells of non-neural lineages, such as macrophages [45]. KP-1 and PG-M1, more commonly known as CD-68, serve as markers of lysosomes, mostly associated with macrophages, but they are also present in neural (schwann) cells that acquire lysosomes during phagocytosis of myelin, a phenomenon which is known to occur, for example, in peripheral nerves showing Wallerian degeneration as well as in traumatic neuromas [28, 46]. This may infer that the interstitial cells contain an intracytoplasmic accumulation of phagolysosomes. There is a possibility that they represent an earlier stage of the granular cells and lose reactivity to S-100 and frequently also to CD-68 during transition to an entirely granular morphology.

In spite of the enigma regarding the cellular origin of a CGCE, it is largely considered to be a non-neoplastic lesion [8, 19, 36, 47, 48]. This can be supported by the clinical observations that the lesion has no growth potential after birth, its ability to regress spontaneously (when small lesions are involved), and the lack of recurrence even after incomplete excision [4, 36, 37, 39]. In light of these features, it has been assumed that a CGCE is either reactive in nature [12–14, 49, 50] or that it is a manifestation of a degenerative process [4, 11, 12, 49]. Moreover, considering the marked predilection of CGCEs for females, hormonal factor (or factors) may be important in the development of the lesion [13]. This theory is further supported by the experimental production of granular cell tumors in the uterine cervix of newborn mice following injection of estrogen [51]. This concept is not proven in CGCEs, since there are no detectable estrogen and progesterone receptors within the lesions [6, 13, 21, 22]. On the other hand, some authors claim that failure to demonstrate estrogen and progesterone receptors in the lesion does not rule out intrauterine growth from other placental or maternal hormones [4, 52].

In summary, the results of the present study have shown that the broad panel of antibodies that characterize different tissues does not confirm any particular cell type for the histogenetic origin of CGCEs, but rather seems to reflect a local metabolic or reactive change, thus, providing supporting evidence that the lesion is of a non-neoplastic nature. This is further supported by the clinical course characterized by lack of growth after birth and even complete regression in cases of small lesions. In spite of the fact that both CGCEs and GCTs are classified as granular cell lesions on the light microscopic level, they present different immunohistochemical profiles, a feature which can aid in separating them into two distinctive entities.

Acknowledgments The study was supported by the Ed and Herb Stein Chair in Oral Pathology, Tel Aviv University. The authors would like to thank Mrs. Hana Vered for technical assistance and Ms. Esther Eshkol for editorial assistance.

Conflict of interest statement The authors declare that they have no conflict of interest.

References

1. van der Waal I (2005) Congenital granular cell epulis. In: Barnes L, Eveson JW, Reichart P, Sidransky D (eds) World health organization classification of tumours. Pathology and genetics. Head and neck tumours. IARC Press, Lyon, p 198
2. Zuker RM, Buenechea R (1993) Congenital epulis: review of the literature and case report. J Oral Maxillofacial Surg 51:1040–1043
3. Odell EW, Morgan PR (1998) Biopsy pathology of the oral tissues. Chapman & Hall Medical, London, pp 131–132
4. Lack EE, Worsham GF, Callihan MD (1981) Gingival granular cell tumors of the newborn (congenital "epulis"). Am J Surg Pathol 5:37–46
5. Koch BL, Myer C, Egelhoff JC (1997) Congenital epulis. Am J Neuroradiol 18:739–741
6. Lapid O, Shaco-Levy R, Krieger Y et al (2001) Congenital epulis. Pediatrics 107:E22

7. Chami RG, Wang HS (1986) Large congenital epulis of newborn. J Pediatr Surg 21:929–930
8. Loyola AM, Gatti AF, Pinto S et al (1997) Alveolar and extra-alveolar granular cell of the newborn: report of case and review of the literature. Oral Surg Oral Med Oral Pathol Oral Radiol Endod 84:668–671
9. Senoo H, Iida S, Kishino M et al (2007) Solitary congenital granular cell lesion of the tongue. Oral Surg Oral Med Oral Pathol Oral Radiol Endod 104:e45–e48
10. Kay S, Elzay RP, Willson MA (1971) Ultrastructural observations on a gingival granular cell tumor (congenital epulis). Cancer 27:674–680
11. Regezi JA, Batsakis JG, Courtney RM (1979) Granular cell tumors of the head and neck. J Oral Surg 37:402–406
12. Rohrer MD, Young SK (1982) Congenital epulis (gingival granular cell tumor): ultrastructural evidence of origin from pericytes. Oral Surg Oral Med Oral Pathol 53:56–63
13. Lack EE, Perez-Atayde AR, McGili TJ et al (1982) Gingival granular cell tumor of the newborn (congenital "epulis"): ultrastructural observations relating to histogenesis. Human Pathol 13:686–689
14. Zarbo RJ, Lloyd RV, Beals TF et al (1983) Congenital gingival granular cell tumor with smooth muscle cytodifferentiation. Oral Surg Oral Med Oral Pathol 56:512–520
15. Kameyama Y, Mizohata M, Takehana S et al (1983) Ultrastructure of the congenital epulis. Virchows Arch A Pathol Anat Histopathol 401:251–260
16. Slootweg P, de Wilde P, Vooijs P et al (1983) Oral granular cell lesions. An immunohistochemical study with emphasis on intermediate-sized filaments proteins. Virchows Arch A Pathol Anat Histopathol 402:35–45
17. Lifshitz MS, Flotte TJ, Greco MA (1984) Congenital granular cell epulis. Immunohistochemical and ultrastructural observations. Cancer 53:1845–1848
18. Nanthrath WB, Remberger K (1986) Immunohistochemical study of granular cell tumors. Demonstration of neuron specific enolase, S100 protein, laminin and alpha-1-antichymotripsin. Virchows Arch A Pathol Anat Histopathol 408:421–434
19. Dastur DK, Manghani DK (1988) Fine structure and possible histogenesis of granular cell 'tumours' of the gum and the labia. Indian J Cancer 25:57–69
20. Takahashi H, Fujita S, Satoh H et al (1990) Immunohistochemical study of congenital gingival granular cell tumor (congenital epulis). J Oral Pathol Med 19:492–496
21. Tucker MC, Rusnock EJ, Azumi N et al (1990) Gingival granular cell tumors of the newborn. An ultrastructural and immunohistochemical study. Arch Pathol Lab Med 114:895–898
22. Damm DD, Cibull ML, Geissler RH et al (1993) Investigation into the histogenesis of congenital epulis of the newborn. Oral Surg Oral Med Oral Pathol 76:205–212
23. Hoshi N, Tsu-ura Y, Watanabe K et al (1995) Expression of immunoreactivities to 75 kDa nerve growth factor receptor, *trk* gene product and phosphotyrosine in granular cell tumors. Pathol Int 45:748–756
24. Filie AC, Lage JM, Azumi N (1996) Immunoreactivity of S100 protein, α-1-antitrypsin, and CD68 in adult and congenital granular cell tumors. Mod Pathol 9:888–892
25. Ugras S, Demirtas I, Bekerecioglu M et al (1997) Immunohistochemical study on histogenesis of congenital epulis and review of the literature. Pathol Int 47:627–632
26. Lazaris AC, Eftychiadis CA, Nicolopoulou P et al (2000) Congenital epulis: an ultrastructural and immunohistochemical case study. Adv Clin Pathol 4:159–163
27. Yavuzer R, Ataoglu O, Sari A (2001) Multiple congenital epulis of alveolar ridge and tongue. Ann Plast Surg 47:199–202
28. Kaiserling E, Ruck P, Xiao J-C (1995) Congenital epulis and granular cell tumor. A histologic and immunohistochemical study. Oral Surg Oral Med Oral Pathol Oral Radiol Endod 80:687–697
29. Junquera LM, de Vicente JC, Vega JA et al (1997) Granular-cell tumours: an immunohistochemical study. Br J Oral Maxillofac Surg 35:180–184
30. Laskin WB, Fetsch JF, Davis CJ et al (2005) Granular cell tumor of the penis: clinicopathologic evaluation of 9 cases. Hum Pathol 36:291–298
31. Williams HK, Williams DM (1997) Oral granular cell tumours: a histological and immunocytochemical study. J Oral Pathol Med 26:164–169
32. Fine SW, Li M (2003) Expression of calretinin and the alpha-subunit of inhibin in granular cell tumors. Am J Clin Pathol 119:259–264
33. Song W-S, Kim J-W, Kim Y-G et al (2005) A case report of congenital epulis in the fetus. J Oral Maxillofac Surg 63:135–137
34. Nakata M, Anno K, Matsumori LT et al (2002) Prenatal diagnosis of congenital epulis: a case report. Ultrasound Obstet Gynecol 20:627–629
35. Kim ES, Gross TL (1999) Prenatal ultrasound detection of a congenital epulis in a triple X female fetus: a case report. Prenat Diagn 19:774–776
36. O'Brian FV, Pielou WD (1971) Congenital epulis: its natural history. Arch Dis Child 46:559–560
37. Sakai VT, Oliveira TM, Silva TC et al (2007) Complete spontaneous regression of congenital epulis in a baby by 8 months of age. Int J Pediatr Dent 17:309–312
38. Welbury RR (1980) Congenital epulis of the newborn. Br J Oral Surg 18:238–243
39. Jenkins HR, Hill CM (1989) Spontaneous regression of congenital epulis of the newborn. Arch Dis Child 64:145–147
40. Vered M, Carpenter WM, Buchner A (2009) Granular cell tumor of the oral cavity: updated immunohistochemical profile. J Oral Pathol Med 38(1):150–159
41. Worsaae N, Schwartz O, Pindborg JJ (1979) Follow-up study of 14 granular cell tumors. Int J Oral Surg 8:133–139
42. Dabbs DJ (2006) Diagnostic immunohistochemistry. Churchill Livingstone, Beijing, p 200, 338
43. Campbell LK, Thomas JR, Lamps LW et al (2003) Protein gene product 9.5 (PGP 9.5) is not a specific marker of neural and nerve sheath tumors: an immunohistochemical study of 95 mesenchymal neoplasms. Mod Pathol 16:963–969
44. Monteil RA, Loubiere R, Charbit Y et al (1987) Gingival granular cell tumor of the newborn: immunoperoxidase investigation with anti-S-100 antiserum. Oral Surg Oral Med Oral Pathol 64:78–81
45. Chan AC, Chan JK, Cheung MM et al (2005) Haematoplymphoid tumours. In: Barnes L, Eveson JW, Reichart P, Sidransky D (eds) World health organization classification of tumours. Pathology and genetics. Head and neck tumours. IARC Press, Lyon, pp 63–64
46. Kurtin PJ, Bonin DM (1994) Immunohistochemical demonstration of the lysosome-associated glycoprotein CD68 (KP-1) in granular cell tumors and schwannomas. Hum Pathol 25:1172–1178
47. Custer RP, Fust JA (1952) Congenital epulis. Am J Clin Pathol 22:1044–1053
48. Dash JK, Sahoo PK, Das SN (2004) Congenital granular cell lesion "congenital epulis"–report of a case. J Indian Soc Pedod Prev Dent 22:63–67
49. Godra A, D'Cruz CA, Labat MF (2004) Pathologic quiz case. A newborn with a midline buccal mucosa mass. Arch Pathol Lab Med 128:585–586
50. McKee PH (1996) Pathology of the skin. Mosby-Wolfe, London, pp 16.42–16.43
51. Sobel HJ, Marquet E (1974) Granular cells and granular cell lesions. Pathol Ann 9:43–79
52. Al-Qattan MM, Clarke HM (1994) Congenital epulis: evidence against the intrauterine estrogen stimulus theory. Ann Plast Surg 33:320–321

Virchows Arch (2009) 454:311–316
DOI 10.1007/s00428-009-0732-z

ORIGINAL ARTICLE

RABGAP1L gene rearrangement resulting from a der(Y)t(Y;1)(q12;q25) in acute myeloid leukemia arising in a child with Klinefelter syndrome

Maria Cristina Roberti · Roberta La Starza · Cecilia Surace · Pietro Sirleto · Rita Maria Pinto · Valentina Pierini · Barbara Crescenzi · Cristina Mecucci · Adriano Angioni

Received: 12 September 2008 / Revised: 2 January 2009 / Accepted: 8 January 2009 / Published online: 28 January 2009

Abstract In this study, we report the molecular cytogenetic characterization of an acute myeloid leukemia with a der(Y)t(Y;1)(q12;q25) in bone marrow cells in a child with Klinefelter syndrome. Conventional cytogenetics demonstrated the unbalanced translocation, i.e., a trisomic 1q25-qter juxtaposed to Yq12 replaced the terminal segment of chromosome Y was acquired and present only on bone marrow cells. Fluorescence in situ hybridization showed that the breakpoint at 1q25 disrupted *RABGAP1L*, a strongly expressed gene in CFU-GEMM, erythroid cells, and megakaryocytes, while the Yq12 breakpoint fell within the heterochromatic region. As der(Y)t(Y;1)(q12;q25) was an isolated cytogenetic change, *RABGAP1L* rearrangement as well as gene(s) dosage effects correlated to 1q25-qter trisomy, and Yq12-qter loss may make a major contribution to leukemogenesis and/or disease progression.

Maria Cristina Roberti and Roberta La Starza should be regarded as joint first authors.

M. C. Roberti · C. Surace (✉) · P. Sirleto · A. Angioni
Cytogenetics and Molecular Genetics,
Bambino Gesù Children's Hospital,
Piazza S. Onofrio 4,
00165 Rome, Italy
e-mail: cecilia.surace@opbg.net

R. La Starza · V. Pierini · B. Crescenzi · C. Mecucci
IbiT Foundation, Fondazione IRCCS Biotecnologie nel Trapianto,
Hematology, University of Perugia,
Perugia, Italy

R. M. Pinto
Department of Hematology,
Bambino Gesù Children's Hospital,
Piazza S. Onofrio 4,
00165 Rome, Italy

Keywords Acute myeloid leukemia · Klinefelter syndrome

Introduction

The Klinefelter syndrome (KS), which is associated with a 47,XXY constitutional karyotype, is often an accidental finding at diagnosis of hematological malignancies. Chromosome and molecular aberrations are currently hypothesized to predispose stem cells to genetic instability, which in turn determines an accumulation of other chromosome changes leading to clonal evolution of malignancies [1]. In fact, although patients with the KS and other constitutional chromosomal abnormalities [2] are at increased risk of diverse neoplasia, the molecular mechanism(s) underlying the predisposition to develop tumors are still unknown.

In describing a patient with KS who developed acute leukemia, Mamunes et al. [3] was the first to report the association between KS and malignant disease. Neoplasms are estimated to develop in 1–2% of KS cases [4] with a high incidence of germ cell tumors and breast cancers [5]. Several studies, however, debated on the association with hematologic malignant diseases [6, 7]. Without well-controlled, prospective studies, definite conclusions are difficult to draw on the risk of malignant disease among persons with KS. The reported cases of acute and chronic leukemia and myelodysplastic syndrome raise concern about increased susceptibility of stem cells to chromosomal damage leading to clonal disorders.

Nevertheless, the association between congenital chromosomal abnormalities and neoplasia was strengthened by the predisposition of patients with constitutional chromosome disorders, as Down syndrome, to the development of

acute leukemia, first reported in 1957 [8]. Interestingly, in a KS patient with mosaic XY/XXY who developed a bronchogenic carcinoma, the XXY fibroblasts in in vitro culture showed a higher susceptibility to transformation by simian virus (SV40) than the XY clone [9].

Structural abnormalities of sexual chromosomes are also rare events in hematological disorders. Frequency of chromosome X abnormalities ranges from 0.4% to 1.5% [10, 11], and only a few are associated with specific leukemic subtypes as primary nonrandom clonal cytogenetic findings [12].

Rearrangements of chromosomes Y and 1 have been observed to date in two patients with solid tumors and in 14 patients with hematological malignancies (Table 1). In seven of 14 with acute myeloid leukemia (AML) and myelodysplastic syndromes (MDS), conventional cytogenetics assigned the breakpoints to bands Yq12 and 1q12–q21 which are close to, or even within, the heterochromatic regions of chromosomes Y and 1.

This case report describes for the first time the molecular cytogenetic characterization of AML with a der(Y)t(Y;1)(q12;q25) in a child with Klinefelter syndrome which was investigated by fluorescence in situ hybridization (FISH) using genomic clones for the centromeres, heterochromatin, and long arms of chromosomes Y and 1.

Clinical history

In December 2001, a 17-month-old boy was admitted to "Bambino Gesù" Children's Hospital, Rome, Italy because of weakness, fever, diffuse bleeding, and hepatosplenomegaly. Upon admission, routine blood tests showed WBC 8.270/mm^3 with 15% uniform vacuolated immature cells, slight anemia (Hb 10.6 g/dl), and severe thrombocytopenia (12.000/mm^3). Bone marrow aspirate showed hypercellularity with erythroid and myeloid lineage dysplasia, decreased megakaryocytes, and 70% agranular large-sized blasts with round nuclei, open chromatin, one or more nucleoli, and moderately basophilic cytoplasm. Immunophenotyping was positive for CD13, CD33, DR, CD4, CD11B, CD7 and negative for CD14, CD15, and MPO. AML-M0 was diagnosed. Karyotyping was 47,XXY[40]/47,XX,der(Y)t(Y;1)(q12;q23-25)[60] (Fig. 1). A constitutional Klinefelter syndrome 47,XXY was diagnosed on peripheral blood T lymphocytes.

The child was treated according to the Italian Association of Pediatric Hematology and Oncology (AIEOP)—AML 2002/01 protocol and, in January 2002, achieved first complete hematological remission (CR). Since the patient had no HLA-matched family donor, he received autologous bone marrow transplantation and remained in first continuous hematological remission for 5 years post-transplant.

Materials and methods

Chromosome studies were performed on unstimulated bone marrow cells after short-term culture. Metaphases were R-banded with acridine orange (RFA) and additional GTG banding was carried out in order to clarify the abnormal karyotype. Chromosome GTG banding was performed also on peripheral blood cells according to standard methods.

Table 1 List of hematologic (1–14) and solid tumors (15–16) carrying rearrangements involving the chromosomes Y and 1 reviewed in literature and reported from the oldest case described to the more recent one

Case	Diagnosis	Chromosome rearrangements	Reference
1	AML-M2	48,X,der(Y)t(Y;1)(q12;q21),+der(Y)t(Y;1)(q12;q21),+8	[22]
2	AML	46,X,t(Y;1)(p11;q21)	[23]
3	Polycythemia vera	t(Y;1)(q12;q12)	[24]
4	Burkitt lymphoma	??,X,t(Y;1),t(8;14)(q?;q?)	[25]
5	Idiopathic myelofibrosis	46,X,t(Y;1)(q12;q12)	[26]
6	MDS	46,X,-Y,+der(Y)t(Y;1)(q12;q21)	[27]
7	MDS	46,X,-Y,+der(Y)t(Y;1)(q12;q21)	[27]
8	Fanconi's anemia and MDS	transient t(Y;1)(q12;q21)	[28]
9	Secondary AML after MDS	t(Y;1)(q12;q12)	[29]
10	Diffuse large B-cell lymphoma	47,X,+X,t(Y;1)(q12;q11),t(1;16)(q11;q11),t(4;20)(q31;q11), t(8;14)(q24;q32),der(13)t(1;13)(q25;p11),del(15)(q11q12)	[30]
11	Myelofibrosis	der(Y)t(Y;1)(q12;q21)	[31]
12	MDS	der(Y)t(Y;1)(q12;q21)	[31]
13	Polycythemia vera	47,X,der(Y)t(Y;1)(q12;q12),+9	[32]
14	CML	46,X,der(Y)t(Y;1)(q11.1 or.2;q12)	[33]
15	Meningioma	46,XY,t(Y;1)(q12;q31)/46,X,der(Y)t(Y;1)	[34]
16	Papilloma	t(Y;1)(q12;q25)	[35]

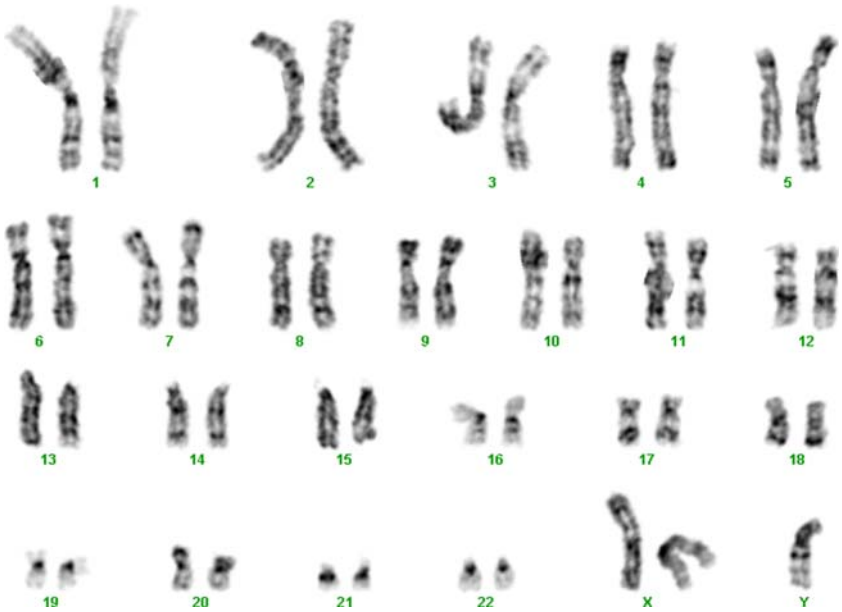

Fig. 1 Karyotype of the patient at G-banding showing the der(Y)t(Y;1)

All karyotypes were described consistent with the International System for Human Cytogenetic Nomenclature (ISCN 1995).

FISH was done as previously described [13] using α-satellite probes for centromeres of chromosomes X/Y (DXZ1, Xp11.1–q11.1/DYZ3, Yp11.1–q11.1; Vysis, Downers Grove, IL, USA) and chromosome 1 (D1Z5, 1p11.1–q11.1; Cytocell, Oxfordshire, UK), satellite III probes for the heterochromatic regions of chromosome Y (DYZ1, Yq12; Vysis) and chromosome 1 (D1Z1, 1q12; Cytocell), and subtelomeric probes for the short arms of chromosomes X and Y (TelVysion Xp/Yp, DXYS129; Vysis). Each FISH experiment was performed both on patient cells and healthy controls; signals were scored in at least 100 cells, determining a cut-off of 2%.

Metaphase FISH was performed with a panel of bacterial and P1 artificial chromosomes (BAC/PAC) clones for the long arm of chromosome 1q23 to q25 ordered from centromere to telomere as shown in Table 2. Breakpoint at chromosome Y was studied by applying the following RP11 clones: centromere-270H4-557B9-1136L22-242E13-57J19-telomere. Analyses were carried out in eight to ten abnormal metaphases.

To monitor 1q trisomy during therapy, clone RP11-210E16/1q42.2 and clone RP11-33G13/1q44 were used in interphase cells. For each probe, 500 nuclei were scored, and all of them showed two signals as normal condition. Analysis was carried out with a fluorescence microscope (Provis, Olympus, Milan, Italy) equipped with a cooled CCD camera (Sensys, Photometrics) run by PathVysion softwares (Vysis, Stuttgart, Germany).

Results

As expected, FISH with the α-satellite probe for the centromere of chromosome X, showed one signal on both chromosomes, and the satellite III probe for chromosome Y heterochromatin displayed one signal on der(Y). Probes for the X and Y p-subtelomeric regions showed the chromosome Y short arm was retained in der(Y).

The centromeric probe and the probe for 1q12 heterocromatin gave a normal hybridization pattern in chromosome 1, indicating the 1q breakpoint did not involve heterochromatin.

Results with BAC/PAC clones for 1q23–25 are summarized in Table 2. Clones from RP11-77M5 to RP11-11B12 were present in two copies, one on each normal 1; clones from RP5-830A10 to RP11-345I18 were present in three copies, one on each normal 1 and on der(Y)t(Y;1). These findings indicated the breakpoint was localized at band 1q25, between two partially overlapping clones, i.e., RP11-11B12 and RP5-830A10 (Fig. 2a and b). These two clones encompass the *RABGAP1L* (RAB GTPase activating protein 1-like) gene which was disrupted and partially translocated to the der(Y)t(Y;1). The chromosome Yq12 breakpoint was narrowed to between clone RP11-242E13 and clone RP11-57J19, indicating it was localized within the heterochromatic sequences (Fig. 2c). After FISH analysis, karyotype was corrected to 47,XX,der(Y)t(Y;1)(q12;q25).

Five years after transplantation, FISH on bone marrow cells with RP11-210E16 and RP11-33G13 gave a normal hybridization pattern excluding the partial trisomy 1q.

Table 2 Summary of FISH findings with 1 and Y BAC clones

BAC clones	Chromosome band	Accession number	Map position on chromosomes 1 and Y	FISH signals
RP11-77M5	1q23.3	AL592435	161,491,930–161,653,608	1,1
RP11-38C18	1q23.3	AL390730	163,428,315–163,546,073	1,1
RP11-7G12	1q24.1	AL606495	164,167,013–164,287,981	1,1
RP11-54B9	1q24.1	AL356005	164,883,011–165,001,435	1,1
RP11-104L21	1q24.2	AL359962	165,654,025–165,721,197	1,1
RP11-184O20	1q24.3	AL512843	170,285,568–170,361,251	1,1
RP11-192B4	1q25.1	AL360002	171,516,461–171,577,864	1,1
RP5-1198E17	1q25.1	AL136170	172,093,126–172,222,566	1,1
RP11-160H22	1q25.1	AL121983	172,222,467–172,387,902	1,1
RP5-970D1	1q25.1	AL021069	172,735,904–172,836,399	1,1
RP11-11B12	1q25.1	AL591108	172,834,400–172,912,159	1,1
RP5-830A10	1q25.1	AL136377	172,874,560–172,990,369	1,1,der(Y)
RP11-64I24	1q25.1	AL161671	172,988,367–173,090,723	1,1,der(Y)
RP11-317A7	1q25.1	ends	173,059,217–173,225,233	1,1,der(Y)
RP11-469L6	1q25.1	ends	173,218,433–173,379,514	1,1,der(Y)
RP11-661N21	1q25.1	ends	173,377,067–173,541,556	1,1,der(Y)
RP11-25D15	1q25.1	ends	173,533,129–173,731,636	1,1,der(Y)
RP11-195C7	1q25.2	ends	174,384,857–174,540,598	1,1,der(Y)
RP11-252L24	1q25.2	AL596254	174,856,272–174,928,479	1,1,der(Y)
RP11-247D3	1q25.2	AL136983	175,271,948–175,311,914	1,1,der(Y)
RP11-65O1	1q25.2	AL356279	176,180,104–176,208,813	1,1,der(Y)
RP11-21M7	1q25.2	AL160281	176,324,673–176,505,626	1,1,der(Y)
RP11-18E13	1q25.2	AL162255	176,964,775–177,047,917	1,1,der(Y)
RP11-177A2	1q25.2	AL139132	177,201,493–177,359,358	1,1,der(Y)
RP11-345I18	1q25.2	AL512326	177,361,347–177,548,616	1,1,der(Y)
RP11-270H4	Yq11.23	AC006991	26,625,200–26,798,441	der(Y)
RP11-557B9	Yq11.23	AC013734	26,906,388–27,086,406	der(Y)
RP11-1136L22	Yq11.23-q12	AC073880	27,194,540–27,228,749	der(Y)
RP11-242E13	Yq12	AC068123	57,228,750–57,327,044	der(Y)
RP11-57J19	Yq12	AC025226	57,305,782–57,372,174	Absent

The clones are listed from centromere to telomere order. The map positions of all the clones are reported according to last UCSC release (2006), except for RP11-57J19 that is present only in the previous UCSC release (2004)

Discussion

This is the first report of a pediatric patient with KS who developed AML-M0 with an unbalanced translocation between chromosomes Y and 1, i.e., der(Y)t(Y;1)(q12;q25). Gene dosage effects due to the 1q25-qter trisomy and/or Yq12-qter loss may have been critical in neoplastic phenotype development. FISH studies characterized both

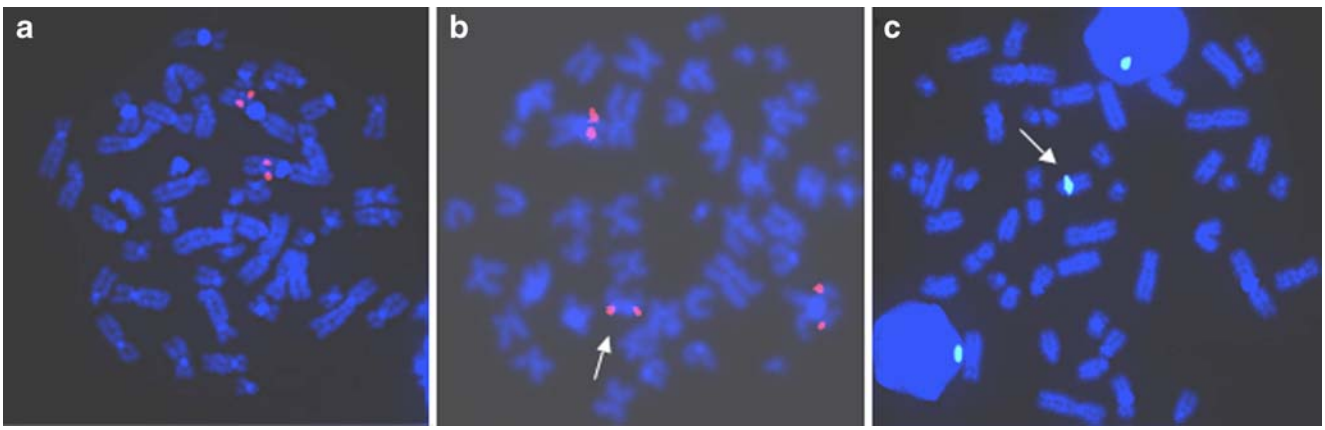

Fig. 2 Metaphase FISH with **a** clone RP11-11B12 gave two signals (*red*) on both normal chromosomes 1; **b** clone RP5-830A10 gave three signals (*red*) on both normal chromosomes 1 and on der(Y) (*arrow*); **c** clone RP11-242E13 gave one hybridization signal (*green*) on der(Y) (*arrow*)

translocation breakpoints. The Yq12 breakpoint was narrowed within heterocromatin, while the chromosome 1 breakpoint fell within the *RABGAP1L* gene.

We were unable to establish whether this rearrangement was specifically linked to the Klinefelter chromosome setting or whether it was an incidental finding in this KS patient but are convinced that cytogenetically, this case is relevant because, for the first time, it reports an unbalanced translocation which juxtaposed the chromosome Yq12 heterochromatin sequences to the *3'RABGAP1L*.

RABGAP1L, also known as *HHL* or *KIAA0471*, encodes for a 298-amino acid protein, which is a GTPase-activating protein, containing a putative phosphotyrosine-binding domain which suggests it is the tyrosine-kinase target in signaling transduction. First cloned in 1997 [14] from a size-fractionated brain cDNA library, *RABGAP1L* is expressed ubiquitously [15]. In mice, it is strongly expressed in erythroid and megakaryocyte lineages, and in multipotential CFU-GEMM (colony forming unit granulocyte, erythrocyte, monocyte, megakaryocyte) colonies [16], indicating *RABGAP1L* has a regulatory function during hematopoietic differentiation.

Deregulated *RABGAP1L* expression was reported in human disease. Downregulation was observed in Alzheimer's disease and in one patient with an *AML1* mutation, while gene expression profiling detected *RABGAP1L* upregulation in human esophageal and oral squamous cell carcinomas [17, 18]. Interestingly, recent molecular studies detected *MLL-AF4*, *AF4-RABGAP1L*, and *RABGAP1L-MLL* fusion transcripts for the first time in one case of ALL. As this case was characterized by a cryptic three-way t(1;4;11)(q25;q21;q23) [19], it was impossible to establish whether the *RABGAP1L* fusion genes played a primary or a secondary role in the leukemogenic pathway. Moreover, *RABGAP1L-MLL* represented in-frame novel gene fusion that was transcribed and able to be translated into chimeric fusion protein, suggesting that this new chimeric protein could be involved in arising and/or progression of hematopoietic diseases.

In the present case, it is still unclear whether *RABGAP1L* was deregulated by juxtaposition to chromosome Y heterochromatic sequences. In fact, many transcriptionally inactive genes are positioned close to constitutive heterochromatin in the nucleus of dividing lymphocytes [20]. This functional compartmentalization is achieved as cells enter the cell cycle and appears to be important in maintaining the heritable repression of a gene subset [21].

Another hypothesis is that *RABGAP1L* had recombined with an unknown gene(s) mapping at Yq12 to produce a new fusion oncogene. Unfortunately, the lack of material from the patient precluded any further studies. However, present molecular cytogenetic evidence together with findings in a case of ALL with *RABGAP1L* fusions [19] suggest that whatever the mechanism, *RABGAP1L* gene deregulation of tyrosine-kinase signaling transduction pathways plays a major role in the pathogenesis of leukemia.

Acknowledgements AIRC (Associazione Italiana Ricerca sul Cancro), MIUR-PRIN (Consiglio Nazionale delle Ricerche-Ministero per l'Istruzione, l'Università e la Ricerca Scientifica); Fondazione Cassa di Risparmio, Perugia, Italy; BAC and PAC clones belong to the Roswell Park Cancer Institute library (http://www.chori.org/bacpac/) and were kindly provided by Dr. Mariano Rocchi (DIGEMI, University of Bari, Italy).

The authors wish to thank Dr. Geraldine Boyd for assistance in the preparation of the manuscript.

The authors declare that they have no conflict of interest.

References

1. Kumar S, Menke DM, Dewald GW et al (2002) Agnogenic myeloid metaplasia associated with Klinefelter syndrome: a case report. Ann Hematol 81:215–218
2. Klinefelter HF (1986) Klinefelter syndrome: historical background and development. South Med J 79:1089–93
3. Mamunes P, Lapidus PH, Abbott JA et al (1961) Acute leukaemia and Klinefelter's syndrome. Lancet 2:26–27
4. Aguirre D, Nieto K, Lazos M et al (2006) Extragonadal germ cell tumors are often associated with Klinefelter syndrome. Human Pathology 37:477–480
5. Keung YK, Buss D, Chauvenet A et al (2002) Hematologic malignancies and Klinefelter syndrome: a chance association? Cancer Genet Cytogenet 139:9–13
6. Horsman DE, Pantzar JT, Dill FJ et al (1987) Klinefelter syndrome and acute leukemia. Cancer Genet Cytogenet 26:375–376
7. Hasle H, Mellemgaard A, Nielsen J et al (1995) Cancer incidence in men with Klinefelter syndrome. Br J Cancer 71:416–420
8. Krivit W, Good RA (1957) Simultaneous occurrence of mongolism and leukemia; report of a nationwide survey. J Dis Child 94:289–293
9. Mukerjee D, Bowen J, Anderson DE (1970) Simian papovavirus 40 transformation of cells from cancer patient with XY-XXY mosaic Klinefelter's syndrome. Cancer Res 30:1769–1772
10. Dewald GW, Brecher M, Travis LB et al (1989) Twenty-six patients with hematologic disorders and X chromosome abnormalities. Frequent idic(X)(q13) chromosomes and Xq13 anomalies associated with pathologic ringed sideroblasts. Cancer Genet Cytogenet 42:173–85
11. Wong KF, Siu LLP, So CC (2000) Deletion of Xq23 is a recurrent karyotypic abnormality in acute myeloid leukemia. Cancer Genet Cytogenet 122:33–36
12. Gray BA, Cornfield D, Bent-Williams A et al (2003) Translocation (X;20)(q13.1;q13.3) as a primary chromosomal finding in two patients with myelocytic disorders. Cancer Genet Cytogenet 141: 169–74
13. Crescenzi B, La Starza R, Romoli S et al (2004) Submicroscopic deletions in 5q- associated malignancies. Haematologica 89:281–285
14. Seki N, Ohira M, Nagase T et al (1997) Characterization of cDNA clones in size-fractionated cDNA libraries from human brain. DNA Res 4:345–349
15. Ishikawa K, Nagase T, Nakajima D et al (1997) Prediction of the coding sequences of unidentified human genes. VIII. 78 new cDNA clones from brain which code for large proteins in vitro. DNA Res 4:307–313

16. Hidaka M, Caruana G, Stanford WL et al (2000) Gene trapping of two novel genes, Hzf and Hhl, expressed in hematopoietic cells. Mech Dev 90:3–15
17. Sharma R, Samantary S, Shukla NK et al (2003) Transcriptional gene expression profile of human esophageal squamous cell carcinoma. Genomics 81:481–488
18. Arora S et al (2005) Identification of differentially expressed genes in oral squamous cell carcinoma. Mol Carcinog 42:97–108
19. Kowarz E, Burmeister T, Lo Nigro L et al (2007) Complex MLL rearrangements in t(4;11) leukemia patients with absent AF4.MLL fusion allele. Leukemia 21:1232–1238
20. Brown KE, Guest SS, Smale ST et al (1997) Association of transcriptionally silent genes with Ikaros complexes at centromeric heterochromatin. Cell 91:845–854
21. Brown KE, Baxter J, Graf D et al (1999) Dynamic repositioning of genes in the nucleus of lymphocytes preparing for cell division. Mol Cell 2:207–217
22. Singh S, Wass J, Devaraj J et al (1993) Translocation (Y;1)(q12; q21) in acute leukemia. Cancer Genet Cytogenet 70:136–139
23. Busson-Le Coniat M, Salomon-Nguyen F, Dastugue N et al (1999) Fluorescence in situ hybridization analysis of chromosome 1 abnormalities in hematopoietic disorders: rearrangements of DNA satellite II and new recurrent translocations. Leukemia 13:1975–1981
24. Rowley JD (1975) Abnormalities of chromosome 1 in myeloproliferative disorders. Cancer 36:1748–1757
25. Prieto F, Badia L, Castell V et al (1981) Citogenética de las leucemias agudas. Sangre 26:738–755
26. GFCH (Groupe Francais de Cytogénétique Hématologique) (1988) Cytogenetics of acutely transformed chronic myeloproliferative syndromes without a Philadelphia chromosome. A multicenter study of 55 patients. Cancer Genet Cytogenet 32:157–168
27. Hollings PE, Giles LM, Rosman I et al (1988) An identical t(Y;1)(q12;q21) in two patients with myelodisplastic syndromes. Cancer Genet Cytogenet 34:285–293
28. Thompson PW, Standers GR, Geddes AD (1991) Transient t(Y;1)(q12;q21) in a patient with Fanconi's anemia and myelodisplastic syndrome. Cancer Genet Cytogenet 52:201–202
29. Wei DC, Wan TSK, Chan LC et al (1993) Der(Y)t(Y;1) is a nonrandom abnormality in myelodysplastic syndrome. Cancer Genet Cytogenet 70:155–156
30. Sawyer JR, Swanson CM, Koller MA et al (1995) Centromeric instability of chromosome 1 resulting in multibranched chromosomes, telomeric fusions, and "jumping translocations" of 1q in a human immunodeficiency virus-related non-Hodgkin's lymphoma. Cancer 76:1238–1244
31. Michaux L, Wlodarska I, Rodrigues Pereira Velloso E et al (1996) Translocation (Y;1)(q12;q12) in hematologic malignancies. Report on two new cases, FISH characterization, and review of the literature. Cancer Genet Cytogenet 86:35–38
32. Raymarkers R, Stellink F, Geurts van Kessel A (1996) Derivative (Y)t(Y;1)(q12;q12), +9 in a patient with polycythemia vera during transition into myelodysplasia. Cancer Genet Cytogenet 88:83–85
33. Ohsaka A, Hisa T (2002) Spectral karyotyping refined the identification of a der(Y)t(Y;1)(q11.1 or.2;q12) in the blast cells of a patient with atypically chronic myeloid leukemia. Acta Haematologica 107:224–229
34. Berra B, Papi L, Bigozzi U et al (1991) Correlation between cytogenetic data and ganglioside pattern in human meningiomas. Int J Cancer 47:329–333
35. Jin C, Jin Y, Wennerberg J et al (1997) Cytogenetic analysis of inverted nasal papillomas and demonstration of genetic convergence during in vitro passaging. Int J Cancer 70:668–673

Virchows Arch (2009) 454:317–325
DOI 10.1007/s00428-008-0720-8

ORIGINAL ARTICLE

VEGF-C and VEGFR-3 in a series of lymphangiomas: Is superficial lymphangioma a true lymphangioma?

Eijun Itakura · Hidetaka Yamamoto · Yoshinao Oda · Masutaka Furue · Masazumi Tsuneyoshi

Received: 15 September 2008 / Revised: 24 November 2008 / Accepted: 10 December 2008 / Published online: 17 January 2009

Abstract Lymphangiomas are commonly regarded as vascular malformations during embryonic development rather than as true neoplasms. VEGF-C and VEGFR-3 are known to be active in the formation of lymphangiomas. However, the significance of the disorders seems to be obscured by confusing different entities. In 114 lymphangiomas, we investigated the clinicopathological features and the expression of VEGF-C and VEGFR-3. The age of patients with lymphangioma circumscriptum or intraabdominal lymphangioma was significantly higher than in patients with cavernous lymphangioma and in patients with cystic hygroma. In cavernous lymphangioma, the age of female patients was significantly higher than in male patients. Five adult cystic hygromas were identified. VEGF-C was detected in 21 of 58 (36%) cavernous lymphangiomas, ten of 28 (36%) cystic hygromas, 0 of 12 (0%) lymphangioma circumscriptum, and four of ten (40%) intraabdominal lymphangiomas. VEGFR-3 was detected in 43 of 58 (72%) cavernous lymphangiomas, 20 of 28 (71%) cystic hygromas, six of 12 (50%) lymphangiomas circumscriptum, and seven of ten (70%) intraabdominal lymphangiomas. VEGF-C was absent from superficial lymphangiomas associated with cavernous lymphangiomas. In typical cases of cavernous lymphangioma, VEGF-C was strongly expressed, suggesting that these cases possessed proliferative activity. In cystic hygroma and intraabdominal lymphangioma, VEGF-C was limited in its distribution. Superficial lymphangiomas more likely represent from peripheral lymphatic dilatation rather than due to growth factor.

Keywords Cystic hygroma · Head and neck neoplasm · Lymphangioma · Skin neoplasm · Soft tissue neoplasm · Vascular neoplasm · VEGF-C · VEGFR-3

E. Itakura · H. Yamamoto · Y. Oda (✉) · M. Tsuneyoshi
Department of Anatomic Pathology,
Graduate School of Medical Sciences, Kyushu University,
3-1-1Maidashi, Higashi-ku,
Fukuoka 812-8582, Japan
e-mail: oda@surgpath.med.kyushu-u.ac.jp

E. Itakura · M. Furue
Department of Dermatology,
Graduate School of Medical Sciences, Kyushu University,
3-1-1 Maidashi, Higashi-ku,
Fukuoka 812-8582, Japan

Present address:
E. Itakura
Department of Pathology and Laboratory Medicine,
David Geffen School of Medicine at UCLA,
10833 Le Conte Ave, CHS 1P-162,
Los Angeles, CA 90095-1732, USA

Introduction

Lymphangiomas are benign tumor-like lesions of lymphatics. Whereas hemangiomas have distinctive proliferative and involutional growth phases that distinguish them from vascular malformation [1–3], lymphangiomas are generally considered to be either hamartomas or the linkage between a malformation and a neoplasm. Some lesions exhibit progressive growth and infiltration, leaving open the question of whether they are true neoplasms or hamartomas [4].

Lymphangiomas are often recognized at birth or during infancy, but may also appear spontaneously in adolescence or later life. Traditionally, they have been divided into several types that differ in clinical and histological characteristics. Cavernous lymphangioma is the most common type and is usually present at birth or in infancy. Cystic hygroma is typically seen in the neck at birth. Intraabdominal lymphangiomas are reported to occur most

commonly in the mesentery, followed by the omentum, mesocolon, and retroperitoneum. Lymphangioma circumscriptum is a superficial lesion commonly involving the axilla, adjacent chest wall, oral cavity, and genitals. It may occur at any age, but usually beyond infancy. This form can be primary and secondary. The secondary form occurs in association with lymph stasis following trauma, surgery, radiation, infection, or chronic immobility [5–7].

Vascular endothelial growth factor-C (VEGF-C), in association with its major receptor, VEGF receptor-3 (VEGFR-3; also known as flt4), plays a role in the regulation of lymphatic system development [8, 9]. During late embryogenesis, VEGFR-3 is exclusively expressed in lymphatic endothelial cells [10], lining a network of vessels that drain interstitial fluid and cells from tissues. Excessive production of VEGF-C is associated with increased lymphangiogenesis, as reported in transgenic mice [11]. It has also been proposed that in solid tumors, VEGF-C secreted by cancer cells induces lymphangiogenesis, possibly leading to an increase in tumor metastasis via the lymphatic system [12]. In a study on a small series of lymphangiomas, co-expression of VEGF-C and VEGFR-3 was found in lymphatic endothelial cells, suggesting a role for the positive regulation of lymphangiogenesis [13]. More recently, experimental evidence has been provided for up-regulation of VEGFR-3 in lymphatic endothelial cells from lymphangiomas [14, 15]. We are now reporting the expression patterns of VEGF-C and VEGFR-3 in a large series of lymphangiomas.

Materials and methods

Sample collection

One hundred fourteen cases of lymphangiomas were selected from the 1981–2001 archival files of Kyushu University. All the histological slides were reviewed and reclassified. A case in this series has been previously reported [16]. Biopsy specimens from three cases of intestinal lymphangiectasia were also included in the study.

Immunohistochemistry

Formalin-fixed, paraffin-embedded sections (4 μm thick) were processed for immunohistochemistry using a standard streptavidin–biotin–peroxidase method. Primary antibodies were obtained from Santa Cruz Biotechnology (Santa Cruz, CA, USA). Slides for VEGF-C were digested in 0.1% trypsin for 30 min, and for VEGFR-3, antigen was retrieved by microwave heating. Sections were incubated with primary antibody (1:200) overnight at 4°C. After the development of antibody-bridge labeling, sections were reacted with diaminobenzidine and counterstained. The number of immunoreactive cells was estimated semi-quantitatively as follows: grade 3+, >50% positive cells; grade 2+, 25–50% positive cells; grade 1+, <25% positive cells; −, negative staining [17].

Statistical analysis

Categorical variables were examined by Fisher's exact test. Age of patients was compared with Welch's *t* test and with Welch's one-way analysis of variance (ANOVA) if comparisons involved more than two groups because normal distributions were not obtained. Welch's ANOVA was followed by *post hoc* Holm–Bonferroni test for multiple comparisons. Twenty precent trimmed mean of age and standard error (SE) were also calculated [18]. Immunohistochemical scores were compared with Mann–Whitney *U* test. Spearman's rank correlation was performed to determine whether the immunohistochemical scores were correlated with age or with each other. "Cystic variant" of cavernous lymphangioma was excluded when Fisher's exact test and Spearman's procedure were applied. All data were analyzed by the statistical package R: a language and environment for statistical computing (http://www.R-project.org/). A probability value less than 0.05 was considered significant. Two-tailed *P* values were quoted throughout.

Results

Clinicopathological findings

The 114 patients whose samples were included in the study ranged in age from birth to 79 years (mean, 19.3 years;

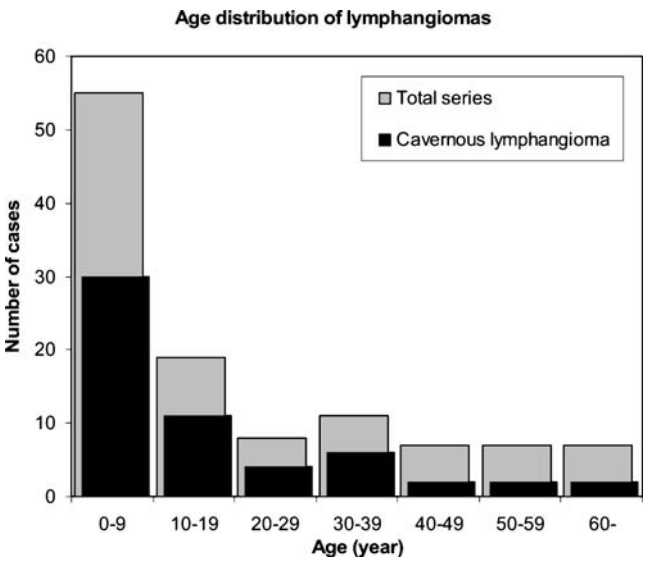

Fig. 1 Age distribution of the total series (n=114) and cavernous lymphangioma (n=58)

Table 1 Comparison of baseline clinical characteristics

		Age (mean, years)	Sex (M:F)
Cavernous lymphangioma	(*n*=58)	15.8	29:29
Cystic hygroma	(*n*=28)	8.5	14:14
Lymphangioma circumscriptum	(*n*=12)	37.1	4:8
Intra-abdominal lymphangioma	(*n*=10)	38.8	5:5
Total series	(*n*=114)	19.3	54:60
P value		*P*=0.0002	*P*=0.77

For continuous variables (age): *P* value for Welch's ANOVA and *post hoc* Holm test
For categorical variables (sex): *P* value for Fisher's exact test
*$P<0.05$, **$P<0.01$

median, 11.5 years; Fig. 1). The 20% trimmed mean was 14.2 years (SE=2.2).

The lesions were classified as cavernous lymphangioma, cystic hygroma, cutaneous lymphangioma, intraabdominal lymphangioma, and other miscellaneous types. Cutaneous lymphangioma was further classified into superficial (lymphangioma circumscriptum) and deep. Baseline clinical and pathological characteristics are summarized in Tables 1 and 2, respectively. The anatomical location of lymphangiomas is shown in Table 3.

Cavernous lymphangioma

Fifty-eight cases were classified as cavernous lymphangioma. They were located in subcutaneous tissue and skeletal muscle. There was no difference in tissue localization among cavernous lymphangiomas of the different locations. Clinically, cavernous lymphangioma of the tongue and lip presented as macroglossia and macrocheilia. The age range of patients with cavernous lymphangioma at the time of diagnosis was 0 to 73 years (mean, 15.8 years; median, 9 years). The 20% trimmed mean age was 13.2 years (SE=2.4). Welch's *t* test revealed a significant difference between the age of male patients (mean, 8.9 years; median, 5 years) and that of female patients (mean, 22.8 years; median, 17 years; *P*=0.0018). The 20% trimmed mean ages of male and female patients were 6.3 years (SE=1.6) and 19.0 years (SE=4.4), respectively.

Gross findings showed that a sponge-like mass consisted of numerous microcysts. Histopathologically, irregular interconnecting lymphatic vessels with a thin and discontinuous smooth muscle layer were seen. Lymphatic spaces contained proteinaceous material, occasional lymphocytes, and few red blood cells. Supporting stroma was composed of collagen. In stroma-rich areas, microscopic lymphatic channels frequently lacked a muscle layer. In some cases, lymphoid aggregates were observed (Fig. 2a).

Five cases (9%) showed prominent cystic change and were classified as cystic variants of cavernous lymphangioma. Gross and histopathological findings showed large multiple cysts in the main mass. The sites involved by this variant were extremities or the lower abdominal region, distinguishable from cystic hygroma, which occurs in the cervicofacial and thoracic areas. Eleven cases (19%) had

Table 2 Comparison of pathological characteristics

Subtypes	Characteristics
Cavernous lymphangioma	Consists of irregular interconnecting lymphatic vessels with a thin and discontonuous smooth muscle layer. In stoma-rich areas, lymphatic channels frequently lack a muscle layer. Lymphoid aggregates may be accompanied.
Cystic variant	Prominent cystic change is seen in the main mass of cavernous lymphangioma.
Accompanying superficial lymphangioma	Occurs on the skin overlying the main mass of cavernous lymphangioma. Hispathological findings are similar to lymphangioma circumsriptum.
Cystic hygroma	Occurs exclusively in the cervicofacial, axillary and pectoral regions. It consists of one or more interconnecting large cysts with a thin wall. Lymphoid aggregates may be accompanied.
Cutaneous lymphangioma	
Lymphangioma circumscriptum	Consists of dilated capillary lymphatic vessels in the papillary dermis. Large vessels are not involved. The overlying epidermis is acanthotic and papillomatous.
Deep type	Locates in the dermis. Similar to but smaller than cavernous lymphangioma. No epidermal involvement.
Intraabdominal lymphangioma	Intraabdominal counterpart of cavernous lymphangioma. It consists of irregular interconnecting lymphatic vessels with a thin and discontinuous smooth muscle layer.

Table 3 Anatomical location of a series of lymphangiomas (114 cases)

Subtypes & anatomical location	Number (%)	Subtotal (%)	Total (%)
Cavernous lymphangioma			58 (51.8%) (11[a], 5[b])
Head and Neck		20 (17.9%) (4[a])	
Cheek	2 (1.8%)		
Lip	3 (2.7%)		
Tongue	4 (3.6%) (3[a])		
Oral cavity	1 (0.9%) (1[a])		
Submandibular region	4 (3.6%)		
Cervical region	6 (5.4%)		
Trunk		16 (14.3%) (2[a], 2[b])	
Pectoral region	4 (3.6%)		
Mediastinum	1 (0.9%)		
Axillary region	4 (3.6%) (2[a])		
Abdominal region	3 (2.7%) (1[b])		
Inguinal region	1 (0.9%) (1[b])		
Back	2 (1.8%)		
Cauda equina	1 (0.9%)		
Upper limb		9 (8.0%) (2[a], 1[b])	
Arm	3 (2.7%) (1[a])		
Forearm	3 (2.7%) (1[b])		
Hand/Thumb/Finger	3 (2.7%) (1[a])		
Lower limb		13 (11.6%) (3[a], 2[b])	
Buttock	1 (0.9%)		
Thigh	8 (7.1%) (2[a], 2[b])		
Popliteal region	1 (0.9%)		
Leg	3 (2.7%) (1[a])		
Cystic hygroma			28 (25.0%)
Submandibular/Cervical/ Axillary/Pectoral regions	28 (25.0%)		
Cutaneous lymphangioma			14 (10.7%) (2[c])
Cheek	1 (0.9%) (1[c])		
Nuchal region	1 (0.9%)		
Axillary region	2 (1.8%)		
Abdominal region	1 (0.9%)		
Lumbar region	1 (0.9%)		
Vulva	4 (3.6%)		
Forearm	1 (0.9%)		
Thigh	1 (0.9%)		
Foot	2 (1.8%) (1[c])		
Intraabdominal lymphangioma			10 (8.9%)
Stomach	1 (0.9%)		
Ileum	2 (1.8%)		
Colon	3 (2.7%)		
Retroperitoneum	4 (3.6%)		
Others			4 (3.6%)
Epicardium	1 (0.9%)		
Lung	1 (0.9%)		
Vertebra	2 (1.8%)		

[a] Number of cavernous lymphangioma with superficial lymphangioma
[b] Number of cystic variant of cavernous lymphangioma
[c] Number of deep type of cutaneous lymphangioma

superficial components resembling lymphangioma circumscriptum. They presented with papules on the skin overlying the main mass of cavernous lymphangioma in deep soft tissue. Histopathologically, these superficial lesions consisted of dilated capillary lymphatic vessels in the papillary dermis. The overlying epidermis was acanthotic and papillomatous.

Cystic hygroma

Twenty-eight cases were classified as cystic hygroma. These were exclusively located in the cervicofacial, axillary, and pectoral regions. In two cases, lesions extended into the mediastinum. The age range at the time of diagnosis was 0 to 44 years (mean, 8.5 years; median,

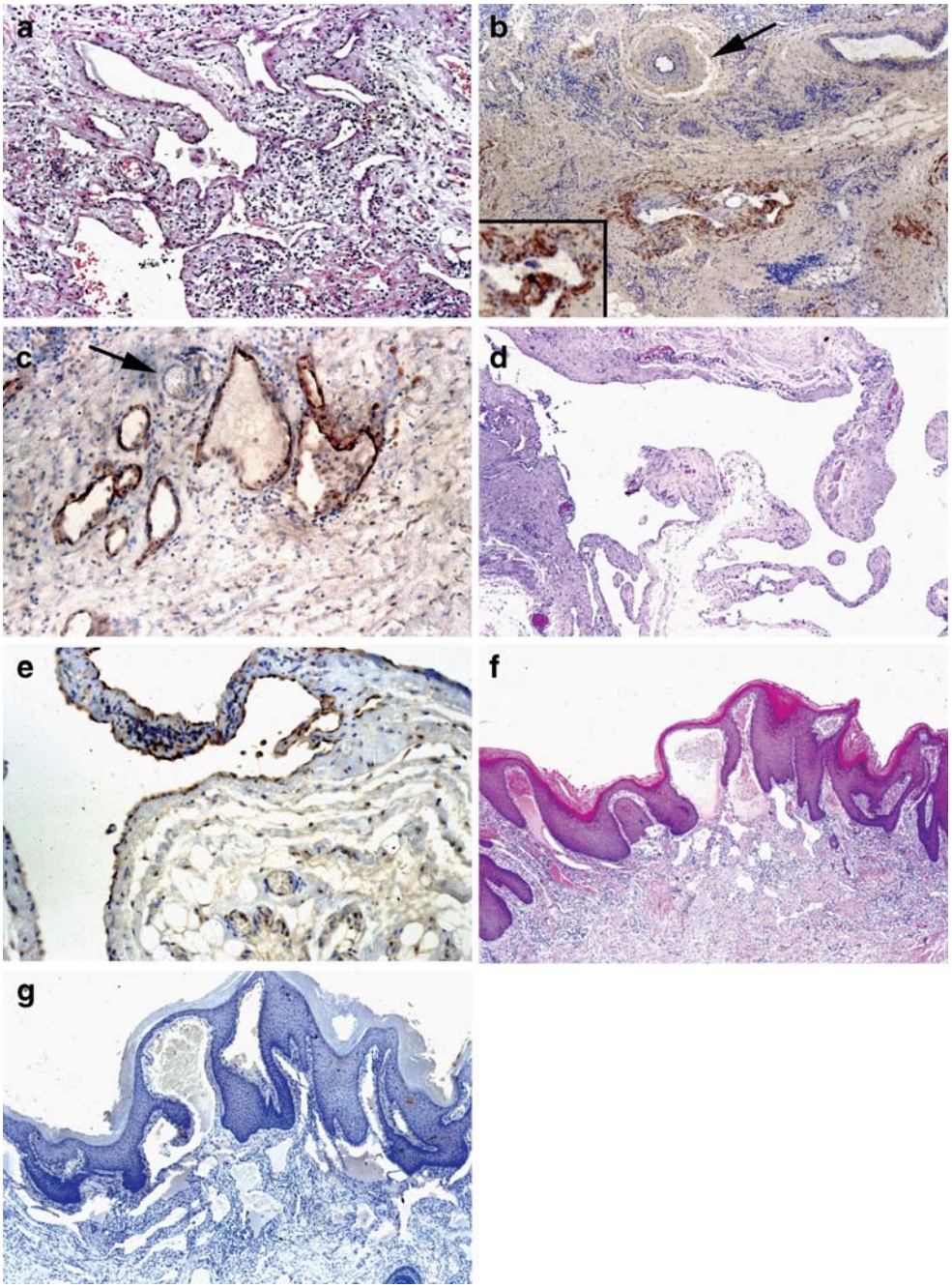

Fig. 2 Cavernous lymphangioma (**a**–**c**). **a** Irregular interconnecting lymphatic channels are located in the collagenous stroma. Lymphoid aggregates are also observed. **b** Strong reactivity for VEGF-C is seen in the lymphatic endothelium and in the smooth muscle cells of irregularly shaped lymphatic vessels. Immunoreactivity for VEGF-C is not detected in normal existing blood vessels (*arrow*). **c** Strong reactivity for VEGFR-3 is seen in the lymphatic endothelium. Immunoreactivity for VEGFR-3 is absent in normal existing blood vessels (*arrow*). Cystic hygroma (**d**–**e**). **d** Cystic lymphatic spaces with a thin and discontinuous smooth muscle layer. **e** Immunoreactivity for VEGFR-3 is detected in the endothelium lining the large cystic lymphatic spaces. Lymphangioma circumscriptum **f**–**g**. **f** The protuberant lesion consists of dilated capillary lymphatic vessels in the papillary dermis. **g** Immunoreactivity for VEGF-C is absent in the superficial lesion

3 years). The 20% trimmed mean age was 4.1 years (SE=1.5). Five cases occurred in adults. Clinical characteristics of adult cystic hygroma are shown in Table 4. There was one case of recurrence 38 years after operation at the age of 6 years. The other adult cases were seen as a new development. There was no significant difference between the age of male patients (mean, 11.8 years; median, 6.5 years) and that of female patients (mean, 5.3 years; median, 1 year; $P>0.05$). The 20% trimmed mean ages of male and female patients were 8.3 years (SE=3.6) and 1.3 years (SE=0.7), respectively.

Gross findings showed one or more interconnecting large cysts with a thin cyst wall. Histopathologically, large irregular lymphatic vessels were seen. The layer of smooth muscle was thin and discontinuous (Fig. 2d). Lymphoid aggregates were occasionally observed. Cavernous lymphangiomas occurring in the head and neck or in the trunk were distinguished from cystic hygroma based on the

Table 4 Clinical features of adult cystic hygroma

Case	Age (years)	Sex	Site of lesion	Previous history
1	18	F	Neck	
2	24	M	Neck	
3	37	M	Mediastinum	
4	43	F	Neck	
5	44	M	Chest wall	Surgery for cystic hygroma at the age of 6 years

predominant presence of microscopic cysts in cavernous lymphangiomas.

Cutaneous lymphangioma

Cutaneous lymphangiomas were classified as superficial and deep. The former represents lymphangioma circumscriptum. In the latter, only the deep dermis was involved without epidermal or superficial dermal changes.

Superficial type (lymphangioma circumscriptum) Twelve cases were classified as lymphangioma circumscriptum. The age range was from 9 to 79 years (mean, 37.1 years; median, 34 years). The 20% trimmed mean age was 34.5 years (SE=8.6). The age of patients with lymphangioma circumscriptum was significantly higher than that of patients with superficial lymphangioma associated with cavernous lymphangioma (mean, 18.5 years; median, 17 years; 20% trimmed mean, 18.1 years [SE=4.6]) (P= 0.022). The patients with lymphangioma circumscriptum presented with papules on the skin. Histopathologically, the lesions consisted of dilated capillary lymphatic vessels positioned within the papillary dermis. Large vessels were not involved. The overlying epidermis was acanthotic and papillomatous (Fig. 2f).

Deep type Two cases were classified as this subtype, one in the cheek, the other in the foot. These presented with small nodules in skin. The histopathological features were similar to cavernous lymphangioma. Irregular interconnecting lymphatic vessels with a thin and discontinuous muscular layer were seen, limited to the deep dermis. Deep type cutaneous lymphangiomas were distinguished from lymphangioma circumscriptum based on absence of superficial dermal lesions and lack of hyperplastic epidermal changes in the deep type.

Intraabdominal lymphangioma

Ten cases were classified as intraabdominal lymphangioma. The age range of patients with intraabdominal lymphangioma at the time of diagnosis was 0 to 62 years (mean, 38.8 years; median, 45 years). The 20% trimmed mean age was 42.5 years (SE=7.1). Gross and histopathological findings were similar to those of cavernous lymphangioma. The lesion consisted of irregular lymphatic vessels with a thin and discontinuous smooth muscle layer.

Others

There were two patients with lymphangioma of the spine and another with lung. The pathological features were similar to those of typical cavernous lymphangioma. A lymphangioma of the epicardium was also identified, composed of relatively uniform microscopic cysts.

Of three cases of intestinal lymphangiectasia, two were from the jejunum and one from the ileocecal valve. The age range of patients with intestinal lymphangiectasia was 55 to 62 years.

Welch's ANOVA revealed a highly significant difference in mean age among cavernous lymphangioma, cystic

Table 5 Results from the immunohistochemical analysis

	VEGF-C	(row %, reactivity: number of cases)		VEGFR-3	(row %, reactivity: number of cases)
Cavernous lymphangioma (excluding the cystic variant)	21/53	(40%, 1+:13, 2+:7, 3+:1)	**	38/53	(72%, 1+:21, 2+:9, 3+:8)
Cystic hygroma	10/28	(36%, 1+:9, 2+:1)	*	20/28	(71%, 1+:13, 2+:3, 3+:4)
Lymphangioma circumscriptum	0/12	(0%)	*	6/12	(50%; 1+:4, 2+:1, 3+:1)
Intra-abdominal lymphangioma	4/10	(40%, 1+:4)		6/10	(60%; 2+:2, 3+:4)
P value	*P*=0.035			*P*=0.45	

P value for Fisher's exact test
*$P<0.05$, **$P<0.01$

hygroma, lymphangioma circumscriptum, and intraabdominal lymphangioma (P=0.0002). The mean age of patients with lymphangioma circumscriptum was significantly higher than cavernous lymphangioma (P=0.034) or cystic hygroma (P=0.0065) by Holm–Bonferroni test. The mean age of patients with intraabdominal lymphangioma was significantly higher than cavernous lymphangioma (P=0.034) or cystic hygroma (P=0.0081) by Holm–Bonferroni test.

Immunohistochemical findings

Immunoreactivity for VEGF-C was detected in lymphatic endothelium and smooth muscle (Fig. 2b). VEGFR-3 was found exclusively in lymphatic endothelium (Fig. 2c). VEGF-C and VEGFR-3 were specific to lymphatic lineage and were not detected in blood vessels (Fig. 2b, c). Results from the immunohistochemical analysis are summarized in Table 5.

In cavernous lymphangioma including the cystic variant, VEGF-C and VEGFR-3 were detected in 21 of 58 cases (36%) and 41 of 58 cases (71%), respectively. Spearman's coefficient between VEGF-C and VEGFR-3 was 0.31 (P= 0.027), suggesting that they were mildly correlated at a significant level. There was no significant correlation between age and either VEGF-C or VEGFR-3. In cavernous lymphangioma excluding the cystic variant, VEGF-C and VEGFR-3 were detected in 21 of 53 cases (40%) and 38 of 53 cases (72%), respectively. In the cystic variant (five cases), VEGFR-3 was detected in three of five cases (60%), but VEGF-C was not detected. There was no significant difference in the reactivity of VEGF-C or VEGFR-3 between male and female patients. VEGF-C was absent from the superficial lymphangioma when associated with cavernous lymphangioma (11 cases). VEGFR-3 was detected in the lymphatic endothelium of the lesion in seven of 11 cases (64%).

In cystic hygroma, VEGF-C and VEGFR were detected in ten of 28 cases (36%) and 20 of 28 cases (71%), respectively. In positive cases, VEGF-C expression was patchy and focal in the lymphatic vessel wall and the positivity score was limited to 1+ except for one case. VEGFR-3 was detected in the lymphatic endothelium of the large cystic lymphatic vessels (Fig. 2e). The degree of expression of VEGFR-3 varied among the cases. Spearman correlation coefficients between age and either VEGF-C or VEGFR-3 were not significant.

In lymphangioma circumscriptum, VEGFR-3 was detected in the lesional endothelium in six of 12 (50%), but VEGF-C was not detected in all cases (Fig. 2g). In the deep type, VEGF-C was detected in one of two cases. VEGFR-3 was detected in both cases.

In intraabdominal lymphangioma, VEGF-C was detected in lesional cells in four of ten (40%). In positive cases, VEGF-C expression was patchy and focal and of limited extent (reactivity, 1+). VEGFR-3 was detected in the lesional endothelium in six of ten (60%). In intestinal lymphangiectasia, VEGFR-3 was detected in the lesional endothelium in two of three (67%), but VEGF-C was absent in all cases.

In the lung lymphangioma, immunoreactivity was detected for both VEGF-C (reactivity, 3+) and VEGFR-3 (reactivity, 3+). In the epicardial lymphangioma, immunoreactivity was also detected for both VEGF-C (reactivity, 2+) and VEGFR-3 (reactivity, 2+). In both vertebral lymphangiomas, neither VEGF-C nor VEGFR-3 was detected.

Fisher exact test revealed a highly significant difference in the positivity of VEGF-C among the four groups (P= 0.0035) as well as between lymphangioma circumscriptum and cavernous lymphangioma excluding the cystic variant (P=0.0063), cystic hygroma (P=0.019), or intraabdominal lymphangioma (P=0.029). There was no significant difference in the positivity of VEGFR-3 among these groups.

Discussion

Lymphangiomas are generally regarded as vascular malformations [4, 7] occurring during embryonic development when VEGF-C and VEGFR-3 are central regulators. Peak VEGF-C expression is seen during the earlier stages of lymphangiogenesis with much less expression during lymphatic capillary organization and functional integration. After embryonic development, VEGF-C expression decreases in most tissues, remaining high in the lymph nodes [8, 19]. VEGF-C promotes survival of the VEGFR-3-expressing lymphatic endothelial cells via the MAPK signaling pathway [20]. However, the role of VEGFR-3 signaling is not very important for the survival of mature lymphatic vessels [21]. Although VEGFR-3 is mostly regarded as a lymphatic marker, it is not exclusive to the lymphatic lineage. VEGFR-3 is exceptionally expressed in blood vascular endothelium during embryogenesis and is essential in the development of the major cardiovascular system before the emergence of the lymphatic vessels [22]. VEGFR-3 may also be present, though to a less extent, in some blood vascular tumors including angiosarcoma [17, 23, 24]. This receptor has been detected in virtually all Kaposi's sarcomas [23–25] which are consequently thought to originate from lymphatic endothelium.

In this study, we found that the expression of the factor and its receptor was different among the various types. VEGF-C was detected in lymphatic endothelium and smooth muscle in 36% cavernous lymphangioma. Positivity was moderately correlated to VEGFR-3 expression, suggesting they both contribute to the development of this lesion, possibly by autocrine and paracrine regulation [13].

VEGFR-3 was detected in 72% of cavernous lymphangiomas. The receptor was expressed in both small and dilated lymphatics, in contrast to D2-40, another lymphatic endothelial cell-specific marker recognizing M2A antigen which has a tendency for better positivity in small lymphatic channels [26]. We hypothesize that VEGF-C and VEGFR-3 might be preferentially expressed in early life and the expression of VEGF-C and VEGFR-3 would tend to decrease in older patients. However, in our study, there was no significant correlation between the immunoreactivity and patient's age. Strong expression of VEGF-C and VEGFR-3 was detected even in older adult patients. Although it is widely regarded as a hamartomatous lesion rather than a true neoplasia, VEGF-C and VEGFR-3 seem to contribute to proliferation in certain cases of cavernous lymphangioma, which may account for some cavernous lymphangiomas being more active and possibly neoplastic, especially in older adult patients.

Cystic hygroma, also called macrocystic lymphatic malformation of the head and neck, is believed to be a consequence of disruption of normal lymphatic development at the lymphovenous connection as a result of defective genes. It is considered that a small portion of the jugular lymphatic sac located laterally in the neck is sequestrated during embryologic life and later becomes cystically dilated. This lesion has been associated with aneuploid chromosomal abnormalities, particularly Turner's syndrome, with poor survival [27–29]. Cystic hygroma is usually present at birth and can be diagnosed by prenatal ultrasound. Spontaneous regression may be observed *in utero*, but this does not preclude abnormal karyotype or fetal anomalies [28]. Meanwhile, cystic hygroma is very rarely seen in adults. It is considered highly unusual for cystic hygroma to present after the fourth decade of life, although there are a few reports in the literature [30–34]. Recurrence after resection is uncommon, but it may occur within a few years. There are only a few case reports of recurrence after more than 20 years [35, 36]. In our study, VEGF-C expression by lesional cells of cystic hygroma was more focal and limited in its distribution. Cystic hygroma may be responsive to VEGF-C, but increase in size may only follow accumulation of fluid after lymphatic sequestration.

It has been proposed that lymphangioma circumscriptum represents dilatation of peripheral lymphatics secondary to absent, inadequate, or obstructed efferents [37]. In our study, VEGF-C was absent, and this growth factor does not seem to be associated with the development of lymphangioma circumscriptum. It may be the lymphatic counterpart of angiokeratoma, which is of a telangiectatic nature shared by different disease entities. The histological features resemble each other and share ectatic vessels in the papillary dermis with overlying hyperplastic epidermis. The nature of this superficial lymphangioma is more likely considered to be lymphangiectatic.

Lymphangiomas in deep soft tissue may accompany superficial lesions in overlying skin [38] or mucosa. In our series, the superficial lesion was also recognized in 11 cases (19%) of cavernous lymphangioma. VEGF-C was absent in the superficial lesion even in the cases in which the main deep component expresses VEGF-C. The superficial lesion may also only follow chronic lymphatic stasis.

Intraabdominal lymphangiomas have been considered the counterpart of cavernous lymphangioma in the trunk or extremities [4]. However, patients with intraabdominal lymphangioma were significantly older than those with cavernous lymphangioma or cystic hygroma. Intraabdominal lymphangioma is apt to be diagnosed later in life, partly because it is clinically less significant. VEGF-C was detected in 40% cases, and in the positive cases, its expression was focal and limited in its distribution. Previous cell proliferation analysis revealed that intraabdominal lymphangiomas are quiescent, manifesting low activity [39]. Enlargement of intraabdominal lymphangiomas may be due to engorgement by chyle and localized secondary reaction, and the contribution of the growth factor seems limited.

In pulmonary lymphangioma, despite a report that the proliferation activity of this type was low [40], our case showed strong VEGF-C reactivity, suggesting high proliferative activity. In bone lymphangioma, expression of VEGF-C and VEGFR-3 was negative. However, immunoreactivity may have been abolished by decalcification.

In summary, we have demonstrated that the expression of VEGF-C was different in the various types of lymphangioma. In some typical cases of cavernous lymphangioma, VEGF-C was strongly expressed, suggesting that these cases possessed proliferative activity. In cystic hygroma and intraabdominal lymphangioma, the expression of VEGF-C was focal and limited in its distribution. VEGF-C was absent from lymphangioma circumscriptum and superficial lymphangiomas associated with cavernous lymphangiomas. The nature of superficial lymphangiomas is more likely considered to be lymphangiectatic.

Acknowledgment The authors would like to thank Dr. Walter F. Coulson, Emeritus Professor, Department of Pathology and Laboratory Medicine, David Geffen School of Medicine at UCLA, for reviewing and editing the manuscript.

Conflict of interest We declare that we have no conflict of interest.

References

1. Takahashi K, Mulliken JB, Kozakewich HP et al (1994) Cellular markers that distinguish the phases of hemangioma during infancy and childhood. J Clin Invest 93:2357–2364

2. Boye E, Yu Y, Paranya G et al (2001) Clonality and altered behavior of endothelial cells from hemangiomas. J Clin Invest 107:745–752
3. Khan ZA, Melero-Martin JM, Wu X et al (2006) Endothelial progenitor cells from infantile hemangioma and umbilical cord blood display unique cellular responses to endostatin. Blood 108:915–921
4. Weiss SW, Goldblum JR (2001) Enzinger and Weiss's soft tissue tumors, 4th edn. Mosby. St. Louis, MO
5. Flanagan BP, Helwig EB (1977) Cutaneous lymphangioma. Arch Dermatol 113:24–30
6. Diaz-Cascajo C, Borghi S, Weyers W et al (1999) Benign lymphangiomatous papules of the skin following radiotherapy: a report of five new cases and review of the literature. Histopathology 35:319–327
7. Sangeza OP, Requena L (2003) Pathology of vascular skin lesions: clinicopathological correlations. Humana, Totowa, NJ
8. Oliver G, Alitalo K (2005) The lymphatic vasculature: recent progress and paradigms. Annu Rev Cell Dev Biol 21:457–483
9. Cueni LN, Detmar M (2006) New insights into the molecular control of the lymphatic vascular system and its role in disease. J Invest Dermatol 126:2167–2177
10. Kaipainen A, Korhonen J, Mustonen T et al (1995) Expression of the fms-like tyrosine kinase 4 gene becomes restricted to lymphatic endothelium during development. Proc Natl Acad Sci U S A 92:3566–3570
11. Jeltsch M, Kaipainen A, Joukov V et al (1997) Hyperplasia of lymphatic vessels in VEGF-C transgenic mice. Science 276:1423–1425
12. Stacker SA, Achen MG, Jussila L et al (2002) Lymphangiogenesis and cancer metastasis. Nat Rev Cancer 2:573–583
13. Huang HY, Ho CC, Huang PH et al (2001) Co-expression of VEGF-C and its receptors, VEGFR-2 and VEGFR-3, in endothelial cells of lymphangioma. Implication in autocrine or paracrine regulation of lymphangioma. Lab Invest 81:1729–1734
14. Norgall S, Papoutsi M, Rossler J et al (2007) Elevated expression of VEGFR-3 in lymphatic endothelial cells from lymphangiomas. BMC Cancer 7:105
15. Kasten P, Schnöink G, Bergmann A et al (2007) Similarities and differences of human and experimental mouse lymphangiomas. Dev Dyn 236:2952–2961
16. Saito T, Terada K, Tsuchiya K et al (1999) Lymphangioma presenting as a dumbbell tumor in the epidural space of the lumbar spine. Spine 24:74–76
17. Itakura E, Yamamoto H, Oda Y et al (2008) Detection and characterization of vascular endothelial growth factors and their receptors in a series of angiosarcomas. J Surg Oncol 97:74–81
18. Wilcox RR (2005) Introduction to robust estimation and hypothesis testing, 2nd edn. Elsevier, Burlington, MA
19. Lymboussaki A, Olofsson B, Eriksson U et al (1999) Vascular endothelial growth factor (VEGF) and VEGF-C show overlapping binding sites in embryonic endothelia and distinct sites in differentiated adult endothelia. Circ Res 85:992–999
20. Mäkinen T, Veikkola T, Mustjoki S et al (2001) Isolated lymphatic endothelial cells transduce growth, survival and migratory signals via the VEGF-C/D receptor VEGFR-3. EMBO J 20:4762–4773
21. Pytowski B, Goldman J, Persaud K et al (2005) Complete and specific inhibition of adult lymphatic regeneration by a novel VEGFR-3 neutralizing antibody. J Natl Cancer Inst 97:14–21
22. Dumont DJ, Jussila L, Taipale J et al (1998) Cardiovascular failure in mouse embryos deficient in VEGF receptor-3. Science 282:946–949
23. Partanen TA, Alitalo K, Miettinen M (1999) Lack of lymphatic vascular specificity of vascular endothelial growth factor receptor 3 in 185 vascular tumors. Cancer 86:2406–2412
24. Folpe AL, Veikkola T, Valtola R et al (2000) Vascular endothelial growth factor receptor-3 (VEGFR-3): a marker of vascular tumors with presumed lymphatic differentiation, including Kaposi's sarcoma, Kaposiform and Dabska-type hemangioendotheliomas, and a subset of angiosarcomas. Mod Pathol 13:180–185
25. Skobe M, Brown LF, Tognazzi K et al (1999) Vascular endothelial growth factor-C (VEGF-C) and its receptors KDR and flt-4 are expressed in AIDS-associated Kaposi's sarcoma. J Invest Dermatol 113:1047–1053
26. Galambos C, Nodit L (2005) Identification of lymphatic endothelium in pediatric vascular tumors and malformations. Pediatr Dev Pathol 8:181–189
27. Chervenak FA, Isaacson G, Blakemore KJ et al (1983) Fetal cystic hygroma. Cause and natural history. N Engl J Med 309:822–825
28. Ganapathy R, Guven M, Sethna F et al (2004) Natural history and outcome of prenatally diagnosed cystic hygroma. Prenat Diagn 24:965–968
29. Gedikbasi A, Gul A, Sargin A et al (2007) Cystic hygroma and lymphangioma: associated findings, perinatal outcome and prognostic factors in live-born infants. Arch Gynecol Obstet 276:491–498
30. Goodman J, McClintock J, Denton GR et al (1963) Cystic hygromas in adults. Arch Surg 86:641–644
31. Nussbaum M, Buchwald RP (1981) Adult cystic hygroma. Am J Otolaryngol 2:159–162
32. Baer S, Davis J (1989) Cystic hygroma presenting in adulthood. J Laryngol Otol 103:976–977
33. Gleason TJ, Yuh WTC, Tali ET et al (1993) Traumatic cervical cystic lymphangioma in an adult. Ann Otol Rhinol Laryngol 102:564–566
34. Morley SE, Ramesar KCRB, Macleod DAD (1999) Cystic hygroma in an adult: a case report. J R Coll Surg Edinb 44:57–58
35. Leipzig B, Rabuzzi DD (1978) Recurrent massive cystic lymphangioma. Otolaryngology 86:758–760
36. Scally CM, Black JH (1990) Cystic hygroma: massive recurrence in adult life. J Laryngol Otol 104:908–910
37. Peachey RD, Lim CC, Whimster IW (1970) Lymphangioma of skin. A review of 65 cases. Br J Dermatol 83:519–527
38. Russell B, Pridie RB (1967) Lymphangioma circumscriptum with involvement of deep lymphatics. Br J Dermatol 79:300
39. Mahle C, Schwartz M, Popek E et al (1997) Intra-abdominal lymphangiomas in children and adults. Assessment of proliferative activity. Arch Pathol Lab Med 121:1055–1062
40. Brown M, Pysher T, Coffin CM (1999) Lymphangioma and congenital pulmonary lymphangiectasis: a histologic, immunohistochemical, and clinicopathologic comparison. Mod Pathol 12:569–575

Virchows Arch (2009) 454:327–331
DOI 10.1007/s00428-008-0715-5

CASE REPORT

Inflammatory fibroid polyp of the small bowel with a mutation in exon 12 of *PDGFRα*

Silvia Calabuig-Fariñas · José Antonio López-Guerrero · M Jesús Nicolau Ribera · Samuel Navarro · David Ramos · Antonio Pellín · Antonio Llombart-Bosch

Received: 18 July 2008 / Revised: 28 October 2008 / Accepted: 4 December 2008 / Published online: 3 February 2009

Abstract Inflammatory fibroid polyp (IFP) is a benign reactive uncommon submucosal lesion of the gastrointestinal tract, the small intestine being the most common site of origin. Histologically, IFPs are characterized by spindle cells, a heavy inflammatory infiltrate including eosinophils and onion-sheet-like formation of lesional cells around blood vessels. We present a case report of an IFP harboring an activation mutation in the *PDGFRα* gene. The lesion was positive for CD34, PDGFRα, and p-PDGFRα immunostaining but was negative for c-KIT and desmin. After a sequencing analysis of *KIT* and *PDGFRα,* a mutation consisting of an in-frame deletion of codons 567-571 and a missense mutation in codon 566 (S566R) of *PDGFRα* was observed. This mutation could activate key cellular pathways with involvement in the pathogenesis of this entity. We concluded that more studies are necessary in order to clarify if this finding is a biologically distinct behavior or, on the contrary, represents a specific feature of the IFP.

Keywords Inflammatory fibroid polyp · PDGFRα · Tyrosine kinase · Mutation · Small intestine

S. Calabuig-Fariñas · S. Navarro · D. Ramos · A. Pellín · A. Llombart-Bosch
Department of Pathology, School of Medicine,
University of Valencia,
Valencia, Spain

J. A. López-Guerrero
Laboratory of Molecular Biology,
Fundacion Instituto Valenciano de Oncologia,
Valencia, Spain

M. J. N. Ribera
Service of Pathology,
Fundacion Intituto Valenciano de Oncologia,
Valencia, Spain

A. Llombart-Bosch (✉)
Department of Pathology,
Universitat de Valencia Estudi General (UVEG),
Avda. Blasco Ibáñez, 17,
46010 Valencia, Spain
e-mail: antonio.llombart@uv.es

Introduction

First described by Vanek [1] in 1949 as "gastric submucosal granuloma with eosinophilic infiltration," inflammatory fibroid polyps have been reported in the literature under a variety of names, the term "inflammatory fibroid polyp" (IFP) being currently the most accepted [2]. The IFP is a benign reactive lesion and occurs predominantly in adults. These polyps have been more frequently seen in the small intestine and stomach. Most IFPs are polypoid masses smaller than 5 cm; nevertheless, sizes of up to 20 cm have been reported [3]. IFPs usually appear as a solitary non-encapsulated, submucosal, polypoid lesion consisting of loosely structured stromal tissue, spindle fibroblastlike cells intermingled with inflammatory cells, and numerous small blood vessels [4]. Morphologically, IFPs can mimic several other tumoral and not tumoral processes of the gastrointestinal tract, including inflammatory myofibroblastic tumors, eosinophilic gastroenteritis, gastrointestinal stromal tumors (GIST), or other mesenchymal lesions [5, 6]. At molecular level, mutations in *PDGFRα* have recently been reported in IFPs [7]. In this report, we present the morphology, immunophenotype, and molecular analysis of a case of IFP, showing the mutation of *PDGFRα* exon 12.

Clinical history

Herein, we describe the case of a 78-year-old white man, who was admitted to the emergency room with abdominal pain of 24 h evolution. He had the following surgical-related events: operated for abdominal hernia (1987); colonic resection for diverticulitis (1988); and ischemic cardiopathy (2001).

Due to the acute abdominal pain, an emergency distal jejuno-ileal resection was performed, confirming an intestinal perforation and finding a fleshy tumor filling the totality of the lumen at a distance of 15 cm distal. Until today, the patient is alive and remains free of disease.

Materials and methods

Tissue samples were collected at surgery and processed for routine histopathology, immunohistochemistry, and molecular biology after formalin fixation and paraffin embedding.

Pathology

Paraffin sections of formalin-fixed tissue (3 μm) were used for conventional hematoxylin and eosin staining and immunohistochemistry. The sections were immunostained following the streptavidin-byotin method (LSAB, Dako, Denmark). The antibodies used were: CD34 (monoclonal, 1:50dilution, DAKO), EMA (monoclonal, 1:200, DAKO), ALK (monoclonal, 1:20, DAKO), vimentin (monoclonal, 1:200dilution, Novocastra), colagen IV (monoclonal, 1:50, DAKO), SMA (monoclonal, 1:2 dilution; DAKO), desmin (monoclonal, 1:2 dilution; DAKO), S-100 protein (polyclonal, 1:2 dilution; DAKO), c-KIT (polyclonal, 1:400 dilution, Dako,Denmark), Ki-67 (mib-1, monoclonal, 1:50, DAKO), CD68 (monoclonal, 1:400, DAKO), PDGFRα (polyclonal, 1:200 dilution; Santa Cruz Biotechnology, Santa Cruz, CA, USA) and p-PDGFRα (Tyr 754) (polyclonal, 1:200, Santa Cruz Biotech). Antigen retrieval was obtained by heating in autoclave (1.5 atm, 3 min) using cytrate buffer pH 6.0 (target retrieval solution, Chem Mate, Dako Denmark). The immunoreaction was evaluated by two different pathologists (SN, ALLB) from zero to +++ depending upon intensity and percentage of stained cells.

DNA sequencing

DNA was isolated from 3 to 5 μm sections of fixed and paraffin-embedded tissue. After deparaffinization, the tumor tissue was resuspended in lysis solution (0.5% sodium dodecyl sulfate, 0.5 mg/mL proteinase K, 10 mmol/L Tris–HCl, pH 8, 0.15 M NaCl, and 5 mmol/L ethylenediamine tetraacetic acid) and incubated overnight at 55°C. DNA was extracted with phenol/chloroform/isoamyl alcohol (25:24:1), precipitated with ethanol and dissolved in 10 to 35 μL of ultrapure water. Intronic polymerase chain reaction (PCR) primers were used to amplify exons 9, 11, 13 [8], and 17 [9] of *c-KIT* and exons 12 and 18 of *PDGFRα* [10]. PCR was performed in a reaction volume of 50 μL containing 1 μL of DNA, 50 mmol/L KCl, 10 mmol/L Tris–HCl, pH 8.3, 2 mmol/L $MgCl_2$, 0.2 mmol/L each dNTP, 0.2 μmol/L for each primer, and two units of AmpliTaq Gold (Perkin Elmer, Norwalk, CT, USA). Amplification reactions were carried out in a DNA Thermal Cycler 9600 (Perkin Elmer) after preheating the samples at 95°C for 10 min. The DNA was amplified over 40 cycles of: 1 min of denaturation at 94°C; 1.5 min of annealing at 56°C for *c-KIT* primers or 2 min at 65°C for *PDGFRα* primers; and 1 min of extension at 72°C with an additional final extension step of 10 min. Ten microliters of the PCR products were visualized in ethidium-bromide—stained 2% UltraPure agarose gels (Life Technologies, Paisley, Scotland) and photographed. Negative controls were included in every set of amplifications. Bidirectional sequencing with specific primers was performed on an ABI 310 sequencer using the BigDye Terminator v1.1 kit (Applied Biosystems, Inc, Foster City, CA, USA).

Results

Macroscopically, the tumor was a polypoid submucosal mass of 2.5×2.5×3 cm, showing an off-white coloration and fibrous consistency without exceeding the serosa causing atrophy, splitting, and fraying of the muscle wall layers. Microscopically, it was composed of conglomerate spindle and stellate cells without atypia or mitosis, loosely distributed in a fibromyxoid stroma with occasional concentric "onionskin"-like arrangement within a prominent vascular network. The spindle-cell component was obscured by the inflammatory elements, which were dominated by eosinophils but which also included plasma cells, lymphocytes, neutrophils, and histiocytes.

The morphology of the lesion was consistent with the diagnosis of IFP; even so, an immunohistochemical panel and molecular studies were performed to confirm the diagnosis and exclude other spindle cell intestinal tumors that could have a worse prognosis. The immunohistochemical study confirmed a stronger and diffuse staining for CD34, vimentin, CD68, and PDGFRα, while SMA, ALK, and S-100

Fig. 1 The tumor appeared as a spindle-cell proliferation and "onionskin"-like arrangement with the inflammatory elements, which are dominated by eosinophils (**a** and **b**). Immunohistochemical studies confirmed positive expression for CD34, PDGFRα, p-PDGFRα, and SMA whereas failed to stain for c-KIT where positivity was only observed in mastocytes (**c** to **h**). **a**, ×200; **b** to **h**, ×400

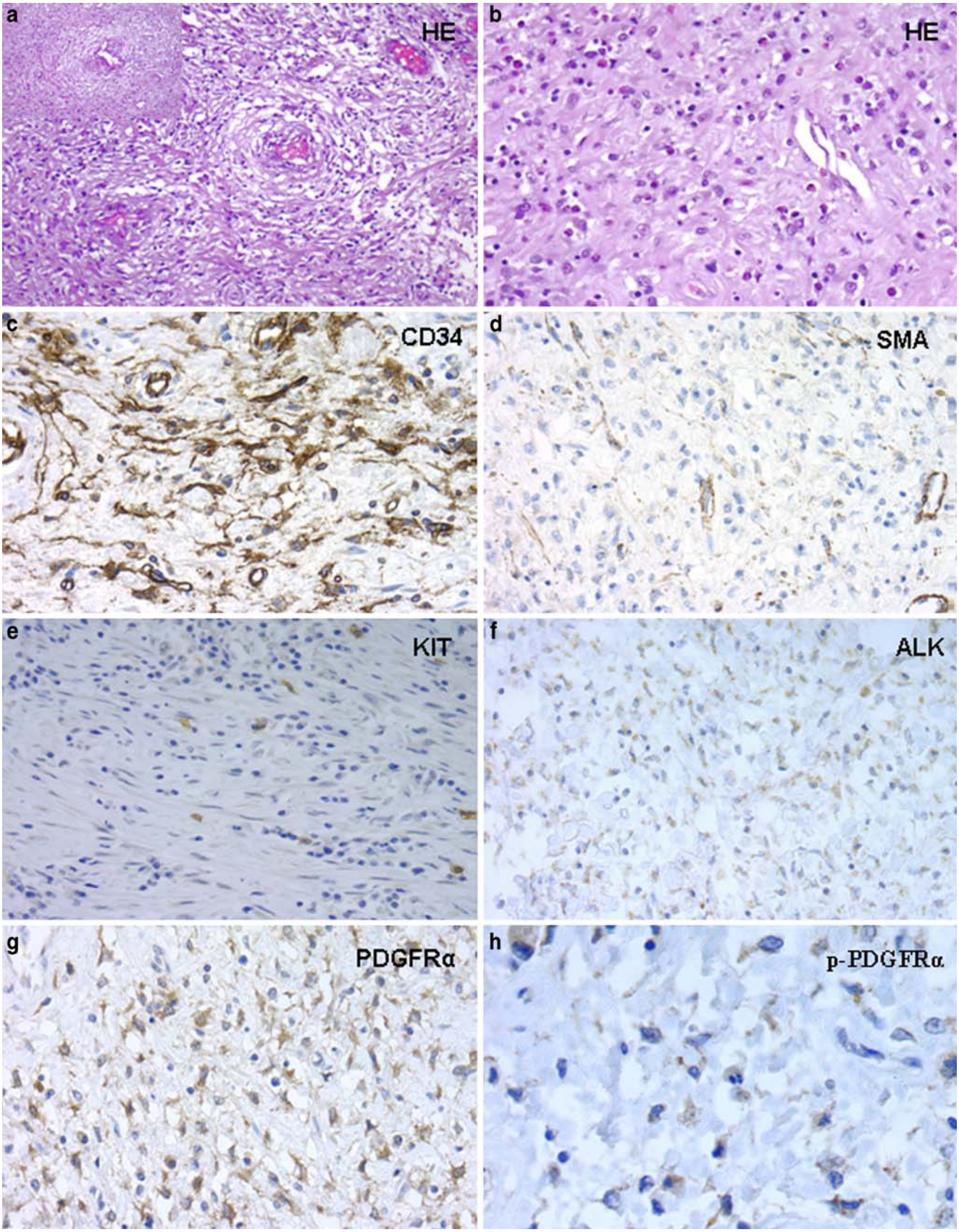
a
HE
b
HE
c
CD34
d
SMA
e
KIT
f
ALK
g
PDGFRα
h
p-PDGFRα

expression was weak; and KIT, EMA, collagen IV, and desmine showed negative staining. The Ki-67 was seen in less than 1% of the spindle cells.

Mutational analysis of exons 9, 11, 13, and 17 of *c-KIT* and exons 12 and 18 of *PDGFRα* revealed a mutation involving the juxtamembrane domain, exon 12 of *PDGFRα*. This genetic alteration was heterozygous and consisted of an in-frame deletion of codons 567–571 and a missense mutation in codon 566 (AGC-AGA) with a change in amino acid serine to arginine. This result was unexpected due to the final histological diagnosis of IFP; we decided to complete the inmunohistochemical study with PDGFRα phosphorylated to confirm the activated state of the receptor in the lesion and repeat the whole molecular analysis to discard contamination or technical pitfalls. p-PDGFRα was low positive in tumor cells and *PDGFRα* mutation confirmed (Figs. 1 and 2).

Discussion

The association of IFP with mutations in *PDGFRα* has been described in a small number of cases in the literature [7, 11]. In our case, the microscopic appearance and immunohistochemical profile are the best evidence for labeling this tumor as an IFP, although the molecular genetic profile is, in contrast, more commonly associated with KIT-negative GIST [5, 12]. Nevertheless, unlike IFP, GIST does not develop in the submucosal layer and does not form onionskin-like sheets around vessels; nor does it have a lot of eosinophilic infiltrate, while CD34 expression is negative. Furthermore, the morphology of GIST cases with mutation in *PDGFRα* usually present epitheloid or mixed cell patterns; in contrast, our mutated case of IFPs was mainly composed of spindle cells with a myxoid stroma and a rich inflammatory infiltrate with eosinophilia [6, 7, 13].

c-KIT and *PDGFRα* genes are proto-oncogenes that map to the long arm of chromosome 4 (4q11–4q12). Both genes belong to the same human type III family of transmembrane receptors with an internal tyrosine kinase component [14]. These genes have been shown to be important for several cellular and tissue processes such as proliferation, apoptosis, chemotaxis, growth, melanogenesis, hematopoiesis, and gametogenesis. *c-KIT* or *PDGFRα* mutations have also been implicated in other non-GIST tumors such as synovial sarcoma (*PDGFRα* 12 deletion 554 to 555) [15], dysgerminomas (*c-KIT* exon 17 codon 816) [16], Ewing's sarcoma (exon 9 of *c-KIT*) [17], melanomas (exon 11 *c-KIT* L576P) [18], Merkel cell carcinoma (exon 10 of the PDGFRα amino acid substitution at codon 478) [19], chronic eosinophilic leukemia and lymphoblastic T-cell lymphoma (*FIP1L1/PDGFRα*) [20], and seminomas (exon 17 of *c-KIT*, D816V, Y823D) [21]. We found one article by Carney et al. that described a combination of multiple GISTs and small intestinal polyps, fibroid tumor, and lipoma with *PDGFRα* mutation (V561D exon 12 of *PDGFRα*) [11], but the most interesting discovery is the previously-reported series of IFP with activating mutations in exons 12 and 18 of *PDGFRα* (70%) [7]. Shildhaus et al. found 16 different mutations (V561D, R560S del.561–567, del.559–561D591H, S566R del.567–571, D842V, D842I, del.842–845, and del. 845–848) including the same mutation herein reported and thus confirming our finding [7]. The authors compared the state of *PDGFRα* mutated in GIST versus IFP, observing that *PDGFRα*-mutated GISTs showed recurrence and metastasis, whereas IFPs do not metastasize. For these reasons, the biological behavior of IFP and GIST is different, despite identical activating *PDGFRα* mutation; consequently, other genetic alterations are required for malignant progression of GIST [7, 8, 22].

The mutation herein described with a constitutive activation of *PDGFRα* could activate key routes for the pathogenesis of this process, as occurs in other tumor entities. This molecular event would not only explain the behavior of IFP, but also suggests potential candidates for molecular target therapies such as imatinib or anti-angiogenic factors [23]. Nevertheless, more studies are needed to clarify whether this finding represents a biologically distinct behavior or to confirm more evidence for the concept that IFP is characterized by this type of mutation.

Acknowledgments The technical assistance of Estela Pons, Elisa Alonso, and Laura Martinez is gratefully acknowledged. This study was supported by grant PI04/0822 from the Instituto Carlos III, Madrid. Spain.

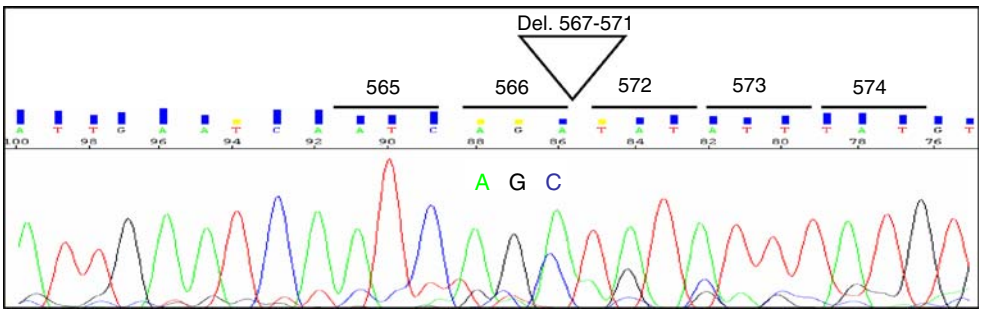

Fig. 2 Molecular analysis revealed a missense mutation in codon 566 AGC-AGA (S566R) plus a deletion of codons 567 to 571 in exon 12 of *PDGFRα*

Conflict of interest statement We declare that we have no conflict of interest.

References

1. Arber DA, Kamel OW, Van de Rijn M et al (1995) Frequent presence of the Epstein–Barr virus in inflammatory pseudotumor. Hum Pathol 26:1093–1098
2. Wysocki AP, Taylor G, Windsor JA (2007) Inflammatory fibroid polyps of the duodenum: a review of the literature. Dig Surg 24:162–168
3. Daum O, Hes O, Vanecek T et al (2003) Vanek's tumor (inflammatory fibroid polyp). Report of 18 cases and comparison with three cases of original Vanek's series. Ann Diagn Pathol 7:337–347
4. Ozolek JA, Sasatomi E, Swalsky PA et al (2004) Inflammatory fibroid polyps of the gastrointestinal tract: clinical, pathologic, and molecular characteristics. Appl Immunohistochem Mol Morphol 12:59–66
5. Kirsch R, Gao ZH, Riddell R (2007) Gastrointestinal stromal tumors: diagnostic challenges and practical approach to differential diagnosis. Adv Anat Pathol 14:261–285
6. Makhlouf HR, Sobin LH (2002) Inflammatory myofibroblastic tumors (inflammatory pseudotumors) of the gastrointestinal tract: how closely are they related to inflammatory fibroid polyps? Hum Pathol 33:307–315
7. Schildhaus HU, Cavlar T, Binot E et al (2008) Inflammatory fibroid polyps harbour mutations in the platelet-derived growth factor receptor alpha (PDGFRA) gene. J Pathol 216:176–182
8. Miettinen M, Lasota J (2001) Gastrointestinal stromal tumors—definition, clinical, histological, immunohistochemical, and molecular genetic features and differential diagnosis. Virchows Arch 438:1–12
9. Corless CL, McGreevey L, Haley A et al (2002) KIT mutations are common in incidental gastrointestinal stromal tumors one centimeter or less in size. Am J Pathol 160:1567–1572
10. Heinrich MC, Corless CL, Demetri GD et al (2003) Kinase mutations and imatinib response in patients with metastatic gastrointestinal stromal tumor. J Clin Oncol 21:4342–4349
11. Carney JA, Stratakis CA (2008) Stromal, fibrous, and fatty gastrointestinal tumors in a patient with a PDGFRA gene mutation. Am J Surg Pathol 32:1412–1420
12. Rossi G, Valli R, Bertolini F et al (2005) PDGFR expression in differential diagnosis between KIT-negative gastrointestinal stromal tumours and other primary soft-tissue tumours of the gastrointestinal tract. Histopathology 46:522–531
13. Santos Gda C, Alves VA, Wakamatsu A et al (2004) Inflammatory fibroid polyp: an immunohistochemical study. Arq Gastroenterol 41:104–107
14. Spritz RA, Strunk KM, Lee ST et al (1994) A YAC contig spanning a cluster of human type III receptor protein tyrosine kinase genes (PDGFRA-KIT-KDR) in chromosome segment 4q12. Genomics 22:431–436
15. Lopez-Guerrero JA, Navarro S, Noguera R et al (2005) Mutational analysis of the c-KIT AND PDGFRalpha in a series of molecularly well-characterized synovial sarcomas. Diagn Mol Pathol 14:134–139
16. Hoei-Hansen CE, Kraggerud SM, Abelar VM, Kaern J et al (2007) Ovarian dysgerminomas are characterised by frequent KIT mutations and abundant expression of pluripotency markers. Mol Cancer 6:12
17. Do I, Santini Araujo E, Kalil RK, Bacchini P et al (2007) Protein expression of KIT and ene mutation of c-KIT and PDGFRs in Ewing sarcomas. Pathology 203:127–134
18. Antonescu CR, Busam KJ, Francone TD et al (2007) L576P KIT mutation in anal melanomas correlates with KIT protein expression and is sensitive to specific kinase inhibition. Int J Cancer 121:257–264
19. Swick BL, Ravdel L, Fitzpatrick JE et al (2008) Platelet-derived growth factor receptor alpha mutational status and immunohistochemical expression in Merkel cell carcinoma: implications for treatment with imatinib mesylate. J Cutan Pathol 35:197–202
20. Metzgeroth G, Walz C, Score J et al (2007) Recurrent finding of the FIP1L1-PDGFRA fusion gene in eosinophilia-associated acute myeloid leukemia and lymphoblastic T-cell lymphoma. Leukemia 21:1183–1188
21. Biermann K, Goke F, Nettersheim D et al (2007) c-KIT is frequently mutated in bilateral germ cell tumours and down-regulated during progression from intratubular germ cell neoplasia to seminoma. J Pathol 213(3):311–318
22. Lasota J, Miettinen M (2006) KIT and PDGFRA mutations in gastrointestinal stromal tumors (GISTs). Semin Diagn Pathol 23:91–102
23. Shor AC, Agresta SV, D'Amato GZ et al (2008) Therapeutic potential of directed tyrosine kinase inhibitor therapy in sarcomas. Cancer Control 15:47–54

Virchows Arch (2009) 454:333–339
DOI 10.1007/s00428-009-0729-7

CASE REPORT

Dendritic cell sarcomas/tumours of the breast: report of two cases

Nilgun Kapucuoglu · Sıbel Percinel · Terenzio Ventura · RongGang Lang · Wael Al-Daraji · Vincenzo Eusebi

Received: 29 September 2008 / Revised: 28 November 2008 / Accepted: 5 January 2009 / Published online: 3 February 2009

Abstract Extranodal follicular dendritic cell sarcoma/tumours (FDCS/Ts) and interdigitating dendritic cell sarcoma/tumours (IDCS/Ts) are rare neoplasms. We present two cases of FDCS/T and IDCS/T of the breast. The FDCS/T case (case 1) presented in a 31-year-old woman and the IDCS/T case (case 2) in a 67-year-old woman who both showed a firm lump in the left breast. The FDCS/T lesion superficially appeared as an anaplastic carcinoma and the IDCS/T was reminiscent of a spindle cell sarcomatoid carcinoma. Nevertheless both lesions were negative for keratins while case 1 displayed neoplastic cells strongly positive for CD21, vimentin and focally for CD68 and S-100 protein. The tumour cells of case 2 were positive for S-100, CD68 and CD45. In breast, an unusual keratin negative tumour composed predominantly of spindle cells arranged in fascicles, storiform pattern or whorls with a lymphoid rich stroma should raise suspicion for FDCS/Ts or IDCS/Ts. The distinction from malignant tumours with similar features is discussed.

Keywords Breast · Follicular dendritic cell sarcoma · Interdigitating dendritic cell sarcoma · Dendritic cell tumour · Immunohistochemistry

N. Kapucuoglu
Department of Pathology, Suleyman Demirel University,
Isparta, Turkey

S. Percinel
Department of Pathology, Ankara University,
Ankara, Turkey

T. Ventura
Department of Pathology, Università dell'Aquila,
SL No 4,
L'Aquila, Italy

R. Lang
Department of Breast Cancer Pathology and Laboratory Medicine,
Cancer Hospital, Tianjin Medical University,
Tianjin, China

W. Al-Daraji
Department of Pathology, University of Nottingham,
Nottingham, UK

V. Eusebi (✉)
Istituto di Anatomia ed Istologia Patologica,
Università di Bologna,
Ospedale Bellaria, Via Altura No 3,
40139 Bologna, Italy
e-mail: vincenzo.eusebi@unibo.it

Introduction

Dendritic cells (DCs) or antigen presenting cells are a heterogeneous group of non-lymphoid, non-phagocytic elements grouped under the generic designation of immune accessory cells of lymphoid and non-lymphoid organs [1]. They are composed of follicular dendritic cells (FDCs); Langerhans' cells (LCs) found primarily in skin; interstitial DCs, representing the counterpart of LCs in parenchymal organs with the exclusion of brain and cornea; veiled cells (VCs), corresponding to LCs, en route to the lymphoid system; and interdigitating dendritic cells (IDCs) confined to T cell areas. They play a key role in both the primary and secondary immune responses by capturing and presenting antigens and immune complexes. Each type differs in function, morphology, ultrastructure and immunophenotype [1–5]. FDCs are confined to the B cell areas (germinal centers) of primary and secondary lymphoid follicles in lymph nodes, as well as in extranodal sites, either as acquired lymphoid tissue or as part of the organised constitutive lymphoid tissue [3, 5]. IDCs are localised in the T-cell-rich areas of peripheral lymphoid tissue, including the paracortex and deep cortex of

Table 1 Summary of extranodal dentritic cell sarcomas reported in the breast

Case no.	Reference	Age/site	Size	Treatment	Follow-up
1	Fisher et al. [7]	41/left	25 mm	Quadrantectomy, mastectomy, radiotherapy	Recurrence after 6 months, NED 3 years
2	Pruneri et al. [8]	40/right	40 mm	Quadrantectomy, sentinel lymph node biopsy	19 months NED
3	Uluoğlu et al. [11]	38/right, bilateral cervical mass	30×20 mm	Chemotherapy, radiotherapy, lumpectomy	32 months breast NED
4 (present case 1)		31/left	50×40×35 mm	Radical mastectomy	13 months NED
5 (present case 2)		67/left	30×27 mm	Wide local excision	3 months D

NED no evidence of disease, *D* dead without evidence of residual disease

lymph nodes and tonsils, splenic periarteriolar lymphoid sheaths and interfollicular areas of mucosa-associated lymphoid tissue. FDCs play a major role in the induction and maintenance of humoral immune responses and IDCs are potent antigen-presenting cells responsible for initiating primary T-lymphocyte immune responses [1–5].

Follicular dendritic cell sarcoma/tumour (FDCS/T) and interdigitating dendritic cell sarcoma/tumour (IDCS/T) are grouped under the heading of dendritic cell neoplasms and their designation sarcoma/tumour is used because of the variable cytological grade and indeterminate clinical behaviour encountered in these neoplasms [3].

Extranodal FDCS/Ts have been reported to involve oral cavity and upper aerodigestive regions, soft tissues of neck, abdominal walls, thigh, liver, tubular gastrointestinal tract (large and small intestine, stomach and rectum), lesser omentum, mesocolon and retroperitoneum, lung, thyroid, pancreas and ampulla of Vater [6]. Two of such cases have been previously reported in the breast (Table 1) [7, 8]. Extranodal IDCS/Ts have been reported to occur in nasopharynx, small intestine and mesentery, liver, testis, skin, tonsil, spleen, bone marrow, chest wall, paraspinal area, bladder and salivary gland [9, 10]. One case has secondarily involved the breast [11].

In this article, we report an additional case of FDCS/T and the first case of IDCS/T primary in the breast and discuss their distinctive morphologic features in view of distinction from similar breast tumours.

Clinical history

Case 1

A 31-year-old woman presented in July 2007 with a firm nodule in the upper internal quadrant of the left breast which at ultrasound examination measured 32 mm in its greatest axis. It was localised superficially and clinically resembled a phyllodes tumour. The lump was excised and a preliminary diagnosis of poorly differentiated carcinoma with lymphocytic rich stroma was rendered. However, the immunohistochemical findings were not consistent with an epithelial lesion and a second look offered the diagnosis of extranodal FDC/T.

In the meantime, the patient had undergone left radical mastectomy with axillary lymph node dissection. No further treatment was administered.

The patient was alive and well when last contacted (August 2008).

Case 2

A 67-year-old demented woman presented with a subcutaneous lump in the upper outer quadrant of the left breast

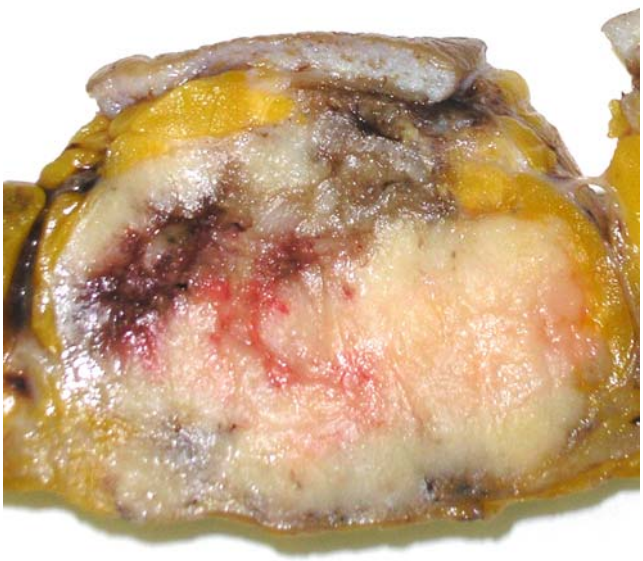

Fig. 1 Case 1. The tumour has macroscopic circumscribed borders. Its cut surface is whitish in colour and has some haemorrhagic and necrotic areas

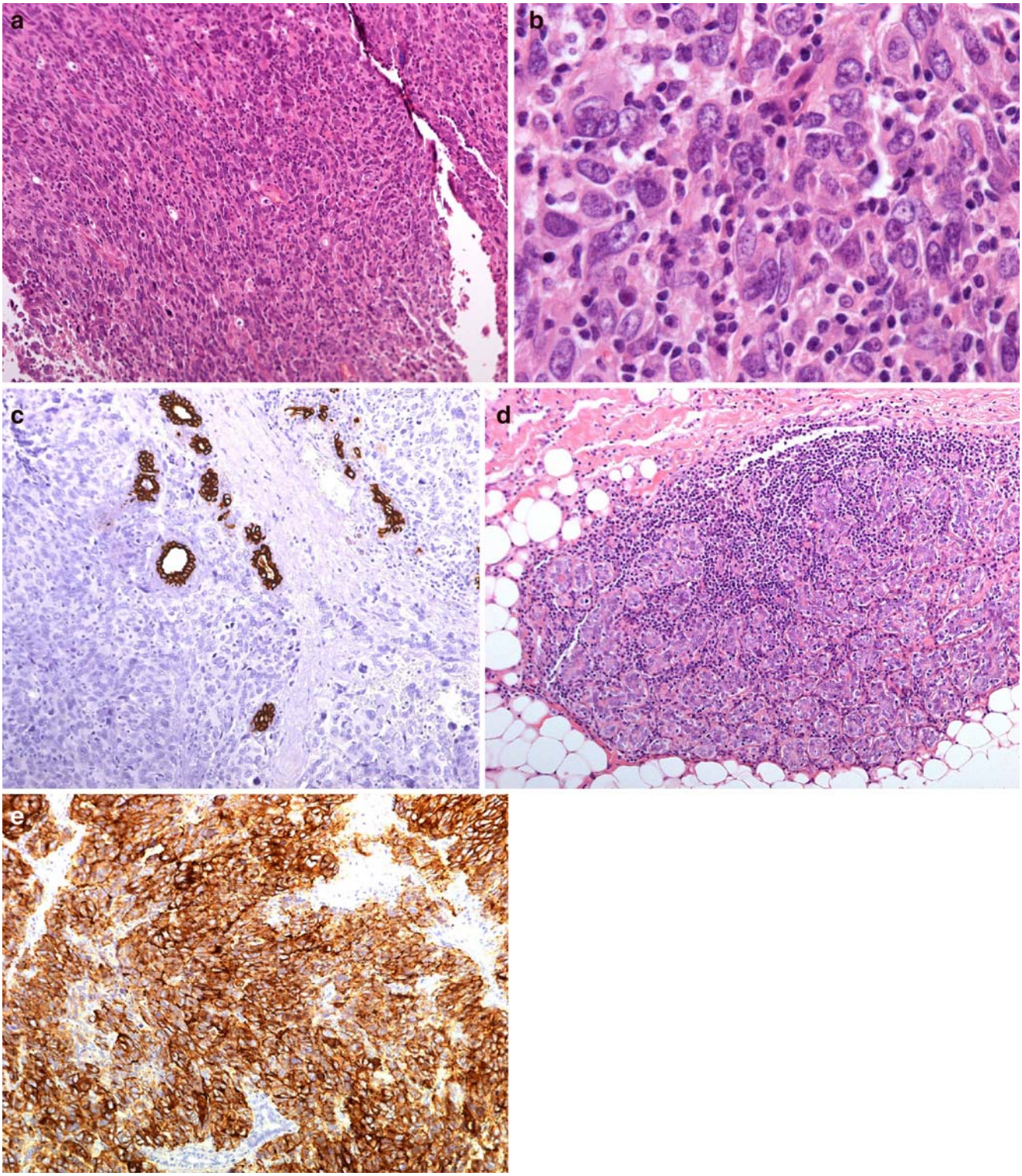

Fig. 2 Case 1. **a** The tumour is composed of oval to spindle shaped cells arranged in sheets and interlacing fascicles. **b** The nuclei are oval or elongated with vesicular or granular finely dispersed chromatin, with prominent nucleoli and thin smooth nuclear membranes. There are occasional giant cells. The tumour cells are intermingled with small lymphocytes. **c** Breast ductules, here highlighted by keratin 7, are scattered among the neoplastic cells. **d** Lobules at the periphery of the tumour show the features of lymphocytic lobulitis. **e** Tumour cells show strong and diffuse cytoplasmic positivity for CD21

which had been discovered in a medical general work up. The family history was that her mother died of breast cancer. Her aunt (from mother's side) and sister all had breast cancer, but are both alive and well. Past history indicated that the patient had developed squamous cell carcinoma of the skin, from the back and one basal cell carcinoma from her nasolabial fold 4 and 1 year respectively before her breast symptoms. The patient was on antihypertensive treatment and statins.

A wide local excision together with the overlying skin was performed. In view of the histological features and immunohistochemical findings, the lesion was regarded as IDCS/T.

The patient died 3 weeks after her operation. The autopsy showed that the cause of death was pulmonary embolism, but no tumour was found anywhere outside breast.

Materials and methods

Both cases were from the consultation files of one of us (VE). Stains were performed on formalin-embedded tissues and immunohistochemical studies were obtained from sections using avidin–biotin complex (ABC) peroxidase method. The following antibodies were employed: CD21 (Dako, clone 1F8, 1:20), vimentin (Dako, clone V9, 1:100), S100 protein, (Ventana), CD68 (Neomarkers, clone MAC 387, 1:200), epidermal growth factor receptor (EGFR) (Zymed, clone 31G7, 1:30), CD1a (Neomarkers, clone 1CA04, 1:50), keratins (AE1/AE3 Dako, 1:100), (MNF 116, Dako, 1:1:200), keratin 7 (Dako, clone Ov-TL 12/30, 1:100), keratin 20 (Dako, clone KS 20.8, 1:40), 34ßE12 (Dako, 1:50), gross cystic disease fluid protein-15 (GCDFP-15) (Signet, clone D6, 1:300), epithelial membrane antigen (EMA) (Dako, clone E29, 1:100), smooth muscle actin (SMA) (Dako, clone 1A4, 1:100), desmin (Neomarkers, clone D33, 1:50), CD34 (Neomarkers, clone QB-END/10, 1:400), CD31 (Ventana), HMB45 (Dako, 1:50), CD45 (Ventana), CD3 (Neomarkers, clone PS1, 1:20), estrogen receptors (Ventana), progesterone receptors (Ventana), her2/neu (Neomarkers, clone CB 11, 1:50). In the lack of additional material for case 2, keratin 14 (Neomarkers, clone 11002, 1:400, WCAP), keratin 5/6 (Neomarkers, clone D5/16 B4, 1:20, WCAP) and p63 (Neomarkers, clone 4A4, 1:1000, WCAP pH:8) were stained in case 1 only, and were all negative.

Results

Case 1

Macroscopically, a circumscribed soft nodule of 50×40×35 mm with a cut surface whitish in colour and having some haemorrhagic and necrotic areas was observed (Fig. 1).

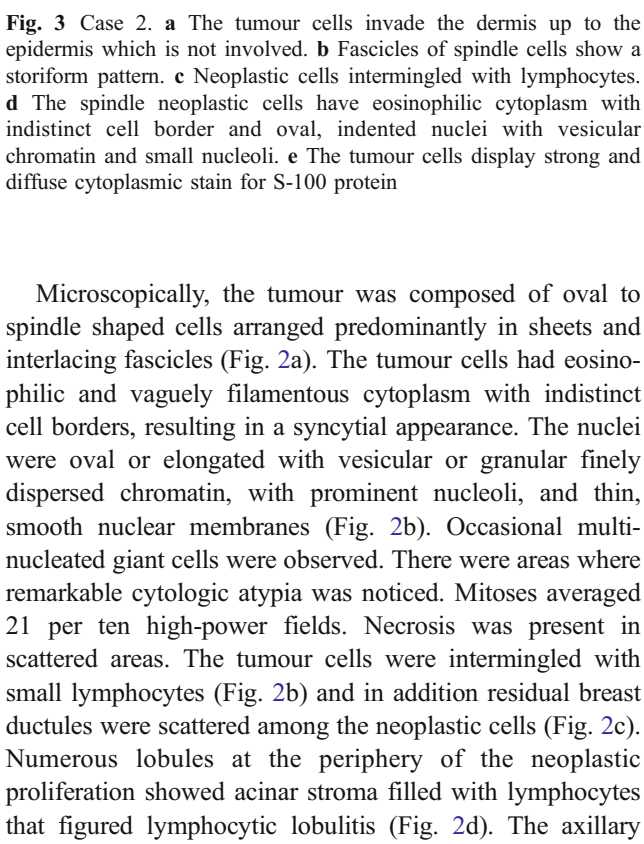

Fig. 3 Case 2. **a** The tumour cells invade the dermis up to the epidermis which is not involved. **b** Fascicles of spindle cells show a storiform pattern. **c** Neoplastic cells intermingled with lymphocytes. **d** The spindle neoplastic cells have eosinophilic cytoplasm with indistinct cell border and oval, indented nuclei with vesicular chromatin and small nucleoli. **e** The tumour cells display strong and diffuse cytoplasmic stain for S-100 protein

Microscopically, the tumour was composed of oval to spindle shaped cells arranged predominantly in sheets and interlacing fascicles (Fig. 2a). The tumour cells had eosinophilic and vaguely filamentous cytoplasm with indistinct cell borders, resulting in a syncytial appearance. The nuclei were oval or elongated with vesicular or granular finely dispersed chromatin, with prominent nucleoli, and thin, smooth nuclear membranes (Fig. 2b). Occasional multinucleated giant cells were observed. There were areas where remarkable cytologic atypia was noticed. Mitoses averaged 21 per ten high-power fields. Necrosis was present in scattered areas. The tumour cells were intermingled with small lymphocytes (Fig. 2b) and in addition residual breast ductules were scattered among the neoplastic cells (Fig. 2c). Numerous lobules at the periphery of the neoplastic proliferation showed acinar stroma filled with lymphocytes that figured lymphocytic lobulitis (Fig. 2d). The axillary lymph nodes were reactive.

Immunohistochemically, the tumour cells showed strong and diffuse cytoplasmic positivity for CD21 (Fig. 2e) and vimentin, while focal positivity for CD68 and S-100 protein was detected. A strong membranous staining for epidermal growth factor receptor was also observed. The tumour cells were negative for the other antibodies employed that included all keratins. On the basis of the morphologic and immunophenotypic findings, the diagnosis of FDCS/T was rendered.

Case 2

The specimen consisted of a 30×27-mm firm nodule with white-grey cut surface.

The tumour was macroscopically circumscribed and histologically reached the skin up to the epidermis which was not involved (Fig. 3a). The neoplastic proliferation consisted of fascicles often showing a storiform pattern of spindle cells intermingled with small lymphocytes (Fig. 3b, c). Cohesive sheets of polygonal or round cells with abundant eosinophilic cytoplasm reminiscent of histiocytes were occasionally noticed. The spindle neoplastic cells had eosinophilic cytoplasm with indistinct cell border that blurred with the stroma. Nuclei were ovoid to round often indented with vesicular chromatin and small nucleoli (Fig. 3d). Nuclear pleomorphism was marked in focal areas and occasional multinucleated tumour giant cells were observed. A deposition of fine to thick bands of collagen was seen between the fascicles of

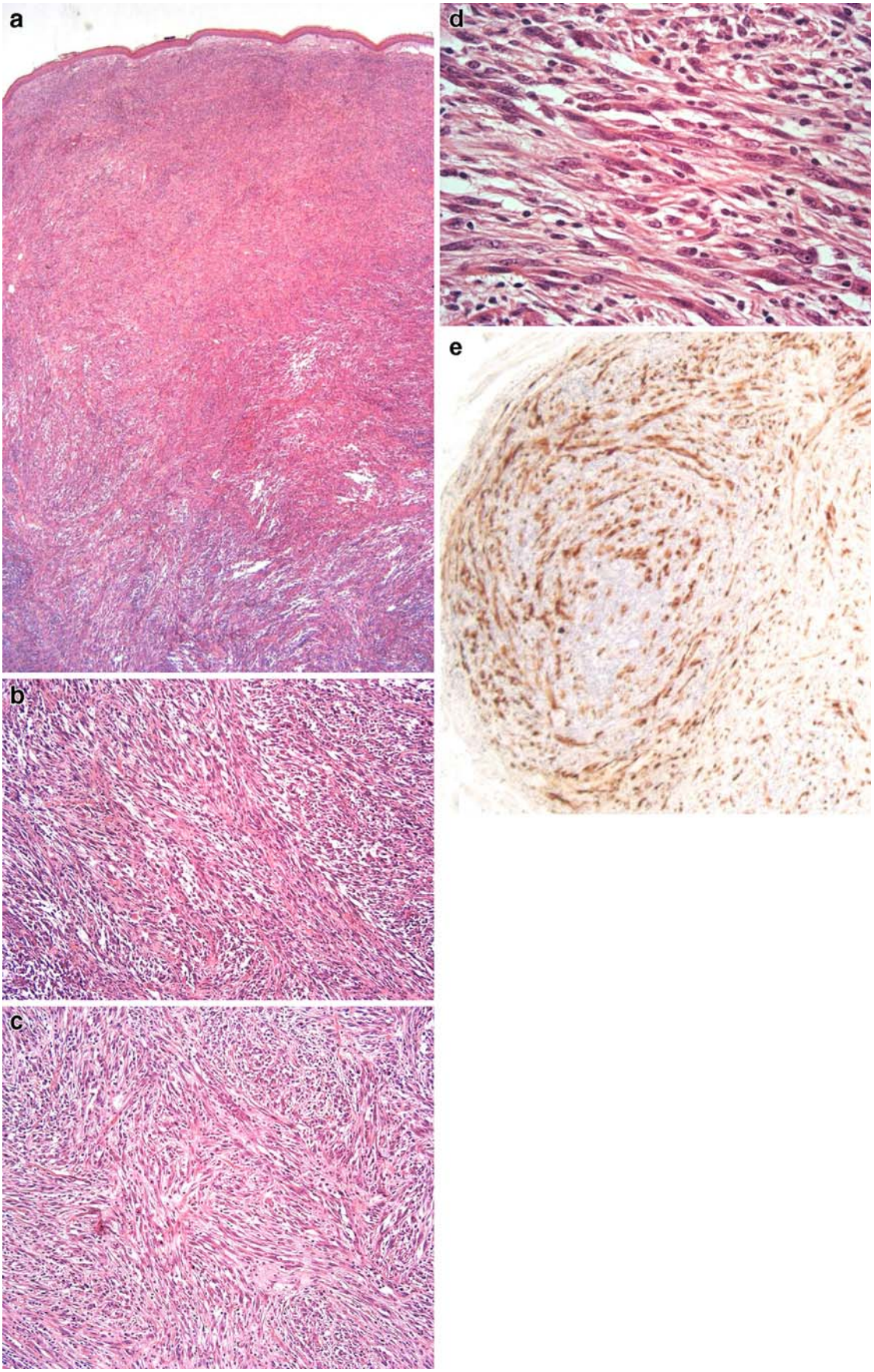
a
b
c
d
e

spindle cells in some areas. Mitotic activity was scanty, but atypical mitoses were observed. Necrotic areas were absent. In the non-neoplastic breast tissue, lobulocentric lymphocytic infiltrate was noticed and perivascular lymphocytic cuffing was occasionally present.

Immunohistochemically, the tumour cells displayed strong and diffuse cytoplasmic expression for S-100 protein (Fig. 3e), CD68 and CD45. The tumour cells were consistently negative for all the other antibodies employed that included CD21, CD1a, HMB45, EGFR and all keratins.

Discussion

Case 1 consisted of spindle to polygonal neoplastic cells intermingled with lymphocytes. The neoplastic cells were negative for keratins and were consistently positive for CD21 and vimentin, all features indicative of FDCS/T [3] that allowed the exclusion of Rosai Dorfman histiocytosis primary in the breast [12] and lymphoepithelial-like carcinoma as originally described by Dadmanesh et al. [13]. The former being invariably CD21 and keratins negative, the latter showing by definition keratin positivity as well as CD21-negative stain. EGFR consistently stained the cells of the present tumour, the expression of which has been shown recently in FDCS/Ts [14–16].

To the best of our knowledge, only two well-documented cases of FDCSs [7, 8] of the breast have been reported in the English literature (Table 1). Consistent with the previous cases, the current case showed same features and in addition a lymphocytic lobulitis was present. The present case 1 showed in addition anaplastic areas and areas of necrosis that are unusual in FDC/T.

In one patient out of the two published, the tumour recurred 6 months later, received radiation therapy and remained disease-free 3 years after the original presentation [7]. The other patient was not subjected to further treatment and remained disease free 19 months after the surgery [8]. The present patient (case 1) is alive and well 13 months after surgery in spite of the anaplastic areas. No further treatment was administered. Admittedly, FU in this case is very short but we feel that the anaplastic features as seen in some areas cast a shade of pessimism on the long-term survival.

Case 2 was composed by a subcutaneous proliferation of neoplastic spindle cells occasionally arranged in a storiform pattern. Neoplastic cells were strongly positive for S-100 protein, CD45 and CD68, while were consistently negative for CD21, keratins and HMB-45. Malignant melanoma was excluded for the integrity of the epidermis and for the lack of staining for HMB-45. Sarcomatoid carcinomas was excluded for the lack of staining for keratins. FDCS/T have CD21 positive elements, are more cellular and show less fasciculated pattern. Malignant schwannomas are rare in breast and lack positivity for CD45. Therefore in view of histology and the immunohistochemical features, the diagnosis of IDCS/T was proposed [1, 3].

In this respect it seems that case 2 is the first case of IDCS/T primary in the breast. Admittedly the lesion involved a small tract of the skin. Nevertheless, the bulk of the lesion was found within the breast parenchyma and this led to the interpretation of coincidental skin involvement. The case previously reported was a secondary localisation of IDCS/T to the breast [11] although having histological features identical to the present case 2 (Table 1).

The diagnosis of IDCS/Ts is challenging and is based on histologic, immunohistochemical and sometimes ultrastructural features [1, 3]. Normal IDCs are positive for ATPase, S-100 protein, HLA-DR, vimentin, CD45 and monocyte–macrophage-associated antigens [1, 3], but there is not a specific marker for these cells.

The pathogenesis and factors involved in the development of FDCS/Ts or IDCS/Ts are not fully understood. The only predisposing factor identified for FDCS/T is hyaline-vascular Castleman's disease [5, 6, 17, 18]. FDC proliferation and dysplastic changes occurring in Castleman's disease can form the background from which a FDSC/T develops [19].

The pathogenesis of IDCS/T in a site that is normally devoid of lymphoid tissue remains speculative. In a case reported in the testis, the presence of lymphoplasmacytic infiltrate in the adjacent non-neoplastic testicular parenchyma raised the possibility that the IDCT might have occurred in a background of an "acquired" lymphoid tissue as a consequence of a preceding inflammatory reaction to a yet unknown stimulus [20]. It is pertinent to note that both the present cases showed lymphocytic lobulitis a feature very often related to autoimmune processes [21].

Recognition of extranodal FDCS/Ts or IDCS/Ts is often difficult. While these lesions are included in the diagnostic list of differential diagnoses in spindle cell tumours of lymph nodes, however these same tumours are not considered in the differential diagnosis list of spindle cell tumours of the breast because sarcomatoid carcinomas and the several other spindle cell lesions are by far more common than dendritic cell neoplasms [22]. Even with immunohistochemical studies, the diagnosis of the tumours may be missed, because FDC markers are not included among the routine panel of antibodies or there is no specific marker to reveal IDCS/T for the investigation of undifferentiated neoplasms.

The clinical course of both dendritic cell neoplasms is variable but IDCS/T seems to be more aggressive than that of FDCS/T [1, 3, 6, 15, 18, 23]. With a median follow-up of 18 months, 43% of the extranodal FDCS/T cases recurred and 7% of them died of disease [18]. Although no definite conclusions can be drawn from the data

available at the current time and prognostically significant pathologic factors can not be identified for both tumours, we think it is wise to follow the approach of WHO which has adopted the non-committal term of sarcoma/tumour.

In conclusion, breast is another extranodal site for FDCS/Ts and IDCS/Ts. An unusual CK-negative tumour composed predominantly of spindle cells arranged in fascicles, storiform pattern or whorls with a lymphoid rich stroma should raise suspicion for FDCS/Ts or IDCS/Ts. An immunohistochemical panel consisting of at least FDC markers, S-100 protein, CD68 and CD45 must be performed to exclude a FDCS/T or IDCS/T. Ultrastructural examination may be required to confirm the diagnosis and to distinguish FDCS/T from IDCS/T.

Conflict of interest statement The authors declare that they have no conflict of interest.

References

1. Pileri SA, Grogan TM, Haris NL et al (2002) Tumors of histiocytes and accessory dendritic cells: an immunohistochemical approach to classification from the International Lymphoma Study Group based on 61 cases. Histopathology 41:1–29
2. Fonseca R, Yamakawa M, Nakamura S et al (1998) Follicular dendritic cell sarcoma and interdigitating reticulum cell sarcoma: a review. Am J Hematol 59:161–167
3. Jaffe ES, Harris NL, Stein H, Vardiman JW (eds) (2001) World Health Organization Classification of Tumors. Pathology and genetics of tumors of haemotopoietic and lymphoid tissues. IARC, Lyon
4. Monda L, Warnke R, Rosai J (1986) A primary lymph node malignancy with features suggestive of dendritic reticulum cell differentiation. A report of 4 cases. Am J Pathol 122:562–572
5. Soriano AO, Thompson MA, Admirand JH et al (2007) Follicular dendritic cell sarcoma: a report of 14 cases and review of the literature. Am J Hematol 82:725–728
6. Shia J, Chen W, Tang LH et al (2006) Extranodal follicular dendritic cell sarcoma: clinical, pathologic, and histogenetic characteristics of an underrecognized disease entity. Virchows Arch 449:148–158
7. Fisher C, Magnusson B, Hardarson S, Smith MEF (1999) Myxoid variant of follicular dendritic cell sarcoma arising in the breast. Ann Diagn Pathol 3:92–98
8. Pruneri G, Masullo M, Renne G et al (2002) Follicular dendritic cell sarcoma of the breast. Virchows Arch 441:194–199
9. Barwell N, Howatson R, Jackson R et al (2004) Interdigitating dendritic cell sarcoma of salivary gland associated lymphoid tissue not associated with HHV-8 or EBV infection. J Clin Pathol 57:87–89
10. Sharma M, Ahsan F, Ah-See KW et al (2006) Interdigitating dendritic cell sarcoma of the parotid gland. J Laryngol Otol 120:244–246
11. Uluoğlu Ö, Akyürek N, Üner A et al (2005) Interdigitating dendritic cell tumor with breast and cervical lymph-node involvement: a case report and review of the literature. Virchows Arch 446:546–554
12. Hammond LA, Keh C, Rowlands DC (1996) Rosai-Dorfman disease in the breast. Histopathology 29:582–584
13. Dadmanesh F, Peterse JL, Sapino A et al (2001) Lymphoepithelioma-like carcinoma of the breast: lack of evidence of Epstein-Barr virus infection. Histopathology 38:54–61
14. Chang KC, Jin YT, Chen FF, Su IJ (2001) Follicular dendritic cell sarcoma of the colon mimicking stromal tumor. Histopathology 38:148–157
15. Han JH, Kim SH, Noh SH et al (2000) Follicular dendritic cell sarcoma presenting as a submucosal tumor of the stomach. Arch Pathol Lab Med 124:1693–1696
16. Hollowood JD, Stamp G, Zouvani J, Fletcher CDM (1995) Extranodal follicular dendritic cell sarcoma of the gastrointestinal tract. Morphologic, immunohistochemical and ultrastructural analysis of two cases. Am J Clin Pathol 103:90–97
17. Chan JKC (1997) Proliferative lesions of follicular dendritic cells: an overview, including a detailed account of follicular dendritic cell sarcoma, a neoplasm with many faces and uncommon etiologic associations. Adv Anat Pathol 4:387–411
18. Chan JKC, Fletcher CDM, Nayler SJ, Cooper K (1997) Follicular dendritic cell sarcoma. Clinicopathologic analysis of 17 cases suggesting malignant porential higher than currently recognized. Cancer 79:294–313
19. Fornelli A, Mureden A, Eusebi V (1998) Tumore a cellule follicolari dendritiche e lesione vascolare insorti in linfonodo con malattia di Castleman. Descrizione di un caso. Pathologica 90: 146–151
20. Luk ISC, Shek TWH, Tang VWL, Ng WF (1993) Interdigitating dendtritic cell tumor of the testis. A novel testicular spindle cell neoplasm. Am J Surg Pathol 23:1141–1148
21. Lammie GA, Bobrow LG, Staunton MDM et al (1991) Sclerosing lymphocytic lobulitis of the breast—evidence for an autoimmune pathogenesis. Histopathology 19:13–20
22. Tavassoli FA, Eusebi V (2008) Tumors of the breast, 4th edn. American Registry of Pathology/AFIP, Washington, DC
23. Chen TC, Kuo TT, Ng KF (2001) Follicular dendritic cell tumor of the liver: a clinicopathologic and Epstein-Barr virus study of the two cases. Mod Pathol 14:354–360

Virchows Arch (2009) 454:341–344
DOI 10.1007/s00428-009-0734-x

CASE REPORT

Turquoise to dark green organs at autopsy

Arne Warth · Benjamin Goeppert · Christian Bopp · Peter Schirmacher · Christa Flechtenmacher · Jürgen Burhenne

Received: 07 January 2009 / Revised: 14 January 2009 / Accepted: 14 January 2009 / Published online: 3 February 2009

Abstract We report the case of a 72-year-old man who died in septic shock following pancreatectomy. At autopsy, organs were discoloured with a rapid colour change from turquoise to dark green, especially of the myocardium. The patient had received 200 mg methylene blue (MB), i.v., for treatment of septic shock 90 min prior to death. Analysis of tissue samples by liquid extraction and liquid chromatography coupled to tandem mass spectrometry demonstrated different concentrations of MB and its metabolites azure A and B in the heart, lungs, kidneys, and liver. Our findings clearly demonstrate the relation of MB administration and organ discolouration at autopsy and shed a new light on MB distribution and accumulation in septic shock.

Keywords Methylene blue · Autopsy · Green organs · Mass spectrometry

Case presentation

A 72-year-old man with a history of arterial hypertension, coronary heart disease, obstructive sleep apnoea syndrome and non-insulin-dependent diabetes mellitus received total pancreatectomy with a combined resection of the distal stomach due to an uncertain mass in the pancreatic head suspected for malignancy. A histologic evaluation resulted in the diagnosis of an intraductal papillary-mucinous neoplasia (IPMN). Postoperatively, the patient developed progressive respiratory and renal failure with septic shock and right heart failure requiring high doses of vasopressors and inotropics. He further underwent splenectomy and resection of the omentum and developed renal failure requiring haemodialysis as well as liver failure. The patient died 6 days after the primary operation with clinical signs of septic multi-organ failure. At autopsy, we discovered turquoise to dark green-coloured organs with predominant discolouration of the heart, brain, pulmonary and renal vessels and bone marrow (Fig. 1). The most prominent finding was a rapid colour change of the myocardium from slight turquoise to dark green within a minute following exposure to air (Fig. 2). This phenomenon was even present at 24 h and in a milder form even after 2 months following formalin fixation of the tissues.

Sulfhaemoglobinaemia is a rare cause for dark green blood and greenish-coloured organs [1]. However, in both intravital and postmortal blood samples, no sulfhaemoglobin was detected (not shown). A recent case report described greenish-discoloured organs at autopsy and the authors suggested that leuco-methylene blue (LMB), a colourless metabolite of methylene blue (MB), caused the discolouration [2] by auto-oxidation of LMB to MB in the presence of atmospheric oxygen [3]. However, the authors describe the discolouration only in the heart and brain and, to a much lesser extent, in the retroperitoneal and perirenal fat.

The patient described herein received 200 mg MB, i.v., 90 min before he died, since highly dosed inotropic agents

A. Warth (✉) · B. Goeppert · P. Schirmacher · C. Flechtenmacher
Institute of Pathology, University Hospital Heidelberg,
Im Neuenheimer Feld 220/221,
69120 Heidelberg, Germany
e-mail: arne.warth@med.uni-heidelberg.de

C. Bopp
Department of Anaesthesiology, University Hospital Heidelberg,
Heidelberg, Germany

J. Burhenne
Department of Internal Medicine VI,
Clinical Pharmacology and Pharmacoepidemiology,
University Hospital Heidelberg,
Heidelberg, Germany

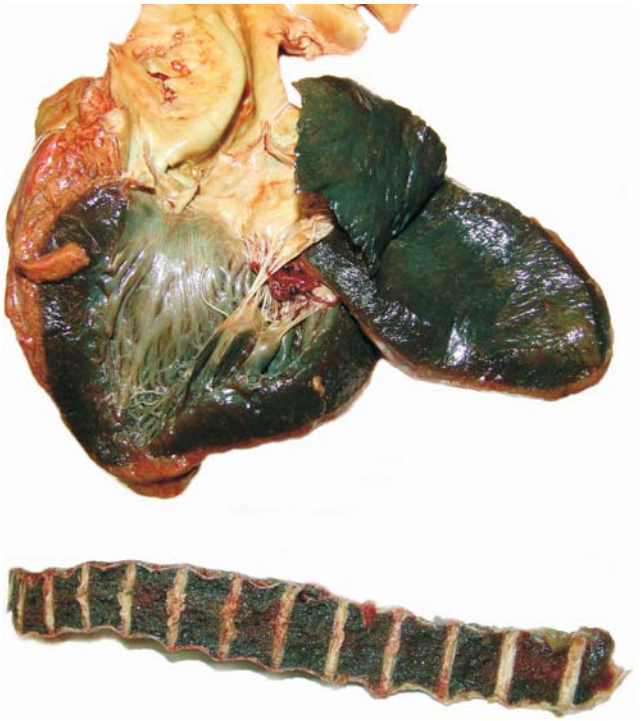

Fig. 1 The dissected heart (*upper part*) and a segment of the vertebral column (*lower part*) following autopsy with turquoise to dark green discolouration

and vasoconstrictors including vasopressin lead to acrocyanosis and were insufficient in maintaining adequate circulation. In order to shed more light on the potential causal relationship of MB administration and the observed discolouration [2], we analysed MB and its metabolites in the patients' tissues.

Materials and methods

For the quantification of MB and its metabolites azure A, B and C in formalin-fixed myocardium, lung, renal and liver tissues, we used liquid extraction and liquid chromatography coupled to tandem mass spectrometry (LC/MS/MS) as already published [4] with slight modifications concerning extraction of tissue material and metabolite quantification.

Table 1 Quantification of methylene blue (MB) and its metabolites by LC/MS/MS

Tissue	Weight (g)	MB (ng/g)	Azure A (ng/g)	Azure B (ng/g)	Total (mg)
Kidney	270	128.1	406.5	1,684	0.6
Heart	520	207.5	924.3	2,943	2.1
Liver	1,600	73.60	122.5	475.1	1.1
Lung	2,570	114.3	441.2	2,056	6.7
Blood[a]	6,000	1,000			6.0
Sum(mg)					16.5
Recovery (%)					8.3

[a] Calculated according to [5]

In brief, calibration, quality control and tissue specimens (~250 mg) were spiked with methylene violet 3RAX (internal standard solution, 25 µL/250 mg sample) and $CaCl_2$ solution (100 mM, 25 µL/250 mg). For extraction and protein precipitation, acetonitrile including 1% trifluoracetic acid (1 mL/250 mg) was added, homogenised by ultraturrax and vortexed for 5 min. Subsequently, samples were centrifuged (10 min, 16,000 *g*, 10°C), and from the clear supernatant 100 µL was transferred to 900 µL LC mobile phase in an autosampler vial. Sample extracts were kept in the autosampler at 15°C for a maximum of 12 h and 25 µL was injected into the LC/MS/MS system.

For ion exchange chromatographic separation, an Uptisphere mixed-mode column (MM1, 5 µm particle size, 120 A pore size, 100 mm length, 2 mm inner diameter) from Interchim S.A. (Montlucon Cedex, France) with integrated guard column was used at 40°C. The solvents consisted of 0.1% acetic acid including 100 mM ammonium acetate (solvent A) and 2.5% formic acid/acetonitrile (1/1) including 500 mM ammonium acetate (solvent B). The gradient elution started isocratic with 95%/5% (solvent

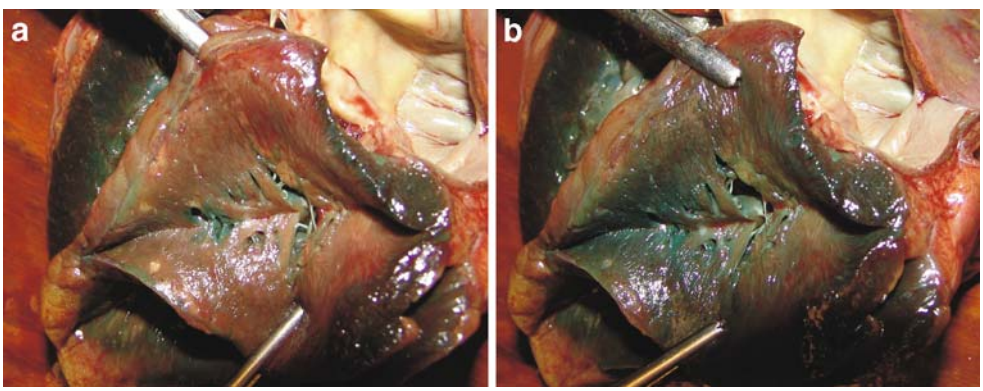

Fig. 2 Myocardium immediately (**a**) and 60 s (**b**) following dissection and contact to air, demonstrating the rapid colour change from a normal brownish red to green

A/B) for 1 min reaching 5%/95% (solvent A/B) at 5 min and was then kept isocratic until 12 min of total elution time. The flow rate was 0.45 mL/min and the eluent was introduced without splitting into the electrospray ion source of the mass spectrometer. Selected reaction monitoring measurements were performed at 1.5 kV multiplier voltage. MS/MS transitions monitored in the positive ion mode were *m*/*z* 284.0 → *m*/*z* 268.0 at 42 V for MB, *m*/*z* 256.0 → *m*/*z* 214.0 at 42 V for azure A, *m*/*z* 270.0 → *m*/*z* 254.0 at 43 V for azure B, *m*/*z* 242.0 → *m*/*z* 200.0 at 44 V for azure C and *m*/*z* 343.0 → *m*/*z* 299.0 at 46 V for methylene violet 3RAX. For MB, the assay was linear at least within 75 ng/g and 10,000 ng/g and the limit of quantification (LOQ) was 75 ng/g. The metabolites were quantified using the response factor of MB. Within-batch accuracy varied between −5.8% and +6.8% with corresponding precision ranging from 0.4% to 2.9% CV.

Results

MB and its metabolites were quantified in different tissues (Table 1). The concentrations of MB varied between 73.60 and 207.5 ng/g. Higher concentrations were found for azure B (475.1 to 2,943 ng/g), which is the main metabolite of MB. For azure A, the concentrations were between MB and azure B, whereas azure C was not detectable above the LOQ. LMB could not be quantified because of its low stability and direct conversion to MB. Considering the organ weights, a recovery could be calculated. Assuming a blood amount of 6 kg and MB blood concentration of 1,000 ng/g (calculated according to [5]), a recovery of about 8% can be calculated for the respective compartments (Table 1).

Discussion

MB is known to increase mean arterial pressure by inhibition of guanylyl cyclase, resulting in a reduction of the vasodilative nitric oxide, and is therefore consistently used in septic shock [6, 7]. MB is further used for treatment of malaria [8], methemoglobinemia, anaphylaxis and vasoplegic syndrome following cardiopulmonary bypass [9]. Consequently, a growing number of greenish-coloured organs should be expected in clinical autopsies, challenging many pathologists to provide a correct diagnosis. To test for the hypothesised correlation of MB administration and greenish discoloured organs [2], we investigated MB and its metabolites in different autopsy tissue specimens using liquid extraction and LC/MS/MS. We demonstrated high concentrations of MB and its metabolites in different tissues. The turquoise to dark green discolouration seems to be the combined effect of the rapid oxidation of LMB to MB as well as the different colours of MB, azure A and azure B alone. These colourations are also used for various histochemical stainings, e.g. the Romanofsky–Giemsa staining [10]. Taking into account the expected concentration in the total blood volume, only about 8% of the applied MB was recovered, demonstrating the high distribution into peripheral compartments. Additionally, an unknown portion of MB might be present as LMB as suggested by the rapid colour change after contact to air.

Although it may be a consequence of the centralised circulation, it is noteworthy that in accordance to the visual impression at autopsy high amounts of both MB and its metabolites were detected in the myocardium and lesser amounts in the kidneys or liver as natural sites of drug elimination. Furthermore, the supposed vasoconstrictive effects of MB may be critical in cardiac vessels due to myocardial ischaemia. Concerning the physiological effects of azure A and B, only little is known. In mice, azure B leads to a decreased TNF production and thereby prevented endotoxic shock whereas MB alone had no protective effects [11].

In summary, we demonstrate the causal relationship of MB administration to the discolouration. Our findings will help pathologists to correctly interpret similar autopsy findings and shed new light on the tissue distribution and accumulation of MB and its metabolites in septic shock.

Acknowledgements A.W. was supported by the Postdoc-Programme of the Medical Faculty of Heidelberg University.

Conflicts of interest statement We (all authors) declare that we have no conflict of interest.

References

1. Flexman AM, Del Vicario G, Schwarz SK (2007) Dark green blood in the operating theatre. Lancet 369:1972
2. Tan CD, Rodriguez ER (2008) Blue dye, green heart. Cardiovasc Pathol. doi:10.1016/j.carpath.2008.06.012
3. Buchholz K, Schirmer RH, Eubel JK et al (2008) Interactions of methylene blue with human disulfide reductases and their orthologues from Plasmodium falciparum. Antimicrob Agents Chemother 52:183–191
4. Burhenne J, Riedel KD, Rengelshausen J et al (2008) Quantification of cationic anti-malaria agent methylene blue in different human biological matrices using cation exchange chromatography coupled to tandem mass spectrometry. J Chromatogr B Analyt Technol Biomed Life Sci 863:273–282
5. Walter-Sack I, Rengelshausen J, Oberwittler H et al (2009) High absolute bioavailability of methylene blue given as an aqueous oral formulation. Eur J Clin Pharmacol 65:179–189

6. Preiser JC, Lejeune P, Roman A et al (1995) Methylene blue administration in septic shock: a clinical trial. Crit Care Med 23:259–264
7. Kwok ES, Howes D (2006) Use of methylene blue in sepsis: a systematic review. J Intensive Care Med 21:359–363
8. Meissner PE, Mandi G, Coulibaly B et al (2006) Methylene blue for malaria in Africa: results from a dose-finding study in combination with chloroquine. Malar J 5:84
9. Levin RL, Degrange MA, Bruno GF et al (2004) Methylene blue reduces mortality and morbidity in vasoplegic patients after cardiac surgery. Ann Thorac Surg 77:496–499
10. Zipfel E, Grezes JR, Seiffert W et al (1981) [Romanowsky dyes and Romanowsky–Giemsa effect. 1. Azure B, purity and content of dye samples, association (author's transl)]. Histochemistry 72:279–290
11. Culo F, Sabolovic D, Somogyi L et al (1991) Anti-tumoral and anti-inflammatory effects of biological stains. Agents Actions 34:424–428

Virchows Arch (2009) 454:345–347
DOI 10.1007/s00428-009-0735-9

CASE REPORT

Multiple malformations: a possible Sonic hedgehog phenotype?

Helen Wainwright · Peter Beighton

Received: 28 October 2008 / Revised: 12 December 2008 / Accepted: 12 January 2009 / Published online: 10 February 2009

Abstract A malformed foetus delivered after 21-week gestation had multiple gross craniofacial, midline and limb abnormalities. At autopsy, obstructive hydrocephalus and colonic atresia were observed. Radiographs revealed extensive epiphyseal stippling which might indicate abnormalities of sterol synthesis. The pattern of malformation in this foetus is similar to the phenotype for mutations in the Sonic hedgehog gene in animal models. It can be speculated that the abnormalities in the foetus could have resulted from disruption of the Sonic hedgehog pathway by molecular, chromosomal or environmental factors.

Keywords Cholesterol · Embryogenesis · Epiphyseal stippling · Malformation

Introduction

The Sonic hedgehog (SHH) gene has been shown in animal models to play a major role in embryogenesis. In particular, the gene is involved in orderly development of the face, heart, gut and limbs. Mice homozygous for a disrupted SHH gene show defects in midline structures (notochord and floorplate), dysplastic distal limb components, cyclopia, neural tube defects and absence of spinal column and ribs [1]. The abnormalities in all tissues extend beyond the normal sites of SHH transcription.

Malformation in humans due to mutations in the SHH gene have not been comprehensively documented, but it is likely that there would be some phenotypical homology with the animal modules.

We have investigated a malformed 21-week foetus in which a wide range of abnormalities were consistent with the effect of interference with full expression of the SHH pathway during embryogenesis. It is unusual to be in a position to demonstrate severe arrested embryonic development at a very early stage, and our findings are presented and discussed in the context of phenotypic delineation.

Clinical history

A malformed female foetus was delivered spontaneously in Cape Town, South Africa in 2003 at the 21st week of gestation. Ultrasound scan a week previously had revealed that the foetus had a possible Dandy Walker cyst and an abnormal spine.

Severe craniofacial arrest of development with bilateral anophthalmia, a large central facial defect and severe limb defects were evident (Fig. 1). Agnathia was a major feature, with the root and bridge of the nose placed superiorly and the central lower lip inferiorly. The nose, palate and upper lip were absent but the tongue was present posteriorly. Laterally, there were symmetrical tissue flaps with two transverse clefts on each side of the face (Fig. 2). The right ear was displaced inferiorly, while the left ear had cutis aplasia, two preauricular sinuses and a skin tag. Cutis aplasia and alopecia were present in the right temporal region. In the skull, the anterior fontanelle was enlarged, the midline was shifted to the left and a supernumerary bone

H. Wainwright
Division of Pathology, Faculty of Health Sciences,
University of Cape Town, Observatory,
7925 Cape Town, South Africa

P. Beighton (✉)
Division of Human Genetics, Faculty of Health Sciences,
University of Cape Town, Observatory,
7925 Cape Town, South Africa
e-mail: Peter.Beighton@uct.ac.za

extended from the anterior to the posterior fontanelle. Other malformations included a posterior fossa cyst with aplasia of the vermis and the anterior limb of the corpus callosum. The limbs were very dysmorphic and a body wall defect extended from the sternum to the perineum with absence of genitalia and anus. Internally, there was bilateral renal agenesis, agenesis of the uterus, and a short bowel with anal agenesis.

The mother was a 31-year-old smoker who attended the antenatal clinic. This was her third pregnancy and she had previously given birth to two normal children. She had polycystic kidney disease and hypertension, for which she had received medicinal therapy of unknown type during pregnancy. There was no history of alcohol or drug abuse.

Materials, methods and results

Radiographs showed agnathia and poorly defined orbital fossae. Scoliosis was evident in the lower thoracic spine. There were 11 thin crowded ribs on the left and 12 on the right. Both clavicles were absent. The right arm ended in a bowed and shortened humerus; the left humerus was angulated. The left foot had ectrodactyly with two toes. In the right leg, the tibia was bowed and shortened with a fibular ray deficiency, and flexion deformity of the three toed foot. Stippling in the paravertebral, femoral and calcaneal regions was a striking feature (Fig. 3).

Histologic studies of the placenta excluded amnion rupture. The epidermis was hypoplastic with absent hair follicles. In the brain, the lateral ventricles were dilated with ependymal rosettes, indicative of obstructive hydrocephalus due to a midline posterior fossa cyst lined by meninges.

The atretic colon had an admixture of anal, rectal and transitional epithelium. No cervix or uterus was identified. The abdominal wall skin was in continuity with the amnion.

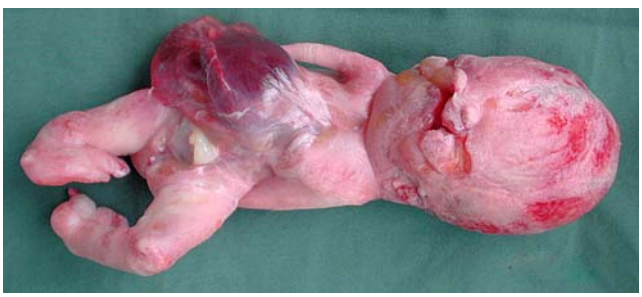

Fig. 1 Anterior view of the foetus showing anophthalmia, a large central facial defect, and a body wall defect extending from mid-sternum and including the perineum. The genitalia are absent and the lower limbs are abnormal

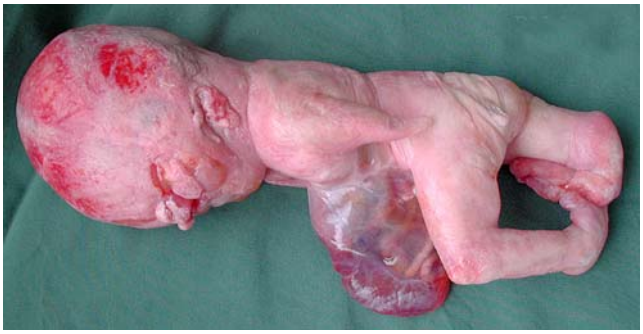

Fig. 2 Lateral view of the head and body showing a central facial defect with lateral skin flaps, agnathia and low-set malformed ears. The arms are shortened and tapered distally

For logistical reasons it was not possible to undertake cytogenetic, molecular or sterol studies.

Case details were submitted to the Washington, USA-based Pediatric Pathology (Pedpath) email discussion list on which problem cases are placed for opinions. A diagnosis of possible Sonic hedgehog gene deficiency was suggested on a basis of the pattern of malformations which were present, and which resembled the corresponding murine phenotype.

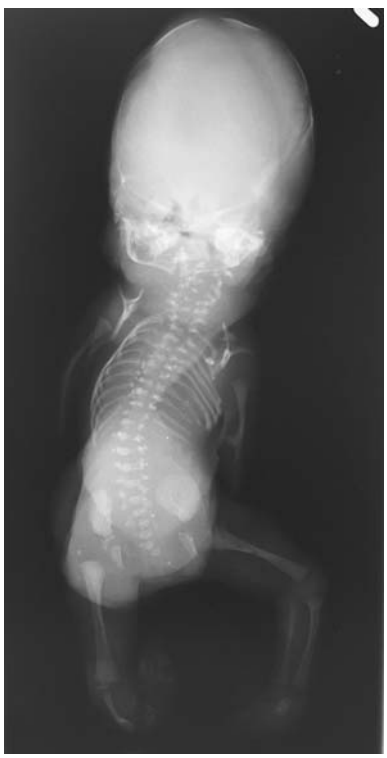

Fig. 3 Antero-posterior radiograph of the affected foetus. Multiple radiodense patches of stippling are evident, maximal in the paravertebral region. The vertebral bodies are very dysplastic

Discussion

The SHH gene is responsible for midline patterning and limb development of the developing embryo via inductive interactions in the mouse. It is involved in brain development, face and palatal development, neurogenesis of brain and retina, limb outgrowth and left–right asymmetry. These murine malformations are similar to those of the foetus which we have documented.

In epiphysial stippling or chondrodysplasia punctata, abnormal endochondral bone formation and the resultant foci of calcification within the cartilage are visible on radiographs [2]. Some skeletal dysplasias and other conditions associated with epiphysial stippling have been shown to have defects in the biosynthesis of cholesterol [3, 4]. Cholesterol is crucial for modification of embryonic signaling proteins, and decreased sterol levels result in abnormal Sonic hedgehog signaling. In the light of these observations, a number of genetic disorders involved in the biosynthesis of cholesterol pathway have been identified because of the common finding of epiphyseal stippling.

A defective response to Sonic hedgehog (SHH) signaling is seen in mouse models with disorders of cholesterol biosynthesis. The decreased levels of cellular sterols result in a decreased response to the SHH signal. Mouse models such as the Insig deficiency double knockout mouse, show midline facial clefting ranging from cleft palate to complete facial clefts [5]. This feature has been shown to be due to sterol precursor accumulation rather than diminished cholesterol or total sterol levels [6].

The foetus which we investigated had a severe midline facial defect, anophthalmia, agnathia, limb abnormalities, a body wall defect and striking epiphyseal stippling. These malformations resemble those in the mouse model, although the craniofacial abnormalities and the extent of disorganization of the embryo in the mouse are much more severe [1]. It is possible that the manifestations in the foetus resulted from interference in the full expression of the SHH gene during embryogenesis. The skeletal epiphyseal stippling in the foetus is also suggestive of a co-existing abnormality in sterol biosynthesis affecting Sonic hedgehog signaling. The foetal malformations could also have resulted from a chromosomal aberration, notably aneuploidy, or environmental and medicinal agents, as in foetal vitamin A toxicity.

For logistical reasons, it was not possible to undertake molecular, cytogenetic or sterol studies in the affected foetus, and the pathogenesis of the malformations remains uncertain. Nevertheless, the developmental abnormalities in the foetus and the SHH mouse are similar and the presence of skeletal stippling is consistent with a disturbance of sterol synthesis. For these reasons, it can be speculated that the affected foetus could represent the human homologue of the murine Sonic hedgehog phenotype.

Acknowledgements We are grateful to Dr. Kerby Oberg for his suggestions concerning the diagnosis and to Professor Judy Hall for her helpful guidance. Our investigations were supported by the Medical Research Council and the National Research Foundation of South Africa.

Conflict of interest statement We declare that we have no conflict of interest.

References

1. Chiang C, Litingtung Y, Lee E et al (1996) Cyclopia and defective axial patterning in mice lacking Sonic hedgehog gene function. Nature 383(6599):407–413
2. Kelley RI, Wilcox WG, Smith M et al (1999) Abnormal sterol metabolism in patients with conradi-hunermann-happle syndrome and sporadic lethal chondrodysplasia punctata. Am J Med Genet 83 (3):213–219
3. Opitz JM, Zanni G, Reynolds JF et al (2002) Defects of blastogenesis. Am J Med Genet 115(4):269–286
4. Porter FD (2003) Human malformation syndromes due to inborn errors of cholesterol synthesis. Curr Opin Pediatr 15(6):607–613
5. Motoyama J (2006) Essential roles of *Gli3* and sonic hedgehog in pattern formation and developmental anomalies caused by their dysfunction. Congen Anom 46(3):123–128
6. Engelking LJ, Evers BM, Richardson JA, Goldstein JL, Brown MS, Liang G (2006) Severe facial clefting in Insig-deficient mouse embryos caused by sterol accumulation and reversed by lovastatin. J Clin Invest 116(9):2356–2365

Virchows Arch (2009) 454:349–351
DOI 10.1007/s00428-008-0716-4

LETTER TO THE EDITOR

CD3+ T large granular lymphocyte leukaemia in a HIV+, HCV+, HBV+ patient

Emanuela Boveri · Roberta Riboni · Pasquale Antico · Alberto Malacrida · Alessandro Pastorini

Received: 25 June 2008 / Revised: 29 November 2008 / Accepted: 5 December 2008 / Published online: 24 January 2009

Keywords T-LGL · HIV · HBV · HCV

Sir, on August 2007, a 50-year-old HIV+, HBV+ and HCV+ male patient presented mild asthenia, splenomegaly (maximum diameter 25 cm by CT scan), hepatomegaly (3 cm below the costal margin), slowly progressing anaemia (haemoglobin 10.8 g/dL), granulocytopenia, lymphocytosis (total white blood cell count 4.340×10^9/L, neutrophils 22%, lymphocytes 74%) and mild thrombocytopenia (PLT 148×10^9/L). He did not complain of significant diseases or complications for his infections and he was not on antiretroviral therapy.

A bone marrow biopsy (BMB), performed to ascertain the cause of the peripheral cytopenia, showed hypercellularity for the age, maturation defects of the erythroid and granulopoietic lineages; no granulomas or histologically identifiable micro-organisms were seen and the reticulin fiber content was mildly, diffusely increased. A discrete lymphoid interstitial infiltrate was observed (30% of the whole cellularity) and composed by small- to medium-sized cells, with round nuclei and a moderate amount of clear cytoplasm (Fig. 1a). By immunohistochemistry, this infiltrate was constituted by mature T-cells, which were CD1−, CD2+, CD3+ (Fig. 1b), CD5−/+, CD7+/−, LAT+ CD4−, CD8+ (Fig. 1c), CD57+/−, TIA1+, perforin+, granzyme B+ (Fig. 1d), CD56− and CD25−, thus expressing an activated cytotoxic phenotype. A constant intra-sinusoidal distribution of the lymphoid component, unapparent by morphology alone, was clearly evidentiated by immunohistochemistry. PCR technique on BMB paraffin sections demonstrated a monoclonal rearrangement of the T-cell receptor (TCR). Cytologic examination of peripheral blood showed an increased number of large lymphocyte with granular cytoplasm; flow cytometry data of peripheral blood were in keeping with the immuno-histochemical findings.

Our case fulfills the criteria for the diagnosis of T-LGL leukaemia [1], a clonal proliferation of cytotoxic T-cells, associated with neutropenia, anaemia and thrombocytopenia, usually following an indolent course; in particular, the clinical picture and peripheral blood data are overlapping with the common clinical presentation of T-LGL leukaemia in immuno-competent population. Moreover, the BMB features are consistent with a neoplastic involvement, because of the entity of the lymphoid component and its peculiar pattern; sinusoidal infiltration is considered specific for different lymphoma subtypes [2], either of B-cell (splenic marginal zone lymphoma, intravascular large B-cell lymphoma) or T-cell origin (T-LGL leukaemia, hepatosplenic T-cell lymphoma), and it has never been described in reactive T-cell proliferations, including reactive expansions of T-LGL [3].

E. Boveri (✉) · R. Riboni
Istituto di Anatomia Patologica,
Fondazione IRCCS Policlinico San Matteo, University of Pavia,
Via Forlanini 14,
27100 Pavia, Italy
e-mail: embover@tin.it

P. Antico
Servizio Tossicodipendenze,
Tirano, Italy

A. Malacrida
Laboratorio Analisi, Ospedale di Sondrio,
Sondrio, Italy

A. Pastorini
Divisione di Ematologia, Ospedale E. Morelli,
Sondalo, Italy

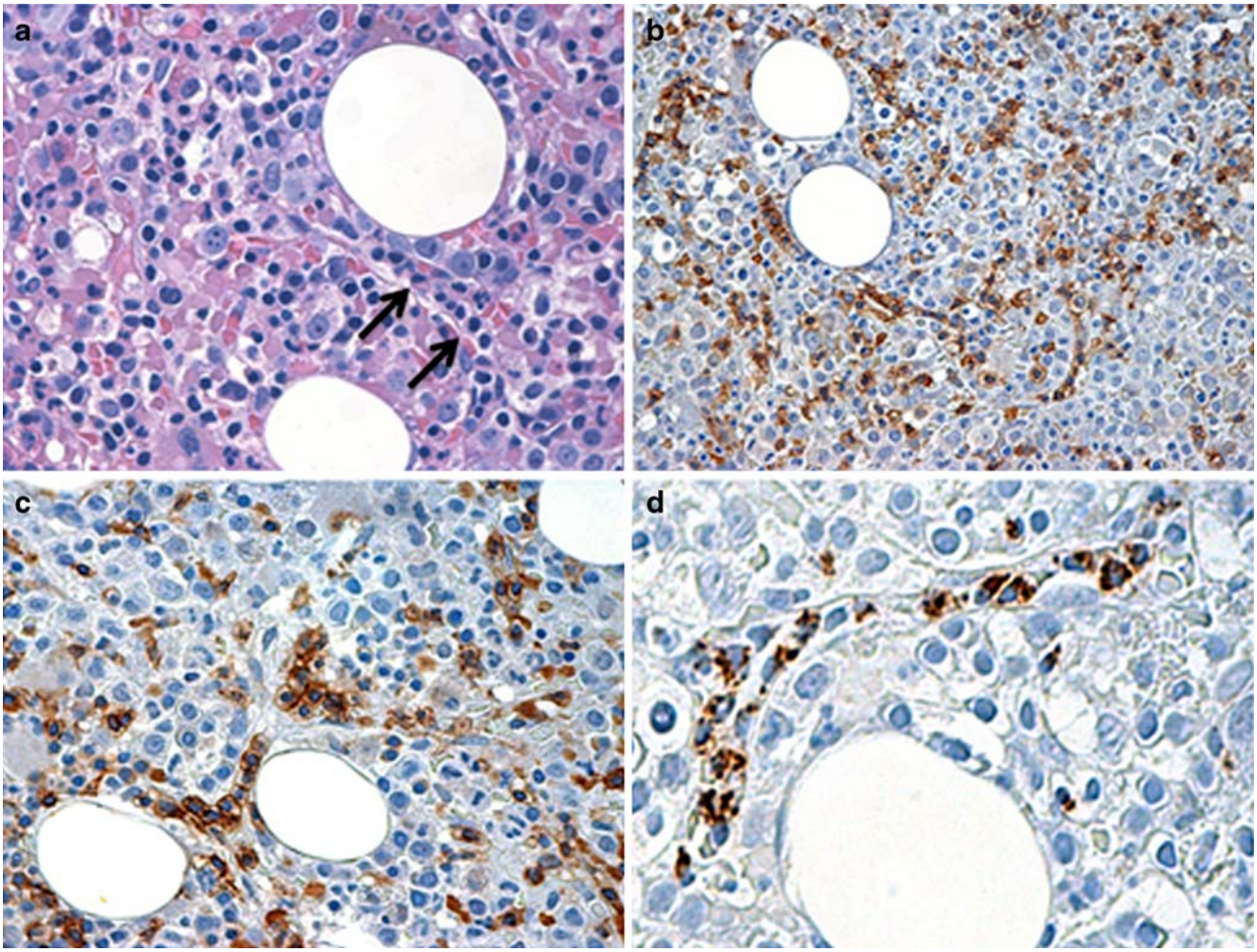

Fig. 1 **a** The BMB showed hypercellularity, maturation defects of erythroid and granulocyte component and a mild lymphoid infiltrate of small cells, with some linear disposition (*arrows*, HE, ×60). **b** CD3 demonstrated the T-cell nature of the lymphoid cells (streptavidin–biotin peroxidase technique, ×40). **c** The intra-sinusoidal pattern of the infiltrate was underlined by CD8 immunostaining (streptavidin–biotin peroxidase technique, ×60). **d** The neoplastic cells expressed the cytotoxic marker granzyme B (streptavidin–biotin peroxidase technique, ×100)

T-LGL can originate from a wide spectrum of proliferations, ranging from reactive, transient expansions to monoclonal indolent or, more rarely, aggressive leukaemias and a non-random association with viral infections or autoimmune disease is well known [1]; on these bases, autoantigens or viral antigens have been supposed to act as a chronic activating immunologic stimulus, leading to expansions and clonal selections of T-LGL.

When considering the possible role of viruses in the pathogenesis of the disease in our patient, an increase of CD8+ LGL can occur during HIV infection and about one third of these subjects carry a monoclonal TCR rearrangement, although without hepato-splenomegaly or clinically malignant course [4]. HBV is also a known cause of CD8+ lymphocytosis and an Italian study reported a higher prevalence of HCV infection than in controls in T-cell neoplasms [5].

In conclusion, although a casual association cannot be excluded, the hypothesis might be raised of a synergistic role of the three viral chronic infections in determining the pathogenesis of the disease in our case.

The patient started anti-retroviral therapy, and 8 months after diagnosis, he is alive, in good general condition, with progressive correction of the peripheral cytopenia.

Conflict of interest The authors declare that they have no conflict of interest.

References

1. Rose MG, Berliner N (2004) T-cell large granular lymphocyte leukemia and related disorders. The Oncologist 9:247–258

2. Costes V, Duchayne E, Taib J, Delfour C, Rousset T, Baldet P, Del sol G, Brousset P (2002) Intrasinusoidal bone marrow infiltration: a common growth pattern for different lymphoma subtypes. Br J Haematol 119:916–922
3. Morice WG, Kurtin PJ, Tefferi A, Hanson CA (2002) Distinct bone marrow findings in T-cell large granular lymphocytic leukemia revealed by paraffin section immunoperoxidase stains for CD8, TIA-1, and granzyme B. Blood 99:268–274
4. S Smith PR, Cavenagh JD, Milne T, Howe D, Wiles SJ, Sinnott P, Forster GE, Helbert M (2000) Benign monoclonal expansion of CD8+ lymphocytes in HIV infection. J Clin Pathol 53:177–181
5. Bianco E, Marcucci F, Mele A, Musto P, Cotichini R, Sanpaolo MG, Iannitto E, De Renzo A, Martino B, Specchia G, Montanaro M, Barbui AM, Nieddu R, Pagano L, Rapicetta M, Franceschi S, Mandelli F, Pulsoni A, Italian Multi-center case–control study (2004) Prevalence of hepatitis C virus infection in lymphoproliferative disease other than B-cell non-Hodgkin's lymphoma, and in myeloproliferative diseases: an Italian Multi-Center case control study. Haematologica 89:70–76

Virchows Arch (2009) 454:353–354
DOI 10.1007/s00428-009-0737-7

LETTER TO THE EDITOR

Tissue microarrays for immunohistochemical determination of oncological biomarkers

Paolo Verderio · Antonino Carbone

Received: 25 November 2008 / Accepted: 17 January 2009 / Published online: 4 February 2009

Dear Editor,

In a recent issue of Virchows Archiv, Marx et al. [1] investigated the potential prognostic impact of the expression of the biomarker alpha-methylacyl-CoA racemase (AMACR) detected in a large series of colorectal cancers (CRC) by immunohistochemistry (IHC) with tissue microarray (TMA) technology. Authors concluded that "AMACR cannot serve as a prognostic biomarker in CRC." This conclusion was in contrast with the results obtained by Lin et al. [2] in a previous study where it was found that there was a striking prognostic role of AMACR detected by IHC using TMA in CRC. In [1], authors stated that "…it appears unlikely that the use of TMA containing only limited amounts of tumor tissue per patient (one spot of 0.6 mm diameter per patient) has led to a significant number of false negative cases." and that "…focal AMACR expression cannot serve as explanation for the discrepancies" between the two studies as both were based on IHC determination of AMACR by TMA. Conversely, we think that the above discrepancies may be better explained by focusing on the potential technical pitfalls involved in TMA construction in the two studies rather than focusing on the data obtained. In fact, although IHC using TMA is substantially faster and at markedly lower costs compared with the conventional approach, its reliability and validity are influenced by many factors, the impact of which have to be put under control. For example, one of the major criticism of TMA technology is that it uses only a small fraction of a tissue specimen, which may not be representative of the whole tissue section. Although various studies [3, 4] have been conducted to optimize the sampling strategy for various solid cancers, actually there are no standardized operative procedures (SOP) for many biomarkers expressed in CRC, including AMACR. For example Marx et al. [1] used TMAs containing one core of 0.6 mm per specimen, whereas Lin et al. [2] used TMAs including three cores of 0.6 mm sampled from each specimen. Which is the minimum core numbers for specimen representativity need for this biomarker? Studies are needed to clarify this as well as many other aspects related to the TMA-based detection by IHC of AMACR in CRC. Among these, an important key issue concerns the antigen survival. It is important to clarify whether archival tissues retain their antigenicity despite long-time storage as paraffin blocks. TMA slides must be cut once and may not be used for staining until months or ever years later. On the other hand, although paraffin should protect the tissue from oxidation or other damage, some authors [5] have reported that, once tissue blocks are sectioned, the antigenicity of proteins on the slides would quickly degraded or even become lost with storage time, resulting in false-negative results. How many false-negative cases were expected for AMACR in [1] and [2] by considering the storage time of the specimens? Again, to answer this question, ad hoc studies are needed.

In general, before clinically validating AMACR as prognostic biomarker in CRC, it should be necessary to validate the methodology (i.e., TMA technology) used for its detection. The workflow involved in the TMA validation should ideally include, as first step, studies aimed to define SOPs for each of the involved phases. In the second step, ad

P. Verderio (✉)
Unit of Medical Statistics and Biometry,
Fondazione IRCCS Istituto Nazionale dei Tumori,
Via Venezian 1,
20133 Milan, Italy
e-mail: paolo.verderio@istitutotumori.mi.it

A. Carbone
Chairman Department of Pathology,
Fondazione IRCCS Istituto Nazionale dei Tumori,
Milan, Italy

hoc studies should be implemented to verify the reliability of the developed SOP in terms of precision, accuracy, and reproducibility by considering as reference values the measures obtained on the conventional whole sections staining.

The above considerations could be made for most biomarkers assessed in the different solid cancers. Coherently, studies have to be carried out to set-up both preanalytical and analytical phases involved in the construction and implementation of TMA for assessing each oncological biomarker. These studies should precede any other kind of investigation.

Finally, as TMA does not actually represent the routine method for most pathologists, prognostic studies based on conventional whole sections should be preferred to clinically validate potential biomarkers. On the other hand, TMA technology, once validated, represents an excellent alternative to other tools, such us cell lines [6], to implement external quality assessment studies focused on the whole process of biomarker determination [7].

References

1. Marx A, Simon P, Simon R, Mirlacher M, Izbicki JR, Yekebas E, Kaifi JT, Terracciano L, Sauter G (2008) AMACR expression in colorectal cancer is associated with left-sided tumor localization. Virchows Arch 453:243–248
2. Lin A, Weiser MR, Klimstra DS, Paty PB, Tang LH, Al-Ahmadie H, Hoo Park S, Guillem JG, Temple L, Wong WD, Gerald WL, Shia J (2007) Differential expression of alpha-methylacyl-coenzyme A racemase in colorectal carcinoma bears clinical and pathologic significance. Human Pathol 38:850–856
3. Rubin MA, Dunn R, Strawderman M, Pienta KJ (2002) Tissue microarray sampling strategy for prostate cancer biomarker analysis. Am J Surg Pathol 26:312–319
4. Su Y, Shrubsole MJ, Ness RM, Cai Q, Kataoka N, Washington K, Zheng W (2006) Immunohistochemical expressions of Ki-67, cyclin D1, beta-catenin, cyclooxygenase-2, and epidermal growth factor receptor in human colorectal adenoma: a validation study of tissue microarrays. Cancer Epidemiol Biomarkers Prev 15:1719–1726
5. DiVito KA, Charette LA, Rimm DL, Camp RL (2004) Long-term preservation of antigenicity on tissue microarrays. Lab Invest 84:1071–1078
6. Paradiso A, Miller K, Marubini E, Pizzamiglio S, Verderio P (2007) The need for a quality control of the whole process of immunohistochemistry human epidermal growth factor receptor 2/neu determination: a United Kingdom National External Quality Assessment Service/Italian Network for Quality Assessment of Tumor Biomarkers pilot experience. J Clin Oncol m25: e27–e28
7. Wasielewski R, Hasselmann S, Rüschoff J, Fisseler-Eckhoff A, Kreipe H (2008) Proficiency testing of immunohistochemical biomarker assays in breast cancer. Virchows Arch 453:537–543

Virchows Arch (2009) 454:355–357
DOI 10.1007/s00428-009-0738-6

LETTER TO THE EDITOR

The Salafia method rediscovered

Dario Piombino-Mascali · Arthur C. Aufderheide · Melissa Johnson-Williams · Albert R. Zink

Received: 10 November 2008 / Revised: 31 December 2008 / Accepted: 19 January 2009 / Published online: 10 February 2009

Keywords Embalming · Formaldehyde · History · Italy · 19th century · 20th century

Sir,

Embalming has played an essential role in human culture for much of history. While religious and cultural beliefs were the main motivators throughout antiquity, Modern Age advances in anatomy, pathology, and chemistry have caused body preservation to become an important tool for funerary purposes and educational and scientific practice [1]. In recent years, the authors have investigated the life and preparation techniques of Professor Alfredo Salafia (1869–1933), a Sicilian embalmer who devised a method of permanent preservation of soft tissue for dissection and funeral preparation (Fig. 1a).

Having started his experiments with animals, Salafia achieved unexpectedly satisfactory results in the early 1900s, after he was granted permission to apply his procedure to unclaimed human bodies, which remained in an excellent state of preservation after arterial injection of a special fluid [2]. From 1902 forward, he was responsible for the embalming of many prominent citizens of Palermo, including Cardinal Michelangelo Celesia (1904), Senator Giacomo Armò (1909), Vice-consul Giovanni Paterniti (1911), and ethnologist Giuseppe Pitrè (1916). Additionally, in 1910, Salafia became established in New York City, where he created a company providing embalming services and fluid manufacturing, and successfully demonstrated his procedure to the public at the Eclectic Medical College. However, his most notable case is undoubtedly Rosalia Lombardo (1920), a 2-year-old child who died of pneumonia, whose body is still exhibited in the Capuchin Catacombs at Palermo (Fig. 1b). Although Rosalia's head is the only exposed area, a recent assessment of her preservation status through conventional X-ray revealed a remarkable preservation of the remainder of the corpse, with only minor deterioration (Fig. 1c).

Salafia never divulged the details of his chemical prior to his death, and the compound of his preservative has remained shrouded in mystery until today. In 2007, after a detailed archival research and the subsequent interview of some living relatives, we were fortunate enough to be able to inspect some relevant material which belonged to this embalmer. Among his notes and papers was an unpublished, beautifully handwritten manuscript, entitled "New special method for the preservation of an entire human cadaver in a permanently fresh state" (Fig. 1d) [3]. Interestingly, this document describes the ingredients of his unknown preservative, namely one part glycerin, one part formalin saturated with both zinc sulfate and chloride, and one part of an alcohol solution saturated with salicylic acid. As far as the embalming procedure is concerned, this was characterized by a great simplicity, consisting of a single-point injection, preferably into the femoral artery via a gravity injector. No other procedures normally adopted in

D. Piombino-Mascali (✉) · A. R. Zink
Institute for Mummies and the Iceman, EURAC,
Viale Druso 1,
39100 Bolzano, Italy
e-mail: dario.piombino@eurac.edu

A. C. Aufderheide
Department of Pathology, University of Minnesota-Duluth,
Duluth, MN, USA

M. Johnson-Williams
American Society of Embalmers,
Forest Park, IL, USA

Fig. 1 **a** A portrait of the late Alfredo Salafia (1869–1933), a long-forgotten Palermo taxidermist and embalmer. **b** Rosalia Lombardo (1918–1920), one of the last bodies to be enshrined in the Capuchin Catacombs by special permission granted by the then mayor of Palermo. **c** Conventional X-ray of the child revealed a well-preserved brain and liver, as well as the presence of a bottle which may have contained an agent to prevent mould growth. The low quality of the image is due to the presence of a lead lining in the coffin, which severely affected the radiological investigation. **d** Salafia's unpublished manuscript, currently held at the Institute for Mummies and the Iceman, EURAC, Bolzano

contemporary embalming, such as drainage or cavity treatment, were in fact recommended for the normal case.

This important discovery certainly provides one of the earliest examples of the use of formaldehyde during the transition from "old" to "modern" embalming chemicals at the turn of the nineteenth century—a process ultimately leading to the replacement of the poisonous, yet widely popular, arsenic and mercury [4, 5]. Formaldehyde was accidentally produced by Alexandr Michajlovič Butlerov (1828–1866) in 1859 and synthesized by August Wilhelm von Hofmann (1818–1892) in 1868. The German chemist Oskar Loew (1844–1941) is credited with having been the first one in recognizing its antiseptic properties in 1888. In 1892, the French biologist Auguste Trillat (1861–1944) revealed to have determined its preservative power, and the following year, German physician Ferdinand Blum (1865–1959) discovered the excellent fixative properties of this chemical. An aqueous solution of formaldehyde—the so-called formalin—was first put on the market in 1893 and was soon adopted in the fields of anatomy, zoology, and histology, but apparently was not suggested as an ingredient used for embalming entire human bodies until 1895 [5–10].

The information described above suggests that Professor Salafia perfected a formaldehyde-based fluid that was successfully used by 1901. Additionally, his precious memoir discloses his occasional use of paraffin wax diluted in ether, hypodermically introduced into the deceased's face in order to keep the features life-like and plump, which

reveals his great attention to the details of cadaver preparation such as the facial expression and the overall appearance of the deceased.

In conclusion, we believe Alfredo Salafia was one of the foremost embalming practitioners of his time, who contributed substantially to the development of modern embalming, and his achievements should not be forgotten.

Acknowledgments We are most grateful to the relatives of Professor Salafia, who enabled us to complete this research, as well as two anonymous reviewers who commented on the original paper. Special thanks are due to Angela Graefen, who patiently edited the text. This article is dedicated to the memory of the embalming historians Edward C. and Gail R. Johnson, who first researched the work of Alfredo Salafia.

References

1. Marinozzi S, Fornaciari G (2005) Le Mummie e l'Arte Medica nell'Evo Moderno. Med Secoli, Supplemento, 1
2. Johnson EC, Johnson GR, Johnson-Williams M (1993) The Salafia method. American Funeral Director, May: 24–25, 54, 66, 68
3. Salafia A (circa 1927–1933) Nuovo metodo speciale per la conservazione del cadavere umano intero allo stato permanentemente fresco. Unpublished manuscript, Palermo
4. Habenstein RW, Lamers WM (2007) The history of American funeral directing, 6th edn. National Funeral Directors Association, Brookfield
5. Mendelsohn S (1940) Embalming fluids. Their historical development and formulation from the standpoint of the chemical aspects of the scientific art of preserving human remains. Chemical, New York
6. Strub CG, Frederick LGD (1967) The principles and practice of embalming, 4th edn. "Darko" Frederick, Dallas
7. Lanzillotti-Buonsanti A (1895) Conservazione dei cadaveri e preparazioni da museo. Tipografia Editrice LF Cogliati, Milan
8. Trillat A (1892) Sur les propriétés antiseptiques de la formaldéhyde. C R Hebd Séances Acad Sci 114:1278–1281
9. Fox CH, Johnson FB, Whiting J, Roller PR (1985) Formaldehyde fixation. J Histochem Cytochem 33(8):845–853
10. Koehler R, Lumière A and L (1895) Sur une nouvelle application de l'aldéhyde formique a la conservation des cadavres et a l'embaumement. Bibl Anatom III:31–32

Virchows Arch (2009) 454:359–367
DOI 10.1007/s00428-009-0751-9

REVIEW AND PERSPECTIVE

The impact of microRNAs on colorectal cancer

Claudius Faber · Thomas Kirchner · Falk Hlubek

Received: 1 December 2008 / Revised: 28 January 2009 / Accepted: 23 February 2009 / Published online: 14 March 2009

Abstract MicroRNAs are small RNAs that regulate gene expression at the post-transcriptional level. After their discovery 15 years ago, a new layer of gene regulation was introduced into every field of human biology and medicine. Considering the strong association between genetic alterations and neoplastic diseases, it is not surprising that there is a special focus on miRNAs and cancer. A multitude of experimental studies on colorectal cancer, the most common cancer site and furthermore the second most common cause of death due to cancer, deliver insight into miRNA-mediated, regulatory links to well-known oncogenic and tumour suppressor signalling pathways. Furthermore, several investigations have described the ability of microRNA expression patterns to predict prognosis in colon cancer and support diagnosis of poorly differentiated tumours. In this short review, we give a comprehensive overview focussed on miRNAs in colorectal cancer research.

Keywords microRNA · Colorectal cancer · Carcinogenesis · Epithelial–mesenchymal transition

Abbreviations

3′UTR	3′ untranslated regions of mRNAs
CRC	Colorectal cancer
CTGF	Connective tissue growth factor
CUP	Cancer of unknown primary
EMT	Epithelial-to-mesenchymal transition
miR/miRNA	microRNA
miRAGE	miRNA serial analysis of gene expression
mRNA	messenger RNA
PDCD4	programmed cell death 4
PI-3-K	Phosphatidylinositol-3-kinase-AKT pathway
PTEN	Phosphatase and tensin homolog
siRNA	Small interfering RNA
SNP	Single nucleotide polymorphism
SIRT1	Silent information regulator 1
TGF-β	Transforming growth factor β
TNF-α	Tumour necrosis factor α
Tsp-1	Thrombospondin-1
UICC	International Union Against Cancer (classification system)
ZEB1/ZEB2	Zinc finger E-box binding homeobox 1/2

C. Faber (✉) · T. Kirchner · F. Hlubek
Institute of Pathology,
Ludwig-Maximilians-University of Munich,
Thalkirchner Strasse 36,
80337 Munich, Germany
e-mail: c.faber@lmu.de

Role of microRNAs in human cells

From the initial discovery of small RNAs in the model organism *Caenorhabditis elegans* [1], it was a long way to appreciate their physiological relevance and their impact on pathological processes in humans. In the first years, small interfering RNAs (siRNA) gained importance in experimental research, owing to the fact that siRNAs are a comfortable tool to silence the expression of a certain protein by translational repression, without the need to engineer genetically modified cells. However, the enzymatic machinery of "RNA interference", exploited by siRNAs, is utilised in vivo by small endogenous RNAs (~22 bp), so-called microRNAs (miRNA). These single-strand RNAs are physiologically expressed in human tissues, some of them in a tissue specific manner. They have important regulatory functions in basic cellular processes like development,

differentiation, proliferation and cell death, affecting major biological systems such as stemness, immunity and cancer [2]. After transcription by the RNA polymerase, primary transcripts (pri-miR) are processed by an enzyme complex (DROSHA) to become precursor-miRNAs (pre-miR; Fig. 1). After their nuclear export, another enzymatic process catalysed by DICER leads to the mature miRNA that ultimately gets integrated into the RNA-induced silencing complex (RISC) [3–5]. This complex inhibits protein expression in two ways. Though the inhibition of translation as well as the degradation of messenger RNAs (mRNA) are both known effects acting on the expression of proteins by miRNAs, recent studies show a preponderance of mRNA destabilisation especially on highly repressed targets [6]. For targeting mRNAs, the 5′-region of a miRNA (seed region) is of special relevance, as it mediates target recognition. However, this recognition shows only an imperfect sequence complementarity, leading to a large number of target mRNAs

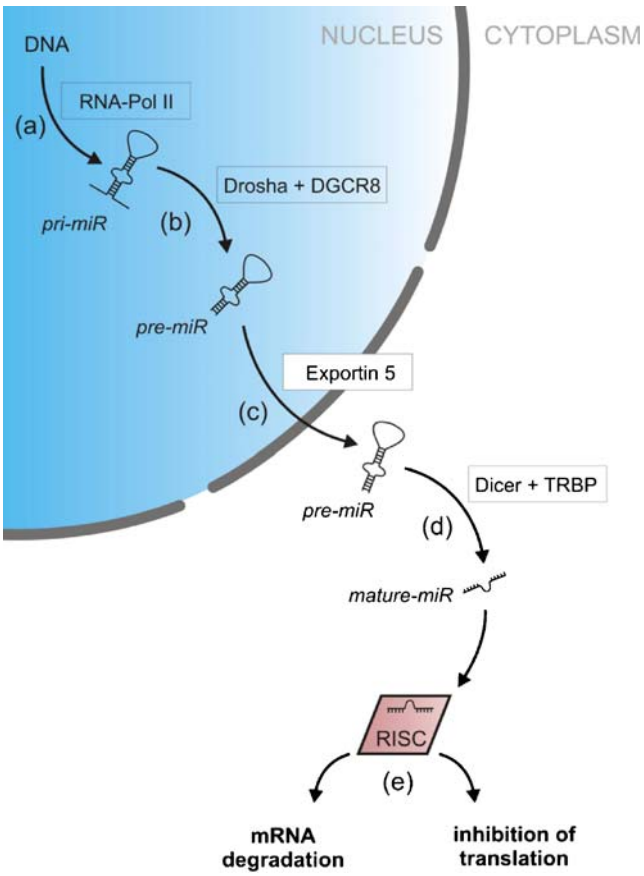

Fig. 1 Diagram of biogenesis and function of miRNAs. *a* Initially, a primary transcript (*pri-miR*) is transcribed from the DNA by RNA-polymerase. In a second step, *b* a nuclear enzyme complex including the protein DROSHA processes the primary transcript leading to a precursor-miRNA (*pre-miR*) that is *c* exported from the nucleus to the cytoplasm. *d* Here, the ribonuclease DICER cleaves the molecule to produce the "mature-miR" that is incorporated into the RISC. Finally, *e* this complex mediates the inhibition of protein translation or the degradation of the target mRNA

[7]. To date (Jan 2009), more than 695 miRNA genes have been identified in the human genome in "non-coding" sequences of the DNA [8], partly residing in previously disregarded genomic areas. They can be arranged in clusters, completely separated or inserted into intronic sequences of coding genes [9]. According to bio-informatical data, miRNAs are supposed to regulate ~30% of all genes [10]. Though a complete picture of miRNA biogenesis and function still lacks many parts of the puzzle, these new regulators of translation have already changed our view of gene expression regulation substantially.

Currently, two different approaches are applied to investigate the connection between miRNA and colorectal cancer (CRC). On the one hand, miRNAs seem to regulate many known oncogenic and tumour suppressor pathways involved in the pathogenesis of CRC. This is of special interest in colorectal neoplasms as many proteins involved in key signalling pathways in this tumour, like p53, RAS and epithelial–mesenchymal transition (EMT) transcription factors as well as members of the PI-3-K and the Wnt/β-catenin pathway seem to be affected by miRNA regulation. Their dissection in functional studies is critical for a better understanding of cancer biology, eventually aiming for the identification of novel pharmaceutical targets. Efforts in this area are discussed in the first part on oncomirs. On the other hand, expression profiles of hundreds of different miRNAs have been shown to bear a much higher potential as biomarkers than their mRNA counterparts. This allows a prediction of prognosis and a distinction of certain disease entities including colorectal cancer sub-types, as discussed in the second part of the article on miRNA profiling.

Oncomirs—tumour suppressor and oncogenic effects of microRNAs

Several miRNAs have been studied in functional experiments. We review experimental data performed on colorectal cancer or CRC cell lines (Fig. 2). When investigations on the regulation of important signalling pathways in CRC are lacking, we will also refer to investigations on other tumours.

p53 and miR-34

p53 is a well-known tumour suppressor gene, mutated in about 51–74% of all CRC and many other human tumours [11]. The protein is activated upon DNA damage and oncogene activation. Recently, several groups have unravelled important aspects of the connection between p53 and the miRNA network (reviewed in [12]). Chang et al. compared miRNA expression patterns in wild-type and $p53^{-/-}$ mutant HCT-116 colon cancer cell lines after

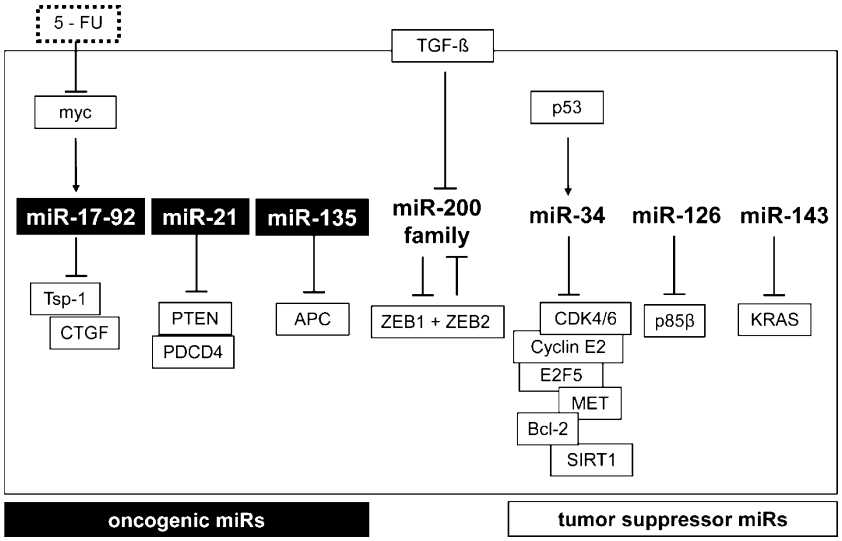

Fig. 2 Overview of microRNAs involved in key signalling pathways in colorectal cancer, their inductors and their targets. The depicted microRNAs affect central factors of colorectal carcinogenesis as p53, RAS and several EMT transcription factors. For details and abbreviations, see text

treatment with DNA damaging agents [13]. They found several miRNAs induced in the wild type but not in the $p53^{-/-}$ mutant cells, suggesting a p53-mediated expression. miR-34a showed the strongest induction. By experimentally over-expressing miR-34a, p53 effects like cell cycle arrest and apoptosis could be phenocopied. Amongst the down-regulated target mRNAs were well-characterised p53 targets like CDK4/6, cyclin E2, E2F5 and bcl-2. Of note, these effects were nearly identical, irrespective of the introduction of miR-34-a, miR-34-b or miR-34-c. Others identified SIRT1, a regulator of apoptosis in response to cellular stress, as an additional target of miR-34a [14]. Interestingly, the suppression of SIRT1 by miR-34a resulted in apoptosis in wild-type colon cancer cells, but not in $p53^{-/-}$ mutants. This suggests a feedback loop between p53 and miR-34. However, the question if miR-34 family members are essential for the promotion of p53-mediated effects that cannot be answered to date, as all the three genes would have to be deleted.

Like p53, members of the miR-34 family can be seen as tumour suppressors to date, making them potential candidates for inactivation in cancer. In fact, decreased levels of miR-34 have been found in many tumours including CRC [13, 15–17]. miR-34a expression was found to be decreased in nine of 25 human colon cancers [18]. One underlying mechanism seems to be CpG island methylation of miR-34a [17], as reported in three of 23 cases of colon cancer, and of miR-34b/c. The latter one was found to be epigenetically silenced in nine of nine examined cell lines and in 101 of 111 primary CRC tumours, but not in normal colonic mucosa. After treatment with demethylating agents, miR-34b/c expression was restored, resulting in inhibition of tumour motility and metastasis formation [19]. These experiments provide a basic mechanism, by which epigenetic alterations can promote oncogenic transformation by directly affecting miRNA genes.

The RAS oncogene

Another key player in colorectal carcinogenesis is the guanosine triphosphatase RAS. Mutations are found in 35–41% of CRCs [11]. In 2004, the let-7 family—containing nine distinct miRNAs—was initially shown to correlate with survival in lung cancer [20]. In colorectal cancer, two of six tumours and one of three colon cancer cell lines showed reduced let-7 levels. Transfection of cell lines with a let-7a-1 precursor miRNA resulted in growth suppression and a decrease in RAS protein levels [21]. This suggests a tumour suppressor effect of let-7 in colon cancer. MiR-143, another miRNA, also acts on RAS expression, as miR-143 and KRAS protein levels show an inverse correlation in CRC in vivo. In in vitro experiments, a direct binding of this specific miRNA to the 3′-untranslated region of the KRAS transcript could be confirmed [22]. Inhibition of miR-143 in cell line experiments resulted in stimulated cell proliferation. Interestingly, a general decrease of miR-143 in CRC and colorectal adenomas compared to normal mucosa was observed in an independent study [23]. Thus, decreased miR-143 expression might contribute to the pathogenesis of CRC by disinhibiting KRAS expression.

The Wnt/β-catenin pathway

The Wnt/β-catenin pathway plays a central role in early colorectal tumour development. More than 60% of all colorectal adenomas and carcinomas carry a mutation in the APC gene, leading to stimulation of the Wnt pathway via free β-catenin [24]. Nagel et al. describe a miR-mediated suppression of APC expression in CRC. miR-135a and miR-135-b decrease the translation of the APC transcript in vitro by targeting its 3′-untranslated region. Of note, miR-135 was also found to be upregulated in vivo in colorectal

adenomas and carcinomas and correlated with low APC levels [25]. Thus, the mir-135 family is dysregulated in neoplastic colorectal tissues. However, the reason for these alterations is still unknown.

Epithelial–mesenchymal transition

One recent study associated the expression of let-7 with two differentiation stages of a panel of cell lines (with an epithelial and a mesenchymal gene signature), linking let-7 to the EMT [26]. EMT describes the downregulation of E-cadherin and the successive loss of cell–cell adhesion, thus leading to a mesenchymal phenotype. Eventually, this contributes to the invasiveness and dissemination of epithelial tumour cells in several carcinomas including colorectal cancer [27]. Another functional link to EMT comes from the members of the miR-200 family (miR-200a, miR-200b, miR-200c, miR-141 and miR-429) that are suppressed by TGF-β-signalling [28]. They, in turn, suppress the EMT transcription factors and E-cadherin suppressors zinc finger E-box binding homeobox 1 (ZEB1; TCF8) and zinc finger E-box binding homeobox 2 (SIP1), important initiators of EMT in colorectal cancer [27, 29]. Interestingly, ZEB1 in turn inhibits the expression of the miR-200 family, thereby stabilising the EMT process. Thus, the miR-200 family members might act as tumour suppressors by inducing an epithelial phenotype. However, there is conflicting data for the putative tumour suppressor miR-200c, as it is predominantly found in CRC, but not in normal mucosa [30, 31] and it has been shown to be a marker of poor prognosis in one of the studies [30]. These observations argue for a more complex role of at least some microRNAs in the regulation of gene expression, as they may act in regulatory circuits with positive and negative feedback loops, instead of mediating uni-directional pathways.

The phosphatidylinositol-3-kinase-AKT pathway

The phosphatidylinositol-3-kinase-AKT (PI3-K-AKT) pathway provides another central oncogenic mechanism. An important gene in this pathway is the regulatory sub-unit p85-alpha, frequently mutated in CRC [32]. Guo et al. found that the functionally related regulatory sub-unit p85-beta is suppressed by miR-126. They could experimentally demonstrate growth suppressive effects on colorectal cancer cells. Additionally, miR-126 was down-regulated in four of four CRC cell lines [33]. The tumour suppressor gene PTEN is an important inhibitor in this pathway, showing genomic mutations in several cancers, but not frequently in sporadic CRC [34]. miR-21 has been identified to be a strong repressor of PTEN in hepatocellular cancer [35]. Interestingly, the same miRNA is upregulated in CRC [36, 37].

Apart from interference with the PI-3-K pathway, miR-21 has been shown to act on PDCD4, a tumour suppressor gene that is an independent prognostic factor in resected colorectal cancer [38]. Silencing of miR-21 by anti-miR-21 resulted in increased levels of PDCD4 in colorectal cell lines and increased invasion in a chicken–embryo–metastasis assay. In addition, 22 resected human tumours showed a higher miR-21 expression than the corresponding normal mucosa and decreased amounts of PDCD4 protein with mRNA levels unchanged [39]. These results argue for an important function of miR-21 in the pathogenesis of CRC, as it also shows a good correlation with prognosis [36, 37].

Regulation of other signalling pathways by miRNAs

The miR-17-92 cluster encodes six miRNAs (miR-17, miR-18a, miR-19a, miR-20a, miR-19b-1 and miR-92-1), located on chromosome 13 [40]. Dews et al. found myc-dependant angiogenesis promoting effects in $p53^{-/-}$ mouse colonocytes. This effect is attributed to a miR-17-92 mediated suppression of the anti-angiogenic factors Tsp1 and connective tissue growth factor, as silencing of the miR-17-92 cluster resulted in restored expression of these two proteins [41]. Thus, the miR-17-92 cluster mediates myc-dependant tumour promoting effects. Furthermore, this signalling pathway also seems to be a target of certain chemotherapeutic agents. 5-Fluorouracil (5-FU) is commonly used for the treatment of colon cancer. A recent study has shown that 5-FU treatment dose dependently decreases the expression of c-myc and, in consequence, of the miR-17-92 cluster [42].

A quite new area of research is the systematic genomic examination of the 3′ untranslated regions of protein coding genes. These regions, responsible for the binding of putative inhibitory small RNAs on the respective mRNAs, are supposed to carry mutations that might affect the affinity for miRNAs. This resistance to miRNA regulation could confer an increased risk for certain diseases, as it has been shown in silico for CRC. Out of eight in silico predicted candidates, the two genes for CD86, a co-stimulatory ligand on lymphocytes, and for the insulin receptor carry a single-nucleotide polymorphism (SNP) that is statistical significantly associated with the risk of sporadic colorectal cancer (odds ratio 2.74 and 1.94, respectively) [43]. However, the biological relevance of these SNPs in vitro has not yet been confirmed.

Prognostic impact of microRNA expression in colorectal cancer

Unlike these functional experiments, several studies focussed on correlations of miRNAs with survival or established bio-pathologic prognostic features (Fig. 3;

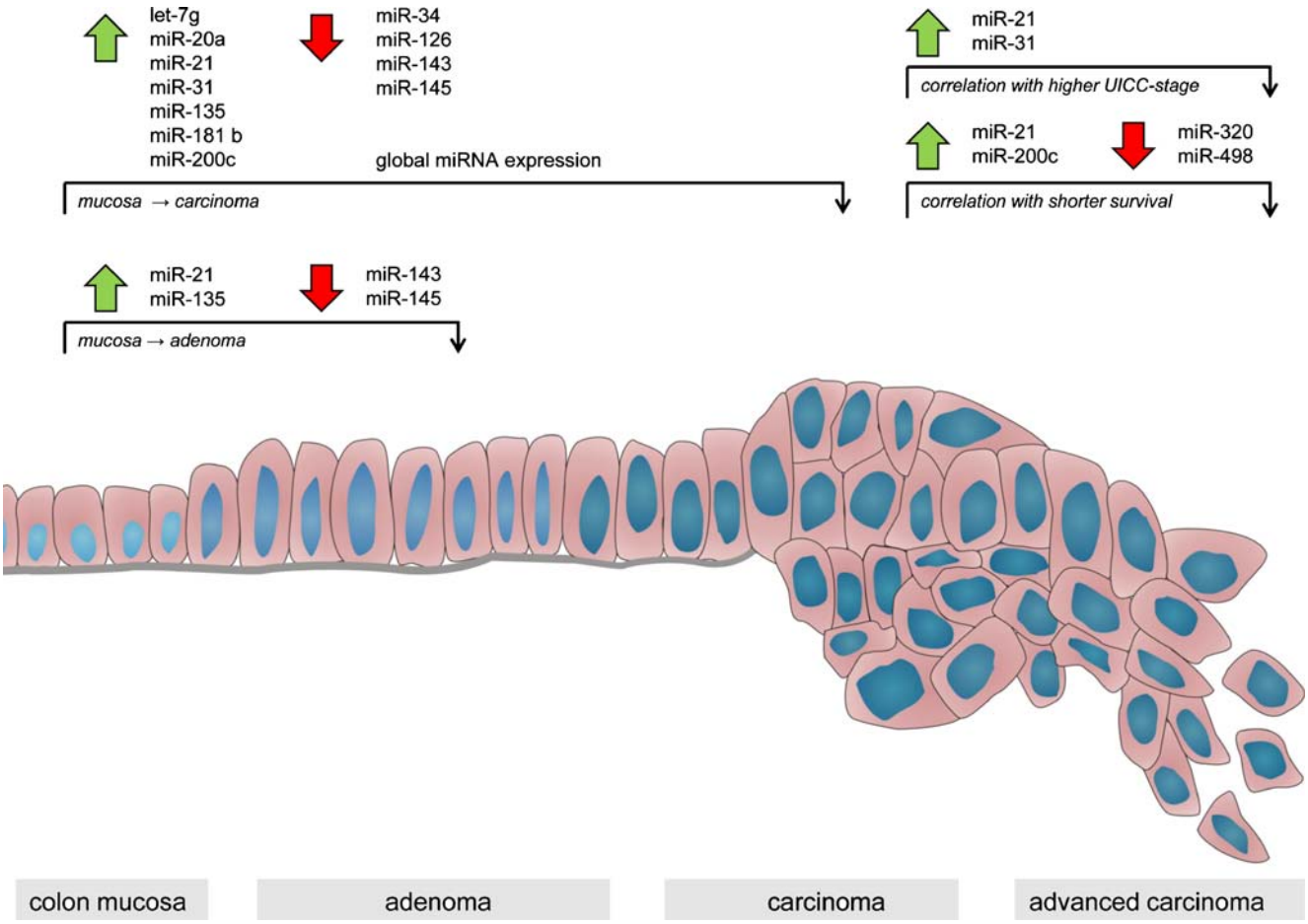

Fig. 3 Changes of miRNA expression in colorectal adenomas, carcinomas and their correlation with UICC stage or survival. Several specific miRNAs are up- or downregulated in adenomas and carcinomas compared to normal colon mucosa, based on expression profiling experiments. Additionally, expression levels of some miRNAs show a correlation with different UICC stages and survival in CRC. Only a selection of miRNAs is shown. For details, see text

Table 1). Studies have been performed on a broad variety of malignant tumours including lung [20], breast [44] and prostate cancer [45] as well as chronic lymphocytic leukaemia [46]. In colon cancer, several studies found a central role for miR-21 over-expression, showing a strong association with the established prognostic factors nodal stage, metastatic disease, International Union Against Cancer (UICC) stage and directly with poor survival [36, 37]. Investigations on 24 resected colorectal cancers demonstrated a significantly shorter survival in patient

Table 1 Selection of study details of publications on CRC or colorectal cancer cell lines investigating miRNA expression with regard to differences from normal samples or prognostic impact

The number (*n*) of tumour samples, normal samples and the number of examined miRNAs is shown

	Tumour (*n*)	Control (*n*)	Cell lines used	miR examined (*n*)
Schetter et al. [36]				
Test cohort	84	84		389
Validation cohort	113	113		
Schepeler et al. [48]	49	10		315
Xi et al. [30]	24	24		10
Slaby et al. [37]	29	6		4
Nakajima et al. [31]	21	21		5
Bandres et al. [47]	12	12	+	156
Michael et al. [23]	14	4	+	28
Cummins et al. [71]	4	2	+	(miRAGE)
Guo et al. [33]	–	–	+	262

samples with high levels of miR-200c [30]. Increased expression of miR-31 has been associated with a higher UICC stage [47]. In contrast, miR-320 and miR-498 have been shown to be positive prognostic markers, showing a strong correlation with recurrence-free survival [48]. Interestingly, adenomas also show an over-expression of miR-21 when compared to normal mucosa [36]. Thus, some miRNAs might also play a role in early tumour development (Table 1).

Additionally, molecular well-defined sub-groups, like microsatellite unstable colorectal cancer (MSI-H) can be distinguished by miRNA profiling. MSI-H colorectal cancers harbour defects in the mismatch repair system. They make up about 15% of all sporadic colorectal cancers. In the inherited disorder Lynch syndrome or hereditary non-polyposis colorectal cancer, certain mismatch repair proteins carry germline mutations. Though these two sub-types are similar in conventional histology, they differ in prognosis and response to chemotherapy [49, 50]. miRNA profiles have been shown to separate MSI-H CRC from microsatellite stable CRC with a specificity of around 80% and a sensitivity of around 90% [48, 51].

Another important prognostic question is the response to therapy. Nakajima et al. found an association for members of the let-7 family of miRNAs and miR-181b with therapy response to the 5-fluorouracil-based anti-metabolite S-1 in a retrospective analysis of tissue samples from CRC patients [31]. According to these preliminary data, let-7 family members might be important in altering chemotherapy response.

Diagnostic potential of microRNA profiles

Apart from this prognostic information, miRNA expression profiles also vary between different tumours and normal tissue. MicroRNAs differ substantially from mRNAs in their degree of effects on protein expression. One mRNA can yield only a small number of polypeptides, varying from each other due to post-transcriptional modifications. On the other hand, miRNAs target mRNAs with an imperfect sequence complementarity. In consequence, a single miRNA can regulate the expression of more than 100 mRNAs simultaneously [10, 52]. This might explain why microarrays of 217 miRNAs have a much higher content of information than ~16,000 mRNAs in distinguishing different tissues and tumours [53, 54]. Significant differences in miRNA expression profiles have now been described in tumours of different developmental lineages and differentiation states including colon cancer [53, 55, 56]. This might prove helpful approaching old clinical problems: The concept of a “cancer of unknown primary” (CUP) describes metastatic lesions without an identified primary tumour. These mostly poorly differentiated tumours make up 2-4% of all cancers [57], with 7% and 12% contributed to by colon cancer due to large autopsy and mRNA studies, respectively [58]. These malignant lesions pose a serious clinical problem, as it is often difficult or impossible to characterise them by histopathological examination including advanced techniques such as immunohistochemistry and electron microscopy. Thus, large studies and therapeutic recommendations are lacking, contributing to a poor prognosis of these patients. Two recent studies examined metastases of known primary tumours with miRNA microarrays for their potential to identify the tissue of origin. After establishing a miRNA classifier (n=68, 11 tumour types, 217 miRNAs), 12 out of 17 poorly differentiated samples were accurately classified by miRNA profiling [53]. A second publication reports an overall accuracy of 90% of classification in more than 400 malignant tumour samples of 22 tissue origins based on a set of only 48 miRNAs [56]. Unfortunately, no information on the tumour differentiation (grading) has been supplied in the latter study, as the poorly differentiated tissues cause the most severe diagnostic problems. A recent study on lymph node metastases of several malignant tumours including CRC identified three specific miRNAs (miR-148a, miR-34b/c and miR-9), specifically downregulated by CpG island hyper-methylation. Re-introducing miRNA function with demethylating agents resulted in reduced tumour growth as well as inhibition of metastasis formation in a xenograft model [59]. To our knowledge, up to now, no one examined miRNA expression in CUP tissue in a larger scale to prove a clinical relevant diagnostic benefit.

The distribution of miRNAs in cancer and normal tissue has been studied by several groups in the last years (Fig. 3; Table 1). In reports on various cancer samples, generally lower miRNA levels were found in tumours compared to normal tissue [53] and lower levels in poorly differentiated compared to well-differentiated tumours in tissue samples [53] as well as in cell lines [60]. Additionally, by targeting key regulators of miRNA biogenesis, cells can be driven towards transformation [61]. However, this could not consistently be confirmed [55]. Investigations on paired colorectal neoplasias and normal mucosa samples demonstrated reduced levels of miR-143 and miR-145 in colonic adenomas and carcinomas [23]. Others confirmed a reduction of these two miRNAs in CRC [37, 47, 48] and added miR-126 an miR-133b to the list [33, 47]. On the other hand, some miRNAs are over-expressed in CRC tissue. Amongst the upregulated miRNAs are let-7 g [62], miR-21 [36, 37], as well as miR-20a [36], a member of the miR-17-92 family. Further, over-expressed transcripts are miR-31 [37, 47], miR-135 [25, 47], miR-181b and miR-200c [30, 31, 36] (for more information about all studies on miRNA expression differences in CRC, see Table 1). A recent publication investigated serum samples of healthy

controls, CRC patients and other common diseases. In CRC serum samples, they found 69 miRNAs that are not expressed in healthy subjects, 55 of them shared with lung cancer [63]. These are promising results for diagnostic purposes. However, larger studies will have to prove if miRNAs really have a higher accuracy in predicting malignancy and prognosis compared to information derived from current standard diagnostic procedures.

Potential for diagnostic applications in surgical pathology

Formalin-fixed paraffin-embedded (FFPE) tissue is a readily available storage medium, well suitable for basic pathologic techniques even after long storage times. However, the application of FFPE for advanced molecular biology techniques is limited due to the poor quality of nucleic acids such as mRNA and DNA [64]. In addition, longer formalin fixation times decrease mRNA amounts extracted from FFPE tissues, thus complicating quantitative analyses [65]. This is of special interest for the surgical pathologist, as the steadily growing application of molecular pathology in many diseases requires new approaches. However, in the case of miRNAs, several studies reveal that they are well preserved in FFPE even after archival times of up to 10 years [66]. One recent examination compared the miRNA-expression profiles from fresh frozen and from FFPE tissues of colorectal cancer. They found a good correlation coefficient of 0.86–0.89. Noteworthy, differing formalin fixation times, inevitable in a routine pathology lab, did not significantly influence the expression of miRNAs in 40 colorectal cancer specimens [66]. Furthermore, miRNAs can also be visualised at the cellular and the sub-cellular level by conventional as well as by fluorescence in situ hybridisation [67, 68]. These practical issues combined with the promising preliminary studies on the diagnostic and prognostic potential of miRNAs, make these small RNAs valuable biomarker candidates for colorectal cancer.

Perspective

The discovery of miRNAs has substantially changed the view on gene regulation. A few gaps that had previously not been deciphered have been closed. However, new questions arise, as the cellular expression pathway from gene to protein has become more complex. miRNAs exert pleiotropic effects on the cell by regulating numerous mRNAs, thus guiding whole programmes of protein expression instead of single genes. Therefore, the classification of all cancer-associated miRNAs into oncogenes or tumour suppressor genes might be an over-simplification.

Recent investigations put another piece of complexity to the situation. Experiments on the tumour necrosis factor α gene have shown that certain miRNAs have the ability to upregulate protein translation under specific circumstances like cell cycle arrest [69, 70]. Apart from this qualitative difference, others have investigated the global impact of miRNAs on protein output [6, 7]. They clearly confirmed a combined action on mRNA levels as well as on translation itself. However, the degree of depression was modest. Therefore, the authors of the latter study suggest a concept of “large-scale fine tuning” of the cell by miRNAs.

These publications demonstrate that there are still many open questions about the impact of miRNAs on the proteome. However, promising preliminary results on the diagnostic and prognostic potential of miRNAs in colorectal cancer have been demonstrated (Fig. 3). On the other hand, functional studies have considerably contributed to a better comprehension of the pathways that drive oncogenic transformation in colorectal cancer (Fig. 2), including new genomic alterations that directly affect miRNA signalling.

Conflict of interest The authors declare that they have no conflict of interest.

References

1. Lee RC, Feinbaum RL, Ambros V (1993) The C. elegans heterochronic gene lin-4 encodes small RNAs with antisense complementarity to lin-14. Cell 75:843–854
2. Sassen S, Miska EA, Caldas C (2008) MicroRNA: implications for cancer. Virchows Arch 452:1–10
3. Esquela-Kerscher A, Slack FJ (2006) Oncomirs—microRNAs with a role in cancer. Nat Rev Cancer 6:259–269
4. Singh SK, Pal Bhadra M, Girschick HJ et al (2008) MicroRNAs—micro in size but macro in function. Febs J 275:4929–4944
5. Akao Y, Nakagawa Y, Naoe T (2007) MicroRNA-143 and -145 in colon cancer. DNA Cell Biol 26:311–320
6. Baek D, Villen J, Shin C et al (2008) The impact of microRNAs on protein output. Nature 455:64–71
7. Selbach M, Schwanhausser B, Thierfelder N et al (2008) Widespread changes in protein synthesis induced by microRNAs. Nature 455:58–63
8. Griffiths-Jones S, Grocock RJ, van Dongen S et al (2006) miRBase: microRNA sequences, targets and gene nomenclature. Nucleic Acids Res 34:D140–D144
9. Ying SY, Lin SL (2006) Current perspectives in intronic micro RNAs (miRNAs). J Biomed Sci 13:5–15
10. Lim LP, Lau NC, Garrett-Engele P et al (2005) Microarray analysis shows that some microRNAs downregulate large numbers of target mRNAs. Nature 433:769–773
11. Leslie A, Carey FA, Pratt NR et al (2002) The colorectal adenoma–carcinoma sequence. Br J Surg 89:845–860
12. Hermeking H (2007) p53 enters the microRNA world. Cancer Cell 12:414–418
13. Chang TC, Wentzel EA, Kent OA et al (2007) Transactivation of miR-34a by p53 broadly influences gene expression and promotes apoptosis. Mol Cell 26:745–752
14. Yamakuchi M, Ferlito M, Lowenstein CJ (2008) miR-34a repression of SIRT1 regulates apoptosis. Proc Natl Acad Sci USA 105:13421–13426

15. Welch C, Chen Y, Stallings RL (2007) MicroRNA-34a functions as a potential tumor suppressor by inducing apoptosis in neuroblastoma cells. Oncogene 26:5017–5022
16. Bommer GT, Gerin I, Feng Y et al (2007) p53-mediated activation of miRNA34 candidate tumor-suppressor genes. Curr Biol 17:1298–1307
17. Lodygin D, Tarasov V, Epanchintsev A et al (2008) Inactivation of miR-34a by aberrant CpG methylation in multiple types of cancer. Cell Cycle 7:2591–2600
18. Tazawa H, Tsuchiya N, Izumiya M et al (2007) Tumor-suppressive miR-34a induces senescence-like growth arrest through modulation of the E2F pathway in human colon cancer cells. Proc Natl Acad Sci USA 104:15472–15477
19. Toyota M, Suzuki H, Sasaki Y et al (2008) Epigenetic silencing of microRNA-34b/c and B-cell translocation gene 4 is associated with CpG island methylation in colorectal cancer. Cancer Res 68:4123–4132
20. Takamizawa J, Konishi H, Yanagisawa K et al (2004) Reduced expression of the let-7 microRNAs in human lung cancers in association with shortened postoperative survival. Cancer Res 64:3753–3756
21. Akao Y, Nakagawa Y, Naoe T (2006) let-7 microRNA functions as a potential growth suppressor in human colon cancer cells. Biol Pharm Bull 29:903–906
22. Chen X, Guo X, Zhang H et al. (2009) Role of miR-143 targeting KRAS in colorectal tumorigenesis. Oncogene. doi:10.1038/onc.2008.474
23. Michael MZ, OC SM, van Holst Pellekaan NG et al (2003) Reduced accumulation of specific microRNAs in colorectal neoplasia. Mol Cancer Res 1:882–891
24. Powell SM, Zilz N, Beazer-Barclay Y et al (1992) APC mutations occur early during colorectal tumorigenesis. Nature 359:235–237
25. Nagel R, le Sage C, Diosdado B et al (2008) Regulation of the adenomatous polyposis coli gene by the miR-135 family in colorectal cancer. Cancer Res 68:5795–5802
26. Shell S, Park SM, Radjabi AR et al (2007) Let-7 expression defines two differentiation stages of cancer. Proc Natl Acad Sci USA 104:11400–11405
27. Spaderna S, Schmalhofer O, Hlubek F et al (2006) A transient, EMT-linked loss of basement membranes indicates metastasis and poor survival in colorectal cancer. Gastroenterology 131:830–840
28. Burk U, Schubert J, Wellner U et al (2008) A reciprocal repression between ZEB1 and members of the miR-200 family promotes EMT and invasion in cancer cells. EMBO Rep 9:582–589
29. Spaderna S, Schmalhofer O, Wahlbuhl M et al (2008) The transcriptional repressor ZEB1 promotes metastasis and loss of cell polarity in cancer. Cancer Res 68:537–544
30. Xi Y, Formentini A, Chien M et al (2006) Prognostic values of microRNAs in colorectal cancer. Biomark Insights 2:113–121
31. Nakajima G, Hayashi K, Xi Y et al (2006) Non-coding MicroRNAs hsa-let-7 g and hsa-miR-181b are associated with chemoresponse to S-1 in colon cancer. Cancer Genomics Proteomics 3:317–324
32. Philp AJ, Campbell IG, Leet C et al (2001) The phosphatidylinositol 3′-kinase p85alpha gene is an oncogene in human ovarian and colon tumors. Cancer Res 61:7426–7429
33. Guo C, Sah JF, Beard L et al (2008) The noncoding RNA, miR-126, suppresses the growth of neoplastic cells by targeting phosphatidylinositol 3-kinase signaling and is frequently lost in colon cancers. Genes Chromosomes Cancer 47:939–946
34. Vivanco I, Sawyers CL (2002) The phosphatidylinositol 3-Kinase AKT pathway in human cancer. Nat Rev Cancer 2:489–501
35. Meng F, Henson R, Wehbe-Janek H et al (2007) MicroRNA-21 regulates expression of the PTEN tumor suppressor gene in human hepatocellular cancer. Gastroenterology 133:647–658
36. Schetter AJ, Leung SY, Sohn JJ et al (2008) MicroRNA expression profiles associated with prognosis and therapeutic outcome in colon adenocarcinoma. JAMA 299:425–436
37. Slaby O, Svoboda M, Fabian P et al (2007) Altered expression of miR-21, miR-31, miR-143 and miR-145 is related to clinicopathologic features of colorectal cancer. Oncology 72:397–402
38. Mudduluru G, Medved F, Grobholz R et al (2007) Loss of programmed cell death 4 expression marks adenoma-carcinoma transition, correlates inversely with phosphorylated protein kinase B, and is an independent prognostic factor in resected colorectal cancer. Cancer 110:1697–1707
39. Asangani IA, Rasheed SA, Nikolova DA et al (2008) MicroRNA-21 (miR-21) post-transcriptionally downregulates tumor suppressor Pdcd4 and stimulates invasion, intravasation and metastasis in colorectal cancer. Oncogene 27:2128–2136
40. Mendell JT (2008) miRiad roles for the miR-17–92 cluster in development and disease. Cell 133:217–222
41. Dews M, Homayouni A, Yu D et al (2006) Augmentation of tumor angiogenesis by a Myc-activated microRNA cluster. Nat Genet 38:1060–1065
42. Zhao HY, Ooyama A, Yamamoto M et al (2008) Down regulation of c-Myc and induction of an angiogenesis inhibitor, thrombospondin-1, by 5-FU in human colon cancer KM12C cells. Cancer Lett 270:156–163
43. Landi D, Gemignani F, Naccarati A et al (2008) Polymorphisms within micro-RNA-binding sites and risk of sporadic colorectal cancer. Carcinogenesis 29:579–584
44. Iorio MV, Ferracin M, Liu CG et al (2005) MicroRNA gene expression deregulation in human breast cancer. Cancer Res 65:7065–7070
45. Porkka KP, Pfeiffer MJ, Waltering KK et al (2007) MicroRNA expression profiling in prostate cancer. Cancer Res 67:6130–6135
46. Calin GA, Ferracin M, Cimmino A et al (2005) A MicroRNA signature associated with prognosis and progression in chronic lymphocytic leukemia. N Engl J Med 353:1793–1801
47. Bandres E, Cubedo E, Agirre X et al (2006) Identification by Real-time PCR of 13 mature microRNAs differentially expressed in colorectal cancer and non-tumoral tissues. Mol Cancer 5:29
48. Schepeler T, Reinert JT, Ostenfeld MS et al (2008) Diagnostic and prognostic microRNAs in stage II colon cancer. Cancer Res 68:6416–6424
49. Popat S, Hubner R, Houlston RS (2005) Systematic review of microsatellite instability and colorectal cancer prognosis. J Clin Oncol 23:609–618
50. Ribic CM, Sargent DJ, Moore MJ et al (2003) Tumor microsatellite-instability status as a predictor of benefit from fluorouracil-based adjuvant chemotherapy for colon cancer. N Engl J Med 349:247–257
51. Lanza G, Ferracin M, Gafa R et al (2007) mRNA/microRNA gene expression profile in microsatellite unstable colorectal cancer. Mol Cancer 6:54
52. Linsley PS, Schelter J, Burchard J et al (2007) Transcripts targeted by the microRNA-16 family cooperatively regulate cell cycle progression. Mol Cell Biol 27:2240–2252
53. Lu J, Getz G, Miska EA et al (2005) MicroRNA expression profiles classify human cancers. Nature 435:834–838
54. Ramaswamy S, Tamayo P, Rifkin R et al (2001) Multiclass cancer diagnosis using tumor gene expression signatures. Proc Natl Acad Sci USA 98:15149–15154
55. Volinia S, Calin GA, Liu CG et al (2006) A microRNA expression signature of human solid tumors defines cancer gene targets. Proc Natl Acad Sci USA 103:2257–2261

56. Rosenfeld N, Aharonov R, Meiri E et al (2008) MicroRNAs accurately identify cancer tissue origin. Nat Biotechnol 26:462–469
57. Pavlidis N, Briasoulis E, Hainsworth J et al (2003) Diagnostic and therapeutic management of cancer of an unknown primary. Eur J Cancer 39:1990–2005
58. Pentheroudakis G, Golfinopoulos V, Pavlidis N (2007) Switching benchmarks in cancer of unknown primary: from autopsy to microarray. Eur J Cancer 43:2026–2036
59. Lujambio A, Calin GA, Villanueva A et al (2008) A microRNA DNA methylation signature for human cancer metastasis. Proc Natl Acad Sci USA 105:13556–13561
60. Gaur A, Jewell DA, Liang Y et al (2007) Characterization of microRNA expression levels and their biological correlates in human cancer cell lines. Cancer Res 67:2456–2468
61. Kumar MS, Lu J, Mercer KL et al (2007) Impaired microRNA processing enhances cellular transformation and tumorigenesis. Nat Genet 39:673–677
62. Nakajima N, Takahashi T, Kitamura R et al (2006) MicroRNA-1 facilitates skeletal myogenic differentiation without affecting osteoblastic and adipogenic differentiation. Biochem Biophys Res Commun 350:1006–1012
63. Chen X, Ba Y, Ma L et al (2008) Characterization of microRNAs in serum: a novel class of biomarkers for diagnosis of cancer and other diseases. Cell Res 18:997–1006
64. Srinivasan M, Sedmak D, Jewell S (2002) Effect of fixatives and tissue processing on the content and integrity of nucleic acids. Am J Pathol 161:1961–1971
65. Bresters D, Schipper ME, Reesink HW et al (1994) The duration of fixation influences the yield of HCV cDNA-PCR products from formalin-fixed, paraffin-embedded liver tissue. J Virol Methods 48:267–272
66. Xi Y, Nakajima G, Gavin E et al (2007) Systematic analysis of microRNA expression of RNA extracted from fresh frozen and formalin-fixed paraffin-embedded samples. RNA 13: 1668–1674
67. Nuovo GJ (2008) In situ detection of precursor and mature microRNAs in paraffin embedded, formalin fixed tissues and cell preparations. Methods 44:39–46
68. Silahtaroglu AN, Nolting D, Dyrskjot L et al (2007) Detection of microRNAs in frozen tissue sections by fluorescence in situ hybridization using locked nucleic acid probes and tyramide signal amplification. Nat Protoc 2:2520–2528
69. Vasudevan S, Tong Y, Steitz JA (2007) Switching from repression to activation: microRNAs can up-regulate translation. Science 318:1931–1934
70. Orom UA, Nielsen FC, Lund AH (2008) MicroRNA-10a binds the 5'UTR of ribosomal protein mRNAs and enhances their translation. Mol Cell 30:460–471
71. Cummins JM, He Y, Leary RJ et al (2006) The colorectal microRNAome. Proc Natl Acad Sci USA 103:3687–3692

Virchows Arch (2009) 454:369–379
DOI 10.1007/s00428-009-0753-7

ORIGINAL ARTICLE

Hedgehog signaling is involved in differentiation of normal colonic tissue rather than in tumor proliferation

Beate Alinger · Tobias Kiesslich · Christian Datz · Fritz Aberger · Felix Strasser · Frieder Berr · Otto Dietze · Klaus Kaserer · Cornelia Hauser-Kronberger

Received: 17 September 2008 / Revised: 25 February 2009 / Accepted: 25 February 2009 / Published online: 12 March 2009

Abstract The Hedgehog (Hh) pathway is a main regulation cascade in embryonic differentiation. It is also present in adult tissues and unusual expression has been associated with formation of benign and malignant lesions. We examined the presence of the Hedgehog pathway in normal and pathological human colon tissue. Components investigated include Sonic (Shh), Indian (Ihh), and Desert Hedgehog (Dhh), Gli1, Gli2, Gli3, and Patched (Ptch). Pathological tissue samples comprised 23 benign and 20 malignant lesions of human colon. The influence of the Hedgehog pathway on differentiation and proliferation has been investigated by analyzing the effect of the pathway inhibitor Cyclopamine on human colon cancer cell lines HT29 and CaCo2. In normal colon, we detected expression of Shh and Dhh within the lining epithelium and Patched, Gli1, and Gli2 along the whole crypts. Within all benign lesions, positive staining of Shh, Dhh, Gli1, Gli2, and Ptch was detected. Expression of Shh and Dhh was restricted to single cell aggregates. Malignant lesions also displayed focal staining pattern for Shh and Dhh but to a much lesser extent. We conclude that Hedgehog signaling is involved rather in constant differentiation and renewing of the colonic lining epithelium than in cancer formation, growth, or proliferation.

Keywords Hedgehog pathway · Colon cancer · Differentiation · Proliferation · Stem cells

Abbreviations

CRC	Colorectal cancer
Shh	Sonic Hedgehog
Ihh	Indian Hedgehog
Dhh	Desert Hedgehog
FFPE	Formalin-fixed paraffin-embedded
CK	Cytokeratin
Hh	Hedgehog
APC	Adenomatous polyposis coli
EGFR	Epidermal growth factor receptor
Ptch	Patched
Smo	Smoothened
DMEM	Dulbecco's modified Eagle's medium
FBS	Fetal bovine serum
DMSO	Dimethyl sulfoxide
PBS	Phosphate-buffered saline
HIER	Heat-induced epitope retrieval
NE	Neuroendocrine
TMA	Tissue microarray

B. Alinger · F. Strasser · O. Dietze · C. Hauser-Kronberger (✉)
Department of Pathology, General Hospital,
Paracelsus Medical University Salzburg,
Muellner Hauptstrasse 48,
5020 Salzburg, Austria
e-mail: c.hauser-kronberger@salk.at

T. Kiesslich · F. Berr
Department of Internal Medicine I,
Paracelsus Medical University Salzburg,
Muellner Hauptstrasse 48,
5020 Salzburg, Austria

C. Datz
Department of Internal Medicine, General Hospital Oberndorf,
Teaching Hospital of Paracelsus Medical University Salzburg,
Paracelsusstraße 37,
5110 Oberndorf, Austria

F. Aberger
Department of Molecular Biology, University of Salzburg,
Hellbrunnerstraße 34,
5020 Salzburg, Austria

K. Kaserer
Department of Pathology, Vienna Medical University,
Währinger Gürtel 18-20,
1090 Vienna, Austria

Introduction

Colorectal cancer (CRC) is one of the most frequently diagnosed cancers and cancer-related mortality remains unacceptably high despite improvements in understanding the events leading to malignant transformation of the colorectal epithelium [1, 2].

Colorectal carcinogenesis occurs as a multistep process that requires sequential or concomitant damage to several genes within and across cellular generations. The pathogenesis of CRC is characterized by a well-defined sequence of events—from aberrant crypt proliferation or hyperplasia over benign adenomas [3] to carcinoma in situ and, finally, metastatic carcinoma [4]. The process of colorectal cancer formation is well described, though the molecular steps are still to be investigated more precisely. Signaling cascades involved in organ development during embryogenesis still play a significant role in tissue maintenance by regulating steadily renewing processes. In the present study, we focused on how Hedgehog (Hh) pathway activity may be correlated with colorectal cancer formation.

The Hh pathway plays an essential role in the embryogenesis of invertebrate and vertebrate species and has been shown to be involved in patterning, growth, and cell-type specification in a wide range of tissues including the gut [5–9]. In mammals, three different forms of the Hedgehog ligand exist comprising Sonic (Shh), Indian (Ihh), and Desert Hedgehog (Dhh). Each of them is able to bind to the receptor Patched (Ptch) on target cells, activating an intracellular signaling cascade which leads to the release of the transcription factors Gli1, Gli2, or Gli3 and therefore expression of particular target genes [10]. Defects in the Hedgehog signaling cascade have been associated to several birth defects like Holoprosencephaly and the Pallister–Hall syndrome, caused by mutations in the shh and the gli3 gene [11, 12]. Both mutations show characteristic gut abnormalities like gut malrotation, esophageal atresia, and imperforate anus. In addition to their function in the embryo, the Hedgehog proteins and the several Hedgehog signal transducing components are expressed in postnatal and adult tissues like stomach [13, 14] and colon [15]. The Hedgehog pathway components Ihh and Ptch were detected in the epithelial lining of the colon [16], possibly being involved in its steadily renewing process by affecting colonic stem cells. Due to activation of the Hedgehog pathway in mature organs, it has been implicated as a possible factor for cancer formation [17–19]. Uncontrolled activation of signaling cascades may lead to uncontrolled proliferation and differentiation and therefore formation of cancer. However, in colonic cancer formation, involvement of Hh pathway is discussed very controversially [20–22].

The current study investigated the relation of Hedgehog pathway activity to normal colon differentiation and analyzed changes in the signaling characteristics during the process of cancer formation. Immunohistochemical detection of several Hedgehog pathway components, including Gli1, 2 and 3, Shh, Ihh, Dhh, and Ptch on normal human colon tissue and selected colonic lesions has been performed. The samples included normal colon tissue samples (n=10), benign lesions of the colon (n=23) comprising tubular, tubulovillous adenoma, and hyperplastic polyps, as well as malignant lesions of G1 to G3 colon adenocarcinoma (n=20), which represent 95% of all arising colon cancers. Additionally to the presence and distribution of the Hh signaling components, all cases were tested for coexpression of the differentiation marker CK20, the proliferation associated protein Ki67, bcl-2 as an indicator for apoptosis resistance, β-catenin, and adenomatous polyposis coli (APC) representative of Wnt signaling. Cdx-2 known as an intestinal transcription factor and positive in colon metastasis and epidermal growth factor receptor (EGFR) were analyzed to show a correlation of Hh activity with routinely therapeutic markers. Additionally, colon cancer tissue arrays including 91 colon cancer cases, each of them represented in triplicate, were investigated immunohistochemically. Main results of protein coexpression were confirmed by double-immunofluorescence staining. The protein expression on tissue was correlated with gene expression analysis in colon cancer cells CaCo2 and HT29. Therefore, quantitative real time polymerase chain reaction (PCR), cyclopamine tolerance assay, and immunohistochemistry were performed.

In summary, we found expression of Hh pathway components Shh, Dhh, Gli1, Gli2, and Ptch in normal, benign, and malignant colonic tissue on protein and mRNA level. Activity seems to correlate with differentiation of normal colon, as Hh expression decreases with increasing tumor stage. Benign colonic lesions as well as low grade carcinomas display more intense Hh expression than high grade carcinomas. In vitro data on the cellular sensitivity toward cyclopamine for the CaCo2 and HT29 cell lines confirm our results.

Material

Human nonpathological and pathological archival tissue samples from colon (n=55) and metastasis (n=4) have been provided by the Department of Pathology, University Hospital Salzburg. The benign lesions (n=23) included tubular, tubulovillous adenomas, hyperplastic polyps, and epithelial dysplasia; malignant lesions comprised adenocarcinoma (n=20). Normal human colon tissue (n=10), received from morphologically normal areas of colectomy specimens, was analyzed as control. All tissue samples were routinely processed by fixation in 7% neutral buffered formalin followed by paraffin embedding.

Tissue arrays with 273 samples of colon cancer, each case spotted in triplicate, and the corresponding normal tissue sections were obtained from the Department of Pathology, Medical University Vienna. The formalin-fixed paraffin-embedded (FFPE) samples were routinely processed.

Histological classification was performed according to the World Health Organization guidelines and tumor staging according to Tumor Node Metastasis System of the International Union against Cancer.

Methods

Immunohistochemistry

Immunohistochemical staining for all antibodies investigated was performed on routinely FFPE tissue and cytoblocks. For detection of Hedgehog pathway activity, goat polyclonal antibodies for Gli1 (N-16), Gli2 (N-20), Gli3 (N-19), Shh (N-19), Ihh (C-15), Dhh (N-19), Ptch (C-20), and Smo (Smoothened, N-17; all Santa Cruz, San Francisco, CA, USA; 1:100) were used and visualized via a standard streptavidin–biotin–peroxidase detection system (S-ABC; StreptABComplex/HRP Duet kit; Dako, Glostrup, Denmark). For preabsorption control, Hh antibodies were incubated with adequate blocking peptides (all from Santa Cruz; 1:10) for 2 h at room temperature. Alternatively, for double-immunofluorescence staining, primary antibodies were applied simultaneously, followed by a biotinylated secondary antibody (1:200) and detection using Alexa Fluor®555 goat antimouse (1:100) or Alexa Fluor®555 goat antirabbit (1:100) and Streptavidin-Alexa Fluor® 488 (1:50; Molecular Probes, Eugene, OR, USA).

Samples were stained for β-catenin (Dako, 1:200), CK20 (NovoCastra, 1:50), Ki67 (Dako, 1:500), bcl-2 (Dako, 1:100), APC (Neo Markers, 1:200), and Cdx-2 (Linaris, 1:20) using the EnVision Detection System (Dako) on a Dako Autostainer. Detection of EGFR was performed using a standardized kit (Dako, EGFR pharm Dx).

Four-micrometer-thick sections were deparaffinized with xylene, hydrated in graded alcohols, followed by heat-induced epitope retrieval in pH9 antigen retrieval buffer (Dako) for all antibodies used.

For all sections stained with goat polyclonal Hedgehog antibodies, avidin–biotin blocking (Dako) was performed. Endogenous peroxidase blocking was carried out for 15 min with 3% H_2O_2 in absolute methanol and normal serum was applied (1:20). Primary antibodies were incubated overnight at 4°C and detection was performed using biotinylated rabbit antigoat antibody (Dako, 1:400) and StreptABComplex/HRP Duet kit (Dako, 1:300), followed by visualization with diaminobenzidine. Slides were counterstained with hematoxylin.

Cell culture

The human colon cancer cell lines HT29 and CaCo2 were grown in Dulbecco's modified Eagle's medium (DMEM; Sigma-Aldrich, Vienna, Austria) supplemented with 10% fetal bovine serum (FBS; Sigma-Aldrich), 100 μg ml^{-1} penicillin–streptomycin (Sigma-Aldrich; 10,000 U ml^{-1} penicillin and 10 mg ml^{-1} streptomycin in 0,9% sodium chloride), 2 mM L-glutamine (Gibco, Stadt, Land) and 1 mM Na-pyruvat (Sigma-Aldrich) at 37°C in a humified atmosphere (5% CO_2).

For immunohistochemical investigations, one nearly confluent 10-cm diameter Petri dish was harvested with trypsin/ethylenediaminetetraacetic acid and washed with sterile phosphate buffered saline (PBS) followed by resuspending in 200 μl citrate plasma and 200 μl thromborel S. After coagulation, cells were fixed for 1 h in neutral buffered saline containing 7% formalin and paraffin-embedded cytoblocks were made.

Cyclopamine treatment

HT29 and CaCo2 cells were seeded in 96-well microplates (Greiner, Kremsmuenster, Austria) in 100 μl DMEM containing 10% FBS at densities of 15,000 per well. Twenty-four hours postseeding, the cells were washed with 100 μl serum-free DMEM and incubated with 10, 7.5, 5, and 2.5 μM cyclopamine (Sigma-Aldrich; stock solution: 5 mM in dimethyl sulfoxide (DMSO)). Control wells were either incubated with serum-free DMEM or with DMEM containing the according amount of DMSO (solvent control). Seventy-two hours postincubation cellular survival was assessed by means of reduction of 3-(4,5-dimethyl-2-thiazolyl)-2,5-diphenyl-2H-tetrazolium bromide (MTT) to the insoluble blue formazan catalyzed by mitochondrial and other cellular dehydrogenases [23, 24]. In brief, 10 μl of PBS containing 5 mg/ml were added to each well of the microplates and incubated at 37°C/5% CO_2 for 45 min; thereafter, the supernatant was removed and the plates were stored at 4°C until measurement. Following solubilization of the formazan by addition of 100 μl 2-propanol, the MTT signal was measured at 565 nm using an Infinite-200 M microplate reader (Tecan, Groedig, Austria). For calculation of the results, the blank values (wells without cells, but similarly processed) were subtracted from the mean values of the control samples (n=20 for each plate), cyclopamine and solvent control samples (each n=10), and the latter two were related to the untreated control samples (=100%). Data represent mean±standard error of the mean (SEM) of three independent experiments.

RNA isolation and cDNA synthesis

Total RNA isolation from cultured cells was performed using Trizol according to the manufacturer's instructions

(Invitrogen; Paisley, UK). RNA was separated by adding chloroform and for precipitation absolute isopropyl alcohol was used, followed by a washing step with 70% EtOH. The pellet was dissolved in 30 µl diethylpyrocarbonate-treated water by gently shaking at 56°C on a heat block. After RNA isolation procedures, RNA quantity was determined at 260/280 nm and RNA purity was proved by gel electrophoresis. cDNA was synthesized with SuperScript II (RNase H) reverse transcriptase (Invitrogen) according to the manufacturer's instructions.

Real-time PCR

Real-time PCR analysis was done on a Rotorgene 6000 (Corbett Research, Sydney, Australia) using SYBR Green Supermix (Bio-Rad Laboratories, Hercules, CA, USA). Primer pairs used were described previously [25, 26]. A total of 10 µl PCR reaction with 5 µl of iQTM SYBR Green Supermix, 0.6 µl of fwd/rev primer mix (10 pmol each) replenished with 4.4 µl cDNA (1:25 diluted) was used. Cycling conditions were 6 min at 95°C, followed by 44 cycles 1 min at 95°C, 15 s at 62°C, and 30 s at 72°C, and a final elongation step (5 min at 72°C).

Statistics

Student's test was used for calculation of significant differences between the samples; ** and * stand for highly (0.01) and significant (0.05) different pairs of values, respectively.

Results

Hedgehog signaling is active in normal and pathological human colonic tissue

Hedgehog pathway components Shh, Dhh, Ptch, Gli1, and Gli2 were expressed in normal colon tissue samples as well as in benign and malignant lesions, concluding an active Hedgehog pathway in the mature colon. The Hedgehog pathway components are present mainly in the epithelial lining of the colon and in colonic neuroendocrine cells. Particularly, the ligands Shh and Dhh showed an intense staining pattern exclusively in the lining epithelium (Fig. 1a, d). The components Gli1, Gli2, and Ptch showed a positive reaction along the whole crypts of the human colon (Fig. 2a–c), though staining was not as strong as for Shh and Dhh, suggesting an active signaling pathway in this part of the colonic wall.

Expression of the Hedgehog pathway members Gli1, Gli2, Shh, Ihh, and Ptch was detected in pathological tissue samples. All cases of tubular and tubulovillous adenoma showed intense positive staining with the antibodies directed against Gli1, Gli2, Shh, Dhh, and Ptch (Figs. 1b, e and 2d–f). Cellular staining pattern for Shh and Dhh was

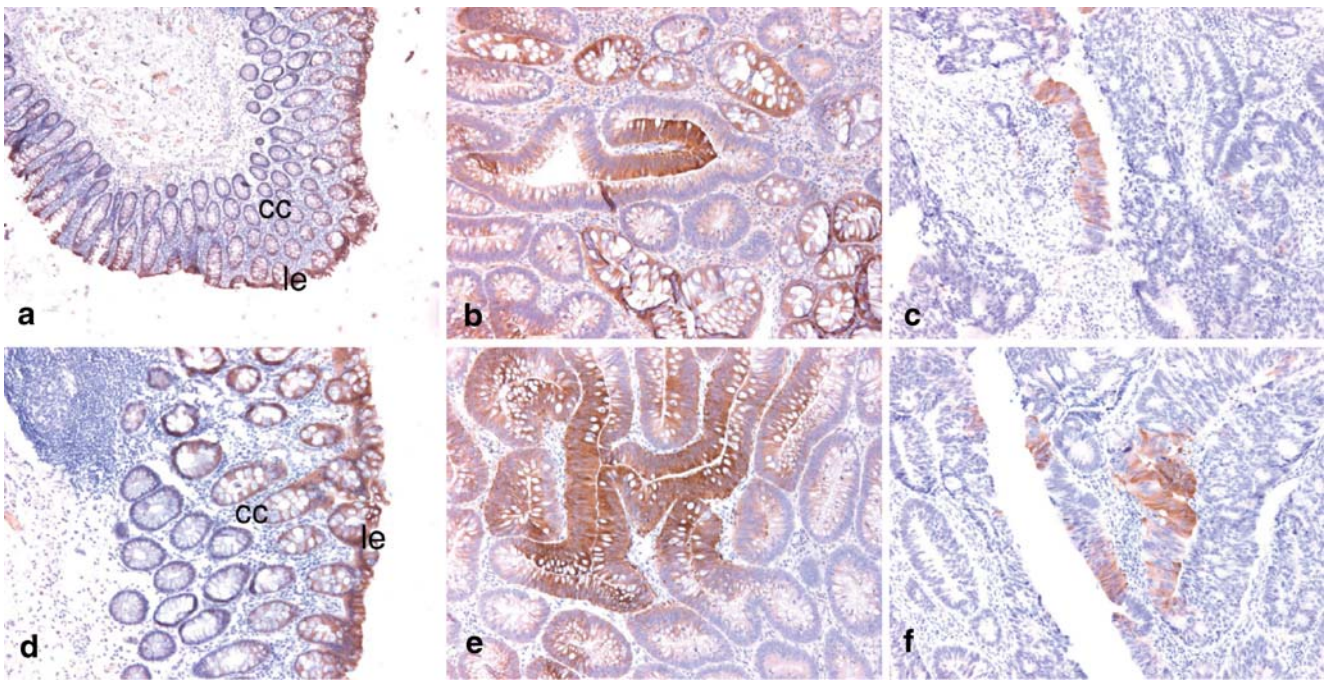

Fig. 1 Expression of the Hedgehog ligands Shh and Dhh in normal and pathological tissue from human colon. **a**–**c** Immunohistochemical staining of the normal colon (**a**, **d**), benign (**b**, **e**), and malignant (**c**, **f**) lesions with an antibody directed against Shh (**a**–**c**) Dhh (**d**–**f**). *le* lining epithelium, *cc* colonic crypts. Magnification ×20

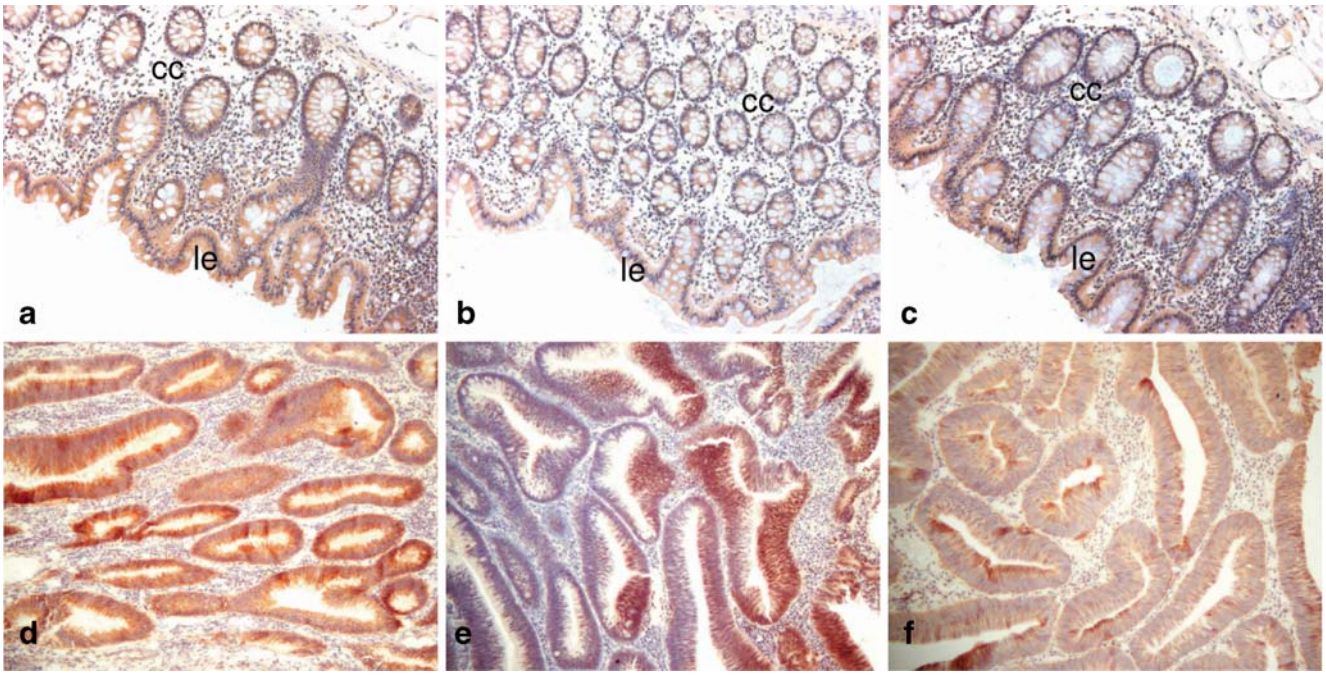

Fig. 2 Expression of Gli1, Gli2, and Ptch in normal and pathological tissue from human colon. Normal colon tissue samples (**a**–**c**) and benign lesions (**d**–**f**) were stained with antibodies against Gli1 (**a**, **d**), Gli2 (**b**, **e**), and Ptch (**c**, **f**). *le* lining epithelium, *cc* colonic crypts. Magnification ×20

not consistently distributed within the pathological tissue samples but showed an area dependent focally variation in protein expression. Expression of Hh ligands was noticeably reduced in adenocarcinoma of the colon. Staining of Gli1, Gli2, and Ptch was absent in nearly all cases of adenocarcinoma; staining of Shh and Dhh was restricted to small cell groups (Fig. 1c, f). Similar results were obtained for analysis of expression of Shh and Dhh on tissue microarray (TMA; Table 1). In contrast to normal epithelium where Shh and Dhh are frequently expressed, the rate of positive staining in malignant colonic tissue is 19% and 7% for Shh and Dhh, respectively.

Hedgehog expression correlates with differentiation in colon

As Hedgehog pathway protein expression in benign and malignant lesions of the colon showed active signaling, the correlation of Hh pathway members with clinically relevant markers was investigated.

Correlation with differentiation using an anti-CK20 and proliferation with an anti-Ki67 antibody was analyzed. These markers showed contrary expression in normal colonic tissue as CK20 is expressed in the colon lining epithelium and Ki67 in the basal crypts where the colonic stem cells are supposed to be located and therefore proliferation occurs. In benign and malignant colon tissue staining, pattern for both CK20 and Ki67 was not consistently distributed but focally as known for Shh and Dhh expression.

Coexpression of the Hh ligands with CK20 (Fig. 3) and inverse coexpression with Ki67 (Fig. 5) in normal and pathological colonic tissue samples was investigated by double-immunofluorescence staining. The Hh ligands Shh and Dhh were coexpressed with CK20 in the epithelial lining of normal human colon (Fig. 3). In benign and malignant colonic tissue samples, all cells that express Shh and Dhh showed positive reaction with CK20. Some cells, however, did express CK20 but not Shh or Dhh. Ki67 expressing cells rather show contrary expression as demonstrated by staining of colon cancer tissue array (Fig. 4)

Table 1 Tissue microarray results in normal and malignant colon tissue samples

Antigen	Malignant colon tissue			Normal colon tissue		
	Evaluable samples	Positive samples	% positive samples	Evaluable samples	Positive samples	% positive samples
Shh	250	48	19.2	162	160	98.7
Dhh	250	17	6.8	120	18	15

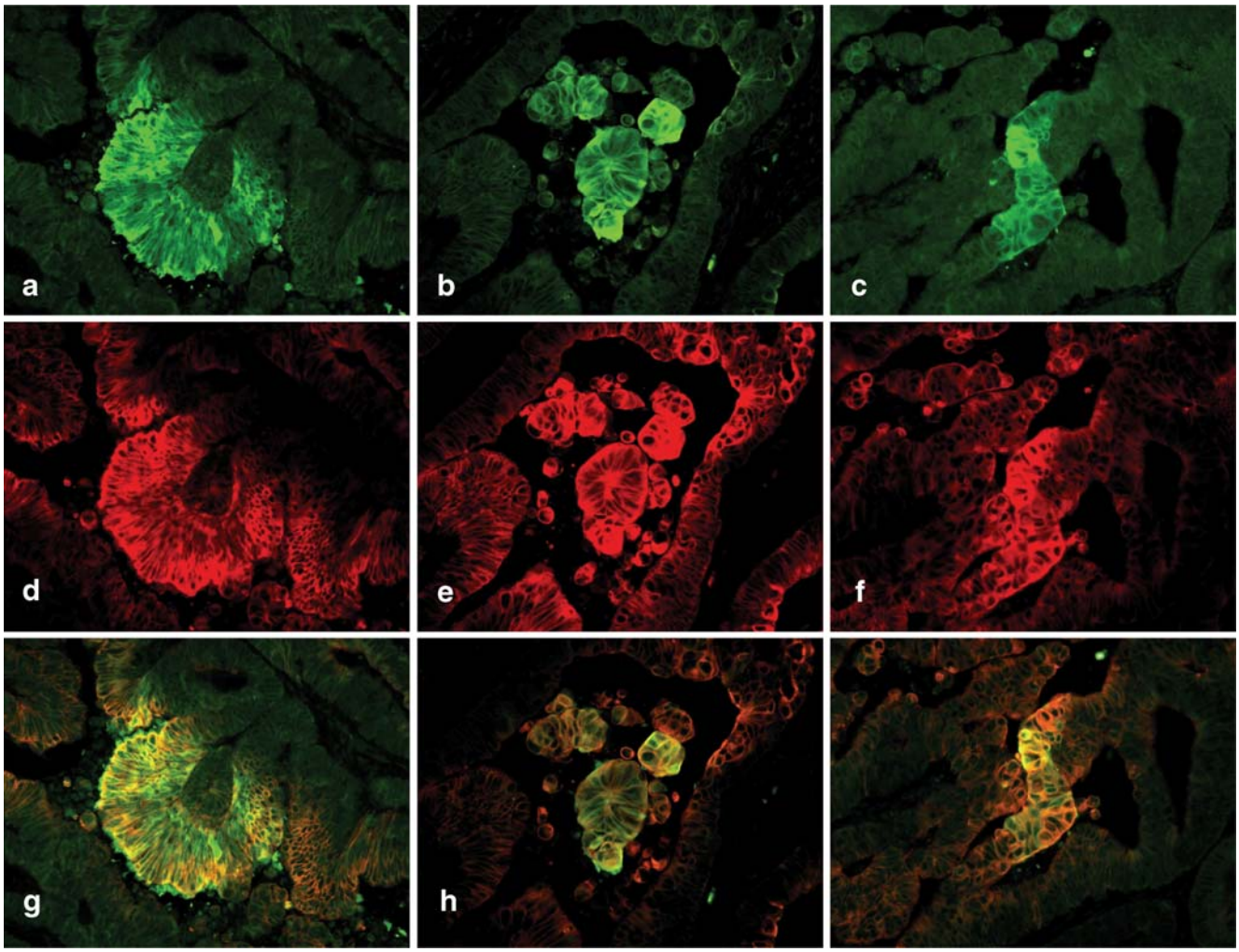

Fig. 3 Representative double-immunofluorescence staining of Shh (*green*) and CK20 (*red*) coexpression. **a**–**c** Typical Shh single staining (*green*) of colonic lesions; **d**–**f** the identical area with CK20 staining; **g**–**i** both staining results combined. Magnification ×20

and double immunofluorescence (Fig. 5). Ki67 expressing cells did not show expression of Shh or Dhh, but within Shh and Dhh positive cell clusters, single cells showed expression of Ki67.

For the anti-apoptotic marker bcl-2, members of the Wnt signaling pathway (β-catenin and APC), EGFR and intestine-specific transcription factor Cdx-2 double-immunofluorescence staining showed no correlation with expression of Hh pathway members neither in normal colon nor in pathological tissue samples (data not shown).

Hedgehog activity is detected in colon cancer cell lines

To confirm our immunohistochemical findings, Hh pathway activity in the human colon adenocarcinoma cell lines CaCo2 and HT29 was studied. Investigations comprised immunohistochemistry on FFPE cytoblocks and quantitative detection of Hh gene expression by real-time PCR. Additionally, a cyclopamine tolerance assay was performed on the cell lines to show if pathway activity is necessary for survival of colon cancer cells. Each cell line showed a particular expression pattern. HT29 cells were positive for CK20 (51%) and Ki67 (40%) and negative (membranous localization) for β-catenin and Cdx-2 (Fig. 6a–d). CaCo2 were negative for CK20 (1%) and positive for Ki67 (95%), β-catenin (34% cytoplasm, 35% nucleus), and Cdx-2 (84%; Fig. 6e–h). Presence of Hh pathway members was detected in both cell lines on protein and mRNA level. Immunohistochemical analysis showed lower Hh protein expression in CaCo2 than in HT29 cells though not as explicit as seen for tissue samples, but on mRNA level expression was notably higher in HT29 than in CaCo2 cells (Figs. 7 and 8). Survival assay with cyclopamine showed that HT29 cells dramatically reduced their cell amount 72 h after addition of cyclopamine, whether CaCo2 seemed to be nearly unaffected (Fig. 9).

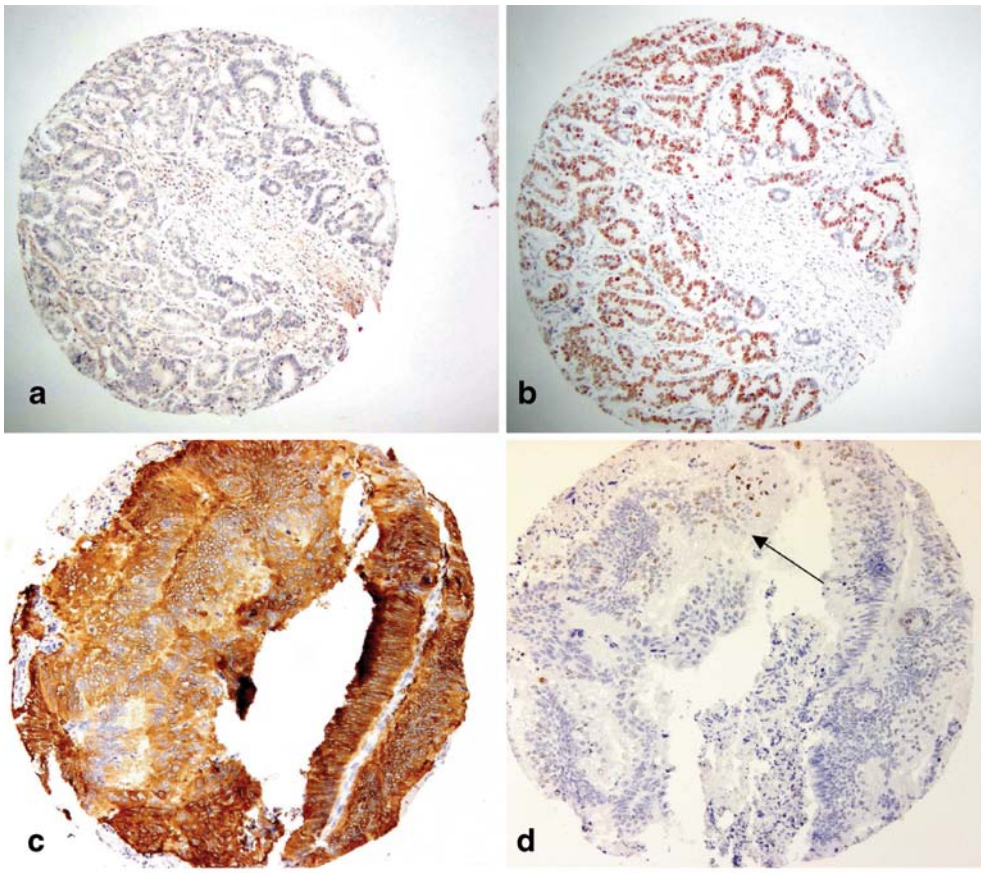

Fig. 4 Colon cancer tissue array staining of Shh and Ki67. **a**–**d** Staining of two different cases of colon cancer with Shh (**a**, **c**) and Ki67 (**b**, **d**). The first case is positive for Ki67 (**b**) but negative for Shh (**a**), contrary the second case shows just few cells positive for Ki67 (**d**, *arrow*) but is positive for Shh (**c**), supporting the findings of a reverse expression. Magnification ×20

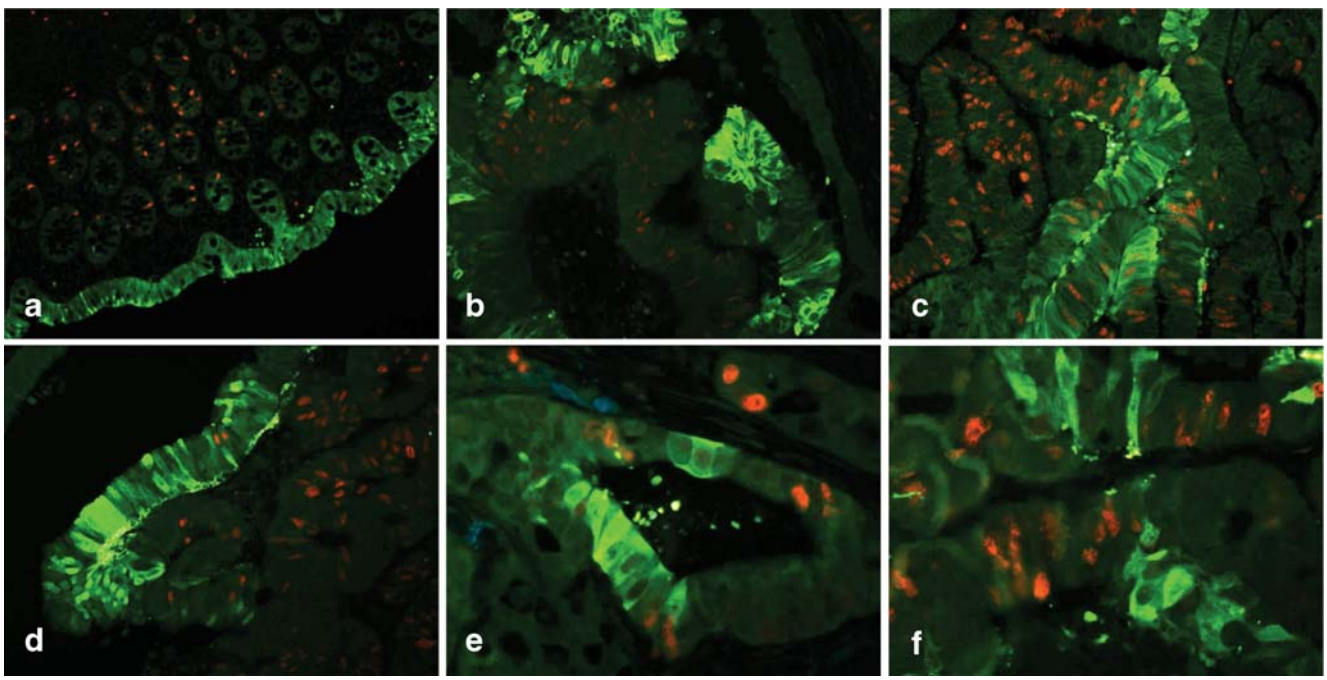

Fig. 5 Double-immunofluorescence staining of Dhh (*green*) with Ki67 (*red*). **a**–**f** Coexpression of Dhh (*green*) with Ki67 (*red*). Dhh and Ki67 are contrary expressed in normal colonic tissue (**a**) and benign and malignant colonic lesions (**b**–**f**). Magnification ×20 (**a**–**d**), ×40 (**e**–**f**)

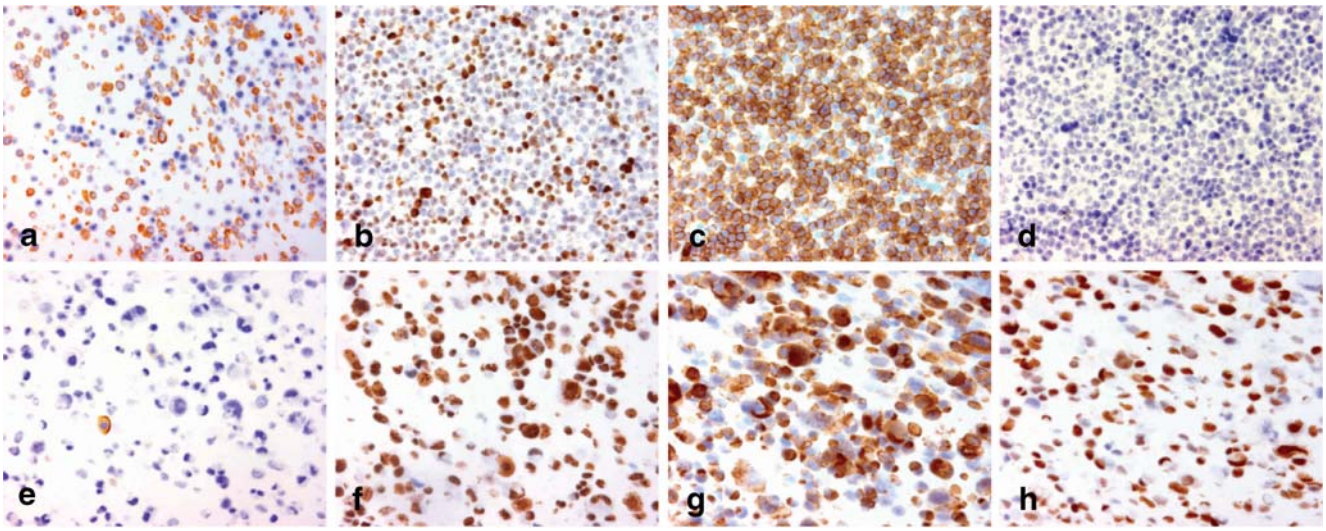

Fig. 6 Immunohistochemical staining of colon cancer cells HT29 and CaCo2 with CK20, Ki67, β-catenin, and Cdx-2. Panels show staining patterns observed for CK20 (**a**, **e**), Ki67 (**b**, **f**), β-catenin (**c**, **g**), and Cdx-2 (**d**, **h**) for both colon cancer cell lines HT29 (**a**–**d**) and CaCo2 (**e**–**h**). Magnification ×20

Discussion

The Hedgehog signaling cascade plays an essential role in correct development of the gut, especially the colon. Expression of the Hh ligand Shh is detected early in the endoderm, suggested to play a key role in gut formation by acting as a signal in epithelial–mesenchymal interaction. Additionally, expression of Ihh is described but later in development and in partially overlapping pattern with Shh [5]. The colonic epithelium is subject to constant renewing, a process of stem cell proliferation and differentiation leading to continuous cellular turnover. It seems reasonable to implicate an involvement of the Hedgehog pathway in this process. Recent data have shown that the Hh pathway is a player in colonic cell proliferation and differentiation and cell regulation by Hh signaling is altered in colonic neoplasia, but the results are discussed controversially [15, 18, 20, 22]. This may be due to variable methodological designs or use of different human colorectal pathological and nonpathological samples. Several studies have been performed on tissue composites consisting of variable fractions of cancer or epithelium cells and also including other tissue components. As active Hh pathway and protein expression in others than normal or cancer epithelial cells have been reported, e.g., in B cell differentiation and angiogenesis, a mix-up of these parameters may lead to diverse results [27, 28]. Studies of the Hh pathway component protein expression and its cellular localization in human colorectal cancer and its paired colorectal normal tissue have not been reported before.

In the present study, the presence and localization of the Hedgehog ligands Shh and Dhh, within the normal colonic epithelium, was restricted to the epithelial lining cells, whereas Gli1 and Gli2 transcription factors and the receptor Patched showed expression along the whole colonic crypts. This expression pattern confirms the presumption that the colonic lining cells are the signaling part of the epithelium producing the Hh ligands. The Hh signal receiving part are cells within the crypts, maybe identical with the colonic stem cells with high differentiating potential into goblet or paneth cells [15]. The distribution of Shh within the normal colonic epithelium is in agreement with the findings from Oniscu et al. [18] but contrary to observations made by van den Brink et al. [15] who detected Ihh expression within the colonic lining epithelium.

Gli1, Gli2, and Ptch expression as indicator of active signaling is not restricted to the basal crypts but rather reaches from the basal crypts to the lining cells. These findings support the assumption of involvement in the ongoing differentiation process along the crypts rather than in the proliferation process that occurs just within the basal crypt cells.

Possible correlation of Hh signaling with cancer formation was analyzed by expression of the Hh members Gli1, Gli2, Shh, Dhh, and Ptch within benign and malignant lesions of the colon. Benign lesions showed an overall protein expression of Hh components, with Shh and Dhh showing a focally but large-area expression pattern. Expression of Gli1, Gli2, and Ptch was consistently distributed within the benign tissue samples. The expression pattern of Shh and Ptch goes along with the findings of Oniscu et al. [18]; other Hh signaling components have not been investigated in that study.

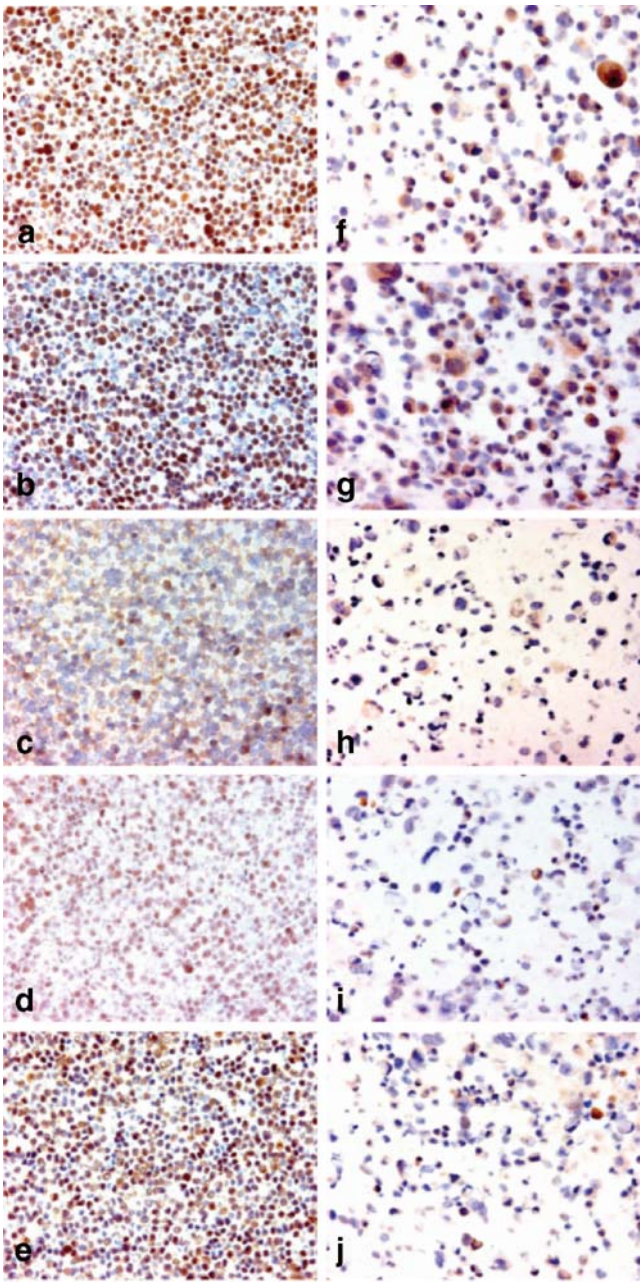

Fig. 7 Expression of Gli1, Gli2, Ptch, Shh, and Dhh in colon cancer cells HT29 and CaCo2. Panels show expression of the Hh pathway members Gli1 (**a**, **f**), Gli2 (**b**, **g**), Ptch (**c**, **h**), Shh (**d**, **i**), and Dhh (**e**, **j**) in HT29 (**a**–**e**) and CaCo2 (**f**–**j**) cells. Magnification ×20

Malignant lesions showed a focally expression of Shh and Dhh but restricted to single cells or small cell groups and only about 20% of all cancer samples investigated with TMA showed ligand expression (Table 1). Gli1, Gli2, and Ptch were absent or slightly expressed in all cases of malignant colon lesions. Our data on a sizeable cohort of colorectal cancer tissue suggest that formation of colon cancer goes along with a loss of Shh and Dhh expression and therefore a decrease of Gli1, Gli2, and Ptch expression and subsequent loss of normal colonic differentiation also becoming obvious with the changes of differentiation marker CK20 (Fig. 3).

Colorectal carcinogenesis occurs as a multistep process that requires sequential or concomitant alterations in signaling mechanisms within and across cellular generations and we propose that Hh pathway is one signaling pathway affected within this process. These initial presumptions were strengthened by double-immunofluorescence staining with proliferation marker Ki67 and differentiation marker CK20. Both markers showed a focal expression within pathological specimens of the colon similar to that of Shh and Dhh. All cells that express Hh ligands also express CK20 but not all CK20 positive cells did express Hh.

Coexpression analysis with Ki67 showed opposite results as the bulk of Shh and Dhh expressing cells are negative for Ki67, but some few separated cells within the Hh positive cell clusters did express Ki67. Colocalization studies in colonic normal and cancer tissue clearly arise that the main proliferating cells are not expressing Hedgehog ligands. Based on these results, we suggest that uncontrolled proliferation and loss of differentiation during the course of colonic tumor genesis goes along with a loss of Shh and Dhh expression which is in agreement with findings of van den Brink et al. [15] of Ihh decrease in dysplastic epithelial cells. They also correlated loss of Hh signaling with loss of differentiation evidenced by decreased expression of various differentiation markers after inhibition with cyclopamine. Additionally, they showed that blocking Hh signaling increased colonic epithelial cell proliferation. Douard et al. [21] demonstrated an involvement of Hh signaling in proliferative processes by positively correlating expression levels of Gli1 with

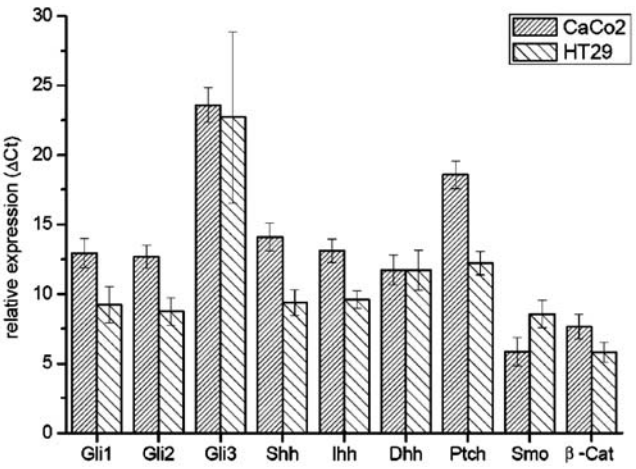

Fig. 8 Real-time PCR results of HT29 and CaCo2 cells. Panel shows average ΔCt values ± Gaussian errors of three independent experiments for each Hh pathway member and β-catenin. ΔCt values are calculated by subtraction of the Ct values of GAPDH (9.5 and 11.5 for CaCo2 and HT29, respectively) from the individual sample's Ct values

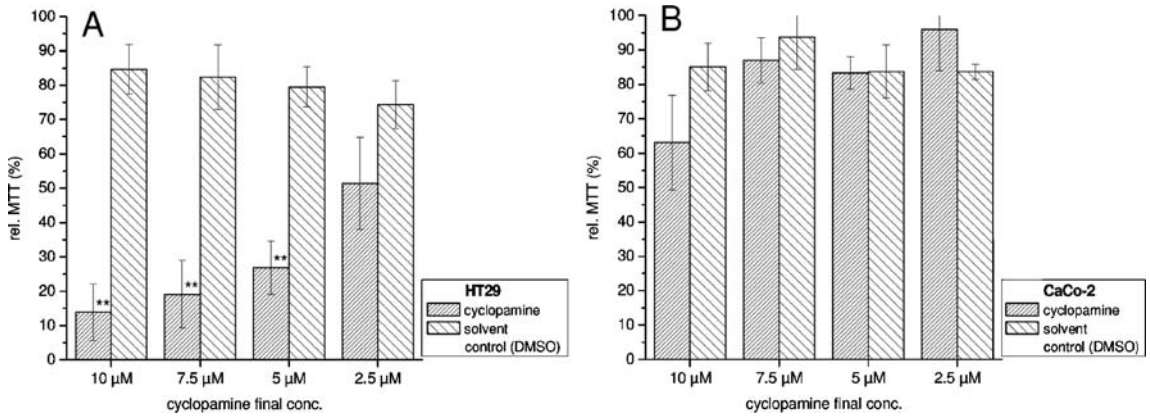

Fig. 9 Effect of cyclopamine treatment on cellular survival (MTT assay) of HT29 (**a**) or CaCo2 (**b**). Solvent controls (*right columns*) indicate the MTT signal of samples incubated with the solvent for cyclopamine (DMSO) at the corresponding concentration. All MTT values are related to untreated control samples; data points represent mean values of three independent experiments ± SEM. *$p<0.05$ or **$p<0.01$ indicate samples significantly or highly significantly different from the related solvent control, respectively

FOXM1, but we detected negative correlation with Ki67 a routinely used marker for proliferation. To further confirm experimental data, we compared Hh activity on protein and mRNA level in the two human colon adenocarcinoma cell lines CaCo2 and HT29.

Expression of Hh pathway members on mRNA level was considerably higher up to four cycles for HT29 cells than for CaCo2 cells except for Smo which showed higher levels in CaCo2 cells. Hh expression was detected also on protein level within both cell lines and difference on protein level was recognized as CaCo2 showed just sparse expression of Gli1, Gli2, Shh, Ihh, and Ptch compared to HT29 cells. Therefore, mRNA levels go along with protein expression in both cell lines. In both cell lines, positive staining for Ki67 was detected but only in single cells of the HT29 cell line. HT29 cells show intense expression of CK20, but no reaction for antibodies directed against β-catenin and Cdx-2. In contrast, CaCo2 cells were negative for CK20 but showed positive nuclear staining of β-catenin and Cdx-2. Since formation of colorectal cancer is characterized by a transient loss of differentiation and nuclear accumulation of the oncoprotein β-catenin and also for the intestine-specific transcription factor Cdx2, these results indicate that the two cell lines are characterized by varying differentiation status and signaling mechanisms. Our data are in contrast with other findings, demonstrating an inactive Hh pathway in colon cancer cell lines [15, 17, 20]. Chatel et al. demonstrated that all seven colon cancer cell lines they investigated show incomplete Hh signaling [20], although high level of Hh proteins were detected in HT29 und CaCo2 cells. In our hands, HT29 and CaCo2 showed combined expression of ligands, transcription factors, and receptors that is concordant with their findings.

HT29 cells are rather well differentiated (positive for CK20, negative for nuclear localization of β-catenin and Cdx-2), show only sparse Ki67 positive staining, and express components of the Hh pathway on mRNA and protein level. In contrast, CaCo2 cells are rather poorly differentiated (loss of CK20, nuclear localization of β-catenin and Cdx-2), show strong Ki67 positive staining, and express Hh pathway proteins and mRNA at a considerably lower level than the HT29 cell line. van den Brink et al. already described a negative correlation between Hh and Wnt pathway as they showed that Ihh expression is downregulated in response to constitutive β-catenin signaling [15].

To prove active Hh signaling in the colon cancer cell lines, a cyclopamine tolerance assay was performed. HT29 cells were more sensitive to the Hh inhibitor as they show significant reduction in viability after treatment for 72 h. CaCo2 cells also show slight reaction on cyclopamine treatment but to a much smaller extent. These data imply that for colon cancer cells with high differentiation status such as HT29, viability and proliferation is dependent on active Hh signaling. In contrast, the poorly differentiated and highly proliferating cell line CaCo2 is rather insensitive toward inhibition of Hh signal transduction by cyclopamine. As demonstrated for colon carcinoma-derived cell lines, inhibition of the Hh signaling pathway by cyclopamine results in cell death by apoptosis [22]. In line with the results obtained from FFPE tissue samples, these facts strengthen the concept that active Hh signaling is involved in differentiation of colonic epithelium, whereas during oncogenesis, only highly differentiated cell types are dependent on active Hh signaling.

In summary, our data demonstrate that Hh signaling is important for differentiation of normal colonic tissue. Hh pathway members Gli1, Gli2, Shh, Dhh, and Ptch are expressed in normal colonic tissue samples as well as in benign lesions, but are reduced or lost in malignant lesions.

In colon cancer cell lines, Hh components show coexpression with markers for differentiation of the colon like CK20 but are inversely expressed with markers of malignant conversion β-catenin and Cdx-2 and proliferation Ki67. Pharmacological inhibition of the Hh pathway in vitro leads to reduction in colon cell viability correlating with the expression level of the pathway members. Taken together, during oncogenesis of colon cancer, the acquisition of a dedifferentiated and highly proliferative phenotype seems to be paralleled by a loss of active Hh signaling.

Acknowledgments This study was supported by the Österreichische Krebshilfe and PMU Salzburg research grant. TK is supported by a research grant of the Österreichische Nationalbank (project No. 12677). We hereby declare that all experiments described in this study comply with the current laws in Austria.

Conflict of interest We declare that we have no conflict of interest.

References

1. Fearon ER, Vogelstein B (1990) A genetic model for colorectal tumorigenesis. Cell 61:759–767
2. Jemal A, Tiwari RC, Murray T et al (2004) Cancer statistics, 2004. CA Cancer J Clin 54:8–29
3. Stryker SJ, Wolff BG, Culp CE et al (1987) Natural history of untreated colonic polyps. Gastroenterology 93:1009–1013
4. Kinzler KW, Vogelstein B (1996) Lessons from hereditary colorectal cancer. Cell 87:159–170
5. de Santa Barbara P, van den Brink GR, Roberts DJ (2003) Development and differentiation of the intestinal epithelium. Cell Mol Life Sci 60:1322–1332
6. Kiefer JC (2003) Molecular mechanisms of early gut organogenesis: a primer on development of the digestive tract. Dev Dyn 228:287–291
7. Ramalho-Santos M, Melton DA, McMahon AP (2000) Hedgehog signals regulate multiple aspects of gastrointestinal development. Development 127:2763–2772
8. Sukegawa A, Narita T, Kameda T et al (2000) The concentric structure of the developing gut is regulated by Sonic hedgehog derived from endodermal epithelium. Development 127:1971–1980
9. van den Brink GR, Hardwick JC, Tytgat GN et al (2001) Sonic hedgehog regulates gastric gland morphogenesis in man and mouse. Gastroenterology 121:317–328
10. Cohen MM Jr (2003) The hedgehog signaling network. Am J Med Genet A 123:5–28
11. Belloni E, Muenke M, Roessler E et al (1996) Identification of Sonic hedgehog as a candidate gene responsible for holoprosencephaly. Nat Genet 14:353–356
12. Nanni L, Ming JE, Bocian M et al (1999) The mutational spectrum of the sonic hedgehog gene in holoprosencephaly: SHH mutations cause a significant proportion of autosomal dominant holoprosencephaly. Hum Mol Genet 8:2479–2488
13. Dimmler A, Brabletz T, Hlubek F et al (2003) Transcription of sonic hedgehog, a potential factor for gastric morphogenesis and gastric mucosa maintenance, is up-regulated in acidic conditions. Lab Invest 83:1829–1837
14. Silberg DG, Kaestner KH (2001) Morphogenesis and maintenance of the gastric epithelium: a role for sonic hedgehog? Gastroenterology 121:485–487
15. van den Brink GR, Bleuming SA, Hardwick JC et al (2004) Indian Hedgehog is an antagonist of Wnt signaling in colonic epithelial cell differentiation. Nat Genet 36:277–282
16. Lees C, Howie S, Sartor RB et al (2005) The hedgehog signalling pathway in the gastrointestinal tract: implications for development, homeostasis, and disease. Gastroenterology 129: 1696–1710
17. Berman DM, Karhadkar SS, Maitra A et al (2003) Widespread requirement for Hedgehog ligand stimulation in growth of digestive tract tumours. Nature 425:846–851
18. Oniscu A, James RM, Morris RG et al (2004) Expression of Sonic hedgehog pathway genes is altered in colonic neoplasia. J Pathol 203:909–917
19. Zhu Y, James RM, Peter A et al (2004) Functional Smoothened is required for expression of GLI3 in colorectal carcinoma cells. Cancer Lett 207:205–214
20. Chatel G, Ganeff C, Boussif N et al (2007) Hedgehog signaling pathway is inactive in colorectal cancer cell lines. Int J Cancer 121:2622–2627
21. Douard R, Moutereau S, Pernet P et al (2006) Sonic Hedgehog-dependent proliferation in a series of patients with colorectal cancer. Surgery 139:665–670
22. Qualtrough D, Buda A, Gaffield W et al (2004) Hedgehog signalling in colorectal tumour cells: induction of apoptosis with cyclopamine treatment. Int J Cancer 110:831–837
23. Gonzalez RJ, Tarloff JB (2001) Evaluation of hepatic subcellular fractions for Alamar blue and MTT reductase activity. Toxicol In Vitro 15:257–259
24. Mosmann T (1983) Rapid colorimetric assay for cellular growth and survival: application to proliferation and cytotoxicity assays. J Immunol Methods 65:55–63
25. Regl G, Kasper M, Schnidar H et al (2004) The zinc-finger transcription factor GLI2 antagonizes contact inhibition and differentiation of human epidermal cells. Oncogene 23:1263–1274
26. Regl G, Neill GW, Eichberger T et al (2002) Human GLI2 and GLI1 are part of a positive feedback mechanism in basal cell carcinoma. Oncogene 21:5529–5539
27. Dierks C, Grbic J, Zirlik K et al (2007) Essential role of stromally induced hedgehog signaling in B-cell malignancies. Nat Med 13:944–951
28. Nagase T, Nagase M, Machida M et al (2008) Hedgehog signalling in vascular development. Angiogenesis 11:71–77

Virchows Arch (2009) 454:381–387
DOI 10.1007/s00428-009-0752-8

ORIGINAL ARTICLE

Comparison of cyclooxygenase-2 and CD44 mRNA expression in colorectal cancer and its relevance for prognosis

Jung Wook Huh · Hyeong Rok Kim · Jae Hyuk Lee · Young Jin Kim

Received: 29 December 2008 / Revised: 16 February 2009 / Accepted: 23 February 2009 / Published online: 10 March 2009

Abstract This study evaluated CD44 and COX-2 expression in colorectal cancer (CRC) and analyzed its relationship with the clinicopathological characteristics. The prognostic impact on patient survival was compared between the two proteins. CD44 and COX-2 mRNA levels in 42 primary CRCs were analyzed using quantitative real-time PCR, with normalization relative to GAPDH. The cycle threshold (Ct) values were measured, and results are expressed as the Ct ratios of CD44 or COX-2 to GAPDH. The COX-2 Ct ratio was much lower in cases of lymphovascular invasion by the tumor than for no invasion (P=0.004). During follow-up for a median of 40 months, there was no significant difference in the median CD44 Ct ratio between survivors and non-survivors (P=0.362), whereas the COX-2 Ct ratio was significantly associated with survival at the time of data analysis (P=0.042). The survival of colorectal cancer patients with a high COX-2 Ct ratio was significantly longer than that of patients with a low COX-2 Ct ratio (P=0.048). This study suggests that COX-2 expression has a more significant impact than CD44 expression on the survival of CRC patients. Further studies are needed to resolve these issues with a large sample size.

Keywords CD44 · COX-2 · Colorectal cancer

J. W. Huh · H. R. Kim (✉) · Y. J. Kim
Department of Surgery, Chonnam National University Hwasun Hospital and Medical School,
160 Ilsimri, Hwasun-eup, Hwasun-gun,
Gwangju 519-809 Jeonnam, South Korea
e-mail: drkhr@chonnam.ac.kr

J. H. Lee
Department of Pathology, Chonnam National University Hwasun Hospital and Medical School,
Gwangju, South Korea

Introduction

Colorectal cancer (CRC) is one of the leading causes of cancer deaths worldwide. Earlier diagnosis, proper treatment, and better knowledge of the clinicopathological prognostic factors of CRC have contributed to improved outcomes. The most significant and independent prognostic factors accepted to date remain the tumor-node-metastasis (TNM) stage and the "potential" residual disease after initial surgery [1]. Several other possibly independent factors have been identified, but only a few of them have been shown to affect the prognosis and survival of CRC patients: tumor grade, venous invasion, perineural invasion, and allelic loss of chromosome 18q [2]. Other some prognostic factors are controversial. Although the TNM classification is useful for staging patients and selecting specific treatment, it is not sufficient as many patients at the same stage may have different clinical outcomes and different responses to adjuvant therapy. Thus, oncologists are interested in finding additional prognostic biomarkers.

CD44 and cyclooxygenase (COX)-2 are two of the most studied proteins involved in the promotion, progression, and treatment of CRC. The transmembrane glycoprotein molecule CD44 is a widely expressed cell surface hyaluronan receptor. CD44 is frequently overexpressed in CRC, where this aberrant expression is closely linked to cancer progression and a poorer prognosis [3–5]. COX-2, a key enzyme in the conversion of arachidonic acid to prostaglandin H_2, is reported to promote tumorigenesis and increase metastatic potential in many types of human cancers, including CRC [6–8]. Specific COX-2 inhibition, using a targeted knockout of the COX-2 gene or pharmacological intervention, has been shown to effectively decrease tumor growth and progression [9, 10]. In the recent study to address directly the relationship between CD44 and COX-2 expression,

Misra et al. [11] showed that through activation of CD44, hyaluronan, which also serves as a ligand for CD44, constitutively regulated pathologic induction of COX-2 in colon cancer. However, relatively few studies have compared the prognostic impact of CD44 and COX-2 expression in terms of the mRNA levels in the tumors of CRC patients.

This study evaluated CD44 and COX-2 expression in CRC using quantitative real-time PCR (qRT-PCR) and analyzed its relationship to the clinicopathological characteristics. The prognostic impact on patient survival was compared between the two markers.

Materials and methods

Tissue samples

This study was based on total RNA extracted from 42 patients who had primary colorectal carcinomas resected at Chonnam National University Hwasun Hospital, South Korea. The non-necrotic portion of the tumors and the surrounding mucosa at a standard distance of 2 cm from the tumors were obtained from each patient and stored frozen in liquid nitrogen at –197°C until use. This study was approved by the appropriate institutional review board, and informed consent was obtained from every patient according to institutional regulations.

RNA extraction and cDNA synthesis

Total RNA was isolated using an RNeasy® mini prep kit (Qiagen, Valencia, CA, USA) according to the manufacturer's protocol. The RNA pellet was dissolved in 30 μL of sterile diethylpyrocarbonate-treated Milli-Q water (Millipore, Burlington, MA, USA) and quantified using a NanoDrop™ ND-1000 spectrophotometer (NanoDrop Technologies, Wilmington, DE, USA) at 260 nm.

Reverse transcription was performed using the Molorey murine leukemia virus reverse transcriptase (M-MLV RT; Promega, Madison, WI, USA). Each total RNA template (2 μg) was reverse-transcribed with 0.5 μg of oligo (dT) primer (Promega). The sample tube was heated to 70°C for 5 min, quickly chilled on ice, and then spun briefly to collect the solution at the bottom of the tube. To this was added 1 μL of RNasin® ribonuclease inhibitor (25 units/μL, Promega), 1× M-MLV reaction buffer, 2.5 mM dNTPs, and 200 units of M-MLV RT, and the mixture was incubated for 60 min at 42°C.

RT-PCR and Western blotting

RT-PCR was performed used Top-Taq™ DNA polymerase (CoreBioSystem, Seoul, Korea). Oligonucleotide primers specific for CD44, COX-2, and GAPDH were designed from their respective GenBank sequences (no. DD055193, no. AJ634912, and no. DQ891557). The GAPDH gene was used as an internal control. The PCR primer sequences are listed in Table 1. The RT-PCR products were electrophoresed in a 1.8% agarose gel at 100 V for 25 min in 1× TAE buffer. After staining with ethidium bromide (5 μg/mL), the gels were photographed under ultraviolet light.

Total protein was extracted from the tissues using RIPA lysis buffer (Santa Cruz Biotechnology, Santa Cruz, CA, USA). First, 40 μg of lysate was subjected to 12% SDS-PAGE (Bio-Rad, Hercules, CA, USA), transferred to polyvinylidene difluoride membranes (Immobilon-p; Millipore), and incubated for 2 h with a 1:2,000 dilution of anti-COX-2 monoclonal antibody (Invitrogen Zymed, Carlsbad, CA, USA), anti-CD44 antibody (R&D), or anti-GAPDH antibody (Santa Cruz Biotechnology). The membranes were washed and treated with mouse anti-goat IgG (1:2,000, Santa Cruz Biotechnology) for 1 h at room temperature. The bands were visualized using Image Reader LAS 3000 (LAS-3000 analytical software, Fuji-Film, NY, USA).

Cloning

The PCR products were transformed into HIT™ DH5α high-efficiency competent cells (Real-Biotech, CA, WI, USA) using pGEM®-T-Easy vector system II (Promega). The PCR products were purified with QIAquick® agarose gel extraction (QIAGEN), ligated into pGem®-T-Easy vector using T4 DNA ligase (Promega), transformed into HIT™ DH5α competent cells, and cultured on LB agar Amp IPTG/X-Gal plates (Becton Dickinson, Franklin Lakes, NJ, USA) to obtain single white clones containing the target fragment. The plasmid concentration was converted into copy number, and a dilution series of each plasmid, from 10^{10} to 10^{2}, was used as the cDNA standard for RT-PCR.

Quantitative real-time RT-PCR

The cDNA generated was used as the template in real-time PCR reactions with QuantiTect™ SYBR Green PCR master mix (QIAGEN) in a Rotor-Gene™ real-time machine (Corbett Research, Mortlake, Australia). The reaction was quantified using the comparative threshold cycle (Ct) method with Rotor-Gene™ real-time analysis software version 6.1 (Corbett Life Science, New South Wales, Australia), according to the manufacturer's protocol [12, 13]. All colorectal specimens were examined simultaneously for each of CD44 or COX-2, and GAPDH, along with the appropriate set of plasmid standards and negative controls (water). The primer sets used for this technique are given in Table 1. All qRT-PCR reactions were performed in triplicate. The crossing

Table 1 Primer sequences used for conventional RT-PCR

Protein	Forward primer (5′→3′)	Reverse primer (5′→3′)	PCR condition[a]	Fragment size (bp)
CD44	CCAATGCCTTTGATGGACCA	TGTGAGTGTCCATCTGATTC	58 (35)	334
COX-2	ACATTCCCTTCCTTCGAAATGC	ACATCATCAGACCAGGCACCAG	62 (35)	590
GAPDH	GTGAAGGTCGGAGTCAAC	GTTGAGGTCAATGAAGGG	55 (35)	116

[a] Annealing Temperature in °C (number of cycles)

point or cycle threshold (Ct) was defined as the maximum of the second derivative from the fluorescence curve. The Ct ratio was calculated as

$$\text{Ct ratio} = \frac{\text{Ct value of target gene (CD44 or COX} - 2)}{\text{Ct value of reference gene (GAPDH)}}$$

The qRT-PCR was conducted with a Rotor-Gene™ real-time centrifugal DNA amplification system (Corbett Research) in a final reaction volume of 25 μL containing 1× QuantiTect™ SYBR Green PCR master mix (QIAGEN), 0.25 μM of each of the forward and reverse primers for the gene (Table 1), 3 μL of template DNA, and RNase-free water. The thermal cycling conditions were 50°C for 2 min and 95°C for 10 min, followed by 50 cycles of 95°C for 15 s; 58°C (for CD44), 62°C (for COX-2), or 55°C (for GAPDH) for 20 s; and 72°C for 25 s.

Statistical analysis

The CD44 and COX-2 gene expression values are expressed as the Ct ratios, which are inversely proportional to the expression level [12, 13]. Thus, the smaller the Ct ratio, the greater the gene expression. The Ct ratios of CD44 and COX-2 were associated with the clinicopathological features using Wilcoxon test, Kruskal–Wallis test, and Fisher's exact test as appropriate.

To evaluate the associations with overall survival, the median values of the CD44 and COX-2 Ct ratios were chosen as the cutoff point for discrimination of the 42 patients into two subgroups, respectively. The overall survival curves were calculated using the Kaplan–Meier method, and the differences between curves were evaluated using the log-rank test. A value of $P<0.05$ was considered statistically significant.

Results

Patient characteristics

This analysis included 25 (59.5%) male and 17 (40.5%) female patients with a median age of 63 years (range, 42–77). Using the 6th International Union against Cancer (UICC) TNM staging system, one, 11, 22, and eight patients had stage I to IV cancers, respectively.

Comparison of CD44 and COX-2 expression between tumor and normal mucosal samples

CD44 and COX-2 were expressed at higher levels in tumor tissue than in surrounding normal tissue (Fig. 1). The mean CD44 and COX-2 Ct ratios were significantly lower, indicating higher expression, in the tumor samples than in the surrounding normal mucosal samples, respectively ($P=0.0089$, $P=0.0186$; Fig. 2a, b).

Correlations between clinicopathological parameters and CD44 and COX-2 Ct ratios in tumors

The correlations between the clinicopathological characteristics and CD44 and COX-2 Ct ratios are shown in Table 2. No significant differences in the CD44 and COX-2 Ct ratios were observed among the variables, with the exception of lymphovascular invasion by the tumor, which had a significantly lower COX-2 Ct ratio than no invasion (1.45± 0.21 versus 1.71±0.29, $P=0.004$; Table 2). A statistically significant association was observed between CD44 and COX-2 Ct ratios ($P=0.005$; Table 3).

Correlation with patient survival

During follow-up for a median of 40 months (range, 2–52), 12 patients died from their cancers. There was no significant difference in the median CD44 Ct ratio between survivors and non-survivors ($P=0.362$; Fig. 3a), whereas the COX-2 Ct ratio was significantly associated with the survival status at the time of the data analysis ($P=0.042$; Fig. 3b).

The median values of the CD44 and COX-2 Ct ratios for 42 patients were 1.298 and 1.590, respectively. The Kaplan–Meier curves for patient survival according to the CD44 and COX-2 Ct ratios (low vs. high) are shown in Fig. 4. There was no significant difference in survival of CRC patients according to the CD44 Ct ratio ($P=0.454$; Fig. 4a). However, the 4-year overall survival rate was significantly higher for patients with a high COX-2 Ct ratio than for those with a low COX-2 Ct ratio ($P=0.048$;

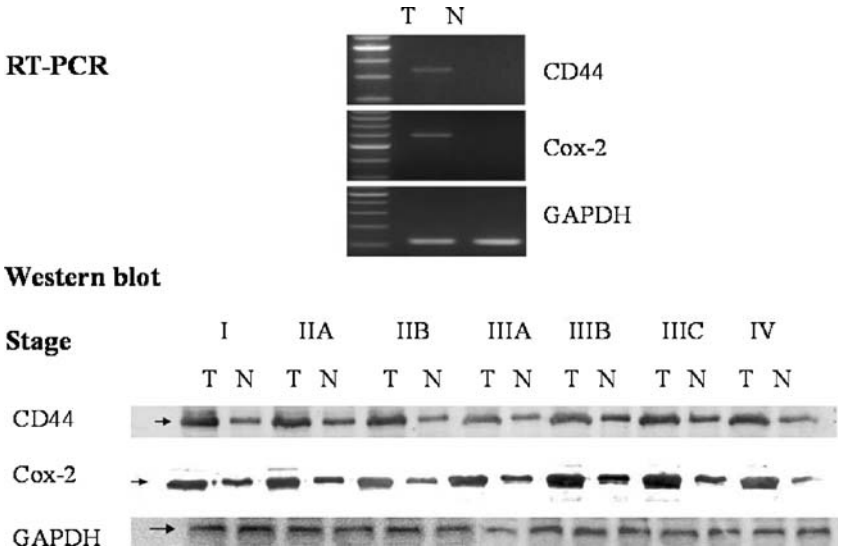

Fig. 1 CD44 and COX-2 expression determined using RT-PCR and Western blot analysis. *T* tumor tissue, *N* surrounding normal mucosal tissue

Fig. 4b). Univariate analysis indicated that among the clinicopathological factors, only lymphovascular invasion was associated with survival according to the COX-2 Ct ratio, at a significance level of 0.004 using the log-rank test (Table 2). For completeness of the analysis, the association between the COX-2 Ct ratio, using the 1.590 cutoff point, and survival was re-examined stratifying for each of the clinicopathological variables. In these analyses, the degree of association (i.e., the observed hazard ratio) was basically unchanged on adjusting for each of the clinicopathological variables (data not shown).

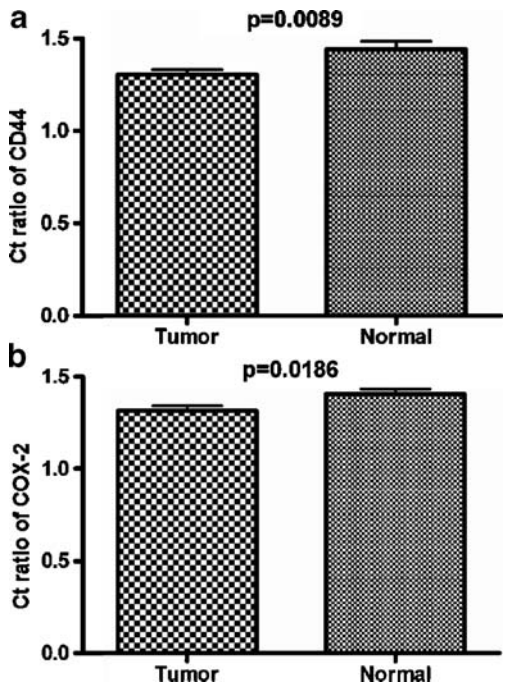

Fig. 2 Comparison of the **a** CD44 and **b** COX-2 Ct ratios between tumor and surrounding normal mucosal samples

Discussion

This study evaluated CD44 and COX-2 mRNA levels based on the Ct values of cDNA as determined by qRT-PCR and explored the relationship between the expression level and the clinicopathological characteristics that may affect patient outcomes. Many studies have provided evidence of decreased survival in CRC patients over-expressing CD44 and COX-2 [4–8, 14–16]. However, relatively few studies have compared the prognostic value of CD44 and COX-2 expression in CRC patients. We found that compared with CD44 overexpression, COX-2 over-expression was more closely correlated with decreased CRC patient survival although the only clinicopathological parameter significantly associated with COX-2 overexpression was lymphovascular invasion (P=0.004).

CD44 is frequently overexpressed in CRC. Nevertheless, the significance of CD44 in CRC is controversial, and findings regarding its prognostic value have been contradictory [3–5, 14, 17]. Bendardaf et al. [3] showed that upregulated CD44 expression in metastases was associated with a shorter disease-free survival in CRC patients. Visca et al. [4] also suggested that the immunohistochemical expression of CD44 may reveal cells that have lost their adhesion ability, resulting in the detection of carcinomas with high metastatic power. Previously, we identified the prognostic value of immunohistochemical CD44 expression in metastatic CRC patients [5]. Sokmen et al. [14] reported that there was no significant association between CD44 expression and recurrence and overall survival in CRC at either stage B or C. In contrast, Asao et al. [17] showed that the loss of CD44 expression in the invaded area of primary tumors was a sensitive marker for metastasis to lymph nodes in CRC patients. In the present study, we used a qRT-PCR assay, which permits a more quantitative measurement

Table 2 Correlation between the clinicopathological parameters and the CD44 and COX-2 Ct ratios

	n	CD44[a]	*P*[b]	COX-2[a]	*P*[b]
Age, years					
<60	17	1.31±0.14	0.969	1.54±0.22	0.617
≥60	25	1.33±0.21		1.62±0.32	
Gender					
Male	25	1.31±0.20	0.420	1.59±0.33	0.828
Female	17	1.34±0.14		1.59±0.23	
Tumor location					
Colon	23	1.31±0.21	0.622	1.57±0.32	0.536
Rectum	19	1.32±0.13		1.61±0.25	
Histology					
Well differentiated	23	1.33±0.20	0.617	1.57±0.32	0.501
Moderately differentiated	14	1.33±0.16		1.64±0.24	
Poorly differentiated	5	1.24±0.10		1.52±0.25	
Tumor size, cm					
<5.0	16	1.34±0.15	0.534	1.57±0.23	0.959
≥5.0	26	1.31±0.19		1.60±0.33	
TNM stage					
Stage I–III	34	1.33±0.19	0.654	1.61±0.30	0.438
Stage IV	8	1.30±0.10		1.52±0.22	
Depth of invasion (T)					
T1–2	4	1.43±0.17	0.170	1.63±0.20	0.635
T3–4	38	1.31±0.18		1.58±0.29	
Lymph node involvement (N)					
Negative	14	1.32±0.24	0.518	1.64±0.40	0.924
Positive	28	1.32±0.14		1.57±0.21	
Perineural invasion					
Negative	28	1.35±0.19	0.272	1.64±0.32	0.180
Positive	14	1.26±0.12		1.49±0.21	
Lymphovascular invasion					
Negative	22	1.35±0.19	0.406	1.71±0.29	0.004
Positive	20	1.28±0.15		1.45±0.21	
Preoperative CEA, ng/ml					
<5.0	19	1.33±0.22	0.791	1.54±0.33	0.211
≥5.0	23	1.31±0.13		1.62±0.25	

CEA carcinoembryonic antigen

[a] CD44 and COX-2 indicate the CD44 and COX-2 Ct ratio, respectively. Values are given as means±SDs

[b] Based on the Wilcoxon or Kruskal–Wallis test

of CD44 expression compared with immunohistochemical method. Our results showed no significant correlation between the CD44 expression and any conventional clinicopathological features. These contradictory results, including ours, may be attributable to different antibodies, variations in the staining techniques, and discrete study populations. The correlation of CD44 with the clinical oncologic outcome in the general population remains unclear.

Table 3 Correlation between the CD44 and COX-2 Ct ratios

	No.	COX-2 Ct ratio		*P*
		Low	High	
CD44 Ct ratio				
Low	21	15	6	0.005
High	21	6	15	

Recent studies have shown that COX-2 expression correlates with the invasiveness of colorectal carcinomas [16, 18–20]. Fujita et al. [18] identified a tumor size- and invasion-dependent increase in the COX-2 level, and Sheehan et al. [19] demonstrated that the extent of COX-2 staining was greater in cases at a more advanced Duke stage, in larger tumors, and in patients with lymph node metastasis. Furthermore, Yamauchi et al. [20] reported that COX-2 expression in the primary lesion may be a useful marker for evaluating prognosis and liver metastasis in CRC patients. By contrast, Tomozawa et al. [21] failed to

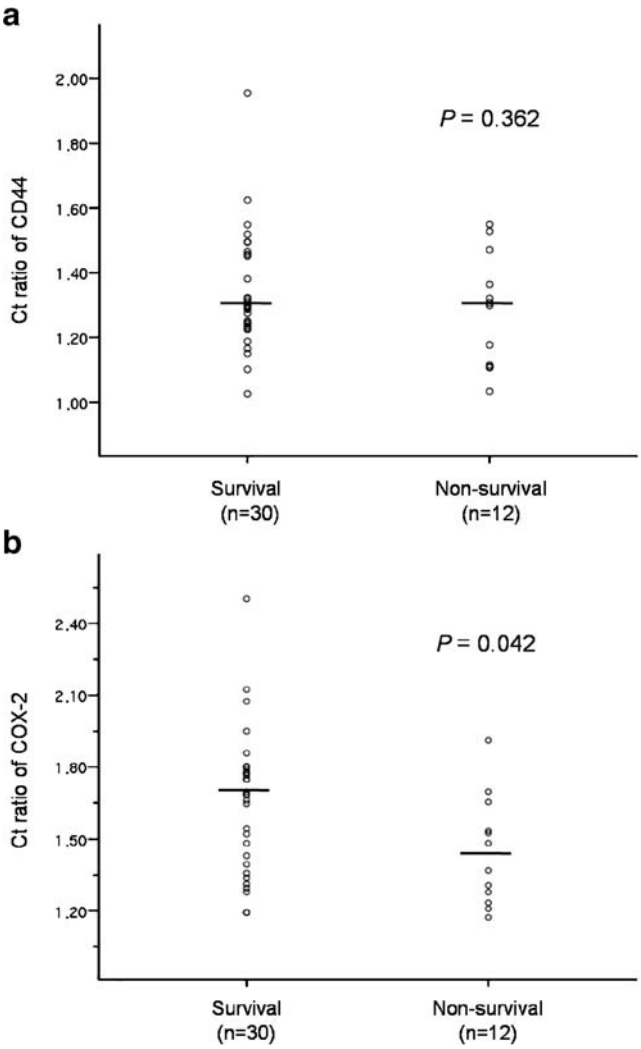

Fig. 3 The **a** CD44 and **b** COX-2 Ct ratios in colorectal tumors according to the survival status. Median values are indicated by the *horizontal bar*

find any correlation between COX-2 expression and clinicopathological variables. Our most relevant finding was a significant association between high COX-2 expression and lymphovascular invasion, suggesting a relationship between COX-2 overexpression and tumor invasion. This finding concurs with the results of Soumaoro et al. [16] and confirms COX-2 expression as a prognostic factor for the survival of CRC patients [6–8, 16, 20].

Evidence suggests that COX-2 contributes to neovascularization and may support vasculature-dependent solid tumor growth and metastasis in animal experiments and in vitro studies [6, 22]. Tomozawa et al. [21] reported that COX-2 overexpression enhanced the development of hematogenous metastasis through the promotion of tumor angiogenesis. The expression of COX-2 is also significantly correlated with the stimulation of metalloproteinases, which aid endothelial cell migration, and the release and activity of vascular endothelial growth factor in CRC [23–25]. In our analysis, the relationship between CD44 and COX-2 Ct ratios was statistically significant. The recent study by Misra et al. [11] on a strong link between hyaluronan–CD44 interaction and COX-2 in CRC may be of considerable value in elucidating the result of our study. These findings indicate that COX-2 is closely related to the invasion and metastasis of CRC, and thus, it may be useful as a biomarker.

Several CD44 isoforms (standard and variant) occur as a result of alternative splicing, thereby providing significant heterogeneity in CD44 expression among different tissues; however, contradictory results have been reported regarding their clinical significances in the progression and metastasis of CRC [5, 15, 26–29]. In this study, we evaluated mRNA expression for the CD44 standard isoform only. Tachikawa et al. [30] reported the extracellular formation of a macromolecular complex and increased antigenicity in patients who express the standard and variant CD44forms simultaneously. In addition, it was considered that patients with the variant CD44 isoform expression are thought to be included in those with immunohistochemical expression of the standard CD44 isoform, depending on the site of the

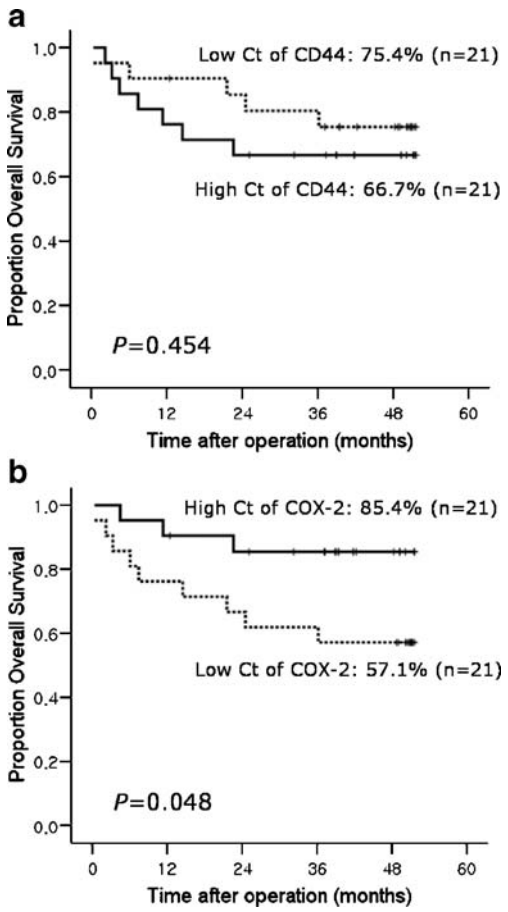

Fig. 4 Survival (Kaplan–Meier) plots indicating the proportion of overall survival for patients with the **a** CD44 and **b** COX-2 Ct ratios for all patients

inserted sequence. For that reason, examination of the standard CD44 form is determined to be useful.

We acknowledge that this study was not a properly randomized trial with a large sample population and had a possible type II error. Although our findings are insufficient for drawing definite conclusions, they still have validity. In conclusion, this study suggests that COX-2 expression has a more significant effect on the survival of CRC patients than CD44 expression. Further studies are needed to resolve these issues with a large sample size.

Acknowledgment This work was supported by a Research Grant (0720570) from the National Cancer Center, South Korea.

Conflict of interest statement We declare that we have no conflict of interest.

References

1. Shepherd NA, Saraga EP, Love SB et al (1989) Prognostic factors in colonic cancer. Histopathology 14:613–620
2. DeVita VT, Hellman S, Rosenberg SA (2001) Cancer: principles and practice of oncology, 6th edn. Lippincott Williams and Wilkins, Philadelphia, pp 1216–1271
3. Bendardaf R, Algars A, Elzagheid A et al (2006) Comparison of CD44 expression in primary tumours and metastases of colorectal cancer. Oncol Rep 16:741–746
4. Visca P, Del Nonno F, Botti C et al (2002) Role and prognostic significance of CD44s expression in colorectal cancer. Anticancer Res 22:2671–2675
5. Huh JW, Kim HR, Kim YJ et al (2009) Expression of CD44s in human colorectal carcinoma: association with prognosis. Pathol Int (in press)
6. Masunaga R, Kohno H, Dhar DK et al (2000) Cyclooxygenase-2 expression correlates with tumor neovascularization and prognosis in human colorectal carcinoma patients. Clin Cancer Res 6:4064–4068
7. Cianchi F, Cortesini C, Bechi P et al (2001) Up-regulation of cyclooxygenase 2 gene expression correlates with tumor angiogenesis in human colorectal cancer. Gastroenterology 121:1339–1347
8. Soumaoro LT, Uetake H, Higuchi T et al (2004) Cyclooxygenase-2 expression: a significant prognostic indicator for patients with colorectal cancer. Clin Cancer Res 10:8465–8471
9. Oshima M, Dinchuk JE, Kargman SL et al (1996) Suppression of intestinal polyposis in Apc delta716 knockout mice by inhibition of cyclooxygenase 2 (COX-2). Cell 87:803–809
10. Kawamori T, Rao CV, Seibert K et al (1998) Chemopreventive activity of celecoxib, a specific cyclooxygenase-2 inhibitor, against colon carcinogenesis. Cancer Res 58:409–412
11. Misra S, Obeid LM, Hannun YA et al (2008) Hyaluronan constitutively regulates activation of COX-2-mediated cell survival activity in intestinal epithelial and colon carcinoma cells. J Biol Chem 283:14335–14344
12. Higuchi R, Fockler C, Dollinger G et al (1993) Kinetic PCR analysis: real-time monitoring of DNA amplification reactions. Biotechnology (N Y) 11:1026–1030
13. Bustin SA (2000) Absolute quantification of mRNA using real-time reverse transcription polymerase chain reaction assays. J Mol Endocrinol 25:169–193
14. Sokmen S, Lebe B, Sarioglu S et al (2001) Prognostic value of CD44 expression in colorectal carcinomas. Anticancer Res 21:4121–4126
15. Fernandez JC, Vizoso FJ, Corte MD et al (2004) CD44s expression in resectable colorectal carcinomas and surrounding mucosa. Cancer Invest 22:878–885
16. Soumaoro LT, Uetake H, Takagi Y et al (2006) Coexpression of VEGF-C and Cox-2 in human colorectal cancer and its association with lymph node metastasis. Dis Colon Rectum 49: 392–398
17. Asao T, Nakamura J, Shitara Y et al (2000) Loss of standard type of CD44 expression in invaded area as a good indicator of lymph-node metastasis in colorectal carcinoma. Dis Colon Rectum 43:1250–1254
18. Fujita T, Matsui M, Takaku K et al (1998) Size- and invasion-dependent increase in cyclooxygenase 2 levels in human colorectal carcinomas. Cancer Res 58:4823–4826
19. Sheehan KM, Sheahan K, O'Donoghue DP et al (1999) The relationship between cyclooxygenase-2 expression and colorectal cancer. JAMA 282:1254–1257
20. Yamauchi T, Watanabe M, Kubota T et al (2002) Cyclooxygenase-2 expression as a new marker for patients with colorectal cancer. Dis Colon Rectum 45:98–103
21. Tomozawa S, Tsuno NH, Sunami E et al (2000) Cyclooxygenase-2 overexpression correlates with tumour recurrence, especially haematogenous metastasis, of colorectal cancer. Br J Cancer 83:324–328
22. Tsujii M, Kawano S, DuBois RN (1997) Cyclooxygenase-2 expression in human colon cancer cells increases metastatic potential. Proc Natl Acad Sci U S A 94:3336–3340
23. Fosslien E (2001) Review: molecular pathology of cyclooxygenase-2 in cancer-induced angiogenesis. Ann Clin Lab Sci 31:325–348
24. Gallo O, Franchi A, Magnelli L et al (2001) Cyclooxygenase-2 pathway correlates with VEGF expression in head and neck cancer. Implications for tumor angiogenesis and metastasis. Neoplasia 3:53–61
25. Xiong B, Sun TJ, Hu WD et al (2005) Expression of cyclooxygenase-2 in colorectal cancer and its clinical significance. World J Gastroenterol 11:1105–1108
26. Ylagan LR, Scholes J, Demopoulos R (2000) Cd44: a marker of squamous differentiation in adenosquamous neoplasms. Arch Pathol Lab Med 124:212–215
27. Ropponen KM, Eskelinen MJ, Lipponen PK et al (1998) Expression of CD44 and variant proteins in human colorectal cancer and its relevance for prognosis. Scand J Gastroenterol 33:301–309
28. Coppola D, Hyacinthe M, Fu L et al (1998) CD44V6 expression in human colorectal carcinoma. Hum Pathol 29:627–635
29. Gotley DC, Fawcett J, Walsh MD et al (1996) Alternatively spliced variants of the cell adhesion molecule CD44 and tumour progression in colorectal cancer. Br J Cancer 74:342–351
30. Tachikawa D, Arima S, Futami K (2000) Do the expression of CD44, apoptosis and thymidylate synthase inhibition rate correlate with the efficacy of chemotherapy in colorectal cancer? Anticancer Res 20:595–60

Virchows Arch (2009) 454:389–399
DOI 10.1007/s00428-009-0740-z

ORIGINAL ARTICLE

Estrogen signaling in colorectal carcinoma microenvironment: expression of ERβ1, AIB-1, and TIF-2 is upregulated in cancer-associated myofibroblasts and correlates with disease progression

Vassiliki Tzelepi · Petros Grivas · Zinovia Kefalopoulou · Haralabos Kalofonos · John N. Varakis · Maria Melachrinou · Georgia Sotiropoulou-Bonikou

Received: 1 July 2008 / Revised: 12 January 2009 / Accepted: 23 January 2009 / Published online: 7 March 2009

Abstract Epidemiological and molecular data suggest the involvement of estrogen signaling in colorectal tissue, mediated mainly through estrogen receptor beta (ERβ). Estrogens may mediate their effects in epithelial cells indirectly by acting on stromal cells. Expression of ERα, ERβ1, and the ER coregulators, amplified in breast cancer-1 (AIB-1) and transcriptional intermediary factor 2 (TIF-2), was evaluated in myofibroblasts of 107 colorectal carcinomas, 77 paired samples of normal mucosa, and 29 adenomas by immunohistochemistry. Double immunostaining with a-SMA was used to identify the myofibroblasts of normal tissue, adenomas, and cancer microenvironment. ERα was not expressed in stromal cells. Nuclear expression of ERβ1, AIB-1, and TIF-2 in myofibroblasts gradually increased from normal mucosa, through adenomas, to carcinomas. Cytoplasmic ERβ1 and TIF-2 expression was enhanced in carcinomas compared to normal mucosa and adenomas. Enhanced nuclear and cytoplasmic ERβ1 expression and elevated nuclear AIB-1 expression were more frequently noted in myofibroblasts of carcinomas of advanced stage. ERβ1 expression in cancer-associated myofibroblasts correlated to AIB-1 and TIF-2 expression. None of the markers correlated with patients' prognosis. Our findings imply that ERβ1-dependent (genomic and non-genomic) and ER-coregulator-dependent (AIB-1, TIF-2) signal transductions in myofibroblasts may be involved in the initiation and progression of colorectal carcinomas.

Keywords Colorectal carcinoma · Myofibroblasts · Estrogen receptors · AIB-1 · TIF-2

V. Tzelepi · Z. Kefalopoulou · M. Melachrinou
Department of Pathology, University of Patras,
26500 Rion, Greece

V. Tzelepi · Z. Kefalopoulou · J. N. Varakis ·
G. Sotiropoulou-Bonikou (✉)
Department of Anatomy and Histology-Embryology,
University of Patras,
26500 Rion, Greece
e-mail: sotiropouloug@yahoo.com

P. Grivas · H. Kalofonos
Department of Internal Medicine-Division of Oncology,
Medical School,
University of Patras,
26500 Rion, Greece

P. Grivas
Department of Internal Medicine, Hahnemann University
Hospital/Drexel University College of Medicine,
Philadelphia, PA 19102, USA

Introduction

Carcinomas are heterogeneous multicellular masses that consist of malignant epithelial cells and various non-malignant host-derived cells [1]. The latter are active participants of tumor initiation, progression, and metastasis [2, 3]. Myofibroblasts are the predominant cells in cancer microenvironment and orchestrate the stromal response [4]. Myofibroblasts are also found, although in reduced numbers, in various normal tissues and have distinct functions [5]. In normal colon mucosa, myofibroblasts reside in the subepithelial and pericryptal area and are connected to the muscularis mucosa [6]. Their location just beneath the basement membrane suggests that they play a critical role in the regulation of epithelial cell functions, through epithelial-mesenchymal crosstalk. Additionally, they are important components of the stem cell niche that regulates proliferation and differentiation of epithelial stem cells [7].

Colorectal carcinomas are characterized by an intense stromal reaction [8]. Activation and transdifferentiation of quiescent (myo)fibroblasts of normal mucosa or recruitment of myofibroblasts occurs early in the multistep process of colorectal carcinogenesis since their presence has been documented in colorectal adenomas [6] and facilitates the invasion of colon cancer cells [9].

Colon cancer represents an important cause of cancer-associated morbidity and mortality in the developed world [10]. Epidemiological and molecular data support a possible role of estrogens in colorectal carcinogenesis. Phytoestrogens (natural compounds with endogenous or acquired estrogenic activity) and postmenopausal hormonal (estrogen and progesterone) replacement therapy have been associated with reduced incidence of colorectal cancer [11–13]. Additionally, colon cancer is more frequent in males than females of the reproductive age [10]. On the other hand, estradiol has been found to increase the proliferation of colon cancer cells [14], and elevated endogenous estradiol levels were independently associated with increased risk of colorectal cancer in a large cohort of postmenopausal women [11]. Thus, the precise role of estrogen signaling in colorectal carcinogenesis remains elusive.

Estrogen effects are mediated by two types of estrogen receptors (ERs), ERα and ERβ. ERs belong to the nuclear receptor superfamily that consists of ligand-dependent transcription factors [15]. ERα protein and mRNA are variably expressed in colorectal carcinomas [16, 17]. However, ERβ seems to be the predominant type of ER in colonic tissue [16, 18]. Its role in colorectal carcinogenesis is controversial [16, 17, 19, 20]. These discrepancies may partly be attributed to the existence of five different isoforms of ERβ protein due to alternative splicing of the codon 8. ERβ isoforms exhibit differential modulation of estrogen action and may have distinct biologic actions in colorectal carcinogenesis [21, 22].

Increasing data support the fact that estrogens may mediate their effects on epithelial cells through paracrine actions and establish a molecular crosstalk between epithelial and stromal cells [23–27]. However, to the best of our knowledge, the expression of ERs in the microenvironment of colorectal carcinomas has not been studied before.

ER-mediated transcription is dependent on the recruitment of coactivators [28]. Coactivators have rather diverse functions and integrate a variety of intracellular signal transduction pathways with transcription [28, 29]. Thus, coactivators serve as master regulators of gene expression and are involved in a variety of human disease states including cancer [30]. Amplified in breast cancer-1 (AIB-1) and transcriptional intermediary factor 2 (TIF-2) belong to the steroid receptor coactivator (SRC) family of nuclear receptor coactivators and are also known as SRC-3 and SRC-2, respectively [28]. AIB-1 and TIF-2 expression is enhanced in epithelial cells of various carcinomas [28, 31, 32] and in endometrial epithelial and stromal cells of patients with polycystic ovary syndrome [33]. However, their role in myofibroblasts of cancer microenvironment remains elusive.

Thus, estrogens may act in a paracrine way in colorectal tissue, modulating the function of stromal cells of normal mucosa, adenomas, and colorectal carcinomas. To test this hypothesis, we investigated the expression of ERs (ERα and ERβ1) and two ER coregulators (AIB-1 and TIF-2) in myofibroblasts of normal mucosa, adenomas, and colorectal carcinomas by immunohistochemistry and correlated their expression to various clinicopathologic parameters and patients prognosis.

Materials and methods

Patients

In the present study, 107 specimens obtained from an equal number of patients suffering from colorectal carcinoma, who had undergone colectomy for therapeutic purposes, were retrieved from the Pathology files of the University Hospital of Patras, Greece. Tissue sections from non-neoplastic mucosa and from concurrent or metachronous adenomas were also evaluated in 77 and 29 patients, respectively.

The clinicopathologic characteristics of the patients are shown in Table 1. All women were in the peri- and postmenopausal age (mean age±standard deviation for women 63±7 years old). None of the patients had received chemo/radiotherapy prior to surgery. Follow-up data were available for 104 patients. Three patients were lost to follow-up. Follow-up period ranged from 7 to 106 months (mean 57, SD 25.5). During the follow-up period, 42 relapses and 32 cancer-related deaths were noted. Regarding adenomas, 20 specimens displayed low-grade dysplasia, and nine specimens displayed high-grade dysplasia.

This study received ethical approval from the Local Research Ethics Committee at University Hospital of Patras according to the principles laid down by Declaration of Helsinki.

Immunohistochemistry

Immunohistochemistry was performed on serial 4 μm formalin-fixed paraffin-embedded tissue sections using mouse monoclonal antibodies against ERα (1:30, NCL-L-6F11, Novocastra, UK), AIB-1 (1:50, Clone 34, BD Biosciences, CA, USA), and TIF-2 (1:50, Clone 29, BD Biosciences) and rabbit polyclonal antibodies against ERβ

Table 1 Clinicopathologic characteristics of patients

Clinicopathologic parameters	*N* (%)
Gender	
Male	68 (63.6%)
Female	39 (36.4%)
Age (years)	30–83 (64±10)
Stage (Dukes)	
B	41 (38.3%)
C	60 (56.1%)
D	6 (5.6%)
T stage	
T2	15 (14%)
T3	82 (76.6%)
T4	10 (9.4%)
Lymph node status	
N0	41 (38.3%)
N1	40 (37.4%)
N2	26 (24.3%)
Metastasis	
M0	101 (94.4%)
M1	6 (5.6%)
Grade	
Grade I	22 (20.6%)
Grade II	74 (69.1%)
Grade III	11 (10.3%)
Histologic type	
Adenocarcinoma	95 (88.8%)
Mucinous adenocarcinoma	12 (11.2%)
Primary site	
Right colon	30 (28%)
Left colon	41 (38.3%)
Rectum	36 (33.7%)

(prediluted, AR385-5R, Biogenex, CA, USA), which recognize the ERβ1 isoform. Sections were deparafinized in xylene and rehydrated in a series of graded ethanol solutions. Endogenous peroxidase activity was blocked with 0.3% hydrogen peroxide for 15 min. For antigen retrieval, sections were heated in 10 mM citrate buffer, pH6 (ERα, ERβ) or 1 mM EDTA–NaOH, pH8 (AIB-1, TIF-2) for 15 min in a microwave oven. After cooling to room temperature, sections were incubated with blocking serum (1% bovine serum albumin Fraction V, Serva Electrophoresis, Germany) for 30 min and then with the primary antibody for 1 h at room temperature. Slides were next incubated with Dako EnVision Labeled Polymer (Dako, CA, USA) for 45 min. Diaminobenzidine (Dako) was used as the chromogen. Nuclei were counterstained with hematoxylin. Serial sections were stained with mouse monoclonal antibodies against a-SMA (prediluted, RTU-SMA, Novocastra) using the same protocol. No antigen retrieval was performed for a-SMA immunostaining. In order to confirm the myofibroblastic nature of the cells under evaluation and ascertain the expression of ERβ and their coregulators in myofibroblasts, double immunostaining with a-SMA was performed in all cases of normal mucosa and adenomas. Recognition of myofibroblasts of carcinomas was feasible due to the intense desmoplastic reaction that accompanies colorectal carcinoma. Additionally, double immunostaining was performed in 53 cases of colorectal carcinomas. After staining with the first antibody (ERβ, AIB-1, or TIF-2), sections were rinsed with distilled water and incubated with doublestaining block for 3 min (Dako). The second primary antibody (prediluted, RTU-SMA, Novocastra) was applied for 30 min, followed by alkaline phosphatase labeled polymer (Dako) for 30 min. Sections were next incubated with Fast Red Chromogen Solution (Dako). Nuclei were counterstained with hematoxylin. Breast cancer tissue sections were used as positive control for ERα and ERβ. Additionally, tumor-associated lymphocytes or follicles of Payer patches, when present, were valuable internal positive controls for ERβ [19]. Known immunostaining positive specimens were used as a positive control for AIB-1 and TIF-2. In negative control slides, the same method was performed, and the primary antibody was substituted by 1% TBS.

Evaluation of immunostaining

Each slide was individually reviewed and scored in a blind fashion by two independent observers. Discrepancies in scoring between the observers were resolved by review of the slides under a double-headed microscope. This study focused on stromal cells and, in particular, on myofibroblasts of normal mucosa, adenomas, and carcinomas. Carcinoma-associated myofibroblasts were evaluated at areas of intense desmoplastic response. Myofibroblasts of the granulation tissue formed at the base of areas of ulceration were ignored.

ERβ functions mainly as a transcription factor and AIB-1 and TIF-2 are transcriptional coregulators. Therefore, they mainly reside in the nuclei of cells. However, cytoplasmic localization has been observed before and may represent non-genomic actions of ER [34] or subcellular dislocation during malignant transformation [35]. Thus, in addition to nuclear staining, cytoplasmic staining was separately evaluated.

In each case, the percentage of myofibroblasts exhibiting positive nuclear staining and the percentage of myofibroblasts exhibiting positive cytoplasmic expression were determined. Cell counts were performed at a ×400 magnification. At least 1,000 cells were counted in tissue sections obtained from carcinomas. In tissue sections obtained from adenomas and normal mucosa, 200–300 cells were counted.

For statistical purposes, nuclear expression was categorized as follows: low expression, <50% positive staining cells; moderate expression, 50–90% positive cells; high expression, >90% positive cells. Cut-off points were selected based on the distribution of protein expression in normal mucosa and carcinomas; 50% represents the upper quartile expression levels in normal mucosa and 90% the median expression levels in carcinomas. Any case exhibiting cytoplasmic staining was considered as positive for cytoplasmic staining.

Statistical analysis

Expression of the markers was analyzed both as categorical and as continuous variables. Since continuous variables did not follow normal distribution (one-sample Kolmogorov–Smirnov test, $p>0.05$ for all markers), non-parametric statistical tests were used. Kruskal–Wallis H test was used in order to record any differences between the staining results, and the tumor features and Mann–Whitney U test was used to compare two different groups. The Spearman rank correlation was used to detect any potential correlations between the expression of the markers and the Wilcoxon test to detect any differences between paired samples of normal mucosa, adenomas, and carcinomas. For categorical values, chi-square test was used to compare between groups; Marginal Homogeneity test to compare paired samples of normal mucosa, adenomas, and carcinomas; and Pearson correlation test to detect any potential correlations between the markers. Univariate analysis of overall and disease-free survival was calculated with Kaplan–Meier curves, and differences in survival between the groups were recorded using the log-rank test. Multivariate analysis taking into account clinicopathologic factors and expression of the proteins studied was performed using Cox proportional hazards method. All data were analyzed with the SPSS program (SPSS® release 14.0, Chicago, IL, USA). Any p value less than 0.05 was considered significant.

Results

ERα

ERα expression was infrequent (<1% of the cells) and was noted only in the nuclei of epithelial cells in two cases of normal mucosa, one case of adenoma, and three carcinomas. Additionally, ERα expression was never seen in stromal cells (myofibroblasts, endothelial cells, lymphocytes). Figure 1a displays a case of colorectal carcinoma with rare epithelial cells positive for ERα. Thus, ERα expression was extremely rare in colorectal tissue, and no further statistical analysis was performed for this marker.

ERβ1

ERβ1 was expressed in the nuclei and cytoplasm of myofibroblasts (Fig. 1b–d). Nuclear expression of ERβ1 was noted in 30±17% of myofibroblasts of normal mucosa, 52±20% of myofibroblasts of adenomas, and 82±24% of cancer-associated myofibroblasts. Low, mod-

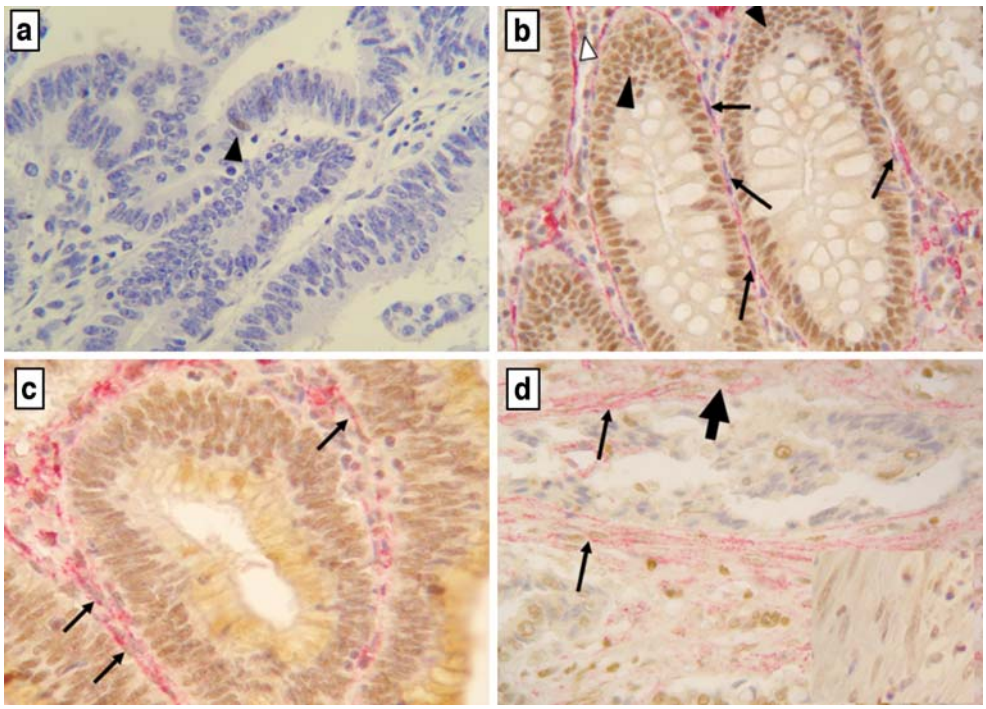

Fig. 1 **a** Rare epithelial cells (*arrowhead*) express ERα in a case of colon carcinoma. **b** Myofibroblasts (*arrows*) of normal mucosa are negative for ERβ1, whereas epithelial cells (*black arrowhead*) and lymphocytes (*white arrowhead*) exhibit positive immunostaining. **c** Most myofibroblasts (*arrows*) of adenomas are positive for ERβ1. **d** Cancer-associated myofibroblasts exhibit nuclear (*arrows*) and cytoplasmic (*thick arrow*) ERβ1 expression. Due to the intense cytoplasmic a-SMA immunostaining, cytoplasmic expression of ERβ1 is better appreciated in single immunostaining for ERβ1 (*inset*; *brown* ERβ1, *red* a-SMA; original magnification ×400)

erate, and high expression of ERβ1 in myofibroblasts of normal colonic mucosa, adenomas, and carcinomas is shown in Table 2. Statistical analysis (Wilcoxon and Marginal Homogeneity tests) revealed that ERβ1 was more frequently expressed in tumor-associated myofibroblasts compared to normal mucosa ($p<0.001$) and adenoma-associated myofibroblasts ($p<0.001$; Fig. 2a). Additionally, ERβ1 was more commonly expressed in myofibroblasts of adenomas compared to myofibroblasts of lamina propria ($p=0.001$; Fig. 2a). Thus, ERβ1 expression in myofibroblasts increased from normal mucosa, through adenomas, to carcinomas. Additionally, high expression of ERβ1 (ERβ1 in >90% of the cells) was more frequently noted in locally advanced carcinomas (T4) since 80% (eight of ten) of T4 tumors displayed high ERβ1 expression, compared to 45% (44 of 97) of T2–T3 tumors (chi-square test, $p=0.048$; Fig. 3a). No correlation was found between nuclear ERβ1 expression and the other clinicopathologic parameters, including gender, degree of dysplasia of adenomas and primary site, stage, lymph node status, grade, and histologic type of carcinomas.

Distinct cytoplasmic staining of ERβ1 in myofibroblasts was noted in 19 of 77 (24.6%) normal mucosa specimens, eight of 29 (27.5%) adenomas, and 59 of 107 (55.1%) carcinomas. Due to intense cytoplasmic expression of a-SMA in double immunostained sections, cytoplasmic expression of ERβ1 was better appreciated in sections stained only for ERβ1 (Fig. 1d). Statistical analysis revealed that cytoplasmic staining was more common in carcinomas compared to normal mucosa ($p<0.001$) and adenomas ($p=0.008$) and was further enhanced in T4 carcinomas (nine of ten) compared to T2/T3 tumors (50 of 97; chi-square test, $p=0.022$; Fig. 3b). No correlation of cytoplasmic staining of ERβ1 with the other clinicopathologic parameters was noted.

ERβ1 was also expressed in other stromal cells such as endothelial cells and lymphocytes and in epithelial cells of normal mucosa, adenomas, and carcinomas (Fig.1b–d). Mean expression levels of ERβ1 in epithelial cells of carcinomas were 92±16% in normal mucosa specimens, 95±45% in adenomas, and 88±23% in carcinomas. No difference regarding the percentage of positive epithelial cells was noted between normal mucosa, adenomas, and carcinomas. In carcinomas, ERβ1 expression in epithelial cells positively correlated with ERβ1 expression in myofibroblasts ($r=0.451$, $p<0.001$).

AIB-1

AIB-1 was expressed only in the nuclei of myofibroblasts. AIB-1 expression was noted in 46±24% of myofibroblasts of normal mucosa, 65±27% of adenoma-associated myofibroblasts, and 81±24% of carcinoma-associated myofibroblasts (Fig. 4a–c). Number of cases with low, moderate, and high expression of AIB-1 in myofibroblasts of lamina propria and adenoma- and carcinoma- associated myofibroblasts is shown in Table 2. Statistical analysis (Wilcoxon and Marginal Homogeneity tests) revealed that AIB-1 was more frequently expressed in myofibroblasts of cancer-associated stroma compared to normal mucosa ($p<0.001$) and adenomas ($p=0.002$; Fig. 2b). Furthermore, adenoma-associated myofibroblasts displayed elevated AIB-1 expression compared to myofibroblasts of normal mucosa ($p=0.007$; Fig. 2b). Thus, AIB-1 expression in myofibroblasts gradually increased from normal mucosa through adenomas to colorectal carcinomas. Additionally, 58 of 60 stage C carcinomas and 30 of 41 stage B carcinomas expressed moderate and high levels of AIB-1. Thus, low expression of AIB-1 in myofibroblasts was rarely seen in stage C carcinomas (chi-square test, $p=0.029$). No correlation of AIB-1 expression in myofibroblasts with other clinicopathologic parameters was noted.

AIB-1 expression was repeatedly seen in other stromal cells such as endothelial cells and lymphocytes as well as in epithelial cells of normal mucosa, adenomas, and carcinomas (Fig. 4a–c). AIB-1 was expressed in 88±18% of epithelial cells of normal mucosa, in 91±20% of epithelial cells of adenomas, and in 88±20% of epithelial cells of

Table 2 Expression of ERβ, AIB-1, and TIF-2 in myofibroblasts of normal mucosa, adenomas, and carcinomas

Marker	Level of expression	Normal mucosa ($N=77$)	Adenoma ($N=29$)	Carcinoma ($N=107$)
ERβ	Low expression	69 (89.6%)	12 (41.4%)	10 (9.4%)
	Moderate expression	8 (10.4%)	17 (58.6%)	45 (42%)
	High expression	0 (0%)	0 (0%)	52 (48.6%)
AIB-1	Low expression	44 (57.1%)	8 (27.5%)	11 (10.2%)
	Moderate expression	33 (42.9%)	19 (65.5%)	48 (44.9%)
	High expression	0 (0%)	2 (7%)	48 (44.9%)
TIF-2	Low expression	56 (72.7%)	10 (34.5%)	10 (9.4%)
	Moderate expression	21 (27.3%)	19 (65.5%)	25 (23.3%)
	High expression	0 (0%)	0 (0%)	72 (67.3%)

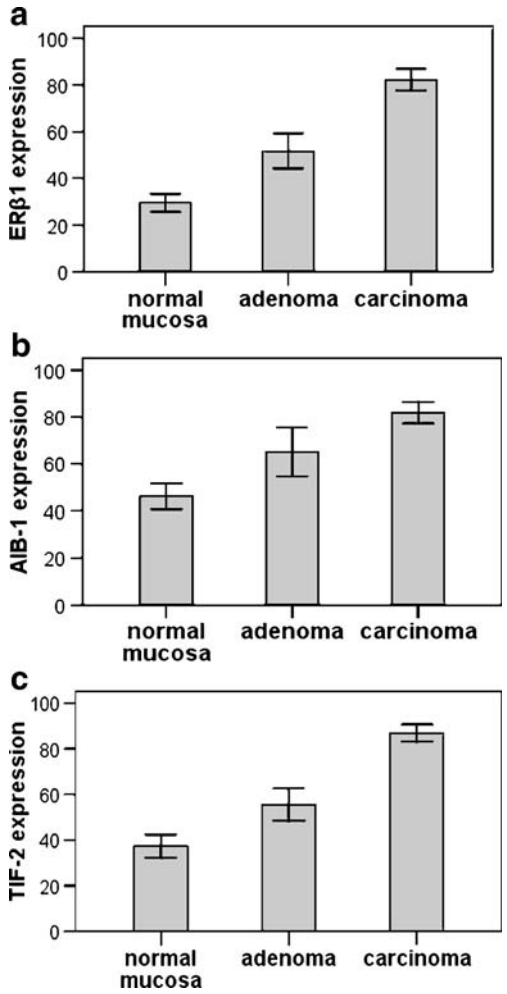

Fig. 2 Expression of ERβ1 (**a**), AIB-1 (**b**), and TIF-2 (**c**) in myofibroblasts increases from normal colonic mucosa through adenomas to colorectal carcinomas

carcinomas. No statistically significant difference was noted regarding the percentage of positive epithelial cells of normal mucosa, adenomas, and carcinomas. A positive correlation between AIB-1 expression in epithelial cells and AIB-1 expression in myofibroblasts was noted in normal mucosa specimens (r=0.237, p=0.042) and carcinomas (r=0.211, p=0.034).

TIF-2

TIF-2 immunostaining was noted in the nuclei and rarely in the cytoplasm of myofibroblasts (Fig. 4d–f). Nuclear expression of TIF-2 was noted in 37±21% of myofibroblasts of normal mucosa, 55±19% of myofibroblasts of adenomas, and 87±19% of myofibroblasts of carcinomas. Table 2 shows the number of cases with low, moderate and high expression of TIF-2. Statistical analysis (Wilcoxon and Marginal Homogeneity tests) revealed that TIF-2 expression was enhanced in tumor-associated myofibroblasts compared to myofibroblasts of normal mucosa ($p<0.001$) and of adenomas ($p<0.001$) and in adenoma-associated myofibroblasts compared to myofibroblasts of normal mucosa ($p=0.005$; Fig. 2c). Thus, like ERβ1 and AIB-1, TIF-2 expression in myofibroblasts increased during malignant transformation of colonic tissue. No correlation of TIF-2 expression in myofibroblasts to any clinicopathologic parameter was noted.

Distinct cytoplasmic expression of TIF-2 was noted in myofibroblasts of one of 77 normal mucosa specimens, zero of 29 adenomas, and 17 of 107 carcinomas and was more commonly seen in cancer-associated myofibroblasts compared to myofibroblasts of normal mucosa ($p=0.001$).

TIF-2 expression was also noted in a high proportion of normal, dysplastic, and malignant epithelial cells, as well as in endothelial cells and lymphocytes of normal mucosa, adenomas, and carcinomas (Fig. 4d–f). Mean expression levels of TIF-2 in epithelial cells were 98±3% in normal mucosa specimens, 98±4% in adenomas, and 96±5% in carcinomas. There was no statistically significant difference regarding the percentage of positive epithelial cells of normal mucosa, adenomas, and carcinomas. Additionally, there was no correlation between TIF-2 expression in epithelial cells and its expression in myofibroblasts.

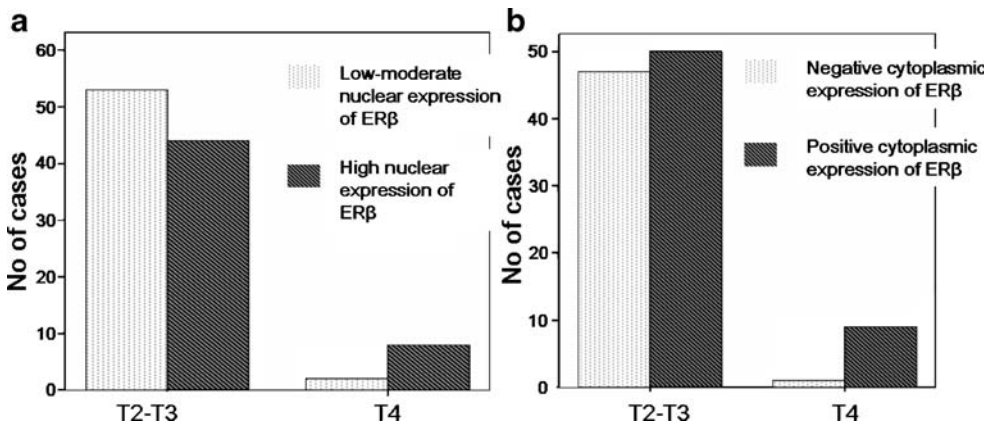

Fig. 3 **a** Locally advanced (*T4*) carcinomas exhibited more commonly high nuclear expression of ERβ in myofibroblasts ($p=0.048$). **b** Cytoplasmic expression of ERβ1 was more frequently seen in myofibroblasts of carcinomas of advanced stage ($p=0.022$)

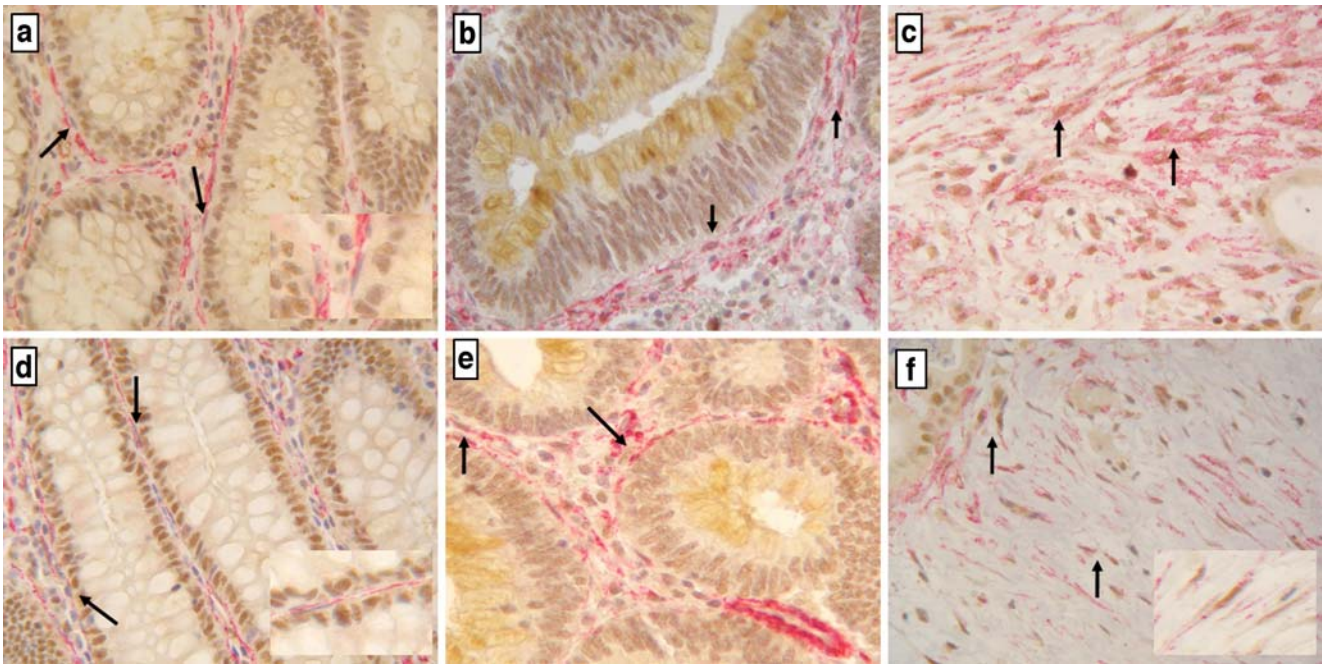

Fig. 4 **a–c** AIB-1 immunostaining in normal mucosa (**a**), adenoma (**b**), and carcinoma (**c**). Low expression of AIB-1 is noted in myofibroblasts (*arrows* and *inset*) of normal mucosa (**a**), whereas high expression is noted in myofibroblasts (*arrows*) of adenoma (**b**) and carcinoma (**c**; *red* a-SMA, *brown* AIB-1; original magnification ×400). **d–f** TIF-2 expression is low in myofibroblasts (*arrows* and *inset*) of normal mucosa (**d**), moderate in myofibroblasts (*arrows*) of adenoma (**e**), and high in cancer-associated myofibroblasts (*arrows* and *inset*; **f**). Cancer-associated myofibroblasts display both nuclear and cytoplasmic expression of TIF-2 (*inset* in **f**; *red* a-SMA, *brown* TIF-2, *arrows* myofibroblasts; original magnification ×400)

Correlation between markers

Since AIB-1 and TIF-2 are ER transcriptional coregulators, the relationship of the expression of these markers in the nuclei of the cells was examined. In myofibroblasts of normal mucosa and adenomas, no correlation between ERβ1, AIB-1, and TIF-2 expression was noted. However, in carcinomas, ERβ1 expression in myofibroblasts correlated with AIB-1 (r=0.359, p< 0.001) and TIF-2 (i=0.255, p= 0.008).

Survival analysis

Advanced Dukes stage and lymph node involvement were associated with shorter disease-free survival (p< 0.001, p= 0.04, respectively) on Kaplan–Meier analysis. Additionally, advanced Dukes stage, lymph node involvement, and poor differentiation were associated with decreased overall survival (p< 0.001, p= 0.021 and p< 0.001, respectively). None of the markers examined was associated with disease-free or overall survival on Kaplan–Meier analysis.

Multivariate Cox analysis that included age, gender, primary site, grade, stage, histologic type, and ERβ1, AIB-1, and TIF-2 expressions showed that stage and age were independently associated with disease-free survival and that stage and grade were independent prognostic factors of overall survival (Tables 3 and 4).

Discussion

Epidemiological and molecular data suggest the involvement of estrogen signaling in colorectal carcinogenesis, mediated mainly through ERβ [36]. In our study, ERβ1 was highly expressed not only in epithelial cells but also in stromal cells of colorectal carcinomas, and this may explain some of the discrepancies between non-morphologic studies regarding the expression of ERβ in normal and malignant colorectal tissue [16, 17, 20]. ERβ1 expression in myofibroblasts was more frequent in adenoma- and cancer-associated myofibroblasts compared to normal mucosa. Additionally, ERβ1 expression was enhanced in myofibroblasts of locally advanced (stage T4) carcinomas. Previous studies have shown that ERβ expression in epithelial cells is downregulated in colorectal carcinomas paralleling tumors' dedifferentiation [19]. Thus, even though ERβ1 is expressed in both epithelial cells and myofibroblasts of colorectal carcinomas, it may have diverse biologic effects, depending on the cell of origin.

Various studies suggest the importance of paracrine actions of estrogens that mediate a molecular crosstalk between epithelial and stromal cells [23–25, 37]. Estrogens can have multiple functions in stromal cells of various organs. Estradiol increases MMP-9 production from mesangial cells of the kidney and collagen production from skin fibroblasts [38, 39]. ER-mediated signaling in stromal cells

Table 3 Cox survival analysis for disease-free survival

Clinicopathologic parameter	*p*	Exp(*B*)	95.0% CI for Exp(*B*)	
			Lower	Upper
Dukes	0.000			
Dukes (B vs D)	0.000	0.033	0.008	0.129
Dukes (C vs D)	0.000	0.057	0.015	0.217
Grade	0.165			
Grade (I vs III)	0.101	0.304	0.074	1.260
Grade (II vs III)	0.837	0.894	0.308	2.599
Histologic type	0.215	0.487	0.156	1.519
Age	0.031	0.961	0.928	0.996
Gender	0.460	1.319	0.633	2.750
ERβ	0.265	1.011	0.992	1.030
AIB-1	0.520	0.995	0.978	1.011
TIF-2	0.877	0.998	0.980	1.018

is crucial for estrogen-dependent growth of epithelial cells in the uterus, mammary gland, and prostate gland [23–25]. Furthermore, estrogens stimulate the proliferation of normal epithelial cells when cocultured with stromal cells but have no effect on epithelial cells when cultured in isolation [40]. Additionally, ERβ expression increases not only in epithelial cells but also in stromal cells of endometrial hyperplasia [41] and in periductal fibroblasts of lobular carcinoma in situ [42]. In the latter case, ERβ immunoreactivity was associated with higher incidence of ipsilateral, concurrent, or metachronous invasive carcinoma. It has been hypothesized that estrogens stimulate ERβ positive periductal fibroblasts to produce growth factors that enhance proliferation of epithelial cells [42]. Thus, it could be speculated that estrogens may mediate their effects on epithelial cells through paracrine mechanisms. Indeed, it has been found that estrogens stimulate the production of hepatocyte growth factor from stromal cells of breast carcinomas and of VEGF from stromal cells of normal endometrium [37, 43, 44]. Stroma-derived factor 1 (SDF-1) is produced by malignant cells and cancer-associated fibroblasts and enhances tumor growth [45]. SDF-1 expression is regulated by ER signaling in breast and ovarian cancer cell lines and depends on coexpression of members of the p160 family of coactivators [46, 47]. Thus, estrogens are important components of epithelial–stromal crosstalk in normal tissues and cancer microenvironment. Further studies are needed to elucidate the exact mechanisms of estrogen-dependent crosstalk between malignant and stromal cells in the microenvironment of colorectal cancer.

To the best of our knowledge, only one study has assessed, in addition to epithelial cells, the expression of ERβ in stromal cells of carcinomas [48]. In this study, no difference in ERβ expression between stromal cells surrounding areas of prostatic hyperplasia and prostate cancer-associated stromal cells was found [48]. However,

Table 4 Cox survival analysis for overall survival

Clinicopathologic parameter	*p*	Exp(*B*)	95.0% CI for Exp(*B*)	
			Lower	Upper
Dukes	0.000			
Dukes (B vs D)	0.000	0.039	0.009	0.166
Dukes (C vs D)	0.001	0.078	0.018	0.339
Grade	0.028			
Grade (I vs III)	0.008	0.073	0.011	0.500
Grade (II vs III)	0.421	0.626	0.200	1.959
Histologic type	0.073	0.260	0.059	1.136
Gender	0.059	2.729	0.961	7.750
Age	0.332	0.979	0.938	1.022
ERβ	0.500	1.007	0.986	1.029
AIB-1	0.353	0.991	0.971	1.011
TIF-2	0.460	0.992	0.972	1.013

the stroma of normal prostate and prostatic carcinomas consists mainly of fibroblasts and smooth muscle cells with few myofibroblasts [49], and this may account for the discrepancies with our study. Additionally, the antibody used in that study recognized the ERβ2 isoform that has no transcriptional activity and acts as a negative regulator of ER signaling [21].

ERβ has been detected in the cytoplasm of normal and malignant epithelial cells in various organs, including colorectal tissue [17, 19], and may mediate non-genomic actions of the receptors [34]. In fact, ERβ has been shown to activate MAPK pathway in epithelial [50] and endothelial cells [51]. Additionally, estradiol increases production of MMP-2 from smooth muscle cells of pulmonary lymphangioleiomyomatosis in an ER-dependent non-genomic pathway and enhances invasion in collagen matrix [52]. Thus, based on our findings of increased cytoplasmic expression of ERβ1 in myofibroblasts of carcinomas, with further increase in carcinomas of stage T4, we might speculate that non-genomic actions of ERβ1 in myofibroblasts are involved in colorectal carcinomas. The pathways activated by cytoplasmic ERβ1 in myofibroblasts of colorectal carcinoma merit further investigation.

Gender-related differences in the expression of ERβ have been described [16, 53], but have not been confirmed by other studies [19, 20, 22]. Additionally, in our study, ERβ1 expression did not differ between male and female patients either in normal mucosa specimens, adenomas, or carcinomas. Discrepancies between findings can be attributed to differences in methodology, the ERβ isoform detected, and the number and age of female patients analyzed. Thus, definite conclusions on the presence of gender-related differences in ERβ expression in colorectal tissue cannot be drawn. However, since our study focused on postmenopausal women and evaluated the ERβ1 isoform separately in epithelial cells and myofibroblasts, it might indicate that estrogen signaling through ERβ1 in colorectal tissue may not be different between males and females.

Transcriptional activation from estrogen-ER complexes is facilitated by recruitment of coactivators [28, 29]. AIB-1 expression in epithelial cells has a well-described oncogenic role in various carcinomas [28]. In colorectal carcinomas, increased AIB-1 expression in malignant cells was associated with lymph node and/or distant metastasis [18] or locally advanced stage (Grivas et al., manuscript in press). However, the expression of AIB-1 in stromal cells was not evaluated in these studies. In our study, AIB-1 expression was increased in myofibroblasts of dysplastic mucosa and was further increased in cancer-associated myofibroblasts paralleling the progression of colorectal carcinomas. Thus, it could be speculated that AIB-1 mediated signaling is increased in myofibroblasts early in colorectal carcinogenesis and might contribute to the initiation and progression of colorectal carcinomas. Additionally, in our study, AIB-1 expression in myofibroblasts of colorectal carcinomas was significantly associated with ERβ1 expression. AIB-1 has been shown to interact with various nuclear receptors (ERα) and other transcription factors (AP1, NFκB, E2F1) [28]. The exact mechanisms of AIB-1 actions in the stroma of carcinomas remain elusive, even though a possible association with ERβ1 could be implied by our results. Further studies will help the clarification of the transcription factor(s) whose transcriptional activity is regulated by AIB-1 expression in cancer-associated myofibroblasts since NF-κB expression is also enhanced in myofibroblasts of colorectal carcinomas [54].

TIF-2 is a member of the SRC family of coregulators and is frequently overexpressed in malignant cells of various neoplasms [31, 32, 55–57]. On the contrary, a recent study using non-morphologic techniques has found a decline of TIF-2 mRNA in colon carcinomas compared to normal colonic tissue [58]. However, to the best of our knowledge, its expression in stromal cells of carcinomas has never been studied before. A previous study in patients with polycystic ovary syndrome (a syndrome associated with increased risk of endometrial hyperplasia and cancer) revealed increased TIF-2 expression in endometrial stromal cells compared to patients without the syndrome [33]. In our study, TIF-2 expression in myofibroblasts increased from normal mucosa through adenomas to carcinomas. These data support a potential role of TIF-2 in epithelial-stromal cell interactions that contribute to malignant transformation. Additionally, even though we cannot exclude the interaction of TIF-2 with other nuclear receptors or transcription factors, it might be speculated that TIF-2 could enhance the transcriptional activity of ERβ1 in myofibroblasts of colorectal carcinomas and facilitate paracrine actions of estrogens on epithelial cells.

The role of cytoplasmic localization of TIF-2 that was observed in our study remains elusive. Differential subcellular localization of TIF-2 during malignant transformation has been described in rabdomyosarcoma cells [35]. In line with these observations, cytoplasmic localization of TIF-2 was more frequently noted in myofibroblasts of colorectal carcinomas compared to myofibroblasts of normal mucosa and adenomas and might represent aberrant nuclear/cytoplasmic shuttling of TIF-2 protein in cancer microenvironment.

In conclusion, the increased expression of ERβ1, AIB-1, and TIF-2 in myofibroblasts of colorectal carcinomas and correlation of elevated levels of ERβ1 and AIB-1 with advanced stage support a possible role of these factors in the initiation and progression of colorectal carcinomas through paracrine actions. The expression of additional coregulators (coactivators and corepressors) and transcrip-

tion factors needs to be investigated both in epithelial cells and stromal cells of colorectal carcinomas in order to elucidate the signaling networks within and among the cells of cancer microenvironment that mediate the effects of estrogens in colorectal carcinogenesis.

Conflict of interest statement The authors declare that they have no conflict of interest.

References

1. Bissell MJ, Labarge MA (2005) Context, tissue plasticity, and cancer: are tumor stem cells also regulated by the microenvironment. Cancer Cell 7:17–23
2. Hu M, Polyak K (2008) Microenvironmental regulation of cancer development. Curr Opin Genet Dev 18:27–34
3. Radisky ES, Radisky DC (2007) Stromal induction of breast cancer: inflammation and invasion. Rev Endocr Metab Disord 8:279–287
4. Schurch W, Seemayer TA, Gabbiani G (1998) The myofibroblast. Am J Surg Pathol 22:141–147
5. Powell DW, Mifflin RC, Valentich JD et al (1999) Mofibroblast I. Paracrine cells important in health and disease. Am J Physiol 277 (1 Pt 1):C1–9
6. Adegboyega PA, Mifflin RC, DiMari JF et al (2002) Immunohistochemical study of myofibroblasts in normal colonic mucosa, hyperplastic polyps and adenomatous colorectal polyps. Arch Pathol Lab Med 126:829–836
7. Yen T-H, Wright NA (2006) The gastrointestinal tract stem cell niche. Stem Cell Rev 2:203–212
8. Nakayama H, Enzan H, Miyazaki E et al (2000) Differential expression of CD34 in normal colorectal tissue, peritumoral inflammatory tissue, and tumor stroma. J Clin Pathol 53:626–629
9. De Wever O, Nguyen OD, Van Hoorde L et al (2004) Tenascin C and SF/HGF produced by myofibroblasts can provide convergent pro-invasive signals to human colon cancer cells through RhoA and Rac. FASEB J 18:1016–1028
10. Boffetta P (2005) Cancer Epidemiology. In: Ahrens W, Pigeot I (eds) Handbook of epidemiology. Springer, Heidelberg, pp 1406–1435
11. Gunter MJ, Hoover DR, Yu H et al (2008) Insulin, insulin-like growth factor-I, endogenous estradiol, and risk of colorectal cancer in postmenopausal women. Cancer Res 68:329–337
12. Kampman E, Potter JD, Slattery ML et al (1997) Hormone replacement therapy, reproductive history, and colon cancer: a multicenter, case-control study in the United States. Cancer Causes Control 8:146–158
13. Lechner D, Kallay E, Cross HS (2005) Phytoestrogens and colorectal cancer prevention. Vitam Horm 70:169–198
14. Di Domenico M, Castoria G, Bilancio A et al (1996) Estradiol activation of human colon carcinoma-derived Caco-2 cell growth. Cancer Res 56:4516–4521
15. Pearce ST, Jordan VC (2004) The biological role of estrogen receptors α and β in cancer. Crit Rev Oncol Hematol 50:3–22
16. Campbell-Thompson M, Lynch IJ, Bhardwaj B (2001) Expression of estrogen receptor (ER) subtypes and ERbeta isoforms in colon cancer. Cancer Res 61:632–640
17. Xie L-Q, Yu J-P, Luo H-S (2004) Expression of estrogen receptor b in human colorectal cancer. World J Gastroenterol 10:214–217
18. Foley EF, Jazaeri AA, Shupnik MA et al (2000) Selective loss of estrogen receptor b in malignant human colon. Cancer Res 60:245–248
19. Konstantinopoulos PA, Kominea A, Vandoros G et al (2003) Oestrogen receptor beta (ERb) is abundantly expressed in normal colonic mucosa, but declines in colon adenocarcinoma paralleling the tumour dedifferentiation. Eur J Cancer 39:1251–1258
20. Cavallini A, Notarnicola M, Giannini P et al (2005) Oestrogen receptor-related receptor alpha (ERRa) and oestrogen receptors (ERa and ERb) exhibit different gene expression in human colorectal tumour progression. Eur J Cancer 41:1487–1494
21. Peng B, Lu B, Leygue E et al (2003) Putative functional characteristics of human estrogen receptor-beta isoforms. J Mol Endocrinol 30:13–29
22. Wong NACS, Malcomson RDG, Jodrell D et al (2005) ERβ isoform expression in colorectal carcinoma: an in vivo and in vitro study of clinicopathological and molecular correlates. J Pathol 207:53–60
23. Cooke PS, Buchanan DL, Young P et al (1997) Stromal estrogen receptors mediate mitogenic effects of estradiol on uterine epithelium. Proc Natl Acad Sci USA 94:6535–6540
24. Cunha GR, Young P, Hom YK et al (1997) Elucidation of a role for stromal steroid hormone receptors in mammary gland growth and development using tissue recombinants. J Mammary Gland Biol Neoplasia 2:393–402
25. Prins GS, Birch L, Couse JF et al (2001) Estrogen imprinting of the developing prostate gland is mediated through stromal estrogen receptor alpha: studies with alphaERKO and betaERKO mice. Cancer Res 61:6089–6097
26. Gupta PB, Proia D, Cingoz O et al (2007) Systemic stromal effects of estrogens promote the growth of estrogen receptor-negative tumors. Cancer Res 67:2062–2071
27. Yamaguchi Y, Hayashi S-I (2008) Estrogen-related cancer microenvironment of breast carcinoma. Endocr J doi:10.1507/endocrj.K08E-099
28. Yan J, Tsai SY, Tsai M-J (2006) SRC-3/AIB1: transcriptional coactivator in oncogenesis. Acta Pharmacol Sin 27:387–394
29. O'Maley BW, Qin J, Lanz RB (2008) Cracking the coregulator codes. Curr Opin Cell Biol 20:310–315
30. Lonard DM, O'Malley BW (2007) Nuclear receptor coregulators: judges, juries and executioners of cellular regulation. Mol Cell 27:691–700
31. Gregory CW, He B, Johnson RT et al (2001) A mechanism for androgen receptor-mediated prostate cancer recurrence after androgen deprivation therapy. Cancer Res 61:4315–4319
32. Hershberger PA, Vasquez AC, Kanterewicz B et al (2005) Regulation of endogenous gene expression in human non–small cell lung cancer cells by estrogen receptor ligands. Cancer Res 65:1598–1605
33. Gregory CW, Wilson EM, Apparao KBC et al (2002) Steroid receptor coactivator expression throughout the menstrual cycle in normal and abnormal endometrium. J Clin Endocrinol Metab 87:2960–2966
34. Bjornstrom L, Sjoberg M (2005) Mechanisms of estrogen receptor signaling: convergence of genomic and nongenomic actions on target genes. Mol Endocrinol 19:833–842
35. Chen SL, Wang M, Hosking B et al (2001) Subcellular localization of the Steroid Receptor Coactivators (SRCs) and MEF2 in muscle and rhabdomyosarcoma cells. Mol Endocrinol 15:783–796
36. Slattery ML, Sweeney C, Murtaugh M et al (2005) Associations between ERα, ERβ, and AE genotypes and colon and rectal cancer. Cancer Epidemiol Biomarkers Prev 14:2936–2942
37. Zhang HZ, Bennett JM, Smith KT et al (2002) Estrogen mediates mammary epithelial cell proliferation in serum-free culture indirectly via mammary stroma-derived hepatocyte growth factor. Endocrinology 143:3427–3434

38. Potier M, Elliot SJ, Tack I et al (2001) Expression and regulation of estrogen receptors in mesangial cells: influence on matrix metalloproteinase-9. J Am Soc Nephrol 12:241–251
39. Surazynski A, Jarzabek K, Haczynski J et al (2003) Differential effects of estradiol and raloxifene on collagen biosynthesis in cultured human skin fibroblasts. Int J Mol Med 12:803–809
40. King KJ, Nicholson HD, Assinder SJ (2006) Effect of increasing ratio of estrogen:androgen on proliferation of normal human prostate stromal and epithelial cells, and the malignant cell line LNCaP. Prostate 66:105–114
41. Villavicencio A, Bacalla K, Avellaira C et al (2006) Androgen and estrogen receptors and co-regulators levels in endometria from patients with polycystic ovarian syndrome with and without endometrial hyperplasia. Gynecol Oncol 103:307–314
42. Middleton LP, Perkins GH, Tucker SL et al (2007) Expression of ERa and ERb in lobular carcinoma in situ. Histopathology 50:875–880
43. Bausero P, Cavaille F, Meduri G et al (1998) Paracrine action of vascular endothelial growth factor in the human endometrium: production and target sites, and hormonal regulation. Angiogenesis 2:167–182
44. Hyder SM, Nawaz Z, Chiappetta C et al (2000) Identification of functional estrogen response elements in the gene coding for the potent angiogenic factor vascular endothelial growth factor 1. Cancer Res 60:3183–3190
45. Orimo A, Gupta PB, Sgroi DC et al (2005) Stromal fibroblasts present in invasive human breast carcinomas promote tumor growth and angiogenesis through elevated SDF-1/CXCL12 secretion. Cell 121:335–348
46. Hall JM, Korach KS (2003) Stromal cell-derived factor 1, a novel target of estrogen receptor action mediates the mitogenic effects of estradiol in ovarian and breast cancer cells. Mol Endocrinol 19:792–803
47. Kishimoto H, Wang Z, Bhat-Nakshari P et al (2005) The p160 family of coactivators regulate breast cancer cell proliferation and invasion through autocrine/paracrine activity of SDF-1a/CXCL12. Carcinogenesis 26:1706–1715
48. Horvath LG, Henshall SM, Lee C-S et al (2001) Frequent loss of estrogen receptor-b expression in prostate cancer. Cancer Res 61:5331–5335
49. Zhang Y, Nojima S, Nakayama H et al (2003) Characteristics of normal stromal components and their correlation with cancer occurrence in human prostate. Oncol Rep 10:207–211
50. Marquez-Garban DC, Chen H-W, Fishbein MC et al (2007) Estrogen receptor signaling pathways in human non-small cell lung cancer. Steroids 72:135–143
51. Klinge CM, Blankenship KA, Risinger KE et al (2005) Resveratrol and Estradiol rapidly activate MAPK signaling through estrogen receptors α and β in endothelial cells. J Biol Chem 280:7460–7468
52. Glassberg MK, Elliot SJ, Fritz J et al (2008) Activation of the estrogen receptor contributes to the progression of pulmonary lymphangioleiomyomatosis via matrix metalloproteinase-induced cell invasiveness. J Clin Endocrinol Metab 93:1625–1633
53. Jassam N, Bell SM, Speirs V et al (2005) Loss of oestrogen receptor β in colon cancer and its association with Dukes' staging. Oncol Rep 14:17–21
54. Vandoros GP, Konstantinopoulos PA, Sotiropoulou-Bonikou G et al (2006) PPAR-gamma is expressed and NF-kB pathway is activated and correlates positively with COX-2 expression in stromal myofibroblasts surrounding colon adenocarcinomas. J Cancer Res Clin Oncol 132:76–84
55. Picard F, Géhin M, Annicotte J et al (2002) SRC-1 and TIF2 control energy balance between white and brown adipose tissues. Cell 111:931–941
56. Mukherjee A, Soyal SM, Fernandez-Valdivia R et al (2006) Steroid Receptor Coactivator 2 is critical for progesterone-dependent uterine function and mammary morphogenesis in the mouse. Mol Cell Biol 26:6571–6583
57. Carroll RS, Brown M, Zhang J et al (2000) Expression of a subset of steroid receptor cofactors is associated with progesterone receptor expression in meningiomas. Clin Cancer Res 6:3570–3575
58. Giannini R, Cavallini A (2005) Expression analysis of a subset of coregulators and three nuclear receptors in human colorectal carcinoma. Anticancer Res 25:4287–4292

Virchows Arch (2009) 454:401–409
DOI 10.1007/s00428-009-0739-5

ORIGINAL ARTICLE

Apoptosis of interstitial cells of Cajal, smooth muscle cells, and enteric neurons induced by intestinal ischemia and reperfusion injury in adult guinea pigs

Feng Mei · Sheng Guo · Yang-tao He · Jiang Zhu · De-shan Zhou · Jian-qin Niu · Han-zhi Wang · Yan-ping Tian

Received: 6 August 2008 / Revised: 17 January 2009 / Accepted: 18 January 2009 / Published online: 12 February 2009

Abstract This study aimed at evaluating whether apoptosis of interstitial cells of Cajal (ICC), smooth muscle cells (SMC), and enteric neurons was involved in a guinea pig model of intestinal ischemia and reperfusion injury. The small intestinal segments were resected at either 6 (I_{60}/R_{6h}) and 12 h (I_{60}/R_{12h}) or 7 (I_{60}/R_{7d}) to 14 (I_{60}/R_{14d}) days after 60 min intestinal ischemia in the adult guinea pigs and studied by immunohistochemistry with anti-Kit, 5-bromo-2′-deoxyuridine (BrdU), α-smooth muscle actin, vimentin, and β-tublin III antibodies. Also, apoptosis was tested by terminal deoxynucleotidyl transferase-mediated dUTP nick end labeling (TUNEL) method. In the I_{60}/R_{12h} injury, there was a ~50% decrease of Kit+ cells in cell numbers at the level of myenteric plexus and a number of Kit-/vimentin-positive cells were labeled by TUNEL. Also, a few SMC and enteric neurons were TUNEL positive. The Kit+ ICC recovered to normal and a number of Kit-/BrdU-double-positive cells were observed in the I_{60}/R_{14d} group. Our results indicated that the intestinal I/R injury could lead to apoptosis of ICC, SMC, and enteric neurons which may contribute to the gastrointestinal motility disorders, and proliferation was involved in the recovery of ICC.

Keywords Proliferation · ICC-MY · ICC-DMP · TUNEL · BrdU

Electronic supplementary material The online version of this article (doi:10.1007/s00428-009-0739-5) contains supplementary material, which is available to authorized users.

Feng Mei and Sheng Guo contributed equally to this work.

F. Mei (✉) · Y.-t. He · D.-s. Zhou · J.-q. Niu · H.-z. Wang · Y.-p. Tian
Department of Histology and Embryology,
Third Military Medical University,
Chongqing 400038, China
e-mail: thethirdmilitary@sohu.com

S. Guo
Department of Immunology, Third Military Medical University,
Chongqing 400038, China

J. Zhu
Department of Pathology, Southwest Hospital,
Third Military Medical University,
Chongqing 400038, China

D.-s. Zhou
Department of Histology and Embryology,
Capital University of Medical Sciences,
Beijing 100054, China

Introduction

The small intestine is one of the most susceptible organs to ischemia and reperfusion (I/R) injury such as is often encountered during hemorrhagic shock or small bowel transplantation. In an intestinal I/R injury model, changes in mucous and systemic inflammatory responses have been documented [1]. Some studies have also shown changes in gastrointestinal motility [2–6]; however, the underlying mechanisms are not well understood yet.

Interstitial cells of Cajal (ICC) play an important role in the regulation of gastrointestinal (GI) motility [7–9]. ICC in the small intestine are divided into two subgroups. One subgroup is located at the level of the myenteric plexus (ICC-MY) and acts as the pacemaker cells that generate and propagate the slow waves in the small intestine [10, 11]. The other is closely associated with the deep muscular plexus (ICC-DMP), and these cells play a role in the mediation of inputs from the enteric nervous system to GI smooth muscles [12–14].

ICC express the product of the *c-kit* gene [11, 15, 16], a proto-oncogene that encodes the receptor tyrosine kinase (Kit) which is considered essential for the development, differentiation, and functional maintenance of ICC [17]. A

recent study has also shown that a downregulated ICC Kit expression is probably associated with the gastrointestinal motility disorders resulting from I/R injury of the small intestine [2]. Other studies have also shown the loss of Kit immunopositivity after intestinal surgical manipulation [18] and gastrointestinal disorders, such as intestinal obstruction [19, 20], and this loss is probably one of the underlying mechanisms associated with intestinal motility dysfunction. However, it is noteworthy that apoptosis is generally observed in the liver [21], kidney [22], intestine [23], and lung [24] after I/R injuries, but it is not clear whether apoptosis of the ICC, smooth muscle cells (SMC), or enteric neurons is also involved in the intestinal I/R injury. Furthermore, a reexpression of Kit protein may contribute to the recovery of ICC networks after disrupted by intestinal disorders [18–20]. Also, a proliferative event has been reported during the recovery of the ICC after disruption by intestinal transection and anastomosis [25], but it is unclear whether the proliferation is linked to the recovery of the ICC after an I/R injury as well as the Kit reexpression. This study investigated alterations in the morphology and number of ICC in an intestinal I/R injury model using immunofluorescence, detection of apoptosis by terminal deoxynucleotidyl transferase-mediated dUTP nick end labeling (TUNEL) methodology, and detection of cell proliferation using 5-bromo-2′-deoxyuridine (BrdU) incorporation.

Materials and methods

Animals

Twenty-four adult guinea pigs (300–350 g, male or female, aged 6–8 weeks) were purchased from the Animal Center of the Third Military Medical University (Chongqing, China) and used in our experiments. All experiments were performed in accordance with our University Health Guide for the Care and Use of Laboratory Animals.

Animal surgery

Operations for experimental animals were performed under pentobarbital sodium anesthesia (Nembutal 50 μg g^{-1}). After the laparotomy by midline incision, the vascular arcades were ligated between the descending branch of the right colic artery and the ascending branch of the ileocolic artery, between the descending branch of the ileocolic artery and the last ileal artery, and between the jejunal arteries just proximal and distal to the point of the superior mesenteric artery in order occlude and interrupt the collateral blood flow. In addition, bulldog clamps were applied to the jejunum and terminal ileum at the same ligation levels as the vascular arcades in order to interrupt collateral flow within the intestinal wall. Then, the superior mesenteric artery was occluded just proximal to the right colic artery by vascular microclip. The right colic artery and vein and the ileocolic artery and vein were also occluded (supplemental Fig. 1). After the planned ischemic period, the vascular microclips and bulldog clamps were removed and blood reperfusion of the intestine confirmed by an immediate change of intestinal color from white to pink and the recovery of mesenteric arterial pulsations. The intestines were carefully returned to the abdomen and the incision was closed by two layers of continuous 3–0 silk sutures.

Experimental groups

Animals were divided into four groups according to the ischemia and reperfusion periods: (1) ischemia for 60 min followed by reperfusion for 6 h (I_{60}/R_{6h}), (2) ischemia for 60 min followed by reperfusion for 12 h (I_{60}/R_{12h}), (3) ischemia for 60 min followed by reperfusion for 7 days (I_{60}/R_{7d}), and (4) ischemia for 60 min followed by reperfusion for 14 days (I_{60}/R_{14d}; N=3 in each group). Sham control animals (N=3 in each group) were treated in an identical fashion except for vascular clamping. At the end of each experiment, the animals were killed by an overdose of pentobarbital and the ileum was harvested.

Immunofluorescence

The ileum was removed and enteric contents were washed away with phosphate-buffered saline (PBS). The small intestine was inflated with acetone for 30 min (room temperature), then opened along the mesenteric border, then the mucosa was removed, and the longitudinal smooth muscle layer containing the ICC-MY (also referred to as the ICC associated with Auerbach's plexus or ICC-MP by some authors) and the circular smooth muscle layer associated with ICC around the deep muscular plexus were prepared with the aid of a dissection microscope. The immunostaining procedures have been described previously [26]. Briefly, ICC were identified by using a rat monoclonal antibody raised against Kit (ACK2, 5 μg ml^{-1}; eBioscience) and immunoreactivity was detected by using a Cy3-conjugated secondary antibody (antirat IgG, 1:100; Zymed). Vimentin or smooth muscle actin was detected with a mouse monoclonal vimentin (1:100; DAKO) or α-smooth muscle actin (α-SMA; 1:100; Santa Cruz) antibody, and enteric neurons were detected with a rabbit polyclonal β-tublin III antibody (1:100; Sigma) respectively using the same procedures. Antibody-positive cells were labeled by a Cy5-conjugated secondary antibody (antimouse IgG, 1:100; Zymed), a fluorescein isothiocyanate (FITC)-conjugated (antimouse IgG, 1:100; DAKO), or a tetramethylrhodamine isothiocyanate (TRITC)-conjugated secondary antibody (antirabbit IgG, 1:100; Zymed). Nega-

tive control specimens were prepared in the same manner, but each primary antibody was omitted. The stained results were examined using a BX51 fluorescence microscope (OLYMPUS, Japan) or with a TCS SP5 confocal laser scanning microscope (Leica, Germany) with an excitation wavelength appropriate for FITC (488 nm), Cy5 (650 nm), Cy3 (552 nm), or TRITC (552 nm). The Z stacking of confocal images at 3- to 5-μm intervals contained all the levels of positively stained cells and processes.

Detection of ICC apoptosis

To detect the apoptosis of ICC, TUNEL labeling was done using an apoptosis detection Kit (Roche). Whole-mount preparations were fixed with 4% paraformaldehyde for 20 min at 25°C, washed twice with PBS for 30 min, and then treated with 0.1% Triton X-100 for 20 min on ice (2–8°C). The whole-mount preparations were incubated with TUNEL reaction buffer containing 45 μL of the labeling solution and 5 μL of the enzyme solution at 37°C for 1 h in a humidified atmosphere in the dark. Sections were then washed three times for 15 min each with PBS to remove unincorporated fluorescein-dUTP. The specimens were observed with a fluorescence microscope with an excitation wavelength in the range of 450–500 nm.

Detection of proliferating ICC

To identify the proliferation of ICC, daily intraperitoneal injection of BrdU (10 mg kg^{-1} day^{-1}, Sigma) was given

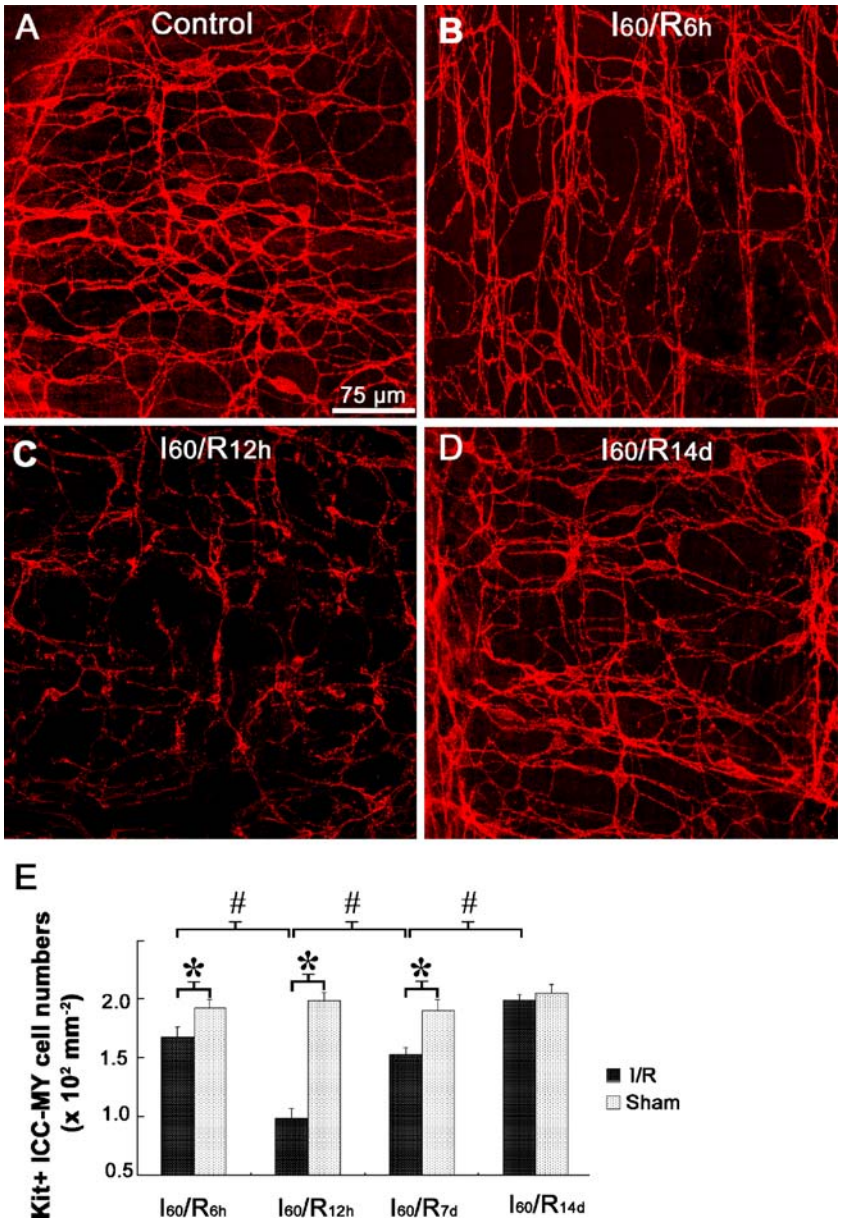

Fig. 1 Confocal images of ICC-MY labeled with ACK2 (*red*) on whole-mount preparations of the small intestine showing the alterations of ICC in the intestinal I/R injury model (**a**–**d**). **a** ICC project their cytoplasmic processes to form an intact cellular network in the control tissue. **b** The Kit+ cells are almost intact after reperfusion for 6 h (I_{60}/R_{6h}; **b**) and these cells are obviously reduced following I_{60}/R_{12h} injury (**c**). **d** A dramatic recovery of ICC is seen in the I_{60}/R_{14d} injury group. **e** The graphs summarized the changes in mean (± SEM) Kit+ ICC-MY cell numbers after I/R insult in guinea pigs. *$P<$ 0.05 indicates significant differences between control and I/R group (n=3; SNK), and #$P<$ 0.05 (SNK) represents significant differences between I/R groups (n=3). *Scale bar* **a** refers to all panels

after I/R to each group of experimental animals. The animals were killed and specimens were stained for ACK2 (Kit) as described above, and then the whole-mount preparations labeled for BrdU as follows: The specimens were additionally fixed in 4% paraformaldehyde in 0.1 M PB at pH 7.2 for 30 min. After rinsing in PBS, the specimens were treated with 2 N HCl for 30 min at 37°C for partial denaturalization of double-stranded DNA. To reveal BrdU, the specimens were incubated with a mouse monoclonal antibody raised against BrdU (3 μg ml^{-1}; DAKO) overnight at 4°C and then a FITC-conjugated secondary antibody (antimouse IgG, 1:100; DAKO).

Measurement and statistical analysis

Photographs of either Kit-positive cells, Kit/TUNEL, or Kit/BrdU double-labeled cells were taken in ten random 0.2607-mm^2 fields (×200 magnification) per whole-mount preparation with a digital camera (SPOT, Diagnostic Instruments, Inc) mounted on a BX51 fluorescence micro-

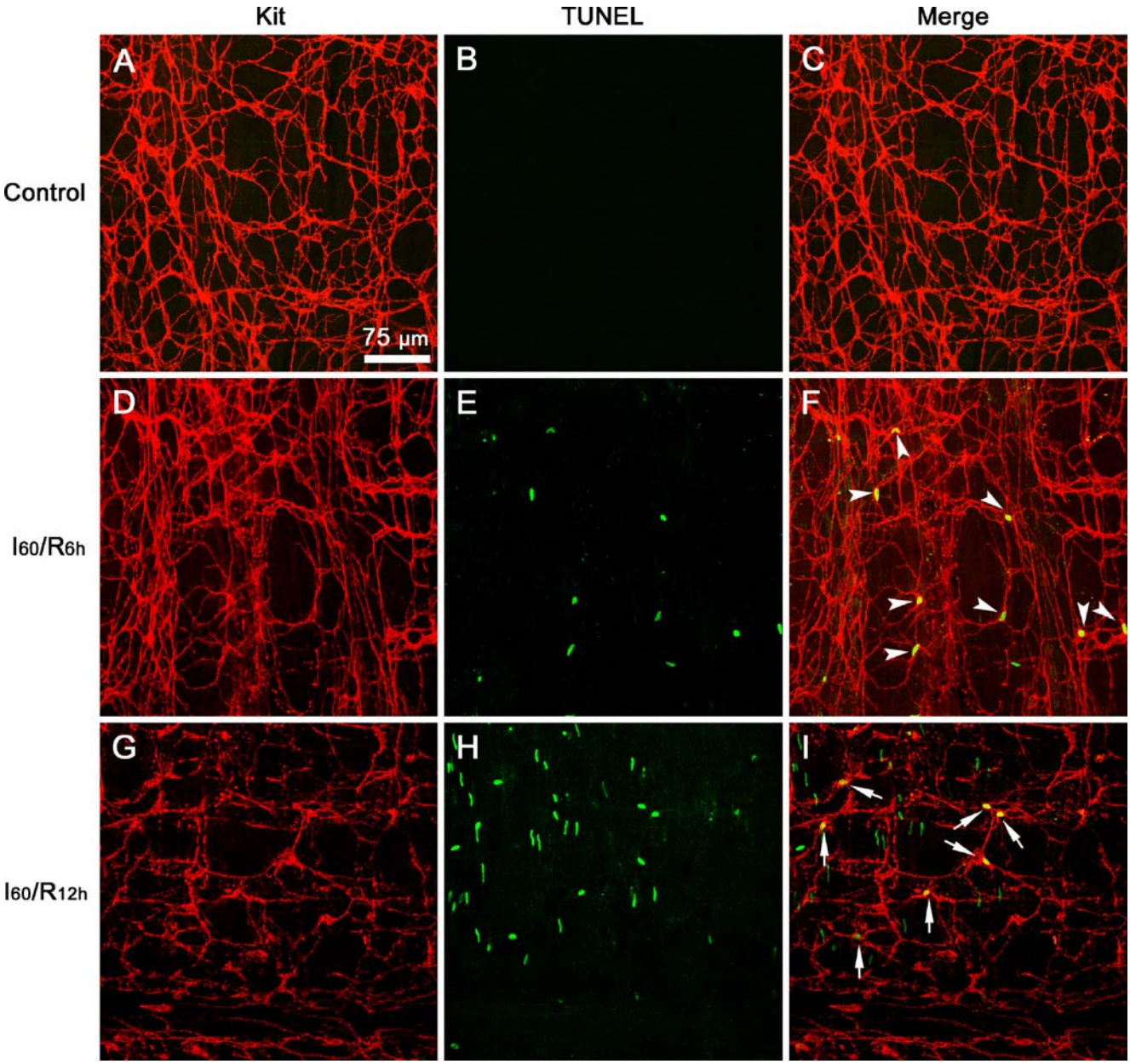

Fig. 2 Confocal photomicrographs showing presumptive apoptotic ICC on whole-mount preparations from the ileum after I/R insult (**a**–**i**). **a**–**c** Kit (*red*)/TUNEL (*green*) double labeling shows that no apoptotic cell is observed in the ICC-MY of control group. **d**–**f** The Kit+(*red*) ICC-MY are almost intact in the I_{60}/R_{6h} group; however, a number of Kit/TUNEL(*green*) double labeling ICC-like cells are visible (*arrowheads*). **g**–**i** The Kit+ ICC-MY networks (*red*) are incomplete following I_{60}/R_{12h} injury with a number of apoptotic ICC (*arrows*). Scale bar **a** refers to all panels

scope (OLYMPUS, Japan). The cell numbers were counted with Image-Pro Plus 5.0 (Media Cybernetics). Five intestinal segments from each experimental animal were sampled for immunofluorescent staining. Data were expressed as means±standard error of the mean (SEM). The *n* value reported in the text refers to the number of animals used. Differences in the data were evaluated by one-way analysis of variance followed by a Student–Newman–Keul's (SNK) post hoc test and $P \leq 0.05$ was taken as a statistically significant difference.

Results

Changes in ICC morphology and density

ICC-MY were located between the longitudinal and circular smooth muscle layers and around the myenteric plexus of the small intestinal wall; cells were revealed by Kit immunohistochemistry in confocal whole-mount preparations (Fig. 1a) that clearly showed ICC processes and numerous branches forming a cellular network in the control. In the I_{60}/R_{6h} group, the density of Kit+ ICC-MY slightly decreased (167.5±8.4 mm^{-2}), and an almost intact cellular networks could be observed (Fig. 1b, e). In the I_{60}/R_{12h} group the density of Kit+ cell numbers were significantly reduced by ~50% compared with the control values (97.6±8.6 mm^{-2}) along with a reduction in the density and thickness of the cellular processes (Fig. 1c, e). Kit+ cell density had partially recovered after 7 days of reperfusion but was still significantly lower than control cell numbers (152.2±6.4 mm^{-2}; Fig. 1e). However, Kit+ cell numbers had recovered to control values and also the cellular networks had restored after 14 days reperfusion (I_{60}/R_{14d} injury; Fig. 1d, e).

Detection of the apoptosis

Apoptosis was detected by the TUNEL method. In control preparations, no cell was labeled by TUNEL method in the intestinal wall on whole-mount preparations (Fig. 2a–c). In the I_{60}/R_{6h} group, the Kit+ ICC-MY networks seemed to be intact; however, a number of Kit+/TUNEL+ (16.7± 3.4 mm^{-2}) were observed which located within the ICC-MY which had identical features with normal ones (Fig. 2d–f; Table 1). The Kit+ cellular networks were incomplete in the I_{60}/R_{12h} injury group, and a number of apoptotic Kit+ ICC were observed (17.4±4.2 mm^{-2}; Fig. 2g–i; Table 1). Kit/vimentin/TUNEL triple labeling showed that those Kit+/TUNEL+ cells were labeled by vimentin in ICC-MY. Some of these cells had long branching processes within ICC-MY (Fig. 3a–d) which were similar in features with normal mature cells, while others had shortened processes with fewer branches (Fig. 3e–h) and probably represented different stages of apoptosis, i.e., those cells with shorter processes were at later stages of apoptosis. In addition, a number of β-tublin III+ enteric neurons which distributed within the myenteric plexus (Fig. 4a–c) and a small number of α-SMA-labeled SMC (Fig. 4d–f) were also marked by TUNEL which hinted that the apoptosis of SMC and enteric neurons were also involved. The quantitative data showed that there were about 17–18 mm^{-2} apoptotic Kit+ cells found in the ICC-MY in either I_{60}/R_{6h} or I_{60}/R_{12h} group (Table 1), and about 10% SMC and 7% enteric neurons were also labeled by TUNEL which suggested that the apoptosis of SMC and enteric neurons was also involved in the I/R injury.

Proliferation of ICC

We used double immunofluorescent staining with anti-Kit/BrdU to reveal the presence of ICC proliferation. Kit/BrdU ICC-MY-like cell labeling was neither seen in the control tissue nor was present 6 and 12 h after reperfusion. However, proliferative cells were frequently seen at 7 days (10.6± 1.1 mm^{-2}) and represented ~5% of the population. This figure was increased by ~2.5 times in the I_{60}/R_{14d} injury group (25.7±4.1 mm^{-2}; Table 1). Cell counting showed that the BrdU+ cells in the ICC-MY represented ~13% of the total Kit-positive cells at the level of myenteric plexus in the I_{60}/R_{14d} injury group. The distribution in many cases was characterized by pairs of cell bodies with processes, and single isolated cells were also observed (Fig. 5a–c). In ICC-DMP, the Kit/BrdU double-labeled cells were often distrib-

Table 1 Mean density of Kit+/TUNEL+ and Kit+/BrdU+ cells in the ICC-MY in the intestinal I/R injury guinea pig model

	I_{60}/R_{6h}	I_{60}/R_{12h}	I_{60}/R_{7d}	I_{60}/R_{14d}
	I/R	I/R	I/R	I/R
Kit+/TUNEL+ cells (mm^{-2}; N=3)	16.7±3.4	17.4±4.2	0*	0
Kit+/BrdU+ cells (mm^{-2}; N=3)	0	0	10.6±1.1*	25.7±4.1

Neither $Kit^+/TUNEL^+$ nor $Kit^+/BrdU^+$ cell was found in control. Data given as mean ± SEM.
N numbers of animals used
*$P<0.05$ (SNK) significantly different to earlier time point (e.g., I_{60}/R_{7d} vs. I_{60}/R_{12h})

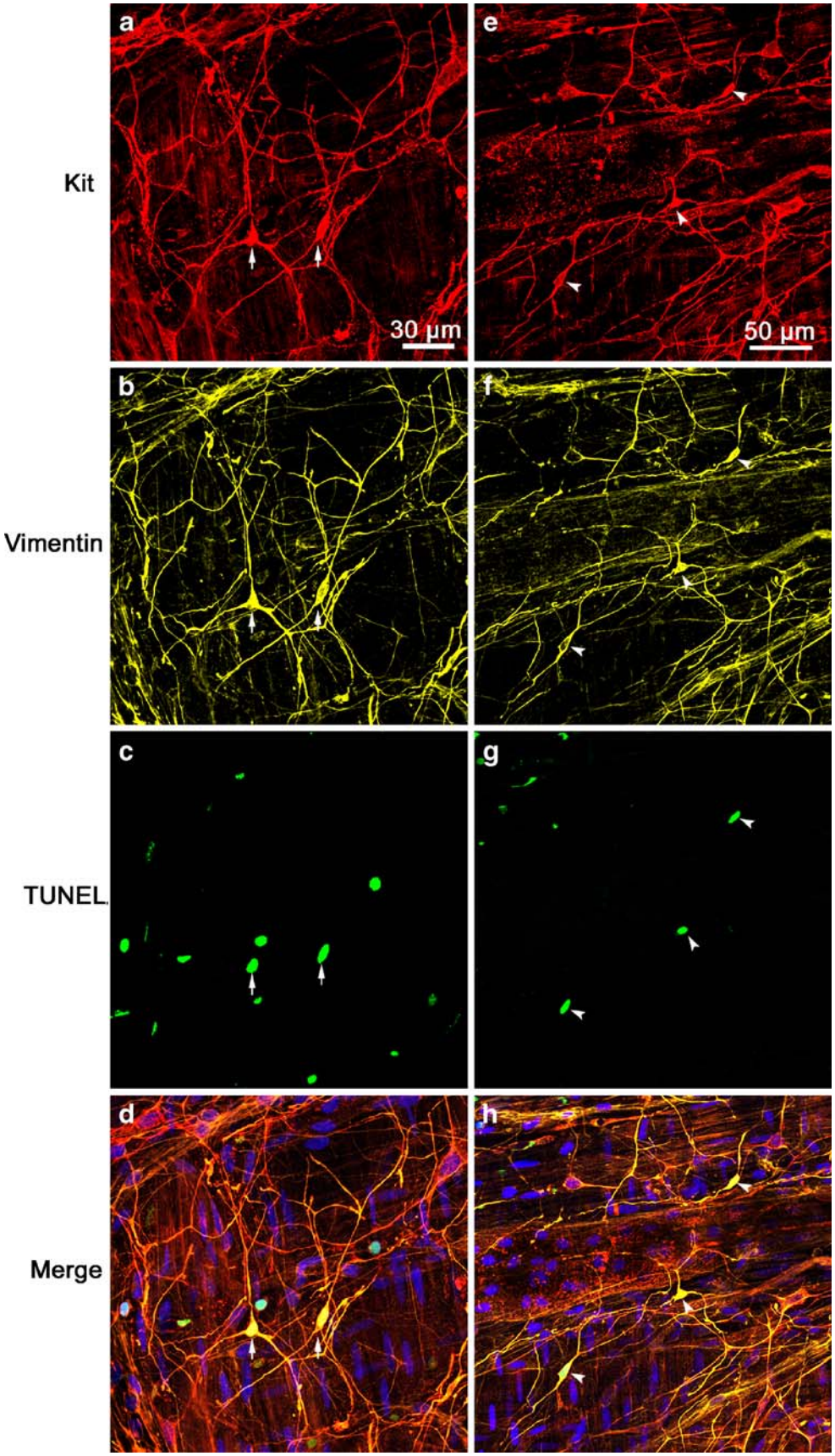

Fig. 3 Confocal images of ICC-MY labeled with Kit (*red*), vimentin (*yellow*), and TUNEL (*green*) on whole-mount preparations of the ileum counterstained with DAPI (*blue*) in the I_{60}/R_{12h} injury group (**a**–**h**). **a**–**d** A few Kit-/vimentin-positive cells are visible with long processes with branches and are labeled by TUNEL (*arrows*). **e**–**h** Tissue is shown at lower magnification that some of the Kit-/vimentin-/TUNEL-positive cells have more shortened processes with fewer branches (*arrowheads*) suggesting a later stage of apoptosis. *Scale bar*=30 (**a**–**d**) and 50 μm (**e**–**h**)

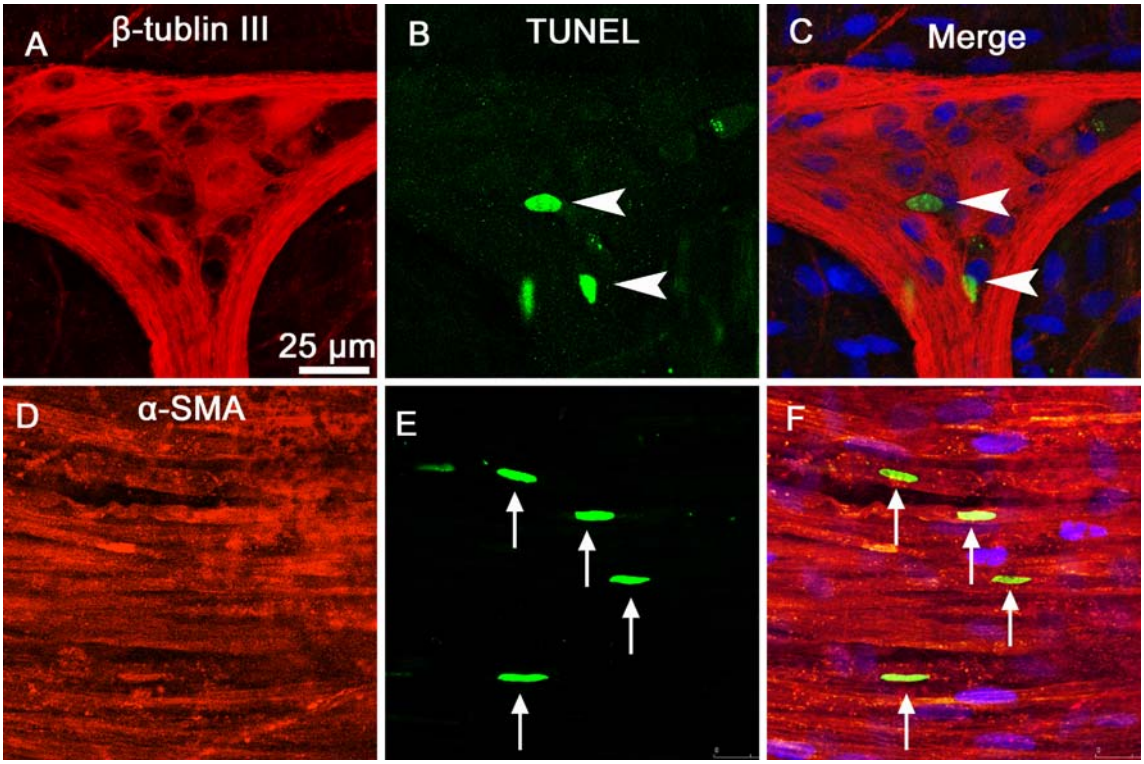

Fig. 4 Confocal photomicrographs showing the TUNEL-positive enteric neurons (**a**–**c**) and smooth muscle cells (**d**–**f**) labeled by anti-β-tublin III and anti-α-SMA antibodies respectively on whole-mount preparations of the ileum counterstained with DAPI (*blue*) from I_{60}/R_{12h} injury animals. **a**–**c** Several β-tublin III (*red*) and TUNEL (*green*)-double-positive cells (*arrowheads*) are present. Note, β-tublin III immunoreactivity does not stain nuclei, thus is clearly differentiated from the nuclear TUNEL label. Cells were also present after double labeling (*arrows*) with α-SMA (*red*) and TUNEL (*green*; **d**–**f**). *Scale bar* **a** refers to all panels

uted in pairs (Fig. 5d–f), and they had relatively round cell bodies and long slender processes which could be identified as ICC-DMP according to their features, although less and thinner processes were seen comparing with mature ones.

Discussion

The present study demonstrates that (1) the Kit-positive ICC numbers are reduced after the intestinal I/R injury but make a dramatic recovery; (2) the I/R injury can lead to the apoptosis of ICC, SMC, and enteric neurons; (3) proliferation of ICC is involved in the recovery of the ICC. It has been reported that I/R injury can lead to gastrointestinal dysfunctions, such as a delay in gastrointestinal transit [3, 4], alterations of the migrating motor complex [5], and alterations in in vivo motor responsiveness to pharmacological stimulation [6]. In addition, in vitro experiments reveal a reduction in mechanical contraction of the smooth muscle layers [1], although the underlying mechanisms are not clearly understood. In partial agreement with the present data, a rat intestinal I/R injury model has revealed that a loss of Kit+ ICC is concomitant with the weakening of spontaneous mechanical contractions, presumably driven by ICC, which subsequently recover to normal as well as ICC Kit labeling. On this basis, it has been suggested that ICC play a central role in I/R-caused motility disorders [2]. In support of this hypothesis, our results also show a 50% decrease of Kit+ cell numbers in ICC-MY in the intestinal I/R guinea pig model. A loss and reappearance of Kit expression maybe one of the underlying mechanisms associated with motility disorders such as that has been suggested by intestinal obstruction [19] and surgical resection models [18]. Others have postulated that the loss of Kit may lead to transdifferentiation of ICC toward a smooth muscle cell phenotype on the basis of Kit signaling blockade experiments in the neonatal mice with an anti-Kit antibody [27]. Therefore, we have stained our tissue using anti-Kit and anti-α-SMA (a special marker of SMC) for cells in a transdifferentiation stage where both proteins might be present. Double-labeled cell is not seen and thus, it seems not to support a case for ICC transdifferentiation toward a SMC phenotype under our experimental conditions (supplemental Fig. 2A–C). However, as α-SMA is not an established marker for those transdifferentiated cells, a further observation under electron microscopy would be necessary to exclude or include this possibility.

Is the switch of Kit expression the only explanation for the alteration of Kit+ ICC as suggested in a rat model of I/R injury? It should be noted that in animal models of I/R injuries

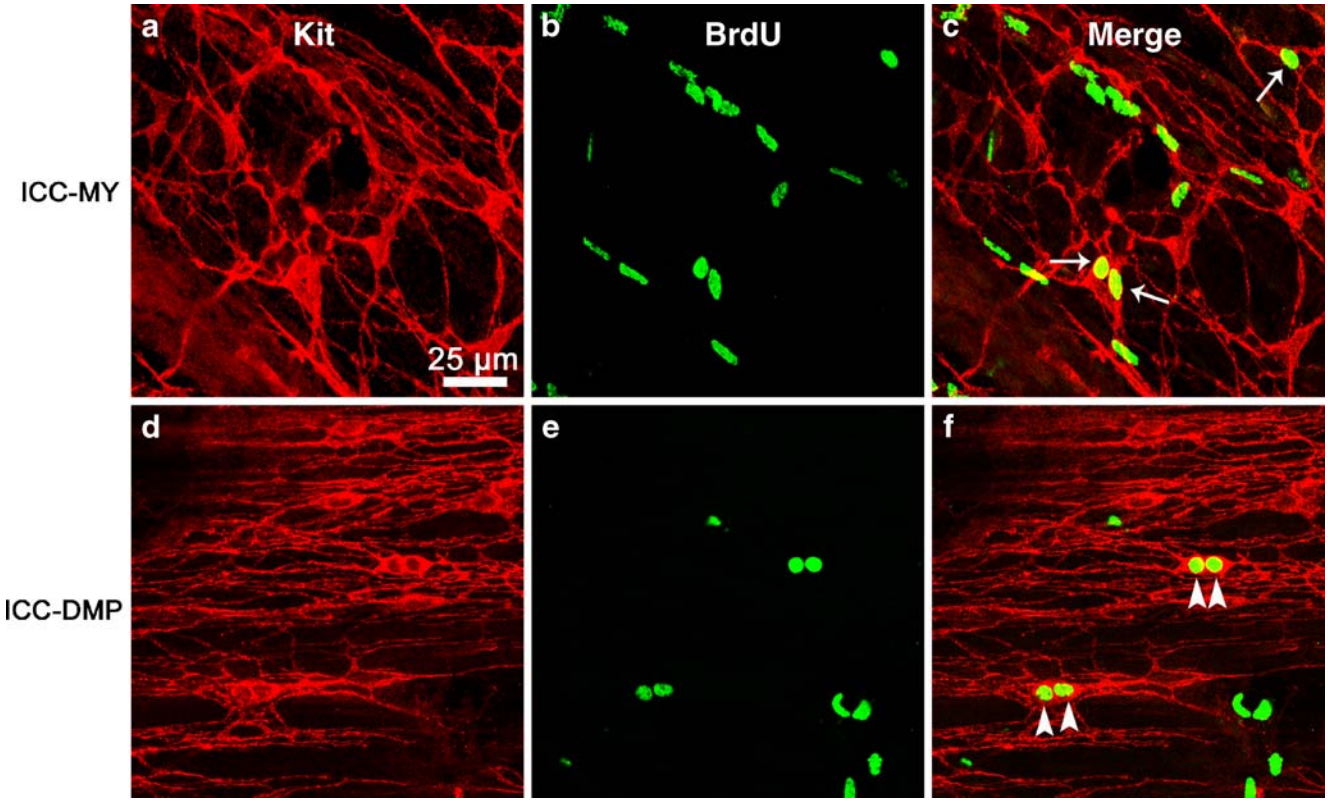

Fig. 5 Confocal photomicrographs showing presumptive proliferating ICC on whole-mount preparations from the ileum in I_{60}/R_{14d} injury group. **a**–**c** A number of double labeled of Kit (*red*) and BrdU (*green*) cells (*arrows*) that have processes with branches are present in the ICC-MY and resemble normal mature cells. **d**–**f** The Kit(+)/BrdU(+) cells often distribute in pairs in ICC-DMP, with closely adjacent cell bodies (*arrowheads*). *Scale bar* **a** refers to all panels

to the liver [21], kidney [22], heart [28], and lung [24], as well as intestine [23], apoptosis is often present in the tissues. We have confirmed these previous results showing cell death by using TUNEL methodology and about 10–15% of the apoptotic Kit+ cells are at an early stage after I/R. Vimentin, structural protein, is colocalized with Kit in ICC [26]. The Kit/vimentin/TUNEL labeling cells further confirm a true loss of ICC which suggests that the apoptosis of ICC is also involved in the cell number reduction as well as the reduction of Kit expression. Besides that, it should be noted that apoptotic ICC might cease Kit expression at certain stage; therefore, those Kit+/TUNEL+ cells may only represent a part of apoptotic ICC. In addition, a number of SMC and enteric neurons are also labeled by TUNEL. Therefore, a conclusion is made that the intestinal motility dysfunctions that caused by I/R injury could be interpreted as a compound result of both the Kit expression reduction and the apoptosis of ICC, SMC, and enteric neurons.

Our findings confirm, by using BrdU incorporation, that there is a restoration of the Kit+ ICC cell numbers in both ICC-MY and ICC-DMP, at least in part, via proliferation for at least 7 days after an I/R insult in the adult guinea pig. We do not find out the presence of cell proliferation (Kit/BrdU double-labeled ICC-like cells) in the control tissue over a similar time period. Similarly, our recent findings also have indicated that an age-dependent proliferation is involved in the expansion of ICC cell number in the murine small intestine aged from postpartum days 0 to 16, and the proliferation vanishes in adult mice [29], and under in vitro culture conditions, only ICC from neonatal mice before day 6 postpartum can proliferate in response to Kit ligand which also suggests a time-limited proliferation of ICC [30]. Therefore, it seems that ICC or ICC progenitor do not proliferate generally in adult animals as shown in our previous work [25].

The present study has shown that proliferation takes a part in the restoration of ICC after loss. One question is what kind of causes probably promote the proliferation? ICC are actually reduced in number by apoptosis and this suggests that the recovery of ICC is due at least in part to generation of new ICC. A number of reduced ICC may cease expression of Kit and change into a kind of intermediate fibroblast-like cells after insult and, in all likelihood, only Kit expression resumption is involved in their recovery.

Another question is what kind of cells may have given rise to the proliferation? A recent study has successfully identified a very small group of $Kit^+/CD44^+/CD34^+$/insulin $receptor^+$/insulin-like growth factor I receptor $(IGF\text{-}IR)^+$ cells in murine stomach as the putative progenitors of ICC

which could be expanded under the stimulation of Kit ligand, stem cell factor, and further transdifferentiate into mature ones [31], and similarly, our recent study has also shown that a number of Kit+/BrdU+ cells (new-emerged ICC) which appear during postnatal development in the murine small intestine are also labeled with anti-CD44, CD34, and IGF-IR antibodies. Therefore, it is likely that those new-emerged ICC (Brdu+/Kit+ cells) after ICC loss in adult animals originate from the proliferation and differentiation of progenitor cells in this case, although this hypothesis needs to be proved by further investigations.

Acknowledgments This work was supported in parts by the national key basic research program of China (2007CB512401), grants no. 30800982 from the National Science Foundation of China (NSFC) and Natural Science Foundation Project of CQ CSTC (2008BB5280). We thank Dr. Thomas FitzGibbon for comments and discussion on earlier drafts of the manuscript, and also, we are grateful to Wei Sun and Li-ting Wang (Central laboratory, Third Military Medical University) for their help with confocal laser scanning microscopy.

Conflict of interest statement We declare that we have no conflict of interest.

References

1. Hierholzer C, Kalff JC, Audolfsson G (1999) Molecular and functional contractile sequelae of rat intestinal ischemia/reperfusion injury. Transplantation 68:1244–1254
2. Shimojima N, Nakaki T, Morikawa Y (2006) Interstitial cells of Cajal in dysmotility in intestinal ischemia and reperfusion injury in rats. J Surg Res 135:255–261
3. Udassin R, Eimerl D, Schiffman J (1995) Postischemic intestinal motility in rat is inversely correlated to length of ischemia. An in vivo animal model. Dig Dis Sci 40:1035–1038
4. Hassoun HT, Weisbrodt NW, Mercer DW (2001) Inducible nitric oxide synthase mediates gut ischemia/reperfusion-induced ileus only after severe insults. J Surg Res 97:150–154
5. Hebra A, Hong J, McGowan KL (1994) Bacterial translocation in mesenteric ischemia–reperfusion injury: is dysfunctional motility the link. J Pediatr Surg 29:280–285
6. Ballabeni V, Barocelli E, Bertoni S (2002) Alterations of intestinal motor responsiveness in a model of mild mesenteric ischemia/reperfusion in rats. Life Sci 71:2025–2035
7. Ward SM, Sanders KM (2001) Physiology and pathophysiology of the interstitial cell of Cajal: from bench to bedside. I. Functional development and plasticity of interstitial cells of Cajal networks. Am J Physiol Gastrointest Liver Physiol 281:G602–G611
8. Rumessen JJ, Thuneberg L (1996) Pacemaker cells in the gastrointestinal tract: interstitial cells of Cajal. Scand J Gastroenterol Suppl 216:82–94
9. Huizinga JD, Berezin I, Chorneyko K (1998) Interstitial cells of Cajal: pacemaker cells. Am J Pathol 153:2008–2011
10. Thomsen L, Robinson TL, Lee JC (1998) Interstitial cells of Cajal generate a rhythmic pacemaker current. Nat Med 4:848–851
11. Huizinga JD, Thuneberg L, Kluppel M (1995) W/kit gene required for interstitial cells of Cajal and for intestinal pacemaker activity. Nature 373:347–349
12. Ward SM, McLaren GJ, Sanders KM (2006) Interstitial cells of Cajal in the deep muscular plexus mediate enteric motor neurotransmission in the mouse small intestine. J Physiol 573:147–159
13. Rumessen JJ, Mikkelsen HB, Thuneberg L (1992) Ultrastructure of interstitial cells of Cajal associated with deep muscular plexus of human small intestine. Gastroenterol 102:56–68
14. Zhou DS, Komuro T (1992) Interstitial cells associated with the deep muscular plexus of the guinea-pig small intestine, with special reference to the interstitial cells of Cajal. Cell Tissue Res 268:205–216
15. Ward SM, Burns AJ, Torihashi S (1994) Mutation of the proto-oncogene c-kit blocks development of interstitial cells and electrical rhythmicity in murine intestine. J Physiol 480:91–97
16. Kluppel M, Huizinga JD, Malysz J (1998) Developmental origin and Kit-dependent development of the interstitial cells of Cajal in the mammalian small intestine. Dev Dyn 211:60–71
17. Beckett EA, Ro S, Bayguinov Y (2007) Kit signaling is essential for development and maintenance of interstitial cells of Cajal and electrical rhythmicity in the embryonic gastrointestinal tract. Dev Dyn 236:60–72
18. Yanagida H, Yanase H, Sanders KM (2004) Intestinal surgical resection disrupts electrical rhythmicity, neural responses, and interstitial cell networks. Gastroenterol 127:1748–1759
19. Chang IY, Glasgow NJ, Takayama I (2001) Loss of interstitial cells of Cajal and development of electrical dysfunction in murine small bowel obstruction. J Physiol 536:555–568
20. Ekblad E, Sjuve R, Arner A (1998) Enteric neuronal plasticity and a reduced number of interstitial cells of Cajal in hypertrophic rat ileum. Gut 42:836–844
21. Nakajima H, Mizuta N, Fujiwara I (2008) Blockade of the Fas/Fas ligand interaction suppresses hepatocyte apoptosis in ischemia–reperfusion rat liver. Apoptosis 13:1013–1021
22. Nogae S, Miyazaki M, Kobayashi N (1998) Induction of apoptosis in ischemia–reperfusion model of mouse kidney: possible involvement of Fas. J Am Soc Nephrol 9:620–631
23. Luo CC, Shih HH, Chiu CH (2004) Reduced apoptosis in newborn compared to adult rat intestine after ischemia–reperfusion injury. Biol Neonate 85:90–93
24. Stammberger U, Gaspert A, Hillinger S (2000) Apoptosis induced by ischemia and reperfusion in experimental lung transplantation. Ann Thorac Surg 69:1532–1536
25. Mei F, Yu B, Ma H (2006) Interstitial cells of Cajal could regenerate and restore their normal distribution after disrupted by intestinal transection and anastomosis in the adult guinea pigs. Virchows Arch 449:348–357
26. Komuro T, Zhou DS (1996) Anti-c-kit protein immunoreactive cells corresponding to the interstitial cells of Cajal in the guinea-pig small intestine. J Auton Nerv Syst 61:169–174
27. Torihashi S, Nishi K, Tokutomi Y (1999) Blockade of kit signaling induces transdifferentiation of interstitial cells of Cajal to a smooth muscle phenotype. Gastroenterol 117:140–148
28. Yoshida H, Zhang JJ, Chao L (2000) Kallikrein gene delivery attenuates myocardial infarction and apoptosis after myocardial ischemia and reperfusion. Hypertens 35:25–31
29. Mei F, Zhu J, Guo S (2009) An age-dependent proliferation is involved in the postnatal development of interstitial cells of Cajal in the small intestine of mice. Histochem Cell Biol 131:43–53
30. Nakahara M, Isozaki K, Vanderwinden JM (2002) Dose-dependent and time-limited proliferation of cultured murine interstitial cells of Cajal in response to stem cell factor. Life Sci 70:2367–2376
31. Lorincz A, Redelman D, Horvath VJ (2008) Progenitors of interstitial cells of Cajal in the postnatal murine stomach. Gastroenterol 134:1083–1093

Virchows Arch (2009) 454:411–419
DOI 10.1007/s00428-009-0726-x

ORIGINAL ARTICLE

The detection of CD14 and CD16 in paraffin-embedded bone marrow biopsies is useful for the diagnosis of chronic myelomonocytic leukemia

Marwan Qubaja · Béatrice Marmey · Agnès Le Tourneau · Stéphanie Haiat · Dominique Cazals-Hatem · Bettina Fabiani · Jacques Diebold · Jean-Pierre Marie · Josée Audouin · Frédéric Geissmann · Thierry Jo Molina

Received: 10 July 2008 / Revised: 17 November 2008 / Accepted: 6 January 2009 / Published online: 26 February 2009

Abstract Histopathological study of bone marrow biopsy (BMB) in chronic myelomonocytic leukemia (CMML) is often difficult and might benefit from an immunohistochemical approach. We immunostained 15 cases of CMML, focusing at two new antibodies staining for CD14 and CD16 on paraffin-embedded tissues. CD68 (KP1), CD68 (PG-M1), and CD163 were not differentially expressed between CMML and chronic myelogenous leukemia (CML). In CMML BMB, we found a significant increase in the number of $CD14^+$ monocytes. This increase was made of dispersed cells in the interstitium, often exhibiting bilobated nuclei, and being difficult to differentiate from neutrophils. There was no expansion of $CD16^+$ monocyte-like cells. However, we found a significant decrease in the number of granulocytes expressing CD16, MPO, and CD15 in CMML compared to CML and control BMB, probably related to dysgranulopoiesis. Indeed, BMB immunohistochemistry can be helpful in CMML by identifying both the monocyte expansion with CD14 and the dysgranulopoiesis with CD16.

Keywords Bone marrow biopsy · Chronic myelomonocytic leukemia · Monocytes · CD14 · CD16 · Dysgranulopoiesis

Introduction

Chronic myelomonocytic leukemia (CMML) is a clinico-pathological entity defined within the World Health

M. Qubaja · B. Marmey · A. Le Tourneau · J. Diebold · J. Audouin · T. J. Molina (✉)
Service d'Anatomie et de Cytologie Pathologiques "Jacques Delarue", AP-HP, Hôtel Dieu,
1, Place du Parvis Notre-Dame,
75181 Paris Cedex 04, France
e-mail: thierry.molina@htd.aphp.fr

M. Qubaja · B. Fabiani · J.-P. Marie
Université Pierre et Marie Curie,
Paris, France

A. Le Tourneau · J. Diebold · J. Audouin · F. Geissmann · T. J. Molina
Faculté de Médecine,
Université Paris Descartes,
Paris, France

S. Haiat · J.-P. Marie
Service d'Hématologie clinique, Hôtel Dieu,
Paris, France

F. Geissmann · T. J. Molina
INSERM, U838, Institut Necker-Enfants Malades,
Paris, France

D. Cazals-Hatem
Service d'Anatomie Pathologique,
Université Paris Diderot; AP-HP, Hôpital Beaujon,
Paris, France

B. Fabiani
Service d'Anatomie Pathologique,
AP-HP, Hôpital Saint-Antoine,
Paris, France

Organization (WHO) category of myelodysplastic/myeloproliferative neoplasms (MDS/MPN) [1, 2]. Indeed, although around 3% of cases have been demonstrated to bear jak2 mutation [3], there are no recurrent genetic abnormalities. This disease is defined as a clonal disorder of a bone marrow stem cell, accompanied by evidence of both effective (myeloproliferative) and ineffective (myelodysplastic) hematopoiesis. The bone marrow of CMML is usually hypercellular and shows a significant increase in granulocytic proliferation with a variable degree of dysgranulopoiesis [1, 4–6]. Prominent dysplastic changes in the erythroid and megakaryocytic lineages may be encountered, but these cell types are often normal in appearance [1]. The WHO diagnostic criteria for CMML are mainly based on findings encountered in the peripheral blood and bone marrow aspirate. The presence of peripheral blood monocytosis is mandatory for the diagnosis of CMML, but is not specific for this entity. Human peripheral blood monocytes are distributed between a major population $CD14^{+}$ $CD16^{-}$ representing 90–95% of total blood monocytes and a minor population $CD14^{low}$ $CD16^{+}$, which represents 5–10% of total blood monocytes [7]. CD14 is considered as a good marker of the major monocyte population and can be now evaluated on paraffin-embedded tissue. Although flow cytometry has demonstrated a moderate increase of $CD14^{+}$ cells in CMML [8], the level and pattern of monocytic proliferation in the marrow of patients has not been clearly established, particularly due to the presence of marked granulocytic proliferation with dysgranulopoiesis difficult to distinguish from the monocytic population particularly on bone marrow biopsy (BMB). The diagnostic features of CMML on BMB are difficult to differentiate from other myelodysplastic syndromes or myeloproliferative neoplasms. Recently, Orazi et al. [9] have demonstrated the interest of BMB for the diagnosis of CMML showing an accumulation of CD123-positive plasmacytoid dendritic cells as a diagnostic feature of this entity. However, although specific, this expansion is not encountered in 80% of CMML cases [9]. In this study, we aimed to examine the value of CD14 and CD16 staining in BMB from patients with CMML and to compare it with other antibodies staining monocyte-derived cells.

Materials and methods

Bone marrow specimens were obtained from the Department of Pathology of Hôtel Dieu Hospital, Paris. All biopsies were fixed in Bouin's solution and decalcified in RDO (Eurobio, France). Fifteen cases of CMML-1 and ten cases of CML classified according to the WHO classification were studied [1]. In addition, eight "normal" bone marrow biopsies performed for the initial staging of either Hodgkin's disease (n=5) or follicular lymphoma (n=3) were used as controls. As immunohistochemical controls, we also studied bone marrow biopsies fixed in buffered formalin and decalcified in EDTA (five CML, four CMML, and five normal).

Single immunostaining procedure

The primary antibodies used are summarized in Table 1. Sections were deparaffinized and pretreated by microwave (750 W, 3×5 mn) in citrate buffer, pH 6, except for MPO, performed without pretreatment. After inhibition of endogeneous peroxidase, sections were immunostained as reported previously [10] using an indirect immunoperoxidase method. The primary antibodies were incubated at dilutions comprised between 1:50 and 1:900. Biotinylated goat anti-rabbit and anti-mouse IgG (AbCys, Paris, France) was added at 1:200 dilution for 20 min, followed by 20 min avidin–biotin–peroxidase complex (AbCys, Paris, France). Peroxidase activity was revealed using diaminobenzidine (DakoCytomation, Trappes, France), and the sections were mounted in Faramount (DakoCytomation). For all the antibodies, we evaluated the percentage of positively stained marrow cells in the most representative areas (with the optimal staining of internal positive control) by counting three consecutive high power fields (magnification ×100 with a total surface of 0.0432 mm^2) using a grid eyepiece. An average of 470 (±6.5) nucleated cells was counted. For CD163 and PG-M1, due to the staining of the long cytoplasmic dendrites of macrophages, only cytoplasmic and/or membrane positivity surrounding visible nuclei have been considered as positive. In addition, for CD15, CD16, and MPO, we also evaluated the percentage of positive cells out of 200 considering only polymorphonuclear granulocytes (pmns). The statistical analyses were performed using paired Student's t test.

Double immunostaining procedure

For CD14/PG-M1 double staining, sections were incubated with anti-CD14 mouse primary antibody for 2 h. The

Table 1 Antibodies used for the immunohistochemical study

Antibody	Dilution	Specificity	Source
NCL-CD14-223	1:50	CD14	Novocastra
Myeloperoxidase	1:400	Myeloperoxidase	Dako
PG-M1	1:50	CD68	Dako
KP1	1:50	CD68	Dako
10D6	1:900	CD163	Novocastra
80H5	1:50	CD15	Beckman Coulter
NCL-CD16	1:100	CD16	Novocastra
Ret40F	1:50	Glycophorin C	Dako

binding of anti-CD14 mouse antibody was revealed by biotinylated goat anti-rabbit and anti-mouse antibody (AbCys, Paris, France), followed by streptavidin–peroxidase complex (AbCys, Paris, France). The peroxidase activity was developed by using diaminobenzidine (DakoCytomation, Trappes, France). The endogeneous alkaline phosphatase was then inhibited by levamizole (SIGMA). Sections were then incubated with anti-CD68 (PG-M1) mouse antibody for 1 h. The binding of anti-CD68 antibody was revealed by rabbit anti-mouse antibody, followed by mouse alkaline phosphatase labeled antialkaline phosphatase (Dakocytomation) for 30 min. The alkaline phosphatase activity was developed using fuchsin substrate (DakoCytomation, Trappes, France). The same procedure described above was performed for the double staining CD14/CD15.

Results

Patient population

The median age of the fifteen CMML patients was 72 years (38–87 years); 11 were males and four were females. The median age of the ten CML was 52 years (25–77 years); six were males and four were females. The median age of the eight patients was 42 years (17–74 years); five were males and three were females.

Blood cell counts

In the CMML cases, the median WBC was 11.7 (±3.6)×10^9/l with a monocytosis median value of 2.7 (±1.5)×10^9/l. In the CML cases, the median WBC was 157 (±94.3)×10^9/l. Platelet counts were 228 (±178)×10^9/l in CMML whereas 825(±386)×10^9/l in CML.

Genetics

None of the CMML cases had the Philadelphia chromosome on caryotype or bcr-abl transcripts, whereas all the CML cases were tested positive.

Bone marrow histology

Most of the CMML cases and all the CML cases showed hypercellular marrow. Increased granulocytic proliferation was a common finding in both groups. Erythropoiesis was decreased significantly in the cases of CML. Dyserythropoiesis was seen in five out of the 15 CMML cases, demonstrated by the presence of numerous normoblasts with a left shift distribution of erythropoiesis. Megakaryocytes were increased in 11 out of the 15 CMML cases and in seven out of the ten CML cases. Dysmegakaryopoiesis was found in 13 out of the 15 CMML cases, which was characterized by the presence of micromegakaryocytes and/or megakaryocytes with abnormal nuclear lobation. Monocytes were, as usual, difficult to identify morphologically in the marrow of all groups. Dysgranulopoiesis was encountered in 12 out of the 15 CMML cases, represented by the presence of abnormal nuclear segmentation however difficult to evaluate on bone marrow biopsy. Neither the CMML nor the CML cases showed the presence of blastic clusters or sheets. Nodules of plasmocytoid monocytes were not seen in any of our CMML cases, confirmed by the absence of significant staining with CD123.

Immunohistochemistry results

Immunohistochemical patterns were comparable on Bouin's fixed and control formalin-fixed samples as shown for CD14 staining (see below) in CMML (Fig. 3e vs g) and CML (Fig. 3f vs h).

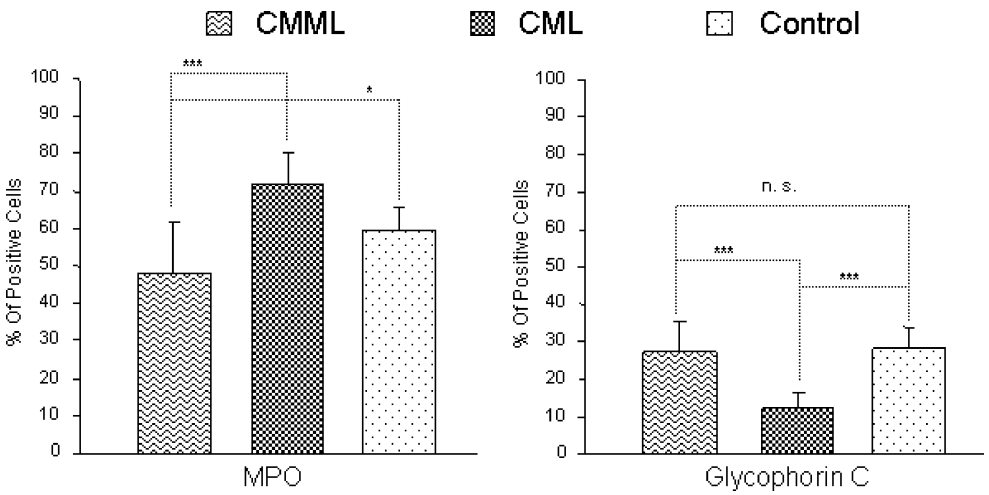

Fig. 1 Percentages of marrow cells positive with myeloperoxidase (*MPO*) and glycophorin C in CMML (n=15), CML (n=10), and control marrow biopsies (n=8). *p<0.05, **p<0.01, ***p<0.001. *n.s.* not significant; p>0.05

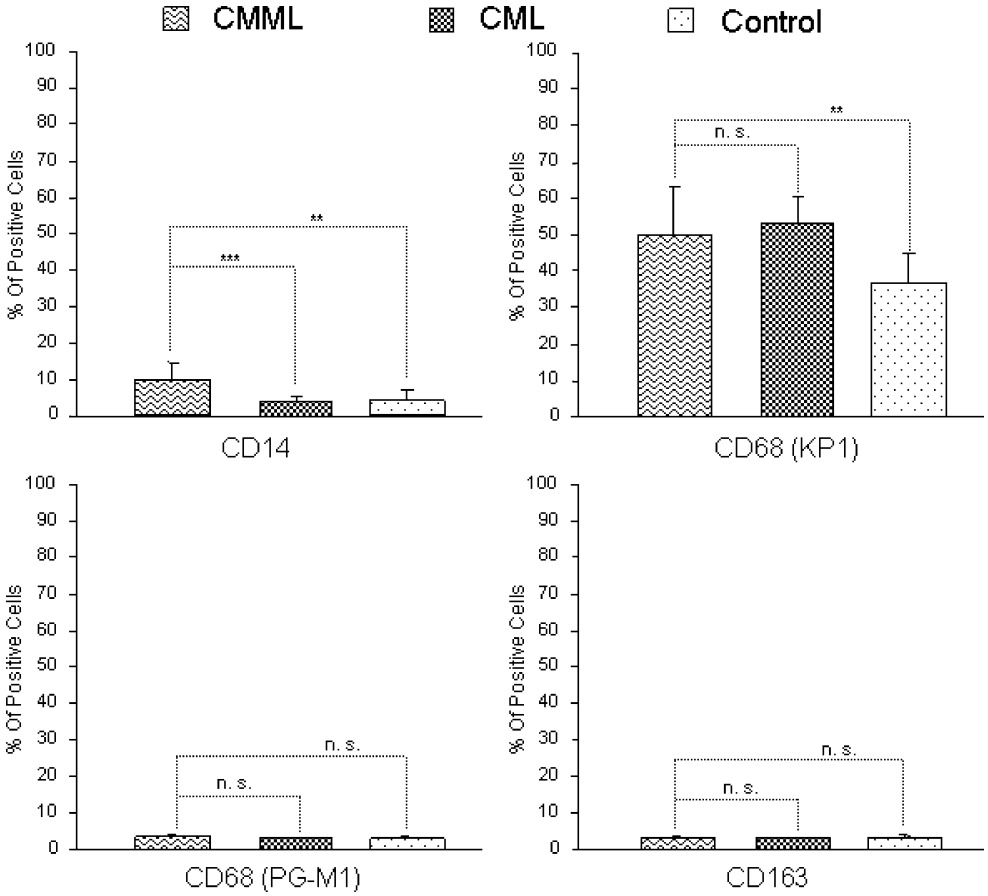

Fig. 2 Percentages of marrow cells positive with CD68/KP1 and CD68/PG-M1, CD163, and CD14 in CMML (n=15), CML (n=10), and control marrow biopsies (n=8). *p<0.05, **p<0.01, ***p<0.001. *n.s.* not significant; p>0.05

Evaluation of myeloid and erythroid populations

The percentage of MPO-positive cells was found to be strongly decreased in CMML (48±13.7%) compared to CML (71.5±8.8%; p<0.001) and even compared to control marrow biopsies (59±6%; p=0.05). Immunostaining with glycophorin C showed a significantly decreased number of erythroblasts only in the cases of CML (12.3±4.4%) compared to CMML (27.6±8%; p<0.001). The number of glycophorin-C-positive nucleated cells was not statistically different between CMML and control marrow biopsies, although dyserythropoiesis was present in one third of the CMML cases, the morphology of positive normoblasts being more left-shifted in CMML (Fig. 1).

Evaluation of macrophagic/monocytic populations

In the control cases, the anti-CD14 antibody stained cells often with indented nuclei or irregular nuclear contour with no signs of phagocytosis and sometimes with bilobated nuclei with a small but well-identified cytoplasm corresponding morphologically to monocytes (Figs. 2 and 3a**)**. These cells were often observed in the interstitium but rarely within the sinusoids. Granulocytes were not stained, and these CD14-positive bilobated cells, which were morphologically difficult to differentiate from neutrophils on sections, did not stain for CD15 as demonstrated by the double staining CD14/CD15 (Fig. 3b). CD14 did not stain macrophages on BMB. PG-M1 demonstrated clear cytoplasmic staining of macrophages but not of CD14-positive monocyte-like cells. Moreover, double staining PG-M1/CD14 identified clearly CD14-positive/PG-M1-negative monocytes (Fig. 3c). In the cases of CMML (Fig. 3d, e, and g**)**, the percentage of CD14-positive cells was significantly higher

Fig. 3 **a** CD14 staining in control marrow. Note the positively stained cells often with irregular nuclear contours or sometimes with bilobated nuclei. Granulocytes are not stained. **b** CD14 (*brown*)/CD15 (*red*) double immunostaining in control BM. Monocytes (*arrows*), including those with bilobated nuclei, are positive for CD14 but negative for CD15, which is expressed by the granulocytes. **c** CD14 (*brown*)/PG-M1 (*red*) double immunostaining in control BM. Macrophages are positive for PG-M1 and negative for CD14. On the other hand, monocytes (*arrows*) are positive for CD14 and negative for PG-M1. **d** CD14 staining in CMML. The positively stained cells are numerous but dispersed and rarely in loose clusters. **e** CD14 staining in CMML. The positively stained cells often have bilobated nuclei. Granulocytes showing dysgranulopoiesis are negative for CD14 (*arrows*). **f** CD14 staining in CML. Few positively stained monocytes are seen. **g** CD14 staining in CMML, formalin-fixed bone marrow. Pattern comparable to **e**. **h** CD14 staining in CML, formalin-fixed bone marrow. Pattern comparable to **f** ▶

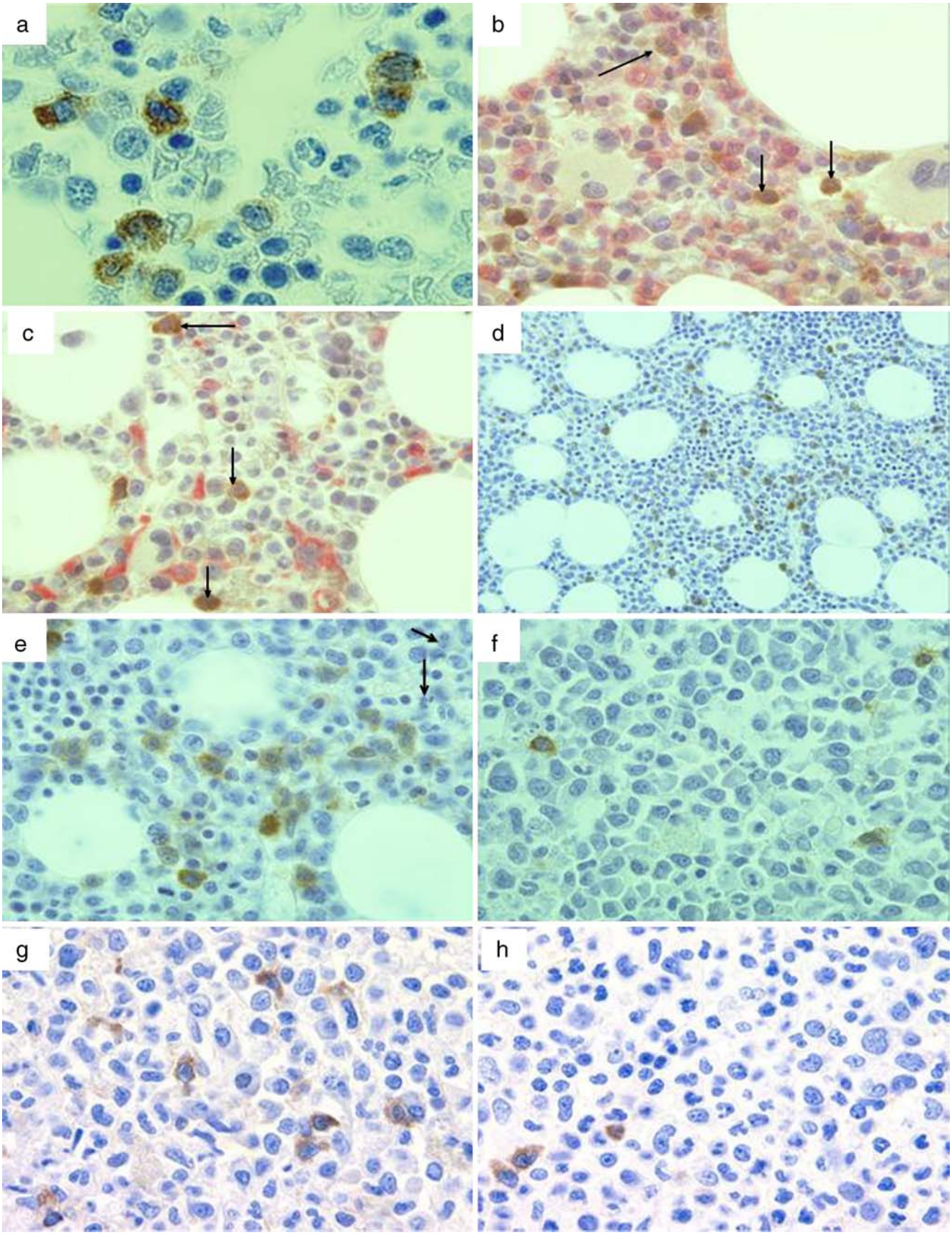
a
b
c
d
e
f
g
h

(10±4.5%) than in the cases of CML (3.6±1.6%; Fig. 3f and h) or control marrow biopsies (4.5±2.6%). This increase in CD14-positive cells in CMML is made of dispersed cells with rarely some loose clusters, but never organized in sheets. However, the CD14-positive cells on sections were very difficult to differentiate morphologically from pmns, particularly because of the dysgranulopoiesis (Fig. 3d, e, and g). The anti-CD16 antibody, although mainly stained granulocytes and in rare cases occasional macrophages, could identify very rare potential monocytes as suggested by the presence of few monocyte-like cells in the control cases. These cells had more or less rounded nuclei, and they represented less than 5% of the mononucleated cells in the control cases. There was no significant increase of these CD16-positive mononuclear cells in CMML (data not shown). The percentage of KP1-positive cells was not statistically different between CMML and CML cases. Numerous cells from the granulocyte lineage were positive with KP1 as well as macrophages, and it was very difficult to clearly identify monocytes. PG-M1 and CD163 staining were mainly restricted to macrophages, both in CMML and in CML and comparable to control.

Evaluation of granulocytic populations

Normal pmns expressed MPO, CD15, and CD16. We found out a significant decrease in the numbers of pmns expressing CD16 (65±21%) and MPO (75±25%) in CMML compared to CML or to control marrow biopsies where around 90% of the cells were positive (Figs. 4) and 5a–d). There was also a slight but significant decrease in the numbers of pmns expressing CD15 in CMML (Fig. 5e and f). Considering all the cases, there was a decrease of one of the three pmns markers in all of the 15 CMML cases and a decrease of two markers in ten out of the 15 CMML cases analyzed.

Discussion

We have evaluated the value of immunohistochemistry on paraffin-embedded tissue sections of BMB to study myeloid markers, particularly CD14 and CD16, comparing CMML, CML, and a control group. Interestingly, we clearly showed a strong decrease of the number of MPO-

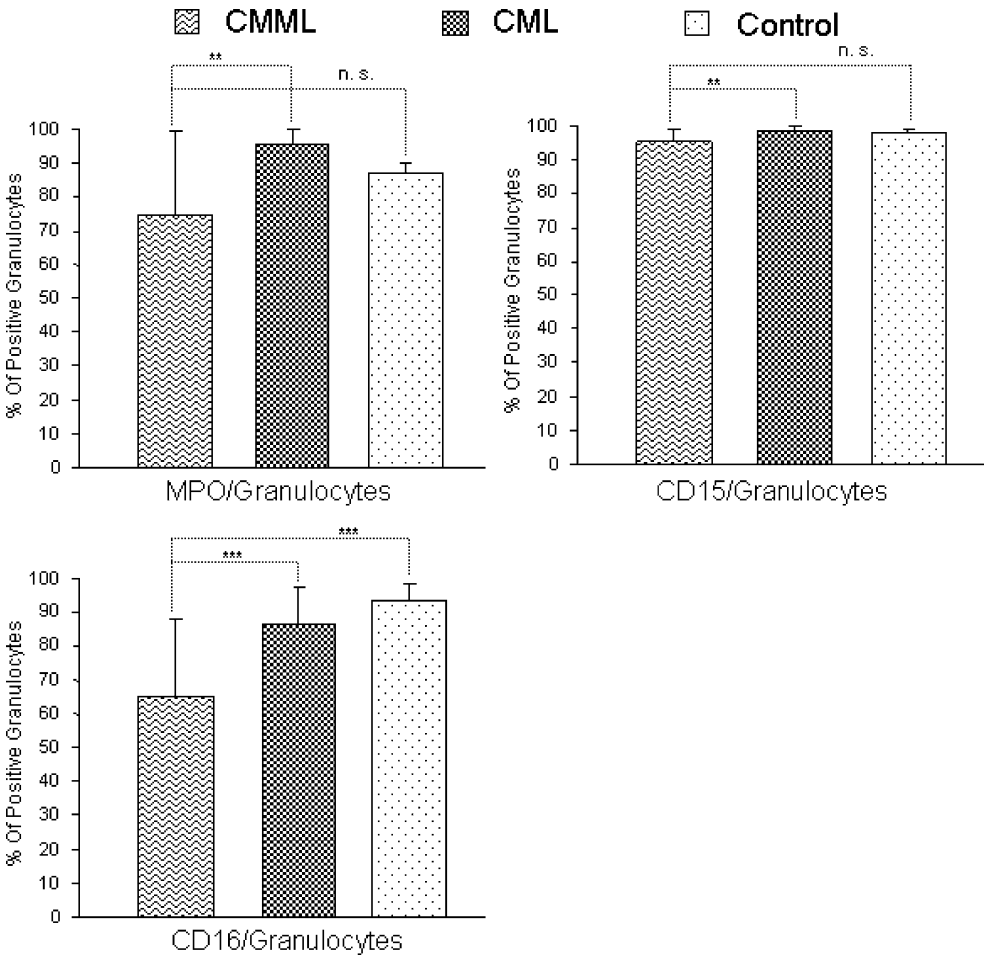

Fig. 4 Percentages of polymorphonuclear cells (pmns) positive with myeloperoxidase (*MPO*), CD15, and CD16 in CMML (n=15), CML (n=10), and control marrow biopsies (n=8). *p<0.05, **p<0.01, ***p<0.001. *n.s.* not significant; p>0.05

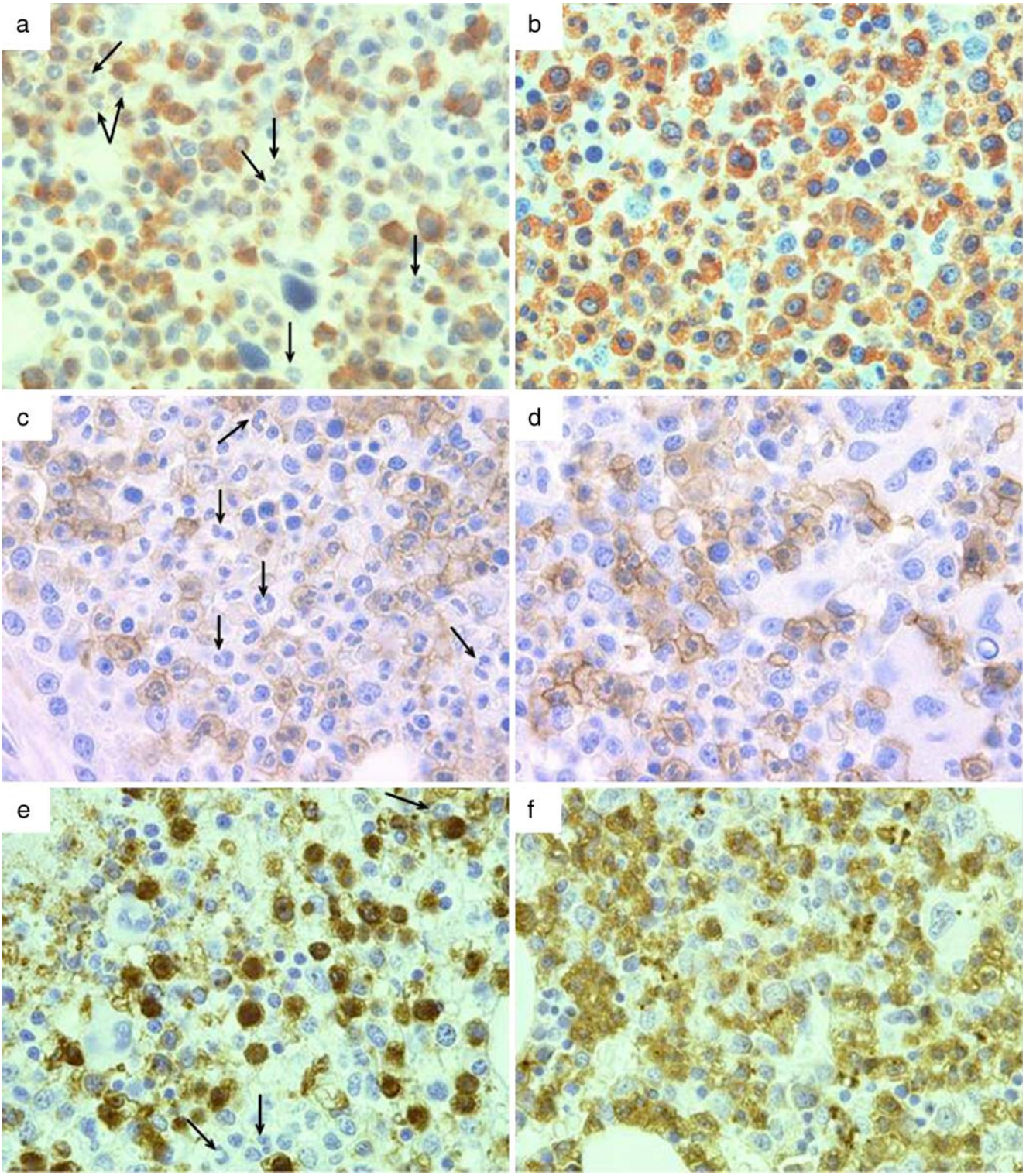

Fig. 5 **a** and **b** MPO staining in CMML **(a)** and in CML **(b)**: Some granulocytes are not stained in CMML (*arrows*). However, in CML, almost all the granulocytes are positively stained. **c** and **d** CD16 staining in CMML **(c)** and in CML **(d)**: Some positively stained granulocytes are seen in CMML with the presence of numerous negative granulocytes (*arrows*). On the other hand, nearly all the granulocytes are stained in CML. **e** and **f** CD15 staining in CMML **(e)** and in CML **(f)**. Presence of a minority of unstained granulocytes (*arrows*) in CMML. By contrast, in CML, almost all granulocytes are positively stained

positive cells in CMML, compared to CML. This is due in part to the absence of erythroblastic hypoplasia in CMML compared to CML. In addition, this drop of cell staining for MPO in CMML is also due to the decrease in the numbers of pmns and probably mononuclear cells from the granulocyte lineage staining for MPO and to the expansion of MPO negative monocytes. Although dysgranulopoiesis has been demonstrated by flow cytometry linked to a decrease of the expression of CD15 and CD16 by pmns [11, 12], this has not been clearly demonstrated, to our knowledge, for MPO. Interestingly, we found particularly for CD16, and at a lower level for CD15 and MPO, a decrease in the number of pmns positive for these markers in the BMB of CMML compared to CML suggesting that this phenotyping of pmns on BMB might help to suggest the dysgranulopoiesis, which is well defined on marrow aspirates, but very difficult to assess on histological slides. Similar to the results observed by Orazi et al. [9] (on formalin-fixed BMB and decalcified in nitric oxide) and others [13–15], both CD163 and CD68 (PG-M1) positive cells were found to be much more restricted to bone marrow macrophages than CD68 (KP1). However, we were able to demonstrate an increase in the numbers of CD14-positive cells compared to PG-M1-positive or CD163-positive cells in CMML. This observation, together with the presence of CD14-positive/PG-M1-negative monocytes, suggests that PG-M1 is not a marker of all monocytes, at least on BMB, or that its expression level is too low to be detected after fixation and decalcification. Our finding is in agreement with the fact that it has been reported, in CMML, a significant increase of the percentage of nonspecific esterase-positive monocytes compared to PG-M1- or CD163-positive cells [9], suggesting that these last two markers did not stain all the monocytes on BMB. This might confirm what has been suggested concerning the lower sensitivity of CD163 and CD68/PG-M1 antibodies for leukemic monocytic cells compared to tissue histiocytes/macrophages [9, 14, 15]. Moreover, PG-M1 has not been found as a good marker in discriminating between the subtypes of acute myeloid leukemia M4/5 and M1/2 [16]. CD14 is known to be expressed by monocytes, interstitial myeloid DC, and various types of tissular macrophages [10, 17, 18]. By flow cytometry analysis of blood or bone marrow, CD14 is used to identify the monocytes [8, 19]. We were able to identify clearly on control bone marrow normal monocytes very difficult to recognize on giemsa staining due to the rarity of these cells and the often irregular sometimes bilobated character of nucleus mimicking some neutrophils on sections. Our ability to identify them using immunohistochemistry is of great potential help for the diagnosis of monocyte pathology. Interestingly, the marrow biopsies in our study showed a moderate, but significant, increase of CD14-positive cells in the cases of CMML compared to those in the cases of CML and control marrow biopsies. This expansion of CD14-positive cells is not made of dense clusters, but of unevenly distributed cells admixed with cells of the granulocytic lineage explaining how difficult it is to identify them on BMB. This pattern is completely different from the pattern of sheets of plasmacytoid dendritic cells observed in 20% of CMML [9] and confirms that CMML is not linked to a proliferation of clusters of monocytes in BMB. Overall, we demonstrate the interest of CD14 and CD16 staining on BMB, particularly when dealing with a clinical suspicion of CMML.

Acknowledgments The authors wish to thank Patricia Bonjour and Pierre-Etienne Bouchet for technical help. Marwan Qubaja is supported by a grant in cooperation between University Pierre et Marie Curie and Al-Quds University—School of Medicine.

Conflict of interest The authors do not identify any conflict of interest to declare.

References

1. Vardiman JW, Imbert M, Pierre R et al (2001) Chronic myelomonocytic leukemia. In: Jaffe ES, Harris NL, Stein H, Vardiman JW (eds) World Health Organization classification of tumors: pathology and genetics of tumours of haematopoietic and lymphoid tissues. IARC, Lyon, pp 49–52
2. Vardiman JW, Harris NL, Brunning RD (2002) The World Health Organization (WHO) classification of the myeloid neoplasms. Blood 100:2292–2302
3. Steensma DP, Dewald GW, Lasho TL et al (2005) The JAK2 V617F activating tyrosine kinase mutation is an infrequent event in both "atypical" myeloproliferative disorders and myelodysplastic syndromes. Blood 106:1207–1209
4. Bennett JM, Catovsky D, Daniel MT et al (1994) The chronic myeloid leukaemias: guidelines for distinguishing chronic granulocytic, atypical chronic myeloid, and chronic myelomonocytic leukaemia. Proposals by the French–American–British Cooperative Leukaemia Group. Br J Haematol 87:746–754
5. Fenaux P, Beuscart R, Lai JL et al (1988) Prognostic factors in adult chronic myelomonocytic leukemia: an analysis of 107 cases. J Clin Oncol 6:1417–1424
6. Martiat P, Michaux JL, Rodhain J (1991) Philadelpia-negative (Ph−) chronic myeloid leukemia (CML): comparison with Ph+ CML and chronic myelomonocytic leukemia. Blood 78:205–211
7. Geissmann F, Jung S, Littman DR (2003) Blood monocytes consist of two principal subsets with distinct migratory properties. Immunity 19:71–82
8. Xu Y, McKenna RW, Karandikar NJ et al (2005) Flow cytometric analysis of monocytes as a tool for distinguishing chronic myelomonocytic leukemia from reactive monocytosis. Am J Clin Pathol 124:799–806
9. Orazi A, Chiu R, O'Malley DP et al (2006) Chronic myelomonocytic leukemia: the role of bone marrow biopsy immunohistology. Mod Pathol 19:1536–1545
10. Marmey B, Boix C, Barbaroux JB et al (2006) CD14 and CD169 expression in human lymph nodes and spleen: specific expansion of CD14+ CD169− monocyte-derived cells in diffuse large B-cell lymphomas. Hum Pathol 37:68–77

11. Lorand-Metze I, Ribeiro E, Lima CS et al (2007) Detection of hematopoietic maturation abnormalities by flow cytometry in myelodysplastic syndromes and its utility for the differential diagnosis with non-clonal disorders. Leuk Res 31:147–155
12. Shao Z, Chen G, Lin Z et al (1998) Immunophenotype of myeloid cells in myelodysplastic syndromes and its clinical implications. Chin Med J 111:28–31
13. Manaloor EJ, Neiman RS, Heilman DK et al (2000) Immunohistochemistry can be used to subtype acute myeloid leukemia in routinely processed bone marrow biopsy specimens. Comparison with flow cytometry. Am J Clin Pathol 113:814–822
14. Lau SK, Chu PG, Weiss LM (2004) CD163: a specific marker of macrophages in paraffin embedded tissue samples. Am J Clin Pathol 122:794–801
15. Nguyen TT, Schwartz EJ, West RB et al (2005) Expression of CD163 (hemoglobin scavenger receptor) in normal tissues, lymphomas, carcinomas, and sarcomas is largely restricted to the monocyte/macrophage lineage. Am J Surg Pathol 29:617–624
16. Horny HP, Wehrmann M, Steinke B et al (1994) Assessment of the value of immunohistochemistry in the subtyping of acute leukemia on routinely processed bone marrow biopsy specimens with particular reference to macrophage-associated antibodies. Hum Pathol 25:810–814
17. Larregina AT, Morelli AE, Spencer LA et al (2001) Dermal-resident CD14+ cells differentiate into Langerhans cells. Nat Immunol 2:1151–1158
18. Buckley PJ, Smith MR, Braverman MF et al (1987) Human spleen contains phenotypic subsets of macrophages and dendritic cells that occupy discrete microanatomic locations. Am J Pathol 128:505–520
19. Yang DT, Greenwood JH, Hartung L et al (2005) Flow cytometric analysis of different CD14 epitopes can help identify immature monocytic populations. Am J Clin Pathol 124:930–936

Virchows Arch (2009) 454:421–429
DOI 10.1007/s00428-009-0749-3

ORIGINAL ARTICLE

A European network for virtual microscopy—design, implementation and evaluation of performance

Mikael Lundin · Janusz Szymas · Ewert Linder · Hans Beck · Peter de Wilde · Han van Krieken · Marcial García Rojo · Ignacio Moreno · Aurelio Ariza · Sitki Tuzlali · Sergülen Dervişoğlu · Heikki Helin · Veli-Pekka Lehto · Johan Lundin

Received: 2 October 2008 / Revised: 10 February 2009 / Accepted: 17 February 2009 / Published online: 12 March 2009

Abstract Web-based virtual microscopy has enabled new applications within pathology. Here, we introduce and evaluate a network of academic servers, designed to maximize image accessibility to users from all regions of Europe. Whole-slide imaging was utilized to digitize the entire slide set (n=154) for the slide seminars of the 21st European Congress of Pathology. The virtual slides were mirrored to five academic servers across Europe using a novel propagation method. Functionality was implemented that automatically selects the fastest server connection in order to optimize the slide-viewing speed (http://www.webmicroscope.net/ECP2007). Results show that during

Electronic supplementary material The online version of this article (doi:10.1007/s00428-009-0749-3) contains supplementary material, which is available to authorized users.

M. Lundin · J. Lundin
Department of Oncology, Institute of Clinical Medicine,
University of Helsinki,
Helsinki, Finland

M. Lundin · J. Lundin
Folkhälsan Research Center,
Helsinki, Finland

J. Szymas
Department of Clinical Pathology,
University of Medical Sciences,
Poznan, Poland

E. Linder
Swedish Institute for Infectious Disease Control (SMI),
Solna, Sweden

E. Linder
Department of Microbiology, Tumor, and Cell Biology (MTC),
Karolinska Institutet,
Stockholm, Sweden

H. Beck · P. de Wilde · H. van Krieken
Department of Pathology,
Radboud University Nijmegen Medical Center,
Nijmegen, the Netherlands

M. García Rojo · I. Moreno
Pathology Department, Hospital General de Ciudad Real,
Ciudad Real, Spain

A. Ariza
Department of Pathology,
Hospital Universitari Germans Trias i Pujol,
Barcelona, Spain

S. Tuzlali
Department of Pathology, Faculty of Medicine,
Istanbul University,
Istanbul, Turkey

S. Dervişoğlu
Cerrahpasa Medical Faculty, Pathology Department,
Istanbul University,
Istanbul, Turkey

H. Helin · V.-P. Lehto
Department of Pathology, Haartman Institute,
University of Helsinki and Helsinki University Central Hospital,
HUCH Laboratory Diagnostics,
Helsinki, Finland

M. Lundin (✉)
Clinical Research Institute HUCH,
Haartmaninkatu 4, P.O. Box 105, 00029 Helsinki, Finland
e-mail: mikael.lundin@helsinki.fi

6 months of monitoring the uptime of the network was 100%. The average viewing speed with the network was 3.1 Mbit/s, as compared to 1.9 Mbit/s using single servers. A good viewing speed (>2Mbit/s) was observed in 32 of 37 countries (86%), compared to 25 of 37 (68%) using single servers. Our study shows that implementing a virtual microscopy network spanning a large geographical area is technically feasible. By utilizing existing academic networks and cost-minimizing image compression, it is also economically feasible.

Keywords Virtual microscopy · Whole-slide imaging · Network · Internet · Pathology

Introduction

Virtual microscopy has over a time scope of only a few years evolved dramatically. Starting from an experimental early phase with the first proofs of useful applications [1–6], virtual microscopy has become an established and accepted tool at university institutions and hospitals. An image server in an intranet can provide a whole campus or hospital area with significant benefits within education and research and increasingly also in routine practices.

Broadening the perspectives outside the campus network firewalls, the most significant advantages of web-based virtual microscopy can be found within education, quality assurance, and consultations: national and international board certification exams, common educational libraries, quality assessment rounds for laboratories, international collaborations for second opinion, and slide seminars of important multinational meetings and congresses [7–9]. However, common to these applications is that they are critically dependent on reliable image server connections and equal functionality for users from different geographical regions.

With a single campus server, most applications will run smoothly in the near perimeter of the server, but, as the distance from the image server increases, loading of image data will become slower. At a certain point, some applications, for example those involving screening of large specimen areas, may cease to be practically functional. It is also known that segments of the global internet can be inaccessible from time to time due to periodical heavy data load and, more often, random problems [10, 11].

It is a clearly recognizable discrepancy that the most useful applications of web-based virtual microscopy are also the ones with a critical dependency on functionality and reliability. Large-scale international projects will not gain widespread acceptance among the community of pathologists and cytologists until the accessibility problem is solved. Our objective is to introduce a solution by designing and implementing a European Virtual Microscopy network, maximizing availability and reliability, and providing high connection speeds to users from all regions. The purpose of this study is to present and to evaluate the performance of a network of academic servers set up to host the slide seminar cases of the 21st European Congress of Pathology, held in Istanbul on September 8th to 13th, 2007.

Materials and methods

Preparation of the whole-slide images and web site

One hundred and fifty-four slides to be presented at the slide seminars during the 21st European Congress of Pathology were digitized with a Zeiss Mirax Scan scanner (Zeiss GmbH, Göttingen, Germany) at a 0.23-μm resolution and compressed to wavelet files. We have previously shown that with a target compression level of 1:9 no visual loss in image quality can be detected with the wavelet image compression technique (either jpg2000 or Enhanced Compressed Wavelets) [4]. Conversion and compression software (Mirax jpg2000 converter from VMscope GmbH, Germany, and Image Compressor from ERDAS Inc., Norcross, US) were used to generate the wavelet files. The wavelet compression deploys regional compression rules where areas uniform in color or pattern compress highly. The actual average compression level in the whole set was therefore 1:57. The average dimension of the virtual slides was 83,000×140,000 pixels, and the average file size was 37 GB uncompressed and 0.64 GB compressed (the entire slide set 5.7 TB and 98 GB, respectively). The hard disk storage space cost for one set of slides was 20€ ($28) but has in less than a year dropped to 12€ ($17) at the time of writing. The slides were indexed on the WebMicroscope web server and added to a web site to be accessed by congress attendants and other users (http://www.webmicroscope.net/ECP2007).

The network of servers

Five existing academic servers connected to the internet from across Europe and maintained by university departments were joined into a virtual microscopy network. All servers were running the Windows Server operating system and represented the same generation of hardware, with similar processing and memory capacity (2.4–3.0 GHz with 4 GB of random access memory). Three servers (Finland, Poland, and Sweden) were connected with a 1-Gbit/s speed to the internet, while the servers in the Netherlands and in Spain were connected at 100 Mbit/s.

The main WebMicroscope server is situated in the National Library of Health Sciences in Helsinki. It is

connected to the global internet through the Finnish University and Research Network academic network. The four other servers acted as mirror servers, located in Stockholm, Sweden (Swedish Institute for Infectious Disease Control), Poznan, Poland (Laboratory of Neurosurgical Pathology, University of Medical Sciences), Madrid, Spain (Spanish Society of Pathology/Spanish Division of the International Academy of Pathology), and in Nijmegen, the Netherlands (Radboud University Medical Center, Department of Pathology).

Mirroring of the slides on the network servers

The purpose of the mirroring was to generate identical sets of the virtual slides on each participating server. A web-based image file propagation application was written and installed on each server. This mirroring program can be initiated from the main server with instructions on what files to download and from where.

Two different experimental download schemas were designed and tested. In the first schema, all servers downloaded image data from the main server. In the other, hierarchical schema, only servers 2 and 3 were instructed to download data from the main server in Helsinki while servers 4 and 5 in turn downloaded data from servers 2 and 3, as data became available. The mirroring application included a function to check each downloaded file for correctness. If the data were incomplete, the loading of the missing pieces would restart.

Automatic speed test and selection of server to use

A core component in the network of mirror servers is a speed test function to select the optimal server for the user. When a web user visits the slide seminar web site, the user's browser automatically executes an integrated script code that measures the current actual internet connection speed from the user's computer to each of the mirror servers around Europe. The server with the fastest internet connection is then automatically selected as the source to load image data from. The speed test was designed so that the results are visible to the user at all times. The speed test can be repeated at any time, and the automatic server selection can be manually overrun to force the use of a specific server of choice.

The integrated speed test used in this study is more advanced than a traditional connection speed test which usually only measures the amount of data transferred over the internet during a specific time. The speed test is instead based on a function that effectively simulates the viewing of virtual slides from a server. In the first phase of the test, a small area from a virtual slide is extracted and displayed on the users' screen. Based on the time taken to conduct this preliminary test (0–2 s), a bigger area is selected in order to conduct a more reliable test during the next 5 s. The results from the second phase are used to select the optimal server for the user. As all servers in the network are tested in parallel, the total time to conduct the speed test is only 5–7 s.

Monitoring of the network

For the purposes of the study, two different monitoring systems were set up. Firstly, the results of the automatic speed tests conducted by the web users were stored in a database. Secondly, a separate server-to-server speed test was set up to internally monitor spatial fluctuations in the network performance and to monitor server uptimes.

The results of the automatic speed tests (in megabit per second) were stored together with information on the country of origin of the user (based on an Internet Protocol (IP) address lookup). In the server-to-server speed monitoring, a timer-based test was conducted from each server to all network servers every 10 min. The servers were synchronized not to conduct overlapping tests by using a 2-min shift in the schedule. Thus, every 2 min, a test from one server to all servers was conducted.

We have previously shown that, with an internet connection speed above 2 Mbit/s, the viewing experience is very smooth [4]. This can be accomplished by a moderately fast home broadband internet connection (xDSL). When comparing connection speeds by region in Europe, variations in this speed by which the end user's own computer is connected to the internet may exist and thus make the average and median of the speed results suboptimal as a comparison instrument. As the purpose of this study was to evaluate how fast are the connections which can be possibly established to the network in each region, the average of only the top half of the conducted tests is likely to give a better estimation of the network functionality. In the interpretations of the results, this measurement method will therefore be emphasized.

Slide viewing and server software

The browser-based viewing and server software have been described in previous reports [4, 5]. It is a robust viewing system originally developed for the satellite and aerial imaging industry (ERDAS Image Web Server by ERDAS Inc., Norcross, USA). A dedicated data protocol and browser plug-in enable the fastest possible transfer speed, loading only the image data currently being viewed on the computer screen of the user. The compression level or the size of the image files does not affect image data transfer rates. The software that has been adapted for virtual microscopy also features an alternative cross-platform-compatible plug-in free viewer.

Results

Mirroring of the virtual slide set on the network

In order to evaluate the reliability and performance of the mirroring function, where the image data (98 GB) propagated from the main server in Helsinki to all the other servers, the two download schemas were repeated three times each. All tests were conducted during late night and early morning hours when internet traffic in Europe is lowest.

With the first schema, where all servers downloaded the image data directly from the main server in Helsinki, the average time to complete mirroring ranged from 2 to 9 h (Stockholm 2 h, Poznan 9 h, Madrid 7 h, and Nijmegen 5 h). With the hierarchical schema, only the servers in Stockholm and Nijmegen were instructed to download data from the main server in Helsinki, while the server in Poznan downloaded data from Nijmegen, and the server in Madrid downloaded data from Stockholm as data became available. With this schema, the time to complete mirroring of data ranged from 1.5 to 6 h (Stockholm 1.5 h, Poznan 6 h, Madrid 5 h, and Nijmegen 4 h).

Monitoring of web user connections

During the congress in September 2007, access to the web site was restricted by personal passwords sent to the participants. After the congress, the website and all virtual slides and the case diagnoses were released for public access, and monitoring of the network was started on October 2007. As planned, results collected from a 3-month period were analyzed in this study. A speed test was conducted automatically when a web user visited any of the congress' web site pages.

Connection speeds to the network

The total number of completed speed tests during the study period was 5,596. Of these, 3,799 users were tracked to 37 European countries based on an IP address lookup. For each individual test, the connection speed to the fastest server was recorded as the result of the network as a whole. The average connection speed to the network was 3.1 Mbit/s (median 2.7 Mbit/s). A connection speed above 2 Mbit/s was recorded for 55.1% of the users, while 72.6% had a connection speed above 1 Mbit/s. The average connection speed of only the top half of the test results was 5 Mbit/s (Table 1). Results from countries outside Europe can be found on the network web site.

Performance of the network of servers compared to single servers

When comparing the servers functioning as single servers to the network as a whole, the network was between 24% and 107% faster than the single servers (Helsinki 24%, Stockholm 55%, Poznan 94%, Madrid 107%, and Nijmegen 55%). The median connection speed as well as the average of the top half increased correspondingly (Table 1). The proportion of web users with a connection speed above 2 Mbit/s increased from 45% to 55% for the server in Helsinki, while it more than doubled for the servers in Poznan and Madrid (from 24.9% and 24.6% to 55%, respectively, Table 2).

Performance of the network according to geographical location

In 23 of the 37 (62%) countries, the average connection speed to the network exceeded 2 Mbit/s while in nine (24%) countries the average connection speed was between 1 and 2 Mbit/s. In five (14%) countries, the average connection speed was found to be below 1 Mbit/s. In 32 of the 37 (86%) countries, the average of the top half was above 2 Mbit/s (Table 3, Supplemental Figure 1). When analyzed as single servers, the average number of countries with a connection speed above 2 Mbit/s was 25 (68%).

Figure 1a shows the average connection speed to the network according to country of the visitor. Correspondingly, Fig. 1b–f shows the connection speeds by country to each server in the network.

Table 1 Connection speeds (average, median, and average of top half) to the virtual microscopy network as a whole and to each single server in the network

	Network	Helsinki		Stockholm		Poznan		Madrid		Nijmegen	
Average (Mbit/s)	3.1	2.5	24%	2	55%	1.6	94%	1.5	107%	2	55%
Median (Mbit/s)	2.7	2.1	29%	1.8	50%	1.4	93%	1.4	93%	1.8	50%
Average of top half (Mbit/s)	5	4	25%	3.2	56%	2.5	100%	2.2	127%	3.2	56%

The proportional benefit of the network is shown as a percentage. For example, the network provided a 24% better average connection speed as compared to the Helsinki server alone while the average connection speed to the network was more than doubled (107%) as compared to the Madrid server alone

Table 2 Proportions of visitors with a connection speed above 1 and 2 Mbit/s to the virtual microscopy network and to each single server in the network

	Network	Helsinki	Stockholm	Poznan	Madrid	Nijmegen
Proportion >1 Mbit/s	72.6%	65.1%	57.7%	54.7%	54.2%	59.9%
Proportion >2 Mbit/s	55.1%	45.1%	32.1%	23.6%	19.8%	38.7%

Server-to-server self-monitoring of the network

From October 2007 to April 2008, the uptime of the network as a whole was 100%, as in each of the set of five tests conducted every 10 min a connection could be established to the network. During the follow-up, a total of 157,258 tests were initiated and thus 786,290 server probes performed. In 152,877 (97.2%) tests, all five servers responded, while in 4,255 (2.7%) and in 123 (0.1%) tests only four or three servers in the network responded. The majority (2,752, 63%) of the failed tests could be tracked to the connection from Stockholm to Poznan.

Table 3 Connection speed (average of top half in megabit per second) to the network and to each server according to country of origin

	Network	Helsinki	Stockholm	Poznan	Madrid	Nijmegen
Austria	5.7	4.9	3.3	4.7	3.1	4.1
Belarus	2	2	1.1	0.8	0	0.7
Belgium	6.2	4.8	4.1	2.4	3.2	5.9
Bulgaria	2.4	2.2	1.2	1.2	1.3	1.5
Croatia	2.8	2.4	1.9	1.8	1.6	2.4
Cyprus	0.3	0.3	0.3	0.3	0.3	0.3
Czech Republic	5.6	4.7	3.6	3.6	2.7	4.7
Denmark	7.5	6.7	6.4	2.7	2.6	5.2
Estonia	7.3	6.3	7.1	4.2	1.9	4.3
Finland	13.8	13.7	8.4	2	2.2	3.6
France	3.8	3.4	2.3	2	2.8	3.1
Georgia	0.2	0	0.2	0	0.1	0
Germany	4.7	3.7	3.3	2.8	2.4	4
Greece	2.5	2.4	1.6	1.3	1.5	1.8
Hungary	4.9	3.6	3.4	2.9	2.6	4.2
Iceland	4.5	3.8	4.1	1.5	2.1	3.9
Ireland	4.1	3.4	2.3	2	2.3	3.1
Italy	3.4	2.4	2.2	2	2.4	2.5
Latvia	2.1	2.1	0.8	1.2	1.9	0.9
Lithuania	7.8	6.6	3.3	5.9	2	3
Luxembourg	6.8	6.8	3.8	5.2	3.8	4.2
Macedonia	0.8	0.8	0.5	0.6	0.7	0.7
Moldova	2.7	2.7	1.4	1.3	1.3	1.3
the Netherlands	13.3	6.5	5	3	3.5	13.1
Norway	7.9	6.7	6.9	2	2.4	3.6
Poland	13.1	5.1	4.3	12.9	0.5	4.3
Portugal	3.1	2.1	1.3	1.1	2.9	1.7
Romania	3.2	3	1.8	2.3	1.9	2.3
Russia	3	2.8	2.6	1.7	1.6	1.9
Slovakia	3	2.9	1.5	3	1.9	2.3
Slovenia	6.1	4.9	4.8	2.9	3.8	6
Spain	4.5	2.4	2	1.7	3.8	2.8
Sweden	12.2	10	10.8	2.4	2.5	4.3
Switzerland	5.7	4.8	3.8	2.8	4.2	5.2
Turkey	1.5	1.1	1.1	0.9	0.8	0.9
Ukraine	1	1	0.7	0.6	0.8	0.8
UK	5.4	4.3	3.4	2.1	3.1	3.1

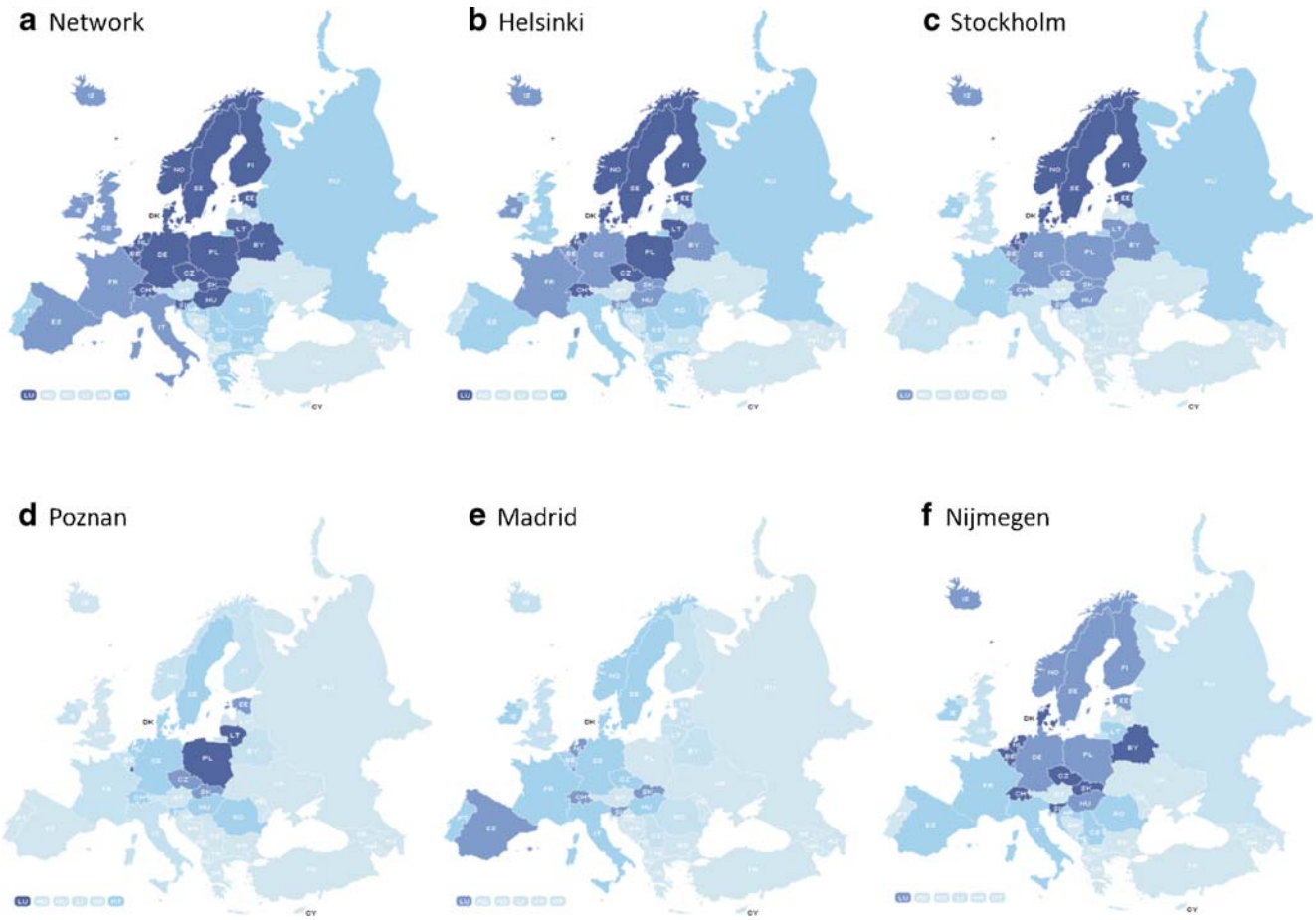

Fig. 1 Connection speed (average of top half, megabit per second) by country. **a** shows the connection speed to the network as a whole, while **b**–**f** show the speed to the single servers. A *darker blue* gradient means a faster connection

During the follow-up time, negligible fluctuations in the average server-to-server connection speeds were seen from month to month (Fig. 2a). Small variations due to weekday were seen, with 3% slower connection speeds on Tuesdays than on average (Fig. 2b). During weekends, the connection speed was 4% above average. These fluctuations were accentuated only in the connection to Poznan, with Tuesdays at 8% below average and Sundays 15% above average (Fig. 2b). A corresponding accentuation was seen for the Poznan server when analyzing the variations according to hour of the day (Fig. 2c). Server-to-server connection speeds were on average fastest in the early morning and slowest in the afternoon.

Discussion

This study shows that it was possible to implement a high-performance academic virtual microscopy network in Europe, and by utilizing existing servers it could be implemented at minimal costs. A 100% uptime of the network during an extensive follow-up time shows that a good reliability and availability can be established for important international applications even with a small network. Regional differences in connection speed within Europe could be eliminated for large areas but not for all peripheral regions with the current network.

The virtual microscopy network described in this article is a novel concept. At the time of writing, the only result returned by web search engines is the present study, and no articles can be found in the medical literature. When we started to design the network in 2006, our goals were firstly to eliminate regional differences in connection speed seen with a single-server setting and secondly to maximize the uptime (availability/reliability) of the web site and image data source. Depending on factors such as distance from the server, traffic load, and random problems on the internet, significant differences in connection speed can be seen when using a single server. Even total failures may occur as a consequence of temporary internet or server problems [10, 11].

To accomplish both goals, the current network was based on mirror servers, where identical sets of the virtual slides were stored on each participating server. The integrated

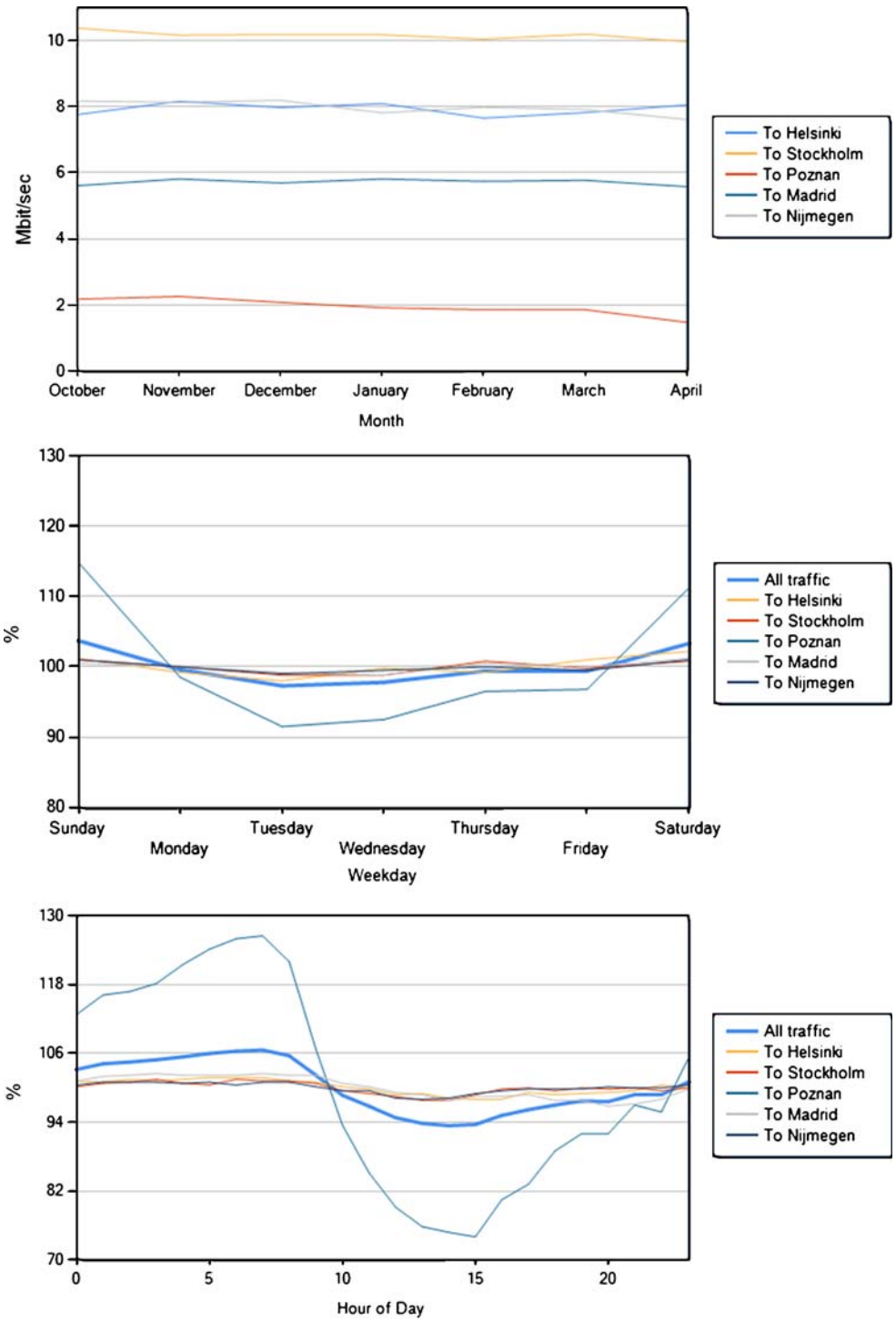

Fig. 2 Fluctuations in connection speed by month (**a**), weekday (**b**), and hour of day (**c**), as measured from all servers to one server

speed test automatically guides the user to load image data from the server with the currently best connection speed. This effectively distributes the traffic and burden on the servers, and if one server or segment of internet fails, the user will be directed to use another server.

The process of mirroring image data was in itself an interesting part of the study. The repeated tests showed that it was possible to conveniently mirror the whole-slide set of this major congress (100 GB of data, 154 slides) during one single night. The positive effect of a hierarchical mirroring schema was demonstrated, decreasing the average time to distribute the slides to all servers from 9 to 6 h. The hierarchical mirroring utilizes the cumulative bandwidth of the involved servers, thus partly resembling a peer-to-peer network [12]. Although it was possible (but slower) to use a single server as the only mirroring data source in this study,

a hierarchical model quickly becomes obligatory in a larger network as the number of servers increase. If all servers would download data from the same server, the connection to this primary server would get saturated and radically slow down the propagation of data. In our experiments, we could decrease the total download time partly because we avoided this saturation effect by having only two servers download data from Helsinki (the fastest server loaded in 1.5 h when the traffic was lower as compared to 2 h when all servers were connected) and partly because the download speed to Poznan from Nijmegen is higher than from Helsinki (6 vs. 9 h).

The current network was implemented with mirror servers, but, in a very early phase, we experimented with an alternative design based on cache servers commonly used on the internet to provide better global access to web sites. By using discrete image tiling from jpg2000 files, image data from within a slide viewed by a user could temporarily be stored on one or several cache (accelerator) servers. When the next user views exactly the same area with the same magnification, image data could be loaded from the cache servers instead of from the primary server. However, in our tests, this method proved unsuccessful. Virtual slides digitized at a high resolution are extremely large files, and, with (seen from a technical perspective) quite limited number of users, exactly the same areas at exactly the same zoom level are viewed too infrequently to be effectively cached. A cache server solution works well if there are tens of thousands of users and only a few images, as for example on popular geographical map web sites. This will however not be the situation even in a large European virtual microscopy network.

The results of the network monitoring show that the mirroring system performed well. In the continuous (every 10 min) server-to-server monitoring, the uptime of the network was 100% during the follow-up. In 97.2% of the 152,877 checks, all servers responded and only in 123 (0.1%) tests did two servers failed to answer. In 63% of the tests with one failing server, the problem was tracked to the Stockholm–Poznan connection (not the other way). The connection to Poznan, from all the other servers, was also the only one with noticeable fluctuation in speed over time, both according to weekday and to hour of day. The reasons for this phenomenon remain unclear, but it demonstrates that internet connections are not always optimal and emphasizes the need to use a network of servers. The server in Poznan is probably ideally located in a region that more than others benefits from its own server. In order to be able to provide adequate connection speeds to a whole continent, it is such regions that must be identified (and equipped with own servers).

With the five servers included in the network, it was possible to enable adequate connection speeds from large parts of Europe (Fig. 1) but, as Table 3 shows, not from all. In 32 of the 37 countries, the average of the top half of the speed tests was >2 Mbit/s, and in 31 countries more than half of the visitors had a connection speed above 2 Mbit/s. In order to totally eliminate regional differences in connection speed, more servers (10+) should be connected to the network in carefully selected areas. As seen in Table 3 and in the speed maps in Fig. 1, such regions can be found in the southeastern parts of Europe. In this study, the effect of a server in a country was clearly seen, providing very high connection speeds to users within the country itself and also to nearby regions (Supplemental Figure 1). The coverage of the major internet cables of the European internet does not precisely match the political country boundaries and distances as seen on a map [13]. The optimal solution would therefore be to place servers by major university regions and user population.

When we designed this network, we had no previous study results to rely on for geographical placement of servers. However, the relatively small network clearly outperformed each server as single servers, indicating a quite successful constellation. On average, the network more than doubled the connection speed as compared to the Madrid server and in 17 countries one of the other servers was faster for the end user than the main server.

With the instruments for monitoring the network in this study, it was not possible to precisely analyze the effect of concurrent users. The very small fluctuations seen in the server-to-server monitoring indicate that such an effect, if there was one, was very well balanced by the automatic user redirection. If one server is under heavy load, the automatic speed test that also takes the work done by the server into consideration will guide the user to use another server. As a single server (with a 100–1,000-Mbit/s internet connection) can handle hundreds of concurrent users, a network of five servers is technically capable of serving a community of 1,000+users. Although no significant fluctuations were detected in the network functionality during the follow-up time, upcoming improvements of the system include more specific monitoring tools for concurrent users, with alarm triggers automatically alerting web administrators (by mail and SMS) of abnormal functionality.

When building a virtual microscopy network, two important sources of costs are the costs for bandwidth and storage space. Both sources could in this study be minimized, as the servers were all connected to academic networks, and the wavelet compression technique reduced file sizes to a minimum. Except for the low bandwidth costs usually offered by academic networks, an advantage as compared to commercial networks is that most end users are likely to have their computers connected to an academic network, generally providing better connection speeds than through links between the commercial and academic

networks. The costs of the hard disk drives for storage of the slide set in this study is at the time of writing (August 2008) around 12€ ($17) per server on high quality disks (0.11€/GB, 0.17$/GB). With file sizes corresponding to the slide set in this study (0.63 GB/slide), close to 10,000 slides could be stored on a 6-TB disk space that today easily can be added to a powerful server that today costs around 3,000€ ($4,150). Mirroring in the network will make local backup systems for the common image data unnecessary. Current levels of storage costs would thus permit comprehensive permanent collections of slides. Further, most common projects would be time-limited, allowing withdrawal of mirroring after a certain time period when the expected number of visitors decreases, for example after an exam.

As the aim of this study was to design and evaluate a novel technique for providing fast and reliable slide-viewing possibilities for a large geographical area, the slide scanning equipment and file formats used were only of secondary importance. Even the choice of viewing technology did not influence the results or conclusions of this study. However, when designing virtual microscopy networks, common imaging and data communication standards will be of high importance [14, 15].

Our virtual microscopy network can be considered as a form of cloud computing [16]. The slide-viewing applications and image data are provided online, allowing users to access services from the Internet ("the cloud") with a common web browser. The user does not need to know from which server the images are being viewed and there is no need to store huge amounts of image data on the user's computer. Another term that has been used for this type of computational resources is grid services [17]. However, grid computing may rather be considered as application of several computers to a single problem at the same time [18, 19]. Cloud computing, on the other hand, does not use all resources simultaneously but rather aims to provide optimal access to web-based software services.

This study shows that implementing a virtual microscopy network spanning a whole continent is technically feasible. By utilizing existing powerful academic networks and cost-minimizing effective image compression techniques, it would also be economically feasible. We conclude that the time is ripe to establish a common academic virtual microscopy network for unifying educational and diagnostic practices within Europe.

Acknowledgments This study has been supported by grants from Biomedicum Foundation, Finska Läkaresällskapet, Instrumentariumin Tiedesäätiö, Medicinska Understödsföreningen Liv och Hälsa, Svenska Kulturfonden, and COST Action IC0604 Euro-Telepath.

Conflict of interest statement We declare that we have no conflict of interest

References

1. Steinberg DM, Ali SZ (2001) Application of virtual microscopy in clinical cytopathology. Diagn Cytopathol 25:389–96
2. Demichelis F, Barbareschi M, Dalla Palma P et al (2002) The virtual case: a new method to completely digitize cytological and histological slides. Virchows Arch 441:159–64
3. Romer DJ, Suster S (2003) Use of virtual microscopy for didactic live-audience presentation in anatomic pathology. Ann Diagn Pathol 7:67–72
4. Lundin M, Lundin J, Helin H et al (2004) A digital atlas of breast pathology: an application of web-based virtual microscopy. J Clin Pathol 57:1288–1291
5. Helin H, Lundin M, Lundin J et al (2005) Web-based virtual microscopy in teaching and standardizing Gleason grading. Hum Pathol 36:381–6
6. Lam AK, Veitch J, Hays R (2005) Resuscitating the teaching of anatomical pathology in undergraduate medical education: web-based innovative clinicopathological cases. Pathology 37:360–363
7. Lundin M, Lundin J, Isola J (2004) Virtual microscopy: applications in diagnostic pathology. J Clin Pathol 57:1250–1251
8. Molnar B, Berczi L, Diczhazy C et al (2003) Digital slide and virtual microscopy based routine and telepathology evaluation of routine gastrointestinal biopsy specimens. J Clin Pathol 56:433–438
9. Furness P (2007) A randomized controlled trial of the diagnostic accuracy of internet-based telepathology compared with conventional microscopy. Histopathology 50:266–273
10. Oppenheimer D, Ganapathi A, Patterson DA (2003) Why do Internet services fail, and what can be done about it? In: 4th Usenix Symposium on Internet Technologies and Systems (USITS '03)
11. Markopoulou A, Iannaccone G, Bhattacharyya S et al (2004) Characterization of failures in an IP backbone. INFOCOM 2004. In: Twenty-third Annual Joint Conference of the IEEE Computer and Communications Societies, vol. 4, pp 2307–2317
12. Steinmetz R, Wehrle K (2005) Peer-to-peer systems and applications (Lecture Notes in Computer Science/Information Systems and Applications, including Internet/Web, and HCI). Springer, Berlin
13. TeleGeography, Inc. (2002) European Terrestrial Networks Map 2002. http://www.telegeography.com/products/map_europe/images/europe_map_large.gif. Accessed 10 Feb 2009
14. Kayser K, Görtler J, Goldmann T et al (2008) Image standards in tissue-based diagnosis (diagnostic surgical pathology). Diagn Pathol 3:17
15. COST Action IC0604 (2009) Telepathology Network in Europe: EURO-TELEPATH. http://www.conganat.org/eurotelepath/. Accessed 10 Feb 2009
16. Miller M (2008) Cloud computing: web-based applications that change the way you work and collaborate online. Que, Upper Saddle River
17. Görtler J, Berghoff M, Kayser G et al (2006) Grid technology in tissue-based diagnosis: fundamentals and potential developments. Diagn Pathol 1:23
18. Wikipedia (2009) Grid computing. http://en.wikipedia.org/wiki/Grid_computing Accessed 10 Feb 2009
19. Foster I, Kesselman C (1998) The grid: blueprint for a new computing infrastructure. Morgan Kaufmann, San Francisco

Virchows Arch (2009) 454:431–439
DOI 10.1007/s00428-009-0750-x

ORIGINAL ARTICLE

Desmoplastic small round cell tumor of the central nervous system: report of two cases and review of the literature

Luciano Neder · Bernd W. Scheithauer · Keki E. Turel · Mark A. Arnesen · Rhett P. Ketterling · Long Jin · Timothy J. Moynihan · Caterina Giannini · Fredric B. Meyer

Received: 19 November 2008 / Revised: 22 January 2009 / Accepted: 16 February 2009 / Published online: 5 March 2009

Abstract Desmoplastic small round cell tumor (DSRCT) is a malignant tumor often involving the abdominal and/or pelvic peritoneum. Only one fully documented example has arisen in the central nervous system (CNS). Herein, we describe two additional examples, fulfilling the morphologic, immunohistochemical, and molecular criteria (EWS/WT1 translocation) of DSRCT. Both arose in the cerebellopontine angle (CPA) and underwent spinal dissemination. Patient 1, a 37-year-old male, underwent a subtotal resection, and 2 years later died of recurrent disease with spinal dissemination. Patient 2, a 39-year-old man, presented with cerebellar and CPA lesions as well as spinal leptomeningeal deposits. After 27 months of adjuvant therapy, he is alive with progressive disease. In conclusion, CNS DSRCT follows a similar aggressive course as do peritoneal examples. Although rare, DSRCT warrants consideration in the differential diagnosis of "malignant small blue cell tumors" of the CNS.

Keywords Central nervous system · Meninges · Desmoplastic small round cell tumor · EWS/WT1 translocation

For consideration of publication in Virchows Archiv.

L. Neder · B. W. Scheithauer (✉) · R. P. Ketterling · L. Jin · C. Giannini
Department of Laboratory Medicine and Pathology, Mayo Clinic, 200 First Street, SW, Rochester, MN 55905, USA
e-mail: scheithauer.bernd@mayo.edu

K. E. Turel
Department of Neurosurgery, Bombay Hospital Institute of Medical Sciences, Mumbai, India

M. A. Arnesen
Department of Laboratory Medicine, Abbott Northwestern Hospital, Minneapolis, MN, USA

T. J. Moynihan
Department of Medical Oncology, Mayo Clinic, 200 First Street, SW, Rochester, MN 55905, USA

F. B. Meyer
Department of Neurosurgery, Mayo Clinic, 200 First Street, SW, Rochester, MN 55905, USA

Introduction

First described in 1989 by Gerald and Rosai [1], desmoplastic small round cell tumor (DSRCT) is a malignant "small blue cell tumor" typically involving the abdominal and/or pelvic peritoneum of children and young adults, especially males [2–5]. DSRCT is a highly aggressive, presumably "primitive" neoplasm. Virtually, nothing is known of its cytogenesis [6]. Histologically, it is characterized by solid nests of small cells embedded in a dense, collagenous stroma. Its rather distinctive immunoprofile includes reactivity for epithelial (cytokeratins and epithelial membrane antigen) and myoid (desmin) markers [7]. Practically all cases exhibit the t(11;22)(p13;q12) chromosomal translocation, its breakpoints being the same as those involved in Ewing sarcoma and Wilms' tumor. This translocation results in fusion of the Ewing sarcoma gene (*EWS*) on chromosome 22 with the Wilms' tumor suppressor gene (*WT1*) on chromosome 11 [6, 8–10].

The presentation of DSRCT at nonperitoneal sites is a rare event. Reported examples have involved pleura [11–13], lung [14], ovary [15, 16], tunica vaginalis [10, 17, 18],

soft tissues and bone [19, 20], as well as the parotid gland [21]. Two possible intracerebral examples have also been reported [22, 23]. Tison et al. [24] described the first example to involve the central nervous system. In this paper, we describe two further examples. In both instances, the tumors arose in the tentorium, extended into the cerebellopontine angle (CPA), and disseminated widely throughout the neuraxis.

Clinical history

Patient 1

A 37-year-old male presented with a 5-month history of left-sided hearing loss and tinnitus. A magnetic resonance imaging (MRI) scan (Fig. 1a, b) and an audiogram suggested an acoustic neuroma. A craniotomy showed the mass to originate in the tentorium and to extend into the CPA. A subtotal resection was performed. An initial histologic diagnosis of "malignant epithelial neoplasm most consistent with metastatic carcinoma" was made on a very limited specimen. No alternative primary lesion was found despite the performance of total body computer tomography (CT) and MRI scans. Stereotactic irradiation was administered to the tumor bed. Six months thereafter, progressive left leg weakness became apparent as did bowel and bladder dysfunction. An MRI scan demonstrated drop metastases throughout the spinal leptomeninges, the largest situated at the S1–S2 level (Fig. 1c–e). At laminectomy, "dirty-looking" intradural tumor nodules were noted. These were debulked, and an optimal specimen was obtained. The patient underwent radiation therapy, including radiosurgery to the CPA (1,000 rads), as well as whole brain (3,600 rads) and spinal irradiation (4,500 rads). Chemotherapy (carboplatinum, temozolomide) was also

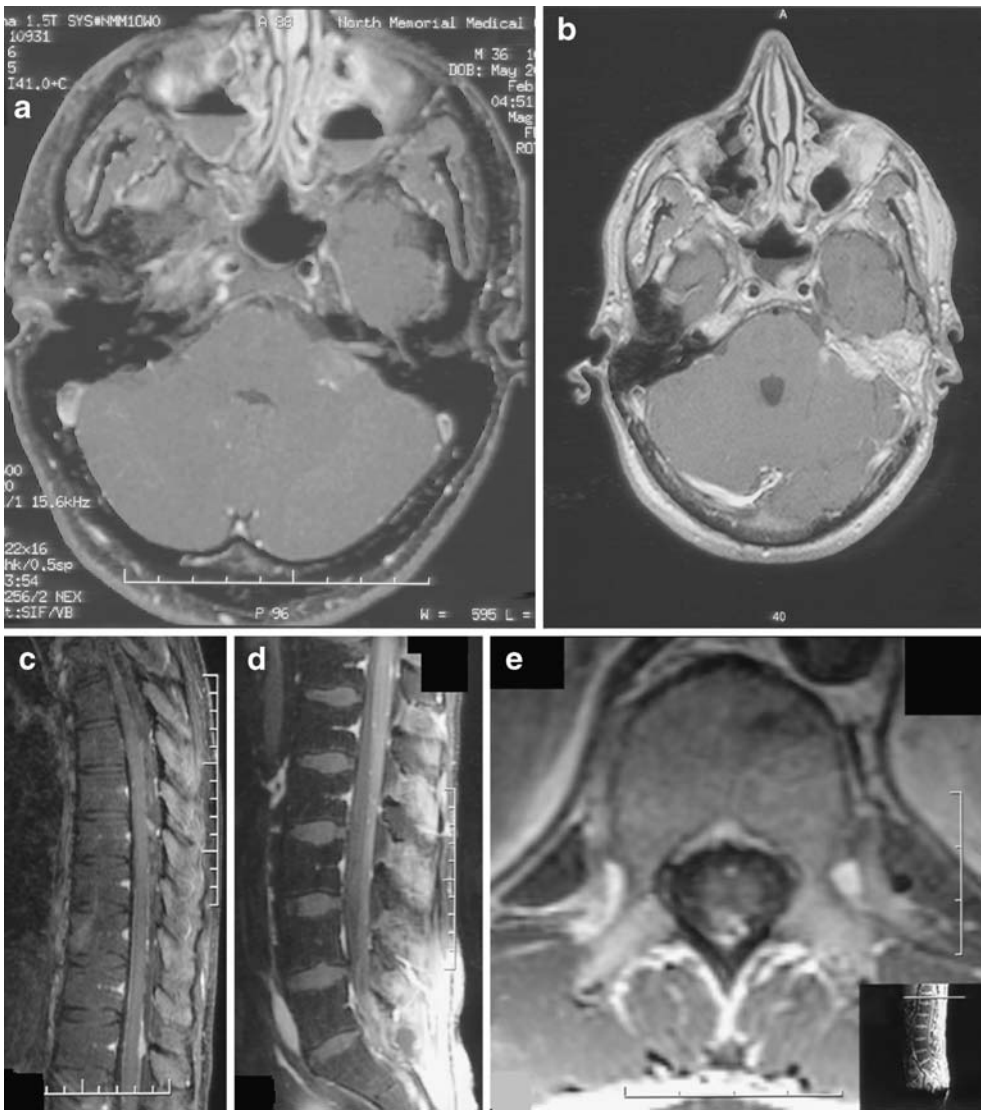

Fig. 1 Case 1. Preoperative MR imaging of the primary posterior fossa tumor showed heterogeneous enhancement and mild mass effect in the left cerebellopontine angle and upon the seventh and eighth cranial nerves (**a**). After a postoperative interval, it became better defined as a nodule with linear enhancement along the tentorium (**b**). Note postoperative fat packing of the left mastoid air cells (**b**). Postcontrast fat saturated T1W midsagittal sections through the thoracic (**c**) and lumbar (**d**) spine shows multiple small enhancing nodules coating the distal spinal cord, conus, and nerve roots of the cauda equina. The axial post-contrast image (**e**) obtained at the level of the distal spinal cord confirms the leptomeningeal location of the tumor deposits

administered. Two years after the initial diagnosis, the patient died of progressive disease.

Patient 2

A 39-year-old man presented with a 4-month history of gait imbalance and bilateral, lower limb weakness. Subsequently, after a fall, he became incapable of sitting, standing, or walking. A neurologic examination revealed hypotonic paraparesis with absent reflexes and a sensory level at L1. The patient then developed urinary and fecal incontinence. An MRI scan showed multiple, patchy, enhancing lesions in the spinal leptomeninges space (Fig. 2a–c), the left cerebellar hemisphere, and both cerebral peduncles (Fig. 2d). Pre-operative evaluation of somatosensory evoked potentials showed severe loss of posterior column conduction; electromyography revealed bilateral L2–S1 radiculopathy. Computed tomography scans of the abdomen and pelvis showed no abnormality. A T12–L5 laminectomy showed cauda equina nerve roots to be studded with gray tumor nodules. Only a decompression of the spinal cord and conus medullaris was achieved. A histopathologic diagnosis of DSRCT was established. The patient underwent both radiotherapy and three courses of chemotherapy (cisplatin, etoposide, and Holoxan). Despite initial improvement, the patient developed lower limb weakness and urinary incontinence. An MRI scan 27 months after initial diagnosis showed an increase in posterior fossa lesions, further tumor spread in the spinal axis, and enlargement of enhancing nerve root deposits, particularly at the C7–T1 level.

Materials and methods

Immunohistochemistry Formalin-fixed, paraffin-embedded specimens were stained by the hematoxylin–eosin, periodic acid-Schiff, and Gomori reticulin methods. Immunohistochemistry (avidin–biotin peroxidase complex method) was performed using antibodies to vimentin (Dako, Carpinteria, CA;1:500, V9), epithelial membrane antigen (EMA) (Dako, 1:50 BRD, E29), S-100 protein (Dako, 1:1600, polyclonal), glial fibrillary acidic protein (GFAP) (Dako, 1:4000, polyclonal), neurofilament protein (NF) (Dako, 1:800 BRD, 2F11), CD 56 (Monsan/Caltag, San Francisco, CA; 1:20, HNK-1), CD 99, (Dako, 1:100, 12E7), desmin (Dako, 1:200, DER11), myogenin (Dako, 1:500, F5D), CAM 5.2 (Becton Dickinson, San Jose, CA; 1:150 BRD, CAM 5.2), PSA (Dako, 1:4000 BRD, polyclonal), TTF-1 (Dako, 1:1000, 8G7G3/1), leukocyte common antigen (LCA) (Dako, 1:50, PD7/26&2B), INI-1 (BD Transduction, 1:100 BRD, 25), MIB-1 (Dako, 1:300, MIB-1), p53 (Dako, 1:200, DO7), synaptophysin (ICN, Costa Mesa, CA; 1:40, SY38), and MyoD1 (Dako, 1:50 BRD, 5.8A).

In case 1, ultrastructural studies were performed upon glutaraldehyde-fixed tissue routinely processed, stained with uranyl acetate and lead citrate, and studied on a Philips CM 12® transmission electron microscope (Philips Corp, Eindhoven, The Netherlands).

PCR analysis RT-PCR studies were performed in both cases. In patient 1, primers designed to amplify cDNA spanning the junction region of the *EWS–WT1* gene fusion site were used to analyze RNA on frozen tissue of the

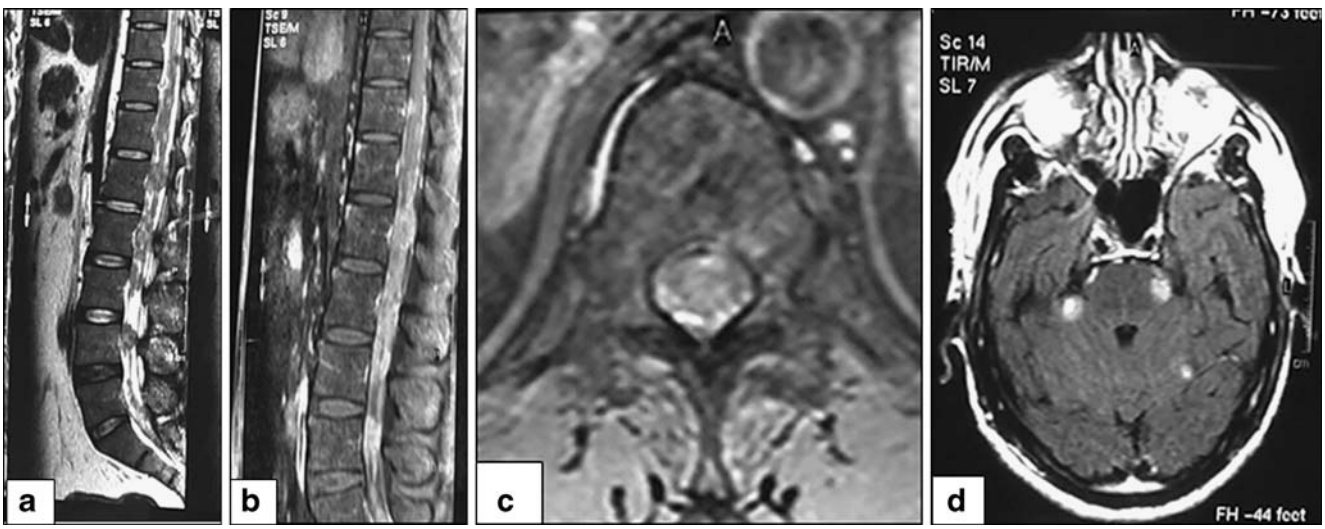

Fig. 2 Case 2. T2W midsagittal lumbar MRI shows multiple leptomeningeal metastases coating the distal spinal cord and cauda equina. The lesions approached 2 cm in size (**a**) and enhanced intensely on this fat saturation, post-contrast T1W sagittal images (**b**) axial views confirmed their leptomeningeal location (**c**). Intracranial tumor is confirmed on postcontrast axial T1W MRI scans of the posterior fossa; note meningeal enhancement due to pial metastasis (**d**)

spinal metastasis. The forward primer corresponded to the EWS exon 7 (5′-TCC TAC AGC CAA GCT CCA AGT C, Genbank accession X66899) and the reverse primer to the WT1 exon 9 (GAC CGG GAG AAC TTT CGC TGA C, Genbank accession X51630). The primer set was designed to detect fusions of EWS–WT1 involving distinct EWS exons. The predictor PCR product had to be one band, i.e., 197-bp product. To verify the presence of intact RNA, the expression of the housekeeping gene phosphoglycerate kinase (*PGK*) was confirmed. To confirm the in-frame exon fusions, automated sequencing (ABI Prism 377 DNA sequencer®) was employed. In patient 2, RT-PCR was performed on paraffin-embedded tissue using two sets of primers. In addition to the previously described primer set (EWS exon 7-WT1 exon 9), a new set of primer (EWS exons-WT1 exon 8) was designed to amplify smaller PCR products. Forward (5′- TCC TAC AGC CAA GCT CCA AGT C) and reverse (5′- ACC TTC GTT CAC AGT CCT TG) RT-PCR detected EWS exon 7-WT1 exon 8 fusion transcript. Thus, primer sets detecting two PCR product sizes (197 and 103 bp) were employed.

FISH analysis In case 1, the disrupted *EWS* gene was also assessed by this method in order to detect rearrangement in the region of the *EWS* gene. A commercially available EWS break-apart FISH probe (Vysis®, Inc. Abbott Park, Illinois) was used. As described by Qian et al. 2005 [25], the probe set was composed of a direct-labeled red probe and a direct-labeled green probe flanking the *EWS* gene region on chromosome 22q12.

Results

Patient 1

Intracranial and spinal biopsies showed similar histologic features. The second more optimal specimen from spinal level L5–S1 consisted of sheets of small- to medium-size cells with high nuclear cytoplasmic ratios and round to oval, hyperchromatic nuclei with inconspicuous nucleoli in addition to a desmoplastic stroma (Fig. 3a–b). Three and five mitoses were noted per 10 high-power (×40) fields (HPF) in the intracranial and spinal biopsies, respectively. Apoptotic bodies were scarce. No rosettes or glandular structures were identified. Foci of necrosis were seen, particularly in the spinal specimen. Reticulin stains were negative among tumor cells, reactivity being perivascular and stromal. The periodic acid-Schiff stain showed no glycogen. Immunohistochemically, both tumors showed a membrane pattern of EMA staining, strong paranuclear reactivity for CAM 5.2 (Fig. 3c), dot-like staining for desmin (Fig. 3d), and nuclear INI-1 positivity. The maximal MIB-1 labeling index (LI) was 17.6% in the spinal sample. Negative stains included synaptophysin, S-100 protein, NF protein, CD 56, CD99, myogenin, PSA, TTF-1, LCA, and MyoD1.

Ultrastructurally, the tumor was composed of oval to round cells with moderate to high nuclear/cytoplasmic ratios (Fig. 4a), no cell processes, round to somewhat irregular nuclei featuring delicate chromatin, and inconspicuous nucleoli. Frequent large cytoplasmic skeins of whorled intermediate filaments (Fig. 4b) and relatively few organelles were noted. These included scattered lamellar mitochondria, single profiles of rough endoplasmic reticulum, occasional Golgi complexes, and very rare electron dense bodies resembling secretory granules. Intercellular junctions were poorly formed and infrequent.

At the molecular genetic level, the tumor cells exhibited fusions of *EWS–WT1* genes involving distinct EWS exons. Unexpectedly, the PCR products consisted of two distinct bands, 197-bp and 416-bp products (Fig. 5). Automated sequencing of PCR products confirmed the in-frame fusion of both EWS exons 7-WT1 exon 8 (197 bp) and EWS exon 9-WT1 exon 8 (416 bp). The disrupted *EWS* gene was also demonstrated by FISH assay, which showed flanking of the *EWS* gene region on chromosome 22q12 (Fig. 6).

Patient 2

The tumor sample obtained from T12–L5 laminectomy showed broad cuffs of viable perivascular tumor cells separated by confluent zones of necrosis (Fig. 7a). As in case 1, the tumor cells featured oval to irregular nuclei with coarse chromatin and scant cytoplasm (Fig. 7b). Mitotic activity reached 5/10 HPF. The immunophenotype was also the same as in case 1. EMA+, CAM 5.2+ (paranuclear) (Fig. 7c); desmin+ (dot-like) (Fig. 7d), and nuclear INI-1+. The maximal MIB-1 LI was 11.5%. Tumor cells were also immunonegative for the same panel of antibodies noted above. In this case, the amplified DNA PCR products consisted of 103-bp (EWS exon 7-WT1 exon 8 fusion transcript) and 197-bp band transcript (EWS exon 7-WT1 exon 9 fusion) as shown in Fig. 8. Finally, RT-PCR for the alveolar rhabdomyosarcoma (ARMS) fusion transcripts PAX3-FKHR and PAX7-FKHR were not detected.

Discussion

In addition to one previously reported example of central nervous system (CNS) DSRCT [24], and a possible second case [23], the two cases reported herein illustrate the challenge of diagnosing undifferentiated small cell neoplasms of the CNS. Patient 1 presented with a relatively circumscribed CPA mass, clinically and radiographically

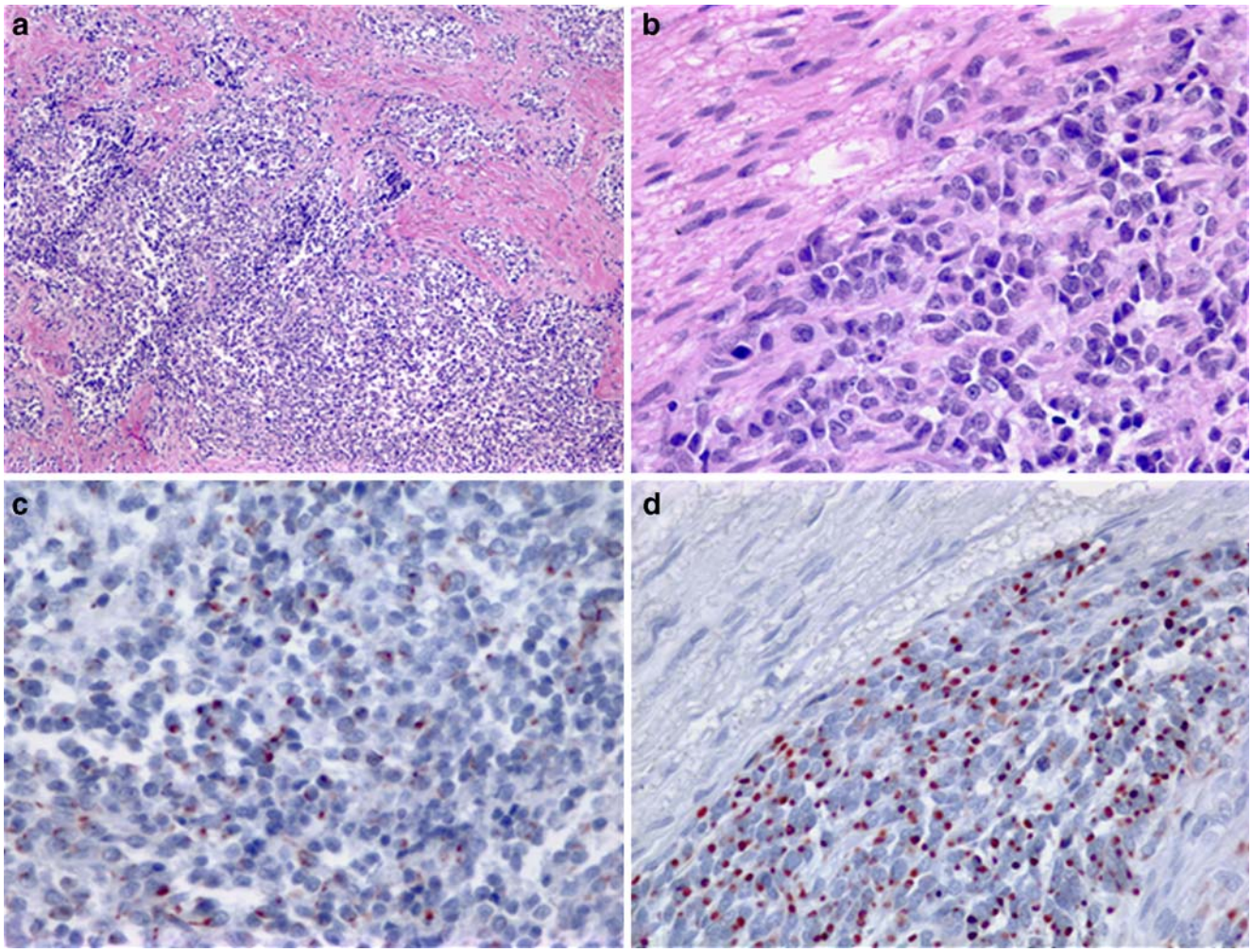

Fig. 3 Case 1. The spinal drop metastases feature solid cellular sheets and lobules separated by a desmoplastic stroma (**a**) H&E, ×100. The small to medium in size cells contain round to oval nuclei with inconspicuous nucleoli (**b**) H&E (×400). Immunohistochemically, they are positive for CAM 5.2 (**c**) and show a characteristic paranuclear dot-like desmin immunoreactivity (**d**) (×400)

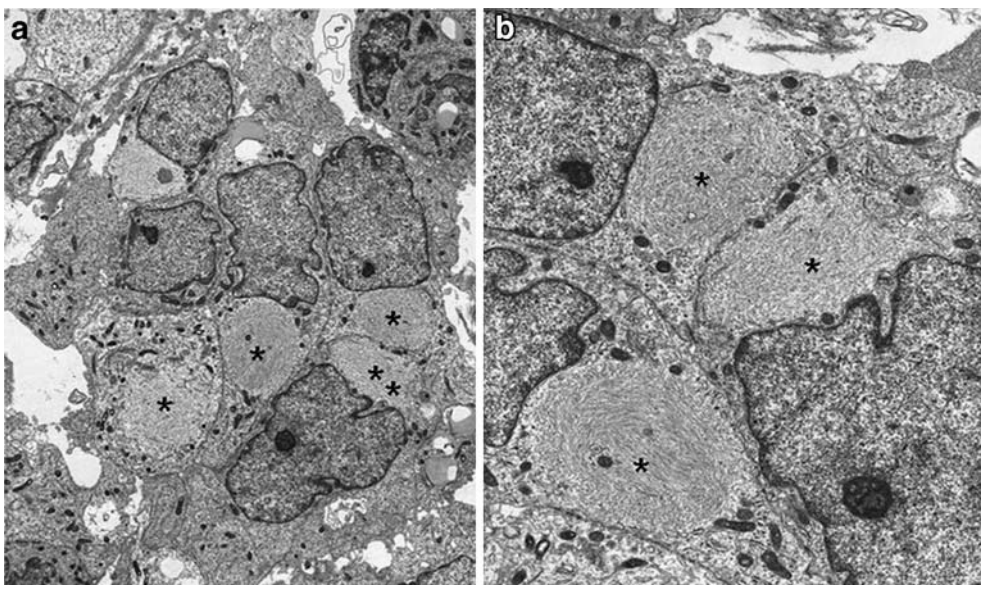

Fig. 4 Case 1. Ultrastructurally, the neoplastic cells of this "drop metastasis" are composed of cells with oval to round nuclei and few organelles (**a**) (×4.000). Note the large skein of whorled intermediate filaments (*asterisk*) displacing the nuclei. No cellular processes are evident (**b**) (×6.000). Intercellular junctions are scant and are poorly formed

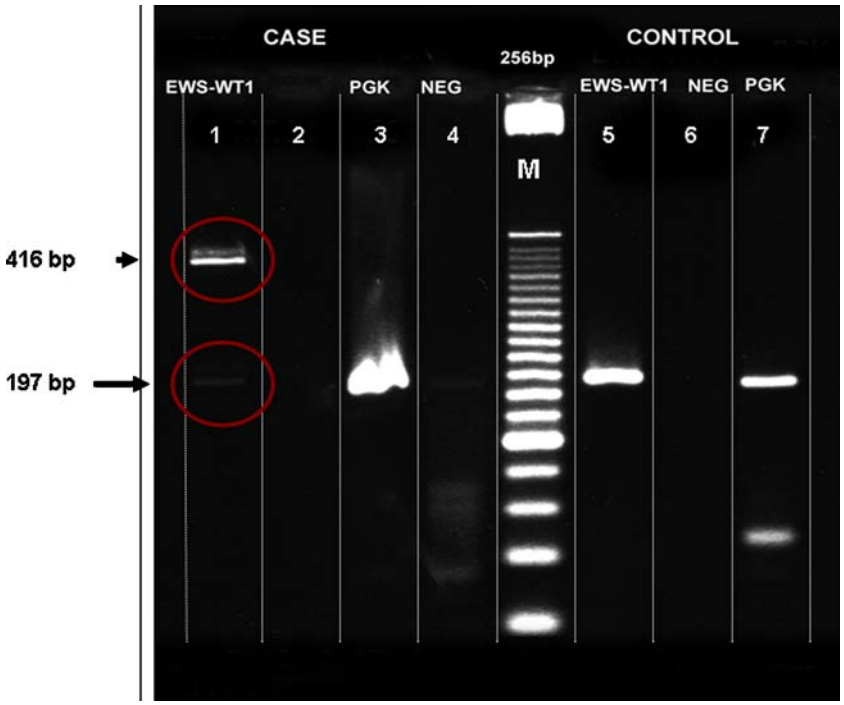

Fig. 5 Case 1. Agarose gel stained with ethidium bromide showing RT-PCR products. *Lane 1* shows a weak but consistent product of expected size (197-bp, *arrow*) as well as a major 416-bp product (*arrowhead*). The housekeeping gene *PGK*, an internal control, was amplified in the same reaction (189-bp, *lanes 3* and *7*). The positive control lane shows the standard 197-bp fragment (*lane 5*). Negative controls were used for each sample (*lanes 2*, *4*, and *6*). A 25-bp DNA ladder was used as a molecular marker (*M*)

mimicking acoustic neuroma. The initial, minute biopsy consisted of densely cellular sheets of round cells unassociated with desmoplastic stroma. In that the only two immunohistochemical markers (CAM 5.2, EMA) were applied, a tentative diagnosis of metastatic carcinoma was made. The correct diagnosis awaited an optimal biopsy of a spinal deposit. In case 2, the patient presented with symptoms of spinal cord compression by what the spinal MRI scans showed to be multiple, enhancing, leptomeningeal metastases; further MRI screening demonstrated intracranial lesions. In both cases, tumor was limited to the CNS. As expected, both showed immunoreactivity for epithelial (cytokeratin) and myogenic (desmin) markers, as well as molecular evidence of the EWS–WT1 translocation, thus confirming the diagnosis of DSRCT.

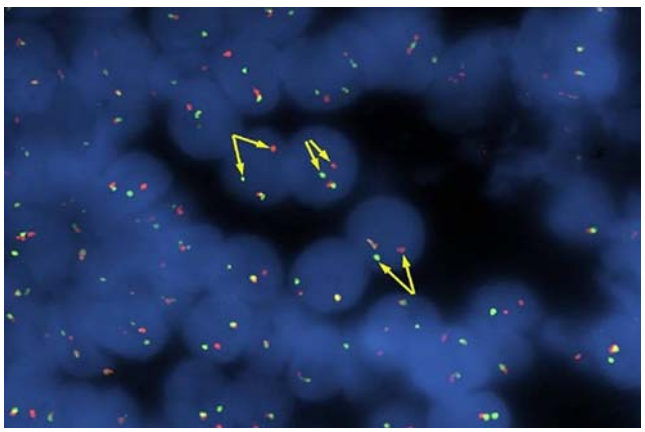

Fig. 6 Case 1. Representative abnormal interphase cells from the tumor specimen using a break-apart FISH probe for the Ewing sarcoma (*EWS*) gene show the normal *EWS* gene (*yellow fusion signal*) due to overlap of the *orange* (centromeric) and *green* (telomeric) probes. The abnormal *EWS* gene is demonstrated by break-apart of the *green* and *orange* FISH signals (see *arrows*) indicating structural disruption of the gene within the common breakpoint region of introns 7 to 10

The principal differential diagnoses of DSRCT of the CNS include medulloblastoma, primitive neuroectodermal tumor (PNET), and atypical teratoid/rhabdoid tumor (AT/RT). Aside from routine histology, which poses a challenge, the distinctions are readily made by immunocytochemical and molecular genetic methods. *Conventional medulloblastomas* consist of densely packed small cells with round to carrot-shaped nuclei. Processes vary in number, but with rare exceptions [2, 26], a fibrillary background or Homer–Wright rosette formation is not seen. Other variants, particularly large cell and anaplastic medulloblastoma are readily distinguished from DSRCT based on immunohistochemical features. Medulloblastomas express neuronal (synaptophysin, NF, class III B-tubulin) and occasionally glial markers (GFAP, S-100 protein) but lacking the epithelial ones (keratin, EMA) and myogenic (desmin, smooth muscle actin). They also show a very different genetic signature, loss of one arm of chromosome 17 ("isochromosome 17q") [27–30]. *Atypical teratoid/rhabdoid tumor* (*AT/RT*), a now well-established entity, often affects the posterior fossa, particularly the CPA. Its cells, which are larger than those of DSRCT, include (a) rhabdoid as well as "large pale cells," possess both vesicular nuclei and prominent nucleoli, (b) immunoreactivity for not only

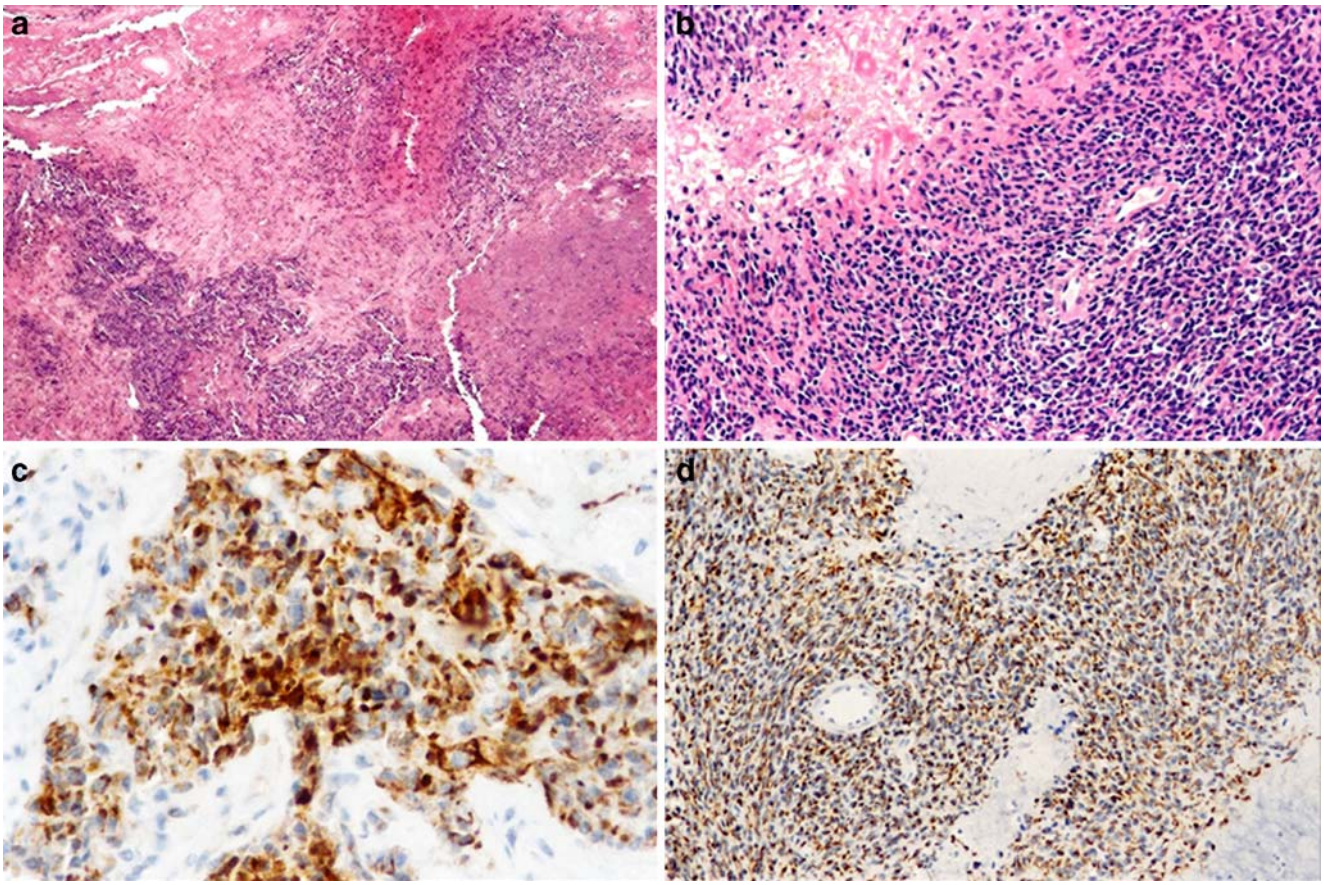

Fig. 7 Case 2. Photomicrographs of spinal drop metastases consisting of broad cuffs of viable perivascular tumor cells separated by confluent necrosis (**a**) H&E (×40). The tumor cells possess often oval nuclei with coarse chromatin as well as scant cytoplasm (**b**) H&E (×200). Note immunoreactivity for CAM 5.2 (**c**) (×400) and dot-like desmin staining (**d**) (×400)

epithelial (keratins, EMA) and myoid (smooth muscle actin, desmin) markers but neuronal/glial markers as well (synaptophysin, GFAP, S-100 protein), (c) loss of function of the *INI-1* gene and its protein product, but no EWS–WT1 translocations [31, 32]. Other differential diagnoses are readily excluded on the basis of histochemical and immunocytologic criteria; these include *small cell melanoma* (HMB-45 and Melan A+), *metastatic carcinoma*, (desmin-),

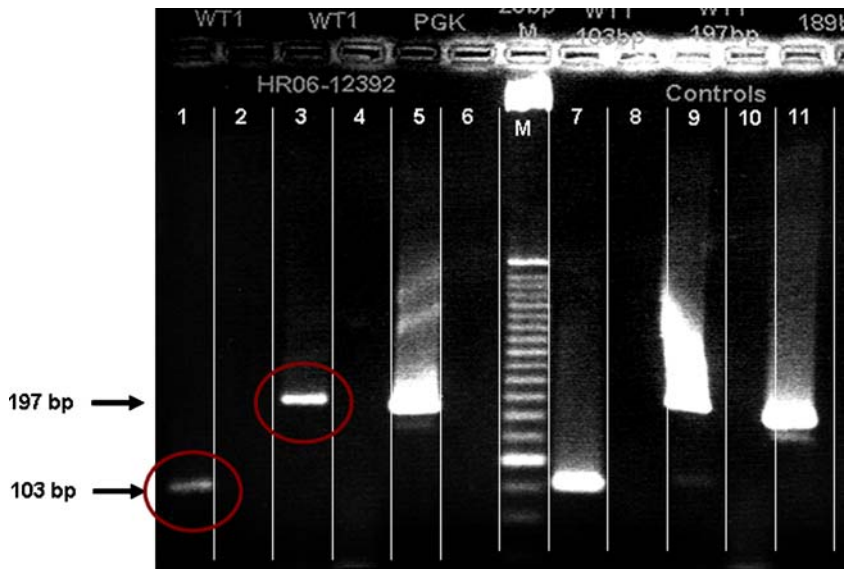

Fig. 8 Case 2. Agarose gel stained with ethidium bromide and showing two amplified PCR products, including small 103-bp (*lane 1*) and a large 197-bp products (*lane 3*). The housekeeping gene *PGK* was amplified in the same reaction as an internal control (189-bp, *lanes 5* and *11*). The positive control shows the standard 103-bp product (*lane 7*) and 197-bp fragment (*lane 9*). Negative controls were used for each sample (*lanes 2*, *4*, *6*, *8*, and *10*). A 25-bp DNA ladder was used as a molecular marker (*M*)

neuroblastoma (synaptophysin+), *Ewing's sarcoma* (PAS+, CD99+), *rhabdomyosarcoma* (MyoD1 and myogenin+), and *Wilms' tumor* (CD56 and WT1+).

Differential diagnoses aside, the histologic features of DSRCT vary considerably. In a series of 39 cases, Ordónez et al. [26] found about one-third to show unusual cytologic features including signet-ring, spindle, rhabdoid, and pleomorphic cells. In addition, pattern variations included "Zell-ballen-like" structures. More recently, even a large cell variant was described [33]. Globular, paranuclear accumulation of intermediate filaments, the basis of the paranuclear dot-like pattern of desmin immunoreactivity, which is a conspicuous ultrastructural feature, are not of themselves diagnostic of DSRCT [4, 34, 35].

The reciprocal chromosomal translocation t(11;22)(p13;q12) that characterizes DSRCT results in fusion of exon 7 of the *EWS* gene on chromosome 22 with exon 8 of the *WT1* suppressor gene on chromosome 11. The breakpoint within the *WT1* gene is usually between exons 7 and 8 [8, 36]. Although the chimeric transcript typically exhibits a breakpoint at EWS exon 7 and WT1 exon 8, our case 1 was unusual in that one breakpoint was in EWS exon 9, the result being in a longer (416 bp) PCR product. This unusual breakpoint was confirmed by automated sequencing, which demonstrated the in-frame fusion of EWS exon 9 to WT1 exon 8. In our second case, the characteristic DSRCT fusion transcript of EWS exon 7 to WT1 exon 8 was present. Since the RT-PCR was performed on paraffin-embedded tissue, our strategy included use of other primer sets designed to amplify smaller products. The sizes of amplified DNA PCR products in the second case were found to be 103-bp and 197-bp band transcripts. Interestingly, translocations involving the N-terminal domain of the *EWS* promoter gene at chromosome 22q12 also underlie other primitive neoplasms, including Ewing's sarcoma t(11;22)(q24;q12), extraskeletal myxoid chondrosarcoma t(9;22)(q22;q12), clear cell sarcoma of soft tissue t(11;22)(q13;q12), and rare cases of myxoid liposarcoma t(12;22)(q13;q12) [37].

The histogenesis of DSRCT remains unclear. Most previously reported cases have involved peritoneum or tunica vaginalis, thus suggesting a histogenetic relationship to mesothelium [38, 39]. A report of a pleural example further supports this notion [13]. The *WT1* gene is normally expressed in structures derived from intermediate mesoderm, for example in the transition of mesenchyme to nephron and of primitive gonadal mesenchyme to sex cord structures [40]. It is of note that submesothelial mesenchyme participates in the formation of several genitourinary organs containing epithelial and myoid elements. Nonetheless, the occurrence of DSRCT in soft tissues and bone [19, 20], parotid gland [21], and the CNS [24], as well as in aged patients, challenges the concept that DSRCT is either mesothelial-derived or blastomatous in nature. Despite some histopathologic overlap and the rare occurrence of focal neuroectodermal differentiation, DSRCT has not been histogenetically linked to peripheral PNET. Indeed, the unique t(11;22)(p13;q12) chromosomal translocation of DSRCT occurs at breakpoints different from that of Ewing's sarcoma/PNET t(11;22)(q24;q12). One plausible explanation for the histogenesis of DSRCT was forwarded by Katz et al. 1997 [41], who suggested that this tumor features polyphenotypism, neuroectodermal differentiation, and desmoplasia being epiphenomena governed by local environmental factors or mediated by various gene products. Indeed, the *WT1* gene products are involved in the expression of PDGFA, a chemo-attractant for fibroblasts that may explain the characteristic desmoplasia seen in DSRCT [42]. The hypothesis might explain one unique tumor occurring in a 37-year-old man with an intra-abdominal small round cell tumor sharing morphologic features of both PNET and DSRCT, as well as exhibiting the EWS/FLI-1 fusion transcript [41].

The only bona fide case of intracranial DSRCT was that of Tison et al. in 1996 who described a tentorial example in a 24-year-old man confirmed by Southern blot analysis [24]. At the time of their report, the patient had undergone chemo- and radiotherapy. Our attempts to obtain long-term follow-up in that case were unsuccessful (Rosai, personal communication, 2007).

In summary, we have described two additional cases of intracranial DSRCT in the CNS. Despite multimodal therapy, they seem to exhibit aggressive behavior similar to that of DSRCT arising in the peritoneal cavity. Our cases highlight the diagnostic challenge posed by poorly differentiated, round cell neoplasms in the CNS. Despite its rarity, DSRCT expands the differential diagnosis of small round cell tumors of the CNS.

Acknowledgments The authors thank Dr. Ricardo V. Lloyd for his critical review of the manuscript, Mrs. Julie Majerus for technical assistance, Mr. James Hopfenspirger for photographic expertise, and Mrs. Denise Chase for excellent secretarial support.

Conflict of interest statement We declare that we have no conflict of interest.

References

1. Gerald WL, Rosai J (1989) Case 2. Desmoplastic small cell tumor with divergent differentiation. Pediatr Pathol 9:177–183
2. Chang F (2006) Desmoplastic small round cell tumors: cytologic, histologic, and immunohistochemical features. Arch Pathol Lab Med 130:728–732
3. Gerald WL, Ladanyi M, de Alava E et al (1998) Clinical, pathologic, and molecular spectrum of tumors associated with t(11;22)(p13;q12): desmoplastic small round-cell tumor and its variants. J Clin Oncol 16:3028–3036

4. Gerald WL, Miller HK, Battifora H et al (1991) Intra-abdominal desmoplastic small round-cell tumor. Report of 19 cases of a distinctive type of high-grade polyphenotypic malignancy affecting young individuals. Am J Surg Pathol 15:499–513
5. Leuschner I, Radig K, Harms D (1996) Desmoplastic small round cell tumor. Semin Diagn Pathol 13:204–212
6. Antonescu CR, Gerald W (2002) Desmoplastic small round cell tumor. In: Fletcher CDM, Unni KK, Mertens F (eds) Tumors of soft tissue and bone. IARC Press, Lyon, pp 216–218
7. Lae ME, Roche PC, Jin L et al (2002) Desmoplastic small round cell tumor: a clinicopathologic, immunohistochemical, and molecular study of 32 tumors. Am J Surg Pathol 26:823–835
8. Gerald WL, Rosai J, Ladanyi M (1995) Characterization of the genomic breakpoint and chimeric transcripts in the EWS–WT1 gene fusion of desmoplastic small round cell tumor. Proc Natl Acad Sci USA 92:1028–1032
9. Ladanyi M, Gerald W (1994) Fusion of the EWS and WT1 genes in the desmoplastic small round cell tumor. Cancer Res 54:2837–2840
10. Rodriguez E, Sreekantaiah C, Gerald W et al (1993) A recurring translocation, t(11;22)(p13;q11.2), characterizes intra-abdominal desmoplastic small round-cell tumors. Cancer Genet Cytogenet 69:17–21
11. Bian Y, Jordan AG, Rupp M et al (1993) Effusion cytology of desmoplastic small round cell tumor of the pleura. A case report. Acta Cytol 37:77–82
12. Choi JK, van Hoeven K, Brooks JJ et al (1995) Desmoplastic small round cell tumor presenting in pleural fluid and accompanied by desmin-positive mesothelial cells. Acta Cytol 39:377–378
13. Parkash V, Gerald WL, Parma A et al (1995) Desmoplastic small round cell tumor of the pleura. Am J Surg Pathol 19:659–665
14. Syed S, Haque AK, Hawkins HK et al (2002) Desmoplastic small round cell tumor of the lung. Arch Pathol Lab Med 126:1226–1228
15. Slomovitz BM, Girotra M, Aledo A et al (2000) Desmoplastic small round cell tumor with primary ovarian involvement: case report and review. Gynecol Oncol 79:124–128
16. Young RH, Eichhorn JH, Dickersin GR et al (1992) Ovarian involvement by the intra-abdominal desmoplastic small round cell tumor with divergent differentiation: a report of three cases. Hum Pathol 23:454–464
17. Kawano N, Inayama Y, Nagashima Y et al (1999) Desmoplastic small round-cell tumor of the paratesticular region: report of an adult case with demonstration of EWS and WT1 gene fusion using paraffin-embedded tissue. Mod Pathol 12:729–734
18. Roganovich J, Bisogno G, Cecchetto G et al (1999) Paratesticular desmoplastic small round cell tumor: case report and review of the literature. J Surg Oncol 71:269–272
19. Adsay V, Cheng J, Athanasian E et al (1999) Primary desmoplastic small cell tumor of soft tissues and bone of the hand. Am J Surg Pathol 23:1408–1413
20. Antonescu CR, Gerald WL, Magid MS et al (1998) Molecular variants of the EWS–WT1 gene fusion in desmoplastic small round cell tumor. Diagn Mol Pathol 7:24–28
21. Wolf AN, Ladanyi M, Paull G et al (1999) The expanding clinical spectrum of desmoplastic small round-cell tumor: a report of two cases with molecular confirmation. Hum Pathol 30:430–435
22. Bouchireb K, Auger N, Bhangoo R et al (2008) Intracerebral small round cell tumor: an unusual case with EWS–WT1 translocation. Pediatr Blood Cancer 51:545–548
23. Yachnis AT, Rorke LB, Biegel JA et al (1992) Desmoplastic primitive neuroectodermal tumor with divergent differentiation. Broadening the spectrum of desmoplastic infantile neuroepithelial tumors. Am J Surg Pathol 16:998–1006
24. Tison V, Cerasoli S, Morigi F et al (1996) Intracranial desmoplastic small-cell tumor. Report of a case. Am J Surg Pathol 20:112–117
25. Qian X, Jin L, Shearer BM et al (2005) Molecular diagnosis of Ewing's sarcoma/primitive neuroectodermal tumor in formalin-fixed paraffin-embedded tissues by RT-PCR and fluorescence in situ hybridization. Diagn Mol Pathol 14:23–28
26. Ordonez NG (1998) Desmoplastic small round cell tumor: I: a histopathologic study of 39 cases with emphasis on unusual histological patterns. Am J Surg Pathol 22:1303–1313
27. Giangaspero F, Chieco P, Ceccarelli C et al (1991) "Desmoplastic" versus "classic" medulloblastoma: comparison of DNA content, histopathology and differentiation. Virchows Arch A Pathol Anat Histopathol 418:207–214
28. Katsetos CD, Herman MM, Frankfurter A et al (1989) Cerebellar desmoplastic medulloblastomas. A further immunohistochemical characterization of the reticulin-free pale islands. Arch Pathol Lab Med 113:1019–1029
29. Kleihues P, Louis DN, Scheithauer BW et al (2002) The WHO classification of tumors of the nervous system. J Neuropathol Exp Neurol 61:215–225 discussion 226–219
30. Louis DN, Ohgaki H, Wiestler OD et al (2007) The 2007 WHO classification of tumours of the central nervous system. Acta Neuropathol 114:97–109
31. Judkins AR, Mauger J, Ht A et al (2004) Immunohistochemical analysis of hSNF5/INI1 in pediatric CNS neoplasms. Am J Surg Pathol 28:644–650
32. Rorke LB, Packer RJ, Biegel JA (1996) Central nervous system atypical teratoid/rhabdoid tumors of infancy and childhood: definition of an entity. J Neurosurg 85:56–65
33. Pasquinelli G, Montanaro L, Martinelli GN (2000) Desmoplastic small round-cell tumor: a case report on the large cell variant with immunohistochemical, ultrastructural, and molecular genetic analysis. Ultrastruct Pathol 24:333–337
34. Backer A, Mount SL, Zarka MA et al (1998) Desmoplastic small round cell tumour of unknown primary origin with lymph node and lung metastases: histological, cytological, ultrastructural, cytogenetic and molecular findings. Virchows Arch 432:135–141
35. Peydro-Olaya A, Llombart-Bosch A, Carda-Batalla C et al (2003) Electron microscopy and other ancillary techniques in the diagnosis of small round cell tumors. Semin Diagn Pathol 20:25–45
36. Lee SB, Haber DA (2001) Wilms tumor and the WT1 gene. Exp Cell Res 264:74–99
37. Palmer RE, Lee SB, Wong JC et al (2002) Induction of BAIAP3 by the EWS–WT1 chimeric fusion implicates regulated exocytosis in tumorigenesis. Cancer Cell 2:497–505
38. Gonzalez-Crussi F, Crawford SE, Sun CC (1990) Intraabdominal desmoplastic small-cell tumors with divergent differentiation. Observations on three cases of childhood. Am J Surg Pathol 14:633–642
39. Ordonez NG, Zirkin R, Bloom RE (1989) Malignant small-cell epithelial tumor of the peritoneum coexpressing mesenchymal-type intermediate filaments. Am J Surg Pathol 13:413–421
40. Pritchard-Jones K, Fleming S, Davidson D et al (1990) The candidate Wilms' tumour gene is involved in genitourinary development. Nature 346:194–197
41. Katz RL, Quezado M, Senderowicz AM et al (1997) An intra-abdominal small round cell neoplasm with features of primitive neuroectodermal and desmoplastic round cell tumor and a EWS/FLI-1 fusion transcript. Hum Pathol 28:502–509
42. Gerald WL, Haber DA (2005) The EWS–WT1 gene fusion in desmoplastic small round cell tumor. Semin Cancer Biol 15:197–205

Virchows Arch (2009) 454:441–449
DOI 10.1007/s00428-009-0748-4

ORIGINAL ARTICLE

Expression of ADAMs ("a disintegrin and metalloprotease") in the human lung

Antoon Dijkstra · Dirkje S. Postma · Jacobien A. Noordhoek · Monique E. Lodewijk · Henk F. Kauffman · Nick H. T. ten Hacken · Wim Timens

Received: 14 September 2008 / Revised: 12 February 2009 / Accepted: 12 February 2009 / Published online: 3 March 2009

Abstract In view of the associations of "a disintegrin and metalloprotease" (ADAM) with respiratory diseases, we assessed the expression of various ADAMs in human lung tissue. Lung tissue was obtained from nine individuals who underwent surgery for lung cancer or underwent lung transplantation for emphysema. Also, 16HBE 14o- (human bronchial epithelial) and A549 (alveolar type II epithelium-like) cell lines were used. Immunohistochemistry was performed with antibodies recognizing different ADAM domains. The ADAMs were typically distributed over the bronchial epithelium. ADAM8 and ADAM10 were expressed diffusely in all layers of the epithelium. ADAM9, ADAM17, and ADAM19 were predominantly expressed in the apical part of the epithelium, and ADAM33 was predominantly and strongly expressed in basal epithelial cells. In smooth muscle, ADAM19 and ADAM17 were strongly expressed, as was ADAM33, though this expression was weaker. ADAM33 was strongly expressed in vascular endothelium. All ADAMs were generally expressed in inflammatory cells. The typical distribution of ADAMs in the lung, especially in the epithelium, is interesting and suggests a localized function. As most ADAMs are involved in release of (pro-) inflammatory mediators and growth factors, they may play an important role in the first line of defense and in initiation of repair events in the airways.

Keywords ADAM (a disintegrin and metalloprotease) · Lung · Epithelium · Inflammatory cells · Immunohistochemistry

A. Dijkstra · D. S. Postma · J. A. Noordhoek · N. H. T. ten Hacken
Department of Pulmonology, University Medical Center Groningen and University of Groningen,
Hanzeplein 1,
9713 GZ Groningen, The Netherlands

M. E. Lodewijk · W. Timens (✉)
Department of Pathology, University Medical Center Groningen and University of Groningen,
Hanzeplein 1,
9713 GZ Groningen, The Netherlands
e-mail: w.timens@path.umcg.nl

H. F. Kauffman
Department of Allergology, University Medical Center Groningen and University of Groningen,
Hanzeplein 1,
9713 GZ Groningen, The Netherlands

Introduction

Although the "a disintegrin and metalloprotease" (ADAM) molecules are known for quite some time, it has more recently become clear that these molecules play a central role in many normal and abnormal biological processes. ADAMs are thought to be implicated in the control of membrane fusion and in cell–cell and cell–matrix interactions by the binding capacity of the disintegrin domain to specific integrins [1]. ADAMs have also been demonstrated to play a role in the shedding of proprotein ectodomains like membrane-anchored cytokines and growth factors [1]. The ADAM molecules are members of a disintegrin and metalloprotease family, which are type I transmembrane zymogen glycoproteins that typically contain a N-terminal secretion signal domain, an epidermal growth factor (EGF)-like-transmembrane part, and a cytoplasmic (C-terminal) domain [2, 3]. The EGF-like transmembrane domain has a prodomain, a metalloprotease-, a disintegrin-, and a cysteine-rich domain. For several ADAMs, the specific substrates have not been identified yet. The most extensively studied ADAM molecule is ADAM17 (also known

as tumor necrosis factor (TNF)-alpha-converting enzyme (TACE)), which cleaves membrane-bound TNF-alpha, thereby releasing this molecule in its active, soluble form [4].

Because of their biological role in humans, further knowledge about the localization and function of ADAM-family members is also of importance to understand their role in disease development. In recent studies, ADAMs have been suggested to play a role in a pulmonary disease like asthma [5–9] but also in interstitial lung disease [10], eosinophilic pneumonia [11], and lung cancer [12]. Moreover, single nucleotide polymorphisms (SNPs) in *ADAM33* have been found to be associated with asthma development and progression [7] as well as with progressive lung function loss in the general population and development of COPD [13, 14]. In view of the association of ADAMs with respiratory diseases, our study was undertaken to assess the expression and localization of various ADAMs with metalloproteinase activity (ADAM8, ADAM9, ADAM10, ADAM17, ADAM19, and ADAM33) in human lung tissue. To verify epithelial localization, ADAM expression was also assessed in a human bronchial and alveolar epithelial cell line.

Materials and methods

Human lung tissue

Lung tissue was obtained from six individuals (age median [range], 65 [62–74]; four men, two women; three current smokers, two ex-smokers, one non-smoker) who underwent surgery for lung cancer and from three patients (age median [range], 61 [53–70]; two men, one woman, all ex-smokers) that underwent lung transplantation for emphysema. Lung tissue was taken as far as possible from the tumor and was normal on inspection. The lung tissue was only included in the study after exclusion of any lung pathology (for the emphysema cases, any lung pathology other than seen in COPD) as based on clinical data, lung function, and routine histological examination of lung tissue performed by an experienced pulmonary pathologist (WT). The procedures followed were in accordance with the ethical local and national guidelines.

Immunohistochemistry

Antibodies recognizing different domains of the ADAMs were commercially obtained (Table 1). Frozen lung sections were cut at 4 μm, dried for 20 min, and fixed in acetone (100%). Sections were incubated for 1 h with rabbit or goat antibodies for ADAMs in a proper dilution as determined previously. Endogenous peroxidase was blocked with 0.075% H_2O_2 in phosphate-buffered saline (PBS, pH7.4) for 30 min. Subsequently, sections incubated with rabbit antibodies were incubated for 30 min with peroxidase conjugated goat-anti-rabbit (GARpo) anti-serum, followed by incubation with rabbit-anti-goat (RAGpo). Sections incubated with goat antibodies were incubated with RAGpo, followed by incubation with GARpo. Sections were rinsed in PBS for 5 min after each incubation step. Peroxidase activity was demonstrated by immersing the slides in sodium acetate buffer containing 0.2 mg/ml 3-amino-9-ethyl-carbazole (Sigma-Aldrich Chemie BV, Zwijndrecht, The Netherlands) and 0.03% H_2O_2 for 15 min. Sections were counterstained with Mayers hematoxylin for 1 min. Immunohistology staining results were evaluated by three independent observers. Staining intensity was for each of the indicated tissue elements (Table 1) graded as − (absent), ± (weak), + (moderate), or ++ (strong).

Cell lines

16HBE 14o- (human bronchial epithelial cell line, a gift of Prof. D.C. Gruenert, University of Vermont, San Francisco, CA, USA) and A549 (alveolar type II epithelium-like cell line, American Type Culture Collection, Rockville, MD, USA) cells were cultured in Earle's MEM (BioWhittaker Europe BV, Cambrex, Verviers, Belgium) and RPMI 1640 (BioWhittaker), respectively. Both culture media were supplemented with 10% heat inactivated fetal bovine serum (BioWhittaker), L-glutamine (2 mM, BioWhittaker), streptomycin (100 μg/ml, BioWhittaker), and penicillin (100 U/ml, BioWhittaker) and cultured at 37°C with 5% CO_2. 16HBE and A549 cells were detached by trypsin-EDTA (BioWhittaker) treatment and cytospins were made. Subsequently, these cytospins were incubated with antibodies against the ADAMs and immunostained as described above.

Results

Expression of ADAMs in bronchial epithelial cells

The expression of the various ADAMs studied in different locations of human lung tissue is shown in Table 1 and illustrated in Fig. 1. There was no difference in expression patterns in the emphysematous lung tissue when compared to the normal lung tissue from the other six patients. All ADAMs were expressed in bronchial epithelium, yet they have a different distribution between basal and apical cells. ADAM9, ADAM17, and ADAM19 are predominantly expressed in the apical part of the epithelium, whereas ADAM33 expression is higher in basal epithelial cells.

Table 1 Location of expression of ADAMs in human lung tissue

ADAM	Designation	Company	Epithelium		Alveolar epithelium (type II)	Smooth muscle	Interstitial inflammatory cells	Endothelium
			Apical	Basal				
ADAM8	Ectodomain	R&D Systems	±	±	±	−	+	−
ADAM9	C-terminal	Biogenesis	+	±	±	±	++	±
	N-terminal	Biogenesis	+	±	+	±	+	±
ADAM10	C-terminal, peptide 732–748	Serotec	+	−/±	±	±	+	±
	N-terminal	Serotec	−/±	++	−	−	±	−
	Catalytic site	Biogenesis	+	+	−/±	±/+	+	−/±
ADAM17	Cytoplasmic domain, peptide 695–824	R&D	++	+	+	+	+	±
ADAM19	C-terminal	Biogenesis	+	+	±	+	++	+
	N-terminal	Biogenesis	+	−/±	−	−/±	+	+
	Catalytic site	Biogenesis	−	−	−	+	±/+	−/±
ADAM33	N-terminal	Serotec	−/±	+	−/±	±	+	+
	Cytoplasmic domain	Sigma-Aldrich	+	+	+	−/±	+	+
	Cytoplasmic domain	Triple Point	+	+	+	−/±	+	+
	Catalytic site	Sigma-Aldrich	−/±	±	−	−/±	+	+
	Prodomain	Sigma-Aldrich	−/±	+	+	±	+	+

Intensity of staining: ++ strong; + moderate; ± weak; − absent. The antiserum to ADAM8 was raised in goat, all others in rabbit. Company details: R&D Systems, Minneapolis, MN, USA; Biogenesis, Poole, UK; Serotec, Oxford, UK; Sigma-Aldrich Chemicals, Zwijndrecht, The Netherlands; Triple Point Diagnostics, Forest Grove, OR, USA. Designation of the antibodies as stated as given by the manufacturers

ADAM10 and ADAM8 are diffusely expressed over the epithelium. Interestingly, staining for the C-terminal end of ADAM10 is mainly seen in the apical part, and for the N-terminal end, this is located in the basal cells of the epithelium.

To verify our tissue findings, we stained ADAMs on the bronchial cell line 16HBE (Table 2), illustrated in Fig. 2. In 16HBE cells, ADAM9 and ADAM10 are most strongly expressed, whereas ADAM33 is weakly expressed. Not all 16HBE cells show expression of all ADAM subdomains; the percentage and intensity of positive cells are given in Table 2. Staining for the catalytic site of ADAM19 and ADAM33 showed no positive cells at all. When comparing the results of epithelial cell lines and lung tissue, expression in the 16HBE cell line matches the findings in bronchial epithelial cells in lung tissue.

Expression of ADAMs in alveolar epithelial cells

All ADAMs are expressed in alveolar epithelium (type II cells); however, expression of ADAM10 and ADAM19 is weaker in alveolar than bronchial epithelial cells. ADAM8, ADAM17, ADAM9, and ADAM33 in contrast are equally expressed in both epithelial cell types.

In the A549 alveolar epithelial type 2 cell line, almost all ADAMs are expressed in all cells (Table 2; illustrated in Fig. 2) although the ADAM33 catalytic site and prodomain show a minor number (5–10%) of negative cells, and ADAM 19 catalytic site shows no staining at all. In general, expression in A549 cells matches the findings in the alveolar type 2 cells.

Expression of ADAMs in bronchial smooth muscle tissue

The expression of ADAM19 is higher in smooth muscle than in bronchial epithelial cells, whereas ADAM17 is equally expressed in smooth muscle and epithelium. ADAM9, ADAM10, and ADAM33 are also expressed in smooth muscle tissue, yet with a weaker staining in smooth muscle cells than in bronchial epithelial cells. ADAM8 is not expressed in smooth muscle tissue.

Expression of ADAMs in vascular endothelium

ADAM33 is the most strongly expressed ADAM in the vascular endothelium. Some weak expression of ADAM9, ADAM10, ADAM17, and ADAM19 is present, yet endothelial expression of these latter ADAMs is not found in all subjects.

Expression of ADAMs in inflammatory cells

All ADAMs are uniformly and very profoundly expressed in interstitial inflammatory cells.

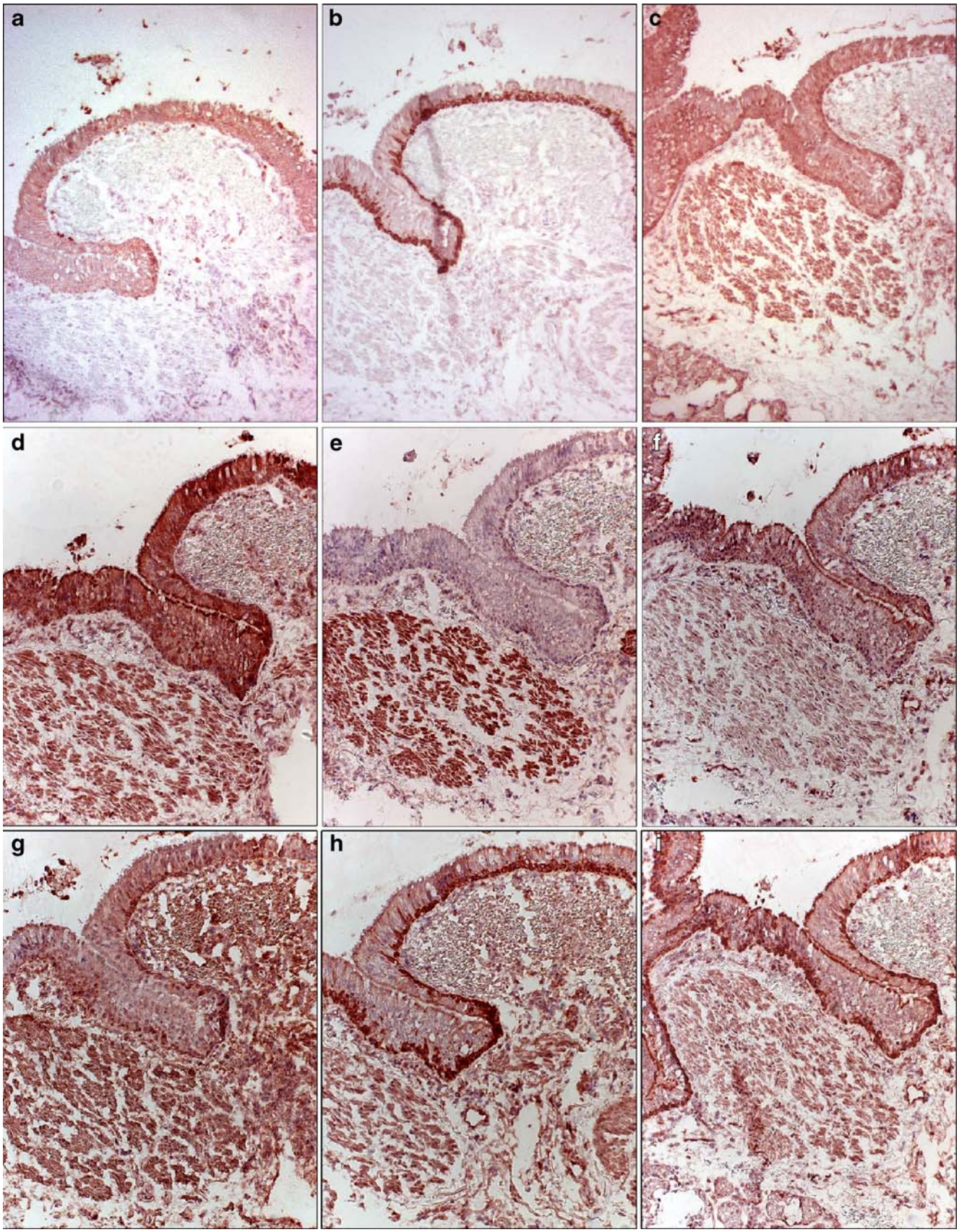
a
b
c
d
e
f
g
h
i

◀ **Fig. 1** Expression of ADAMs in normal human lung, immunostaining with antibodies designated to different domains of ADAMs (as indicated by manufacturers): **a** ADAM8 ectodomain, **b** ADAM10 N-terminal domain, **c** ADAM10 catalytic site, **d** ADAM17 cytoplasmic domain, **e** ADAM19 catalytic site, **f** ADAM19 N-terminal domain, **g** ADAM33 prodomain, **h** ADAM33 N-terminal domain, **i** ADAM33 cytoplasmic domain. Note specific localization patterns in different tissue compartments, in particular in different parts of the bronchial epithelium (immunoperoxidase, original magnification ×200)

Glandular cells and nerves

ADAMs are incidentally expressed in glandular cells and nerves that are present in some of the specimen.

Discussion

ADAMs have been suggested to play an important role in lung diseases [11–15]. As a starting point to understand the role of ADAMs in lung disease, it is important to note that we have found several ADAMs expressed specifically in both bronchial epithelium and alveolar type 2 epithelial cells, interstitial inflammatory cells, smooth muscle, and endothelium. Individual ADAMs showed specific distribution patterns in these cell types, whereas some ADAMs showed remarkable co-localization, suggestive for similar or mutual interacting functions. ADAM expression in a human lung bronchial and alveolar type epithelial cell line confirmed the expression in epithelium in human lung tissue. Interestingly, several ADAMs had a very topical (predominantly apical or basal) expression, in bronchial epithelium, suggesting that the more precise localization of individual ADAM molecules may signify their functional relevance.

Table 2 Expression of ADAMs in a human bronchial and a human alveolar epithelial cell line

ADAM	Designation	16HBE (% of total cells)	A549 (% of total cells)
ADAM8	Ectodomain	+ (100%)	+ (100)
ADAM9	C-terminal	++ (60);+(40)	+ (100)
	N-terminal	+ (100)	+ (100)
ADAM10	C-terminal	++ (60);+(40)	+ (100)
	N-terminal	++ (10);+(80);±(10)	± (100)
	Catalytic site	+ (80)	+ (100)
ADAM17	Cytoplasmic domain	+ (70)	+ (100)
ADAM19	C-terminal	+ (50)	+ (100)
	N-terminal	+ (50)	± (100)
	Catalytic site	−	−
ADAM33	N-terminal	± (70)	+ (100)
	Cytoplasmic domain	± (60)	+ (100)
	Catalytic site	−	+ (90)
	Prodomain	+ (80)	+ (95)

Intensity of staining: ++ strong; + moderate; ± weak; − absent

Given the apical localization in airway epithelial cells, ADAM17, ADAM19, and ADAM9 may play a role in early immune defense mechanisms. This is exemplified by both ADAM17 and ADAM19, which are both capable of shedding TNF-alpha. ADAM17 plays a key role in this release of soluble TNF-alpha by cleavage of the membrane-anchored precursor of TNF-alpha [16–18]. TNF-alpha is a proinflammatory cytokine and a key mediator in immune defense with a role in induction and amplification of inflammation, as a response to external, potential threatening stimuli. The prominent apical distribution of ADAM17 in the bronchial epithelium may thus enable easy activation and hence a low threshold for rapid and early release of TNF-alpha in the airway lumen in the defense to disease-initiating inhaled substances. In addition, cigarette smoke exposure of human airway epithelial cells has been shown to lead to ADAM17-mediated release of amphiregulin, which is a ligand for the epidermal growth factor receptor (EGFR) [19]. This can be of clinical relevance since stimulation of EGFR on epithelial cells contributes to mucus production and epithelial cell proliferation.

ADAM19 can, besides TNF-alpha, release tumor necrosis factor-related activation-induced cytokine (TRANCE) [20]. TRANCE is part of the tumor necrosis factor superfamily and has an immunity-modulating role as well. The joint apical expression of ADAM17 and ADAM19 is of interest and raises the question of whether this represents ability of coordinated action of the two molecules or that the regulation of each molecule is individually organized and may thus indicate their different roles in pathogenesis of disease. ADAM17, but in particular ADAM19, was also strongly expressed in smooth muscle. It is conceivable that particularly with chronic airway wall inflammation, as in asthma, these ADAMs may become activated and contribute to the perpetuation of the inflammatory process.

ADAM9, which also is apically expressed in epithelial cells, has a quite different function. It is capable of shedding of heparin-binding epidermal growth factor (HB-EGF) from bronchial epithelial cells via protein kinase C-delta (PKC-delta) activation [21]. HB-EGF is an important growth factor, not only for epithelial cells but also for smooth muscle cells and fibroblasts. This particular apical localization could then represent low threshold ability to early tissue (epithelial) repair, in conjunction with the other local defense mechanisms at the epithelial interface. Furthermore, ADAM9-mediated cellular adhesion by integrin binding has been described in fibroblasts, which leads to induction of fibroblast motility [22]. This capacity suggests

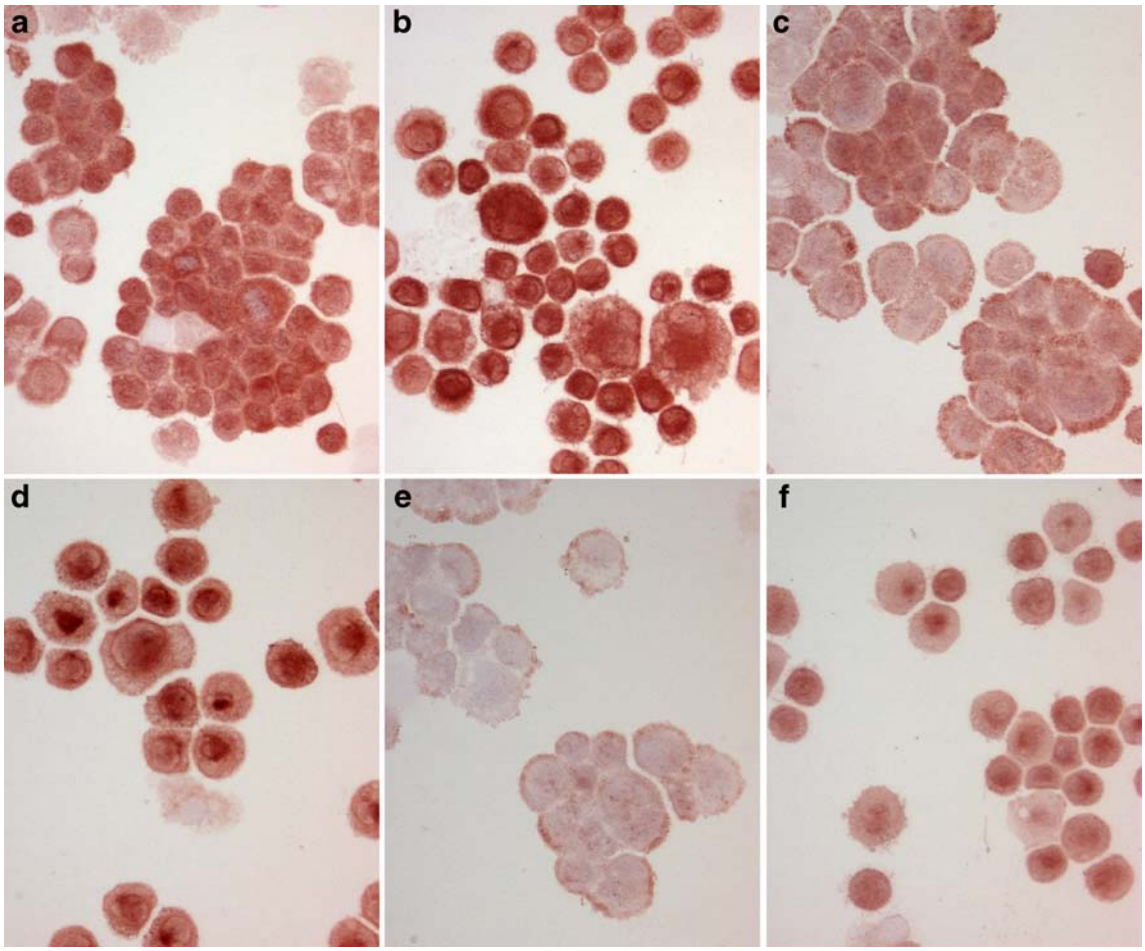

Fig. 2 Expression of ADAMs in bronchial epithelial cell line 16HBE (**a**, **c**, **e**) and alveolar epithelial cell line A549 (**b**, **d**, **f**): **a**, **b** ADAM17 cytoplasmic domain; **c**, **d** ADAM33 prodomain; **e**, **f** ADAM33 N-terminal domain (immunoperoxidase)

that ADAM9 also may play a role in remodeling of the airway wall by regulating motility and migration of fibroblasts and smooth muscle cells.

ADAM10 was diffusely expressed in the bronchial epithelium, and the N-terminal domain showed especially strong staining in basal epithelial cells. ADAM10 was also weakly expressed in smooth muscle. Similar to ADAM9, ADAM10 is capable of HB-EGF shedding. Considering the differences in distribution between these two ADAMs, it is tempting to speculate that once repair has set in by activating apically located ADAM9, ADAM10 in basal cells may be responsible for sustained repair effects, possibly also affecting underlying submucosal structures.

Human ADAM8 has been clustered as a human leukocyte differentiation antigen, CD156, and is thought to play a role in cell adhesion and infiltration of inflammatory cells [23, 24]. ADAM8 was expressed in bronchial and alveolar type II epithelium and interstitial inflammatory cells, predominantly with morphology of neutrophils and macrophages, without smooth muscle expression. These findings are consistent with its published expression in the epithelium and increased gene transcription in peribronchial and perivascular inflammatory cells in an allergen induced murine model of asthma [5]. ADAM8 can cleave CD23, the low-affinity IgE receptor (FcεRIIb) [25], which is involved in up regulation of IL-4 induced synthesis of IgE in B-cells [26]. CD23 shedding would counteract IgE-mediated immune responses, next to inducing release of proinflammatory mediators from macrophages [27].

ADAM33 was the only ADAM that was predominantly (and strongly) expressed in the basal cells of bronchial epithelium (Fig. 1g, h, i). Furthermore, ADAM33 was expressed in bronchial smooth muscle. A recent study showed several SNPs in the *ADAM33* gene to be associated with susceptibility of asthma and bronchial hyperresponsiveness [6]. The latter study showed ADAM33 to be expressed in human pulmonary fibroblasts and bronchial smooth muscle tissue, yet not in epithelial cells. Our findings are in line with more recent publications that

showed ADAM33 to be localized in epithelium [8, 28]. Low mRNA levels of ADAM33 are shown in bronchial biopsies although no mRNA was found in epithelial cells from bronchial brushes [29]. Considering our present findings, the latter might be explained by the content of the brushes, in which generally abundant ciliated cells and little basal epithelial cells are present. Yang et al. recently described a lack of ADAM33 mRNA in bronchial epithelium samples [30]. They suggested ADAM33 repression by a cell type-selective expression of ADAM33, which was epigenetically controlled by DNA methylation.

Our findings of basal epithelial cell expression of ADAM33 support its possible involvement in remodeling process, as in asthma [31]. This may well be initiated by shedding of c-kit ligand. Not only ADAM33 [32] but also ADAM8 [33], ADAM9 [34], ADAM17 [35, 36], and ADAM19 [20] are capable of shedding of c-kit ligand, also known as stem cell factor (SCF). SCF plays, apart from its main role as hemopoietic growth factor, a role in recruitment and in maturation of mast cell progenitors [37], sustaining the survival and maintaining phenotypic properties of mast cells in mucosal tissues [38, 39]. Furthermore, SCF may play a role in eosinophil migration and/or retention in activated tissue compartments [31], given its expression on human peripheral blood cells. Eosinophils express a functional c-kit receptor that stimulates very late antigen 4 (VLA-4)-mediated cell adhesion to fibronectin and vascular cell adhesion molecule 1 (VCAM-1). As mast cells and eosinophils are thought to play a key role in the pathogenesis of asthma [40, 41] and possibly also to be implicated in COPD [42, 43], the extensive presence of ADAMs capable of release of c-kit ligand in the airways suggests a regulatory role for these molecules in manifestation of these diseases.

Another issue of importance is that a large number of alternatively spliced forms of ADAM33 have been identified [44, 45]. Some show structural similarity to a synthetic ADAM12-S that induces myogenesis [46], in turn suggesting ADAM33 to be able to induce airway smooth muscle proliferation and hypertrophy [44].

Interestingly, strong expression of ADAM33 was observed in vascular endothelial cells, whereas other ADAMs were more weakly expressed. This may reflect their role in adhesion, extravasation, and possibly activation of inflammatory cells, especially eosinophils. Furthermore, it might contribute to angiogenesis, which is thought to play a role in asthma and COPD as well [47, 48]. Furthermore, angiogenesis is important in tumor development; EGFR-signaling of ADAMs may contribute in this way [3].

We used commercially available antibodies that are designed to bind to different domains of the ADAM proteins. We found similar localization in expression of different antibodies to subdomains of the same ADAM and for some, like ADAM33, also for different antibodies to the same (cytoplasmic) subdomain. Interestingly, there is a lack of staining for the catalytic (metalloproteinase) site of ADAM19 and ADAM33, which may implicate that these ADAMs are lacking the metalloproteinase site and therefore are present in an inactive form. For ADAM33, there is suggestive evidence that this is indeed the case since alternative splice variants have been described that mostly lack the metalloproteinase site [44].

Our present study is the first to investigate expression of several ADAM proteins in lung tissue and discusses the findings as to their putative role in the pathogenesis of respiratory diseases. As emphysematous lung tissue shows a similar expression pattern as the other lung tissues from patients that underwent surgery for lung cancer, there seems to be no obvious effect of the lung tumors on the lung tissue with respect to ADAMs expression. Clearly, this survey should be expanded, including much more diseased lung tissue to get further information about possible ADAMs variations that may play a role in lung disease. ADAMs appear to have a typical, specific distribution over the bronchial epithelium and other parts of the bronchial wall like smooth muscle and vascular endothelium. This specific localization of ADAMs, especially in the apical and basal epithelial cells, is interesting as to their individual and joint contribution toward defense against inhaled substances. Given the current knowledge on their functional properties, the distribution suggests that ADAMs play a main regulatory role in the first line of defense at the epithelial barrier by coordinated release of proinflammatory mediators as well as in remodeling and tissue repair by topic release of various growth factors. A next step is to dissect the exact functional role of ADAMs and subtle functional expression differences of ADAMs and their splice variants in the development and progression of pulmonary diseases.

Acknowledgment This work was supported by the Netherlands Asthma Foundation, grant number 3.2.00.38.

Conflict of interest We declare that we have no conflict of interest.

References

1. Primakoff P, Myles DG (2000) The ADAM gene family: surface proteins with adhesion and protease activity. Trends Genet 16:83–87
2. Black RA, White JM (1998) ADAMs: focus on the protease domain. Curr Opin Cell Biol 10:654–659

3. Blobel CP (2005) ADAMs: key components in EGFR signalling and development. Nat Rev Mol Cell Biol 6:32–43
4. Peschon JJ, Slack JL, Reddy P et al (1998) An essential role for ectodomain shedding in mammalian development. Science 282:1281–1284
5. King NE, Zimmermann N, Pope SM et al (2004) Expression and regulation of a disintegrin and metalloproteinase (ADAM) 8 in experimental asthma. Am J Respir Cell Mol Biol 31:257–265
6. Van Eerdewegh P, Little RD, Dupuis J et al (2002) Association of the ADAM33 gene with asthma and bronchial hyperresponsiveness. Nature 418:426–430
7. Jongepier H, Boezen HM, Dijkstra A et al (2004) Polymorphisms of the ADAM33 gene are associated with accelerated lung function decline in asthma. Clin Exp Allergy 34:757–760
8. Lee JY, Park SW, Chang HK et al (2006) A disintegrin and metalloproteinase 33 protein in patients with asthma: relevance to airflow limitation. Am J Respir Crit Care Med 173:729–735
9. Holgate ST, Holloway J, Wilson S et al (2006) Understanding the pathophysiology of severe asthma to generate new therapeutic opportunities. J Allergy Clin. Immunol 117:496–506
10. Edwards ST, Cruz AC, Donnelly S et al (2005) c-Kit immunophenotyping and metalloproteinase expression profiles of mast cells in interstitial lung diseases. J Pathol 206:279–290
11. Matsuno O, Miyazaki E, Nureki S et al (2007) Elevated soluble ADAM8 in bronchoalveolar lavage fluid in patients with eosinophilic pneumonia. Int Arch Allergy Immunol 142:285–290
12. Rocks N, Paulissen G, Quesada-Calvo F et al (2006) Expression of a disintegrin and metalloprotease (ADAM and ADAMTS) enzymes in human non-small-cell lung carcinomas (NSCLC). Br J Cancer 94:724–730
13. van Diemen CC, Postma DS, Vonk JM et al (2005) A disintegrin and metalloprotease 33 polymorphisms and lung function decline in the general population. Am J Respir Crit Care Med 172:329–333
14. Gosman MM, Boezen HM, van Diemen CC et al (2007) A disintegrin and metalloprotease 33 and chronic obstructive pulmonary disease pathophysiology. Thorax 62:242–247
15. Holgate ST, Yang Y, Haitchi HM et al (2006) The genetics of asthma: ADAM33 as an example of a susceptibility gene. Proc Am Thorac Soc 3:440–443
16. Black RA, Rauch CT, Kozlosky CJ et al (1997) A metalloproteinase disintegrin that releases tumour-necrosis factor-alpha from cells. Nature 385:729–733
17. Moss ML, Jin SL, Milla ME et al (1997) Cloning of a disintegrin metalloproteinase that processes precursor tumour-necrosis factor-alpha. Nature 385:733–736
18. Zheng Y, Saftig P, Hartmann D et al (2004) Evaluation of the contribution of different ADAMs to tumor necrosis factor alpha (TNFalpha) shedding and of the function of the TNFalpha ectodomain in ensuring selective stimulated shedding by the TNFalpha convertase (TACE/ADAM17). J Biol Chem 279:42898–42906
19. Lemjabbar H, Li D, Gallup M et al (2003) Tobacco smoke-induced lung cell proliferation mediated by tumor necrosis factor alpha-converting enzyme and amphiregulin. J Biol Chem 278:26202–26207
20. Chesneau V, Becherer JD, Zheng Y et al (2003) Catalytic properties of ADAM19. J Biol Chem 278:22331–22340
21. Izumi Y, Hirata M, Hasuwa H et al (1998) A metalloprotease-disintegrin, MDC9/meltrin-gamma/ADAM9 and PKCdelta are involved in TPA-induced ectodomain shedding of membrane-anchored heparin-binding EGF-like growth factor. EMBO J 17:7260–7272
22. Nath D, Slocombe PM, Webster A et al (2000) Meltrin gamma (ADAM-9) mediates cellular adhesion through alpha(6) beta(1) integrin, leading to a marked induction of fibroblast cell motility. J Cell Sci 113(Pt 12):2319–2328
23. Yoshiyama K, Higuchi Y, Kataoka M et al (1997) CD156 (human ADAM8): expression, primary amino acid sequence, and gene location. Genomics 41:56–62
24. Higuchi Y, Yasui A, Matsuura K et al (2002) CD156 transgenic mice. Different responses between inflammatory types. Pathobiology 70:47–54
25. Fourie AM, Coles F, Moreno V et al (2003) Catalytic activity of ADAM8, ADAM15, and MDC-L (ADAM28) on synthetic peptide substrates and in ectodomain cleavage of CD23. J Biol Chem 278:30469–30477
26. Nakamura T, Kloetzer WS, Brams P et al (2000) In vitro IgE inhibition in B cells by anti-CD23 monoclonal antibodies is functionally dependent on the immunoglobulin Fc domain. Int J Immunopharmacol 22:131–141
27. Bonnefoy JY, Plater-Zyberk C, Lecoanet-Henchoz S et al (1996) A new role for CD23 in inflammation. Immunol Today 17:418–420
28. Foley SC, Mogas AK, Olivenstein R et al (2007) Increased expression of ADAM33 and ADAM8 with disease progression in asthma. J Allergy Clin Immunol 119:863–871
29. Haitchi HM, Powell RM, Shaw TJ et al (2005) ADAM33 expression in asthmatic airways and human embryonic lungs. Am J Respir Crit Care Med 171:958–965
30. Yang Y, Haitchi HM, Cakebread J et al (2008) Epigenetic mechanisms silence a disintegrin and metalloprotease 33 expression in bronchial epithelial cells. J Allergy Clin Immunol 121 (1393–9):1399
31. Yuan Q, Austen KF, Friend DS et al (1997) Human peripheral blood eosinophils express a functional c-kit receptor for stem cell factor that stimulates very late antigen 4 (VLA-4)-mediated cell adhesion to fibronectin and vascular cell adhesion molecule 1 (VCAM-1). J Exp Med 186:313–323
32. Zou J, Zhu F, Liu J et al (2004) Catalytic activity of human ADAM33. J Biol Chem 279:9818–9830
33. Amour A, Knight CG, English WR et al (2002) The enzymatic activity of ADAM8 and ADAM9 is not regulated by TIMPs. FEBS Lett 524:154–158
34. Roghani M, Becherer JD, Moss ML et al (1999) Metalloprotease-disintegrin MDC9: intracellular maturation and catalytic activity. J Biol Chem 274:3531–3540
35. Mohan MJ, Seaton T, Mitchell J et al (2002) The tumor necrosis factor-alpha converting enzyme (TACE): a unique metalloproteinase with highly defined substrate selectivity. Biochemistry 41:9462–9469
36. Cruz AC, Frank BT, Edwards ST et al (2004) Tumor necrosis factor-alpha-converting enzyme controls surface expression of c-Kit and survival of embryonic stem cell-derived mast cells. J Biol Chem 279:5612–5620
37. Da Silva CA, Reber L, Frossard N (2006) Stem cell factor expression, mast cells and inflammation in asthma. Fundam Clin Pharmacol 20:21–39
38. Iemura A, Tsai M, Ando A et al (1994) The c-kit ligand, stem cell factor, promotes mast cell survival by suppressing apoptosis. Am J Pathol 144:321–328
39. MacDonald AJ, Thornton EM, Newlands GF et al (1996) Rat bone marrow-derived mast cells co-cultured with 3T3 fibroblasts in the absence of T-cell derived cytokines require stem cell factor for their survival and maintain their mucosal mast cell-like phenotype. Immunology 88:375–383
40. Boyce JA (2003) The role of mast cells in asthma. Prostaglandins Leukot Essent Fatty Acids 69:195–205

41. Oliveira SH, Lukacs NW (2003) Stem cell factor: a hemopoietic cytokine with important targets in asthma. Curr Drug Targets Inflamm Allergy 2:313–318
42. Grashoff WF, Sont JK, Sterk PJ et al (1997) Chronic obstructive pulmonary disease: role of bronchiolar mast cells and macrophages. Am J Pathol 151:1785–1790
43. Zhu J, Qiu YS, Majumdar S et al (2001) Exacerbations of Bronchitis: bronchial eosinophilia and gene expression for interleukin-4, interleukin-5, and eosinophil chemoattractants. Am J Respir Crit Care Med 164:109–116
44. Powell RM, Wicks J, Holloway JW et al (2004) The splicing and fate of ADAM33 transcripts in primary human airways fibroblasts. Am J Respir Cell Mol Biol 31:13–21
45. Umland SP, Garlisi CG, Shah H et al (2003) Human ADAM33 messenger RNA expression profile and post-transcriptional regulation. Am J Respir Cell Mol Biol 29: 571–582
46. Gilpin BJ, Loechel F, Mattei MG et al (1998) A novel, secreted form of human ADAM 12 (meltrin alpha) provokes myogenesis in vivo. J Biol Chem 273:157–166
47. Hashimoto M, Tanaka H, Abe S (2005) Quantitative analysis of bronchial wall vascularity in the medium and small airways of patients with asthma and COPD. Chest 127:965–972
48. Santos S, Peinado VI, Ramirez J et al (2002) Characterization of pulmonary vascular remodelling in smokers and patients with mild COPD. Eur Respir J 19:632–638

Virchows Arch (2009) 454:451–456
DOI 10.1007/s00428-009-0754-6

ORIGINAL ARTICLE

Infant and perinatal pulmonary hypoplasia frequently associated with brainstem hypodevelopment

Giulia Ottaviani · Rosaria Mingrone · Anna M. Lavezzi · Luigi Matturri

Received: 16 August 2008 / Revised: 15 November 2008 / Accepted: 27 February 2009 / Published online: 14 March 2009

Abstract Recent anatomo-pathological studies have revealed a frequent associated hypoplasia of both arcuate nucleus and lungs in stillbirths. The purpose of this study is to analyze the lung and brainstem development in sudden unexplained perinatal death and sudden infant death syndrome (SIDS). A total of 51 cases were investigated. A complete autopsy was performed in each case. Anatomo-pathologic examination of the central autonomic nervous system included an in-depth study on histological serial sections of the brains where the main structures participating in control of the vital functions are located. The stage of lung development was evaluated by macroscopic and microscopic criteria. In 52.9% of cases, a pulmonary hypoplasia was detected. The pulmonary hypoplasia was significantly more frequent in the SIDS group compared to the sudden perinatal unexplained death groups ($p<0.05$). In 72.5% of cases, histological examination of the brainstem on serial sections showed hypodevelopment of the brainstem nuclei, particularly hypoplasia, of the arcuate nucleus (60.8%). In 47.1% of cases, pulmonary hypoplasia was associated with brainstem hypodevelopment.

Competing interests statement No benefits in any form have been received or will be received from a commercial party related directly or indirectly to the subject of this article. In particular, there are no competing interests related to this article. All authors have no conflict to disclose.

G. Ottaviani · R. Mingrone · A. M. Lavezzi · L. Matturri
"Lino Rossi" Research Center for the study and prevention of the unexpected perinatal death and SIDS, University of Milan, Milan, Italy

G. Ottaviani (✉)
MED08—Anatomic Pathology,
Dipartimento di Scienze Materno-Infantili, University of Milan,
Via della Commenda 9,
Milan 20122, Italy
e-mail: giulia.ottaviani@unimi.it
URL: http://users.unimi.it/giuliaottaviani/

Keywords SIDS · Sudden perinatal unexplained death · Pulmonary hypoplasia · Brainstem hypodevelopment.

Introduction

In the final stages of fetal life, the stimulatory effect on respiration is nullified by the dominant inhibitory input from nervous structures located in the upper portion of the brainstem, in particular the pre-Bötzinger and the parabrachial/Kölliker–Fuse complex [1–3]. Our recent anatomo-pathologic study of sudden fetal deaths after the 25th week of gestation has revealed frequent association of hypoplasia of the arcuate nucleus, an important chemoreceptorial respiratory center located on either side of the medullary ventral surface, and lung hypoplasia. The incidence of this associated pulmonary and brainstem nuclei hypoplasia is 31% in stillbirth [4].

We investigated the development of pulmonary parenchyma and correlated the possible presence of pulmonary hypoplasia with hypodevelopment of the brainstem nuclei in sudden unexplained perinatal victims. The purpose of this study was to analyze the physio-pathologic relationship between the brainstem and pulmonary development, with regard to unexplained perinatal death and sudden infant death syndrome (SIDS). Preliminary findings have been reported in abstract form [5].

Material and methods

Selection and classification of cases

A total of 51 consecutive cases (31 sudden perinatal unexplained death and 20 SIDS) were investigated over the time of three years. Clinical information regarding

symptoms, familial history, electrocardiograms, and circumstances of death, as well as pregnancy runs and parents' habits were requested. Mothers' pregnancy in all cases had run a normal course. None of the mothers had any significant pathology.

A case was classified as sudden intrauterine unexplained death (SIUD) when a fetus died suddenly with no explained cause after the 22nd gestational week, before complete expulsion or extraction of the fetus from the mother, resulting in a stillbirth for which there was no explanation despite postmortem examinations [6–8].

A case was classified as Sudden Neonatal Unexplained Death (SNUD) when a newborn died suddenly with no explained cause, from birth to the end of the first postnatal month of life [8, 9].

A case was classified as SIDS when an infant death was sudden, completely unexpected and unexplained after a thorough case investigation, including performance of a complete autopsy, examination of the death scene, and a review of the clinical history [10].

Accordingly, in this study, a diagnosis of SIUD was established for 18 fetuses (ten males and eight females, ranging in age from 33 to 41 gestational weeks), of SNUD for 13 newborns (six males and seven females, ranging in age from 7 h to 24 days) and of SIDS for 20 infants (eight males and 12 females, ranging in age from 1 to 9 months).

Necropsy investigational protocol

A complete autopsy was performed on all cases, including close examination of the cardiac conduction system, as well of the central and peripheral autonomic nervous structures involved in cardio-respiratory reflexogenesis, according to our investigational protocol [11–13].

A complete autopsy examination was carried out, including a systemic gross and microscopic evaluation of the body. The placental disk, the umbilical cord, and the membranes were accurately examined in fetuses. All organs were fixed in 10% phosphate-buffered formalin, processed and embedded in paraffin. Five-micrometer sections from myocardium and cardiac conduction system were stained with hematoxylin–eosin and Heidenhain's trichrome (Azan).

The brainstem and the lung were the particular focus of this study.

Examination of the brainstem included sampling of three specimens. The first specimen, ponto-mesencephalic, includes the upper third of the pons and the adjacent portion of midbrain. The second extends from the upper third of the medulla oblongata to the portion adjacent to the pons. The third specimen took as reference point the obex and extends 2–3 mm above it and below it. Transverse serial sections were made at intervals of 60 μm. For each level, 12 5-μm sections were obtained, two of which were routinely stained for histological examination alternately using hematoxylin-eosin and Klüver-Barrera stains and three additional sections at each level were placed on slides for immunohistochemistry if required. The remaining sections are saved and stained as deemed necessary for further investigations. The histological evaluation of the brainstem was focused on the locus coeruleus, the parafacial nucleus, the parabrachial/Kölliker–Fuse complex in the pons/mesencephalon, and on the hypoglossus, the dorsal motor vagal, the tractus solitarius, the ambiguus, the pre-Bötzinger, the inferior olivary and the arcuate nuclei in the medulla oblongata [11–13].

The stage of lung development in each case was evaluated based on a autopsy macroscopic criterion, namely the correlation between lung weight and body weight (LW/BW), and according to microscopic criteria, that is, the presence of cartilaginous bronchi up to the distal peripheral level and the radial alveolar count (RAC). This parameter involves examining at least ten fields for each case with a 40× lens to estimate the number of alveoli transected by a perpendicular line drawn from the center of the most peripheral bronchiole (recognizable by not being completely covered by epithelium) to the pleura or the nearest interlobular septum. In order to carry out this examination, we used samples of fetal lung sectioned parallel to the frontal plane and passing through the hilus [14]. According to the macroscopic criterion, a LW/BW ratio below 0.012 was diagnostic for lung hypoplasia. The normal reference values for the microscopic criterion of RAC varies at different ages [14, 15].

Ethical approval

Ethical consent was not required for our study as the former Institute of Pathology is the referral national center for the study of sudden unexpected and unexplained infant and perinatal death, according to the Italian Law no. 31 of 2-02-2006 "Regulations for Diagnostic Post Mortem Investigation in Victims of Sudden Infant Death Syndrome (SIDS) and Unexpected Fetal Death".

Statistical analysis

Age was expressed as mean ± SEM. The histological findings in SIUD and controls were expressed as absolute value to total case number. The significance of differences between group parameters was evaluated by Fisher's test. The level of significance was set at $p<0.05$, two-tailed.

Results

At autopsy, examination of all the 51 victims were described as well developed, with body length and weight

corresponding to postconceptional age (gestational age + postnatal age), according to standard allometric growth patterns [16].

The 51 victims were subdivided into three age-related groups: 18 SIUD, 13 SNUD, and 20 SIDS, as shown in Table 1.

Overall, in 27 of the 51 cases (52.9%), pulmonary hypoplasia was observed, characterized by a decrease indices of pulmonary development, with a LW/BW value below 0.012 and/or a RAC index below the normal ranges for the given range group (Fig. 1). The pulmonary hypoplasia was detected in four of the 18 SIUD cases (22.2%), in six of the 13 SNUD cases (46.1%), and in 17 of the 20 SIDS cases (85%). The pulmonary hypoplasia was significantly more frequent in the SIDS group compared to the SNUD and SIUD groups ($p<0.05$; Table 1).

In 37 of the 51 cases (72.5%), the microscopic examination of serial sections of the brainstem showed hypodevelopmental abnormalities. Precisely, in 31 cases (60.8%), a hypoplasia of the arcuate nucleus was evident (Fig. 1); in three cases (5.9%), the nucleus was completely absent (agenesis); and in five cases (9.8%), there was neuronal immaturity of the arcuate nucleus. In four cases (7.8%), there was a hypoplasia of the reticular formation. Hypoplasia of the raphe obscurus was found in three cases (5.9%) of SIUD. Agenesis of the facial–parafacial complex was detected in two cases (3.9%). The solitary tract nucleus was found to be hypoplasic in two cases (3.9%) and presented neuronal immaturity in another case. The dorsal vagal nucleus was hypoplasic in one case (1.9%) and presented neuronal immaturity in another case (1.9%). Neuronal immaturity of the inferior olivary nucleus was detected in one case (1.9%). Neuronal immaturity and hypoplasia of the hypoglossus nucleus was identified in one case of SIDS (1.9%). Hypoplasia of the parabrachial/Kölliker–Fuse complex was detected in one case of SIUD (1.9%). Hypoplasia of the pre-Bötzinger complex was detected in one case of SIUD (1.9%). Table 1 shows the distribution of the brainstem among the SIUD, SNUD, and SIDS groups. In two cases, severe inflammatory infiltrates were observed, and in one case, gliosis of the brainstem was observed. In 13 victims (25.5%), one or more combined brainstem developmental abnormalities were detected in the same case.

In 24 of the 51 cases (47.1%), the pulmonary hypoplasia was associated with hypodevelopment of the brainstem nuclei (Fig. 1). A total of ten cases (19.6%) presenting with both pulmonary hypoplasia and hypodeveloped brainstem nuclei had smoking parents (Table 1).

Among the 18 fetuses, examination of the placenta, together with the membranes and umbilical cord revealed chorioamnionitis in eight cases (44.4%), villitis in three cases

Table 1 Demographic data and histopathological findings of the 51 analyzed cases, divided by SIUD, SNUD, and SIDS groups

	SIUD	SNUD	SIDS	Total
No. of cases	18	13	20	51
Sex (M/F)	10/8	6/7	8/12	24/27
Age range	33-41 gw	7 h–24 days	1–9 months	33 gw–9 months
Pulmonary hypoplasia[a]	4/18 (22.2%)	6/13 (46.1%)	17/20 (85%)	27/51 (52.9%)
Arcuate nucleus hypoplasia	9/18 (50%)	8/13 (61.5%)	14/20 (70%)	31/51 (60. 8%)
Arcuate nucleus agenesis	1/18 (5.5%)	1/13 (7.7%)	1/20 (5%)	3/51 (5.9%)
Arcuate nucleus neuronal immaturity	1/18 (5.5%)	2/13 (15.4%)	2/20 (10%)	5/51 (9.8%)
Reticular formation hypoplasia	–	2/13 (15.4%)	2/20 (10%)	4/51 (7.8%)
Raphe obscurus hypoplasia	3/18 (16.7%)	–	–	3/51 (5.9%)
Facial/parafacial complex agenesis	2/18 (11.11%)	–	–	2/51 (3.92%)
Solitary tract nucleus hypoplasia	1/18 (5.5%)	1/13 (7.7%)	–	2/51 (3.9%)
Solitary tract nucleus neuronal immaturity	–	1/13 (7.7%)	–	1/51 (1.9%)
Dorsal vagal nucleus hypoplasia	–	1/13 (7.7%)	–	1/51 (1.9%)
Dorsal vagal nucleus neuronal immaturity	–	1/13 (7.7%)	–	1/51 (1.9%)
Inferior olivary nucleus neuronal immaturity	–	1/13 (7.7%)	–	1/51 (1.9%)
Hypoglossus nucleus hypoplasia and neuronal immaturity	–	–	1/20 (5%)	1/51 (1.9%)
Parabrachial/Kölliker-Fuse complex hypoplasia	1/18 (5.5%)	–	–	1/51 (1.9%)
Pre-Bötzinger complex hypoplasia	1/18 (5.5%)	–	–	1/51 (1.9%)

Subgroups: SIUD before birth; SNUD 0–30 days; SIDS 1–12 months

SIUD sudden intrauterine unexplained death, *SNUD* sudden neonatal unexplained death, *SIDS* sudden infant death syndrome

[a] Statistically significant: SIUD vs. SIDS and SNUD vs. SIDS, $p<0.05$

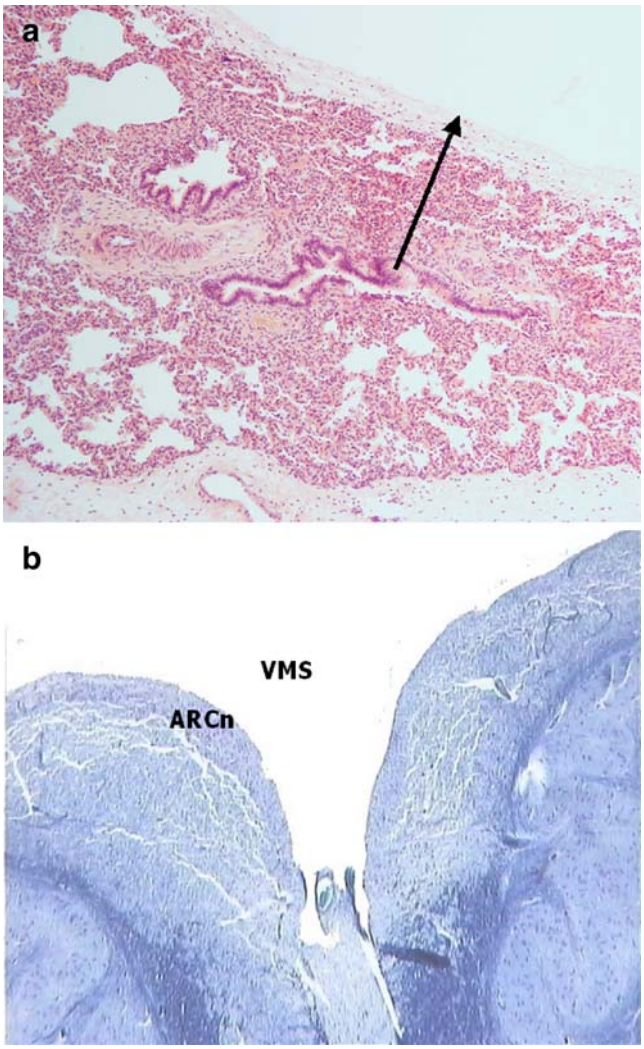

Fig. 1 Case no. 7. A 2-day-old female newborn deceased suddenly and unexpectedly. **a** The *line* illustrates the method for determining the radial alveolar count (RAC). The lungs are hypoplasic being the RAC<4.4. H–E, 100×; **b** Right monolateral hypoplasia of the arcuate nucleus (*ARCn*). *VMS* ventral medullary surface. Klüver-Barrera, 25×

(16.7%), and malposition of the umbilical cord in two cases (11.1%). Precisely, in one case, the umbilical cord was around the neck of the fetus but without causing constriction; in the other case, it was positioned around the foot.

Other pathological findings were fibromuscular hyperplasia of the pulmonary artery in 12 cases (23.5%), pneumonia in two cases (3.9%), and all these observations were not considered as primary pathology and possible causes of perinatal or infant death themselves.

Discussion

Our recent anatomo-pathological studies have revealed a correlation between pulmonary hypoplasia and abnormalities of the brainstem nuclei in stillbirth. In particular, a frequent hypoplasia of both arcuate nucleus and lungs in stillbirth has been reported [4].

In the human fetus, episodic rapid and irregular respiratory movements have been found and can be detected by ultrasound from the 11th week of gestation, becoming more marked as pregnancy progresses [17]. Fetal breathing regulates release of tracheal fluid in the lung and consequently regulates alveolar expansion and seems favoring lung development [18]. Lack of fetal respiratory movements could result in impaired development of the alveoli and in pulmonary hypoplasia [1, 19].

It has been reported that the predominating absence of ventilation in utero is determined by the inhibitory effect exerted mainly by the Kölliker–Fuse nucleus, located at the rostral level of the pons. Thus, in the fetus, there is a periodic disinhibition of the Kölliker–Fuse nucleus to allow breathing movements which favor pulmonary development [1, 2, 20, 21].

Aim of this work was to study the correlation between pulmonary hypoplasia and hypodevelopmental abnormalities of the brainstem nuclei deputed to vital functions control in fetuses, newborns, and infants dying suddenly and unexpectedly.

Sudden unexplained perinatal death and SIDS have been considered to have common morphological substrates [11, 12, 22]. Besides the abnormalities of the cardiac conduction system, histopathological substrates for sudden perinatal unexpected death and SIDS should be looked for in the wide field of neuropathology, based on the study on serial sections of the brainstem nuclei. In particular, hypoplasia of the arcuate nucleus, detected in this work in 60.8% of SIDS and sudden unexpected perinatal death victims (Fig. 1), is of great interest, particularly in view of its frequency and pathogenic implications [4, 11–13]. In 5.9% agenesis of the arcuate nucleus was detected, and in 9.80% of cases, there was neuronal immaturity of the arcuate nucleus. Hypodevelopment of the reticular formation, raphe obscurus, facial–parafacial complex, solitary tract, dorsal vagal, inferior olivary, hypoglossus nuclei, parabrachial Kölliker–Fuse, and pre-Bötzinger complexes were also detected. Subtle lesions involving these structures, isolated or associated, are likely responsible for disruption of neuronal pathways. The observations of similar anomalies in the SIDS and sudden unexplained perinatal deaths demonstrate that they are congenital in nature and that there is a clear continuity between SIDS and unexpected perinatal death. They are the morphological substrate for the releases of lethal nervous reflexes and/or of malignant arrhythmias. In particular, the neuropathological involvement of the cardiorespiratory, upper digestive and arousal centers may underline lethal reflexogenic mechanisms of sudden perinatal death and SIDS, without any clinically evident neurological dysfunctions.

Using specific macro- and microscopic criteria, we have hereby demonstrated the presence of pulmonary hypoplasia in 52.9% cases, with higher distribution among SIDS (85%) compared to SNUD (46.1%) and SIUD (22.2%) victims. In 47.1% of our cases, the lung hypoplasia was associated with hypodevelopment of the brainstem nuclei (Fig. 1). This suggests that the brainstem hypodevelopment exerts a negative effect on respiratory movements and on lung development already in utero. The pulmonary hypoplasia, associated with similar brainstem abnormalities among SIUD, SNUD, and SIDS, becomes then more frequent after birth and increases in SIDS group compared with sudden perinatal unexplained death (Table 1).

Our results show that 85% of SIDS cases have pulmonary hypoplasia. This finding raises the question as to whether the normal values we adopted are set too high. The population studied by Emery and Mithal [14, 15] are not specified other than they were normally formed. Presumably though, many of their infant deaths were SIDS even if they were not defined as such.

Furthermore, it is also important to underline that pulmonary disorders, in particular infections as detected in two of our cases, are related to the delayed pulmonary development during the antenatal, neonatal, and infantile period [23].

It was previously discussed for fetuses the importance to analyze the fetal development in utero by magnetic resonance making a prenatal diagnosis of lung hypoplasia associated with hypoplasia of brainstem nuclei could be applied in prenatal counseling, allowing early therapeutic planning [1, 24–27].

In conclusion, all the findings of our study confirm the hypothesis that hypopdevelopment of the brainstem nuclei, which modulate cardiorespiratory, upper digestive, and arousal activities, lead to disturbances in the lungs development, with increasing incidence in neonatal and infant age. The herein presented results confirm a continuum of lung hypoplasia associated with sudden death, not only in fetuses but, at increasing incidence, also in newborns and infants dying suddenly and unexpectedly. Further studies on the interactive normal and abnormal lung and brainstem development will lead to a better understanding of complex interactions involved in the pathophysiology of SIDS and sudden unexplained perinatal death. The cases presented here seem to usefully contribute research orientation and literature information in this field.

Acknowledgements Dr. Giulia Ottaviani, MD, PhD, is supported by PUR personal funding, University of Milano, project "Cardiovascular pathology of sudden infant and perinatal death with clinico-pathological correlations".

Conflict of interests The authors declare that have no conflict of interest. No benefits in any form have been received or will be received from a commercial party related directly or indirectly to the subject of this article.

References

1. Lavezzi AM, Ottaviani G, Ballabio G et al (2004) Preliminary study on the cytoarchitecture of the human parabrachial/Kölliker-fuse complex, with reference to sudden infant death syndrome and sudden intrauterine unexplained death. Pediatr Dev Pathol 7:171–179
2. Lavezzi AM, Ottaviani G, Rossi L et al (2004) Hypoplasia of the parabrachial/Kölliker-Fuse complex in perinatal death. Biol Neonate 86:92–97
3. Lavezzi AM, Matturri L (2008) Functional neuroanatomy of the human pre-Bötzinger complex with particular reference to sudden unexplained perinatal and infant death. Neuropathology 28:10–16
4. Matturri L, Lavezzi AM, Minoli I et al (2003) Association between pulmonary hypoplasia and hypoplasia of arcuate nucleus in stillbirth. J Perinatol 23:328–332
5. Matturri L, Ottaviani G, Minoli I et al (2007) Neonatal pulmonary hypoplasia frequently associated with brainstem hypodevelopment. 8th World Congress of Perinatal Medicine. September 9–13th, Florence, Italy. J Perinat Med Suppl 35:209
6. Frøen JF, Arnestad M, Frey K et al (2001) Risk factors for sudden intrauterine unexplained death: epidemiologic characteristics of singleton cases in Oslo, Norway, 1986–1995. Am J Obstet Gynecol 184:694–702
7. Ottaviani G, Matturri L (2008) Histopathology of the Cardiac Conduction System in Sudden Intrauterine Unexplained Death (SIUD). Cardiovasc Pathol 17:146–155
8. Lavezzi AM, Ottaviani G, Mauri M et al (2006) Alterations of biological features of the cerebellum in sudden perinatal and infant death. Curr Mol Med 6:429–435
9. Lavezzi AM, Ottaviani G, Matturri L (2007) Ontogenesis of human cerebellar cortex and biopathological characterization in sudden unexplained fetal and infant death. Virchows Arch 450:31–40
10. Willinger M, James LS, Catz C (1991) Defining the sudden infant syndrome (SIDS): deliberations of an expert panel convened by the National Institute of Child Health and Human Development. Pediatr Pathol 11:677–684
11. Matturri L, Ottaviani G, Alfonsi G et al (2004) Study of the brainstem, particularly the arcuate nucleus, in sudden infant death syndrome (SIDS) and sudden intrauterine unexplained death (SIUD). Am J Forensic Med Pathol 25:44–48
12. Matturri L, Ottaviani G, Lavezzi AM (2005) Techniques and criteria in pathologic and forensic-medical diagnostics in sudden unexpected infant and perinatal death. Am J Clin Pathol 124:259–268
13. Matturri L, Ottaviani G, Lavezzi AM (2008) Guidelines for neuropathologic diagnostics of perinatal unexpected loss and sudden infant death syndrome (SIDS) - A technical protocol. Virchows Arch 452:19–25
14. Emery JL, Mithal A (1960) The number of alveoli in the terminal respiratory unit of man during late intrauterine life and childhood. Arch Dis Child 35:544–547
15. Emery JL, Mithal A (1969) The weight of the lungs. In: Emery J (ed) The Anatomy of the Developing Lung. Heinemann Medical, London, pp 203–205
16. Weller U, Jorch G (1993) Current percentile curves for body weight, body length and head circumference of newborn infants after the 25th week of pregnancy. Monatsschr Kinderheilkd 141:665–669
17. Boddy K, Dawes GS (1975) Fetal breathing. Br Med Bull 31:3–7
18. Harding R, Bocking AD, Sigger JN (1986) Influence of upper respiratory tract on liquid flow to and from fetal lungs. J Physiol 61:68–71
19. Barness EG (1997) Respiratory system. In: Barness EG (ed) Potter's pathology of the fetus and infant. Mosby, St.Louis, MI, pp 712–773

20. Teitel DF (1996) Fetal chemoreception: a developing story. Reprod Fertil Dev 8:471–482
21. Blanco CE, Hanson MA, Kumar P (1995) Breathing and sleep states in the fetus and at birth. In: Loughlin GM, Carrol JL, Marcus CL (eds) Sleep and Breathing in Children. A Developmental Approach. Marcel Dekker. Inc. New York, pp, pp 161–179
22. Ottaviani G (2007) Crib death: sudden unexplained death of infants—the pathologist's viewpoint. Springer, Heidelberg
23. Nakamura Y (1993) Pulmonary disorders in infants. Acta Pathol Jpn 43:347–359
24. Lan LM, Yamashita Y, Tang Y et al (2000) Normal fetal brain development: MR Imaging with a half-Fourier rapid acquisition with relaxation enhancement sequence. Radiology 215:205–210
25. Inder TE, Huppi PS (2000) In vivo studies of brain development by magnetic resonance techniques. Ment Retard Dev Disabil Res Rev 6:59–67
26. Kuwashima S, Nishimura G, Timura F et al (2001) Low-intensity fetal lungs on MRI may suggest the diagnosis of pulmonary hypoplasia. Pediatr Radiol 31: 669–672
27. Duncan KR, Gowland PA, Moore RJ et al (1999) Assessment of fetal lung growth in utero with echo-planar MR imaging. Radiology 210:197–200

Virchows Arch (2009) 454:457–466
DOI 10.1007/s00428-009-0742-x

ORIGINAL ARTICLE

Salivary type tumors seen in consultation

Simion I. Chiosea · Robert Peel · E. Leon Barnes · Raja R. Seethala

Received: 8 December 2008 / Revised: 27 January 2009 / Accepted: 29 January 2009 / Published online: 7 March 2009

Abstract The aim of this study is to characterize personal consultation practice in salivary pathology and to identify most common diagnostic challenges. Seven hundred sixty consultation requests were prospectively indexed over 12 months, and 205 cases of salivary type tumors were identified. The following data were recorded: anatomic site, patients' age and gender, geographic origin of cases, diagnoses by submitting pathologist and consultant, and turn-around time. Final diagnosis was offered by submitting pathologist in 77 of 205 cases (37.5%). The definitive diagnosis was provided to contributors in 188 of 205 cases (91.7%); diagnostic limitations and potential adequacy issues were addressed in 17 remaining cases. The average turn-around time was 4.4 days. The three most common diagnostic problems were acinic cell carcinoma, epithelial myoepithelial carcinoma, and adenoid cystic carcinoma. Pathologists' adherence to recommendations by Association of Directors of Anatomic and Surgical Pathology regarding consultation practice is described.

Keywords Personal consultations · Salivary gland pathology

Introduction

Pathology consultation cases usually originate from two main sources: referral cases, also known as institutional consults (IC), in which the patient had been referred to a tertiary center for therapy or second opinion; and *consultation-only cases or personal consults* (PC), in which a second opinion was being sought but the patient was not being referred for therapy. These practices are summarized by the Association of Directors of Anatomic and Surgical Pathology (ADASP) in a 1993 report [1].

IC have been the subject of numerous studies [2–6] and included head and neck subsites [7, 8]. The focus of such studies is fairly concrete: accuracy with respect to an expert "gold standard" and impact of expert reclassification on patient management and outcome. Studies of PC are far more challenging, uncommon [9–11], always retrospective, and to date have not been performed in head and neck pathology. For PC, a final diagnosis is not rendered by the contributor, and thus is not exactly "reversed" by an expert. Therefore, assessment of concordance and accuracy is less meaningful here. Thus, a more pragmatic approach to analysis of PC would be to identify problematic areas and document the approach to resolution.

In order to describe the commonly encountered challenges in a head and neck consultative practice, we prospectively collected data on PC received by the Head and Neck Division at University of Pittsburgh Medical Center (UPMC) over a 1-year period. This real-time evaluation of PC revealed that salivary type tumors represent a major diagnostic dilemma. In this study, we focus on the commonly encountered problems in salivary gland pathology.

Electronic supplementary material The online version of this article (doi:10.1007/s00428-009-0742-x) contains supplementary material, which is available to authorized users.

S. I. Chiosea (✉) · R. Peel · E. L. Barnes · R. R. Seethala
Department of Pathology, Presbyterian Hospital,
University of Pittsburgh Medical Center,
PUH A616.2, 200 Lothrop Street,
Pittsburgh, PA 15213, USA
e-mail: chioseasi@upmc.edu

R. Peel
e-mail: peelrl@upmc.edu

E. L. Barnes
e-mail: barnesel@upmc.edu

R. R. Seethala
e-mail: seethalarr@upmc.edu

Materials and methods

About 40,000 surgical specimens are accessioned annually at UPMC-Presbyterian University Hospital (PUH), and 5,000 are from the head and neck organs. Three pathologists have extensive expertise in Head and Neck Pathology. Two Head and Neck Pathology fellows were in training during the academic year of this study (2007–2008). PC cases referred to UPMC Head and Neck Division were prospectively identified—760 cases over a 12-month period (Aug 2007 to July 2008; excluding endocrine cases). Of 760 cases, 205 cases were salivary type tumors, which are characterized in this study. This study is approved by Institutional Review Board (no. 0601084).

Indexed data The following data were recorded prospectively: age, gender, geographic location, and type of pathology practice where cases originated from academic, community, or commercial laboratory, number of slides and blocks submitted for review, and anatomic site. We categorized initial diagnoses as "none", "preliminary", or "final". In cases where final diagnosis was made, we further looked for the presence of a comment "case sent for additional extradepartmental review, addendum to follow". When no such a comment was present, we recorded who requested the consultation (e.g., clinician, patient) and how much time passed between the original sign out date and the date case was received at UPMC. Turn-around time (TAT) was measured in days, including weekends and holidays. When tissue block was required and was not submitted initially, TAT was calculated from the day block was received. If consultation was delayed for more than 7 days (n=36 cases), a written explanation of the delay was included in the report (e.g., conference time, extensive immunohistochemical [IHC] work-up). Most consultation cases were submitted by the pathologist within 6-week period after tissue was collected. All information was extracted from documentation submitted with pathology material. Since we were not involved in gross evaluation of consultation cases, we generally did not comment on adequacy of excision.

If necessary, *additional information* sometimes unavailable to the referring pathologist, such as radiologic appearance or clinical symptoms, was provided to us by clinician at our request. IHC studies were performed as previously described [12]. Most commonly used abbreviations of salivary type tumors are as follows: acinic cell carcinoma (ACC), adenoid cystic carcinoma (AdCC), epithelial myoepithelial carcinoma (EMCa), mucoepidermoid carcinoma (MEC), pleomorphic adenoma (PA), hyalinizing clear cell carcinoma of salivary origin (HCCC), low-grade cribriform cystadenocarcinoma (LGCCAC), polymorphous low-grade adenocarcinoma (PLGA).

Cost: A $250 fee was charged per consultation case.

Results

General characteristics of consult cases

The demographic and geographic features, submitted material, and TAT along with other general features of consultation cases are summarized in Table 1. The diagnoses rendered by consultants and anatomic distribution of cases are summarized in Table 2. Hematoxylin and eosin (H&E) slides alone were sufficient for diagnosis in only 27% of cases (55 of 205). Tissue blocks were initially submitted along with H&E slides in 43% of cases (89 of 205). Blocks were requested in 30% of cases following the review of initial H&E slides (61 of 205) and were received on average within 4.5 days.

Final or preliminary diagnoses were rendered in 153 of 205 cases (75%). Fifty-two cases were received without pathologists' interpretation: 25% of cases from community practices (36 of 142), 47% of cases from commercial laboratories (eight of 17), and 17% from academic institutions (eight of 46). Most of the cases with a final diagnosis (50 of 73, 68%) had a "disclaimer" in the final diagnosis or diagnostic comment field—"consultation pending".

Adherence to recommendations by Association of Directors of Anatomical and Surgical Pathology [1] All cases were accepted for consultation. The rendered diagnosis was always communicated to the submitting pathologist as a written report transmitted via fax. If the case was sent to more consultants after our opinion was rendered, we were not made aware of this fact. Gross description with cassette summary accompanied all cases. Fifty-one of 205 cases did not include the cover letter explaining the reason for consultation, specific questions to be answered, or working diagnosis. All slides were shipped in an adequate manner—No glass slide was received broken [13]. All materials that cannot be duplicated (tissue blocks and cytology slides) were returned. All recuts and special studies performed at UPMC PUH were retained.

Most common diagnostic challenges: epithelial myoepithelial carcinoma

General features of 21 EMCa are summarized in Table 3. Nineteen EMCas were located in the parotid gland (90.4%), one in submandibular gland (4.3%), and one in sublingual gland (4.3%). Tissue blocks/blank slides were provided in ten cases and requested by consultants after initial H&E evaluation in nine additional cases. Two cases were signed out based on H&E and IHC performed by submitting pathologists. Preliminary and final diagnoses rendered by submitting pathologists in cases diagnosed by consultants

Table 1 Demographic and other characteristics of patients and material

Demographic features	Men (number)/average age (years), %	86/56 (42%)
	Women (number)/average age (years), %	119/59 (58%)
Practice type (number, %)	Academic	46 (22%)
	Commercial	17 (8%)
	Community	142 (70%)
Slides per case, average		10
Cases received with accompanying blocks		89 (43%)
Cases with blocks requested following review of original H&E slides		61 (30%)
Turn-around time		4.4 days
Contributors' diagnoses	Final, with comment "consultation pending" [a]	50 (25%)
	Final, without the comment "consultation pending"	23 (11%)
	Preliminary	80 (39%)
	None	52 (25%)
Geography[b]	31 states; 125 different departments; top 5 contributors—PA (49[c]), CA (15), OH (14), FL (11); ≥5 cases were received from 17 states	

[a] Consultation was requested by clinicians in nine cases and patients in two cases

[b] One international case was received

[c] Of 49 PA cases, 11 were sent by University of Pittsburgh Medical Center-affiliated hospitals.

as EMCa are summarized in Table 4 (Electronic supplementary material).

Histologically, the majority of EMCa (17 of 21, 81.0%) showed a biphasic tubular proliferation of pale eosinophilic cuboidal inner/luminal cell layer surrounded by an often clear cell outer myoepithelial layer (Fig. 1a). However, in this series, clear cells dominated in only 11 of 21 cases (52.3%). Immunohistochemically, luminal cell layer was strongly positive for low molecular weight cytokeratin cocktail CAM5.2 (Fig. 1b), while the outer myoepithelial cell layer was positive for p63 (Fig. 1c), actin, and/or calponin (Fig. 1d). Of note, nine of 21 (42.8%) cases showed at least partial encapsulation (Fig. 1a). Of the named variants of EMCa, oncocytic and apocrine variants were noted in six of 21 (28.6%) cases (Fig. 1e). Here, the bi-layered appearance was maintained. However, the epithelial layer and often, the myoepithelial cell layers, showed abundant granular eosinophilic cytoplasm. In the apocrine EMCa, the epithelial component also showed periapical snouts, large nuclei with vesicular chromatin, and prominent nucleoli. This cell layer was positive for androgen receptor (Fig. 1f).

Adenoid cystic carcinoma

AdCC comprised 20 of 205 (9.8%) of salivary consultation cases. General features of AdCC are summarized in Table 3. Site distribution was as follows: parotid gland—five (25%), palate—two (10%), tongue—two (10%), buccal mucosa—one (5%), maxillary sinus—three (15%), submandibular gland—two (10%), ear—two (10%), nasal cavity—one (5%), nasopharynx—one (5%), neck, and not otherwise specified—one (5%). Preliminary and final diagnoses rendered by submitting pathologists in cases diagnosed as AdCC by consultants are summarized in Table 5 (Electronic supplementary material).

All AdCC were infiltrative basaloid tumors with basement membrane type material deposition (Fig. 2a). These tumors were also biphasic, consisting of an outer myoepithelial and inner ductal layers. However, unlike EMCa, both cell layers were comprised of cells with scant cytoplasm and small angulated, but relatively monomorphic hyperchromatic cells (Fig. 2b and d). Ten of 20 (50%) cases had a tubular or cribriform predominant morphology, while seven of 20 (35%) had solid predominant (Fig. 2c) morphology. The myoepithelial contribution to the tumor diminished as the solid component increased. Additionally, three of 20 (15%) cases had evidence of high-grade transformation (HGT) [14].

Acinic cell carcinoma

Twenty ACC were diagnosed over the period of this study. General features of ACC are summarized in Table 3. Seventeen carcinomas arose in the parotid gland, two in the upper lip (biopsies), and one in submandibular gland. Tissue blocks were provided in seven cases and requested by consultants after initial H&E evaluation in three additional cases. Preliminary and final diagnoses rendered by submitting pathologists in cases diagnosed as ACC by consultants are summarized in Table 6 (Electronic supplementary material).

ACC in this series were characterized by a variety of growth patterns: papillary cystic (n=5; Fig. 3d), solid (n=2; Fig. 3a),

Table 2 Diagnoses and anatomic distribution of salivary lesions

Diagnosis	Anatomic site, number of cases							
	(Para)nasal	Ear	Naso pharynx	Neck	Major salivary glands	Oral cavity	Thorax	Total
Acinic cell carcinoma					18	2		20
Adenoid cystic carcinoma	4	2	1	1	7	5		20
Adenoma, NOS					4			4
Atypical PA					5			5
Basal cell adenocarcinoma			1		3			4
Basal cell adenoma				1	4			5
Carcinoma ex PA					12			12
Carcinosarcoma ex PA					1			1
Canalicular adenoma					2	1		3
Cautery artifact					1			1
Cystadenoma					1			1
EMCA					21			21
HCCC						1		1
LGCCAC					3			3
Lymphadenoma					1			1
MEC					9	8		18[a]
Mucocele						3		3
No definitive diagnosis	1		1	1	1	11	2	17
Oncocytic hyperplasia					1			1
Myoepithelial carcinoma	1				8			9
Myoepithelioma					8			8
Normal histology					1			1
Oncocytoma					4			4
PA			1		12	4		19[b]
PLGA	1				1	5		7
Salivary duct carcinoma					10			10
Sialadenoma papilliferum						2		2
Warthin tumor				1	3			4
Total	7	2	4	4	140	42	2	205[a,b]

Of 140 cases located in major salivary glands, 117 cases involved parotid gland, 21 submandibular gland, one submandibular and parotid glands, one sublingual gland

NOS not otherwise specified, *PA* pleomorphic adenoma, *EMCA* epithelial myoepithelial carcinoma, *HCCC* hyalinizing clear cell carcinoma of salivary origin, *LGCCAC* low-grade cribriform cystadenocarcinoma, *PLGA* polymorphous low-grade adenocarcinoma

[a] One MEC was located at base of skull

[b] One additional PA was located in lacrimal gland and one in the larynx

and mixed microcystic and follicular (n=13; Fig. 1e; Table 7, Electronic supplementary material). The key histologic feature of ACC is the presence of zymogene granules, sometimes more obvious on Periodic Acid Schiff stain with diastase (PASD; Fig. 3b). In all but two cases, granules were smaller, fewer, and less basophilic than in classic cases (a combination of features more commonly seen in ACC arising in minor salivary glands). No case showed dedifferentiation or significant areas of clear cells. Prominent tumor-associated lymphoid response was present and mentioned in the diagnostic line in ten of 20 cases. In four cases, the prominence of vacuolated mucous-like cells (Fig. 3c) prompted the differential diagnosis of a mucoepidermoid carcinoma and "sebaceous" differentiation. In all of these cases, mucin appeared to be intraluminal rather than intracytoplasmic. Four cases were further complicated when the predominant cells were "intercalated duct-type cells" (Fig. 3f).

Consultation cases with no definitive diagnosis

In 8% of cases (17 of 205), no definitive confident diagnosis was rendered by consultants. General features of

Table 3 General features of epithelial myoepithelial carcinomas, adenoid cystic carcinomas, acinic cell carcinomas (three most common diagnostic challenges sent for consultation) and cases with no conclusive diagnosis

Feature, total cases	EMCa, 21	AdCC, 20	ACC, 20	No conclusive diagnosis
Average age, years	61.4	59.8	46[a]	57
Men to women ratio	9:12	11:9	8:12	9:8
Type of practice	C-15; Com–2; U-4	C-13; Com-2; U-5	C-12; Com -5; U -3	C-15; Com-1; U-1
TAT, days	4.8	4	2.6	6

Type of practice: C—community, Com—commercial laboratory, U—university

EMCa epithelial myoepithelial carcinoma, *AdCC* adenoid cystic carcinoma, *ACC* acinic cell carcinoma, *TAT* turn-around time (days)

[a] Four patients were younger than 21 [youngest—12 years of age]

these cases are summarized in Table 3. In 13 cases, it was impossible to distinguish between a benign and malignant process. In four cases, while the malignant nature of the process was apparent, the exact type of the cancer remained unclear. This subset of cases required a more extensive review by more than one consultant within our department, leading to a TAT of 6 days (versus 4.1 days TAT in cases where definitive diagnosis was provided). Preliminary and final diagnoses rendered by submitting pathologists in these cases are summarized in Table 8 (Electronic supplementary material). The anatomic distribution of this subset of cases is summarized Table 9 (Electronic supplementary material). Follow-up excisions were sent for two cases with inconclusive diagnosis: One case was confidently diagnosed as a PA. In another case, although the malignant nature of the neoplasm was firmly established (due to the presence of an invasive growth pattern), further classification was still impossible.

Discussion

The popularity of PC can be potentially attributed to many factors, but among the most prominent is the progressive evolution of sub-specialization in medicine. The refinement of clinical oncology and surgery practice places increasing demands on pathologists to provide a level of expertise and sophistication that satisfies this new and changing "standard of care". Unfortunately, the scope of material encountered by most practicing pathologists is still very broad and general. To address the challenge of providing improved expertise in each area, some academic centers adopt subspecialty sign out practice, but for most practices, this is not feasible. Thus, PC to designated experts in subspecialty area has become a viable option.

The current study is the first prospective analysis of a PC practice. While our data collection included all head and neck lesions (excluding endocrine), for this study, we have chosen to report on our experience with salivary type pathology, as this was the most prominent area of our consultative service (205 of 760 cases). The broad geographic distribution of contributors and demographic features of patients allow us to conclude that the problematic diagnostic patterns documented by this study are representative of challenges experienced by a larger pathology community. Regarding the breadth of material received during this 12-month period, almost all salivary type entities (as described in Head and Neck WHO Classification of Tumors) were represented (with the exception of sebaceous tumors, oncocytic carcinoma, and sialoblastoma). Furthermore, the demographic features of more common salivary neoplasms are similar to those described in the largest studies on the topic. For instance, the female predominance, age and anatomic distribution, and prevalence of ACC in this series mirrors those summarized in Armed Force Institute of Pathology atlas of tumors of the salivary glands [15].

For the first time, adherence to the ADASP recommendations for personal consultations is described. Twenty-five percent of consultation requests were NOT accompanied by final or preliminary diagnoses. This is one area for future improvement. Some criteria of consultation practice were never studied before. For instance, the TAT presented here was 4.4 days. For comparison, in this study, the average time required to receive the block once it was requested was 4.5 days. The only other benchmarks for comparison in the literature are the TAT provided by two retrospective European studies conducted by referring institutions (rather than consultants as in the present analysis): 22 days [16] and 32.8 days [17]. The TAT does depend on the diagnostic difficulty of the consult case. For instance, the recognition of classic H&E features of ACC resulted in faster TAT: these cases were signed out on average in 2.6 days. For comparison, the general TAT for all salivary type consultation cases was 4.4 days, and for cases were definitive diagnosis was not rendered, TAT was 6 days (waiting for additional clinical information, imaging studies, deeper H&E levels, IHC).

In 92% of cases (188 of 205 cases), expert pathologist provided the final diagnosis. It is difficult to appreciate the clinical and financial impact of this service.

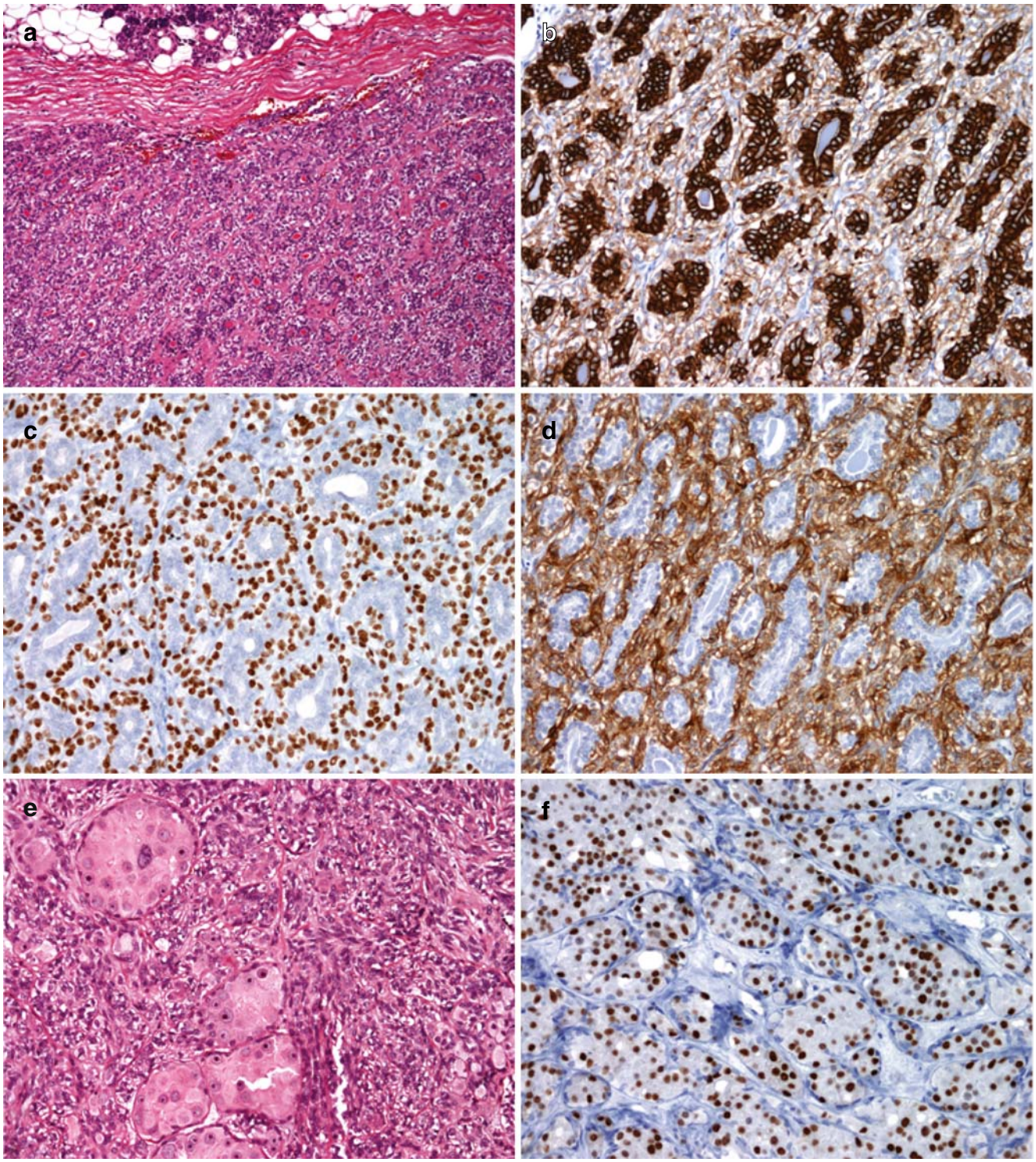

Fig. 1 Epithelial myoepithelial carcinoma diagnostic features. **a** Partially encapsulated EMCa showing a biphasic ductular proliferation of eosinophilic inner cells and clear outer myoepithelial cells, H&E, ×100. **b** CAM5.2 highlights luminal cells, IHC, ×200. **c** The outer myoepithelial cell layer is positive for p63, IHC, ×200. **d** Myoepithelial cells are highlighted by calponin, IHC, ×200. **e** Apocrine variant of EMCa with epithelial layer showing abundant granular eosinophilic cytoplasm, prominent nucleoli, H&E, ×400. **f** Luminal cells with apocrine features are positive for androgen receptor, IHC, ×200

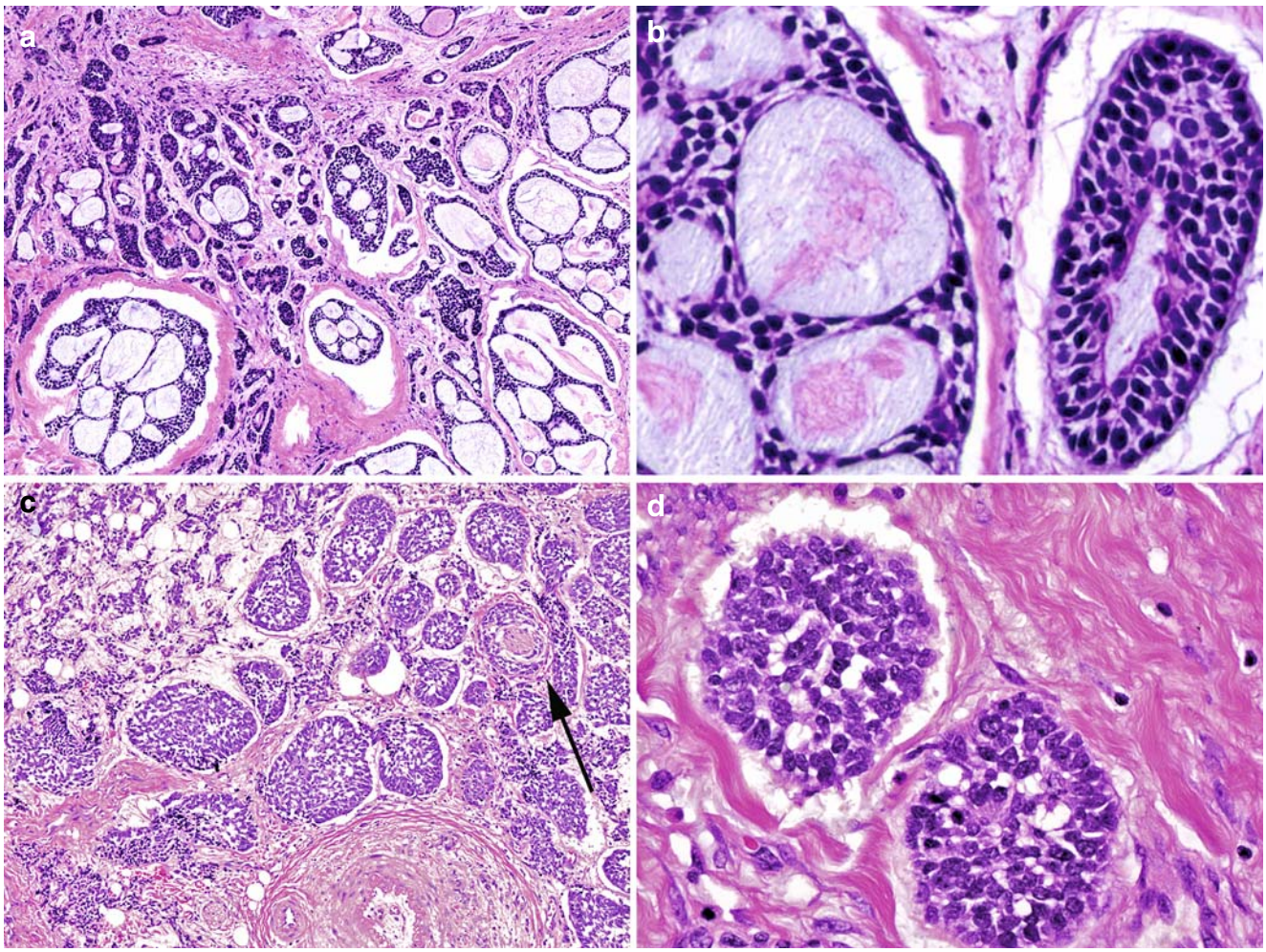

Fig. 2 Adenoid cystic carcinoma diagnostic features. **a** AdCC showing a basaloid cribriform patterned proliferation of tumor cells in myxohyaline matrix, H&E, ×100. **b** The distinguishing nuclear characteristics of AdCC are hyperchromasia, angulation, and monomorphism shown here. Also present is the characteristic clefting of tumor nests from stroma, H&E, ×400. **c** Solid AdCC showing perineural invasion, H&E, ×100. **d** The nuclear features are similar to the cribriform AdCC in Fig. 2b, H&E, ×400

Epithelial myoepithelial carcinoma

These tumors have proved historically to be difficult to recognize and categorize [15]. One of the major challenges in the accurate diagnosis is the rarity of this tumor. Additionally, the biphasic arrangement of tumor cells can show numerous patterns and variants [12]. Occasionally, one component may predominate, obscuring the biphasic nature of the tumor. As shown above, IHC stains can "unmask" the biphasic nature.

Another issue encountered here was the deceptively bland appearance of this low-grade malignancy. These tumors usually infiltrate in a multinodular fashion rather than angulated infiltrative nests. In our consult experience, at least partial encapsulation is relatively common, raising the possibility of a benign biphasic tumor, most notably of a cellular PA. As we noted in our previous series [12], this distinction may be extremely challenging particularly if the EMCa had arisen from PA, as noted in two cases in this study. Distinguishing features from PA include documentation of invasion, even if nodular or minimal, and absence of chondromyxoid stroma in EMCa.

Another perhaps less apparent reason for diagnostic difficulty is the restrictive nature of the AFIP definition requiring that the outer cell myoepithelial cell layer shows clear cytoplasm [15]. We characterized oncocytic and apocrine variants of EMCa that defy the classic definition and yet to date behave in a fashion similar to "classic" EMCa [12]. In this study, oncocytic and apocrine variants comprised over one fourth of our EMCa. This high prevalence of "non-classic" EMCa is likely reflective of "consult bias" towards unusual cases.

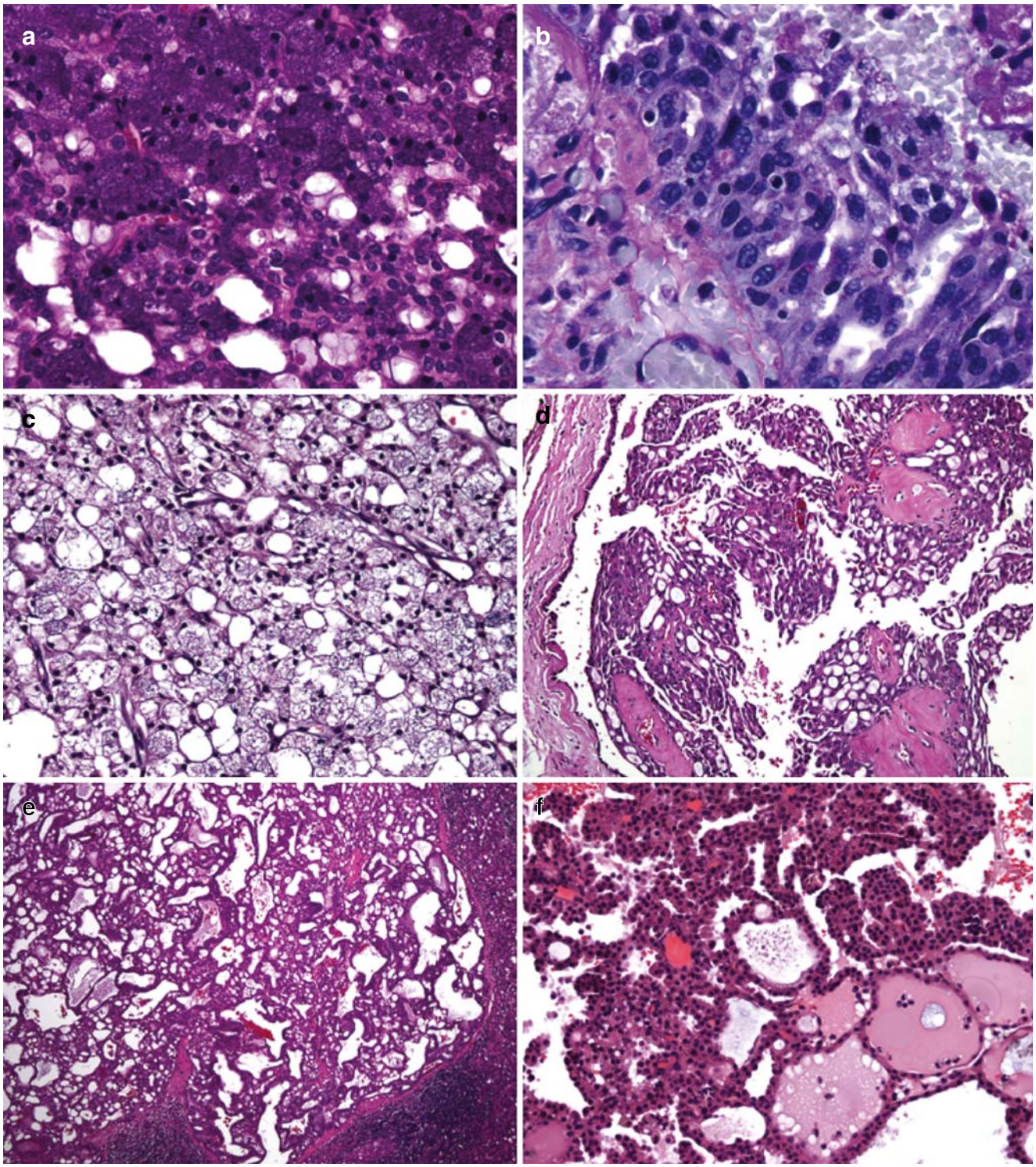

Fig. 3 Acinic cell carcinoma diagnostic features. **a** Classic well-differentiated acinic cell carcinoma with acinic cells with basophilic granular cytoplasm arranged in a solid pattern, H&E, ×200. **b** Rare cytoplasmic zymogene granules highlighted by periodic acid shift stain with diastase treatment (PASD resistant; PASD, ×400). **c** A representative area of acinic cell carcinoma with numerous modified serous/acinic cells showing vacuolated cytoplasm, H&E, ×200. **d** Papillary-cystic pattern of acinic cell carcinoma, H&E, 100×. **e** Mixed follicular and microcystic pattern of acinic cell carcinoma and tumor-associated lymphoid stroma, H&E, 100×. **f** Cuboidal intercalated duct-type cells arranged in mixed follicular and microcystic patterns; minimal to none acinic serous differentiation, H&E, ×200

Once the biphasic nature of a tumor is recognized and is confirmed to be malignant by its permeative growth, perineural, and/or angiolymphatic invasion, the differential diagnosis narrows to AdCC, basal cell adenocarcinoma, and oncocytic carcinoma (with respect to the oncocytic EMCa variant). Both EMCa and AdCC are biphasic tumors with the same phenotype—inner ductal and outer myoepithelial layers. However, AdCC tends to be more infiltrative and comprised of cells with more hyperchromatic and angulated nuclei with scanter cytoplasm. We have also noted clefting of tumor nests from the surrounding stroma/basement membrane type material to be more common in AdCC. In EMCa, the retraction artifact is more commonly seen between the luminal and outer layers (personal observations). Basal cell adenocarcinomas to some extent are biphasic tumors that may show central ducts and some outer myoepithelial cells. A key distinguishing morphologic features from EMCa is the presence of peripheral palisading of the outermost layer in basal cell adenocarcinomas. Only some of the outer basal cells in basal cell adenocarcinoma are myoepithelial (expressing p63 *and* actin/calponin); the rest express p63 only. Oncocytic carcinomas may show p63 positive cells; however, in contrast to a bona fide oncocytic EMCa, these cells are small, indistinct, and randomly distributed [18]. Apocrine EMCa, a newly described variant [19], is also oncocytoid in appearance but the ductal component has vacuolated cytoplasm, periapical snouts, and nuclear pleomorphism typical of apocrine change and reminiscent of salivary duct carcinoma. Additionally, these areas express androgen receptor similar to salivary duct carcinoma [20, 21].

Adenoid cystic carcinoma

AdCC, though more easily recognized, is still a significant part of our consult practice. Contributors are aware that not all basaloid or cribriform patterned salivary gland malignancies are automatically AdCC. To some extent, the predominant growth pattern dictates the differential diagnosis. For tubular/cribriform patterns, the biphasic tumor differential mentioned above comes into play, in addition to low-grade salivary gland malignancies such as PLGA, and rarely benign entities such as a cellular PA or basal cell adenoma. In contrast, solid AdCC and AdCC with HGT evoke high-grade diagnostic considerations, including carcinoma ex PA, salivary duct carcinoma, and non-salivary lesions such as neuroendocrine carcinoma, basaloid squamous cell carcinoma, or even a lymphoma. Our consult data appear to support this concept (see Table 5, Electronic supplementary material).

For the tubular and cribriform patterned AdCC, key diagnostic features are the recognition of the biphasic growth pattern and angulated dark nuclei. A historical differential diagnostic consideration is PLGA. It is interesting to note that this was not a significant issue in our consult practice. In our opinion, this consideration has diminished greatly with the characterization of salient morphologic features of PLGA [22]. PLGA is not a biphasic tumor; it is polymorphous in pattern, but fairly uniform in cell type with characteristic ovoid nuclei with open, "papillary thyroid carcinoma"-like chromatin [22]. PLGA is strongly positive for S100 [22].

For solid conventional AdCC, an epithelial phenotype predominates; however, immunostains will show a residual outer abluminal myoepithelial cell. AdCC with HGT, on the other hand, has the appearance of a high-grade adenocarcinoma or undifferentiated carcinoma, and there is no longer an abluminal myoepithelial layer. If the transformed component is present alone, it would be indistinguishable from an adenocarcinoma, not otherwise specified, or a high-grade carcinoma ex PA. Thus, one important diagnostic criterion is the recognition of a residual conventional AdCC component [14].

Acinic cell carcinoma

We have identified three sources of problems in diagnosis of ACC: abundance of mucous and vacuolated cells, tumor-associated lymphoid response, and predominance of non-specific intercalated ductal-type cells.

The importance of tumor-associated lymphoid response as a potential diagnostic pitfall was previously highlighted by Auclair [23]. Unlike acinic cell carcinoma, benign salivary tissue inclusions within lymph nodes are present in parotid gland only and demonstrate *both* ducts and acini [24]. A careful search for zymogene granules on PASD stain, combination of solid, follicular, microcystic, and papillary-cystic pattern along with the predominantly negative p63 immunostain (i.e., absence of epidermoid cells) will lead to the correct diagnosis of ACC.

In addition to highlighting common diagnostic challenges presented by recognizable nosologic entities, we outline here a *subset of biopsies with inconclusive diagnosis* following expert review. When the cytologic features are bland, the mitotic rate is low, and the classic morphologic features for a malignant category (e.g., ACC) are absent, the delineation of benign versus malignant process relies on evaluation of the periphery of the lesion to assess for invasiveness. In the absence of the tumor/normal tissue interface, it is essentially impossible to evaluate for defining features of malignancy: invasive growth, perineural, or angiolymphatic invasion. This does not imply that useful data cannot be gleaned from such biopsies. Here, morphologic characterization and immunohistochemical studies can at least narrow the differential diagnostic considerations, which were offered in all cases. The most common diagnostic line employed in this group of lesions was "biphasic salivary neoplasm". The differential diagnosis of

biphasic salivary tumors included AdCC, EMCa, and cellular PA. Of note, even when malignant nature of the biphasic carcinoma is obvious, reliably distinguishing between an AdCC and EMCa might still be a difficult task (one case in this series). Clear cell neoplasms were another perennial problem encountered on this biopsy. The differential diagnosis here is broad and occasionally includes non-salivary/metastatic lesions. Again here, characterizing the immunophenotype of the clear cells (i.e., epithelial versus myoepithelial) may exclude several categories. In some cases, the prohibitively small size of the biopsy results in the diagnostic line "insufficient for diagnosis". Thus, in summary, our general practice is not to make the "line diagnosis" of carcinoma unless at least one of the following criteria is met:

1. High-grade cytologic features, including severe atypia, abundant/atypical mitoses, and/or necrosis.
2. Perineural or angiolymphatic invasion.
3. Infiltration as seen at tumor/adjacent normal tissue (stroma) interface.
4. Morphologic features absolutely classic for a malignant category (i.e., adenoid cystic carcinoma, acinic cell carcinoma).

Further prospective studies with follow-up are required to validate these or other "adequacy" criteria for biopsies of salivary type lesions.

In summary, this prospectively accrued study of personal consultations originating from head and neck sites offers insights into the challenges commonly encountered in salivary gland pathology. Demographic characteristics and TAT benchmarks are established, and adherence by both contributor and consultant to most of ADASP recommendations is described. The commonly encountered named entities in this PC practice include AdCC, EMCa, and ACC. We also herein formalize a problem that is commonly encountered in salivary gland pathology, namely the biopsy of a cytologically bland neoplasm without tumor stromal interface, and offer recommendations on reporting for these biopsies.

Acknowledgments The authors would like to thank all the pathologists who contributed their cases, and Mai Phan, Kimberly Onder, Kim Marie Adams, and Donna Bowen for secretarial support. The authors declare that they have no competing interests.

References

1. ADASP (1993) Consultations in surgical pathology. Association of directors of anatomic and surgical pathology. Am J Surg Pathol 17:743–745
2. Abt AB, Abt LG, Olt GJ (1995) The effect of interinstitution anatomic pathology consultation on patient care. Arch Pathol Lab Med 119:514–517
3. Kronz JD, Westra WH, Epstein JI (1999) Mandatory second opinion surgical pathology at a large referral hospital. Cancer 86:2426–2435
4. Boiko PE, Piepkorn MW (1994) Reliability of skin biopsy pathology. J Am Board Fam Pract 7:371–374
5. Santoso JT, Coleman RL, Voet RL et al (1998) Pathology slide review in gynecologic oncology. Obstet Gynecol 91:730–734
6. Epstein JI, Walsh PC, Sanfilippo F (1996) Clinical and cost impact of second-opinion pathology. Review of prostate biopsies prior to radical prostatectomy. Am J Surg Pathol 20:851–857
7. Westra WH, Kronz JD, Eisele DW (2002) The impact of second opinion surgical pathology on the practice of head and neck surgery: a decade experience at a large referral hospital. Head Neck 24:684–693
8. Kronz JD, Westra WH (2005) The role of second opinion pathology in the management of lesions of the head and neck. Curr Opin Otolaryngol Head Neck Surg 13:81–84
9. Bruner JM, Inouye L, Fuller GN et al (1997) Diagnostic discrepancies and their clinical impact in a neuropathology referral practice. Cancer 79:796–803
10. Chan TY, Epstein JI (2005) Patient and urologist driven second opinion of prostate needle biopsies. J Urol 174:1390–1394 discussion 1394; author reply 1394
11. Herawi M, Parwani AV, Irie J et al (2005) Small glandular proliferations on needle biopsies: most common benign mimickers of prostatic adenocarcinoma sent in for expert second opinion. Am J Surg Pathol 29:874–880
12. Seethala RR, Barnes EL, Hunt JL (2007) Epithelial-myoepithelial carcinoma: a review of the clinicopathologic spectrum and immunophenotypic characteristics in 61 tumors of the salivary glands and upper aerodigestive tract. Am J Surg Pathol 31:44–57
13. Rosen PP (1989) Special report: perils, problems, and minimum requirements in shipping pathology slides. Am J Clin Pathol 91:348–354
14. Seethala RR, Hunt JL, Baloch ZW et al (2007) Adenoid cystic carcinoma with high-grade transformation: a report of 11 cases and a review of the literature. Am J Surg Pathol 31:1683–1694
15. Ellis G, Auclair, PL (1996) Tumors of the Salivary Glands. Washington 1996
16. Cormier B, Bonneau C, Kerdraon R et al (2007) Request of second opinion for difficult diagnosis in surgical pathology. Assessment of a one year activity in a general hospital. Ann Pathol 27:345–351
17. Cook IS, McCormick D, Poller DN (2001) Referrals for second opinion in surgical pathology: implications for management of cancer patients in the UK. Eur J Surg Oncol 27:589–594
18. McHugh JB, Hoschar AP, Dvorakova M, et al. (2008) p63 immunohistochemistry differentiates salivary gland oncocytoma and oncocytic carcinoma from metastatic renal cell carcinoma. Head and Neck Pathology 1(2):1–9
19. Seethala RR, Richmond JA, Hoschar AP, et al. (2009) New variants of epithelial-myoepithelial carcinoma: oncocytic-sebaceous and apocrine. Arch Pathol Lab Med (in press)
20. Fan CY, Melhem MF, Hosal AS et al (2001) Expression of androgen receptor, epidermal growth factor receptor, and transforming growth factor alpha in salivary duct carcinoma. Arch Otolaryngol Head Neck Surg 127:1075–1079
21. Kapadia SB, Barnes L (1998) Expression of androgen receptor, gross cystic disease fluid protein, and CD44 in salivary duct carcinoma. Mod Pathol 11:1033–1038
22. Castle JT, Thompson LD, Frommelt RA et al (1999) Polymorphous low grade adenocarcinoma: a clinicopathologic study of 164 cases. Cancer 86:207–219
23. Auclair PL (1994) Tumor-associated lymphoid proliferation in the parotid gland. A potential diagnostic pitfall. Oral Surg Oral Med Oral Pathol 77:19–26
24. Martinez-Madrigal F, Micheau C (1989) Histology of the major salivary glands. Am J Surg Pathol 13:879–899

Virchows Arch (2009) 454:467–474
DOI 10.1007/s00428-009-0761-7

ORIGINAL ARTICLE

Disturbance of circadian gene expression in breast cancer

Shou-Jen Kuo · Shou-Tung Chen · Kun-Tu Yeh · Ming-Feng Hou · Ya-Sian Chang · Nicholas C. Hsu · Jan-Gowth Chang

Received: 27 November 2008 / Revised: 4 March 2009 / Accepted: 5 March 2009 / Published online: 19 March 2009

Abstract To explore the mechanism of the disruption of circadian rhythm in breast cancer, we examined the expression of nine circadian genes in 53 newly diagnosed breast cancers by immunohistochemical staining, mutational analysis, and methylation analysis of the promoter of circadian genes. Our results showed that 37 of the 53 breast cancer tissues had hypermethylation on the promoters of PER1, PER2, CRY1, or BMAL1. Twenty-five out of 53 paired noncancerous (normal) tissues had methylation on the promoter of PER1 or CRY1. Our results indicated a higher frequency of concurrent methylation of PER1 and CRY1 promoters in cancerous and normal tissues. Promoter methylation of the PER1 correlates with c-erbB2 immunohistochemical reaction of ≥2+ (p=0.012) and has a strong inverse correlation with estrogen receptor positivity (p=0.016). We further analyzed the patterns of circadian gene expression by immunohistochemical methods and found that homogeneous expression of PER2 or BMAL1 is significantly associated with lymph node metastasis and poor prognosis. PER2 heterogeneous expression correlates with <2+ c-erbB2 immunohistochemical reaction. Heterogeneous expression of CLOCK is associated significantly with 3-year survival. In conclusion, the expression pattern of circadian genes might be a biomarker for the prognosis of breast cancer.

Keywords Circadian genes · Promoter methylation · Immunohistochemical analysis · Breast cancer

Electronic supplementary material The online version of this article (doi:10.1007/s00428-009-0761-7) contains supplementary material, which is available to authorized users.

S.-J. Kuo · M.-F. Hou · Y.-S. Chang · N. C. Hsu · J.-G. Chang (✉)
Department of Laboratory Medicine,
Kaohsiung Medical University Hospital,
Kaohsiung, Taiwan
e-mail: jgchang@ms.kmuh.org.tw

S.-J. Kuo · M.-F. Hou · Y.-S. Chang · N. C. Hsu · J.-G. Chang
Institute of Clinical Research, College of Medicine,
Kaohsiung Medical University,
Kaohsiung, Taiwan

S.-J. Kuo · S.-T. Chen · K.-T. Yeh
Department of Surgery and Pathology,
Changhua Christian Hospital,
Changhua, Taiwan

M.-F. Hou
Department of Surgery, Kaohsiung Medical University Hospital,
Kaohsiung, Taiwan

J.-G. Chang
Center for Excellence in Environmental Medicine,
Kaohsiung Medical University,
Kaohsiung, Taiwan

Introduction

In mammals, physiological and hormonal processes as well as behavioral reactions that follow circadian rhythms are driven by an endogenous master clock. The master clock is located in the suprachiasmatic nucleus (SCN) of the hypothalamus and produces self-sustaining circadian rhythms that are synchronized by external cues. Recent studies have shown that the circadian system is a master and slave structure: the master pacemaker (SCN) synchronizes the slave oscillators (peripheral tissues) of mammals [1–7]. Recently, circadian rhythms similar to those operating in the SCN have been found in most mammalian cells and peripheral tissues, and these peripheral circadian rhythms may be driven or synchronized by the central pacemaker in SCN [4, 5]. The human circadian rhythm is

controlled by at least nine circadian genes, viz. period 1 (PER1), period 2 (PER2), period 3 (PER3), cryptochrome 1 (CRY1), cryptochrome 2 (CRY2), CLOCK, BMAL1, casein kinase 1ε (CK1ε), and timeless (TIM) [6–8]. The three PER genes encode PER–ARNT–SIM (PAS) domain nuclear proteins but do not directly bind DNA. The CLOCK and BMAL1 genes encode PAS helix–loop–helix transcription factors. The products of these genes are assembled into a molecular clockwork which is composed of interlocking feedback loops in gene expression [1–10].

A study conducted in Norway where the daylight and corresponding winter darkness each rules in different halves of the year demonstrated an annual dynamic change of histology in breast cancer patients [11]. Circadian rhythms regulate many functions in the human body, including sleep and wakefulness, body temperature, blood pressure, hormone production, digestive secretion, and immune activity. Disruption of these rhythms can have profound influence on human health [12–16]. The disruption of circadian rhythm is already known as a risk factor in the development of breast cancer [16–20] but molecular changes involving circadian genes in breast cancer cells are rarely explored. In this study, we used immunohistochemical staining, mutational analysis, and methylation analysis of the promoter to study nine circadian genes in paired breast cancer tissues in order to explore the contribution of circadian genes in breast tumorigenesis.

Materials and methods

Samples

Fifty-three resected breast cancer and paired noncancerous (normal) tissue samples were obtained from 53 newly diagnosed female breast cancer patients (who had not received neoadjuvent chemotherapy) at the Changhua Christian Hospital. Women who work at night or work night shifts occasionally were not included in this study. The paired breast parenchyma showed fibrocystic change and atrophy of terminal ductal lobular units. All patients were staged as defined by the 2002 American Joint Committee on Cancer staging system. The age of the patients ranged from 27 to 84 years old with a mean of 51.4 years old. The tissues were frozen immediately after surgical resection and stored in liquid nitrogen until extraction of either DNA or RNA. DNA extraction was performed as previously described [21, 22]. Clinically, eight cases were stage I, 35 cases were stage II, eight cases were stage III, and two cases were stage IV. Pathologically, four cases were grade I, 34 cases were grade II, and 15 cases were grade III. Histopathologically, 51 cases were infiltrating ductal carcinoma and two cases were infiltrating lobular carcinoma. This study was approved by the Institute Review Board of the Changhua Christian Hospital.

Analysis of circadian-related, cell cycle-related, estrogen receptor, progesterone receptor, P53, and c-erbB-2 protein levels by immunohistochemistry

Paraffin-embedded breast cancer tissue sections (4 μ) on poly-1-lysine-coated slides were deparaffinized. After treatment with 3% H_2O_2 in methanol, the sections were hydrated with gradient alcohols and phosphate-buffered saline (PBS), incubated with 10 mM citrate buffer, and finally, heated at 100°C for 20 min in PBS. After incubation with the mouse monoclonal antibodies for estrogen receptor (1:50 dilution, Novo Castra, UK), progesterone receptor(1:40 dilution, Novo Castra, UK), P53 (1:100 dilution, Dako, Denmark), rabbit polyclonal antibody for c-erbB-2 (1:600 dilution, Dako, Denmark), nine circadian proteins (1:75 dilution for PER1, PER2, and CRY1; 1:50 dilution for PER3, CLOCK, CK1ε, BMAL1, and TIM1; 1:75 dilution for CRY2; Santa Cruz, CA, USA), cyclin A, cyclin B, and cyclin D (1:50 dilution, Novo Castra, UK) for 20 min at room temperature, the sections were incubated with an HRP/Fab polymer conjugate for another 30 min after being thoroughly washed three times with PBS. The sites of peroxidase activity were visualized using 3,3′-diaminobenzidine tetrahydrochloride as a substrate. Hematoxylin was used as the counter stain. The paired normal breast tissues were used as positive controls for the circadian proteins. The expression patterns of circadian proteins in breast cancerous cells were examined. Cytoplasmic staining in more than 10% of cells was considered positive. A homogeneous pattern indicates that more than 90% of cells are positive while heterogeneous pattern marks that less than 90% of cells are positive. For nuclei staining of estrogen receptor, progesterone receptor, and P53, staining in more than 10% of cells was considered positive. Anti-c-erbB-2 antibody was utilized to stain cell membrane with guidelines published by ASCO/CAP. Briefly, the scoring system was as follows: no staining or membrane staining in fewer than 10% of tumor cells, 0; faint, barely perceptible membrane staining in more than 10 % of tumor cells, the cells are stained only in part of the membrane, 1+; weak to moderate complete membrane staining observed in more than 10% of tumor cells or strong complete membrane staining in less than 30% of tumor cells, 2+; and strong, complete membrane staining in more than 30% tumor cells, 3+. The immunohistochemical results were evaluated by two investigators scoring independently.

Mutational analysis of nine circadian genes

Amplification of the coding regions of nine circadian genes was carried out by polymerase chain reaction (PCR). The PCR primers and the primer sequences were as described [21]. PCR was performed in a 50 μL final volume containing 200 nM of each primer, 200 μM of each dNTP, 3.5 mM $MgCl_2$, 2 U *Taq* DNA polymerase (Promega, Medison, WI, USA), and 1X PCR buffer. The amplification procedure was carried out as follows: 35 cycles of PCR reactions including denaturing at 95°C for 1 min annealing at the temperature depending on the melting temperature (T_m) of each primer set for 1 min and an extension cycle at 72°C for 2 min. The PCR products were subjected to gel purification, and direct sequencing DNA sequencing was performed by ABI Prism 310 Genetic Analyzer and the BigDye Terminator Cycle sequencing kit (Applied Biosystem, USA) according to the manufacturer's protocol.

Methylation-specific PCR analysis of circadian genes

Genomic DNA was modified with sodium bisulfite and methylation-specific PCRs were performed as described [21–23] with some modifications. Two pairs of primers for the promoter of each circadian gene were used to determine the methylation status of the promoter. The sequences of primers are as described [21]. Briefly, approximately 4 μg of genomic DNA in 40 μL H_2O was denatured by incubation with 10 μL of 1 N NaOH at 37°C for 10 min and then modified with 30 μL of 10 mM hydroquinone and 520 μL 1.5 M sodium bisulfite (pH 5.0) at 50°C for 16 h. DNA samples were eluted with 100 μL prewarmed H_2O (65–70°C) in a Wizard DNA purification kit (Promega, Madison, WI, USA). We then added 50 μL 1 N NaOH to the eluent and incubated the mixture at room temperature for 5 min. After the pellet was precipitated with 150 μL 100% isopropanol and washed with 70% ethanol, it was resuspended in 45 μL H_2O. Modified DNA was amplified in a total volume of 20 μL solution containing 1X PCR buffer, 1.0 mM $MgCl_2$, 100 ng of each primer, 0.2 mM of each dNTP, and 2.5 U *Taq* polymerase. PCR was performed in a thermal cycler for 35 cycles; each cycle consisted of denaturation at 94°C for 1 min, annealing at 60°C for both methylated and unmethylated primers for 1 min, extension at 72°C for 1 min, and a final 5-min extension at 72°C. PCR products were then loaded and electrophoresed on a 3.5% agarose gel, stained with ethidium bromide, and visualized under UV illumination.

CpG methylase (SssI)-treated genomic DNA was used as a positive control for methylation-specific primers. DNA samples extracted from the blood of healthy individuals who had been tested negative for methylation in the promoters of the nine circadian genes were used as positive controls for unmethylated status. To ensure methylation specificity, unmodified genomic DNA samples from both the cancerous and noncancerous parts of each breast cancer patient were used as negative controls. To confirm the results of the methylation-specific and unmethylation-specific PCR experiments, all the suspected PCR products were subjected to direct sequencing.

Statistical analysis

Comparison between methylation status and clinicopathological analysis were analyzed by Fisher's exact test or chi square test on SPSS for Windows Release 15.0 (SPSS, Chicago, IL, USA). Variables with a p value of less than 0.05 were considered statistically significant.

Results

Mutational analysis of coding areas of nine circadian genes

To elucidate the mechanism of the disruption of circadian genes in breast cancer, we performed direct sequencing on cases with abnormal expression patterns for possible mutations in the coding region of the circadian genes. No function-related changes were found, but 15 polymorphisms of the circadian genes were detected in cancerous and normal tissues (Supplement Table 1). Eleven of the 15 polymorphic sites were silent changes; the remaining four sites resulted in changes in amino acid residues of similar characteristics. We found no correlation between the detected polymorphisms and the circadian gene expression patterns. These results suggest that circadian gene mutations do not play a significant role in the perturbed expression patterns of the circadian genes in breast cancerous cells.

Analysis of the methylation status of the promoter of nine circadian genes

The results of methylation-specific PCR analysis of the promoters of the nine circadian genes are shown in Fig. 1. Using methylation-specific PER1 primers, the methylated promoter yielded a 298-bp PCR product which was not present in cases of the unmethylated promoter. Similarly, the unmethylated promoter produced a 318-bp PCR product and none was generated for the methylated promoter using the nonmethylation-specific primers (Fig. 1a). Using the same principle, methylation-specific and nonmethylation-specific primers for the promoters of eight other circadian genes were used for determining the methylation status of the promoter of each gene (Fig. 1b–i). In total, 53 pairs of breast cancerous and normal tissues were examined for

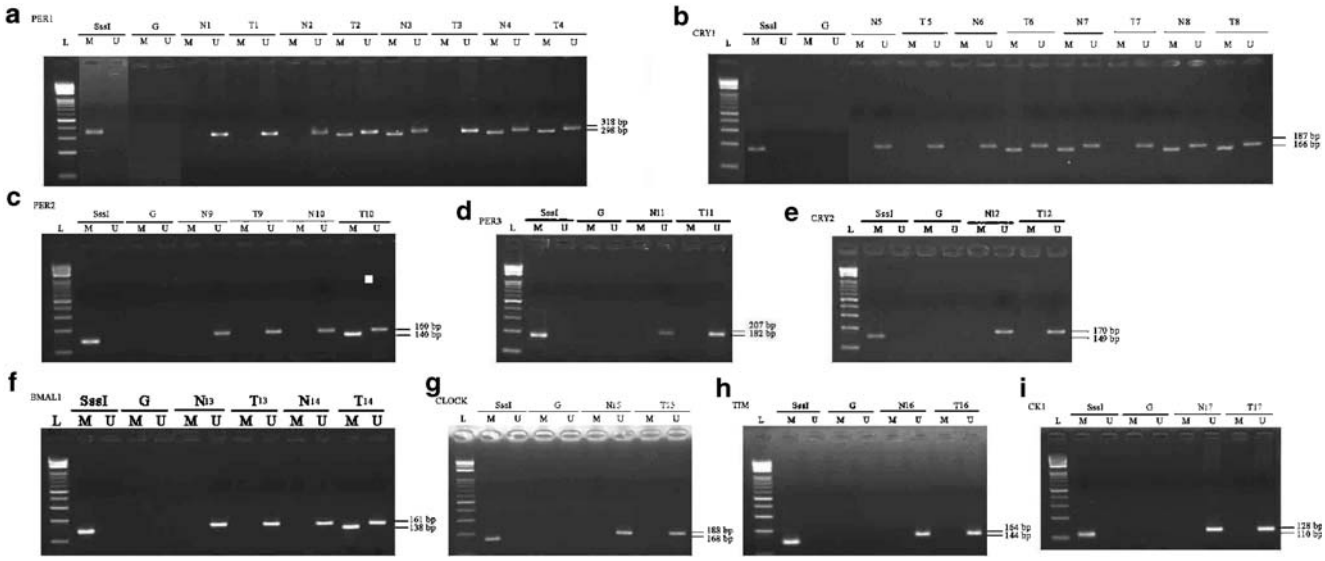

Fig. 1 Methylation analysis of nine circadian genes in primary breast cancers. Representative MS-PCR analysis of PER1 (**a**), CRY1 (**b**), PER2 (**c**), PER3 (**d**), CRY2 (**e**), BMAL1 (**f**), CLOCK (**g**), TIM (**h**), and CK1ε (**i**) in primary breast cancerous tissues are shown. Parallel amplification reactions were carried out using primers specific for unmethylated (*U*) or methylated (*M*) DNA. *L* 100-bp ladder markers, *N1* to *N17* noncancerous tissue, *T1* to *T17* cancerous tissue; *SssI* CpG methylase-treated DNA, *G* unmodified genomic DNA, *M* and *U* PCR using methylation-specific PCR primers for bisulfite-modified DNA, *U* PCR using nonmethylation-specific PCR primers for bisulfite-modified DNA

promoter methylation of the nine circadian genes. No methylation was found in the promoters of PER3, CRY2, CLOCK, CK1ε, and TIM in both cancerous and normal tissues of the 53 breast cancer patients. Fourteen out of 53 of the normal tissues had PER1 promoter methylation (11 cases showed similar methylation status in their paired cancerous tissues), and 26 out of 53 of the cancerous tissues had methylation in the PER1 promoter. Two cases (out of 53) of breast cancerous tissues had promoter methylation in the PER2 promoter. Twenty-five out of 53 of the cancerous tissues had CRY1 promoter methylation. Twenty-one out of 53 of the normal tissues had CRY1 promoter methylation (11 cases had similar methylation in their paired cancerous tissues). One case (out of 53) of breast cancerous tissue revealed promoter methylation of both BMAL1 and PER1 genes. Results of the methylation-specific PCR experiments were confirmed by direct sequencing of the PCR products.

The results of methylation analysis of the promoters of the nine circadian genes are summarized in Table 1. Thirty-seven out of the 53 breast cancerous tissues had methylation in the promoter of at least one circadian gene. Twenty-five out of 53 paired normal tissues had methylation in the promoter of at least one circadian gene. In these 25 cases, 11 cases showed methylated PER1 and CRY1 promoters, three cases had methylation in PER1 promoter, and 11 cases had methylation in CRY 1 promoter. A higher frequency of concurrent methylation of PER1 and CRY1 promoters in cancerous and normal tissues was indicated.

Correlation between the methylation status of the circadian genes and clinical–pathological features in the breast cancer patients

We attempted to correlate circadian gene promoter methylation with clinical–pathological features in the breast cancer patients. No correlation was observed between circadian gene promoter methylation and progesterone receptor, P53, tumor grade, tumor size, and clinical stage. However, promoter methylation of the PER1 correlates with ≥2+ c-erbB2 immunohistochemical reaction (p=0.012) and has a strong inverse correlation with estrogen receptor positivity (p=0.016) (Table 2).

Table 1 Methylation-specific PCR analysis of four circadian gene promoters in 53 breast cancers

Tissue	Promoter methylation					
	P1+P2+C1	P1+C1	P1+P2	P1+B1	P1	C1
Noncancerous	0	11	0	0	3	11
Cancerous	1	14[a]	1	1	10[b]	10[c]

P1 PER1, *P2* PER2, *C1* CRY1, *B1* BMAL1

[a] Six cases also had methylation at their paired noncancerous tissues

[b] Three cases also had methylation at their noncancerous tissues

[c] Three cases had methylation at their paired noncancerous tissues

Table 2 PER1 promoter methylation status and clinical–pathological features in breast cancer patients

Clinical parameters		PER1 promoter methylation		*p* value
		Positive	Negative	
Age	<50	13	16	0.498
	≥50	13	11	
ER	−	20	12	0.016[a]
	+	6	15	
PR	−	17	14	0.317
	+	9	13	
c-erbB2	<+	8	14	0.012
	≥++	15	5	
P53	−	11	13	0.571
	+	14	12	
Grade	I, II	19	19	0.827
	III	7	8	
Tumor size (cm)	<2	2	4	0.413
	≥2	24	23	
Stage	I, II	22	20	0.482
	III, IV	4	6	

ER estrogen receptor, *PR* progesterone receptor

[a] Chi square test

Immunohistochemical analysis of circadian proteins

In order to understand the expression patterns of circadian proteins in breast carcinoma cells and paired normal cells, we examined cellular circadian protein expression levels by immunohistochemical staining. The cancerous and normal tissues were obtained simultaneously and processed under the same conditions. Hence, both the cancerous and the paired normal tissues are theoretically at the same circadian clock. The results showed that most of the duct cells in the normal parts of the breast were positively and homogenously stained for antibodies directed against the circadian proteins, indicating that the normal cells are indeed in a similar status of circadian rhythm. In contrast, heterogeneously and negatively staining patterns were frequently found in the breast carcinoma cells for one or several antibodies of the circadian proteins. We compared the expression of nine circadian proteins with the clinical–pathological features of breast cancer patients (Fig. 2) and found that the expression patterns of circadian proteins correlates with clinical features. The results showed that the homogeneous expression of PER2 or BMAL1 is associated with lymph node metastasis ($p<0.05$) and PER2 heterogeneous expression correlates with <2+ c-erbB2 immunohistochemical reaction. The heterogeneous expression of CLOCK was associated with higher 3-year survival ($p=0.006$) (Table 3).

Discussion

DNA methylation in the CpG-rich regions known as CpG islands located in promoter regions is associated with gene silencing [23–29]. Aberrant methylation or hypermethylation of normally unmethylated CpG islands in promoter regions has been shown to occur in important cancer-related genes in immortalized, transformed, or cancer cells

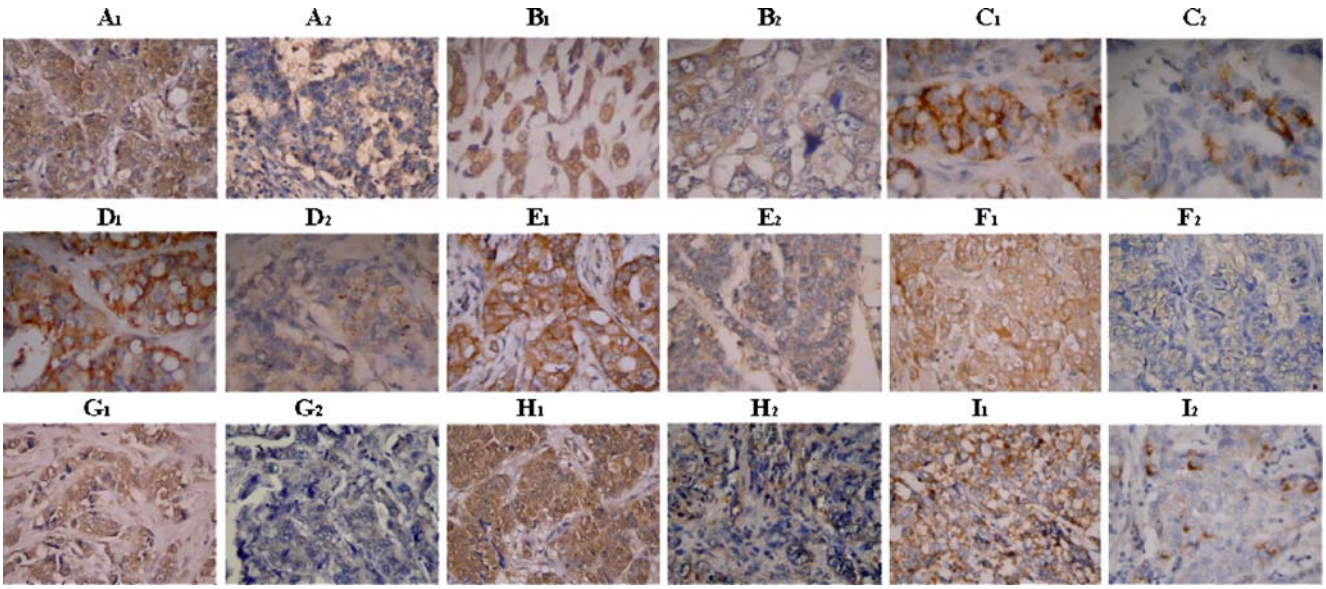

Fig. 2 Immunohistochemical staining of the circadian proteins in breast cancerous tissues was shown. The expression of representative cases of nine circadian proteins were shown in **a** PER1, **b** PER2, **c** PER3, **d** CRY1, **e** CRY2, **f** CLOCK, **g** BMAL1, **h** CK1ε, and **i** TIM. The numbers *1* and *2* represent homogeneous expression and heterogeneous expression, respectively

Table 3 The correlation between the clinicopathological features and the expression patterns of PER2, CLOCK, and BMAL1

		PER2				CLOCK				BMAL1			
		He	Ho	Total	*p* value	He	Ho	Total	*p* value	He	Ho	Total	*p* value
Tumor size (cm)	≤2	8	2	10	0.155	6	4	10	1.000	4	6	10	0.233
	>2	20	19	39		22	17	39		8	31	39	
Grade	Well	3	0	3	0.268	1	2	3	0.632	1	2	3	0.914
	Moderate	15	11	26		16	10	26		6	20	26	
	Poor	9	9	18		10	8	18		4	14	28	
Survival (years)	≤3	3	6	9	0.153	1	8	9	0.006[a]	1	8	9	0.662
	>3	24	15	39		26	13	39		10	29	39	
LN	−	15	5	20	0.040[b]	13	7	20	0.382	8	12	20	0.034[c]
	+	12	16	28		14	14	28		3	25	28	
c-erbB2	<2+	21	6	27	0.002[d]	18	9	27	0.184	8	19	27	0.510
	≥2+	7	14	21		10	11	21		4	17	21	

p value by chi square test or Fisher's exact test when appropriated

He heterogeneous expression, *Ho* homogeneous expression

[a] Clock heterogeneous expression was significantly associated with 3-year survival

[b] Per2 homogeneous expression was significantly associated with lymph node metastasis

[c] BMAL1 homogeneous expression was significantly associated with lymph node metastasis

[d] Per2 heterogeneous expression was significantly associated with c-erbB2 immunohistochemical reaction of <2+

[27, 28, 30, 31]. Changes in promoter methylation have been studied in several common human cancers including breast cancer [21, 30–33]. In this study, we employed the methylation-specific PCR to investigate the methylation status of the promoters of nine circadian genes in breast cancer. Our results revealed promoter methylation of PER1 and CRY1 genes in cancerous tissues and paired normal breast tissues which suggests that methylation of PER1 or CRY1 promoter may be functionally important in providing survival benefit for cancer cells. This phenomenon has been previously noted in other cancer-related genes such as E-cadherin and CAV-1 [31, 34–36].

PER1, PER2, BMAL1, and CRY1 are important genes that regulate the circadian clock [1–3]. Activation of these genes is regulated by BMAL1 and CLOCK through the E-box of PER, which enhances the expression of PER and CRY. Then, PER and CRY enter into the nucleus to inhibit the activity of BMAL1 and CLOCK in feedback. The downregulation of BMAL1 and CLOCK results in decreased expression of PER and CRY leading to the formation of the circadian clock. Interestingly, homozygous PER1, PER2, and CRY1 mutant displayed a shorter circadian period with reduced precision and stability [37–40]. Thus, inactivation of these genes results in the deregulation of breast cancer cells from the control of the central pacemaker. Matsuo et al. [41] have shown that the circadian clock controls the expression of cell cycle-related genes and the intracellular circadian rhythm. They also noted that the intracellular circadian clockwork can control the cell-division cycle directly and unidirectionally in proliferating cells. Inactivation of the PER1, PER2, and CRY1 genes in breast cancer cells may result in deregulation of cell cycle control which favors the proliferation of breast cancer cells.

Recent studies have shown that a large number of genes are controlled by the circadian clock in a tissue-specific manner and that many of these circadian control genes function in the rate-limiting steps of major physiological processes [3, 13]. PER1, PER2, BMAL1, and CRY1 are critical components in the formation of the circadian clock; suppressed expression of these genes may have profound effects on the development of breast cancer.

Clinicopathological analysis shows a strong inverse correlation between PER1 promoter methylation and estrogen receptor expression. Since no expression of estrogen receptor may result in an aggressive tumor phenotype and reduced survival, our results suggest that PER1 inactivation may play an important role in the development of breast cancer. Whether methylation of the PER1 gene influences the estrogen receptor expression, or vice versa, needs to be further investigated. In accordance with our previous study [42], PER1 methylation status has strong correlation with the expression of the c-erB2 oncogene.

We compared the circadian protein expression patterns with clinical features of breast cancer patients, and the results showed that the heterogeneous and homogeneous expression patterns of different circadian proteins in

cancerous tissues correlates closely with lymph node metastasis and survival time. The homogeneous expression of PER2 or BMAL1 in breast cancer tissue is strongly associated with lymph node metastasis and poor prognosis. PER2 heterogeneous expression correlates with <2+ c-erbB2 immunohistochemical reaction which is a good indicator of better survival than those with ≥2+ in breast cancer. The heterogeneous expression of CLOCK in breast cancer tissues has significantly higher 3-year survival. PER2 is considered as a tumor suppressor gene, homogeneous expression of PER2 may be the result of clonal selection of terminal tumor evolution. This dominant clone may overcome the control of PER2 results in a more aggressive nature, such as lymph node invasion. BMAL1 corporate with PER2 to control the circadian rhythm, homogeneous expression of BMAL1 has a similar effect on the prognosis of breast cancer cells. The heterogeneous expression of CLOCK in breast cancer tissues may indicate that the cancer cells are still controlled by circadian CLOCK in comparison with homogeneous CLOCK expression of the more aggressive cancer cells.

In conclusion, this study shows that promoter methylation of the circadian genes occurs frequently in breast cancer tissues. Promoter methylation likely inactivates the expression of the affected circadian genes and disrupts the circadian rhythm of breast cancer cells. This further results in a different mode of circadian clock regulation from that of normal cells. Our results may provide a basis of chronotherapy in breast cancer that is based on the differences in the expression of circadian genes in the cancerous and normal tissues.

Acknowledgements We thank Miss W. L. Chan for editing the manuscript. This study was supported in part by grants from Nation Science Council, Taiwan (NSC93-2314-B-039-006 and NSC93-2314-B-039-028) and a grant from Changhua Christian Hospital, Taiwan.

Conflicts of interest statement We have no conflicts of interest.

References

1. Reppert SM, Weaver DR (2002) Coordination of circadian timing in mammals. Nature 418:935–941
2. Yamaguchi S, Isejima H, Matsuo T et al (2003) Synchronization of cellular clocks in the suprachiasmatic nucleus. Science 302:1408–1412
3. Morse D, Sassone-Corsi P (2002) Time after time: inputs to and outputs from the mammalian circadian oscillators. Trends Neurosci 25:632–637
4. Balsalobre A (2002) Clock genes in mammalian peripheral tissues. Cell Tissue Res 309:193–199
5. Stratmann M, Schibler U (2006) Properties, entrainment, and physiological functions of mammalian peripheral oscillators. J Biol Rhythms 21:494–506
6. Ko CH, Takahashi JS (2006) Molecular components of the mammalian circadian clock. Hum Mol Genet 15(Spec No 2): R271–R277
7. Barnes JW, Tischkau SA, Barnes JA et al (2003) Requirement of mammalian Timeless for circadian rhythmicity. Science 302:439–442
8. Albrecht U (2002) Invited review: regulation of mammalian circadian clock genes. J Appl Physiol 92:1348–1355
9. Gallego M, Virshup DM (2007) Post-translational modifications regulate the ticking of the circadian clock. Nat Rev Mol Cell Biol 8:139–148
10. Sato TK, Yamada RG, Ukai H et al (2006) Feedback repression is required for mammalian circadian clock function. Nat Genet 38:312–319
11. Hartveit F (2000) Annual rhythm in the growth of human breast carcinomas as reflected in the histology of their growing edge. Int J Surg Pathol 8:39–47
12. Cermakian N, Boivin DB (2003) A molecular perspective of human circadian rhythm disorders. Brain Res Brain Res Rev 42:204–220
13. Fu L, Lee CC (2003) The circadian clock: pacemaker and tumour suppressor. Nat Rev Cancer 3:350–361
14. Hastings MH, Reddy AB, Maywood ES (2003) A clockwork web: circadian timing in brain and periphery, in health and disease. Nat Rev Neurosci 4:649–661
15. Roenneberg T, Merrow M (1999) Circadian clocks—from genes to complex behaviour. Reprod Nutr Dev 39:277–294
16. Stevens RG, Rea MS (2001) Light in the built environment: potential role of circadian disruption in endocrine disruption and breast cancer. Cancer Causes Control 12:279–287
17. Hansen J (2006) Risk of breast cancer after night- and shift work: current evidence and ongoing studies in Denmark. Cancer Causes Control 17:531–537
18. Keith LG, Oleszczuk JJ, Laguens M (2001) Circadian rhythm chaos: a new breast cancer marker. Int J Fertil Womens Med 46:238–247
19. Rafnsson V, Tulinius H, Jonasson JG et al (2001) Risk of breast cancer in female flight attendants: a population-based study (Iceland). Cancer Causes Control 12:95–101
20. Schernhammer ES, Laden F, Speizer FE et al (2001) Rotating night shifts and risk of breast cancer in women participating in the nurses' health study. J Natl Cancer Inst 93:1563–1568
21. Lin YM, Chang JH, Yeh KT et al (2008) Disturbance of circadian gene expression in hepatocellular carcinoma. Mol Carcinog 47:925–933
22. Su TH, Wang JC, Tseng HH et al (1998) Analysis of FHIT transcripts in cervical and endometrial cancers. Int J Cancer 76:216–222
23. Herman JG, Graff JR, Myohanen S et al (1996) Methylation-specific PCR: a novel PCR assay for methylation status of CpG islands. Proc Natl Acad Sci U S A 93:9821–9826
24. Baylin SB (1997) Tying it all together: epigenetics, genetics, cell cycle, and cancer. Science 277:1948–1949
25. Bird AP (1986) CpG-rich islands and the function of DNA methylation. Nature 321:209–213
26. Costello JF, Plass C (2001) Methylation matters. J Med Genet 38:285–303
27. Das PM, Singal R (2004) DNA methylation and cancer. J Clin Oncol 22:4632–4642
28. Jones PA, Baylin SB (2002) The fundamental role of epigenetic events in cancer. Nat Rev Genet 3:415–428
29. Laird PW (2003) The power and the promise of DNA methylation markers. Nat Rev Cancer 3:253–266
30. Baylin SB, Herman JG, Graff JR et al (1998) Alterations in DNA methylation: a fundamental aspect of neoplasia. Adv Cancer Res 72:141–196
31. Rashid A, Issa JP (2004) CpG island methylation in gastroenterologic neoplasia: a maturing field. Gastroenterology 127:1578–1588
32. Belinsky SA (2004) Gene-promoter hypermethylation as a biomarker in lung cancer. Nat Rev Cancer 4:707–717
33. Esteller M, Corn PG, Baylin SB et al (2001) A gene hypermethylation profile of human cancer. Cancer Res 61:3225–3229

34. Chan TF, Su TH, Yeh KT et al (2003) Mutational, epigenetic and expressional analyses of caveolin-1 gene in cervical cancers. Int J Oncol 23:599–604
35. Leung WK, Yu J, Ng EK et al (2001) Concurrent hypermethylation of multiple tumor-related genes in gastric carcinoma and adjacent normal tissues. Cancer 91:2294–2301
36. Waki T, Tamura G, Tsuchiya T et al (2002) Promoter methylation status of E-cadherin, hMLH1, and p16 genes in nonneoplastic gastric epithelia. Am J Pathol 161:399–403
37. Cermakian N, Monaco L, Pando MP et al (2001) Altered behavioral rhythms and clock gene expression in mice with a targeted mutation in the Period1 gene. EMBO J 20:3967–3974
38. Vitaterna MH, Selby CP, Todo T et al (1999) Differential regulation of mammalian period genes and circadian rhythmicity by cryptochromes 1 and 2. Proc Natl Acad Sci U S A 96:12114–12119
39. Zheng B, Albrecht U, Kaasik K et al (2001) Nonredundant roles of the mPer1 and mPer2 genes in the mammalian circadian clock. Cell 105:683–694
40. Zheng B, Larkin DW, Albrecht U et al (1999) The mPer2 gene encodes a functional component of the mammalian circadian clock. Nature 400:169–173
41. Matsuo T, Yamaguchi S, Mitsui S et al (2003) Control mechanism of the circadian clock for timing of cell division in vivo. Science 302:255–259
42. Chen ST, Choo KB, Hou MF et al (2005) Deregulated expression of the PER1, PER2 and PER3 genes in breast cancers. Carcinogenesis 26:1241–1246

Virchows Arch (2009) 454:475–478
DOI 10.1007/s00428-009-0744-8

CASE REPORT

A primary malignant ependymoma of the abdominal cavity: a case report and review of the literature

Carolin Mogler · Patricia Kohlhof · Roland Penzel · Lars Grenacher · Georg M. Haag · Peter Schirmacher · Wolf Mueller

Received: 19 December 2008 / Revised: 29 January 2009 / Accepted: 8 February 2009 / Published online: 24 February 2009

Abstract Ependymomas generally arise in the central nervous system (CNS). Rare primary extraneural ependymomas have been observed. Here, we describe the first case of an overt malignant primary extraneural ependymoma in a young female patient. Careful reevaluation together with extensive review of the literature and comparison of related cases established the diagnosis after treatment failure and tumor progression. The tumor was large and firm with some small cysts and showed pseudorosettes with strong glial fibrillary acidic protein (GFAP) expression. In conclusion, primary extraneural ependymomas have to be included into the differential diagnosis of abdominal tumors with pseudorosette-formation, even in unusual sites, and GFAP-immunohistochemistry (IHC) supports the diagnosis.

C. Mogler · R. Penzel · P. Schirmacher
Department of General Pathology, University Hospital, Heidelberg, Germany

P. Kohlhof · W. Mueller
Department of Neuropathology, University Hospital, Heidelberg, Germany

L. Grenacher
Department of Radiology, University Hospital, Heidelberg, Germany

G. M. Haag
Department of Clinical Oncology, National Center for Tumor Disease, University Hospital, Heidelberg, Germany

C. Mogler (✉)
IPH Heidelberg,
INF 220/21,
69120 Heidelberg, Germany
e-mail: Carolin.Mogler@med.uni-heidelberg.de

Keywords Ependymoma · GFAP · EMA

Introduction

Ependymomas generally arise in the central nervous system, though primary extraneural ependymomas have been observed. To date, only three intraabdominal cases have been reported.

Clinical history

We present a 27-year-old female patient with a four year history of a primary extraneural anaplastic ependymoma (WHO III) arising in the abdominal cavity. Tumor therapy included several extensive tumor-debulking operations, a high-dose imatinib chemotherapy (400 and 800 mg daily), and an ependymoma-targeted combined carboplatin/etoposide chemotherapy which resulted in stabilization of the disease. One month after completion of the chemotherapy and 4 years after the initial tumor diagnosis, disease progressed again. Tumor debulking resulted in an improved quality of life with reduced need of pain medication. Of note, the ependymoma-targeted therapy was delayed for 6 months by misdiagnosing the tumor as a gastrointestinal autonomic nerve tumor (GANT). An i.v.-contrast-enhanced portal-venous phase of a standard abdominal CT was performed in the course of re-evaluation using a MD-CT Philips Brilliance (64-row). The tumor was mostly hypodense and showed an inhomogeneous contrast enhancement. Tumor growth extended around the liver with evidence of tumor infiltration into the caudate lobe and stenosis of the hepatic veins near the inferior caval vein.

Materials and methods

Automated IHC was performed on a Benchmark XT by Ventana, Strasbourg, France for c-kit (CD117; pH 6, 1:50), Ki-67 (MIB1; pH 6, 1:200), GFAP (pH 6, 1:25) and epithelial membrane antigen (EMA; pH 6, 1:100) according to standard protocols.

Results

We present the tumor specimen, which was obtained during the first debulking operation and which was reviewed 6 months after surgery following the failure of GANT-targeted imatinib chemotherapy. The specimen measured 13×12×7 cm in size and was macroscopically well-delineated from surrounding peritoneum. The surface was brownish to yellowish in appearance and featured both dense and knotty parts with some small cysts (Fig. 1a, b). Microscopically, the tumor featured a high cellularity. Nuclear morphology was mostly monomorphic and characterized by round to oval nuclei with "salt and pepper" speckling of the chromatin. Intratumoral areas of more extensive fibrillarity were present. Key histological features of ependymoma were identified, consisting of perivascular pseudorosettes (Fig. 1c) with perivascular anuclear zones of dense fibrillary processes. True ependymal rosettes were not identified, but focally tumor-derived tubules, which can be seen in ependymomas were present (Fig. 1d). Nuclear atypia was moderate in some parts of the tumor, but mitotic activity was high (>25 mitoses/ten high-power fields; Fig. 1e). Foci of geographic and palisading necroses were present (Fig. 1f). In contrast to the macroscopic impression of tumor delineation from surrounding tissues, widespread tumor invasion into the adjacent peritoneum was seen microscopically. IHC showed a homogenous strong positive reaction for GFAP (Fig. 1g, h) which was more pronounced in the perivascular pseudorosettes. Consistent with the diagnosis of an ependymoma, the staining pattern for EMA was dot-like in some and cytoplasmatic in other tumor areas (Fig. 1i, j). The proliferation index clearly exceeded 4%, and the mitotic activity was brisk with up to 25 mitotic figures/ten high-power fields. Nuclear atypia and palisading necroses together with the brisk mitotic activity were considered as features of malignancy and the tumor was classified as an anaplastic ependymoma WHO grade III. Of note, focal c-kit expression was reported in the tumor tissue misleading to the initial diagnosis of a GANT. We repeated c-kit IHC on all surgical specimens of the patient and compared the results to three anaplastic ependymomas with typical histology. We found c-kit expression in comparable frequencies and locations in both the patient's tumor specimens and the three anaplastic ependymomas confined to single hematopoetic cells within the tumor stroma (data not shown). The tumor specimen removed 4 years later upon tumor progression largely shared morphology and immunohistochemical behavior with the primary tumor.

Discussion

Ependymomas usually develop in the brain or spinal cord possibly by neoplastic transformation of ependymal cells of the ventricular wall or the spinal canal. Extraneural metastases have been well described in the literature. They may appear sporadically at many sites in the body [1, 2] including the abdominal cavity [2]. Primary extraneural ependymomas are very rare, and to date, only isolated cases have been documented [3, 4]. Primary extraneural ependymomas may originate from remnant embryonic neuroectodermal cells due to incomplete regression [5]. Accordingly, most extraneural ependymomas were found in or near structures of the neural axis, i.e., mediastinal, coccygeal locations or in the filum terminale, where ependymal rests can be found after birth [5]. Other discussed mechanisms include upfront unidirectional teratomas [6], remnants of neural tissue following the involution of the other two germ-layer components of a teratoma [6] or the incomplete closure of the neural arch [7], which, similar to the findings in the ovary, would allow for the development of a neometaplasia of heterotopic Muellerian duct-derived tissue [8] or a heterotopic monodermal tumor [9] outside the central nervous system. The latter may explain why extraneural ependymomas are common in the ovary [10]. In the abdominal cavity, however, only three cases of primary extraneural ependymomas have been reported, to date [11–13]. Even though the number of reported cases is very low, they seem to have features in common with the presented case, both morphologically and clinically. All patients were female. Age ranged from 27 to 41 years. The initial finding usually was a big solitary tumor mass exceeding 10 cm in diameter causing unspecific abdominal complaints. Macroscopically, these tumors tended to be firm and solid with small intratumoral cysts. Diagnostic difficulties were encountered in two cases [11] including the current case. In both, the diagnosis ependymoma was established only after recurrence and therapeutic failure. Histomorphology of the case presented here was dominated by a "glial" picture. Tumor cell morphology and nuclear chromatin speckling were suggestive of an ependymoma respecting the fact that extraneural ependymomas can demonstrate a wider architectural variability compared to ependymomas of the CNS [14]. Perivascular pseudorosettes were reported in all published cases, whereas true ependymal rosettes were

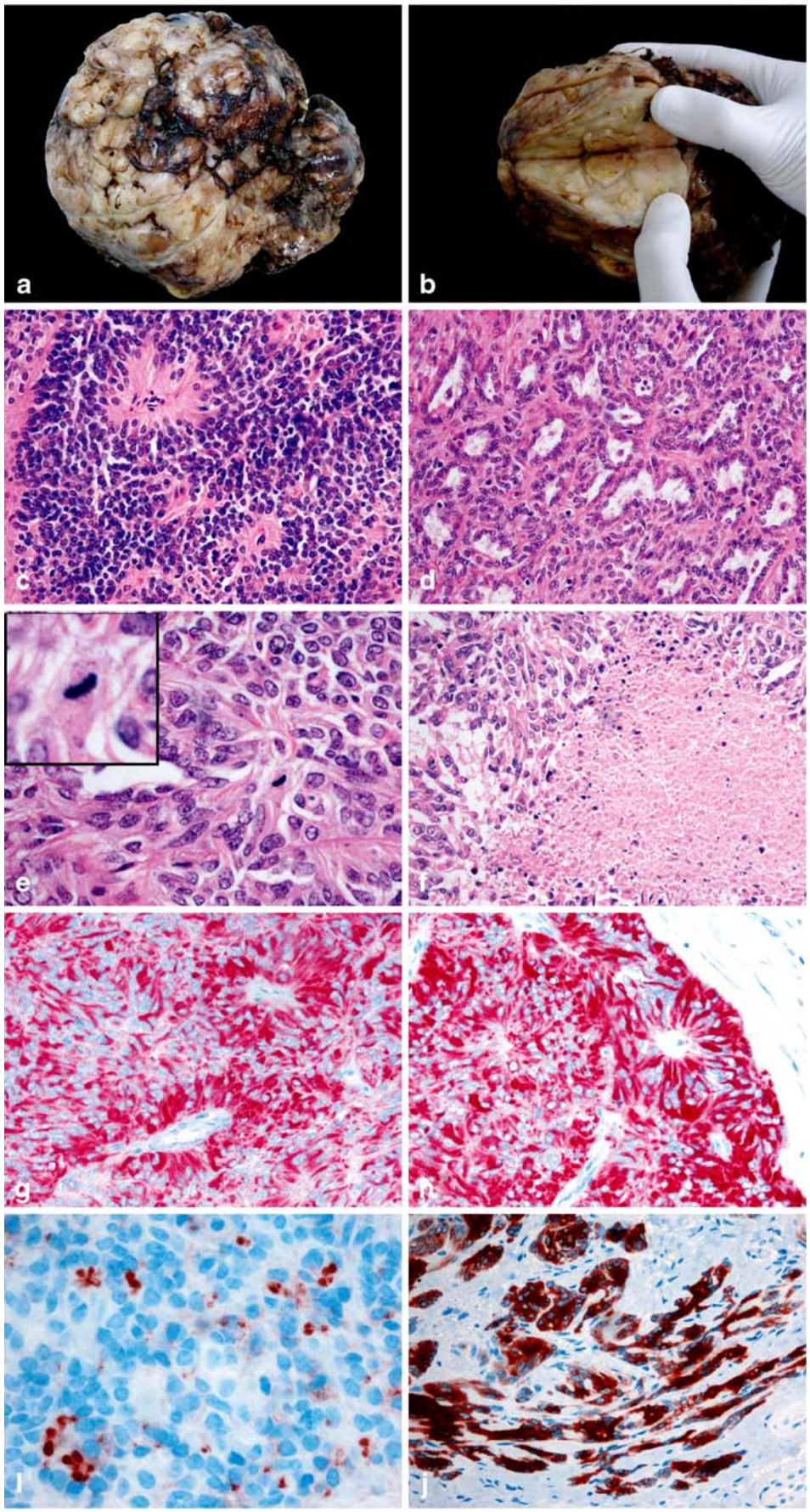

Fig. 1 Macroscopic, microscopic and immunohistochemical findings. **a**–**b** Macroscopy: firm and solid tumor mass (**a**) with heterogeneous cutting surface (**b**). **c**–**f** Histology with **c** pseudorosettes (HE; ×100), **d** intra-tumoral tubules (HE, ×100), **e** brisk mitotic activity (HE, ×100), and **f** necrosis. **g**–**j** Immunohistochemistry, **g**, **h** strong GFAP-expression in tumor cells highlighting pseudorosettes (×200), **i** ependymoma-typical dot-like EMA-expression in some (×400) and (**j**) cytoplasmatic EMA expression in other tumor areas (×200)

mentioned only in one report [11]. Strong positive reaction for GFAP, highlighting the pseudorosettes as in our case, is a feature common to all ependymomas including the intraabdominal variants. However, it needs to be considered that ovarian carcinomas can also show a remarkable GFAP expression which might lead to diagnostic predicament especially including tumors in the lower abdomen [14]. Here, tumor location especially in relation to the ovary, the identification of perivascular pseudorosettes and additional immunohistochemical investigations may help to clarify the diagnostic dilemma [14]. The majority of the tumor mass of the presented case was found in the abdominal cavity, and only marginal pelvic tumor extension was evident. Debulking operations did not necessitate ovariectomy indicating tumor-free ovaries and leading us to the assumption of a primary extraneural ependymoma arising from the abdominal peritoneum. The EMA staining-pattern with intracytoplasmic in some and dot-like in other tumor parts was typical of ependymomas [15]. Extensive imaging investigations aimed at excluding the possibility of an extraneural metastasis of a primary cerebral ependymoma. No further lesions were found, neither intracerebral nor extraneural throughout a period of 4 years demonstrating the intraabdominal origin of the ependymoma. Clinically, the three documented primary extraneural ependymomas of the abdominal cavity were benign tumors. Complete surgical tumor resection with or without adjuvant ependymoma-targeted chemotherapy resulted in long-term recurrence-free intervals. However, recurrences as late as 13 years after primary surgery did occur [11], and as the presented case illustrates, malignant transformation seems possible. In conclusion, this is the first report demonstrating a primary extraneural anaplastic ependymoma (WHO grade III) arising from the peritoneum in the abdominal cavity.

Conflict of interest statement We declare that we have no conflict of interest.

References

1. Graf M, Blaeker H, Otto HF (1999) Extraneural metastasizing ependymoma of the spinal cord. Pathol Oncol Res 5(1):56–60
2. Newton HB, Henson J, Walker RW (1992) Extraneural metastases in ependymoma. J Neuro-oncol 14(2):135–142
3. Morantz RA, Kepes JJ, Batnitzky S et al (1979) Extraspinal ependymomas. Report of three cases. J Neurosurg 51(3):383–391
4. Prabhakar V, Rao BD, Subrahmanian MV et al (1969) Extraspinal ependymoma. Neurol India 17(2):82–84
5. Fassett DR, Schmidt MH (2003) Lumbosacral ependymomas: a review of the management of intradural and extradural tumors. Neurosurg Focus 15(5):E13
6. Aguirre P, Scully RE (1982) Malignant neuroectodermal tumor of the ovary, a distinctive form of monodermal teratoma: report of five cases. Am J Surg Pathol 6(4):283–292
7. Vagaiwala MR, Robinson JS, Galicich JH et al (1979) Metastasizing extradural ependymoma of the sacrococcygeal region: case report and review of literature. Cancer 44(1):326–333
8. Guerrieri C, Jarlsfelt I (1993) Ependymoma of the ovary. A case report with immunohistochemical, ultrastructural, and DNA cytometric findings, as well as histogenetic considerations. Am J Surg Pathol 17(6):623–632
9. McCluggage WG, Young RH (2005) Immunohistochemistry as a diagnostic aid in the evaluation of ovarian tumors. Semin Diagn Pathol 22(1):3–32
10. Kleinman GM, Young RH, Scully RE (1993) Primary neuroectodermal tumors of the ovary. A report of 25 cases. Am J Surg Pathol 17(8):764–778
11. Dekmezian RH, Sneige N, Ordonez NG (1986) Ovarian and omental ependymomas in peritoneal washings: cytologic and immunocytochemical features. Diagn Cytopathol 2(1):62–68
12. Hofman V, Isnard V, Chevallier A et al (2001) Pelvic ependymoma arising from the small bowel. Pathology 33(1):26–29
13. Wiendl H, Feiden W, Scherieble H et al (2003) March 2003: a 41 - year-old female with a solitary lesion in the liver. Brain Pathol (Zurich, Switzerland) 13(3):421–423
14. Idowu MO, Rosenblum MK, Wei XJ et al (2008) Ependymomas of the central nervous system and adult extra-axial ependymomas are morphologically and immunohistochemically distinct–a comparative study with assessment of ovarian carcinomas for expression of glial fibrillary acidic protein. Am J Surg Pathol 32 (5):710–718
15. Mahfouz S, Aziz AA, Gabal SM et al (2008) Immunohistochemical study of CD99 and EMA expression in ependymomas. Medscape J Med 10(2):41

Virchows Arch (2009) 454:479–480
DOI 10.1007/s00428-009-0741-y

LETTER TO THE EDITOR

Renal angiomyoadenomatous tumor: morphologic, immunohistochemical, and molecular genetic study of a distinct entity

J. Verine

Received: 6 December 2008 / Accepted: 22 January 2009 / Published online: 10 February 2009

Dear Editor,

In a recently published article in *Virchows Archiv*, Michal et al. [1] described a very nice and detailed study of five new cases of renal angiomyoadenomatous tumor (RAT) resulting from their consultation activity. These authors had already reported a first case of this new entity of renal tumors [2].

I highly appreciate the attempt to describe in detail the histological, immunohistochemical, cytogenetic, and ultrastructural features of this tumor. RAT is characterized macroscopically by a sharply circumscribed tumor with microcystic or macrocystic changes. Microscopic examination reveals a leiomyomatous stroma often forming abortive vascular structures surrounding and encasing a distinctive and characteristic epithelial component. This latter is represented by adenomatous structures composed of cells with small deeply basophilic nuclei alienated along the basal membrane. The cytoplasm of the cells is frequently covered by clear snouts responsible for a clear cell appearance. The whole realizes focally a characteristic aspect of a "shark's smile". Immunohistochemically, the epithelial component of RAT is mainly positive for cytokeratin 7 (CK7), EMA, vimentin, and carbonic anhydrase IX (CA-IX), whereas CD10 is negative. Analysis of the *VHL* gene mutation and 3p LOH reveals both no mutation of coding sequence of the *VHL* gene and any copy number changes.

The authors discussed several differential diagnosis represented essentially by angiomyolipomas, mixed epithelial and stromal tumors of the kidney, and clear cell renal cell carcinoma (RCCs) particularly with an angioleiomyomatous stroma. Unfortunately, the authors simply mention clear cell papillary RCC (ccpRCC) as a distinct histopathological and molecular genetic entity without comparing it to RAT. Nevertheless, RAT shares many histopathological features of ccpRCC [3, 4] also described as sporadic clear cell renal cell carcinoma with diffuse cytokeratin 7 immunoreactivity (ccRCC CK7+) [5]. CcpRCC is a recently reported entity of renal epithelial tumors which is not described in current World Health Organization classification system. At gross examination, ccpRCC is a well-circumscribed tumor defined by fibrous capsule with microcystic–macrocystic appearance. Histologically, this tumor is composed of tubular, cystic, and/or papillary structures lined by clear cells. Having reviewed figures of all articles cited in this letter, it seems that clear snouts and shark's smile are also present in some cases of ccpRCC (see Figs. 3 and 4g–h, pp 149 and 150 of article by Tickoo et al. [3]). The immunoprofile of this tumor is similar to RAT, i.e., CK7+, CA-IX+, and CD10−, and cytogenetic findings revealed also no alterations of the *VHL* gene. The follow-up of patients with ccpRCC suggests a biologically indolent tumor as RAT, but further follow-up studies are needed to better understand its clinical behavior.

I think therefore that these tumors could correspond in fact to different morphological aspects of the same but distinctive entity of renal tumors depending on the cystic or papillary predominant architecture and the abundance of

J. Verine (✉)
AP-HP, Service d'Anatomie Pathologique, Hôpital Saint-Louis,
1 Avenue Claude Vellefaux,
75010 Paris, France
e-mail: jerome.verine@sls.aphp.fr

J. Verine
Inserm, U728,
75010 Paris, France

J. Verine
Université Paris 7, U728, Institut Universitaire Hématologie,
75010 Paris, France

stroma. The gathering of reported cases of ccpRCC, ccRCC CK7+, and RAT is important from this point of view and could also allow to better determine their clinical behavior.

References

1. Michal M, Hes O, Nemcova J, Sima R, Kuroda N, Bulimbasic S, Franco M, Sakaida N, Danis D, Kazakov DV, Ohe C, Hora M (2009) Renal angiomyoadenomatous tumor: morphologic, immunohistochemical, and molecular genetic study of a distinct entity. Virchows Arch 454:89–99 doi:10.1007/s00428-008-0697-3
2. Michal M, Hes O, Havlicek F (2000) Benign renal angiomyoadenomatous tumor: a previously unreported renal tumor. Ann Diagn Pathol 4:311–315
3. Tickoo SK, dePeralta-Venturina MN, Harik LR, Worcester HD, Salama ME, Young AN, Moch H, Amin MB (2006) Spectrum of epithelial neoplasms in end-stage renal disease: an experience from 66 tumor-bearing kidneys with emphasis on histologic patterns distinct from those in sporadic adult renal neoplasia. Am J Surg Pathol 30:141–153
4. Gobbo S, Eble JN, Grignon DJ, Martignoni G, MacLennan GT, Shah RB, Zhang S, Brunelli M, Cheng L (2008) Clear cell papillary renal cell carcinoma: a distinct histopathologic and molecular genetic entity. Am J Surg Pathol 32:1239–1245
5. Mai KT, Kohler DM, Belanger EC, Robertson SJ, Wang D (2008) Sporadic clear cell renal cell carcinoma with diffuse cytokeratin 7 immunoreactivity. Pathology 40:481–486

Virchows Arch (2009) 454:481–495
DOI 10.1007/s00428-009-0766-2

REVIEW AND PERSPECTIVE

Mitochondria and cancer

Valdemar Máximo · Jorge Lima · Paula Soares · Manuel Sobrinho-Simões

Received: 15 January 2009 / Revised: 6 March 2009 / Accepted: 17 March 2009 / Published online: 3 April 2009

Abstract The authors review the role played by mutations in mitochondrial DNA and in nuclear genes encoding mitochondrial proteins in cancer development, with an emphasis on the alterations of the oxidative phosphorylation system and glycolysis.

Keywords Mitochondria · mtDNA · Tumourigenesis · Glycolysis · OXPHOS

Introduction

The last decades witnessed the intensive utilisation of genetics in the understanding of the etiopathogenesis of neoplastic processes. The identification of oncogenes and tumour-suppressor genes has allowed major advances in prevention of hereditary cancers and early and precise diagnosis of numerous tumour types. Cancer genetics has also provided valuable information for prognostic and therapy selection purposes.

Despite such advances, the limitations of the molecular approaches, even reinforced by high throughput technologies with all their "omics" derivatives, to disentangle the complexity of cancer development, turned progressively obvious and have been leading to other approaches. Some of these approaches are leading to an increased complexity of cancer genetics models being grouped under the umbrella descriptive terms of systems or integrative biology, whereas others are based on the rediscovery of developmental and organismal biology models of cancer.

Whatever the model used as a conceptual frame for addressing carcinogenesis, it has to incorporate a number of imposing observational data: pronounced genotypic heterogeneity of most cancers, crucial role of host cells in every neoplastic growth, key function of angiogenesis (and vasculogenesis?) in cancer development, importance of 3D modelling for understanding cancer initiation and cancer progression.

The aforementioned data support the concept that cancer is an extremely complex, chimeric new growth, a sort of highly regulated, successful, invasive clone of our own tissues.

To address the dynamics of such "new tissue", it is necessary to combine genetics and epigenetics with metabolic data. One of the most interesting (and consistent) characteristics of neoplastic tissues from a metabolic standpoint is the overproduction of lactic acid as a consequence of elevated glycolysis [1, 2]. As Warburg [1] claimed, more than 50 years ago "*mutation* and *carcinogenic* agent are not alternatives, but empty words unless metabolically specified". He also pointed out that tumour cells obtained their energy by fermentation rather than by respiration [3] and that the damage to respiration should be irreversible since the respiration of cancer cells never returned to normal [1]. Elaborating on this, Warburg advanced that "in cancer, the inhibition of respiration continues through all the following divisions. This originally mysterious phenomenon has been explained…the

V. Máximo · J. Lima · P. Soares · M. Sobrinho-Simões
Department of Pathology, Medical Faculty, University of Porto, Porto, Portugal

V. Máximo · J. Lima · P. Soares · M. Sobrinho-Simões (✉)
Institute of Molecular Pathology and Immunology of the University of Porto (IPATIMUP),
Rua Dr. Roberto Frias, S/N,
4200-465 Porto, Portugal
e-mail: ssimoes@ipatimup.pt

M. Sobrinho-Simões
Department of Pathology, Hospital S. João,
Porto, Portugal

respiratory *grana* are *autonomous organisms*… The respiration connected with the *grana* remains damaged; when it has once been damaged, it is for the same reason that properties linked with genes remain damaged when genes have been damaged" [1]. The *grana* are today's mitochondria and Warburg's insights, in 1956, are almost unbelievable taking into consideration the date of the double helix discovery by Watson and Crick.

A last point to refer that Warburg also anticipated that "the injury to respiration must not be so great that the cells are killed for then no cancer cells could result" [1]. It took almost 50 years to demonstrate that germline mutations in subunits B, C and D of succinate dehydrogenase account for the vast majority of hereditary paragangliomas [4–6], whereas mutations in SDHA, the flavoprotein subunit that forms the catalytic core of complex II of mitochondrial respiratory chain, leads to Leigh syndrome, a neurodegenerative condition [7]. These findings support Warburg's educated guess and show that mitochondrial alterations may be involved in the two extremes of the disease spectrum: degenerative conditions caused by cell death and neoplastic conditions apparently caused by a blockage of cell death.

In the present review, we will try to highlight the links between mitochondrial alterations and carcinogenesis using the available epidemiological and experimental data. For the sake of simplicity, the review will be divided into the following sections:

(a) "Mitochondrial DNA (mtDNA) mutations and human tumours"
(b) "Mutations in nuclear genes encoding mitochondrial proteins and human tumours"
(c) "In vitro models (cybrids) and animal models"
(d) "Mitochondrion-rich and oncocytic (Hürthle cell) tumours"
(e) "Genetic and biochemical alterations in oncocytic tumours"
(f) "Therapeutic hints"
(g) "Summary and conclusions"

Mitochondrial DNA mutations and human tumours

Although the vast majority of human genes are located in the nucleus and are inherited equally from both parents, there is one vital set of genes that resides in the cytoplasm and is inherited exclusively from the mother—the mitochondrial DNA (mtDNA). mtDNA is located within the mitochondria, which are double-membrane organelles, once free-living bacteria and are responsible for producing most of the cellular ATP (adenosine-5′-triphosphate) via the oxidative phosphorylation (OXPHOS) in an oxygen-dependent process [8, 9]. In the human species, there are 37 genes which are encoded by the mtDNA: two ribosomal RNAs, 22 transfer RNAs, and 13 genes—*ND1*, *ND2*, *ND3*, *ND4*, *ND4L*, *ND5*, *ND6*, *CytB*, *COI*, *COII*, *COIII*, *ATPase6* and *ATPase8*—that encode proteins of the OXPHOS system (Fig. 1) [8, 9].

In addition to OXPHOS, cells can also produce ATP through glycolysis, which takes place in the cytosol and does not require O_2. OXPHOS is more efficient in generating ATP than glycolysis; therefore, this is the preferred cellular process, provided there is enough O_2 available. Whenever there is a decrease in O_2 levels, there is a shift from OXPHOS to glycolysis and the ATP is generated mainly through glycolysis (Pasteur effect).

In the first half of the twentieth century, Otto Warburg [1, 2] made an outstanding discovery: Cancer cells prefer to metabolise glucose by glycolysis, not using OXPHOS, even in the presence of O_2 (Warburg effect or aerobic glycolysis). He further hypothesised that this phenomenon was attributable to irreversible damages in cancer cells OXPHOS [1]. The Warburg effect has since been demonstrated in different types of tumours and the concomitant increase in glucose uptake has been exploited clinically for the detection of tumours by fluorodeoxyglucose positron emission tomography [10]. Although aerobic glycolysis has now been generally accepted as a metabolic hallmark of cancer, its cause and its causal relationship with cancer progression are still unclear.

This metabolic shift may be due to defects in OXPHOS that force cancer cells towards glycolysis. Genetic evidence for OXPHOS defects has been provided, during the past 10 years, with the identification of mutations in mtDNA-encoded OXPHOS genes in most types of human cancers [11–32].

Although most of the studies on record report homoplasmic mtDNA mutations in cancer cells, there is evidence that mtDNA mutations do not need to reach homoplasmy in order to influence tumour cell growth [19, 33]. The dynamics of this process, i.e. the putative existence of a trend towards homoplasmy in most neoplastic settings [34], remains to be fully clarified.

The first comprehensive study on mtDNA alterations in tumours was made by Polyak et al. in 1998 [16], who screened the entire mtDNA genome and detected mutations in seven out of ten colon cancer cell lines, which were also present in the corresponding primary tumours. Various studies followed the report of Polyak et al. [16] and it became clear that mtDNA mutations were frequent events in carcinomas of the breast, stomach, liver, prostate, kidney, bladder, head and neck and lung [35, 36].

The mtDNA is a hotspot for mutations because the mutation rate of mtDNA is ten to 20 times higher than that of

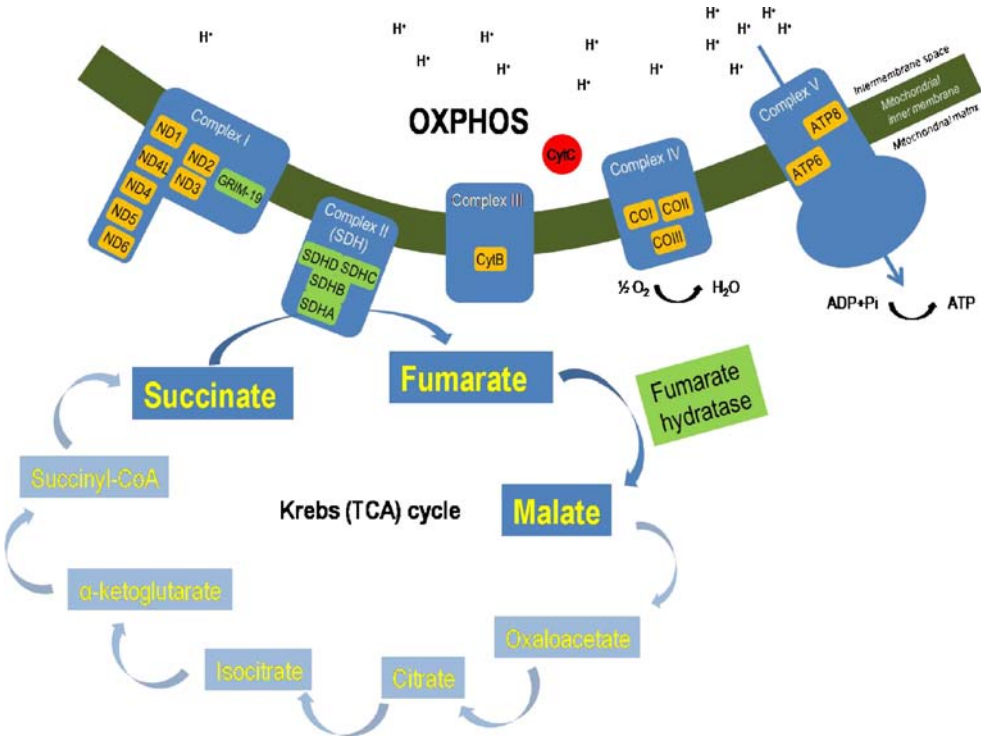

Fig. 1 Schematic representation of the OXPHOS system and the Krebs cycle in the mitochondria. We have highlighted the genes/proteins addressed in the present review. MtDNA-encoded OXPHOS proteins are depicted in *orange* and nuclear-encoded mitochondrial proteins are depicted in *green*

nuclear DNA for a number of reasons: The mtDNA polymerase γ replicates mtDNA with poor fidelity; there is a high concentration of reactive oxygen species (ROS) in the mitochondrial inner membrane (close to the mtDNA molecule); there are no efficient mtDNA repair mechanisms and there are no mtDNA-coating proteins like the histones in the nucleus [9]. The mutations seem to be present throughout the mtDNA molecule, even though the D-loop—a regulatory non-coding region where transcription factors encoded by the nuclear DNA bind to mtDNA—is where mutations are more frequent. The carcinogenic significance of D-loop alterations is unknown and, although D-loop alterations correlate, in some studies, with clinical parameters [37], it remains to be confirmed their role in tumourigenesis.

Mutations in the 13 protein-encoding mtDNA genes may, in turn, have a direct effect on the protein function, hence in the OXPHOS system. There appears not to exist a particularly affected gene, even though the seven complex I genes seem to accumulate more mutations. This is the case for thyroid tumours, which are amongst the best studied in terms of mtDNA mutations. Yeh et al. in 2000 [18] and Maximo et al. in 2002 [21] described somatic mutations in 23% and 51.5% of thyroid tumours, respectively. In the study by Maximo et al. [21], a significant association between mutations in complex I genes and malignancy was observed. Furthermore, Yeh et al. [18] found, in comparison with a control population, a significant association between germline polymorphisms in complex I genes and the occurrence of thyroid tumours, whereas Maximo et al. [21] observed that germline polymorphisms in complexes I and IV were associated with the development of malignant thyroid tumours [18, 21].

The importance of complex I and its dysfunction in thyroid tumourigenesis advanced by Yeh et al. [18] and Maximo et al. [21] has been supported by more recent studies. Abu-Amero et al. [22] identified seven somatic mutations in 19 thyroid tumours samples (36.8%), most of them being located in complex I genes, and four mutations in four thyroid tumour-derived cell lines, all in complex I genes. The authors also observed that in two thyroid cancer cell lines, there was a severe defect in complex I activity [22], possibly due to the mutations in complex I genes. Another thyroid cancer cell line—the XTC.UC1, derived from a Hürthle cell thyroid carcinoma—was found to harbour a frameshift mutation in *ND1* gene (complex I) and a missense mutation in *CytB* gene (complex III) [23]. These alterations were associated with a marked reduction in the enzymatic activity of complexes I and III in conjunction with a enhanced production of ROS [23].

The functional tumourigenic role played, in vivo, by mtDNA mutations has been demonstrated in 2005, using prostate and cervical cancer models, by two groups [38, 39]. The results obtained by Shidara et al. [39] support the conclusion that the cancer-promoting effect of mtDNA

pathogenic mutations is achieved through blockage of apoptosis, whereas Petros et al. [38] point to the influence of mtDNA mutations in ROS overproduction, which, in turn, would stimulate cell proliferation.

It has also been shown that mitochondrial respiration defects in cancer cells cause activation of the AKT survival pathway through a redox-mediated mechanism [40].

Reviewing the evidence on record, Gottlieb and Tomlinson [41], advanced that mitochondrial dysfunction may lead to carcinogenesis through several mechanisms: decrease in apoptosis, increase in the production of ROS and activation of a hypoxia-like pathway (pseudo-hypoxia; see below).

Mutations in nuclear genes encoding mitochondrial proteins and human tumours

Whilst the aforementioned studies focussed on mtDNA alterations, others have reported that nuclear-encoded mitochondrial proteins of the OXPHOS system and Krebs cycle might also be involved in mitochondrial dysfunction and tumourigenesis.

The most compelling evidence showing that defects in nuclear-encoded mitochondrial proteins are involved in tumourigenesis came out in 2000 when Baysal et al. [4] demonstrated that germline loss-of-function mutations in *SDHD*, a gene that encodes the homonym subunit of the mitochondrial enzyme succinate dehydrogenase (SDH—also known as complex II of the OXPHOS) cause familial paragangliomas (PGL). Besides its role in the OXPHOS, SDH is also involved in the Krebs cycle (Fig. 1). Immediately after the publication of Baysal et al. [4], other studies showed that also *SDHB* and *SDHC*, which encode two other subunits of SDH, are mutated in familial PGL and phaeochromocytomas [5, 6]. Furthermore, SDH alterations may be involved in other types of tumours. Lima et al. [42] studied a case of familial C-cell hyperplasia [thought to be a pre-malignant lesion of medullary thyroid carcinoma (MTC)] where the affected individuals presented a germline alteration in *SDHD*. Subsequent studies found that individuals with MTC presented more frequently *SDHB* or *SDHD* polymorphisms than a control population [43] and that MTC patients harbouring germline *SDHD* polymorphisms had lower mean age at diagnosis than MTC patients without germline *SDHD* polymorphisms [44]. These results suggest that SDH alterations may act as modulators of MTC tumourigenesis.

In a recent paper, Ricketts et al. [45] investigated whether germline mutations in *SDHB*, *SDHC* or *SDHD* were associated with renal cell carcinoma (RCC) susceptibility in 68 patients with no clinical evidence of a RCC susceptibility syndrome. No mutations in *SDHC* or *SDHD* were identified, but three of the 68 (4.4%) probands had a germline *SDHB* mutation. Patients with germline *SDHB* mutations presented with familial RCC (n=1) or bilateral RCC (n=2) without any personal or family history of phaeochromocytoma or head and neck PGL [45]. This finding suggests that *SDHB* may represent a susceptibility gene for non-syndromic RCC [45]. Curiously, downregulation of *GRIM-19*, another nuclear-encoded OXPHOS gene, has been associated with RCC (see below).

SDHB, *SDHC* and *SDHD* (SDH genes) were the first nuclear genes encoding mitochondrial proteins to be considered as tumour-suppressor genes. Another nuclear-encoded mitochondrial enzyme—fumarate hydratase (FH)—was also found to fit into that category. Tomlinson et al. [46] reported that heterozygous *FH* mutations predispose to dominantly inherited uterine fibroids, skin leiomyomata and type II papillary renal cell cancer, the so-called hereditary leiomyomas and renal cell carcinoma (HLRCC) syndrome. In contrast to this and partially mimicking the different outcome of *SDHA* mutations, homozygous mutations of *FH* are associated with fumarase deficiency, a degenerative condition [47].

In addition to the involvement in apparently opposed diseases, such as cancer and degenerative disorders, SDH and FH share other important features. They are both part of the Krebs cycle, where they catalyse subsequent steps (Fig. 1) and although there is no clear overlap of the tumour spectrum associated with SDH and *FH* mutations (possibly with the exception of renal cell carcinoma), both neoplastic syndromes give rise to tumours showing increased microvessel density and activation of the hypoxia pathway [48]. It is thus possible that failure of the Krebs cycle in PGL and HLRCC tumours causes inappropriate signalling of a hypoxic state of the neoplastic cells, leading to angiogenesis and, perhaps, to clonal expansion and tumour growth.

Maximo et al. [49] analysed a nuclear gene—*GRIM-19*—which encodes a mitochondrial complex I protein [50] in Hürthle and non-Hürthle thyroid tumours and identified three *GRIM-19* missense somatic mutations in three Hürthle cell thyroid tumours, as well as a germline mutation in a Hürthle cell papillary carcinoma arising in a thyroid with multiple Hürthle cell tumours and familial clustering [49]. No mutations were detected in any of the 20 non-Hürthle cell carcinomas tested, nor in any of the 96 blood donor samples. It was proposed that such mutations may be tumourigenic through the dual function of GRIM-19 in mitochondrial metabolism (as part of OXPHOS complex I) and cell death (being involved in retinoic acid and interferon-β induced apoptosis) [49]. In the chapter on oncocytic tumours (below), the pathogenic meaning of *GRIM-19* mutations in thyroid oncology will be discussed. Herein, we just want to stress that the expression of GRIM-19 is lost or severely downregulated in a number of primary RCC, regardless of the histotype of the tumours

[51]. We have confirmed these findings in two clear cell RCCs we have recently analysed (Portugal and Máximo, unpublished results).

The evidence obtained in the setting of tumourigenesis associated with mutations in nuclear genes encoding OXPHOS proteins (e.g. SDH and *GRIM-19*) fits with the results obtained with mtDNA mutations (see above). It remains to be better clarified the functional role, from a tumourigenic standpoint, of the mutations in Krebs cycle genes (SDH and *FH*).

Conceptually, any alteration that disrupts either the OXPHOS system or the Krebs cycle will have a direct effect on the cell's metabolism: If ATP production through OXPHOS is no longer viable, glycolysis remains the only way to obtain energy. There are two consequences of this metabolic shift that constitute important advantages to tumour cells: overproduction of lactic acid and acidification of the media with concomitant injury to "normal" cells, as well as oxygen-independent growth and survival. Classical oncogenes and tumour suppressor genes such as Ras, Myc, Akt and p53 can also drive metabolic changes and promote glycolysis [52–55]. The altered metabolism of cancer cells may confer a selective advantage for survival and proliferation in the unique tumour microenvironment, an adaptation in which the hypoxia-inducible factor (HIF) probably plays a major role [52–55].

Summing up, aerobic (and anaerobic) glycolysis is constitutively upregulated in cancer cells through both genetic and epigenetic changes caused by mitochondrial alterations [52, 56]. It represents an evolved solution to common environmental constraints (i.e. space) [56]. Upregulation of glycolysis leads to microenvironmental acidosis thus creating a powerful growth advantage for the acid-resistant neoplastic cells over "normal" cells (see Summary and conclusions).

In vitro models (cybrids) and animal models

Cybrids

The means to assess the phenotypic effects of mtDNA mutations are not the standard cloning/transfection methods used to study nuclear DNA genes because the mitochondrial genome has its own genetic code and because it is not possible to make stable transfections directed to mtDNA. Another major drawback is the existence of hundreds or thousands of mtDNA copies inside one cell. Instead, it is possible to substitute the mtDNA content of one cell line with foreign mtDNA that contains a mutation of interest, leading to the establishment of cybrid cell lines. These cybrid cell lines are obtained from the fusion of a recipient ρ0 cell line that is devoid of mitochondrial DNA and a donor cell line (that has to be removed of the nucleus but maintains mitochondria and mtDNA) that contains the mtDNA of interest (Fig. 2). The major advantage of cybrid cell lines is that they allow the distinction of the phenotypic effects caused by mtDNA mutations from those caused by the nuclear background of the donor cells, i.e. should the mtDNA mutation confer a selective advantage in the donor cell line (independently of the nuclear background), this effect will be observed in the resulting cybrid cells lines.

This methodology has already been performed to study mtDNA mutations, namely those that are found in human tumours. Petros et al. [38] introduced a pathogenic *ATPase6* mutation (T8993G) in a prostate cancer cell line and observed that the resulting cybrids induced the formation of tumours in nude mice that were seven times larger than those tumours induced by the same cell line with wt mtDNA. Similarly, Shidara et al. [39] established cybrids derived from HeLa cells and mtDNA containing either the T8993G or T9176C pathogenic *ATPase6* muta-

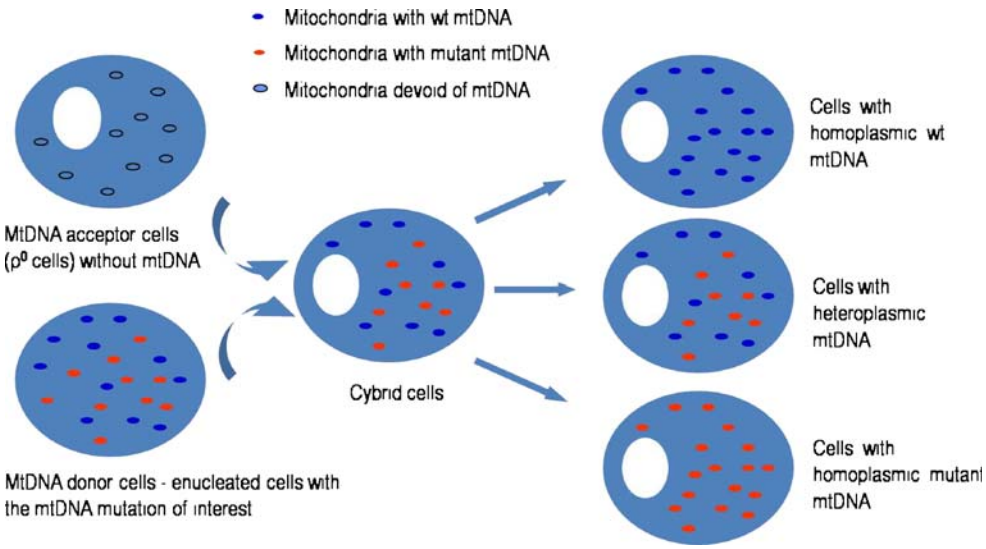

Fig. 2 Schematic representation of the cybrid production method. Starting from a cell line without mtDNA (but with mitochondria) and from enucleated cells that contain the mtDNA mutation of interest, it is possible to perform cell fusion resulting in a cybrid cell line that harbours the mtDNA mutation in a varying degree of heteroplasmy. After culturing this cybrid cell line, it is possible to obtain a homoplasmic wt or homoplasmic mutant mtDNA cell line and a heteroplasmic cell line

tions and observed that mutant cybrids grew faster than the wt in culture and that the ATP6 mutations conferred an advantage in the early stage of tumour growth when the cybrids were transplanted into nude mice. Interestingly, upon transfection of a wt nuclear version of the *ATPase6* gene in the mutant cybrids, these reverted the phenotype, thus reinforcing the functional effects of the mtDNA mutations [39]. Recently, the importance of mtDNA mutations in the metastatic process was disclosed by Ishikawa et al. [57], who analysed two mouse tumour cell lines, one highly metastatic and the other poorly metastatic, observing the results of interchanging their mtDNA; the recipient tumour cells acquired the metastatic potential of the transferred mtDNA, i.e. the poorly metastatic cell line acquired metastatic potential when its mtDNA was replaced by the mtDNA from the metastatic cell line and vice versa [57]. Additionally, the mtDNA conferring high metastatic potential contained two *ND6* mutations—G13997A and 13885insC—that produced a deficiency in complex I activity and were associated with overproduction of ROS [57]. ROS appear to play a major role in the metastatic potential, since pre-treatment with ROS scavengers abolished metastasis formation [57].

Animal models

The generation of animal models has provided some insights on the effects of OXPHOS inactivation. Piruat et al. [58] generated knockout mice for the *SDHD* gene and observed that the homozygous null mice died at early embryonic stages (7.5 days post-conception) whereas heterozygous mice developed without morphological abnormalities or major physiological dysfunction. The authors looked in detail at the carotid body function, which is one of the most affected organs in PGL syndrome type 1, and detected an overactivity of the carotid body cells due to a decrease of K^+ conductance and persistent Ca^{2+} influx into glomus cells [58]. This overactivity was accompanied by a subtle hypertrophy and hyperplasia of the carotid body, meaning that the inheritance of a heterozygous defect in *SDHD* leads to a state of cellular "overactivation" and, therefore, to an increased susceptibility to tumourigenesis upon subsequent genetic alterations [58]. In this way, OXPHOS inactivation would be an initial step in tumour development conferring tumourigenic potential to the cells. Piruat et al. [58] did not observe the occurrence of tumours in this mouse model, but it is possible that tumours would only appear later on [58].

In addition to *SDHD*, the functional importance of *GRIM-19* has also been highlighted by knock-out experiments. Huang et al. [50] generated mice deficient in *GRIM-19* by gene targeting and showed that homologous deletion of *GRIM-19* causes embryonic lethality at embryonic day 9.5. Interestingly, *GRIM-19*$^{-/-}$ blastocysts display abnormal mitochondrial structure, morphology and cellular distribution [50].

Mitochondrion-rich and oncocytic (Hürthle cell) tumours

The accumulation of huge numbers of abnormal mitochondria as seen by electron microscopy and immunohistochemistry is the hallmark of oncocytic cells regardless of the organ of origin (thyroid, parathyroid, kidney, salivary gland,…) and of the benign or malignant nature of the lesions [25, 59–66]. Such accumulation may also reflect a "normal" process; for example, the parathyroid glands normally present a variable percentage of oncocytic cells, most probably related with cell ageing [67]. Besides the role played by increased proliferation of mitochondria in the cytoplasm without cell division, it is not known whether a decreased turnover of the mitochondria may also contribute to their accumulation in oncocytic cells [21, 68].

Oncocyte is a descriptive term for a neoplastic or non-neoplastic cell stuffed with mitochondria that give a granular eosinophilic appearance to its large cytoplasm. In many instances, oxyphilic transformation is used as a synonym for oncocytic transformation, thus leading to the utilisation of oxyphilic tumour as a synonym for oncocytic tumour or oncocytoma. In the thyroid, other terms are used: Hürthle cell transformation and Hürthle cell tumours [61, 62, 69]. The question of who first described oncocytic cells in the thyroid gland is still open, although most authors acknowledge the 1907 *Virchows Archiv* article of Theodor Langhans as the first clear report of oxyphilic cells in a thyroid tumour [70]. Finally, there are, in some organs, tumours composed by oncocytes that carry specific designations (e.g. Warthin's tumour of the salivary glands).

The prominence of oncocytic cells in endocrine organs, salivary glands, kidney and other parenchymatous organs (and in their respective tumours), in contrast to the rarity of oncocytic cells in the mucosa and respective tumours of the digestive and respiratory tract, suggests that this alteration occurs in tissues with low proliferative index and reduced turnover, i.e. in stable cells with a very long intermitotic interval.

Following this *rationale*, the accumulation of mitochondria in neoplastic lesions indicates a low proliferative turnover and is thus associated, in most instances, to benign neoplasms or malignant tumours of low malignancy (as if the cells of the digestive and respiratory tract and of their tumours divide too quickly or die/desquamate too soon to allow the accumulation of abnormal mitochondria) [21, 25]. It takes many years before the accumulation of mitochondria reaches the "oncocytic" threshold (three or four thousand mitochondria per cell) thus justifying the utilisation, in some circumstances, of the term "oncocytoid".

The great majority of oncocytic tumours are epithelial-derived tumours, but there are also on record examples of oncocytomas occurring in non-epithelial settings. In a recent review, we have summarised the different sites, other than the thyroid, where oncocytomas have been reported to occur in 499 papers published in English in the last 55 years. During the same period, more than 600 papers on thyroid oncocytic tumours have been published [34].

Hürthle cells can be observed in all sorts of thyroiditis (and are prominent in Hashimoto's thyroiditis of adult and elderly patients), nodular goitre, adenoma, follicular carcinoma, papillary carcinoma (PTC) and poorly differentiated carcinoma of the thyroid. Undifferentiated (anaplastic) carcinomas composed of Hürthle cells are extremely rare probably because the neoplastic cells divide too rapidly to allow the accumulation of mitochondria. With the exception of undifferentiated carcinoma, every type of benign or malignant thyroid tumour has its oncocytic counterpart. This concept has been incorporated in the third edition of the WHO Book on Endocrine Tumours in which the "old" Hürthle cell (oncocytic) carcinoma has been substituted by the oncocytic variants of follicular carcinoma, PTC and poorly differentiated carcinoma [71].

In the thyroid, Hürthle cells are not restricted to follicular cell-derived tumours. There are also some medullary carcinomas composed of Hürthle cells that are morphologically indistinguishable from those derived from the follicular cells [72]. The occurrence of Hürthle cell transformation in medullary thyroid carcinoma fits with its occurrence in other neuroendocrine tumours throughout the body [73–75].

The presence of abundant mitochondria in the cytoplasm of the neoplastic cells may be seen throughout the entire tumour ("primary" oxyphilia, indicating that the carcinogenic hit has occurred in cells with pre-existing mitochondrial abnormalities) or just in some parts of the tumour ("secondary" oxyphilia, indicating that the mitochondrial abnormalities have occurred after tumour development) [25].

The criteria used in the diagnosis of the oncocytic variant of PTC and of follicular carcinoma are those used in the diagnosis of conventional tumours [76]. Although it is now widely accepted that most oncocytic tumours of the thyroid are benign, one should search actively for capsular and vascular invasion and for PTC nuclei, whenever dealing with any oncocytic tumour [76]. It has also been shown that the typical molecular features of conventional PTC and follicular carcinoma are also present in their oncocytic counterparts [77, 78]. This has been recently confirmed with regard to the *BRAF* V600E mutation, which is detected in about 50% cases of conventional PTC, as well as in about 50% of cases of the oncocytic variant of PTC [79]. This mutation is also very prevalent in Warthin's like PTC which is characteristically composed by oncocytic cells [80].

The prognostic factors associated to Hürthle cell carcinomas do not differ from those that were found to carry meaningful information in non-Hürthle cell carcinomas [81–85]. It remains, however, controversial whether the category of Hürthle cell variant of follicular carcinoma carries per se a worse prognosis. Some authors claim that these carcinomas spread to the perithyroid soft tissues and give rise to metastases more often than do conventional follicular carcinomas [85], but it remains to be seen whether or not the higher prevalence of nodal metastases in this setting reflects the inclusion, in the series, of cases of Hürthle cell variant of PTC erroneously classified as follicular carcinoma. The overall mortality rate of patients with Hürthle cell carcinoma [81] appears to be higher than those of patients with papillary or follicular carcinoma [86] without Hürthle cell features, as a consequence, partly at least, of the poor responsiveness of Hürthle cells to radioiodine therapy [86, 87].

Parathyroid adenomas composed predominantly (more than 90%) or exclusively of oxyphilic cells are uncommon. According to Apel and Asa [88], they constitute 4.4% to 8.4% of all parathyroid adenomas and usually remain clinically silent, whereas Giorgadze et al. [89] advanced that oxyphilic parathyroid adenomas, although rare, tend to be large and are often associated with minimal hyperparathyroidism.

Oxyphilic carcinomas of the parathyroid are frequently functional tumours, associated with high serum calcium, presenting higher Ki-67 and lower p27 than oxyphilic adenomas [90]. Oxyphilic carcinomas are associated with recurrent disease and death in about 50% of the cases. These figures do not substantially differ from those of patients with chief cell carcinoma of the parathyroid [90].

Warthin's tumour is the second most common salivary gland tumour, arising almost always in the parotid gland (accounts for about 15% of all epithelial tumours of the parotid gland), occasionally causing pain or facial nerve paralysis [91]. Warthin's tumours are constituted by cystic spaces, lined by a double layer of oncocytic cells of questionable neoplastic nature that rest on a lymphoid stroma [92]. Some are multi-focal and about 10% are bilateral but malignant transformation is very rare [91]. Smokers have approximately eight times higher risk for developing these tumours than non-smokers [93]. Oncocytic carcinoma of the salivary glands is a very rare high-grade carcinoma.

Renal oncocytomas, the most common benign solid renal tumour, are thought to originate from the intercalated cells of the renal collecting duct and account for about 3–7% of all renal tumours [94]. About 2–12% of oncocytomas are multifocal, and 4–14% are bilateral [95]. Almost all cases of oncocytoma behave in a benign fashion with no recurrence, metastasis or mortality. Some atypical features, such as nuclear pleomorphism, perinephric fat involvement, focal

necrosis and even extension to branches of the renal vein, do not seem to worsen significantly the prognosis [95].

Genetic and biochemical alterations in oncocytic tumours

The best studied oncocytic tumours in terms of mtDNA are those of the thyroid. A large deletion encompassing 4,977 bp of mtDNA, known as the mtDNA common deletion (CD), is almost always detected and was proposed as a hallmark of oncocytic thyroid tumours [21, 25, 96, 97]. This deletion removes seven OXPHOS genes (*ATPase6*, *ATPase8*, *COIII*, *ND3*, *ND4L*, *ND4* and *ND5*) and five tRNAs (glycine, arginine, histidine, serine and leucine), thus resulting in severe impairment of the OXPHOS system.

The mtDNA CD was found in every thyroid tumour with oncocytic features, irrespectively of the histological subtypes; the mtDNA CD was also present in non-oncocytic thyroid tumours, but with significantly lower frequency and relative lower amount [21].

Traditionally, the association between mtDNA CD and oncocytic phenotype has been explained through a positive feedback mechanism: The severe impairment of the OXPHOS system (as a consequence of the mtDNA CD) would engage and activate nuclear genes that control mitochondrial number, resulting in an increase in the mitochondrial mass [98, 99].

The analysis of the prevalence of mtDNA mutations has shown that missense somatic mutations in complex I genes (without any apparent concentration in a single gene) were more frequently detected in malignant tumours than in adenomas [21]. A significant association was also observed between D-loop somatic mutations and the occurrence of somatic mutations in other mtDNA genes [21]. We have summarised in Fig. 3 all but silent mtDNA somatic mutations reported to date in oncocytic tumours. A large number (n=253) of mtDNA variants (alterations present both in tumour and adjacent thyroid tissue) were disclosed in all tumour types. The variants affecting genes of complex I and IV were significantly more frequent in patients with malignant tumours than in patients with benign tumours, whereas those affecting complex V genes—almost all in *ATPase6* (34/37) and most of them missense (27/34)—were associated with the presence of oncocytic features in the tumours of the patients [21]. For a thorough review on mitochondria and oncocytic tumours, see Lima et al. [34].

Gasparre et al. [29] analysed breast and thyroid oncocytic tumours and found that 26 of the 45 (57.8%) oncocytic thyroid samples harboured 30 somatic mtDNA mutations, 25 of which were located in complex I genes; in 12 of the 45 cases (26.7%), the mutations were considered as disruptive (either frameshift or non-sense), and they were all located in complex I genes [29]. The association of disruptive complex I mutations with the Hürthle cell phenotype was strengthened by the finding that the only breast tumour that presented a disruptive somatic mtDNA mutation (also located in a complex I gene) was a mitochondrion-rich tumour [29].

To address the correlation between mtDNA mutations and oncocytic phenotype, Gasparre et al. [29] established primary cultures from two thyroid tumours, each with a disruptive mtDNA mutation. Intriguingly, none of the primary cultures showed evidence of the disruptive mtDNA mutations found in the original biopsies and, moreover, the oncocytic phenotype was lost during culture [29]. It was suggested that mtDNA mutations are negatively selected under the culture conditions [29], thus reinforcing the assumption that, in vivo, hypoxic conditions play a major role in the positive selection of the mtDNA mutations and the oncocytic phenotype.

Few publications have analysed mtDNA alterations in renal oncocytomas. Welter et al. [100] used restriction endonucleases to search for mtDNA abnormalities in six renal oncocytomas and observed that every tumour displayed an extra band, which was not noted in the corresponding normal tissue; these findings were not reproduced by Brooks et al. [101], who did not observe any mtDNA alterations in five renal oncocytomas. Tallini et al. [20] did not find alterations in *COXI* and D-loop region in ten renal oncocytomas. In addition, these authors also analysed the presence of the mtDNA CD, but failed to detect an increased frequency in comparison to controls [20]. Recently, we observed the mtDNA CD in 11 of 14 renal oncocytomas (79%) and in seven of the 14 cases (50%) in the respective adjacent normal parenchyma (Portugal et al., unpublished observation).

Simonnet et al. [102] observed that renal oncocytomas displayed a normal or slightly elevated activity of complexes II–V of the OXPHOS system, whereas complex I was not detectable in two-dimension electrophoresis; in addition, renal oncocytomas also showed a fivefold increase in citrate synthase (an indicator of mitochondrial proliferation) [102]. The absence of complex I, together with an increase in the remaining complexes and citrate synthase, led to the conclusion that the mitochondrial proliferation in renal oncocytomas might be a compensatory mechanism for a decreased OXPHOS activity [102, 103]. Mayr et al. [104] confirmed the observations of Simonnet et al. [103], showing that the enzymatic activity of complex I was undetectable or greatly reduced in the tumour samples as well as lack of assembled complex I. Furthermore, mtDNA mutation analysis showed frameshift mutations either in *ND1*, *ND4* or *ND5* in nine of 15 tumours [104].

Muller-Hocker et al. [67] showed that defects of the respiratory chain are present during cell ageing in the oncocytic cells of normal parathyroids. Muller-Hocker [59]

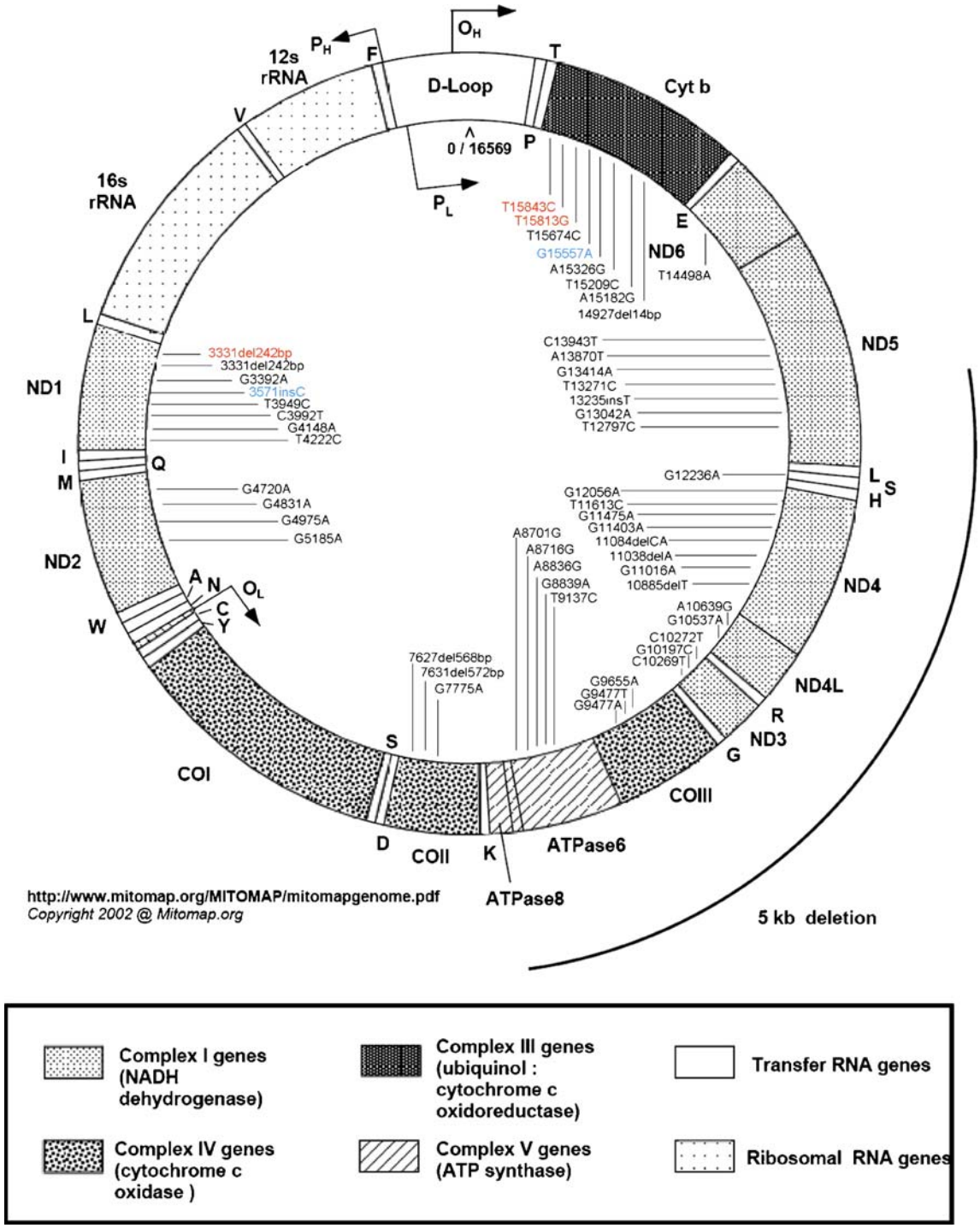

Fig. 3 Schematic representation of mtDNA somatic mutations found in human oncocytomas and in the XTC.UC1 thyroid oncocytoma cell line. Only missense, non-sense or frameshift mutations are depicted. *Numbers* indicate the mutation position according to the Cambridge reference sequence; mutations in thyroid oncocytomas are represented in *black*, in breast oncocytomas in *red* and in the thyroid oncocytoma cell line in *blue*. Picture taken and adapted with permission from MITOMAP [121] and Lima et al. [34]

described also random cytochrome-C-oxidase deficiency in oncocytic parathyroid adenomas, whereas no abnormalities were detected in other enzymes of the respiratory chain (SDH and ATP synthase). Genetic studies are necessary to see if the aforementioned mitochondrial protein alterations reflect mtDNA alterations.

Lewis et al. [19] observed, using two-colour fluorescent in situ hybridisation, that all oncocytic cells in Warthin's

tumours contained mitochondria showing a reduction on normal mtDNA signal and that oncocytic cells had mixed populations of normal and deleted mtDNA (heteroplasmy), but no cells had exclusively deleted mtDNA. Lewis et al. [19] also found the presence of a low level of mtDNA deletions in normal parotid epithelial cells of smoker patients, a finding that supports the assumption that these deletions may precede the oncocytic phenotype.

Biochemical analyses of oncocytic thyroid tumours revealed that the ATP synthesis in the tumour cells is impaired, suggesting an inactivation of the OXPHOS system [28, 105]. Savagner et al. [28] studied seven fresh oncocytic thyroid tumours and respective controls, having found that the ATP synthesis was lower in all the tumours, with a parallel overexpression of uncoupling protein 2, which is a protein that uncouples the electron flow in the OXPHOS system from the ATP production in complex V. Savagner et al. [28] also found that two mitochondrial genes—*ND2* and *ND5*—were overexpressed in relation to normal thyroid tissue. Confirming these observations, two other studies, using microarrays, have found that the majority of the peptide-encoding mtDNA genes were overexpressed in thyroid oncocytic tumours [106, 107]. These results suggest that the defective ATP production observed in this setting may explain the characteristic mitochondrial proliferation of oncocytic cells.

Using differential display, it was disclosed, amongst other alterations, an overexpression of the gene encoding the core I subunit of the complex III of the mitochondrial OXPHOS system in a follicular carcinoma composed of Hürthle cells [108]. However, in a large series of thyroid tumours, *core I* overexpression was found to be associated with benign and malignant tumours of the thyroid with microfollicular growth pattern, independently of the presence of Hürthle cells [108].

A last point to refer is that the association between *GRIM-19* mutations and Hürthle cell phenotype [49] has not been confirmed in renal oncocytomas, nor in Warthin's tumour of the salivary glands (Portugal, Guimarães et al., unpublished results). In the thyroid, familial forms of benign and malignant Hürthle cell tumours may be due to a germline mutation in *GRIM-19* (see above) [49]. Downregulation of GRIM-19 has been shown to confer a growth advantage on cells and to reduce the likelihood that they will enter apoptosis [51]. The detection of a RET/PTC1 re-arrangement in one case of the oncocytic variant of PTC in which there was also a *GRIM-19* mutation [49] suggests that the latter mutation may serve as a predisposing alteration for the occurrence of tumours with cell oxyphilia; other alterations such as RET/PTC rearrangement or *BRAF* mutation may be necessary for the acquisition of the malignant phenotype (for a thorough review, see [109]).

Therapeutic hints

Although the cause of the metabolic shift towards glycolysis of cancer tissues remains to be fully clarified, the glycolytic phenotype is such a common end product of diverse molecular abnormalities that the Warburg effect may turn into the Achilles' heel of cancer cells from a therapeutic standpoint [52, 56, 110, 111]. Since early carcinogenesis is thought to occur in a hypoxic microenvironment, Gatenby and Gillies [56] proposed that the transformed cells initially have to rely on glycolysis for energy production. As discussed above, this early metabolic adaptation appears to offer a proliferative advantage, suppressing apoptosis. Furthermore, the "byproducts" of glycolysis (i.e. lactate and acidosis) contribute to the breakdown of the extracellular matrix, facilitate cell mobility and increase the metastatic potential [56, 112]. In a recent study, Bonnet et al. [113] compared several cancer cell lines with normal cell lines and found that cancer cells had more hyper-polarised mitochondria, having hypothesised that if this metabolic-electrical remodelling is an adaptive response, then its reversal might increase apoptosis and inhibit cancer growth [113]. Bonnet et al. [113] used dichloroacetate (DCA), a small molecule and a well-characterised inhibitor of pyruvate dehydrogenase kinase (PDK). Inhibition of PDK by DCA in A549 cells shifts pyruvate metabolism from glycolysis and lactate production to glucose oxidation in the mitochondria. This metabolic shift was associated with increased production of ROS, efflux of pro-apoptotic mediators from the mitochondria, induction of mitochondria-dependent apoptosis and decreased tumour growth [113].

In 2001, Ko et al. [111] showed that a small molecule named 3-bromopyruvate (3BrPA) was a potent inhibitor of the glycolytic activity in tumour cells [111]. 3-BrPA is not only an analogue of lactic acid but also highly reactive. Due to its structural analogy to lactic acid, it is believed that 3-BrPA may take advantage of the Warburg effect by selectively entering cancer cells via the enhanced number of lactic acid transporters that are present in such cells and, once inside, using its alkylating properties to block energy production. Ko et al. [111] showed that 3BrPA had little or no effect on normal hepatocytes used as control population, but destroyed almost all the hepatoma cells; it has been shown, moreover, that 3-BrPA works also in vivo [111, 112].

Summary and conclusions

Mitochondria are key organelles in cellular homeostasis taking part in vital processes, such as ATP production via the OXPHOS system, and programmed cell death (apoptosis) via cytochrome C release from the mitochondrial intermembrane space. In 1956, Otto Warburg [114] showed that

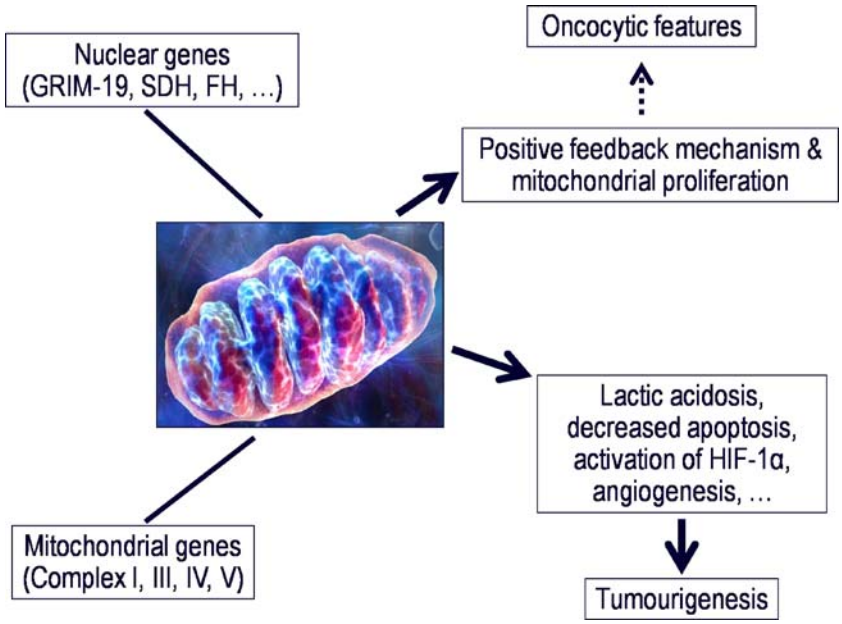

Fig. 4 Schematic representation of the putative role of alterations in nuclear or mtDNA-encoded mitochondrial proteins both in the oncocytic phenotype and in tumourigenesis. Picture adapted from Sobrinho-Simoes et al. [69]

human tumours displayed elevated glycolysis and reduced rate of OXPHOS, even in the presence of oxygen and suggested that defects in OXPHOS could underlie many forms of cancer. In the last decade, the finding of mtDNA mutations, as well as of mutations in nuclear genes encoding mitochondrial proteins in many types of sporadic and familial human tumours with and without oncocytic (Hürthle cell) features, has provided a genetic basis for the mitochondrial dysfunction observed in human tumourigenesis.

The mechanisms by which mtDNA and nuclear DNA mutations and the resulting defective mitochondrial proteins involved in OXPHOS and/or Krebs cycle can lead to or promote tumourigenesis are not fully understood. It has been advanced that the outcome of such mechanisms would be enhanced glycolysis, with a concomitant survival advantage in hypoxic and acidic microenvironments, as well as an escape from the excessive ROS formation (which may lead to apoptosis) of a malfunctioning OXPHOS.

There is epidemiological and experimental evidence showing that some pathogenic mtDNA mutations, as well as mutations in a few mitochondrial coding nuclear genes (*GRIM-19*, SDH, *FH*), create a favourable environment for tumour development by conferring growth advantage to cells. However, extra-hits, such as LOH and mutations in other oncogenes and/or tumour-suppressor genes, appear to be required for tumour progression, including malignant transformation.

There is also emerging evidence suggesting that mitochondrial dysfunction may lead to the activation of HIF 1-alpha (HIF-1α), therefore triggering the hypoxia pathway in the tumourigenic process. The activation of this pathway would result in the transcription of a number of genes known to be associated with human tumourigenesis, such as those involved in glucose metabolism, angiogenesis, extra-cellular matrix modification, motility and survival [115–119].

The two cartoons shown in Figs. 4 and 5 summarise the way the relationship between mitochondrial alterations, hypoxia (and pseudo-hypoxia) and carcinogenesis may be envisaged using the available epidemiological and experimental evidence.

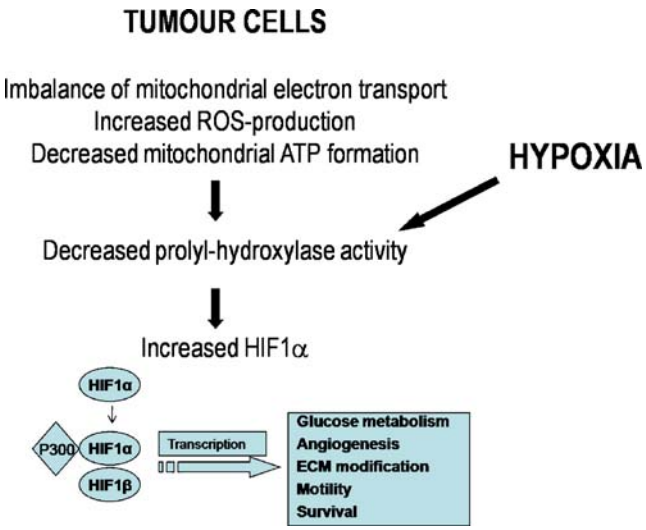

Fig. 5 Schematic representation of the possible mechanisms of HIF-1α stabilisation due to mitochondrial dysfunction in tumour cells

The role played by the increased activity of HIF-1α in cancer development has been repeatedly aknowledged both in connection with mitochondrial alterations [32, 57, 120] and in other settings [115–119]. The discussion of such role rests beyond the scope of the present review.

Acknowledgments This work was supported by the Portuguese Science and Technology Foundation through the grant SFRH/BPD/29197/2006 (Jorge Lima) and by the Late David and Esther Bernstein Halpern Fund.

Conflict of interest statement We declare that we have no conflict of interest.

References

1. Warburg O (1956) On the origin of cancer cells. Science 123:309–314
2. Warburg O (1930) The metabolism of tumours. London Constable, London
3. Warburg O, Wind F, Negelein E (1927) The metabolism of tumors in the body. J Gen Physiol 8:519–530
4. Baysal BE, Ferrell RE, Willett-Brozick JE et al (2000) Mutations in SDHD, a mitochondrial complex II gene, in hereditary paraganglioma. Science 287:848–851
5. Astuti D, Latif F, Dallol A et al (2001) Gene mutations in the succinate dehydrogenase subunit SDHB cause susceptibility to familial pheochromocytoma and to familial paraganglioma. Am J Hum Genet 69:49–54
6. Niemann S, Muller U (2000) Mutations in SDHC cause autosomal dominant paraganglioma, type 3. Nat Genet 26:268–270
7. Horvath R, Abicht A, Holinski-Feder E et al (2006) Leigh syndrome caused by mutations in the flavoprotein (Fp) subunit of succinate dehydrogenase (SDHA). J Neurol Neurosurg Psychiatry 77:74–76
8. Wallace DC (1999) Mitochondrial diseases in man and mouse. Science 283:1482–1488
9. Wallace DC (2005) A mitochondrial paradigm of metabolic and degenerative diseases, aging, and cancer: a dawn for evolutionary medicine. Annu Rev Genet 39:359–407
10. Rohren EM, Turkington TG, Coleman RE (2004) Clinical applications of PET in oncology. Radiology 231:305–332
11. Habano W, Sugai T, Nakamura SI et al (2000) Microsatellite instability and mutation of mitochondrial and nuclear DNA in gastric carcinoma. Gastroenterology 118:835–841
12. Richard SM, Bailliet G, Paez GL et al (2000) Nuclear and mitochondrial genome instability in human breast cancer. Cancer Res 60:4231–4237
13. Maximo V, Soares P, Seruca R et al (2001) Microsatellite instability, mitochondrial DNA large deletions, and mitochondrial DNA mutations in gastric carcinoma. Genes Chromosomes Cancer 32:136–143
14. Burgart LJ, Zheng J, Shu Q et al (1995) Somatic mitochondrial mutation in gastric cancer. Am J Pathol 147:1105–1111
15. Habano W, Sugai T, Yoshida T et al (1999) Mitochondrial gene mutation, but not large-scale deletion, is a feature of colorectal carcinomas with mitochondrial microsatellite instability. Int J Cancer 83:625–629
16. Polyak K, Li Y, Zhu H et al (1998) Somatic mutations of the mitochondrial genome in human colorectal tumours. Nat Genet 20:291–293
17. Fliss MS, Usadel H, Caballero OL et al (2000) Facile detection of mitochondrial DNA mutations in tumors and bodily fluids. Science 287:2017–2019
18. Yeh JJ, Lunetta KL, Van Orsouw NJ et al (2000) Somatic mitochondrial DNA (mtDNA) mutations in papillary thyroid carcinomas and differential mtDNA sequence variants in cases with thyroid tumours. Oncogene 19:2060–2066
19. Lewis PD, Baxter P, Paul GA et al (2000) Detection of damage to the mitochondrial genome in the oncocytic cells of Warthin's tumour. J Pathol 191:274–281
20. Tallini G, Ladanyi M, Rosai J et al (1994) Analysis of nuclear and mitochondrial DNA alterations in thyroid and renal oncocytic tumors. Cytogenet Cell Genet 66:253–259
21. Maximo V, Soares P, Lima J et al (2002) Mitochondrial DNA somatic mutations (point mutations and large deletions) and mitochondrial DNA variants in human thyroid pathology: a study with emphasis on Hurthle cell tumors. Am J Pathol 160:1857–1865
22. Abu-Amero KK, Alzahrani AS, Zou M et al (2005) High frequency of somatic mitochondrial DNA mutations in human thyroid carcinomas and complex I respiratory defect in thyroid cancer cell lines. Oncogene 24:1455–1460
23. Bonora E, Porcelli AM, Gasparre G et al (2006) Defective oxidative phosphorylation in thyroid oncocytic carcinoma is associated with pathogenic mitochondrial DNA mutations affecting complexes I and III. Cancer Res 66:6087–6096
24. Lohrer HD, Hieber L, Zitzelsberger H (2002) Differential mutation frequency in mitochondrial DNA from thyroid tumours. Carcinogenesis 23:1577–1582
25. Maximo V, Sobrinho-Simoes M (2000) Hurthle cell tumours of the thyroid. A review with emphasis on mitochondrial abnormalities with clinical relevance. Virchows Arch 437:107–115
26. Maximo V, Lima J, Soares P et al (2005) Mitochondrial D-loop instability in thyroid tumours is not a marker of malignancy. Mitochondrion 5:333–340
27. Rogounovitch T, Saenko V, Yamashita S (2004) Mitochondrial DNA and human thyroid diseases. Endocr J 51:265–277
28. Savagner F, Franc B, Guyetant S et al (2001) Defective mitochondrial ATP synthesis in oxyphilic thyroid tumors. J Clin Endocrinol Metab 86:4920–4925
29. Gasparre G, Porcelli AM, Bonora E et al (2007) Disruptive mitochondrial DNA mutations in complex I subunits are markers of oncocytic phenotype in thyroid tumors. Proc Natl Acad Sci U S A 104:9001–9006
30. Gasparre G, Iommarini L, Porcelli AM et al (2008) An inherited mitochondrial DNA disruptive mutation shifts to homoplasmy in oncocytic tumor cells. Hum Mutat 30:391–396
31. Jeronimo C, Nomoto S, Caballero OL et al (2001) Mitochondrial mutations in early stage prostate cancer and bodily fluids. Oncogene 20:5195–5198
32. Zhou S, Kachhap S, Sun W et al (2007) Frequency and phenotypic implications of mitochondrial DNA mutations in human squamous cell cancers of the head and neck. Proc Natl Acad Sci U S A 104:7540–7545
33. Park JS, Sharma LK, Li HZ et al. (2009) A heteroplasmic, not homoplasmic, mitochondrial DNA mutation promotes tumorigenesis via alteration in reactive oxygen species generation and apoptosis. Hum Mol Genet (in press)
34. Lima J, Maximo V, Soares P et al (2009) Mitochondria and oncocytomas. In: Singh KK, Costello LC (eds) Mitochondria and cancer. Springer, New York, pp 193–209
35. Copeland WC, Wachsman JT, Johnson FM et al (2002) Mitochondrial DNA alterations in cancer. Cancer Invest 20:557–569

36. Czarnecka AM, Golik P, Bartnik E (2006) Mitochondrial DNA mutations in human neoplasia. J Appl Genet 47:67–78
37. Tamori A, Nishiguchi S, Nishikawa M et al (2004) Correlation between clinical characteristics and mitochondrial D-loop DNA mutations in hepatocellular carcinoma. J Gastroenterol 39:1063–1068
38. Petros JA, Baumann AK, Ruiz-Pesini E et al (2005) mtDNA mutations increase tumorigenicity in prostate cancer. Proc Natl Acad Sci U S A 102:719–724
39. Shidara Y, Yamagata K, Kanamori T et al (2005) Positive contribution of pathogenic mutations in the mitochondrial genome to the promotion of cancer by prevention from apoptosis. Cancer Res 65:1655–1663
40. Pelicano H, Xu RH, Du M et al (2006) Mitochondrial respiration defects in cancer cells cause activation of Akt survival pathway through a redox-mediated mechanism. J Cell Biol 175:913–923
41. Gottlieb E, Tomlinson IP (2005) Mitochondrial tumour suppressors: a genetic and biochemical update. Nat Rev Cancer 5:857–866
42. Lima J, Teixeira-Gomes J, Soares P et al (2003) Germline succinate dehydrogenase subunit D mutation segregating with familial non-RET C cell hyperplasia. J Clin Endocrinol Metab 88:4932–4937
43. Montani M, Schmitt AM, Schmid S et al (2005) No mutations but an increased frequency of SDHx polymorphisms in patients with sporadic and familial medullary thyroid carcinoma. Endocr Relat Cancer 12:1011–1016
44. Cascon A, Cebrian A, Pollan M et al (2005) Succinate dehydrogenase D variants do not constitute a risk factor for developing C cell hyperplasia or sporadic medullary thyroid carcinoma. J Clin Endocrinol Metab 90:2127–2130
45. Ricketts C, Woodward ER, Killick P et al (2008) Germline SDHB mutations and familial renal cell carcinoma. J Natl Cancer Inst 100:1260–1262
46. Tomlinson IP, Alam NA, Rowan AJ et al (2002) Germline mutations in FH predispose to dominantly inherited uterine fibroids, skin leiomyomata and papillary renal cell cancer. Nat Genet 30:406–410
47. Eng C, Kiuru M, Fernandez MJ et al (2003) A role for mitochondrial enzymes in inherited neoplasia and beyond. Nat Rev Cancer 3:193–202
48. Pollard PJ, Briere JJ, Alam NA et al (2005) Accumulation of Krebs cycle intermediates and over-expression of HIF1alpha in tumours which result from germline FH and SDH mutations. Hum Mol Genet 14:2231–2239
49. Maximo V, Botelho T, Capela J et al (2005) Somatic and germline mutation in GRIM-19, a dual function gene involved in mitochondrial metabolism and cell death, is linked to mitochondrion-rich (Hurthle cell) tumours of the thyroid. Br J Cancer 92:1892–1898
50. Huang G, Lu H, Hao A et al (2004) GRIM-19, a cell death regulatory protein, is essential for assembly and function of mitochondrial complex I. Mol Cell Biol 24:8447–8456
51. Alchanati I, Nallar SC, Sun P et al (2006) A proteomic analysis reveals the loss of expression of the cell death regulatory gene GRIM-19 in human renal cell carcinomas. Oncogene 25:7138–7147
52. Hsu PP, Sabatini DM (2008) Cancer cell metabolism: Warburg and beyond. Cell 134:703–707
53. Ramanathan A, Wang C, Schreiber SL (2005) Perturbational profiling of a cell-line model of tumorigenesis by using metabolic measurements. Proc Natl Acad Sci U S A 102:5992–5997
54. Matoba S, Kang JG, Patino WD et al (2006) p53 regulates mitochondrial respiration. Science 312:1650–1653
55. Kaelin WG Jr, Ratcliffe PJ (2008) Oxygen sensing by metazoans: the central role of the HIF hydroxylase pathway. Mol Cell 30:393–402
56. Gatenby RA, Gillies RJ (2004) Why do cancers have high aerobic glycolysis? Nat Rev Cancer 4:891–899
57. Ishikawa K, Takenaga K, Akimoto M et al (2008) ROS-generating mitochondrial DNA mutations can regulate tumor cell metastasis. Science 320:661–664
58. Piruat JI, Pintado CO, Ortega-Saenz P et al (2004) The mitochondrial SDHD gene is required for early embryogenesis, and its partial deficiency results in persistent carotid body glomus cell activation with full responsiveness to hypoxia. Mol Cell Biol 24:10933–10940
59. Muller-Hocker J (1992) Random cytochrome-C-oxidase deficiency of oxyphil cell nodules in the parathyroid gland. A mitochondrial cytopathy related to cell ageing? Pathol Res Pract 188:701–706
60. Rosai J, Carcangiu ML, DeLellis RA (1992) Tumours of the thyroid gland. Armed Force Institute of Pathology, Washington, DC
61. Sobrinho-Simoes MA, Nesland JM, Holm R et al (1985) Hurthle cell and mitochondrion-rich papillary carcinomas of the thyroid gland: an ultrastructural and immunocytochemical study. Ultrastruct Pathol 8:131–142
62. Nesland JM, Sobrinho-Simoes MA, Holm R et al (1985) Hurthle-cell lesions of the thyroid: a combined study using transmission electron microscopy, scanning electron microscopy, and immunocytochemistry. Ultrastruct Pathol 8:269–290
63. Ebner D, Rodel G, Pavenstaedt I et al (1991) Functional and molecular analysis of mitochondria in thyroid oncocytoma. Virchows Arch B Cell Pathol Incl Mol Pathol 60:139–144
64. Muller-Hocker J, Jacob U, Seibel P (1998) Hashimoto thyroiditis is associated with defects of cytochrome-c oxidase in oxyphil Askanazy cells and with the common deletion (4, 977) of mitochondrial DNA. Ultrastruct Pathol 22:91–100
65. Ortmann M, Vierbuchen M, Koller G et al (1988) Renal oncocytoma. I. Cytochrome c oxidase in normal and neoplastic renal tissue as detected by immunohistochemistry—a valuable aid to distinguish oncocytomas from renal cell carcinomas. Virchows Arch B Cell Pathol Incl Mol Pathol 56:165–173
66. Muller-Hocker J (2000) Expression of bcl-2, Bax and Fas in oxyphil cells of Hashimoto thyroiditis. Virchows Arch 436:602–607
67. Muller-Hocker J, Aust D, Napiwotzky J et al (1996) Defects of the respiratory chain in oxyphil and chief cells of the normal parathyroid and in hyperfunction. Hum Pathol 27:532–541
68. Cheung CC, Ezzat S, Ramyar L et al (2000) Molecular basis off Hurthle cell papillary thyroid carcinoma. J Clin Endocrinol Metab 85:878–882
69. Sobrinho-Simoes M, Maximo V, Castro IV et al (2005) Hurthle (oncocytic) cell tumors of thyroid: etiopathogenesis, diagnosis and clinical significance. Int J Surg Pathol 13:29–35
70. Langhans T (1907) Über die epithelialen Formen der malignen Struma. Virchows Arch 189:69–153
71. DeLellis RA LR, Heitz PU, Eng C (eds) (2004) World Health Organization classification of tumours. Pathology and genetics of tumours of endocrine glands. IARC, Lyon
72. Dominguez-Malagon H, Delgado-Chavez R, Torres-Najera M et al (1989) Oxyphil and squamous variants of medullary thyroid carcinoma. Cancer 63:1183–1188
73. Volante M, La Rosa S, Castellano I et al (2006) Clinicopathological features of a series of 11 oncocytic endocrine tumours of the pancreas. Virchows Arch 448:545–551
74. Moran CA, Suster S (2000) Primary neuroendocrine carcinoma (thymic carcinoid) of the thymus with prominent oncocytic features: a clinicopathologic study of 22 cases. Mod Pathol 13:489–494

75. Baloch ZW, LiVolsi VA (1999) Oncocytic lesions of the neuroendocrine system. Semin Diagn Pathol 16:190–199
76. DeLellis RA (2006) Pathology and genetics of thyroid carcinoma. J Surg Oncol 94:662–669
77. Soares P, Trovisco V, Rocha AS et al (2003) BRAF mutations and RET/PTC rearrangements are alternative events in the etiopathogenesis of PTC. Oncogene 22:4578–4580
78. Castro P, Rebocho AP, Soares RJ et al (2006) PAX8-PPARgamma rearrangement is frequently detected in the follicular variant of papillary thyroid carcinoma. J Clin Endocrinol Metab 91:213–220
79. Trovisco V, Vieira DCI, Soares P et al (2004) BRAF mutations are associated with some histological types of papillary thyroid carcinoma. J Pathol 202:247–251
80. Trovisco V, Soares P, Preto A et al (2005) Type and prevalence of BRAF mutations are closely associated with papillary thyroid carcinoma histotype and patients' age but not with tumour aggressiveness. Virchows Arch 446:589–595
81. Carcangiu ML, Bianchi S, Savino D et al (1991) Follicular Hurthle cell tumors of the thyroid gland. Cancer 68:1944–1953
82. Evans HL, Vassilopoulou-Sellin R (1998) Follicular and Hurthle cell carcinomas of the thyroid: a comparative study. Am J Surg Pathol 22:1512–1520
83. McDonald MP, Sanders LE, Silverman ML et al (1996) Hurthle cell carcinoma of the thyroid gland: prognostic factors and results of surgical treatment. Surgery 120:1000–1004
84. Papotti M, Botto Micca F, Favero A et al (1993) Poorly differentiated thyroid carcinomas with primordial cell component. A group of aggressive lesions sharing insular, trabecular, and solid patterns. Am J Surg Pathol 17:291–301
85. Watson RG, Brennan MD, Goellner JR et al (1984) Invasive Hurthle cell carcinoma of the thyroid: natural history and management. Mayo Clin Proc 59:851–855
86. Lang W, Choritz H, Hundeshagen H (1986) Risk factors in follicular thyroid carcinomas. A retrospective follow-up study covering a 14-year period with emphasis on morphological findings. Am J Surg Pathol 10:246–255
87. Valenta LJ, Michel-Bechet M, Warshaw JB et al (1974) Human thyroid tumors composed of mitochondrion-rich cells: electron microscopic and biochemical findings. J Clin Endocrinol Metab 39:719–733
88. Apel RL, Asa SL (2002) The parathyroid glands. In: LiVolsi V, Asa SL (eds) Endocrine pathology. Churchill Livingstone, Philadelphia, pp 103–137
89. Giorgadze T, Stratton B, Baloch ZW et al (2004) Oncocytic parathyroid adenoma: problem in cytological diagnosis. Diagn Cytopathol 31:276–280
90. Erickson LA, Jin L, Papotti M et al (2002) Oxyphil parathyroid carcinomas: a clinicopathologic and immunohistochemical study of 10 cases. Am J Surg Pathol 26:344–349
91. Yoo GH, Eisele DW, Askin FB et al (1994) Warthin's tumor: a 40-year experience at The Johns Hopkins Hospital. Laryngoscope 104:799–803
92. Honda K, Kashima K, Daa T et al (2000) Clonal analysis of the epithelial component of Warthin's tumor. Hum Pathol 31:1377–1380
93. Kotwall CA (1992) Smoking as an etiologic factor in the development of Warthin's tumor of the parotid gland. Am J Surg 164:646–647
94. Zambrano NR, Lubensky IA, Merino MJ et al (1999) Histopathology and molecular genetics of renal tumors toward unification of a classification system. J Urol 162:1246–1258
95. Kuroda N, Toi M, Hiroi M et al (2003) Review of renal oncocytoma with focus on clinical and pathobiological aspects. Histol Histopathol 18:935–942
96. Maximo V, Soares P, Rocha AS et al (1998) The common deletion of mitochondrial DNA is found in goiters and thyroid tumors with and without oxyphil cell change. Ultrastruct Pathol 22:271–273
97. Maximo V, Sobrinho-Simoes M (2000) Mitochondrial DNA 'common' deletion in Hurthle cell lesions of the thyroid. J Pathol 192:561–562
98. Attardi G, Yoneda M, Chomyn A (1995) Complementation and segregation behavior of disease-causing mitochondrial DNA mutations in cellular model systems. Biochim Biophys Acta 1271:241–248
99. Heddi A, Faure-Vigny H, Wallace DC et al (1996) Coordinate expression of nuclear and mitochondrial genes involved in energy production in carcinoma and oncocytoma. Biochim Biophys Acta 1316:203–209
100. Welter C, Kovacs G, Seitz G et al (1989) Alteration of mitochondrial DNA in human oncocytomas. Genes Chromosomes Cancer 1:79–82
101. Brooks JD, Marshall FF, Isaacs WB et al (1999) Absence of HinfI restriction abnormalities in renal oncocytoma mitochondrial DNA. Mol Urol 3:1–3
102. Simonnet H, Alazard N, Pfeiffer K et al (2002) Low mitochondrial respiratory chain content correlates with tumor aggressiveness in renal cell carcinoma. Carcinogenesis 23:759–768
103. Simonnet H, Demont J, Pfeiffer K et al (2003) Mitochondrial complex I is deficient in renal oncocytomas. Carcinogenesis 24:1461–1466
104. Mayr JA, Meierhofer D, Zimmermann F et al (2008) Loss of complex I due to mitochondrial DNA mutations in renal oncocytoma. Clin Cancer Res 14:2270–2275
105. Savagner F, Chevrollier A, Loiseau D et al (2001) Mitochondrial activity in XTC.UC1 cells derived from thyroid oncocytoma. Thyroid 11:327–333
106. Baris O, Savagner F, Nasser V et al (2004) Transcriptional profiling reveals coordinated up-regulation of oxidative metabolism genes in thyroid oncocytic tumors. J Clin Endocrinol Metab 89:994–1005
107. Jacques C, Baris O, Prunier-Mirebeau D et al (2005) Two-step differential expression analysis reveals a new set of genes involved in thyroid oncocytic tumors. J Clin Endocrinol Metab 90:2314–2320
108. Maximo V, Preto A, Crespo A et al (2004) Core I gene is overexpressed in Hurthle and non-Hurthle cell microfollicular adenomas and follicular carcinomas of the thyroid. BMC Cancer 4:12
109. Sobrinho-Simoes M, Preto A, Rocha AS et al (2005) Molecular pathology of well-differentiated thyroid carcinomas. Virchows Arch 447:787–793
110. Pedersen PL (2007) Warburg, me and Hexokinase 2: multiple discoveries of key molecular events underlying one of cancers' most common phenotypes, the "Warburg effect", i.e., elevated glycolysis in the presence of oxygen. J Bioenerg Biomembr 39:211–222
111. Ko YH, Pedersen PL, Geschwind JF (2001) Glucose catabolism in the rabbit VX2 tumor model for liver cancer: characterization and targeting hexokinase. Cancer Lett 173:83–91
112. Geschwind JF, Ko YH, Torbenson MS et al (2002) Novel therapy for liver cancer: direct intraarterial injection of a potent inhibitor of ATP production. Cancer Res 62:3909–3913
113. Bonnet S, Archer SL, Allalunis-Turner J et al (2007) A mitochondria-K+ channel axis is suppressed in cancer and its normalization promotes apoptosis and inhibits cancer growth. Cancer Cell 11:37–51

114. Warburg O (1956) On respiratory impairment in cancer cells. Science 124:269–270
115. Pouyssegur J, Dayan F, Mazure NM (2006) Hypoxia signalling in cancer and approaches to enforce tumour regression. Nature 441:437–443
116. Bristow RG, Hill RP (2008) Hypoxia and metabolism. Hypoxia, DNA repair and genetic instability. Nat Rev Cancer 8:180–192
117. Higgins DF, Kimura K, Bernhardt WM et al (2007) Hypoxia promotes fibrogenesis in vivo via HIF-1 stimulation of epithelial-to-mesenchymal transition. J Clin Invest 117:3810–3820
118. Yang MH, Wu MZ, Chiou SH et al (2008) Direct regulation of TWIST by HIF-1alpha promotes metastasis. Nat Cell Biol 10:295–305
119. Chiang AC, Massague J (2008) Molecular basis of metastasis. N Engl J Med 359:2814–2823
120. Selak MA, Armour SM, MacKenzie ED et al (2005) Succinate links TCA cycle dysfunction to oncogenesis by inhibiting HIF-alpha prolyl hydroxylase. Cancer Cell 7:77–85
121. MITOMAP (2007) A human mitochondrial genome database www.mitomap.org.

Virchows Arch (2009) 454:497–503
DOI 10.1007/s00428-009-0746-6

ORIGINAL ARTICLE

Unison or cacophony: postgraduate training in pathology in Europe

Fred T. Bosman · Jan G. van den Tweel

Received: 8 February 2009 / Accepted: 10 February 2009 / Published online: 3 March 2009

Abstract With the free movement of people in the European Union, medical mobility has increased significantly. This is notably the case for disciplines for which shortage of well-trained staff has occurred. Pathology is among those specialties and effectively the discipline is confronted with a striking increase in mobility among trainees and qualified specialists. The presumption underlying unlimited mobility is that the competencies of the medical specialists in the European countries are more or less equal, including significant similarities in the postgraduate training programs. In order to assess whether reality corresponds with this presumption, we conducted a survey of the content and practice requirements of the curricula in the EU and affiliated countries. The results indicate a striking heterogeneity in the training program content and practice requirements. To name a few elements: duration of the training program varied between 4 and 6 years; the number of autopsies required varied between none at all and 300; the number of biopsies required varied between none at all and 15,000. We conclude that harmonization of training outcomes in Europe is a goal that needs to be pursued. This will be difficult to reach through harmonization of training programs, as these are co-determined by political, cultural, and administrative factors, difficult to influence. Harmonization might be attained by defining the general and specific competencies at the end of training and subsequent testing them through a test to which all trainees in Europe are subjected.

Keywords Postgraduate education · Europe

F. T. Bosman (✉)
Institut Universitaire de Pathologie,
Centre Hospitalier Universitaire Vaudois,
Rue du Bugnon 25,
1011 Lausanne (CH), Switzerland
e-mail: fred.bosman@chuv.ch

J. G. van den Tweel
Department of Pathology, University of Utrecht Medical Center,
Utrecht, The Netherlands

Introduction

The European Union and its affiliates counts about 30 countries that are all entirely autonomous regarding under- and postgraduate medical education, licensing, specialty diplomas, and CME. In these countries postgraduate training programs for the medical specialties are usually under regulation by government supervised governing bodies, in which (a variety) of medical specialties are represented. Representatives tend to be delegated by a professional society, which typically has created a committee for postgraduate education, in charge of defining program content and monitoring training outcome, the latter often in the format of an examination. The responsible professional societies may be largely practice oriented, or more academically or both. In practice, those who bear academic responsibility for postgraduate education are often not necessarily represented in these governing bodies.

According to EU legislation, any member-country is obliged to recognize the medical certificates of any other member-country as equivalent. This has stimulated reflection as to how to get to an integrated European approach, within the Union Européenne des Médecins Spécialistes (UEMS). The backbone of UEMS are the 37 Specialist Sections and the corresponding European Boards, representing the majority of European specialties. Specialist Sections, including pathology, are composed of two

delegates per member state who represent the national professional organization for medical specialists in a particular specialty. How delegates are appointed varies per country. Sections may admit additional members with specific expertise. For example the Section/Board of Pathology includes representatives of the European Society of Pathology, the European Association of Junior Doctors, the European Federation of Cytological Societies in combination with the International Academy of Cytology, Forensic Pathology and the European Confederation of European Neuropathological Societies (Euro-CNS).

As yet, the Section/Board has made several attempts to harmonize training programs and developed the European Pathology Board Examination, an MCQ test assessing basic knowledge and morphological recognition skills that every practicing pathologist should dispose of. The examination was originally only intended for pathologists certified in one of the EU countries. For several reasons they hardly participate in this examination. As a matter of fact, nearly all participants are non EU (in the 2008 test 32 out of 35) candidates who hope to gain access to pathology practice in an EU member state. This raises the question whether this examination still makes sense as a European test.

How pathology trainees in the EU acquire their knowledge and skills is left entirely up to the specialty boards in the individual member-countries. As evidence-based principles in diagnostic pathology are far from universally applied [1] this potentially constitutes and important risk for heterogeneous pathology practice. The EU has no common definition of basic training requirements nor have common rules for the accreditation of training institutions been developed.

In this structure, primary responsibility for the conception of a European framework for supranational curriculum planning is formally confided to UEMS pathology. In practice, however, UEMS pathology is lacking in executive power. The pathologists representing national governing bodies or professional societies in the UEMS Section and Board are not necessarily those directly responsible for the national training program and do not necessarily have key academic affiliations or responsibilities. Consequently, the Section/Board disposes of little means to impose a supranational vision on national governing bodies, which remain largely autonomous. This complexity, the significant lack of congruence between academic and administrative responsibilities and the prevalence of national regulations over supranational aspirations, has hampered the development of a common blueprint for postgraduate education in pathology.

However, harmonization remains an important goal, as increasing mobility in the pathology field is a reality, given the shortage of pathologists in most European countries. A recent initiative to overcome this problem has been the creation of the European Association of Pathology Chairs and Program Directors (EAPCP), which has brought together those directly responsible for under- and postgraduate pathology education.

Curious as to the real bandwidth of qualifying criteria, against the background of this lack of common ground, we set out to obtain details of the postgraduate training programs in pathology for the member countries and (potentially) affiliated countries of the European Union. A questionnaire was sent to national representatives, for a number of countries several representatives, with the aim to verify if within a single country 'unity of doctrine' exists in reality. This paper reports on the results of this survey and proposes strategies that might be explored in order to attain the necessary harmonization in training outcomes.

Materials and methods

A questionnaire was developed (Table 1) and sent to a representative of each country represented in the European Section/Board of Pathology. In case of non-response, a reminder was sent and for some countries additional contacts were addressed in order to obtain a complete data set. Personal interactions with representatives from most countries clarified open issues and provided additional detail where deemed necessary.

Results

The response rate was high: we obtained an appropriately completed questionnaire from 26 of 30 EU and affiliated countries. In some countries, we received several slightly different responses in view of their decentralized approach to postgraduate training regulation (e.g., in Germany, confided to the 'Länder'). The complete dataset is provided as supplementary information (supplement 1). From eight countries, we obtained the URL of a website where detailed information concerning qualifying requirements and training programs can be obtained. These are likewise contained in the supplementary information.

Program duration, overall structure

The minimum required duration of postgraduate training varies between 4 (eight countries) and 6 (one country) years (Table 2). In most (17) countries the duration is 5 years, but 6 years in one country. In eight countries, clinical training is required (mostly 1 year, but 6 months in one country), which may (for 6-year training programs) or may not (for 4-year training programs) be included in the overall listed duration. Remarkably, the 4-year programs are mostly in the 'new' European member countries.

Table 1 Survey EAPCP

Structure of the postgraduate training program in Pathology in the European countries

1. Is pathology one specialty in your country or are there recognized subspecialties: one ____ several _____
   if subspecialties which: cytopathology
   neuropathology
   molecular pathology
   other

2. How long is postgraduate training in pathology (general anatomic/diagnostic pathology) in your country? 4 ____ 5 ____ 6 ____ 7 ____ years

3. Is a year of clinical training required? yes ____ no ____

4. Has your specialty governing board developed detailed guidelines for specialty training, including learning objectives and practice requirements? yes ____ no ____

   If yes, are these available in English? yes ____ no ____

   Accessible on a Website? yes ____ no ____

   If yes, what is the URL of the site: _____

5. What are the practice requirements
   autopsies how many _____
   are foetal autopsies counted? yes ____ no ____
   cytology how many _____
   biopsies how many _____
   frozen sections how many _____

   Are there set minimum numbers for subspecialty areas? yes ____ no ____
   If yes, please specify: _____

6. For which of the following techniques is hands on experience required in your programme:
   - routine histology _____
   - immunohistochemistry _____
   - morphometry _____
   - in situ hybridization _____
   - molecular biology _____
   - electron microscopy _____

7. Are theoretical courses an important part of your postgraduate programme yes ____ no ____
   If yes, what is the number of course hours required per year? _____
   Can you provide a course programme?

8. Are residents supervised during the entire training period or do they develop an increasing level of autonomy during their residency?
   - supervised all along yes ____ no ____
   - gradual increase in autonomy yes ____ no ____
   - do they independently sign reports yes ____ no ____

9. Are residents required to participate in a research project? yes ____ no ____
   Do they have to publish (a)paper(s) in order to qualify for a specialist diploma? yes ____ no ____

Table 1 (continued)

10. Does your country require a specialty examination? yes ____ no ____

    If yes, how is this composed?
    MCQ theoretical test _____
    Open question test _____
    Slide seminar histology _____
    Slide seminar cytology _____
    Cutting in with histology and writing a full report _____
    Autopsy, including writing a full report _____

11. How are residents selected (match, interview)
    Are residents regularly evaluated, how (specify) _____
    Is there a nationwide regular (for example annual) progress examination (anonymous or nominative)
    Do residents have to participate in quality control surveys
    Do residents perform the histological examinations for all the cases examined macroscopically?
    Are residents required to present cases in clinico-pathological conferences?
    Do residents regularly participate in international courses/conferences?
    Any other comments?

Please provide documentation (in English preferably) whenever available.

In 20 countries, obligatory courses are part of the training program, eight of these without specification of the number of course hours for the total training program. For the other eight, the number of course hours varied between 48 and 300 per year.

With few exceptions, the reaction to the question whether or not the trainee developed a certain level of autonomy during the program was affirmative. Strikingly, however, on the question whether or not the trainee was allowed to sign out cases without supervision, the response was mostly negative: in only eight countries residents are allowed to sign out cases autonomously before final qualification.

Practice requirements

Remarkable heterogeneity characterizes the practice requirements for certification (Table 3). Most countries specify some level of activity for specific fields, although in six countries no numbers are set. This obviously does not imply that a trainee can qualify without having practiced diagnostic pathology; the responsibility for judging an adequate level of proficiency may be ultimately left to the director of the training program and/or the final program examination (Table 4).

For autopsies the required numbers varies between 60 and 300. In most countries fetal autopsies are included in the autopsy count, although for some countries a maximum number of fetal autopsies in the total count has been set. In at least two countries (France and Greece), qualification as specialist pathologist can be obtained (almost) without any autopsy practice. For biopsies the required number varies between 600 and 15,000. In two countries (Switzerland and Lithuania) the number of biopsies within subspecialty fields is defined. For cytology the numbers required varies between 500 and 10,000. In several countries a specified

Table 2 Program duration and overall structure

	Number of countries
Duration of training	
4 year	8
5 year	17
6 year	1
Clinical year required	
Yes	8 (one 6 months)
No	18
Development of autonomy	
Yes	22
No or ?	4
Independent sign out before graduation	
Yes	8
No or ?	18
Obligatory courses	
Yes	18
No or ?	8

Table 3 Practice requirements

	Number of countries
Autopsies	
None specified	4
<100	1
100–200	19
>200	2
Biopsies	
None specified	6
<3,000	3
3,000–10,000	13
>10,000	2
Frozen sections	
None specified	16
<100	2
>100	5
Cytology	
None specified	6
<3,000	7
>3,000	11
Technical competencies	
Histology	12
Immunohistochemistry	10
Electron microscopy	7
Morphometry	5
Molecular pathology	3
FISH	1

number has been set for gynecological and non-gynecological cytology.

In most countries with explicit practice requirements, no numbers have been set for frozen section diagnosis. Effectively, in several countries frozen sections are not performed by trainees but only by qualified pathologists. In countries with specified numbers, these vary between 50 and 500.

Exposure to laboratory methods in pathology

The questionnaire specified 'hands on' experience in laboratory methods. What exactly this implies is difficult to grasp from the survey documents. It can be assumed that in case of an affirmative answer at least some personal practice in the specific laboratory method is required. Many countries (14) require some practice in histological techniques and about the same proportion in immunohistochemistry (12). The number of countries requiring experience in electron microscopy (seven) or morphometry (five) is lower. Of note is that experience in molecular pathology is required in only five countries and in fluorescent in situ hybridization (FISH) in only 3.

Examination

The majority of the countries have over time adopted an examination system for quality control towards the end of the training period (Table 4). Nonetheless, in six countries, no central examination system exists and the director of the training program bears full responsibility for the certification of the candidate. In many countries the examination has a strong practice-oriented content. This might imply some form of testing of macroscopical examination skills and specimen sampling, included in nine countries. Reporting an autopsy, based upon a combination of examination of macroscopical specimens and the accompanying histology is included in 11 countries. Cytology slides and histology slides are almost invariably included in the examination (16 and 18, respectively; 14 out of 20 examining countries). Knowledge is tested through multiple choice questions in eight countries and through open questions in 13. Oral examinations were explicitly stated by two countries, although in reality this figure is probably higher as most practice-oriented examination parts tend to be conducted through direct interaction between an examiner and the candidate, which can be considered as a form of an oral examination.

Table 4 Final examination

	Number of countries	Type of examination	Number of countries
Without final examination	6		
With final examination	20	MCQ	8
		Open questions	13
		Of which oral	2
		Cutting in	9
		Histology	18
		Cytology	16
		Autopsy	11
With intermediate progress examinations	4 (of which 1 anonymous)		

In only four countries, intermediate 'progress' tests are organized, one of which anonymous underlining its formative character.

Research, selection, international exchange, and cpc participation

Research is not universally considered a priority: in only nine countries active participation in a research project is required and in only four countries a published paper is required in order to qualify as a specialist.

Selection of trainees is very different between the different countries. The extremes are, on the one end of the spectrum, the countries where freshly graduated physicians have to sit a national ranking test. Ranking according to the score determines access to specialty training: the higher the ranking, the more options are open. In this system, usually the trainees are assigned to a program and the director of the program has limited influence on the choice of candidate trainees. On the other end of the spectrum, fresh graduates apply for open trainee positions and the decision as to who to enlist is entirely taken by the director of the program. We do consider how graduates are selected for a training program an important issue. It is highly likely that the evolution of a training program is at least in part determined by the composition of the trainee group and therefore the selection process might have significant impact on the outcome of training.

International exchange seems not to be a priority, although many countries do promote and support participation in international courses. Most countries (20) advocate active participation of trainees in clinicopathological conferences, usually with the responsibility to present and discuss cases.

A final question was whether or not trainees perform microscopical examinations of all the cases for which they had assumed the macroscopical examination. The importance of the question is the tendency in some departments to use residents as an easy labor force for tasks regarded as less qualified, but that do not necessarily provide added value to the training program. In nine countries, residents routinely perform macroscopical examination of specimens which they do not see again for microscopical examination and of which they do not edit the report.

Discussion

Harmonization of pathology training has for nearly 20 years been the main aim of the Specialist Section/Board of Pathology of the UEMS. Despite the fact that the members of this body repeatedly agreed upon a common training and testing program, and were willing to support this in their national bodies, the proposed measures did not result in the intended harmonization and implementation of these initiatives in the national programs largely failed. In the meantime, in the EU the reciprocal recognition of certificates has resulted in a significant movement of European doctors, among whom many were pathologists, and the need for new initiatives to achieve the harmonization goal have become more and more evident [2]. We felt that detailed insight in the present training situation would allow us to develop more balanced efforts and better targeted actions. So what does the survey tell us?

First of all, heterogeneity in the training programs is striking. For none of the investigated items any sign of effective harmonization was perceived. The differences in training duration, training content, responsibilities of the trainees, research experience, and testing and examination appear to be enormous. It is evident that none of the well-intended initiatives in the past has resulted in any improvement of the existing diversity. The reasons for this failure lie primarily in the decentralized responsibility for postgraduate training and specialist certification: entirely at a national level. Most countries (understandingly) want to stick to their own concept of a program, which in their judgment has functioned well for decades. A striking conclusion is that some pathologists trained in Europe cannot assure adequate autopsy practice. This calls for explicit measures, as has been proposed for example in the form of a distinct subspecialty for autopsy pathology [3].

Secondly, pathology curricula in the European countries are still largely oriented towards classical pathology practice. The amount of exposure to new methods in diagnostic pathology (notably molecular pathology) is very limited and that in an era full of new challenges and plenty more to come in the 30 or so years that the average trainee will practice the discipline. Training programs ideally should continuously identify new needs and develop effective approaches towards responding efficiently to new requirements [4, 5]. A more balanced mixture of formal teaching and the prototypical 'learning by doing' might need to be considered [6].

Thirdly, validation of training outcome is very heterogeneous. National exams, which are not even universally applied as a measure of quality control of training outcome, are very different in structure and content. This might be one reason why the gradual increase in autonomy, proclaimed by most countries, has not resulted in much functional autonomy: rare are the training programs allowing advanced trainees to sign out cases independently, the ultimate reflection of autonomy. Longitudinal case-based evaluation [7] might provide a formal basis for allowing an advanced resident to gain professional independence. A European approach towards pathology training outcome validation might also facilitate transatlantic competence recognition, as has been called for in this era of globalization [8].

We must conclude that harmonization of training programs is an illusion and should no longer be pursued. Moreover it is not the program, but the outcome that counts. Since the practice of pathology is relatively uniform in Europe (and around the world) a much more pragmatic and realistic approach would be to agree upon the competencies at the end of training and to develop tools to measure competencies all along the training period, as has been implemented elsewhere [7, 9–11]. The Resident in Service Examination, a similar approach, is now implemented in 100% of the training programs in the United States [12]. Following such approaches the profile of the European pathologist has been conceived by the EAPCP and tools to monitor training outcomes, aiming at the European profile, are in full swing development. The main tool for monitoring of training outcome will consist of a formative progress test that is histo- and cytopathology practice-oriented, deployed through the internet as was already advocated long ago [13], can be used by the residents on a voluntary and anonymous basis for self-evaluation, and by institutions for comparing overall outcome of their program with that of others. Moreover, such a test can also be used by practicing pathologists to compare their knowledge with that of their peers.

What to do? Sensing the need to face these challenges the EAPCP was created with as primary aim to mount a European network of professionals responsible for the quality and the execution of the pathology training program in their institutes. The survey this paper is based upon is one of the initiatives taken by the EAPCP. The results obtained have helped the EAPCP in developing a description of the profile of the European pathologist at the end of her/his training, in terms of general and specific learning objectives. The document includes general guidelines as to how to develop these outcome parameters into a curriculum and how to evaluate in a structured way the progress of the trainee all along the training period and provides the basis for a European progress test, which will allow trainees to self-evaluate and training bodies all over Europe to compare training outcomes. As the UEMS Section/Board of Pathology remains an important professional-political platform to consolidate such initiatives and increase their impact, the EAPCP needs to collaborate with it and in fact the UEMS Section/Board of Pathology has agreed to collaborate. This will assure proper input from the relevant stakeholders and allow adequate representation of the interests of pathology as a medical discipline. The EAPCP might eventually act as a bridge between the bodies that determine the fate of pathology in Europe: the European Society of Pathology providing scientific and educational input with its annual congresses and postgraduate education programs, the UEMS Section/Board of Pathology providing professional and political input at a European level and the national pathology organizations, powerful third party in this complex process.

Acknowledgements The authors wish to thank the representatives of the national postgraduate pathology training bodies for their help in collecting the data.

Conflicts of Interest None.

References

1. Wick MR, Bourne TD, Patterson JW et al (2005) Evidence-based principles and practices in pathology: selected problem areas. Semin Diagn Pathol 22:116–125
2. Ruiter DJ, Roald B, Underwood J, Prat J, UEMS Section of Pathology/European Board of Pathology (2004) Histopathology training in Europe: a lesson for other specialties? Virchows Arch 444:278–282
3. Van den Tweel JG (2008) Autopsy pathology should become a recognised subspecialty. Virchows Arch 452:585–587
4. Saikia B, Gupta K, Saikia UN (2008) The modern histopathologist: in the changing face of time. Diagn Pathol. 3:25–28
5. Marchevsky AM, Wick MR (2004) Evidence-based medicine, medical decision analysis, and pathology. Hum Pathol 35:1179–1188
6. Gallagher PJ, Dixon MF, Heard S, Moore JK, West KP (2003) An initiative to reform senior house officer training in histopathology. Hosp Med. 64:302–305
7. Ducatman BS, Ducatman AM (2006) Longitudinal case-based evaluation of diagnostic competency among pathology residents: a statistical approach. Arch Pathol Lab Med 130:188–193
8. Van Den Tweel J, Taylor CR (2002) Globalization of pathology training and examination: the time to begin is now. Hum Pathol 33:861–862
9. Lockard WT Jr, Lunz ME, Burke MD et al (1989) The first six years' experience with the pathology residents' in-service examination, 1983–1988. Am J Clin Pathol 92(4 Suppl 1):S11–S22
10. Association of Directors of Anatomic, Surgical Pathology (2003) Curriculum content and evaluation of resident competency in anatomic pathology: a proposal. Hum Pathol 34:1083–1090
11. Wick MR (2003) Curricula for pathology training: an editorial comment. Hum Pathol 34:1091
12. Alexander CB (2006) Pathology graduate medical education (overview from 1926 to 2005). Hum Pathol 37:923–928
13. Hamza S, Anderson P, Reddy VV et al (2001) Use of the Internet in pathology resident training and education. Adv Anat Pathol 8:290–297

Virchows Arch (2009) 454:505–511
DOI 10.1007/s00428-009-0763-5

ORIGINAL ARTICLE

Histopathology report of cutaneous melanoma and sentinel lymph node in Europe: a web-based survey by the Dermatopathology Working Group of the European Society of Pathology

Anna Batistatou · Martin G. Cook · Daniela Massi · On behalf of the ESP Dermatopathology Working Group

Received: 11 December 2008 / Revised: 14 March 2009 / Accepted: 17 March 2009 / Published online: 8 April 2009

Abstract In order to survey the diagnostic reporting of melanomas by European pathologists and assess their current practice and opinions on the information required in the final report, a web-based questionnaire was diffused through the members of the Dermatopathology Working Group of the European Society of Pathology. Forty replies from different pathology laboratories were collected (49%). Main prognostic parameters related to the primary tumor, including Breslow thickness, presence of ulceration, and Clark's level, as well as additional features, are reported by a large majority of laboratories. Presence of regression is reported by 90% of respondents but with different recording items. For sentinel lymph node (SLN) biopsy for melanoma, the conventional panel of antibodies includes S-100, Melan A, and HMB45. Dissection of the SLN is performed by "bivalve" or "bread loaf" approach. The number of sections cut and stained varies. Forty-four percent of respondents report depths of metastases from the capsule, while the majority report maximum dimension of the largest deposit. Results indicate that pathology reports for primary cutaneous melanoma and SLN vary between laboratories across Europe. Although the most important prognostic features are universally reported, key features which impact on prognosis and treatment are often omitted and others still require standardization.

Keywords Melanoma · Histopathology report

A. Batistatou (✉)
Department of Pathology, University of Ioannina,
Medical School, University Campus,
P.O. Box 1186, 451 10 Ioannina, Greece
e-mail: abatista@cc.uoi.gr

M. G. Cook
Department of Histopathology,
Royal Surrey County Hospital and University of Surrey,
Guildford, UK

D. Massi
Department of Human Pathology and Oncology,
University of Florence,
Florence, Italy

Introduction

Melanoma is the major cause of skin cancer mortality, with its incidence rising worldwide [1,2]. The progress in public education has made the early detection of the disease possible, so pathologists today are dealing with an increasing load of skin biopsies with melanoma. Since many specialties are involved in the management of melanoma, integral components of high-quality care of melanoma patients are effective communication of appropriate information. When dealing with a melanoma, an accurate histological diagnosis is only the first step towards a rational and effective treatment. Besides diagnosis, several histopathological parameters constitute accepted prognostic factors and should also be included in the final pathology report [3–9]. Features not currently included in the latest editions of the American Joint Committee on Cancer (AJCC) and the International Union Against Cancer staging manuals might be also important [5,8,10].

In many pathology laboratories, standardized synoptic reports for melanoma have been formulated, so that key elements of the histological assessment are not overlooked

and clear communication with the clinician is achieved. Following such a proforma could assist the pathologist to provide all the information that is relevant and important for the clinical approach to the patient. A report could be also used as a means of education of pathologists, in order to pay attention to clinically important features. It is beyond doubt that pathologists who sign the report have the responsibility for the communicated information and that practices vary due to personal beliefs and demands by the referring clinician and institutional policies. Therefore, pathology reports for primary cutaneous melanoma vary between laboratories in Europe.

The aim of the present study is to record these differences, as well as to assess the beliefs of pathologists as to what is the essential information that should be included in the final pathology report for cutaneous melanoma.

Material and methods

In order to survey the European pathologists who diagnose melanomas, assess their current practice, and record their opinions on the essential information to be included in the final pathology report, a 50-point questionnaire was prepared ("Appendix"). This was sent to all 81 current members of the European Society of Pathology Dermatopathology Working Group, by e-mail or by regular mail, if the former was not available.

The questions were related to six areas:

1. Details of respondents with respect to country and practice (specialized melanoma and/or active sentinel lymph node surgical unit or not, number of melanomas diagnosed per year)
2. Pathologists' practice regarding standardized pathologist report and reporting of accepted prognostic factors
3. Pathologists' opinions regarding standardized pathology report and accepted prognostic factors
4. Pathologists' practice and opinions regarding parameters not included in the AJCC 2002
5. Pathologists' practice and beliefs regarding sentinel lymph node (SLN).
6. Free text comments and opinions were sought regarding other features that should be included in the final pathology report for melanoma

Results

Respondents

In total, 40 replies were received (49%). The response rate is attributed in part to the fact that occasionally pathologists from the same laboratory completed only one questionnaire. The preliminary results from this survey were presented during the 21st European Congress of Pathology in Istanbul, Turkey, on September 2007. Respondents who reported their opinion and practice were based in the following European Countries: Croatia, Czech Republic, Finland, France, Germany, Greece, Italy, Netherlands, Portugal, Romania, Serbia, Slovenia, Spain, Switzerland, and UK. In addition, a few respondents/members were located in countries outside Europe at the time of the questionnaire: Canada, Israel, Turkey, and USA. Regarding activity, 18/40 (~32%) respondents work at units/hospitals diagnosing <50 cutaneous melanomas per year; 11/40 (~28%) diagnose 50–100 melanomas per year; ten of 40 (~25%) diagnose 100–300 melanomas per year and six of 40 (15%) diagnose >300 melanomas per year. Fifty-eight percent (23/40) of respondents regularly assess SLN for melanoma metastases. Fifteen percent (six of 40) does not assess SLN at all and has not answered the relevant questions.

Pathology report, relevant histopathological parameters

Forty-five percent of respondents (18/40) do not use a standardized pathology report, but only 18% (7/40) thinks that a standardized pathology report is not necessary (Table 1). The anatomic site is reported by 68% (27/40) of respondents and some propose to include it in the clinical data. The histological subtype is reported by 90% (36/40) of respondents. It is pointed by respondents that the histological subtype is of debatable/uncertain/limited importance and that originally described histotypes do not reflect the morphological profile of currently diagnosed melanomas. Twenty-eight percent (11/40) of respondents do not include the growth phase in the pathology report. All respondents report Breslow thickness. It is usually measured with an ocular micrometer and less often by computer-assisted methods (8%, three of 40). All but two respondents (38/40) believe that the Clark level of invasion should be reported. All but one respondent (39/40) believe that ulceration should be included in the final pathology report and reports it. However, there is disagreement on the report of the extent of ulceration since the majority (60%, 24/40) does not report it. Those who report the extent of ulceration follow variable methods for its estimation. They estimate it in millimeter or as a percentage or they categorize it as focal–extensive or superficial–deep. Many respondents (72%, 29/40) include the predominant cell type in their report, while 35% (14/40) believes that it should not be included. The dermal mitotic rate is reported by 80% (32/40) of respondents. Methods of assessing and reporting vary: some count mitoses and report them as number per square millimeter or per high-power fields (HPF) or per

Table 1 Summarized results of the survey

Question number	Yes	No
5	55% (22/40)	45% (18/40)
6	82% (33/40)	18% (7/40)
7	68% (27/40)	32% (13/40)
8	90% (36/40)	10% (4/40)
9	90% (36/40)	10% (4/40)
10	85% (34/40)	15% (6/40)
11	72% (29/40)	28% (11/40)
12	78% (31/40)	22% (9/40)
13	100% (40/40)	0% (0/40)
14	100% (40/40)	0% (0/40)
16	95% (38/40)	5% (2/40)
17	95% (38/40)	5% (2/40)
18	97% (39/40)	3% (1/40)
19	97% (39/40)	3% (1/40)
20	40% (16/40)	60% (24/40)
21	45% (18/40)	55% (22/40)
22	72% (29/40)	28% (11/40)
23	65% (26/40)	35% (14/40)
24	80% (32/40)	20% (8/40)
25	72% (29/40)	28% (11/40)
26	100% (40/40)	0% (0/40)
27	92% (37/40)	8% (3/40)
28	100% (40/40)	0% (0/40)
29	92% (37/40)	8% (3/40)
30	78% (31/40)	22% (9/40)
31	72% (29/40)	28% (11/40)
32	90% (36/40)	10% (4/40)
33	90% (36/40)	10% (4/40)
34	100% (40/40)	0% (0/40)
35	95% (38/40)	5% (2/40)
36	100% (40/40)	0% (0/40)
37	97% (39/40)	3% (1/40)
38	87% (35/40)	13% (5/40)
39	85% (34/40)	15% (6/40)
41	58% (23/40)	42% (17/40)
42	88% (30/34)	12% (4/34)
47	44% (15/34)	56% (19/34)
48	68% (23/34)	32% (11/34)
49	71% (24/34)	29% (10/34)
50	97% (33/34)	3% (1/34)

5HPF; others initially screen for hot spots at ×10 and then use rougher estimates (high, moderate, low mitotic activity). Vascular or lymphatic invasion is reported, if present, by all respondents, usually without differentiation between lymphatic or vascular (95%). Only two of 40 (5%) use immunohistochemistry in order to identify the vessel type (CD34, D2-40). Perineural invasion is reported if present. The presence of tumor-infiltrating lymphocytes (TILs) is usually included (78%, 31/40) in the pathology report and graded as brisk, nonbrisk, and absent. Most respondents do not attempt immunosubtyping, while others do (5%) and report the subpopulations identified. Regression is usually reported (90%, 36/40). There is great variation on the mode of reporting: present/absent, absent/scarce/moderate/severe, present/partial/complete, in millimeter, or as a percentage. The presence of associated nevus and satellite lesions is reported if they are present. Thirteen percent (five of 40) does not report the distance from the nearest margins. The summarized results of this survey are presented in Table 1. Other features that respondents have proposed that could be included in the pathology report are: the presence of second cell-type component, the percentage of MIB-1-positive neoplastic cells, the density of pigmentation, the presence of necrosis, the presence of sun damage in surrounding skin, an estimate of metastatic potential, the immunohistochemical expression of p16 and β-catenin, results of other immunostaining if it is done, the presence of adnexal infiltration, the names of second opinions when done, as well as the pathological staging (T, TNM).

Sentinel lymph node biopsy for melanoma

Immunohistochemistry is usually used as an additional aid in identifying metastases (Table 1). The conventional panel of antibodies included S-100 (74%), Melan A (65%), and HMB45 (62%). Some respondents use additional markers, i.e., CD68, antityrosine, microphthalmia transcription factor, and melanoma cocktail. There is discrepancy on the dissection procedure of the SLN. Most respondents "bivalve" it (48%); others "bread loaf" it (42%), while 10% takes random sections.

The number of sections cut and stained also varies as follows: 9% takes only one section; 47% takes one to five sections; 29% takes five to ten and 15% examines ten to 20 sections. The cutting of sections is done sequentially by 33% and at steps by 66% of respondents. Forty-four percent (15/34) of respondents report on the depths of the metastases from the capsule, while 68% (23/34) reports of the maximum dimension of the largest deposit. All but one report on the presence of nevus cells within SLN.

Discussion

While there is considerable published information on the features of melanoma that are important for its progression and clinical management, there is very little information about the current practice of reporting melanoma in Europe [1,11,12]. This is the first comprehensive assessment on

European pathologists' views and practice and demonstrates the lack of consensus on several important issues.

Of the most important microscopic features, there is agreement on the measurement and reporting of Breslow thickness, which is the strongest prognostic index for melanoma [13]. In fact, the T attribute of the TNM staging system is primarily defined by the thickness of the melanoma, measured at a right angle to the adjacent normal skin, from the top of the granular layer of the overlying skin epidermis (or the base of the ulcer, if the lesion is ulcerated) to the deepest invading melanoma cell. In the 2002 AJCC staging system, it is grouped in 1-mm intervals.

The Clark level of invasion is believed by many respondents to be important for reporting, even if only for historical reasons, since, as some point out, it is less important than thickness [14,15]. Increasing levels of invasion correlate with a decrease in survival, although this feature has most value if analyzed as a single variable and not as part of a multivariate analysis [9].

Ulceration is based on microscopic examination and is defined in the literature proposed by the AJCC as the absence of intact epidermis over any part of the primary melanoma. Its presence is regarded as an indicator of biological aggressiveness. Ulceration is a dominant prognostic factor in cutaneous melanoma without metastasis and a significant stage-modifying factor in the 2002 AJCC classification [6,16]. There is positive correlation between ulceration and melanoma thickness. Pathologists have understood the significance of ulceration, but, as shown in our survey, there is considerable discrepancy on the mode of measuring and reporting it [17,18]. It has been reported that the disagreement between pathologists on reporting ulceration can be significantly lowered if a more precise definition of ulceration is used, i.e., full-thickness epidermal defect, evidence of host response and thinning, and effacement or reactive hyperplasia of the surrounding dermis [18].

Recognition and definition of the growth phase of melanoma is important for understanding the multistep model (Clark model) of melanoma progression [11]. Furthermore, vertical growth phase is an adverse prognostic factor. However, in our survey, growth phase is not reported by approximately one third of pathologists. The histological subtype is often reported although its prognostic significance is uncertain and less important than the growth patterns and depth of invasion [19–22]. Furthermore, it is known in clinical practice that several cases do not fit well in any certain category, creating the need for new candidate entities.

The dermal mitotic rate is not currently included in the accepted prognostic parameters and the 2002 AJCC classification; however, it is believed to be of high prognostic value and is important particularly in thin melanomas [23–25]. A recent study on thin cutaneous melanoma ($\leq$ 1 mm) has identified level, tumor cell mitotic rate, and sex as additional prognostic factors and suggested that tumor cell mitotic rate should be incorporated into the next iteration of AJCC staging [26]. The majority of respondents report the mitotic rate in invasive melanomas; however, there is discrepancy in the mode of reporting. Based on published studies, the most desirable mode of reporting mitoses is in terms of number of mitoses per square millimeter.

The presence of regression in primary melanomas is a well-known phenomenon, but its prognostic significance has been disputed [27–31]. Some investigators consider regression as an indicator of poor prognosis, particularly in thin melanomas, while more recent reports have shown that regression is actually a favorable process, especially in thin melanomas [31]. Respondents are obviously aware of the significance of regression since the vast majority includes its presence in the final report. However, the unfamiliarity of observers with the pathological features of regression is reflected in the variability of reporting its extent. This is possibly due to the variable microscopic features in various stages of regression. A prominent mononuclear infiltrate is followed by destruction of melanoma cells and the appearance of melanophages, fibrosis, and vascular changes. A staging scheme has been recently proposed, with stage 1 including cases with loss of part of the dermal component, stage 2 including cases with complete loss of the dermal and retaining of the junctional component, and stage 3 including cases with loss of both dermal and junctional components in the involved segment of melanoma [31].

The host immune responses are important for melanoma, but they are difficult to evaluate and standardize. The presence of TILs is of debatable/doubtful value until redefined, but pathologists generally report them [32,33].

The presence of vascular or lymphatic invasion does not affect the T category but is reported [34,35]. Furthermore, vascular invasion may be difficult to identify with the routine hematoxylin–eosin stain, requiring aid by immunohistochemistry. The presence of perineural invasion is reported if present since it may correlate with increased risk for local recurrence.

Sentinel lymph node biopsy is a widely accepted indicator of patient prognosis and has been established as an important factor in clinical management of melanoma patients [36–39]. Regarding SLN, an encouraging result from this survey is that standardized gross and microscopic assessment is followed [37,38]. Most pathologists follow accepted protocols for dissection and microscopic examination [38]. Further microscopic features, such as the microanatomic location and the size of the metastases, are reported, and this practice indicates that respondents

understand the importance of prediction of nonsentinel lymph node involvement.

In conclusion, the evidence gathered and presented herein supports the notion that pathologist members of the European Society of Pathology who report cutaneous melanomas mostly follow common practices, although with individualization. There is some controversy about the features that are essential and those that are desirable; however, overall, the most important features are reported. However, passive distribution of practice guidelines seems to be insufficient to accomplish community-wide quality improvement in melanoma pathology reporting.

The next step for achieving the best clinical practice would be the development of Europe-wide guidelines for the optimal pathology report of melanoma. Currently formulated pathology reports are followed locally or nationally in some countries. The goal is to achieve, through active communication between all members of the Dermatopathology Working Group of the European Society of Pathology, a consensus statement on an acceptable and adequate pathology report to be used in all Europe.

Conflict of interest statement We declare that we have no conflict of interest.

Appendix: Questionnaire

1. In which country is your pathology laboratory?
2. Are you working in a specialized Melanoma Unit?
3. Do you have an active sentinel lymph node Surgical Unit in your hospital?
4. How many primary cutaneous melanomas do you diagnose per year?
5. Do you use a standardized pathology report for melanoma?
6. Do you think that a standardized pathology report for melanoma is necessary?
7. In your final pathology report for melanoma, is the anatomic site included?
8. Do you think that the anatomic site should be included in the final pathology report for melanoma?
9. In your final pathology report for melanoma, is the histological subtype included?
10. Do you think that the histological subtype should be included in the final pathology report for melanoma?
11. In your final pathology report for melanoma, is growth phase included?
12. Do you think that the growth phase should be included in the final pathology report for melanoma?
13. In your final pathology report for melanoma, is the Breslow thickness included?
14. Do you think that the Breslow thickness should be included in the final Pathology report for melanoma?
15. For measuring Breslow thickness, do you use an ocular micrometer or other tools?
16. In your final pathology report for melanoma, is the Clark level of invasion included?
17. Do you think that the Clark level of invasion should be included in the final pathology report for melanoma?
18. In your final pathology report for melanoma, is the presence of ulceration included?
19. Do you think that the presence of ulceration should be included in the final pathology report for melanoma?
20. In your final pathology report for melanoma, is the extent of ulceration included?

Comment: If the answer is YES, please specify how do you measure and how do you report the extent of ulceration (in millimeter, as a percentage of the melanoma surface, etc.)

21. Do you think that the extent of ulceration should be included in the final pathology report for melanoma?
22. In your final pathology report for melanoma, is the predominant cell type included?
23. Do you think that the predominant cell type should be included in the final pathology report for melanoma?
24. In your final pathology report for melanoma, is the dermal mitotic rate included?

Comment: If the answer is YES, please specify how do you measure and how do you report the mitotic rate (per square millimeter, high–low, etc.)

25. Do you think that the dermal mitotic rate should be included in the final pathology report for melanoma?
26. In your final pathology report for melanoma, is the vascular or lymphatic invasion included?

Comment: If the answer is YES, please specify if you try to separate between blood or lymphatic vascular invasion and how.

27. Do you think that the vascular or lymphatic invasion should be included in the final pathology report for melanoma?
28. In your final pathology report for melanoma, is the perineural invasion included?
29. Do you think that the perineural invasion should be included in the final pathology report for melanoma?
30. In your final pathology report for melanoma, is the presence of tumor-infiltrating lymphocytes (TILs) included?

Comment: If the answer is YES, please specify how do you report it (e.g., brisk–nonbrisk–absent) and if you try to separate the subpopulations (e.g., with immunohistochemistry).

31. Do you think that the presence of tumor-infiltrating lymphocytes (TILs) should be included in the final pathology report for melanoma?
32. In your final pathology report for melanoma, is the regression included?

Comment: If the answer is YES, please specify how do you measure and how do you report the extent of regression (in millimeter, as a percentage of the tumor, etc.)

33. Do you think that regression should be included in the final pathology report for melanoma?
34. In your final pathology report for melanoma, is the presence of associated nevus included?
35. Do you think that the presence of associated nevus should be included in the final pathology report for melanoma?
36. In your final pathology report for melanoma, is the presence of satellite lesions included?
37. Do you think that the presence of satellite lesions should be included in the final pathology report for melanoma?
38. In your final pathology report for melanoma, is the distance from the nearest lateral and deep margins included?
39. Do you think that the distance from the nearest lateral and deep margins should be included in the final pathology report for melanoma?
40. What other features do you think that should be included in the final pathology report for primary cutaneous melanoma?
41. Do you regularly assess SLN for melanoma metastases?
42. Do you use immunohistochemistry to help identify metastases?
43. If yes, which antibodies do you use?
44. How do you dissect the lymph node?
    a. "Bread loaf"
    b. "Bivalve"
    c. Random
45. How many sections do you request to be cut and stained?

(a) 1
(b) 1–5
(c) 5–10
(d) 10–20

46. If more than 1, are they:

(a) Sequential
(b) At steps

47. Do you measure and report the depths of the metastases from the capsule?
48. Do you measure and report the maximum dimension of the largest deposit?
49. Do you report the site of the metastasis within the SLN?

(e.g., subcapsular, subcapsular and parenchymal, parenchymal only, multifocal, extensive)

50. Do you report the presence of nevus cells within SLN?

References

1. Thompson JF, Scolyer RA, Kefford RF (2005) Cutaneous melanoma. Lancet 365:687–701
2. Tsao H, Atkins MB, Sober AJ (2004) Management of cutaneous melanoma. N Engl J Med 351:998–1012
3. Newton Bishop JA, Corrie PG, Gore ME et al (2002) UK guidelines for the management of cutaneous melanoma. Br J Plast Surgery 55:46–54
4. Cochran AJ, Bailly C, Cook MG et al (1997) Recommendations on the reporting of tissues removed as part of the surgical treatment of cutaneous melanomas. Virchows Arch 431:79–81
5. Clark WH Jr, Elder DE, IV GD et al (1989) Model predicting survival in stage I melanoma based on tumour progression. J Natl Cancer Inst 81:1893–1904
6. Balch CM, Buzaid AC, Soong SJ et al (2001) Final version of the American Joint Committee on cancer staging system for cutaneous melanoma. J Clin Oncol 19:3635–3648
7. Balch CM, Soong SJ, Atkins MB et al (2004) An evidence based staging system for cutaneous melanoma. CA Cancer J Clin 54:131–149
8. Association of Directors of Anatomic and Surgical Pathology (1998) Recommendations for the reporting of tissues removed as part of the surgical treatment of cutaneous melanoma. Pathol Int 48:168–170
9. Calonje E (2000) Best practice no 162 The histological reporting of melanoma. J Clin Pathol 53:587–590
10. Cook MG, Clarke TJ, Humphreys S et al (1997) A nationwide study of observer variation in the diagnosis of thick cutaneous malignant melanoma including the MIN terminology. J Clin Pathol 50:202–203
11. Miller AJ, Mihm MC Jr (2006) Melanoma. N Engl J Med 355:51–65
12. Cook MG, Clarke TJ, Mumphreys S et al (1996) The evaluation of diagnostic and prognostic criteria and the terminology of thin cutaneous malignant melanoma by the CRC Melanoma Pathology panel. Histopathology 28:497–512
13. Breslow A (1980) Prognosis in cutaneous melanoma: tumour thickness as a guide to treatment. Pathol Ann 15:1022
14. Clark WH Jr, From L, Bernardino EA et al (1969) The histogenesis and biological behavior of primary human malignant melanomas of the skin. Cancer Res 29:705–727
15. Matghoob AA, Koenig K, Bittercourt FV et al (2000) Breslow thickness and Clark level in melanoma support for including level in pathology report and in the American Joint Committee on Cancer Staging. Cancer 88:589–585
16. Balch CM, Soong SJ, Gershenwald JE et al (2001) Prognostic factors analysis of 17,600 melanoma patients: validation of the American Joint Committee on Cancer Melanoma Staging System. J Clin Oncol 19:3635–3648
17. Balch CM, Wilkerson JA, Murad TM et al (1980) The prognostic significance of ulceration of cutaneous melanoma. Cancer 45:3012–3017

18. Spatz A, Cook MG, Elder DE et al (2003) Interobserver reproducibility of ulceration assessment in primary cutaneous melanomas. Eur J Cancer 39:1861–1865
19. McGovern VJ (1970) The classification of melanoma and its relationship with prognosis. Pathology 2:85–98
20. Barnhill RL, Mihm MC Jr (1993) The histopathology of cutaneous malignant melanoma. Semin Diagn Pathol 10:47–75
21. Forman SB, Ferringer TC, Peckham SJ et al (2008) Is superficial spreading melanoma still the most common form of malignant melanoma? J Am Acad Dermatol 58:1013–1020
22. Banerjee SS, Harris M (2000) Morphological and immunophenotypic variations in malignant melanoma. Histopathology 36:387–402
23. Azzola MF, Shaw HM, Thompson JF et al (2003) Tumour mitotic rate is a more powerful prognostic indicator than ulceration in patients with primary cutaneous melanoma. Cancer 97:1488–1498
24. Francken AB, Shaw HM, Thompson JF et al (2004) The prognostic importance of tumor mitotic rate confirmed in 1317 patients with primary cutaneous melanoma and long follow-up. Ann Surg Oncol 11:426–433
25. Gimotty PA, Guerry D, Ming ME et al (2004) Thin primary cutaneous malignant melanoma: a prognostic tree for 10-year metastasis is more accurate than American Joint Committee on Cancer Staging. J Clin Oncol 22:3668–3676
26. Gimotty PA, Elder DE, Fraker DL et al (2007) Identification of high-risk patients among those diagnosed with thin cutaneous melanomas. J Clin Oncol 25:1129–1134
27. Cook MG (1992) The significance of inflammation and regression in melanoma. Virchows Archiv A Pathol Anat 420:113–115
28. Gromet MA, Epstein WL, Blois MS (1978) The regressing thin malignant melanoma. Cancer 42:2282–2292
29. Kelly JW, Sagebie RW, Blois MS (1985) Regression in malignant melanoma. Cancer 56:2287–2291
30. Cook MG, Spatz A, Brocker EB et al (2002) Identification of histological features associated with metastatic potential in thin (<1.0 mm) cutaneous melanoma with metastases. A study on behalf of EORTC melanoma group. J Pathol 197:183–193
31. Kaur C, Thomas RJ, Desai MA et al (2008) The correlation of regression in primary melanoma with sentinel lymph node status. J Clin Pathol 61:297–300
32. Clemente CG, Mihm MC Jr, Bufalino R et al (1996) Prognostic value of tumor infiltrating lymphocytes in the vertical growth phase of primary cutaneous melanoma. Cancer 77:1303–1310
33. Busam KJ, Antonescu CR, Marghoob AA et al (2001) Histologic classification of tumor-infiltrating lymphocytes in primary cutaneous malignant melanoma: a study of interobserver agreement. Am J Clin Pathol 115:856–860
34. Straume O, Akslen LA (1996) Independent prognostic importance of vascular invasion in nodular melanomas. Cancer 78:1211–1219
35. Clark WH Jr, Elder DE, Guerry DG 4th et al (1989) A model predicting survival in stage I melanoma based on tumor progression. J Natl Cancer Inst 81:1893–1904
36. WHO (1999) WHO declares lymphatic mapping to be the standard of care for melanoma. Oncology 13:288
37. Cook MG, Green MA, Anderson B et al (2003) EORTC Melanoma Group: the development of optical pathological assessment of sentinel lymph nodes for melanoma. J Pathol 200:314–319
38. Cook MG, Di Palma S (2008) Pathology of sentinel lymph nodes for melanoma. J Clin Pathol 61:897–902
39. Scoyler RA, Murali R, McCarthy SW et al (2008) Pathologic examination of sentinel lymph nodes from melanoma patients. Semin Diagn Pathol 25:100–111

Virchows Arch (2009) 454:513–517
DOI 10.1007/s00428-009-0762-6

ORIGINAL ARTICLE

Esophageal melanomas harbor frequent *NRAS* mutations unlike melanomas of other mucosal sites

Shigeki Sekine · Yukihiro Nakanishi · Reiko Ogawa · Satoko Kouda · Yae Kanai

Received: 4 January 2009 / Revised: 26 February 2009 / Accepted: 8 March 2009 / Published online: 25 March 2009

Abstract Mucosal melanomas have genetic alterations distinct from those in cutaneous melanomas. For example, *NRAS*- and *BRAF*-activating mutations occur frequently in cutaneous melanomas, but not in mucosal melanomas. We examined 16 esophageal melanomas for genetic alterations in *NRAS*, *BRAF*, and *KIT* to determine whether they exhibit genetic features common to melanomas arising from other mucosal sites. A sequencing analysis identified *NRAS* mutations in six cases; notably, four of these mutations were located in exon 1, an uncommon mutation site in cutaneous and other mucosal melanomas. *BRAF* and *KIT* mutations were found in one case each. Immunohistochemistry showed KIT expression in four cases, including the tumor with a *KIT* mutation and two other intramucosal tumors. The low frequency of *BRAF* mutations and the presence of a *KIT* mutation-positive case are findings similar to those of mucosal melanomas of other sites, but the prevalence of *NRAS* mutations was even higher than that of cutaneous melanomas. The present study implies that esophageal melanomas have genetic alterations unique from those observed in other mucosal melanomas.

Keywords *NRAS* · *BRAF* · *KIT* · Esophageal melanoma

Introduction

Melanomas show distinct patterns of genetic alterations depending on their sites of origin. The anatomical site-specific patterns of genetic alterations have been discussed in relation to the extent of ultraviolet exposure. *NRAS* and *BRAF* are the most frequently mutated oncogenes in melanomas. Both mutant N-Ras and B-Raf promote tumorigenesis through the constitutive activation of the MAP kinase pathway. Earlier studies suggested that *NRAS* mutations were frequent among melanomas arising from sun-exposed skin [1, 2]. Subsequently, *BRAF*-activating mutations were also identified in a significant proportion of melanomas [3]. Curtin et al. analyzed *NRAS* and *BRAF* mutations as well as DNA copy number changes in a large cohort of melanomas [4]. They utilized the presence of solar elastosis as a histological hallmark of chronic sun exposure and indicated that the majority of melanomas occurring on skin without chronic sun-induced damage had either *NRAS* or *BRAF* mutations whereas melanomas arising on skin with chronic sun-induced damage, acral sites, and mucosal membranes had mostly wild-type *NRAS* and *BRAF*. At the same time, they demonstrated that each group of melanomas exhibited distinct patterns of DNA copy number changes.

In addition to *NRAS* and *BRAF* mutations, a subset of melanomas contains *KIT* mutations [5–7]. Remarkably, the prevalence of *KIT* mutations also varies depending on the site of tumor origin, with the highest prevalence observed in mucosal melanomas [5]. Thus, genetic alterations in melanomas show site/organ-specific patterns and mucosal melanomas have distinct genetic features from those of cutaneous melanomas.

Esophageal melanomas are exceedingly rare, but highly aggressive neoplasms [8–10]. Previous studies have reported that melanomas constitute only 0.1–0.3% of all esophageal tumors [11, 12]. The rarity of this tumor is reasonable, considering the fact that the esophagus usually lacks melanocytes [13]. In addition, the esophagus is not

S. Sekine · Y. Nakanishi · R. Ogawa · S. Kouda · Y. Kanai (✉)
Pathology Division, National Cancer Center Research Institute,
5-1-1, Tsukiji, Chuo-ku,
Tokyo, Japan
e-mail: ykanai@ncc.go.jp

exposed to ultraviolet radiation, a major risk factor for melanomas. Because of the rarity of this lesion, data on genetic alterations in esophageal melanomas is scarce. However, the characterization of their genetic features, including how they differ from cutaneous melanomas and melanomas of other mucosal sites would contribute to the understanding of site/organ-specific genetic alterations in melanomas. Furthermore, considering the development of specific kinase inhibitors, such information could be critical for choosing an appropriate treatment. In this paper, we present the results of a mutational analysis of *NRAS*, *BRAF*, and *KIT* in 16 cases of esophageal melanomas.

Materials and methods

Sixteen surgically resected esophageal melanomas were examined in the present study (Table 1). The samples were routinely fixed with 10% formalin and embedded in paraffin. Five-micrometer-thick sections of each specimen were stained briefly with hematoxylin and eosin and used for DNA extraction. The tumor and nontumor areas were separately dissected using sterilized toothpicks under a microscope. Tissues obtained from the proper muscle layer distant from the tumors were used as nontumor samples. The dissected samples were incubated in 100 μL of DNA extraction buffer (50 mmol/L Tris–HCl, pH 8.0, 1 mmol/L ethylenediaminetetraacetic acid, 0.5% (*v*/*v*) Tween 20, 200 μg/mL proteinase K) at 37°C overnight. Proteinase K was inactivated by heating at 100°C for 10 min. The DNA samples were subjected to polymerase chain reaction (PCR) directly or after purification. When required, the samples were purified using a QIAquick PCR Purification Kit (Qiagen, Hilden, Germany). PCR was performed for 3 min at 95°C for initial denaturing, followed by 35 or 40 cycles at 94°C for 15 s, 58°C for 20 s, and 72°C for 60 s and a final extension at 72°C for 5 min. The primers that were used are listed in Table 2. The PCR products were electrophoresed in a 2% (*w*/*v*) agarose gel, visualized under UV light with ethidium bromide staining, and recovered using a QIAquick Gel Extraction Kit (Qiagen). Isolated PCR products were sequenced bidirectionally on an Applied Biosystems 3130 Genetic Analyzer (Applied Biosystems, Foster, CA, USA) using the same primers used for amplification. Each experiment, including DNA extraction, was done at least twice.

Immunohistochemical staining was performed using the avidin–biotin complex method. The primary antibody used was polyclonal anti-KIT (A4502; 1:100 dilution; Dako, Denmark). 3-3′-Diaminobenzidine tetrahydrochloride was used as a chromogen. The sections were counterstained with hematoxylin. Mast cells in the sections were used as positive controls. For negative controls, the tissue was processed in the same way but the primary antibody was omitted. The staining

Table 1 Results of mutational analysis and immunohistochemistry

Case no.	Age/sex	Depth of invasion	*BRAF*		*NRAS*		*KIT*		KIT IHC
			Nucleotide	Amino acid	Nucleotide	Amino acid	Nucleotide	Amino acid	
1	62/M	Mucosa	–		–		–		+++ (membranous)
2	67/M	Mucosa	–		–		–		+++ (membranous)
3	48/M	Submucosa	–		–		–		–
4	57/F	Submucosa	–		A183T	Q61H	–		–
5	64/M	Submucosa	–		–		–		–
6	67/M	Submucosa	–		–		–		–
7	72/M	Submucosa	–		G35C	G12A	–		–
8	73/M	Submucosa	–		–		–		–
9	48/M	Muscularis propria	–		–		C1727T	L576P	+++ (cytoplasmic)
10	68/M	Muscularis propria	T1799A	V600E	–		–		–
11	69/M	Muscularis propria	–		G34C	G12R	–		–
12	70/M	Muscularis propria	–		G38C	G13A	–		–
13	63/M	Adventitia	–		A183T	Q61H	–		–
14	64/M	Adventitia	–		–		–		–
15	68/M	Adventitia	–		G37C	G13R	–		–
16	71/M	Adventitia	–		–		–		++ (membranous)

IHC immunohistochemistry

Table 2 Primers used in the present study

	Forward primer	Reverse primer
BRAF exon15	TGTTTGCTCTGATAGGAAAATG	CTGATGGGACCCACTCCAT
NRAS exon 1	CAGGTTCTTGCTGGTGTGAAATGACTGAG	CTACCACTGGGCCTCACCTCTATGG
NRAS exon 2	AACAAGTGGTTATAGATGGTGA	CGTTAGAGGTTAATATCCGCA
KIT exon 11	TTTCCCTTTCTCCCCACAG	AAAGCCCCTGTTTCATACTGAC
KIT exon 13	TGCTAAAATGCATGTTTCCAAT	CAGCTTGGACACGGCTTTAC
KIT exon 17	TTTCTTTTCTCCTCCAACCTAA	TGTCAAGCAGAGAATGGGTACT

results were evaluated based on the amount of immunopositive tumor cells as follows: − [<5%], + [5–25%], ++ [25–75%], +++ [>75%]. When KIT is expressed, the staining intensity and the subcellular localization were also evaluated.

Results

The results of the mutational analysis are summarized in Table 1. A *BRAF* mutation was found in one case, while *NRAS* mutations were observed in six cases (Fig. 1). Four of six *NRAS* mutations were located in exon 1, and all these mutations were G to C transversions. All *BRAF* and *NRAS* mutations were missense mutations that had been previously identified as being oncogenic. A missense *KIT* mutation was observed in one case. The mutation affected the juxtamembrane domain of KIT. The wild-type sequence signal was very low for this mutation, suggesting that it was a homozygous mutation. All samples from nontumor areas showed wild-type sequences, indicating the somatic nature of the mutations. All the mutations that were observed were mutually exclusive.

Immunohistochemistry showed no or only focal and equivocal KIT expression in 12 cases (Fig. 2a). The case with the *KIT* mutation showed strong cytoplasmic expression (Fig. 2b), and another case showed heterogeneous staining with approximately 70% of the area exhibiting moderate membranous expression (Fig. 2c). Based on the heterogeneous KIT expression, we performed an additional mutational analysis. The KIT-positive and KIT-negative areas were separately subjected to sequencing analysis, but no *KIT* mutations were observed in either sample. Two early-stage melanomas limited to the mucosal layer exhibited strong and diffuse membranous KIT expression (Fig. 2d).

Discussion

NRAS and *BRAF* mutations are the most common genetic alterations in melanomas. An extensive literature review by Hocker and Tsao reported overall mutation rates of 26% for *NRAS* and 42% for *BRAF* in cutaneous melanomas [14]. In contrast, several studies concurred that these mutations are significantly less prevalent in mucosal melanomas with reported frequencies of 5–14% for *NRAS* and 0–10% for *BRAF* [2, 4, 15–17].

Our results showed that *BRAF* mutations are uncommon among esophageal melanomas as in mucosal melanomas of other organs. Unexpectedly, however, six of the 16 melanomas were found to harbor *NRAS*-activating mutations. While our series may not be sufficiently large to determine the mutational frequency conclusively, the prevalence of *NRAS* mutation-positive cases in the present series was even higher than that observed in cutaneous melanomas. Notably, four of the six mutations were located in exon 1 of *NRAS* and all these mutations were G to C transversions. This finding is intriguing as *NRAS* mutations in melanomas predominantly affect codon 61 within exon 2 and G to C transversion is a rare type of mutations for these sites [14].

Furthermore, previous studies showed that a few recurrent mutations are responsible for the vast majority of *NRAS* mutations in melanomas. The literature review by Hocker and Tsao showed that three mutations, G35A, C181A, and A182G, accounted for 82% of *NRAS* mutations of the 255 substitutions at the *NRAS* locus [14]. However, surprisingly, none of the six mutations identified in this study were identical to these most common *NRAS* mutations. These observations suggest that esophageal melanomas have a high frequency of *NRAS* mutations with a unique mutation spectrum.

Our literature review identified only one study analyzing *NRAS* and *BRAF* mutations in esophageal melanomas. Wong et al. examined three cases of esophageal melanomas, two of which had *NRAS*-activating mutations affecting codons 12 and 61, respectively [17]. On the other hand, only two *BRAF* and three *NRAS* mutations were identified in 33 mucosal melanomas arising outside of the esophagus in their series. While the number of subjects in their study was small, their result is consistent with our finding that esophageal melanomas have a high prevalence of *NRAS* mutations.

A *KIT* mutation was identified in one case, indicating that a subset of esophageal melanomas harbor *KIT*-activating mutations as in other mucosal melanomas. An identical mutation has been reported in gastrointestinal

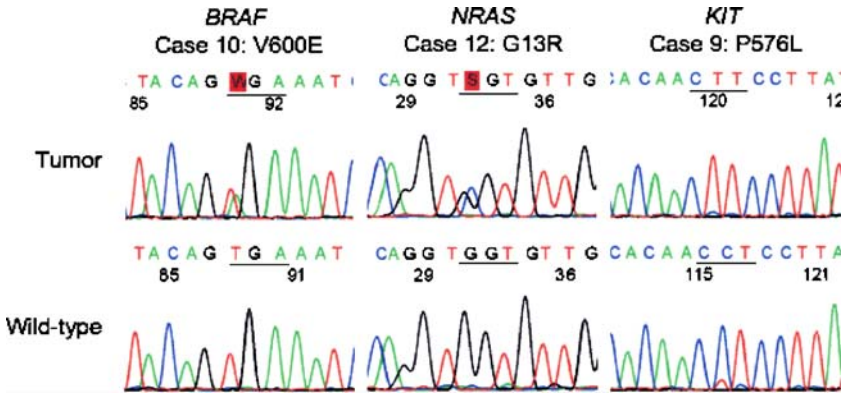

Fig. 1 Representative mutations of *BRAF*, *NRAS*, and *KIT* in esophageal melanomas. Heterozygous *BRAF* V600E and *NRAS* G13R mutations and homozygous P576L *KIT* mutation are shown

stromal tumors and anal melanomas [7, 18], and this mutation has been shown to be associated with a sensitivity to dasatinib and imatinib, inhibitors of SRC/ABL and KIT [7]. While the frequency of this mutation was not high in the present series, the identification of a *KIT* mutation is important, since it provides an immediate therapeutic application. Indeed, the successful treatments of melanomas with *KIT* mutations by imatinib have been recently reported [19, 20].

Of note, the case with the *KIT* mutation also exhibited the strong expression of KIT protein, whereas the majority of the mutation-negative melanomas did not express KIT, as determined using immunohistochemistry. This finding agrees with the results of previous studies on mucosal melanomas of other sites and suggests that immunohistochemistry is useful for excluding *KIT* mutation-negative cases prior to genetic testing [6, 7]. We also found KIT expression in two early-stage tumors. The expression of KIT in early-stage cutaneous melanomas has also been previously reported [21, 22]. Since non-neoplastic melanocytes express KIT, the expression of KIT in early-stage melanomas might be regarded as the retention of physiological expression in melanocytes [21]. Overall, our observations suggest that immunohistochemistry for KIT may be useful for prescreening *KIT* mutation-positive cases among advanced esophageal melanomas.

The present study indicates that esophageal melanomas have a high frequency of *NRAS* mutations unlike mucosal melanomas of other sites. Furthermore, the mutational spectrum of *NRAS* is distinct from those commonly observed in melanomas. Even among mucosal melanomas, the patterns of genetic alterations are likely distinct between

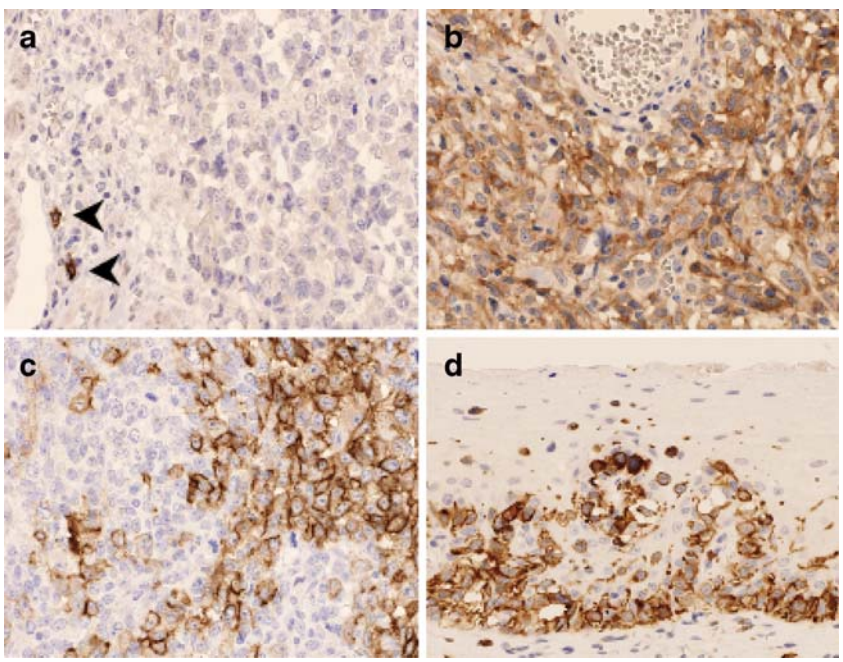

Fig. 2 KIT expression in esophageal melanomas. **a** This case lacks KIT expression. Few mast cells show positive staining (*arrowheads*; case 13). **b** Tumor cells show diffuse cytoplasmic staining (case 9). **c** An area of the tumor cells shows membranous expression (case 16). **d** Tumor cells proliferating within the epithelial layer show membranous expression (case 2)

differing sites of origin. Our observations also suggest that not only the degree of ultraviolet exposure, but also organ-specific factors may significantly influence the mutational spectrum in melanomas.

Acknowledgements This work was supported by a Grant-in-Aid for the Third Term Comprehensive 10-Year Strategy for Cancer Control, a Grant-in-Aid for Cancer Research from the Ministry of Health, Labor and Welfare of Japan, and a program for promotion of Fundamental Studies in Health Sciences of the National Institute of Biomedical Innovation (NiBio), Japan.

Conflicts of interest The authors declare that they have no conflicts of interest.

References

1. van't Veer LJ, Burgering BM, Versteeg R et al (1989) N-ras mutations in human cutaneous melanoma from sun-exposed body sites. Mol Cell Biol 9:3114–3116
2. Jiveskog S, Ragnarsson-Olding B, Platz A et al (1998) N-ras mutations are common in melanomas from sun-exposed skin of humans but rare in mucosal membranes or unexposed skin. J Invest Dermatol 111:757–761
3. Davies H, Bignell GR, Cox C et al (2002) Mutations of the BRAF gene in human cancer. Nature 417:949–954
4. Curtin JA, Fridlyand J, Kageshita T et al (2005) Distinct sets of genetic alterations in melanoma. N Engl J Med 353:2135–2147
5. Curtin JA, Busam K, Pinkel D et al (2006) Somatic activation of KIT in distinct subtypes of melanoma. J Clin Oncol 24:4340–4346
6. Rivera RS, Nagatsuka H, Gunduz M et al (2008) C-*kit* protein expression correlated with activating mutations in KIT gene in oral mucosal melanoma. Virchows Arch 452:27–32
7. Antonescu CR, Busam KJ, Francone TD et al (2007) L576P KIT mutation in anal melanomas correlates with KIT protein expression and is sensitive to specific kinase inhibition. Int J Cancer 121:257–264
8. Kato H, Watanabe H, Tachimori Y et al (1991) Primary malignant melanoma of the esophagus: report of four cases. Jpn J Clin Oncol 21:306–313
9. Li B, Lei W, Shao K et al (2007) Characteristics and prognosis of primary malignant melanoma of the esophagus. Melanoma Res 17:239–242
10. Lohmann CM, Hwu WJ, Iversen K et al (2003) Primary malignant melanoma of the oesophagus: a clinical and pathological study with emphasis on the immunophenotype of the tumours for melanocyte differentiation markers and cancer/testis antigens. Melanoma Res 13:595–601
11. Turnbull AD, Rosen P, Goodner JT et al (1973) Primary malignant tumors of the esophagus other than typical epidermoid carcinoma. Ann Thorac Surg 15:463–473
12. Scotto J, Fraumeni JF Jr, Lee JA (1976) Melanomas of the eye and other noncutaneous sites: epidemiologic aspects. J Natl Cancer Inst 56:489–491
13. Tateishi R, Taniguchi H, Wada A et al (1974) Argyrophil cells and melanocytes in esophageal mucosa. Arch Pathol 98:87–89
14. Hocker T, Tsao H (2007) Ultraviolet radiation and melanoma: a systematic review and analysis of reported sequence variants. Hum Mutat 28:578–588
15. Cohen Y, Rosenbaum E, Begum S et al (2004) Exon 15 BRAF mutations are uncommon in melanomas arising in nonsun-exposed sites. Clin Cancer Res 10:3444–3447
16. Edwards RH, Ward MR, Wu H et al (2004) Absence of BRAF mutations in UV-protected mucosal melanomas. J Med Genet 41:270–272
17. Wong CW, Fan YS, Chan TL et al (2005) BRAF and NRAS mutations are uncommon in melanomas arising in diverse internal organs. J Clin Pathol 58:640–644
18. Lasota J, Jasinski M, Sarlomo-Rikala M et al (1999) Mutations in exon 11 of c-*Kit* occur preferentially in malignant versus benign gastrointestinal stromal tumors and do not occur in leiomyomas or leiomyosarcomas. Am J Pathol 154:53–60
19. Hodi FS, Friedlander P, Corless CL et al (2008) Major response to imatinib mesylate in KIT-mutated melanoma. J Clin Oncol 26:2046–2051
20. Lutzky J, Bauer J, Bastian BC (2008) Dose-dependent, complete response to imatinib of a metastatic mucosal melanoma with a K642E KIT mutation. Pigment Cell Melanoma Res 21:492–493
21. Montone KT, van Belle P, Elenitsas R et al (1997) Proto-oncogene c-*kit* expression in malignant melanoma: protein loss with tumor progression. Mod Pathol 10:939–944
22. Janku F, Novotny J, Julis I et al (2005) KIT receptor is expressed in more than 50% of early-stage malignant melanoma: a retrospective study of 261 patients. Melanoma Res 15:251–256

Virchows Arch (2009) 454:519–524
DOI 10.1007/s00428-009-0760-8

ORIGINAL ARTICLE

Association of hormone receptor status with grading, age of onset, and tumor size in *BRCA1*-associated breast cancer

M. Graeser · K. Bosse · M. Brosig · C. Engel · R. K. Schmutzler · on behalf of the German Consortium for Hereditary Breast and Ovarian Cancer

Received: 6 January 2009 / Revised: 3 March 2009 / Accepted: 6 March 2009 / Published online: 21 April 2009

Abstract *BRCA1*-associated breast cancer frequently presents with estrogen-receptor (ERα) and progesterone-receptor (PR) negativity, grade 3, and early onset. In contrast, in *BRCA1*-deficient mice, ERα is highly expressed in early tumorigenesis. In a retrospective cohort study on 587 breast cancer patients with deleterious *BRCA1* mutations, the correlation of ER, PR status, grading, age of onset, and tumor size was investigated. ERα and PR expression decreased from 62% in ductal carcinoma in situ (DCIS) to 20% and 16% in pT3, respectively (p value for ER 0.025 and PR 0.035, Fisher's exact test). The percentage of grade 1/2 tumors decreased from 44% in DCIS to 17% in pT3 (p value 0.074). Moreover, ER/PR positivity increased with increasing age. Our data suggest that early stage *BRCA1*-associated breast cancers are more frequently ERα and PR positive and low grade than advanced stages.

Keywords *BRCA1* · Breast cancer · Estrogen receptor · Progesterone receptor

M. Graeser and K. Bosse contributed equally to this paper.

M. Graeser (✉) · K. Bosse · R. K. Schmutzler
Department of Gynecology and Obstetrics,
Center for Familial Breast and Ovarian Cancer,
University Hospital of Cologne,
Kerpenerstrasse 34,
50931 Cologne, Germany
e-mail: monika.graeser@uk-koeln.de

M. Brosig · C. Engel
Institute of Medical Informatics, Statistics, and Epidemiology,
University of Leipzig,
Leipzig, Germany

Introduction

Women with deleterious mutations in the breast cancer susceptibility gene *BRCA1* are predisposed to breast and ovarian cancer with an estimated lifetime risk of about 80% [1–3].

As *BRCA1* acts as a tumor-suppressor gene, the inactivation of the wild-type allele is thought to be mandatory for cancer development. Although the potential for disruption of function of the second *BRCA1* allele exists in all somatic cells with inherited germ-line mutations, the increased risk of cancer in mutation carriers is most evident in hormone-sensitive tissues, such as breast and ovarian tissue in women and prostate tissue in men. The BRCA1 protein has been implicated in DNA damage repair, cell cycle checkpoint control, and transcriptional regulation [4]. The specific suppression of breast and ovarian carcinogenesis by the *BRCA1* gene has been attributed to its regulation of estrogen receptor alpha (ERα) and progesterone receptor (PR) [5, 6], which play important roles in breast development [7, 8]. BRCA1 directly interacts with ER and down regulates ligand-dependent and -independent transcription activities [9, 10]. In line with these findings, it could be shown that ERα is highly expressed in the premalignant mammary gland and initiation stages of tumorigenesis in a mouse model lacking the full-length form of *BRCA1* [11]. In contrast, normal breast tissue of human *BRCA1* mutation carriers stains positive for ER to the same extent as in women with wild-type *BRCA1*. The majority of BRCA related breast cancers are ERα and PR negative and of high grade [12, 13]. Clinical observations, however, indicate that reduced exposure to steroidal hormones after removal of the ovaries leads to a reduction in breast cancer risk around 50% [14]. Additionally, tamoxifen reduces contralateral breast cancer risk in *BRCA* mutation carriers [15].

King et al. presented data indicating that PR is highly and aberrantly expressed in normal breast epithelium of *BRCA1* mutation carriers [16]. They could show that this is due to the diminution of PR ubiquitination and degradation in the absence of functional *BRCA1*. Furthermore, the treatment of the *BRCA1*-deficient mice with the progesterone antagonist mifepristone (RU 486) prevented mammary tumorigenesis [17]. These observations indicate that ovarian hormones contribute to breast cancer development in *BRCA1* mutation carriers. Therefore, the purpose of this study was to analyze ERα and PR expression during breast cancer development in *BRCA1* mutation carriers.

Study population and methods

The German Consortium for Hereditary Breast and Ovarian Cancer (GCHBOC) comprises 12 university centers. Using uniform inclusion criteria and standard operating procedures, families with clustering or early onset of breast or ovarian cancer are registered and tested for the presence of deleterious germ line mutations in *BRCA1* and *BRCA2*. Comprehensive data on familial cancer history including a detailed pedigree, pathology reports, and results of molecular testing are documented in a central database using standardized electronic case report forms. Inclusion criteria and methods for genetic testing are described elsewhere [18]. All patients gave their written informed consent to be enrolled in the registry. The registry has been approved by the institutional review boards of each participating center.

Between 1997 and 2008, 8,622 women underwent *BRCA* genetic testing. Overall, 2,655 women were identified with a polymorphism, 340 women with an unclassified variant (UV), and 1,853 with a deleterious mutation in the *BRCA1* gene. Of the *BRCA1* mutation carriers, 1,042 had developed breast cancer between 1976 and 2008. Of the latter, medical reports were available from 587 women.

In order to exclude a potential recruitment bias, we compared the median age of onset of the 587 women included in our study with the median age of onset of 455 women who could not be included in the study because of missing data. The median age of onset for the study group is 39 years (range 23–80 years) and for the 455 excluded women, 40 years (range 17–81 years), i.e., there was no difference in menopausal status which may have exerted a major effect on hormonal receptor status.

In the case of metachronous tumors, only the first breast cancer was considered. Patients with pT4 tumors were excluded because these tumors represent a small and inhomogeneous group of malignancies with different tumor extent and partially inflammatory component. A total of 587 patients with complete clinical and pathology reports including ERα, PR status, pT status, and age at diagnosis were analyzed. In 541 patients, information on tumor grading was available.

We stratified the patients by tumor size, histological grade, and age and calculated the percentage of ER/PR-positive tumors for each stratum. The median age of onset our study participants was 39 years (range 23 to 80 years), 38 years (25 to 66 years) for patients with ductal carcinoma in situ (DCIS), 39 years (23 to 80 years) for patients with T1, 38 years (23 to 79 years) for patients with T2, and 39 years (24 to 54 years) for patients with T3. There was no significant difference in the age pattern between tumor sizes. Sixty-five patients were younger than 30 years at the time of the first breast cancer diagnosis; 251 were between 30 and 39 years, 193 between 40 and 49 years, 51 between 50 and 59 years, and 27 above 60 years of age.

Tumor pathology

Information regarding the histological type of breast cancer, ER and PR status, and grading were obtained from institutional pathology reports and were reviewed by reference pathologists. All carcinoma in situ and invasive breast cancer specimens were routinely evaluated for ER and PR status using immunohistochemistry. Monoclonal antibodies were used to stain for ERα and PR. Three classification systems, i.e., percentage of positive-stained nuclei, Remmele score, and Allred score, have been applied according to the current S3 guideline [19]. Tumors were considered hormone-responsive in the case of >10% positive cell nuclei, Allred score >=4, or Remmele score >=2. As the revised St. Gallen guideline 2005 considers tumors exhibiting 1% to 10% positive nuclei of uncertain endocrine responsiveness, there remained some impreciseness in the categorization of tumors with very low ERα and PR expression.

Statistical analysis

Two-sided Fisher's exact test was used to asses the association between hormone receptor positivity, tumor size, grading, and age at diagnosis. A p value equal to or less than 0.05 was considered statistically significant. All statistical analyses were performed using SPSS 15.0.1.1 (SPSS Inc., Chicago, IL, USA) for Windows.

Results

Thirteen women were diagnosed with DCIS, 321 women with pT1-size tumors, 228 women with pT2 tumor, and 25 women with pT3 tumor. Detailed characteristics are given in Table 1. The ERα and PR expression gradually diminished (Fig. 1) from 62% in pTis to 20.0% in pT3 for ERα and from 61.5% to 16.0% for PR, respectively (p=0.025 and p=0.035). In

Table 1 Clinicopathological characteristics of *BRCA1*-associated breast cancer cases

Characteristics	*BRCA1* mutation carriers (n=587)
Tumor size, no. (%)	
pTis	13 (2.3)
T1	321 (54.7)
T2	228 (38.7)
T3	25 (4.3)
Grading, no. (%)	
G1	7 (1.2)
G2	147 (25.1)
G3	387 (65.9)
Not specified	46 (7.8)
Estrogen receptor status, no. (%)	
Positive	158 (26.9)
Negative	429 (73.1)
Progesterone receptor status, no. (%)	
Positive	159 (27.0)
Negative	428 (73.0)
Age (years) at first breast cancer, no. (%)	
<29	65 (11.0)
30–39	251 (42.9)
40–49	193 (32.8)
50–59	51 (8.7)
>60	27 (4.6)

541 patients, we had information on histological grade, ERα, and PR status. The proportion of cancers that were ERα-positive decreased considerably from grade 1 to 3 (grade 1, 57.1% ERα positive; grade 2, 45.6%; and grade 3, 17.8% ERα positive; p value <0.001). A similar relationship was found for PR status and grading (grade 1, 42.9% PR positive; grade 2, 39.5%; and grade 3, 20.7% PR positive; p value <0.001; Fig. 2). It is well known that ERα and PR are expressed in an age-dependent manner in sporadic breast cancer which was seen in our cohort of *BRCA1* mutation carriers as well. We observed an increase in ERα and PR positivity for tumors diagnosed under 30 years (24.6% ERα and 20.0% PR) to tumors diagnosed above 60 years (55.6% ER and 40.7% PR; Fig. 3; p_{trend}=0.009 and p_{trend}=0.004, respectively).

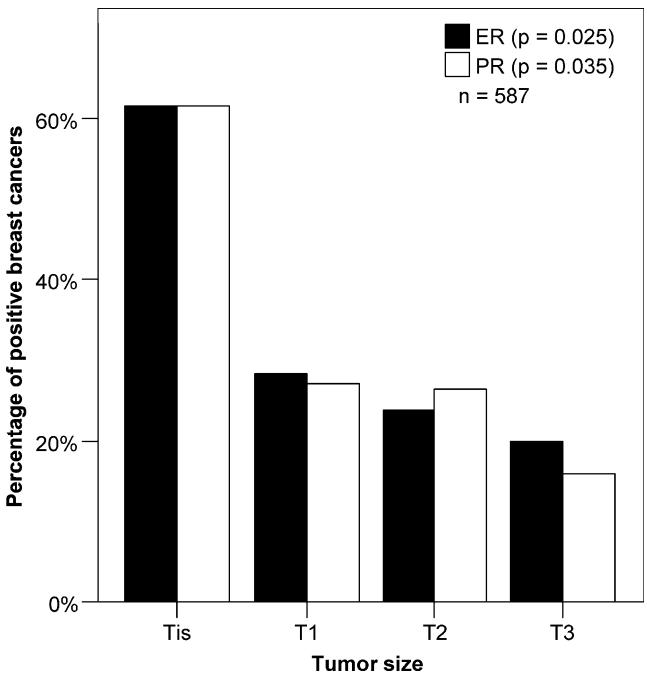

Fig. 1 Percentage of ER and PR positive breast cancer by tumor size in 587 *BRCA1* mutation carriers

Additionally, we found a trend for an association between histological grading and tumor size. Grade 1/2 tumors decreased from 44.4% in DCIS to 16.7% in pT3 tumors (p value 0.074; Fig. 4).

Discussion

Numerous studies pointed out that 70–90% of invasive *BRCA1*-associated breast cancers do not express ERα which is in line with our observation [20, 21]. The overall frequency of high-grade tumors (G3) in our study population was 71.5% which is slightly lower than that reported by Atchley et al. (85.4%) but consistent with the results by Foulkes et al. (73.6%) [20, 21]. However, most studies did not stratify the patients according to tumor size. For

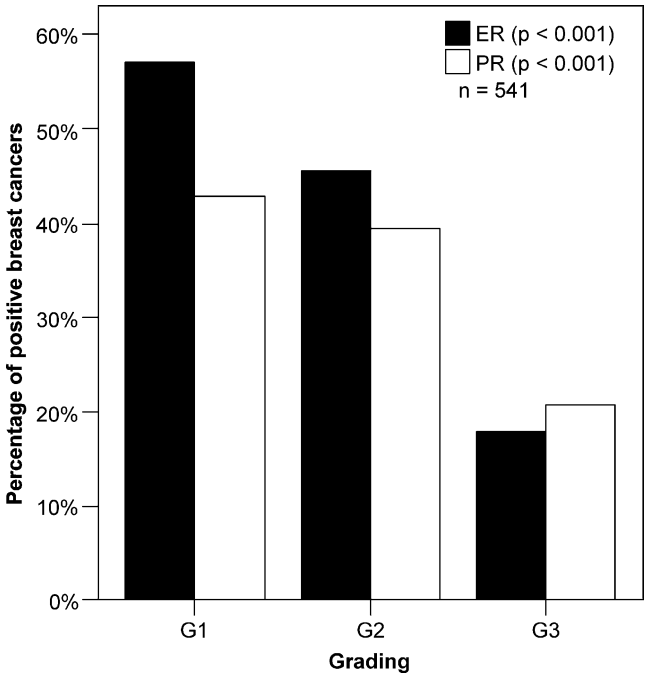

Fig. 2 Percentage of ER and PR positive breast cancer by grading in 541 *BRCA1* mutation carriers

instance, among 56 *BRCA1* mutation carriers described by Atchley et al., 71.5% presented with advanced tumor stage (pT2–3) compared to only 43.0% (pT2–3) in our study population [20]. Foulkes et al. even excluded patients with preinvasive stages (DCIS) from their evaluation [21].

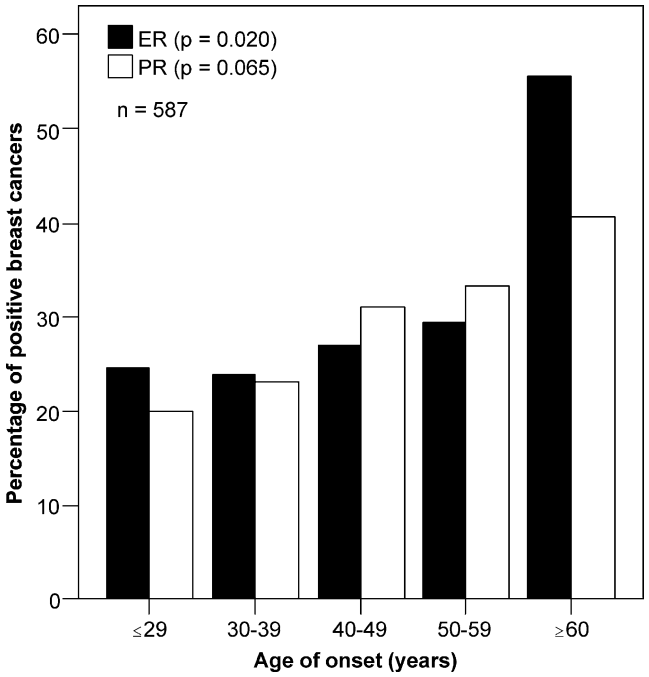

Fig. 3 Percentage of ER and PR positive breast cancer by age of onset in 587 *BRCA1* mutation carriers

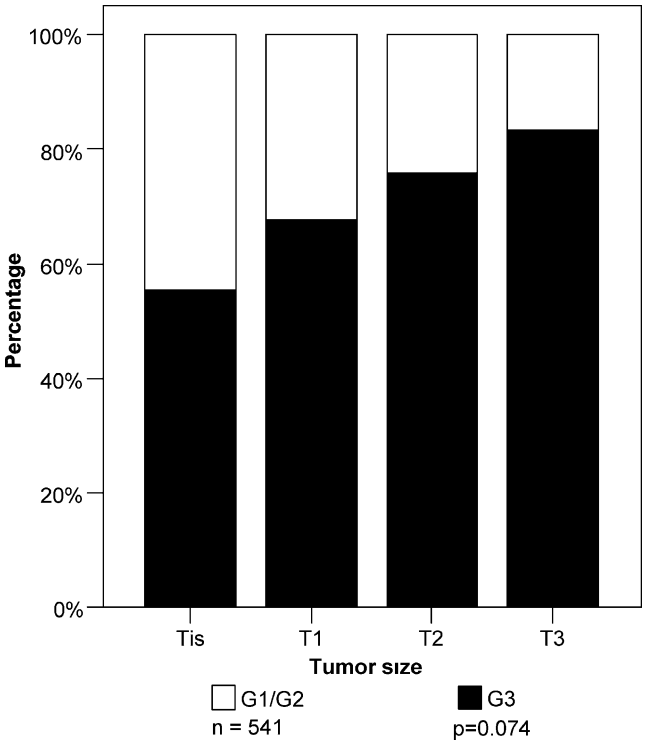

Fig. 4 Association of grading and tumor size in 587 *BRCA1* mutation carriers

In our study, we found an inverse correlation between hormone receptor status and tumor size. In agreement with our data, Li et al. found that ERα is highly expressed in initiation stages of tumorigenesis in *BRCA1*-deficient mice [11]. The majority of cells in hyperplasia (95.8%), carcinoma in situ (94.7%), and small tumors <0.5 cm in diameter (82.4%) were ERα positive and gradually decreased to less than 1% positivity in larger tumors of approximately 2 cm in size.

We detected an inverse correlation between ERα and PR expression and grading which is in agreement with Atchley et al. who found that the proportion of tumors that were ERα-positive decreased as the histological grade increased [20].

Finally, we observed an increase in the percentage of tumors that were ERα/PR positive with increasing age. Accordingly, Vaziri et al. found that ERα and PR were less frequently expressed in tumors of *BRCA1* mutation carriers (25% ERα/PR) than in controls (59.5% ERα and 57.1% PR) if breast cancer appeared before age 50 [22]. A similar trend was observed by Foulkes et al. who found that 19% of *BRCA1*-related breast cancers were ERα-positive cancers occurring in women in their premenopausal years compared to 38.0% in postmenopausal years after age 55 [21].

A potential limitation of our study is the impreciseness in the classification of tumors with very low hormone receptor

levels, i.e., tumors with 1–10% positively stained nuclei have been considered non-endocrine responsive in the past while they are considered of uncertain responsiveness since 2005 (St. Gallen, S3 GL). Therefore, the percentage of hormone responsive *BRCA1*-associated tumors might have been slightly higher which should not have a major influence on the observed association between hormone receptor levels and tumor progression.

Our observations point to a role of hormones in early BRCA1-associated carcinogenesis rather than in tumor progression. This is further supported by the observation that oophorectomy in human *BRCA1* mutation carriers and in mouse mutants significantly reduced the frequency of breast cancer formation [23, 24]. Taken together, these data suggest that *BRCA1*-related breast carcinogenesis is sensitive to anti-hormonal prevention.

In this context, Narod et al. and Metcalfe et al. demonstrated that prophylactic tamoxifen intake significantly reduced the risk for contralateral breast cancer in *BRCA1* mutation carriers [15, 23]. However, these observations conflict with results by Jones et al. [25]. They described a proliferative effect of tamoxifen on mammary cancer development in *BRCA1*-depleted mice while oophorectomy was protective. This was explained by an agonistic activity of tamoxifen in the absence of functional *BRCA1*.

An alternative strategy may therefore be the targeting of PR which showed a concomitant expression with ERα in our cohort. PR expression is even elevated in benign tissue adjacent to BRCA1-associated breast cancers [16]. This is further supported by Poole et al. who pointed out that *BRCA1* deficiency in mice correlates with PR accumulation [17]. They were able to show that functional *BRCA1* leads to degradation of PR by ubiquitination. Consequently, administration of the progesterone antagonist mifepristone (RU 486) substantially reduced branching and tumor development in these mice. Our finding of predominantly PR positive staining in early tumor formation in *BRCA1* mutation carriers supports the assumption that progesterone is involved in breast cancer development. Therefore, PR is a promising new target for the prevention of *BRCA1*-associated carcinogenesis that deserves further investigation.

Acknowledgements We thank all centers of the German Consortium for Hereditary Breast and Ovarian Cancer (GCHBOC) for their excellent work: Dorothea Gadzicki (Hannover), Ulrich Bick (Berlin), Karin Kast (Dresden), Ursula G. Froster (Leipzig), Bettina Schlehe (Heidelberg), Astrid Bechthold (Würzburg), Norbert Arnold (Kiel), Sabine Preisler-Adams (Münster), Carolin Nestle-Kraemling (Düsseldorf), Marion Kiechle (München), Dominic Varga (Ulm), Hans-Heinrich Kreipe (Reference Pathology, Hannover), Reinhard Büttner (Reference Pathology, Bonn), and Markus Loeffler (central documentation and biometry). The GCHBOC is supported by grants from the Deutsche Krebshilfe.

Conflict of interest None.

References

1. Ford D, Easton DF, Stratton M et al (1998) Genetic heterogeneity and penetrance analysis of the *BRCA1* and *BRCA2* genes in breast cancer families. The Breast Cancer Linkage Consortium. Am J Hum Genet 62:676–689
2. Ford D, Easton DF, Bishop DT et al (1994) Risks of cancer in BRCA1-mutation carriers. Breast Cancer Linkage Consortium. Lancet 343:692–695
3. Miki Y, Swensen J, Shattuck-Eidens D et al (1994) A strong candidate for the breast and ovarian cancer susceptibility gene *BRCA1*. Science 266:66–71
4. Turner N, Tutt A, Ashworth A (2004) Hallmarks of 'BRCAness' in sporadic cancers. Nat Rev Cancer 4:814–819
5. Fan S, Wang J, Yuan R et al (1999) BRCA1 inhibition of estrogen receptor signaling in transfected cells. Science 284: 1354–1356
6. Razandi M, Pedram A, Rosen EM et al (2004) BRCA1 inhibits membrane estrogen and growth factor receptor signaling to cell proliferation in breast cancer. Mol Cell Biol 4:5900–5913
7. Korach KS (1994) Insights from the study of animals lacking functional estrogen receptor. Science 266:1524–1527
8. Li X, Lonard DM, O'Malley BW (2004) A contemporary understanding of progesterone receptor function. Mech Ageing Dev 125:669–678
9. Ma Y, Katiyar P, Jones LP et al (2006) The breast cancer susceptibility gene *BRCA1* regulates progesterone receptor signaling in mammary epithelial cells. Mol Endocrinol 20:14–34
10. Zheng L, Annab LA, Afshari CA et al (2001) BRCA1 mediates ligand-independent transcriptional repression of the estrogen receptor. Proc Natl Acad Sci USA 98:9587–9592
11. Li W, Xiao C, Vonderhaar BK et al (2007) A role of estrogen/ERalpha signaling in BRCA1-associated tissue-specific tumor formation. Oncogene 26:7204–7212
12. Johannsson OT, Idvall I, Anderson C et al (1997) Tumour biological features of BRCA1-induced breast and ovarian cancer. Eur J Cancer 33:362–371
13. Eisinger F, Jacquemier J, Nogues C et al (1999) Steroid receptors in hereditary breast carcinomas associated with *BRCA1* or *BRCA2* mutations or unknown susceptibility genes. Cancer 1585:2291–2295
14. Rebbeck TR, Lynch HT, Neuhausen SL et al (2002) Prophylactic oophorectomy in carriers of BRCA1 or BRCA2 mutations. N Engl J Med 346:1616–1622
15. Narod SA, Brunet JS, Ghadirian P et al (2000) Tamoxifen and risk of contralateral breast cancer in BRCA1 and BRCA2 mutation carriers: a case-control study. Hereditary Breast Cancer Clinical Study Group. Lancet 356:1876–1881
16. King TA, Gemignani ML, Li W et al (2004) Increased progesterone receptor expression in benign epithelium of BRCA1-related breast cancers. Cancer Res 64:5051–5053
17. Poole AJ, Li Y, Kim Y et al (2006) Prevention of BRCA1-mediated mammary tumorigenesis in mice by a progesterone antagonist. Science 314:1467–1470
18. Meindl A (2002) Comprehensive analysis of 989 patients with breast or ovarian cancer provides BRCA1 and BRCA2 mutation profiles and frequencies for the German population. Int J Cancer 97:472–480
19. Remmele W, Schicketanz KH (1993) Immunohistochemical determination of estrogen and progesterone receptor content in human breast cancer. Computer-assisted image analysis (QIC score) vs. subjective grading (IRS). Pathol Res Pract 189:862–866

20. Atchley DP, Albarracin CT, Lopez A et al (2008) Clinical and pathologic characteristics of patients with BRCA-positive and BRCA-negative breast cancer. J Clin Oncol 1026:4282–4288
21. Foulkes WD, Metcalfe K, Sun P et al (2004) Estrogen receptor status in BRCA1- and BRCA2-related breast cancer: the influence of age, grade, and histological type. Clin Cancer Res 10:2029–2034
22. Vaziri SA, Krumroy LM, Elson P et al (2001) Breast tumor immunophenotype of BRCA1-mutation carriers is influenced by age at diagnosis. Clin Cancer Res 7:1937–1945
23. Metcalfe K, Lynch HT, Ghadirian P et al (2004) Contralateral breast cancer in BRCA1 and BRCA2 mutation carriers. J Clin Oncol 22:2328–2335
24. Kauff ND, Satagopan JM, Robson ME et al (2002) Risk-reducing salpingo-oophorectomy in women with a BRCA1 or BRCA2 mutation. N Engl J Med 346:1609–1615
25. Jones LP, Li M, Halama ED et al (2005) Promotion of mammary cancer development by tamoxifen in a mouse model of BRCA1-mutation-related breast cancer. Oncogene 24:3554–3562

Virchows Arch (2009) 454:525–529
DOI 10.1007/s00428-009-0755-5

ORIGINAL ARTICLE

Status of HER1 and HER2 in peritoneal, ovarian and colorectal endometriosis and ovarian endometrioid adenocarcinoma

C. Uzan · E. Darai · A. Valent · O. Graesslin · A. Cortez · R. Rouzier · P. Vielh

Received: 15 January 2009 / Revised: 24 February 2009 / Accepted: 27 February 2009 / Published online: 18 March 2009

Abstract A role for the EGF system, in particular HER1 and 2, in growth of the endometrium has been suggested but HER1 and 2 have not been studied in all locations of endometriosis and in ovarian endometrioid adenocarcinoma (OEC) which is a rare form of malignant transformation of endometriosis. Immunohistochemistry (IHC) was used for studying HER1 and HER2 in ovarian (n=10), peritoneal (n=10), colorectal endometriosis (n=20) and OEC (n=10). Fluorescent in situ hybridisation (FISH) was used for analysing the status of HER2 gene in colorectal endometriosis and OEC. All samples were negative for HER2 in both glandular and stromal cells and in glandular cells for HER1 by IHC. In 15 out of 20 colorectal endometriosis, there was a weak expression in stromal cells. Following FISH, two colorectal samples had a partial 17 aneusomy and three OEC, a 17 polysomy. The other samples were 17 disomic without HER2 amplification; HER1 and 2 do not seem to have a role in endometriosis physiopathology.

C. Uzan (✉) · A. Valent · P. Vielh
Research Translational Laboratory, Histocytopathology Unit,
Institute Gustave Roussy,
39, rue Camille Desmoulins,
94805 Villejuif, France
e-mail: catherine.uzan@igr.fr

E. Darai · A. Cortez · R. Rouzier
Obstetrics and Gynecology Department, Tenon Hospital,
75020 Paris, France

O. Graesslin
Obstetrics and Gynecology Department,
Institute Alix de Champagne,
51092 Reims, France

Keywords Endometriosis · HER · Endometrioid ovarian cancer · Immunohistochemistry · Fluorescent in situ hybridisation

Introduction

Growth factors receptors are crucial in regulating growth, differentiation and motility of various tumour cells [1]. One of the most studied growth factor receptor systems is the epidermal growth factor receptor (EGFR) family. This family consists of four distinct, but structurally similar, transmembrane tyrosine kinase (TK) receptors, named HER1/erbB-1 (better known as epidermal growth factor receptor [EGFR]), HER2/erbB-2, HER3/erbB-3 and HER4/erbB-4. HER2 gene is located on the 17 chromosome.

Gene amplification and/or protein overexpression of EGFR have been observed in a variety of solid epithelial tumours. Examples include the lung, colorectal, urinary tract, bladder, breast, head and neck, oesophageal and gastric carcinomas. In breast carcinomas, approximately 6% show HER1 amplification with EGFR protein overexpression [2]. Overexpression of HER1 has been correlated with high grade and progression of tumours [3] and expression of HER2 (cerb-B2 protein) has been demonstrated in normal as well as in malignant epithelial cells of the female genital tract [4–6]. Ejskjaer et al. observed cyclical expression of the four EGF receptors and two of their ligands, and localised all four receptors and four ligands in endometrial biopsies [7]. The highest expression of HER1 has been observed during the proliferative phase and during the early secretory phase for HER2 [7]. Niikura et al. reported EGFR expression in 58.3% of normal endometrium, in 100% of endometrial hyperplasia, and in 67.5% of

endometrial carcinoma [8]. Three receptors (HER1, HER2 and HER4) and two detectable ligands (TGF-alpha and HB-EGF) were found significantly higher expressed in endometrial cancer than in healthy menopausal endometrium [9]. These results suggest a fundamental role for the EGF system in the cyclical growth of the endometrium and, potentially, in the development of endometriosis.

Endometriosis is defined by the presence of endometrial glands and stroma outside the cavity of the uterus. The incidence of endometriosis in the female population ranges from 5% to 15%, reaching 50% in women with infertility [10, 11]. The most frequent locations of endometriosis are the peritoneum and ovaries (endometriomas), followed by deep infiltrating endometriosis (DIE) [12]. Among DIE, colorectal endometriosis is one of the most severe form altering quality of life [13]. Although molecular mechanisms remain to be defined, an increasing body of data suggests the possible transformation of endometriotic cells in endometrioid or clear cell carcinoma [14]. In addition, one EGFR gene polymorphism has been recently associated with susceptibility to endometriosis [15], and Melega et al. reported that about 21% of endometriosis are EGFR positive and oestrogen receptor negative, suggesting a potential role of epidermal growth factor in the growth and maintenance of endometrial ectopia [16]. Finally, the development of new therapeutic agents targeting EGFR has attracted attention to treat various HER positive tumours. So far, few data concerning HER1 and HER2 expression in endometriosis are available and the small published series which only include peritoneal or ovarian endometriosis, but no DIE lesions, report contradictory results [17, 18].

These data prompted us to evaluate the status of HER1 and HER2 by immunohistochemistry (IHC) and by fluorescent in situ hybridisation (FISH) in a large series of lesions consisting of peritoneal, ovarian and colorectal endometriosis and ovarian endometrioid adenocarcinomas.

Materials and methods

Materials

Tissue samples were obtained from women undergoing surgery in the Gynecology Department of Tenon Hospital, Paris, between 2001 and 2003. Specimens consisted of ten ovarian endometriotic cysts, ten peritoneal endometriosis, 20 colorectal endometriosis and ten endometrioid ovarian adenocarcinomas. Diagnosis of endometriosis was first made by direct visualisation (laparoscopy or laparotomy) during surgery then confirmed by histological examination of the corresponding specimens. All the samples were provided by scheduled surgery, no sample was retrieved specifically for the study. None of the women were receiving hormone therapy at the time of sampling. All the patients with colorectal endometriosis had surgery for chronic pains.

Immunohistochemistry

Sections (4 μm thick) were deparaffinated in xylene and rehydrated through a graded series of ethanol solutions. For HER1, after antigen retrieval with protease I (37°C, 8 min), sections were automatically immunostained (benchmark Ventana®) using a prediluted antibody (Ventana®) followed by incubation with the Ultraview Universal kit (Ventana®) containing the secondary antibody. For HER2, after antigen retrieval with citrate buffer pH 7.3 (98°C, 20 min), sections were automatically immunostained (Dakoautostainer®) with the polyclonal antibody from DAKO® (dilution of 1/850) followed by incubation with the N-histofine kit containing the secondary antibody.

Each slide consisted of one pathologic specimen and an external positive control. Positive controls for HER1 and HER2 were sections of placenta and of breast cancer, respectively. Samples were considered negative when no labelled cells were observed on the tissue section, and positive in all other cases. Expression was studied in both glandular and stromal cells.

Fluorescent in situ hybridisation

FISH was performed using direct-labelled probes (DAKO®) specific for HER2. Sections (4 μm thick) were deparaffinated in xylene and rehydrated through a graded series of ethanol solutions. We followed the procedure as recommended by manufacturers with only one modification: slides and probes were denaturated separately (slides in formamide at 72°C during 8 min, probes at 85°C during 6 min). Cells were counterstained with 18 μl of 4,6-diamidino-2-phenylindole (DAPI) for 5 min and then viewed under a fluorescent microscope equipped with multi-bandpass filters to visualise colours simultaneously. One hundred nuclei were counted.

Results

HER1 and HER2 immunohistochemistry

HER1 immunostaining showed that glandular and stromal cells were both negative in all cases of ovarian and peritoneal endometriosis as well as in tumour cells of endometrioid adenocarcinomas. In 15 out of the 20 samples of colorectal endometriosis, glandular cells were also found negative, whereas a weak expression was observed in stromal cells (in the other five colorectal samples, both glandular and stromal cells were negative).

HER2 immunostaining showed that glandular and stromal cells were both negative in all cases of ovarian, peritoneal and colorectal endometriosis as well as in tumour cells of endometrioid adenocarcinomas.

HER2 fluorescent in situ hybridisation

HER2 gene is located on the 17 chromosome. HER2 gene status was studied by FISH and showed: (1) 18 colorectal endometriosis with a 17 disomy and no gene amplification (Fig. 1); (2) two colorectal samples with a partial 17 aneusomy: one sample with 20% of glandular cells with 17 trisomy and a second sample with 50% cells of glandular cells with 17 trisomy (Fig. 2) and (3) three cases of endometrioid adenocarcinoma had a 17 polysomy: one sample with 80% cells with three to four copies of the chromosome 17, one with 40% cells with 17 trisomy and one with 60% cells with 17 trisomy and 20% cells with four to six copies of the chromosome 17. The seven other cases of endometrioid adenocarcinoma were all disomic.

Discussion

The intimate mechanisms of endometriosis pathogenesis are still poorly understood and, as a consequence, medical treatments are usually quite limited and surgery is often the only option for advanced stages or deep infiltrating endometriosis. On the other hand, aggressive locations of endometriosis share similarities with tumour characteristics and targeted therapies could represent an interesting therapeutic alternative. Ovarian endometrioid adenocarcinoma can be a rare form of malignant transformation of endometriosis, which is the reason why it seemed interesting to study both types of specimens.

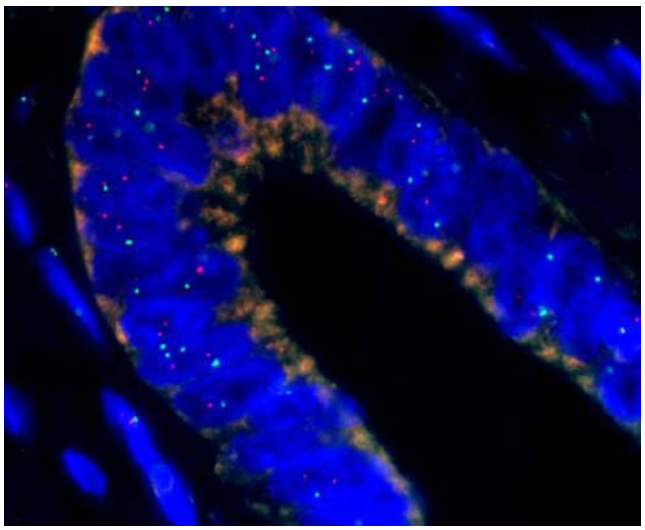

Fig. 1 Colorectal endometriosis with 17 disomy (centromere probes in *red* and HER2 probe in *green*)

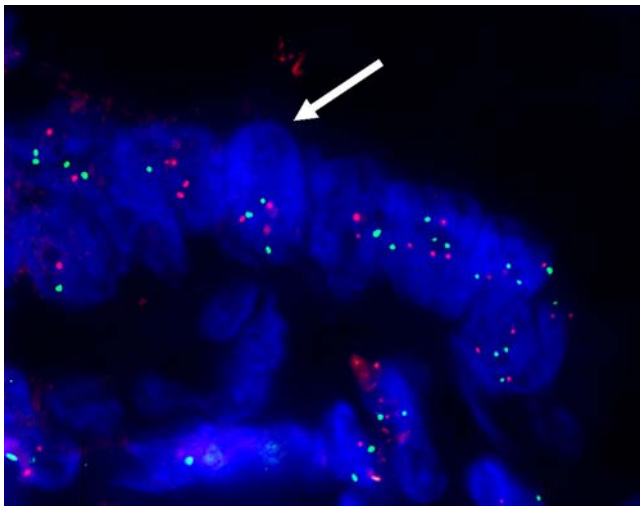

Fig. 2 Trisomy 17 in glandular cells of colorectal endometriosis (three spots *green* and *red* in the cell indicated with the *white arrow*)

We found no expression of HER1 or HER2 in glandular and stromal cells in the three principal locations of endometriosis, namely ovarian, peritoneal and colorectal (besides a weak expression in stromal cells in 15/20 colorectal samples which are difficult to interpret). These results are in line with those of Schneider et al. showing the absence of HER2 expression in a small series of endometriotic samples which, however, did not include severe forms of the disease [18]. In the same way, Nasu et al. also found no HER2 expression in epithelial and stromal cells, in a limited series of six endometriomas [17]. To the best of our knowledge, no expression of these two receptors was observed in ovarian endometrioid adenocarcinoma, a rare form of malignant transformation of endometriosis. This suggests that the EGF system may not be a target of interest for the treatment of endometriosis, but contrasts with the data of Marwah et al. showing that HER-2/neu expression was positive in 8% of benign ovarian cases and 38% of ovarian cancer and that HER-2/neu expression was significantly associated with high-grade ovarian tumours [19]. However, no case of endometriotic cyst was included in this series. Our data are also in keeping with in vitro study showing that Trastuzumab did not inhibited cell proliferation in an ovarian cell line (SKOV3) expressing low level of HER2 and in accordance with those of Malamou-Mitsi et al. finding a positive immunostaining for HER2 in only 18% of ovarian cancer which had no prognostic relevance after multivariate analysis [20, 21]. Nevertheless, in a preliminary study, Sasaki et al. suggested that ovarian cancer with an overexpression of HER-2/neu had a trend for chemoresistance [22].

The study of HER2 status was performed by IHC and FISH since although usually well correlated, the results of both techniques have been recently discordant in 8% to 10% of tumours [23, 24]. Moreover, even if it is used for targeting therapy, monosomy of the 17 chromosome or loss of HER2 if found (showed by FISH and not by IHC) could have been useful to better understand pathogenesis of endometriosis. In the present study, 18 of 20 colorectal endometriosis exhibited a 17 disomy with no HER2 gene amplification and the remaining two colorectal samples had a partial 17 aneusomy. To our knowledge, no similar results have been previously reported raising the issue of the implication of 17 aneusomy in the pathogenesis of deep infiltrating endometriosis. Inagaki et al. found no significant differences in the frequency and genotype distribution of the EGFR+2073 A/T and EGF+61 G/A polymorphisms between endometriosis patients with all disease stages and controls suggesting that these alterations are not associated with an increased risk of endometriosis [25]. These results partly contrast with those of Hsieh et al. suggesting that EGFR, a regulator of angiogenesis and mediator of sex steroid-induced cell growth and differentiation, particularly gene 2073*T-related genotypes and allele are associated with higher susceptibilities to endometriosis and leiomyoma [15]. We also observed a 17 polysomy in three cases of endometrioid adenocarcinoma while the other seven cases were all disomic. In a previous study, the HER-2/neu status was not found to correlate with progression of disease during first-line chemotherapy. Gene amplification of the HER-2/neu gene was found in all 3+-scored ovarian carcinomas [26]. Noack et al. have evaluated the expression of the same onco-protein in ovarian endometrioid adenocarcinoma arising in an endometriotic cyst [27]. Evaluating genomic instability by comparative genomic hybridization, apart from HER-2, all onco-proteins tested (bcl-2, c-MYC, cyclin D1, p53 and KIT) were more strongly expressed in epithelial cells of the adenocarcinoma than in cells of the endometriotic cyst. These results reinforce data suggesting that HER2 was not implicated in the malignant transformation of endometriotic cyst [27].

The best way to assess HER1 status is a matter of debate. In lung adenocarcinomas, the two known types of genetic alterations, namely mutations and amplifications, are so frequently associated that the optimal testing approach between mutation analysis and gene copy number analysis (by FISH or CISH) is under discussion [28]. Li et al. reported that, among EGFR-mutated cases, approximately 50% show increased EGFR gene copy number [29]. Conversely, 75% of cases with increased EGFR gene copy number show mutations [30]. Detection of EGFR mutation seems however to be a better predictor of outcome in patients treated with EGFR tyrosine kinase inhibitors (EGFR TKI) than EGFR copy number [31]. Therefore, for some authors, HER1 study by immunochemistry plays little role in selecting patients. In spite of this, the Tarceva (erlotinib, EGFR TKI) package only mentions EGFR IHC for determining treatment eligibility. In gastric carcinoma, patients with EGFR overexpression had unfavourable prognosis and correlation between IHC and FISH results was highly statistically significant since only one of the 371 cases was negative by IHC and positive by FISH [32]. This is why we decided to study the HER1 status only by IHC.

In conclusion, HER1 and HER2 are neither overexpressed in endometriosis, whatever its location, nor in ovarian endometrioid adenocarcinoma suggesting that the EGF pathway may not be a relevant target for medical therapy in these two pathological entities.

Acknowledgements The authors want to thank P. Duvillard and F. Drusch for their efficient help in this study

Conflicts of interest statement We declare that we have no conflicts of interest.

References

1. Casalini P, Iorio MV, Galmozzi E et al (2004) Role of HER receptors family in development and differentiation. J Cell Physiol 200:343–350
2. Bhargava R, Gerald WL, Li AR et al (2005) EGFR gene amplification in breast cancer: correlation with epidermal growth factor receptor mRNA and protein expression and HER-2 status and absence of EGFR-activating mutations. Mod Pathol 18:1027–1033
3. Pérez-Soler R (2004) HER1/EGFR targeting: refining the strategy. Oncologist 9:58–67
4. Brumm C, Rivière A, Wilckens C et al (1990) Immunohistochemical investigation and northern blot analysis of c-erB-2 expression in normal, premalignant and malignant tissues of the corpus and cervix uteri. Virchows Arch A Pathol Anat Histopathol 417:477–484
5. Press MF, Cordon-Cardo C, Slamon DJ (1990) Expression of the *HER-2/neu* proto-oncogene in normal human adult and fetal tissues. Oncogene 5:953–962
6. Wang DP, Fujii S, Konishi I et al (1992) Expression of c-erbB-2 protein and epidermal growth factor receptor in normal tissues of the female genital tract and in the placenta. Virchows Arch A Pathol Anat Histopathol 420:385–393
7. Ejskjaer K, Sørensen BS, Poulsen SS et al (2005) Expression of the epidermal growth factor system in human endometrium during the menstrual cycle. Mol Hum Reprod 11:543–551
8. Niikura H, Sasano H, Kaga K et al (1996) Expression of epidermal growth factor family proteins and epidermal growth factor receptor in human endometrium. Hum Pathol 27:282–289
9. Ejskjaer K, Sørensen BS, Poulsen SS et al (2007) Expression of the epidermal growth factor system in endometrioid endometrial cancer. Gynecol Oncol 104:158–167
10. Stovall DW, Bowser LM, Archer DF et al (1997) Endometriosis-associated pelvic pain: evidence for an association between the stage of disease and a history of chronic pelvic pain. Fertil Steril 68:13–18
11. Vercellini P, Trespidi L, De Giorgi O et al (1996) Endometriosis and pelvic pain: relation to disease stage and localization. Fertil Steril 65:299–304

12. Jenkins S, Olive DL, Haney AF (1986) Endometriosis: pathogenetic implications of the anatomic distribution. Obstet Gynecol 67:335–338
13. Dubernard G, Piketty M, Rouzier R et al (2006) Quality of life after laparoscopic colorectal resection for endometriosis. Hum Reprod 21:1243–1247
14. Vigano P, Somigliana E, Chiodo I et al (2006) Molecular mechanisms and biological plausibility underlying the malignant transformation of endometriosis: a critical analysis. Human Reprod Update 12:77–89
15. Hsieh YY, Chang CC, Tsai FJ et al (2005) T homozygote, allele of epidermal growth factor receptor 2073 gene polymorphism are associated with higher susceptibility to endometriosis and leiomyomas. Fertil Steril 83:796–799
16. Melega C, Balducci M, Bulletti C et al (1991) Tissue factors influencing growth and maintenance of endometriosis. Ann N Y Acad Sci 622:256–265
17. Nasu K, Hayata T, Takai N et al (1995) Immunohistochemical study of c-erb B-2 protein expression in endometriosis. Hum Reprod 10:935–937
18. Schneider J, Jimenez E, Rodriguez F et al (1998) c-myc, c-erb-B2, nm23 and p53 expression in human endometriosis. Oncol Rep 5:49–52
19. Marwah N, Bansal C, Gupta S et al (2007) Immunohistochemical study of the expression of HER-2/neu oncogene in ovarian lesions. Indian J Pathol Microbiol 50:489–492
20. Berek JS, Schultes BC, Nicodemus CF (2003) Biologic and immunologic therapies for ovarian cancer. J Clin Oncol 21:168–174
21. Malamou-Mitsi V, Crikoni O, Timotheadou E (2007) Prognostic significance of HER-2, p53 and Bcl-2 in patients with epithelial ovarian cancer. Anticancer Res 27:1157–1165
22. Sasaki N, Kudoh K, Kita T et al (2007) Effect of HER-2/neu overexpression on chemoresistance and prognosis in ovarian carcinoma. J Obstet Gynaecol Res 33:17–23
23. Tubbs RR, Pettay JD, Roche PC et al (2001) Discrepancies in clinical laboratory testing of eligibility for trastuzumab therapy: apparent immunohistochemical false-positives do not get the message. J Clin Oncol 19:2714–2721
24. Gong Y, Yan K, Lin F et al (2007) Determination of oestrogen-receptor status and ERBB2 status of breast carcinoma: a gene-expression profiling study. Lancet Oncol 8:203–211
25. Inagaki M, Yoshida S, Kennedy S et al (2007) Association study between epidermal growth factor receptor and epidermal growth factor polymorphisms and endometriosis in a Japanese population. Gynecol Endocrinol 24:1–5
26. Tuefferd M, Couturier J, Penault-Llorca F et al (2007) HER2 status in ovarian carcinomas: a multicenter GINECO study of 320 patients. PLoS ONE 2:1138
27. Noack F, Schmidt H, Buchweitz O (2004) Genomic imbalance and onco-protein expression of ovarian endometrioid adenocarcinoma arisen in an endometriotic cyst. Anticancer Res 24:151–154
28. Bunn PA Jr, Dziadziuszko R, Varella-Garcia M et al (2006) Biological markers for non-small cell lung cancer patient selection for epidermal growth factor receptor tyrosine kinase inhibitor therapy. Clin Cancer Res 12:3652–3656
29. Li AR, Chitale D, Riely GJ et al (1995) Immunohistochemical study of c-erb B-2 protein expression in endometriosis. Hum Reprod 10:935–937
30. Ladanyi M (2008) EGFR mutations in lung adenocarcinomas: clinical testing experience and relationship to EGFR gene copy number and immunohistochemical expression. J Mol Diagn 10:242–248
31. Ichihara S, Toyooka S, Fujiwara Y et al (2007) The impact of epidermal growth factor receptor gene status on gefitinib-treated Japanese patients with non-small-cell lung cancer. Int J Cancer 120:1239–1247
32. Kim MA, Lee HS, Lee HE et al (2008) EGFR in gastric carcinomas: prognostic significance of protein overexpression and high gene copy number. Histopathology 52:738–746

Virchows Arch (2009) 454:531–539
DOI 10.1007/s00428-009-0747-5

ORIGINAL ARTICLE

Diagnosis of autoimmune pancreatitis by core needle biopsy: application of six microscopic criteria

Sönke Detlefsen · Asbjørn Mohr Drewes · Mogens Vyberg · Günter Klöppel

Received: 30 December 2008 / Revised: 10 February 2009 / Accepted: 11 February 2009 / Published online: 24 February 2009

Abstract Autoimmune pancreatitis (AIP) has been established as a special entity of chronic pancreatitis (CP). However, its clinical distinction from pancreatic cancer and other types of CP is still difficult. The aim of this study was to evaluate the efficacy of pancreatic core needle biopsy for the diagnosis of AIP. In 44 core needle biopsy specimens, we assessed the following microscopic features: granulocytic epithelial lesions (GELs), more than ten IgG4-positive plasma cells/HPF, more than ten eosinophilic granulocytes/HPF, cellular fibrosis with inflammation, lymphoplasmacytic infiltration, and venulitis. All biopsies that showed four or more of the six features (22 of 44) were obtained from 21 of 26 patients whose clinical diagnosis and follow-up were consistent with AIP. All non-AIP CP patients (n=14) showed three or less than three of the features in their biopsies. GELs were only observed in biopsy specimens from AIP patients. In conclusion, our data indicate that the six criteria we applied were able to recognize AIP in 76% of biopsy specimens using a cut-off level of four. When the specimens that revealed only three features but showed GELs were added, the sensitivity rose to 86%. Pancreatic core needle biopsy can therefore make a significant contribution to the diagnosis of AIP.

Keywords Autoimmune pancreatitis · Diagnosis · Pancreatic biopsy · Granulocytic epithelial lesion · IgG4

S. Detlefsen (✉) · G. Klöppel
Department of Pathology,
University Hospital Schleswig-Holstein,
Campus Kiel, Arnold-Heller-Str.3, Haus 14,
24105 Kiel, Germany
e-mail: S.Detlefsen@gmx.net

S. Detlefsen · A. Mohr Drewes
Department of Gastroenterology, Mech-Sense, Aalborg Hospital,
Aalborg, Denmark

S. Detlefsen · M. Vyberg
Department of Pathology, Aalborg Hospital,
Aalborg, Denmark

Introduction

Autoimmune pancreatitis (AIP) has been established as a special entity of chronic pancreatitis (CP) that is responsive to steroid treatment. However, its clinical distinction from pancreatic cancer and other entities of CP is difficult because of the similarity of these diseases and the lack of a reliable marker of AIP [1].

According to the criteria of the Japan Pancreas Society, AIP can be diagnosed on the basis of imaging findings together with *either* laboratory findings (elevated levels of serum gammaglobulin and/or IgG or presence of autoantibodies) or histopathological findings (marked lymphoplasmacytic infiltration and fibrosis) [2, 3]. The criteria of the Korean working group include imaging, laboratory findings, histological findings, and response to steroid treatment. For the diagnosis of AIP, the imaging criterion is required along with any one of the other three features [4]. The criteria of the Mayo Clinic (HISORt criteria) are histopathology (marked lymphoplasmacytic infiltration and infiltration of more than ten IgG4-positive plasma cells per high power field (HPF)), imaging, serology, presence of other organ involvement, and response to steroid treatment [5]. In contrast to the other working groups, the Mayo Clinic group already diagnoses AIP if only the histology is positive. The fact that with the HISORt criteria AIP can be diagnosed on the basis of typical histopathological features alone gives pancreatic core needle biopsy a special significance. However, the role of pancreatic

core needle biopsy in the diagnosis of AIP is still controversial because the available data are sparse and its usefulness is not generally accepted. In a previous study, we found diagnostically relevant lesions in three of four core needle biopsy specimens [6]. In other studies, the effectiveness of core needle biopsy in diagnosing AIP was less significant [5, 7, 8]. This also held for fine-needle aspiration cytology, which was even thought to be barely suggestive of or even inadequate for the diagnosis of AIP [9–13].

We studied 44 pancreatic core needle biopsy specimens from 40 patients, which were obtained to establish the diagnosis of AIP or pancreatic cancer or alcoholic chronic pancreatitis. Most of the histopathological features we used for the diagnosis of AIP were recently established in resection specimens [6, 13–15]. Using six microscopic features of AIP, we wanted to know how many of these features are needed in a biopsy specimen to enable the diagnosis of AIP. In addition, we attempted to identify features whose presence in a biopsy enables the diagnosis of AIP also in those cases that lack significant infiltration with IgG4-positive plasma cells.

Materials and methods

Core needle biopsies

Forty-four pancreatic core needle biopsy specimens with CP were reviewed from 40 patients whose history, symptoms, and imaging criteria were suggestive of either AIP, pancreatic cancer, or alcoholic CP. Thirty-one specimens were retrieved from the consultation files of the Department of Pathology, University Hospital Schleswig-Holstein, Campus Kiel, Germany, and 13 from the files of the Department of Pathology, Aalborg Hospital, Denmark. The core needle biopsy specimens were obtained by transabdominal ultrasound (US)-guided core needle biopsy (n=33), intraoperative core needle biopsy (n=7), endoscopic US-guided core needle biopsy (n=3), and transabdominal computed-tomography-guided core needle biopsy (n=1). The biopsies were obtained from lesions localized in the pancreatic head (n=37), the pancreatic head–body (n=3), the pancreatic body (n=1), the pancreatic tail (n=2), and the entire pancreas (n=1). The mean length of the biopsy cylinders (with a width of approximately 1.2 mm) was 16.5 mm (range 4 to 48 mm). All biopsy specimens were fixed in formalin and embedded in paraffin. The sections were stained with hematoxylin and eosin. The mean number of slides evaluated per biopsy was 2.1 (range 1 to 11).

Immunohistochemistry

One slide from every biopsy specimen was immunostained for IgG4 using a monoclonal mouse antibody (The Binding Site, Birmingham, UK, clone HP6025) and the EnVision staining technique (Dako A/S, Glostrup, Denmark) with a working dilution of 1:100. The slides were first pretreated by boiling in citrate-buffered saline for 3.5 min. Endogenous phosphatase activity was blocked with 1 mM levamisole in the substrate solution. Normal tonsillar tissue served as controls.

Patients

Clinical information was obtained from either the medical and surgical records of the patients, from a questionnaire answered by the clinician and/or pathologist in charge, and/or by direct consultation with the clinician in charge.

During follow-up, 26 of the 40 patients fulfilled the criteria of the Mayo Clinic (HISORt criteria) and were diagnosed with AIP (16 men and ten women; mean age 51.2 years; range 10 to 79 years; Table 1) [5]. None of these patients developed malignant disease or had evidence of pancreatic pseudocysts or calculi. The mean follow-up period was 24 months, range 3 to 48 months. Eight of the 26 patients had other autoimmune-related diseases. Nineteen of the 26 patients were later treated with steroids, 18 of whom showed a clear-cut response. IgG4 serum levels were available in 12 patients (they were elevated in three and normal in nine).

Fourteen of the 40 patients (seven men and seven women; mean age 53.1 years; range 29 to 72 years) had non-AIP CP. These patients were diagnosed with alcoholic CP (n=7) or tumor-associated, obstructive CP (n=7; Table 2). In none of the seven tumor-associated core needle biopsy specimens, there was malignant cell infiltration. They derived from the margin of the tumor showing only fibrosis and inflammation. The mean follow-up period was 22.9 months, range 4 to 48 months.

Histopathological examination

Each core needle biopsy was evaluated for the presence of six microscopic AIP features [6, 13, 15–19]:

1. Granulocytic epithelial lesion (GEL): Focal disruption and destruction of the duct epithelium resulting from invasion of neutrophilic granulocytes into the lumen of medium- or large-sized interlobular ducts and/or invasion of neutrophilic granulocytes into the lumen of three or more small intralobular ducts together with neutrophilic infiltration between acinar cells (Fig. 1a).
2. IgG4-positive plasma cell infiltration: more than ten IgG4-positive plasma cells in at least one HPF at a magnification of ×400 (0.2 mm^2; Fig. 1b).
3. Eosinophilic infiltration: more than ten eosinophilic granulocytes in at least one HPF at a magnification of ×400 (0.2 mm^2; Fig. 2a).

Table 1 Clinicopathological features of 26 patients whose pancreatic core needle biopsy specimen was suggestive of AIP and whose follow-up was consistent with this diagnosis

CASE no.	Age	Sex	Other autoimmune disease	Total no. of AIP features in the specimen	GELs present in the specimen	>10 IgG4-positive plasma cells/HPF in the specimen	Serum IgG4	Steroid therapy
1	62	M	No	3	No	No	ND	ND
2	10	M	Chronic glomerulonephritis, Evan's syndrome	4	Yes	No	N	EF
3	46	M	No	5	No	Yes	ND	EF
4	50	M	Chronic parotitis	4	No	No	ND	EF
5	40	F	No	4	No	Yes	ND	EF
6	73	F	No	4	Yes	No	N	EF
7	46	F	No	5	Yes	No	ND	ND
8	75	M	No	4	No	Yes	E	NCE
9	64	M	No	4	No	Yes	ND	ND
10	72	F	No	4	Yes	No	ND	EF
11	51	M	Inflammatory subcutaneous pseudotumor	5	Yes	No	ND	ND
12	59	M	No	3	No	No	E	EF
13a[a]	36	F	No	4	Yes	No	N	EF
13b[a]	36	F	No	5	Yes	No	N	EF
14	32	M	No	3	Yes	No	N	EF
15	26	M	Suspected autoimmune hepatitis	6	Yes	Yes	ND	EF
16	53	M	Ulcerative colitis, Hashimoto's thyroiditis	5	No	Yes	N	EF
17	58	M	No	3	No	Yes	E	EF
18	79	F	No	4	No	Yes	N	EF
19	53	M	No	5	Yes	No	N	EF
20	19	F	No	3	Yes	No	N	EF
21	54	F	Hashimoto's thyroiditis	4	Yes	No	N	EF
22a[a]	57	M	No	3	No	Yes	ND	ND
22b[a]	57	M	No	5	No	Yes	ND	ND
23a[a]	38	M	Intrahepatic cholangiogram with PSC-like changes	3	Yes	No	ND	EF
23b[a]	38	M	Intrahepatic cholangiogram with PSC-like changes	4	Yes	No	ND	EF
24	60	F	Wegener's granulomatosis	4	No	Yes	ND	EF
25	53	F	No	4	No	Yes	ND	ND
26	65	M	No	4	No	No	ND	ND

F female, *M* male, *PSC* primary sclerosing cholangitis, *E* elevated, *N* normal, *ND* not determined, *EF* effective, *NCE* no clear-cut effect

[a] Patients from whom two biopsy specimens were obtained at an interval of several weeks.

4. Cellular fibrosis with inflammation: Fibrotic tissue usually arranged in a perilobular pattern and intermingled with myofibroblasts and at least 20 lymphocytes and/or plasma cells, if present in at least one field of view at a magnification of ×200 (0.6 mm^2; Fig. 2b).
5. Lymphoplasmacytic infiltration: two patterns were distinguished, periductal lymphoplasmacytic infiltration and diffuse infiltration. The diffuse infiltrate covered >30% of the total area of the biopsy specimen (Fig. 3a).
6. Venulitis: Dense lymphocytic infiltration in the tissue surrounding one or several venules, often accompanied by vessel obliteration and endothelial damage (Fig. 3b).

Statistical analysis

Statistical analysis was carried out using SigmaStat 3.0. Results obtained in core biopsy specimens from AIP patients and core biopsy specimens from patients diagnosed

Table 2 Clinicopathological features of 14 patients whose pancreatic core needle biopsy specimen met three or less features for the diagnosis of autoimmune pancreatitis and whose follow-up was consistent with the diagnosis of either alcoholic chronic pancreatitis (CP) or tumor-associated obstructive CP

CASE no.	Age	Sex	No. of AIP features observed per specimen	Main clinical features	Treatment	Diagnosis
1	50	M	2	Intake of >80 g alcohol/day for at least 10 years/recurrent acute bursts of CP	Conservative	Alcoholic CP
2[a]	57	M	1	Intake of >80 g alcohol/day for several years/recurrent acute bursts of CP	Conservative	Alcoholic CP
3	29	M	0	Intake of >80 g alcohol/day for several years/recurrent acute bursts of CP	Cholecystectomy/stenting of bile duct/pain treatment with opioids	Alcoholic CP
4	48	F	0	Intake of >80 g alcohol/day for several years/recurrent acute bursts of CP	Percutaneous drainage of pseudocysts/ gastrocystostomy/oral antidiabetics	Alcoholic CP
5	46	F	0	Intake of >80 g alcohol/day for several years/ERCP with short stenoses of the main pancreatic duct	Subcutaneous insulin/choledocho-duodenostomy	Alcoholic CP
6a[b]	47	F	3	Intake of >80 g alcohol/day for several years/recurrent acute bursts of CP/abdominal US: intrapancreatic calcifications	Percutaneous drainage of pseudocysts/ subcutaneous insulin/enzyme substitution/ pain treatment with opioids	Alcoholic CP
6b[b]	50	F	2	Intake of >80 g alcohol/day for several years/recurrent acute bursts of CP/abdominal US: intrapancreatic calcifications	Percutaneous drainage of pseudocysts/ subcutaneous insulin/enzyme substitution/ pain treatment with opioids	Alcoholic CP
7	51	F	3	Intake of >80 g alcohol/day for several years/recurrent acute bursts of CP/abdominal US: pseudocysts	Pain treatment with opioids	Alcoholic CP
8	60	M	3	Pancreatic mucinous cystadenoma[c]	Whipple resection/reoperation for intraabdominal abscesses with poor overall outcome	Obstructive CP
9	53	F	2	Metastasizing pancreatic ductal adenocarcinoma	Palliation	Obstructive CP
10	71	F	1	Metastasizing pancreatic ductal adenocarcinoma	Palliation	Obstructive CP
11	72	M	0	Metastasizing pancreatic ductal adenocarcinoma[c]	Gastroenterostomy/palliation	Obstructive CP
12	56	F	0	Pancreatic solid-pseudopapillary tumor[c]	Whipple resection/good outcome	Obstructive CP
13	38	M	3	Metastasizing pancreatic ductal adenocarcinoma	Chemotherapy	Obstructive CP
14[a]	69	M	2	Advanced pancreatic ductal adenocarcinoma w. infiltration of superior mesenteric vein[c]	Cholangio- and gastrojejunostomy/palliation	Obstructive CP

ERCP endoscopic retrograde cholangio-pancreaticography, *US* ultrasound

[a] Specimens showing IgG4 positivity (more than ten IgG4-positive plasma cells/HPF) as one criterion

[b] Patient from whom two biopsy specimens were obtained at an interval of 3 years

[c] Final diagnosis in resection specimen

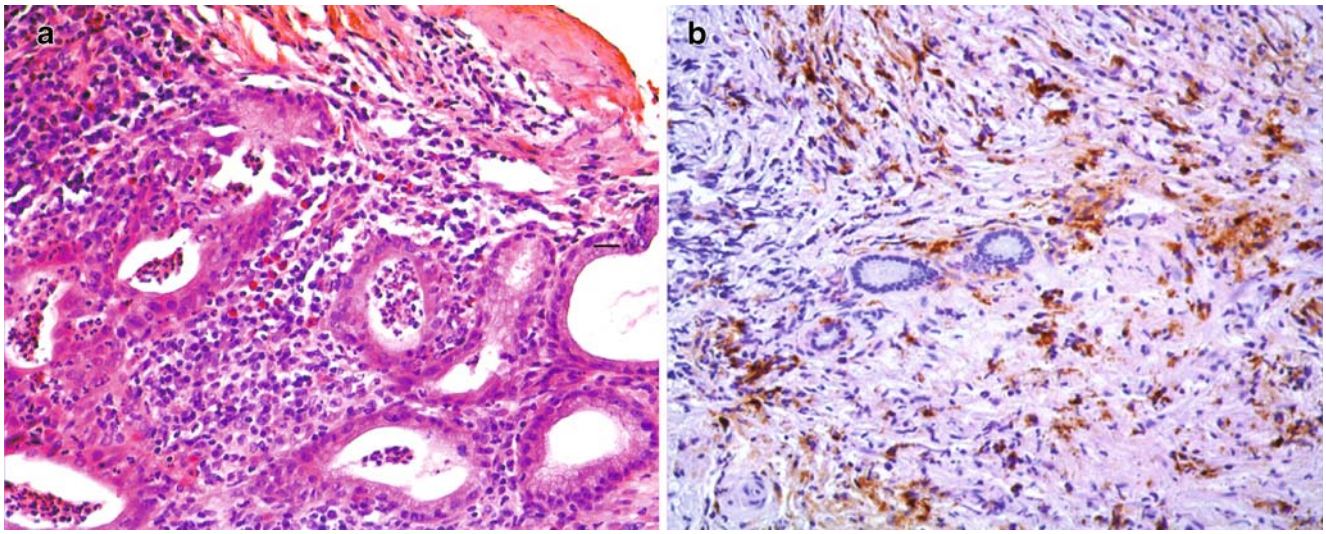

Fig. 1 Pancreatic core needle biopsy specimens from AIP patients. **a** Granulocytic epithelial lesions (hematoxylin and eosin, ×200). **b** Increased numbers of IgG4 immunopositive plasma cells (×200)

with other types of CP were evaluated using Fisher's exact test (Table 3) and the χ^2 test for tabulated data (Table 4). The level of significance was set at $p<0.05$.

Results

In 22 of the 44 pancreatic core biopsy specimens, four or more of the six features were present Table 3. There was no clear correlation between the length of the biopsy cylinder and the number of features observed in the tissue. The 22 specimens were obtained from 21 of 26 patients whose clinical diagnosis was consistent with AIP (Table 1). In the remaining 22 of 44 specimens, 11 showed three features. Seven of these were from seven of 26 patients with the clinical diagnosis of AIP. Only four of 11 specimens with three features were associated with non-AIP CP (Table 2). All biopsy specimens with two or fewer features were from non-AIP CP patients (Table 3). Among the 29 biopsy specimens from the 26 AIP patients, there were 14 biopsy specimens that revealed GELs, a feature that was not observed in any of the 15 non-AIP CP biopsy specimens (Table 1; Fig. 1a). If the three biopsy specimens that showed only three features, including GELs, were added to the 22 specimens showing four or more criteria, all of which came from 21 of 26 AIP patients, a total of 25 of 29

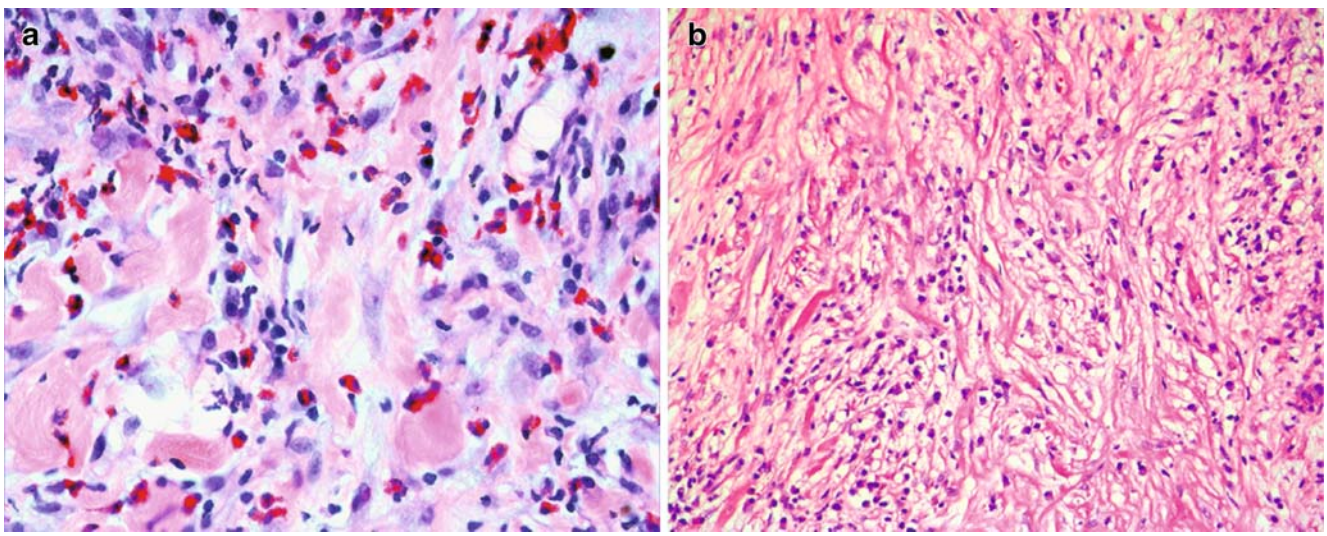

Fig. 2 Pancreatic core needle biopsy specimens from AIP patients. **a** Infiltration by eosinophilic granulocytes (hematoxylin and eosin, ×400). **b** Cellular fibrosis with an inflammatory infiltrate replacing acinar tissue (hematoxylin and eosin, ×200)

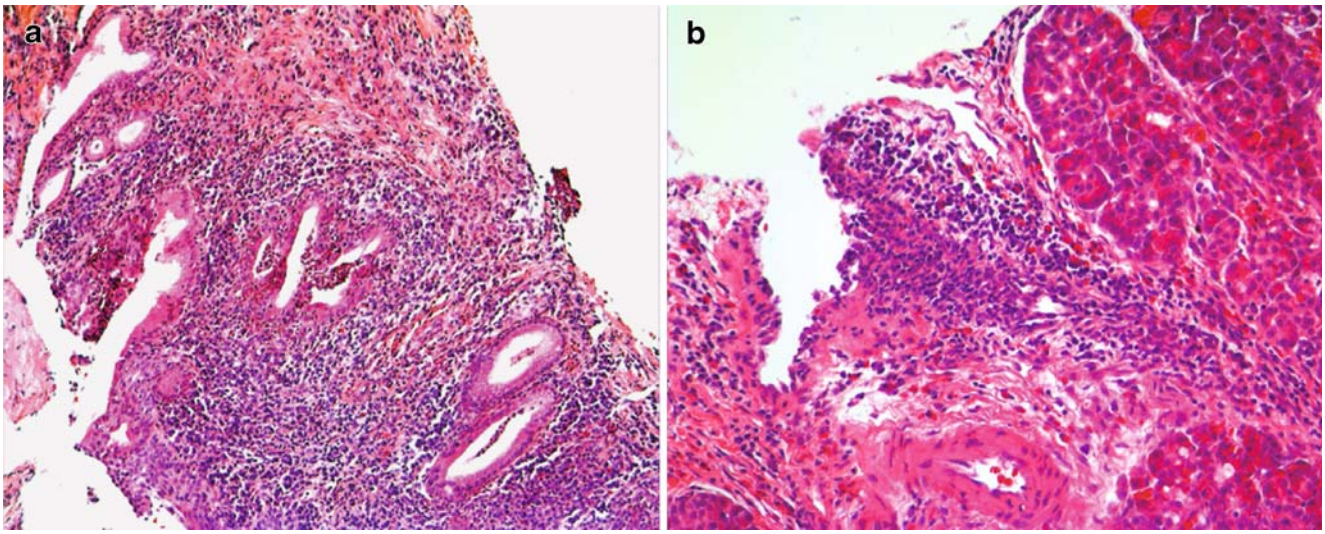

Fig. 3 Pancreatic core needle biopsy specimens from AIP patients. **a** Periductal lymphoplasmacytic infiltration (hematoxylin and eosin, ×100). **b** Venulitis (hematoxylin and eosin, ×200)

(86%) biopsy specimens (from 23 of 26 AIP patients) were associated with AIP.

More than ten IgG4-positive cells were found in 14 of 44 biopsy specimens (Fig. 1b), of which 12 of 29 were from 11 of 26 AIP patients (Table 4). These 12 of 29 specimens were negative for GELs and eosinophilic granulocytes (>10/HPF), except for one case that revealed both IgG4-positive plasma cells and GELs (Table 1). Of the 17 IgG4-negative AIP specimens, on the other hand, 11 revealed positivity for eosinophils and 13 for GELs. Among the seven AIP specimens that showed only three features, five showed either GELs (three of seven) or more than ten IgG4-positive plasma cells (two of seven). In the remaining two of seven specimens, other features were present. Cellular fibrosis was found in almost all AIP specimens (28 of 29; Table 4; Fig. 2b). However, it was also found in six of 15 specimens from non-AIP CP patients (Table 4). Next in frequency were lymphoplasmacytic infiltration (27 of 29; Fig. 3a) and venulitis (19 of 29; Fig. 3b), but both features were also recorded in biopsy specimens from non-AIP CP patients, though only in a few instances (Table 4). The number of AIP features noted in the AIP core needle biopsy specimens was significantly higher than the frequency recorded in the biopsy specimens from the non-AIP CP patients ($p<0.001$).

In 11 of the 44 pancreatic core needle biopsy specimens, two or fewer of the six features were present (Tables 2 and 3). All 11 specimens were obtained from 11 of 14 patients whose clinical diagnosis was consistent with non-AIP CP. In addition, there were four specimens obtained from non-AIP CP patients that contained three of the features. Hence, none of the 15 core biopsy specimens from 14 patients diagnosed

Table 3 Number of microscopic features per specimen observed in 29 core needle biopsy specimens from 26 patients whose clinical diagnosis and follow-up were consistent with autoimmune pancreatitis (AIP) and in 15 core needle biopsy specimens from 14 patients with symptoms consistent with non-AIP chronic pancreatitis (non-AIP CP) consisting of alcoholic CP and tumor-associated, obstructive CP

Number of features per specimen	AIP	Non-AIP CP
0	0% (0/29)	33.3% (5/15)
1	0% (0/29)	13.3% (2/15)
2	0% (0/29)	26.7% (4/15)
3	24.1% (7/29)	26.7% (4/15)
4	48.3% (14/29)	0% (0/15)
5	24.1% (7/29)	0% (0/15)
6	3.5% (1/29)	0% (0/15)

Table 4 Frequency of the individual features in pancreatic core needle biopsy specimens

Feature	AIP	Non-AIP CP
Granulocytic epithelial lesion (GEL)	48.3% (14/29)	0% (0/15)
>10 IgG4 positive plasma cells/HPF	41.4% (12/29)	13.3% (2/15)
>10 eosinophilic granulocytes/HPF	62.1% (18/29)	33.3% (5/15)
Cellular fibrosis with inflammation	96.6% (28/29)	40.0% (6/15)
Lymphoplasmacytic infiltration	93.1% (27/29)	33.3% (5/15)
Venulitis	65.5% (19/29)	26.7% (4/15)

Twenty-nine specimens derived from 26 patients whose clinical diagnosis and follow-up were consistent with autoimmune pancreatitis (AIP). The remaining 15 specimens were from 14 patients with symptoms consistent with non-AIP chronic pancreatitis (non-AIP CP), consisting of alcoholic CP and tumor-associated, obstructive CP

with other types of CP showed more than three of the features or GELs (Table 3). Infiltration by more than ten IgG4-positive plasma cells/HPF was observed in two of the non-AIP CP specimens (Table 4). Cellular fibrosis and lymphoplasmacytic infiltration were seen in six of 15 and five of 15 cases, respectively. The latter feature was lacking a periductal association, but instead showing a diffuse pattern. Infiltration by more than ten eosinophilic granulocytes/HPF and changes compatible with venulitis were recorded in five of 15 and four of 15 specimens, respectively. The difference in frequency of each of the six features between AIP and non-AIP CP specimens was not statistically significant (p=0.8; Table 4).

Discussion

AIP shows distinct histopathological features that allow it to be diagnosed in pancreatic resection specimens without great difficulty and that distinguish it clearly from other types of CP and also from ductal adenocarcinoma [6, 15, 20, 21]. However, in pancreatic biopsy specimens, AIP seems to be difficult to recognize [5, 7, 9, 22]. Hence, the usefulness of pancreatic biopsy for the diagnosis of AIP has been debated [23]. In this study, we reviewed 44 pancreatic core needle biopsy specimens from 40 patients. These specimens were obtained to establish the diagnosis of AIP or alcoholic CP or pancreatic cancer. Most of the histopathological AIP features that we used in this study had been recently defined in pancreatic specimens obtained by surgical resection [6]. Our data show that with the six chosen microscopic features, we were able to recognize AIP in 76% (22 of 29) of core needle biopsy specimens from 21 of 26 patients whose clinical diagnosis was compatible with AIP, when we used a cut-off level of four features. Moreover, this figure rose to 86% (25 of 29), when we added those specimens that showed three features but contained GELs. On the other hand, all cases that showed two or fewer features came from non-AIP CP patients. The number of features observed was not clearly correlated to the length of the biopsy cylinder.

Few data exist on the usefulness of pancreatic core needle biopsy for the diagnosis of AIP. In 2004, we evaluated five wedge biopsy specimens and four core needle biopsy specimens [6]. Among the core needle biopsy specimens, one was regarded as diagnostic, two as "suggestive of AIP", and one as "inconclusive" [6]. In a series of five core needle biopsy specimens, Deshpande found only one to be diagnostic because the two histological hallmarks of AIP, periductal collar of inflammation and venulitis, were only present in this specimen [8]. Levy reported on three AIP cases for which trucut biopsy specimens were available. They were able to establish the diagnosis of AIP in two of the three cases [24]. In another study including 16 pancreatic core needle biopsy specimens deriving from AIP patients, seven showed the "full spectrum" of characteristic histological changes [5]. The largest survey of core biopsy specimens so far came from 22 Japanese AIP patients [7]. In this study, which relied on the presence of periductal lymphoplasmacytic infiltrates, cellular fibrosis and venulitis as well as the demonstration of more than ten IgG4-positive plasma cells per HPF as a diagnostic criterion of AIP, the diagnosis was only made in six of 22 (27%) cases.

In our series of 44 core needle biopsy specimens from the pancreas, 22 showed four of the six features we had chosen. All of these 22 biopsy specimens were obtained from 21 patients whose clinical diagnosis and follow-up were consistent with AIP. In contrast, the specimens obtained from patients with non-AIP CP never displayed more than three of the six features, and seven of 15 (obtained from seven patients) revealed none or only one of them. This suggests that the presence of four or more of the microscopic features that we chose is highly diagnostic of AIP in a pancreatic core needle biopsy specimen.

Among the applied features, most crucial and discriminative were the presence of GELs and the demonstration of more than ten IgG4-positive plasma cells per HPF (Table 4). GELs were not noted in non-AIP CP cases, suggesting that GELs can be regarded as diagnostic of AIP. Apart from the AIP cases, more than ten IgG4-positive plasma cells were also seen in two of 15 non-AIP CP cases, implying that the abundance of IgG4-positive plasma cells is suggestive of, but not specific to, AIP. Although these two features, the presence of GELs and the abundance of IgG4-positive plasma cells, play a crucial role in the diagnosis of AIP, they also have their limitations in view of the two types of AIP that can be currently distinguished. As we and others have shown, GELs and IgG4 positivity are features that may distinguish two subgroups of AIP [6, 25, 26]. One subgroup displays GELs and seems to lack increased numbers of IgG4-positive plasma cells in the pancreas and probably also elevated serum IgG4 levels. This AIP subtype has also been called "ductocentric AIP" [27] or "idiopathic duct destructive pancreatitis" [25]. In our series of resection specimens, it accounted for almost 45% of the AIP cases [6]. In the present study, 13 of 29 (45%) AIP core needle biopsies from 11 of 26 patients were IgG4−/GEL+, while one of 29 AIP biopsies from ten of 26 patients were IgG4+/GEL+, and 11 of 29 AIP biopsies were IgG4+/GEL−. Importantly, we took into account GELs not only when present in medium- and large-sized interlobular ducts but also when seen in small intralobular ducts.

The second subtype, which was found to be GEL negative, appears to correspond to the AIP subtype that has been called "lymphoplasmacytic sclerosing pancreatitis"

[25] or "lobulocentric AIP" [27]. This subtype seems to present with abundant IgG4-positive plasma cells within the lymphoplasmacytic infiltrates [26]. These data provide an explanation why in our current study almost half of the AIP specimens were IgG4 negative, but at the same time GEL positive, or vice versa. The features IgG4 positivity and GEL may therefore be complementary to each other as they appear to characterize two different subtypes of AIP. It is interesting to note that the relative frequency of the two AIP subtypes in Europe and the US seems to differ from that in East Asia. While in Europe each subtype can be expected in about 40–50% of the cases (in our present biopsy series they amount to 38% and 45%, respectively), the GEL-positive AIP subtype seems to be rare in East Asia [1, 28–35].

Because the presence of GELs seems to be specific to one subtype of AIP, a diagnosis of AIP can be made if GELs are recognized in a biopsy specimen, regardless of the number of other features found. Among the microscopic features that were less discriminative were the demonstration of a lymphoplasmacytic infiltration, cellular perilobular fibrosis with inflammation, venulitis, and increased numbers of eosinophilic granulocytes because each of these changes were also identified in a small number of non-AIP CP cases. Therefore, it was necessary to set a cut-off level for the number of criteria that are required for the diagnosis of AIP in a pancreatic core needle biopsy specimen.

In conclusion, our microscopic criteria were able to recognize AIP in 22 of 29 (76%) core needle biopsy specimens from 21 of 26 AIP patients when using a cut-off level of four features and in 25 of 29 biopsies (86%) from 23 of 26 AIP patients when the GEL-positive cases were added. Core needle biopsy is therefore in many patients a useful adjunct for recognizing AIP and distinguishing it from other diseases such as alcoholic CP or obstructive CP secondary to pancreatic cancer. However, our criteria for the diagnosis of AIP in pancreatic core needle biopsies have to be tested on a larger number of patients in a prospective study before the utility of our findings can be fully appreciated.

Acknowledgments This study was supported by the Danish Medical Association Research Fund/The Johanne Dorthe Due Estate.

Conflict of interest statement The authors declare that they have no conflict of interest.

References

1. Löhr M (2007) What are the useful biological and functional markers of early-stage chronic pancreatitis? J Gastroenterol 42 (Suppl 17):66–71
2. Japan Pancreas Society (2002) Diagnostic criteria for autoimmune pancreatitis. J Jpn Pancreas Soc 17:585–587
3. Okazaki K, Uchida K, Matsushita M et al (2007) How to diagnose autoimmune pancreatitis by the revised Japanese clinical criteria. J Gastroenterol 42(Suppl 18):32–38
4. Kim KP, Kim MH, Kim JC et al (2006) Diagnostic criteria for autoimmune chronic pancreatitis revisited. World J Gastroenterol 12:2487–2496
5. Chari ST, Smyrk TC, Levy MJ et al (2006) Diagnosis of autoimmune pancreatitis: the Mayo Clinic experience. Clin Gastroenterol Hepatol 4:1010–1016
6. Zamboni G, Lüttges J, Capelli P et al (2004) Histopathological features of diagnostic and clinical relevance in autoimmune pancreatitis: a study on 53 resection specimens and 9 biopsy specimens. Virchows Arch 445:552–563
7. Bang SJ, Kim MH, Kim dH et al (2008) Is pancreatic core biopsy sufficient to diagnose autoimmune chronic pancreatitis? Pancreas 36:84–89
8. Deshpande V, Mino-Kenudson M, Brugge W et al (2005) Autoimmune pancreatitis: more than just a pancreatic disease? A contemporary review of its pathology. Arch Pathol Lab Med 129:1148–1154
9. Deshpande V, Mino-Kenudson M, Brugge WR et al (2005) Endoscopic ultrasound guided fine needle aspiration biopsy of autoimmune pancreatitis: diagnostic criteria and pitfalls. Am J Surg Pathol 29:1464–1471
10. Farrell JJ, Garber J, Sahani D et al (2004) EUS findings in patients with autoimmune pancreatitis. Gastrointest Endosc 60:927–936
11. Pace A, Topalidis T, Bläker M et al (2007) Autoimmune pancreatitis with normal IgG4-levels: 4 case reports and review of the literature. Z Gastroenterol 45:1245–1251
12. Salla C, Chatzipantelis P, Konstantinou P et al (2007) EUS-FNA contribution in the identification of autoimmune pancreatitis: a case report. JOP 8:598–604
13. Weber SM, Cubukcu-Dimopulo O, Palesty JA et al (2003) Lymphoplasmacytic sclerosing pancreatitis: inflammatory mimic of pancreatic carcinoma. J Gastrointest Surg 7:129–137
14. Klimstra DS, Adsay NV (2004) Lymphoplasmacytic sclerosing (autoimmune) pancreatitis. Semin Diagn Pathol 21:237–246
15. Klöppel G, Lüttges J, Löhr M et al (2003) Autoimmune pancreatitis: pathological, clinical, and immunological features. Pancreas 27:14–19
16. Abraham SC, Leach S, Yeo CJ et al (2003) Eosinophilic pancreatitis and increased eosinophils in the pancreas. Am J Surg Pathol 27:334–342
17. Klöppel G, Lüttges J, Sipos B et al (2005) Autoimmune pancreatitis: pathological findings. JOP 6:97–101
18. Klöppel G, Sipos B, Zamboni G et al (2007) Autoimmune pancreatitis: histo- and immunopathological features. J Gastroenterol 42(Suppl 18):28–31
19. Detlefsen S, Sipos B, Zhao J et al (2008) Autoimmune pancreatitis: expression and cellular source of profibrotic cytokines and their receptors. Am J Surg Pathol 32:986–995
20. Finkelberg DL, Sahani D, Deshpande V et al (2006) Autoimmune pancreatitis. N Engl J Med 355:2670–2676
21. Ectors N, Maillet B, Aerts R et al (1997) Non-alcoholic duct destructive chronic pancreatitis. Gut 41:263–268
22. Levy MJ, Wiersema MJ, Chari ST (2006) Chronic pancreatitis: focal pancreatitis or cancer? Is there a role for FNA/biopsy? Autoimmune pancreatitis. Endoscopy 38(Suppl 1):S30–S35
23. Kwon S, Kim MH, Choi EK (2007) The diagnostic criteria for autoimmune chronic pancreatitis: it is time to make a consensus. Pancreas 34:279–286
24. Levy MJ, Reddy RP, Wiersema MJ et al (2005) EUS-guided trucut biopsy in establishing autoimmune pancreatitis as the cause of obstructive jaundice. Gastrointest Endosc 61:467–472
25. Notohara K, Burgart LJ, Yadav D et al (2003) Idiopathic chronic pancreatitis with periductal lymphoplasmacytic infiltration: clinicopathologic features of 35 cases. Am J Surg Pathol 27:1119–1127
26. Zhang L, Notohara K, Levy MJ et al (2007) IgG4-positive plasma cell infiltration in the diagnosis of autoimmune pancreatitis. Mod Pathol 20:23–28

27. Deshpande V, Chicano S, Finkelberg D et al (2006) Autoimmune pancreatitis: a systemic immune complex mediated disease. Am J Surg Pathol 30:1537–1545
28. Pearson RK, Longnecker DS, Chari ST et al (2003) Controversies in clinical pancreatology: autoimmune pancreatitis: does it exist? Pancreas 27:1–13
29. Kleeff J, Welsch T, Esposito I et al (2006) Autoimmune pancreatitis–a surgical disease? Chirurg 77:154–165
30. Aparisi L, Farre A, Gomez-Cambronero L et al (2005) Antibodies to carbonic anhydrase and IgG4 levels in idiopathic chronic pancreatitis: relevance for diagnosis of autoimmune pancreatitis. Gut 54:703–709
31. Kojima M, Sipos B, Klapper W et al (2007) Autoimmune pancreatitis: frequency, IgG4 expression, and clonality of T and B cells. Am J Surg Pathol 31:521–528
32. Choi EK, Kim MH, Lee TY et al (2007) The sensitivity and specificity of serum immunoglobulin G and immunoglobulin G4 levels in the diagnosis of autoimmune chronic pancreatitis: Korean experience. Pancreas 35:156–161
33. Hamano H, Kawa S, Horiuchi A et al (2001) High serum IgG4 concentrations in patients with sclerosing pancreatitis. N Engl J Med 344:732–738
34. Nahon UK, Levy P, O'Toole D et al (2005) Is idiopathic chronic pancreatitis an autoimmune disease? Clin Gastroenterol Hepatol 3:903–909
35. Hochwald SN, Hemming AW, Draganov P et al (2008) Elevation of serum IgG4 in Western patients with autoimmune sclerosing pancreatocholangitis: a word of caution. Ann Surg Oncol 15:1147–1154

Virchows Arch (2009) 454:541–548
DOI 10.1007/s00428-009-0764-4

ORIGINAL ARTICLE

β_{III}-tubulin at the invasive margin of colorectal cancer: possible link to invasion

A. Portyanko · P. Kovalev · J. Gorgun · E. Cherstvoy

Received: 6 November 2008 / Revised: 14 March 2009 / Accepted: 18 March 2009 / Published online: 10 April 2009

Abstract Cell locomotion, including cancer cell invasion, is closely associated with the dynamics of cytoskeletal structures. Previous in vitro studies indicated that tubulin isotype composition may affect polymerization properties and dynamics of microtubules. Colorectal cancer is a good model for studying tumour invasion because of the easily detectable invasive front. Hence, we investigated the localization of β_{III}-tubulin in colorectal cancer specimens. Immunohistochemical staining for β_{III}-tubulin was evident in cancer cells apparently budding from adjacent malignant cells with a higher differentiation and negative staining. An association between β_{III}-tubulin immunoreactivity and tumour budding grade was demonstrated. To the best of our knowledge, this is the first report documenting a preferential localization of β_{III}-tubulin in the invading epithelium. From this finding arises the possibility that changes in tubulin isotypes could modulate the invading activity of cancer cells. Further investigations are needed to determine whether our findings have clinical implications.

Keywords Colorectal cancer · Immunohistochemistry · β_{III}-tubulin · Tumour budding · Cytoskeleton · Invasion

A. Portyanko (✉) · E. Cherstvoy
Department of Pathology, Belarusian State Medical University,
220116 Dzerzhynsky Ave. 83,
Minsk, Belarus
e-mail: aportyanko@yahoo.com

P. Kovalev
Department of Oncomorphology, City Pathological Bureau,
220116 Semashko St. 8/5,
Minsk, Belarus

J. Gorgun
Department of Gastroenterology and Nutrition,
Belarusian Medical Academy of Postgraduate Education,
220013 P Brovky st 3-3,
Minsk, Belarus

Introduction

The treatment of cancer is a worldwide problem. Unfortunately, the anticancer drugs that are presently used in the clinic have only limited success. To provide a significant clinical advance, new concepts have to be introduced to aid the design of new tools for therapy. The understanding of mechanisms of tumour growth and progression is critical for development of novel anticancer drugs. Metastatic dissemination of the cancer is primarily responsible for treatment failure, morbidity and death in cancer patients. Once cancer cells have spread and formed secondary masses (metastases), cancers are largely incurable despite the progress in medicine.

Invasion is a significant step in metastasing cascade in malignant tumours. Cell locomotion, including cancer cell invasion, is closely associated with the dynamics of cytoskeletal structures. Microtubules are indispensable for the directional migration of cells. Tubulin, the major constituent protein of microtubules, is a heterodimer of α and β subunits. Both α and β exist in multiple isotypic forms. Previous in vitro studies indicated that tubulin isotype composition may affect polymerization properties and dynamics of microtubules. It was shown in vitro that the growing and shortening dynamics of microtubules depends on the isotypic composition of the tubulin itself [1–4]. Microtubules assembled from the purified $\alpha\beta_{III}$ isotype were considerably more dynamic than microtubules made from the $\alpha\beta_{II}$ or $\alpha\beta_{IV}$ isotypes or from unfractionated phosphocellulose-purified tubulin [4]. Furthermore, increasing the proportion of the $\alpha\beta_{II}$ isotype in a mixture of the $\alpha\beta_{II}$ and $\alpha\beta_{III}$ isotypes suppressed microtubule dynamics, demonstrating that microtubule dynamics can be influenced by the tubulin isotype composition [4]. Moreover, different tubulin isotypes are associated with different sensitivity of cancer cells to chemotherapeutic agents. Microtubules composed of either β_{III}- or β_{IV}-tubulin

are considerably less sensitive to the suppressive effects of Taxol on microtubule dynamics, than microtubules assembled from β_{II} or unfractionated tubulin [5]. Studies with taxol, colchicine and estramustine indicate that drug interactions with tubulin isotypes differ [2, 6–9] and might contribute to cell resistance to antimitotics [10–12].

Colorectal cancer (CRC) is a major global health problem with more than a million new cases diagnosed worldwide every year. Moreover, colorectal cancer is a good model for studying tumour invasion because of the easily detectable invasive front. The invasive edge of human CRC is characterised in most cases by presence of tumour budding which is associated with poor prognosis [13, 14].

In the present study, we report the localization of β_{III}-tubulin in human CRC specimens.

Materials and methods

Tissue samples

For this study, formalin-fixed, paraffin-embedded surgical specimens of 32 tumours from 31 patients with non-mucous well- and moderately differentiated colorectal adenocarcinomas were retrieved (Table 1). The tissue specimens were dissected from the edge of the tumours to ensure that they contained the invasive part of the tumours. All tumour samples were examined histopathologically. Tumour stage was defined according to the TNM classification (sixth edition) [15]. Tumour budding was defined as the presence of isolated cells or small cell clusters scattered in the stroma at the invasive margin of the tumour [13].

Table 1 Patients and clinicopathological data

Tumour	Patient	Age	Gender	TNM	Localization	Number of tumour buds per field
1	1	66	F	T2 N0 M0	Rectum	21
2	2	54	F	T3 N0 M0	Ascending	30
3	3	62	M	T3 N0 M0	Sigmoid	40
4	4	78	M	T3 N0 M0	Sigmoid	5
5	5	73	M	T3 N0 M0	Sigmoid	49
6	6	77	F	T4 N2 M0	Sigmoid	4
7	6	77	F	T3 N2 M0	Rectum	32
8	7	47	M	T3 N2 M0	Transverse	58
9	8	80	M	T2 N0 M0	Rectum	74
10	9	68	F	T3 N0 M0	Sigmoid	106
11	10	67	F	T3 N0 M0	Rectum	46
12	11	71	F	T1 N0 M0	Sigmoid	25
13	12	77	F	T3 N0 M0	Sigmoid	141
14	13	65	M	T4 N0 M0	Transverse	51
15	14	65	M	T3 N2 M1	Rectum	42
16	15	70	M	T3 N1 M0	Ascending	12
17	16	74	F	T3 N0 M0	Sigmoid	21
18	17	79	M	T4 N1 M1	Sigmoid	32
19	18	60	M	T4 N1 M0	Sigmoid	11
20	19	77	M	T3 N1 M1	Caecum	24
21	20	57	F	T3 N1 M0	Ascending	16
22	21	67	F	T3 N0 M0	Rectum	10
23	22	50	M	T4 N2 M0	Sigmoid	21
24	23	66	F	T3 N0 M0	Rectum	0
25	24	50	F	T2 N1 M0	Sigmoid	38
26	25	70	F	T4 N2 M0	Sigmoid	45
27	26	77	F	T3 N0 M0	Transverse	38
28	27	57	F	T3 N2 M0	Sigmoid	17
29	28	56	M	T3 N2 M0	Rectum	39
30	29	60	M	T3 N1 M0	Descending	5
31	30	76	M	T3 N0 M0	Transverse	0
32	31	81	F	T3 N0 M0	Rectum	57

Antibodies

Monoclonal mouse antibodies to β_{III}-tubulin (clone 5G8 [16–18] 1:1,000, Promega, Madison, WI) and cytokeratin (clone AE1/AE3, DAKO Inc., Denmark) were used at the working dilution of 1:1,000 and 1:100, respectively. The anti-β_{III}-tubulin was raised against a peptide (EAQGPK) corresponding to the C-terminus of β_{III}-tubulin.

Immunohistochemical-staining procedures

Sections (4 μm thick) were cut from the tissue blocks and mounted on silane-coated slides and later deparaffinized in xylene and rehydrated in alcohol. Antigen retrieval was carried out using citrate buffer (pH 6.0) in a microwave oven at 850 W for 16 min. After antigen retrieval, sections were cooled for 20 min. After washing twice in Tris-buffered saline (TBS), the endogenous peroxidase activity was suppressed by a solution of 3% hydrogen peroxide for 20 min. After three washes in TBS, nonspecific reaction was blocked by incubating with 1% bovine serum albumin for 30 min. Sections were incubated with anti-β_{III}-tubulin antibody overnight at 4°C. Sections were then rinsed twice with TBS. Bound antibodies were detected with EnVision system (DAKO Inc., Denmark). Diaminobenzidine (DAB) was used as the chromogen, and sections were lightly counterstained with Mayer's haematoxylin and mounted. As a negative control, the same procedure was applied omitting the primary antibody. Sections of CRC slides with intense reactivity were used as a positive control for the immunohistochemical reaction. Sections were stained in the same manner with anti-cytokeratin antibody to confirm the presence of tumour budding.

Budding

Tumour budding was quantified on slides stained with anti-cytokeratin antibody. An isolated undifferentiated cell or cancer cell cluster in the deepest invasive margin composed of fewer than five cancer cells was defined as budding focus. After selecting a field in which budding intensity was considered maximal, the number of budding foci was counted using a ×20 objective lens (the field of vision was 0.933 mm^2). Cancers were then divided into three groups: low-, moderate- and high-grade budding. Cut-offs were estimated along 33rd and 66th percentile.

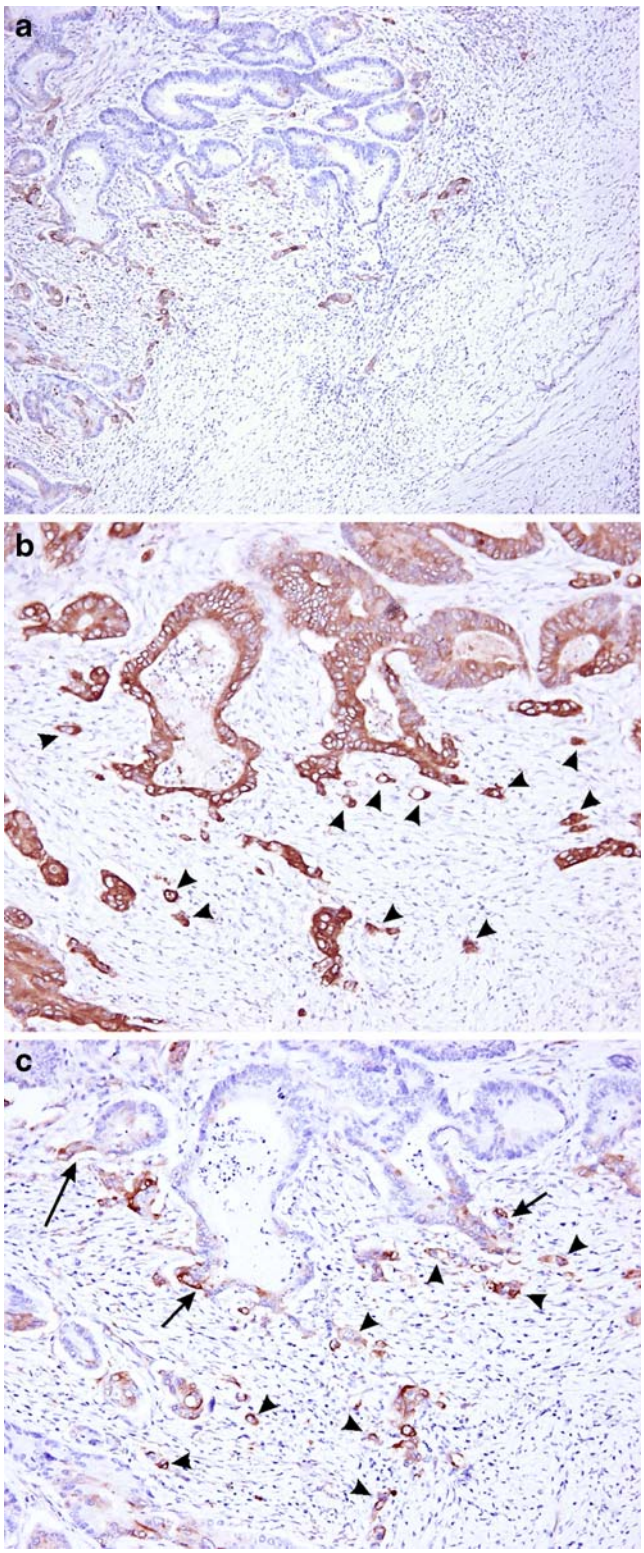

Fig. 1 Immunohistochemical staining of β_{III}-tubulin (**a**, **c**) and cytokeratin AE1/AE3 (**b**) in sections of colorectal cancer detected by peroxidase-mediated DAB staining (*brown*). **a** Colonic adenocarcinoma showing non-homogeneous staining of epithelial cells with foci of more intense labelling at the invasion front (original magnification× 100). **b** Tumour budding identified by anti-cytokeratin antibody (*arrowheads*). **c** The same area stained by anti-β_{III}-tubulin antibody. Here, strong cytoplasmic staining for β_{III}-tubulin is evident in a number of cancer cells apparently budding from adjacent malignant epithelium showing a higher differentiation and negative β_{III}-tubulin. Note positive staining of tumour buds (*arrowheads*) and the "invading" parts of tumour glands (*arrows*; **b**, **c** original magnification×200)

Evaluation of immunohistochemical stainings

All specimens were evaluated using a Leica DMLB microscope with N PLAN objectives. Images were acquired at ×200 using a DC200 Leica digital camera [1,798×1,438 pixels] from ten noncoincident random fields from the central area and 10 noncoincident consecutive fields from invasive margin of each tumour. The most peripheral areas of each tumour within one field of vision (×200) were considered as the invasive margin, the remaining part was defined as the centre. In order to exclude the possibility of any coincidence of the acquired fields all images were printed and compared by pathologists. No coincidence was revealed.

The obtained images were analysed by the image analysis software, ImageScope v. 9.0.19.1516 (Aperio Technologies, Inc.). The epithelial compartment was drawn out using Bamboo pen tablet (Wacom Co. Ltd.). Epithelial compartments were outlined using Pen Tool of ImageScope and thus selected for subsequent analysis. Artefacts, glands lumens, areas of necrotic and apoptotic debris were excluded from analyses with Negative Pen Tool. Small

Table 2 Expression of β_{III}-tubulin in central area and invasive margin of human CRC: Quantitative IHC evaluation

Tumour	n	Positivity, %	Invasive margin			Central area				
			wP, %	mP, %	sP, %	n	Positivity, %	wP, %	mP, %	sP, %
1	147	96.06*	18.41	28.46	49.19*	244	83.27	28.27*	31.24*	23.76
2	174	80.78*	25.72*	31.62*	23.45*	210	26.17	14.41	9.25	2.50
3	126	53.55*	20.95*	20.48*	12.12*	228	12.31	7.32	3.48	1.52
4	173	66.07*	25.45	23.25	17.38*	308	55.82	25.79	22.85	7.17
5	124	21.63*	13.67	6.62*	1.35*	179	20.26	12.90	5.85	1.51
6	145	29.60	14.43	9.75	5.41	198	30.83	18.67*	9.43	2.73
7	303	72.59*	35.81	24.86*	11.93*	269	66.39	43.83*	18.12	4.44
8	210	37.03	18.52	14.22*	4.29*	264	29.25	20.54*	7.29	1.42
9	253	60.57*	20.92	26.39*	13.27*	268	45.68	19.75	17.85	8.08
10	164	74.73*	26.54*	33.48*	14.71*	181	22.92	14.77	6.77	1.38
11	181	41.22	16.46	14.57	10.20	148	39.49	17.70	14.60	7.19
12	201	16.79*	4.62*	8.37*	3.80*	188	5.70	2.32	2.94	0.44
13	317	46.94*	19.88*	23.77*	3.29*	135	11.43	7.15	4.09	0.18
14	157	78.25*	17.82	46.72*	13.71*	260	49.82	17.02	28.05	4.74
15	135	69.26*	37.53	21.55*	10.19*	147	59.28	37.29	16.47	5.51
16	103	1.57*	1.14*	0.31*	0.12*	143	0.49	0.19	0.21	0.10
17	115	69.58*	33.97*	22.25*	13.36*	123	36.89	15.81	14.54	6.54
18	199	29.42*	19.35*	9.14*	0.93*	197	15.26	10.84	3.93	0.50
19	201	23.09*	9.80*	9.80*	3.49*	149	17.85	5.16	8.49	4.21
20	96	67.36*	30.91*	24.09*	12.36*	129	10.87	8.11	1.86	0.91
21	133	15.70*	2.84*	4.60*	8.27*	172	6.91	1.16	1.95	3.80
22	149	5.53*	1.55*	3.28*	0.70*	232	0.45	0.17	0.25	0.03
23	175	3.98*	0.92*	1.51*	1.55*	264	0.75	0.18	0.22	0.35
24	157	3.23*	1.47*	1.24*	0.52*	270	2.45	1.38	0.86	0.22
25	110	11.96*	1.30*	8.10*	2.56*	180	4.59	0.42	2.65	1.53
26	186	16.63*	1.27*	4.51*	10.84*	103	6.66	0.46	1.64	4.56
27	131	65.80*	3.20*	20.02*	42.58*	177	9.19	0.50	5.02	3.67
28	110	17.94*	6.51*	9.34*	2.09*	146	5.81	2.96	2.38	0.47
29	271	26.83*	3.40*	12.46*	10.98*	218	7.80	1.55	3.88	2.36
30	216	35.19*	7.19*	19.23*	8.77*	249	8.91	3.18	4.37	1.36
31	126	3.10	1.87	0.88	0.35	434	6.19*	4.71*	1.36*	0.12
32	194	24.32*	3.78*	11.01*	9.53*	250	6.07	1.22	2.60	2.25

* Significantly higher values (Mann–Whitney's *U*-test $p<0.05$)

n Number of epithelial regions

glands, nests and clusters of epithelial cells were selected as an entire region, whereas larger glands and sheets of epithelium were divided into separate regions according to the opportunity to draw a curve without break.

The Positive Pixel Count Algorithm v.9 was used for quantitative evaluation of IHC. The thresholds for weak, medium and strong intensity of staining were set as default. From the automatically calculated parameters, the following were selected for our study:

Number of weak positive pixels (Nwp),
Number of positive pixels (Np),
Number of strong positive pixels (Nsp),
Total number (number positive + number negative) (TN),
Positivity (number positive/TN).

Using the above-mentioned parameters we have calculated some additional ones according to formulas

$$\text{Weak positivity (wP)} = \text{Nwp/TN} \times 100$$
$$\text{Moderate positivity (mP)} = \text{Np/TN} \times 100$$
$$\text{Strong positivity (sP)} = \text{Nsp/TN} \times 100$$

were wP, mP and sP denotes the percentage of weakly, moderately and strongly stained pixels correspondingly. All

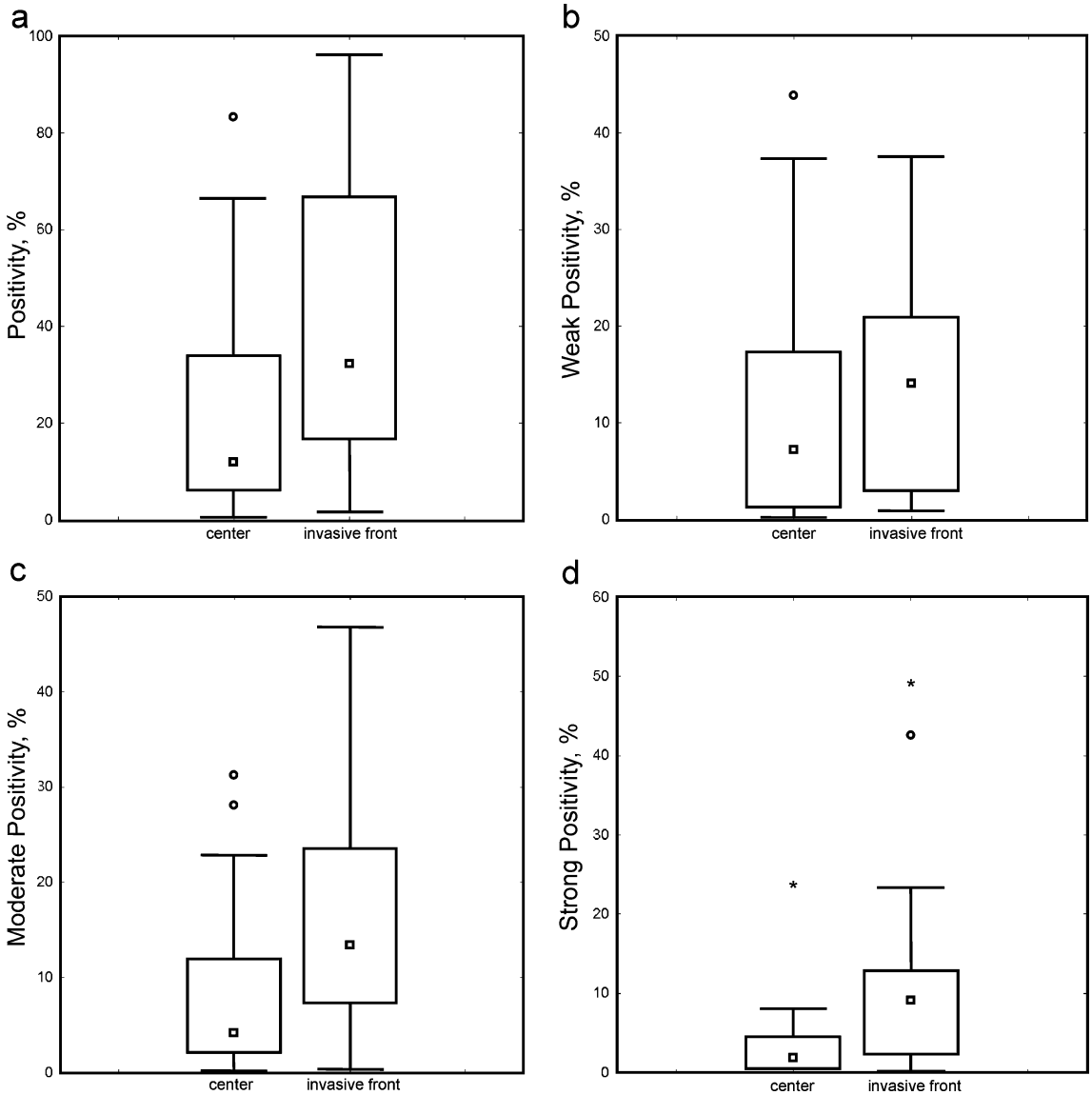

Fig. 2 β_{III}-tubulin positivity (total, weak, moderate and strong positivity) in central areas and invasive margin in CRCs. **a** Higher overall positivity in the invasive margin (Wilcoxon test, p=0.000002); **b** Higher weak positivity in the invasive margin (Wilcoxon test, p=0.007); **c** Higher moderate positivity in the invasive margin (Wilcoxon test, p=0.000004); **d** Higher strong positivity in the invasive margin (Wilcoxon test, p=0.000002). Median values are shown by an *empty square*; the *box* represents values between the 25th and the 75th percentiles; and the *lower* and *upper bars* indicate non-outlier range; an *open circle* and *asterisk* represent outliers and extremes, respectively

parameters were calculated for every epithelial region separately.

Statistics

Mann–Whitney's *U*-test, Wilcoxon matched pairs test and Kruskal–Wallis test were used to analyse data. A p-value <0.05 was considered to indicate statistical significance.

Results

Tumour budding was detected in 29 cases (90.6%) by AE1/AE3 immunohistochemistry. The results of quantitative evaluation of tumour budding are shown in Table 1. The cut-offs along the 33rd and 66th percentile were established as 20 and 40 budding foci per field of vision, respectively.

Positive staining with anti-β_{III}-tubulin antibody was observed in all cases. While normal colonic epithelium was negative, heterogeneous labelling of tumour tissue, with weakly, moderately, strongly stained and negative areas was observed. The reactivity was most prominent at the invasion front of tumours (Fig. 1a). In four cases, β_{III}-tubulin expression was weak and limited to a few tumour cells. Malignant cells in the region of tumour budding expressed β_{III}-tubulin in 28/29 cases. Staining for β_{III}-tubulin was evident in cancer cells apparently budding from adjacent malignant cells which exhibited a higher degree of differentiation and negative staining for β_{III}-tubulin (Fig. 1b and c).

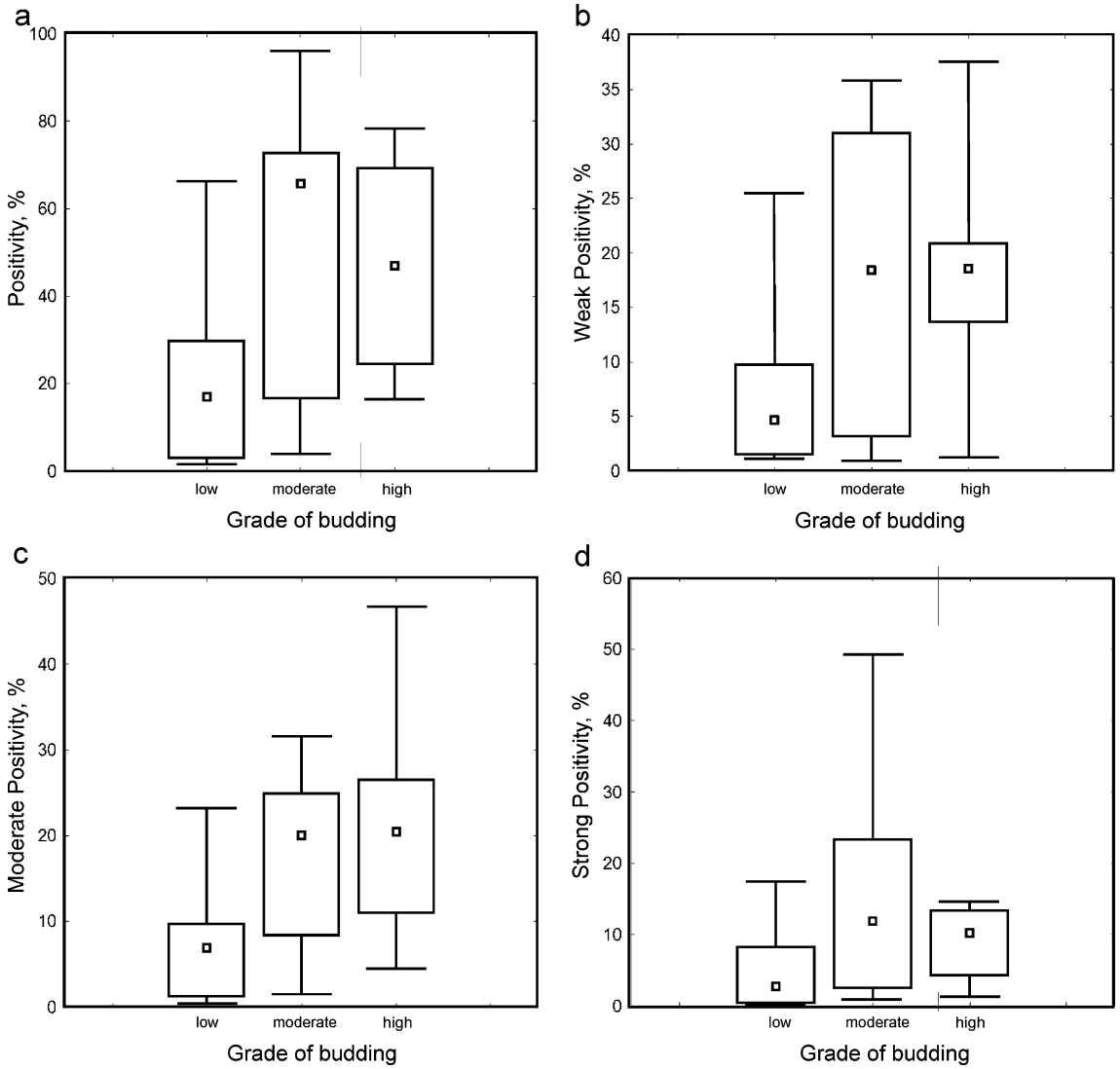

Fig. 3 Box plots featuring β_{III}-tubulin positivity (total, weak, moderate and strong positivity) after stratification according to tumour budding grade. Differences were significant by Kruskal–Wallis test for total, moderate and strong positivity. **a** $p=0.0218$; **b** $p=0.0911$; **c** $p=0.0280$; **d** $p=0.0399$. Median values are shown by an *open square*; the *box* represents values between the 25th and the 75th percentiles; and the *lower* and *upper bars* indicate non-outlier range

The results of quantitative IHC evaluation of β_{III}-tubulin staining are detailed in Table 2 and Fig. 2. Total, weak, moderate and strong positivity of tumour cells at the invasive front was significantly higher in 28, 21, 27 and 29 cases, respectively. In one case, there were no differences between central and invasive parts and in two cases the immunostaining was stronger in the central area of the tumours. We considered the expression to be upregulated if total positivity or intensive positivity (moderate or strong) were significantly higher. In general, we can say that the expression of β_{III}-tubulin was upregulated at the invasive front in 29/32 tumours. Wilcoxon matched pairs test also revealed the significant ($p<0.05$) upregulation of β_{III}-tubulin expression at the invasive margin of tumours (Fig. 2).

Tumours with higher grade of tumour budding had significantly more intensive staining of the invasive margin with anti-β_{III}-tubulin antibodies (Fig. 3). No difference was revealed for the central areas of cancers.

Discussion

A consistent finding in our study was the prominent β_{III}-tubulin immunoreactivity in cancer cells at the invasion front of most cases of CRC. In these cancers, the strongest staining was found in the cancer cells that appeared to be budding from the adjacent neoplastic glands. Moreover, we have demonstrated here that β_{III}-tubulin immunoreactivity is associated with tumour budding grade. In CRC, budding is associated with more aggressive behaviour. Because of the amoeboid morphology of budding cells and the presence of dendritic processes or pseudopodia extending from cancer cells [19, 20], we believe that these buds consist of migrating cells and that β_{III}-tubulin expression in these cells is linked to their motility.

Previously, β_{III}-tubulin was considered to be located exclusively in nervous tissue and even was used as a marker of neuronal origin [21–23]. Later works have shown that β_{III}-tubulin is expressed in a variety of tumours, particular those that are aggressive and likely to metastasize [24–26]. Furthermore, tumours with β_{III}-tubulin expression were found to be more resistant to several chemotherapy drugs (estramustine, taxol, paclitaxel, docetaxel) [8, 10, 11, 27–29]. As was already mentioned, microtubules assembled from β_{III} isotype are significantly more dynamic than others.

Little is known about regulation of β_{III}-tubulin expression. It is coded by TUBB3 gene. Recently, it was shown that hypoxia increases the expression of this gene [30] and that aberrant expression of β_{III}-tubulin might be regulated by epigenetic modulation (DNA methylation and chromatin acetylation) [31].

To the best of our knowledge, this is the first report documenting a preferential localization of β_{III}-tubulin in the invading epithelium of CRC. This finding raises the possibility that changes in tubulin isotype composition could play a role in the invasive activity of cancer cells. Moreover, if the invasive and the central tumour cells contain different tubulin isotypes then drugs targeting those in the invasive cell would prevent metastasis more effectively than others. We believe that the results obtained from colorectal cancer studies could appear to be fundamental for all malignancies of epithelial origin. Further investigations are needed to determine whether our findings have clinical implications.

Acknowledgements We thank Professor Richard F. Ludueña, University of Texas Health Science Center at San Antonio, USA, for the critical review of the manuscript and Svetlana Klimovich for excellent technical support.

Conflict of interest statement We declare that we have no conflict of interest.

References

1. Banerjee A, Roach MC, Trcka P, Ludueña RF (1990) Increased microtubule assembly in bovine brain tubulin lacking the type III isotype of beta-tubulin. J Biol Chem 265:1794–1799
2. Lu Q, Ludueña RF (1993) Removal of the β_{III} isotype enhances taxol induced microtubule assembly. Cell Struct Funct 18:173–182
3. Lu Q, Ludueña RF (1994) In vitro analysis of microtubule assembly of isotypically pure tubulin dimers. Intrinsic differences in the assembly properties of $\alpha\beta_{II}$, $\alpha\beta_{III}$, and $\alpha\beta_{IV}$ tubulin dimers in the absence of microtubule-associated proteins. J Biol Chem 269:2041–2047
4. Panda D, Miller HP, Banerjee A et al (1994) Microtubule dynamics in vitro are regulated by the tubulin isotype composition. Proc Natl Acad Sci USA 91:11358–11362
5. Derry WB, Wilson L, Khan IA et al (1997) Taxol differentially modulates the dynamics of microtubules assembled from unfractionated and purified β-tubulin isotypes. Biochemistry 36:3554–3562
6. Banerjee A, Ludueña RF (1992) Kinetics of colchicine binding to purified β-tubulin isotypes from bovine brain. J Biol Chem 267:13335–13339
7. Banerjee A, D'Hoore A, Engelborghs Y (1994) Interaction of desacetamidocolchicine a fast binding analogue of colchicine with isotypically pure tubulin dimers $\alpha\beta_{II}$, $\alpha\beta_{III}$ and $\alpha\beta_{IV}$. J Biol Chem 269:10324–10329
8. Laing N, Dahllof B, Hartley-Asp B et al (1997) Interaction of estramustine with tubulin isotypes. Biochemistry 36:871–878
9. Banerjee A, Engelborghs Y, D'Hoore A et al (1997) Interaction of a bicyclic analogue of colchicine with purified β-tubulin isoforms from bovine brain. Eur J Biochem 246:420–424
10. Kavallaris M, Kuo D, Burkhart CA et al (1997) Taxol-resistant epithelial ovarian tumous are associated with altered expression of specific β-tubulin isotypes. J Clin Invest 100:1282–1293
11. Ranganathan S, Benetatos CA, Colarusso PJ et al (1998) Altered β-tubulin isotype expression in paclitaxel-resistant human prostate carcinoma cells. Br J Cancer 77:562–566
12. Sangrajrang S, Denoulet P, Laing NM et al (1998) Association of estramustine resistance in human prostatic carcinoma cells with modified patterns of tubulin expression. Biochem Pharmacol 55:325–331
13. Ueno H, Murphy J, Jass JR et al (2002) Tumour 'budding' as an index to estimate the potential of aggressiveness in rectal cancer. Histopathology 40:127–132

14. Okuyama T, Oya M, Ishikawa H (2003) Budding as a useful prognostic marker in pT3 well- or moderately-differentiated rectal adenocarcinoma. J Surg Oncol 83:42–47
15. Wittekind CH, Meyer HJ, Bootz F (2002) International Union Against Cancer (UICC): TNM-Klassifikation maligner Tumoren, 6th edn. Springer, Berlin
16. Wachs FP, Couillard-Despres S, Engelhardt M et al (2003) High efficacy of clonal growth and expansion of adult neural stem cells. Lab Invest 83:949–962
17. Ohishi Y, Oda Y, Basaki Y et al (2007) Expression of beta-tubulin isotypes in human primary ovarian carcinoma. Gynecol Oncol 105:586–592
18. Packer MA, Stasiv Y, Benraiss A et al (2003) Nitric oxide negatively regulates mammalian adult neurogenesis. Proc Natl Acad Sci USA 100:9566–9571
19. Shinto E, Mochizuki H, Ueno H et al (2005) A novel classification of tumour budding in colorectal cancer based on the presence of cytoplasmic pseudo-fragments around budding foci. Histopathology 47:25–31
20. Prall F, Ostwald C (2007) High-degree tumor budding and podiaformation in sporadic colorectal carcinomas with K-ras gene mutations. Hum Pathol 38:1696–1702
21. Katsetos CD, Frankfurter A, Christakos S et al (1993) Differential localization of class III β-tubulin isotype (β_{III}) and calbindin-D28k identifies distinct neuronal types in the developing human cerebellar cortex. J Neuropathol Exp Neurol 52:655–666
22. Katsetos CD, Karkavelas G, Herman MM et al (1998) Class III β-tubulin isotype in the adrenal medulla, I: localization in the developing human adrenal medulla. Anat Rec 250:343–349
23. Moody SA, Quigg MS, Frankfurter A (1989) The development of the peripheral trigeminal system in the chick revealed by an isotype-specific anti-β-tubulin monoclonal antibody. J Comp Neurol 279:567–580
24. Katsetos CD, Del Valle L, Geddes JF et al (2001) Aberrant localization of the neuronal class III β-tubulin in astrocytomas. A marker for anaplastic potential. Arch Pathol Lab Med 125:613–624
25. Katsetos CD, Herman MM, Mörk SJ (2003) Class III β-tubulin in human development and cancer. Cell Motil Cytoskeleton 55:77–96
26. Katsetos CD, Del Valle L, Geddes JF et al (2002) Localization of the neuronal class III β-tubulin in oligodendrogliomas: comparison with Ki-67 proliferative index and 1p/19q status. J Neuropathol Exp Neurol 61:307–320
27. Dumontet C, Isaac S, Souquet PJ et al (2002) Expression of class III β tubulin in non-small cell lung cancer is correlated with resistance to taxane chemotherapy. Elect J Oncol 1:58–64
28. Urano N, Fujiwara Y, Doki Y et al (2006) Clinical significance of class III β -tubulin expression and its predictive value for resistance to docetaxel-based chemotherapy in gastric cancer. Int J Oncol 28:375–381
29. Gan PP, Pasquier E, Kavallaris M (2007) Class III β -tubulin mediates sensitivity to chemotherapeutic drugs in non small cell lung cancer. Cancer Res 67:9356–9363
30. Raspaglio G, Filippetti F, Prislei S et al (2008) Hypoxia induces class III β-tubulin gene expression by HIF-1alpha binding to its 3′ flanking region. Gene 409:100–108
31. Izutsu N, Maesawa C, Shibazaki M et al (2008) Epigenetic modification is involved in aberrant expression of class III β-tubulin, TUBB3, in ovarian cancer cells. Int J Oncol. 32:1227–1235

Virchows Arch (2009) 454:549–555
DOI 10.1007/s00428-009-0771-5

ORIGINAL ARTICLE

Transcription factors Snail, Slug, Twist, and SIP1 in spindle cell carcinoma of the head and neck

Nika Kojc · Nina Zidar · Nina Gale · Mario Poljak · Kristina Fujs Komloš · Antonio Cardesa · Heinz Höfler · Karl-Friedrich Becker

Received: 31 January 2009 / Revised: 9 March 2009 / Accepted: 1 April 2009 / Published online: 21 April 2009

Abstract Spindle cell carcinoma (SpCC) is a biphasic tumor composed of squamous cell carcinoma (SCC) and malignant spindle cells. There is mounting evidence that epithelial–mesenchymal transition (EMT) plays an important role in the pathogenesis of SpCC. Transcription repression has recently emerged as a fundamental mechanism triggering EMT in experimental models. Our aim is to analyze the expression of transcription repressors Snail, Slug, Twist, and SIP1 in SpCC of the head and neck in comparison to SCC, matched for location and stage. Thirty cases of SpCC and 30 cases of SCC of the head and neck were included. Snail, Slug, Twist, and SIP1 expression was analyzed on mRNA and protein levels, using real-time reverse transcription–polymerase chain reaction (RT-PCR) and immunohistochemistry. By RT-PCR, we found upregulation of mRNA for transcription factors Snail, Slug, Twist, and SIP1 in SpCC when compared to SCC. This upregulation was statistically significant for Slug, Twist, and SIP1 but nonsignificant for Snail. Immunohistochemistry was performed for Snail, Slug, and SIP1 and demonstrated a positive reaction for Slug and SIP1 in all cases and for Snail in two thirds of SpCC cases. Our finding of upregulation of all four tested transcription factors supports the hypothesis that EMT plays an important role in the pathogenesis of SpCC of the head and neck.

Keywords Spindle cell carcinoma · Pathogenesis · Transcription repression · Snail · Slug · SIP1 · Twist

N. Kojc (✉) · N. Zidar · N. Gale
Institute of Pathology, Faculty of Medicine,
University of Ljubljana,
Korytkova 2,
1000 Ljubljana, Slovenia
e-mail: nika.kojc@mf.uni-lj.si

M. Poljak · K. Fujs Komloš
Institute of Microbiology and Immunology, Faculty of Medicine,
University of Ljubljana,
Zaloška 4,
1000 Ljubljana, Slovenia

A. Cardesa
Department of Pathology, Hospital Clinic, IDIBAPS,
University of Barcelona,
Villaroel 170,
08036 Barcelona, Spain

H. Höfler · K.-F. Becker
Institute of Pathology, Technical University of Munich,
Trogerstrasse 18,
81675 Munich, Germany

H. Höfler
Helmholtz Zentrum München—Deutsches Forschungszentrum für Gesundheit und Umwelt, GmbH, Institut für Pathologie,
Neuherberg 85764, Germany

Introduction

Spindle cell carcinoma (SpCC) is a rare variant of epithelial neoplasm composed of squamous cell carcinoma (SCC) and a malignant spindle cell component. It has been detected in various sites throughout the body, including the respiratory tract, breast, skin, urogenital and gastrointestinal tract, and salivary glands. In the head and neck, it is most often localized in the larynx and oral cavity, followed by the skin, tonsils, sinonasal tract, and pharynx [1, 2].

SpCC is characterized by spindle cells usually forming the bulk of the tumor and the SCC component represented by in situ carcinoma and/or invasive SCC. The histogenesis of SpCC has not been elucidated, but there is increasing evidence indicating a monoclonal neoplasm derived from a

single stem cell giving rise to epithelial and mesenchymal components [3, 4]. Little is known about the mechanisms triggering the spindle cell phenotype as well as an altered immunoprofile in SpCC. It has recently been suggested that epithelial–mesenchymal transition (EMT) might play an important role in the pathogenesis of SpCC [5–9]. EMT has been postulated as a versatile mechanism that facilitates cellular reposition during embryonal development and contributes to the pathogenesis of diseases such as tissue fibrosis, carcinogenesis, and metastasis formation [10–13]. The key step of EMT is believed to be the downregulation of E-cadherin expression leading to disruption of adherens junctions, which results in marked phenotypic changes and a highly motile fibroblastoid, mesenchymal phenotype, allowing them to move through the extracellular matrix [10].

There are several mechanisms that might be responsible for the loss of E-cadherin in EMT, but hypermethylation of the E-cadherin promoter and transcription repression are emerging as predominant in most carcinomas [14]. Several factors have been described as transcription repressors of E-cadherin gene and other genes encoding proteins involved in EMT as well as in cell proliferation, cell survival, and angiogenesis. These factors include members of the zinc finger transcription repressor superfamily (e.g., Snail, Slug), the basic helix–loop–helix (bHLH) family (e.g., Twist), and the ZEB family (e.g., ZEB1 and ZEB2, also known as SIP1) [14–16].

Apart from Snail, little is known about other transcription repressors in SpCC. The aim of our study was, therefore, to analyze the expression of transcription repressors Snail, Slug, Twist, and SIP1 in SpCC, compared to conventional SCC, in order to establish their significance in the pathogenesis of SpCC.

Materials and methods

Tissue samples

The study included 30 patients with SpCC of the head and neck and 30 patients with moderately differentiated SCC of similar locations. The same patients were described in our previous study [9]. Among patients with SpCC, there were 25 men and five women, aged 39 to 91 years (mean 66.2± 12.1 years). Among patients with SCC, there were 24 men and six women, aged 38 to 84 years (mean 55.4±8.8 years). Tumors were located in the larynx (14 cases), hypopharynx (four cases), oropharynx (four cases), oral cavity (four cases), skin (two cases), and paranasal sinuses (two cases). Tissue samples were fixed in 10% buffered formalin, embedded in paraffin, and cut at 4 μ for hematoxylin and eosin slides.

Immunohistochemistry

Antigen retrieval and staining with monoclonal antibodies against Snail (Dr. E. Kremmer, GSF—National Research Centre for Environment and Health, Munich; clone Sn9H2), Slug (Santa Cruz Biotechnology, Santa Cruz, CA, USA), and SIP1 (Santa Cruz Biotechnology, Santa Cruz, CA, USA) was performed in an automatic immunostainer (Discovery, Ventana, Tucson, Arizona, USA). We did not perform an immunohistochemical analysis of Twist because there was no suitable specific and sensitive antibody available. Sections were treated with biotinylated secondary antibody, followed by incubation with peroxidase conjugated streptavidin. Visualization of the immunoreaction was carried out with 3.3′-diaminobenzidine and counterstained with hematoxylin. Fibrosarcoma served as a positive control for Snail, Slug, and SIP1. Only cells exhibiting nuclear reaction were considered positive [17, 18]. Negative controls omitting the primary antibodies were also included.

The percentage of positive cells was estimated using an image analysis system (Cell and Tissue Analysis, Leica, Germany) and graded as 0, no staining; 1, up to 10% of positive cells; 2, 11–50% of positive cells; 3, 51–80% of positive cells; and 4, more than 80% of positive cells.

Isolation of total RNA

For molecular investigation, 30 paired tumor/normal tissue samples of SpCC and SCC were chosen. Total RNA was extracted from formalin-fixed, paraffin-embedded tissue using 8 μm sections with a RNeasy FFPE Kit (Qiagen, Hilden, Germany), according to the manufacturer's instructions. The RNeasy FFPE Kit is optimized to reverse formaldehyde modification providing recovery of RNA fragments for application such as quantitative polymerase chain reaction (PCR). RNA concentrations were measured with a BioPhotometer (Eppendorf AG, Hamburg, Germany) at 260 and 280 nm (A260/280). Only samples with A260/280 value higher than 1.8 were used for further study.

Usually, 80–300 ng RNA were isolated and 50–100 ng RNA was used for each one-step real-time reverse transcription–polymerase chain reaction (RT-PCR) reaction.

Quantitative real-time PCR

One-step quantitative real-time PCR analyses of mRNA for Snail, Slug, Twist, and SIP1 were performed using the LightCycler 2.0 Instrument and Software (Roche, Mannheim, Germany). Intron-spanning primers and probes for the TaqMan system designed to exclude annealing to genomic DNA were used, as previously described (Table 1)

Table 1 Sequence of the TaqMan primers and probes used

Target gene	Sequence 5′–3′	Size of PCR product (bp)	Reference
Snail	fw TGCAGGACTCTAATCCAAGTTTACCC r GTGGGATGGCTGCCAGC p TCCAGCAGCCCTACACCAGGCC	71	Rosivatz et al. [19]
Slug	fw TGTGTGGACTACCGCTGC r TCCGGAAAGAGGAGAGAGG p TTCCACGCCCAGCTACCCAATG	63	Castro Alves et al. [20]
Twist	fw TGTCCGCGTCCCACTAGC r TGTCCATTTTCTCCTTCTCTGGA p CAGCAGGGCCGGAGACCTAGATGT	92	Rosivatz et al. [19]
SIP1	fw GCGGCATATGGTGACACACAA r CATTTGAACTTGCGATTACCTGC p CAGATCAGCACCAAATGCTAACCCAAGG	80	Rosivatz et al. [19]

fw forward, *r* reverse, *p* probe

[19, 20]. One-step quantitative real-time PCR was performed with QuantiTect Probe RT-PCR Kit (Qiagen, Hilden, Germany) using 0.2 μL RT Mix, 0.4 μL of the primers, 0.2 μL of the probe, and 50–100 ng template RNA in a 20-μL final reaction mixture. After 20 min incubation at 50°C for reverse transcription, HotStar Taq DNA Polymerase was activated by incubation for 15 min at 95°C. Each of the 45 PCR cycles consisted of quick denaturation at 95°C and hybridization of the probe and primers for 1 min at 60°C.

Quantitation of expression

Relative expression levels of target sequences were determined by the calibrator-normalized relative quantification with efficiency correction. This method calculates the relative amount of target to reference in all samples and compares this ratio to the relative amount of target and reference in a positive sample called calibrator.

The quantity of target and reference gene is a function of the real-time PCR efficiencies and the crossing point deviation of a target gene versus a reference gene. HPRT1 was most constitutively expressed in the majority of samples and was, therefore, included as a reference gene. Amplification efficiency of the target and reference genes was determined by using relative standards, serially fivefold dilutions of a calibrator and analyzed in triplicate for the genes of interest and a reference gene. The resulting data were used to generate standard curves for calculation of PCR efficiencies.

The relative expression of the target gene was expressed as the target/reference ratio of each sample divided by the target/reference ratio of the calibrator. First, the relative ratio of target to reference was calculated to adjust variances in the quality of the RNA and the amount of the cDNA input. The target/reference ratio of each sample was then divided by the target/reference ratio of the calibrator providing a constant point between PCR runs.

The ratio of Snail, Slug, Twist, and SIP1 expression between tumor and corresponding normal tissue greater than 2 were termed upregulation and those less than 0.5 were termed downregulation.

Statistical analysis

The results were analyzed by Mann–Whitney test and chi-square test using SPSS for Windows 16.0; p values less than 0.05 were considered statistically significant.

Results

Expression of Snail, Slug, Twist, and SIP1 mRNA in spindle cell carcinoma

Analyzing 30 cases of SpCC in comparison to nontumorous tissue, relative upregulation of Snail, Slug, Twist, and SIP1 was found in 14 (47%), 22 (73%), 20 (67%), and 12 (40%) cases, respectively. In 17 (57%) cases, there were no differences in SIP1 expression between SpCC and matched normal tissue. The ratio of the relative expression levels of Snail, Slug, Twist, and SIP1 between tumor and normal tissue is shown in Fig. 1.

The ratio of relative expression levels between tumor and nontumorous tissue (T/N), particularly of Snail, showed a broad range due to the very low expression of Snail in nontumorous tissue in six cases. In these cases, the slope of PCR curves reflecting PCR efficiency were characteristically distinguished from the expected value

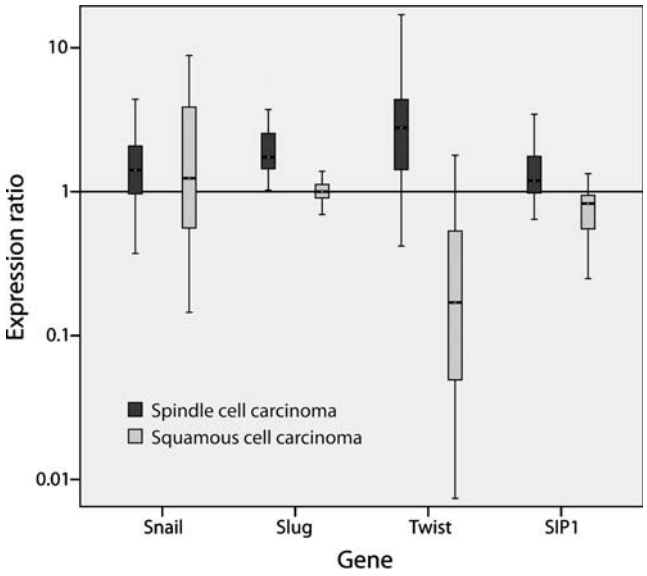

Fig. 1 Relative expression ratio of Snail, Slug, Twist, and SIP1 comparing tumor with matched normal tissue. *Horizontal bars* (mean of expression ratio) represent the expression patterns of Snail, Slug, Twist, and SIP1 (logarithmically scaled) for SpCC and SCC

calculated from serial dilutions of the calibrator, although threshold cycles were detected around 30–32 cycles. We, therefore, concluded that these samples expressed a very low level of Snail mRNA rather than considering the calculated value.

Expression of Snail, Slug, Twist, and SIP1 mRNA in squamous cell carcinoma

In 30 cases of SCC, the relative expression of Slug and SIP1 was comparable to normal mucosa in 27 (87%) cases and 21 (68 %) cases. The relative expression of Snail showed upregulation in nine (29%) cases, while SIP1 was not upregulated in any case of SCC compared to non-tumorous tissue. There was marked downregulation of mRNA expression compared to normal tissue in 11 (35%) cases for Snail, 21 (68%) cases for Twist, and nine (29%) cases for SIP1.

Expression of Snail, Slug, Twist, and SIP1 mRNA in spindle cell carcinoma compared to squamous cell carcinoma

Comparing the T/N ratio of Snail, Slug, Twist, and SIP1 expression in SpCC versus the T/N ratio in SCC, we found different expressions of all examined transcription factors as shown in Fig. 1. Statistically significant upregulation was confirmed for Slug ($p<0.00$), Twist ($p<0.00$), and SIP1 ($p<0.00$).

Immunohistochemical analysis of Snail, Slug, and SIP1 in spindle cell carcinoma

A summary of immunohistochemical results is shown in Table 2. Positive reaction for Snail was found in the spindle cells of 19 SpCC cases (Fig. 2a), while a positive reaction for Slug (Fig. 3a) and SIP1 was detected in all cases.

Snail, Slug, and SIP1 were also expressed in numerous mononuclear inflammatory cells and endothelial cells in blood vessels within the tumors and in stromal myofibroblasts.

In the SCC component of SpCC, the expression patterns were similar to those in SCC described in the next section.

Immunohistochemical analysis of Snail, Slug, and SIP1 in squamous cell carcinoma

A summary of immunohistochemical results is shown in Table 2. Positive reaction for Snail (Fig. 2b) was found in four cases and for Slug (Fig. 3b) and SIP1 in the majority of SCC cases. Snail, Slug, and SIP1 were also expressed in numerous mononuclear inflammatory cells and endothelial cells in blood vessels within the tumors and in stromal myofibroblasts.

Immunohistochemical analysis of Snail, Slug, and SIP1 in normal mucosa

In the normal mucosa, there was no positive staining for Snail. Slug and SIP1 exhibited a nuclear reaction and

Table 2 Immunohistochemical results for Snail, Slug, and SIP1 in SpCC and SCC

Percentage of positive tumor cells	Number of Snail positive cases		Number of Slug positive cases		Number of SIP1 positive cases	
	SpCC	SCC	SpCC	SCC	SpCC	SCC
0	11	26	0	5	0	7
1–10	8	4	5	14	9	19
11–50	9	0	11	9	13	4
51–80	2	0	11	2	7	0
>80	0	0	3	0	0	0

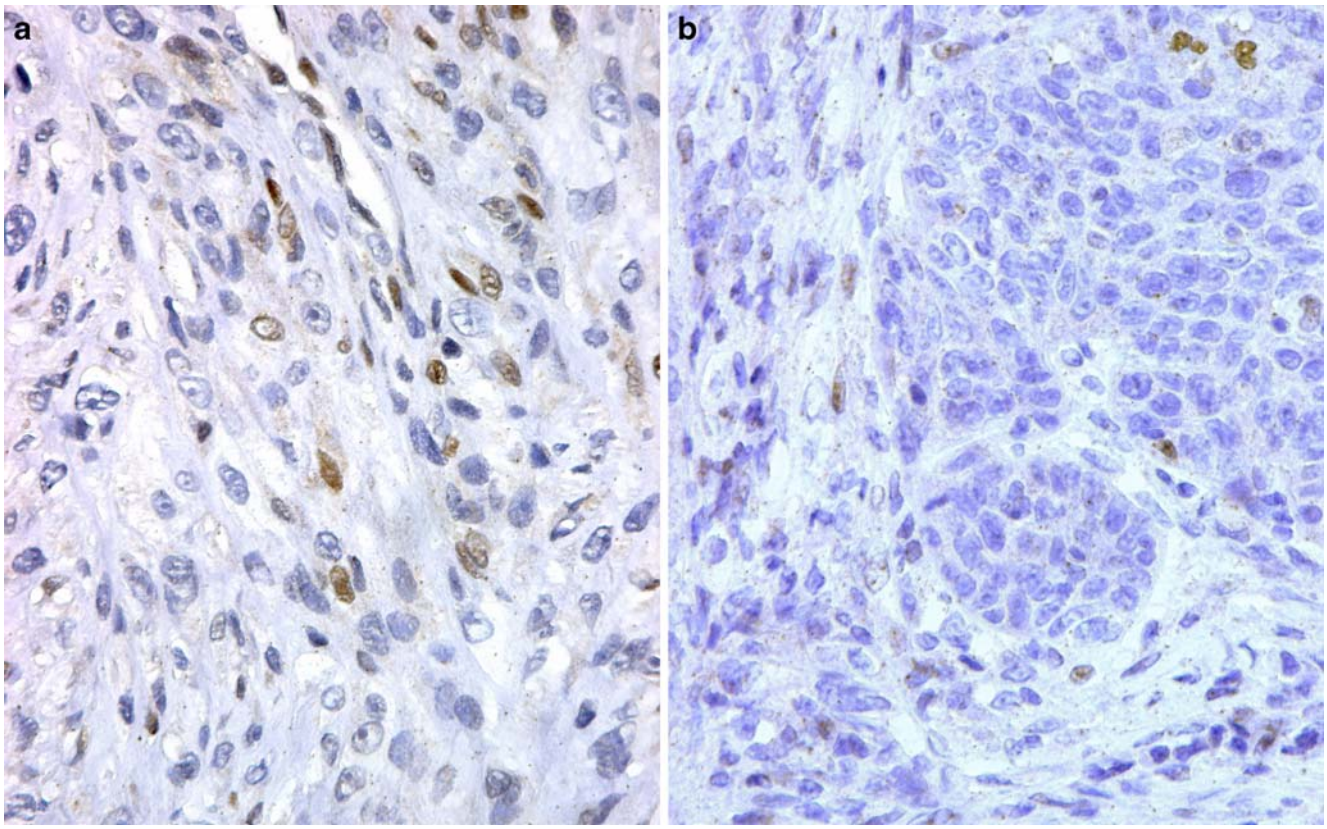

Fig. 2 Immunohistochemistry for Snail. **a** SpCC: positive reaction in approximately 20% of tumor cells. Original magnification ×40. **b** SCC: positive reaction in rare tumor cells. Original magnification ×40

showed similar distribution patterns: they were expressed in the basal and suprabasal layers of the squamous epithelium, in scattered mononuclear inflammatory cells in the lamina propria, in occasional stromal cells, and faintly in endothelial cells.

Statistical analysis

The frequency and intensity of Snail, Slug, and SIP1 expression was significantly higher in SpCC than in SCC (p=0.0001 for Snail, p=0.001 for Slug, and p<0.000 for SIP1). In SpCC, no significant correlation was observed between Snail, Slug, and SIP1 versus cadherins, keratin, and vimentin (data not shown).

Discussion

EMT is a process that allows epithelial cells to separate from their neighbors and migrate to distal regions. During EMT, epithelial cells turn off epithelial genes and turn on mesenchymal genes. They lose the apical–basal polarity, reorganize the actin cytoskeleton, and change to a spindle, mesenchymal phenotype. EMT is fundamental during normal development in processes such as mesoderm and neural crest formation. It is also reactivated in a variety of pathologic conditions in later life, including wound healing, fibrosis, and progression of carcinoma [10, 11, 21]. Our study provides further evidence that EMT might also play an important role in the pathogenesis of SpCC of the head and neck. This is based on our finding of upregulation of transcription repressors Snail, Slug, SIP1, and Twist, important inducers of EMT, on both mRNA and protein levels.

Using RT-PCR, we found upregulation of mRNA for transcription factors Snail, Slug, Twist, and SIP1 in SpCC of the head and neck when compared to SCC with a similar stage and tumor location. This upregulation was statistically significant for Slug, Twist, and SIP1 but nonsignificant for Snail. Immunohistochemistry was performed for Snail, Slug, and SIP1 and demonstrated a positive reaction for Slug and SIP1 in all cases and for Snail in two thirds of SpCC cases. There was, thus, a rough correlation between mRNA and protein expression.

In SCC, by RT-PCR, we found upregulation of Snail and downregulation of Twist, whereas SIP1 and Slug expression was similar as in the normal tissue. The results for Slug and SIP1 were further supported by immunohisto-

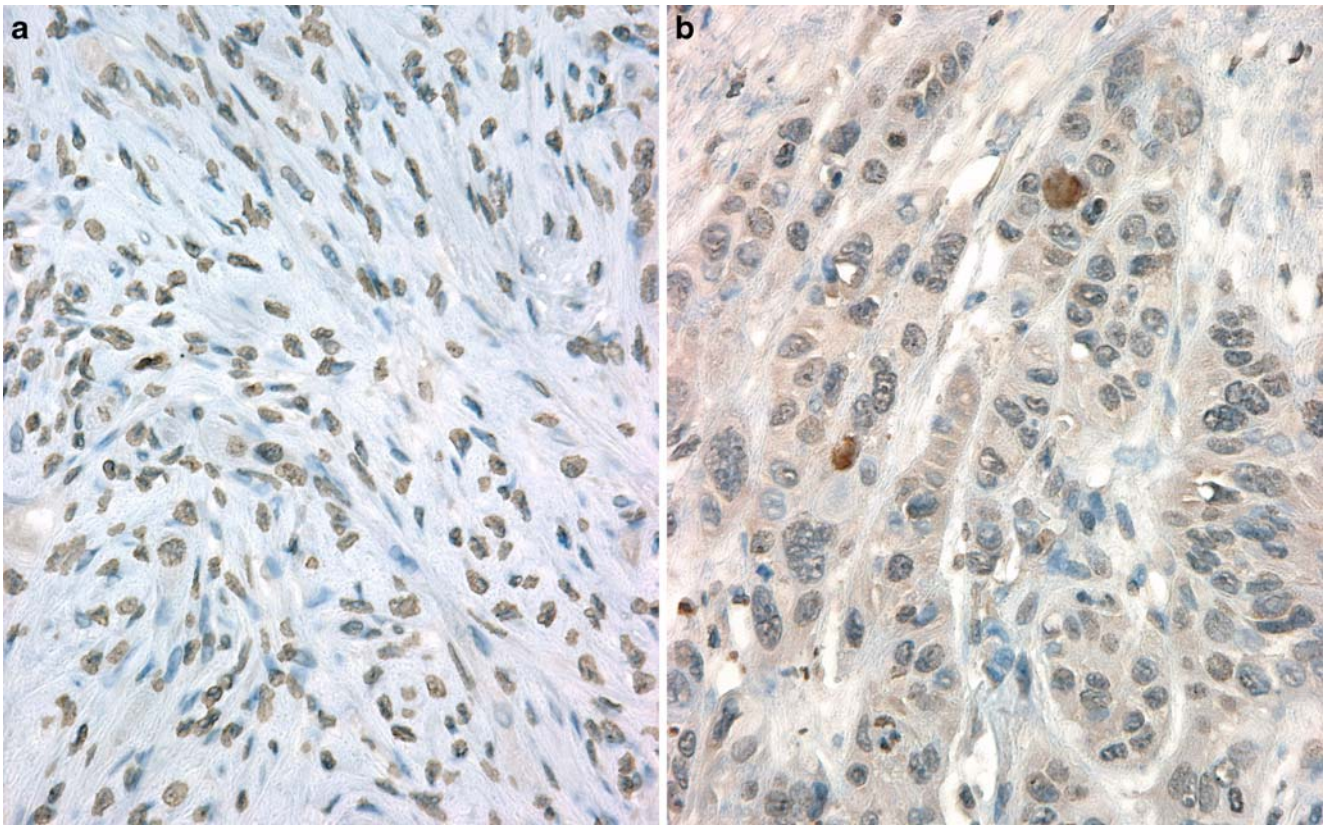

Fig. 3 Immunohistochemistry for Slug. **a** SpCC: positive reaction in approximately 90% of tumor cells. Original magnification ×40. **b** SCC: positive reaction in rare tumor cells. Original magnification ×40

chemistry, which showed only focal staining for SIP1 and Slug in the majority of SCC cases. Upregulation of Snail is consistent with previous studies, describing various patterns of transcription factors expression in many carcinomas, presumably the result of transient EMT, which has been postulated to be responsible for tumor progression and metastasizing [16, 22].

Transcription repression has recently emerged as a fundamental mechanism for the induction of EMT. Other mechanisms include gene mutation, promoter hypermethylation, enhanced degradation, chromatin rearrangements, and post-translational truncation or modification [20, 23, 24]. Transcription repression can be mediated by factors from the Snail, ZEB, and bHLH families. The Snail superfamily of zinc finger transcription repressors includes Snail and Snail-2, also known as Slug, Snail-like, Scratch1, and Scratch2 [25]. The ZEB family includes ZEB1 (also known as TCF8 and δEF1) and ZEB2 (also known as ZFXH1B and SMAD interacting protein 1 [SIP1]). The most important members of the bHLH family are Twist, E47 (also known as TCF3), and E2-2 (also known as TCF4) [26].

In experimental models, these factors all induce a similar phenotype when overexpressed, eliciting complete EMT at both morphologic and behavioral levels [27]. The exact mechanisms of transcription repressors have not been completely elucidated, but one of the most important targets is E-cadherin. Transcription factors bind to consensus E-box sequences in the E-cadherin gene promoter and downregulate E-cadherin transcription [26]. The result is a functional loss of E-cadherin, which is believed to be one of the hallmarks of EMT. Some studies indicate that Snail and Slug repress E-cadherin in different ways: Snail binds to E-cadherin with a higher affinity than Slug and leads to initiation of EMT through downregulation of E-cadherin, whereas Slug may contribute to the maintenance of the mesenchymal phenotype by sustained repression of E-cadherin [28].

The majority of studies have focused on E-cadherin in EMT in general and on E-cadherin as a target for transcription repressors in particular. However, there is emerging evidence that transcription repressors not only repress E-cadherin, thus affecting adherens junctions, but also induce the disassembly of other cell junctional complexes, such as tight junctions, desmosomes, and gap junctions [22, 29–31]. Moreover, Savagner et al. demonstrated in an experimental model of EMT that adherens junction components, such as E-cadherin, were only modestly relocalized but still present, whereas desmosomal

components disappeared completely from cell–cell contact areas [29].

Our observations in SpCC are consistent with the results of experimental studies. We found a loss of desmosomal cadherins (Zidar, unpublished observation) and altered expression of classical cadherins in all cases [9]. Our finding of the strongest Slug expression among transcription repressors in SpCC is consistent with the suggested role of Slug in EMT [28]: Slug is supposed to be necessary for the maintenance of the spindle phenotype, which is the main morphologic feature of SpCC.

In conclusion, our finding of upregulation of all tested transcription factors further supports the hypothesis that EMT might play an important role in the pathogenesis of SpCC, as suggested by some previous studies [5–9].

Conflict of interest statement We declare that we have no conflict of interest.

References

1. Cardesa A, Zidar N (2005) Spindle cell carcinoma. In: Barnes L, Eveson JW, Reichart PA, Sidransky D (eds) Larynx, hypopharynx and trachea, pathology and genetics of tumours of the head and neck. WHO classification of tumours. IARC, Lyon, pp 111–113
2. Gale N, Zidar N (2006) Benign and potentially malignant lesions of the squamous epithelium and squamous cell carcinoma. In: Cardesa A, Menzel T, Rudolf P (eds) Head and neck, soft tissues, retroperitoneum and skin. Pathologie, 3rd edn. Springer, Berlin, pp 1–38
3. Thompson L, Chang B, Barsky SH (1996) Monoclonal origins of malignant mixed tumors (carcinosarcomas). Evidence for a divergent histogenesis. Am J Surg Pathol 20:277–285
4. Choi HR, Sturgis EM, Rosenthal DI et al (2003) Sarcomatoid carcinoma of the head and neck. Molecular evidence for evolution and progression from conventional squamous cell carcinoma. Am J Surg Pathol 27:1216–1220
5. Navarro P, Lozano E, Cano A (1993) Expression of E- or P-cadherin is not sufficient to modify the morphology and the tumorigenic behaviour of murine spindle carcinoma cells. J Cell Sci 105:923–934
6. Islam S, Carey TE, Wolf GT et al (1996) Expression of N-cadherin by human squamous carcinoma cells induces a scattered fibroblastic phenotype with disrupted cell–cell adhesion. J Cell Biol 135:1643–1654
7. Kim JB, Islam S, Kim YJ et al (2000) N-cadherin extracellular repeat 4 mediates epithelial to mesenchymal transition and increased motility. J Cell Biol 151:1193–1206
8. Chuang R, Crowe DL (2007) Understanding genetic progression of squamous cell carcinoma to spindle cell carcinoma in a mouse model of head and neck cancer. Int J Oncol 30:1279–1287
9. Zidar N, Gale N, Kojc N et al (2008) Cadherin–catenin complex and transcription factor Snail-1 in spindle cell carcinoma of the head and neck. Virchows Arch 453:267–274
10. Thiery JP (2003) Epithelial–mesenchymal transitions in development and pathologies. Curr Opin Cell Biol 15:740–746
11. Peinado H, Portillo F, Cano A (2004) Transcriptional regulation of cadherins during development and carcinogenesis. Int J Dev Biol 48:365–375
12. Becker KF, Rosivatz E, Blechschmidt K et al (2007) Analysis of the E-cadherin repressor Snail in primary human cancers. Cells Tissues Organs 185:204–212
13. Moustakas A, Heldin CH (2007) Signaling networks guiding epithelial–mesenchymal transitions during embryogenesis and cancer progression. Cancer Sci 98:1512–1520
14. Bolós V, Peinado H, Pérez-Moreno MA et al (2003) The transcription factor Slug represses E-cadherin expression and induces epithelial to mesenchymal transitions: a comparison with Snail and E47 repressors. J Cell Sci 116:499–511
15. Perez-Moreno M, Jamora C, Fuchs E (2003) Sticky business: orchestrating cellular signals at adherens junctions. Cell 112:535–548
16. Cano A, Pérez-Moreno MA, Rodrigo I et al (2000) The transcription factor snail controls epithelial–mesenchymal transitions by repressing E-cadherin expression. Nat Cell Biol 2:76–83
17. Parent AE, Choi C, Caudy K et al (2004) The developmental transcription factor Slug is widely expressed in tissues of adult mice. J Histochem Cytochem 52:959–965
18. Francí C, Takkunen M, Dave N et al (2006) Expression of Snail protein in tumor–stroma interface. Oncogene 25:5134–5144
19. Rosivatz E, Becker I, Specht K et al (2002) Differential expression of the epithelial–mesenchymal transition regulators Snail, SIP1, and Twist in gastric cancer. Am J Pathol 161:1881–1891
20. Castro Alves C, Rosivatz E, Schott C et al (2007) Slug is overexpressed in gastric carcinomas and may act synergistically with SIP1 and Snail in the down-regulation of E-cadherin. J Pathol 211:507–515
21. Barrallo-Gimeno A, Nieto MA (2005) The Snail genes as inducers of cell movement and survival: implications in development and cancer. Development 132:3151–3161
22. De Craene B, Gilbert B, Stove C et al (2005) The transcription factor Snail induces tumor cell invasion through modulation of the epithelial cell differentiation program. Cancer Res 65:6237–6244
23. de Moraes RV, Oliveira DT, Landman G et al (2008) E-cadherin abnormalities resulting from CPG methylation promoter in metastatic and nonmetastatic oral cancer. Head Neck 30:85–92
24. Rosivatz E, Becker KF, Kremmer E et al (2006) Expression and nuclear localization of Snail, an E-cadherin repressor, in adenocarcinoma of the upper gastrointestinal tract. Virchows Arch 448:277–287
25. Nieto MA (2002) The snail superfamily of zinc-finger transcription factors. Nat Rev Mol Cell Biol 3:155–166
26. Moreno-Bueno G, Cubillo G, Sarrió D et al (2006) Genetic profiling of epithelial cells expressing E-cadherin repressors reveals a distinct role for Snail, Slug, and E47 factors in epithelial–mesenchymal transition. Cancer Res 66:9543–9556
27. Peinado H, Olmeda D, Cano A (2007) Snail, ZEB and bHLH factors in tumour progression: an alliance against the epithelial phenotype? Nat Rev 7:415–428
28. Hotz B, Arndt M, Dullat S et al (2007) Epithelial to mesenchymal transition: expression of the regulators Snail, Slug, and Twist in pancreatic cancer. Clin Cancer Res 13:4769–4776
29. Savagner P, Yamada KM, Thiery JP (1997) The zinc-finger protein Slug causes desmosome dissociation, an initial and necessary step for growth factor-induced epithelial–mesenchymal transition. J Cell Biol 137:1403–1419
30. Vandewalle C, Comijn J, De Craene B et al (2005) SIP1/ZEB2 induces EMT by repressing genes of different epithelial cell–cell junctions. Nucleic Acids Res 33:6566–6578
31. Aigner K, Descovich L, Mikula M et al (2007) The transcription factor ZEB1 (deltaEF1) represses plakophilin 3 during human cancer progression. FEBS Lett 581:1617–1624

Virchows Arch (2009) 454:557–562
DOI 10.1007/s00428-009-0743-9

ORIGINAL ARTICLE

Extranodular background liver parenchyma of focal nodular hyperplasia: histopathological characteristics

Utaroh Motosugi · Shin-ichi Murata · Michio Shimizu · Masanori Yasuda · Takaki Sakurai · Yoshihiko Shimizu · Shinichi Ban · Kohji Nagata · Hiroshi Yamaguchi · Seiya Sannohe

Received: 18 November 2008 / Revised: 3 February 2009 / Accepted: 6 February 2009 / Published online: 22 April 2009

Abstract Focal nodular hyperplasia (FNH) of the liver is considered to develop as a hyperplastic response to a preexisting vascular abnormality. From the pathogenic point of view, we studied histological alterations in the extranodular background liver tissue of FNH (FNH-bg-liver). We compared ten FNH-bg-livers with ten non-FNH cases (non-FNH-liver) and found small uniform nodule formations with ring-like siderosis in the FNH-bg-livers (4/7, 57%) but not in the non-FNH-livers. Abnormal small arteries not accompanied by portal tracts were observed in six of six FNH-bg-livers for which immunohistochemical study was available, while this was observed in only three of the ten non-FNH-livers. CD34-positive sinusoids around the portal tracts were observed in only the FNH-bg-livers (3/6, 50%). Further, two of ten FNH-bg-livers had ectopic pancreatic tissue. Ring-like siderosis, abnormal small arteries, CD34-positive sinusoids, and ectopic pancreatic tissue were characteristic in the extranodular background liver tissue in cases of FNH.

Keywords Focal nodular hyperplasia · Liver · Siderosis · Ectopic pancreas

U. Motosugi · S. Murata (✉) · M. Shimizu · M. Yasuda · T. Sakurai · Y. Shimizu · S. Ban · K. Nagata · H. Yamaguchi · S. Sannohe
Department of Pathology, Saitama Medical University International Medical Center,
1397–1 Yamane,
Hidaka-shi, Saitama-ken 350-1298, Japan
e-mail: smurata@saitama-med.ac.jp

Introduction

Classical focal nodular hyperplasia (FNH) is a well-circumscribed lesion that is composed of proliferating benign hepatocytes with a characteristic stellate central fibrous scar, and it includes vascular abnormalities such as stenotic portal veins, thickened arteries, and numerous smaller vessels. The stellate central fibrous scar, however, is seen in less than 50% of cases [1, 2]. The vascular abnormality exists exclusively in FNH and is the most important diagnostic clue for FNH [3, 4]. The scar may be the result of ischemic changes or necrosis because of the vascular abnormalities. Therefore, it has recently been accepted that FNH is a hyperplastic response to a preexisting vascular abnormality rather than a neoplastic mass despite a study reporting the monoclonal nature of FNH [5–9].

On the other hand, the formation of multiple masses is another characteristic feature of FNH, and this feature is found in about 30% of cases [2]. Occasionally, however, the lesions are inconspicuous, which makes their identification difficult. A case of progression of multiple FNH after resection of a solitary FNH has also been reported [4].

Although most past reports have noted that the extranodular background liver tissue of FNH patients is normal or nearly normal, the existence of vascular abnormalities and multiple FNH masses in liver implies that the background liver tissue of FNH may undergo subtle alterations, and precursory changes that are caused by factors are the same as those that cause FNH. In fact, there is one report that simply mentions that the extranodular area in 73% of FNH cases exhibited changes that were similar to but milder than those in the nodule [10]. Here, we studied the histological alterations and precursory changes that occur in the extranodular background liver tissue of FNH from the pathogenic viewpoint.

Materials and methods

Case selection

Liver tissue specimens were obtained by partial hepatectomy or tumorectomy from ten patients with FNH (two male patients and eight female patients with a mean age at diagnosis of 41.0 years). All ten FNHs had macroscopic stellate scars and fibrous septa in the lesions. The pathological diagnosis of FNH was confirmed by two experienced pathologists. As control cases, ten non-cirrhotic tissues were surgically resected from patients with metastasis from colorectal carcinoma. The extranodular background liver tissue of the FNH (FNH-bg-livers) and metastatic liver tumor (non-FNH-livers) was obtained from an area at a distance of at least 1 cm from the masses.

Histopathological features after staining with hematoxylin–eosin and Berlin blue

The liver tissues were fixed in 10% neutral-buffered formalin and then embedded in paraffin. The histopathological features of 4-μm-thick sections that were stained with hematoxylin–eosin were studied. Further, additional 4-μm-thick sections were stained with Berlin blue for visualizing iron deposits.

Immunohistochemistry

To detect abnormal arteries and alterations in the sinusoidal endothelium, immunohistochemical analysis was performed. The Ventana XT System Benchmark (Ventana Japan, Tokyo, Japan) was used to stain additional 4-μm-thick sections with a primary antibody against mouse monoclonal antibodies to CD34 Class II (1:50; clone QBEnd-10, DAKO Japan, Tokyo, Japan) and smooth-muscle actin (SMA; 1:100; clone 1A4, DAKO Japan, Tokyo, Japan) after antigen retrieval with CC1 (Ventana Japan, Tokyo, Japan). To visualize the reaction, labeling was carried out using the streptavidin–biotin complex technique (I-VIEW DAB Universal Kit, Ventana Japan, Tokyo, Japan) that was performed according to the manufacturer's instructions. Four FNH-bg-livers were not available for immunohistochemistry.

Statistical analysis

Fisher's exact test was used to compare the frequency of appearance of the findings examined between FNH-bg-livers and non-FNH-livers. A two-sided p value of less than 0.05 was considered to indicate a statistically significant difference.

Results

Small uniform nodule formation with accentuating hepatic lobule

We found small uniform nodule formations that accentuated the hepatic lobule in seven (7/10, 70%) FNH-bg-livers (Figs. 1 and 2, Tables 1 and 2) but only two (2/10, 20%) non-FNH-livers. The small uniform nodules accentuating the hepatic lobules were composed of clear swollen hepatocytes in the central area around the central vein (zone 3) and dark small hepatocytes in peripheral areas (zone 1) of the hepatic lobule.

No fibrous septum was found. Staining with Berlin blue revealed ring-like iron deposits along the periphery of the nodules (ring-like siderosis) in four of eight cases in which Berlin blue staining was available (4/8, 50%; Fig. 2b). On the other hand, no ring-like siderosis was observed in the non-FNH-livers. The frequency of appearance of ring-like siderosis was significantly different between FNH-bg-liver and non-FNH-liver ($p=0.021$).

In a case in which partial hepatectomy was performed, the nodule formation and ring-like siderosis was observed more than 8 cm from the lesion (Fig. 1).

Abnormal unpaired arteries and alteration of sinusoidal endothelium

An abnormal unpaired small artery was defined as a muscular small artery not accompanied by a bile duct or portal vein (Fig. 3a, b). The presence of SMA in the artery was confirmed by an immunohistochemical staining with an antibody to SMA. Abnormal small arteries were present in FNH-bg-livers in six of six cases in which immunohistochemical study was available (6/6, 100%). However, only three cases with non-FNH-livers had abnormal small arteries (3/10, 30%; Table 1). The difference of frequency of appearance was statistically significant ($p=0.021$). Three FNH-bg-livers had more than five abnormal arteries per ten high-power fields; these livers are indicated as double positive (++) in Table 1.

Trait alteration of the sinusoidal endothelium as revealed by the immunoactivity with CD34 was observed only around the portal tracts in FNH-bg-livers (3/6, 50%; Fig. 3c).

Other findings

In other findings, two of ten FNH-bg-livers had ectopic pancreatic tissue intermingled with the intrahepatic peribiliary glands in medium-sized portal tracts (2/10, 20%). No pancreatic ectopia was detected in the non-FNH-livers (Tables 1 and 2, Figs. 1 and 3d).

Fig. 1 Gross findings of focal nodular hyperplasia and extranodular background liver tissue obtained with partial hepatectomy. Histological findings of areas *a* and *b* are shown in Fig. 2a, b and 3d

Discussion

An international working party defined FNH as a lesion supplied by large arteries [2]. Abnormal hepatic circulation is a key feature that precedes the development of FNH [3, 4]. A common histopathological finding is stenosis and/or dilatation of portal veins and muscular thickening of the arterial wall in FNH nodules. Further, a radiological finding of FNH was a hypervascular tumor with intense staining of the capillaries during the parenchymal phase of the angiogram. A central feeding blood supply through an anomalously enlarged artery is also a characteristic angiographic finding [11, 12]. The radiological as well as histopathological findings support the preexistence of histological alterations in the extranodular background liver tissue of FNH. Only one report studied the histological alterations in FNH-bg-livers, but it lacked a detailed description [10].

Abnormal unpaired small arteries that were not accompanied by obvious fibrous tissue or bile ducts were highlighted by immunohistochemical staining for SMA. The incidence of abnormal unpaired small arteries was considerably higher in FNH-bg-livers (100%) than in non-FNH-livers (30%). Abnormal unpaired small arteries are rarely seen in normal or even cirrhotic livers, but increased numbers of abnormal unpaired arteries are frequently observed in hepatocellular carcinoma [13, 14]. In hepatocellular carcinoma, abnormal unpaired arteries are believed to arise from the blood vessels in the fibrous septa and extend into the nodule as neovasculization. However, it is not clear whether the abnormal unpaired small arteries in an FNH-bg-liver are a result of neovasculization or congenital malformation.

Further, a high incidence (50%) of CD34-positive sinusoidal endothelium around the portal tracts was only seen in the FNH-bg-livers. Only a few sinusoidal endothelial cells in acinar zone 1 of normal liver parenchyma express CD34, while the sinusoidal endothelium among tumor cell nests in hepatocellular carcinomas frequently express CD34 [13, 15]. It has been reported that in FNH nodules, the sinusoids along the periphery of the central scar express CD34 [16]. CD34 expression is considered to be indicative of capillarization of the sinusoids that are in the process of developing into the predominant arterial blood supply [13, 17]. Therefore, we consider CD34 expression in FNH-bg-livers as an indication of hemodynamic alteration in the extranodular area as well as the intranodular area.

The small uniform nodules in the FNH-bg-livers of 70% of FNH cases are also an interesting finding. These nodules

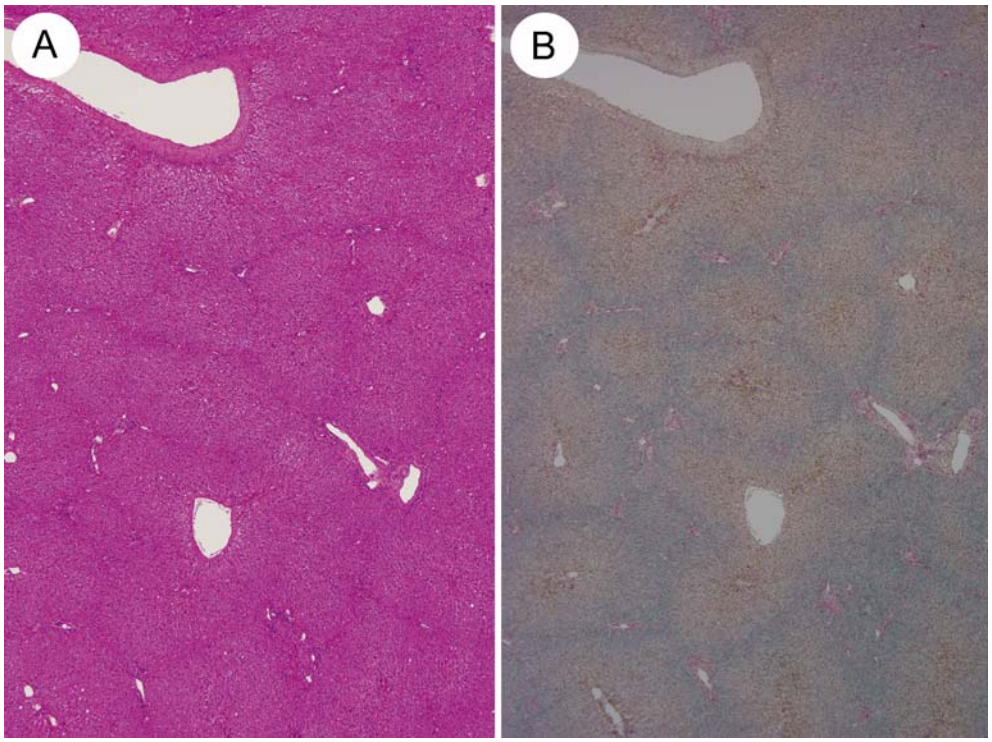

Fig. 2 Nodular formation and ring-like siderosis in the extranodular background liver of focal nodular hyperplasia. **a** Hepatic lobules are accentuated by relatively eosinophilic liver parenchyma of zone 1. **b** Berlin blue stain enhances the nodular pattern by staining the siderosis of zone 1. The findings defined as ring-like siderosis were observed in half the FNH-bg-livers

resemble those found in nodular regenerative hyperplasia (NRH). It has been proposed that FNH and NRH may be related to abnormal hepatic circulation [18]. However, the nodules in FNH-bg-livers accentuate the hepatic lobule and have a central vein, whereas a portal tract is present at the center of the nodules in NRH. Although nodules were also observed in 20% of the non-FNH livers, ring-like siderosis was only observed in the nodules in FNH-bg-livers. Secondary siderosis is usually found in patients with neonatal iron overload, hematological disorders, chronic hepatitis, cirrhosis, alcoholic liver disease, or steatosis. Apart from HFE gene mutation in primary hemochromatosis, the precise cause of iron deposition in various liver diseases is unknown [19]. Iron deposition in the extranodular background liver with FNH has not been reported. We propose the following pathogenesis for the ring-like siderosis in FNH-bg-liver: (1) FNH alters blood perfusion and leads to microhemorrhage and/or local iron overload, or (2) preexisting iron deposition causes FNH development. One case report in which it was found that iron overload led to a significant increase in the size of the FNH nodules supports the second proposal [20].

Ectopic pancreatic tissue in the liver is rare. In a study of 1,000 consecutive autopsy cases, heterotopic pancreatic

Table 1 Nodular formation, ferrugination, and immunohistochemistry in background liver tissue of FNH

No.	Age	Sex	Abnormal small artery	CD34-positive sinusoid	Nodular formation	Ring-like siderosis	Ectopic pancreas
1	34	F	+	−	+	+	+
2	39	F	+	+	−	−	+
3	38	F	+ +	+	+	−	−
4	41	M	+ +	−	+	+	−
5	60	F	+ +	−	+	+	−
6	64	F	+	+	−	−	−
7	38	M	N/A	N/A	+	+	−
8	36	F	N/A	N/A	+	−	−
9	35	F	N/A	N/A	+	N/A	−
10	25	F	N/A	N/A	−	N/A	−
Total			100% (6/6)	50% (3/6)	70% (7/10)	50% (4/8)	20% (2/10)

Table 2 Comparison of FNH-liver with non-FNH liver

	Abnormal small artery	CD34-positive sinusoid	Nodular formation	Ring-like siderosis	Ectopic pancreas
FNH	100% (6/6)	50% (3/6)	70% (7/10)	50% (4/8)	20% (2/10)
Non-FNH	30% (3/10)	0% (0/10)	20% (2/10)	0% (0/10)	0% (0/10)
p value[a]	0.021	N.S.	N.S.	0.045	N.S.

N.S. not significant

[a] Two-sided *p* value of Fisher's exact test

tissue was found in only 4.1% of livers [21]. Surprisingly, we found pancreatic heterotopias in two of ten (20%) FNH patients. Although that could be incidental, the high incidence of heterotopic pancreatic tissue might support the hypothesis that some congenital malformation is related to the pathogenesis of FNH.

In summary, we found abnormal unpaired arteries, CD34-positive sinusoidal endothelium, small uniform nodular formation with ring-like siderosis, and ectopic pancreatic tissue in the extranodular liver parenchyma of FNH patients. These are characteristic histopathologic findings in liver parenchyma around FNH.

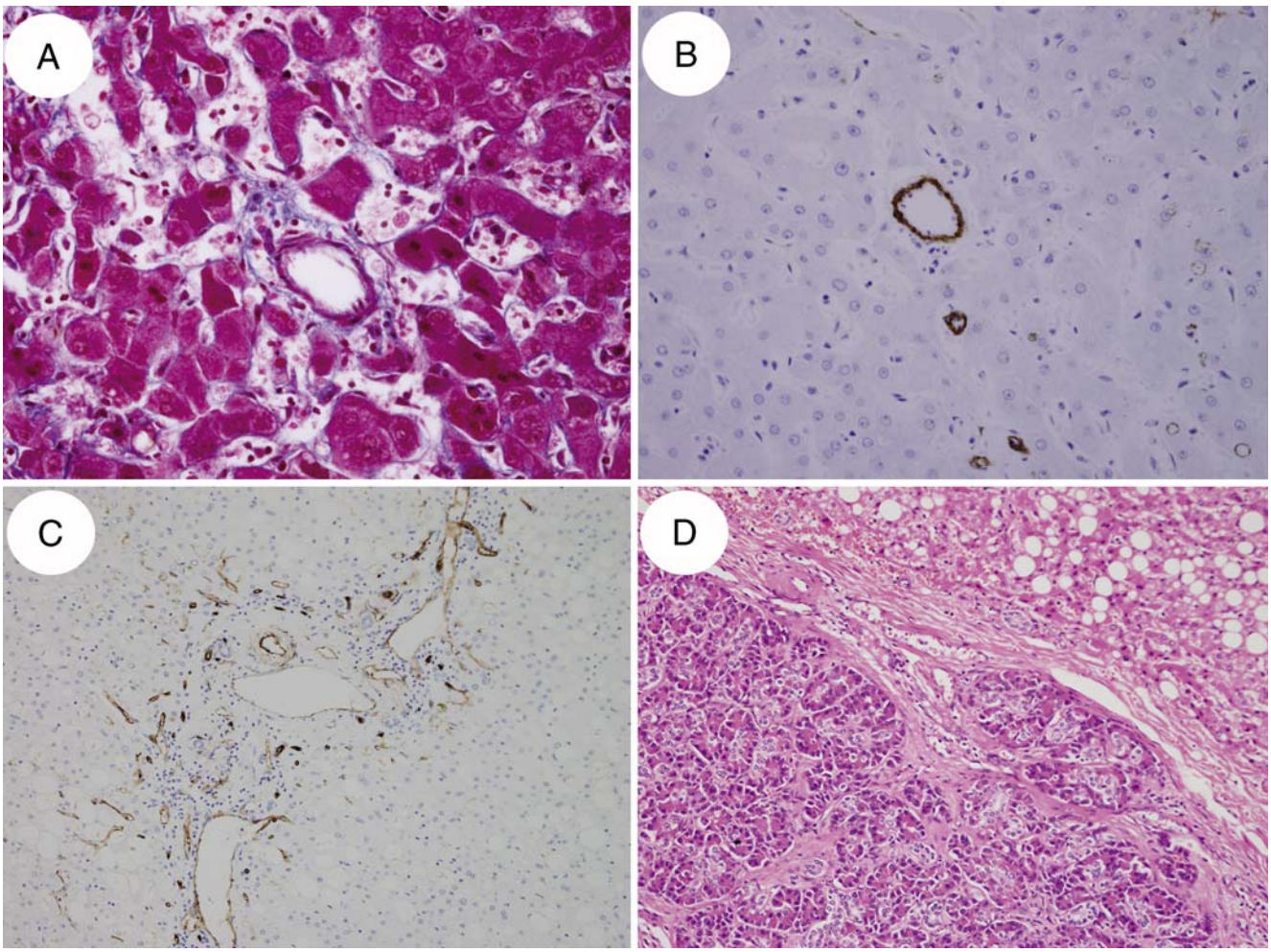

Fig. 3 Other findings of FNH-bg-livers. **a** Abnormal unpaired small artery that was not accompanied by a bile duct or portal vein was observed in all FNH-bg-livers. **b** The wall of the abnormal unpaired small artery is positive for smooth muscle actin. **c** CD34-positive sinusoids were observed around the portal tract in half of FNH-bg-livers. **d** Ectopic pancreas tissue presented in two of ten FNH-bg-livers

Conflict of interest statement We declare that we have no conflict of interest.

References

1. Nguyen BN, Flejou JF, Terris B et al (1999) Focal nodular hyperplasia of the liver: a comprehensive pathologic study of 305 lesions and recognition of new histologic forms. Am J Surg Pathol 23:1441–1454
2. International Working Party (1995) Terminology of nodular hepatocellular lesions. Hepatology 22:983–993
3. Kaji K, Kaneko S, Matsushita E et al (1998) A case of progressive multiple focal nodular hyperplasia with alteration of imaging studies. Am J Gastroenterol 93:2568–2572
4. Sadowski DC, Lee SS, Wanless IR et al (1995) Progressive type of focal nodular hyperplasia characterized by multiple tumors and recurrence. Hepatology 21:970–975
5. Bioulac-Sage P, Balabaud C, Wanless IR (2001) Diagnosis of focal nodular hyperplasia: not so easy. Am J Surg Pathol 25:1322–1325
6. Paradis V, Laurent A, Flejou JF et al (1997) Evidence for the polyclonal nature of focal nodular hyperplasia of the liver by the study of X-chromosome inactivation. Hepatology 26:891–895
7. Gaffey MJ, Iezzoni JC, Weiss LM (1996) Clonal analysis of focal nodular hyperplasia of the liver. Am J Pathol 148:1089–1096
8. Bioulac-Sage P, Rebouissou S, Sa Cunha A et al (2005) Clinical, morphologic, and molecular features defining so-called telangiectatic focal nodular hyperplasias of the liver. Gastroenterology 128:1211–1218
9. Rebouissou S, Bioulac-Sage P, Zucman-Rossi J (2008) Molecular pathogenesis of focal nodular hyperplasia and hepatocellular adenoma. J Hepatol 48:163–170
10. Kondo F, Nagao T, Sato T et al (1998) Etiological analysis of focal nodular hyperplasia of the liver, with emphasis on similar abnormal vasculatures to nodular regenerative hyperplasia and idiopathic portal hypertension. Pathol Res Pract 194:487–495
11. Welch TJ, Sheedy PF, Johnson CM et al (1985) Radiographic characteristics of benign liver tumors: Focal nodular hyperplasia and hepatic adenoma. Radiographics 5:673–682
12. Hussain SM, Terkivatan T, Zondervan PE et al (2004) Focal nodular hyperplasia: findings at state-of-the-art MR imaging, US, CT, and pathologic analysis. Radiographics 24:3–17, discussion 18–19
13. Park YN, Yang CP, Fernandez GJ et al (1998) Neoangiogenesis and sinusoidal "capillarization" in dysplastic nodules of the liver. Am J Surg Pathol 22:656–662
14. Roncalli M, Roz E, Coggi G et al (1999) The vascular profile of regenerative and dysplastic nodules of the cirrhotic liver: implications for diagnosis and classification. Hepatology 30:1174–1178
15. Scoazec JY, Racine L, Couvelard A et al (1994) Endothelial cell heterogeneity in the normal human liver acinus: in situ immunohistochemical demonstration. Liver 14:113–123
16. Scoazec JY, Flejou JF, D'Errico A et al (1995) Focal nodular hyperplasia of the liver: composition of the extracellular matrix and expression of cell-cell and cell-matrix adhesion molecules. Hum Pathol 26:1114–1125
17. Ruck P, Xiao JC, Kaiserling E (1995) Immunoreactivity of sinusoids in hepatocellular carcinoma. An immunohistochemical study using lectin UEA-1 and antibodies against endothelial markers, including CD34. Arch Pathol Lab Med 119:173–178
18. Kondo F (2001) Benign nodular hepatocellular lesions caused by abnormal hepatic circulation: etiological analysis and introduction of a new concept. J Gastroenterol Hepatol 16:1319–1328
19. Bonkovsky HL, Banner BF, Rothman AL (1997) Iron and chronic viral hepatitis. Hepatology 25:759–768
20. Hohler T, Lohse AW, Schirmacher P (2000) Progressive focal nodular hyperplasia of the liver in a patient with genetic hemochromatosis–growth promotion by iron overload? Dig Dis Sci 45:587–590
21. Terada T, Nakanuma Y, Kakita A (1990) Pathologic observations of intrahepatic peribiliary glands in 1000 consecutive autopsy livers. Heterotopic pancreas in the liver. Gastroenterology 98:1333–1337

Virchows Arch (2009) 454:563–571
DOI 10.1007/s00428-009-0757-3

ORIGINAL ARTICLE

Semaphorin3A immunohistochemical expression in human meningiomas: correlation with the microvessel density

Valeria Barresi · Enrica Vitarelli · Serenella Cerasoli

Received: 13 January 2009 / Revised: 2 March 2009 / Accepted: 4 March 2009 / Published online: 19 March 2009

Abstract The immunoexpression of the antiangiogenic factor semaphorin3A (SEMA3A) was evaluated in a series of meningiomas. Then, its correlations with the microvessel density (MVD) of the tumors and with the clinicopathological parameters as well with the survival time or recurrence-free interval were investigated. A positive SEMA3A immunostaining was found in most of meningiomas and a significant association was found between a high expression of this protein and a low MVD of the tumors. Moreover, a low SEMA3A immunoexpression was significantly correlated with a higher recurrence rate of meningiomas. In conclusion, our findings suggest a role for SEMA3A as an antiangiogenic factor in meningiomas with its decrease being associated with the development of recurrences. The supplementation of SEMA3A might be used in novel therapeutic antiangiogenic strategies to prevent the recurrence of highly vascularized meningiomas.

Keywords SEMA3A · CD105 · Neoangiogenesis · Meningioma · Prognosis

Dedicated to my son Alessandro who was born on the 3rd of October 2008.

V. Barresi · E. Vitarelli
Department of Human Pathology, University of Messina, Messina, Italy

S. Cerasoli
Unit of Pathology, M. Bufalini Hospital, Cesena, Italy

V. Barresi (✉)
Dipartimento di Patologia Umana, Policl. Univ. G. Martino, Pad D, Via Consolare Valeria, 98125 Messina, Italy
e-mail: vbarresi@unime.it

Introduction

Meningiomas represent frequent neoplasms [1] mainly characterized by a benign histology and an indolent clinical course. The most powerful prognosticators for these neoplasias include the histological grade and the extent of surgical resection; nonetheless, an adverse clinical course in terms of mortality and morbidity has been also associated with the degree of tumor vascularity and with the extent of peritumoral vasogenic edema [2, 3]. In particular, we have recently shown that the quantity of intratumoral neoangiogenesis, reflected by the microvessel density (MVD) quantified through the specific marker CD105, is significantly correlated with a high histological grade and growth fraction as well as with a shorter overall and recurrence-free survival in human meningiomas [3]. As known, neoangiogenesis is dependent on the balance between angiogenic and antiangiogenic regulators [4]. Among the antiangiogenic factors, attention has been recently focused on semaphorin3A (SEMA3A), which belongs to the class 3 semaphorins (SEMAs), a class of proteins secreted by vertebrates with a role in axon guidance [5]. SEMA3A exerts its action through the binding to neuropilin-1 (NRP-1), a protein initially identified on neuronal cells but which is also expressed on the endothelial cells as a transmembrane receptor. SEMA3A inhibits the proliferation of endothelial cells and induces their apoptosis following its binding to NRP-1 [6]. NRP-1 also functions as an additional receptor for the vascular endothelial growth factor (VEGF). It is known that VEGF is an activator of neoangiogenesis via the binding to VEGF receptors (VEGF-R), but it has been shown that, in the absence of VEGF-R expression, VEGF activity may be mediated by NRP-1 [7]. In addition, NRP-1 may also enhance the effects of VEGF binding to

VEGF-R2 [8]. Therefore, SEMA3A behaves as an antiangiogenic factor both directly, through the binding to NRP-1, and indirectly, through the competitive inhibition of VEGF binding to NRP-1 [9, 10]. In the present study, we analyzed for the first time SEMA3A immunohistochemical expression in a series of human meningiomas of different histotype and histological grade and correlated it with the MVD revealed in the same tumors by CD105 immunohistochemical detection. Our purpose was to verify whether the quantity of neoangiogenesis differed together with the amount of SEMA3A expression in human meningiomas, in coherence with a possible role of SEMA3A as a negative regulator of neoangiogenesis in these tumors. The correlations between SEMA3A expression and the clinicopathological parameters, such as the histological grade or the proliferation index, as well as the overall and recurrence-free survival of these neoplasias were also assessed in an attempt to evaluate the eventual histoprognostic value of this marker in human meningiomas.

Materials and methods

Forty-five cases of surgically resected meningiomas, obtained from 21 female (47%) and 24 male (53%) patients (age range 31–84 years; mean age 64 years) and occurred between 1996 and 1998, were taken from the files of the Unit of Pathology, M. Bufalini Hospital, Cesena, Italy. More precisely, 18 cases, diagnosed as atypical meningiomas, were randomly selected. Subsequently, a comparable number of cases comprising meningothelial, transitional, and fibrous histotypes were considered. Moreover, cases of meningiomas displaying a more unusual histotype and occurring in the same years were also recruited. Finally, three anaplastic meningiomas were added to the cohort. All cases were histologically re-evaluated according to the World Health Organization (WHO) 2007 classification system [11]. Finally, the cohort of the study comprised: eight meningothelial (17%), seven transitional (15%), three fibrous (6%), three microcystic (6%), two secretory (4%), one chordoid (2%), 18 (40%) atypical, and three anaplastic (6%) meningiomas. Thus, according to the WHO 2007 classification [1], 23 cases displayed a histological grade I, 19 a histological grade II, and three a histological grade III. The tumor localization was subdivided into three sites: convexity (40%), parasagittal (35%), and basal (25%). For each case, Simpson's grade of surgical resection [11] was available. On the basis of Simpson's grade, two main groups were considered: the first one (66%) representing grade 1 tumors (complete excision, including dura and bone), the second group (34%) comprising both grade 2 (complete excision plus apparently reliable coagulation of dural attachments) and grade 3 (complete excision of the solid tumor, but with insufficient dural coagulation or bone excision) meningiomas. The Ki-67 labeling index (LI), reflecting the tumor growth fraction, was available in all cases, whereby the follow-up data, including the patients survival and recurrences, were available in 42 out of 45 (93%) cases. Recurrence was defined as the detection of a recurrent tumor by neuroradiological investigations in those patients with a previous complete surgical excision. In the meningiomas of the cohort, the tumor neoangiogenesis was quantified through the assessment of MVD performed by using the immunohistochemical detection of the specific marker for neoangiogenesis CD105 (endoglin) as previously described [3, 12–14].

Immunohistochemistry

All meningiomas were fixed in 10% neutral formalin for 24 h at room temperature, embedded in paraffin at 55°C, and cut into parallel consecutive 4-μm thick sections for the subsequent immunohistochemical study. Briefly, the endogenous peroxidase activity was blocked with 0.1% H_2O_2 in methanol for 20 min; then, normal sheep serum was applied for 30 min to prevent unspecific adherence of serum proteins. The SEMA3A antigen was unmasked by microwave oven pretreatment in 10 mM, pH 6.0 sodium citrate buffer for three cycles for 5 min, whereas for CD105 epitope retrieval, specimens were pretreated with proteinase K (S3020, Dako Cytomation) at room temperature for 15 min. Sections were successively incubated at 4°C overnight with the primary polyclonal antibody against SEMA3A sc-10720 (Santa Cruz Biotechnology, Santa Cruz, CA; w.d. 1:25) and with the primary monoclonal antibody against CD105 (Dako, Denmark; clone SN6h, w.d. 1:50). The bound primary antibodies were visualized by avidin–biotin–peroxidase detection using the Vectastain Rabbit/Mouse Elite Kit, according to the manufacturer's instructions. To reveal the immunostaining, the sections were incubated in darkness for 10 min with 3,3′-diaminobenzidine tetrahydrochloride (Sigma Chemical, St. Louis, MO, USA) in the amount of 100 mg in 200 mL 0.03% hydrogen peroxide in phosphate-buffered saline (PBS). Nuclear counterstaining was performed by Mayer's haemalum. Specificity of the binding was assessed by omitting the primary antiserum or replacing it with normal rabbit serum or PBS solution (pH 7.4). Moreover, renal tubules within specimens of fetal kidney and the syncytiotrophoblast present in specimens of human term placenta were used as positive controls for SEMA3A [15] and CD105 [16] immunohistochemical reactions, respectively. In parallel sections obtained from the same tissue blocks, Ki-67 antigen was

unmasked by retrieval procedures (10 mM, pH 6.0 sodium citrate buffer heated in a microwave oven for three cycles for 5 min) and then Ki-67 antiserum (clone MIB-1, Dako, Glostrup, Denmark; w.d. 1:50) was applied for 30 min at room temperature.

Quantification and statistics

With reference to SEMA3A immunohistochemical assay, sections were estimated by a light microscopy with ×20 and ×40 objective lens and ×10 eyepiece. The assessment of the immunostained section was performed by two independent pathologists blinded to the clinicopathological data. SEMA3A expression was based on the presence of a cytoplasmic staining. Staining intensity (SI) was graded as 0 (negative), 1 (weak), 2 (moderate), and 3 (strong); the area of staining positivity (ASP), recorded as the percentage of positive cells, was assessed by providing the following values: 0 (<5%), 1 (5–25%), 2 (26–50%), 3 (51–75%), and 4 (76–100%). Then, an intensity distribution (ID) score was generated for each case by multiplying the values of SI and ASP. Cases displaying a score of 0 were considered as negative for SEMA3A.

The quantification of microvessels was performed as previously described [12–14]. Briefly, the three most vascularized areas detected by CD105 were initially selected (so-called hot spots) under ×40 field. Then, microvessels were counted in each of these areas under a ×400 field. Single endothelial cells or clusters of endothelial cells, with or without a lumen, were considered to be individual vessels. The mean value of three ×400 field (0.30 mm^2) counts was recorded as the MVD of the section. Then, the MVD value was converted into the mean number of microvessels per square millimeter for the statistical analyses. The vessels were counted using a Zeiss microscope by two independent observers blinded to the clinicopathological data.

The Ki-67 LI was calculated as the mean percentage by counting the stained nuclei of tumor cells for 1,000 cells in three representative neoplastic fields; all degrees of nuclear SI were taken into consideration. A Ki-67 value of 4% was utilized as a cut-off point to determine low and high Ki-67 expression, as suggested by Perry et al. [17].

The median ID score value (ID score of 3) was used as the cut-off to define low (ID score of 0–2) and high (ID score of 3–12) SEMA3A expression and the Fisher's exact and chi-squared tests were performed in order to analyze the statistical correlations between SEMA3A immunohistochemical expression and the clinicopathological parameters of the meningiomas. Mann–Whitney and Kruskal–Wallis tests were used to evaluate the correlations between the MVD and the clinicopathological variables of the tumors.

Overall survival and recurrence-free survival were assessed by the Kaplan–Meier method, with the date of primary surgery as the entry data. Patients that died of diseases independent from the meningioma (myocardial infarction, other malignant neoplasias not involving the central nervous system) were censored. The endpoint for the recurrence-free survival analysis was the length of survival to the detection of a recurrent tumor. The Mantel–Cox log–rank test was applied to assess the strength of association between survival time or recurrence-free interval and each of the parameters (age and gender of the patient, site, Simpson's grade, histologic grade, MVD, Ki-67 LI, and SEMA3A expression of the tumor) as a single variable. Successively, a multivariate analysis (Cox regression model) was utilized to determine the independent effect of each variable on survival.

For SEMA3A and MVD overall and recurrence-free survival analyses, cases were subdivided into two groups by using the median MVD value (CD105-MVD median value=20) and the median SEMA3A ID score, respectively, as the cut-off values.

A probability (P) value less than 0.05 was considered statistically significant. Data were analyzed using the SPSS package version 6.1.3 (SPSS, Chicago, IL, USA).

Results

The clinicopathological characteristics, the MVD counts, and the SEMA3A immunohistochemical data relative to the 45 analyzed meningiomas are shown in Table 1. SEMA3A immunohistochemical expression, with a variable ID score, was identified in 42 out of 45 (93%) cases. The immunostaining, demonstrated by the presence of stained brown granular immunoreaction products, was evident in the cytoplasm of the neoplastic cells (Fig. 1).

CD105-positive vessels were identified in 33 out of 45 (73%) meningiomas. A high (ID score of 3–12) SEMA3A immunoexpression was present in ten out of 12 (83%) of the CD105-negative cases, which were all but one grade I tumors (Table 1). Besides, among grade I meningiomas, the microcystic displayed a low (ID score of 0–2) SEMA3A expression, in association with a high MVD (above 20 vessels/mm^2) (Table 1). A significant association was found between a high SEMA3A immunohistochemical expression and a MVD below 20 vessels/mm^2 (P=0.0365) (Table 2). Correspondingly, significantly lower MVD counts were evidenced in SEMA3A highly expressing tumors (P=0.0106) (Table 3) (Fig. 2).

A variously represented Ki-67 nuclear reactivity was found in meningiomas, with a rate of stained cells ranging from 0.5% to 30% (mean value of 6.8%). Despite the high (20% or 30%) Ki-67 LI value encountered, some cases

Table 1 Clinicopathological characteristics, MVD, and SEMA3A immunohistochemical data of 45 analyzed meningiomas

Case	Sex	Age (years)	Site	Histotype	Grade	Ki-67 (%)	Simpson	SEMA3A ID score	CD105-MVD (vesels/mm^2)	Status	FU (months)	Recurrences	DFI
1	F	31	B	Atypical	2	8	1	12	20.00	NED	93	Not	93
2	M	38	S	Atypical	2	10	3	1	23.33	DOD	97	–	
3	M	57	S	Atypical	2	5	2	2	30.00	NED	104	–	89
4	F	76	B	Transitional	1	3	1	4	4.33	DID	5	Not	5
5	M	60	B	Meningothelial	1	0.5	2	1	0.00	NED	112	–	
6	M	75	B	Secretory	1	0.5	2	4	30.00	DOD	2	–	119
7	F	49	C	Meningothelial	1	0.5	1	1	5.33	NED	117	Not	117
8	F	71	C	Atypical	2	6	1	1	66.66	AWD	89	Yes	60
9	M	67	C	Atypical	2	10	1	6	0.00	NED	120	Not	120
10	F	76	C	Microcystic	1	1	2	0	83.33	DID	76	–	
11	M	54	B	Meningothelial	1	0.5	1	12	5.33	NED	114	Not	114
12	F	73	S	Atypical	2	5	3	1	20.00	NED	114	–	
13	M	65	B	Meningothelial	1	4	1	8	0.00	DID	0	–	–
14	M	64	C	Atypical	2	5	1	6	93.33	NED	94	Not	94
15	M	56	S	Atypical	2	5	1	1	51.00	DOD	91	Yes	16
16	M	66	S	Atypical	2	6	1	8	26.66	NED	108	Not	108
17	F	54	C	Transitional	1	0.5	1	1	0.00	NED	100	Not	100
18	M	63	C	Transitional	1	2	1	0	4.33	NED	118	Not	118
19	M	80	S	Transitional	1	0.5	1	1	5.33	NED	119	Not	119
20	M	75	C	Meningothelial	1	4	1	6	0.00	DID	50	Not	50
21	M	63	C	Meningothelial	1	0.5	1	6	0.00	NED	115	Not	115
22	F	70	B	Transitional	1	0.5	2	12	0.00	NED	119	–	119
23	F	70	C	Atypical	2	10	1	1	27.66	DOD	47	Yes	39
24	F	79	B	Meningothelial	1	1	1	4	0.00	NED	119	Not	119
25	M	73	S	Atypical	2	30	2	1	55.33	DID	111	–	
26	F	47	B	Secretory	1	1	3	9	5.33	NED	96	–	7
27	M	53	S	Microcystic	1	4	1	1	106.66	NED	110	Not	110
28	F	60	C	Atypical	2	10	1	2	23.33	DOD	7	Yes	7
29	F	70	B	Fibroblastic	1	1	1	4	0.00	NED	96	Not	96
30	F	64	S	Fibroblastic	1	3	1	4	0.00	NED	108	Not	108
31	M	40	S	Atypical	2	3	1	3	20.00	NED	108	Not	108
32	F	84	S	Atypical	2	30	2	8	23.33	DOD	9	–	
33	F	66	C	Transitional	1	0.5	1	0	4.33	NED	117	Not	117
34	F	75	C	Atypical	2	5	1	2	30.00	NED	105	Not	105
35	F	74	C	Atypical	2	15	1	2	85.33	NED	91	Not	91

36	M	71	B	Transitional	1	4	2	12	18.66	DID	7	–	
37	M	75	S	Atypical	2	20	2	6	40.00	DOD	41	–	14
38	M	65	C	Meningothelial	1	0.5	1	6	0.00	NED	111	Not	111
39	M	75	C	Chordoid	2	5	1	12	63.33	DOD	1	Not	1
40	F	59	C	Fibroblastic	1	2	1	6	0.00	NED	103	Not	103
41	F	62	S	Atypical	2	5	1	2	83.33	NED	71	Not	71
42	M	43	C	Microcystic	1	1	1	2	36.66	NED	97	Not	97
43	F	71	S	Anaplastic	3	20	2	0	27.66		NA		NA
44	M	68	S	Anaplastic	3	30	3	1	51		NA		NA
45	M	75	S	Anaplastic	3	30	3	3	66.66		NA		NA

LI labeling index, *MVD* microvessel density, *FU* follow-up, *DFI* disease-free interval, *B* basal, *S* sagittal, *C* convexity, *NED* not evidence of disease, *DOD* dead of disease, *DID* dead of independent disease, *NA* not available

were classified as atypical and not as malignant meningiomas since the criterion of 20 or more mitoses per ten high-power fields in order to classify them as grade 3 tumors was not fulfilled [22].

No significant correlations were found between SEMA3A immunoexpression amount and the age and gender of the patients or the site, the grade, the Ki-67 LI, and the Simpson's grade of the tumors (Table 2). By contrast, when the statistical correlations between the MVD counts and the various clinicopathological parameters were investigated, a significantly higher MVD was found in the meningiomas characterized by a sagittal site (P=0.0091) and a high histological grade (P=0.0003) and Ki-67 LI (P=0.0001) (Table 3). Regarding the clinical course, univariate analyses identified a high histological grade, a Ki-67 LI higher than 4% (Fig. 2), and a MVD count equal or higher than 20 vessels/mm^2 as significant negative prognostic factors for the patients' specific survival to meningiomas (Tables 4 and 5). Multivariate analysis indicated that only Ki-67 LI was an independent prognostic factor (Tables 4 and 5).

Among the 30 patients with a Simpson's grade 1 meningioma, four had developed recurrences. Follow-up ranged from 5 to 120 months. Univariate analyses showed that a MVD ≥20 vessels/mm^2, a Ki-67 LI >4%, a high histologic grade, and a low SEMA3A immunoexpression (Fig. 2) were significant prognostic factors for recurrence (Table 6).

Discussion

The quantity of neoangiogenesis, reflected by the MVD, has been demonstrated as a prognostic parameter, correlated with a higher biological aggressiveness, in several types of human neoplasias, including meningiomas [3, 18, 19]. Actually, as long as a neoplastic mass is supplied by the only host vessels, it retains a limited volume and a low doubling time. By contrast, when the formation of new capillaries is induced by the neoplastic cells through the secretion of proangiogenic factors, the nutrients provided by the newly formed vessels allow a more rapid growth and the progression of the tumor [20, 21]. In meningiomas, neoangiogenesis appears to be positively regulated by VEGF produced by the neoplastic cells; indeed, the expression of this factor significantly increases together with the MVD of these neoplasms [22, 23]. It has been recently demonstrated that the proangiogenic activity of VEGF may be antagonized by the antiangiogenic factor SEMA3A [5, 9]; nonetheless, the expression of SEMA3A has been never investigated in meningiomas up to now. In view of this, in the present study, we analyzed SEMA3A immunohistochemical expression in a series of human

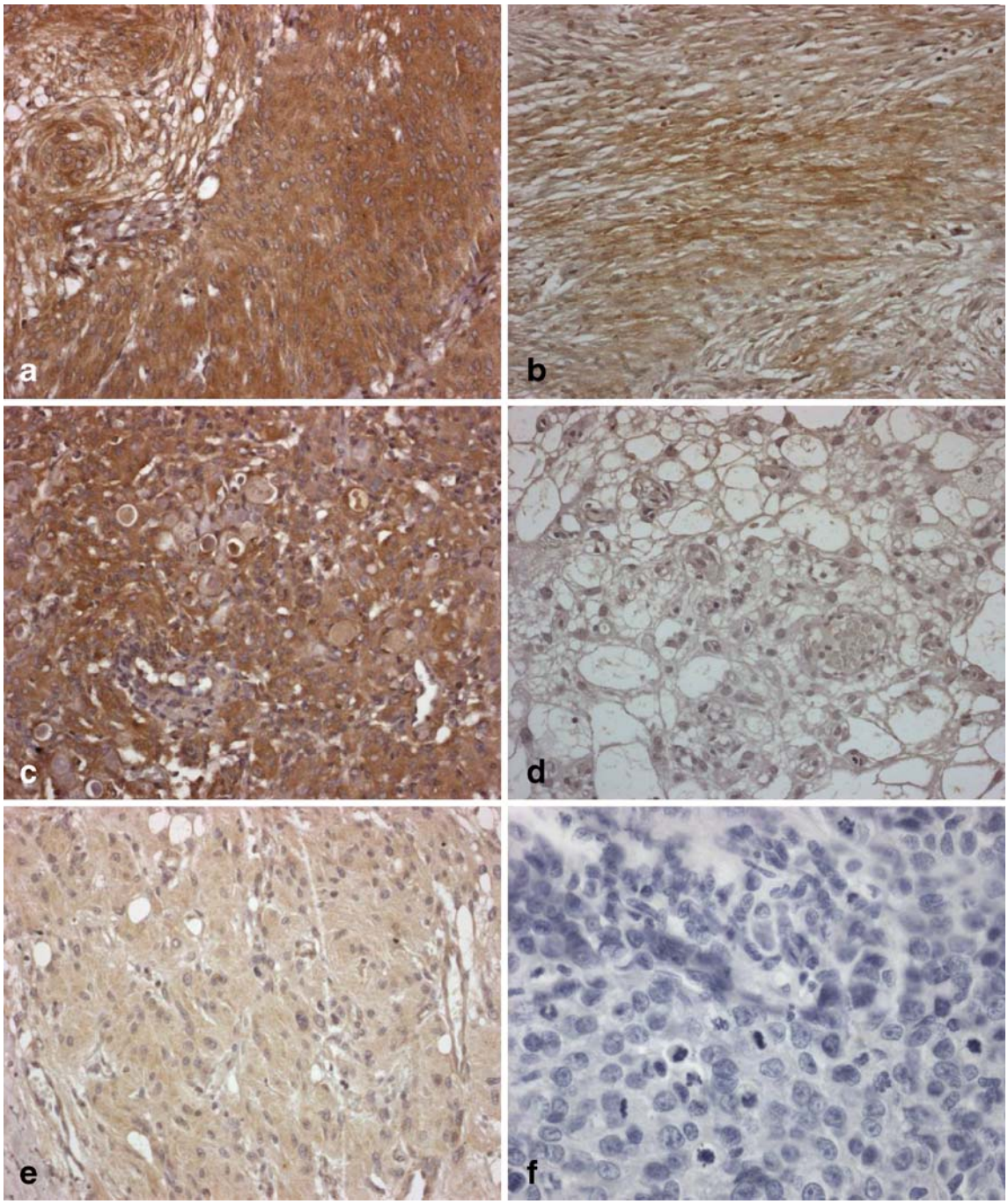

Fig. 1 A meningothelial (**a**; SEMA3A stain; original magnification, ×100), a fibrous (**b**; SEMA3A stain; original magnification, ×100), and a secretory (**c**; SEMA3A stain; original magnification, ×100) meningioma showing a strong SEMA3A immunostaining. **d** A microcystic meningioma negative for SEMA3A (SEMA3A stain; original magnification, ×100) **e** An atypical meningioma with a grade 1 intense SEMA3A staining in the cytoplasm of the neoplastic cells (SEMA3A stain; original magnification, ×200). **f** No SEMA3A immunostaining was evidenced in the neoplastic cells of an anaplastic meningioma (SEMA3A stain; original magnification, ×400)

meningiomas and evaluated its eventual correlations with the MVD quantified in the same tumors.

A positive SEMA3A immunostaining was evidenced in 93% of meningiomas; among the positive tumors, 49% exhibited a low SEMA3A expression, whereas a high immunoexpression was encountered in 51% of cases. The expression of SEMA3A in neoplastic elements is not a novel finding; indeed, SEMA3A expression had been previously demonstrated in glioma [24] and mesothelioma [25] cell lines as well as in neoplastic tissues such as clear cell renal cell carcinoma [26] and pancreatic [27] and ovarian neoplasms [28].

Table 2 Statistical correlations between SEMA3A ID score and clinicopathological parameters as well as MVD investigated through Fisher's exact test and the chi-squared test

Variable	SEMA3A ID score		*P* value
	0–2	3–12	
Gender			0.376
Male	10	14	
Female	12	9	
Age			0.768
≤65 years	11	10	
>65 years	11	13	
Site			0.009
Convexity	11	7	
Sagittal	10	6	
Basal	1	10	
Grade			0.392
1	9	14	
2	11	8	
3	2	1	
Ki-67 LI			0.236
≤4%	10	15	
>4%	12	8	
Simpson's grade			0.757
Grade 1	14	16	
Grade 2–3	8	7	
MVD			0.0365
<20 vessels/mm^2	6	14	
≥20 vessels/mm^2	16	9	

In the present study, CD105 was chosen for the assessment of the MVD of the analyzed tumors for its previously demonstrated higher specificity in comparison to pan-endothelial markers in the evaluation of meningiomas neoangiogenesis [3]. It is a 180-kDa transmembrane glycoprotein predominantly expressed on the endothelial cells of newly formed vessels in tissues undergoing active angiogenesis, such as tumors [29]. On the whole, CD105 immunostained vessels were found in 73% of the meningiomas of our cohort. Interestingly, a high SEMA3A immunohistochemical expression was encountered in the majority of CD105-negative cases; in addition, a significant correlation was found between a low MVD and a high SEMA3A expression, with the highly SEMA3A-expressing tumors characterized by significantly lower MVD counts in comparison to the meningiomas showing a low SEMA3A expression. These data seem to indicate the existence of a negative correlation between the expression of SEMA3A and the MVD, consistently with a hypothetic antiangiogenic role of this protein in meningiomas. Besides, the microcystic meningiomas, which, in spite of their histological grade I, are highly vascularized tumors [3, 30], displayed a low SEMA3A immunohistochemical expression in association with an intense neoangiogenesis, as reflected by their high MVD. A tendency towards a negative correlation between SEMA3A expression and MVD had been already reported in ovarian neoplasms [28], but it was not significant. Nonetheless, it is tempting to speculate that MVD did not actually reflect neoangiogenesis in this study [28]; indeed, the pan-endothelial marker CD34, and not a specific marker for neoangiogenesis, such as CD105, had been used for the MVD assessment.

When the tumors of our cohort were stratified by the histological grade, no significant differences in terms of SEMA3A expression were found between grades 1, 2, and 3 meningiomas. By contrast, as already observed in a previous study [3], significantly higher MVD counts were evidenced in higher-grade tumors. Thus, in grades 2 and 3 tumors, neoangiogenesis might be stimulated by an increase in the secretion of VEGF, as already suggested by other studies [23, 24], without a significant difference in the semaphorin expression. Hence, if the antiangiogenic role of SEMA3A in human meningiomas is confirmed in future studies, it is suitable that an exogenous supplementation of

Table 3 Statistical correlations between MVD and clinicopathological parameters as well as SEMA3A ID score analyzed through Mann–Whitney and Kruskal–Wallis tests

Variable	*n*	Mean rank	*P*
Gender			0.446
Male	24	24.39	
Female	21	21.40	
Age			0.284
≤65 years	21	20.76	
>65 years	24	24.95	
Site			0.009
Convexity	18	22.67	
Sagittal	16	28.53	
Basal	11	14.05	
Grade			0.0003
1	23	0.63	
2	19	29.31	
3	3	34.50	
Ki-67 LI			0.0001
≤4%	25	16.28	
>4%	20	31.40	
Simpson's grade			0.1815
Grade 1	30	21.15	
Grade 2–3	15	26.70	
SEMA3A ID score			0.010
0–2	22	28.11	
3–12	23	18.10	

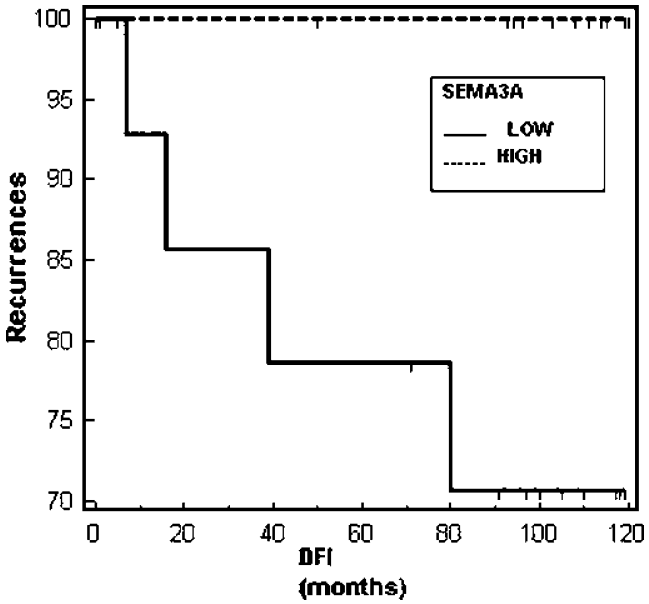

Fig. 2 Kaplan–Meier meningioma recurrence-free survival curve. Cases characterized by a low (ID score of 0–2) SEMA3A expression displayed a significantly higher recurrence rate in comparison to meningiomas showing a high SEMA3A immunoexpression (ID score of 3–12)

this protein would tip the balance towards antiangiogenesis in the higher-grade meningiomas. If so, SEMA3A might be used, together with anti-VEGF antibodies, as a novel antiangiogenic therapy to reduce the blood supply to these tumors.

In our study, we also analyzed the prognostic value of SEMA3A expression on the patients overall and recurrence-free survival to meningiomas. Whereas no association emerged with the former, a low SEMA3A expression was significantly associated to the development of recurrences in the group of patients harboring a Simpson's grade 1 meningioma. It has been suggested that the development of recurrences of totally resected (Simpson's grade 1) meningiomas may be related to the presence of microscopic clusters of neoplastic cells left in the dura mater or in the arachnoid membrane [31, 32] and we may hypothesize that this event depends upon the biological activity of these cells. As specified above, we found that the recurrent tumors of our series displayed a significantly lower SEMA3A expression, as well as significantly higher MVD and growth fraction. Thus, we may speculate that surgically unremoved neoplastic foci of these tumors may grow and give rise to recurrent tumors for their higher capability to stimulate the neoangiogenic process in relationship to a low level of SEMA3A expression. Unfortunately, due to the small number of recurrent cases in our cohort, multivariate analysis could not be performed in order to assess whether the SEMA3A ID score is an independent factor for meningioma-specific recurrence rate.

In conclusion, this pilot study suggests that SEMA3A may negatively regulate neoangiogenesis in meningiomas and that a low SEMA3A expression behaves as a negative prognostic factor for the development of recurrences in these tumors. If further studies confirm these findings, the supplementation of SEMA3A may be used in novel therapeutic antiangiogenic strategies to prevent the recurrence of highly vascularized meningiomas.

Table 5 Multivariate survival analyses in 42 patients with meningioma

Variable	Multivariate analysis			
	β	SE	Exp (β)	P
Ki-67 LI	2.4630	1.0730	11.7398	0.0217

Table 4 Univariate survival analyses in 42 patients with meningioma

Parameter	Univariate analysis		
	χ^2	df	P
Gender	0.3330	1	0.5639
Age	0.9585	1	0.3276
Site	0.9522	2	0.6212
Grade	6.1852	1	0.0129
Ki-67 LI	8.4092	1	0.0037
Simpson's grade	2.1688	1	0.1408
MVD	8.1966	1	0.0042
SEMA3A ID score	0.02569	1	0.8727

Table 6 Univariate analysis for recurrences in 30 patients with a Simpson's grade 1 meningioma

Parameter	Univariate analysis		
	χ^2	df	P
Gender	0.9251	1	0.3361
Age	0.1055	1	0.7454
Site	0.8171	2	0.6646
Grade	5.8306	1	0.0157
Ki-67 LI	8.2699	1	0.0040
MVD	4.9424	1	0.0262
SEMA3A ID score	4.2018	1	0.0404

Acknowledgements We gratefully acknowledge the precious technical assistance of Dr. C.M. Nunnari, MLT, in the study.

Conflicts of interest statement We declare that we have no conflicts of interest.

References

1. Perry A, Louis DN, Scheithauer BW et al (2007) Meningiomas. In: Louis DN, Ohgaki H, Wiestler OD, Cavenee WK (eds) WHO classification of tumors of the central nervous system. IARCC Press, Lyon, pp 164–172
2. Perry A, Stafford SL, Scheithauer BW et al (1999) "Malignancy" in meningiomas: a clinico-pathological study of 116 patients with grading implications. Cancer 85:2046–2056
3. Barresi V, Cerasoli S, Vitarelli E et al (2007) Density of microvessel positive for CD105 (endoglin) is related to prognosis in meningiomas. Acta Neuropathol 114:147–156
4. Folkman J, Shing Y (1992) Angiogenesis. J Biol Chem 267:10931–10934
5. Luo Y, Raible D, Raper JA (1993) Collapsin: a protein in brain that induces the collapse and paralysis of neuronal growth cones. Cell 75:217–227
6. Guttmann-Raviv N, Shraga-Heled N, Varshavsky A et al (2007) Semaphorin-3A and semaphoring-3F work together to repel endothelial cells and to inhibit their survival by induction of apoptosis. J Biol Chem 282:26294–26305
7. Soker S, Takashima S, Miao HQ et al (1998) Neuropilin-1 is expressed by endothelial and tumor cells as an isoform specific receptor for vascular endothelial growth factor. Cell 92:735–745
8. Soker S, Maio HQ, Nomi M et al (2002) VEGF165 mediates formation of complexes containing VEGFR-2 and neuropilin-1 that enhance VEGF165 receptor binding. J Biol Chem 85:357–368
9. Miao HQ, Soker S, Feiner L et al (1999) Neuropilin-1 mediates collapsin-1/semaphorin III inhibition of endothelial cell motility: functional competition of collapsin-1 and vascular endothelial growth factor-165. J Cell Biol 12:233–242
10. Narazaki M, Tosato G (2006) Ligand-induced internalization selects use of common receptor neuropilin-1 by VEGF165 and semaphorin3A. Blood 107:3892–3901
11. Simpson D (1957) The recurrence of intracranial meningiomas after surgical treatment. J Neurol Neurosurg Psychiatry 20:22–39
12. Barresi V, Grosso M, Vitarelli E et al (2008) Endoglin (CD105) immuno-expression in human foetal and neonatal lungs. Histol Histopathol 23:701–708
13. Barresi V, Cerasoli S, Tuccari G (2008) Correlative evidence that tumor cell-derived caveolin-1 mediates angiogenesis in meningiomas. Neuropathology 28:472–478
14. Barresi V, Vitarelli E, Tuccari G et al (2008) Correlative study of microvessel density and 5-lipoxygenase expression in human sporadic colorectal cancer. Arch Pathol Lab Med 132:1807–1812
15. Villegas G, Tufro A (2002) Ontogeny of semaphorins 3A and 3F and their receptors neuropilins 1 and 2 in the kidney. Gene Expr Patterns 2:151–155
16. Gougos A, St Jacques S, Greaves A et al (1992) Identification of distinct epitopes of endoglin, an RGD-containing glycoprotein of endothelial cells, leukemic cells, and syncytiotrophoblasts. Int Immunol 4:83–92
17. Perry A, Stafford SL, Scheithauer BW et al (1998) The prognostic significance of MIB-1, p53, and DNA flow cytometry in completely resected primary meningiomas. Cancer 82:2262–2269
18. Ding S, Li C, Lin S et al (2006) Comparative evaluation of micorvessel density determined by CD34 or CD105 in benign and malignant gastric lesions. Hum Pathol 37:861–866
19. Saad RS, El-Gohary Y, Memari E et al (2005) Endoglin (CD105) and vascular endothelial growth factor as prognostic markers in esophageal adenocarcinoma. Hum Pathol 36:955–961
20. Folkman J (1995) Clinical applications of angiogenic research. N Eng J Med 333:1757–1763
21. Hanahan D, Folkman J (1996) Patterns and emerging mechanisms of the angiogenic switch during tumorigenesis. Cell 86:353–364
22. Pistolesi S, Boldrini L, Gisfredi S et al (2004) Angiogenesis in intracranial meningiomas: immunohistochemical and molecular study. Neuropathol Appl Neurobiol 30:118–25
23. Provias J, Claffey K, delAguila L et al (1997) Meningiomas: role of vascular endothelial growth factor/vascular permeability factor in angiogenesis and peritumoral edema. Neurosurgery 40:1016–1026
24. Rieger J, Wick W, Weller M (2003) Human malignant glioma cells express semaphorins and their receptors, neuropilins and plexins. Glia 42:379–389
25. Catalano A, Caprari P, Rodilossi S et al (2004) Crosstalk between vascular endothelial growth factor and semaphorin-3A pathway in the regulation of normal and malignant mesothelial cell proliferation. FASEB J 18:358–360
26. Catalano A, Caprari P, Moretti S et al (2006) Semaphorin-3A is expressed by tumour cells and alters T-cell signal transduction and function. Blood 107:3321–3329
27. Müller MW, Giese NA, Swiercz JM et al (2007) Association of axon guidance factor Semaphorin 3A with poor outcome in pancreatic cancer. Int J Cancer 121:2421–2433
28. Osada R, Horiuchi A, Kikuchi N et al (2006) Expression of semaphorins, vascular endothelial growth factor and their common receptor neuropilins and allelic loss of semaphorin locus in epithaelial ovarian neoplasms: increased ratio of vascular endothelial growth factor to semaphoring is a poor prognostic factor in ovarian carcinomas. Hum Pathol 37:1414–1425
29. Miller DW, Graulich W, Karges B et al (1999) Elevated expression of endoglin, a component of the TGF-ß receptor complex, correlates with proliferation of tumour endothelial cells. Int J Cancer 81:568–572
30. Christov C, Lechapt-Zalcman E, Adle-Biassette H et al (1999) Vascular permeability factor/vascular endothelial growth factor (VPF/VEGF) and its receptor flt-1 in microcystic meningiomas. Acta Neuropathol 98:414–420
31. Kamitani H, Masuzawa H, Kanazawa I et al (2001) Recurrence of convexity meningiomas: tumour cells in the arachnoid membrane. Surg Neurol 56:228–235
32. Kinjo T, al-Mefty O, Kanaan I (1993) Grade zero removal of supratentorial convexity meningiomas. Neurosurgery 33:394–399

Virchows Arch (2009) 454:573–579
DOI 10.1007/s00428-009-0759-1

ORIGINAL ARTICLE

Expression of prostatic acid phosphatase (PSAP) in transurethral resection specimens of the prostate is predictive of histopathologic tumor stage in subsequent radical prostatectomies

Sven Gunia · Stefan Koch · Matthias May · Manfred Dietel · Andreas Erbersdobler

Received: 27 January 2009 / Revised: 23 February 2009 / Accepted: 4 March 2009 / Published online: 20 March 2009

Abstract Clinical management of incidental prostate cancer (IPC) remains challenging since its clinical course cannot be predicted by conventional histopathology. Aiming to define predictive factors in IPC, we correlated the immunohistochemically detected expression of prostate-specific antigen (PSA), prostatic acid phosphatase (PSAP), alpha-methylacyl-CoA racemase (AMACR, p504s), and androgen receptor in transurethral resection specimens with Gleason scores and histologic staging on the corresponding radicals in a cohort of 54 patients (mean age, 65.9 years; range, 49–80 years). PSAP expression showed a significant correlation with tumor staging (ρ=−0.37; p=0.02) but not with Gleason scores (ρ=−0.06; p=0.69). K-statistics revealed a highly significant moderate interobserver agreement concerning the evaluation of PSAP staining (K=0.47; $p<$ 0.001). In contrast, the other markers assessed failed to correlate with conventional histopathology. Therefore, PSAP might be predictive of tumor stage in IPC and represent a valuable adjunct for clinical decisions in terms of individual therapeutic management.

S. Gunia (✉) · S. Koch
Department of Pathology, HELIOS Clinic Bad Saarow,
Charité-University Medicine Teaching Hospital,
Pieskower Straße 33,
15526 Bad Saarow, Germany
e-mail: sven.gunia@helios-kliniken.de

M. May
Department of Urology,
Clinic St. Elisabeth,
Straubing, Germany

M. Dietel · A. Erbersdobler
Department of Pathology, Campus Charité Mitte,
Charité-University Medicine,
Berlin, Germany

Keywords Incidental prostate cancer · Radical prostatectomy · Histopathologic tumor staging · Immunohistochemistry · Prostatic acid phosphatase (PSAP)

Introduction

Incidental prostate cancer (IPC) is defined as a clinically unapparent tumor discovered after histologic examination of the specimen obtained by open prostatectomy or transurethral resection of the prostate (TURP) [1]. Its overall incidence in TURPs performed for clinically benign prostatic hypertrophy is estimated to range between 13% and 22% and varies with age and section technique employed [2].

Since the original appreciation of the heterogeneity of IPC by Jewett in 1975, numerous staging systems have been advanced, and subdivision of the disease into two histopathologic stages (T1a and T1b) according to the latest TNM classification system has gained wide acceptance in oncologic practice nowadays [3, 4].

However, clinical management of individual patients with IPC remains challenging due to considerable overlap in the natural history of the disease. Since separating tumors that will follow a long natural history from those that will progress rapidly is not possible at present, the frequently encountered indolent course of the disease has led to a policy of conservative treatment, although a significant number of patients suffer rapid progression and eventual death from what initially began as IPC [2]. Therefore, advanced prognostic parameters are clearly needed, since conventional histopathology seems to be of limited value in predicting individual outcome in IPC.

Focusing on markers commonly established in diagnostic surgical pathology practice, we present the first

comprehensive study aiming to hint at so far neglected predictive factors in IPC. Therefore, prostate-specific antigen (PSA), prostatic acid phosphatase (PSAP), alpha-methylacyl-CoA racemase (AMACR, p504s), and androgen receptor (AR) were immunohistochemically assessed in transurethral resection specimens (TURP) and correlated with Gleason scores and histologic staging performed on the corresponding radical prostatectomies (RPs) in a cohort of 54 patients.

Materials and methods

Selection of patients

Retrospective computerized database analysis was performed in order to identify all patients with newly diagnosed clinically unapparent (neither palpable nor visible by imaging using transrectal 7-MHz ultrasonography) IPC based on the histopathologic examination of TURP specimens resected due to symptomatic prostatic hypertrophy. In all cases, the transurethral resected tissue was entirely subjected to histopathologic examination in order to enable proper tumor staging, which was straightforward in all cases based upon the estimation of tumor spread because equivocal cases (still T1a versus just T1b) did not occur. All patients subsequently underwent RP in the period of time between 1999 and 2008 at the Departments of Urology affiliated to two hospitals in Berlin (Charité-University Medicine and Vivantes Clinic am Urban) and five hospitals in Brandenburg (HELIOS Clinic Bad Saarow, Clinic Hoyerswerda, Röhn Clinic Frankfurt (Oder), Clinic Bautzen, and Ernst-von-Bergmann Clinic Potsdam). This analysis yielded a total of 54 patients (mean age, 65.9 years; range, 49–80 years). None of the patients received radiotherapy, androgen deprivation, 5-alpha-reductase inhibitor (i.e., Finasteride) therapy, repeat TURP, or needle biopsy before radical surgery. The following data were recorded: serum PSA level at the time of TURP (unavailable in three patients), histopathologic staging (performed on TURP chips and RPs) and Gleason scores (performed on RPs) as well as surgical margin and nodal status. Since histologic examination of TURP chips revealed only limited foci of cancer in a subset of patients investigated, Gleason scores assigned on RP specimens were used for statistical correlations. In radicals harboring multifocal cancer, the composition of the dominant tumor nodule was appropriate for assigning the Gleason score representative of the entire tumor. Additionally, Gleason scores were assigned in 17 (31.5%) of the transurethral resected specimens. The remaining 37 (68.5%) TURP specimens harbored only limited foci of cancer, which were considered inappropriate for any Gleason score to be reliably assigned. Intervals of serum PSA levels at the time of TURP and pertinent histopathologic parameters of the study cohort are summarized in Table 1.

Central review of histopathology and TMA construction

Hematoxylin and eosin (HE)-stained TURP chips were reviewed by two independent clinical pathologists (S.G. and A.E.) in order to select one representative section from each patient to be used for tissue microarray (TMA) construction. During this review, special attention was paid to the presence and distribution of electrocautery artifacts, which might affect immunohistochemical results. However, cautery artifacts were negligible in the tumor-bearing areas of all TURP chips investigated. Prostatic intraepithelial

Table 1 Pertinent histopathologic parameters of the study cohort and intervals of serum PSA levels at the time of TURP (n=54; serum PSA unavailable in three patients)

Intervals of serum PSA levels at the time of TURP	Absolute (relative) number of cases
Serum PSA≤4.0 ng/ml/4.1–10 ng/ml/>10 ng/ml	24(47%)/13(25.5%)/14(27.5%)
Histopathologic staging (n=54) and Gleason scores (n=17) performed on TURP chips	
T1a/1b	27(50%)/27(50%)
Gleason scores 4–6	17(100%)
Gleason score 7	0
Gleason scores 8–10	0
Histopathologic staging (n=54) and Gleason scores (n=54) performed on RP specimens	
Gleason scores 4–6	45(83.3%)
Gleason score 7	5(9.3%)
Gleason scores 8–10	4(7.4%)
pT2	48(88.9%)
pT3a/3b	2(3.7%)/4(7.5%)
pN0/pN1	54(100%)/0(0%)
R0/R1	54(100%)/0(0%)

neoplasia was not present in any of the specimens assessed. Histopathologically, all specimens assessed represented acinar adenocarcinomas. Ductal adenocarcinomas or any other variants of prostate cancer were not investigated in our study.

Then, the corresponding wax-embedded tissue blocks were retrieved from the pathology archives of the different hospitals involved. Tumor-bearing areas for tissue retrieval were marked on HE-stained sections, punched out of the paraffin block (1.5-mm punch diameter), and inserted into a recipient block as previously described [5]. The tissue array was cut into 4-μm sections without any sectioning aids like tapes or additionally coated slides.

Owing to tissue loss during arraying and sectioning, a total of 44 samples (81.5%) were still available for immunostaining of PSA, PSAP, and AR. For staining of AMACR, 43 samples (79.6%) were retained, respectively.

Immunohistochemistry

Freshly cut 4-μm-thick TMA sections were used for immunohistochemistry. Following deparaffinization with graded alcohols and xylene, antigen demasking was achieved by heat retrieval (100°C) in 0.01 M citrate buffer for 30 min, automatically performed by Bond™ system (Visionbiosystems, Australia). Then, primary antibodies directed against PSA (1:100 dilution; monoclonal; Dako-Cytomation, Denmark A/S), PSAP (1:80 dilution; monoclonal; BioGenex, San Ramon, CA, USA), AR (1:100 dilution; polyclonal; Medac, Hamburg, Germany), and AMACR (1:100 dilution; monoclonal; BioLogo, Seattle, WA, USA) were employed and incubated at room temperature for 1 h.

Subsequently, sections were washed with PBS and incubated with rabbit anti-mouse IgG 1:50 and following that mouse peroxidase–antiperoxidase conjugate 1:200. The enzymatic reaction was developed in a freshly prepared solution of diaminobenzidine (0.5 mg/ml; Sigma, Deisenhofen, Germany) and 0.01% hydrogen peroxide in water.

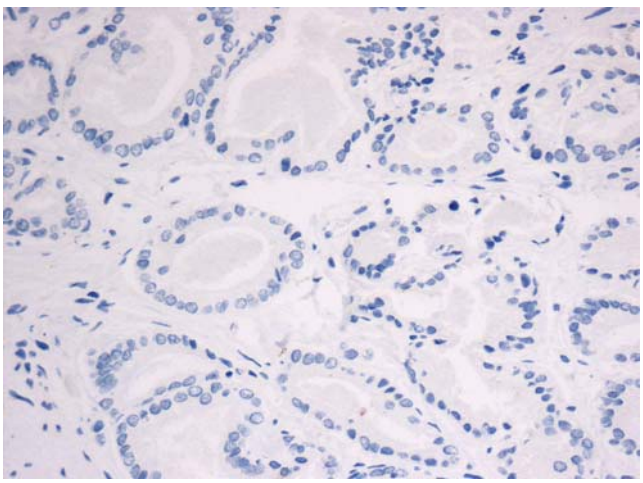

Fig. 1 IPC without PSAP expression (grade 0). Anti-PSAP, ×20 objective

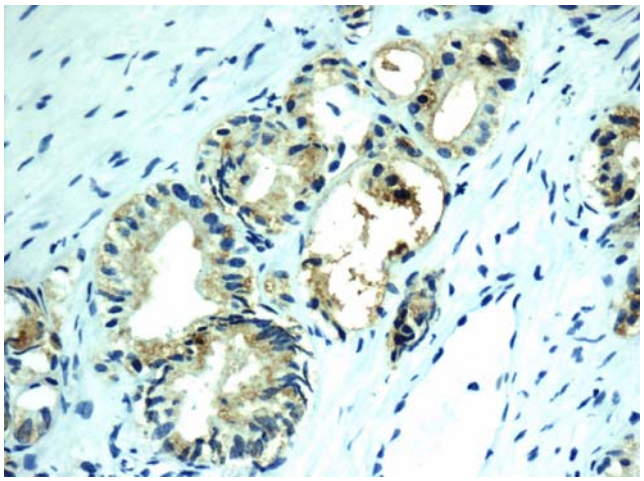

Fig. 2 IPC showing weak cytoplasmic PSAP expression (grade 1+). Anti-PSAP, ×20 objective

For each marker studied, negative controls were prepared by omitting the primary antibody. Sections from a RP specimen not belonging to the study cohort that contained acinar adenocarcinoma as well as benign prostatic glands served as positive controls.

The immunostained sections were evaluated in succession by two independent clinical histopathologists (S.G. and A.E.) blinded with respect to the specimens and to the staining grade previously signed out by the other pathologist. Semiquantification of marker expression was accomplished using the ×20 objective. Briefly, positive staining was defined as to having more than 5% of tumor cells showing cytoplasmic (PSA, PSAP, and AMACR) or nuclear (AR) staining. For all markers assessed, the staining intensity was graded as negative (0), weak (1+), moderate (2+), or strong (3+). Different examples of PSAP expression are illustrated in Figs 1, 2, 3, and 4 (×20 objective).

Statistical analysis

For each marker evaluated, mean values calculated from the data obtained from both independent pathologists for each tumor sample were used for statistical correlations. The Spearman correlation was used to determine the magnitude and direction of the association between marker expression and histopathologic grading and staging performed on RP specimens. Cohen weighted kappa (K)-statistics were used to assess the interobserver variability concerning staining evaluation of PSAP, AMACR, and AR expression. Briefly, K-statistics are a measure of overall agreement without requiring assumptions concerning the "correct" grade of

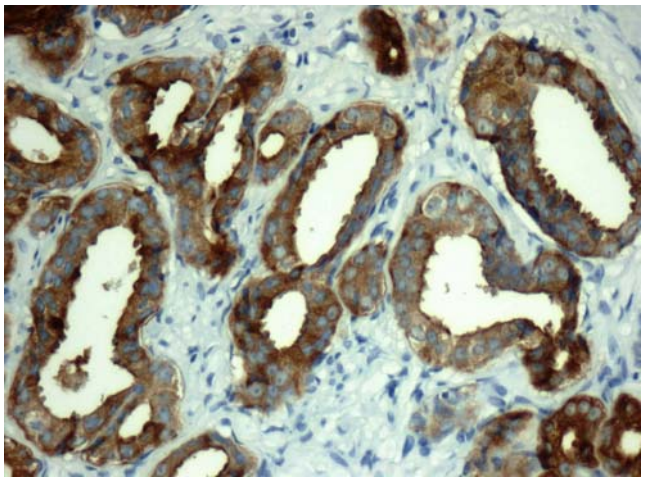

Fig. 3 IPC displaying moderate cytoplasmic PSAP expression (grade 2+). Anti-PSAP, ×20 objective

marker expression. The value of K ranges from –1.0 to +1.0. A value of 0 indicates chance agreement only, while a value of +1.0 indicates perfect agreement. A negative value implies systematic disagreement between observers. It is generally accepted that a value of 0.001–0.20 indicates slight agreement, 0.201–0.40 fair agreement, 0.401–0.60 moderate agreement, 0.601–0.80 substantial agreement, and 0.801–0.99 excellent agreement, respectively.

Since one pathologist involved did not assign score 3+ to any of the PSA immunostained specimens, K-statistics could not be employed and were replaced by the Spearman correlation in order to asses interobserver agreement concerning evaluation of PSA staining.

p Values <0.05 were considered significant. All calculations were performed using the statistical software package SPSS 13.0.

Results

Correlation between conventional histopathologic parameters and serum PSA levels at the time of TURP

All tumors were found to be at least stage pT2a on the corresponding RP specimens.

Gleason scores assigned on a subset of TURP chips (n=17) failed to correlate with histologic staging performed on all TURP chips (ρ=−0.13; p=0.6) and on the corresponding RPs (ρ=0.33; p=0.2) but showed a significant positive correlation with Gleason scores assigned on the corresponding radicals (ρ=0.97; p<0.001), respectively. Among the 17 cases in which Gleason scores have been assigned on TURP chips, one case (5.9%) revealed higher Gleason score on its corresponding RP specimen (TURP chips, Gleason pattern 3+3; subsequent RP specimen, Gleason pattern 3+4, respectively). The remaining 16 cases (94.1%) were found to have identical Gleason scores on their subsequent RPs, respectively.

There was a significant positive correlation between Gleason scores assigned on the RPs and histologic staging on the RPs in our cohort (correlation coefficient ρ=0.27; p=0.04). However, histologic staging performed on TURP chips (T1a and T1b) failed to significantly correlate with Gleason scores (ρ=0.08; p=0.6) and with histologic staging (ρ=0.03; p=0.8) performed on the RP specimens, respectively.

Serum PSA levels at the time of TURP failed to correlate with Gleason scores (ρ=0.19; p=0.17) and with histologic staging (ρ=0.23; p=0.12) performed on the RP specimens.

Marker expression in the tumor samples

PSA and PSAP showed uniform expression at the apical portion of the glandular epithelium in 36 (81.8%) and 40 (91%) of the IPC investigated. AMACR showed cytoplasmic subluminal circumferential staining in 38 (88.4%) of the tumors assessed. In contrast, nuclear AR expression was found to be slightly heterogeneous in terms of distribution and staining intensity and was observed in 43 (97.7%) of the IPC evaluated. The distribution of marker expression is summarized in Tables 2 and 3.

Correlation between marker expression and conventional histopathologic criteria as well as reproducibility of staining evaluation

PSAP expression showed a significant inverse correlation with histologic staging (ρ=−0.37; p=0.02) but not with Gleason scores (ρ=−0.06; p=0.69) performed on RPs. In contrast, there was no significant correlation between conventional histopathology and expression of PSA (staging,

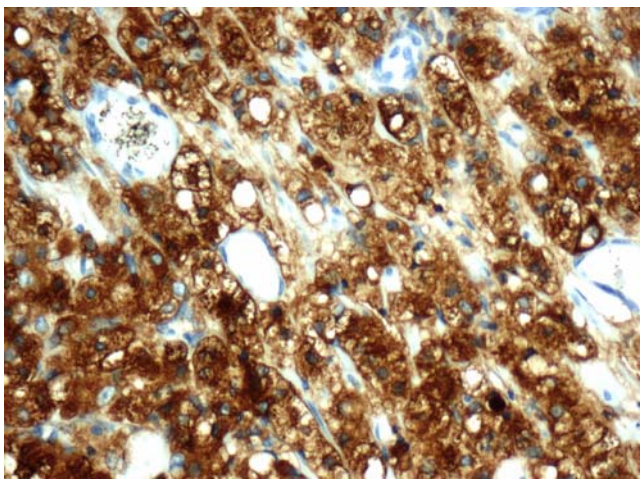

Fig. 4 IPC with strong cytoplasmic PSAP expression (grade 3+). Anti-PSAP, ×20 objective

Table 2 Distribution of marker expression in dependence on histopathologic tumor staging performed on TURP chips (T1a and T1b) and on the corresponding RP specimens (pT2a–3b; n=44 for PSA, PSAP, and AR staining; n=43 for AMACR staining)

Grade of marker staining	T1a	T1b	pT2a	pT2b	pT2c	pT3a	pT3b
PSA							
0	2	6	2	2	3	1	0
1	6	7	7	1	3	0	2
2	7	7	8	1	4	0	1
3	6	3	5	0	3	0	1
PSAP							
0	3	1	2	0	1	1	0
1	2	4	2	0	2	0	2
2	5	3	2	0	5	0	1
3	11	15	16	4	5	0	1
AMACR (p504s)							
0	2	3	1	1	3	0	0
1	4	3	4	1	0	0	2
2	7	6	11	0	1	1	0
3	7	11	6	2	8	0	2
AR							
0	0	1	0	0	1	0	0
1	4	3	3	1	3	0	0
2	6	5	5	1	3	0	2
3	11	14	14	3	5	1	2

ρ=−0.12, p=0.42; grading, ρ=−0.11, p=0.49), AR (staging, ρ=−0.19, p=0.22; grading, ρ=0.02; p=0.92), and AMACR (staging, ρ=0.09, p=0.55; grading, ρ=0.24, p=0.13).

K-Statistics revealed a highly significant moderate agreement for PSAP staining (K=0.47, p<0.001), a highly significant fair agreement for AMACR staining (K=0.34, p<0.001) and a significant slight agreement for AR staining (K=0.18, p=0.03). Concerning PSA staining, the staining grades independently assigned by both pathologists showed a highly significant correlation (ρ=0.88; p< 0.001), respectively.

Discussion

Although the majority of IPC are clinically insignificant, the speed of progression of individual tumors remains unpredictable [6]. Paul et al. recommended RP to be performed in patients who are candidates for curative therapy, since according to their findings, TURP did not represent an adverse prognostic factor compared with patients who were diagnosed by needle biopsy, and recent studies reported the mortality rate for transurethral prostate resection to be 0.1% [7, 8]. In light of this, RP might be advocated at least in a subgroup of patients suffering from aggressive IPC.

Only few studies have previously assessed the prognostic role of conventional histomorphology in IPC. The results of these investigations are summarized in Table 4

Table 3 Distribution of marker expression in dependence on the Gleason scores assigned on RP specimens (n=44 for PSA, PSAP, and AR staining; n=43 for AMACR staining)

Grade of marker staining	Gleason scores 4–6	Gleason score 7	Gleason scores 8–10
PSA			
0	5	3	0
1	10	0	3
2	12	1	1
3	8	1	0
PSAP			
0	3	1	0
1	2	2	1
2	7	0	1
3	23	2	2
AMACR (p504s)			
0	1	0	0
1	6	1	0
2	7	2	2
3	21	2	2
AR			
0	4	1	0
1	4	1	2
2	11	2	0
3	15	1	2

Table 4 Prognostic implications of conventional histopathologic parameters in IPC

Study	Conclusion
[9]	Stage T1a IPC appears to have low progression potential compared with T1b IPC
[10]	Stage T1b IPC shows a progression rate of approximately 33%
[11]	The greatest threat of patients with IPC seems to be involvement of the peripheral rather than the transition zone resected during TURP
[12]	Evidence of residual disease at repeat TURP is a hallmark of high progression
[13]	Larger tumor volume and high histologic grade are associated with greater tumor aggressiveness

and suggest that the prognostic role of conventional histopathology seems to be of limited value [9–13]. Therefore, efforts should be directed at defining the natural history of individual IPC.

Since RP is only rarely performed after the detection of IPC in TURP specimens, we decided to collect cases from several institutions in the region of Berlin and Brandenburg. With this material, we are able to present the first comprehensive immunohistochemical study aiming to correlate the expression of markers established in diagnostic surgical pathology practice with conventional histopathologic outcome parameters in a cohort of 54 patients who underwent RP due to IPC.

Looking at our cohort, three notions merit discussion. First, approximately 11.2% of clinically unapparent tumors were found to be at least stage pT3a on subsequent RP. This figure might be explained by the frequent multicentricity of ICP and is in keeping with the well-known low sensitivity of digital rectal examination [14, 15]. Second, approximately 17% of IPC were assigned with Gleason score ≥7 on RP in our cohort. Although definite allocation of the zonal origin of cancer is felt to be inappropriate in our cohort, these tumors might have arisen in the peripheral zone of the gland with subsequent intraglandular spread toward the transition zone. This hypothesis is supported by the significant correlation between Gleason scores and histologic staging on RPs observed in our study. Finally, due to the limited foci of cancer available for histologic examination, assigning Gleason scores was felt to be appropriate only in a subset of 17 (31.5%) TURP chips assessed. Despite the significant correlation between grading assigned on TURP chips and on their corresponding radicals, this figure strongly limits conventional grading to be used as a prognostic parameter in IPC in our cohort and, therefore, underscores the role of PSAP expression as a possible adjunct for predicting histologic staging on the subsequent radicals in this scenario in order to enable individual prognostic ramification.

The inverse correlation between PSAP expression and tumor stage observed in our cohort might be explained by a gradual loss of cellular enzyme synthesis occurring during tumor spread and is felt to be in keeping with the less intense PSAP staining encountered in poorly differentiated prostate cancer [16]. The lacking correlation between PSAP expression and Gleason scores in our series might be attributable to the limited number of cases assessed. Therefore, larger studies are clearly needed in order to confirm our findings and to determine reliable cut-point values of marker expression for identification of aggressive cancer.

In accordance with previous studies, PSA staining intensity decreased from moderately to poorly differentiated IPC and was found to be inversely correlated with tumor staging in our study, although both findings failed to be significant probably due to the limited number of cases evaluated [17].

Our data failed to establish any significant correlation between AR expression and histologic staging or grading of IPC. However, we observed decreased AR expression in advanced IPC, which might be functionally involved in the accompanying decline in PSA expression by the AR-mediated control of cellular PSA production by circulating androgens [18].

AMACR, a peroxisomal and mitochondrial enzyme involved in the oxidation of branched-chain fatty acids and cholesterol metabolites, correlates with histopathologic grading in noninvasive bladder cancer and proved to be a sensitive and specific biomarker for the diagnosis of prostate cancer (PC) [19, 20]. However, its diagnostic utility in IPC has not been evaluated yet. In our cohort, AMACR expression was immunohistochemically detectable in 88.4% of IPC assessed but failed to correlate with Gleason scores and with histologic staging performed on the corresponding RPs. The interpretation of these data remains speculative. However, AMACR is known to display less intense and more heterogeneous staining in uncommon variants of PC (e.g., atrophic, foamy gland, and pseudohyperplastic PC) [21]. Therefore, owing to the heterogeneity previously described to occur in IPC, larger studies are needed aiming to clarify the diagnostic and prognostic role of AMACR expression in IPC [3].

Conclusion

Conventional histomorphology appears to be of limited predictive value in IPC. Our data suggest that PSAP might be a so far neglected prognostic marker in IPC since its immunohistochemically semiquantified expression in TURP chips might be predictive of the histopathologic tumor stage on the subsequent RP specimen. This novel

finding might be a valuable adjunct for clinical decisions concerning individual therapeutic management.

However, this encouraging step toward defining individual outcome parameters in IPC awaits to be confirmed by larger studies, which should aim to define reliable cut-point values of marker expression for separating clinically aggressive tumors from those which will probably not progress during the expected lifetime of the patient concerned.

Acknowledgements The authors gratefully thank Frank Dietrich, MD, Conrad Flössel, MD, Jan Jander, MD, Helmut Knispel, MD, Hartmut Lobeck, MD, Volker Loy, MD, Roland Pauli, MD, Volkmar Rosenthal, MD, and Wilko Weichert, MD, for their contribution to this work.

Conflict of interest statement All authors and participants involved in this study have no conflict of interest.

References

1. Van Andel G, Vleeming R, Kurth KH et al (1995) Incidental carcinoma of the prostate. Semin Surg Oncol 11:36–45
2. Sheldon CA, Williams RD, Fraley EE (1980) Incidental carcinoma of the prostate: a review of the literatur and critical reappraisal of classification. J Urol 124:626–631
3. Jewett HJ (1975) The present status of radical prostatectom for stages A and B prostatic cancer. Urol Clin North Am 2:105–124
4. Sobin LH, Wittekind CH (2002) TNM classification of malignant tumors, 6th edn. Wiley-Liss, New York, pp 172–175
5. Kononen J, Bubendorf L, Kallioniemi A et al (1998) Tissue microarrays for high-throughput molecular profiling of tumor specimens. Nat Med 4:844–847
6. Mazzuchelli R, Barbisan F, Scarpelli M et al (2009) Is incidentally detected prostate cancer in patients undergoing radical cystoprostatectomy clinically significant? Am J Clin Pathol 131:279–283
7. Paul R, Knebel C, van Radenborgh H et al (2005) [Incidental carcinoma of the prostate: can we and should we recommend radical prostatectomy?]. Urologe A 44:1054–1058
8. Reich O, Gratzke C, Bachmann A et al (2008) Morbidity, mortality and early outcome of transurethral resection of the prostate: a prospective multicenter evaluation of 10, 654 patients. J Urol 180:246–249
9. Martino P, Palazzo S, Battaglia M et al (2004) Incidental prostatic cancer: repeat TURP or biopsy? Urol Int 73:193–197
10. Miller JS, Donovan JF Jr, Williams RD et al (1990) Evaluation and treatment of stage A prostate cancer. In: Williams RD, Carroll PR (eds) Treatment perspectives in urologic oncology. Pergamon, Elmsford, pp 113–134
11. Greene DR, Egawa S, Neerhut G et al (1991) The distribution of residual cancer in radical prostatectomy specimens in stage A prostate cancer. J Urol 145:324–328
12. Zhang G, Wassermann NF, Kapoor DA et al (1992) Early detection of local progressive disease from stage A1 prostate carcinoma by transrectal ultrasonography. Cancer 69:2300–2305
13. Barnes R, Hirst A, Rosenquist R (1976) Early carcinoma of the prostate: comparison of stages A and B. J Urol 115:404–405
14. Bostwick DG (1995) The pathology of incidental carcinoma. Cancer Surv 23:7–18
15. Friedman GD, Hiatt RA, Quesenberry CP Jr et al (1991) Case-control study of screening for prostate cancer by digital rectal examination. Lancet 337:1526–1530
16. Varma M, Berney DM, Jasani B et al (2004) Technical variations in prostatic immunohistochemistry: need for standardisation and stringent quality assurance in PSA and PSAP immunostaining. J Clin Pathol 57:687–690
17. Ablin RJ (1997) A retrospective and prospective overview of prostate-specific antigen. J Cancer Res Clin Oncol 123:583–594
18. Kim J, Coetzee GA (2004) Prostate specific gene regulation by androgen receptor. J Cell Biochem 93:233–241
19. Gunia S, May M, Scholman K et al (2008) Expression of alpha-methylacyl-CoA racemase correlates with histopathologic grading in noninvasive bladder cancer. Virchows Arch 453:165–170
20. Zha S, Ferdinadusse S, Hicks JL et al (2005) Peroxisomal branched chain fatty acid beta-oxidation pathway is upregulated in prostate cancer. Prostate 63:316–323
21. Hameed O, Humphrey PA (2005) Immunohistochemistry in diagnostic surgical pathology of the prostate. Semin Diagn Pathol 22:88–104

Virchows Arch (2009) 454:581–588
DOI 10.1007/s00428-009-0745-7

ORIGINAL ARTICLE

Intraosseous lymphocytic infiltrates after hip resurfacing arthroplasty

A histopathological study on 181 retrieved femoral remnants

Jozef Zustin · Michael Amling · Matthias Krause · Stefan Breer · Michael Hahn · Michael M. Morlock · Wolfgang Rüther · Guido Sauter

Received: 11 December 2008 / Revised: 28 January 2009 / Accepted: 4 February 2009 / Published online: 19 February 2009

Abstract To identify a possible role of lymphocytic infiltrates in failure mechanism of the metal-on-metal hip resurfacing arthroplasty, the extent of lymphocytic infiltration was compared with reasons for prosthesis failure in a series of retrieval specimens. One hundred eighty-one femoral head and neck remnants were subjected to thorough analysis of histological findings and clinical data. Lymphocytic infiltrates were considered weak to moderate in 52 (28.7%) and excessive in ten (5.5%) cases. Six cases with excessive lymphocytic infiltrates belonged to the group of 33 (18.2%) revisions without obvious cause (periprosthetic fracture, component loosening, and infection) for prosthesis failure. Excessive lymphocytic infiltrates were strongly linked to the presence of proliferative desquamative synovitis ($p<0.0001$). Both the excessive lymphocytic infiltrates and proliferative desquamative synovitis were associated with female gender ($p<0.05$). We hypothesize that a specific cause of groin pain might be related to excessive intraosseous lymphocytic infiltrates and explained possibly by the hypersensitivity reaction of the delayed type after the hip resurfacing arthroplasty. Proliferative desquamative synovitis might constitute another morphologic feature associated with the delayed type hypersensitivity reaction.

Keywords Hip resurfacing · Arthroplasty failure · Hypersensitivity · Groin pain · Metal-on-metal · T lymphocyte

J. Zustin (✉) · G. Sauter
Institute of Pathology,
University Medical Center of Hamburg Eppendorf,
Martinistr.52,
20246 Hamburg, Germany
e-mail: j.zustin@uke.uni-hamburg.de

M. Amling · M. Krause · S. Breer · M. Hahn
Center for Biomechanics and Skeletal Biology,
University Medical Center Hamburg Eppendorf,
Hamburg, Germany

M. Amling
Department of Trauma, Hand and Reconstructive Surgery,
University Medical Center Hamburg Eppendorf,
Hamburg, Germany

M. M. Morlock
Biomechanics Section,
TUHH Hamburg University of Technology,
Hamburg, Germany

W. Rüther
Department of Orthopaedics,
University Medical Center Hamburg Eppendorf,
Hamburg, Germany

Introduction

With the application of metal-on-metal bearings, surface arthroplasty is being performed in a growing number of centers worldwide [1]. Short-term clinical follow-up reports have been encouraging [2, 3] although femoral neck fractures [4, 5] and femoral component loosening [6] have been identified as causes of its early- to medium-onset failure. Other clinically and macroscopically clearly defined causes of the revision surgery are failure of the acetabular component and infection. Other clinically less well-defined causes for groin pain and consecutive revision surgery include metal hypersensitivity in an unknown fraction of cases after metal-on-metal hip replacements [7, 19–21, 23]. Some of these cases may

manifest themselves as unexplained groin pain, joint effusions leading to enlarged bursae or groin masses, and periprosthetic osteolysis after 2 or 3 years [7, 8].

We had recently observed cases with extensive lymphocytic infiltrates in femoral head remnants removed after prosthesis failure involving metal-on-metal bearings. To identify possible causes for such extensive lymphocytic infiltrates after failure of hip resurfacing arthroplasty, the extent of lymphocytic infiltration was compared with morphologically or clinically defined causes for prosthesis failure. The results of our analysis suggest that excessive lymphocytic infiltrations might constitute a feature of metal hypersensitivity of the delayed type.

Materials and methods

Patient cohort Formalin-fixed material from 181 femoral head remnants submitted to our laboratories from January 2004 to September 2008 were examined. Data on clinical diagnosis of the index surgical procedure were submitted in 127 (70.2%) cases, including 98 advanced stages of osteoarthritis, 13 hip dysplasia, nine avascular osteonecrosis of femoral head, and seven posttraumatic lesions. Clinical diagnosis of rheumatoid arthritis (seven cases) was an exclusion criterion for present study. The cohort included 81 male (age 55.5 years±8.9) and 76 female patients (54.7±9.8). Data on implantation time was available on 148 (81.8%) of our patients.

Femoral head bone tissue of 26 females (age 71.1 years±7.0) and 14 male patients (69.4±6.8) who underwent total hip arthroplasty for advanced stages of primary osteoarthritis was also used as a control.

Methods A central 4-mm-thick slice was cut from the revised hips in the femoral neck plane using a water-cooled diamond coated saw (EXACT 310). The slice was macroscopically photographed, X-rayed, and then embedded in methyl methacrylate (Fig. 1). The remaining bone tissue of the femoral head and when provided also the femoral neck remnant was removed using acetone and used for further histological analysis [9]. One other slice perpendicular to the former was completely plastic embedded and stained with Kossa, toluidine blue, and Goldner trichrome dyes. When some soft tissue from synovial membrane adhered to the femoral neck, this was plastic-embedded and reviewed histologically. When required, additional parallel sections from plastic-embedded tissue as well as additional paraffin-embedded specimens were prepared after EDTA decalcification in order to perform further histological analyses including immunohistochemistry.

Femoral head specimens were cut in parallel sections in the medial–lateral plane and macroscopically photographed and X-rayed (Fig. 2). From each femoral head, four sections were plastic-embedded and stained with toluidine blue in addition to Goldner trichrome dyes.

Histopathology The lymphocyte content of the bone (Fig. 3) was estimated as negative (no evident lymphocytic infiltration), weak to moderate (less 300 lymphocytes per high power field (HPF)), and excessive (≥300 lymphocytes per HPF) in areas with maximum intraosseous lymphocytic

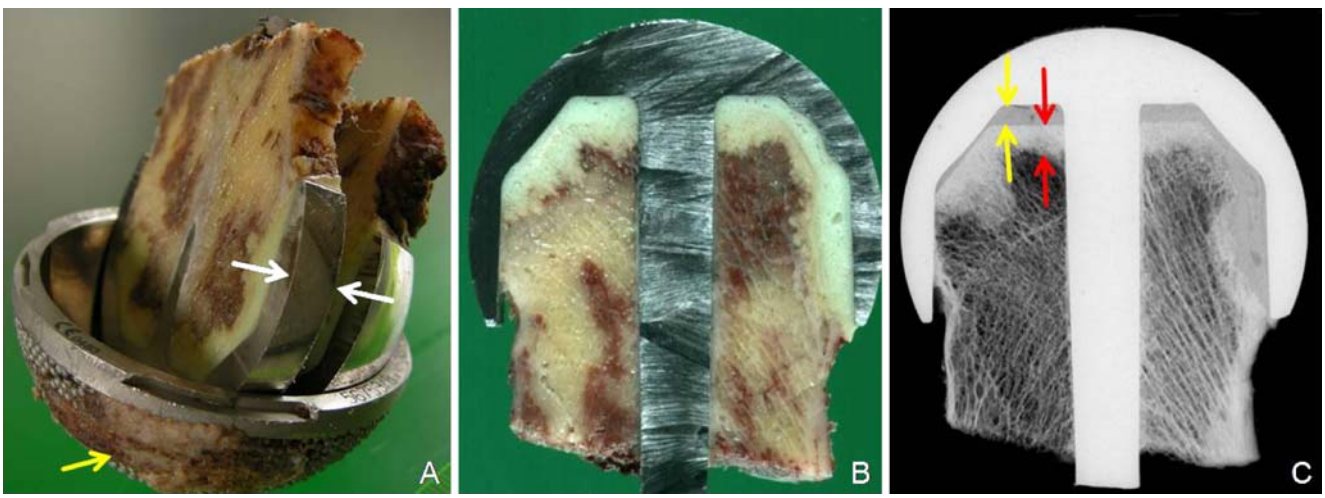

Fig. 1 Macroscopic and contact X-ray analysis of the retrieved femoral remnant. A central slice (*white arrows*) with in situ femoral component (**a**) was cut by means of a water-cooled diamond band coated saw. At the surface of non-cemented acetabular component, adherent fibrous tissue (*yellow arrow*) was evident. Macroscopic (**b**) and contact X-ray analysis of the slice were performed in order to identify osseous changes and patterns of cementation. On the contact radiography (**c**), cement mantle thickness at the dome (*yellow arrows*) and the depth of cement penetration (*red arrows*) can be well documented in addition to possible osteolytic as well as osteosclerotic osseous lesions

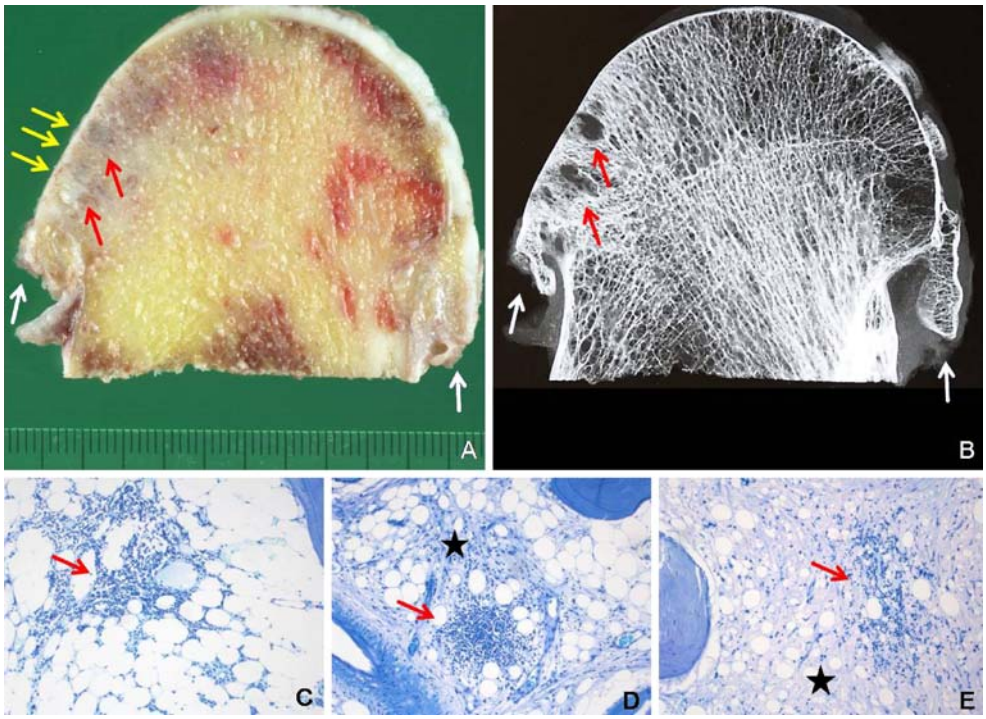

Fig. 2 Control tissues. A central slice was cut in medial-lateral plane by means of a water-cooled diamond band coated saw. Macroscopically (**a**), femoral head with focal complete loss of hyaline cartilage (*yellow arrows*), initial formation of subchondral pseudocysts (*red arrows*), and osteophyte at the margins (*blue arrows*) were evident. Contact radiography (**b**) highlighted the osteolytic pseudocystic defects (*red arrows*) and marginal osteophyte formations (*blue arrows*). The amount and morphologic patterns of intraosseous lymphocytic infiltration were analyzed histologically. In the majority of cases, smaller perivascular lymphocytic infiltrations (*red arrows* in **c**–**e**) were found throughout the bone marrow with depleted hematopoesis (**c**). Several cases showed also diffuse homogenous eosinophilic colored interstitium of the bone marrow (*star*), consistent with bone marrow edema (**d**/**e**)

infiltration both under the bone–cement interface and within the deeper osseous tissue of femoral remnant.

Representative sections of bone tissue with lymphocytic infiltrates were immunohistochemically analyzed using a panel of antibodies to lymphocytes (CD45), B lymphocytes (CD20), T lymphocytes (CD3, CD4), follicular dendritic cells (CD23), and macrophages (CD68). Proliferative activity of lymphocytes was also analyzed immunohistochemically (Ki67).

In addition, the type of the inflammatory or reactive changes of adherent soft tissue (Fig. 4) was classified as follows. Reactive synovitis was considered in cases with only discrete lymphocytic infiltrates and/or histiocytic infiltrates as well as some low degree of synovial stromal proliferation in addition to focal finding of osseous or cartilaginous detritus. Fibrinous synovitis was diagnosed when some discrete proliferation of synoviocytes was seen in addition to fibrinoid exsudation without signs of infectious genesis. Proliferative desquamative synovitis showed florid proliferation of synoviocytes with only blunt recognizable superficial border of activated synovium and abundant exsudation and scattered desquamated synoviocytes in addition to discrete to abundant lymphocytic infiltrates within deeper synovial membrane. Histological examination did not reveal any cement or metal particles within cytoplasm of synoviocytes. Purulent synovitis was diagnosed in cases with moderate degree of stromal and synovial proliferation in addition to edema and fibrinous exsudation. Furthermore, synovial and periprosthetic membrane tissue with one or more polymorph neutrophile leukocytes per HPF on average after examination of ten fields was considered infectious [10].

Statistics Statistical analyses were performed using SPSS 15.0 for Windows (SPSS, Chicago, IL, USA) software. Since time to revision surgery deviated clearly from a normal distribution, non-parametric analytical methods were applied (Kruskal–Wallis test, Chi-squared test). The standard deviation (SD) is used throughout to describe the spread around the mean. The type I error probability was set to 5%.

Results

The review of all available sections of our 181 cases in combination with clinical information revealed evidence for femoral head and neck fractures in 119 (65.7%), femoral

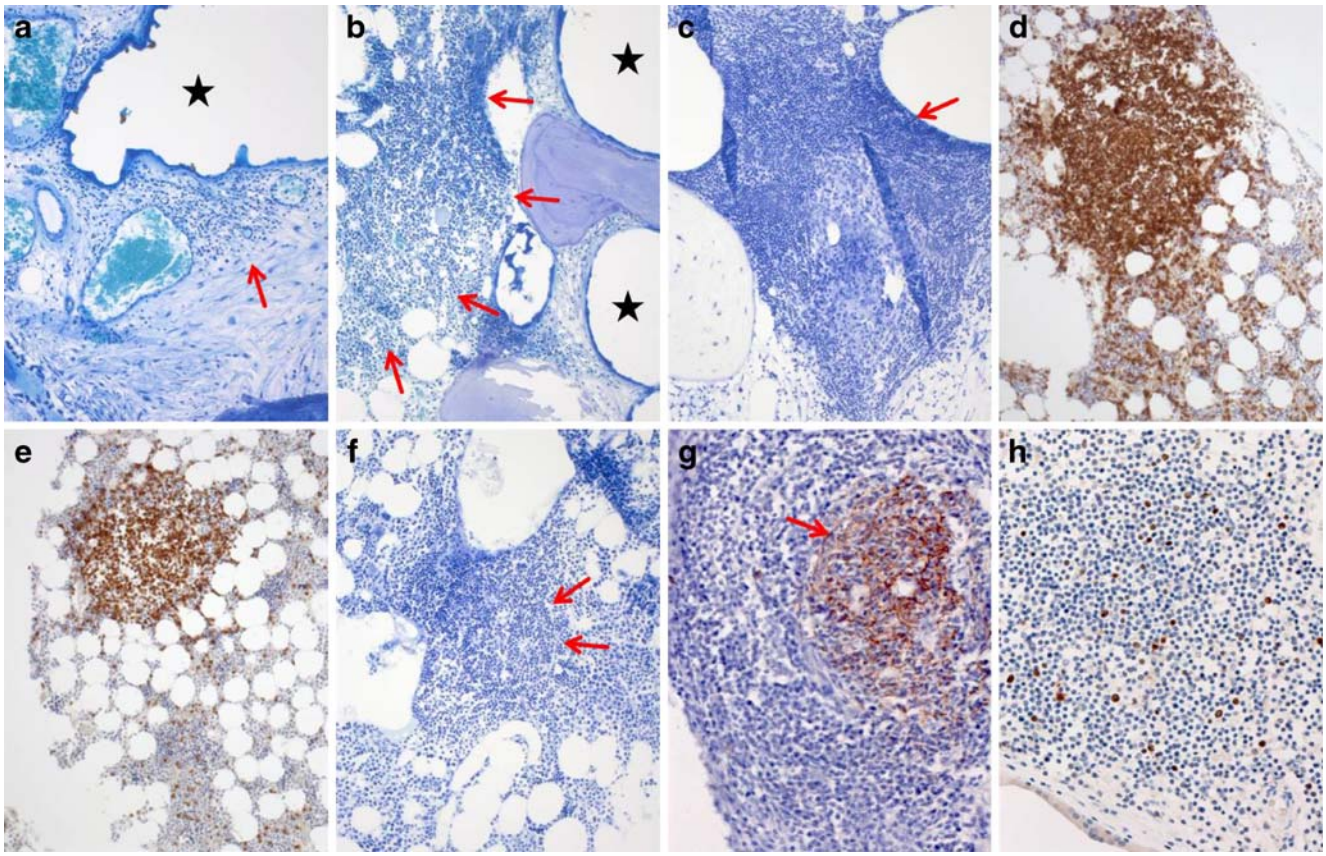

Fig. 3 Intraosseous lymphocytic infiltration. Deep cement interdigitations (*star*) were frequently surrounded by hyperemic fibrous tissue and scattered lymphocytic infiltrates (*red arrow*; **a**). Excessive lymphocyte infiltration (*red arrows*) almost completely displacing the bone marrow was apparent in several bone tissue remnants after hip resurfacing arthroplasty (**b**). Lymphocyte infiltrate was located adjacent to cement interdigitations (*stars*; **b**). Within the deeper bone marrow tissue, both excessive perivascular and irregular nodular lymphocytic infiltrates (*red arrow*) were identified (**c**; toluidine blue, ×50). Immunohistochemical reactions exhibited positive reaction against lymphocyte marker (CD45; **d**). Clearly, T lymphocytes (CD3) dominated (**e**). Rarely, lymph follicle germinative center (*red arrows*) was apparent (**f**). In the latter, CD23-positive follicular dendritic cells (*red arrows*) were demonstrated immunohistochemically (**g**). Proliferative activity (Ki67) of lymphocyte infiltration (**h**)

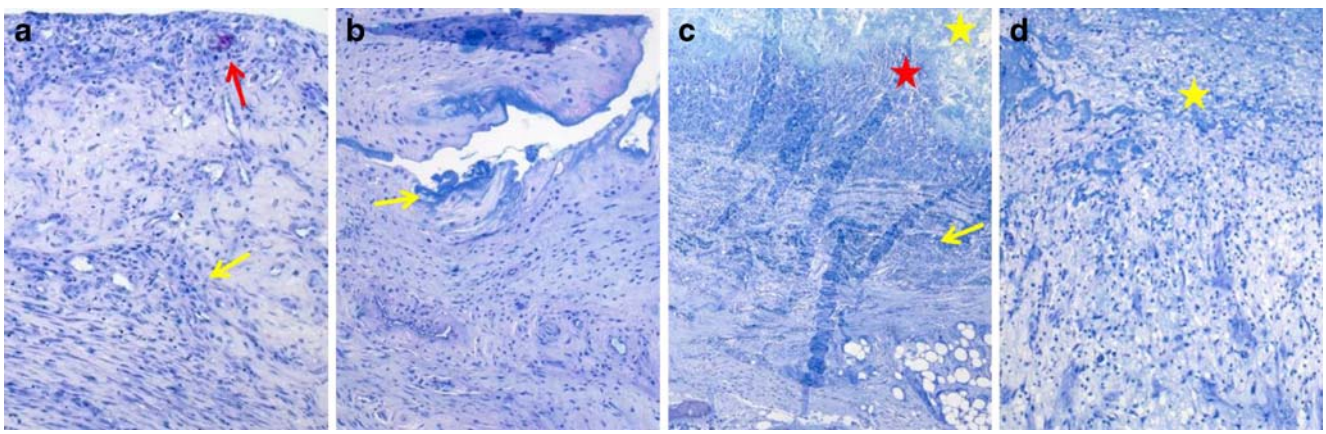

Fig. 4 Morphological changes of synovial tissue after the hip resurfacing arthroplasty. Few scattered lymphocytes and histiocytes (*yellow arrow*) in addition to several particles of osseous detritus (*red arrows*) were characteristic for reactive synovitis (**a**). Fibrinous exsudate (*yellow arrow*) in the absence of inflammatory infiltrates were found in cases with fibrinous synovitis (**b**). Cases with desquamated synoviocytes within the bluish exsudate (*yellow star*), marked proliferation of synoviocytes (*red star*), and moderate histiocytic as well as lymphocytic infiltration of deeper soft tissues (*yellow arrow*) were referred to as the proliferative desquamative synovitis (**c**). Severe edema, infiltration of polymorph neutrophile leucocytes (*yellow star*), and purulent exsudation were characteristic for infectious/purulent synovitis (**d**; toluidine blue, ×50)

component instability in 34 (18.8%), acetabular component failure in 13 (7.2%), and infection in six (3.3%) cases. A total of 24 (13.3%) cases showed multiple of these features. Finally, there were 33 cases (18.2%) in those macroscopic and X-ray examination of specimen that did not provide an evidence for specific causes of resurfacing arthroplasty failure.

Hips with acetabular failure (in situ, 418.4 days±362.9) were revised later than cases with periprosthetic fracture (157.5±189.7) but earlier than other non-fractural failures (605.8±502.2; $p<0.0001$). Similarly, cases with well-defined cause for revision surgery (246.1±323.2) were implanted significantly shorter than hips with non-obvious cause for revision (491.7±475.3; $p=0.0007$; Table 1).

The quantitation of lymphocytic infiltrations revealed no lymphocytes in 119 (65.7%), weak to moderate in 52 (28.7%), and excessive infiltrates in ten (5.5%) patients. A comparison with identified causes for prosthesis failure revealed that excessive lymphocytic infiltrates were strongly linked to the absence of macroscopically or clinically identifiable causes for prosthesis failure ($p<.0001$; Table 1). Excessive lymphocyte infiltrates were seen in six (18.2%) of 33 patients without identified causes of revision as compared to four (3.1%) of 127 patients with at least one identified cause of prosthesis failure.

The finding of intraosseous excessive lymphocytic infiltration was significantly associated with female gender ($p=0.0231$). Among patients with known gender, excessive lymphocytic infiltration was found in only one of 71 males (1.2%) but in seven of 76 (9.2%) female patients. Excessive lymphocytic infiltrates were mostly located immediately underneath the bone–implant interface (ten cases). Furthermore, both the intramedullary perivascular (seven specimens) and diffuse dense (six cases) lymphocytic infiltrates were apparent in most specimens. Excessive pseudolymphomatous infiltrates presented with positivity for CD45 and CD3, characteristic for T lymphocytes. Germinative center of intraosseous lymph follicles containing CD23 positive follicular dendritic cells were demonstrated immunohistochemically in two cases. Proliferative activity of intraosseous lymphocyte infiltration defined as Ki 67-positivity was <5%.

Two (5.9%) femoral remnants with excessive lymphocytic infiltrates belonged into the group of 34 hips with instability of the femoral component, and eight (5.2%) cases were found in the group of 147 well-fixed implants ($p=0.5927$).

Eosinophile granulocytic infiltration or vasculitis with fibrinoid necrosis of the vessel wall was not apparent within both osseous and soft synovial tissue in our series. In one case, focal superficial necrobiosis at the lateral edge of the prosthesis (Fig. 5) was found. In the same case, one arteriole within the inflammatory infiltrate was demonstrated.

The mean time to revision surgery in cases with excessive intraosseous lymphocytic infiltrates was approximately 13 months (390.3 days±202.6).

In the control group, focal intramedullary and perivascular intraosseous lymphocytic infiltrates (44.9 lymphocytes/HPF± 62.7; Fig. 2) were detected in 35 cases. Lymph follicles with germinative centers or CD23 positive follicular dendritic cells were not apparent.

While the synovium was not available in the majority of cases with head fractures, adherent synovial soft tissue was found in 107 (59.1%) submitted femoral remnant specimens. Histological changes within the synovium were classified as reactive in 80 (74.8%), fibrinous in 12 (11.2%), proliferative desquamative in 12 (11.2%), and as purulent synovitis in three (2.8%) patients. There was a close relationship between excessive lymphocytic intraosseous infiltrates and proliferative desquamative type of synovitis ($p<0.0001$; Table 2). Accordingly, proliferative desquamative synovitis was also more frequent in female (nine (18.4%) of 49) than in male (two (4.8%) of 42) patients ($p=0.0255$).

The mean time to revision surgery in cases with desquamative synovitis was approximately 11.5 months (351.8 days±204.5) in the present study.

Discussion

To learn more on the significance of excessive lymphocytic infiltrates in revision specimens after the hip resurfacing arthroplasty with metal-on-metal bearings, we quantified

Table 1 Failure patterns of the hip resurfacing arthroplasty and intraosseous lymphocytic infiltrates

	Lymphocyte Infiltration			Samples	Mean in situ time [days]	SD
	Absent	Weak to moderate	Excessive			
Periprosthetic fracture	103 (86.6%)	14 (11.8%)	2 (1.7%)	119	157.5	189.7
Femoral instability	15 (44.1%)	17 (50.0%)	2 (5.9%)	34	488.6	480.9
Acetabular failure	6 (46.4%)	7 (53.8%)	0 (0%)	13	418.4	362.9
Sepsis/arthritis	3 (50.0%)	3 (50%)	0 (0%)	6	453.0	320.1
Not obvious diagnosis	7 (21.2%)	20 (60.6%)	6 (18.2%)	33	491.7	475.3

Significant differences are highlighted in the body of text

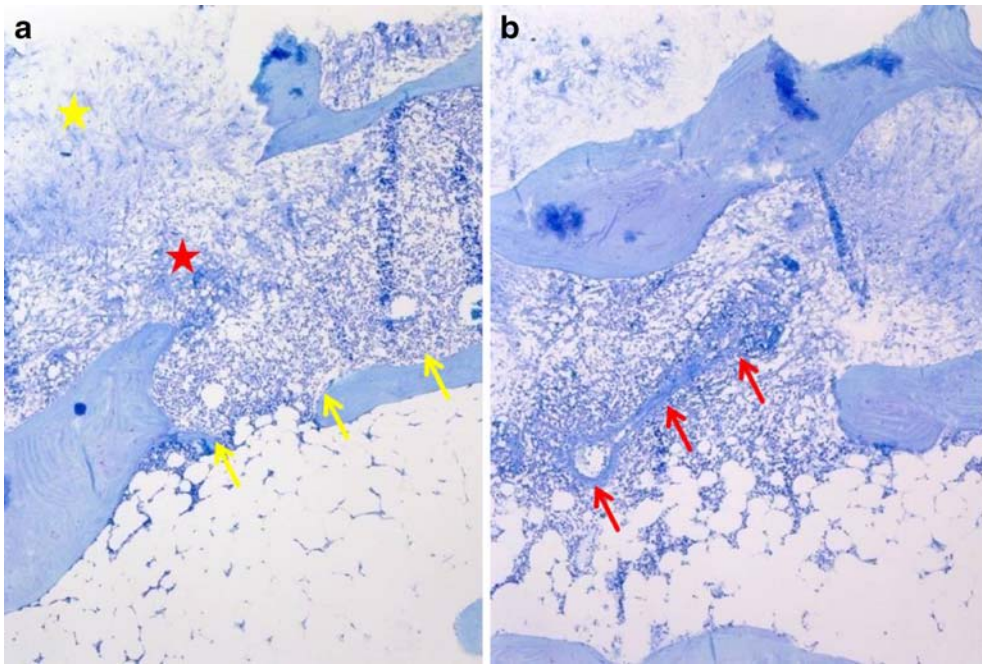

Fig. 5 Bone tissue necrobiosis. Zone of necrobiosis (*yellow star*) was located close to the lateral edge of the prosthesis. Edema and dilated blood vessels in addition to scattered histiocytes were found at the border of necrosis (*red star*). Excessive lymphomatous infiltrates (*yellow arrows*) displaced the adjacent fatty bone marrow (**a**). Muscular arteriole (*red arrows*) was detected within dense pseudolymphomatous infiltrate of the femoral remnant (**b**; toluidine blue, ×100)

intraosseous lymphocytic infiltrates and compared these findings with clinico-pathological data.

The categorization of potential causes for prosthesis failure was based on the available clinical data and the results of our pathology work-up. At least one condition (fractural failure, instability of the femoral or acetabular component, infectious complications) that could potentially explain prosthesis failure was identified in 148 of 181 patients. We assume that the 33 remaining patients without identifiable cause for arthroplasty failure mostly presented with unexplained groin pain, probably caused by implantation-related intra- and periarticular complications, including femoro-acetabular and iliopsoas impingement as well as metal wear or hypersensitivity reaction [7].

Based on the strong association found between excessive lymphocytic infiltrates and the absence of a defined cause for prosthesis failure, we speculate that abundant lymphocytic infiltration is a characteristic feature for one "non-visible" cause for implant failure associated with groin pain after hip replacement. Among clinically and macroscopically non-visible causes for groin pain after the index surgical procedure, hypersensitivity reaction might be the most conveniently linked to abundant lymphocytic infiltrates. Excessive lymphocytic infiltrates were located predominantly superficially under the bone–implant interface in our series. Clearly, T lymphocytes dominated. Accumulation of lymphocytes is a common feature of hypersensitivity reactions in contact dermatitis [11–13], adverse tattoo [14, 15], drug [16], and orthodontic reactions [17, 18]. Most recently, other authors had also described excessive lymphocytic infiltrates in periprosthetic iliopsoas muscle and deep connective tissues from patients with suggested metal hypersensitivity [7, 19–21]. These lesions were described as "aseptic lymphocyte-dominated vascular associated lesion" by some investigators [22–24]. We have found similar lesion only in one of our ten cases with excessive lymphocyte infiltration. Interestingly, superficial bone tissue necrobiosis [25] at margin of the implant appeared in the same case. As tissue necrosis does not belong to specific histological findings by dermatological

Table 2 Relationship between intraosseous lymphocytic infiltrations and distinct types of synovitis

		Synovis				
		Reactive	Fibrinous	Proliferative desquamative	Purulent	Total
Intramedullary Lymphocyte Infiltration	Absent	42 (76.4%)	9 (16.4%)	3 (5.5%)	1 (1.8%)	55
	Weak to moderate	37 (84.1%)	3 (6.8%)	2 (4.5%)	2 (4.5%)	44
	Excessive	1 (12.5%)	0 (0%)	7 (87.5%)	0 (0%)	8
	Total	80 (74.8%)	12 (11.2%)	12 (11.2%)	3 (2.8%)	107

Significant relationships are highlighted in the body of text

or other organ hypersensitivity reactions, we suggest that it can be at least partly caused by the impaired blood supply of tissues located close to the joint cavity, which is filled with inflammatory exsudate under pressure in typical cases suggestive of metal hypersensitivity [7, 19–21]. At the border of the described necrobiosis and in some other cases with excessive osseous lymphocytic infiltrates, a few scattered histiocytes were found close to the bone–implant interface. Ingested wear particles were visible within a cytoplasm of some of these cells. However, histiocytic infiltration was not apparent within deeper intramedullary spaces.

Our hypothesis that metal hypersensitivity might cause excessive intraosseous lymphocytic infiltrates is further supported by the strong association of lymphocytic infiltrations with female gender. Seven of eight patients with dense lymphocytic infiltrates were female in our study. Several studies had found a two- to tenfold higher frequency of metal hypersensitivity in females than in male patients [20–24]. It is believed that the female preponderance is caused by the more frequent exposure of women to metals by using earrings, ear piercing [11, 26–32], and other jewelry [11, 26–30].

In contrast to some recent studies on lymphocyte infiltrations within periprosthetic membranes and neocapsular tissues [33, 34], the majority of failures obtained in the current study were revised for periprosthetic fractures. Periprosthetic membrane at the bone–cement interface was minimal or virtually absent in some specimens. Furthermore, lymphocyte infiltration of deeper osseous tissues was also taken into account, and even more conservative criterion (300 lymphocytes/HPF) was defined to characterize the excessive lymphocytic infiltrate within the femoral remnant bone tissue. Interestingly, seven of 35 control cases with primary osteoarthritis showed more than 100 intraosseous lymphocytes per high power field (maximum 260 lymphocytes/HPF).

Similarly, with the recently proposed classification of chronic synovitis from native joint biopsies [35], besides the extent of inflammatory lympho-histiocytic infiltration of periprosthetic synovium, both the degree of the proliferation of synoviocytes and character of inflammatory exsudate were used as diagnostic criteria for synovial changes for the purpose of the current study. In the presence of joint replacement device, such high-grade synovitis [35]/proliferative desquamative synovitis suggestive of hypersensitivity reaction might possibly cause higher pressure of the joint effusion and facilitate its propagation into damaged or weakened soft and bone tissues. This might be another important mechanism of intraosseous influx of wear particles facilitating the osteolysis and prosthesis loosening [36, 37] as well as the enlargement of periarticular bursae, consistent with other compartments of the effective joint space [36, 37].

The association found between the excessive lymphocytic infiltrates and proliferative desquamative synovitis is also consistent with the suggestion that metal hypersensitivity might possibly cause both changes. Several recent reports have described marked joint effusion leading to enlarged bursae or groin masses in patients with unexplained groin pain caused possibly by metal hypersensitivity [7, 19–21]. It appears to be likely that desquamative synovitis has caused effusions in these cases. Again, this hypothesis would fit with the strong female predominance of proliferative desquamative synovitis as nine of 11 of these patients were female in our cohort.

Prevalence of the suggested hypersensitivity reaction of delayed type to metal after the hip resurfacing arthroplasty is not known. Based on the assumption that up to 5% of the hip replacements eventually fail and excessive lymphocytic infiltrates were found in ten of 181 failed prostheses in this study, one could speculate that significant metal hypersensitivity leading to revision surgery may occur in about ten of 3,600 resurfacing hip arthroplasties. A recent report described four patients who had underwent exploratory surgery for unexplained groin pain out of a total of approximately 1,500 implantations with finding of dense lymphocytic infiltration of periprosthetic soft tissues and large straw or brown watery to creamy fluid joint effusion under pressure [7].

Independent of the origin of lymphocytic infiltrates in the bone from patients with prosthesis failure, it is noteworthy that lymphocytic populations can be excessive and mimic lymphoma in some patients. Dense pseudolymphomatous infiltrates had indeed led to the suspicion of diagnosis of lymphoma in three patients of our series. While one of these patients was lost of follow-up, no evidence for lymphoma was clinically seen after a careful work-up and a follow-up period of 18 and 24 months in the remaining two patients.

In summary, the present study might possibly provide an additional evidence for a link between morphologic features like the excessive intraosseous lymphocytic infiltrates at the bone–implant interface or severe proliferative desquamative synovitis and the metal hypersensitivity of delayed type. Histological analysis of explanted bone may be instrumental for diagnosing an important cause for prosthesis failure and help to avoid implantation of other metal materials in affected patients.

Conflict of interest statement We declare that we have no conflict of interest.

References

1. Campbell P, Beaule PE, Ebramzadeh E et al (2006) A study of implant failure in metal-on-metal surface arthroplasties. Clin Orthop Relat Res 453:35–46

2. De Smet KA, Pattyn C, Verdonck R (2002) Early results of primary Birmingham hip resurfacing using a hybrid metal-on-metal couple. Hip Int 12:158–162
3. Daniel J, Pynsent PB, McMinn DJW (2004) Metal-on-metal resurfacing of the hip in patients under the age of 55 years with osteoarthritis. J Bone Joint Surg Br 86-B:177–184
4. Shimmin AJ, Bare J, Back DL (2005) Complications associated with hip resurfacing arthroplasty. Orthop Clin North Am 36:187–193
5. Steffen RT, Pandit HP, Palan J et al (2008) The five-year results of the Birmingham Hip Resurfacing arthroplasty. J Bone Joint Surg Br 90-B:436–441
6. Amstutz HC, Beaule PE, Dorey FJ et al (2004) Metal-on-metal hybrid surface arthroplasty: two to six years follow-up study. J Bone Joint Surg Am 86-A:28–39
7. Campbell P, Shimmin A, Walter L et al (2008) Metal sensitivity as a cause of groin pain in metal-on-metal hip resurfacing. J Arthroplasty 23(7):1080–1085
8. Shimmin A, Beaule P, Campbell P (2008) Metal-on-metal resurfacing arthroplasty. J Bone Joint Surg Am 90-A:637–654
9. Morlock M, Bishop N, Ruether W et al (2006) Biomechanical, morphological, and histological analysis of early failures in hip resurfacing arthroplasty. Proc Inst Mech Eng [H] 220(2):333–344
10. Pandey R, Drakoulakis E, Athanasou NA (1999) An assessment of the histological criteria used to diagnose infection in hip revision arthroplasty tissues. J Clin Pathol 52(2):118–123
11. Blanco-Dalmau L, Carrasquillo-Alberty H, Silva-Parra J (1984) A study of nickel allergy. J Prosthet Dent 52:116–119
12. Fyhrquist-Vanni N, Alenius H, Lauerma A (2007) Contact dermatitis. Dermatol Clin 25(4):613–623
13. Gober MD, Gaspari AA (2008) Allergic contact dermatitis. Curr Dir Autoimmun 10:1–26
14. Blumental G, Okun MR, Ponitch JA (1982) Pseudolymphomatous reaction to tattoos. Report of three cases. J Am Acad Dermatol 6:485–488
15. Balfour E, Olhoffer I, Leffell D et al (2003) Massive pseudoepitheliomatous hyperplasia: an unusual reaction to a tattoo. Am J Dermatopathol 25(4):338–340
16. Schmidt DA, Depta JP, Pichler WJ (2006) T-cell mediated hypersensitivity to quinolones: mechanisms and cross-reactivity. Clin Exp Allergy 36(1):59–69
17. Skoglund A, Torbjörn E (1991) Hypersensitivity reactions to dental materials in patients with lichenoid oral mucosa lesions and in patients with burning mouth syndrome. Scand J Dent Res 99:320–328
18. Torgerson RR, Davis MD, Bruce AJ et al (2007) Contact allergy in oral disease. J Am Acad Dermatol 57(2):315–321
19. ChSJ Fang, Harvie P, Gibbons CL et al (2008) The imaging spectrum of peri-articular inflammatory masses following metal-on-metal hip resurfacing. Skeletal Radiol 37(8):715–722
20. Pandit H, Vlychou M, Whitwell D et al (2008) Necrotic granulomatous pseudotumours in bilateral resurfacing hip arthroplasties: evidence for a type IV immune response. Virchows Arch 453(5):529–534
21. Pandit H, Glyn-Jones S, McLardy-Smith P et al (2008) Pseudotumours associated with metal-on-metal resurfacings. J Bone Joint Surg Br 90(7):847–851
22. Davies AP, Willert HG, Campbell PA et al (2005) An unusual lymphocytic perivascular infiltration in tissues around contemporary metal-on-metal joint replacements. J Bone Joint Surg Am 87:18–27
23. Jacobs JJ, Hallab NJ (2006) Loosening and osteolysis associated with metal-on-metal bearings: a local effect of metal hypersensitivity? J Bone Joint Surg Am 88:1171–1172
24. Willert HG, Buchhorn GH, Fayyazi A et al (2005) Metal-on-metal bearings and hypersensitivity in patients with artificial hip joints. A clinical and histomorphological study. J Bone Joint Surg Am 87:28–36
25. Doorn PF, Mirra JM, Campbell PA et al (1996) Tissue reaction to metal on metal total hip prostheses. Clin Orthop Relat Res 329-Suppl.:187–205
26. Prystowsky SD, Allen AM, Smith RW et al (1979) Allergic contact hypersensitivity to nickel, neomycin, ethylenediamine and benzocaine. Arch Dermatol 115:959–962
27. Kerusuo H, Kullaa A, Kerusuo E et al (1996) Nickel allergy in adolescents in relation to orthodontic treatment and piercing of ears. Am J Orthodont Dentofacial Orthop 109:148–154
28. Jensen CS, Lisby S, Baadsgaard O et al (2002) Decrease in nickel sensitization in a Danish schoolgirl population with ears pierced after implementation of a nickel-exposure regulation. Br J Dermatol 146(4):636–642
29. McDonagh AJG, Wright AL, Cork MJ et al (1992) Nickel sensitivity: the influence of ear piercing and atopy. Br J Dermatol 126:16–18
30. Fors R, Persson M, Bergström E et al (2008) Nickel allergy-prevalence in a population of Swedish youths from patch test and questionnaire data. Contact Dermatitis 58(2):80–87
31. Suzuki H (1998) Nickel and gold in skin lesions of pearced earlobes with contact dermatitis. A study using scanning electron microscopy and x-ray microanalysis. Arch Dermatol Res 290:523–527
32. Jones TK, Hansen CA, Singer MT et al (1996) Dental implications of nickel hypersensitivity. J Prosthet Dent 56:507–509
33. Morawietz L, Classen RA, Schröder JH et al (2006) Proposal for a histopathological consensus classification of the periprosthetic interface membrane. J Clin Pathol 59:591–597
34. Witzleb WC, Hanisch U, Kolar N et al (2007) Neo-capsule tissue reactions in metal-on-metal hip arthroplasty. Acta Orthop 78 (2):211–220
35. Krenn V, Morawietz L, Burmeister GR et al (2006) Synovitis score: discrimination between chronic low-grade and high-grade synovitis. Histopathology 49:358–364
36. Schmalzried TP, Jasty M, Harris WH (1992) Periprosthetic bone loss in total hip arthroplasty. Polyethylene wear debris and the concept of the effective joint space. J Bone Joint Surg Am 74 (6):849–863
37. Beaule PE, Campbell P, Mirra J et al (2001) Osteolysis in a cementless, second generation metal-on-metal hip replacement. Clin Orthop Relat Res 386:159–165

Virchows Arch (2009) 454:589–594
DOI 10.1007/s00428-009-0767-1

CASE REPORT

Biliary intraductal papillary mucinous neoplasia: three case reports

Banu Yaman · Deniz Nart · Funda Yilmaz · Ahmet Coker · Murat Zeytunlu · Murat Kilic

Received: 3 January 2009 / Revised: 5 March 2009 / Accepted: 19 March 2009 / Published online: 4 April 2009

Abstract Intrahepatic cholangiocarcinoma is subdivided as mass-forming, periductal-infiltrating, and intraductal-growing types. Intraductal-growing type is an entity described in recent years as mucin-producing intrahepatic cholangiocarcinoma or intrahepatic (biliary) intraductal papillary mucinous neoplasia (b-IPMN). b-IPMN is classified as adenoma, borderline tumor, carcinoma in situ, and carcinoma, from benign to malignant. Using a different classification, b-IPMNs are subdivided into intestinal, pancreatobiliary, gastric, or oncocytic based on morphology of the cells forming the lesion and expression of MUC1, MUC2, and MUC5 gene proteins in the mucin family. The clinical and histopathological features of b-IPMN diagnosed in three cases are presented herein. Case 1 was classified as borderline. Case 2 was diagnosed as carcinoma in situ. Case 3 had large invasive areas, and was diagnosed as carcinoma. In all three cases, immunohistochemical investigation revealed MUC1 and MUC5AC to be positive, and MUC2 to be negative. We present herein three cases diagnosed with the clinical and pathological findings of a new entity in the literature, b-IPMN, and we discuss the macroscopic, histological, and immunohistochemical features.

Keywords Papillary neoplasia · Bile ducts · Liver · Mucin · Cholangiocarcinoma

B. Yaman (✉) · D. Nart · F. Yilmaz
Department of Pathology, Faculty of Medicine, University of Ege, Izmir, Turkey
e-mail: drbanuyaman@yahoo.com

A. Coker · M. Zeytunlu · M. Kilic
Department of General Surgery, Faculty of Medicine, University of Ege, Izmir, Turkey

Introduction

Cholangiocarcinoma (CC) arises from intrahepatic or extrahepatic bile ducts and shows various histological types and growth patterns [1]. Intrahepatic CC is subdivided into three groups as mass-forming, periductal-infiltrating, and intraductal-growing types [2–5]. Intraductal-growing type is an entity that has been described in recent years, and designated as mucin-producing intrahepatic CC or intrahepatic (biliary) intraductal papillary mucinous neoplasia (b-IPMN) [3, 6, 7]. b-IPMN comprises a histological spectrum that ranges from benign to malignant and can be seen as adenoma, borderline tumor, carcinoma in situ, and carcinoma [2, 3]. Using a different classification, b-IPMN is subdivided on the basis of histology and mucin gene protein (MUC1, MUC2, and MUC5) expression into four subtypes as pancreatobiliary, gastric, intestinal, or oncocytic [2, 8–11]. We present three cases with the diagnosis of b-IPMN together with their clinical and histopathological findings.

Clinical history

Two male patients (cases 1 and 2; 54 and 65 years old), both without biliary disease, presented with icterus and pain and sensitivity on the epigastrium and right upper quadrant. Liver function tests were elevated in both patients, both albumin (3.3 and 3 g/dl, respectively) and total protein (5.4 and 5.3 g/dl) levels were decreased, and bilirubin and lactate dehydrogenase levels were slightly elevated. In addition, CEA and CA 19-9 elevation and leukocytosis were determined in case 2. Ultrasonographic radiological examination in case 1 revealed left lobe hypoplasia of the liver and a 2-cm lesion in the 4A segment next to the portal

vein, which made pressure, cystic at the periphery and hyperechoic in the center.

In case 2, dilated intrahepatic bile ducts in the left lobe of the liver and a 4-cm lobulated echogenicity in the left common bile duct were noted.

In cases 1 and 2, the liver masses were examined clinically and radiologically and, respectively, segmentectomy and left lobectomy were applied.

The third case was a 60-year-old male who underwent liver transplantation because of hepatitis B cirrhosis.

Materials and methods

The specimens were fixed in 10% buffered formalin, embedded in paraffin, routinely processed, cut in 4-μm-thick sections, and stained with hematoxylin and eosin (H & E) as well as periodic acid-Schiff–Alcian blue (PAS–AB) stain according to standard procedures.

Immunohistochemical studies using the biotin–streptavidin peroxidase technique were performed using antibodies against cytokeratin 7 (CK7), cytokeratin 20 (CK20), MUC1, MUC2, and MUC5AC.

Results

Macroscopic examination of the segmentectomy specimen in case 1 measuring 10×8×4 cm revealed dilated intrahepatic bile ducts containing mucinous material. The bile ducts were dilated and a papillary lesion of 2 cm was observed within the dilated bile duct.

Microscopic examination of the tumor in case 1 showed that dilated bile ducts were lined by biliary epithelium displaying papillary structures. The cells showed oncocytic properties, large eosinophilic granular cytoplasm, and prominent nucleoli. Some of them showed moderate to severe degree of dysplastic changes. The tumor showed intraductal growth pattern and no liver parenchymal invasion was seen. Normal hepatic parenchyma was observed among the papillary structures. In the immunohistochemical analysis, MUC1, MUC5AC, and patchy cytokeratin7 immunopositivities were observed. Immunostaining for MUC2 and cytokeratin20 was negative. Based on these properties, case 1 was classified as borderline and showed oncocytic properties (Fig. 1).

At the lobectomy specimen in case 2, measuring 20×8.5×6 cm, a mucoid and papillary lesion of 4 cm were seen in the dilated left common bile duct. The tumor had a large amount of mucin. The other bile ducts in the lobectomy were dilated too (Fig. 2).

Microscopic evaluation showed a largely exophytic tumor containing intra- and extracellular mucinous material which with periodic acid-Schiff–Alcian blue staining positive concluded. The dilated bile ducts were lined by biliary epithelium displaying simple and complex papillary structures. The papillae were lined by one to several layers of cuboidal to low columnar cells with acidophilic cytoplasm and round nuclei with prominent nucleoli. There was cytologic dysplasia but no evidence of stromal invasion was noted. He was diagnosed as carcinoma in situ. The tumor cells showed immunohistochemical staining for MUC1, MUC5AC, and cytokeratin7; however, cells were negative for MUC2 and cytokeratin20 (Fig. 3). With these histomorphological and immunohistochemical properties, the tumor was evaluated as pancreatobiliary type.

At the explant material of the third case developed an irregular 2.2-cm mass on cirrhosis base and four satellite lesions were seen. Microscopic examination of the third tumor showed large invasive areas, and tubulary and papillary development of cuboidal cells with acidophilic cytoplasm, round nuclei, and prominent nucleoli was seen. This invasive tumor was immunohistochemically positive for MUC1, MUC5AC, and cytokeratin7 and the others negative for MUC2 and cytokeratin20 (Fig. 4). Based on this histological and immunohistochemical findings, case 3 was diagnosed as pancreatobiliary type and as carcinoma.

Twelve months after the surgery, all three cases were alive without any evidences of tumor recurrence after excision.

In this report, three cases diagnosed with the clinical and pathological findings of a new entity in the literature, b-IPMN, are presented and the macroscopic, histological, and immunohistochemical features are discussed.

Discussion

Biliary dysplasia is described as multilayering, piled-up nuclei, an increased nucleo-cytoplasmic ratio, a partial loss of nuclear polarity, and nuclear hyperchromasia in biliary epithelial cells [3, 12]. According to the WHO classification of liver tumors, biliary intraductal lesions are divided into flat-type biliary dysplasia and papillary-type biliary intraepithelial neoplasia.

Intraductal papillary neoplasia has a good prognosis and mucin production compared with the others [1, 13, 14]. The most important factors in the etiology of intraductal papillary neoplasia are stone, infection, pancreatic injury, and biliary hyperplasia on the base [1, 3, 15, 16].

Cholangiocarcinoma arises from intrahepatic or extrahepatic bile ducts and shows various histological types and growth patterns [1]. Intrahepatic CC is the second most frequently seen liver malignancy after hepatocellular carcinoma and is known to develop in patients with hepatolithiasis [3, 12]. Intrahepatic CC is divided into three

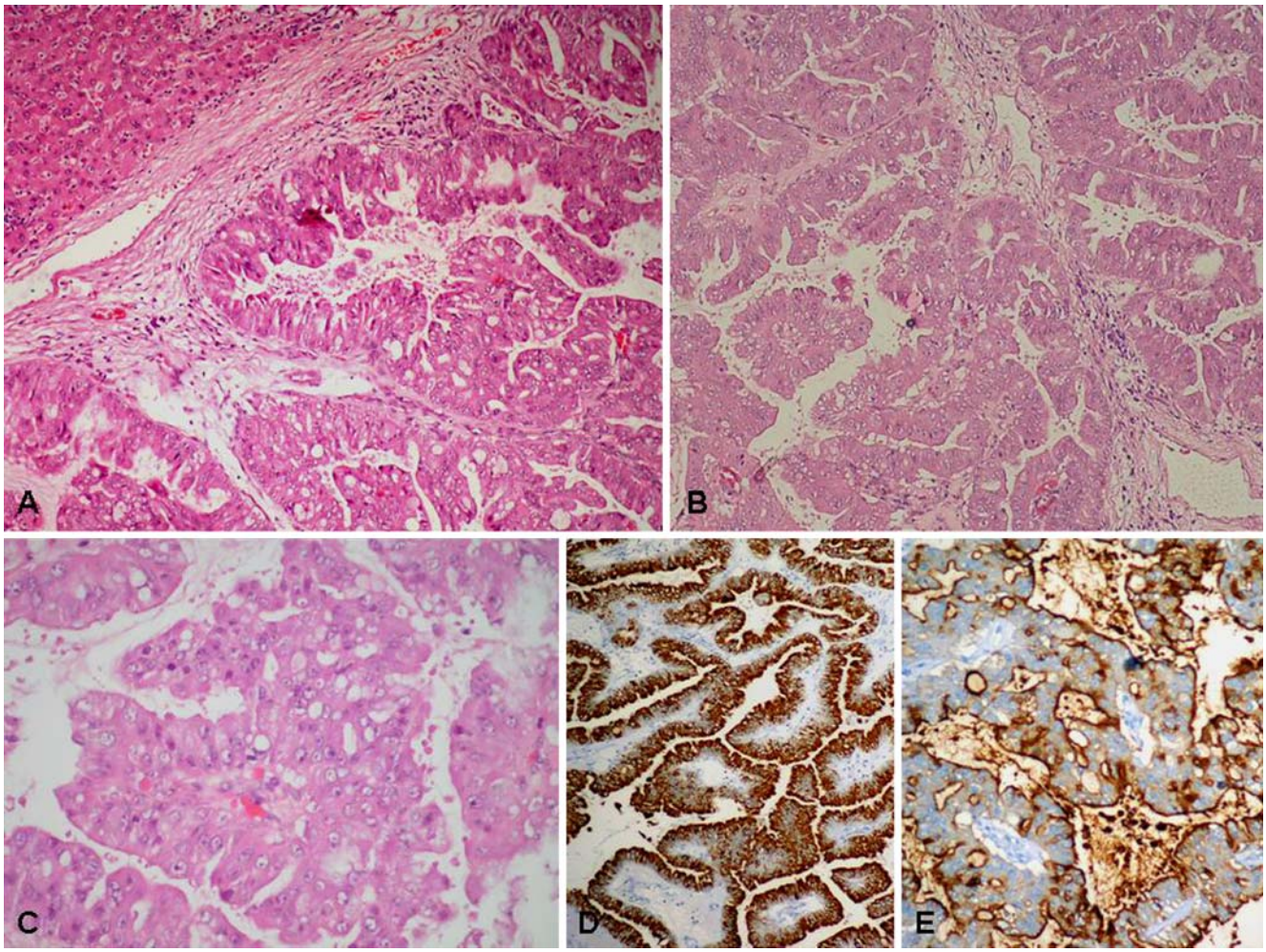

Fig. 1 Borderline tumor in case 1. **a** The tumor showed oncocytic properties and intraductal growth pattern. HE, ×200. **b** HE, ×200. **c** Papillary structures composed of cells with large eosinophilic cytoplasm and prominent nucleoli. HE, ×400. **d** MUC1, ×100. **e** MUC5AC, ×200

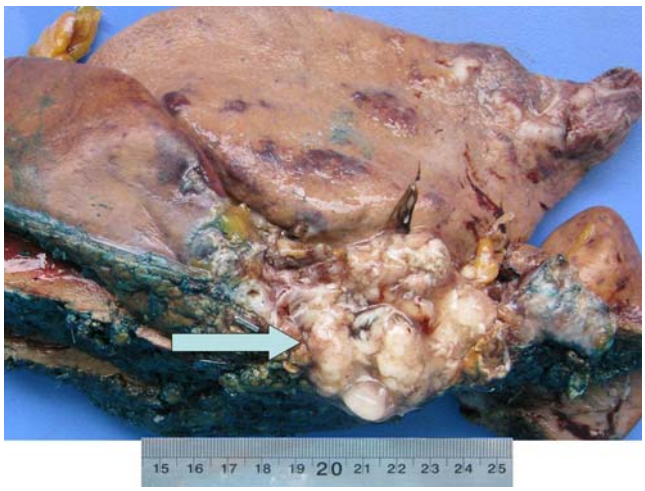

Fig. 2 Macroscopic evaluation of the tumor in case 2 shows a 4-cm lobulated, mucoid, and papillary mass (*arrow*) in the dilated intrahepatic bile duct

types as mass forming, periductal infiltrating, and intraductal growing [2–5]. The mass-forming type has a regular shape and forms an expansile and solid nodule or mass in the hepatic parenchyma. The periductal-infiltrating type is diffusely infiltrative around the portal tractus. The intraductal-growing type has a better prognosis, and has no bile wall invasion or is located in minimally dilated intrahepatic large bile ducts. The affected bile ducts usually show marked localized dilatation [3–5].

Biliary papillomatosis and intraductal intrahepatic CC, known as liver biliary intraductal papillary neoplasia, show the spectrum of papillary biliary neoplasia [1, 2]. Biliary papillomatosis is a rare entity and is classified as either mucin-hypersecreting type or non-mucin-producing type [1, 17]. Intraductal intrahepatic CC is the least common type and is known as mucin-producing intrahepatic CC or b-IPMN [3, 6, 7]. Recent studies revealed striking similarities between b-IPMN and intraductal papillary mucinous neoplasia of the pancreas (p-IPMN) in its histopathological

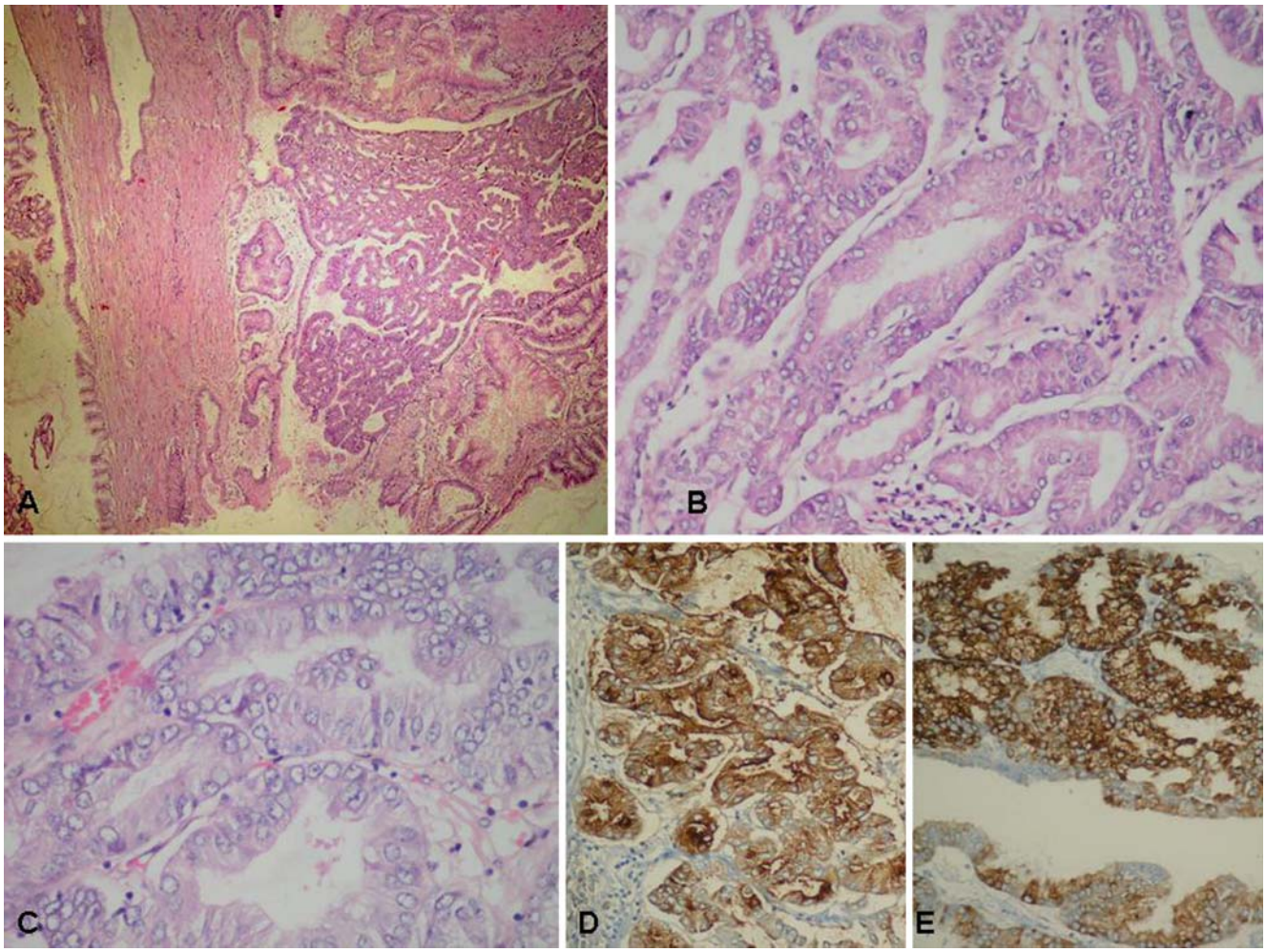

Fig. 3 Carcinoma in situ in case 2. **a** The tumor had an intra- and extracellular mucin component, prominent papillary formation. HE, ×100. **b** The papillae with cuboidal cells. HE, ×200. **c** The cells with round nuclei with prominent nucleoli. HE, ×400. **d** MUC1, ×100. **e** MUC5AC, ×200

features, production of a large amount of mucin, pathophysiological characteristics, and clinical findings [2, 3, 8–10, 14, 18, 19].

Biliary intraductal papillary neoplasia of the liver has a histological spectrum from low- and high-grade papillary growing to in situ and invasive carcinoma and sometimes to a mucinous carcinoma [2, 3, 19]. b-IPMN is classified as adenoma, borderline tumor, carcinoma in situ, and carcinoma, from benign to malignant [2, 14, 18–20]. The three cases that we presented in this study showed a wide range of spectrum as borderline tumor, carcinoma in situ, and carcinoma. In one study, Chen et al. [3] divided biliary intraductal papillary neoplasia into four groups, defined as: type 1 = low-grade dysplasia, type 2 = high-grade dysplasia, type 3 = in situ and microinvasive adenocarcinoma, and type 4 = types 2 and 3 biliary lesions with variable invasion of adenocarcinoma. Type 3 is similar to intraductal-growing type of intrahepatic CC. Type 4 includes the intraductal-growing type with variable stromal invasion and intraductal papillary carcinoma foci of periductal-infiltrating type or mass-forming type [1, 3].

Shibahara et al. [9] showed the criteria for diagnosis of mucin-producing bile duct tumors to be similar to those of IPMN of the pancreas: (1) radiographic fluid retention in cystic lesion and/or dilated bile ducts; (2) confirmation of the fluid as mucin by percutaneous transhepatic biliary drainage and/or endoscopic retrograde cholangiography and/or surgical specimens; (3) development from intrahepatic or extrahepatic bile ducts; and (4) cystic formation and/or dilatation of bile ducts.

Some studies have reported consistently different histological appearance and mucin core proteins (MUC) of b-IPMN, similar to p-IPMN [2, 8–10, 14, 18]. As a result, on the basis of their histology and mucin expression, four subtypes of b-IPMN are currently defined: gastric, intestinal, pancreatobiliary, or oncocytic type [2, 8–11, 14, 18, 21].

The gastric type includes the cells resembling gastric foveola. They have eosinophilic cytoplasm and nuclei

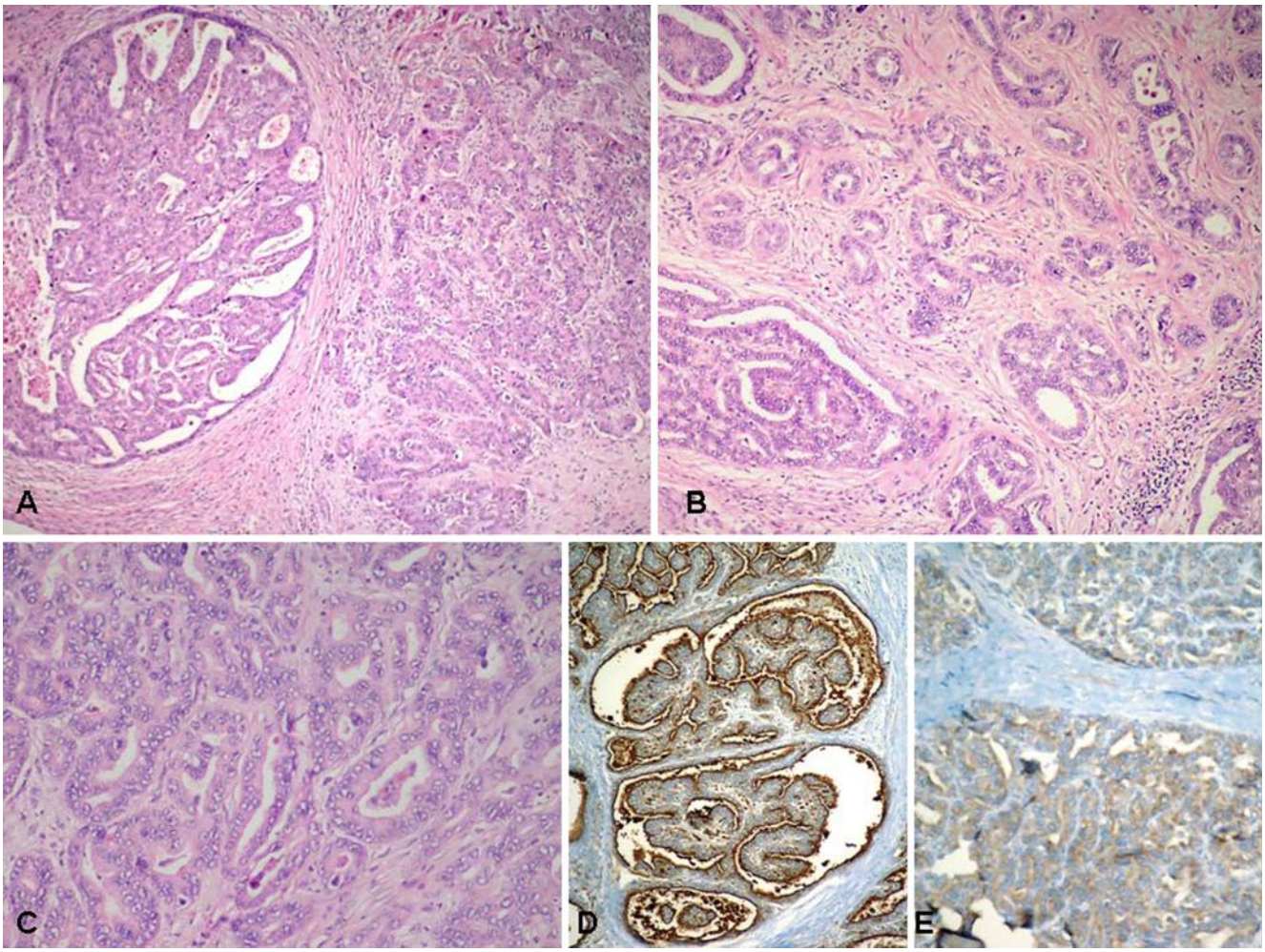

Fig. 4 Tubulary and papillary development of invasive carcinoma in case 3. **a** HE, ×100. **b** HE, ×200. **c** Cuboidal cells with acidophilic cytoplasm, round nuclei, and prominent nucleoli. HE, ×400. **d** MUC1, ×100. **e** MUC5AC, ×200

located at the basal layer. The intestinal type consists of cells with basophilic cytoplasm and oval nuclei with pseudostratification like intestinal villous neoplasia [8, 11, 14, 18, 22, 23]. The pancreatobiliary and oncocytic types have both cuboidal cells, but the histological appearances are different [9]. The pancreatobiliary type has a complex papillary structure, and includes cuboidal cells with hyperchromatic nuclei resembling cholangio-papillary carcinoma. The cells of the oncocytic type with abundant eosinophilic granular cytoplasm and big rounded nuclei and prominent nucleoli resemble oncocytic carcinoma cells [8, 11, 14, 18, 22, 23].

The mucin core protein expressions of these subtypes are variable [2, 8, 11, 14, 18]. Furukawa et al. [11] published in a consensus study the MUC expressions in the different subtypes of IPMN (Table 1).

MUC1 is expressed in invasive ductal adenocarcinoma of the pancreas. It is positive in the pancreatobiliary type of p-IPMN and focal positive in the oncocytic type. MUC2 is found in intestinal gland secretion and is considered to be a marker of intestinal differentiation [2, 8, 11, 14, 18]. It is generally negative in pancreatobiliary and oncocytic subtypes, but Zen et al. [18] showed some of pancreatobiliary IPMNs were focally positive with MUC2. MUC5AC is not detected in the normal pancreas and is expressed by mucous surface cells of the stomach. MUC5AC is

Table 1 The four histological types of biliary intraductal papillary mucinous neoplasia according to mucin core protein contents, a consensus study [11]

	MUC1	MUC2	MUC5AC
Gastric	−	−	+
Intestinal	−	+	+
Pancreatobiliary	+	−	+
Oncocytic	+	−	+

consistently detected in all types of IPMN [2, 8, 11, 14, 18, 22, 23].

Results of MUC staining in oncocytic variant of IPMN are variable. Some researchers showed focal MUC1 and MUC2 positivity; on the other hand, others have reported little or no MUC1 and MUC2 expression [9, 14, 18]. Rouzbahman et al. [19] found MUC2 focal positive in two cases in four oncocytic-type biliary tract neoplasia.

In the three cases we present here, MUC1 and MUC5AC were positive, MUC2 was negative. The diagnosis was oncocytic type in the first case because of their oncocytic properties and in the other two cases the diagnoses were pancreatobiliary type.

In recently published studies, patients with biliary tract malignancies who were MUC1-positive and MUC2-negative immunohistochemically showed poorer survival than MUC1-negative and MUC2-positive patients [9, 10]. Furthermore, IPMN expressing MUC5AC alone had a good prognosis [19]. MUC5AC expression is correlated with tumors that show an expansive growth pattern and low degrees of invasion and metastasis [9, 10]. Ishida et al. [21] showed that the gastric type IPMN is less aggressive clinically and patients with intestinal type IPMNs had poor prognoses.

All of our cases were alive after 12 months and have no evidence of tumor recurrences.

In conclusion, we report herein three cases diagnosed as the new entity of b-IPMN, and we describe the different histological spectrum as borderline, carcinoma in situ, and invasive carcinoma. Examination of the cell morphology showed development from the oncocytic cells in one, while the others developed from the pancreatobiliary cells; development from intestinal type cells is seen less. MUC1 and MUC5AC were positive on immunohistochemical examination in all three tumors, while MUC2 was negative.

Conflict of interest statement We declare that we have no conflict of interest.

References

1. Güllüoğlu MG, Ozden I, Poyanlı A et al (2007) Intraductal growth-type mucin-producing peripheral cholangiocarcinoma associated with biliary papillomatosis. Ann Diagn Pathol 11(1):34–38
2. Ji Y, Fan J, Zhou J et al (2008) Intraductal papillary neoplasms of bile duct. A distinct entity like its counterpart in pancreas. Histol Histopathol 23(1):41–50
3. Chen TC, Nakanuma Y, Zen Y et al (2001) Intraductal papillary neoplasia of the liver associated with hepatolithiasis. Hepatology 34(4 Pt 1):651–658
4. Liver Cancer Study Group of Japan (1997) Classification of Primary Liver Cancer. Tokyo: Kanehara-Shuppan 6-7.
5. Yamamoto M, Takasaki K, Yoshikawa T et al (1998) Does gross appearance indicate prognosis in intrahepatic cholangiocarcinoma? J Surg Oncol 69(3):162–167
6. Chen MF, Jan YY, Chen TC (1998) Clinical studies of mucin-producing cholangiocellular carcinoma: a study of 22 histopathology-proven cases. Ann Surg 227(1):63–69
7. Kim YI, Yu ES, Kim ST (1989) Intraductal variant of peripheral cholangiocarcinoma of the liver with *Clonorchis sinensis* infection. Cancer 63(8):1562–1566
8. Klöppel G, Kosmahl M (2006) Is the intraductal papillary mucinous neoplasia of the biliary tract a counterpart of pancreatic papillary mucinous neoplasm? J Hepatol 44(2):249–250
9. Shibahara H, Tamada S, Goto M et al (2004) Pathologic features of mucin-producing bile duct tumors: two histopathologic categories as counterparts of pancreatic intraductal papillary-mucinous neoplasms. Am J Surg Pathol 28(3):327–338
10. Uchiyama S, Chijiiwa K, Hiyoshi M et al (2007) Mucin-producing bile duct tumor of the caudate lobe protruding into the common hepatic duct. J Gastrointest Surg 11:1570–1572
11. Furukawa T, Klöppel G, Adsay V et al (2005) Classification of types of intraductal papillary-mucinous neoplasm of the pancreas: a consensus study. Virchows Arch 447(5):794–799
12. Nakanuma Y, Sripa B, Vatanasapt V et al (2000) Intrahepatic cholangiocarcinoma. In: Hamilton SR, Aaltonen LA (eds) WHO classification of tumors, pathology and genetics, tumours of the digestive system. IARC, Lyon, pp 173–180
13. Ishikawa A, Sasaki M, Ohira S et al (2004) Aberrant expression of CDX2 is closely related to the intestinal metaplasia and MUC2 expression in intraductal papillary neoplasm of the liver in hepatolithiasis. Lab Invest 84(5):629–638
14. Zen Y, Fujii T, Itatsu K et al (2006) Biliary cystic tumors with bile duct communication: a cystic variant of intraductal papillary neoplasm of the bile duct. Mod Pathol 19(9):1243–1254
15. Abraham SC, Lee JH, Hruban RH et al (2003) Molecular and immunohistochemical analysis of intraductal papillary neoplasms of the biliary tract. Hum Pathol 34:902–910
16. Zen Y, Sasaki M, Fujii T et al (2006) Different expression patterns of mucin core proteins and cytokeratins during intrahepatic cholangiocarcinogenesis from biliary intraepithelial neoplasia and intraductal papillary neoplasm of the bile duct—an immunohistochemical study of 110 cases of hepatolithiasis. J Hepatol 44 (2):350–358
17. Lee SS, Kim M, Lee SK et al (2004) Clinicopathologic review of 58 patients with biliary papillomatosis. Cancer 100:783–793
18. Zen Y, Fujii T, Itatsu K et al (2006) Biliary papillary tumors share pathological features with intraductal papillary mucinous neoplasm of the pancreas. Hepatology 44(5):1333–1343
19. Rouzbahman M, Serra S, Adsay NV et al (2007) Oncocytic papillary neoplasms of the biliary tract: a clinicopathological, mucin core and Wnt pathway protein analysis of four cases. Pathology 39(4):413–418
20. Kim HJ, Kim MH, Lee SK et al (2000) Mucin-hypersecreting bile duct tumor characterized by a striking homology with an intraductal papillary mucinous tumor (IPMT) of the pancreas. Endoscopy 32(5):389–393
21. Ishida M, Egawa S, Aoki T et al (2007) Characteristic clinicopathological features of the types of intraductal papillary-mucinous neoplasms of the pancreas. Pancreas 35(4):348–352
22. Nakamura A, Horinouchi M, Goto M et al (2002) New classification of pancreatic intraductal papillary-mucinous tumour by mucin expression: its relationship with potential for malignancy. J Pathol 197:201–210
23. Yonezawa S, Horinouchi M, Osako M et al (1999) Gene expression of gastric type mucin (MUC5AC) in pancreatic tumors: its relationship with the biological behavior of the tumor. Pathol Int 49:45–54

Virchows Arch (2009) 454:595–598
DOI 10.1007/s00428-009-0756-4

CASE REPORT

Leiomyomatous nodules in a cellular angiofibroma: a hitherto unreported finding

Juan C. Tardío

Received: 21 January 2009 / Revised: 23 February 2009 / Accepted: 2 March 2009 / Published online: 20 March 2009

Abstract Cellular angiofibroma is a benign tumor of the superficial soft tissues of the vulvovaginal and inguinoscrotal regions of adult patients. Histologically, it is characterized by bland spindle cells arranged without any pattern in a stroma with thin collagen fibrils and evenly distributed small- to medium-sized blood vessels with hyalinized walls. The case of a 44-year-old female with a perineal cellular angiofibroma containing small leiomyomatous nodules is described in this case report. These nodules could probably be originated from smooth muscle differentiation of the spindle cell component of an otherwise conventional cellular angiofibroma. To our knowledge, the finding of distinct leiomyomatous nodules within a cellular angiofibroma has not been previously reported.

Keywords Cellular angiofibroma · Leiomyomatous nodules · Immunohistochemistry · Perineal tumor

Introduction

Cellular angiofibroma was first described by Nucci et al. in 1997 [1]. Since the original report, only three series and some case reports have been published [2–4]. Cellular angiofibroma typically presents in the superficial soft tissues of the vulvovaginal region of females and the inguinoscrotal region of males. In the latter, it has also been called angiomyofibroblastoma-like tumor. Histologically, it is characterized by a moderately cellular proliferation of bland spindle cells randomly distributed within a richly vascularized stroma.

Hereby, a case of cellular angiofibroma containing nodular foci of leiomyomatous differentiation is presented. To our knowledge, this feature has not been previously reported.

J. C. Tardío (✉)
Servicio de Anatomía Patológica,
Hospital Universitario de Fuenlabrada,
Camino del Molino, 2,
28942 Fuenlabrada, Madrid, Spain
e-mail: jtardio.hflr@salud.madrid.org

Clinical history

A 44-year-old female presented to our hospital with a perineal mass of 1-year duration. An ultrasound and magnetic resonance examination revealed a soft tissue tumor located in the posterior right perineal region. A needle biopsy was performed. After the diagnosis of the biopsy was rendered, the patient underwent a surgical resection of the mass. During the procedure, a well-demarcated tumor located between the rectum and the vagina and adhered to the elevator muscle of the anus was found. A marginal tumorectomy was performed.

Material and methods

The biopsy and the surgical specimen were fixed in 10% buffered formalin and embedded in paraffin. Sections of 4 μm were obtained for conventional histopathological stainings and immunohistochemical study. Immunohistochemistry was performed using the EnVision detection system (Dako, Glostrup, Denmark), diaminobenzidine as chromogen, and antibodies against the following antigens: muscle-specific actin (MSA; clone HHF35, dilution 1/400; Dako), smooth muscle actin (SMA; clone 1A4, dilution 1/100; Master Diagnóstica, Granada, Spain), desmin (clone D33, dilution 1/200; Dako), h-caldesmon (clone h-CD,

dilution 1/50; Dako), calponin (clone CALP, dilution 1/200; Dako), CD34 (clone QBend-10, dilution 1/50; Dako), S100 protein (polyclonal, dilution 1/2,000; Dako), estrogen receptor alpha (ER; clone 1D5, dilution 1/100; Dako), and progesterone receptor (PR; clone PgR 636, dilution 1/50; Dako). Heat-induced epitope retrieval was achieved by pressure cooker in citrate buffer at pH 6.0 boiling for 2 min before incubation with anti-SMA or by water bath in Tris/EDTA buffer at pH 9.0 for 30 min before incubation with the remaining primary antibodies. All of them were cooled for 15 min in the buffer before incubation with the primary antibody. Incubation with all primary antibodies was performed at room temperature for 30 min. Sections were counterstained with hematoxylin.

Results

The biopsy consisted of a moderately cellular mesenchymal proliferation composed of spindle cells with a short fusiform, bland nucleus, and a palely acidophilic cytoplasm with bipolar dendritic processes. The cells were disposed without any pattern within a stroma containing slightly eosinophilic, delicate collagen fibers and numerous evenly distributed thin-walled blood vessels. Mitotic figures were not seen. A diagnosis of cellular angiofibroma was rendered.

The surgical specimen was grossly formed by a 95×65×45 mm bilobated, grayish white, elastic mass. The cut surface was bright and showed several small white protruding nodules (Fig. 1), the largest one measuring 4 mm in diameter. No areas of necrosis were found.

Histologically, the nodules were composed of spindle cells with a uniform ovoid to fusiform nucleus and an eosinophilic fibrillary cytoplasm with poorly delimited borders. The cells were arranged in fascicles separated by scarce fibrous stroma without a prominent vascular component (Fig. 2). No cytological atypia was observed. The mitotic index was lower than one mitosis per ten high-power fields. The rest of the tumor had the same morphology as that seen in the biopsy, a classical cellular angiofibroma (Fig. 3). The borders between the two areas were well-demarcated (Fig. 4).

The immunohistochemical study showed reactivity for ER and PR in the two components of the tumor. The cells in the small nodules strongly and diffusely coexpressed MSA, SMA, desmin, h-caldesmon (Fig. 4b), and calponin.

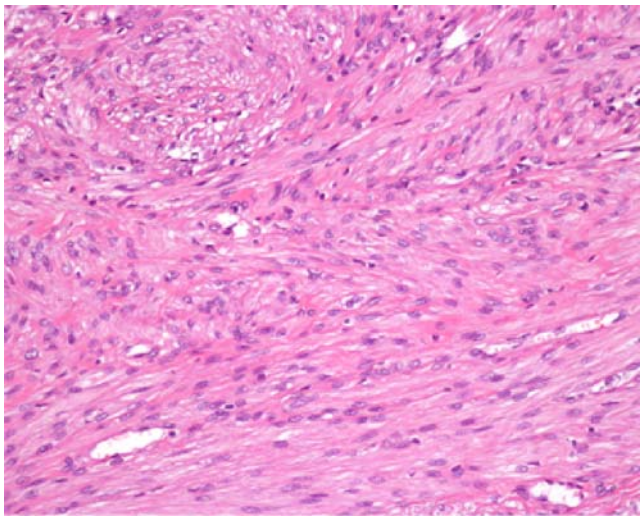

Fig. 2 Nodule composed of mature smooth muscle cells arranged in a fascicular pattern

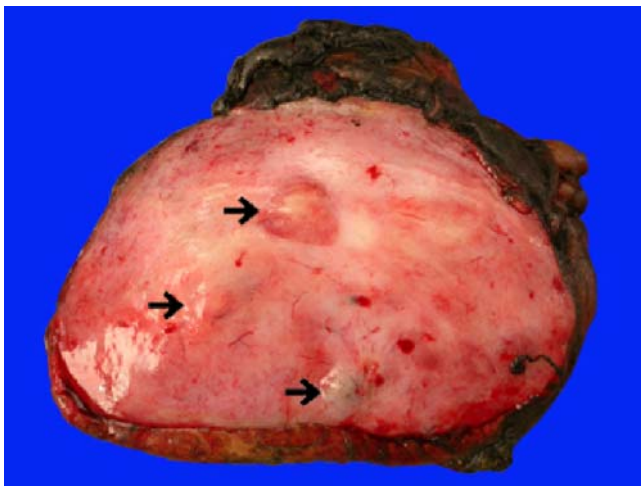

Fig. 1 Gross view showing three small white nodules (*arrows*) protruding from the cut surface of the lesion

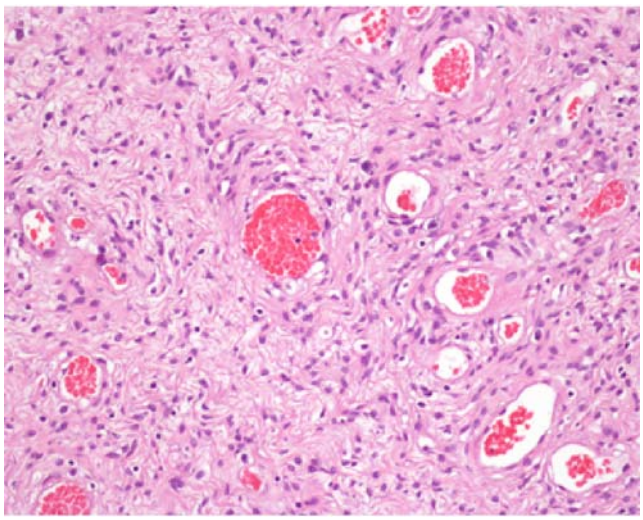

Fig. 3 Bland spindle cells disposed without any pattern amongst numerous blood vessels within a fibrillary stroma

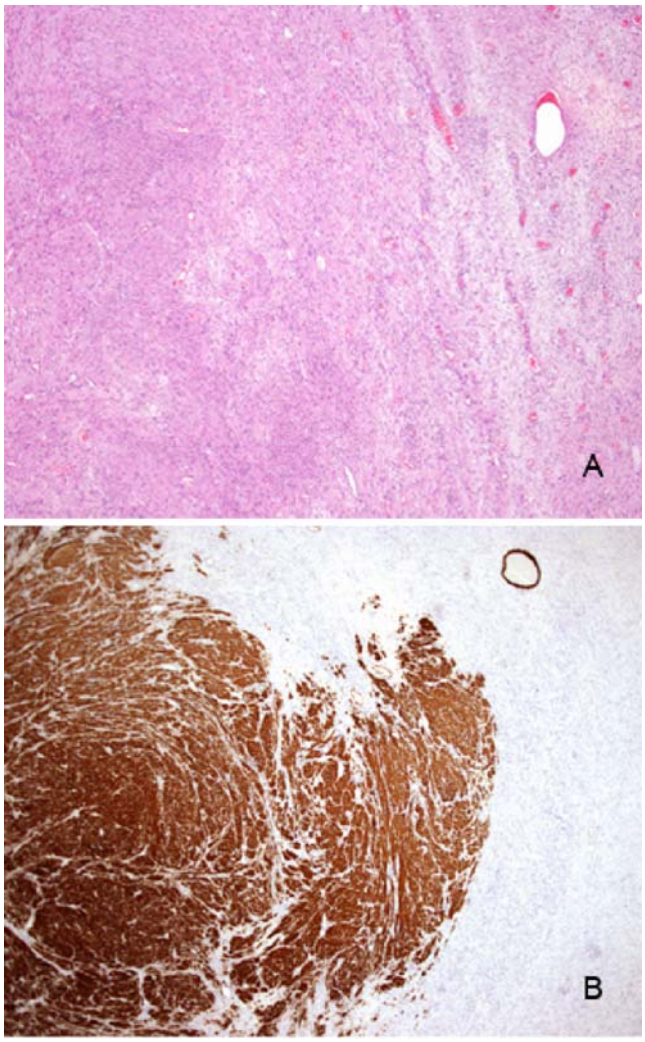

Fig. 4 The well-demarcated limit between a leiomyomatous nodule (*on the left*) and the conventional cellular angiofibroma (*on the right*) is shown by hematoxylin–eosin staining (**a**) and immunohistochemistry for h-caldesmon (**b**)

The muscle markers were negative in the remainder of the tumor. CD34 highlighted the vascular component staining the endothelia and was negative in the spindle cells. S100 protein expression was not present.

Discussion

Cellular angiofibroma is a benign tumor of the superficial soft tissues of the vulvovaginal and the inguinoscrotal regions of adult patients. Other superficial and deep pelvic and extrapelvic locations have rarely been documented. Cellular angiofibroma usually presents as a well-delimited mass, histologically characterized by two components: bland spindle cells and numerous blood vessels. The spindle cells are randomly distributed throughout the lesion without any particular pattern. The vascular component is composed of evenly distributed small- to medium-sized vessels with frequent mural hyalinization [2–4]. Immunohistochemically, cellular angiofibroma is positive for vimentin and variably expresses CD34 (50–60% of the cases), ER (35–40%), PR (55%), MSA (35%), SMA (20%), and desmin (10%) [2,4].

In our case, nodules with histological and immunophenotypical features of leiomyomatous differentiation were found within a conventional cellular angiofibroma. Whether they were originated from smooth muscle differentiation of the spindle cell component or derived from the vessel walls can be speculated. However, since the morphology of the nodules was not consistent with angioleiomyomas, the former possibility is favored. Leiomyomatous differentiation had not been previously described in cellular angiofibromas, although it has rarely been reported in mammary myofibroblastoma [5], a tumor that shows overlapping histological features with cellular angiofibroma. A more common feature is the presence of a variable number of adipocytic cells within cellular angiofibromas. It occurs in approximately one fourth of the cases and, in most of them, the fat component is scarce and located in the periphery of the tumors. However, it can occasionally be abundant and randomly distributed. A typical cellular angiofibroma containing a distinct nodule of pleomorphic liposarcoma has been reported [4].

Although an origin from or a differentiation to hormonally responsive subepithelial stromal cells has been suggested for some mesenchymal tumors of the lower female genital tract, based on their selective location and their coexpression of desmin and hormonal receptors, the line of differentiation of cellular angiofibroma remains to be clarified. Recently, genetic aberrations involving chromosomes 13q and 16, common to spindle cell lipoma and mammary-type myofibroblastoma of soft tissue have been reported in three cases of cellular angiofibroma [6,7]. The close relationship between these three lesions is further supported by their overlapping histological and immunophenotypical features. Fibroblastic and preadipocytic lines of differentiation have previously been postulated for spindle cell lipoma [4].

In conclusion, a case of a perineal cellular angiofibroma with leiomyomatous nodules in an adult female patient is presented. A focal smooth muscle differentiation of the spindle cell component of the cellular angiofibroma is proposed as the pathogenetic mechanism. To the best of our knowledge, this finding has not been previously reported.

Conflict of interest statement I declare that I have no conflict of interest.

References

1. Nucci MR, Granter SR, Fletcher CDM (1997) Cellular angiofibroma: a benign neoplasm distinct from angiomyofibroblastoma and spindle cell lipoma. Am J Surg Pathol 21:636–644
2. Laskin WB, Fetsch JF, Mostofi FK (1998) Angiomyofibroblastoma-like tumor of the male genital tract: analysis of 11 cases with comparison to female angiomyofibroblastoma and spindle cell lipoma. Am J Surg Pathol 22:6–16
3. McCluggage WG, Ganesan R, Hirschowitz L et al (2004) Cellular angiofibroma and related fibromatous lesions of the vulva: report of a series of cases with a morphological spectrum wider than previously described. Histopathology 45:360–368
4. Iwasa Y, Fletcher CDM (2004) Cellular angiofibroma. Clinicopathologic and immunohistochemical analysis of 51 cases. Am J Surg Pathol 28:1426–1435
5. Thomas TMM, Myint A, Mak CKL et al (1997) Mammary myofibroblastoma with leiomyomatous differentiation. Am J Clin Pathol 107:52–55
6. Maggiani F, Debiec-Rychter M, Vanbockrijck M et al (2007) Cellular angiofibroma: another mesenchymal tumour with 13q14 involvement, suggesting a link with spindle cell lipoma and (extra)-mammary myofibroblastoma. Histopathology 51:410–412
7. Hameed M, Clarke K, Amer HZ et al (2007) Cellular angiofibroma is genetically similar to spindle cell lipoma: a case report. Cancer Genet Cytogenet 177:131–134

Virchows Arch (2009) 454:599–622
DOI 10.1007/s00428-009-0784-0

REVIEW AND PERSPECTIVE

Cancer invasion and metastasis: interacting ecosystems

Marc Mareel · Maria J. Oliveira · Indira Madani

Received: 6 March 2009 / Accepted: 30 April 2009 / Published online: 27 May 2009

Abstract Malignant tumors invade and metastasize. They consist of cancer cells, evolving through genetic and epigenetic modulation, mixed with tumor-associated host cells, emerging from resident or bone marrow-derived precursors. These cells establish ecosystems to activate cellular programs for local invasion and distant metastasis. Characteristic of such malignancy-related activities is communication inside ecosystems between cells, ligands, receptor protein complexes, and signaling pathways as well as between ecosystems comprising the primary tumor, lymph node and distant metastasis, bone marrow and blood and lymph circulation. Complexity is another characteristic, resulting from: heterogeneity of the cell populations; the numbers of promoter and suppressor genes, their levels of regulation, and the pleiotropic activities of their products; biological redundancy of the molecular mechanisms underpinning invasion-related activities. Clinical attention is paid to putative new targets, namely host cells, individual molecules and their signaling pathways, as well as the effects of current treatment on invasion and metastasis.

Keywords Tumor-associated host cells · Metastatic site · Circulation · Bone marrow · Promoter and suppressor genes · Therapy guidance

M. Mareel · I. Madani (✉)
Department of Radiotherapy, Ghent University Hospital,
De Pintelaan 185,
9000 Ghent, Belgium
e-mail: indira.madani@ugent.be

M. Mareel
e-mail: marc.mareel@ugent.be

M. J. Oliveira
Divisão de Biomateriais, INEB,
Instituto de Engenharia Biomédica,
Rua do Campo Alegre, 823,
4150-180 Porto, Portugal

M. J. Oliveira
Faculty of Medicine, Porto University,
Al. Prof. Hernâni Monteiro,
4200-319 Porto, Portugal
e-mail: moliveira@ipatimup.pt

Introduction

Tumors are malignant when they grow and invade into neighboring tissues, e.g. brain gliomas, or when they metastasize, e.g. melanoma of the skin. Accordingly, tumor volume, depth of invasion, and presence of metastases in lymph nodes or in distant organs, as characterized by the TNM staging system, are major prognostic factors. Tumors consist of cancer cells and tumor-associated host cells. The cancer cells originate from cancer initiating cells, also called cancer stem cells; they grow without restriction following genomic alterations that serve as founder mutations. Genetic instability causes further mutations making the cancer cell population heterogeneous with respect to many characteristics, including invasion and metastasis. Various concepts are launched to explain progression of the malignant phenotype emphasizing selection or adaptation, late or early acquisition of metastatic capability, transient or permanent changes of the cell populations, evolution of cancer cells inside or outside the primary tumor (Fig. 1). The tumor-associated host cells represent about half of the total number of cells in malignant tumors. They comprise endothelial cells, leukocytes and macrophages, fibroblasts, nerve cells, and adipocytes. Some of these host cells are resident, building together with the cancer cells a "recognizable caricature of the histology of the organ from which the tumor derives" [1]. Others come from the bone marrow moving in through the tumor vasculature.

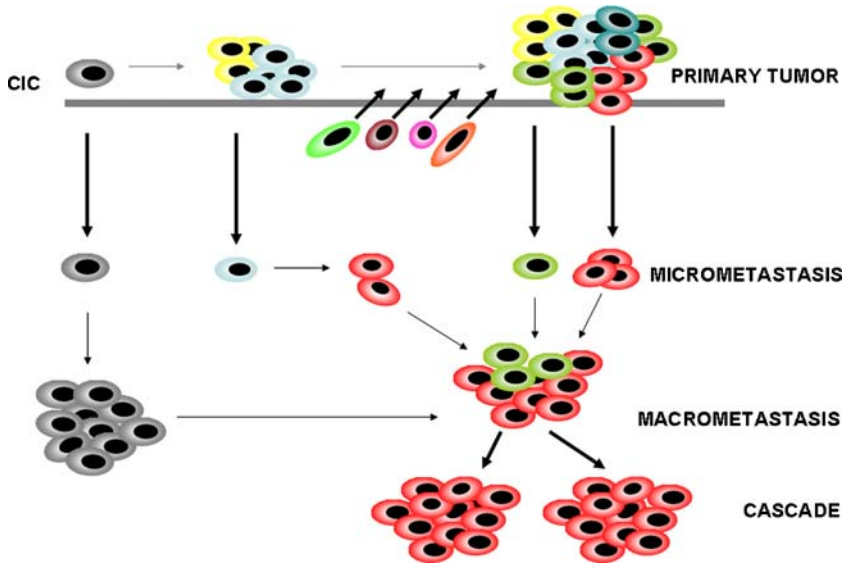

Fig. 1 Models of tumor development. Cancer initiating cells (*CIC*), also called cancer stem cells, can self-renew and initiate tumor formation by generating a heterogeneous population of noninvasive (*yellow* and *light blue*) and further invasive, nonmetastatic (*lime* and *turquoise*) and metastatic (*red*) cells. Darwinian selection of rare genetic variants produces metastases in a later stage of tumor development [8]. Metastasis form cascades of secondary metastasis, displaying increasing homogeneity. Inherently nonmetastatic (*green*) cells may contribute to metastasis [119]. Nonmetastatic (*light blue*) cells may escape at an early stage of tumor development and undergo progression at the site of metastasis [123, 165]. Some authors suggest that CIC may serve as seeds for metastasis [136, 148]. Joining the cancer cell population before the acquisition of invasive capacity are tumor-associated host cells, a. o. myofibroblasts (*bright green*), macrophages (*brown*), leukocytes (*rose*), and endothelial cells (*orange*). *Thin arrows, transition between cell types; thick arrows, displacement; thick gray line, epithelial basement membrane*

All of these host cells influence tumor behavior at both the primary and the metastatic sites.

New methodology has facilitated the direct observation of the activities of invasive and metastatic cells including their interaction with the host, in vivo as well as in vitro. High throughput genomic and proteomic analysis has forced us to consider the enormous molecular complexity and the surprising biological redundancy of the mechanisms underlying these cellular activities. Covering, be it only a minor part of, the molecular aspects of invasion and metastasis is beyond the scope of the present review. We will compare former lists of invasion and metastasis suppressor and promoter genes [2, 3] with the genes found in metastatic signatures resulting from high throughput microarray analysis. At the proteomic level, protein complexes, their levels of regulation, and their signaling pathways will be discussed using examples that already have clinical applications.

The ecosystem concept considers cancer as a system operating inside a living organism; all its elements are continuously interacting and changes in a single element may dramatically alter the whole system. Central to the concept is the idea that the cancer cells and the tumor-associated host cells are continually engaged in interrelationships with every other element of the ecosystem. When analyzing cancer as a disease, we will consider five ecosystems situated inside the human body, namely the primary tumor, the bone marrow, the circulation, the sites of lymph node, and of distant metastases. It is our working hypothesis that, like inside the individual ecosystems, there is a continuous interaction between these ecosystems. To invade, tumors, i.e. cancer cells interacting with host cells, activate programs that implicate a number of cellular activities, namely: homotypic cell–cell adhesion, heterotypic cell–cell and cell–matrix adhesion, hydrolysis, migration, survival, and growth. Although none of these activities per se is cancer specific, it is conceivable that spatio-temporal programs combining different activities may well be so. Carcinoma invasion results in interruption of the basement membrane and intermingling of epithelial cells with tumor-associated host cells from the stroma. At the molecular level, protein complexes involved in these activities interact with one another underpinning the invasion programs. We will consider metastasis as a multistep process of invasion engaging similar programs that bring cancer cells into lymph nodes and distant organs, where they establish secondary tumors similar to the primary ones.

New insights into the molecular cell biology of cancer raise clinically important questions. Are markers of invasion and metastasis applicable to diagnosis and to individualization and image-guidance of therapy? Can anti-invasive and anti-metastatic strategies be applied to the treatment of cancer? Are tumor-associated host cells effective targets for therapy, both local and systemic, next to or as an alternative for the cancer cells? We have recently discussed the question whether

or not radiotherapy might stimulate invasion and metastasis [4]. Here, we shall extend this question to other forms of therapy, namely surgery, hormonal therapy, and chemotherapy.

The present review is not meant to be comprehensive. The examples discussed are chosen for their putative clinical application. We will concentrate on recent references (2003–2008) with preference for reviews that contain extensive lists of original references.

Methodology

Ecosystems of invasion and metastasis

Various in vivo and in vitro assays are used to analyze mechanisms of invasion and metastasis. Such assays allow manipulations and read outs that are not possible in the patient. Clinical observations and data from surgical pathology remain, nevertheless, invaluable sources of information. Some assays aim at a close mimic of the natural situation whereas others are limited to invasion-or metastasis-associated cellular phenotypes. Each of these assays is considered as an ecosystem that is defined by the nature and the position of its elements, each of which may influence the outcome. The relevance of an assay depends upon its capability to distinguish between "noninvasive" and "invasive" or "nonmetastatic" and "metastatic", the final test being the application of the results to the natural situation in human cancer. Seeding of cancer cells onto extracellular matrices is the most widely used in vitro method. The matrigel chemoinvasion assay evaluates the capacity of cells to invade from an upper chamber through a reconstituted basement membrane into a lower chamber that contains a chemoattractant. Similarly, the collagen invasion assay evaluates the capacity of cells to penetrate into a major constituent of the stromal matrix, namely collagen type 1. The system consists of a 3D gel made from a biological preparation of collagen type 1 that may contain other matrix components as well as pleiotropic matrix-associated factors. The need for reconstitution of the natural ecosystem is illustrated by the finding that human cancer cells fail to invade into such matrices unless they are added with tumor-associated host cells or factors produced by these [5]. Confrontations of cancer cells with tissue fragments in organotypical culture are less popular than the matrix assays because of the time-consuming histological analysis [6].

In vivo models comprise spontaneous and chemically induced tumors, transplantation of cells into syngeneic or immunosuppressed animals and constitutional or conditional tumorigenesis in transgenic animals [7]. A paradigm syngeneic model of metastasis is the B16 melanoma that originated spontaneously in an inbred C57/BL6 mouse [8]. For human cancer cells, researchers use immunosuppressed mice: nude mice lacking functional T cells with T-cell-independent B-cell immune response being preserved, or severe combined immunodeficiency (SCID) mice, lacking both T and B cells with macrophages and NK cells present. The site of transplantation is a major determinant of the invasive and metastatic phenotype. Orthotopic transplantation, at a site that is representative of the origin of the cell line or the tumor, results in invasive and eventually metastatic tumors, whereas paratopic, usually subcutaneous, injection of the same cells produces noninvasive tumors. Humanization of the mouse orthotopic site was realized through injection of human fibroblasts into the cleared mammary fat pad of SCID mice before implantation of the mammary epithelial cells [9]. The organization of the inoculum is another determinant of invasion and metastasis, as illustrated by the Surgical Orthotopic Implantation model [10]. Here, implantation of tissue fragments has a much higher rate of invasion and metastasis than injection of cell suspensions.

Genetically engineered mice permit alteration of suppressor and promoter genes characteristic of human tumors, e. g. brain glioma [11]. Tumor progression can be followed in the *Pb-Tag* transgenic adenocarcinoma of the mouse prostate model, where expression of SV40 early genes (Tag) is directed to prostate epithelium by the promoter of rat probasin (*Pb*). Here, progression is predictable in time from mild hyperplasia to severe hyperplasia to adenocarcinoma GI and GIII and finally metastasis frequently in lymph nodes and lungs, sometimes also in the bone [12]. Progression from the noninvasive towards the invasive and metastatic phenotype through downregulation of E-cadherin was demonstrated in the Rip Tag mouse model [13]. A specific metastasis gene was demonstrated by Ambartsumian et al. [14]. GRS/A mice have a high incidence of mammary tumors that are locally invasive but rarely metastasize. When successfully bred to phenotypically normal transgenic mice that overexpress the mts1 gene under a mouse mammary tumor virus long terminal repeat promoter in the lactating mammary gland, the hybrid GRS/Amts1 females do develop also metastases.

Methods of observation

Fluorescent labeling has greatly facilitated the observation of cancer cells inside living tissues in vivo and in 3-D cultures (Fig. 2). With dual-color cells, expressing red fluorescent protein in the cytoplasm and histone H2B-linked green fluorescent protein (GFP) in the nucleus, highly sensitive whole-mouse imaging systems like epifluorescence and multiphoton laser scan permit the visualization in the live animal of the subcellular changes that occur during circulation, arrest in the capillaries, and extravasation [10]. Visualization of pro-invasive hydrolases

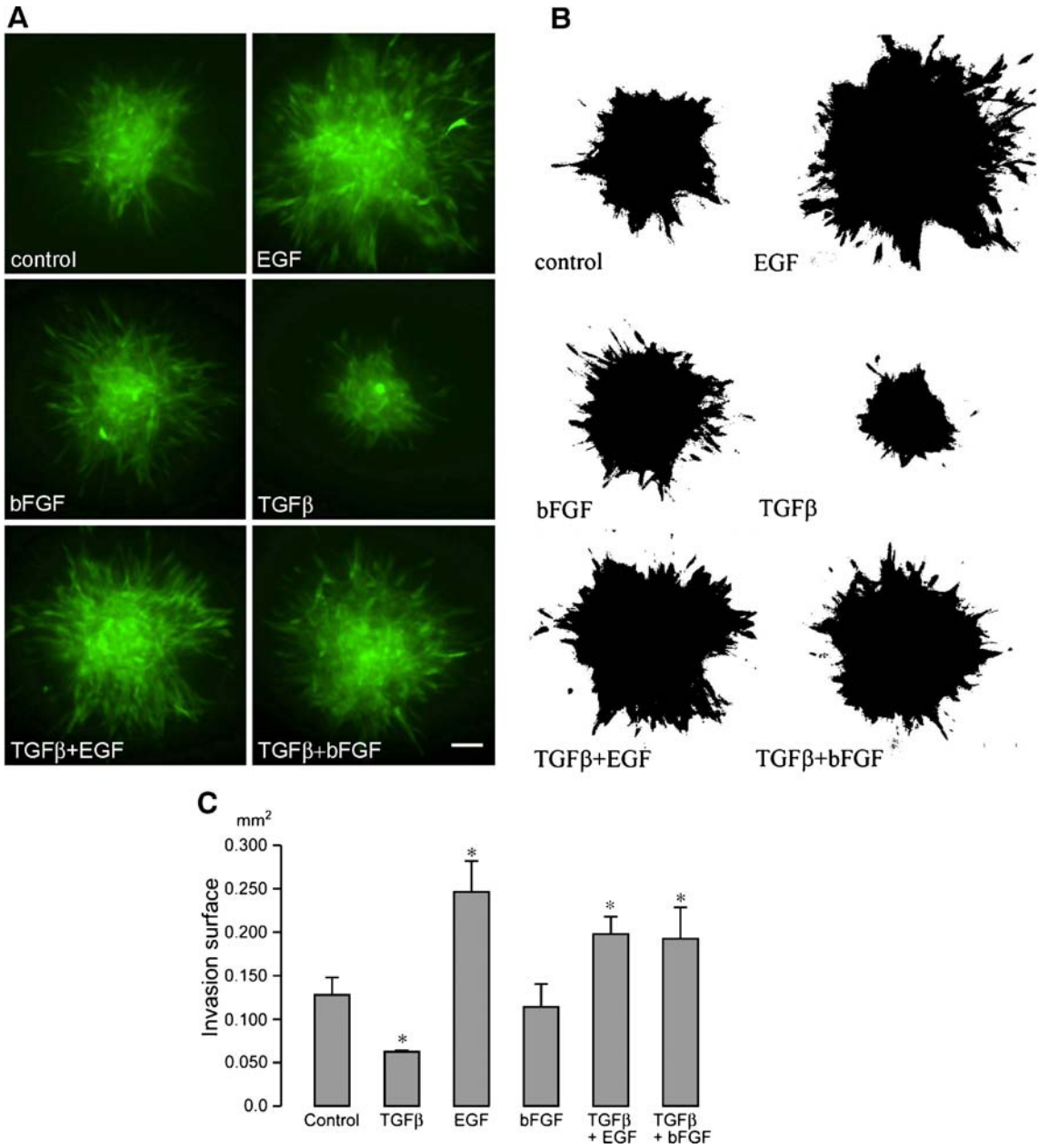

Fig. 2 Imaging of in vitro invasion in 3-D culture. **a** Spheroids of GFP-labeled iHDF (immortalized human dermal fibroblasts) are inside collagen type 1 gels for 24 h without (control) or with EGF, bFGF, TGF-β or combinations of these as indicated. **b** Binary images were generated from fluorescent cultures with Image J for quantitation, which is not achievable by phase contrast microscopy. **c** Invasion is quantified as surface occupied by the cells that invaded centripetally from the spheroid. From Denys et al. with permission [166]

like matrix metalloproteinases is possible with contrast agents linked to matrix metalloproteinase (MMP) inhibitors or to MMP selective and specific substrates combined with optical probes that emit in a spectrum where tissues have low absorption and reduced scattering [15]. Laser capture microdissection collects defined cell populations from heterogeneous ecosystems. It so provides histologically enriched cell populations and brings molecular analysis to the tissue level [16]. High throughput screening techniques such as oligonucleotide microarrays and proteomic analysis have become very popular for the identification of genes and their proteins implicated in metastasis because they are applicable to both experimental and clinical material. The interpretation of the overwhelming amount of data generated in this way is, however, debated because of striking differences between results from different laboratories studying the same type of tumors with little overlap in individual genes and because of the very high numbers of genes differentially expressed between nonmetastatic and metastatic cells [17–19].

Molecular aspects of invasion and metastasis

Genomics

Molecular alterations implicated in invasion and metastasis have been described at the genomic (genetic and epigenetic), transcriptional, translational, and post-translational level. Cancer is a genomic disease, implicating inactivation of tumor suppressor genes and activation of promoter genes. Some of these genes are more specifically involved in invasion and metastasis (Tables 1 and 2). Mechanisms of gene inactivation in human cancer comprise loss of heterozygosity, deletion, mutation, chromatin modification, and promoter methylation, the latter being reversible through reactivation of silenced genes [20]. Mechanisms of gene activation comprise mutation, multiplication, translocation, and promoter acetylation. A glance at Tables 1 and 2 shows that invasion and metastasis genes encode proteins that serve at various steps of cell signaling, namely as autocrine and paracrine ligands, receptors, signal transducers, transcription factors, or their modulators and mediators of cellular response.

These genes were selected on the basis of the following observations (references in [3]): (1) the genomic change is present in invasive (metastatic) lesions or their precursors and not in benign lesions or normal precursor tissues of a given tumor type; more rigorously, in invasive and benign areas that are obtained by microdissection from the same tumor. (2) The genomic change marks the difference between invasive and noninvasive variants of a cell line derived from the same tissue. (3) Transfection of cells with sense or anti-sense cDNA or siRNA causes conversion of the invasive (metastatic) phenotype. (4) Transgenic animals expressing or silencing the gene of interest in a specific tissue develop tumors with different invasive (metastatic) behavior. Given the criteria for the choice of the genes listed in Tables 1 and 2, one would expect a broad overlap with the genes that emerged from the microarray expression profiles of primary tumors as compared to metastases or of tumors with a better versus a worse prognosis.

Why relatively few genes, originally described as promoters and suppressors of invasion and metastasis are found in the poor prognosis or metastasis signatures is hard to explain. Neither do we have an explanation for the lack of overlap in signatures obtained by different workers for the same type of tumors [18]. A signature of 79 differentially expressed genes correctly separated primary tumors and lymph node metastases in breast cancer and predicted clinical outcome in the 20–30% of node-positive patients that remain free of metastasis within the next 15–30 years [21]. Surprisingly, there is only one overlapping gene, namely TGF-β3, with the 70 gene Amsterdam signature [22] and none with the 76 gene Rotterdam signature [23].

Table 1 Promoter genes implicated in invasion and metastasis

Gene[a]			Protein function	Microarray[b]
Acronym	**Locus**	**Name**		
CTNNB1	3p22–p21.3	Catenin, Beta-1	Transcriptional regulator	
EIF4E	4q21–q25	Eukaryotic translation initiation factor 4E	mRNA cap-binding protein	[171]
ERBB2 (HER2)	17q21.1	Avian erythroblastic leukemia viral homolog 2	Receptor tyrosine kinase	[172, 173]
EZH2	7q35–q36	Enhancer of zeste homolog 2	Transcriptional regulator	[25, 174]
FGF3	11q13	Fibroblast growth factor 3	Heparin-binding growth factor	[172]
KRAS	12p12.1	Kirsten rat sarcoma viral oncogene homolog	Small GTPase	
HRAS	11p15.5	Harvey rat sarcoma viral oncogene homolog	Small GTPase	
MET (HGFR)	7q31	Hepatocyte growth factor receptor	Receptor tyrosine kinase	[38]
MTA1	14q32.3	Metastasis-associated protein 1	Transcriptional regulator	[38]
MYC	8q24.12	Myelocytomatosis viral oncogene homolog	Transcription factor	[172, 175]
PIK3CG	7q22.3	Phosphatidylinositol 3-kinase catalytic gamma	Protein and lipid tyrosine kinaseS100	
S100A4 (mts1)	1q21	S100 calcium-binding protein A4	Calcium-binding protein	
SMAD2	18q21	Sma- and Ma-related protein 2 MAD homolog	Transcription factor	[176]
SNAI1	20q13.1	Snail homolog 1	Zn-finger transcription factor	
SRC	20q12–q13	Rous sarcoma virus protein	Non-receptor tyrosine kinase	[38]
TIAM1	21q22.1	T-cell lymphoma invasion and metastasis 1	Rho GEF	

[a] Involvement of genes in invasion and metastasis are in references [2, 3, 161]

[b] Genes found to be implicated in metastasis by cDNA microarray. We found no overlap in the lists published by Eccles et al. [17], Montel et al. [19], van 't Veer et al. [22], Eckhardt et al., and [24] Suzuki et al. [26]

Table 2 Suppressor genes implicated in invasion and metastasis

Gene[a]			Protein function	Microarray[b]
Acronym	**Locus**	**Name**		
AKAP12	6q24–q25	A-kinase Anchor Protein 12	Concentrates and immmobilizes protein	
ARHGDIB (RhoGDI2)	12p12.3	Rho GDP dissociation inhibitor beta	Adaptor protein	
BRMS1	11q13.1–q13.2	Breast cancer metastasis-suppressor 1	Transcriptional regulator	[177]
CASP8	2q33	Caspase-8	Cysteine aspartate-specific protease	
CBX5	12q13.13	Chromobox homolog 5	DNA-binding protein	
CD44	11p13	CD44 antigen	Hyaluronate and osteopontin receptor	[23]
CDH1	16q22.1	Cadherin 1	Adherens junction protein	[38]
CLDN1	3q28–q29	Claudin-1	Tight junction protein	[25]
CRMP1	4p16.1	Collapsin response mediator protein 1	Signal transducing phosphoprotein	
CRSP3	6q22.33–q24.1	Cofactor required for Sp1 transcriptional activation subunit 3	Transcriptional regulator	
DRG1	22q12.2	Developmentally regulated GTP-binding protein 1	High molecular mass GTPase	
GPR68 (OGR1)	14q31	G-protein-coupled receptor 68	G-protein-coupled receptor	[174]
GSN	9q34	Gelsolin	Actin-severing protein	
KAI1	11p11.2	Prostate cancer antimetastasis gene	TCR/CD3 Tetraspanin coreceptor	
KISS1	1q32	KISS1 metastasis suppressor	Multifunctional peptide	
MAP2K4	17p11.2	Mitogen-activated protein kinase kinase 4	Serine/threonine kinase	[178]
NME1 (NM23)	17q21.3	Nonmetastatic cells, protein expressed in	Nucleoside diphosphate kinase	[179]
PEBP1 (RKIP)	12q24.23	Phosphatidylethanolamine-binding protein 1	Raf kinase inhibitor	
PTEN	10q23.3	Phosphatase and tensin homologue deleted on chromosome 10	Protein and lipid phosphatase	[175]
PTPN11	12q24.1	Protein-tyrosine phosphatase, non-receptor-type 11	Tyrosine phosphatase	
RB1	13q14.2	Retinoblastoma 1	Transcriptional regulator	
RRM1	11p15.5	Ribonucleotide reductase, M1 subunit	Cell cycle regulator	
SERPINB5	18q21.3	Serpin peptidase inhibitor 5	Protease inhibitor	
SMAD4	18q21.1	Sma- and Ma-related protein 4	Transcription factor	
TIMP2	17q25	Tissue inhibitor of metalloproteinase 2	Protease inhibitor	
TP53	17p13.1	Tumour protein p53	Transcriptional regulator	
VDUP (TXNIP)	1q21.1	Vitamin D3-upregulated protein	Thioredoxin-binding protein	[21]
VHL	3p26–p25	Von Hippel–Lindau tumor suppressor	Ubiquitinylation	

[a] Involvement of genes in invasion and metastasis are in references [2, 3, 161]

[b] Genes found to be implicated in metastasis by cDNA microarray. We found no overlap in the lists published by Eccles et al. [17], Montel et al. [19], van 't Veer et al. [22], Eckhardt et al. [24], Suzuki et al. [26]

Microarray-based profiling has reopened the discussion about tumor progression (Fig. 1). The conclusion that similarities between primary tumor and distant metastasis plead for an early escape of cancer cells and progression at the site of metastasis whereas differences support late escape and clonal selection at the primary site is considered as an oversimplification that does not match clinical and autopsy findings [1, 17]. The problem words here are "differences" and "similarities". Are numerical values easier to interpret? In a xenogeneic breast cancer model (MDA-MB453), matched pairs of metastasis-competent and metastasis-incompetent human clonal cell lines derived from the same breast cancer cell line, as confirmed by chromosome analysis and by fingerprinting, were inoculated in the mammary fat pad. Primary tumors differed from their lymph node and lung metastasis by 26 and 114 transcripts, respectively [19]. In a spontaneous BALB/cfC3H breast cancer model, metastatic to lymph nodes and bone, 125 know genes differed significantly more than twofold with 36 and 89 genes expressed at higher levels in weakly metastatic and in highly metastatic tumors, respectively [24]. In a comparison between primary ovarian

tumors and their omental metastases 35 differences, out of 20,000 cDNAs on the chip, are interpreted as both lesions being "essentially alike" [25]. Suzuki et al. found "very similar" expression signatures between lymph node metastases and matched primary breast carcinomas [26]. They do, however, emphasize that a small number of genes are differentially expressed between tumors and metastases in a consistent manner, suggesting that these genes are mechanistically important. Several genes identified in the metastasis signatures are stromal in origin, presumably pertaining to the cohort of tumor-associated host cells. Examples for breast cancer are the wound response signature [27] and the 26-gene stroma-derived predictor of prognosis [28].

Single nucleotide polymorphisms (SNPs) are variations in DNA sequence across the gene that are common in the population. SNPs within promoters affect the expression of invasion promoter and suppressor genes, such as MMPs/tissue inhibitors of metalloproteinases (TIMPs) [29], E-cadherin [30], and integrin β4 [31]. Analysis of germ line SNPs addresses the question whether or not some people are genetically predisposed to metastasis [32]. Signal-induced proliferation-associated gene 1 (SIPA1) is such a metastasis efficiency gene, in which SNPs are associated with metastasis [33].

Taken together the microarray analyses have greatly increased the number of candidate promoter and suppressor genes implicated in invasion and metastasis, but had not yet deepened our understanding of its mechanisms.

Proteomics

The number of proteins involved in invasion and metastasis is much larger than the number of promoter and suppressor genes, many of which encode transcriptional and translational regulators. The transcription of CDH1 encoding the invasion-suppressor E-cadherin is regulated by Snail, Slug, ZEBs (ZEB1=δEF1; ZEB2=SIP1), and bHLH, receiving signals from more than 20 autocrine and paracrine ligands that reach them via multiple signal transduction pathways [34]. These transcription factors are themselves regulated post-transcriptionally through phosphorylation and sumoylation; their transcriptional repression is mediated through interaction with corepressors like HDAC. Adding to the complexity is the fact that CDH1 transcription factors also modulate other genes.

Micro(mi)RNAs are small noncoding RNAs that regulate target gene expression post-transcriptionally. They may silence target genes either by degrading mRNA molecules or by inhibiting their translation [35]. miRNAs influence invasion and metastasis, as they modulate the translation of suppressor genes, such as PTEN, CD44, SERPINB5, or of promoter genes, such as RAS, respectively [36]. The mRNA cap-binding protein eLF-4E, engaged with elF-4F in the translation initiation complex, contributes to metastatic progression by selectively upregulating the translation of key malignancy-related proteins [37]. Translational modulation may explain also why, in the study of breast cancer primary tumors and lymph node metastases, expression at other transcriptional level, as shown by cDNA microarrays, does not always match the expression at the protein level, as evident from tissue microarray and from immunohistochemistry performed on selected markers [38].

N- or *O*-glycosylation of membrane surface receptors may modulate their function, altering tumor cell adhesion or motility, and promoting or inhibiting invasion and metastasis [39]. E-cadherin glycosylation by GlcNAc-TIII prolongs its turnover rate and increases its stability at the plasma membrane, so enhancing cell–cell adhesion and inhibiting invasion and metastasis [40].

Phosphorylation/dephosphorylation on tyrosine (Y) and serine/threonine (S/T) residues is a major regulator of the activity of invasion- and metastasis-related proteins. Receptor tyrosine kinases, such as epidermal growth factor receptor (EGFR), vascular EGFR (VEGFR), mesenchymal-epithelial transition factor (c-MET), and many others, are transmembrane glycoproteins autophosphorylating Y residues upon binding of ATP and activation of their kinase domain. Such Y-phosphorylation initiates the signal transduction that leads to the cellular activities implicated in invasion and metastasis. Constitutive activation of such receptors also occurs upon mutation of Y residues that are responsible for silencing of the kinase domain. Upon Y-phosphorylation, modulated by receptor and non-receptor Y-kinases and Y-phosphatases [41], β-catenin may leave the invasion-suppressor E-cadherin complex and serve pro-invasive signaling through the Wnt signaling pathway. By contrast, S/T-phosphorylation by GSK-3β in the APC complex directs β-catenin towards the ubiquitin-proteasome degradation pathway, suppressing pro-invasive signaling.

Proteolysis not only serves degradation but also activates latent forms of ligands. For TGF-β, integrins offer common docking points for latent TGF-β and activating proteinases bringing both into close vicinity. Alternatively, the interaction between integrins and LLC results in conformational changes that liberates active TGF-β [42]. Proteolysis has a major role in the production of soluble forms of receptors, such as sE- and N-cadherin, sVEGFR, etc.

Most proteins implicated in invasion- and metastasis-related cellular activities belong to larger families, members of which serve different activities and which may switch from one isotype to another during tumor progression. In the cadherin family of transmembrane glycoproteins, E (epithelial)-cadherin is an invasion suppressor, N(eural)-cadherin is an invasion promoter, whereas P(placental)-cadherin is a promoter in some types of tumors and a

suppressor in other types. P-cadherin enhances invasion and migration in experimental breast cancer models and correlates with high-grade, poor-prognosis human breast tumors [43]. In melanoma, P-cadherin functions as a pro-adhesive molecule, linking melanocytes to keratinocytes, and inhibiting invasion and metastasis [44]. Switching increases aggressiveness as exemplified by the change from E- to N-cadherin expression in melanoma, prostate, breast, and pancreatic cancer in line with its stimulation of motility in vitro and metastasis in vivo [45]. N-cadherin favors the interaction between cancer cells and tumor-associated host cells, such as endothelial cells and myofibroblasts [46]. Transcriptional repression of E-cadherin and upregulation of N-cadherin by the same transcription factor Twist is reported in prostate cancer cells [47]. Alternatively, transcriptional repression of E-cadherin may free p120 catenin to bind and stabilize N-cadherin.

In the epidermal growth factor family, heterotypic dimerization between members serves activation of the orphan receptor EGFR2 (Neu; HER2) [48]. In the pro-angiogenic vascular endothelial growth factor family [49], the four members bind preferentially to one of four receptors and stimulate either blood or lymph angiogenesis. The family of MMPs contains 23 metzincin proteinases capable of degrading extracellular matrix proteins and of processing many bioactive molecules [50, 51]. They differ in substrate specificity, in source, being produced by tumor-associated host cells or by cancer cells, in cellular localization, being secreted or membrane-linked, in ecosystem, occupying the primary tumor as well as distant metastasis.

Proteins form complexes, bearing an ever growing number of molecules, from which depart numerous signaling pathways evoking several cellular responses [52]. Such dynamic complexes, called proteomes, are based on domains that interact with modified peptides (e.g. SH2 with p-Tyr), with peptides (e.g. PDZ with Val-COOH), with the same domain (e.g. PDZ with PDZ), or with phospholipids (e.g. FYVE with PI-3-P) [53].

Ecosystems of invasion and metastasis

Tumors: cancer cells and host cells

Malignant tumors are not just collections of genetically altered cancer cells but consist also of tumor-associated host cells [17, 54] (Fig. 3). Interaction between these various cell types produces ecosystems at the level of the primary tumor, lymph node metastases, and distant metastases. Communication between the latter implicates two other, tumor-related, ecosystems, namely the bone marrow and the lymph and blood circulation, the latter serving as a transport system for cells and signals. All the above-mentioned ecosystems pertain to another ecosystem, namely the host organism.

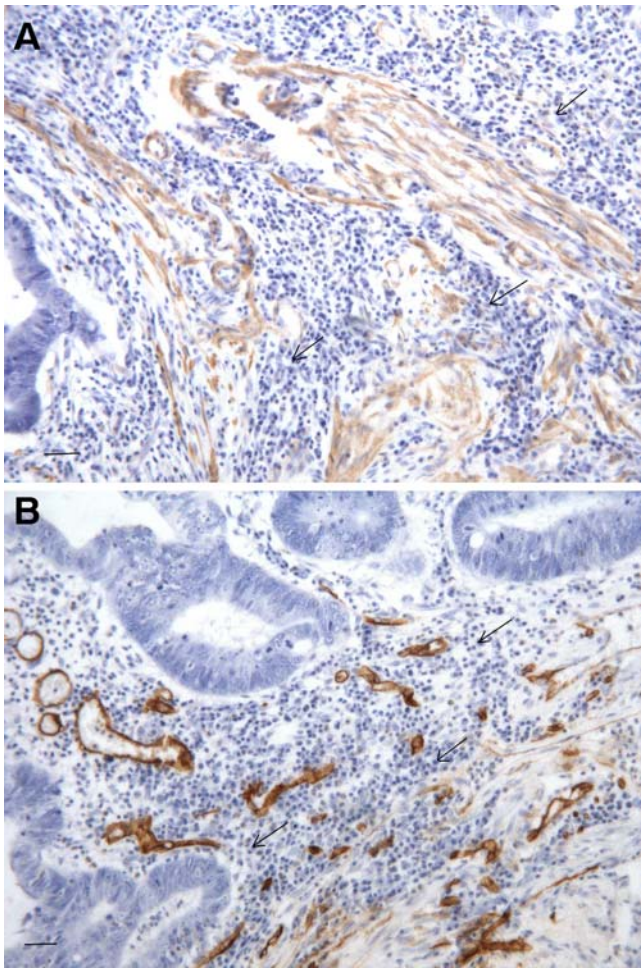

Fig. 3 Tumor-associated host cells in colorectal cancer. Parafine sections from a colorectal cancer, removed after neoadjuvant chemo-radiotherapy; immunolabeling with an antibody against a-SMA (smooth muscle actin) recognizing myofibroblasts (**a**) and against CD34 recognizing endothelial cells (**b**); counterstaining with hematoxylin. Note numerous inflammatory cells (*arrows*). Scale bar= 10 μm. Unpublished results in collaboration with P. Demetter, Department of Pathology, Erasmus Hospital, ULB, Brussels. ELSEVIER license number to reprint Figure 2 [166] is 2190781177416

That host elements influence invasion and metastasis is suggested by a number of observations both in vivo and in vitro. Metastasis is organ-specific as first described by Paget who launched the "seed and soil" concept [55]. Recruitment of host cells by disseminated cancer cells is necessary to create the organotypic histological organization that is reminiscent of the primary tumor [1]. In transplanted tumors, the site of implantation determines malignancy; orthotopic implantation, at the site of origin of the transplant, gives rise to invasive and metastatic tumors whereas ectopic implants, usually in the subcutis, produce noninvasive and nonmetastatic tumors. The lack of inva-

siveness of cancer cells in vitro fails to predict their invasive behavior upon transplantation into immunosuppressed mice [56, 57]. Epithelial cancer cells isolated from a rat colon tumor failed to invade into tissue fragments or into extracellular matrices in vitro, whereas fresh tumor isolates, containing the cancer cells and host cells, were invasive in the same in vitro systems [58].

Given that a founder genetic alteration of the epithelial cancer initiating cell serves as the momentum of tumor formation, the question arises at what time host cells become associated with the tumor. Circumstantial evidence suggests that the association starts before the tumor becomes invasive (Fig. 4). However, when during premalignant development the tumors start to send specific signals to the host is completely unknown. Such signals may initiate a chain reaction, such as described for noninvasive tumors activating macrophages and so causing the angiogenic switch that leads to malignant transformation [59]. As a working hypothesis we accept that, in all the above-mentioned ecosystems of noninvasive and invasive primary tumors or metastases, phenotypic changes may be initiated by tumor-associated host cells as well as by cancer cells.

Tumor-associated host cells

Tumor-associated host cells do communicate not only with cancer cells but also with each other (Fig. 5a, b). They are abundant in the more invasive tumors with a worse prognosis and poor treatment possibilities, such as pancreatic cancer, which is characterized by extensive host cell reaction comprising fibroblasts, pancreatic stellate cells, leukocytes and macrophages, aberrant endothelial cells, nerve fibers, and other bone marrow-derived progenitor cells [60].

Endothelial cells

Endothelial cells are recruited by the tumor from progenitor cells or from resident vessels to form a new network of blood and lymph vessels. Direct intravital observations showed that blood angiogenesis precedes lymphangiogenesis [61]. The vessels sustain the tumor's metabolism with nutrients and oxygen; they open the way for the extravasation, into the tumor, of circulating host cells and for the intravasation, into the circulation, of metastatic cancer cells. The pro-invasive and pro-metastatic role of angiogenesis is supported by ample clinical and experimental evidence. Angiogenesis is a sign of worse prognosis, as exemplified dramatically by cutaneous melanoma [62]. In nonmetastatic breast cancer vascularization measured by Chalkley morphometry is a predictor of micrometastasis in the bone marrow [63]. Accordingly, overexpression of pro-angiogenic molecules like VEGF marks a poor prognosis in melanoma, in gastric, colorectal, pancreatic, breast, prostate, and lung cancer [64]. Like blood angiogenesis, lymph angiogenesis is a marker of worse prognosis in breast cancer and melanoma [65, 66]. In inflammatory breast cancer, which is associated with regional lymph node metastasis in most cases, there are a higher number of lymph vessels than in the noninflammatory counterparts, suggesting a contribution of lymph angiogenesis to nodal spread. In most experimental models, peritumoral lymphangiogensis is a prerequisite for metastasis to regional lymph nodes [67].

Angiogenesis is modulated in a paracrine manner by the balance between suppressors such as angiostatin, and promoters mostly belonging to the VEGF family, comprising (receptors): VEGF-A (VEGFR-1 and VEGFR-2), VEGF-B (VEGFR-1), VEGF-C (VEGFR-2 and 3), VEGF-D (VEGFR-2 and 3), placental growth factor (PlGF), and

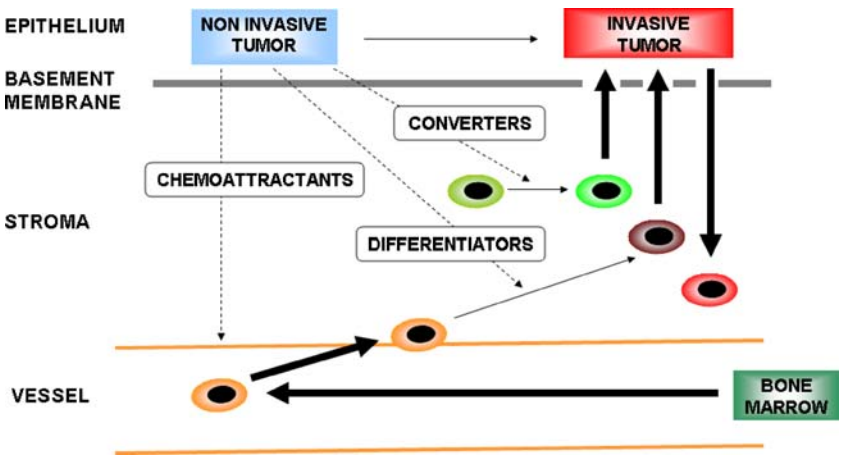

Fig. 4 Tumor-associated host cells and the pro-invasive switch during cancer progression. Chemoattractants divert bone marrow-derived cells (*orange*) towards the tumor, where they undergo differentiation. Resident host cells (*green*) are converted to another cell type. Invasive cancer cell (*red*). *Thin arrows* cellular or tumoral transition. *Thick arrow* displacement or invasion

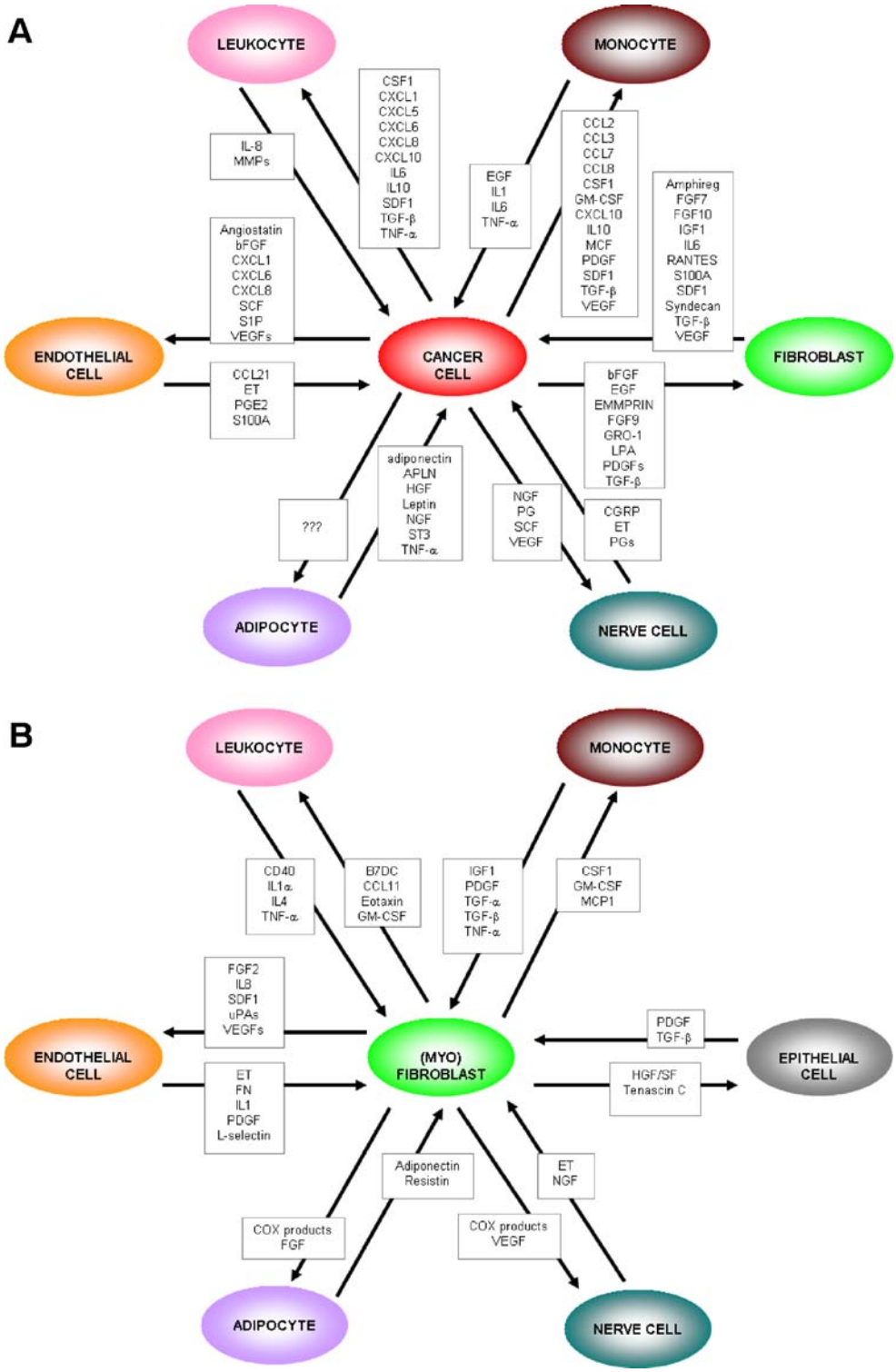

(VEGFR-1) [49, 62]. A generally accepted scenario is that VEGFs, produced upon genetic or epigenetic induction mainly by cancer cells, though also by tumor-associated host cells, binds to VEGFRs on endothelial cells and so elicits responses like proliferation, migration, and ectopic survival, all of which are implicated in mobilization of endothelial precursors and angiogenesis. Genetic induction comprises inactivation of tumor suppressors p53 and VHL and activation of tumor promoters Ras, EGFR, and ErbB-2. Epigenetic inducers of VEGF-A comprise: hypoxia (through

◀ **Fig. 5** Molecular conversation between cancer cells and tumor-associated host cells (**a**) and between myofibroblasts and other tumor-associated host cells (**b**). Lists of molecules participating at communication between cells are not exhaustive. *APLN* apelin, *B7DC* programmed death ligand 2, *bFGF* basic fibroblast growth factor, *CCL* chemokines with the first two cysteins not separated by another amino acid, *CD40* tumor necrosis factor receptor 5, *CGRP* calgranulin-related protein, *COX* cyclo-oxygenase, *CSF1* colony-stimulating factor 1, *CXCL* chemokines with the first two cysteins separated by another amino acid, *EGF* epidermal growth factor, *EMMPRIN* extracellular matrix metalloproteinase inducer, *ET* endothelin, *FGF* fibroblast growth factor, *GM-CSF* granulocyte-macrophage colony-stimulating factor, *GRO-1* (= CXCL1) GRO protein alpha, *HGF* (= *SF*) hepatocyte growth factor (= scatter factor), *IGF1* insulin-like growth factor 1, *Il* interleukin, *LPA* lysophosphatidic acid, *MCF* MCF cell line-derived transforming sequence, *MCP1* (= CCL2) monocyte chemotactic protein 1, *NGF* nerve growth factor, *PDGF* platelet-derived growth factor, *PGE2* prostaglandin E2, *RANTES* (= CCL5) regulated upon activation, normally T-expressed and presumably secreted, *S100A* S100 calcium-binding protein, *S1P* sphyngosine 1 phosphate, *SCF* MGF stem cell factor, *SDF1* (= CXCL12) stromal cell-derived factor 1, *ST3* (= MMP11) stromelysin 3; *TGF-β* transforming growth factor β, *TNF* tumor necrosis factor, *uPA* urokinase type plasminogen activator, *VEGFs* vascular endothelial growth factors. Adapted from [49, 54, 62, 68, 71, 77, 85, 90, 167, 168], where detailed literature can be found. Lists are not meant to be exhaustive; they illustrate the multiplicity of signals between cells of the ecosystems

HIF-1α and 2α), cytokines e.g. IL-6, sex hormones, growth factors, e.g. bFGF, and chemokines, e.g. SDF-1 (= CXCL12). Lymphangiogenesis is driven by the following ligand/receptor complexes: VEGF-C and D/VEGFR-3; angiopoietin-1 and 2/Tie2; HGF/c-MET; PDGF-BB/PDGFRα/β; IGF-1 and 2 /IGF-1R [68]. Particular for melanoma is the cell surface mimicry between cancer cells and endothelial cells both expressing the same receptors binding their cognate ligands, namely: VEGF to VEGFR-2; PlGF to NP-1/2 and to VEGFR-1; uPA to uPAR; IL-8 to CXCR-1; FGF to FGFR-1. Issuing signaling activates similar cellular activities implicated in growth, invasion, and metastasis of the cancer cells and in recruitment of bone marrow precursors and angiogenesis of the endothelial cells [62]. There are several circulating bone marrow-derived cell populations that stimulate or amplify tumor angiogenesis and that home in the perivascular zone, namely: F4/80+, CD11b+ macrophages; VEGFR+, CXCR4+, CD11b+ myeloid cells; CD11b+, Tie-2-expressing monocytes; VEGFR-1+, CXCR4+ hemangiocytes; CD11b+, VE-cad+ vascular leukocytes; Gr1+, CD11B+ neutrophils; and myeloid-derived suppressor cells [49]. Implicated also are platelets, directing site-specific recruitment of bone marrow-derived progenitor cells to sites of vasculogenesis [69].

Leukocytes and macrophages

A large variety of hematopoietic cells and their progeny is associated with tumors [70–72]. Some of these cells, e. g. macrophages, definitely modulate invasion and metastasis, while the role of others, e. g. dendritic cells and T lymphocytes, is less clear. The Dr. Jekyll and Mr. Hyde conundrum applies to the diversity of inflammatory cell phenotypes that infiltrate primary tumors and metastasis [72]. Contributing to a worse prognosis, by facilitating invasive growth and metastasis are: macrophages, myeloid-derived suppressor cells, and CD4+ T lymphocytes. A better prognosis is associated with: dendritic cells inducing Ag-specific T lymphocyte responses; CD8+ T lymphocytes. Opposite effects on invasion and metastasis are exemplified by cytokine-mediated monocyte differentiation into suppressor M1 macrophages, expressing the pro-inflammatory cytokines TNF-α, IL-1β, and COX-2, or promoter M2 macrophages, expressing the anti-inflammatory cytokines IL-10, arginase-1, PPARγ. In the same monocyte lineage, mature dendritic cells (CD208-positive) and immature dendritic cells (CD1α-positive) act as suppressors and promoters, respectively. In most human cancers, tumor-associated macrophages (TAM) are considered as promoters of invasion and metastasis and markers of a worse prognosis [73]. Some authors consider TAMs as obligate partners for invasion and metastasis as they promote cancer cell invasion, inflammation, extracellular matrix (ECM) modeling, and angiogenesis [74]. TAMs produce pro-invasive enzymes, like MMPs. Multiphoton microscopy and transgenic fluorescent labeling permitted direct visualization of macrophage-assisted intravasation in mouse mammary tumors [75]. The origin of TAMs is in the bone marrow, where CD34-positive progenitors expand, are committed and mobilized into circulation; they differentiate into monocytes, invade into the noninvasive tumor and undergo maturation into macrophages. Dendritic cells are among the first to invade the tumor [70].

Scenarios for the mechanisms by which leukocytes and macrophages modulate invasion and metastasis, shall take into consideration that these tumor-associated host cells do communicate not only with the cancer cells but also with other types of host cells [73]. Chemoattraction of leukocytes and macrophages elicits an inflammatory reaction favoring growth and invasion of cancer cells [59]. TAMs neighboring the noninvasive primary tumor secrete proteinases (MMPs, uPA, cathepsins) that breakdown the basement membrane and open the way for cancer cell invasion. MMPs also remodel the ECM favoring stromal invasion. TAMs, in collaboration with cancer cells, produce factors (VEGF, bFGF, PDGF, MMPs, IL-8, Ang1) that promote angiogenesis as described above. Intravasation is assisted by a paracrine loop between EGF expressed by TAMs associated with tumor vessels and binding to EGFR on cancer cells and through cancer cell CSF-1 binding to CSF-1R on TAMs. Both receptors signal via WASP to form invadopodia on the cancer cells and podosomes on the

TAMs [74]. Extravasation of cancer cells is assisted by macrophages through production of cytokines (IL-1, IL-18, TNF) that stimulate the expression of heterotypic cell–cell adhesion molecules on endothelial cells (VCAM-1, E-selectin, and ICAM-1) arresting cancer cells at the site of distant metastasis. In the circulation, macrophages may kill cancer cells. By contrast, in primary tumors and metastases TAMs secrete PGE2, IL-10, and TGF-β causing immunosuppression.

(Myo)fibroblasts

Fibroblasts found in the tumor stroma are called peritumoral fibroblasts, cancer-associated fibroblasts and myofibroblasts; they constitute a heterogeneous cell population, awaiting the kind of subtyping that was performed for the above-mentioned leukocytes and macrophages. The formation of such stroma may be driven by mutated epithelial cancer cells, by mutated fibroblast or by the extracellular matrices produced by both [76]. We have reviewed previously the impact of myofibroblasts on invasion [5, 77]. Comparison of both reviews reveals a dramatic increase in the elements of this host cell compartment as evident from the number of precursor cells, of ligands released from the noninvasive tumor and received by the stromal fibroblasts, and of pro-invasive signals sent to the cancer cells by the myofibroblasts (Fig. 4). Crucial in the interaction between cancer cells and (myo)fibroblasts remains TGF-β influencing both the cancer cells and the myofibroblasts [78].

Myoepithelial cells

In breast cancer the pro-invasive activities of myofibroblasts are counteracted by myoepithelial cells, both modulating the basement membrane [79]. The diagnostic criterion that distinguishes invasive from in situ carcinoma is the disappearance of the organized myoepithelium and of the basement membrane [80], though myoepithelial cells associated with ductal carcinoma in situ are already abnormal [81, 82]. The interaction between luminal epithelial cells and myoepithelial cells occurs through TGF-β, hedgehog, and p63, loss of which causes disappearance of the myoepithelium and progression to invasion. Myoepithelial cells suppress invasion through their effects on growth, invasion, angiogenesis via secretion of TIMPs, and downregulation of MMPs [83, 84].

Nerve cells

Perineural invasion is an indication of poor prognosis in cancer of the prostate, the bile duct, the pancreas, and the head and neck mucosa, where it is held responsible for local spread. Nerve cells receive from the tumor afferent signals that do not only evoke pain but also stimulate the formation of new nerves (neurogenesis); they produce efferent signals, such as CGPR, endothelin, histamine, prostaglandins, and substance P, stimulating inflammation, angiogenesis, and invasion [85]. In prostate cancer neurogenesis starts, probably from stem cells, at the stage of high-grade prostatic intraepithelial neoplasia, i.e. before the acquisition of invasion [86]. Recent coculture experiments and observations on human cancer put forward possible mechanisms of neurogenesis and perineural invasion: chemoattraction of neurons towards cancer cells by SF4 [86]; chemoattraction by NGF and by CX3CL of pancreatic cancer cells expressing p75(NGFR) and CXCR4, respectively [87, 88] and by CXCL12 of prostate cancer cells expressing CXCR4 [89].

Adipocytes

Given the link between obesity and cancer, it is not surprising that adipocytes, highly abundant in the stroma where tumors originate are found on the list of tumor-associated host cells that influence invasion. In breast tumors, the crosstalk between cancer cells and adipocytes or their precursor preadipocytes marks the early steps of stromal invasion. Cancer cells induce adipocytes to express ST3 (MMP11), a MMP that does not require extracellular activation as it is cleaved in the Golgi system before secretion. It contributes to cancer cell survival during early invasion into the adipose tissue, where it is, indeed, highly expressed in human cancers. It is speculated that some of these adipocytes convert into myofibroblasts during further development of desmoplasia, explaining why the fibroblast/adipocyte ratio is higher in tumor than in normal stroma [90]. In the bone marrow, adipocytes support the progression of multiple myeloma, in concert with the fibroblasts, as they inhibit apoptosis and stimulate proliferation, cell adhesion, and migration [91].

Adipocytes produce a number of cytokines (Fig. 5a), termed adipokines [92]. They display a broad spectrum of activities, including stimulation of invasion and angiogenesis. The pro-angiogenic effect of apelin, a bioactive peptide and a ligand of the G-protein-coupled receptor APJ was demonstrated with human vascular endothelial cells in culture. The activities of adipocyte-derived apelin are upregulated by hypoxia and neutralized by APJ siRNA [93]. In breast cancer cells, leptin stimulated growth, angiogenesis, invasion, and migration [94]. In human colon cancer cell lines, expressing the Ob receptor, leptin induced invasion and the formation of lamillepodial structures through activation of Cdc42, Rac1, and Src kinase [95]. In human renal cancer cell lines, leptin stimulated Matrigel invasion via Rho and MEK pathways [96]. Adiponectin

counteracts the pro-invasive and pro-angiogenesis activities of adipokines like leptin, as it is antimitogenic, enhances apoptosis, and inhibits angiogenesis. Adipocyte-produced leptin stimulates macrophages to secrete pro-inflammatory cytokines, like IL1α and TNF-α and this is counteracted by adiponectin [92].

Osteoblasts/osteoclasts

Osteoclasts/osteoblasts are the first and the most extensively studied tumor-associated host cells. They participate at the bone metastasis ecosystem. For recent reviews, the reader is referred to references [91, 97, 98].

Microorganisms

Bacteria are elements of the tumor ecosystem in the colon and the stomach; they play a role in invasion, at least in experimental systems [99–101]. *Listeria monocytogenes* stimulates colon cancer cell invasion and motility through the release of soluble pro-invasive peptides that activate ErbB2/ErbB3 receptors or modulate the activity of PI3K and of small GTPases. *Helicobacter pylori*, a bacterium that colonizes the stomach of half of the world population, stimulates invasion of gastric cancer cells through activation of c-Met receptor and of its downstream signaling targets, the metalloproteases MMP-2 and MMP-9. Inducing cells to express the invasion-suppressor molecule E-cadherin promotes the formation of a complex that abrogates *Helicobacter*-mediated cancer cell invasion.

Primary tumors and metastases

Primary tumor

The primary tumor is the ecosystem in which the metastatic disease does originate. Once it reaches the invasive phenotype, a primary tumor contains a heterogeneous population of cancer cells and most of the above-mentioned tumor-associated host cells, except osteoclasts that are typical for bone metastases. Survival of the cancer cell population depends on the stem cell compartment, that might be situated within the constraints of the primary tumor or belong to a separate ecosystem.

Lymph node metastasis

Lymph nodes are ecosystems vital for metastatic epithelial tumors. Sentinel lymph nodes have a direct lymphatic connection to the site of the primary tumor. They contain the cells that express the ligands and the receptors to communicate with cancer cells, namely macrophages and B and T lymphocytes. Lymph nodes are primarily implicated in immune responses in a highly dynamic way as illustrated by two-photon imaging of lymphocyte motility and dendritic cell-mediated antigen response [102]. Sentinel lymph nodes host the first contact of the immune system with the tumor through soluble antigens presented by dendritic cells and this sometimes precedes the arrest of cancer cells in the peripheral sinus of these lymph nodes. Lymph node metastasis is very common in most human cancers, where it is considered as a crucial prognostic factor [66]. Exceptions are carcinoids of the gastro-intestinal tract and papillary thyroid cancer, which, for unknown reasons, are relatively benign despite the presence of lymph node metastasis [103]. Sentinel lymph nodes are used for staging of e.g. breast cancer and melanoma, because they are important transit sites for spread to regional lymph nodes and to distant organs. The procedure includes the search for single or small clusters of cancer cells by immunohistochemistry with antibodies that do not recognize host cells [104]. Transgenic animals manipulated genetically to produce lymph node metastasis are reviewed by Nathanson [67]. Experimental and clinical analysis emphasizes the role of the chemokines and their receptors that were first described for the homing of leukocytes [105]. These molecular interactions, e. g. between CXCR4 and CCR7 on breast and colon cancer cells and their ligands CXCL12 (= SDF-1) and CCL21 (= 6Ckine) in the nodes explain why cancer cells home to lymph nodes but less so why they survive and grow there. Lymphangiogenesis in the sentinel lymph nodes, such as observed in VEGF transgenic mice, promotes further spread [106], in line with observations in breast cancer patients [107].

Distant metastasis

Metastasis in distant organs has been covered by many reviews [8, 17, 108]. Major attention is paid to the site of such metastasis with, as for lymph nodes, much emphasis on chemokine receptors and their ligands. André et al. analyzed by immunohistochemistry the relationship between chemokine expression in the primary tumor and the site of distant metastasis in 142 node-positive breast cancer patients that did not receive chemotherapy [109]. They found site specificity of CXCR4 for liver, CX3CR1 for brain, CCR6 for pleura, and CCR7 for skin. The types of tumor-associated host cells that occupy the primary tumor are also found in distant metastasis. Some interactions are, however, specific for the site of metastasis. Liver metastases from breast and colorectal cancer in some patients, but not in others, display a non-angiogenic growth pattern with cancer cells replacing hepatocytes and co-opting sinusoidal blood vessel. In such metastases, there are no signs of hypoxia or vessel leakage [110]. In brain metastasis, astrocytes may dominate the host cell compartment [111]. In bone metastasis, starting from

cancer cells arrested in the bone marrow, osteoclasts/osteoblasts, and their precursors are major players.

Of particular interest are the observations in favor of the preparation of a niche at the putative site of metastasis by cells recruited from the bone marrow upon signals (VEGF-A, TNF-α, TGF-α) received from the primary tumor [112–114].

The bone marrow

The bone marrow (BM) is of interest for metastasis because it reacts to growth of a tumor by enhanced myelopoiesis and mobilization of the above-mentioned inflammatory tumor-associated host cells. More specifically, the bone marrow releases the hematopoietic progenitor cells that prepare the niche for metastasis [112–114]. Furthermore, the BM is a representative site of micrometastases, called BM-DTC for BM distant tumor cells. Questions of interest are: how and when does micrometastasis occur? Are micrometastatic cells metastatic progenitors? How is micrometastatic dormancy regulated? Are micrometastases composed of cancer stem cells? There is convincing evidence to accept that the presence of BM-DTC has a negative prognostic value, provided the correct detection molecular and morphological techniques are combined [115–117].

The circulation

The lymph and blood circulation serves as the principal way by which the above-mentioned ecosystems do communicate (Fig. 6). The peritoneal and pleural cavity is part of this circulation in pelvic tumors, gynecological and colon cancer, and in thoracic tumors, respectively [118]. The circulation constitutes by itself a separate ecosystem containing important elements of the metastatic disease, namely: metastatic and nonmetastatic cancer cells [119]; bone marrow-derived precursors of tumor-associated host cells [49, 120]; premetastatic niche cells [112]; ligands and soluble receptors modulating invasion and metastasis (VEGF, bFGF, angiostatin, endostatin, sVEGFR-1, and sHER-2). Clinicians have only started to explore this ecosystem, which poses methodological problems because of the high dilution of the elements of interest by the blood. There are indications to accept that the detection of circulating tumor cells has a prognostic value and may serve as an indicator of metastatic propensity in individual tumors [117, 118].

The invasion program

The multistep process of metastasis

Displacement of tumor cells, mainly of cancer cells but also of tumor-associated host cells, is the essence of metastatic disease. Such spread over the tumor-bearing organism has been subdivided following the behavior of the cancer cells into primary invasion, intravasation, transport within circulation, arrest at the site of metastasis, extravasation, and homing, together called the multistep process of metastasis (Fig. 7). Metastases repeat the multistep process to form secondary metastases, a phenomenon called the metastatic cascade. Metastases manifest themselves clinically when they grow to a volume that disturbs the function of the harboring organ. Invasion from the primary tumor into the surrounding stroma, characterized by perforation of the epithelial basement membrane marks the onset of malignancy. Considering the assistance of tumor-associated host cells discussed above, one might raise the question who invades whom. Invasion is not necessarily followed by metastasis, as exemplified by primary tumors of the brain. Invasion is, however, considered as a prerequisite for metastasis, though early release of cancer cells from the primary tumor may be missed on routine pathological examination (Fig. 1). Intravasation brings cancer cells into the lymph or the blood circulation. Note that at the site of cancer cell intravasation bone marrow-derived tumor-associated host cells do extravasate. Both processes are considered to be active, implicating chemotactic migration [121]. At least for lymphatics, passive intravasation should not be excluded [67]. Lack of a functional intratumoral lymphatic network, neoangiogenesis, and increased permeability of new blood vessels create interstitial hypertension and an increased centrifugal lymphatic flow. The latter carries peripheral cancer cells towards the vast network of open peritumoral lymph vessels that lack endothelial junctions and are anchored to the extracellular matrix to avoid collapse. Transport in the circulation is considered to be passive. Arrest in the capillaries implicates binding of cancer cells onto the apical surface of the endothelium, and the vascular extracellular matrix, a phenomenon that is facilitated by platelets through formation of thrombi and activation of the endothelium [122]. After extravasation, cancer cells find a niche where they can survive (homing) and eventually grow. A surprising finding is that apparently normal mouse mammary cells, injected intravenously, survived in the lungs and started to proliferate once the oncogenes (transgenes) they carried were activated [123]. The question is whether or not such cells can reach the circulation spontaneously. What the experiment demonstrates is that the tumorigenic capacity conferred on mouse mammary cells by coexpression of the oncogenes Myc and Ras can be realized in the ecosystem of the lung and that this activation may even start 17 weeks after the i.v. injection. A similar phenomenon occurs also with cancer cells and is called dormancy [124, 125]. It explains recurrences several years, even decades, after removal of the primary tumor with complete local control,

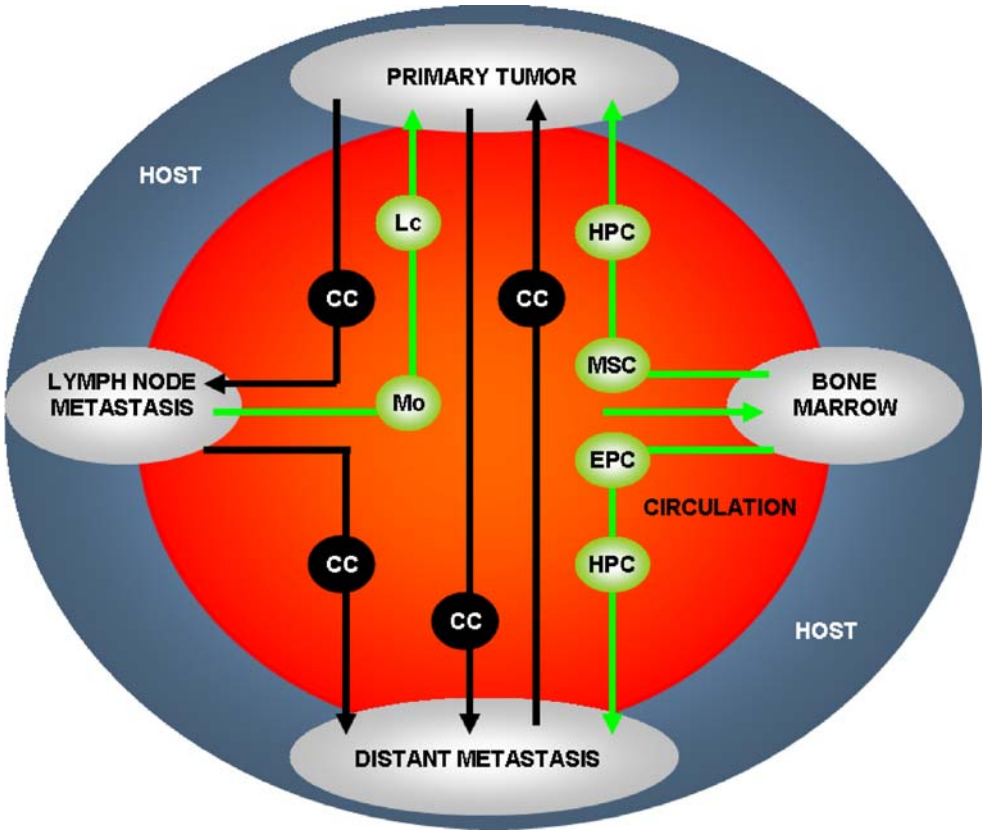

Fig. 6 Translocation of cancer cells and tumor-associated host cells between the ecosystems of a metastatic tumor. *HPC* hematopoietic precursor cells (VEGFR1-positive; CXCR4-positive), *EPC* endothelial progenitor cells (VEGFR2-positive; CXCR4-positive), both retained by CXCL12 (= SDF-1). *CC* cancer cells; note return from distant metastasis to primary tumor [127]. *Lc* leucocytes, Mo monocytes. *MSC* mesenchymal stem cells. For bone marrow-derived cells present in the circulation and participating at angiogenesis, see [49]. Adapted from [59, 114]

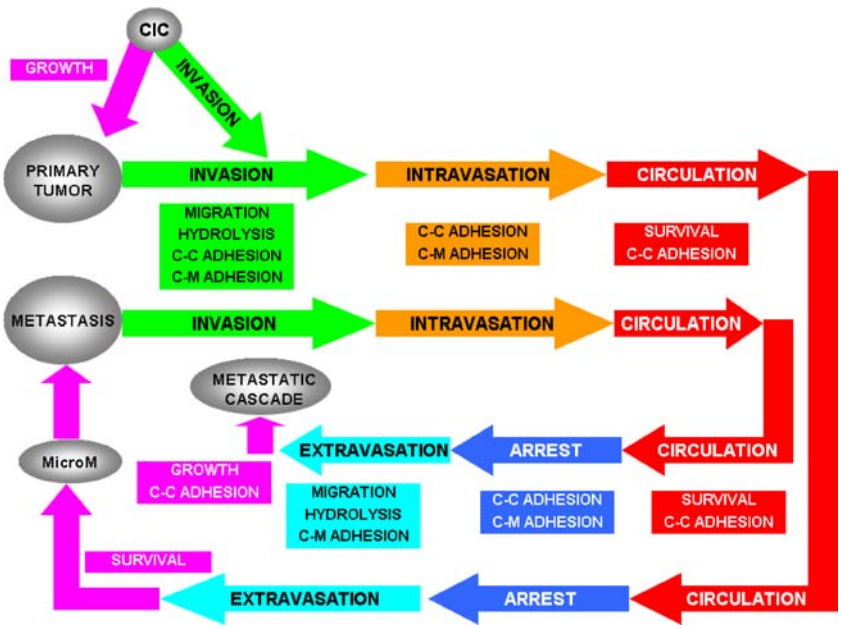

Fig. 7 The multistep process of invasion and metastasis. At each step we mention the cellular activities implicated, with emphasis on the cancer cells. When the cancer initiating cells (*CIC*) perform the multistep process without growth at the primary site metastases may also develop, a phenomenon called CUP (cancer unknown primary). Lack of growth of micrometastases is called dormancy, a phenomenon that may explain late metastasis. *C-C* cell–cell, *C-M* cell–matrix, *MicroM* micrometastasis

as typically observed in the bone with breast cancer and in the liver with ocular melanoma. Mechanisms of dormancy include: G0–G1 arrest; dominance of anti-angiogenic over pro-angiogenic factors, exemplified by the dramatic growth of lung metastases after removal of the primary tumor in Folkman's experiments [126]; immunosurveillance. Distant metastases give rise to metastases through the multistep process by which they are themselves generated from primary tumors. Compelling experimental evidence comes from parabiosed C57BL/6 mice in which lung metastases in tumor-amputated mice gave rise to lung metastases in the parabiosed normal syngeneic partner [8]. Return of metastasized cells to the primary tumor is a novel aspect of the metastatic cascade [127]. Such reseeding might explain the pattern of local relapses in breast cancer patients [128].

Cellular activities of invading cells

The cellular activities implicated in invasion and metastasis comprise homotypic cell–cell adhesion; heterotypic cell–cell and cell–matrix adhesion; hydrolysis; migration; survival; and growth [129, 130]. We will discuss these activities one by one, though it is quite clear that they are connected to one another at various levels (Fig. 8). The latter is quite obvious from an analysis of the molecular pathways that modulate these cellular activities. One receptor, e.g. an integrin, that is sensitive to multiple extracellular ligands and to interaction with other receptors, may modulate several of the above-mentioned invasion-related cellular activities [62]. Binding of one ligand, e. g. TGF-β to its cognate receptor on cancer cells and on various tumor-associated host cells results in stimulation or inhibition of various cellular responses [78]. Similarly, one transcription factor binds to several promoters, activates several genes encoding different molecules and altering several cellular activities, as exemplified by Snail, affecting cell–cell adhesion, motility, survival, and proliferation. Downregulation of molecules that are key regulators in one cellular activity, e.g. E-cadherin in cell–cell adhesion, is influenced by activation of receptors, e.g. c-Met, and integrins, that regulate other activities, migration, and cell–matrix adhesion, respectively [131].

Homotypic cell–cell adhesion

The E-cadherin/catenin/actin complex maintains the structure of the epithelium by homophilic (E-cadherin to E-cadherin), homotypic (epithelial cell to epithelial cell) adhesion. In models in vitro and in vivo, loss of E-cadherin induced invasion in line with clinical observations

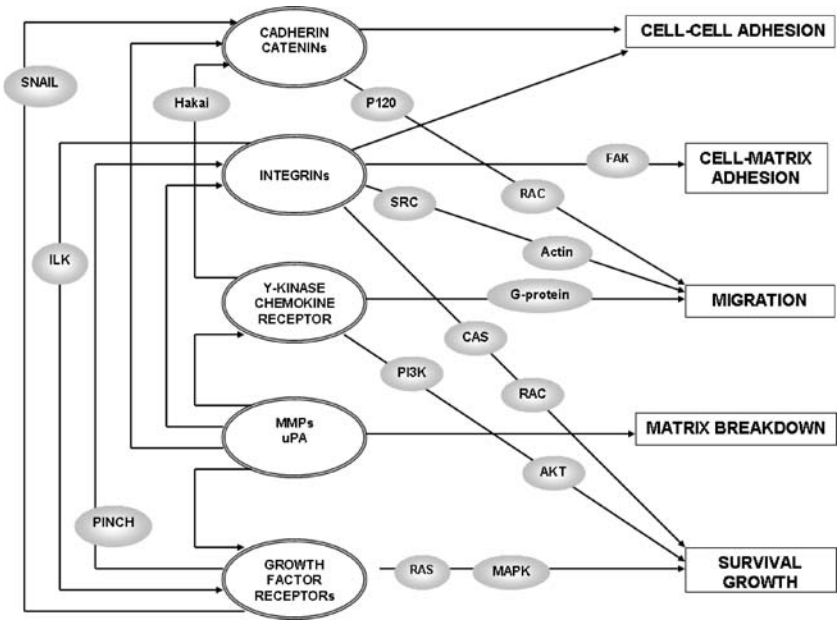

Fig. 8 Crosstalks between invasion- and metastasis-related cellular activities and their associated molecular complexes and pathways. Selected examples illustrate the relationship between the cellular activities that establish invasion programs. *AKT* (= PKB) protein kinase B, *CAS* Crk-associated substrate, *FAK* focal adhesion kinase, *G-protein* guanine nucleotide-binding protein, *Hakai* E3 ubiquitin-protein ligase, *ILK* integrin-linked (serine/threonine) kinase, *MAPK* mitogen-activated proteoin kinase, *MMP* matrix metalloproteinase, *p120* p120 catenin, *PI3K* phosphatidylinositol 3,4,5,-triphosphate, *PINCH* particularly interesting new cysteine-histidine rich protein, *RAC* RAC GTPase-activating protein 1, *RAS* RAS GTPase-activating protein, *SRC* protooncogene SRC, *uPA* urokinase type plasminogen activator, *Y* tyrosine. Adapted from [49, 62, 130, 131, 155]

[34, 132]. In these experiments, neutralization of E-cadherin by specific antibodies changed the cells' morphotype from epithelioid to mesenchymal in a reversible manner. A more definite form of such transition is described as epithelial-mesenchymal transition (EMT) characterized not only by morphotypic but also by molecular changes, namely: disappearance of E-cadherin, claudins, occludins, desmoplakin, cytokeratins, mucin-1; expression of fibronectin, vitronectin FSP1, vimentin, smooth muscle actin, and FGFR2 IIIb and IIIc splice variants [133]. The prototype EMT is seen in early embryonic development during gastrulation when epithelial cells invade through the primitive streak to form the mesenchyme. Complex molecular networks, signaling to E-cadherin as well as to the cytoskeleton, regulate EMT. Interestingly, ligands triggering EMT reveal the participation of (myo)fibroblasts, via FGF, HGF, and TGF-α of macrophages, via EGF and of inflammatory cells, via TNF-α [134]. EMT is considered to be reversible: the process is called mesenchymal-epithelial transition and is initiated by upregulation of E-cadherin leading to homotypic cell–cell adhesion. Such phenomenon expressed fully or partly explains the epithelial differentiation in metastases [135, 136]. Compatible with reversible downregulation of E-cadherin is its transcriptional regulation [131].

The clinical relevance of EMT has been questioned by Tarin et al. stating that there is no pathological evidence for the conversion of epithelial to mesenchymal cells in invasive cancers and that the static pictures of such cancers are compatible with invasion and metastasis of epithelial cells without EMT [137]. One of the problems is that we have no marker to tell us which mesenchymal cells in the tumor are derived from an epithelial cancer cell [138]. Taken together there is convincing evidence to accept that loss of homotypic cell–cell adhesion favors invasion at the primary tumor, whereas gain of homotypic cell–cell adhesion supports growth of metastases in epithelial tumors.

Heterotypic cell–cell adhesion

Homophilic heterotypic adhesion may suppress invasion, as exemplified by E-cadherine-mediated adhesion of melanoma cells to keratinocytes in the skin, or promote invasion, as demonstrated for N-cadherin-mediated adhesion of myofibroblasts to epithelial breast cancer cells [139]. The paradigm heterotypic heterophilic cell–cell adhesion is at the site of metastasis between circulating cancer cells and endothelial cells in a multistep manner that was first described for leukocytes. Chemokines produced at the metastatic niche direct cancer cells bearing their cognate receptors to the endothelium where they bind to selectins. This low affinity binding causes the cells to roll over the inner surface of the vessel, providing an opportunity for a higher affinity interaction through IgCAMs on the endothelium and integrins on the cancer cell. Similar interactions occur also during implantation of cancer cells onto body cavities [118]. Next to this single cell, leukocyte-like, scenario, cancer cell thrombi execute the arrest in the circulation that precedes extravasation and homing. Thrombi are formed through interaction between cancer cells and platelets and endothelial cells, implicating thrombin for activation of the participating cells and P-selectin and its ligands for cell–cell adhesion [122].

Cell–matrix adhesion

Interaction between tumor cells and the extracellular matrix occurs during invasion through epithelial and endothelial basement membranes as well as through the stroma. Integrins are major orchestrators of cellular activities that are involved in adhesion, migration, and survival of cancer cells and of tumor-associated host cells. Integrin inside-out signaling occurs through tyrosine kinase growth factor receptors. Outside-in signaling involves components of the extracellular matrix and secretory molecules such as small integrin-binding ligand, N-linked glycoproteins. The latter family of secretory phosphoglycoproteins comprises osteopontin (OPN), bone sialoprotein (BSP), dentin matrix protein 1 (DMP1), dentin sialophosphoprotein, matrix extracellular phosphoprotein that do participate at all steps of metastasis in an autocrine or a paracrine manner [140]. Binding to their specific receptors, integrins and/or CD44, on cancer cells, promotes uPA and MMP-mediated proteolysis. OPN promotes migration and adhesion of endothelial cells during angiogenesis at the primary tumor as well as at distant metastasis [62]; it serves as a chemotactic factor for macrophages. Expression of BSP, DMP1, and OPN helps cancer cells inside the circulation to sequester complement factor H, so protecting them from complement-mediated cytolysis. Cell–matrix adhesion at sites of integrin clustering is crucial also in the formation of locomotory structures such as podosomes and invadopodia in tumor-associated macrophages and cancer cells, respectively [141].

Hydrolysis

Most proteases, such as MMPs and uPA, used by cancer cells to create space in the extracellular matrix to invade, are recruited from tumor-associated host cells. At the primary tumor, producer host cells are: pericytes, endothelial cells, macrophages, neutrophils, mast cells, and (myo) fibroblasts [51]. At the premetastatic niche, hematopoietic/endothelial progenitor cells produce MMP9 preparing the site for the development of extravasating metastastatic cells. The lytic activity of MMPs is not limited to components of

the extracellular matrix but concerns also cell surface molecules, such as cadherins and integrins, and soluble ligands, such as growth factor binding proteins, chemokines and cytokines, and proteases and protease inhibitors. Polarized delivery of proteases occurs at podosomes and invadopodia through intracellular trafficking mediated by microtubules and Golgi complexes [142]. Remarkably, proteases, mostly MMPs produced by the stroma, have also anti-tumor activities, inhibiting also invasion and metastasis by induction of apoptosis, inhibition of proliferation, and suppression of angiogenesis [143, 144]. Substrates targeted by anti-tumor proteases include extracellular matrix proteins, chemokines, and cytokines, all serving as invasion promoters.

Motility

Studies of invasion have paid major attention to cell migration, an activity which is frequently used as a surrogate for invasion in vitro [145]. Such assays mostly score for migration of single cells, for example through pores in a filter that initially separates cells and chemoattractants in a two-compartment chamber. It is important to realize that invading cancer cells use other types of migration as well and that they are able to switch from one type to another. Most obvious in invasive cancers is migration in group, with (cohort migration) or without separation from the primary tumor (coordinated migration). Protease-dependent solitary cell migration shows a mesenchymal phenotype at the front of invasion that is characteristic of EMT, whereas protease-independent solitary cell migration shows an amoeboid phenotype. Blocking proteolysis converts HT-1080 fibrosarcoma cells in gels from the mesenchymal to the amoeboid type of migration [146]. These four modes are underpinned by different molecular mechanisms, displaying a high degree of plasticity [145, 147–149]. Minimum motility pathways were determined by gene profiling in cells collected by chemotaxis in a microcapillary tube from the front of an experimental rat tumor in vivo [23]. They confirm the role of autocrine and paracrine motility factors and chemokines recognizing respectively tyrosine kinase receptors and G-protein-coupled receptors on both cancer cells and tumor-associated host cells and signaling through small GTPases of the Rho family to elements of the actin cytoskeleton [150, 151]. One of the first and best characterized motility factors is HGF/SF binding to the c-MET tyrosine kinase receptor [129, 152]. c-Met is an invasion and metastasis promoter gene that is activated by mutations in human cancers [153]. Chemokines, e.g. CXCL12(= SDF-1), present in the ecosystem of distant metastases bind to their G-protein-coupled receptors, in this case CXCR4, on breast cancer cells and this leads to actin polymerization, pseudopodia formation, and chemotactic migration [105]. In a 3D culture model of the tumor-lymph vessel ecosystem, cancer cells secrete both CCR7, and its ligands CCL21 and CCL19. The ligands are drained towards the lymphatics and concentrate downstream of cancer cells ensuring that the latter migrate towards the lymphatics [121]. Another member of the G-protein-coupled receptor family binds autocrine motility factor AMF/gp78, signaling not only via the small GTPase pathway to promote migration but also via the Akt pathway to stimulate proliferation and inhibit apoptosis [154]. AMF is also a paracrine factor affecting host elements of the tumor ecosystem as exemplified by its pro-angiogenic activity.

Survival

When epithelial cells leave their normal ecosystem where they receive signals from and signal to their neighboring cells and extracellular matrix, they undergo a particular form of apoptosis called anoikis. It is clear that ectopic survival with resistance to anoikis is a prerequisite for invasion and metastasis. Cancer cells realize such resistance through the integrin-actin-receptor tyrosine kinase network, in which integrin-linked kinase (ILK) plays a major role [155]. Implicated also are: activation of survival pathways via TrkB (neurotrophic tyrosine kinase receptor), PI3K, and Akt; breakdown of death receptors; release of growth factors through increased MMP activity; overexpression of anti-apoptotic molecules such as BCL-2; and inactivation of p53 [17, 156, 157].

Clinical implications

Few recent papers on the mechanisms of invasion and metastasis fail to speculate about clinical applications: diagnostic, prognostic, and therapeutic. New insights into the communicating ecosystem concept have lead to the selection of patients for therapy following biomarkers for angiogenesis [120] or circulating tumor cells [158]. In metastasized breast cancer patients (stage IV) surgical removal of the primary tumor increases survival [159]. Successful aggressive treatment of smaller numbers of metastases (oligometastasis) illustrates the cascade concept [160]. Molecular pathways of invasion and metastasis, implicating cancer cells and tumor-associated host cells, have been suggested as targets for anti-invasive therapy and lists of anti-invasive compounds used pre-clinically and clinically can be found in various publications [17, 161]. Specific targets such as EMT and integrins are discussed by Sabbah et al. [132] and by Hehlgans et al. [155]. A single target is approached by various agents, as illustrated for the invasion promoter tyrosine kinase receptor MET: ligand

antagonists, such as uncleavable HGF and anti-HGF monoclonal antibodies; receptor competitors, such as Sema (a domain necessary for MET dimerization) recombinant proteins, decoy MET, anti-MET antibodies; kinase inhibitors; SH2 competitor peptides; and shRNAs [129].

Cancer cells are the major targets for therapy, though tumor-associated host cells are considered more and more frequently. Therapeutic strategies and lists of agents were published recently for blood and lymph angiogenesis [49, 68, 162], for myofibroblasts [5] and for small integrin-binding ligand N-linked glycoproteins [140] among others.

An equally intriguing question concerns the influence of current treatments on invasion and metastasis (Fig. 9). Ionizing radiation shows a hormetic dose–response with stimulation at lower doses and inhibition at higher doses. Pro-invasive and pro-metastatic activities of cancer cells are promoted by ionizing radiation, pending upon the dose and the nature of the radiation beam [4]. It also stimulates the tumor-associated host cells that are involved in invasion and metastasis, namely endothelial cells, myofibroblasts, leukocytes, and macrophages. Clonogenic survival of cancer cells still serves as the main biological rationale for radiotherapy of cancer, with DNA as the key target molecule. It became, however, quite clear that ionizing radiation affects also other molecules, such as tyrosine kinase receptors (EGFR, VEGFR, PDGFR, c-MET), TGF-β, integrins, and tenascin C, all of which are modulators of invasion and should be taken into account by the radiotherapist. Chemotherapy mobilizes hematopoietic progenitor cells from the bone marrow and this is exploited for peripheral stem cell transplantation. Similarly, it causes vasculogenic rebounds by bone marrow-derived circulating cells (CEPs) within hours to weeks, justifying anti-angiogenic treatment in strict chronological combination with chemotherapy [163]. Surgery causes wound healing reactions that activate host reaction, such as inflammation, angiogenesis, and fibrosis, all of which may promote invasion [118, 164]. In the peritoneal cavity surgical wounds may favor adhesion of cancer cells to the mesothelial stroma. Surgeons are actually considering prevention of traumatic promotion of invasion and metastasis through prevention of surgical trauma, extensive intraoperative peritoneal lavage, hyperthermic intraoperative chemoperfusion, anti-inflammatory drug treatment, and inhibition of cancer cell adhesion to the mesothelial wall by heparin or by monoclonal antibodies against cell–cell or cell–matrix adhesion molecules.

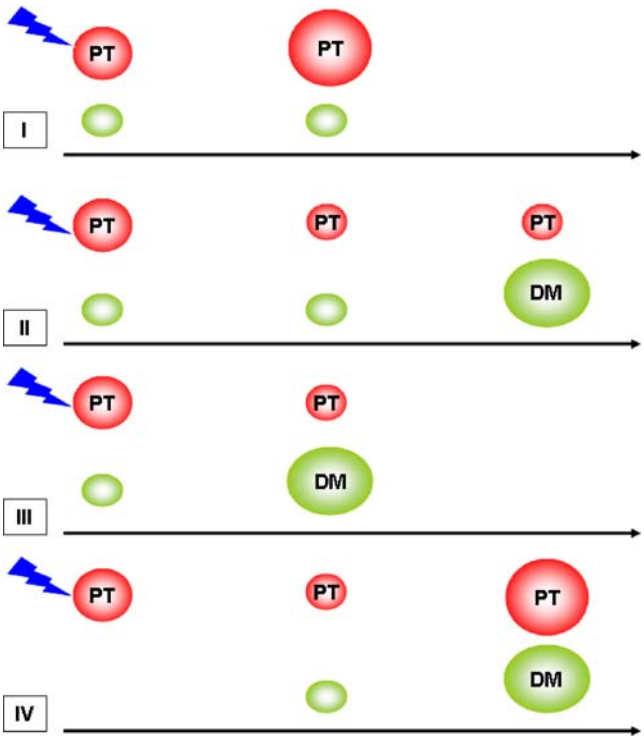

Fig. 9 Treatment of primary tumor (*PT*) and development of distant metastasis (*DM*). *I* Locoregional failure causes death of the patient before growth of DM; example: older textbooks (before WW II) considered cancers of the head and neck mucosa as nonmetatstatic in distant organs. *II* Local control prolongs survival permitting growth of metastasis; example: small cell lung cancer [169]. *III* Local control stimulates growth of metastases; example: radiotherapy or surgery of mouse 3LL carcinoma changes the angiogenic balance at the site of metastasis, through elimination of angiostatin [126, 170]. *IV* Local treatment stimulates invasion and metastasis through its effect on the cancer cells, the tumor-associated host cells or both [4]. *Arrows* indicate time, *flashes* treatment

Conclusions and perspectives

Malignant, i.e. invasive and metastatic, tumors involve communicating ecosystems, namely: a primary tumor, lymph node metastases, distant metastases, a reactive bone marrow, and the circulation. Each of these ecosystems contains cancer cells and tumor-associated host cells that are in continuous molecular conversation with each other. Multiple autocrine and paracrine ligands signaling through multiple and branching pathways, together with activation of promoter genes and inactivation of suppressor genes, modulate programs of cellular activities, comprising cell–cell adhesion, cell–matrix adhesion, breakdown of extracellular matrix, migration, survival, and growth. These programs take tumor cells through the multistep process of metastasis, comprising: invasion into foreign tissues, intravasation, survival in the circulation, arrest at distant organs, extravasation, homing, survival, and growth. It is our hope that future therapeutic strategies will take into account the dynamic molecular complexity of invasion and metastasis

implicating both cancer cells and tumor-associated host cells.

Conflict of interest statement We declare that we have no conflict of interest.

References

1. Tarin D (2006–2007) New insights into the pathogenesis of breast cancer metastasis. Breast Dis 26:13–25
2. Stafford LJ, Vaidya KS, Welch DR (2008) Metastasis suppressors genes in cancer. Int J Biochem Cell Biol 40:874–891
3. Oliveira MJ (2004) The effect of bacteria on colon cancer cell invasion: molecular mechanisms associated. Faculty of Medicine and Health Sciences. Ghent University. PhD thesis
4. Madani I, De Neve W, Mareel M (2008) Does ionizing radiation stimulate cancer invasion and metastasis? Bull Cancer 95:292–300
5. De Wever O, Mareel M (2003) Role of tissue stroma in cancer cell invasion. J Pathol 200:429–447
6. Bracke ME, Vanhoecke BW, Derycke L et al (2008) Plant polyphenolics as anti-invasive cancer agents. Anticancer Agents Med Chem 8:171–185
7. Ottewell PD, Coleman RE, Holen I (2006) From genetic abnormality to metastases: murine models of breast cancer and their use in the development of anticancer therapies. Breast Cancer Res Treat 96:101–113
8. Langley RR, Fidler IJ (2007) Tumor cell-organ microenvironment interactions in the pathogenesis of cancer metastasis. Endocr Rev 28:297–321
9. Kuperwasser C, Chavarria T, Wu M et al (2004) Reconstruction of functionally normal and malignant human breast tissues in mice. Proc Natl Acad Sci U S A 101:4966–4971
10. Hoffman RM (2006) Real-time subcellular imaging in live animals: new visible targets for cancer drug discovery. IDrugs 9:632–635
11. Fomchenko EI, Holland EC (2006) Mouse models of brain tumors and their applications in preclinical trials. Clin Cancer Res 12:5288–5297
12. Gingrich JR, Barrios RJ, Morton RA et al (1996) Metastatic prostate cancer in a transgenic mouse. Cancer Res 56:4096–4102
13. Perl AK, Wilgenbus P, Dahl U et al (1998) A causal role for E-cadherin in the transition from adenoma to carcinoma. Nature 392:190–193
14. Ambartsumian N, Grigorian M, Lukanidin E (2005) Genetically modified mouse models to study the role of metastasis-promoting S100A4 (mts1) protein in metastatic mammary cancer. J Dairy Res 72:27–33
15. Scherer RL, McIntyre JO, Matrisian LM (2008) Imaging matrix metalloproteinases in cancer. Cancer Metastasis Rev 27:679–690
16. Espina V, Heiby M, Pierobon M et al (2007) Laser capture microdissection technology. Expert Rev Mol Diagn 7:647–657
17. Eccles SA, Welch DR (2007) Metastasis: recent discoveries and novel treatment strategies. Lancet 369:1742–1757
18. Brenton JD, Carey LA, Ahmed AA et al (2005) Molecular classification and molecular forecasting of breast cancer: ready for clinical application? J Clin Oncol 23:7350–7360
19. Montel V, Huang TY, Mose E et al (2005) Expression profiling of primary tumors and matched lymphatic and lung metastases in a xenogeneic breast cancer model. Am J Pathol 166:1565–1579
20. Karpf AR, Jones DA (2002) Reactivating the expression of methylation silenced genes in human cancer. Oncogene 21:5496–5503
21. Feng Y, Sun B, Li X et al (2007) Differentially expressed genes between primary cancer and paired lymph node metastases predict clinical outcome of node-positive breast cancer patients. Breast Cancer Res Treat 103:319–329
22. van ‘t Veer LJ, Dai H, van de Vijver MJ et al (2002) Gene expression profiling predicts clinical outcome of breast cancer. Nature 415:530–536
23. Wang Y, Klijn JG, Zhang Y et al (2005) Gene-expression profiles to predict distant metastasis of lymph-node-negative primary breast cancer. Lancet 365:671–679
24. Eckhardt BL, Parker BS, van Laar RK et al (2005) Genomic analysis of a spontaneous model of breast cancer metastasis to bone reveals a role for the extracellular matrix. Mol Cancer Res 3:1–13
25. Adib TR, Henderson S, Perrett C et al (2004) Predicting biomarkers for ovarian cancer using gene-expression microarrays. Br J Cancer 90:686–692
26. Suzuki M, Tarin D (2007) Gene expression profiling of human lymph node metastases and matched primary breast carcinomas: clinical implications. Mol Oncol 1:172–180
27. Chang HY, Nuyten DS, Sneddon JB et al (2005) Robustness, scalability, and integration of a wound-response gene expression signature in predicting breast cancer survival. Proc Natl Acad Sci U S A 102:3738–3743
28. Finak G, Bertos N, Pepin F et al (2008) Stromal gene expression predicts clinical outcome in breast cancer. Nat Med 14:518–527
29. Clark IM, Swingler TE, Sampieri CL et al (2008) The regulation of matrix metalloproteinases and their inhibitors. Int J Biochem Cell Biol 40:1362–1378
30. Li Y, Liang J, Kang S et al (2008) E-cadherin gene polymorphisms and haplotype associated with the occurrence of epithelial ovarian cancer in Chinese. Gynecol Oncol 108:409–414
31. Brendle A, Lei H, Brandt A et al (2008) Polymorphisms in predicted microRNA-binding sites in integrin genes and breast cancer: ITGB4 as prognostic marker. Carcinogenesis 29:1394–1399
32. Hunter KW, Crawford NP (2006) Germ line polymorphism in metastatic progression. Cancer Res 66:1251–1254
33. Crawford NP, Ziogas A, Peel DJ et al (2006) Germline polymorphisms in SIPA1 are associated with metastasis and other indicators of poor prognosis in breast cancer. Breast Cancer Res 8:R16
34. van Roy F, Berx G (2008) The cell-cell adhesion molecule E-cadherin. Cell Mol Life Sci 65:3756–3788
35. Bartel DP, Chen CZ (2004) Micromanagers of gene expression: the potentially widespread influence of metazoan microRNAs. Nat Rev Genet 5:396–400
36. Ma L, Weinberg RA (2008) Micromanagers of malignancy: role of microRNAs in regulating metastasis. Trends Genet 24:448–456
37. Graff JR, Zimmer SG (2003) Translational control and metastatic progression: enhanced activity of the mRNA cap-binding protein eIF-4E selectively enhances translation of metastasis-related mRNAs. Clin Exp Metastasis 20:265–273
38. Hao X, Sun B, Hu L (2004) Differential gene and protein expression in primary breast malignancies and their lymph node metastases as revealed by combined cDNA microarray and tissue microarray analysis. Cancer 100(6):1110–1122
39. Hakomori S (1996) Tumor malignancy defined by aberrant glycosylation and sphingo(glyco) lipid metabolism. Cancer Res 56:5309–5318
40. Yoshimura M, Ihara Y, Matsuzawa Y et al (1996) Aberrant glycosylation of E-cadherin enhances cell–cell binding to suppress metastasis. J Biol Chem 271:13811–13815
41. McLachlan RW, Yap AS (2007) Not so simple: the complexity of phosphotyrosine signaling at cadherin adhesive contacts. J Mol Med 85:545–554

42. Wipff PJ, Hinz B (2008) Integrins and the activation of latent transforming growth factor beta1—an intimate relationship. Eur J Cell Biol 87:601–615
43. Paredes J, Correia AL, Ribeiro AS et al (2007) P-cadherin expression in breast cancer: a review. Breast Cancer Res 9:214
44. Van Marck V, Stove C, Van Den Bossche K et al (2005) P-cadherin promotes cell–cell adhesion and counteracts invasion in human melanoma. Cancer Res 65:8774–8783
45. Wheelock MJ, Shintani Y, Maeda M et al (2008) Cadherin switching. J Cell Sci 121:727–735
46. De Wever O, Westbroek W, Verloes A et al (2004) Critical role of N-cadherin in myofibroblast invasion and migration in vitro stimulated by colon-cancer-cell-derived TGF-beta or wounding. J Cell Sci 117:4691–4703
47. Alexander NR, Tran NL, Rekapally H et al (2006) N-cadherin gene expression in prostate carcinoma is modulated by integrin-dependent nuclear translocation of Twist1. Cancer Res 66:3365–3369
48. Stove C, Bracke M (2004) Roles for neuregulins in human cancer. Clin Exp Metastasis 21:665–684
49. Kerbel RS (2008) Tumor angiogenesis. N Engl J Med 358:2039–2049
50. Chabottaux V, Noel A (2007) Breast cancer progression: insights into multifaceted matrix metalloproteinases. Clin Exp Metastasis 24:647–656
51. Noël A, Jost M, Maquoi E (2008) Matrix metalloproteinases at cancer tumor–host interface. Semin Cell Dev Biol 19:52–60
52. Jones RB, Gordus A, Krall JA et al (2006) A quantitative protein interaction network for the ErbB receptors using protein microarrays. Nature 439:168–174
53. Pawson T, Nash P (2003) Assembly of cell regulatory systems through protein interaction domains. Science 300:445–452
54. Kopfstein L, Christofori G (2006) Metastasis: cell-autonomous mechanisms versus contributions by the tumor microenvironment. Cell Mol Life Sci 63:449–468
55. Paget S (1889) The distribution of secondary growths in cancer of the breast. Lancet 1:571–573
56. Mareel MM, Behrens J, Birchmeier W et al (1991) Down-regulation of E-cadherin expression in Madin Darby canine kidney (MDCK) cells inside tumors of nude mice. Int J Cancer 47:922–928
57. Creighton CJ, Bromberg-White JL, Misek DE et al (2005) Analysis of tumor–host interactions by gene expression profiling of lung adenocarcinoma xenografts identifies genes involved in tumor formation. Mol Cancer Res 3:119–129
58. Dimanche-Boitrel MT, Vakaet L Jr, Pujuguet P et al (1994) In vivo and in vitro invasiveness of a rat colon-cancer cell line maintaining E-cadherin expression: an enhancing role of tumor-associated myofibroblasts. Int J Cancer 56:512–521
59. Lin EY, Pollard JW (2007) Tumor-associated macrophages press the angiogenic switch in breast cancer. Cancer Res 67:5064–5066
60. Korc M (2007) Pancreatic cancer-associated stroma production. Am J Sur 194(4 Suppl):S84–S86
61. He Y, Rajantie I, Pajusola K et al (2005) Vascular endothelial cell growth factor receptor 3-mediated activation of lymphatic endothelium is crucial for tumor cell entry and spread via lymphatic vessels. Cancer Res 65:4739–4746
62. Mahabeleshwar GH, Byzova TV (2007) Angiogenesis in melanoma. Semin Oncol 34:555–565
63. Benoy IH, Salgado R, Elst H et al (2005) Relative microvessel area of the primary tumour, and not lymph node status, predicts the presence of bone marrow micrometastases detected by reverse transcriptase polymerase chain reaction in patients with clinically non-metastatic breast cancer. Breast Cancer Res 7: R210–R219
64. Hicklin DJ, Ellis LM (2005) Role of the vascular endothelial growth factor pathway in tumor growth and angiogenesis. J Clin Oncol 23:1011–1027
65. Schoppmann SF, Bayer G, Aumayr K, Austrian Breast and Colorectal Cancer Study Group et al (2004) Prognostic value of lymphangiogenesis and lymphovascular invasion in invasive breast cancer. Ann Surg 240:306–312
66. Tobler NE, Detmar M (2006) Tumor and lymph node lymphangiogenesis—impact on cancer metastasis. J Leukoc Biol 80:691–696
67. Nathanson SD (2007) Preclinical models of regional lymph node tumor metastasis. In: Leong S (ed) Cancer metastasis and the lymphvascular system: basis for rational therapy. Springer, New York, pp 129–156
68. Wissmann C, Detmar M (2006) Pathways targeting tumor lymphangiogenesis. Clin Cancer Res 12:6865–6868
69. Rafii DC, Psaila B, Butler J et al (2008) Regulation of vasculogenesis by platelet-mediated recruitment of bone marrow-derived cells. Arterioscler Thromb Vasc Biol 28:217–222
70. Mantovani A, Sica A et al (2004) The chemokine system in diverse forms of macrophage activation and polarization. Trends Immunol 25:677–686
71. Mantovani A, Romero P, Palucka AK et al (2008) Tumour immunity: effector response to tumour and role of the microenvironment. Lancet 371:771–783
72. Talmadge JE, Donkor M, Scholar E (2007) Inflammatory cell infiltration of tumors: Jekyll or Hyde. Cancer Metastasis Rev 26:373–400
73. Lewis CE, Pollard JW (2006) Distinct role of macrophages in different tumor microenvironments. Cancer Res 66:605–612
74. Condeelis J, Pollard JW (2006) Macrophages: obligate partners for tumor cell migration, invasion, and metastasis. Cell 124:263–266
75. Wyckoff JB, Wang Y, Lin EY et al (2007) Direct visualization of macrophage-assisted tumor cell intravasation in mammary tumors. Cancer Res 67:2649–2656
76. Mahadevan D, Von Hoff DD (2007) Tumor–stroma interactions in pancreatic ductal adenocarcinoma. Mol Cancer Ther 6:1186–1197
77. De Wever O, Demetter P, Mareel M et al (2008) Stromal myofibroblasts are drivers of invasive cancer growth. Int J Cancer 123:2229–2238
78. Massaguè J (2008) TGFbeta in cancer. Cell 134:215–230
79. Hu M, Yao J, Carroll DK et al (2008) Regulation of in situ to invasive breast carcinoma transition. Cancer Cell 13:394–406
80. Lerwill MF (2004) Current practical applications of diagnostic immunohistochemistry in breast pathology. Am J Surg Pathol 28:1076–1091
81. Allinen M, Beroukhim R, Cai L et al (2004) Molecular characterization of the tumor microenvironment in breast cancer. Cancer Cell 6:17–32
82. Hu M, Yao J, Cai L et al (2005) Distinct epigenetic changes in the stromal cells of breast cancers. Nat Genet 37:899–905
83. Barsky SH, Karlin NJ (2005) Myoepithelial cells: autocrine and paracrine suppressors of breast cancer progression. J Mammary Gland Biol Neoplasia 10:249–260
84. Polyak K, Hu M (2005) Do myoepithelial cells hold the key for breast tumor progression? J Mammary Gland Biol Neoplasia 10:231–247
85. Mantyh PW, Clohisy DR, Koltzenburg M et al (2002) Molecular mechanisms of cancer pain. Nat Rev Cancer 2:201–209
86. Ayala GE, Dai H, Powell M et al (2008) Cancer-related axonogenesis and neurogenesis in prostate cancer. Clin Cancer Res 14:7593–7603
87. Wang W, Zhao H, Zhang S, et al (2008) Patterns of expression and function of the p75(NGFR) protein in pancreatic cancer cells and tumours. Eur J Surg Oncol Nov 26 (in press)

88. Marchesi F, Piemonti L, Fedele G et al (2008) The chemokine receptor CX3CR1 is involved in the neural tropism and malignant behavior of pancreatic ductal adenocarcinoma. Cancer Res 68:9060–9069
89. Zhang S, Qi L, Li M et al (2008) Chemokine CXCL12 and its receptor CXCR4 expression are associated with perineural invasion of prostate cancer. J Exp Clin Cancer Res 27:62
90. Andarawewa KL, Motrescu ER, Chenard MP et al (2005) Stromelysin-3 is a potent negative regulator of adipogenesis participating to cancer cell-adipocyte interaction/crosstalk at the tumor invasive front. Cancer Res 65:10862–10871
91. Caers J, Van Valckenborgh E, Menu E et al (2008) Unraveling the biology of multiple myeloma disease: cancer stem cells, acquired intracellular changes and interactions with the surrounding micro-environment. Bull Cancer 95:301–313
92. Vona-Davis L, Rose DP (2007) Adipokines as endocrine, paracrine, and autocrine factors in breast cancer risk and progression. Endocr Relat Cancer 14:189–206
93. Kunduzova O, Alet N, Delesque-Touchard N et al (2008) Apelin/APJ signaling system: a potential link between adipose tissue and endothelial angiogenic processes. FASEB J 22:4146–4153
94. Cirillo D, Rachiglio AM, la Montagna R et al (2008) Leptin signaling in breast cancer: an overview. J Cell Biochem 105:956–964
95. Jaffe T, Schwartz B (2008) Leptin promotes motility and invasiveness in human colon cancer cells by activating multiple signal-transduction pathways. Int J Cancer 123:2543–2556
96. Horiguchi A, Sumitomo M, Asakuma J et al (2006) Leptin promotes invasiveness of murine renal cancer cells via extracellular signal-regulated kinases and rho dependent pathway. J Urol 176:1636–1641
97. Bussard KM, Gay CV, Mastro AM (2008) The bone microenvironment in metastasis; what is special about bone? Cancer Metastasis Rev 27:41–55
98. Vakaet LA, Boterberg T (2004) Pain control by ionizing radiation of bone metastasis. Int J Dev Biol 48:599–606
99. Oliveira MJ, Van Damme J, Lauwaet T et al (2003) Beta-casein-derived peptides, produced by bacteria, stimulate cancer cell invasion and motility. EMBO J 22:6161–6173
100. Oliveira MJ, Costa AC, Costa AM et al (2006) *Helicobacter pylori* induces gastric epithelial cell invasion in a c-Met and type IV secretion system-dependent manner. J Biol Chem 281:34888–34896
101. Oliveira MJ, Costa AM, Costa AC, et al (2009) CagA associates with c-Met, E-cadherin, and p120-catenin in a multiproteic complex that suppresses *Helicobacter pylori*-induced cell invasive phenotype. J Infect Dis (in press)
102. Miller MJ, Wei SH, Parker I et al (2002) Two-photon imaging of lymphocyte motility and antigen response in intact lymph node. Science 296:1869–1873
103. Mullen JT, Wang H, Yao JC et al (2005) Carcinoid tumors of the duodenum. Surgery 138:971–977
104. Hoon DS, Kitago M, Kim J et al (2006) Molecular mechanisms of metastasis. Cancer Metastasis Rev 25:203–220
105. Müller A, Homey B, Soto H et al (2001) Involvement of chemokine receptors in breast cancer metastasis. Nature 410:50–56
106. Hirakawa S, Brown LF, Kodama S et al (2007) VEGF-C-induced lymphangiogenesis in sentinel lymph nodes promotes tumor metastasis to distant sites. Blood 109:1010–1017
107. Van den Eynden GG, Vandenberghe MK, van Dam PJ et al (2007) Increased sentinel lymph node lymphangiogenesis is associated with nonsentinel axillary lymph node involvement in breast cancer patients with a positive sentinel node. Clin Cancer Res 13:5391–5397
108. DiMeo TA, Kuperwasser C (2006) The evolving paradigm of tissue-specific metastasis. Breast Cancer Res 8:301
109. Andre F, Cabioglu N, Assi H et al (2006) Expression of chemokine receptors predicts the site of metastatic relapse in patients with axillary node positive primary breast cancer. Ann Oncol 17:945–951
110. Stessels F, Van den Eynden G, Van der Auwera I et al (2004) Breast adenocarcinoma liver metastases, in contrast to colorectal cancer liver metastases, display a non-angiogenic growth pattern that preserves the stroma and lacks hypoxia. Br J Cancer 90:1429–1436
111. Mendes O, Kim HT, Lungu G et al (2007) MMP2 role in breast cancer brain metastasis development and its regulation by TIMP2 and ERK1/2. Clin Exp Metastasis 24:341–351
112. Kaplan RN, Psaila B, Lyden D (2006) Bone marrow cells in the 'pre-metastatic niche': within bone and beyond. Cancer Metastasis Rev 25:521–529
113. Hiratsuka S, Watanabe A, Aburatani H et al (2006) Tumour-mediated upregulation of chemoattractants and recruitment of myeloid cells predetermines lung metastasis. Nat Cell Biol 8:1369–1375
114. Kaplan RN, Psaila B, Lyden D (2007) Niche-to-niche migration of bone-marrow-derived cells. Trends Mol Med 13:72–81
115. Pantel K, Brakenhoff RH (2004) Dissecting the metastatic cascade. Nat Rev Cancer 4:448–456
116. Vincent-Salomon A, Bidard FC, Pierga JY (2008) Bone marrow micrometastasis in breast cancer: review of detection methods, prognostic impact and biological issues. J Clin Pathol 61:570–576
117. Bidard FC, Vincent-Salomon A, Gomme S, Institut Curie Breast Cancer Study Group et al (2008) Disseminated tumor cells of breast cancer patients: a strong prognostic factor for distant and local relapse. Clin Cancer Res 14:3306–3311
118. Ceelen WP, Bracke ME (2009) Peritoneal minimal residual disease in colorectal cancer: mechanisms, prevention, and treatment. Lancet Oncol 10:72–79
119. Bidard FC, Pierga JY, Vincent-Salomon A et al (2008) A "class action" against the microenvironment: do cancer cells cooperate in metastasis? Cancer Metastasis Rev 27:5–10
120. Bertolini F, Mancuso P, Shaked Y et al (2007) Molecular and cellular biomarkers for angiogenesis in clinical oncology. Drug Discov Today 12:806–812
121. Shields JD, Fleury ME, Yong C et al (2007) Autologous chemotaxis as a mechanism of tumor cell homing to lymphatics via interstitial flow and autocrine CCR7 signaling. Cancer Cell 11:526–538
122. Nierodzik ML, Karpatkin S (2006) Thrombin induces tumor growth, metastasis, and angiogenesis: evidence for a thrombin-regulated dormant tumor phenotype. Cancer Cell 10:355–362
123. Podsypanina K, Du YC, Jechlinger M et al (2008) Seeding and propagation of untransformed mouse mammary cells in the lung. Science 321:1841–1844
124. Aguirre-Ghiso JA (2007) Models, mechanisms and clinical evidence for cancer dormancy. Nat Rev Cancer 7:834–846
125. Brackstone M, Townson JL, Chambers AF (2007) Tumour dormancy in breast cancer: an update. Breast Cancer Res 9:208
126. O'Reilly MS, Holmgren L, Shing Y et al (1994) Angiostatin: a novel angiogenesis inhibitor that mediates the suppression of metastases by a Lewis lung carcinoma. Cell 79:315–328
127. Norton L, Massagué J (2006) Is cancer a disease of self-seeding? Nat Med 12:875–878
128. Bidard FC (2008) Interactions en coopérations cellulaires dans le processus métastatique. MSc thesis. L'Université Paris XI
129. Benvenuti S, Comoglio PM (2007) The MET receptor tyrosine kinase in invasion and metastasis. J Cell Physiol 213:316–325

130. Mareel M, Leroy A (2003) Clinical, cellular, and molecular aspects of cancer invasion. Physiol Rev 83:337–376
131. Christofori G (2006) New signals from the invasive front. Nature 441:444–450
132. Sabbah M, Emami S, Redeuilh G et al (2008) Molecular signature and therapeutic perspective of the epithelial-to-mesenchymal transitions in epithelial cancers. Drug Resist Updat 11:123–151
133. Thiery JP, Sleeman JP (2006) Complex networks orchestrate epithelial-mesenchymal transitions. Nat Rev Mol Cell Biol 7:131–142
134. Yang J, Weinberg RA (2008) Epithelial-mesenchymal transition: at the crossroads of development and tumor metastasis. Dev Cell 14:818–829
135. Christiansen JJ, Rajasekaran AK (2006) Reassessing epithelial to mesenchymal transition as a prerequisite for carcinoma invasion and metastasis. Cancer Res 66:8319–8326
136. Brabletz T, Jung A, Spaderna S et al (2005) Opinion: migrating cancer stem cells—an integrated concept of malignant tumour progression. Nat Rev Cancer 5:744–749
137. Tarin D, Thompson EW, Newgreen DF (2005) The fallacy of epithelial mesenchymal transition in neoplasia. Cancer Res 65:5996–6000
138. Garber K (2008) Epithelial-to-mesenchymal transition is important to metastasis, but questions remain. J Natl Cancer Inst 100:232–239
139. De Wever O, Derycke L, Hendrix A et al (2007) Soluble cadherins as cancer biomarkers. Clin Exp Metastasis 24:685–697
140. Bellahcène A, Castronovo V, Ogbureke KU et al (2008) Small integrin-binding ligand N-linked glycoproteins (SIBLINGs): multifunctional proteins in cancer. Nat Rev Cancer 8:212–226
141. Gimona M, Buccione R (2006) Adhesions that mediate invasion. Int J Biochem Cell Biol 38:1875–1892
142. Gimona M, Buccione R, Courtneidge SA et al (2008) Assembly and biological role of podosomes and invadopodia. Curr Opin Cell Biol 20:235–241
143. López-Otín C, Matrisian LM (2007) Emerging roles of proteases in tumour suppression. Nat Rev Cancer 7:800–808
144. Martin MD, Matrisian LM (2007) The other side of MMPs: protective roles in tumor progression. Cancer Metastasis Rev 26:717–724
145. Sahai E (2005) Mechanisms of cancer cell invasion. Curr Opin Genet Dev 15:87–96
146. Wolf K, Mazo I, Leung H et al (2003) Compensation mechanism in tumor cell migration: mesenchymal-amoeboid transition after blocking of pericellular proteolysis. J Cell Biol 160:267–277
147. Wolf K, Friedl P (2006) Molecular mechanisms of cancer cell invasion and plasticity. Br J Dermatol 154(Suppl 1):11–15
148. Yilmaz M, Christofori G, Lehembre F (2007) Distinct mechanisms of tumor invasion and metastasis. Trends Mol Med 13:535–541
149. Wicki A, Christofori G (2007) The potential role of podoplanin in tumour invasion. Br J Cancer 96:1–5
150. Yamaguchi H, Condeelis J (2007) Regulation of the actin cytoskeleton in cancer cell migration and invasion. Biochim Biophys Acta 1773:642–652
151. Sahai E, Garcia-Medina R, Pouysségur J et al (2007) Smurf1 regulates tumor cell plasticity and motility through degradation of RhoA leading to localized inhibition of contractility. J Cell Biol 176:35–42
152. Gentile A, Trusolino L, Comoglio PM (2008) The Met tyrosine kinase receptor in development and cancer. Cancer Metastasis Rev 27:85–94
153. Lengyel E, Sawada K, Salgia R (2007) Tyrosine kinase mutations in human cancer. Curr Mol Med 7:77–84
154. Funasaka T, Raz A (2007) The role of autocrine motility factor in tumor and tumor microenvironment. Cancer Metastasis Rev 26:725–735
155. Hehlgans S, Haase M, Cordes N (2007) Signalling via integrins: implications for cell survival and anticancer strategies. Biochim Biophys Acta 1775:163–180
156. Douma S, Van Laar T, Zevenhoven J et al (2004) Suppression of anoikis and induction of metastasis by the neurotrophic receptor TrkB. Nature 430:1034–1039
157. Geiger TR, Peeper DS (2005) The neurotrophic receptor TrkB in anoikis resistance and metastasis: a perspective. Cancer Res 65:7033–7036
158. Sandri MT (2007) Circulating tumor cells. IEO—Scientific Report 2007—Ongoing research 2008; pp 192–194
159. Gnerlich J, Jeffe DB, Deshpande AD et al (2007) Surgical removal of the primary tumor increases overall survival in patients with metastatic breast cancer: analysis of the 1988–2003 SEER data. Ann Surg Oncol 14:2187–2194
160. Salama JK, Chmura SJ, Mehta N et al (2008) An initial report of a radiation dose-escalation trial in patients with one to five sites of metastatic disease. Clin Cancer Res 14:5255–5259
161. Dollé L, Depypere HT, Bracke ME (2006) Anti-invasive/anti-metastasis strategies: new roads, new tools and new hopes. Curr Cancer Drug Targets 6:729–751
162. Fox SB, Generali DG, Harris AL (2007) Breast tumour angiogenesis. Breast Cancer Res 9:216
163. Shaked Y, Kerbel RS (2007) Antiangiogenic strategies on defense: on the possibility of blocking rebounds by the tumor vasculature after chemotherapy. Cancer Res 67:7055–7058
164. Formenti SC, Demaria S (2008) Local control by radiotherapy: is that all there is? Breast Cancer Res 10:215
165. Hüsemann Y, Geigl JB, Schubert F et al (2008) Systemic spread is an early step in breast cancer. Cancer Cell 13:58–68
166. Denys H, Derycke L, Hendrix A et al (2008) Differential impact of TGF-beta and EGF on fibroblast differentiation and invasion reciprocally promotes colon cancer cell invasion. Cancer Lett 266:263–274
167. Milas L, Mason K, Liao Z et al (2003) Role of cyclooxygenase-2 (COX-2) and its inhibition in tumor biology and radiotherapy. In: Nieder C, Milas L, Ang KK (eds) Modification of radiation response. Springer, Berlin, pp 241–258
168. Opdenakker G, Van Damme J (2004) The countercurrent principle in invasion and metastasis of cancer cells. Recent insights on the roles of chemokines. Int J Dev Biol 48:519–527
169. Nugent JL, Bunn PA Jr, Matthews MJ et al (1979) CNS metastases in small cell bronchogenic carcinoma: increasing frequency and changing pattern with lengthening survival. Cancer 44:1885–1893
170. Camphausen K, Moses MA, Beecken WD et al (2001) Radiation therapy to a primary tumor accelerates metastatic growth in mice. Cancer Res 61:2207–2211
171. Ramaswamy S, Ross KN, Lander ES et al (2003) A molecular signature of metastasis in primary solid tumors. Nat Genet 33:49–54
172. Chen YJ, Lin SC, Kao T et al (2004) Genome-wide profiling of oral squamous cell carcinoma. J Pathol 204:326–332
173. Perou CM, Sørlie T, Eisen MB et al (2000) Molecular portraits of human breast tumours. Nature 406:747–752
174. LaTulippe E, Satagopan J, Smith A et al (2002) Comprehensive gene expression analysis of prostate cancer reveals distinct transcriptional programs associated with metastatic disease. Cancer Res 62:4499–4506
175. Lapointe J, Li C, Giacomini CP et al (2007) Genomic profiling reveals alternative genetic pathways of prostate tumorigenesis. Cancer Res 67:8504–8510

176. Lips EH, van Eijk R, de Graaf EJ et al (2008) Integrating chromosomal aberrations and gene expression profiles to dissect rectal tumorigenesis. BMC Cancer 8:314
177. Cromer A, Carles A, Millon R et al (2004) Identification of genes associated with tumorigenesis and metastatic potential of hypopharyngeal cancer by microarray analysis. Oncogene 23:2484–2498
178. Couvelard A, Hu J, Steers G et al (2006) Identification of potential therapeutic targets by gene-expression profiling in pancreatic endocrine tumors. Gastroenterology 131:1597–1610
179. Bertucci F, Finetti P, Rougemont J et al (2004) Gene expression profiling for molecular characterization of inflammatory breast cancer and prediction of response to chemotherapy. Cancer Res 64:8558–8565

Virchows Arch (2009) 454:623–628
DOI 10.1007/s00428-009-0768-0

ORIGINAL ARTICLE

Activity-based differentiation of pathologists' workload in surgical pathology

G. A. Meijer · J. J. Oudejans · J. J. M. Koevoets · C. J. L. M. Meijer

Received: 14 December 2007 / Revised: 17 March 2009 / Accepted: 21 March 2009 / Published online: 28 April 2009

Abstract Adequate budget control in pathology practice requires accurate allocation of resources. Any changes in types and numbers of specimens handled or protocols used will directly affect the pathologists' workload and consequently the allocation of resources. The aim of the present study was to develop a model for measuring the pathologists' workload that can take into account the changes mentioned above. The diagnostic process was analyzed and broken up into separate activities. The time needed to perform these activities was measured. Based on linear regression analysis, for each activity, the time needed was calculated as a function of the number of slides or blocks involved. The total pathologists' time required for a range of specimens was calculated based on standard protocols and validated by comparing to actually measured workload. Cutting up, microscopic procedures and dictating turned out to be highly correlated to number of blocks and/or slides per specimen. Calculated workload per type of specimen was significantly correlated to the actually measured workload. Modeling pathologists' workload based on formulas that calculate workload per type of specimen as a function of the number of blocks and slides provides a basis for a comprehensive, yet flexible, activity-based costing system for pathology.

G. A. Meijer (✉) · J. J. Oudejans · J. J. M. Koevoets · C. J. L. M. Meijer
Department of Pathology, VU University Medical Center, Amsterdam, The Netherlands
e-mail: ga.meijer@vumc.nl

Keywords Pathology · Workload · Cost · Benchmarking

Introduction

To the outside world, including other hospital departments and hospital management, the pathology department often appears to function as a black box system with a specimen as input and a diagnosis as output. In reality, for each specimen, a complex number of activities are carried out at the macroscopic, microscopic, and molecular level. The kind and number of activities performed vary per type of specimen (e.g., liver biopsy, appendectomy, etc.), and are defined by protocols based on scientific evidence. Each of the individual activities (e.g., specimen reception, cutting up, microscopy, immunohistochemistry, electron microscopy, etc.) is to be carried out according to good laboratory practice (GLP) standards and requires the usage of resources like staff, consumables, and equipment. In turn, the type and amount of resources required varies per type of activity.

Obviously, the consumption of resources is not standard for each specimen, but depends on the type and number of activities required according to the protocol and carried out according to GLP guidelines.

Changes in types and numbers of specimens handled as well as changes of protocols (e.g., due to new clinical or scientific insights) will have direct consequences for workload. Successful management of a pathology laboratory requires a good insight in these processes and is essential for allocation of resources [1–5]. In the present study, we aimed to develop a model for measuring the pathologists' workload that can take into account such changes in types of specimens or protocols.

Materials and methods

Study design

The hypothesis tested was that pathologists' workload (i.e., the work within the scope of the diagnostic process) can be measured and defined in an activity-based manner. This requires measuring workload (i.e., average time spent on a specimen) for an adequate series of cases of each diagnostic category occurring in a pathology practice. For common specimen types (e.g., gall bladder resection, breast lumpectomy, etc.), this is feasible; for many other less common types of specimens, this is a problem. However, when for different types of specimens the actual activities performed are listed (e.g., macroscopy: reading clinical data, describing macroscopic aspect of specimen, measuring size and weight, taking pictures, sampling frozen material, cutting blocks, etc.) appear to be common to many specimen types, albeit in different combinations and magnitude. Taking this approach, the diagnostic process for all specimen types occurring can be analyzed and broken down into separate activities (i.e., a product breakdown). So, times were scored not as a total time per type of specimen, but time per product breakdown activity; and in this way, adequate sample sizes can be obtained for each of these defined activities. Both macroscopic and microscopic procedures were broken down to separate activities. This also included communication by phone on individual cases. Clinicopathological conferences were not included. Examples of items scored for macroscopy and microscopy are given in Table 1.

Next, a list of specimen types occurring in our laboratory was constructed. This list consisted of 91 organ sites. Specimens were considered to be either biopsies or resections, thus yielding 182 specimen types. Importantly, all pathology diagnoses in the Netherlands are registered in the nationwide pathology registry PALGA, including SNOMED like codes for organ site and type of specimen [6]. Therefore, all individual laboratories in this way already document these relevant production variables.

Measurements

Second, the time needed to perform the product breakdown activities was measured. To this end, on consecutive days during a period of 12 weeks, a time-scoring form was added to each specimen received that day, and during the complete diagnostic process (from the inspection of the gross pathology to the final authorization of the report) the time required for each product breakdown activity was scored. During cutting up, times were scored by an independent observer; while during microscopy, time was scored by the pathologist for each product breakdown activity using a stopwatch. Data were provided by eight consultant pathologists and eight registrars. Times for consultants and registrars were scored and analyzed separately. In total, approximately 700 forms, covering a period of 12 weeks, were received and analyzed. In total, times for 11,200 ($700 \times 2 \times 8$) product breakdown activities were scored.

Data analysis

Results of the measurements were entered in a specifically designed database. The data analysis aimed at finding a

Table 1 List of items in product breakdown of pathologists tasks that were scored individually for time needed during cutting up gross specimens and microscopy, respectively

Cutting up	
1	Analyzing and dictating clinical information
2	Consulting clinician
3	Consulting supervisor
4	Gross inspection and dictating
5	Specimen photography
6	Judging radicality of resection
7	Painting specimens
8	Dissecting resection margins
9	Taking frozen sample/biobanking
10	Weighing specimen
11	Simple total embedding
12	Split in half and embed
13	Lamellate/multiple blocks
14	Cut up and inspect
15	Prepare for overnight fixation/pin down specimen
16	Prepare for decalcification
17	Exploring specimen (e.g., for harvesting lymph nodes)
Microscopy	
1	Analyzing clinical information
2	Retrieving archival slides from the patient
3	Microscopy <5 slides H&E
4	Microscopy 5–10 slides H&E
5	Microscopy >10 slides H&E
6	Requesting additional stains
7	Microscopy of step sections
8	Microscopy of special stains
9	Microscopy of immunohistochemical stains
10	Electron microscopy
11	Quantitative pathology
12	Peer consultation, literature searches
13	Discuss case with clinician

Time was only scored when items occurred, not all items occurred in all cases. In cases where consultant pathologists supervised registrars, relevant items (e.g. microscopy items) were scored twice, i.e., when registrars evaluated slides on their own as well as during supervision by the consultant pathologist

relation between a specimen feature which is fixed (within certain limits) and the time cost per activity. The fixed variable used was the number of slides or tissue blocks. These data were based on the standard protocols used in our laboratory [7] and checked against the actual counting of the numbers of slides and blocks for the cases measured.

Using linear regression analysis, the relationship between the time needed for each activity, and the number of slides or blocks was analyzed. Based on this, for each activity, the time needed was calculated as a function of the number of slides or blocks involved, as prescribed by the protocol.

Given the calculated time per activity, the total pathologists' time required for a range of specimens was calculated based on the involved activities, again, as prescribed by the protocol.

To test the validity of this approach, for 22 specimen types that occurred with adequate frequency in the database, the correlation between these virtual specimen times and the actually measured times was computed. These 22 were biopsies of urinary bladder, bone marrow, uterine cervix, colon, rectum, endometrium, larynx, liver, stomach, duodenum, esophagus, breast, and prostate; and gross specimens of appendix, large intestine, gall bladder, lymph node, pancreas, ovary, placenta, prostate, and uterus. All statistical analyses were carried out using the SPSS 9.5 software.

Results

For all activities, significant correlations were found between the number of slides or the number of blocks and the time the pathologist needed for completing this activity. This was also the case in the situation where a pathologist was supervising a registrar. For instance, for the activities 'interpretation of H&E slides', 'interpretation of extra stains' (i.e. PAS, deeper, etc.), and 'interpretation of immunohistochemical stains' the time required appeared to be significantly correlated to the number of slides involved in these activities (Fig. 1a–c). Interestingly, the graph for interpretation of H&E sections slows a steeper

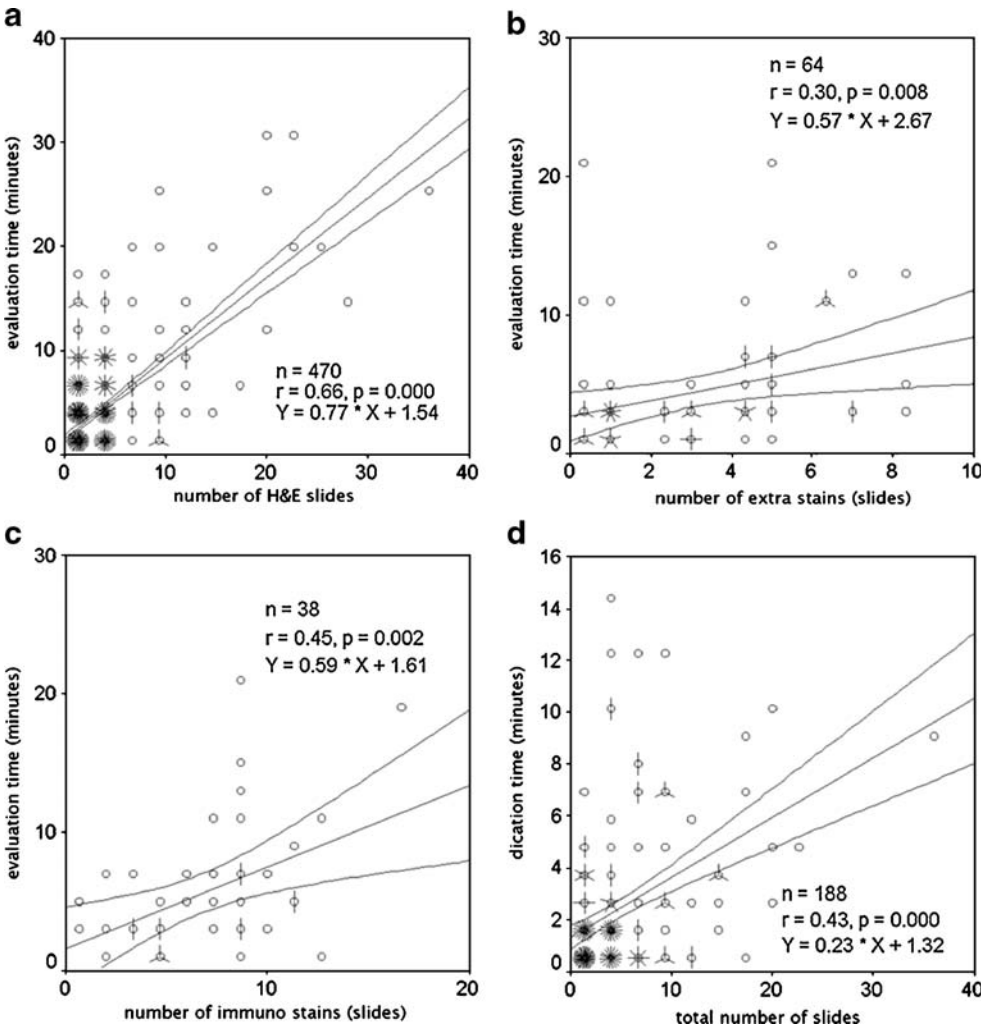

Fig. 1 Correlation between pathologist activities and number of slides involved. For the activities 'interpretation of H&E slides', 'interpretation of extra stains' (i.e. PAS, step sections, etc.), and 'interpretation of immunohistochemical stains' the time required appeared to be significantly correlated to the number of slides involved in these activities (Fig. 1a–c). The time required for report dictating includes validation (Fig. 1day). Time is indicated as minutes and refers to times calculated for pathologists working on their own. The fact that the regression lines intercept the Y-axis at values>0 reflects the start-up time involved when beginning a new task. Similar analyses were performed for situations where pathologists supervised registrars (not shown)

slope than the graphs for extra stains and immunohistochemical stains. This can be explained by the fact that when judging these latter stains, morphology of the lesions is already familiar to the pathologist from the H&E sections and time is mainly spent on scoring histochemical or immunohistochemical features, which takes less time per slide. The time required for 'report dictating' was significantly correlated to the total number of slides per case (Fig. 1d).

Then, as described above, for all organs (as far as practically relevant), the virtual total pathologists' time involved was calculated from the regression function for each activity, and this result was multiplied with a factor that corrected for the frequency with which each activity occurred for every individual type of specimen. For example, in our laboratory, immunohistochemistry was applied in 10% of colorectal biopsies with an average of five slides. So, on average, for colorectal biopsies, the time involved for the activity 'evaluating immunohistochemical stains' is given by the equation $0.10 \times 5 \times A+B$, where A=the factor of the regression function and B the constant. Another example are bone marrow biopsies where immunohistochemistry is performed in 95% of cases with an average of eight markers and one negative control, which gives $0.95 \times 9 \times A+B$.

For 22 specimen types, enough actual measurements were present in the database to compare the calculated 'virtual pathologists' time' needed to evaluate and report a specimen with the times actually measured. Again, with linear regression analysis, the calculated times showed a high correlation with the actually measured total interpretation times. This was true for specimens that were handled by a consultant alone, and for specimens that were handled by a registrar who was supervised by a pathologist (Fig. 2a–b).

Discussion

Successful management of a pathology laboratory requires a good insight in these processes and is essential for allocation of resources. This insight is difficult mostly because pathologists find it difficult to obtain a realistic and quantitative economical perception of their everyday diagnostic practice. However, obtaining good insight is essential in particular in a period of increasing complexity of lab organization and technical processes with increasing costs. Here, we describe a comprehensive yet flexible approach for activity-based cost modeling that provides this insight in these processes and may be of help in mastering increasing budget constraints.

Knowledge of the workload that is involved with the products delivered is one of the basics of enterprise resource planning. Pathologists do not tend to regard their diagnostic reports as products, but from a management perspective, it is well defensible to compare the diagnostic process with a production process. From the specimen as raw material, using multiple resources, the pathologist makes a diagnosis, the end product. While nowadays, on one hand, the resources available are limited by budget constraints, the input (specimens) is not, neither in number nor in complexity. This may lead to serious budgetary problems. Budget control then is essential but this requires accurate information on the consumption of resources.

Medicine is a rapidly evolving profession, and this certainly goes for pathology. Several causes can be identified for the increase of pathologists' workload in the recent past. These include an increase in number of presented specimens as a result of an aging population with more possible cancer patients, and an ever increasing arsenal of diagnostic procedures available to the clinician continues to increase, and many of these, like new

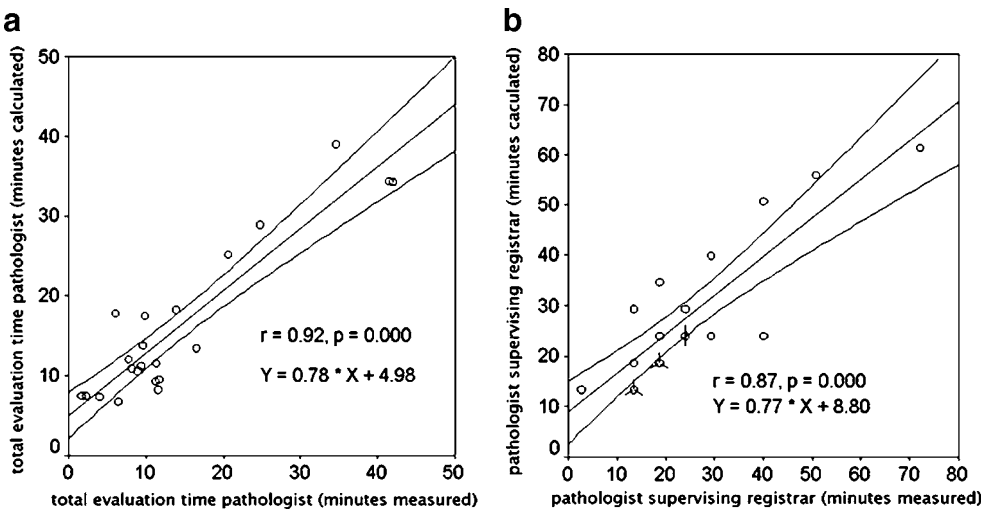

Fig. 2 Validation of calculated time consumption versus actually measured time consumption. For 22 specimen types enough actual measurement were present in the database to compare the calculated 'virtual pathologist's time' with the actually measured times. The calculated times showed a high correlation with the actually measured times, both in the case the specimens were handled by a pathologist alone, as well as in those cases where the specimens were handled by a registrar who was supervised by a pathologist (Fig. 2a–b)

endoscopic techniques, allow for taking biopsies. In addition, rapid advances in biomedical science have tremendously increased our understanding of the biology of disease with considerably implications for clinical practice. A most prominent example is the development of targeted therapies in oncology (e.g., against *her2neu*, *egfr*, and *c-kit*), which require dedicated diagnostic procedures like immunohistochemistry, in situ hybridization, and mutation analysis. As a result, diagnostic reports become increasingly complex which leads to increasing demand for interdisciplinary meetings of clinicians and pathologists for discussing these cases.

Approaches to measuring pathologists' workload

The most simple approach is by just counting the number of specimens handled per period, but this has serious limitations. With an increase of laborious specimens, as discussed above, and a decrease of simple specimens, the total number of specimens may remain stable while the consumption of pathologists' resources has considerable increased. Also systems counting different diagnostic categories have their limitations [2, 4]. Such trends can be detected when consumption of resources is measured in a differentiated way. Here, we present an activity-based, differentiated method to measure pathologists' labor, which is one of the major resources used in diagnostic pathology.

A protocol-based pathology practice, as is common in many institutions, enables to split the diagnostic process associated with different types of specimens in common activities, i.e. a product break down. However, in the same way as protocols should not be applied too rigidly, leaving room for a certain variation in the individual case and the individual pathologist, a workload measuring or costing system should be able to cope with variation. The system presented here was based on measuring a large number of cases handled by 16 different pathologists and registrars, thus covering a large variation in cases and pathologists. The results of the calculated workload correlated very well with the actual measurements, for individual activities as well as complete cases.

It should be noted, however, that the present study only focused on pathologists' workload, which in itself is largely insufficient to calculate a global budget of a lab. This requires an integrated approach that takes into account information on other resources (e.g., other staff like technicians, and secretaries, equipment, and consumables), to generate a model that, when fed with data of the actual numbers of the different types of specimens handled, can compute the theoretical budget in terms of staff, consumables, and equipment required to do the job. These data can be compared with the allowed budgets and the results could facilitate an optimized management of the pathology department.

Of course, real life is always more complicated than a simple computer model, but the aim of the current approach is not to produce virtual reality, but rather to have an adequate tool for workload and cost measurement in pathology. The method presented here is more flexible than the more classical approach of classifying cases in range groups of diagnoses, as is common in a number of countries. With the presented method, a change in the protocol is immediately reflected in the final calculations.

For implementing the presented approach in interested laboratories, several conditions should be met. The method used requires the coding of specimens. In our laboratory, histopathology specimens are coded according to site or organ (using a limited thesaurus) and type of procedure. As to the latter, we only use biopsy or resection. It turned out that in this way, the variation of workload within a certain type specimen was limited for almost all types of specimens. The major exception was skin pathology that showed a large variation in workload per specimen, and this variation did not segregate with biopsy or resection. To handle this point, skin specimens were divided in four groups (simple (naevi, basal cell carcinoma, etc.), inflammatory skin diseases, difficult differential diagnoses between benign and malignant, larger resection specimens (not difficult but many slides), and the mean workload for each group was calculated. Within these four groups, variation in workload per case was only limited. Moreover, groups 2 to 4 showed similar results so these could be taken together, leaving a group with "easy" skins and a group with "difficult" skins. For all four groups, again, a good correlation was found between the measured and calculated figures. To still allow the overall calculation of workload, an average time for skin specimens can be used applying a correction factor for the ratio of "easy" and "difficult" skins in a given department.

Limitations of the present approach

The present approach focused on measuring pathologists' workload, which is the production component that is most difficult to quantify. However, in itself, this is insufficient to calculate a global laboratory budget. For an adequate calculation of costs, it is also necessary to take into account the idle time lost during a working day. In an activity-based costing system, like the one presented here, this is not automatically included, in contrast to the "total absorption"-based costing systems that primarily aim at recovering all costs made, but that are less suitable to detect changes in workload. So, in an activity-based costing system, a correction has to be included for idle time, e.g., by using a factor for the overall percentage of idle time. In addition, apart from surgical pathology, also other pathology tasks like cytology, autopsies, conferences, teaching, and re-

search needs to be covered by the system. This can be done in way similar to that applied for surgical pathology. In principle, the methodology we used for calculating pathologists' workload can be implemented in every interested laboratory. The product breakdown items scored are listed in Table 1. The work reported here is limited to surgical pathology but we have applied similar strategies to cytology and post-mortem pathology (unpublished results).

In conclusion, we present an activity-based approach to measure pathologists' workload in surgical pathology that can be used as basis of a costing system. By applying formulas that calculate workload per type of specimen as a function of the number of blocks and slides, based on standard protocols, a reliable estimation of pathologists' workload per type of specimen can be made. With this approach, including also data on other resources like non-pathologist staff, consumables, and equipment, it is possible to have a comprehensive, yet flexible, activity-based costing system.

Acknowledgments The pathologists and registrars of the Department of Pathology, VU University Medical Center are acknowledged for their participation in performing the workload measurements.

Conflict of interest statement We declare that we have no conflict of interest.

References

1. Freeman R (2002) Microbiology workload. J Clin Pathol 55:734
2. Parham DM (1996) The hidden increase in histopathologists' workload. J Clin Pathol 49:689–690
3. Riordan T, Cartwright K, Logan M et al (2002) How do microbiology consultants undertake their jobs? A survey of consultant time and tasks in South West England. J Clin Pathol 55:735–740
4. Tarbit IF (1990) Laboratory costing system based on number and type of test: its association with the Welcan workload measurement system. J Clin Pathol 43:92–97
5. Bellocq JP, Biron N, Kessler S et al (2001) Activity and cost analysis in surgical pathology. Experience of a French university laboratory using the activity-based costing method. Ann. Pathol. 21:215–232
6. Casparie M, Tiebosch AT, Burger G et al (2007) Pathology databanking and biobanking in The Netherlands, a central role for PALGA, the nationwide histopathology and cytopathology data network and archive. Cell Oncol 29:19–24
7. Anonymous (1995) Protocollenboek pathologie. Department of Pathology, Free University Hospital, Amsterdam, The Netherlands

Virchows Arch (2009) 454:629–637
DOI 10.1007/s00428-009-0769-z

ORIGINAL ARTICLE

Altered expression of CD44 and DKK1 in the progression of Barrett's esophagus to esophageal adenocarcinoma

T. Darlavoix · W. Seelentag · P. Yan · A. Bachmann · F. T. Bosman

Received: 30 December 2008 / Revised: 26 March 2009 / Accepted: 30 March 2009 / Published online: 25 April 2009

Abstract Barrett's esophagus (BE) is an acquired condition in which the normal lining of the esophagus is replaced by intestinal metaplastic epithelium. BE can evolve to esophageal adenocarcinoma (EAC) through low-grade dysplasia (LGD) and high-grade dysplasia (HGD). The only generally accepted marker for increased risk of EAC is the presence of HGD, diagnosed on endoscopic biopsies. More specific markers for the prediction of EAC risk are needed. A tissue microarray was constructed comprising tissue samples from BE, LGD, HGD, and EAC. Marker expression was studied by immunohistochemistry using antibodies against CD44, DKK1, CDX2, COX2, SOX9, OCT1, E-cadherin, and β-catenin. Immunostaining was evaluated semi-quantitatively. CD44 expression decreased in HGD and EAC relative to BE and LGD. DKK1 expression increased in HGD and EAC relative to BE and LDG. CDX2 expression increased in HGD but decreased in EAC. COX2 expression decreased in EAC, and SOX9 expression increased only in the upper crypt epithelial cells in HGD. E-cadherin expression decreased in EAC. Nuclear β-catenin was not significantly different between BE, LGD, and HGD. Loss of CD44 and gain of DKK1 expression characterizes progression from BE and LGD to HGD and EAC, and their altered expression might indicate an increased risk for developing an EAC. This observation warrants inclusion of these immunohistochemically detectable markers in a study with a long patient follow-up.

Keywords Barrett's esophagus · Esophageal adenocarcinoma · Dysplasia

T. Darlavoix
Academic Medical Center, University of Amsterdam, Amsterdam, The Netherlands

W. Seelentag
Unilabs Lausanne-Cypa, Laboratory of Cytology and Pathology, Lausanne, Switzerland

P. Yan · A. Bachmann · F. T. Bosman (✉)
University Institute of Pathology, University of Lausanne, Rue du Bugnon 25, 1011 Lausanne, Switzerland
e-mail: fred.bosman@chuv.ch

Introduction

Barrett's esophagus (BE) is an acquired condition defined as the replacement of normal stratified squamous epithelium by metaplastic columnar epithelium in the distal esophagus [1–3]. BE is acquired due to prolonged gastro-esophageal reflux disease (GERD) which is increasing in incidence [4]. BE is a preneoplastic condition as it predisposes to the development of esophageal adenocarcinoma (EAC) via progression along low-grade dysplasia (LGD) and high-grade dysplasia (HGD). EAC is rapidly increasing in the western world; the incidence has increased over 70% in the last 20 years [5]. Almost without exception, EAC develops in BE [6] and, therefore, early recognition of this condition and endoscopic follow-up are potentially effective ways to prevent EAC.

BE evolves into EAC stepwise through increasing grades of dysplasia. As yet, the marker used for clinical decision making on eventual therapeutic intervention in a BE patient is the presence of HGD in endoscopic biopsies (during the follow-up of BE patients or a newly diagnosed GERD patient). In the presence of HGD, the patient runs a risk of over 40% to develop an EAC, and HGD is therefore an indication for an intervention, which used to be esophagectomy, but lately, more conservative approaches

such as photodynamic therapy or mucosectomy have been developed [7, 8]. An important problem, however, is that of all patients with BE, only about 0.5% per year will eventually develop an adenocarcinoma [9]. A large number of patients are therefore kept under surveillance for the detection of a relatively small number of cancers. Consequently, markers are needed for the prediction of cancer risk in BE patients before HGD has developed.

Various attempts have been made to identify markers that can predict whether or not a BE patient will develop an EAC. Approaches chosen have included morphometry, cell adhesion molecule expression, DNA ploidy analysis, loss of heterozygosity at the chromosomal level, p53 mutations and immunohistochemical overexpression, proliferative activity (through immunohistochemical staining of the Ki-67 antigen), p16 anomalies (including promoter methylation, mutations, and loss of heterozygosity), activation of the Wnt pathway (through adenomatous polyposis coli mutations, β-catenin mutations, or one of the other players in Wnt signaling), analysis of patterns of promoter methylation, and more [10–16]. Although a voluminous literature exists on this subject, as yet, the only clinically used biomarker with a high predictive value is the presence of HGD [10].

In this study, we addressed this problem by examining the expression of genes involved in the Wnt pathway, Wnt downstream genes and key homeobox signaling pathway genes in the normal esophagus, BE with and without dysplasia, and EAC. The genes included in the study were selected based on their involvement in directing differentiation, including tissue architecture, in the gastrointestinal tract. The importance of these genes in gastrointestinal cancer has been repeatedly stipulated but almost never in BE or in EAC [13, 17–23]. Their expression was studied in retrospectively collected tissue samples selected from surgical resection specimens. The potentially predictive markers must subsequently be validated in a study on Barrett patients with long-term follow-up.

Materials and methods

Selection of cases

The cases selected concerned a consecutive series of esophagectomy specimens received by the University Institute of Pathology in Lausanne, diagnosed as EAC between 1995 and 2007 (52 cases). Cases with insufficient tissue available (either having been used in previous studies or used in the diagnostic work-up) were excluded. In all, 44 cases were available for study. After re-assessment of the diagnosis by two experienced pathologists (WS and FB), 31 cases were retained based upon the following criteria: presence of at least one or more areas of adenocarcinoma and/or HGD and/or LGD and/or intestinal metaplasia. The use of human tissues in this study was according to the criteria for the use of archival specimens as established by the local ethics review board.

Tissue microarray creation

Tissue samples to be included in the tissue microarray (TMA), notably with EAC, HGD, LGD, and BE, were identified on H&E stained tissue sections. From the 31 cases, 122 different tissue samples were included. Control tissue samples included in each TMA block comprised samples randomly selected from surgical resection specimens (normal ileum, normal duodenum, normal colon, normal esophagus, adenocarcinoma of the colon, and diffuse type and intestinal type adenocarcinoma of the stomach).

The TMAs were created in paraffin-embedded blocks of 2% agarose (Sigma A5093) mounted on a cassette using a manual TMA maker (Beecher Instruments Inc., Sun Prairie, WI, USA), as described previously [24]. Each TMA consisted of a 6×7 grid of 2 mm cores, allowing up to 41 tissue cores per TMA (one varying position was left empty for TMA recognition and proper orientation). Overall, four TMA blocks were constructed including 158 cores (64 EAC, 17 HGD, 19 LGD, and 22 BE samples and 36 control tissue samples). Sections (4 μ) were cut, stretched on a 56°C water bath, and mounted on SuperFrost Plus microscope slides (Menzel GmbH & Co KG, Braunschweig, Germany). On one H&E stained section, a final reference diagnosis was made for each tissue core (WS and FTB); this diagnosis was used in the study.

Selection of antibodies

Our selection of the target proteins was based upon the hypothesis that Wnt signaling and Wnt downstream genes play a key role in EAC development, in analogy to gastric and colorectal cancer. A first selection was made on the involvement of Wnt target genes in human gastrointestinal carcinogenesis as mentioned on the Wnt homepage (http://www.stanford.edu/~rnusse/wntwindow.html). A final selection was made based upon the published literature supporting potential involvement of the various proteins in gastrointestinal mucosa differentiation or in intestinal carcinogenesis [13, 18, 19, 25–31] and on the available antibodies applicable to routinely processed tissue specimens. As a readout protein for Wnt pathway activation, nuclear localization of β-catenin was used. As Wnt downstream proteins, we chose CD44, COX2, E-cadherin, CDX2, DKK1, and SOX9. Two homeobox proteins (CDX2 and OCT1) were included in the study, based on earlier reports indicating involvement of these proteins in intestinal metaplasia/dysplasia [21, 25, 30, 31].

Immunohistochemistry

Immunohistochemistry (IHC) was performed either manually or using an automated system (as indicated in Table 1). The choice of using one system or the other was based upon the quality of the staining obtained, some antibodies requiring a specially adapted protocol not easily adaptable to the staining machine.

Manual immunoperoxidase staining was performed, after dewaxing, quenching of endogenous peroxidase activity (by incubation with 3% hydrogen peroxide in demineralized water for 5 min), and antigen retrieval (2 min in a pressure cooker in ethylenediaminetetraacetic acid (EDTA) buffer, pH 9.0), using Envision+ (DAKO, Glostrup, Denmark) as detection system [24]. Exposure to primary antibodies, diluted as indicated in Table 1, was 2 h at room temperature. Visualization was performed with diaminobenzidine tetrachloride as chromogen. Sections were counterstained with hematoxylin.

Automated IHC was performed using the Bond IHC stainer (Vision BioSystems, Mount Waverley, Australia) with as secondary reagent, anti-goat Histofine max polymer (Nichirei Biosciences, Tokyo, Japan). Key program sequences were antigen retrieval (with EDTA buffer pH 9.0 for 20 min at 95°C or citrate buffer pH 9.0 for 20 min at 100°C), primary antibody incubation for 30 min, and incubation with the polymer kit for 15 min. In all experiments, negative control incubations (omission of the primary antibody) and positive control tissues were included.

Assessment of immunoreactivity

The immunoreactivity was microscopically evaluated independently by two observers (WS and PY) in terms of the percentage of cells stained (in deciles). Given the zonal architecture of BE mucosa, the percentage of positive cells was noted separately for the upper crypt half and the lower crypt half in BE, LGD, and HGD but only as a percentage of all cells in EAC. No major discrepancies occurred between the two assessors; the mean of the two assessments was used for statistical calculations.

Data was entered in SPSS version 15.0 for Windows (SPSS Inc., Chicago, IL, USA), and descriptive analysis was undertaken, together with a one-way ANOVA test to assess statistical significance between the values obtained for localization and diagnostic category. For comparison between BE, LGD, and HGD, upper and lower crypt half were considered separately. For comparisons with EAC, the highest (either upper of lower) crypt value was used. Differences between diagnostic categories were analyzed using Tukey's honestly significant difference post hoc test, graphically visualized by box-plot graphs. In the graphs, for the sake of clarity, outliers have been indicated separately (with the symbols *white circle* or *filled star* in the figures, the numbers referring to the outlying sample number), but the data points were included in the statistical calculations. The number of samples available precluded the use of validated statistical approaches (receiver operating characteristic (ROC) analysis) to determine eventual cut-points. To explore potential diagnostic use of these markers, we arbitrarily chose 30% loss of CD44 (absence of membranous immunostaining in at least 30% of the cells) and 30% gain of DKK1 (cytoplasmic staining of at least 30% of cells) as cut-points.

Results

The results obtained by scoring of the immunostained TMAs are illustrated in the figures and summarized in Table 2. We will briefly describe immunoreactivity patterns per studied antigen.

CD44 and DKK1

In general, CD44 immunoreactivity was found on the plasma membrane of epithelial cells. A minority of the

Table 1 Antibodies used with their dilution, antigen retrieval method, and immunohistochemistry method

Antigen	Source	Clone	Species	Concentration	IHC method
ß-catenin	Novocastra	17C2	Mouse	1:100	A
CD44	CHUV	Wild-type PCA	Mouse	1:50	A
COX2	Cayman	synth pept	Mouse	1:1,000	B
DKK1	Lifespan	PCA	Rabbit	1:100	B
E-cadherin	DAKO	NCH-3.8	Mouse	1:40	A
CDX2	Novocastra	AMT28	Mouse	1:50	A
OCT1	LabVision	PCA	Rabbit	1:50	A
SOX9	Chemicon	PCA	Rabbit	1:400	A

A: manual Envision system (DAKO, Glostrup, Denmark), heat-induced epitope retrieval: pressure cooker 2 min EDTA pH 9.0

B: bond automated IHC system (Vision BioSystems, Mount Waverley, Australia), heat-induced epitope retrieval in EDTA pH 9.0

PCA polyclonal antibody

Table 2 Semiquantitative results of immunohistochemical staining

Antibody		BE		LGD		HGD		EAC		*p* value	Significant between diagnoses
		Mean	SD	Mean	SD	Mean	SD	Mean	SD		
CD44	Crypt	86	18	85	13	53	30			<0.001	BE and LGD vs HGD
	Upper	44	33	46	36	40	36			0.843	
	Total	86	18	85	13	47	36	48	37	<0.001	BE and LGD vs HGD and EAC
DKK1	Crypt	19	12	21	20	49	28			0.001	BE and LGD vs HGD
	Upper	11	13	19	26	29	33			0.084	
	Total	16	15	21	25	35	37	51	35	<0.001	BE and LGD vs EAC
CDX2	Crypt	50	27	59	23	61	26			0.264	
	Upper	32	25	43	33	63	23			0.005	BE vs HGD
	Total	48	28	48	33	66	23	33	34	0.002	HGD vs EAC
OCT1	Crypt	33	26	42	28	47	27			0.320	
	Upper	20	23	26	28	32	30			0.349	
	Total	28	29	35	31	41	32	29	30	0.446	
SOX9	Crypt	95	4	94	2	95	5			0.720	
	Upper	81	11	79	21	93	5			0.010	BE and LGD vs HGD
	Total	95	4	89	22	96	4	89	15	0.100	
COX2	Crypt	93	15	93	21	94	12			0.982	
	Upper	91	14	90	23	96	10			0.582	
	Total	95	8	93	21	96	10	73	24	<0.001	BE, LGD, and HGD vs EAC
E-cadherin	Crypt	100	1	100	0	100	0			0.480	
	Upper	100	1	100	0	100	0			0.490	
	Total	100	1	100	0	100	0	79	31	<0.001	BE, LGD, and HGD vs EAC
β-catenin	Cytoplasm	97	11	96	18	72	33	63	34	<0.001	BE and LGD vs EAC
	Nuclear	0	0	1	3	1	3	6	14	0.150	

Results of descriptive and statistical analysis for obtaining *p* values using ANOVA test. A Tukey's honestly significant difference post hoc test was performed for assessing the significance of the differences between diagnoses. As statistically significant, we considered $p<0.05$. Mean and SD values are noted in percentages

epithelial cells expressed CD44 circumferentially; the vast majority showed focal membrane expression. Stromal cells also stained strongly but were not included in the cell count. Significant loss of CD44 staining of crypt epithelial cells was found in HGD in comparison with BE and LGD (Fig. 1a–c). This was also found for CD44 staining in HGD and EAC vs BE and LGD, as graphically illustrated in Fig. 1d.

DKK1 stained the cytoplasm with appreciable differences in intensity between samples. EAC showed more intense immunoreactivity (Fig. 2a–c). More lower crypt cells expressed DKK1 in HGD than in BE and LGD. In EAC, strong diffuse cytoplasmic immunoreactivity was noted. Overall, DKK1 expression was significantly higher in HGD and EAC than in BE and LGD (Fig. 2d; Table 2).

Given the consistent differences in CD44 and DKK1 expression notably between LGD and HGD, we chose as arbitrary cut-points 30% loss of CD44 and 30% gain of DKK1 expression. With these parameters, the combination of loss of CD44 and gain of DKK1 was only found in HGD samples but with low (29%) sensitivity for HGD (Table 3). Altered expression of at least one marker attained high specificity and sensitivity (94% and 80%, respectively).

CDX2

CDX2 was only expressed in the nuclei of epithelial cells. EAC often stained diffusely. CDX2 expression was significantly higher in upper crypt epithelium in HGD than in upper crypt epithelium in BE (Fig. 3a–c; Table 2). Overall, CDX2 expression was significantly lower in EAC than in HGD (Fig. 3d; Table 2).

SOX9

SOX9 showed a nuclear staining pattern with limited variation between tissue samples. In some HGD cases, strong SOX9 staining was noted in upper crypt epithelium (Fig. 4a, b). SOX9 expression was not strikingly increased in each HGD case but, overall, significantly higher in HGD than in BE or LGD (Fig. 4c).

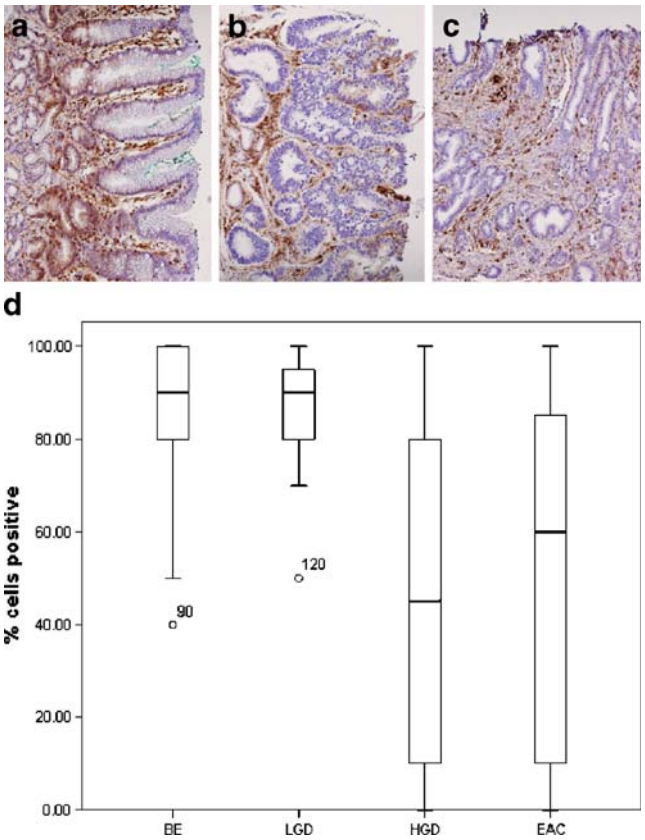

Fig. 1 CD44 staining in BE (a), HGD (b), and EAC (c). Crypt cells in BE show strong membranous staining, which is lost in HGD and EAC. Note that stromal cells also show CD44 immunoreactivity. **d** Box plot of the percentage of CD44 positive cells per diagnostic category (BE and LGD vs HGD and EAC, $p<0.001$)

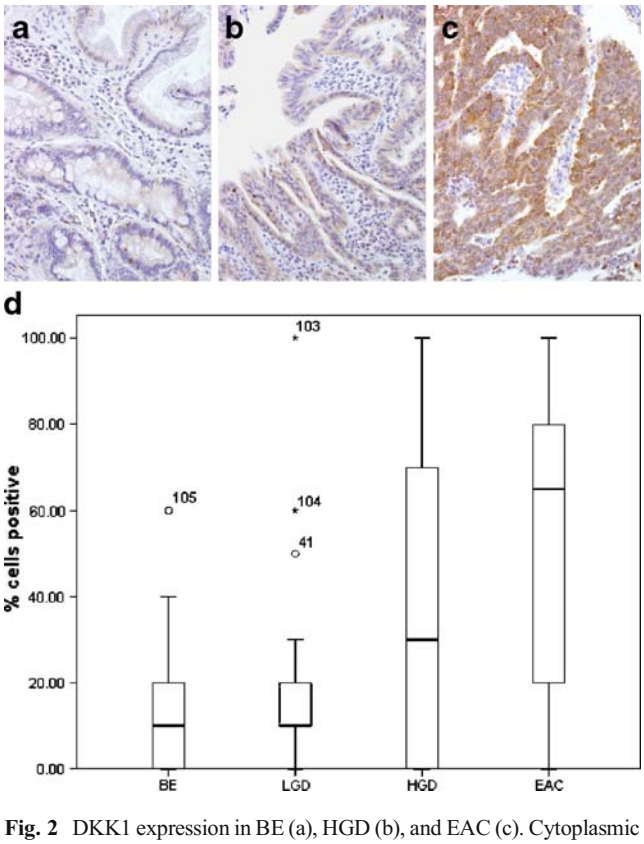

Fig. 2 DKK1 expression in BE (a), HGD (b), and EAC (c). Cytoplasmic DKK1 expression was focal and weak in BE, more widespread in HGD, and strong in EAC. **d** Box plot of percentage of cells expressing DKK1 per diagnostic category (BE and LGD vs EAC, $p<0.001$)

COX2

COX2 showed strong immunoreactivity in the cytoplasm of epithelial cells (Fig. 5a, b). In EAC, expression was lower (Fig. 5c). In BE, LGD, and HGD, COX2 expression was significantly higher than in EAC (Fig. 5d). COX2 was also expressed in inflammatory cells, notably macrophages, but this was not taken into account in scoring the results.

OCT1

OCT1 was expressed in nuclei of epithelial and stromal cells. In BE, crypt cell nuclei were most intensely stained. Significant differences were not noted between LGD and HGD or EAC (data not shown).

E-cadherin

E-cadherin was strongly immunostained with a membranous pattern in all samples with the exception of EAC. In EAC, staining was decreased and very heterogeneous (data not shown), some areas retaining E-cadherin expression and others with complete loss. In the invasion front in EAC, individual invasive cells did not show membranous staining but occasionally cytoplasmic staining.

Table 3 Sensitivity and specificity of CD44 loss and DKK1 gain for the differentiation between LGD and HGD

Marker expression	Histology		
	HGD	LGD	Total
CD44L/DKK1G	5	0	5
CD44L/DKK1N or CD44N/DKK1G	11	4	15
CD44N/DKK1N	1	15	16
Total	17	19	36

CD44L=CD44 loss (more than 30% of cells)
CD44N=normal pattern of CD44 expression
DKK1G=gain in DKK1 expression (more than 30% of the cells)
DKK1N=less than 30% DKK1 expression
Specificity of CD44L/DKK1G for HGD 5/5=100%
Sensitivity of CD44L/DKK1G for HGD 5/17=29%
Specificity of at least one aberrant marker for HGD 16/17=94%
Sensitivity of at least one aberrant marker for HGD 16/20=80%
Specificity of CD44N/DKK1N for LGD 15/19=79%

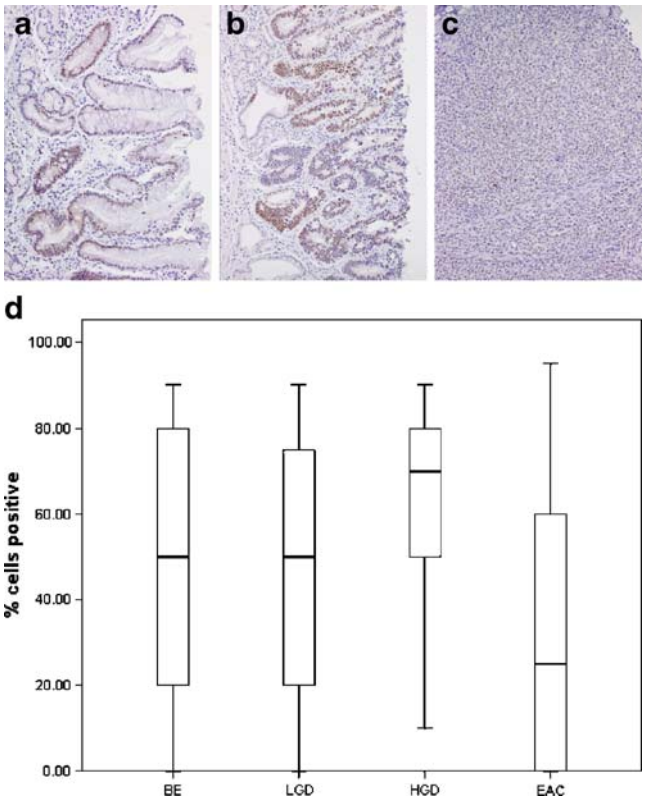

Fig. 3 CDX2 expression in BE (a), HGD (b), and EAC (c).Nuclear expression was observed in BE in the crypt epithelium, extending to upper crypt epithelium all the way to the surface in HGD. CDX2 expression was decreased in EAC. **d** Box plots of the percentage of CDX2 positive cells per diagnostic category (BE vs HGD, $p=0.005$; HGD vs EAC, $p=0.002$)

β-catenin

In BE and LGD, strong membranous staining was found. BE and LGD showed a higher percentage of β-catenin positive cells than EAC. Nuclear staining was found almost exclusively in EAC (Fig. 6). Statistical analysis indicated a significant decrease in membranous β-catenin expression in EAC (Table 2).

Discussion

The aim of this study was to identify proteins that show altered expression during the progression of BE to EAC, with as final goal the definition of markers that will allow the identification of BE patients with a high risk for EAC development. Gene expression profiling studies with this aim have been published [32] but, as yet, have not resulted in significant progress.

In the design of the study, several elements merit brief consideration. Firstly, the choice of the material studied: we conducted the study on a limited number of tissue samples (122) from 31 patients. We do not consider the small number of patients an important limitation in our study, as the intention was to identify promising markers rather than validating them in a long-term follow-up case control approach. Therefore, the endpoint we used was not patient outcome but histological diagnosis per sample. Further studies would have to include BE and LGD samples from patients who did not develop HGD or EAC.

A second consideration is our choice to score immunoreactivity in BE, LGD, and HGD separately in the lower and the upper crypt. This division is somewhat arbitrary and could be subject to inter-observer variation. We attempted to improve the reproducibility of the scoring results through implication of two independent observers. These obtained very similar results, confirming the reliability of our observations. A further consideration is the way we compared BE, LGD, and HGD with EAC. As in EAC, mucosal architecture is completely lost, rendering lower and upper crypt scores without meaning; we compared scores in EAC with the highest score (either upper crypt or lower crypt) in LGD and HGD for our statistical evaluations. We

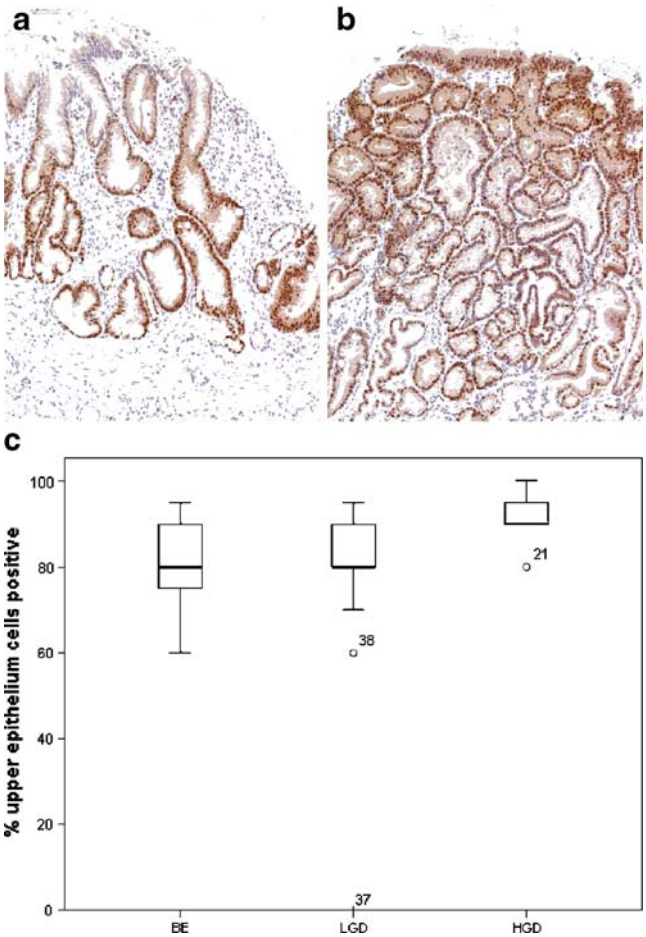

Fig. 4 Nuclear SOX9 expression was observed in BE mainly in the lower crypt region (a) but in HGD, extended all the way to the surface (b). **c** Box plot of the percentage SOX9 positive cells per diagnostic category (BE and LGD vs HGD and EAC, $p=0.01$)

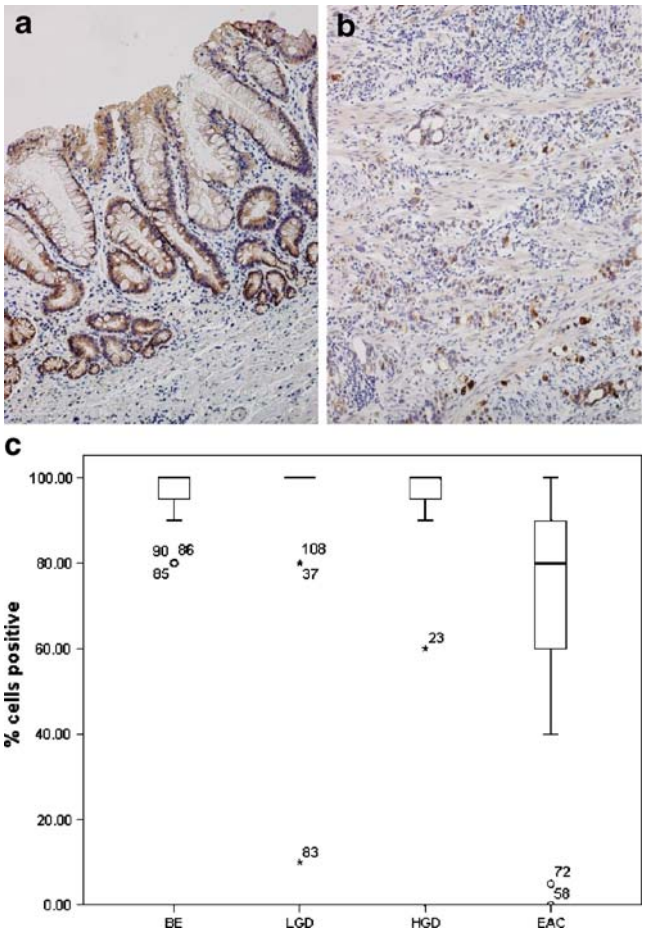

Fig. 5 Diffuse cytoplasmic COX2 expression was found in BE (a), LGD, and HGD. The percentage of COX2 positive cells was decreased in EAC (b). **c** Box plot of the percentage of COX2 positive cells per diagnostic category (BE, LGD and HGD vs EAC, $p<0.001$)

deem this justified as no important differences were noted when the mean of the two values was used.

Finally, we scored immunoreactivity as a continuous variable rather than in terms of positive or negative, as cut-points could not be established using validated statistical approaches (e.g., ROC analysis). Using this experimental design, we found the expression of several of the studied markers to differ significantly between BE, LGD, HGD, and EAC. Taking as an arbitrary cut-point 30% loss of CD44 and 30% gain of DKK1 expression, the combination of these two markers seems promising.

CD44 and DKK1

CD44 has been extensively studied in colorectal cancer [33] and, also, in BE where decreased expression of wild-type CD44 in glandular epithelium was reported [34, 35] with a shift from focal in BE to more diffuse in BE with dysplasia. We found wild-type CD44 expression to have significantly decreased in the crypt base epithelium only in HGD, which is in contrast to the findings of Menges et al. [35, 36]. Also, in EAC, we noted a decreased level.

Dickkopf-1 (DKK1) is a Wnt antagonist protein that specifically inhibits Wnt canonical signaling by interacting with the co-receptor Lrp-5/6 and, thus, prevents Wnt and Frizzled from forming a ternary complex with Lrp-5/6 [37]. Expression of members of the DKK1 family has been studied before in colorectal cancer, showing a differential expression pattern between normal colon epithelium and colorectal cancer [29]. However, epigenetic silencing of DKK1 has been reported in colorectal cancer [38, 39]. DKK1 has been studied before in reflux esophagitis and in BE but not in EAC [40]. We found DKK1 expression to have increased significantly in HGD and EAC in comparison with BE and LGD. This result is counterintuitive, as silencing of its repressor conceptually should to go along with activated Wnt signaling. Overexpression of a repressor could, however, also signify activation downstream of its site of action, sustained expression being the result of a defective feedback loop. It has in addition been reported that DDK1 may inhibit tumorigenesis through Wnt pathway independent mechanisms.

In all, loss of CD44 and gain of DKK1 expression might be taken as indicators of the progression from LGD to HGD. This is a novel finding and warrants detailed study, including confirmation by western blotting and reverse transcription polymerase chain reaction, as a marker for progression of BE to EAC.

CDX2, OCT1, SOX9, and COX2

The caudal-related homeobox gene CDX2 encodes an intestine-specific transcription factor crucial for the regulation of differentiation of intestinal cells [21]. Immunostaining of CDX2 has been proposed as a useful marker for the identification of intestinal metaplasia in BE [15, 25, 31, 41]. Overall, we observed increased CDX2 expression in

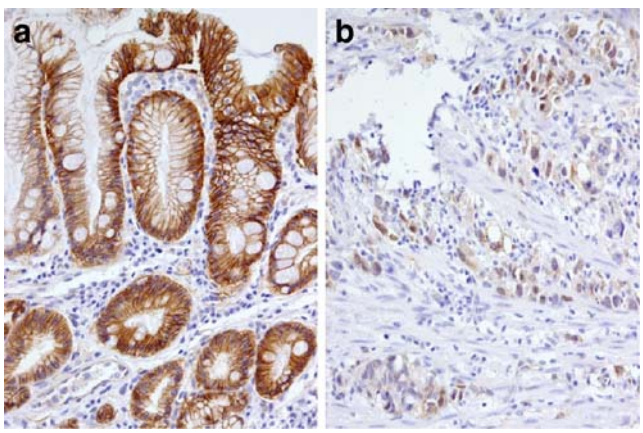

Fig. 6 β-catenin expression shows a strong membranous immunostaining pattern in BE (a) but a nuclear staining pattern in EAC (b)

HGD relative to BE and LGD, which then decreases in EAC. The widely varying values in individual cases preclude the use of CDX2 for the diagnosis of HGD. Our observations match those of Villanacci et al. [25]. It has been reported that CDX2 expression is modulated by OCT1, but we did not find OCT1 expression to differ significantly between the diagnostic categories, suggesting that the changes in CDX2 expression we observed are not due to concomitant changes in OCT1 expression, as previous research suggests [21]. How CDX2 and OCT1 interact remains largely unclear, and more research on this subject has to be conducted.

SOX genes constitute a family of transcription factors, belonging to a super-family known as the high mobility group box and play an important role in, among others, the development of the intestinal tract [42]. SOX9 has been reported to be regulated by the Wnt pathway, and it represses CDX2 expression in intestinal crypts [43].

We found SOX9 expression to have slightly but significantly increased in upper crypt epithelium in HGD. For SOX9 and CDX2 to both show increased expression in the upper crypt epithelium in HGD was an unexpected result, given the repressive influence of SOX9 on CDX2 expression [43]. In the regulation of CDX2 expression, evidently, other factors than only SOX9 are involved. The wide variation in expression of SOX9 in individual cases precludes its use for diagnostic purposes.

COX2 was shown to be functionally active in BE since treatment with COX2 inhibitors reduced proliferative activity of BE cells in culture as well as of EAC cells [2]. COX2 polymorphisms have been reported to be associated with increased risk for EAC [44]. An effect of the polymorphism studied (the 8473 C allele) on the immunohistochemical expression level was, however, not reported. We found the percentage of COX2 expressing cells were significantly reduced in EAC, relative to the other disease categories. This matches the results obtained by Villanacci et al. [25], who attributed the lower expression of COX2 to the poor differentiation grade of the EAC in their series. In our group of EAC, the number of poorly differentiated EACs was also high. Our data, notably the absence of any difference in COX2 expression between BE, LGD, and HGD, imply that COX2 is not a potential marker for progression of BE towards EAC.

E-cadherin and β-catenin

E-Cadherin belongs to the family of the cadherin transmembrane proteins, which play an important role in cell adhesion notably in the formation of adherence junctions through homotypic interactions. Earlier studies on the involvement of E-cadherin in the development of EAC suggest that there is decreased expression with progressive degrees of dysplasia [26, 45]. Although we were unable to reproduce the differences between LGD and HGD, we did find a significant decrease in EAC relative to HGD. E-cadherin is more likely related to the development of invasive activity and, as such, a marker of EAC. A role in the discrimination between BE and LGD on one hand and HGD on the other is unlikely.

Nuclear β-catenin is an indicator of canonical Wnt activation. When accumulating in the nucleus, β-catenin forms a complex with lymphoid enhancer factor (LEF1), T-cell factor (TCF4), and other transcription factors [13]. Unlike in many other carcinomas, mutations in the β-catenin gene do not play a role in EAC [46], the mechanisms involved in Wnt activation having been incompletely resolved to date. The key regulators of the Wnt pathway in EAC are probably different from those in other carcinomas as is stated by Clement et al. [12]. We found no statistically significant differences in β-catenin expression between BE and LGD or HGD. The Wnt pathway is likely to be involved in the development of EAC [12, 13] but in EAC invasion rather than in the progression from BE to dysplasia.

In conclusion, our data indicate that loss of CD44 and gain of DKK1 expression characterizes the transition from LGD to HGD, which might go along with an increased risk for developing an EAC. This observation warrants their inclusion into a follow-up study. The first goal of this study would be to confirm our findings in a larger series of cases. Ultimately, when these findings are confirmed, these markers should be included in a prospective clinicopathological study with long-term patient follow-up to confirm their significance as indicators for an increased risk for the development of EAC from BE.

Conflict of interest We declare that we have no conflict of interest.

References

1. Flejou JF (2000) Barrett's oesophagus: from metaplasia to dysplasia and cancer. Gut 54(Suppl 1):i6–i12
2. Koppert LB, Wijnhoven BP, van Dekken H et al (2005) The molecular biology of esophageal adenocarcinoma. J Surg Oncol 92:169–190
3. Playford RJ (2006) New British society of gastroenterology (BSG) guidelines for the diagnosis and management of Barrett's oesophagus. Gut 55:442
4. el-Serag HB, Sonnenberg A (1998) Opposing time trends of peptic ulcer and reflux disease. Gut 43:327–333
5. Blot WJ, McLaughlin JK (1999) The changing epidemiology of esophageal cancer. Semin Oncol 26(5 Suppl 15):2–8
6. Farrow DC, Vaughan TL (1996) Determinants of survival following the diagnosis of esophageal adenocarcinoma (United States). Cancer Causes Control 7:322–327
7. Falk GW, Rice TW, Goldblum JR et al (1999) Jumbo biopsy forceps protocol still misses unsuspected cancer in Barrett's esophagus with high-grade dysplasia. Gastrointest Endosc 49:170–176

8. Heitmiller RF, Redmond M, Hamilton SR (1996) Barrett's esophagus with high-grade dysplasia. An indication for prophylactic esophagectomy. Ann Surg 224:66–71
9. Shaheen NJ, Crosby MA, Bozymski EM et al (2000) Is there publication bias in the reporting of cancer risk in Barrett's esophagus? Gastroenterology 119:333–338
10. Flejou JF, Svrcek M (2007) Barrett's oesophagus—a pathologist's view. Histopathology 50:3–14
11. Morales CP, Souza RF, Spechler SJ (2002) Hallmarks of cancer progression in Barrett's oesophagus. Lancet 360:1587–1589
12. Clement G, Braunschweig R, Pasquier N et al (2006) Alterations of the Wnt signaling pathway during the neoplastic progression of Barrett's esophagus. Oncogene 25:3084–3092
13. Doucas H, Garcea G, Neal CP et al (2005) Changes in the Wnt signalling pathway in gastrointestinal cancers and their prognostic significance. Eur J Cancer 41:365–379
14. Shi XY, Bhagwandeen B, Leong AS (2008) p16, Cyclin D1, Ki-67, and AMACR as markers for dysplasia in Barrett esophagus. Appl Immunohistochem Mol Morphol 16:447–452
15. Shi XY, Bhagwandeen B, Leong AS (2008) CDX2 and villin are useful markers of intestinal metaplasia in the diagnosis of Barrett esophagus. Am J Clin Pathol 129:571–577
16. Nair KS, Naidoo R, Chetty R (2005) Expression of cell adhesion molecules in oesophageal carcinoma and its prognostic value. J Clin Pathol 58:343–351
17. Taketo MM (2006) Wnt signaling and gastrointestinal tumorigenesis in mouse models. Oncogene 25:7522–7530
18. Okamoto R, Watanabe M (2004) Molecular and clinical basis for the regeneration of human gastrointestinal epithelia. J Gastroenterol 39:1–6
19. Johnson ML, Rajamannan N (2006) Diseases of Wnt signaling. Rev Endocr Metab Disord 7:41–49
20. van Es JH, van Gijn ME, Riccio O et al (2005) Notch/gamma-secretase inhibition turns proliferative cells in intestinal crypts and adenomas into goblet cells. Nature 435:959–963
21. Almeida R, Almeida J, Shoshkes M et al (2005) OCT-1 is overexpressed in intestinal metaplasia and intestinal gastric carcinomas and binds to, but does not transactivate, CDX2 in gastric cells. J Pathol 207:396–401
22. Bian YS, Osterheld MC, Fontolliet C et al (2002) p16 inactivation by methylation of the CDKN2A promoter occurs early during neoplastic progression in Barrett's esophagus. Gastroenterology 122:1113–1121
23. Brantjes H, Barker N, van Es J et al (2002) TCF: lady justice casting the final verdict on the outcome of Wnt signalling. Biol Chem 383:255–261
24. Yan P, Seelentag W, Bachmann A et al (2007) An agarose matrix facilitates sectioning of tissue microarray blocks. J Histochem Cytochem 55:21–24
25. Villanacci V, Rossi E, Zambelli C et al (2007) COX-2, CDX2, and CDC2 immunohistochemical assessment for dysplasia-carcinoma progression in Barrett's esophagus. Dig Liver Dis 39:305–311
26. Bailey T, Biddlestone L, Shepherd N et al (1998) Altered cadherin and catenin complexes in the Barrett's esophagus-dysplasia-adenocarcinoma sequence: correlation with disease progression and dedifferentiation. Am J Pathol 152:135–144
27. Pinto D, Clevers H (2005) Wnt, stem cells and cancer in the intestine. Biol Cell 97:185–196
28. Clevers H, Batlle E (2006) EphB/EphrinB receptors and Wnt signaling in colorectal cancer. Cancer Res 66:2–5
29. Gregorieff A, Pinto D, Begthel H et al (2005) Expression pattern of Wnt signaling components in the adult intestine. Gastroenterology 129:626–638
30. Mutoh H, Sakamoto H, Hayakawa H et al (2006) The intestine-specific homeobox gene Cdx2 induces expression of the basic helix-loop-helix transcription factor Math1. Differentiation 74:313–321
31. Liu T, Zhang X, So CK et al (2007) Regulation of Cdx2 expression by promoter methylation, and effects of Cdx2 transfection on morphology and gene expression of human esophageal epithelial cells. Carcinogenesis 28:488–496
32. Greenawalt DM, Duong C, Smyth GK et al (2007) Gene expression profiling of esophageal cancer: comparative analysis of Barrett's esophagus, adenocarcinoma, and squamous cell carcinoma. Int J Cancer 120:1914–1921
33. Ngan CY, Yamamoto H, Seshimo I et al (1996) Expression of CD44H and CD44v3 in normal oesophagus, Barrett mucosa and oesophageal carcinoma. J Clin Pathol 49:489–492
34. Lagorce-Pages C, Paraf F et al (1998) Expression of CD44 in premalignant and malignant Barrett's oesophagus. Histopathology 32:7–14
35. Menges M, Goebel R, Pueschel W et al (2002) Expression of CD44v5 and -v6 in Barrett's carcinoma is not increased compared to that in nondysplastic Barrett's mucosa. Exp Mol Pathol 72:207–212
36. Niehrs C (2006) Function and biological roles of the Dickkopf family of Wnt modulators. Oncogene 25:7469–7481
37. Sato H, Suzuki H, Toyota M et al (2007) Frequent epigenetic inactivation of DICKKOPF family genes in human gastrointestinal tumors. Carcinogenesis 28:2459–2466
38. Aguilera O, Fraga MF, Ballestar E et al (2006) Epigenetic inactivation of the Wnt antagonist DICKKOPF-1 (DKK-1) gene in human colorectal cancer. Oncogene 25:4116–4121
39. Ali I, Rafiee P, Hogan WJ et al (2006) Dickkopf homologs in squamous mucosa of esophagitis patients are overexpressed compared with Barrett's patients and healthy controls. Am J Gastroenterol 101:1437–1448
40. Van Baal JW, Bozikas A, Pronk R et al (2008) Cytokeratin and CDX-2 expression in Barrett's esophagus. Scand J Gastroenterol 43:132–140
41. Wegner M (1999) From head to toes: the multiple facets of Sox proteins. Nucleic Acids Res 27:1409–1420
42. Blache P, van de Wetering M, Duluc I et al (2004) SOX9 is an intestine crypt transcription factor, is regulated by the Wnt pathway, and represses the CDX2 and MUC2 genes. J Cell Biol 166:37–47
43. Ferguson HR, Wild CP, Anderson LA et al (2008) Cyclooxygenase-2 and inducible nitric oxide synthase gene polymorphisms and risk of reflux esophagitis, Barrett's esophagus, and esophageal adenocarcinoma. Cancer Epidemiol Biomarkers Prev 17:727–731
44. Feith M, Stein HJ, Mueller J et al (2004) Malignant degeneration of Barrett's esophagus: the role of the Ki-67 proliferation fraction, expression of E-cadherin and p53. Dis Esophagus 17:322–327
45. Wijnhoven BP, Nollet F, De Both NJ et al (2000) Genetic alterations involving exon 3 of the beta-catenin gene do not play a role in adenocarcinomas of the esophagus. Int J Cancer 86:533–537
46. Williams LJ, Guernsey DL, Casson AG (2006) Biomarkers in the molecular pathogenesis of esophageal (Barrett) adenocarcinoma. Curr Oncol 13:33–43

Virchows Arch (2009) 454:639–646
DOI 10.1007/s00428-009-0772-4

ORIGINAL ARTICLE

Overexpression of Dickkopf 3 in hepatoblastomas and hepatocellular carcinomas

Yihua Pei · Junko Kano · Tatsuo Iijima · Yukio Morishita · Yukinori Inadome · Masayuki Noguchi

Received: 4 January 2009 / Revised: 3 April 2009 / Accepted: 7 April 2009 / Published online: 13 May 2009

Abstract Dickkopf 3 (Dkk3) is a protein expressed at a very early stage of hepatogenesis. In this study, we examined whether Dkk3 was related to a premature or dedifferentiated nature in hepatoblastomas (HBLs) and hepatocellular carcinomas (HCCs). It was demonstrated that Dkk3 was overexpressed in HBLs and HCCs and that its expression was more frequent in the former than in the latter, being consistent with the fact that most HBLs show an embryonal or fetal hepatic histology, whereas there was no distinct relationship between Dkk3 expression and clinical data or histology. All of the HBLs expressed Dkk3, alpha-fetoprotein (AFP), or both proteins, suggesting that, similar to AFP, Dkk3 is another potentially useful biomarker detecting a wide range of HBLs. Furthermore, Dkk3 and AFP were expressed reciprocally in the tumors. These results suggest that Dkk3 may be related to the premature or dedifferentiated nature of HBLs and HCCs, whereas AFP may be related to a more differentiated nature. Thus, assessment of Dkk3 and AFP may be useful in the diagnosis of hepatic tumors.

Keywords Dickkopf 3 · Hepatoblastoma · Hepatocellular carcinoma · Heterogeneity

Electronic supplementary material The online version of this article (doi:10.1007/s00428-009-0772-4) contains supplementary material, which is available to authorized users.

Y. Pei · J. Kano (✉) · M. Noguchi
Department of Pathology, Institute of Basic Medical Sciences,
Graduate School of Comprehensive Human Sciences,
University of Tsukuba,
1-1-1 Tennodai,
Tsukuba, Ibaraki 305-8575, Japan
e-mail: junkano@md.tsukuba.ac.jp

Y. Morishita
Department of Clinical Pathology, Institute of Clinical Medicine,
Graduate School of Comprehensive Human Sciences,
University of Tsukuba,
1-1-1 Tennodai,
Tsukuba, Ibaraki 305-8575, Japan

T. Iijima
Ibaraki Prefectural Central Hospital,
6528 Koibuchi,
Kasama, Ibaraki 309-1793, Japan

Y. Inadome
Hitachi Ltd. Hitachi General Hospital,
2-1-1 Jonan,
Hitachi, Ibaraki 309-1793, Japan

Introduction

Dickkopf (Dkk) 3 is a member of the Dkk family of four genes (Dkk1, Dkk2, Dkk3, and Dkk4) that encode secreted proteins. Dkk1, Dkk2, and Dkk4 are considered to be modulators of the Wnt signaling pathway known to be involved in embryonic and cancer development and bind to the same effectors such as lipoprotein receptor-related protein 5/6. In contrast, it has not been established whether Dkk3 functions in Wnt signaling, and it has been reported that Dkk3 does not bind to the effectors recognized by the other Dkk family members. Therefore, Dkk3 seems to be a divergent member of the Dkk family, and its function is poorly understood [1]. It has been demonstrated that the Dkks, including Dkk3, show regionalized expression and control cell fate during development in vertebrates [2–7]. In normal adult human tissues, Dkk3 is expressed at higher levels in the deep gastric glands/colonic crypt bases, where gastrointestinal stem cells reside [8], and more recently, it has been shown that only a subset of pancreatic beta cells contain Dkk3 [9]. These results suggest that Dkk3 may be expressed by only a distinct subpopulation of cells in these

tissues. In our previous study using porcine models, we demonstrated that Dkk3 was expressed differentially and characteristically in adult hepatic stem-like cells and was up-regulated in the fetal liver at the fifth gestational week (GW) and also in regenerating liver in an 80% hepatechtomy model, suggesting that Dkk3 plays a role in liver development and regeneration [10]. The available data suggest that Dkk3 is likely involved in development and differentiation, not only in embryos but also in some adult tissues.

On the other hand, Dkk3 has been shown to be down-regulated and hypermethylated in some tumor tissues and cells, a state designated reduced expression in immortalized cells [11]. It has been also reported that transfection of Dkk3 in some tumor cells influences their invasion capacity and leads to apoptosis, suggesting that Dkk3 may act as a tumor suppressor [12–16], whereas Dkk3 mutant mice show no enhanced tumorigenesis [17]. It is well known that the Wnt pathway plays an important role in carcinogenesis, and there is considerable evidence for the involvement of Dkks in cancer development [18], although the precise mechanism has not been established. Dkk1is known to be overexpressed in some tumor cell lines and tissues, such as myeloma and ovarian endometrioid adenocarcinomas [19, 20]. Wirths et al. have reported that Dkk1 is overexpressed in hepatoblastomas (HBLs) and Wilms' tumors relative to normal tissues and suggested that ß-catenin mutation might result in a negative feedback mechanism against activated Wnt signaling [21]. HBLs of early childhood and hepatocellular carcinomas (HCCs) are major malignant tumors of the liver associated with high mortality. HBL, an embryonal tumor, contains embryonal, fetal, or undifferentiated small hepatic cells. On the other hand, HCC shows various histological appearances reflecting hepatic differentiation due to dedifferentiation of the original tumor cells. Although the histological appearance is thought to be an important prognostic factor in malignant liver tumors, it does not reflect the outcome sufficiently [22]. Therefore, it has been considered important to establish the molecular characteristics of HBLs and HCCs that best represent their biological properties. Recently, Luo et al. demonstrated that HBLs and HCCs show differences in gene expression, although some specific genes and types of genomic instability are common to both [23].

In the present study, we hypothesized that Dkk3 may be related to a premature or dedifferentiated nature that is reflected in the histological appearance of HBLs and HCCs and that it might be a useful biomarker of hepatic malignancy. To assess this hypothesis, we analyzed the expression pattern of Dkk3 in these tumors by in situ hybridization (ISH) and immunohistochemistry (IHC), along with some hepatic and cell proliferation markers. Some HBLs and HCCs have ß-catenin mutations and show nuclear accumulation of ß-catenin [24]. Dkk1 is considered to be a downstream target gene of ß-catenin [25], and a recent report has suggested that Dkk3 is a positive regulator of Wnt signaling that is suppressed by Dkk1 [26]. We then examined the nuclear accumulation of ß-catenin and Dkk1expression in relation to Wnt/ß-catenin signaling and the role of other Dkks. Finally, we analyzed the characteristics of Dkk3-expressing cells in HBLs and a HCC cell line.

Materials and methods

Tissue samples and cell culture

The present study was approved by the Ethics Committee of Tsukuba University (Ibaraki, Japan). Samples of HBLs and HCCs obtained surgically or by biopsy from 14 patients and 72 patients, respectively, at Tsukuba University Hospital (Ibaraki, Japan) between 1981 and 2006, together with corresponding paired samples of non-cancerous liver parenchyma, were investigated. The clinical data for the samples are summarized in Table 1. KYN-3, a HCC cell line [27], was maintained in RPMI-1640 (Invitrogen, Carlsbad, CA, USA) supplemented with 10% fetal bovine serum (Sigma-Aldrich, St. Louis, MO, USA), 100 U/ml penicillin, and 100 µg/ml streptomycin (Invitrogen) in a type I collagen-coated dish (Asahi Techno Glass, Tokyo, Japan).

Dkk3 in situ hybridization

T7 RNA polymerase promoter-attached primers for Dkk3 were designed on the basis of the sequence in the GeneBank database (accession no. NM_015881, sense: 5′-GGAGACGAAGAAGGCAGAAGGA-3′; anti-sense; 5′-TCCCAGGTGATGAGGTCCAGAA-3′). Then, the PCR products were transcribed to anti-sense and sense cRNA probes labeled with digoxigenin (DIG) with a DIG RNA Labeling Kit (Roche Diagnostics GmbH, Penzberg, Germany) in accordance with the manufacturer's instructions. Formalin-fixed and paraffin-embedded liver tissues were cut into 3-µm-thick sections and mounted on silane-coated slides (Matsunami Glass Ind., Osaka, Japan). Hybridization was performed at 50°C for 16 h in DAKO mRNA In Situ Hybridization Solution (DakoCytomation, Carpinteria, CA, USA) containing either 0.6 µg/ml heat-denatured DIG-labeled anti-sense probe, the labeled probe with a 100-fold excess of the unlabeled probe, or the sense probe. Hybridization assays with the last two probes were used as negative controls. Detection of hybridized cRNA probes was performed with horseradish peroxidase-conjugated rabbit anti-DIG antibody (DakoCytomation) and a GenPoint™ Tyramide Signal Amplification System (DakoCytomation). Tumors were assessed as positive on the basis of more than two positively staining areas.

Table 1 Clinical data for the hepatoblastomas (HBLs) and hepatocellular carcinomas (HCCs) investigated

		HBL	HCC
Average age		3 years and 11 months	64 years
Male/female		7/7	56/16
Viral infection	HBV positive	0/14	12/72
	HCV positive	0/14	45/72
	HVB + HVC positive	0/14	2/72
Chronic hepatitis		0/14	39/72
Cirrhosis		0/14	26/72
	Embryonal	8/14	
	Fetal	5/14	
Histologic differentiation	Mixed	1/14	
	Poorly differentiated		14/72
	Moderately differentiated		49/72
	Well differentiated		9/72

IHC and immunocytochemistry

Formalin-fixed, paraffin-embedded sections and methanol-fixed KYN-3 cells cultured in chamber slides were used for immunochemical analyses. IHC was performed with the DAKO Envision™ System (DakoCytomation). Immunocytochemistry (ICC) was performed with a FITC- or TRITC-conjugated second antibody. Sections were pretreated in an autoclave (121°C, 10 min) in 10 mM sodium citrate (pH 7.0), except for the case of alpha-fetoprotein (AFP). The primary antibodies used were rabbit anti-human Dkk3 (1:300, H-130, Santa Cruz Biotechnology, Santa Cruz, CA, USA) and Dkk1 (1:50, H-120, Santa Cruz Biotechnology) and mouse anti-human AFP (1:200, Nichirei Biosciences, Tokyo, Japan), beta-catenin-1 (1:200, DakoCytomation), nestin (1:100, Santa Cruz Biotechnology), cytokeratin 19 (CK19; 1:1, Progen Biotechnik Gmbh, Heidelberg, Germany), and Ki67 (1:100, DakoCytomation). Sections were incubated with the first antibody at 4°C overnight, and the reactants were developed with 3,3'-diaminobenzidine (for IHC) or fluorescence-conjugated second antibody (for ICC). Normal rabbit and mouse immunoglobulin G were used as negative controls. Positive assessment was determined as described for ISH. Numbers of Ki67-positive cells per 100 cells in liver tissues were calculated using images of 20 fields/tissue selected randomly, which were captured by a CCD camera with an IPAP-WIN image processor for analytical pathology (Sumika Technoservice Corporation, Osaka, Japan).

Statistical analysis

Results were expressed as the number of cases, percentage, or mean ± SD. Comparison between groups was performed using Fisher's exact test or Student's *t* test. Differences at $p<0.05$ were considered statistically significant.

Results

Dkk3 expression in HBLs and HCCs

Dkk3 expression was detected by ISH in 11 of 14 HBLs (79%) and ten of 72 HCCs (14%) and by IHC in 11 of 14 HBLs (79%) and 14 of 72 HCCs (19%). The counterpart non-cancerous parenchymas were negative for Dkk3. The frequency of Dkk3 expression was significantly higher in HBLs than in HCCs (Table 2 and Fig. 1). Dkk3-positive cases included six of eight embryonal types, four of five fetal types, and one mixed type among the HBLs and five of 14 poorly differentiated, eight of 49 moderately differentiated, and one of nine well-differentiated tumors among the HCCs. Although there was a tendency for Dkk3 staining to be stronger in embryonal-type than in fetal-type HBLs, and Dkk3 positivity was found more frequently in poorly differentiated (five of 14, 36%) than in well or moderately differentiated (nine of 58, 16%) HCCs, there was no significant relationship between Dkk3 expression and clinical parameters or the histological appearance of HBLs and HCCs. In portal areas of the cirrhotic parenchyma, IHC demonstrated scattered Dkk3 expression in some

Table 2 Dkk3 expression in hepatoblastomas (HBLs) and hepatocellular carcinomas (HCCs) revealed by in situ hybridization (ISH) and immunohistochemistry (IHC)

Dkk3	ISH		IHC[a]	
	HBL (%)	HCC (%)	HBL (%)	HCC (%)
+	11 (79)	10 (14)	11 (79)	14 (19)
–	3 (21)	62 (86)	3 (21)	58 (81)
Total	14	72	14	72

[a] Fisher's exact test, $p<0.05$

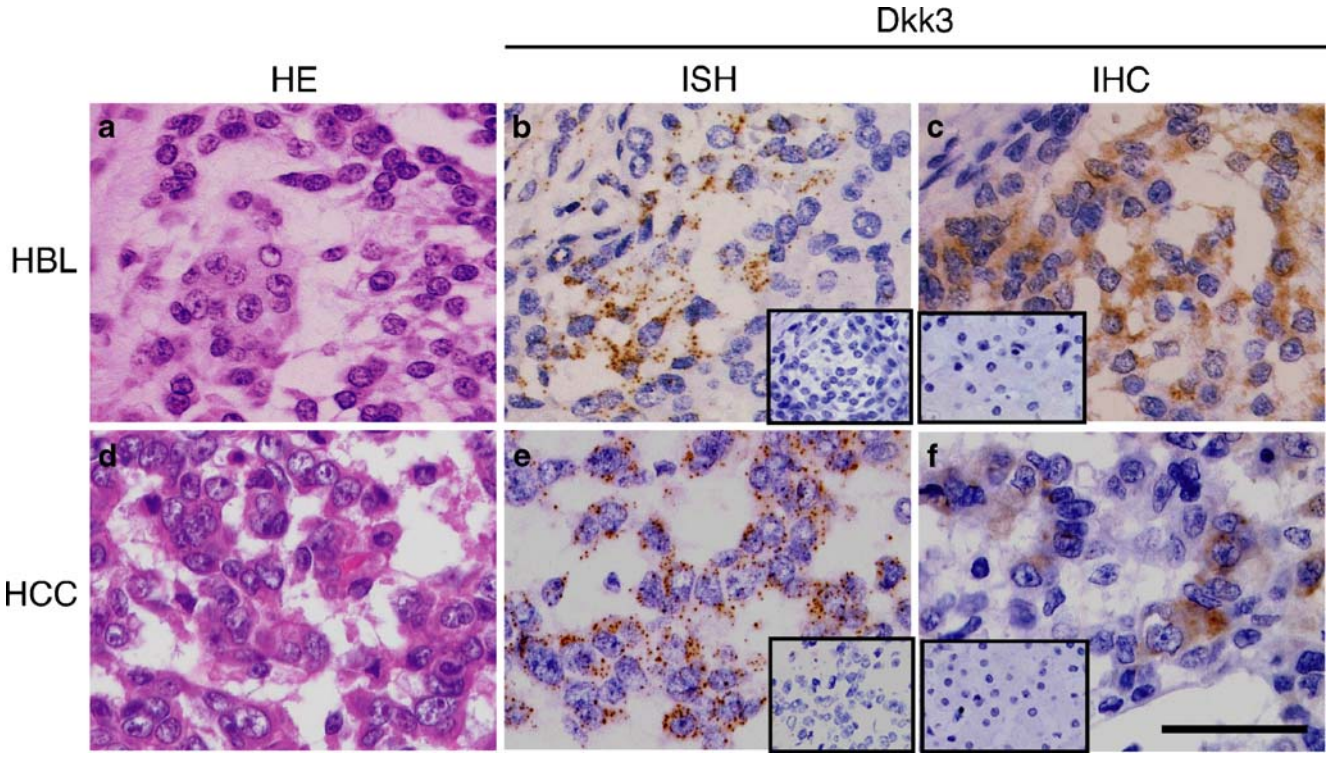

Fig. 1 Expression of Dickkopf 3 (*Dkk3*) in hepatoblastomas (*HBL*: *a–c*) and hepatocellular carcinomas (*HCC*: *d–f*) revealed by in situ hybridization (*ISH*; *b* and *e*) and immunohistochemistry (*IHC*; *c* and *f*). *a* and *d* are stained with hematoxylin and eosin. Micrographs for HBL and HCC groups show the same tumor area, respectively. The *insets* in *b* and *e* are the sense-probe controls, and those in *c* and *f* are the counterpart samples of non-cancerous parenchyma corresponding to the samples of tumor tissue. These are negative for Dkk3. Scale bar, 50 μm

endothelial cells that constituted developing vessels (Fig. 2).

Expression of Dkk3 and AFP in HBLs and HCCs by IHC

AFP is a widely used marker of HBLs and HCCs. Nine of 14 HBLs (64%) expressed both Dkk3 and AFP, whereas six of 72 HCCs (8%) did so. Two of the HBLs (14%) expressed Dkk3, but not AFP, whereas eight of the HCCs (11%) did so. Additionally, three of the HBLs (22%) expressed AFP but not Dkk3, whereas 28 of the HCCs (39%) did so. None of the HBLs lacked expression of both Dkk3 and AFP, whereas 30 of the HCCs (42%) did so (Fig. 3).

Dkk3 expression and cell proliferation in HBLs and HCCs

Dkk3 has been suggested to function as a tumor suppressor, and it has been shown that its overexpression in some cells causes apoptosis. Therefore, cell proliferation in Dkk3-positive tumors was evaluated by IHC with anti-human Ki67 antibody. This revealed that 33±17% of tumor cells in Dkk3-positive and 32±25% in Dkk3-negative HBLs were Ki67 positive. In HCCs, 20±14% of tumor cells in Dkk3-positive cases and 23±12% in Dkk3-negative cases were Ki67 positive. There was no significant difference in the ratio of Ki67 expression between Dkk3-positive and Dkk3-negative tumors.

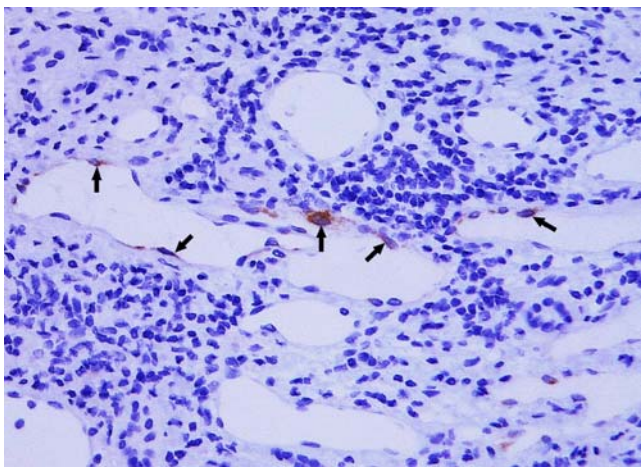

Fig. 2 Immunohistochemical expression of Dkk3 in tumor-surrounding liver cirrhosis in hepatocellular carcinomas. In portal areas of the cirrhotic parenchyma, Dkk3 expression is observed in some endothelial cells (*arrows*) that constitute developing vessels. Original magnification, ×200

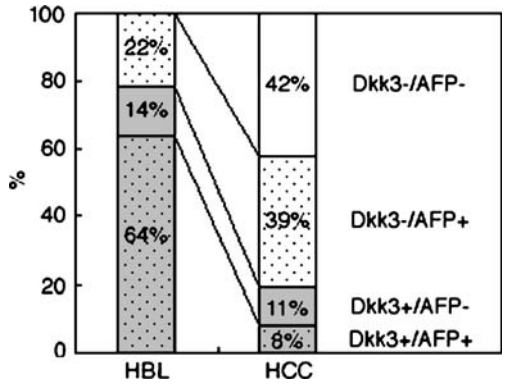

Fig. 3 Frequencies of expression of Dickkopf 3 (*Dkk3*) and alpha-fetoprotein (*AFP*) in hepatoblastomas (*HBL*) and hepatocellular carcinomas (*HCC*) by immunohistochemistry. All of the BHLs express Dkk3, AFP, or both. Forty-two percent of HCCs express neither

Expression of Dkk3 and Dkk1 and nuclear accumulation of ß-catenin in HBLs and HCCs by IHC

To examine whether Dkk3 expression in HBLs and HCCs is related to Wnt signaling, we first analyzed the expression of Dkk1 and the nuclear accumulation of ß-catenin and then investigated the relationship between Dkk3 and Dkk1 expression using IHC. The data are shown in Table 3. There were no statistically significant relationships between Dkk3 expression and nuclear accumulation of ß-catenin or between Dkk3 expression and Dkk1 expression.

Characterization of Dkk3-positive tumor cells by IHC

IHC of HBLs showed that Dkk3 and AFP were stained positively in reciprocal tumor cells. Additionally, some Dkk3-positive cells in HBLs were also positive for CK19, which is expressed by hepatic progenitor or stem-like cells [28, 29], in sequential sections (Fig. 4). Co-expression of Dkk3 and nestin in tumor cells was not conclusive. The character of the protein expression was confirmed in cultured cells by double immunofluorescence staining (Fig. 5).

Discussion

In this study, we demonstrated that Dkk3 was overexpressed in some HBLs and HCCs, whereas the non-cancerous counterpart samples were Dkk3 negative and that the ratio of Dkk3-positive cases was higher in HBLs than in HCCs by both ISH and IHC analyses. Considering that Dkk3 is differentially expressed in porcine adult hepatic stem-like cells and early fetal liver [10], this result seems to be consistent with the fact that hepatic cancers dedifferentiate and that most HBLs show an embryonal or fetal hepatic histology. There was some numerical discrepancy between the rates of positivity for Dkks revealed by ISH and IHC, which may have been due to technical problems such as the probe design in ISH and the antibody specificity in IHC. Furthermore, all of the HBLs analyzed expressed Dkk3, AFP, or both, suggesting that Dkk3 is a useful biomarker of HBLs and would enable detection of a wide range of HBL types. Although Dkk3 is suggested to be a suppressor of tumorigenesis, to have an anti-proliferative effect and to induce apoptosis in various tumors [12–16], Dkk3 expression was independent of clinical data or histology or tumor-proliferative activity detected by Ki67 expression in both HBLs and HCCs. One possible reason may be an inactivating mutation of Dkk3 in hepatic tumors or alteration of Dkk3 activity depending on cell type [12].

It is known that pathogenetic ß-catenin mutation is present in about 80% of HBLs and 20% of HCCs, and this is considered to affect hepatocarcinogenesis [24]. Our results for the nuclear accumulation of ß-catenin seem to be consistent with this concept. Although Dkk1 is hypothesized to work in a negative feedback role and be up-regulated in the presence of active ß-catenin mutation, Dkk1 was not up-regulated in about the half of the cases showing nuclear accumulation of ß-catenin. Because Dkk3 expression was not always suppressed in cases showing Dkk1 expression and nuclear accumulation of ß-catenin, it remained uncertain whether Dkk3 expression has any relation to other members of the Dkk family and Wnt signaling. Further analyses such as manipulation of Dkk expression will be needed in order to clarify the relationship between Dkks and Wnt signaling in HBLs and HCCs. In the present study, Dkk1 expression was not detected in the non-cancerous counterpart samples of liver parenchyma, but it was expressed more frequently in HCCs than in HBLs. In normal pig, Dkk1 expression was observed in fifth GW-fetal liver, but not in seventh GW or 13th GW-

Table 3 Expression of Dkk3 and Dkk1 proteins and nuclear accumulation of ß-catenin protein in hepatoblastomas (HBLs) and hepatocellular carcinomas (HCCs) by immunohistochemistry

Dkk1/Dkk3	Nuclear accumulation of ß-catenin			
	HBL		HCC	
	+	−	+	−
+/+	4	1	2	6
+/−	0	0	5	18
−/+	4	2	1	5
−/−	3	0	4	31
Subtotal	11 (79%)	3 (21%)	12(17%)	60 (83%)
Total	14		72	

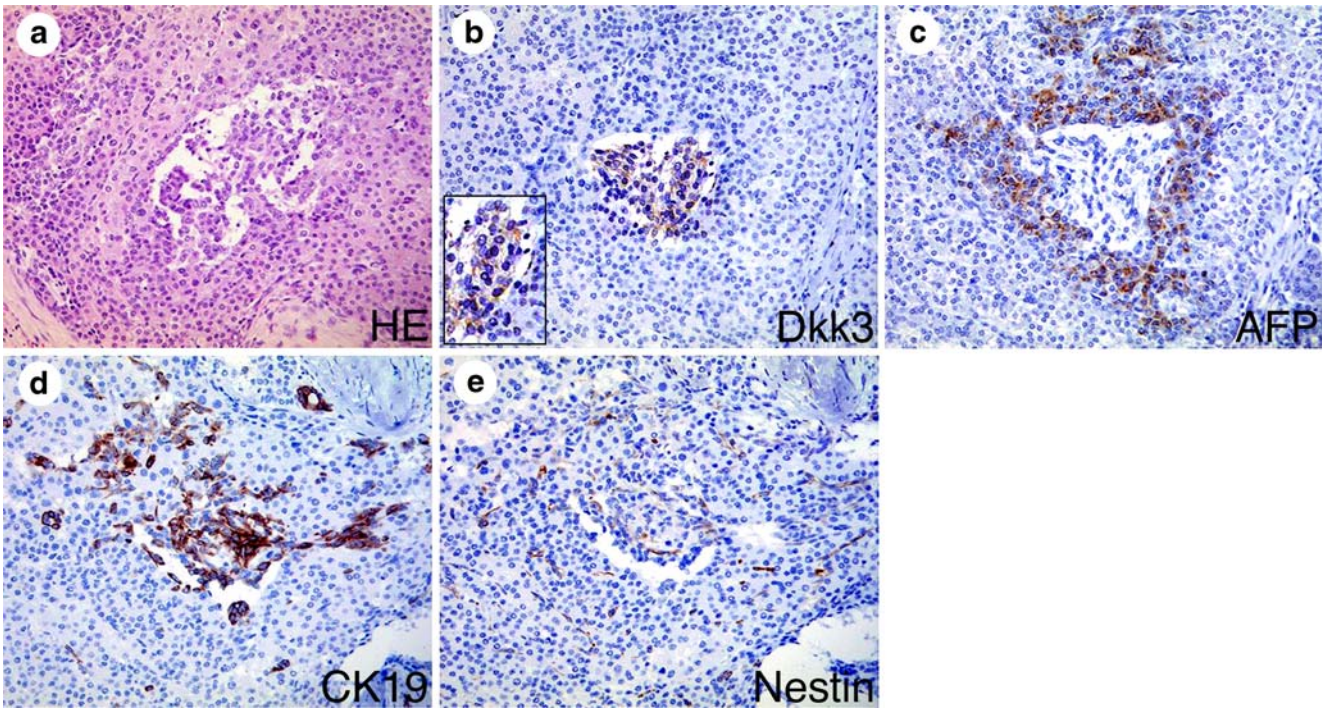

Fig. 4 Immunohistochemical staining for Dickkopf 3 (*Dkk3*, **b**, *inset* shows high-magnification image of positive cells), alpha-fetoprotein (*AFP*, **c**), cytokeratin 19 (*CK19*, **d**), and nestin (**f**) in serial sections of hepatoblastoma. **a** Stained with hematoxylin and eosin. Original magnification, ×200

fetal liver or adult liver by IHC, consistent with Dkk3 expression (Supplementary Fig. 1), suggesting that Dkk1, like Dkk3, was also expressed by immature hepatic cells, although the two may play different roles.

Hepatic cancers are known to be heterogeneous, and interestingly, recent studies have suggested that cancer heterogeneity, including the presence of cancer stem cells, may be involved in the biological properties of cancer such as

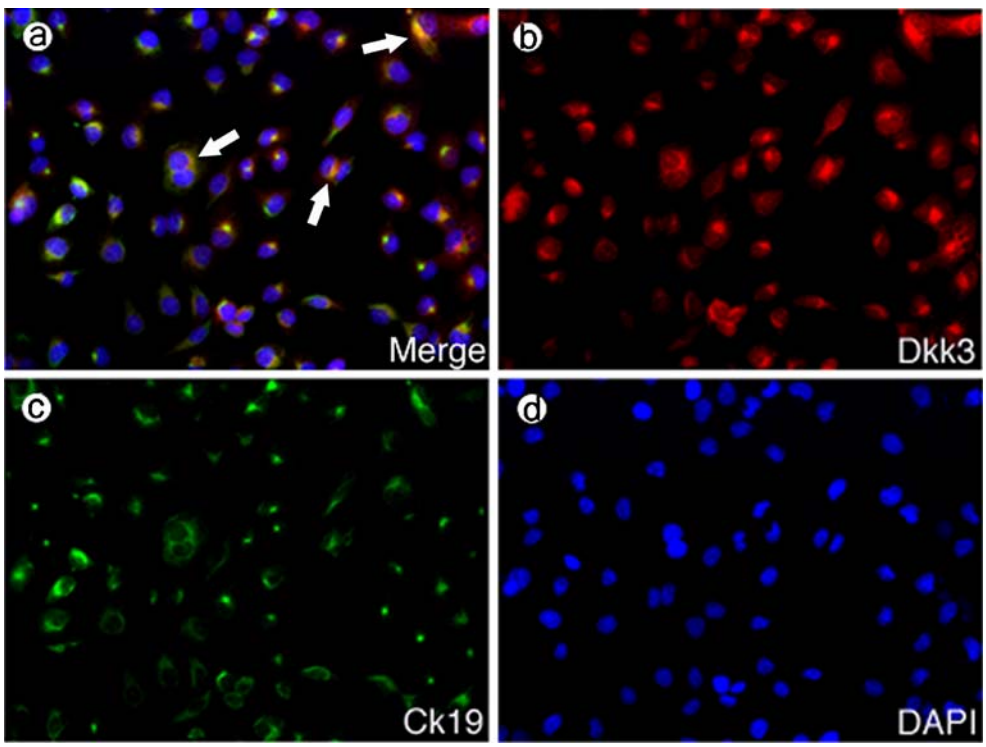

Fig. 5 Dickkopf 3 (*Dkk3*) and cytokeratin 19 (*CK19*) expression in KYN-3 cells revealed by immunocytochemistry. Some cells co-express (**a**, *arrows*) Dkk3 (**b**) and CK19 (**c**). **d** DAPI staining. Original magnification, ×200

resistance to chemotherapy and radiotherapy [30–32]. In this study, it was demonstrated that Dkk3-positive tumor cells were different from AFP-positive tumor cells and that some of them co-expressed CK19, suggesting that Dkk3 may distinguish a certain population of HBLs, which may be rather more immature than cancer cells expressing AFP. Dkk3 may be useful as a marker for detecting this distinct subpopulation.

In conclusion, the present study has demonstrated that Dkk3 is up-regulated in HBLs and HCCs and that the expression is more frequent in HBLs than in HCCs, being consistent with the fact that most HBLs show an embryonal or fetal hepatic histology, whereas there was no distinct relationship between Dkk3 expression and clinical data or histology of HBLs and HCCs. All of the HBLs expressed Dkk3, AFP, or both proteins, suggesting that Dkk3 may be a useful biomarker capable of detecting a wide range of HBLs by simultaneous use of AFP. Furthermore, reciprocal expression of Dkk3 and AFP was found in the hepatic malignant tumors examined, suggesting that Dkk3 can identify tumor cells different from those expressing AFP. Accordingly, Dkk3 may be related to a premature or dedifferentiated nature and might be useful for detection of this distinct subpopulation. Further study is required to reveal the mechanism responsible for overexpression of Dkk3 and its role in hepatic malignant tumors, providing a new insight into the molecular mechanism of carcinogenesis and the prognostic factors of HBLs and HCCs.

Acknowledgments This work was supported in part by Grants-in-Aid for Scientific Research from the Ministry of Education, Culture, Sports, Science, and Technology of Japan (nos. 14570178 and 17590335) to J.K., T.I., and M.N.

Conflict of interest statement We declare that we have no conflict of interest.

References

1. Niehrs C (2006) Function and biological roles of the Dickkopf family of Wnt modulators. Oncogene 25:7469–7481
2. Monaghan AP, Kioschis P, Wu W et al (1999) Dickkopf genes are co-ordinately expressed in mesodermal lineages. Mech Dev 87:45–56
3. Suwa T, Chen M, Hawks CL et al (2003) Zonal expression of dickkopf-3 and components of the Wnt signaling pathways in the human adrenal cortex. J Endocrinol 178(1):149–158
4. Ang SJ, Stump RJ, Lovlcu FJ et al (2004) Spatial and temporal expression of Wnt and Dickkopf genes during murine lens development. Gene Expr Patterns 4(3):289–295
5. Diep DB, Hoen N, Backman M et al (2004) Characterisation of the Wnt antagonists and their response to conditionally activated Wnt signaling in the developing mouse forebrain. Dev Brain Res 153(2):261–270
6. Fjeld K, Kettunen P, Furmanek T et al (2005) Dynamic expression of Wnt signaling-regulated Dickkopf1, -2, and -3 mRNAs in the developing mouse tooth. Dev Dyn 233(1):161–166
7. Nie X (2005) Dkk-1, -2, and -3 expression in mouse craniofacial development. J Mol Histol 36(5):367–372
8. Byun T, Karimi M, Marsh JL et al (2005) Expression of secreted Wnt antagonists in gastrointestinal tissues: potential role in stem cell homeostasis. J Clin Pathol 233(1):515–519
9. Hermann M, Pirkebner D, Draxl A et al (2007) Dickkopf-3 is expressed in a subset of adult human pancreatic beta cells. Histochem Cell Biol 127:513–521
10. Kano J, Ishiyama T, Iijima T et al (2008) Differentially expressed genes in a porcine adult hepatic stem-like cell line and their expression in developing and regenerating liver. Lab Invest 88:132–143
11. Tsuji T, Miyazaki M, Sakaguchi M et al (2000) REIC gene shows down-regulation in human immortalized cells and human tumor-derived cell lines. Biochem Biophys Res Commun 268:20–24
12. Hoang BH, Kubo T, Healey JH et al (2004) Dickkopf 3 inhibits invasion and motility of Saos-2 osteosarcoma cells by modulating the Wnt-ß-catenin pathway. Cancer Res 64:2734–2739
13. Abarzua F, Sakaguchi M, Takaishi M et al (2005) Adenovirus-mediated overexpression of REIC/Dkk-3 selectively induces apoptosis in human prostate cancer cells through activation of c-Jun-NH2-kinase. Cancer Res 65(21):9617–9622
14. Kuphal S, Lodermeyer S, Bataille F et al (2006) Expression of *Dickkopf* genes is strongly reduced in malignant melanoma. Oncogene 25:5027–5036
15. Koppen A, Ait-Aissa R, Koster J et al (2008) *Dickkopf-3* expression is a marker for neuroblastic tumor maturation and is down-regulated by MYCN. Int J Cancer 122:1455–1464
16. Yue W, Sun Q, Dacic S et al (2008) Downregulation of Dkk3 activates ß-catenin/TCF-4 signaling in lung cancer. Carcinogenesis 29(1):88–92
17. Barrantes IB, Montero-Pedrazuela A, Guadano-Ferraz A et al (2006) Generation and characterization of *dickkopf3* mutant mice. Mol Cell Biol 26(6):2317–2326
18. Taipale J, Beachy PA (2001) The Hedgehog and Wnt signaling pathway in cancer. Nature 411:349–354
19. Tian E, Zhan F, Walker R et al (2003) The role of the Wnt-signaling antagonist DKK1 in the development of osteolytic lesions in multiple myeloma. N Engl J Med 349:2483–2494
20. Chamorro MN, Schwartz DR, Vonica A et al (2005) FGF-20 and DKK1 are transcriptional targets of beta-catenin and FGF-20 is implicated in cancer and development. EMBO J 24:73–84
21. Wirths O, Waha A, Weggen S et al (2003) Overexpression of human dicckopf-1, an antagonist of wingless/WNT signaling, in human hepatoblastomas and Wilms' tumors. Lab Invest 83 (3):429–434
22. Crawford JM (1999) The liver and the biliary tract. In: Cotran RS, Kumar V, Collins T (eds) Pathologic basis of disease, 6th edn. Saunders, Pennsylvania, pp 845–901
23. Luo JH, Ren B, Keryanov S et al (2006) Transcriptomic and genomic analysis of human hepatocellular carcinomas and hepatoblastomas. Hepatology 44:1012–1024
24. Taniguchi K, Roberts LR, Aderca IN et al (2002) Mutational spectrum of ß-catenin, AXIN1, and AXIN2 in hepatocellular carcinomas and hepatoblastomas. Oncogene 21:4863–4871
25. Gonzalez-Sancho jm, Aguilera O, Garcia JM et al (2005) The Wnt antagonist DICKKOPF-1 gene is a downstream target of beta-catenin/TCF and is downregulated in human colon cancer. Oncogene 24:1098–1103
26. Nakamura R, Hunter DD, Yi H et al (2007) Identification of two novel activities of the Wnt signaling regulator Dickkopf 3 and characterization of its expression in the mouse retina. BMC Cell Biol 8:52
27. Ogasawara S, Yano H, Iemura A et al (1996) Expressions of basic fibroblast growth factor and its receptors and their relationship to proliferation of human hepatocellular carcinoma cell lines. Hepatology 24(1):198–205

28. Koenig S, Probst I, Becker H et al (2006) Zonal hierarchy of differentiation markers and nestin expression during oval cell mediated rat liver regeneration. Histochem Cell Biol 126:723–734
29. Sell S, Leffert HL (2008) Liver cancer stem cells. J Clin Oncology 28(17):2800–2805
30. Thorgeirsson T, Grisham JW (2002) Molecular pathogenesis of human heptocellular carcinoma. Nat Genet 31:339–346
31. Katoh H, Ojima H, Kokubu A et al (2007) Genetically distinct and clinically relevant classification of hepatocellular carcinoma: putative therapeutic targets. Gastroenterology 133:1475–1486
32. Fuchs B, Fujii T, Dorfman JD et al (2008) Epithelial-to-mesenchymal transition and integrin-linked kinase mediate sensitivity to epidermal growth factor receptor inhibition in human hepatoma cells. Cancer Res 68(7):2391–2399

Virchows Arch (2009) 454:647–656
DOI 10.1007/s00428-009-0770-6

ORIGINAL ARTICLE

Claudins 1, 3, and 4 protein expression in ER negative breast cancer correlates with markers of the basal phenotype

Anne A. Blanchard · George P. Skliris · Peter H. Watson · Leigh C. Murphy · Carla Penner · Ladislav Tomes · Tamara L. Young · Etienne Leygue · Yvonne Myal

Received: 19 January 2009 / Revised: 16 March 2009 / Accepted: 1 April 2009 / Published online: 23 April 2009

Abstract In the present study we investigated the protein expression of claudins 1, 3, and 4 and their relationship to clinical variables and outcome in a cohort of ER−ve and ER+ve human invasive breast cancers. Immunohistochemical analysis was performed on tissue microarrays representing a total of 412 tumors and interpretable data was derived from 314, 299, and 306 tumors for claudins 1, 3, and 4, respectively. In the ER+ve subset, 5%, 89%, and 52%, and in the ER−ve subset, 39%, 79%, and 79% of tumors stained positively for claudins 1, 3, and 4, respectively ($p<0.0001$, $p=0.026$, $p<0.0001$). Thus, in the two subsets, a significantly higher number of tumors were positive for claudins 3 and 4, compared to claudin 1. In addition, protein expressions of claudins 1 and 4 were significantly higher in those tumors that displayed characteristics of the basal-like subtype of breast cancers (ER−ve, Her-2−ve, EGFR+ve, CK5/6+ve). This study shows a unique pattern of expression for the different claudins in ER−ve and ER+ve tumors. Our data also suggests that increased expression of claudins 1 and 4 was associated with the basal-like subtype of breast cancers, a subtype generally linked to poor outcome.

Keywords Claudin 1, 3, 4 · Tissue microarray · Invasive breast cancer · Basal-like subtype · Immunohistochemistry · Estrogen receptor

Abbreviations

EGFR	Epithelial derived growth factor receptor
EMT	Epithelial mesenchymal transition
ER	Estrogen receptor

A. A. Blanchard · C. Penner · L. Tomes · T. L. Young · Y. Myal (✉)
Department of Pathology, University of Manitoba,
770 Bannatyne Avenue,
Winnipeg, Manitoba, Canada R3E0W3
e-mail: myal@cc.umanitoba.ca

A. A. Blanchard
e-mail: ablanch@cc.umanitoba.ca

C. Penner
e-mail: crpenner@exchange.hsc.mb.ca

L. Tomes
e-mail: latomes@yahoo.com

T. L. Young
e-mail: umyoun88@cc.umanitoba.ca

A. A. Blanchard · Y. Myal
Department of Physiology, University of Manitoba,
Winnipeg, Manitoba, Canada

G. P. Skliris · L. C. Murphy · E. Leygue
Department of Biochemistry and Medical Genetics,
University of Manitoba,
Winnipeg, Manitoba, Canada

G. P. Skliris
e-mail: skliris@cc.umanitoba.ca

L. C. Murphy
e-mail: lcmurph@cc.umanitoba.ca

E. Leygue
e-mail: eleygue@cc.umanitoba.ca

G. P. Skliris · L. C. Murphy · E. Leygue
Manitoba Institute of Cell Biology,
Winnipeg, Manitoba, Canada

P. H. Watson
BC Cancer Agency, Vancouver Island Center,
Deeley Research Center,
Victoria, BC, Canada
e-mail: pwatson@bccancer.bc.ca

IHC	Immunohistochemistry
LBA	Ligand-binding assay
OS	Overall survival
RFS	Relapse-free survival
TMA	Tissue microarray

Introduction

The claudins belong to a family of tight junction proteins which are involved in maintaining the differentiated state of epithelial cells [1, 2]. Tight junctions, which are the most apical intercellular junctions in epithelial cells, are also crucial for the organization of epithelial cell polarity, separating the plasma membrane into apical and basolateral domains and preventing diffusion of lipids and proteins between these domains, a property necessary for the functionally developed epithelia [1, 3]. These properties constitute the "gate" and "fence" function of the tight junctions [2]. Claudins, specifically claudin 1, form the backbone of tight junctions, and, aside from maintaining cell polarity and paracellular functions, are also involved in recruiting signaling proteins [4]. Thus, claudins are also hypothesized to be involved in the regulation of proliferation, differentiation, and other cellular functions [4].

To date, 24 members of the claudin family have been identified [5]. Although the expression patterns of the claudins are tissue specific, most tissues express multiple claudins which can interact in a homotypic or heterotypic fashion to form the tight junction strand. It is believed that the exact combination of claudin proteins within a given tissue can determine the selectivity and strength of the tight junction [6].

The role of claudin 1 in breast tumorigenesis is not known nor well-explored, but an absence of tight junctions or defective tight junction has been associated with the development of the neoplastic phenotype in epithelial cells [6–8]. Through microarray analysis of gene expression of the normal involuting mammary gland, we identified the claudin 1 gene as the most highly upregulated gene during early involution [9, 10]. Gene expression of claudins 3 and 4 were also found to be significantly upregulated. As involution represents a period of dynamic tissue regression and remodeling in the mammary gland, it was hypothesized that if deregulated, these proteins may play a role in breast tumorigenesis. Evidence in support of this hypothesis comes from recent studies which show that claudins 3 and 4 are overexpressed in breast cancer and in contrast, claudin 1 (as well as claudin 7, another family member) are downregulated, or, in some studies, completely absent [11–13]. It has been proposed that downregulation of claudin 1 in breast cancer may promote tumorigenesis, possibly through increasing mammary epithelial proliferation [14]. Further support for the above hypothesis has come from two additional reports: a decreased expression of claudin 1 was recently shown to correlate with recurrence in breast cancer [15] and the demonstration that a re-expression of claudin 1 into a metastatic breast cancer cell line induced apoptosis [16]. In addition to lateral membrane staining of claudin 1, basal membrane staining as well as cytoplasmic, was also evident [10] within the tumor cells. Such mislocalization of claudin 1 during tumor progression has also been reported by others [13, 17, 18]. In the present study we investigated claudins 1, 3, and 4 protein expression in a cohort of ER+ve and ER−ve invasive breast tumors as there currently exists very limited data on their protein expression in clinical samples. The two previous studies addressing the expression of these claudins in human invasive breast cancer used relatively small sample sizes, 52 [13] and 15 breast tumors [18], in their analysis. In this study a much larger cohort was evaluated, and in addition, we also examined the clinico-pathological parameters of these tumors to determine whether alterations in claudins 1, 3, or 4 protein levels could be used as a predictor of survival or prognosis.

Materials and methods

Breast tumor tissue microarrays

All invasive breast cancers used in the current study were obtained from the Manitoba Breast Tumour Bank (MBTB, Department of Pathology, University of Manitoba), which operates with the approval from the Faculty of Medicine, University of Manitoba, Research Ethics Board [19]. Collection, handling, and histopathological assessment of tumor tissues had been previously described [20, 21]. The clinico-pathological characteristics of the patient cohorts from which the ER+ve and ER−ve tissue microarrays (TMAs) were derived and the criteria used in the case selection for this study have been previously described [21]. Only those tumor biopsies whose ER status was determined by both ligand-binding assay (LBA; ER positive >3 fmol/mg protein) and by immunohistochemistry (IHC, H >0) were included in this study. The original cohorts consisted of a total of 412 tumor samples, 220 ER+ve and 192 ER−ve tumors. However, due to some exhaustion of the TMAs, some tumor cores were not available for analysis, and therefore interpretable data could not be derived from the entire cohort. Overall 125, 148, and 139 ER+ve tumors were evaluated for claudins 1, 3, and 4 and 189, 151, and 167 ER−ve tumors were analyzed for claudins 1, 3, and 4 protein expression, respectively. The combined cohort evaluated for claudins 1, 3, and 4 were 314, 299, and 306 tumors, respectively.

Validation of claudin antibodies

Claudin 1 polyclonal antibody (Zymed, CA, USA) has been validated at the IHC level in a previous study [10] and by other laboratories [13, 22]. Immuno-neutralization experiments confirmed the specificity of the claudins 3 and 4 antibodies. Claudin 3 (Zymed, CA, USA) polyclonal antibody was validated by pre-incubating the antibody overnight at 4°C with 60 ul of the synthetic peptide (1 mg/ml), derived from the C-terminal region of mouse claudin 3 (Zymed, CA, USA). The claudin 4 (Abcam, Cambridge, MA, USA) polyclonal antibody was validated by pre-incubating the antibody overnight at 4°C with 60 μl of a custom-made peptide, corresponding to the immunogen (CKPYSAKYSAARSAAASNYV, Alpha Diagnostic International, TX, USA) reconstituted at 2 mg/ml.

Immunohistochemical analysis of TMAs

Serial sections (5 μm) of the TMAs were stained with rabbit polyclonal antibodies to claudin 1 (Zymed, San Francisco, CA, USA), claudin 3 (Zymed, San Francisco, CA, USA), or claudin 4 (Abcam, Cambridge, MA, USA) at a dilution of 1:100, 1:200, and 1:400, respectively. IHC was performed as recently reported [21]. Commercially available antibodies to Ki67, CK5/6, EGFR, Her-2, caspase 3, CAIX, ERβ, and p53 have been previously used by us for IHC analysis of the TMAs [21]. The IHC data has been compiled into the database maintained by the MBTB and was made available for correlation analyses and other statistical comparisons [20, 23].

Quantification and cut-off selection

Cut-off selection and the generation of *H*-scores were as previously described [20, 21]. Briefly, *H*-scores were derived from a semi-quantitative assessment of both staining intensity (scale 0–3) and the percentage of positive cells (0–100%), which when multiplied, generated a score ranging from 0–300. Antibody staining was evaluated independently by three investigators for claudin 1 (GPS, CP, and PHW) and by two investigators for claudins 3 and 4 (AB and CP). Where discordance (i.e. different scores given by different investigators) was found (5–10% discordant cases for each claudin), cases were re-evaluated in common and a consensus reached. Primary categorical analysis was as follows: breast cancers were considered claudin 1 positive with an IHC-score of >0, while the median *H*-scores were used to categorize claudins 3 and 4 tumors into high and low expressors (corresponding to claudin 3, $H \geq 40$; claudin 4, $H \geq 20$ for the ER−ve TMA; claudin 3, $H \geq 40$; claudin 4, $H > 0$ for the ER+ve TMA). Positivity for CK5/6 was set at >0, for Ki67 at ≥30 (corresponding to the median of the ER−ve TMA), while for EGFR and Her-2, only cancers that showed membrane-staining intensity of 3+ were considered positive, as used and recommended for routine clinical assessment [20].

Statistical analysis

Analysis was carried out as previously described [20, 21]. Correlations were assessed by the Spearman's rank correlation test (*r*), while associations between claudins 1, 3, and 4 and other clinical-pathological variables were tested using contingency methods (Fisher's exact test). Univariate survival analyses were performed using the Log-rank test to generate Kaplan–Meier curves. Overall survival (OS) was defined as the time from initial surgery to the date of death attributable to breast cancer only. Relapse-free survival (RFS) was defined as the time from initial surgery to the date of clinically documented local or distant disease recurrence or death attributed to breast cancer. The Mann–Whitney test was used to compare the median *H*-scores for each claudin in the basal-like tumor subgroup with the median scores of the tumors that did not meet the criteria for that subtype. Statistical analyses were carried out using GraphPad Prism 4.02 version (GraphPad, San Diego, CA, USA) statistics software.

Results

Immunohistochemical analysis of claudin protein expression in ER+ve and ER−ve TMAs

Specificity for all three claudin antibodies had been established in our previous study [10]. Since a high percentage of tumors stained positively with the claudins 3 and 4 antibodies, the specificity of these antibodies was additionally verified through neutralization experiments with the corresponding peptides. Pre-incubation of the claudins 3 and 4 antibodies with their respective peptides, abolished claudins 3 and 4 specific staining (Fig. 1).

Serial TMA sections were stained with specific antibodies for claudin 1, claudin 3, and claudin 4. Both membrane and cytoplasmic staining was observed and considered when scoring (Fig. 2). Although membrane staining was detected in all positive tumors, cytoplasmic staining was observed only in some tumors. Also, within the same core sample of some tumors there were a number of cells with positive cytoplasmic staining but without distinct membranous staining.

TMAs consisted of a total of 412 tumor biopsies. However, only those tumors from which we were able to retrieve interpretable data (intact, unfolded tumor sections) were considered for analysis. Protein expression data was

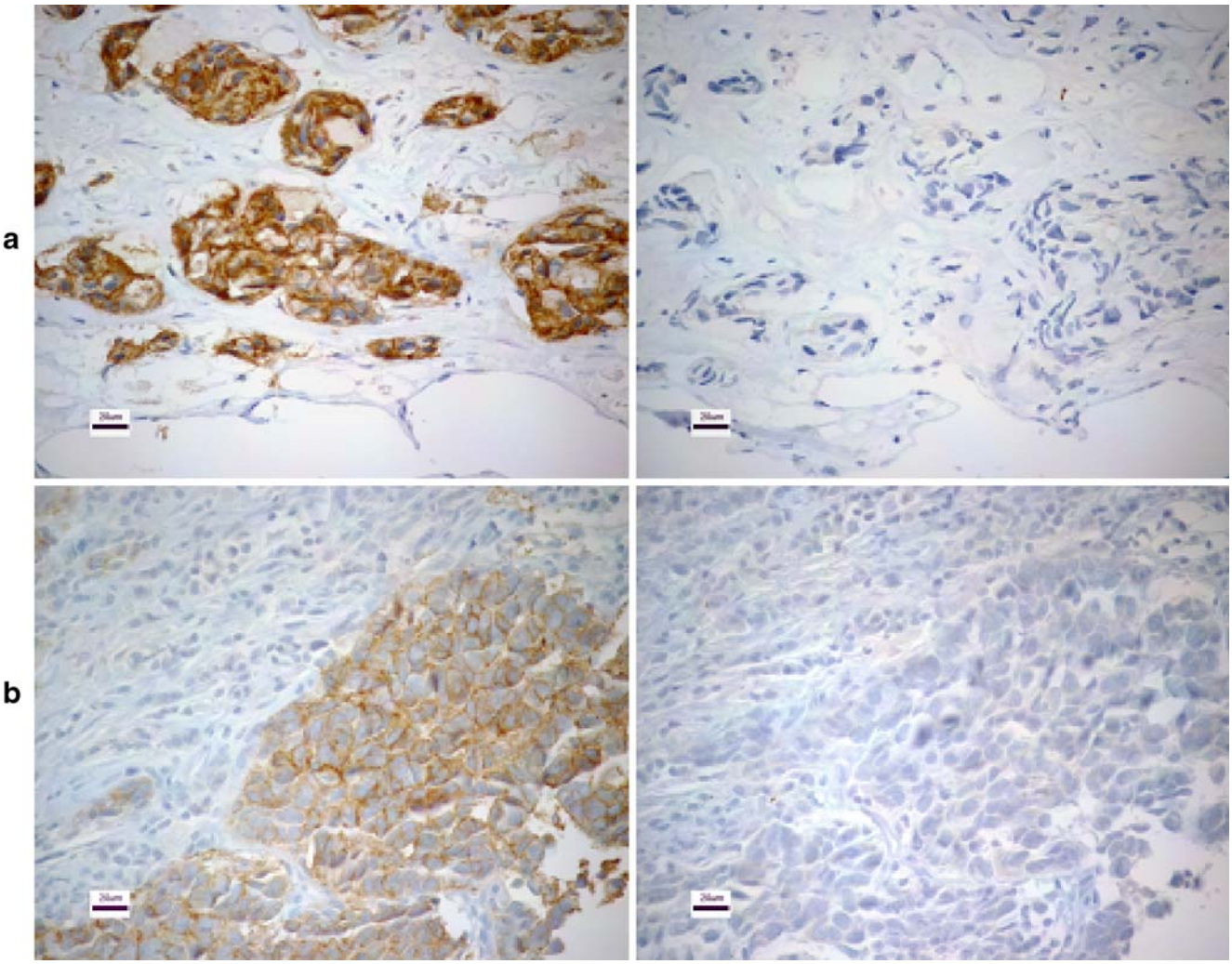

Fig. 1 Confirmation of antibody specificity by immunoneutralization. **a** Claudin 3 immunostaining of an ER+ve invasive breast carcinoma (*left panel*). The rabbit anti-claudin 3 antibody (Zymed, USA) was neutralized overnight with 60 μl of claudin 3 immunizing peptide abolishing the specific signal (serial section, *right panel*, *Bar*=20 μm). **b** Claudin 4 immunostaining of an ER−ve invasive breast carcinoma (*left panel*). The rabbit antibody (Abcam, Cambridge, MA, USA) was neutralized with 60 μl of claudin 4 immunizing peptide during overnight incubation, abolishing the specific signal (serial section, *right panel*, *Bar*=20 μm)

derived from 314 tumors for claudin 1; claudin 3, 299 tumors; and for claudin 4, 306 breast cancer tumors. In the combined cohort, a total of 25% of tumors were stained positively with the claudin 1 antibody, 84% with claudin 3, and 66% with claudin 4. In the ER+ve cohort, 5%, 89%, and 52% tumors stained positively for claudins 1, 3, and 4, while in the ER−ve cohort 39%, 79%, and 79% tumors stained positively for claudins 1, 3, and 4, respectively (Table 1). The differences in positivity between the ER+ve and the ER−ve cohorts were statistically significant for all three claudins: claudin 1 ($p<0.0001$), claudin 3 ($p=0.026$), and claudin 4 ($p<0.0001$; Fisher's exact test). The median *H*-score was also higher in the ER−ve tumors (median *H*-scores of 5 for claudin 1 and 20 for claudin 4) when compared with the ER+ve cohort (median *H*-scores of 0 and 5, respectively, $p<0.0001$, Mann–Whitney test).

Correlation analysis of claudins 1, 3, and 4 protein expression

In the ER+ve cohort, only six tumors were claudin 1 positive (6/125 or 5%, Table 1). Consequently, further correlation analysis was not carried out for this group as the numbers were too small to provide meaningful data. However, a positive and statistically significant correlation was found between claudins 3 and 4 with ERα (Spearman r coefficients 0.179, $p<0.05$; 0.253, $p<0.01$, respectively) ERβ (Spearman r coefficients 0.214, $p<0.05$; 0.231, $p<0.01$, respectively) and with each other (Spearman *r* coefficient 0.554, $p<0.001$) in this cohort.

In the ER−ve cohort a significant positive correlation with claudin 1 and EGFR, p53, CK5/6, caspase 3, and claudin 3 was observed (Table 2). Furthermore, claudin 3

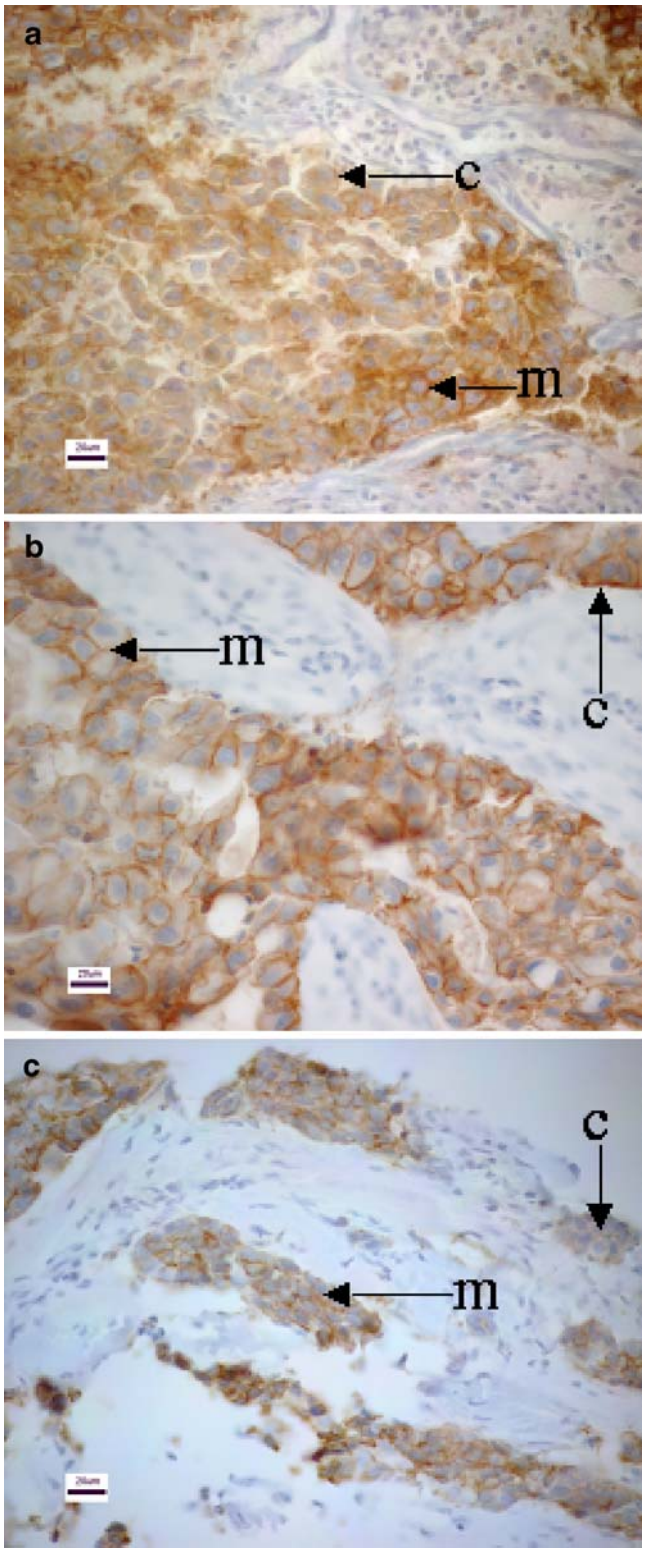

Fig. 2 Representative immunostaining of breast tumors with the claudins 1, 3, and 4 antibodies. **a** claudin 1, **b** claudin 3, and **c** claudin 4. Staining was specific for tumor tissue and both membrane (*m*) and cytoplasmic staining (*c*) was observed. *Bar*=20 μm

expression showed a significant correlation with Ki67 and caspase 3 protein expression in the ER−ve tumors. Claudin 4 expression also showed a significant correlation with Ki67 expression (Table 2).

Categorical analyses of claudins 1, 3, and 4 expressing tumors in the ER+ve and ER−ve cohort

In the ER+ve group, as with the categorical analysis, correlation analysis was not carried out for claudin 1, since only 5% of the ER+ve cases were claudin 1 positive. Further analysis of claudin 3 and 4 expressing ER+ve tumors did not reveal any associations with age, grade, tumor size, and nodal status (not shown). However, tumors that were high in Ki67 expression were also high for claudin 3 protein expression (*H*-score ≥40, $p=0.027$, Fisher's exact test) and claudin 4 protein expression ($p<0.0001$).

Categorical analyses of claudins 1, 3, and 4 expressing tumors in the ER−ve cohort are shown in Table 3. Protein expression data used for claudins 1, 3, and 4 analyses were obtained from 189, 151, and 167 breast tumors, respectively (Table 3). An *H*-score value >0 was used as the cut-off for claudin 1 positive tumors. Claudin 1 was found to be positively associated with EGFR ($p=0.024$), CAIX ($p=0.014$), and caspase 3 ($p=0.012$), Fisher's exact test, Table 3). Since a large majority of tumors stained positively for claudins 3 and 4 (79.0% and 79.0%, respectively) in the ER−ve cohort, we further divided them into two staining categories: high and low. Categorical analyses for high and low claudin staining was performed using the median *H*-scores (40 and 20, respectively) as the cut-off value in these tumor samples (Table 3). As with claudin 1, both claudins 3 and 4 showed a statistically significant association with EGFR ($p=0.011$ and $p=0.014$, respectively) and, as with the ER+ve cohort, there were no associations with age, tumor grade, tumor size, or nodal status.

Correlation between claudins 1, 3, and 4 expression and disease outcome

Using the log-rank test to generate Kaplan–Meier curves, we found no statistical difference in disease outcome (overall survival (Fig. 3) and relapse-free survival not shown) in either the ER−ve or the ER+ve cohort, for all three claudins.

Claudins 1, 3, and 4 protein expression in basal-like tumors

The criteria of Nielsen et al. [24]: ER−ve, Her-2−ve, EGFR+ve, and CK5/6+ve was used to identify a basal-like tumor subset of breast cancers within the ER−ve

Table 1 Comparison between claudin protein expression in ER+ve and ER−ve breast cancer TMAs

		ER+ve TMA		ER−ve TMA		p value
		No. of cases	%	No. of cases	%	
Claudin 1	+ve	6	5	74	39	<0.0001
	−ve	119	95	115	61	
Claudin 3	+ve	132	89	120	79	0.026
	−ve	16	11	31	21	
Claudin 4	+ve	72	52	132	79	<0.0001
	−ve	67	48	35	21	

Positivity for claudins 1, 3, and 4 had an *H*-score of >0; (Fisher's exact test)

cohort. We identified 18 tumors which met these criteria in this cohort. Within this subgroup, there was 61% positivity (11/18 tumors) for claudin 1, markedly higher than that observed (39%) in the entire ER−ve cohort. Positivity for claudin 3 and claudin 4 were 93% (13/14) and 88% (15/17), respectively in this subgroup compared with the 79% positivity observed for each claudin in the ER−ve cohort. The Mann–Whitney test was used to compare the median *H*-scores for each claudin in the basal-like tumor subgroup versus the rest of the cohort from which data for all four selection criteria were obtained (Table 4). The median *H*-scores for claudins 1 and 4 expression were significantly higher in the basal-like subgroup when compared with the non-basal-like subgroup ($p=0.0142$, $p=0.0028$, respectively), while there was a higher (although not statistically significant, $p=0.0962$) median *H*-score for claudin 3 in the basal-like subgroup.

Discussion

The present study was undertaken to evaluate the protein expression of claudins 1, 3, and 4 in a cohort of human invasive breast cancers using TMA analysis. The findings presented here represent the largest number of breast cancers to our knowledge that have been evaluated for protein expression of these claudins. We also investigated the relationship of claudins 1, 3, and 4 with known clinical markers of human invasive breast cancer as well as the association of claudin expression with patient outcome.

The TMAs used in this study are well-characterized [20, 21]. The TMAs were constructed with duplicate cores (0.6 mm) derived from each tumor sample. Whether two cores are entirely representative of gene expression in a large tumor sample sometimes presents concern, as they could result in both over and under scoring of protein expression. However, although such a possibility cannot be entirely excluded, studies have shown that with use of the standard breast cancer prognostic markers (ER, PR, and HER-2/neu), two cores were sufficient and have resulted in >95% accuracy [25–27]. Two cores were also shown to provide a high level of accuracy in the TMA analysis of other cancers, including metastatic prostate and ovarian cancers [28, 29].

IHC analysis of TMAs

Both cytoplasmic and membranous staining of tumor tissues was evident with all three claudin antibodies (Fig. 2). These observations are consistent with the studies of Tokes et al. and Swisshelm et al. [13, 15]. In addition, cytoplasmic mislocalization of other membranous proteins, E cadherin, catenin as well as some other claudin family members during cancer progression, was reported [17, 30–33]. With regards to E cadherin, it has been suggested that such cytoplasmic mislocalization may be an indirect consequence due to the loss of an interacting protein, palladin [34], resulting in its inability to transport E cadherin to the membrane. Other factors such as epigenetic and post-translational modifications as well as alternate

Table 2 Correlation analysis of claudins 1, 3, and 4 protein expression with markers of poor prognosis in the ER−ve TMA

	EGFR	Ki67	p53	CK5/6	Caspase 3
Claudin 1	0.2405** $n=141$	N.S.	0.1857* $n=181$	0.1757* $n=159$	0.1869* $n=188$
Claudin 3	N.S.	0.1757* $n=150$	N.S.	N.S.	0.1918* $n=151$
Claudin 4	N.S.	0.1706* $n=165$	N.S.	N.S.	N.S.

Values are Spearman r coefficients

N.S. $p>0.05$; *$p<0.05$; **$p<0.01$

Table 3 Categorical analyses of claudins 1, 3, and 4 expressing tumors in the ER−ve cohort

Markers and clinical parameters	Subgroup cut-offs	Claudin 1				Claudin 3				Claudin 4			
		+ve	−ve	*n*	*p* value	High	Low	*n*	*p* value	High	Low	*n*	*p* value
EGFR	+	18	14	140	**0.024***	21	7	123	**0.011***	23	9	131	**0.014***
	−	36	72			45	50			45	54		
Her-2	+	4	9	107	0.37	8	2	93	0.11	8	5	102	0.72
	−	45	49			43	40			50	39		
Ki67	≥30	37	55	187	0.77	44	37	150	0.51	47	38	165	0.53
	<30	36	59			33	36			40	40		
CK5/6	+	47	50	159	0.032	44	37	150	0.51	50	38	144	0.39
	−	19	43			33	36			27	29		
CAIX	+	44	47	178	**0.014***	38	38	147	0.74	42	42	160	0.43
	−	26	61			38	33			43	33		
Caspase 3	+	46	49	188	**0.012***	44	33	151	0.19	49	35	167	0.22
	−	28	65			34	40			40	43		
p53	+	49	55	181	0.033	47	38	146	0.31	53	43	162	0.43
	−	24	53			28	33			32	34		
Node	+	29	46	189	0.75	43	35	151	0.42	44	43	167	0.54
	−	40	55			35	38			45	35		
Age	>50	27	40	189	0.88	53	45	151	0.5	58	46	167	0.43
	≤50	47	75			25	28			31	32		
Grade	Low (3 to 5)	2	10	189	0.23	6	2	151	0.37	3	8	167	0.16
	Mod (6 to 7)	27	43			28	30			31	29		
	High (8 to 9)	45	62			44	41			55	41		
Size	>2 cm	50	84	189	0.42	57	52	151	0.86	65	55	167	0.73
	≤2 cm	24	31			21	21			24	23		

An *H*-score >0 was determined as positive for claudin 1. The median *H*-scores were used to separate claudins 3 and 4 positive tumors into high and low expressing tumors ($H \geq 40$, high claudin 3; $H \geq 20$, high claudin 4). Analysis was carried out using Fisher's exact test

*$p<0.025$; ***$p<0.025$**

splicing can also play a role in protein redistribution [35, 36].

Claudin 1

Interpretable information on protein expression was derived from 314 breast cancers for claudin 1. IHC analysis revealed that fewer tumors (25%) stained positively for claudin 1 compared to claudin 3 (84%) and claudin 4 (66%). This study therefore lends support to earlier studies which show that in human invasive breast tumors, claudin 1 is under expressed whereas claudins 3 and 4 are overexpressed [13, 15].

However, when ER status was considered, a significant increase in the number of claudin 1 positive tumors in the ER−ve cohort compared to the ER+ve cohort was observed. Since ER−ve tumors represent a more invasive subtype of breast cancer with poorer prognosis [37] and based on earlier reports, the observed increase in claudin 1 protein expression in the ER negative breast cancers was unexpected. However, differences in claudin 1 expression in ER−ve and ER+ve tumors have not been previously addressed. It is plausible that such increase in claudin 1 positivity in the ER−ve cohort may be attributed to a re-expression of the protein in the more aggressive phenotype. Such mechanisms have been described for some proteins during different stages of tumorigenesis and are thought to be associated with epithelial mesenchymal transition process (EMT) [38]. For example, E cadherin, a junctional protein like claudin 1, and a key player in EMT, is regulated and often absent during cancer invasion, but is re-expressed once a secondary tumor site is established and the cancer has metastasized [39].

Claudin 3

Interpretable information on protein expression was derived from 299 breast cancers for claudin 3. In the combined

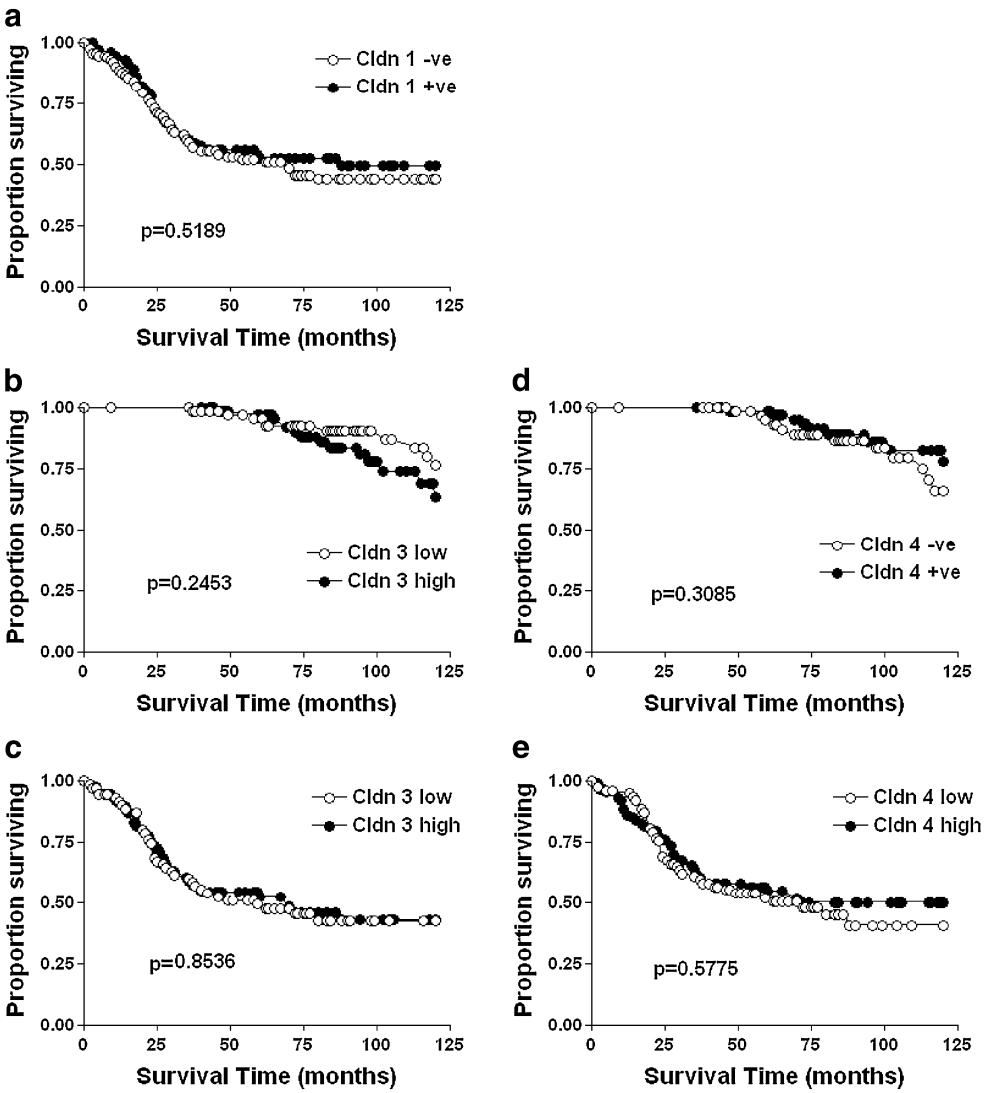

Fig. 3 Kaplan–Meier graphs for OS (overall survival) for claudins 1, 3, and 4 expression in ER−ve tumors (**a**, **c**, and **e**) and ER+ve (**b** and **d**) tumors. *Symbols* on the graph lines represent censored data; *p* values are given for log-rank tests. **a** *n*=189; −ve (*H*=0) claudin 1 events=58;+ve (*H*>0) claudin 1 events=35; **b** *n*=149, low (*H*<40) claudin 3 events=10, high (*H*≥40) claudin 3 events=14; **c** *n*=193; low (*H*<40) claudin 3 events=38, high (*H*≥40) claudin 3 events=39; **d** *n*=139; −ve (*H*=0) claudin 4 events=12,+ve (*H*>0) claudin 4 events=9; **e** *n*=167; low (*H*<20) claudin 4 events=40, high (*H*≥20) claudin 4 events=41. *Cldn* claudin

Table 4 Claudins 1, 3, and 4 protein expression in the basal and non-basal-like breast tumors

	Basal-like tumors		Non-basal-like tumors		*p* value
	Median *H*-score	*n*	Median *H*-score	*n*	
Claudin 1	5	18	0	128	0.0142
Claudin 3	85	14	40	146	0.0962
Claudin 4	40	17	5	144	0.0028

The Mann–Whitney test was used to compare the median *H*-scores for each claudin in the basal-like tumor group (ER−ve, Her-2−ve, EGFR+ve and CK5/6+ve) versus non-basal-like tumors. The median *H*-scores for both claudins 1 and 4 were significantly higher in the basal-like tumors as compared with the non-basal-like tumors. *n*= number of tumors

cohort 84% of tumors stained positively for claudin 3. Thus, there was a higher number of tumors staining for claudin 3 compared to claudin 1 and claudin 4 in the same cohorts. In the ER+ve group the number of tumors that were claudin 3 positive increased to 89% and this fell to 79% positivity in the ER−ve cohort. Overall, there was a significant difference in claudin 3 expression within the two groups when ER status was considered.

Claudin 4

Interpretable information on protein expression was derived from 306 breast cancers for claudin 4. In the combined cohort of invasive breast cancers, 66% of tumors stained positively for claudin 4. The higher percentage of positively stained tumors is similar to that observed for claudin 3. But, as observed for claudin 1, the number of claudin 4 positive tumors decreased (52%) in the ER+ve cohort but increased in the ER−ve cohort (79%).

Overall, our data showed that the expression profiles of the three claudins are unique. Analysis of the combined cohort showed that a higher percentage of invasive breast tumors expressed claudins 3 and 4 proteins compared to claudin 1. However, when ER status was considered, a higher number of ER−ve tumors compared to the ER+ve tumors were claudins 1 and 4 positive, whereas fewer tumors were claudin 3 positive in the ER−ve cohort. These data suggest that claudins 1, 3, and 4 may have different roles during different stages of breast tumorigenesis.

Further analysis of the ER−ve cohort showed a significant correlation between claudin 1 and EGFR, p53, CK5/6, and caspase 3, but not between claudins 3 and 4 and these tumor markers. Conversely, both claudins 3 and 4, but not claudin 1, showed a correlation with Ki67. Although these correlations appear small, they are nonetheless statistically significant and noteworthy in a cancer environment where there are numerous confounding factors. In the ER+ve cohort there was a correlation between claudins 3 and 4 with each other and with ERα and ERβ, suggesting a possible interaction with the claudins and the ER pathway.

Univariate analysis revealed a significantly positive association between all three claudins and EGFR, in the ER−ve cohort. The overexpression of EGFR in breast cancer is well-established and has been associated with the aggressive phenotype and metastasis [40].

The observed increased expression of claudin 1 in the ER−ve tumors and its correlation with prognostic indicators of poor survival prompted us to examine whether the claudins expression were associated with the basal-like subtype of breast cancer. The basal-like subtype of breast cancers, a subgroup of tumors from patients expected to have a worse prognosis and shorter survival [24, 41, 42], are usually characterized by EGFR positivity in addition to ER and Her2 negativity, and CK5/6 overexpression [24, 41, 42]. We found a significant association with claudins 1 and 4 with this subtype. Coincidentally, following this observation in our laboratory, another group reported a high level of claudin 4 protein expression to be associated with the basal-like subset of breast carcinomas [43], lending support to the results of the present study. Also recently, a potential new ER negative "claudin-low" subtype of human breast cancers has been described [44] which exhibit low expression of claudins 3, 4, and 7. However, no information is provided for claudin 1. This subtype may yet be distinct from the one we propose in the present study. It is interesting to note that claudin 1 has also been shown to be upregulated in some cancers such as colon cancer [45] and downregulated in others when the invasive carcinoma develops [46]. It is intriguing to speculate that claudin 1 may function as a tumor suppressor or oncogene at different stages of tumor progression, or, in different types of cancers.

Despite the observed association with the basal subtype of breast cancers, we found no association with patient survival for all three claudins. Tumor stage was not considered as this data was not available for all patients and may be a possible confounder for the survival data.

In summary, this study shows that protein expression of claudins 1, 3, and 4 are altered in breast cancer, have unique expression profiles, and increased expression is associated with a subtype of breast cancers that is generally linked to poor outcome. The association of these claudins with the basal-like subgroup of breast cancers is novel and interesting and warrants further conformation through the analysis of a larger cohort of this subtype of tumors. As well, the correlation observed with claudins 1, 3, and 4 and ER status is important, since ER status is a key indicator of disease progression [47]. Thus, these studies also set the basis for further investigations to determine the relationship between ERs and claudins.

Acknowledgements The authors would like to thank the personnel at the MBTB for technical support. GPS was funded by a Postdoctoral Fellowship from the Manitoba Health Research Council (MHRC) and previously from the CancerCare Manitoba Foundation (CCMF). TLY was formerly funded by a Manitoba Graduate Scholarship, and is currently funded by a Manitoba Health Research Council Studentship. YM is a Manitoba Medical Service Foundation Career Awardee. This study was supported by a grant from the Health Sciences Research Foundation. Biostatistical consultation was kindly provided by M. Cheang, Sr. Systems Analyst, Department of Community Health Sciences, Faculty of Medicine, University of Manitoba.

Conflicts of interest The authors have no known conflicts of interests either financial or personal between themselves and others that might bias the work.

References

1. Anderson JM, Balda MS, Fanning AS (1993) The structure and regulation of tight junctions. Curr Opin Cell Biol 5:772–778
2. Diamond JM (1977) Twenty-first Bowditch lecture. The epithelial junction: bridge, gate, and fence. Physiologist 20:10–18
3. Tsukita S, Furuse M (2002) Claudin-based barrier in simple and stratified cellular sheets. Curr Opin Cell Biol 14:531–536
4. Mitic LL, Anderson JM (1998) Molecular architecture of tight junctions. Annu Rev Physiol 60:121–142
5. Gonzales-Mariscal L. Tight Junctions. [2nd ed.]. 1-1-0001. Boca Raton, CRC
6. Morin PJ (2005) Claudin proteins in human cancer: promising new targets for diagnosis and therapy. Cancer Res 65:9603–9606
7. Tobioka H, Isomura H, Kokai Y et al (2004) Occludin expression decreases with the progression of human endometrial carcinoma. Hum Pathol 35:159–164
8. Kaihara T, Kawamata H, Imura J et al (2003) Redifferentiation and ZO-1 reexpression in liver-metastasized colorectal cancer: possible association with epidermal growth factor receptor-induced tyrosine phosphorylation of ZO-1. Cancer Sci 94:166–172
9. Blanchard A, Shiu R, Booth S et al (2007) Gene expression profiling of early involuting mammary gland reveals novel genes

potentially relevant to human breast cancer. Front Biosci 12:2221–2232
10. Blanchard AA, Watson PH, Shiu RP et al (2006) Differential expression of claudin 1, 3, and 4 during normal mammary gland development in the mouse. DNA Cell Biol 25:79–86
11. Hewitt KJ, Agarwal R, Morin PJ (2006) The claudin gene family: expression in normal and neoplastic tissues. BMC Cancer 6:186
12. Kominsky SL, Argani P, Korz D et al (2003) Loss of the tight junction protein claudin-7 correlates with histological grade in both ductal carcinoma in situ and invasive ductal carcinoma of the breast. Oncogene 22:2021–2033
13. Tokes AM, Kulka J, Paku S et al (2005) Claudin-1, -3 and -4 proteins and mRNA expression in benign and malignant breast lesions: a research study. Breast Cancer Res 7:R296–R305
14. Swisshelm K, Macek R, Kubbies M (2005) Role of claudins in tumorigenesis. Adv Drug Deliv Rev 57:919–928
15. Morohashi S, Kusumi T, Sato F et al (2007) Decreased expression of claudin-1 correlates with recurrence status in breast cancer. Int J Mol Med 20:139–143
16. Hoevel T, Macek R, Swisshelm K et al (2004) Reexpression of the TJ protein CLDN1 induces apoptosis in breast tumor spheroids. Int J Cancer 108:374–383
17. Arabzadeh A, Troy TC, Turksen K (2007) Changes in the distribution pattern of Claudin tight junction proteins during the progression of mouse skin tumorigenesis. BMC Cancer 7:196
18. Soini Y (2005) Expression of claudins 1, 2, 3, 4, 5 and 7 in various types of tumours. Histopathology 46:551–560
19. Watson PH, Snell L, Parisien M (1996) The NCIC-Manitoba Breast Tumor Bank: a resource for applied cancer research. CMAJ 155:281–283
20. Skliris GP, Leygue E, Curtis-Snell L et al (2006) Expression of oestrogen receptor-beta in oestrogen receptor-alpha negative human breast tumours. Br J Cancer 95:616–626
21. Skliris GP, Hube F, Gheorghiu I et al (2008) Expression of small breast epithelial mucin (SBEM) protein in tissue microarrays (TMAs) of primary invasive breast cancers. Histopathology 52:355–369
22. Takala H, Saarnio J, Wiik H et al (2007) Claudins 1, 3, 4, 5 and 7 in esophageal cancer: loss of claudin 3 and 4 expression is associated with metastatic behavior. APMIS 115:838–847
23. Emberley ED, Niu Y, Njue C et al (2003) Psoriasin (S100A7) expression is associated with poor outcome in estrogen receptor-negative invasive breast cancer. Clin Cancer Res 9:2627–2631
24. Nielsen TO, Hsu FD, Jensen K et al (2004) Immunohistochemical and clinical characterization of the basal-like subtype of invasive breast carcinoma. Clin Cancer Res 10:5367–5374
25. Camp RL, Charette LA, Rimm DL (2000) Validation of tissue microarray technology in breast carcinoma. Lab Invest 80:1943–1949
26. Gillett CE, Springall RJ, Barnes DM et al (2000) Multiple tissue core arrays in histopathology research: a validation study. J Pathol 192:549–553
27. Rimm DL, Camp RL, Charette LA et al (2001) Amplification of tissue by construction of tissue microarrays. Exp Mol Pathol 70:255–264
28. Mucci NR, Akdas G, Manely S et al (2000) Neuroendocrine expression in metastatic prostate cancer: evaluation of high throughput tissue microarrays to detect heterogeneous protein expression. Hum Pathol 31:406–414
29. Rosen DG, Huang X, Deavers MT (2004) Validation of tissue microarray technology in ovarian carcinoma. Mod Pathol 17:790–797
30. Chetty R, Jain D, Serra S (2008) p120 catenin reduction and cytoplasmic relocalization leads to dysregulation of E-cadherin in solid pseudopapillary tumors of the pancreas. Am J Clin Pathol 130:71–76
31. Kim MJ, Jang SJ, Yu E (2008) Loss of E-cadherin and cytoplasmic-nuclear expression of beta-catenin are the most useful immunoprofiles in the diagnosis of solid-pseudopapillary neoplasm of the pancreas. Hum Pathol 39:251–258
32. Schmeiser K, Grand RJ (1999) The fate of E- and P-cadherin during the early stages of apoptosis. Cell Death Differ 6:377–386
33. Zhang K, Yao HP, Wang MH (2008) Activation of RON differentially regulates claudin expression and localization: role of claudin-1 in RON-mediated epithelial cell motility. Carcinogenesis 29:552–559
34. Tay PN, Lan Y, Leung CH et al (2008) Genes associated with metastasis and epithelial-mesenchymal transition (EMT)-like phenotype in human colon cancer cells. Palladin in colon cancer metastasis, AACR
35. Chan WY, Soloviev MM, Ciruela F et al (2001) Molecular determinants of metabotropic glutamate receptor 1B trafficking. Mol Cell Neurosci 2001(17):577–588
36. Stamm S, Ben-Ari S, Rafalska I et al (2005) Function of alternative splicing. Gene 344:1–20
37. Putti TC, El-Rehim DM, Rakha EA et al (2005) Estrogen receptor-negative breast carcinomas: a review of morphology and immunophenotypical analysis. Mod Pathol 18:26–35
38. Guarino M, Rubino B, Ballabio G (2007) The role of epithelial-mesenchymal transition in cancer pathology. Pathology 39:305–318
39. Heimann R, Lan F, McBride R, Hellman S et al (2000) Separating favorable from unfavorable prognostic markers in breast cancer: the role of E-cadherin. Cancer Res 60:298–304
40. Mendelsohn J, Baselga J (2000) The EGF receptor family as targets for cancer therapy. Oncogene 2000(19):6550–6565
41. bd El-Rehim DM, Ball G, Pinder SE et al (2005) High-throughput protein expression analysis using tissue microarray technology of a large well-characterised series identifies biologically distinct classes of breast cancer confirming recent cDNA expression analyses. Int J Cancer 116:340–350
42. Jones C, Ford E, Gillett C et al (2004) Molecular cytogenetic identification of subgroups of grade III invasive ductal breast carcinomas with different clinical outcomes. Clin Cancer Res 10:5988–5997
43. Kulka J, Szasz AM, Nemeth Z et al (2008) Expression of Tight Junction Protein Claudin-4 in Basal-Like Breast Carcinomas. Pathol Oncol Res
44. Herschkowitz JI, Simin K, Weigman VJ et al (2007) Identification of conserved gene expression features between murine mammary carcinoma models and human breast tumors. Genome Biol 8:R76
45. Dhawan P, Singh AB, Deane NG et al (2005) Claudin-1 regulates cellular transformation and metastatic behavior in colon cancer. J Clin Invest 115:1765–1776
46. Sobel G, Paska C, Szabo I et al (2005) Increased expression of claudins in cervical squamous intraepithelial neoplasia and invasive carcinoma. Hum Pathol 36:162–169
47. Nicholson RI, Johnston SR (2005) Endocrine therapy—current benefits and limitations. Breast Cancer Res Treat 93(Suppl 1):S3–S10

Virchows Arch (2009) 454:657–666
DOI 10.1007/s00428-009-0765-3

ORIGINAL ARTICLE

Melatonin prevents the development of hyperplastic urothelium induced by repeated doses of cyclophosphamide

Daša Zupančič · Gaj Vidmar · Kristijan Jezernik

Received: 16 October 2008 / Revised: 14 February 2009 / Accepted: 19 March 2009 / Published online: 21 April 2009

Abstract Repeated cyclophosphamide (CP) chemotherapy increases the risk of developing bladder cancer, which could be due to the extremely rapid proliferation of urothelial cells observed in hyperplastic urothelium induced by CP treatment. We investigated the effect of melatonin on the development of urothelial hyperplasia induced by repeated CP treatment. Male ICR mice were injected with CP (150 mg/kg) or melatonin (10 mg/kg) with CP once a week for 3, 4 and 5 weeks. Transmission and scanning electron microscopy, immunohistochemistry and Western blot analysis were used to study the ultrastructure, apoptosis, proliferation and differentiation of urothelial cells. Repeated doses of CP caused the development of hyperplastic urothelium with up to ten cell layers and increased proliferation and apoptotic indices regarding Ki-67 and active caspase-3 immunohistochemistry, respectively. Scanning electron microscopy observations, cytokeratin and asymmetrical unit membrane immunohistochemistry and Western blot analysis showed a lower differentiation state of superficial urothelial cells. Melatonin co-treatment prevented the development of hyperplastic urothelium, statistically significantly decreased proliferation and apoptotic indices after four and five doses of CP and caused higher differentiation state of superficial urothelial cells.

D. Zupančič (✉) · K. Jezernik
Institute of Cell Biology, Faculty of Medicine,
Lipičeva 2,
1000 Ljubljana, Slovenia
e-mail: dasa.zupancic@mf.uni-lj.si

G. Vidmar
Institute for Rehabilitation,
Linhartova cesta 51,
1000 Ljubljana, Slovenia

Keywords Urothelium · Cyclophosphamide · Hyperplasia · Melatonin

Introduction

The three-layered mammalian urinary bladder urothelium is a normally very stable and highly differentiated epithelium [1]. Nevertheless, it shows a great capacity for regeneration after a mechanically or chemically induced damage [1–3]. Urothelial regeneration usually gives rise to hyperplasia and can contribute to a wide range of neoplasms [2]. Hicks and Chowaniec [2] and our unpublished data showed that repeated intraperitoneal doses of cyclophosphamide (CP) cause persistent urothelial hyperplasia. Cohen et al. have developed a model of carcinogenesis which incorporates several basic principles: cancer results from genetic errors within normal cells; carcinogenesis is a multi-stage process, requiring more than one genetic event; and a chance of a genetic event occurring per cell division is a finite quantity and, therefore, that increased cell division increases the chance for a genetic event [4]. Based on this model, they then postulate that changes which lead to increased cell proliferation in the urothelium should be carefully evaluated as a possible contributing factor to carcinogenesis [5–7]. CP has long been known to produce severe hyperplasia following cytotoxic damage to the urothelium [8, 9]. However, it is also a weak complete carcinogen and after prolonged application will produce cancer of the urothelium, but its hyperplastic action is probably associated with its late-stage carcinogenic activity rather than with its first-stage initiating activity [10]. In a lifelong experiment of the carcinogen action of CP, low-dose oral application of CP led to the induction of bladder cancer in 30% to 43% of rats [11]. However, in the last few months of the experiments,

repeated intraperitoneal injections of CP were given to rats and mice and no bladder tumours were observed [2, 12]. Nevertheless, it is known that patients treated with cyclophosphamide have up to a ninefold increased risk of developing bladder cancer [13, 14].

Urothelial carcinogenesis in the rat and mouse proceeds through a sequence of morphologic changes beginning as simple hyperplasia [15]. In the rat, it then progresses to nodular and papillary hyperplasia, while in the mouse nodular hyperplasia is considerably more common than papillary proliferations [4]. The rat model then progress to papillomas and strongly resembles low-grade papillary urothelial neoplasia in humans, whereas the mouse model resembles the high-grade, highly malignant disease of humans [15].

A single-dose CP treatment causes a destruction of the bladder urothelium [8, 9, 16, 17], followed by rapid proliferation of urothelial cells resulting in reversible hyperplasia and gradual restoration of normal three-layered urothelium [6, 18–20]. It is documented that reversible hyperplasia is accompanied not only by an increased proliferation activity of urothelial cells but also by an increased number of apoptotic cells [20] and lower differentiation state of superficial urothelial cells [16, 21, 22]. In the hyperplastic urothelium, most of the urothelial cells undergo apoptosis within the superficial layer and are exfoliated into the lumen of the urinary bladder [20] and subsequently removed from the body with urine and lost for detection. Thus, it is important to identify apoptotic cells before classical features of apoptosis are present, which can be achieved by immunohistochemical detection of active caspase-3 [19, 23, 24]. Specific antisera allow a reliable detection of apoptotic cells without overlap with necrotic cell population [25, 26]. Caspase-3 is an effector caspase and when activated by initiator caspases, such as caspase-8, it cleaves various substrates, leading to the apoptotic cell death [24, 27].

The terminally differentiated superficial urothelial cells–umbrella cells have two unique characteristics: a subapical trajectorial network of cytokeratins [22] and membrane–protein plaques, which cover the apical surface of the umbrella cells, forming a rigid-looking asymmetrical unit membrane (AUM) [28–31]. Immunostaining against AUM proteins may serve as a well-defined marker of cell differentiation, since it shows no labelling signal in the undifferentiated cells with microvilli, whereas strong labelling in the umbrella cells with rigid-looking microridges can be observed [21, 22]. Anti-AUM antibody is made against highly purified bovine AUM and reacts strongly with uroplakin III (47 kDa) [32]. Differentiation of urothelial cells can also be characterised by changes in the cytokeratin (CK) expression patterns. For example, CK 7 is expressed in differentiated and undifferentiated cells, whereas CK 20 is present exclusively in terminally differentiated umbrella cells [33–37].

In the last decade, research has specifically addressed the role of melatonin, the main secretory product of the pineal gland, in controlling the proliferation of neoplastic cells [38]. Both in vitro and on different animal models of tumorigenesis, melatonin has been found to inhibit cell proliferation and to delay tumour progression [39, 40]. Most studies exploring the relationship between melatonin and oncogenesis have focused on melanoma and breast cancer, but more recently melatonin has been shown to influence neoplastic growth in many other cancers including carcinomas of the urinary bladder [41]. Furthermore, increasing evidence indicates that melatonin may exert its anticancer effects not only via inhibition of cell proliferation but also by stimulation of differentiation and apoptosis [39]. Moreover, it is documented that melatonin has a protective effect against single-dose CP-induced urothelial damage [42, 43] and a favourable impact on regeneration and restoration of normal urothelium, since it reduces the number of apoptotic and proliferating urothelial cells and results in their earlier differentiation [43].

Repeated doses of CP cause the development of urothelial hyperplasia, which could lead to bladder cancer development [6]. In different studies, melatonin has been found to inhibit cell proliferation and also influence differentiation and apoptosis. The aim of this study was therefore to examine the effect of melatonin on the development of hyperplastic urothelium and on the proliferation, apoptosis and differentiation of urothelial cells after repeated doses of CP.

Materials and methods

Animals and treatment

The animal experiments were approved by the Slovenian veterinary administration of the Ministry of Agriculture, Forestry and Food according to the Animal Health Protection Act and Introductions for Granting Permits for Animal Experimentation for Scientific Purposes. Forty albino ICR (CD-1) adult male mice were divided into ten groups by a simple random sampling method. They were housed in plastic cages at 23±2°C and 50% to 60% relative humidity. Basal diet and water were available ad libitum.

Group 1 (control) animals were injected with saline once a week for 3 weeks and they served as controls, whereas group 2 (Mel) received 15 mg/kg of body weight of melatonin once a week for 3 weeks and served as control for melatonin administration only. All the animals from groups 3 to 10 were injected with CP (Sigma) at a dose of 150 mg/kg of body weight once a week for 3, 4 and 5 weeks and half of them (groups 7 to 10) also received 15 mg/kg of body weight of melatonin with CP, before and the day after CP injection. All the drugs were administered

intraperitoneally (i.p.). Animals were sacrificed after three (3×), four (4×) and five (5×) doses of CP or melatonin and CP co-treatment (Mel+CP) and 1 month after five doses (1 m) of CP or melatonin and CP co-treatment (Mel+CP).

From each group, the bladders were processed for electron microscopy, for active caspase-3, Ki-67, CK 7, CK 20 and AUM immunohistochemistry and for Western blot analysis.

Electron microscopy

The tissue was fixed in 4.5% paraformaldehyde and 2% glutaraldehyde for 3 h. For transmission electron microscopy, the samples were then postfixed in osmium tetroxide, dehydrated in ethanol and embedded in Epon. Ultrathin sections were stained with lead citrate and uranyl acetate and examined with a Jeol 100 CX electron microscope (Jeol Ltd., Tokyo, Japan). For scanning electron microscopy, the samples were postfixed in osmium tetroxide and critical-point dried. After sputter-coating with gold, they were examined at 15 kV with a Jeol JSM 840 A scanning electron microscope (Jeol Ltd., Tokyo, Japan).

Immunohistochemical detection of active caspase-3, Ki-67 and AUM

The tissue was fixed in 4% paraformaldehyde overnight and embedded in paraffin. After deparaffinisation, the endogenous peroxidase activity was blocked by 3% H_2O_2 in methanol. For detection of Ki-67, sections were microwave-heated. Non-specific labelling was blocked by 2.5% bovine serum albumin (Sigma, Taufkirchen, Germany) for Ki-67 or by 20% normal swine serum for active caspase-3 and AUM. Sections were incubated with primary monoclonal anti-Ki-67 (clone MIB-5, Dako, Glostrup, Denmark; 1:50 dil.), polyclonal anti-active-caspase-3 (R&D Systems, Wiesbaden, Germany; 1:1,500 dil.) or polyclonal rabbit antibodies raised against highly purified bovine AUM (a kind gift from Prof. T.-T. Sun, Department of Dermatology, New York University Medical School, New York, NY 10016; 1:10,000 dil.) overnight at 4°C. For negative controls, the incubation with primary antibody was omitted or the specific primary antibody was replaced by a non-relevant antibody. For secondary antibodies, biotinylated rabbit anti-mouse (Dako, Glostrup, Denmark; 1:100 dil.) or swine anti-rabbit immunoglobulins (Dako, Glostrup, Denmark; 1:400 dil.) were applied for 1 h at room temperature, followed by ABC/HRP complex (Dako, Glostrup, Denmark) incubation. After the standard DAB (Sigma, Taufkirchen, Germany) development procedure, sections were counterstained with haematoxylin and examined with a Nikon Eclipse TE300 fluorescence microscope (Nikon Corporation, Tokyo, Japan).

Immunohistochemical detection of CK 7 and CK 20

The tissue was frozen and cut into 7-μm-thick cryosections and fixed in absolute ethanol (−20°C) for 20 min. After blocking with 2% BSA in PBS, incubation with primary monoclonal anti-CK 7 (clone OV/TL 12/30, Dako, Glostrup, Denmark; 1:20 dil.) and anti-CK 20 (clone KS20.8, Dako, Glostrup, Denmark; 1:100 dil.) was performed overnight at 4°C. For negative controls, the incubation with primary antibody was omitted or the specific primary antibody was replaced by a non-relevant antibody. Adequate secondary antibodies conjugated with TRITC (Sigma, Taufkirchen, Germany) were incubated for 1 h at 37°C. After washing, the sections were mounted in mounting medium Vectashield with DAPI (Vector Laboratories, Burlingame, CA, USA) and examined with a Nikon Eclipse TE300 fluorescence microscope (Nikon Corporation, Tokyo, Japan).

Western blot analysis

Urothelial cells were scraped from the wall of the urinary bladder and homogenised in ice-cold buffer (0.8 M Tris–HCl, 7.5% SDS, 1 mM phenylmethylsulfonyl fluoride). The lysate was centrifuged and the protein concentration in the supernatant was determined by using a BCA™ protein assay kit (Pierce, Rockford, IL, USA). Sample proteins (30 μg/lane) were size-fractionated on 12% SDS–polyacrylamide gels and then transferred to Hybond ECL nitrocellulose membranes (Amersham Biosciences, Little Chalfont, UK) by electroblotting. After blocking overnight at 4°C in 5% skim milk in PBS-Tween, membranes were incubated for 2 h at room temperature with primary polyclonal rabbit antibodies raised against highly purified bovine AUM (a kind gift from Prof. T.-T. Sun, Department of Dermatology, New York University Medical School, New York, NY 10016, USA; 1:10,000 dil.) or monoclonal anti-CK 7 (Santa Cruz Biotechnology, Inc., Santa Cruz, CA, USA; 1:200 dil.). After washing in PBS-Tween, membranes were incubated for 1 h with adequate secondary antibodies horseradish peroxidase-conjugated goat anti-rabbit (Sigma, Taufkirchen, Germany), diluted 1:1,000, or anti-mouse (Dako, Glostrup, Denmark), diluted 1:1,000. Membranes were finally probed with enhanced chemoluminescence reagent (Amersham Biosciences, Little Chalfont, UK) and exposed to X-ray films. Rabbit anti-actin antibodies, diluted 1:1,000 (Sigma, Taufkirchen, Germany), were used to confirm an equal loading of protein in each lane.

Methods and counting for quantitative analysis

Four animals of each group were used for immunohistochemical detection of active caspase-3 and detection of Ki-67 on paraffin sections. Urinary bladders were cut into serial tissue sections and three sections of each urinary

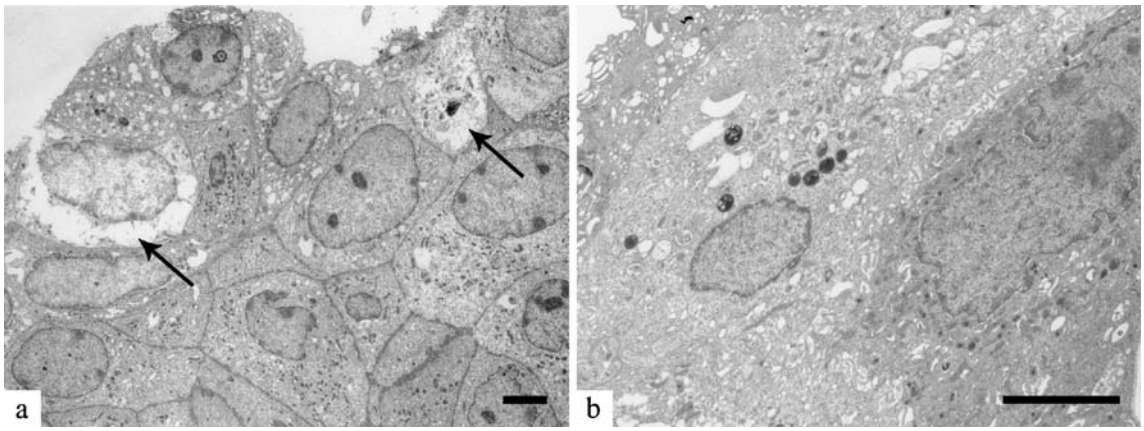

Fig. 1 TEM micrograph. **a** Necrotic cells with swollen cytoplasm and nucleus in the superficial layer of the urothelium (*arrows*) after five doses of CP. **b** Normal urothelium after five doses of melatonin and CP co-treatment. *Scale bar* 5 μm

bladder were examined. Cells with a positive immunohistochemical reaction against active caspase-3 and Ki-67 were accepted as labelled and used for scoring of apoptotic and proliferation indices, respectively. All urothelial cells per tissue section were counted and the indices for each tissue section were defined as a percentage ratio of labelled urothelial cells to the total number of counted cells.

Statistical analysis

For each animal, the mean of the three slices was used for further analysis of apoptotic index and of proliferation index. First, the distributions of both indices were plotted for each group using boxplots. Because of departures from normality, and because of non-homogeneous variances, the data were analysed using two-way analysis of variance on ranks instead of on original observations, which is a robust yet efficient solution [44].

Since the effect of different doses of CP was found to be highly statistically significant, post-hoc comparisons were performed between different doses of CP using the Scheffe procedure on the ranked data (it should be noted that other methods, such as Sidak's, or Dunnet's method for planned comparisons with baseline, lead to equivalent conclusions). Since the effect of group was also highly statistically significant, while the (non-)significance of the interaction

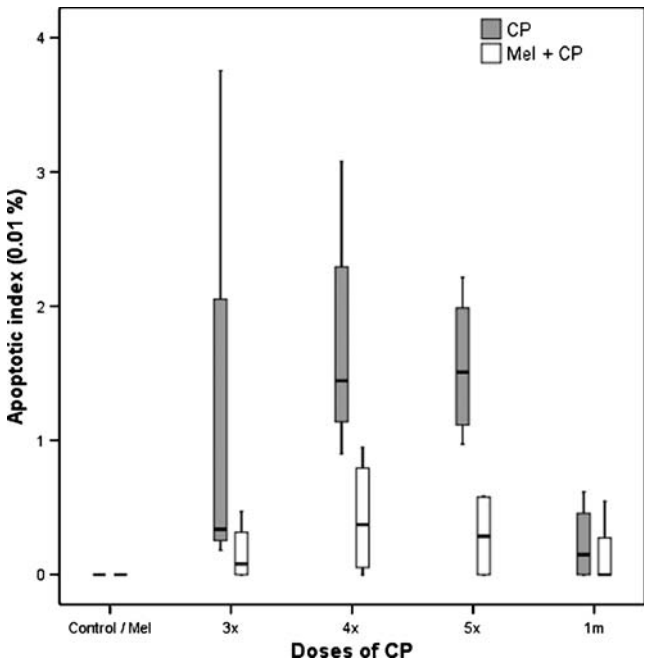

Fig. 2 Boxplot of apoptotic index distribution (*thick line* denotes median, *box* denotes 1st and 3rd quartile and *whiskers* denote the smallest and the largest observation within 1.5 interquartile range from the 1st and the 3rd quartile, respectively)

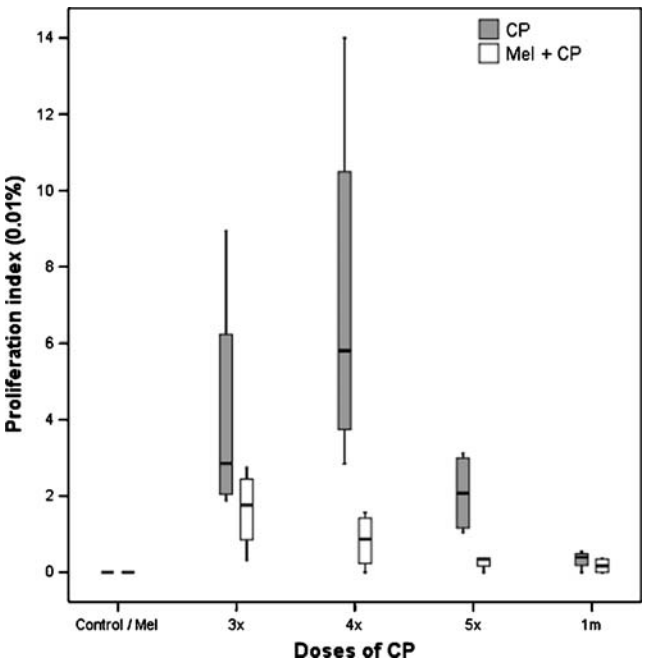

Fig. 3 Boxplot of proliferation index distribution (*thick line* denotes median, *box* denotes 1st and 3rd quartile and *whiskers* denote the smallest and the largest observation within 1.5 interquartile ranges from the 1st and the 3rd quartile, respectively)

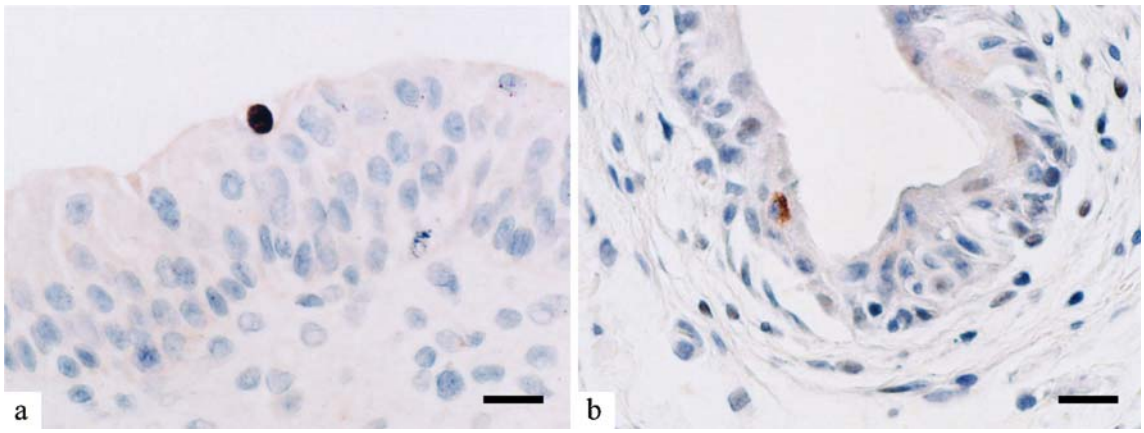

Fig. 4 Active caspase-3 immunohistochemistry. **a** Active caspase-3-positive cell (*brown*) in the urothelium after four doses of CP and **b** after four doses of melatonin and CP co-treatment. *Scale bar* 10 μm

effect should be treated with caution in ANOVA on ranked data [45], the groups with or without melatonin co-treatment were compared after different doses of CP using the exact Mann–Whitney test.

For morphological data (urothelial differentiation markers and hyperplasia appearance), which were in the form of ratings of four-point scale (from 1 = least present to 4 = maximum presence), the median value of the three sections was calculated and analysed in the same way as that for apoptotic and proliferation indices.

Results

In control and melatonin-treated animals, the urothelium was composed of three cell layers and was ultrastructurally normal. Repeated CP treatment at 3, 4 and 5 weeks caused the development of hyperplastic urothelium with up to ten cell layers. After three, four and five doses of CP, prominent dilatations in the intercellular spaces were observed and some necrotic cells were perceived in the superficial layer of the urothelium (Fig. 1a). Melatonin co-treatment resulted in the normal appearance of the urothelium (Fig. 1b). One month after five doses of CP and 1 month after five doses of melatonin and CP co-treatment, the urothelium was composed of three cell layers and was ultrastructurally similar to normal urothelium.

Active caspase-3-positive and Ki-67-positive cells in control and melatonin-treated animals were extremely rare and the mean for all indices was zero (Figs. 2 and 3). After repeated doses of CP (3×, 4× and 5×), substantial elevation of apoptotic and proliferation index was detected, while melatonin co-treatment resulted in much less apoptotic and proliferation index increase (Figs. 2 and 3). An active caspase-3 and Ki-67 reaction positive signal was observed mainly in the cytoplasm of the superficial urothelial cells and in the nuclei of the basal cell layer, respectively (Figs. 4 and 5). One month after five doses of CP and 1 month after five doses of melatonin and CP co-treatment, the apoptotic and proliferation indices returned to near the initial zero level.

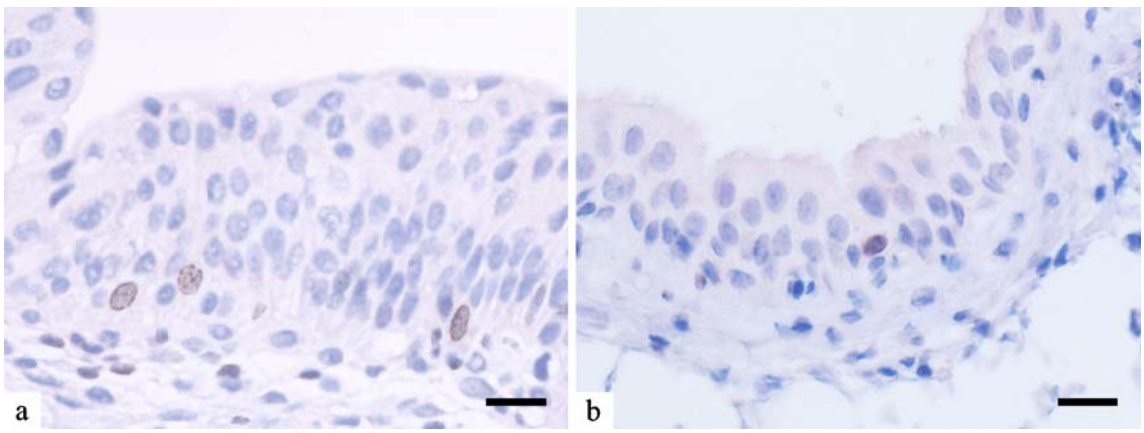

Fig. 5 Ki-67 immunohistochemistry. **a** Ki-67-positive cells (*brown nuclei*) are most abundant in the basal layer of the urothelium after four doses of CP and **b** after four doses of melatonin and CP co-treatment. *Scale bar* 10 μm

Table 1 Summary of the statistical analyses of differentiation markers and hyperplasia appearance in urothelial cells after repeated doses of CP and after repeated melatonin and CP co-treatment

		Mean (range)					*p* values for effects of dose, group and interaction	Summary of post-hoc comparisons regarding CP dose[a]
		Control/ Mel	3×	4×	5×	1m		
CK 7	CP	4.0 (4–4)	4.0 (4–4)	4.0 (4–4)	4.0 (4–4)	4.0 (4–4)	NA	All CP doses equal
	Mel + CP	4.0 (4–4)	4.0 (4–4)	4.0 (4–4)	4.0 (4–4)	4.0 (4–4)		
CK 20	CP	4.0 (4–4)	1.0 (1–1)[b]	1.0 (1–1)[b]	1.0 (1–1)[b]	4.0 (4–4)	<0.001, <0.001, <0.001	4×, 5×, 3× < Control/ Mel, 1 m
	Mel + CP	4.0 (4–4)	2.2 (2–3)[b]	2.0 (2–2)[b]	2.0 (2–2)[b]	4.0 (4–4)		
AUM	CP	4.0 (4–4)	2.2 (2–3)	2.0 (2–2)[b]	2.0 (2–2)[b]	4.0 (4–4)	<0.001, <0.001, <0.001	3×, 4×, 5× < Control/ Mel, 1 m
	Mel + CP	4.0 (4–4)	2.2 (2–3)	3.0 (3–3)[b]	4.0 (3–3)[b]	4.0 (4–4)		
Microvilli	CP	1.0 (1–1)	3.5 (3–4)[b]	2.0 (2–2)	2.0 (2–2)	1.0 (1–1)	<0.001, 0.001, 0.005	Control/Mel, 1 m<5×, 4× < 3×
	Mel+ CP	1.0 (1–1)	2.2 (2–3)[b]	1.8 (1–2)	1.5 (1–2)	1.0 (1–1)		
Ropy ridges	CP	1.0 (1–1)	2.8 (2–3)	2.5 (2–3)	3.0 (3–3)	1.0 (1–1)	<0.001, 0.009, 0.039	Control/Mel, 1 m<3×, 4×, 5×
	Mel + CP	1.0 (1–1)	2.0 (2–2)	2.5 (2–3)	2.2 (2–3)	1.0 (1–1)		
Microridges	CP	4.0 (4–4)	1.0 (1–1)[b]	1.5 (1–2)[b]	2.0 (2–2)[b]	4.0 (4–4)	<0.001, <0.001, <0.001	3×, 4×, 5× < Control/ Mel, 1 m
	Mel + CP	4.0 (4–4)	3.5 (3–4)[b]	3.2 (3–4)[b]	3.5 (3–4)[b]	4.0 (4–4)		
Hyperplasia	CP	1.0 (1–1)	3.0 (3–3)[b]	3.0 (3–3)[b]	3.2 (3–4)[b]	1.0 (1–1)	<0.001, <0.001, <0.001	Control/Mel, 1 m<5×, 4×, 3×
	Mel+ CP	1.0 (1—1)	1.8 (1–2)[b]	1.2 (1–2)[b]	1.0 (1–1)[b]	1.0 (1–1)		

Because the sample size is four in all cells, the distribution of scores is completely captured by mean and range

NA not applicable

[a] Post-hoc comparisons regarding dose are summarised using homogeneous subsets, which are separated by the < (less than) symbol, whereby ordering within homogeneous subsets corresponds to observed means across the two groups. For example, for CK 20, scores were significantly higher at baseline and after 1 month then after all three CP doses, whereby observed scores were higher on average at 1 month than at baseline (though not significantly), while the average score was the lowest after 3× dose, somewhat higher after 4× dose, followed by 5× dose (with those differences not appearing to be significant)

[b] Significant difference between groups for the given dose

Statistical analyses of urothelial differentiation markers and hyperplasia appearance are summarised in Table 1. They show that CK 7 was present in the urothelium of all groups of animals. CK 7 labelling was observed in all cell layers of hyperplastic urothelium and normal three-layered urothelium after repeated doses of CP and after repeated melatonin and CP co-treatment, respectively (Fig. 6a, b). Western blot analysis confirmed the equal presence of CK 7 in all samples (Fig. 7). All superficial urothelial cells of control, melatonin-treated and 1 month after five doses of CP or melatonin- and CP-treated animals were CK 20 positive and AUM positive (Table 1). After repeated doses of CP, CK 20 labelling of superficial cells was completely negative (Fig. 6c), while some superficial cells were CK 20 positive after melatonin and CP co-treatment (Fig. 6d). Labelling with antibodies against AUM exhibited a similar pattern to CK 20 labelling. Weak anti-AUM staining was apparent after repeated doses of CP (Fig. 6e), whereas melatonin and CP co-treatment resulted in stronger AUM staining of the superficial urothelial cells (Fig. 6f). The results of Western blot analysis proved the higher expression of UP III (detected with anti-AUM antibody) in urothelial cells after four and five doses of melatonin and CP co-treatment than after four and five doses of CP (Fig. 7). Scanning electron microscopy revealed that cells with microvilli and ropy ridges were present on the luminal surface of the urothelium after repeated doses of CP (Fig. 6g), while cells with microridges were rare. Co-treatment with melatonin diminished the appearance of microvilli on the luminal surface and resulted in prevailing of cells with ropy ridges and microridges (Fig. 6h).

Fig. 6 Differentiation markers. **a** CK 7 labelling in hyperplastic urothelium after five doses of CP. **b** CK 7 labelling in normal three-layer urothelium after five doses of melatonin and CP co-treatment. **c** No CK 20 labelling in urothelium after three doses of CP. **d** Positive CK 20 labelling in superficial cells of urothelium after three doses of melatonin and CP co-treatment. **e** Weak AUM labelling of superficial urothelial cells after four doses of CP. **f** Strong AUM labelling of all superficial cells after four doses of melatonin and CP co-treatment. **g** After five doses of CP, urothelial cells are covered by microvilli (*arrow*) and ropy ridges (*arrowhead*). **h** After five doses of melatonin and CP co-treatment, cells are covered by microridges. *Scale bar* 10 μm ▶

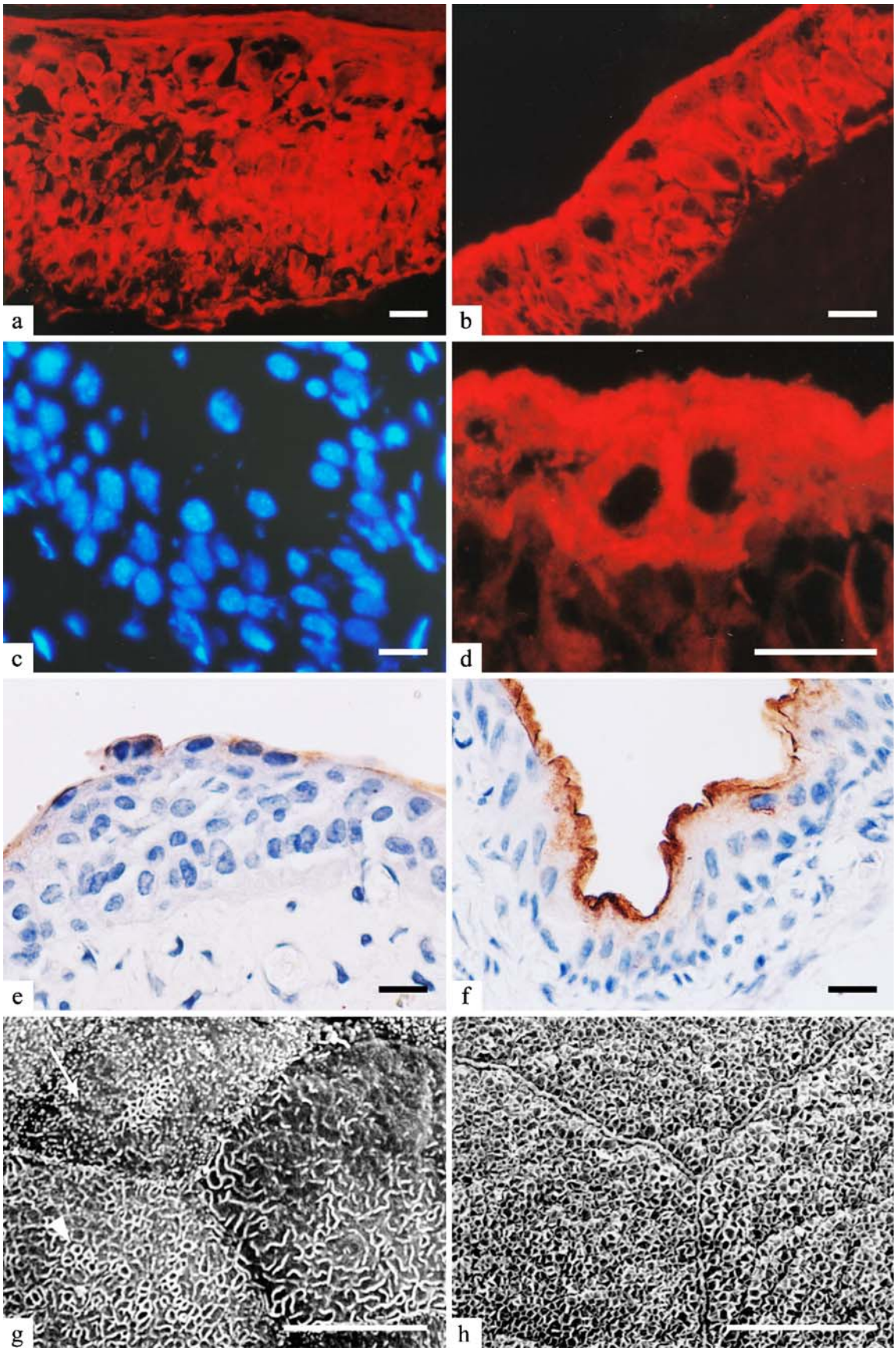
a
b
c
d
e
f
g
h

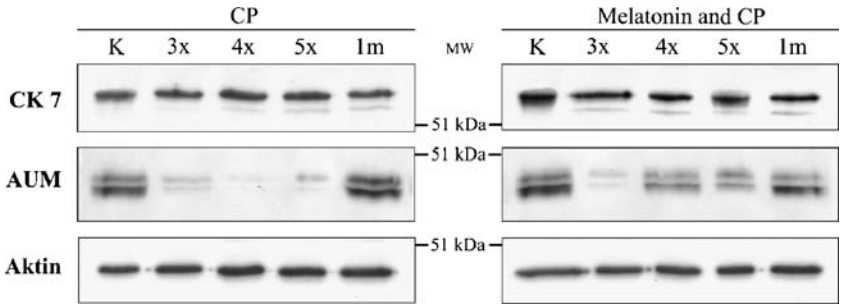

Fig. 7 Western blot analysis of CK 7 and AUM. CK 7 (54 kDa) is equally present in urothelial cells after repeated doses of CP and after repeated doses of melatonin and CP co-treatment. After four and five doses of melatonin and CP co-treatment, the expression of UP III (47 kDa; detected with anti-AUM antibody) is higher than after four and five doses of CP. The immunoblot experiments were performed twice with similar results. *MW* molecular weight standards

The distributions of apoptotic index and proliferation index are depicted in Figs. 2 and 3, respectively.

For apoptotic index and for proliferation index, the main effects of different doses of CP and of CP only or melatonin and CP co-treatment were statistically significant ($p<0.001$ from two-way ANOVA on ranked data), while the interaction effect was not ($p=0.161$ and $p=0.053$ for apoptotic and proliferation indices, respectively).

Post-hoc comparisons between different doses of CP indicate that, for both apoptotic and proliferation index, the average does not differ statistically significantly between control/Mel and 1-m groups ($p=0.605$ and $p=0.175$ for apoptosis and proliferation index, respectively), while that level differs significantly from the 3×, 4× and 5× doses of CP ($p<0.05$), which, in turn, do not differ significantly among themselves ($p>0.05$).

Comparisons between the CP and Mel+CP groups after different doses showed that the groups differed most notably at 4× and 5× ($p=0.029$ for apoptosis and proliferation index at both doses). They differed less at 3× without reaching statistical significance ($p=0.029$ for apoptosis and proliferation index), they were practically equal at 1 m ($p=0.686$ and $p=0.200$ for apoptosis and proliferation index, respectively), and they were identical at the onset of the study as expected ($p=1.000$ for both indices). It should be noted that the p values for comparisons between groups after different doses of CP might have been adjusted for multiple tests, but they are conservative enough because of data aggregation (and thus a reduced sample size, which is very small).

Discussion

Hicks and Chowaniec [2] and our previous unpublished experiments showed that repeated doses of CP cause urothelial hyperplasia. In the present study, we demonstrated that melatonin prevents the development of hyperplastic urothelium induced by repeated CP treatment.

Cohen and co-workers [4–7, 46, 47] proposed a model of carcinogenesis which takes into account the proliferative effects of agents in carcinogenesis. In the current experiment, we demonstrated that urothelial hyperplasia induced by repeated-dose CP is accompanied by increased proliferation activity of urothelial cells. Cohen et al. assumed that, every time a cell undergoes a cell division, there is a low probability, but not zero, of a genetic error occurring [4, 6]. It is, in general, accepted that at least two irreversible genetic events must occur for tumour formation. Thus, the extremely rapid proliferation of urothelial cells seen following repeated CP treatment greatly increased the likelihood of at least one genetic error occurring (initiation). If the increased cell proliferation would be continued for a long period of time, the likelihood of a second promoting event would increase sufficiently that a significant incidence of tumours would occur. Persistent high-proliferation indices observed after repeated CP doses could increase the probability of bladder carcinogenesis and therefore explain the fact that patients treated with repeated CP chemotherapy have up to ninefold increased risk of developing bladder cancer [13, 14].

In numerous experiments in vitro and in different animal models of tumorigenesis, melatonin has been found to inhibit proliferation and neoplastic growth [38, 40, 48]. Some studies also documented that melatonin reduced the cell proliferation in neoplastically unchanged cells [49–51]. It is therefore not surprising that, in the present experiment, melatonin significantly decreased the proliferation activity of urothelial cells and therefore prevented hyperplasia from developing. Since the rapid proliferation of urothelial cells seen after repeated doses of CP could increase the likelihood of bladder carcinogenesis [4–7], melatonin might prevent the development of bladder tumours by decreasing the proliferation activity of urothelial cells.

Experimentally induced urothelial hyperplasia is accompanied by an increased number of apoptotic cells [20, 52–54]. It happened similarly in the present experiment, since not only increased proliferation but also increased apoptotic

indices were found in the hyperplastic urothelium after repeated doses of CP. Melatonin co-treatment significantly decreased not only the proliferation but also the apoptosis of urothelial cells. Numerous reports documented the role of melatonin in inhibiting apoptosis in different cells after ischemia [55–57], hyperoxia [58] or oxidative stress [59]. Moreover, melatonin also decreased the apoptosis of urothelial cells after a single-dose CP treatment [43]. All these experiments investigated the acute injury in which melatonin diminished cell death, while in the present study the anti-apoptotic effect of melatonin was observed in chronic hyperplastic state. It is possible that since melatonin inhibited the proliferation activity of urothelial cells and prevented the development of hyperplastic urothelium, decreased apoptosis of urothelial cells appeared per se and not as a consequence of direct melatonin action.

The scanning electron microscopy observations and expression of urothelial key differentiation markers, the CK 7, CK 20 and AUM, showed that the differentiation state of superficial urothelial cells of hyperplastic urothelium, induced by repeated doses of CP, was lower than in control and resembled the differentiation of superficial urothelial cells during reversible hyperplasia following the destruction of the urothelium after a single dose of CP [16, 21, 22, 60]. Melatonin co-treatment resulted in the higher differentiation state of superficial urothelial cells as indicated by the appearance of urothelial apical surface and confirmed by the expression of analysed differentiation markers. These results are similar to a variety of in vivo and in vitro experimental models of neoplasia, in which evidence was shown that melatonin influences the differentiation of tumour cells [39, 61]. Although it is documented that melatonin is capable of promoting differentiation of neoplastically unchanged osteoblasts and ovarian cells [49, 62], we do not know whether melatonin influences urothelial cell differentiation directly or through its preventive effect against CP-induced hyperplasia. Further studies will be needed to gain a complete insight into this question.

In conclusion, our results document that repeated doses of CP cause the development of hyperplastic urothelium with rapid proliferation of urothelial cells, which could lead to an increased risk of bladder cancer. Melatonin co-treatment prevents the development of hyperplastic urothelium, statistically significantly decreases proliferation and apoptotic indices and causes higher differentiation state of superficial urothelial cells. Despite the lack of clinical studies testing its clinical relevance, the present results suggest that supplementing patients treated with repeated CP chemotherapy with adjuvant melatonin therapy may decrease their risk of developing bladder cancer.

Acknowledgement The authors would like to thank Prof. T.-T. Sun for providing the anti-AUM antibody used in this study.

Conflict of interest statement We declare that we have no conflict of interest.

References

1. Hicks RM (1975) The mammalian urinary bladder: an accommodating organ. Biol Rev 50:215–246
2. Hicks RM, Chowaniec J (1978) Experimental induction, histology, and ultrastructure of hyperplasia and neoplasia of the urinary bladder epithelium. Int Rev Exp Pathol 18:199–280
3. Liang DS (1962) Bladder regeneration following subtotalcystectomy. J Urol 88:503–505
4. Cohen SM, Ellwein LB (1991) Genetic errors, cell proliferation, and carcinogenesis. Cancer Res 51:6493–6505
5. Cohen SM (1983) Promotion in urinary bladder carcinogenesis. Environ Health Perspect 50:51–59
6. Cohen SM (1989) Toxic and nontoxic changes induced in the urothelium by xenobiotics. Toxicol Appl Pharmacol 101:484–498
7. Cohen SM, Greenfield RE, Ellwein LB (1983) Multistage carcinogenesis in the urinary bladder. Environ Health Perspect 49:209–215
8. Koss LG (1967) A light and electron microscopic study of the effects of a single dose of cyclophosphamide on various organs in the rat. Lab Invest 16:44–65
9. Locher GW, Cooper EH (1970) Repair of rat urinary bladder epithelium following injury by cyclophosphamide. Investig Urol 8:116–123
10. Hicks RM (1983) Effect of promoters on incidence of bladder cancer in experimental animal models. Environ Health Perspect 50:37–49
11. Schmähl D, Habs M (1979) Carcinogenic action of low-dose cyclophosphamide given orally to Sprague–Dawley rats in a lifetime experiment. Int J Cancer 23:706–712
12. Tokuoka S (1965) Induction of tumor in mice with *N*,*N*-bis(2-chloroethyl)-*N*′,*O*-propylenephosphoric acid ester diamide (cyclophosphamide). Gann 56:537–541
13. Jung I, Messing E (2000) Molecular mechanisms and pathways in bladder cancer development and progression. Cancer Control 7:325–334
14. Tuttle TM, Williams GM, Marshall FF (1988) Evidence for cyclophospamide-induced transitional cell carcinoma in a renal transplant patient. J Urol 140:1009–1011
15. Cohen SM (2002) Comparative pathology of proliferative lesions of the urinary bladder. Toxicol Pathol 30:663–671
16. Fukushima S, Arai M, Cohen SM et al (1981) Scanning electron microscopy of cyclophosphamide-induced hyperplasia of the rat urinary bladder. Lab Invest 44:89–96
17. Philips FS, Sternberg SS, Cronin AP et al (1961) Cyclophosphamide and urinary bladder toxicity. Cancer Res 21:1577–1589
18. Farsund T (1976) Cell kinetics of mouse urinary bladder epithelium. II. Changes in proliferation and nuclear DNA content during necrosis regeneration, and hyperplasia caused by a single dose of cyclophosphamide. Virchows Arch 21:279–298
19. Jezernik K, Romih R, Mannherz HG et al (2003) Immunohistochemical detection of apoptosis, proliferation and inducible nitric oxide synthase in rat urothelium damaged by cyclophosphamide treatment. Cell Biol Int 27:863–869
20. Romih R, Koprivec D, Stiblar Martincic D et al (2001) Restoration of the rat urothelium after cyclophosphamide treatment. Cell Biol Int 25:531–537
21. Romih R, Jezernik K (1996) Reorganization of the urothelial luminal plasma membrane in the cyclophosphamide treated rats. Pflugers Arch Suppl 431:R241–R242

22. Romih R, Veranic P, Jezernik K (2002) Appraisal of differentiation markers in urothelial cells. Appl Immunohisto M M 10:339–343
23. Hoshi T, Sasano H, Kato K et al (1998) Immunohistochemistry of caspase3/CPP32 in human stomach and its correlation with cell proliferation and apoptosis. Anticancer Res 18:4347–4353
24. Stadelmann C, Lassmann H (2000) Detection of apoptosis in tissue sections. Cell Tissue Res 301:19–31
25. Armstrong RC, Aja TJ, Hoang KD et al (1997) Activation of the CED3/ICE-related protease CPP32 in cerebellar granule neurons undergoing apoptosis but not necrosis. J Neurosci 17:553–562
26. Sirinivasan A, Roth KA, Sayers RO et al (1998) In situ immunodetection of activated caspase-3 in apoptotic neurons in the developing nervous system. Cell Death Differ 5:1004–1016
27. Bratton SB, MacFarlane M, Cain K et al (2000) Protein complex activate distinct caspase cascades in death receptor and stress-induced apoptosis. Exp Cell Res 256:27–33
28. Hicks RM (1965) The fine structure of the transitional epithelium of rat ureter. J Cell Biol 26:215–246
29. Kachar B, Liang F, Lin SU et al (1999) Three-dimensional analysis of the 16 nm urothelial plaque particle: luminal surface exposure, preferential head-to-head interaction, and hinge formation. J Mol Biol 285:595–608
30. Koss LR (1969) The asymmetric unit membrane of the epithelium of the urinary bladder of the rat. An electron microscopy study of a mechanism of epithelial maturation and function. Lab Invest 21:154–168
31. Staehelin LA, Chlapowski FJ, Bonneville MA (1972) Lumenal plasma membrane of the urinary bladder: 1. Three-dimensional reconstruction from freeze-etch images. J Cell Biol 53:73–91
32. Wu XR, Manabe M, Yu J et al (1990) Large scale purification and immunolocalization of bovine uroplakins I, II and III. Molecular markers of urothelial differentiation. J Biol Chem 265:19170–19179
33. Harnden P, Allam A, Joyce AD et al (1995) Cytokeratin 20 expression by non-invasive transitional cell carcinomas: potential for distinguishing recurrent from non-recurrent disease. Histopathology 27:169–174
34. Moll R, Achtstätter T, Brecht E et al (1988) Cytokeratins in normal and malignant transitional epithelium. Maintenance of expression of urothelial differentiation features in transitional cell carcinomas and bladder carcinoma cell culture lines. Am J Pathol 132:123–144
35. Moll R, Schiller DL, Franke WW (1990) Identification of protein IT of the intestinal cytoskeleton as a novel type I cytokeratin with unusual properties and expression patterns. J Cell Biol 77:685–697
36. Romih R, Jezernik K, Mašera A (1998) Uroplakins and cytokeratins in the regenerating rat urothelium after sodium saccharin treatment. Histochem Cell Biol 109:263–269
37. Schaafsma HE, Ramaeker FCS, Vanmujien GNP et al (1989) Distribution of cytokeratin polypeptides in epithelial of the adult human urinary tract. Histochemistry 91:151–191
38. Zachary I, Woll PJ, Rozengurt A (1987) A role for neuropeptides in the control of cell proliferation. Dev Biol 124:295–308
39. Blask DE, Dauchy RT, Sauer LA (2005) Putting cancer to sleep at night: the neuroendocrine/circadian melatonin signal. Endocr 27:179–188
40. Hill SM, Blask DE (1988) Effects of the pineal hormone on the proliferation and morphological characteristics of human breast cancer (MCF-7) in culture. Cancer Res 48:6121–6126
41. Blask DE (1993) Melatonin in oncology. In: Yi HS, Reiter RJ (eds) Melatonin. CRC, Boca Raton, pp 447–476
42. Topal T, Oztas Y, Korkmaz A et al (2005) Melatonin ameliorates bladder damage induced by cyclophosphamide in rats. J Pineal Res 38:272–277
43. Zupančič D, Jezernik K, Vidmar G (2008) Effect of melatonin on apoptosis, proliferation and differentiation of urothelial cells after cyclophosphamide treatment. J Pineal Res 44:299–306
44. Hora SC, Conover WJ (1984) The F-statistic in the two-way layout with rank-score transformed data. J Am Stat Assoc 79:668–673
45. Conover WJ (1999) Practical nonparametric statistics, 3rd edn. Wiley, New York
46. Ellwein LB, Cohen SM (1988) A cellular dynamics model of experimental bladder cancer: analysis of the effect of sodium saccharin in the rat. Risk Anal 8:215–221
47. Greenfield RE, Ellwein LB, Cohen SM (1984) A general probabilistic model of carcinogenesis: analysis of experimental urinary bladder cancer. Carcinogenesis 5:437–445
48. Cini G, Coronnello M, Mini E et al (1998) Melatonin's growth/inhibitory effect on hepatoma AH 130 in the rat. Cancer Lett 125:51–59
49. Sainz RM, Mayo JC, Tan D-X (2003) Antioxidant activity of melatonin in Chinese hamster ovarian cells: changes in cellular proliferation and differentiation. Biochem Biophys Res Commun 302:625–634
50. Lewinski A, Rybicka I, Wajs E et al (1991) Influence of pineal indoleamines on the mitotic activity of gastric and mucosa epithelial cells in the rat: interaction with omeprazole. J Pineal Res 10:104–108
51. Yu HS, Hernandez V, Haywood M et al (1993) Melatonin inhibits the proliferation of retinal pigment epithelial (RPE) cells in vitro. In Vitro Cell Dev Biol Anim 29:415–418
52. Otori K, Yano Y, Takada N et al (1997) Reversibility and apoptosis in rat urinary bladder papillomatosis induced by uracil. Carcinogenesis 18:1485–1489
53. Santarosa R, Colombel MC, Kaplan S et al (1994) Hyperplasia and apoptosis. Opposing cellular processes that regulate the response of the rabbit bladder to transient outlet obstruction. Lab Invest 70:503–510
54. Shirai T, Shibata M-A, Takahashi S et al (1995) Differences in cell proliferation and apoptosis between reversible and irreversible mucosal lesions associated with uracil-induced urolithiasis in *N*-butyl-*N*-(4-hydroxybutyl) nitrosamine-pretreated rats. Carcinogenesis 16:501–505
55. Bertuglia S, Marchiafava PL, Colantuoni A (1996) Melatonin prevents ischemia reperfusion injury and hamster cheek pouch microcirculation. Cardiovasc Res 31:947–952
56. Kunduzova OR, Escourrou G, Seguelas M-H et al (2003) Prevention of apoptotic and necrotic cell death, caspase-3 activation, and renal dysfunction by melatonin after ischemia/reperfusion. FASEB J 17:872–874
57. Osborne NN, Nash MS, Wood JP (1998) Melatonin counteracts ischemia-induced apoptosis in human retinal pigment epithelial cells. Invest Ophthalmol Vis Sci 39:2374–2383
58. Shaikh AY, Xu J, Wu Y et al (1997) Melatonin protects bovine cerebral endothelial cells from hyperoxia-induced DNA damage and death. Neurosci Lett 229:193–197
59. Jou MJ, Peng TI, Reiter RJ et al (2004) Visualization of the antioxidative effects of melatonin at the mitochondrial level during oxidative stress-induced apoptosis of rat brain astrocytes. J Pineal Res 37:55–70
60. Veranič P, Romih R, Jezernik K (2004) What determines differentiation of urothelial umbrella cells? Eur J Cell Biol 83:27–34
61. Cos S, Fernandez R, Guezmes A et al (1998) Influence of melatonin on invasive and metastatic properties of MCF-7 human breast cancer cells. Cancer Res 58:4383–4390
62. Roth JA, Kim B-G, Lin W-L (1999) Melatonin promotes osteoblast differentiation and bone formation. J Biol Chem 274:22041–22047

Virchows Arch (2009) 454:667–676
DOI 10.1007/s00428-009-0777-z

ORIGINAL ARTICLE

Microsomal prostaglandin E synthase protein levels correlate with prognosis in colorectal cancer patients

Tsuguhiko Seo · Atsushi Tatsuguchi · Seiichi Shinji · Masaoki Yonezawa · Keigo Mitsui · Shu Tanaka · Shunji Fujimori · Katya Gudis · Yuh Fukuda · Choitsu Sakamoto

Received: 20 November 2008 / Revised: 2 April 2009 / Accepted: 14 April 2009 / Published online: 2 May 2009

Abstract The aim of this study is to investigate the expression of three prostaglandin E synthase (PGES) isomers in colorectal cancer (CRC) tissue and to evaluate their relationship to clinicopathological factors and patient prognosis. Microsomal PGES (mPGES)-1, mPGES-2, cytosolic PGES (cPGES) and cyclooxygenase (COX)-2 protein expression were analyzed by real-time polymerase chain reaction and Western blot. The localization of each PGES and COX-2 protein was examined by immunohistochemistry in 155 surgical resections and correlated to clinicopathological factors and patient prognosis. mPGES-1 mRNA and protein levels were significantly higher in CRC than in paired normal tissues. mPGES-1 immunoreactivity localized in cancer cells in 43% of cases. mPGES-2 immunoreactivity was significantly more pronounced in cancer cells than in adjacent normal epithelium in 36% of cases. cPGES immunoreactivity was homogeneous in cancer cells and thus determined constitutive. mPGES-1 and mPGES-2 correlated with significantly worse prognosis in stage I–III patients. These results indicate that mPGES-1 and mPGES-2 may each play a role in CRC progression.

Keywords Colorectal neoplasm · Cyclooxygenase-2 · Prognosis · Prostaglandin E synthase · Immunohistochemistry

T. Seo · A. Tatsuguchi (✉) · M. Yonezawa · K. Mitsui · S. Tanaka · S. Fujimori · K. Gudis · C. Sakamoto
Department of Medicine, Division of Gastroenterology,
Nippon Medical School,
1-1-5 Sendagi, Bunkyo-ku,
Tokyo, 113-8603, Japan
e-mail: tachan@nms.ac.jp

A. Tatsuguchi · Y. Fukuda
Department of Analytic Human Pathology,
Nippon Medical School,
1-1-5 Sendagi, Bunkyo-ku,
Tokyo, 113-8602, Japan

S. Shinji
Surgery for Organ Function and Biological Regulation,
Department of Surgery I, Graduate School of Medicine,
Nippon Medical School,
1-1-5 Sendagi, Bunkyo-ku,
Tokyo, 113-8603, Japan

Introduction

Nonsteroidal anti-inflammatory drugs (NSAIDs) have been shown to reduce the incidence of carcinogen-induced colon tumors in rodents and have been associated with reduced incidence of gastrointestinal cancer in epidemiological studies [1]. NSAIDs inhibit cyclooxygenase (COX), the rate-limiting enzyme catalyzing the metabolism of arachidonic acid (AA) into prostaglandins (PGs), prostacyclin, and thromboxanes. There are two forms of COX, a constitutively produced COX-1 and an inducible COX-2. Several lines of evidence indicate that the anti-neoplastic effect of NSAIDs is attributable to COX-2 inhibition [2]. Selective COX-2 inhibitors have been shown to reduce the incidence, multiplicity, and size of colonic carcinomas in the azoxymethane rat model [3]. A recent series of randomized control trials reported that selective COX-2 inhibitors significantly reduced the risk of colorectal adenomas and were effective agents in the prevention of colorectal adenomas [4–6]. Moreover, regular use of aspirin reduced the incidence rate of colorectal cancer (CRC) overexpressing COX-2 but not the incidence rate of CRC with weak or absent COX-2 expression [7]. Thus, COX-2 has received much attention as a molecular target for the prevention and treatment of CRC [8].

PGE_2 has a wide range of biological activities and plays essential roles in a variety of processes linked to tumor progression, including tumor cell proliferation, invasion, angiogenesis, and immunosuppression [9]. PGE_2 is produced via three sequential enzymatic reactions: release of AA from membrane glycerophospholipids by phospholipase A_2, conversion of AA to the unstable intermediate prostanoid prostaglandin H_2 (PGH_2) by COX, and isomerization of PGH_2 to PGE_2 by the cell-specific PGE synthase (PGES). At least three distinct isoforms of PGES have been isolated: one cytosolic PGES (cPGES) and two microsomal fractions, microsomal PGES (mPGES)-1 and mPGES-2 [10–12]. Studies have shown that cPGES is constitutively expressed and functionally coupled to COX-1 [11], whereas mPGES-1 is inducible and preferentially coupled to COX-2 [13, 14]. mPGES-2 has yet to be well characterized, though studies suggest that mPGES-2 promotes PGE_2 production via both COX-1 and COX-2 with modest preference for COX-2 [15].

mPGES-1 functions downstream of COX-2 in the PGE_2-biosynthetic pathway. A number of studies have already shown that mPGES-1 is expressed in various cancers that also express COX-2, suggesting that the COX-2/mPGES-1/PGE_2 pathway is linked to the genesis and growth of cancers [16–20]. Recently, it has been reported that genetic deletion of mPGES-1 results in the marked suppression of intestinal cancer growth [21]. Although the expression of the two mPGES isomers has been reported in CRC, their clinical significance remains unclear [16, 22]. This study aims to investigate the expression of each of the PGES proteins in CRC tissue and to examine the relationship between their expression and various clinicopathological factors and patient prognosis

Materials and methods

Patients and tissue samples

We obtained 155 colon and rectum adenocarcinoma tissue samples from archives of the Department of Pathology at Nippon Medical School Hospital for immunohistochemical analysis of COX-2, mPGES-1, mPGES-2 and cPGES protein expression. Patients included 90 men and 65 women ranging in age from 44 to 91 years (average age, 66.1 years; median, 66.0 years). In addition, ten consecutive colorectal and paired nonneoplastic biopsies were analyzed by Western blot for COX-2 and PGES protein expression. Patients included six men and four women ranging in age from 55 to 71 years (average age, 64.1 years; median, 64 years). We excluded patients who had undergone chemotherapy or radiation. Patients were traced via hospital and pathology records. Disease-free survival (DFS) was defined as the interval from the date of the first surgery until relapse, the appearance of a second primary cancer, or death, whichever occurred first. At the time of analysis, 47 patients had died, and 108 still survived. The median follow-up time for the whole series was 42 months (mean, 46 months; range, 3 to 111 months) and the median survival 62 months (mean, 56 months; range, 1 to 111 months). All subjects gave informed consent, and the project was approved by the Ethics Committee of Nippon Medical School. All staging criteria were defined according to International Union Against Cancer TNM classifications.

Antibodies

Antihuman mouse monoclonal antibodies (mAb) against mPGES-1 and COX-2; and antihuman rabbit polyclonal antibodies (pAb) against mPGES-1, mPGES-2, and cPGES were all from Cayman Chemical (Ann Arbor, MI, USA). Antihuman rabbit pAb against cPGES was compliments of Professor Ichiro Kudo (Showa University; Tokyo, Japan). These antibodies have all been tested in previous studies [11, 15, 20, 23].

Reagents and standards

mPGES-1 protein Recombinant human mPGES-1 protein, kindly donated by Japan Tobacco Central Pharmaceutical Research Institute, was prepared as microsomal proteins of *Escheria coli* transfected with mPGES-1 cDNA.

Polymerase chain reaction analysis RNeasy Mini Kit (Qiagen; Hilden, Germany), Moloney murine leukemia virus (M-MLV) reverse transcriptase (GIBCO Life Technologies; Gaithersburg, MD, USA), random Hexamers (Pharmacia; Freiburg, Germany), and a Taq Man probe and β-actin primer/probe set from Applied Biosystems (Foster City, CA) were used.

Western blot Protein Assay Standard II kit and Precision Plus Protein Standard (Bio-Rad Laboratories; Hercules, CA, USA), Hybond polyvinylidene difluoride (PVDF) membrane, and enhanced chemiluminescence (ECL) reagent (Amersham; High Wycombe, UK) were used.

Real-time polymerase chain reaction analysis of mPGES-1, mPGES-2, and cPGES mRNA

mPGES-1, mPGES-2, and cPGES mRNA expression levels in cancer and non-cancerous tissues were determined by quantitative real-time polymerase chain reaction (PCR) analysis. The PCR primer sequences for targeted genes are summarized in Table 1. Briefly, total RNA was isolated

Table 1 Primer sequences for real-time PCR

Gene	Accession No.	Sequence
mPGES-1	NM_004878	5′-GGAACGACATGGAGACCATCTAC-3′
		5′-TCCAGGCGACAAAAGGGTTA-3′
mPGES-2	NM_025072	5′-GCAAGGAGGTGACCGAGTTC-3′
		5′-CACTGCCGCCACTTCATCTC-3′
cPGES	NM_006601	5′ -AAGACTGGGAAGATGATTCAGATG-3′
		5′ -GAACAACCCTCATCACCACCCATGTTGTTC-3′

following RNeasy Mini Kit instructions. Reverse transcription was conducted for 60 min at 37°C using 2 μg RNA in 25 μl of reaction mixture, 200 U of M-MLV reverse transcriptase, and random Hexamers as primer. cDNA amplification was conducted with a sequence-detection system (GenAmp 5700). A β-actin primer/probe set was used in separate wells as internal control for input cDNA. Thermal cycling conditions included 2 min at 50°C and 10 min at 95°C, followed by 40 cycles for 15 s at 95°C and 1 min at 60°C. Real-time fluorescence measurements and cycle threshold values were determined. Each PGES isomer and β-actin mRNA level was calculated using Primer Express software. To control total cDNA input variations, mPGES-1, mPGES-2, and cPGES mRNA levels for each sample were normalized to β-actin mRNA levels and expressed as arbitrary units.

Western blot analysis

Colonic tissue biopsies were homogenized in protein lysis/sample buffer (RIPA buffer: 50 mM Tris, pH8.0, 0.1% sodium dodecyl sulfate, 1% Nonie P-40, 0.5% deoxycholate, 150 mM NaCl, 1 mM phenylmethylsulfonyl fluoride), iced for 15 min, centrifuged at 15,000 rpm for 20 min, and the resultant supernatants used as protein lysates. Recombinant mPGES-1 protein served as positive control. Lysates were solubilized in sodium dodecyl sulfate (sample buffer), separated on 15% sodium dodecyl sulfate-polyacrylamide gels, subjected to electrophoresis, and transferred onto Hybond PVDF membranes. Membranes were blocked overnight at 4°C in 5% powdered milk in Tris buffered saline Tween (TBST), then incubated with mPGES-1 pAb (Cayman; 1:50), mPGES-2 pAb (Cayman; 1:200) or cPGES mAb (Cayman; 1:100) in TBST for 1 h. Blots were washed with TBST and probed with anti-mouse or anti-rabbit horseradish peroxidase conjugated secondary antibody at concentrations of 1:2,000 for 1 h and developed with ECL reagent.

Immunohistochemical analysis

Specimens were fixed in 10% formalin, embedded in paraffin wax, cut into 3 μm sections, and immersed in 0.3% H_2O_2–methanol for 30 min to block endogenous peroxidase activity. Sections were then microwaved in 0.01 mol/l citrate phosphate buffer (pH6.0) for antigen retrieval and incubated with 10% normal horse or goat serum for 10 min at 37°C to block nonspecific immunoglobulin (IgG) binding. After, sections were incubated for 18 h at 4°C with COX-2 mAb (Cayman; 1:250), mPGES-1 mAb (Cayman; 1:250), mPGES-2 pAb (Cayman; 1:200) or cPGES pAb (Showa 1:100); then incubated for 1 h at 25°C with their respective biotinilated anti-mouse or anti-rabbit IgGs (1:200). Antibody binding sites were visualized by treating the sections with avidin biotinilated peroxidase complex for 1 h at 25°C, then immersing them in 3,3′-diaminobenzidine tetrahydrochloride solution containing 0.03% H_2O_2. Nuclei were counterstained with Mayer's hematoxylin.

Negative control immunohistochemical procedures included omission of the primary antibody and its replacement with normal rabbit or mouse IgG. mPGES-1 antibody specificity was determined by preadsorption of the primary antibody with human mPGES-1 protein for 1 h at 37°C prior to staining procedures.

Evaluation of immunohistochemical staining

Each case was evaluated blindly by two independent observers (T.S. and A.T.). Any disagreement was resolved using a multi-headed microscope. Cases showing COX-2 immunoreactivity in over 10% of cancer cells were considered positive, as previously described [24, 25]. Cases showing mPGES-1 immunoreactivity in over 5% of cancer cells were considered positive, as previously described [20]. Cases in which mPGES-2 immunoreactivity in cancer cells was significantly more pronounced in intensity than its expression in the adjacent glandular epithelium were defined as positive for mPGES-2 expression [20].

Statistical analysis

Immunostaining results for each protein were compared with clinicopathological factors including age, gender, location, vessel invasion, node metastasis, depth of invasion, and stage, using the chi-square test or Fisher's exact test as appropriate. The association among each protein immunostaining was also assessed by the chi-square test or

Fisher's exact test as appropriate. Wilcoxon's signed rank test was used to analyze significant differences in real-time PCR data. The distribution of DFS was estimated by Kaplan–Meier methodology, and the log-rank test was used to test for significant differences in DFS. A Cox proportional hazard model was used to assess the effect of tumor variables on overall survival. In multivariate analysis, variables with $P<0.05$ in the univariate analysis were included. A P value of <0.05 was considered significant.

Results

mPGES-1, mPGES-2 and cPGES mRNA expression levels in colorectal tissue

We first determined mPGES-1, mPGES-2, and cPGES mRNA expression levels in human colorectal mucosa by quantitative real-time PCR. mPGES-1/β-actin and mPGES-2/β-actin mRNA ratios were significantly higher in CRC than in paired normal tissues. In contrast, cPGES/β-actin mRNA expression levels in CRC tissues did not vary significantly from those in paired normal tissues (Fig. 1).

COX-2, mPGES-1, mPGES-2, and cPGES protein levels in colorectal tissue

We analyzed colorectal biopsies by Western blot to determine COX-2 protein levels and those of each of the three PGES proteins. CRC samples showed significantly higher levels of the COX-2 and mPGES-1 proteins than their paired nonneoplastic tissues, where protein levels were low and not significant. In contrast, protein levels for mPGES-2 and cPGES did not vary significantly between cancer and paired nonneoplasitc tissues, although the intensity of their bands varied among cases (Fig. 2).

mPGES-1, mPGES-2, cPGES, and COX-2 localization in CRC

We analyzed the CRC surgical resections by immunohistochemistry to determine which cells expressed the PGES proteins. mPGES-1 immunoreactivity was predominantly detected in cancer cells and was most evident at the advancing edge of cancer cells in invasive carcinoma. It was found in cancer cells in 43% of cases (67/155) (Fig. 3b) but was nearly absent in glandular epithelial cells of colorectal mucosa adjoining cancer tissue (Fig. 3a). mPGES-2 immunoreactivity localized in both cancer cells and glandular epithelial cells of noncancerous colorectal mucosa (Figs. 3c, d), where both the intensity and distribution range of mPGES-2 immunostaining appeared heterogeneous. However, when mPGES-2 immunoreactivity in cancer cells was more closely compared to its expression in the adjacent glandular epithelium, mPGES-2 expression was found to be significantly more pronounced in CRC cells in 36% (56/155) of cases. We classified these cases as having increased mPGES-2 expression. cPGES immunoreactivity was seen in both glandular epithelial cells in noncancerous colorectal mucosa (Fig. 3e) and in the cytoplasm of cancer cells. cPGES immunostaining was diffused and homogeneous (Fig. 3f) in all cases examined and thus determined constitutive. COX-2 immunoreactivity was found in cancer cells in 91% of cases (141/155), consistent with previous reports [24, 25].

Relationship between mPGES-1 and mPGES-2 and Clinicopathological factors

Because certain cases exhibited higher levels of mPGES-1 and mPGES-2 protein, we then explored the clinical significance of the protein expression of these two enzymes in CRC. The relationship between immunohistochemical results and clinicopathological factors is shown in Table 2. mPGES-1 immunoreactivity was significantly higher in differentiated than in poorly differentiated cancers and correlated with vascular invasion. mPGES-2 immunoreactivity was also higher in differentiated than in poorly differentiated cancers, but the difference in protein levels was not significant. However, mPGES-2 immunoreactivity correlated with vascular invasion and tumor recurrence.

Relationship between mPGES-1, mPGES-2, and COX-2

mPGES-1 and COX-2 have been found to coexpress in a variety of cancers. However, studies suggest that these enzymes are regulated differently; thus, their localizations would not necessarily coincide. mPGES-2 has also been

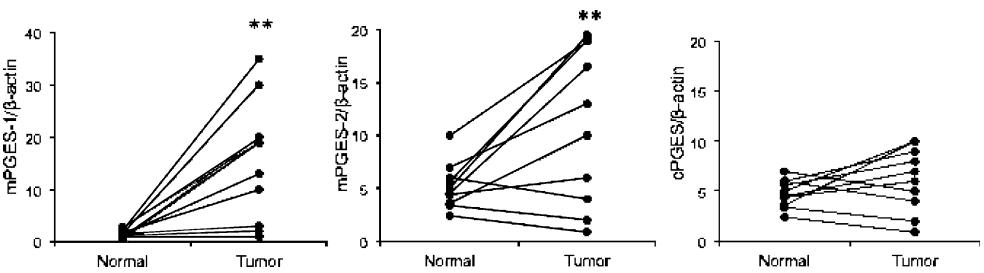

Fig. 1 mPGES-1, mPGES-2, and cPGES mRNA expression in colorectal cancer. mPGES-1/β-actin and mPGES-2/β-actin mRNA ratios were significantly higher in tumor than in paired normal tissues (**$P<0.05$, Wilcoxon's signed rank test)

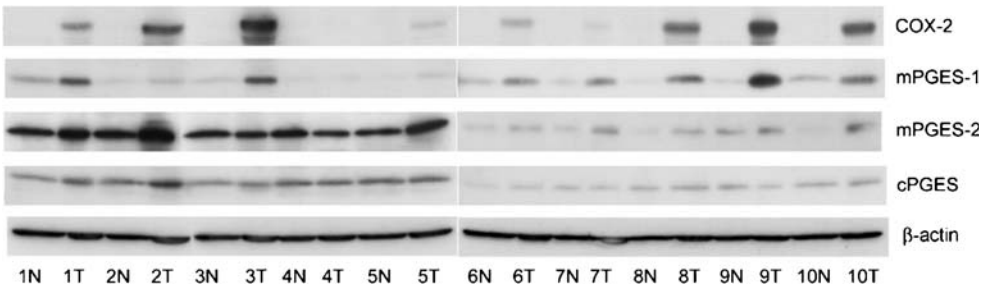

Fig. 2 Western blot analyses of COX-2, mPGES-1, mPGES-2, and cPGES protein levels in colorectal tissue samples from colorectal cancer patients

reported in human CRC tissues and cell lines, yet no study has focused on the relationship between this enzyme and COX-2 in human CRC. Therefore, we investigated the relationship between mPGES-1, mPGES-2, and COX-2 protein localization. There was no significant relationship between mPGES and COX-2 statistically (Table 3). Nevertheless, it was still to be expected that mPGES and COX-2 should colocalize in the same cells for the generation of PGE_2. Thus, we examined immunohistochemical localization of mPGES and COX-2 in each case using serial sections. Generally, the number of COX-2-positive cells was much higher than that seen for mPGES-1. Immunostaining of serial sections revealed that the staining patterns for COX-2 and mPGES-1 differed from each other; COX-2 was basically diffuse and homogeneous, whereas mPGES-1 was focal and preferentially distributed at the invasive edge

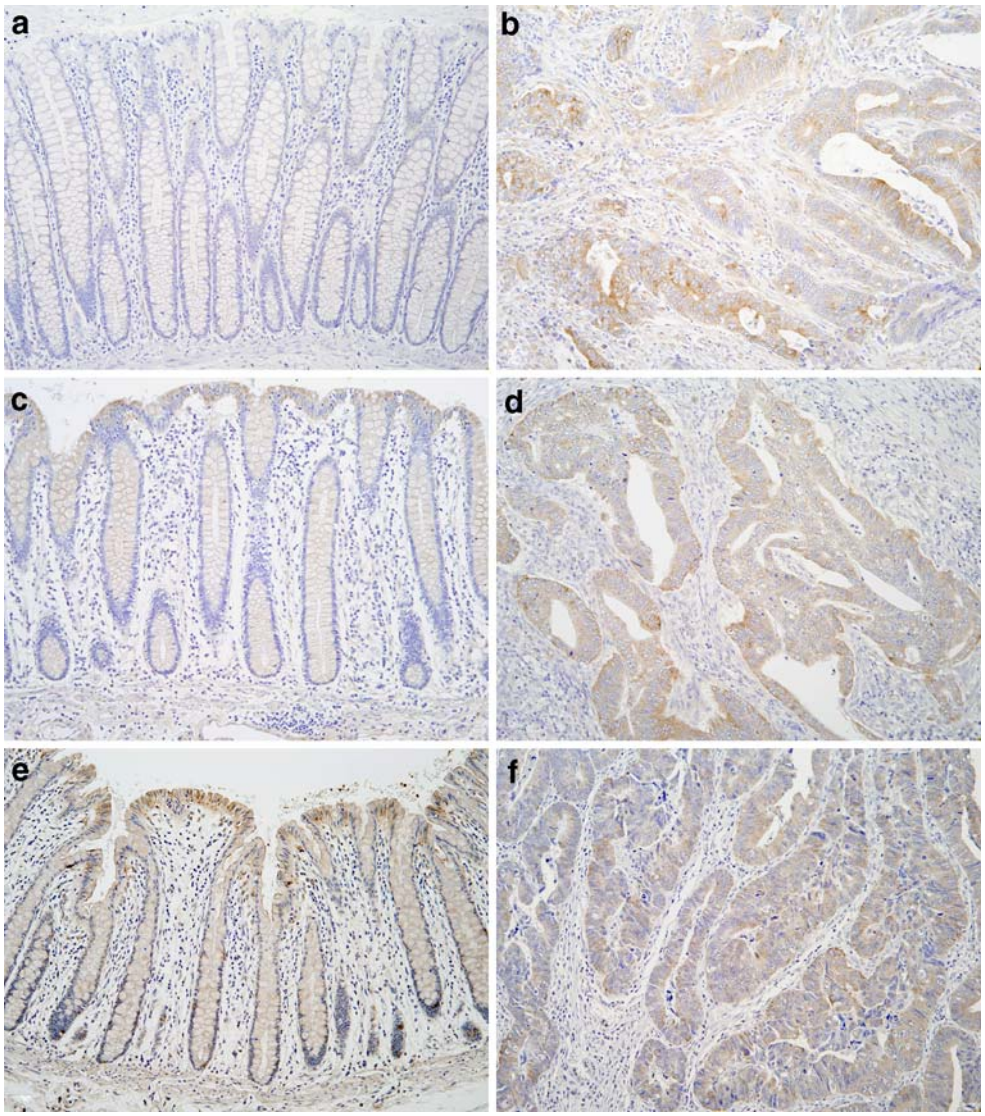

Fig. 3 Immunohistochemical localization of mPGES-1 (**a**, **b**), mPGES-2 (**c**, **d**), and cPGES (**e**, **f**) in normal colorectal mucosa (**a**, **c**, **e**) and in adenocarcinoma (**b**, **d**, **f**). **a** mPGES-1 in normal colorectal mucosa. mPGES-1 was negative in all cells. **b** mPGES-1 in colorectal cancer. mPGES-1 was stained in adenocarcinoma cells and in stromal cells. **c** mPGES-2 in normal colorectal mucosa. mPGES-2 was weakly stained in glandular epithelial cells but not in lamina propria inflammatory cells. **d** mPGES-2 in colorectal cancer. mPGES-2 was stained in adenocarcinoma cells. **e** cPGES in normal colorectal mucosa. cPGES showed weak staining in glandular epithelial cells but strong staining in endocrine cells from the neck to the base of crypts in colorectal mucosa. **f** cPGES was stained in adenocarcinoma cells

Table 2 Relationship between mPGES-1, mPGES-2, COX-2, and clinicopathologic factors

	No.	COX-2		mPGES-1		mPGES-2	
		No. (percent)	*P* value	No. (percent)	*P* value	No. (percent)	*P* value
Age							
<66	78	69 (88)	NS	37 (47)	NS	26 (33)	NS
≥66	77	72 (94)		30 (39)		30 (39)	
Gender							
Male	90	85 (94)	NS	40 (44)	NS	34 (38)	NS
Female	65	56 (86)		27 (42)		22 (34)	
Site							
Colon	106	95 (90)	NS	48 (45)	NS	36 (34)	NS
Rectum	49	46 (94)		19 (39)		20 (41)	
Histology							
Well	89	79 (89)	0.0482	38 (43)	0.0454	28 (31)	NS
Moderate	59	57 (97)		29 (49)		27 (46)	
Poor	7	5 (71)		0		1 (14)	
Depth							
pT1	12	12 (100)	NS	4 (33)	NS	2 (17)	NS
pT2	29	24 (83)		11 (38)		9 (31)	
pT3	105	97 (92)		48 (46)		40 (38)	
pT4	9	8 (89)		4 (44)		5 (56)	
Lymphatic invasion							
Negative	31	28 (90)	NS	10 (32)	NS	8 (26)	NS
Positive	124	113 (91)		57 (46)		48 (39)	
Vascular invasion							
Negative	61	53 (87)	NS	19 (31)	0.0199	14 (23)	0.0064
Positive	94	88 (94)		48 (51)		42 (45)	
Lymph node status							
pN0	85	76 (89)	NS	36 (42)	NS	25 (29)	NS
pNx	70	65 (93)		31 (44)		31 (44)	
TNM stage							
I	36	31 (86)	NS	13 (36)	NS	7 (19)	NS
II	43	40 (93)		19 (44)		15 (35)	
III	52	48 (92)		23 (44)		23 (44)	
IV	24	22 (92)		12 (50)		11 (46)	
Recurrence							
Negative	118	107 (91)	NS	46 (39)	NS	33 (28)	0.003
Positive	37	34 (92)		21 (57)		23 (62)	

Table 3 Correlation between COX-2, mPGES-1, and mPGES-2

	Number	COX-2		*P* value	mPGES-2		*P* value
		Negative (*N*=14)	Positive (*N*=141)		Negative (*N*=99)	Positive (*N*=56)	
mPGES-1							
Negative	88	8	80	NS	64	24	0.0113
Positive	67	6	61		35	32	
mPGES-2							
Negative	99	11	88	NS			
Positive	56	3	53				

of cancer cells. There was no association between COX-2 immunostaining and mPGES-2 immunostaining in cancer cells statistically, although mPGES-1 and mPGES-2 immunostaining correlated with each other (Table 3).

Comparative survival analysis

Survival rates were significantly lower for stage I–III patients with mPGES-1-positive tumors than for patients with mPGES-1-negative tumors according to log-rank analysis (Fig. 4a). Similar results were obtained for mPGES-2 expression (Fig. 4b).

Univariate analysis using the Cox proportional hazards model showed that lymphatic invasion, vascular invasion, lymph nodes status, depth, mPGES-1 expression, and mPGES-2 expression each had significant prognostic value (Table 4). Multivariate analysis performed by introducing all the above variables in the Cox proportional hazards model showed that lymphatic invasion, lymph nodes status, depth, mPGES-1 expression, and mPGES-2 expression retained independent prognostic significance (Table 4).

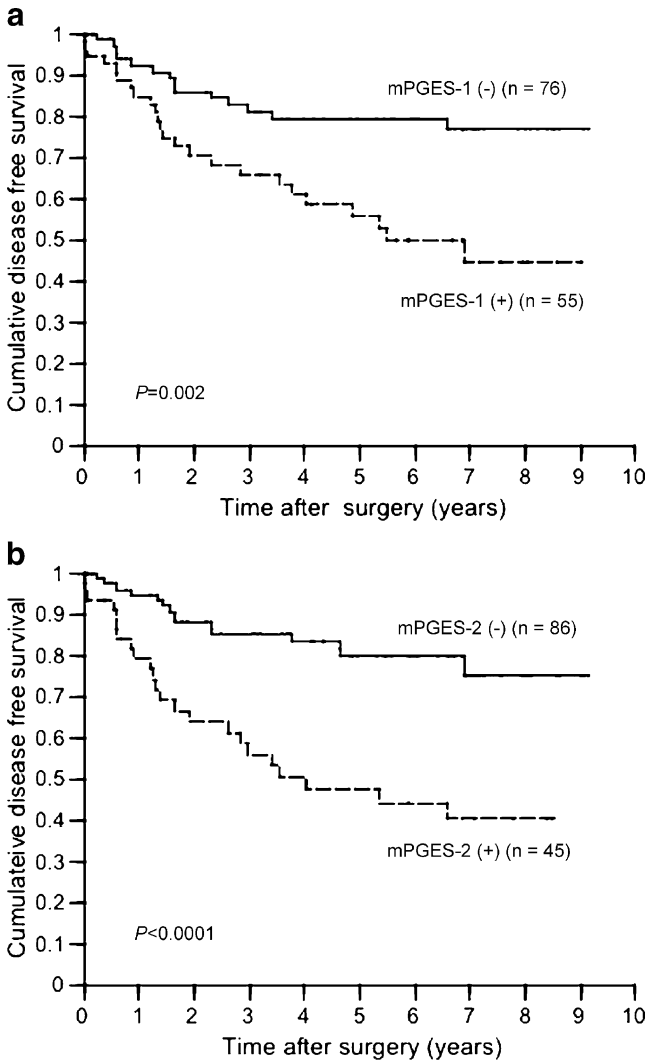

Fig. 4 **a** Kaplan–Meier disease-free survival curve for mPGES-1 expression in stage I–III patients. **b** Kaplan–Meier disease-free survival curve for mPGES-2 expression in stage I–III patients

Discussion

We examined the expression and localization of mPGES-1, mPGES-2, and cPGES in CRC patients and correlated their expression to COX-2, clinicopathological factors, and patient prognosis.

We found for the first time that mPGES-1 expression correlated with histological type, vascular invasion, and patient prognosis in CRC. However, there was no correlation between mPGES-1 expression and TNM stage, suggesting that mPGES-1 induction may be an early event in colorectal carcinogenesis. In addition, although mPGES-1 functions downstream of COX-2 in the PGE_2-biosynthetic pathway, there was no correlation between mPGES-1 and COX-2 expression in CRC. This coincides with previous in vitro data showing that mPGES-1 and COX-2 are regulated differently. For example, chenodeoxycholate markedly induces COX-2 but not mPGES-1 in colorectal cancer cells. Tumor necrosis factor-α induces both mPGES-1 and COX-2, but the time course and magnitude of induction differ [16]. A similar difference in timing of induction is observed following interleukin-1β treatment of synoviocytes [26].

COX-2 expression alone did not correlate with patient survival, consistent with previous studies [24, 27]. In contrast, survival rates were significantly lower for stage I–III patients with mPGES-1-positive tumors than for patients with mPGES-1-negative tumors. This prognostic value of mPGES-1 was confirmed by multivariate Cox proportional hazards analysis to be independent of depth of invasion and lymph node metastasis. The reason for the negative effect of mPGES-1 on the prognosis of CRC patients is not clear. Since mPGES-1 expression tended to be more pronounced at the advancing edge of cancer cells, it could be that mPGES-1 modulates CRC progression through the induction of angiogenic factors such as vascular endothelial growth factor, conferring to cancer cells their aggressive characteristics as has been shown for COX-2 in other studies [28–30].

cPGES expression is considered constitutive and to functionally couple with COX-1 [11]. This correlates with our real-time PCR and Western blot analysis of biopsy samples, where we found no significant differences in cPGES expression levels between cancer tissues and their nonneoplastic counterparts for the same patients. Moreover, the intensity of cPGES immunoreactivity in cancer cells did not differ significantly from that of the normal epithelium.

Table 4 Univariate and multivariate Cox proportional hazards analysis for disease-free survival

Variables	Categories	Univariate analysis		Multivariate analysis	
		HR (95% CI)	*P* value	HR (95% CI)	*P* value
Lymphatic invasion	Positive vs. negative	3.88 (1.18–12.6)	0.024	4.26 (1.10–16.5)	0.035
Vascular invasion	Positive vs. negative	2.23 (1.10–4.50)	0.025	0.81 (0.38–1.77)	NS
Lymph nodes	Positive vs. negative	4.72 (2.37–9.41)	<0.001	2.58 (1.28–5.22)	0.008
Depth (T factor)	Continuous	3.62 (2.00–6.55)	<0.001	4.41 (1.99–9.80)	<0.001
mPGES-1 expression	Positive vs. negative	3.50 (1.82–6.72)	0.002	2.89 (1.46–5.72)	0.002
mPGES-2 expression	Positive vs. negative	4.04 (2.28–7.16)	<0.001	3.22 (1.62–6.40)	<0.001

Thus, results so far do not indicate a specific role for cPGES expression in CRC progression, though that possibility cannot be excluded.

Studies in vitro suggest that mPGES-2 may also be constitutive [31]. However, our results indicate that, although mPGES-2 expression appeared to be ubiquitous, in reality, its expression was not entirely uniform. Although it is difficult to conclude from our Western blot analysis alone that mPGES-2 protein levels are higher in cancer than in normal tissue, our immunohistochemical analysis of mPGES-2 immunoreactivity in colorectal epithelium shows that in 36% of cases mPGES-2 immunoreactivity was significantly more pronounced in CRC cells than in adjacent glandular epithelium. Furthermore, mPGES-2/β-actin mRNA ratios were significantly higher in CRC than in paired normal tissues. This result correlates with reports of mPGES-2 overexpression in CRC [15]. Although mPGES-2 is known to be constitutive in a variety of cells, it can be activated by lipopolysaccharide [15], glutathione, lipoic acid and other reducing agents [32], and interferon-γ [33]. We also examined the relationship between mPGES-2 immunoreactivity and clinicopathological factors and found for the first time that mPGES-2 expression correlated with vascular invasion and tumor recurrence in CRC.

So far, all these data largely correspond with that of a parallel study we recently conducted in gastric cancer; where mPGES-1 and mPGES-2 were also found to correlate with clinicopathological factors and patient prognosis [20]. However, in contrast to that study, in the present study, COX-2 expression did not correlate with mPGES-1 or mPGES-2 expression statistically. This may be explained in part by the fact that, in this study, the positivity rate for COX-2 was almost 100%, while the immunostaining patterns for mPGES-1 and COX-2 differed from each other, consistent with in vitro studies by others, indicating that the induction of COX-2 and mPGES-1 is under different regulatory mechanisms in CRC [16, 17, 34]. It thus follows that cases that express COX-2 do not necessarily express mPGES-1. At first, we hypothesized that mPGES-2 would act to compensate for the lack of mPGES-1 expression. But contrary to our expectations, the relationship between mPGES-1 and mPGES-2 was not correlative. We actually found a significant number of cases (21 out of 155 cases) where neither mPGES-1 nor mPGES-2 was expressed in COX-2-positive CRC patients. In this case, the clinical significance of COX-2 expression alone in CRC patients remains to be elucidated.

There is a great body of evidence showing the benefit of PGE_2 inhibition in CRC prevention and therapy [8, 9]. However, COX-2 selective inhibitors have been found to increase the risk of cardiovascular events, curtailing their use as therapeutics for colorectal neoplasms in the clinical setting [5, 35]. COX-2 selective inhibitors are believed to exert their beneficial effect through the suppression of COX-2-derived PGE_2 and their adverse effects through the inhibition of prostacyclin (PGI_2) and disruption of the thromboxane A_2/PGI_2 equilibrium. It has been suggested that mPGES-1 inhibitors may retain the anti-inflammatory efficacy of COX-2 selective inhibitors by depressing PGE_2 production while avoiding the adverse cardiovascular events associated with COX-2-mediated PGI_2 suppression [36]. Taking all these data into consideration, our results suggest that mPGES-1 and mPGES-2 may be novel targets for clinical therapy and that selective inhibitors of these PGE synthases could replace the selective COX-2 inhibitors.

Recently, two studies examined the role of mPGES-1 in colon cancer using *Apc*-mutant animal models with deletions of the *mPGES-1* gene and reported contradictory results [21, 37]. Nakanishi et al. reported that *mPGES-1* deletion reduced the total number and size of intestinal polyps in $Apc^{\Delta 14/+}$ mice, whereas Elander et al. reported that the absence of this enzyme significantly increased the total number and size of intestinal polyps in Apc^{Min} mice. These studies suggest that suppression of mPGES-1 induces the overexpression of other bioactive prostanoids/thromboxanes (thromboxane B_2, PGD_2, and 6-keto-$PGF_{1\alpha}$) that may themselves be involved in carcinogenesis. Clearly, further studies in vivo on the roles of these mediators in carcinogenesis are warranted. However, it could simply be

that the controversial results of these two studies rose from the fact that different types of *Apc*-mutant mice were used by the two groups. Furthermore, the *Apc*-mutant mice model is clearly imperfect because polyp formation is much more pronounced in the small intestine than in the large intestine. Finally, the adenomatous polyps in these animals rarely progress into invasive carcinomas. Thus, one problematic issue is that *mPGES-1* deletion only affected polyp formation in the colon, where the polyp numbers are so small that limited statistical confidence can be achieved.

To conclude, we found for the first time that mPGES-1 and mPGES-2 expression in CRC significantly correlated with clinicopathological factors, indicating a role for these enzymes in the modulation of CRC progression.

Conflict of Interest The authors declare that they have no conflict of interest.

Reference

1. Ulrich CM, Bigler J, Potter JD (2006) Non-steroidal anti-inflammatory drugs for cancer prevention: promise, perils and pharmacogenetics. Nat Rev Cancer 6:130–140
2. Sinicrope FA, Gill S (2004) Role of cyclooxygenase-2 in colorectal cancer. Cancer Metastasis Rev 23:63–75
3. Kawamori T, Rao CV, Seibert K et al (1998) Chemopreventive activity of celecoxib, a specific cyclooxygenase-2 inhibitor, against colon carcinogenesis. Cancer Res 58:409–412
4. Rahme E, Barkun AN, Toubouti Y et al (2003) The cyclooxygenase-2-selective inhibitors rofecoxib and celecoxib prevent colorectal neoplasia occurrence and recurrence. Gastroenterology 125:404–412
5. Bertagnolli MM, Eagle CJ, Zauber AG et al (2006) Celecoxib for the prevention of sporadic colorectal adenomas. N Engl J Med 355:873–884
6. Arber N, Eagle CJ, Spicak J et al (2006) Celecoxib for the prevention of colorectal adenomatous polyps. N Engl J Med 355:885–895
7. Chan AT, Ogino S, Fuchs CS (2007) Aspirin and the risk of colorectal cancer in relation to the expression of COX-2. N Engl J Med 356:2131–2142
8. Sinicrope FA (2006) Targeting cyclooxygenase-2 for prevention and therapy of colorectal cancer. Mol Carcinog 45:447–454
9. Wang D, Dubois RN (2006) Prostaglandins and cancer. Gut 55:115–122
10. Jakobsson PJ, Thoren S, Morgenstern R et al (1999) Identification of human prostaglandin E synthase: a microsomal, glutathione-dependent, inducible enzyme, constituting a potential novel drug target. Proc Natl Acad Sci U S A 96:7220–7225
11. Tanioka T, Nakatani Y, Semmyo N et al (2000) Molecular identification of cytosolic prostaglandin E2 synthase that is functionally coupled with cyclooxygenase-1 in immediate prostaglandin E2 biosynthesis. J Biol Chem 275:32775–32782
12. Tanikawa N, Ohmiya Y, Ohkubo H et al (2002) Identification and characterization of a novel type of membrane-associated prostaglandin E synthase. Biochem Biophys Res Commun 291:884–889
13. Han R, Tsui S, Smith TJ (2002) Up-regulation of prostaglandin E2 synthesis by interleukin-1beta in human orbital fibroblasts involves coordinate induction of prostaglandin-endoperoxide H synthase-2 and glutathione-dependent prostaglandin E2 synthase expression. J Biol Chem 277:16355–16364
14. Murakami M, Naraba H, Tanioka T et al (2000) Regulation of prostaglandin E2 biosynthesis by inducible membrane-associated prostaglandin E2 synthase that acts in concert with cyclooxygenase-2. J Biol Chem 275:32783–32792
15. Murakami M, Nakashima K, Kamei D et al (2003) Cellular prostaglandin E2 production by membrane-bound prostaglandin E synthase-2 via both cyclooxygenases-1 and -2. J Biol Chem 278:37937–37947
16. Yoshimatsu K, Golijanin D, Paty PB et al (2001) Inducible microsomal prostaglandin E synthase is overexpressed in colorectal adenomas and cancer. Clin Cancer Res 7:3971–3976
17. van Rees BP, Sabula A, Thorne S et al (2003) Expression of microsomal prostaglandin E synthase-1 in intestinal type gastric adenocarcinoma and in gastric cancer cell lines. Int J Cancer 107:551–556
18. Mehrotra S, Morimiya A, Agarwal B et al (2006) Microsomal prostaglandin E2 synthase-1 in breast cancer: a potential target for therapy. J Pathol 208:356–363
19. Rask K, Zhu Y, Wang W et al (2006) Ovarian epithelial cancer: a role for PGE2-synthesis and signalling in malignant transformation and progression. Mol Cancer 5:62
20. Gudis K, Tatsuguchi A, Wada K et al (2007) Clinical significance of prostaglandin E synthase expression in gastric cancer tissue. Hum Pathol 38:1826–1835
21. Nakanishi M, Montrose DC, Clark P et al (2008) Genetic deletion of mPGES-1 suppresses intestinal tumorigenesis. Cancer Res 68:3251–3259
22. Kamei D, Murakami M, Nakatani Y et al (2003) Potential role of microsomal prostaglandin E synthase-1 in tumorigenesis. J Biol Chem 278:19396–19405
23. Gudis K, Tatsuguchi A, Wada K et al (2005) Microsomal prostaglandin E synthase (mPGES)-1, mPGES-2 and cytosolic PGES expression in human gastritis and gastric ulcer tissue. Lab Invest 85:225–236
24. Guo H, Tatsuguchi A, Shinji S et al (2006) Cyclooxygenase-2 expression correlates with membrane-type-1 matrix metalloproteinase expression in colorectal cancer tissue. Dis Colon Rectum 49:1184–1192
25. Tatsuguchi A, Kishida T, Fujimori S et al (2006) Differential expression of cyclo-oxygenase-2 and nuclear beta-catenin in colorectal cancer tissue. Aliment Pharmacol Ther 24(Suppl 4):153–159
26. Stichtenoth DO, Thoren S, Bian H et al (2001) Microsomal prostaglandin E synthase is regulated by proinflammatory cytokines and glucocorticoids in primary rheumatoid synovial cells. J Immunol 167:469–474
27. Fux R, Schwab M, Thon KP et al (2005) Cyclooxygenase-2 expression in human colorectal cancer is unrelated to overall patient survival. Clin Cancer Res 11:4754–4760
28. Tsujii M, Kawano S, Tsuji S et al (1998) Cyclooxygenase regulates angiogenesis induced by colon cancer cells. Cell 93:705–716
29. Tatsuguchi A, Matsui K, Shinji Y et al (2004) Cyclooxygenase-2 expression correlates with angiogenesis and apoptosis in gastric cancer tissue. Hum Pathol 35:488–495
30. Tanaka S, Tatsuguchi A, Futagami S et al (2006) Monocyte chemoattractant protein 1 and macrophage cyclooxygenase 2 expression in colonic adenoma. Gut 55:54–61
31. Kudo I, Murakami M (2005) Prostaglandin e synthase, a terminal enzyme for prostaglandin E2 biosynthesis. J Biochem Mol Biol 38:633–638

32. Watanabe K, Ohkubo H, Niwa H et al (2003) Essential 110Cys in active site of membrane-associated prostaglandin E synthase-2. Biochem Biophys Res Commun 306:577–581
33. Hu J, Meng Q, Roy SK et al (2002) A Novel Transactivating Factor That Regulates Interferon-gamma-dependent Gene Expression. J Biol Chem 277:30253–30263
34. Wright KL, Weaver SA, Patel K et al (2004) Differential regulation of prostaglandin E biosynthesis by interferon-gamma in colonic epithelial cells. Br J Pharmacol 141:1091–1097
35. Bresalier RS, Sandler RS, Quan H et al (2005) Cardiovascular events associated with rofecoxib in a colorectal adenoma chemoprevention trial. N Engl J Med 352:1092–1102
36. Cheng Y, Wang M, Yu Y et al (2006) Cyclooxygenases, microsomal prostaglandin E synthase-1, and cardiovascular function. J Clin Invest 116:1391–1399
37. Elander N, Ungerbäck J, Olsson H et al (2008) Genetic deletion of mPGES-1 accelerates intestinal tumorigenesis in APC(Min/+) mice. Biochem Biophys Res Commun 372:249–253

Virchows Arch (2009) 454:677–683
DOI 10.1007/s00428-009-0778-y

ORIGINAL ARTICLE

Gross genomic alterations differ between serous borderline tumors and serous adenocarcinomas—an image cytometric DNA ploidy analysis of 307 cases with histogenetic implications

Manohar Pradhan · Ben Davidson · Claes Göran Tropé · Håvard Emil Danielsen · Vera Maria Abeler · Björn Risberg

Received: 7 January 2009 / Revised: 6 April 2009 / Accepted: 14 April 2009 / Published online: 8 May 2009

Abstract Our objective was to study the gross genomic alterations in serous borderline tumors and serous adenocarcinomas of the ovary. A retrospective analysis of 245 serous borderline tumors and 62 serous adenocarcinomas from 249 patients was performed using high-resolution image cytometric DNA ploidy analysis. DNA ploidy status, S-phase fraction, and DNA index were evaluated. The majority of serous borderline tumors were diploid (225/245 cases, 92%). The remaining 8% showed an aneuploid peak predominantly with DNA index of less than 1.4. Grades 2 and 3 serous adenocarcinomas were more often (80%) nondiploid, mostly with DNA index exceeding 1.4. Grade 1 serous adenocarcinomas were an intermediate group, more similar to serous borderline tumors. The S-phase fraction increased from serous borderline tumors (mean=0.6%) through grade 1 serous adenocarcinomas (mean=2.8%), being highest in grades 2 and 3 adenocarcinomas (mean=6.8%). Our findings support the hypothesis that serous borderline tumors and grades 2 and 3 serous adenocarcinomas are genomically different lesions, with grade 1 serous adenocarcinomas being an intermediate group more close to borderline tumors.

Keywords Gross genomic alteration · Serous borderline tumor · Serous adenocarcinoma · Ovary · DNA ploidy · Image cytometry · S-phase fraction · Histogenesis

M. Pradhan · B. Davidson · V. M. Abeler · B. Risberg
Division of Pathology, Norwegian Radium Hospital,
Oslo University Hospital,
Oslo, Norway

C. G. Tropé
Division of Gynecological Oncology,
Norwegian Radium Hospital,
Oslo University Hospital,
Oslo, Norway

H. E. Danielsen · B. Risberg
Institute for Medical Informatics, Norwegian Radium Hospital,
Oslo University Hospital,
Oslo, Norway

H. E. Danielsen
Center for Cancer Biomedicine, University of Oslo,
Oslo, Norway

B. Davidson · C. G. Tropé
Faculty Division Radiumhospitalet, the Medical Faculty,
University of Oslo,
Oslo, Norway

B. Risberg (✉)
Institute for Medical Informatics and Division of Pathology,
Oslo University Hospital, Norwegian Radium Hospital,
Montebello,
0310 Oslo, Norway
e-mail: bjorn.risberg@radiumhospitalet.no

Introduction

The World Health Organization (WHO) classification categorizes ovarian tumors into different histologic types, with serous tumors accounting for approximately 40% of all cases [1]. Serous tumors are further classified into benign lesions, borderline tumors (SBTs), and adenocarcinomas (SACs). The SBT category also includes infrequent cases showing microinvasion and the recently recognized subtype characterized by micropapillary growth pattern [1].

Patients with SBTs have excellent prognosis, with 10-year survival ranging from 77% to 99% depending on the International Federation of Gynecology and Obstetrics (FIGO) stage [2]. In contrast, patients with SACs have 5-year survival ranging from 15% to 85% depending on FIGO stage [3]. In addition to its prognostic value, the differentiation of SBTs from SACs is critical for the choice of treatment (conservative surgery vs. radical surgery and chemotherapy) [4].

It is not conclusively established whether SAC develops from benign or borderline serous tumors. A recent review on this issue suggests the existence of two types of malignant ovarian tumors—the first consisting of slow-growing tumors that are generally confined to the ovary at diagnosis and develop from precursor borderline tumors, the second type characterized by rapidly growing and highly aggressive neoplasms without any known precursor lesion [5]. There are comparative genomic hybridization [6] and oligonucleotide microarray analysis [7] studies indicating that SBTs and SACs have different genetic aberrations, supporting the view that the progression from SBT to SAC is unlikely. However, a recent study using cytogenetics reported on common chromosomal alterations in different types of ovarian tumors, suggesting that progression may occur from SBT to SAC [8].

New high-resolution image cytometric DNA ploidy analysis of paraffin-embedded material provides information regarding gross genomic alterations, as well as the possibility to assess proliferation through S-phase fraction (SPF) calculation. Our hypothesis was that DNA ploidy analysis may aid in elucidating the relation between ovarian SBTs and SACs of different histological grade. In the present study, we analyzed the DNA ploidy status of these two diagnostic entities in a large group of well-characterized tumors. Our results support a dualistic view of ovarian serous tumors.

Materials and methods

Patients and material

The cohort of this retrospective study consisted of patients diagnosed with ovarian SBT or SAC whose tumors were subjected to DNA ploidy analysis at the Oslo University Hospital between April 2003 and April 2007. The material consisted of paraffin-embedded tumor blocks from in-house patients and patients operated upon at other hospitals. A total of 307 tumors from 249 patients were analyzed in the study, of which 245 were diagnosed as SBT and 62 as SAC. The 245 SBTs from 198 patients (bilateral in 47 cases) consisted of 222 ordinary SBTs, 11 specimens with a micropapillary growth pattern, and 12 tumors with microinvasion. The 62 SACs were from 51 patients (bilateral in 11 cases) and consisted of 22 grade 1, 21 grade 2, and 19 grade 3 tumors. The mean diameter of SBTs and SACs was 8.0 and 8.6 cm, respectively.

Data regarding FIGO stage were available for 127 SBT and 43 SAC cases and were as follows: SBT: Ia–b 76, Ic 30, SBT with implants in omentum and/or uterus and/or tubes 21; SAC: Ia–b 13, Ic 16, IIa 3, IIb 3, IIIa 4, IIIc 4.

Histological classification

All hematoxylin and eosin (H&E)-stained control sections from the paraffin-embedded tissue used for DNA ploidy analysis were reviewed by an experienced gynecological pathologist (VA). Histological subtyping and grading were performed according to WHO classification of tumors [1]. Pathology records were reviewed in order to determine tumor size, laterality, and age.

DNA image cytometry

Monolayer preparation, Feulgen staining, and measurement of DNA content

DNA ploidy analysis was performed on cells from the area of interest identified by a mark on the H&E-stained slide. One to three 50-μm sections were cut from the paraffin-embedded blocks. Monolayer preparations were made and stained using the Feulgen method, as previously described [9]. Briefly, sections were deparaffinized, rehydrated, and incubated with protease to disaggregate the cells. The enzymatic digestion was then stopped and the cell suspensions were filtered. Monolayer preparations were made from the filtrate on poly-L-lysine-coated glass slides, which were air-dried and fixed in 4% formaldehyde.

To stain with Feulgen stain, the preparations were hydrolyzed in 5 M HCl for 60 min and were afterward stained with Schiff solution for 2 h. The preparations were then washed and treated with 0.5% sodium disulfite in 0.05 M HCl. Finally, the slides were washed in running tap water, dehydrated in increasing alcohol gradient, cleared in xylene, and coverslipped.

Measurement of DNA content

The measurement of nuclear DNA content was performed using the Fairfield DNA ploidy system (Fairfield Imaging Ltd., Nottingham, England), consisting of a Zeiss Axioplan microscope (Zeiss, Jena, Germany) equipped with a black-and-white high-resolution digital camera (model C4742-95; Hamamatsu Photonics K. K., Hamamatsu, Japan). The optical density and the nuclear area were measured, and the integrated optical density of each nucleus was calculated. The background optical density was corrected for each

nucleus. Images were collected into galleries, with nuclei-of-interest used for measurement and with lymphocytes, plasma cells, and fibrocytes as reference cells. Galleries were edited to discard cut, overlapped, and pyknotic nuclei. Histogram Draftsman 1.4 program (Fairfield Imaging Ltd.) was used to create a histogram from the integrated optical density of the nuclear images. The reference cell nuclei were used as an internal diploid control.

Criteria for the classification of DNA ploidy

A tumor was classified as diploid if only one G0/G1 peak (2c) was present; the number of nuclei at the G2 peak (4c) did not exceed 10% of the total number of nuclei, and the number of nuclei with DNA content more than 5c did not exceed 1%. A tumor was defined as tetraploid if a 4c peak (DNA index; DI=1.9–2.1) was present (with a higher number of nuclei at the 4c peak than at the SPF and consisting of more than 10% of the total nuclei); the number of nuclei at the G2 peak (8c) did not exceed 10% of the total number of nuclei, and the number of nuclei with a DNA content more than 9c did not exceed 1%. A tumor was defined as polyploid when more than 10% of the total number of nuclei was present at the 8c peak and/or when the number of nuclei with DNA content more than 9c exceeded 1%. A tumor was defined as aneuploid when noneuploid peak(s) were present or when the number of nuclei with DNA content exceeding 5c (not representing euploid populations) exceeded 1% [9]. In cases in which multiple peaks existed, the DI of the most prominent aneuploid peak was regarded as the DI of the tumor. DNA aneuploid tumors were divided into two groups, one with DI 1.05–1.4 and another with 1.4–1.89 or DI>2.1.

The SPF was manually calculated in the following way: the number of channels between mid-G0/G1 and the mid-G2/M peak was multiplied by the mean number of registrations within an even part of the S-phase region. This number was divided by the total number of nuclei between the beginning of G0/G1 and the end of G2/M peak and multiplied by 100. However, in nine cases, these parameters could not be estimated because of overlapping or small stem lines. The DI and coefficient of variation (CV) of all the tumors were registered.

Statistical analysis

Statistical analysis was performed applying the SPSS-PC package (version 13, Chicago, IL, USA). Statistical significance was considered as $p<0.05$. Analysis of variance (ANOVA) and post hoc Tukey tests were performed.

Results

Patient age ranged from 18 to 92 (mean=55.2) years. All 307 tumors had adequate material for analysis. The mean number of nuclei analyzed was 1,233 (range 382–1,636). The mean CV for the main stem line was 2.59% (range 1.12–8.09). The distribution of DNA ploidy status and mean SPF in SBTs of different subtype and SACs of different histological grade is detailed in Table 1 and examples are shown in Fig. 1.

The percentage of cases with DI>1.4 increased stepwise from SBT through grade 1 SAC to grades 2 and 3 SAC (Table 1). DNA tetraploid distribution was seen only in grades 2 and 3 SAC. The mean SPF was similar in the different SBT subtypes (Table 1). The SPF differed significantly between SBT, grade 1 SAC, and grades 2 and 3 SAC (Table 2).

Presentation of DI values and SPF in a scatter diagram illustrates how grades 2 and 3 SACs differ from SBTs and grade 1 SACs, whereas the latter two tumor groups are more similar (Fig. 2). Thus, grades 2 and 3 SACs are dominated by cases with DI>1.4 and SPF>5%, while the majority of the SBTs and grade 1 SACs have DI<1.4 and SPF<5% (Fig. 2).

Table 1 DNA ploidy distribution and S-phase fraction in serous borderline tumors (SBT) and serous adenocarcinomas (SAC) of the ovary

Histology	Diploid (%)	Aneuploid (%)		Tetraploid (%)	Mean S-phase (95% CI)	Total
		DI (1.05–1.4)	DI (1.4–1.89 and >2.1)	DI (1.9–2.1)		
Ordinary SBT	208 (93.7)	12(5.4)	2 (0.9)	0 (0)	0.61 (0.52–0.7)	222
Micropapillary SBT	7 (63.6)	4 (36.4)	0 (0)	0 (0)	1.23 (0.8–1.7)	11
SBT with microinvasion	10 (83.3)	1 (8.3)	1 (8.3)	0 (0)	0.62 (0.04–1.2)	12
SAC grade 1	13 (59.1)	4 (18.2)	5 (22.7)	0 (0)	2.8 (1.24–4.35)	22
SAC grades 2 and 3	8 (20)	4 (10)	21 (52.5)	7 (17.5)	6.76 (5.44–8.08)	40

DI DNA index, *CI* confidence interval

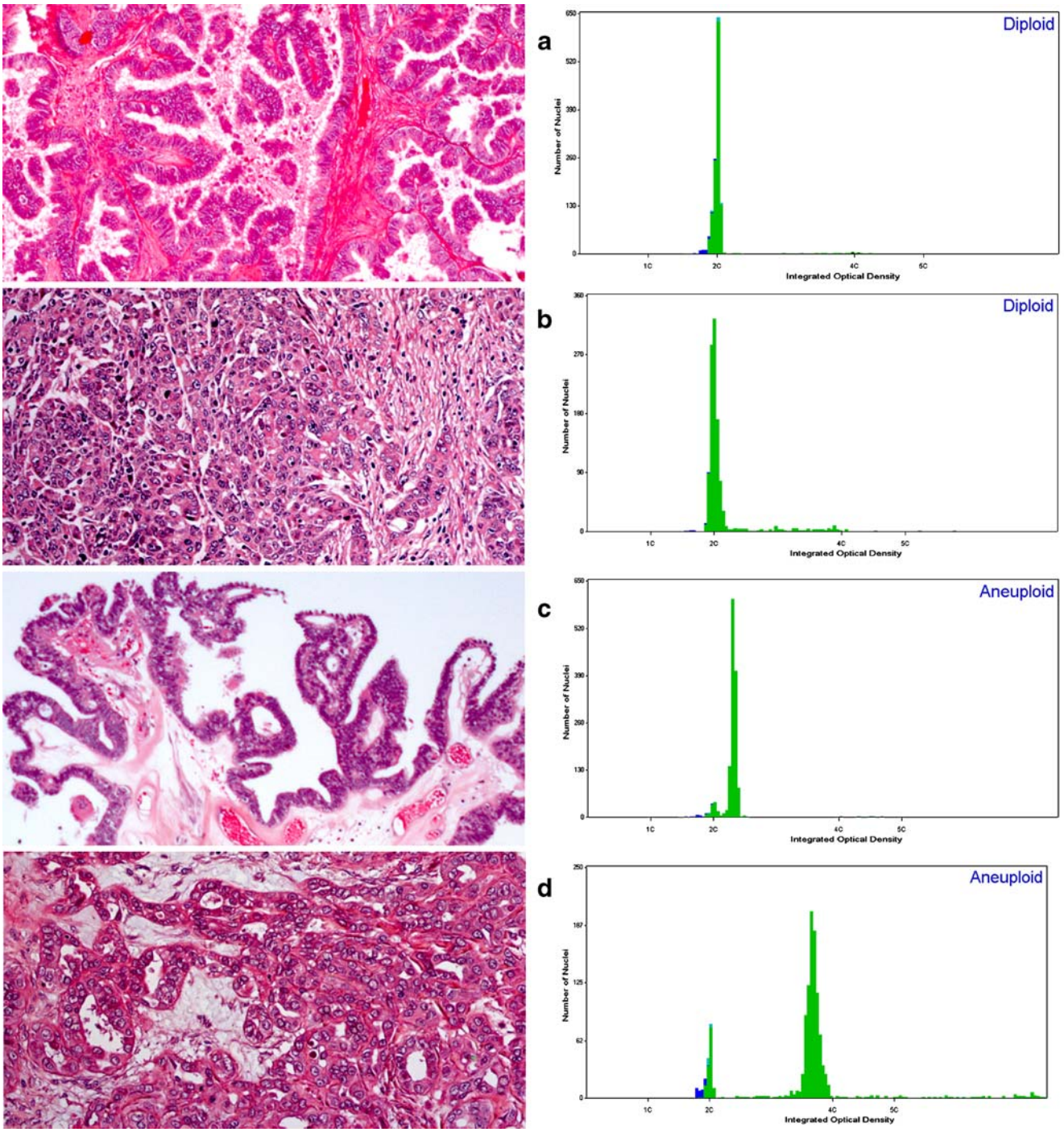

Fig. 1 DNA ploidy in serous borderline tumors and serous adenocarcinoma. DNA diploid tumors: diploid serous borderline tumor (**a**) showing lower S-phase fraction and coefficient of variation of the diploid peak compared to a diploid serous adenocarcinoma (**b**). DNA aneuploid tumors: serous borderline tumor (**c**) with aneuploid histograms showing DNA index of the aneuploid peaks <1.2 and aneuploid serous adenocarcinoma (**d**; DNA index=1.84) showing higher number of nuclei in the S-phase fraction

Discussion

There are different opinions concerning the histogenesis of serous ovarian tumors, some supporting a progression from SBT to SAC [8, 10] and others favoring a dualistic model [5, 11–14]. We studied this issue using high-resolution DNA ploidy image analysis in different subgroups of SBT and grades of SAC in a large and well-characterized retrospective material. Based on DI and SPF measurements, we found that SBTs and grades 2 and 3 SACs are

Table 2 *p* values of ANOVA post hoc Tukey HSD comparisons of S-phase fraction between different DNA ploidy groups and different histological types

Comparison	*p* value
Diploid vs. aneuploid with DI <1.4	<0.001
Diploid vs. aneuploid with DI >1.4	<0.001
Diploid vs. tetraploid	<0.001
Aneuploid with DI<1.4 vs. aneuploid with DI>1.4	<0.001
Aneuploid with DI <1.4 vs. tetraploid	<0.001
Aneuploid with DI >1.4 vs. tetraploid	0.074
SBT vs. SAC grade 1	<0.001
SBT vs. SAC grades 2 and 3	<0.001
SAC grade 1 vs. SAC grades 2 and 3	<0.001

DI DNA index, *SBT* serous borderline tumor, *SAC* serous adenocarcinoma

genomically different lesions, with grade 1 SACs being an intermediate group with a genotype that resembles SBTs more than high-grade SACs.

The DNA ploidy status of ovarian tumors has been extensively studied in the last decades. These previous studies have focused on the prognostic importance of this analysis rather than on close correlation to histological subgroups or on histogenetic aspects [15–19]. Evaluation of the latter aspect has been limited by the fact that many of these previous studies have analyzed limited and histologically less well-defined material. Additionally, the DNA ploidy analysis methods have been less precise compared to current technology. This issue is critical, as the information gained from DNA ploidy analyses differs greatly depending on the method used. Earlier crude measurements using image analysis on Feulgen-stained histological sections [17–20] were unable to evaluate DI and thus cannot be compared to modern image analysis data. In one study of SBTs using Feulgen-stained sections [20], a very high frequency (23/44) of DNA aneuploidy was found, although it had no impact on prognosis. This high incidence of DNA aneuploidy in SBT has not been demonstrated in other studies.

Another technical issue of importance is the fact that the majority of previous studies have used flow cytometry rather than image analysis, analyzing nuclear suspensions from 50-μm paraffin sections. The results of these analyses are sometimes difficult to interpret due to high background and the presence of cut nuclei and nuclear fragments. To the best of our knowledge, the study by Klemi et al. [21] using flow cytometry is the only one performed on a substantial number of SBT and SAC to date. In this study, DI had a prognostic role for patients with SAC based on a cutoff of 1.3. In addition, the authors found that all the DNA aneuploid SBTs had DI<1.4 in contrast to SACs, in which with the majority of DNA aneuploid cases had DI>1.4. No other DNA ploidy parameter was analyzed in their study.

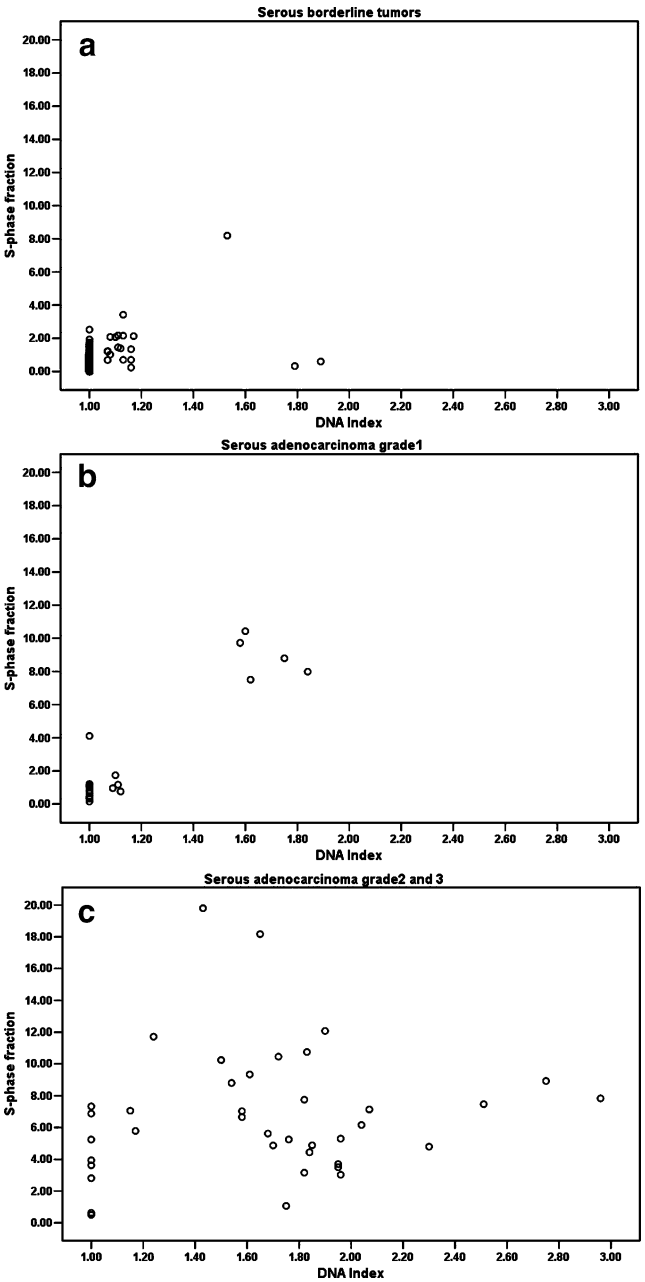

Fig. 2 *Scatter plots* of DNA index and S-phase fraction. *Scatter plots* are shown for **a** serous borderline tumors, **b** serous adenocarcinoma grade 1, and **c** serous adenocarcinoma grades 2 and 3

Other investigators [22–24] have similarly reported that DNA aneuploid SBTs had rather low DNA index (<1.4) using flow cytometry. Additionally, other reports have demonstrated that DNA index >1.4 is associated with worse prognosis in early-stage ovarian carcinoma [25] and mucinous ovarian borderline tumors [26]. Our data are in agreement with these previous reports with respect to the difference in DI between SACs and SBTs.

Our data concord with several studies in which other molecular techniques have been used. A comparative genomic hybridization study showed that the average number of

genetic changes per tumor greatly differs between SBTs (1.9) and SACs (9.2) [27]. Meinhold-Heerlein et al. [7] reported striking similarities between SBT and grade 1 SAC, both being different from SAC grades 2 and 3, using oligonucleotide arrays. Our image analysis technique provides additional data, such as SPF values.

We noted a distinct correlation between DI and SPF. Thus, tumors with DI up to 1.4, such as most DNA aneuploid SBTs, have low SPF. It is interesting to compare these data with the results of experimental findings of Duesberg et al., who found a close correlation between the degree of aneuploidy and genomic instability in studies on tumor cell lines [28, 29]. In these studies, near-diploid tumor cell lines (DI ≤1.4) were relatively stable, whereas those with DI of 1.6–1.7 were highly genomically unstable. The majority of the DNA aneuploid SBTs have DI values corresponding to a genomically stable tumor population, while aneuploid SACs have DI values corresponding to unstable tumor cell populations.

The findings in the above-discussed clinical [21–26] and experimental studies [28, 29] were the reason for using a cutoff of DI=1.4 in our grouping of DNA aneuploid tumors, as shown in Table 1. The tumors deviating from this concept, such as SBTs with DI>1.4 and SACs with DI <1.4, are thus of special interest. They are however too few in this series, and larger material with clinical follow-up needs to be analyzed before any conclusions can be drawn concerning this group.

In conclusion, the present study demonstrates that measuring nuclear DNA content and SPF by high-resolution image analysis of paraffin-embedded material provides data supporting the dualistic model of serous ovarian tumor histogenesis.

Acknowledgements We thank Mrs. Signe Eastgate and Mrs. Erika Thorbjørnsen for their skillful technical assistance.

Conflict of interest statement We declare that we have no conflict of interest.

References

1. Lee KR, Tavassoli FA, Prat J et al (2003) Tumors of the ovary and peritoneum. In: Tavassoli FA, Devilee P (eds) World Health Organization classification of tumours: pathology and genetics. Tumours of the breast and female genital organs. IARC, Lyon, pp 117–124
2. Trimble CL, Kosary C, Trimble EL (2002) Long-term survival and patterns of care in women with ovarian tumors of low malignant potential. Gynecol Oncol 86:34–37
3. Heintz AP, Odicino F, Maisonneuve P et al (2003) Carcinoma of the ovary. Int J Gynaecol Obstet 83(Suppl 1):135–166
4. Aletti GD, Gallenberg MM, Cliby WA et al (2007) Current management strategies for ovarian cancer. Mayo Clin Proc 82:751–770
5. Kurman RJ, Shih IeM (2008) Pathogenesis of ovarian cancer: lessons from morphology and molecular biology and their clinical implications. Int J Gynecol Pathol 27:151–160
6. Hauptmann S, Denkert C, Koch I et al (2002) Genetic alterations in epithelial ovarian tumors analyzed by comparative genomic hybridization. Hum Pathol 33:632–641
7. Meinhold-Heerlein I, Bauerschlag D, Hilpert F et al (2005) Molecular and prognostic distinction between serous ovarian carcinomas of varying grade and malignant potential. Oncogene 24:1053–1065
8. Tibiletti MG, Bernasconi B, Taborelli M et al (2003) Genetic and cytogenetic observations among different types of ovarian tumors are compatible with a progression model underlying ovarian tumorigenesis. Cancer Genet Cytogenet 146:145–153
9. Kristensen GB, Kildal W, Abeler VM et al (2003) Large-scale genomic instability predicts long-term outcome for women with invasive stage I ovarian cancer. Ann Oncol 14:1494–1500
10. Wolf NG, Abdul-Karim FW, Farver C et al (1999) Analysis of ovarian borderline tumors using fluorescence in situ hybridization. Genes Chromosomes Cancer 25:307–315
11. Blegen H, Einhorn N, Sjövall K et al (2000) Prognostic significance of cell cycle proteins and genomic instability in borderline, early and advanced stage ovarian carcinoma. Int J Gynecol Cancer 10:477–487
12. Dodson MK, Hartmann LC, Cliby WA et al (1993) Comparison of loss of heterozygosity patterns in invasive low-grade and high-grade epithelial ovarian carcinomas. Cancer Res 53:4456–4460
13. Hu J, Khanna V, Jones MM, Surti U (2002) Genomic imbalances in ovarian borderline and mucinous tumors. Cancer Genet Cytogenet 139:18–23
14. Pejovic T, Iosif CS, Mitelman F et al (1996) Karyotypic characteristics of borderline malignant tumors of the ovary: trisomy 12, trisomy 7, and r(1) as nonrandom features. Cancer Genet Cytogenet 92:95–98
15. Kaern J, Tropé CG, Kristensen GB et al (1993) DNA ploidy; the most important prognostic factor in patients with borderline tumors of the ovary. Int J Gynecol Cancer 3:349–358
16. Verbruggen MB, van Diest PJ, Baak JP et al (2009) The prognostic and clinical value of morphometry and DNA cytometry in borderline ovarian tumors: a prospective study. Int J Gynecol Pathol 28:35–40
17. Erhardt K, Auer G, Björkholm E et al (1984) Prognostic significance of nuclear DNA content in serous ovarian tumors. Cancer Res 44:2198–2202
18. Dietel M, Arps H, Rohlff A et al (1986) Nuclear DNA content of borderline tumors of the ovary: correlation with histology and significance for prognosis. Virchows Arch 409:829–836
19. Padberg BC, Arps H, Franke U et al (1992) DNA cytophotometry and prognosis in ovarian tumors of borderline malignancy. A clinicomorphologic study of 80 cases. Cancer 69:2510–2514
20. deNictolis M, Montironi R, Tommasoni S et al (1992) Serous borderline tumors of the ovary—a clinicopathological, immunohistochemical, and quantitative study of 44 cases. Cancer 70:152–160
21. Klemi PJ, Joensuu H, Kilholma P et al (1988) Clinical significance of nuclear DNA content in serous ovarian tumors. Cancer 62:2005–2010
22. Demirel D, Laucirica R, Fishman A et al (1996) Ovarian tumors of low malignant potential. Correlation of DNA index and S-phase fraction with histopathologic grade and clinical outcome. Cancer 77:1494–1500
23. Seidman JD, Norris HJ, Griffin JL et al (1993) DNA flow cytometric analysis of serous ovarian tumors of low malignant potential. Cancer 71:3947–3951
24. Fležar MS, But I, Kavalar R et al (2003) Flow and image cytometric DNA ploidy, including 5c exceeding cells, of serous borderline malignant ovarian tumors. Correlation with clinicopathologic characteristics. Anal Quant Cytol Histol 25:139–145

25. Scheuler JA, Trimbos JB, Burg MVD et al (1996) DNA index reflects biological behavior of ovarian carcinoma stage I–IIa. Gynecol Oncol 63:59–66
26. Lai C-H, Hseuh S, Chang T-C et al (1996) The role of DNA flow cytometry in borderline malignant ovarian tumors. Cancer 78:794–802
27. Österberg L, Åkeson M, Levan K et al (2006) Genetic alterations of serous borderline tumors of the ovary compared to stage I serous ovarian carcinomas. Cancer Genet Cytogenet 167:103–108
28. Duesberg P, Rausch C, Rasnick D et al (1998) Genetic instability of cancer cells is proportional to their degree of aneuploidy. Proc Natl Acad Sci U S A 95:13692–13697
29. Fabarius A, Hehlmann R, Duesberg PH (2003) Instability of chromosome structure in cancer cells increase exponentially with degree of aneuploidy. Cancer Genet Cytogenet 143:59–72

Virchows Arch (2009) 454:685–694
DOI 10.1007/s00428-009-0780-4

ORIGINAL ARTICLE

The antimicrobial peptide HBD-2 and the Toll-like receptors-2 and -4 are induced in synovial membranes in case of septic arthritis

D. Varoga · E. Klostermeier · F. Paulsen · C. Wruck · S. Lippross · L. O. Brandenburg · M. Tohidnezhad · A. Seekamp · B. Tillmann · T. Pufe

Received: 6 April 2009 / Revised: 15 April 2009 / Accepted: 16 April 2009 / Published online: 3 May 2009

Abstract Septic arthritis is frequently observed especially in immune-compromised or chronically diseased patients and leads to functional impairment due to tissue destruction. Recently, production of antimicrobial peptides (AMP) was observed in articular cartilage after exposure to bacteria. This report examines the role of synoviocyte-derived AMPs in innate defense mechanisms of articular joints. Samples of healthy, low-grade synovialitis and septic synovial membranes were assessed for the expression of human β-defensin-2 (HBD-2) and Toll-like receptor-2 and -4 (TLR) by immunohistochemistry and enzyme-linked immunosorbent assay (ELISA). A stable synoviocyte line (K4IM) was used for in vitro experiments and assayed for endogenous HBD-2 and TLR production after exposure to inflammatory cytokines or bacterial supernatants by reverse transcription polymerase chain reaction (RT-PCR), real-time RT-PCR, Western blot, ELISA, and dual luciferase assay. Healthy human synovial membranes and cultured synoviocytes are able to produce HBD-2 and TLR-1–5 at basal expression levels. Samples of bacteria-colonized synovial membranes produce higher levels of HBD-2 when compared with samples of healthy tissues. K4IM synoviocytes exposed to *Staphylococcus aureus*, *Pseudomonas aeruginosa*, or proinflammatory cytokines demonstrated a clear HBD-2 transcription and protein induction. TLR-2 and -4 are known to have a critical role in the recognition of gram-positive and gram-negative bacteria in epithelia and are induced in mesenchymal synoviocytes after bacterial exposure on transcription and on protein level. This report demonstrates an unappreciated role of synovial membranes: samples of septic synovial membranes and cultured synoviocytes exposed to bacteria produce increased amounts of the AMP HBD-2 and the bacteria recognition receptors TLR-2 and -4. The induction of anti-inflammatory pathways in infected synoviocytes suggests involvement in intra-articular defense mechanisms.

Keywords Bacterial infection · Antimicrobial peptide · Human β-defensin-2 · Toll-like receptor

The experiments comply with the current laws of Germany.

D. Varoga · S. Lippross · A. Seekamp
Department of Orthopaedic Trauma Surgery, UKSH Campus Kiel, Kiel, Germany

D. Varoga · E. Klostermeier · C. Wruck · L. O. Brandenburg · B. Tillmann · T. Pufe
Department of Anatomy, Christian-Albrechts-University, Kiel, Germany

F. Paulsen
Institute of Anatomy and Cell Biology, Martin-Luther-University of Halle-Wittenberg, Halle, Germany

C. Wruck · L. O. Brandenburg · M. Tohidnezhad · T. Pufe (✉)
Department of Anatomy and Cell Biology, RWTH Aachen University, Wendlingweg 2, 52074 Aachen, Germany
e-mail: tpufe@ukaachen.de

Introduction

Septic arthritis frequently results from hematogenous spread of bacteria or traumatic or surgical bacterial contamination. The most common isolated bacteria in this case are *Staphylococcus aureus* [1, 2]. Once the bacteria invade the synovial membrane, bacterial toxins stimulate the release of multiple cytokines such as tumor necrosis factor (TNF-α) or interleukin-1 (IL-1). These cytokines, in

turn, induce the production of proteolytic enzymes in synovial membrane and support the destruction of articular cartilage [3–5].

In general, the synovium consists of a thin lining layer of macrophages and fibroblasts [6, 7]. In healthy organisms, the predominant cell type is of mesenchymal origin and demonstrates fibroblast-like features [8, 9]. In pyogenic arthritis, the synovial lining thickens, and the sublining tissue becomes infiltrated with T cells, B cells, and macrophages.

The host response to bacterial infection is dependent on both innate (non-antibody-mediated) and adaptive (antibody-mediated) immune systems. The adaptive immune system is primarily cellular in composition and relies on the actions of B and T cells. The innate immune response is more immediate and depends on the activity of phagocytic cells and the expression of a number of antimicrobial proteins and peptides (AMP) [10, 11]. Defensins are an important subfamily of AMP and are able to kill microbes by destructing their cell membranes. To date, six human β-defensin (HBDs), HBD-1 through -6, have been identified in human tissues [10, 11]. The HBDs differ in tissue distribution and expression profile after stimulation with proinflammatory cytokines or bacteria [12–16]. The HBD-2 was first isolated from human skin and displays potent antimicrobial activity in the gram-negative and -positive range as well [12]. The importance of AMP in host defense becomes evident in mice overexpressing the human alpha-defensin-5 gene and the subsequent resistance to oral application of *Salmonella typhimurium* [17]. Other studies revealed that mice with disrupted AMP genes are prone to infection in the affected organs [18].

Toll-like receptors (TLR) are a family of transmembrane receptors [19–21]. They were regarded as key regulators of both innate and adaptive immune response and recognize pathogen-associated molecular patterns (PAMPs) from gram-positive and -negative bacteria [22]. The interaction of TLRs with PAMPs results in the nuclear translocation of the transcription factor nuclear factor kappa B (NF-κB) and a subsequent increase of AMP production [9, 10, 23]. Studies on epithelia demonstrate that TLR-4 and its accessory molecule lymphocyte antigen 96 (MD-2) are required for the recognition of lipopolysaccharide found in the membranes of gram-negative bacteria [24]. By contrast, TLR-2 is required for the recognition of bacterial lipopeptide, and in combination with TLR-6, for the detection of peptidoglycan and lipoteichoic acid, which are components of gram-positive bacteria [23]. Up to now, reports are missing concerning the expression and regulation of TLRs in mesenchymal synoviocytes in case of bacterial exposure.

Recent studies of our group have demonstrated that synovial membranes have the ability to produce HBDs in case of inflammatory or bacterial joint disease [25, 26]. Moreover, expression pattern of these peptide antibiotics changed, dependent on the kind of joint disease, thus, suggesting a regulative AMP production after being challenged by inflammatory mediators [26].

The aim of the current study was to determine inflammatory production and regulation of HBD-2 in human synovial membranes and to evaluate the findings in an in vitro model with immortalized synoviocytes called K4IM and primary synoviocytes.

Material and methods

Tissues

Healthy synovial membranes (n=6) were collected from knee joints without signs of degeneration. The articular joints were dissected from body donors, donated to the Institute of Anatomy. Infected synovial membranes (high-grade synovialitis; n=6) and low-grade synovialitis synovial membrane (n=6) were collected from patients who underwent revision surgery due to bacterial infection at the Department of Trauma, University of Kiel. All samples from patients suffering from septic arthritis showed positive microbiological cultures for gram-positive bacteria such as *S. aureus* (n=3) or *S. epidermidis* (n=3). The study was approved by the institutional review board.

Human cell culture

To analyze parameters that lead to the activation of synovial fibroblasts, we cultured a stable human synoviocyte line (K4IM, a generous gift from Christian Kaps, Charite, Berlin, Germany) which is immortalized with the SV40 T antigen [27]. Several studies confirmed that the immortalized K4IM cell line represents a valuable tool to study mechanisms that induce synoviocyte activation [27, 28]. For Western blot analysis, primary synoviocytes were collected from healthy synovial membranes of body donors and prepared for in vitro examinations, as recently described by Ralph et al. [29]. For in vitro experiments, synoviocytes were cultured in monolayers in RPMI-1640 media supplemented with 10% (v/v) fetal calf serum, 2 mM glutamine, and 50 μg/ml penicillin-streptomycin (Gibco BRL). At 80% confluency, stimulation experiments were performed in serum-free RPMI-1640 medium in humidified 5% CO_2 atmosphere.

Stimulants

Synoviocytes in monolayer culture were exposed to IL-1/-6 (10 ng/ml), TNF-α (10 ng/ml) or supernatants of *Pseudomonas aeruginosa* (PAS) or *S. aureus* (diluted 1:50) for 6 or

24 h. The supernatants were generated from clinical isolates, as recently described by Gläser et al. [30].

RNA preparation and cDNA synthesis

Frozen tissue samples (20 mg) of healthy and infected synovial membranes were crushed in an achate mortar under liquid nitrogen. RNA from tissues was generated by Trizol reagent. Moreover, RNA from cultured synoviocytes was extracted with the RNeasy Total RNA kit (Qiagen, Hilden, Germany) according to the manufacturer's instructions. Contaminating DNA was destroyed by digestion with RNase-free DNase-I (20 min at 25°C, Boehringer, Mannheim, Germany). After inactivation of DNase (15 min at 65°C), complementary DNA (cDNA) was generated with 1 µl (20 pmol) of oligo (dt) primer (Amersham Pharmacia, Uppsala, Sweden) and 0.8 µl of superscript RNase H-reverse transcriptase (Gibco, Paisley, UK) for 60 min at 37°C.

Reverse transcription polymerase chain reaction

For PCR, 4 µl of cDNA were incubated with 30.5 µl water, 4 µl 25 mM $MgCl_2$, 1 µl dNTP, 5 µl 10 × PCR buffer, and 0.5 µl (2.5 U) platinum *Taq* DNA polymerase (Gibco), and the following pairs of primers: HBD-2-for1 5′-CCAGCCAT CAGCCATGAGGGT-3′, HBD-2-ra 5′-GGAGC CCTTT CTGAATCCGCA-3′, 57°C, 255 bp; TLR-1-for1 5′-CTATA CACCAAGTTGTCAGC-3′, TLR-1-ra 5′-GTC TCCAACT CAGTAAGGTG-3′, 56°C, 210 bp; TLR-2-for1 5′-GCCAA AGTCTTGATTGATTGG-3′, TLR-2-ra 5′-TTG AAGTTCT CCAGCTCCTG-3′, 56°C, 347 bp; TLR-3-for1 5′-GATCT GTCTCATAATGGCTTG-3′, TLR-3-ra 5′-GAC AGATTCCG AATGCTTGTG-3′, 56°C, 300 bp; TLR-4-for1 5′-TGGATACGTTTCCTTATAAG-3′, TLR-4-ra 5′-GAAATGGAGGCACCCCTTC-3′, 56°C, 548 bp; TLR-5-for1 5′-CTAGCTCCTAATCCTGATG-3′, TLR-5-ra 5′-C CATGTGAAGTCTTTGCTGC-3′, 56°C, 400 bp. A glyceraldehyde-3-phosphate dehydrogenase (GAPDH)-specific intron-spanning primer pair (forward primer: 5′TGA AGGTCGGAGTCAACGGA TTTGGT-3′; reverse primer: 5′-CATGTGGGCCATGAGGTCCACCAC -3′), which yielded a 983-bp amplified product, served as the internal control for equal amounts of cDNA. Thirty-five cycles were performed with each primer pair. All primers were synthesized by MWG-Biotech AG, Ebersberg, Germany. For the negative control reaction, the cDNA was replaced with water.

Real-time reverse transcription polymerase chain reaction

Real-time reverse transcription polymerase chain reaction (RT-PCR) was carried out using a one-step RT-PCR system (Qiagen; QuantiTect SYBR Green RT-PCR). For this purpose, 100 ng of total RNA was added. Real-time RT-PCR was used to monitor gene expression using an i-Cycler (Biorad, München, Germany) according to the standard procedure. PCR was performed, as recently described by our group [31, 32]. I-Cycler Data Analysis software (Biorad, München, Germany) was used for PCR data analysis. The used TaqMan primers and probes had the following identification numbers: GAPDH: Hs99999905_m1, HBD-2: Hs00823638_m1, TLR-2: Hs00610101_m1, and TLR-4: Hs00370853_m1 (Applied Biosystems, Darmstadt, Germany). Relative quantification was performed by normalizing the signals of the different genes against those of GAPDH. The assessed data included three independent experiments with triplicates.

Western blot

For Western blots, samples were reduced in the presence of 10 mM dithiothreitol, proteins separated by sodium dodecyl sulphate-polyacrylamide gel electrophoresis (10% gels), transferred onto nitrocellulose membranes that were blocked and incubated with antibodies according to standard techniques as described [33]. Signals were detected by chemiluminescence reaction (ECL-Pus; Amersham Pharmacia, Uppsala, Sweden).

HBD-2 enzyme-linked immunosorbent assay

For enzyme-linked immunosorbent assay (ELISA), 100 mg fresh weight of healthy and infected synovial membranes was crushed in an achate mortar under liquid nitrogen and homogenized in 150 mM NaCl, 20 mM Tris HCl buffer, pH 7.4, using a polytron homogenizer (Kinematica, Luzern, Switzerland). A soluble fraction was obtained by centrifugation at 48.000×g for 60 min. Subsequently, 50 µl aliquots of this homogenates and aliquots of the collected cell supernatants from the stimulation experiments were examined by sandwich ELISA. Ninety-six well immunoplates (MaxiSorp™, Nunc, Roskilde, Denmark) were coated at 4°C for 24 h with 100 µl (0.5 µg/ml) goat anti-HBD-2 antibody (Acris, Hiddenhausen, Germany; PP1125P2) diluted 1:500 in 0.05 M carbonate buffer, pH 9.6. Subsequently, wells were blocked with 200 µl 1% bovine serum albumin in phosphate buffer solution (PBS) for 10 min at room temperature. After three times washing with 200 µl PBS+0.1% Tween 20, 100 µl per well of cell culture supernatants were incubated for 30 min at room temperature. Plates were washed thrice with PBS+0.1% Tween 20, and wells were incubated for 30 min at room temperature with 50 µl of biotinylated goat anti-HBD-2 antibody (Acris, Hiddenhausen, Germany, PP1125B1) diluted 1:2.500 to 0.2 µg/ml in PBS+0.1% Tween 20. Plates were washed again three times with PBS+0.1%

Tween and filled with 50 µl/well of streptavidin-POD (Roche Diagnostics, Mannheim, Germany; 1:10.000 in PBS+0.1% Tween 20). The plates were then incubated for 30 min at room temperature, washed three times as described above, and incubated with 2.2′-azino-bis-3-ethyl-benzthiazoline-6-sulfonic acid (Roche Diagnostics) as the development agent for 15–45 min at room temperature in the dark. Absorbance was measured at 405 nm with a multichannel photometer (Sunrise; Tecan, Crailsheim, Germany). Human recombinant HBD-2 (PeproTec, Rocky Hill, CT, USA) served as the standard with the following concentrations: 0, 0.16, 0.32, 0.64, 1.25, 2.5, and 5 ng/ml.

Dual luciferase assay

The luciferase assay was carried out as described in Harder et al. [34].

Statistical analysis

Differences between the groups were evaluated using the *t* test. Group differences were considered significant if $P < 0.05$. All statistical analyses were carried out using the JMP statistics package (SAS Institute, Cary, NC, USA).

Results

Human β-defensin-2 is induced in septic synovial membrane

To evaluate HBD-2 expression in low-grade synovialitis and in healthy and inflamed human synovial membranes (high-grade synovialitis), RT, PCR, immunohistochemistry, and ELISA experiments were performed.

RT-PCR revealed HBD-2 transcripts in all examined tissue samples of bacteria-infected synovial membranes (Fig. 1a). Immunohistochemistry was used to analyze expression pattern of HBD-2 in healthy and infected tissues. Neglectable immunostaining was demonstrated in tissue samples of low-grade synovialitis or healthy synovial membranes (Fig. 1b), but bacterial colonization results in a significant upregulation of HBD-2. The observed immunostaining was primarily visible in the extracellular matrix of fibroblasts, as detected by their characteristic shape (Fig. 1b).

ELISA experiments were performed to analyze quantitative amounts of HBD-2 protein in the collected tissue samples of healthy, low-grade synovialitis and high-grade synovialitis (bacteria-infected synovial membranes). In case of gram-positive infections, HBD-2 expression levels clearly raised to 1.5 ng/100 mg fresh tissue, thus demonstrating a microbial influence in the regulation of synovial membrane-derived AMP (Fig. 1c). The amount of HBD-2 in healthy and in low-grade synovialitis was similar (Fig. 1c).

IL-1, IL-6, TNF-α, *P. aeruginosa*, and *S. aureus* stimulate HBD-2 expression in cultured synoviocytes

To assess inducers of HBD-2 in synovial membranes, K4IM synoviocytes were taken into cell culture and stimulated with different proinflammatory cytokines and supernatants of a clinical isolate of *S. aureus* or *P. aeruginosa*. After 6 or 24 h of stimulation, RNA or cell supernatants were collected and assayed by RT-PCR, real-time RT-PCR, or ELISA experiments. Similar to recent results in chondrocytes, cultured K4IM synoviocytes strongly induce HBD-2 transcripts after exposure to IL-1/-6 or TNF-α (Fig. 2a, b). Among these inflammatory cytokines, TNF-α has the greatest impact on HBD-2 gene expression in K4IM cells (Fig. 2b). Protein analysis with a HBD-2 sandwich ELISA revealed gram-positive bacteria of *S. aureus* and gram-negative *P. aeruginosa* as additional stimulators, because 24 h after exposure amounts of secreted HBD-2 protein raised up to 160 ng/300.000 cells. Interestingly, induction of HBD-2 was not dependent on the specification of the bacteria and did not exceed amounts of cytokine-exposed synoviocytes (Fig. 2c).

The Toll-like receptors 1–5 are expressed in healthy synovial membranes

To investigate the expression of TLRs, which are known to be involved in the regulation of AMPs in epithelia, RT-PCR, immunohistochemistry, and Western blot investigations were performed. RT-PCR revealed transcripts of TLR-1–5 in homogenates of healthy synovial membranes (Fig. 3), indicating a role in the regulation of AMP in mesenchymal synovial membranes. Because of their key role in bacteria-mediated anti-inflammatory pathways in epithelia, production of TLR-2 and -4 was additionally demonstrated by immunohistochemistry in samples of septic synovial membranes (Fig. 1b). Regulation of TLR-4 was examined in primary synoviocytes after exposure to *P. aeruginosa.* Western blot analysis revealed induction of gram-negative specialized TLR-4 after 24 h of bacterial stimulation.

Bacterial induction of TLR-2 and -4 in cultured synoviocytes

To test the inducibility of TLR-2 and -4 in cultured synoviocytes, K4IM cells were challenged by TNF-α or supernatants of *P. aeruginosa* and *S. aureus.* After 6 h of co-culturing, RT-PCR and real-time RT-PCR examinations were performed. Addition of the proinflammatory cytokine

TNF-α (10 ng/ml) resulted in an increased transcription of TLR-4 (Fig. 4a). Real-time RT-PCR demonstrated a clear induction of TLR-2 and -4-messenger RNA after 6 h of exposure to gram-negative *P. aeruginosa* and gram-positive *S. aureus* (Fig. 4b). Interestingly, bacterial specification did not significantly influence TLR-2 gene expression, but quantitative TLR-4-RT-PCR revealed more transcripts in case of gram-positive bacterial stimulation with *S. aureus* (Fig. 4b).

Proinflammatory cytokines and supernatant of *P. aeruginosa* and *S. aureus* increase promoter activity of HBD-2

In order to verify the ELISA and real-time RT-PCR data, we performed dual luciferase assays. IL-1 leads to an 11-fold, TNF-α to an eightfold, and IL-6 to a twofold increase of the HBD-2 promoter activity (Fig. 5a). *P. aeruginosa* leads to a 1.2-fold and *S. aureus* to a 2.2-fold increase of the HBD-2 promoter activity (Fig. 5b). After 12 h, 10 ng/ml IL-1 leads to a maximum of HBD-2 promoter activity (Fig. 5c; control=1). All experiments were performed with $n=8$.

Discussion

Defensins are an essential part of the host innate immune system responsible for the first line of defense against pathogenic microorganisms [10, 11]. In case of bacterial arthritis, many cell types neighboring to synoviocytes (for instance chondrocytes, osteocytes, and osteoblasts) were

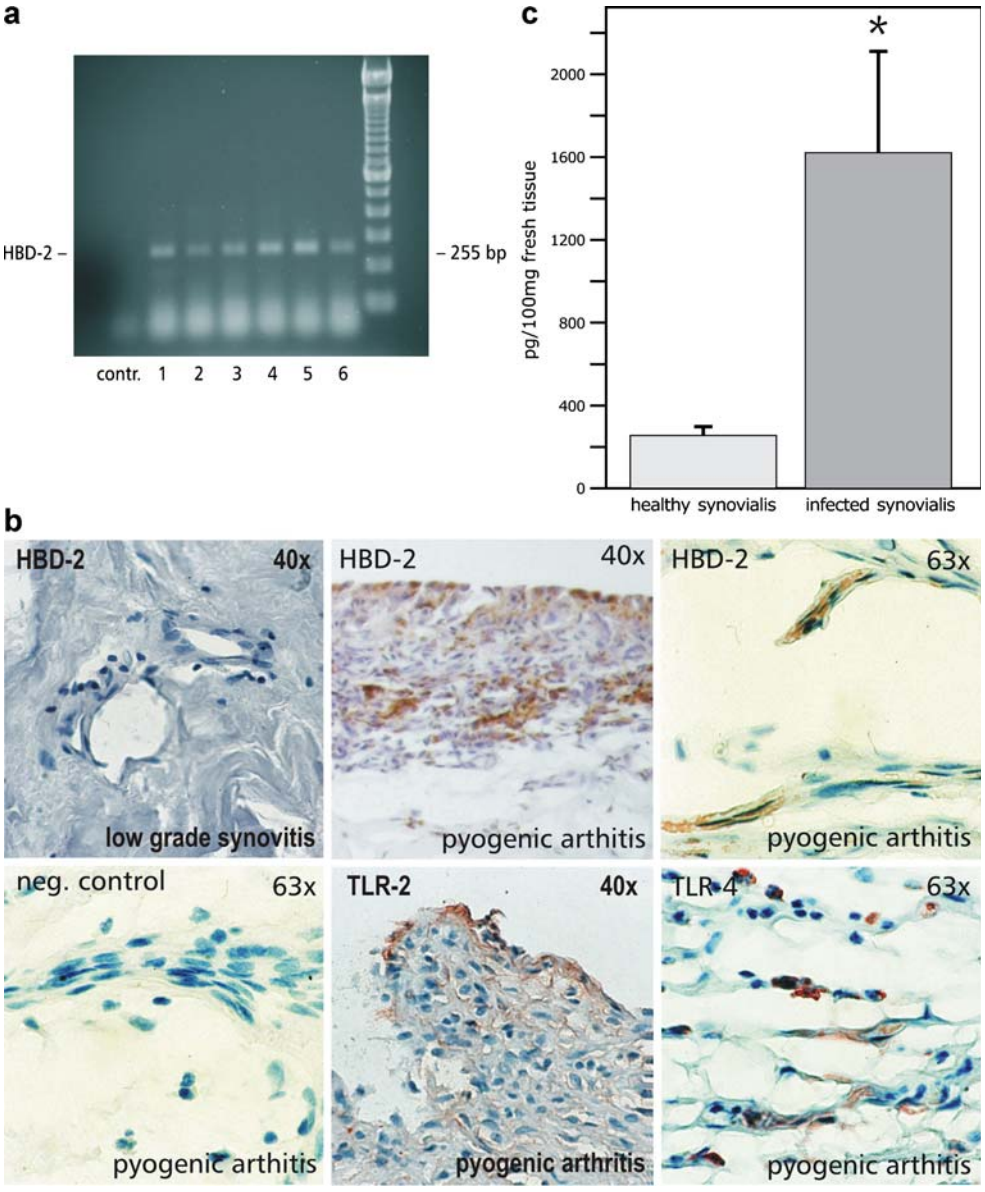

Fig. 1 **a**–**c** Human β-defensin-2 is expressed and induced in bacteria-infected synovial membranes. To assess production of HBD-2 in synovial membranes after bacterial infection, RT-PCR, immunohistochemistry, and ELISA experiments were performed. RT-PCR revealed HBD-2 transcripts in all examined bacteria-colonized tissue samples (**a**). Immunohistochemical examinations confirmed increased staining activity in samples of infected synovial membranes. Staining was primarily found in the extracellular matrix of fibroblasts, as detected by their characteristic cigar-shape (**b**). ELISA experiments approved increased expression of the endogenous antibiotic. In case of bacterial colonization with staphylococci, HBD-2 amounts peaked to 1.5 ng/100 mg fresh tissue (**c**). Values are the mean ± standard deviation, *$P<0.05$ versus controls

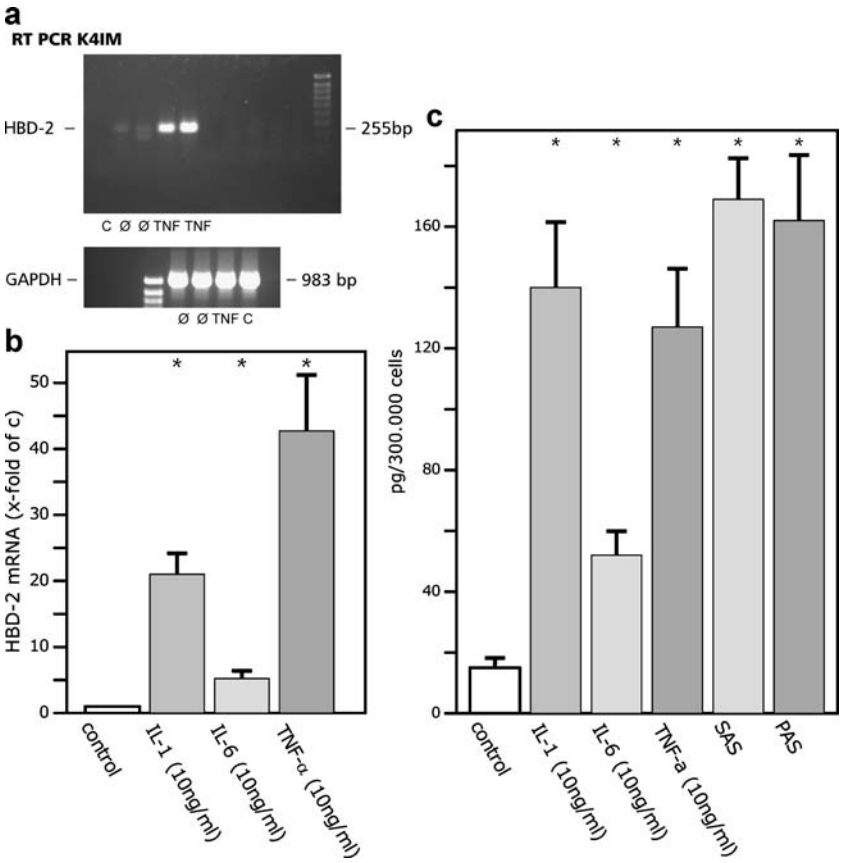

Fig. 2 **a**–**c** Proinflammatory cytokines such as IL-1, IL-6, or TNF-α and bacterial supernatants of *Staphylococcus aureus* and *Pseudomonas aeruginosa* were transcriptional inducers of human β-defensin-2. Proinflammatory cytokines such as IL-1, IL-6, or TNF-α are known to be involved in inflammatory joint disease. To assess their influence on HBD-2 gene expression in cultured K4IM synoviocytes, RT-PCR, real-time RT-PCR, and ELISA experiments were performed. After 6 h of stimulation, TNF-α (10 ng/ml) stimulation resulted in a more than 40-fold increased transcription rate when compared to controls (**a**, **b**). To examine secreted HBD-2 protein levels in cultured K4IM synoviocytes, ELISA experiments were done. After 24 h of stimulation, cell culture supernatants were collected and revealed increased HBD-2 expression in case of IL-1, IL-6, TNF-α, or bacterial exposure (**c**). Interestingly, induction of HBD-2 was not dependent on the specification of the bacteria and did not significantly exceed amounts of cytokine-exposed synoviocytes. Values are the mean ± standard deviation, *$P<0.05$ versus controls. *c* negative control; *Ø* unstimulated cells

affected, but Typ-A and -B-synoviocytes were regarded as the most immunocompetent cells from all. Therefore, we analyzed the production and regulation of the antimicrobial peptide HBD-2 in samples of healthy and infected synovial membranes and evaluated these findings in a model of cultured K4IM synoviocytes after inflammatory or bacterial exposure.

The transcriptional induction of HBD-2 in mesenchymal synovial membrane after contact with proinflammatory cytokines or *S. aureus* is in accordance with previous results on epithelial tissues, which examine the antibacterial role of defensins. Harder et al. [12] were the first who describe the induction of HBD-2 after inflammatory challenge of human skin. Other studies confirmed upregulation in several epithelial tissues such as the lungs or the gastrointestinal or urogenital tract [13, 35–38]. Typical stimulators include the cytokines TNF-α, IL-1/-6, or the gram-negative bacteria *P. aeruginosa* [12, 34, 38, 39]. Many studies failed to observe HBD-2 induction following gram-positive bacterial stimulation, but it is reasonable to propose that AMP induction differs dependent on the examined tissues and the pathogenicity of the used bacteria [12, 39].

The induction of synoviocyte-secreted HBD-2 protein was measured after 24 h of inflammatory or bacterial stimulation. In contrast, AMP secretion of blood cells is induced within a few minutes as a result of storage in cellular granules. The continuous expression of HBD-2 from synoviocytes after inflammatory challenge seems to be more likely a result of a de novo synthesis [10, 11]. Only

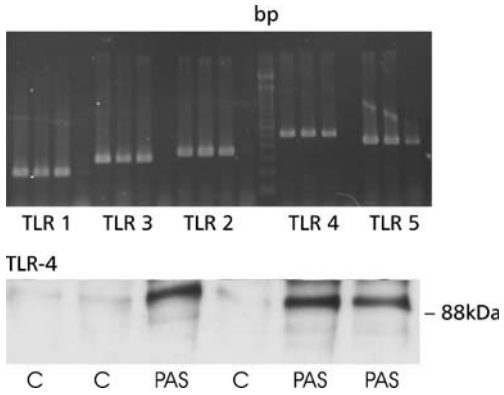

Fig. 3 Toll-like receptors 1–5 were expressed in healthy synovial membranes. To determine putative receptors for bacterial recognition in synovial membranes, RT-PCR and Western blot investigations of Toll-like receptors were performed. RT-PCR revealed transcripts of TLR-1 to -5 in samples of healthy tissues. To assess the inducibility of TLRs after bacterial exposure, primary synoviocytes were challenged by supernatants of *Pseudomonas aeruginosa.* Western blot analysis revealed increased expression of TLR-4 after gram-negative bacterial stimulation, thus suggesting a potential relationship between bacterial recognition via Toll-like receptors and subsequent induction of antimicrobial peptides in synovial membranes. *c* unstimulated cells; *PAS P. aeruginosa*-stimulated cells

two studies have already focused on the expression and regulation of HBD-2 in mesenchymal tissues such as articular cartilage or synovial membranes [26, 32]. Paulsen et al. discovered HBD-2 only in situ in some samples of pyogenic synovial membranes by means of immunohistochemistry [26]. In contrast to our study, all examined tissue samples were tested positive for *S. aureus* colonization and thus may explain their observed incontinuous production of HBD-2.

The induction of HBD-2 in synovial membrane is not merely connected with antibacterial tasks. The secreted protein levels, as measured by ELISA, were at low antibacterial levels, but concomitant expression of cartilage- or neutrophil-released AMPs may increase intra-articular defense levels. In addition to their antimicrobial activity, HBD-2 provides a link to the adaptive immune system by attracting immature dendritic cells and memory T cells via the chemokine receptor CCR-6 [40]. Interestingly, for chemotactic tasks, HBD-2 is needed in much lower concentrations. Recently, two reports describe intra-articular accumulation of AMPs in human joints following abacterial rheumatoid arthritis (RA) [41, 42]. Without immediate threat of bacterial colonization, bactericidal/permeability-increasing protein (BPI) and human neutrophil peptides (HNP-1–3) increased in joint fluid samples of patients with RA. Moreover, they observed a significant correlation between joint destruction and intra-articular accumulation of BPI and HNP, thus suggesting additional tasks of AMPs than the antimicrobial [42]. Previous results of our group may provide an explanation. After co-incubation of chondrocytes or cartilage discs with HBD-3 protein, levels of tissue destructive matrix metalloproteinases raises, and levels of their endogenous inhibitors (tissue inhibitors of metalloproteinases) dropped [31]. Especially, the observed sub-antimicrobial protein levels support our hypothesis that synoviocyte-derived HBD-2 expression following inflammatory exposure may modify migration pattern of blood cells into the joint cavity via CCR-6 receptor or interferes with tissue remodeling processes in articular cartilage.

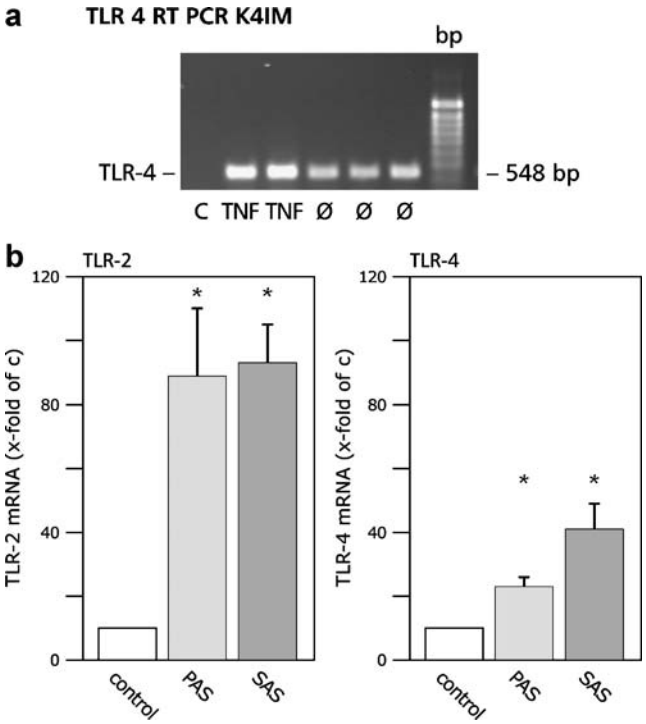

Fig. 4 Toll-like receptor-2 and -4 were induced in cultured K4IM synoviocytes after bacterial stimulation. To determine K4IM synoviocytes as an appropriate in vitro model for studying mechanisms that induce synoviocyte activation, real-time RT-PCR was performed. After 6 h of stimulation, TLR-2 gene expression increased nearly tenfold after gram-positive or -negative bacterial stimulation. Interestingly, TLR-2 is primarily involved in the recognition of gram-positive bacteria in epithelia, but bacterial specification does not influence TLR-2 transcription rate in mesenchymal synoviocytes. The same observation is made in case of TLR-4 real-time analysis. Studies on epithelia suggest that TLR-4 is primarily involved in the recognition of gram-negative bacteria, but mesenchymal synoviocytes induce TLR-4 also after gram-positive bacterial challenge. Values are the mean ± standard deviation, $*P<0.05$ versus controls

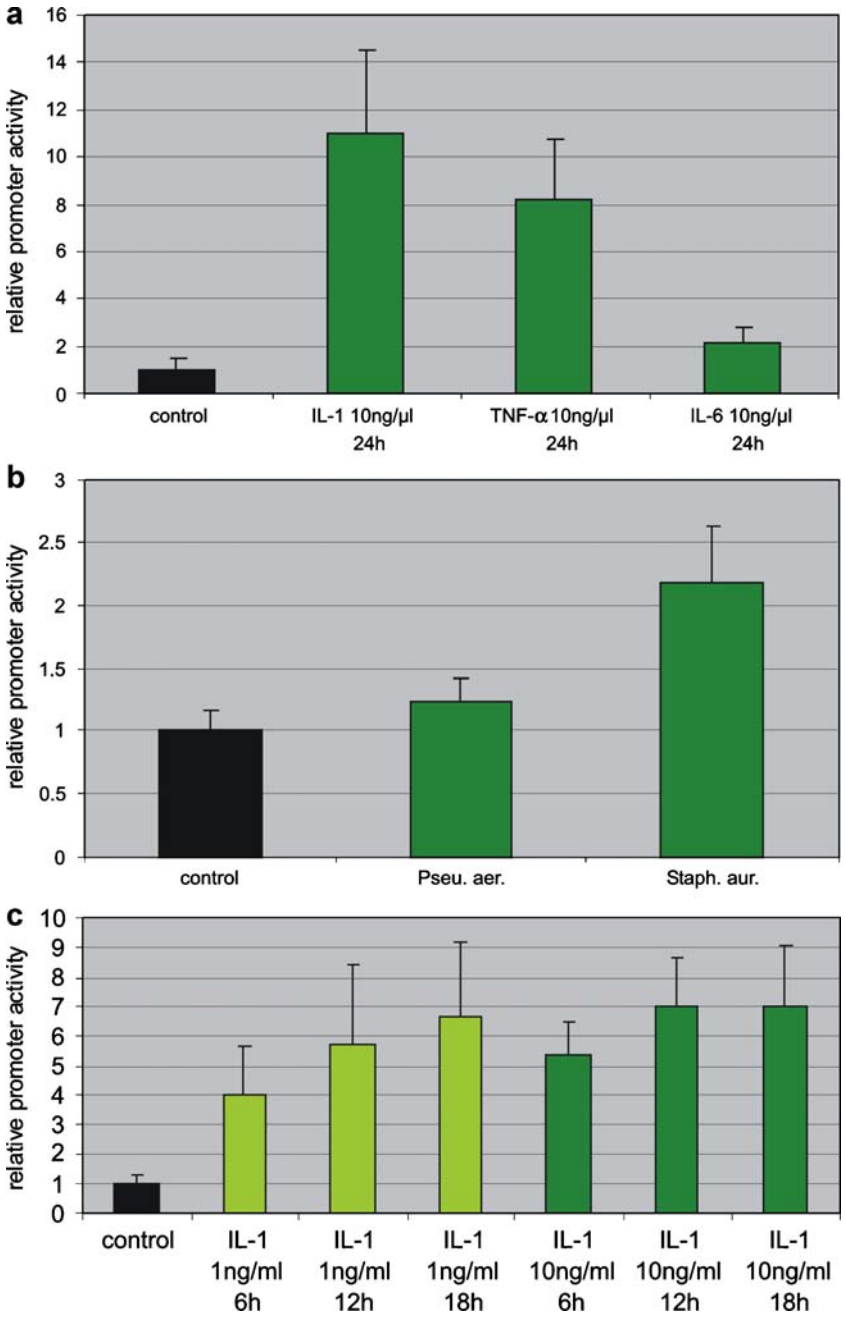

Fig. 5 Dual luciferase assay revealed strong increase of HBD-2 promoter activity due to proinflammatory cytokines or *Staphylococcus aureus* supernatant. IL-1 leads to an 11-fold, TNF-α to an eightfold, and IL-6 to a twofold increase of the HBD-2 promoter activity (**a**). *Pseudomonas aeruginosa* leads to a 1.2-fold and *S. aureus* to a 2.2-fold increase of the HBD-2 promoter activity (**b**). After 12 h, 10 ng/ml IL-1 leads to a maximum of HBD-2 promoter activity (**c**; control=1). All experiments were performed with $n=8$. *Error bars* indicate SEM. *Significant difference versus control

The receptor, which mediates bacteria- or inflammatory-dependent upregulation of AMP in infectious arthritis, has not yet been characterized. The induction of TLR-2 and -4 in cultured synoviocytes suggest a possible involvement in host AMP production following bacterial stimulation. TLR recognize specific pathogen-associated molecules that are associated with a variety of bacteria, viruses, and fungi [21–23]. Interaction of TLR and bacterial pathogens resulted in an enhanced production of antimicrobial proteins and secretion of proinflammatory cytokines in epithelial tissues, but the role of TLRs in bacteria-infected mesenchymal tissues has to be evaluated in future experiments [21].

Conclusion

Taken together, this is the first report which describes the induction of HBD-2 and the PAMP receptors TLR-2 and -4 in synovial membranes after inflammatory and bacterial exposure and suggests involvement either in innate defense mechanism or in the regulation of the destructive course of septic arthritis.

Acknowledgments We wish to thank Susanne Echterhagen, Christiane Jaeschke, Patrycja Kozak, Inka Kronenbitter, Ursula Mundt, Michaela Nicolau, Angela Rüben, Sonja Seiter, and Kirsten Vosen for their expert technical assistance and Clemens Franke for the drawing. The K4IM and the HSE cells were a courtesy from Christian Kaps. This work was supported by grants of the Deutsche Forschungsgemeinschaft (SFB 617, project A22; DFG Va 220/2-1, Pu 214/3-2, Pu 214/4-2, Pu 214/5-2, and PA 738/9-1), from the "Stiftung zur Förderung der Medizinischen Forschung" of the Medical Faculty of the University of Kiel (to D V and TP), from the Hensel Stiftung (to DV and FP), and by the "Verein zur Förderung der Erforschung und Bekämpfung rheumatischer Erkrankungen Bad Bramstedt e.V.", and by BMBF/Wilhelm-Roux (FKZ 9/16 to FP).

Conflicts of interest We declare that we have no conflict of interest.

Authors' contributions

DV, TP, EK, CW, LB, FP, MT, and SL performed the experiments, and BT and AS contributed to the draft manuscript; DV and TP contributed equally to the present work. The manuscript has been read and approved by all authors.

References

1. Goldenberg DL (1999) Septic arthritis. Lancet 351:197–202
2. Ross JJ (2005) Septic arthritis. Infect Dis Clin North Am 4:799–817
3. Jasin HE (1983) Bacterial lipopolysaccharides induce in-vitro degradation of cartilage matrix through chondrocyte activation. J Clin Invest 72:2014–2019
4. Deng GM, Verdrengh M, Liu ZQ et al (2000) The major role of macrophages and their product tumor necrosis factor alpha in the induction of arthritis triggered by bacterial DNA containing CpG motifs. Arthritis Rheum 43:2283–2289
5. Hsieh YS, Yang SF, Lue KH et al (2006) Clinical correlation with the PA/plasmin system in septic arthritis of the knee. Clin Orthop Relat Res 447:172–178
6. Castor CW (1960) The microscopic structure of normal human synovial tissue. Arthritis Rheum 3:140–151
7. Barland P, Novikoff AB, Hamerman D (1962) Electron microscopy of the human synovial membrane. J Cell Biol 14:207–220
8. Wilkinson LS, Pitsillides AA, Worrall JG et al (1992) Light microscopic characterization of the fibroblast-like synovial intimal cell (synoviocyte). Arthritis Rheum 35:1179–1184
9. Stevens CR, Mapp PI, Revell PA (1990) A monoclonal antibody (Mab 67) marks type B synoviocytes. Rheumatol Int 10:103–106
10. Zasloff M (2002) Antimicrobial peptides of multicellular organisms. Nature 415:389–395
11. Ganz T (2003) Defensins: antimicrobial peptides of innate immunity. Nat Rev Immunol 3:710–720
12. Harder J, Bartels J, Christophers E et al (1997) A peptide antibiotic from human skin. Nature 387:861
13. Valore EV, Park CH, Quale AJ et al (1998) Human β-defensin-1: an antimicrobial peptide of urogenital tissue. J Clin Invest 101:1633–1642
14. Harder J, Bartels J, Christophers E et al (2001) Isolation and characterization of human β-defensin-3, a novel human inducible peptide antibiotic. J Biol Chem 276:5707–5713
15. Garcia JR, Krause A, Schulz S et al (2001) Human beta-defensin 4: a novel inducible peptide with a specific salt-sensitive spectrum of antimicrobial activity. FASEB J 15:1819–1821
16. Garcia JR, Jaumann F, Schulz S et al (2001) Identification of a novel, multifunctional beta-defensin (human beta-defensin 3) with specific antimicrobial activity. Its interaction with plasma membranes of *Xenopus* oocytes and the induction of macrophage chemoattraction. Cell Tissue Res 306:257–264
17. Salzman NH, Ghosh D, Huttner KM et al (2003) Protection against enteric salmonellosis in transgenic mice expressing a human intestinal defensin. Nature 422:522–526
18. Nizet V, Ohtake T, Lauth X et al (2001) Innate antimicrobial peptide protects the skin from invasive bacterial infection. Nature 414:454–457
19. Muzio M, Polentarutti N, Bosisio D et al (2000) Toll-like receptors: a growing family of immune receptors that are differentially expressed and regulated by different leukocytes. J Leukoc Biol 67:450–455
20. Mushegian A, Medzhitov R (2001) Evolutionary perspective on innate immune recognition. J Cell Biol 155:705–711
21. Akira S, Takeda K, Kaisho T (2001) Toll-like receptors: critical proteins linking innate and acquired immunity. Nat Immunol 2:675–678
22. Cook DN, Pisetsky DS, Schwartz DA (2004) Toll-like receptors in the pathogenesis of human disease. Nat Immunol 5:975–979
23. Takeda K, Kaisho T, Akira S (2003) Toll-like receptors. Annu Rev Immunol 21:335–376
24. Suzuki M, Hisamatsu T, Podolsky K (2003) Y interferon augments intracellular pathway for LPS recognition in human intestinal epithelial cells through coordinated up-regulation of LPS uptake and expression of the intracellular TLR-4-MD-2 complex. Infect Immun 71:3503–3511
25. Paulsen F, Pufe T, Petersen W et al (2001) Expression of natural peptide antibiotics in human articular cartilage and synovial membrane. Clin Diagn Lab Immunol 8:1021–1023
26. Paulsen F, Pufe T, Conradi L et al (2002) Antimicrobial peptides are expressed and produced in healthy and inflamed human synovial membranes. J Pathol 198:369–377
27. Haas C, Aicher WK, Dinkel A et al (1997) Characterization of SV40T antigen immortalized human synovial fibroblasts: maintained expression patterns of EGR-1, HLA-DR and some surface receptors. Rheumatol Int 16:241–247
28. Hess S, Rheinheimer C, Tidow F et al (2001) The reprogrammed host: *Chlamydia trachomatis*-induced up-regulation of glycoprotein 130 cytokines, transcription factors, and antiapoptotic genes. Arthritis Rheum 44:2392–2401
29. Ralph JA, McEvoy AN, Kane D et al (2005) Modulation of orphan nuclear receptor NURR1 expression by methotrexate in human inflammatory joint disease involves adenosine A2A receptor-mediated responses. J Immunol 175:555–565
30. Gläser R, Harder J, Lange H et al (2005) Antimicrobial psoriasin (S100A7) protects human skin from *Escherichia coli* infection. Nat Immunol 1:57–64
31. Varoga D, Pufe T, Harder J et al (2005) Human β-defensin-3 mediates tissue remodelling processes in articular cartilage by increasing metalloproteinases and reducing their endogenous inhibitors. Arthritis Rheum 52:1736–1745
32. Varoga D, Paulsen FP, Kohrs S et al (2006) Expression and regulation of human beta-defensin-2 in osteoarthritis. J Pathol 209:166–173
33. Pufe T, Petersen W, Tillmann B et al (2001) The angiogenic peptide vascular endothelial growth factor is expressed in foetal and ruptured tendons. Virchows Arch 439:579–585
34. Harder J, Meyer-Hoffert U, Teran LM et al (2000) Mucoid *Pseudomonas aeruginosa*, TNF-alpha, and IL-1-beta, but not IL-6, induce human beta-defensin-2 in respiratory epithelia. Am J Respir Cell Mol Biol 22:714–721
35. Liu L, Roberts AA, Ganz T (2003) By IL-1 signaling, monocyte-derived cells dramatically enhance the epidermal antimicrobial response to lipopolysaccharide. J Immunol 170:575–580

36. Bals R, Wang X, Wu Z et al (1998) Human beta-defensin 2 is a salt-sensitive peptide antibiotic expressed in human lung. J Clin Invest 102:874–880
37. Becker MN, Diamond G, Verghese MW et al (2000) CD-14-dependent lipopolysaccharide-induced beta-defensin-2 expression in human tracheobronchial epithelium. J Biol Chem 275:29731–29736
38. O'Neil DA, Porter EM, Elewaut D et al (1999) Expression and regulation of the human beta-defen-sins hBD-1 and HBD-2 in intestinal epithelium. J Immunol 163:6718–6724
39. Varoga D, Pufe T, Harder J et al (2004) Production of endogenous antibiotics in articular cartilage. Arthritis Rheum 50:3526–3534
40. Yang D, Chertov O, Bykovskaia SN et al (1999) Beta-defensins: linking innate and adaptive immunity through dendritic and T cell CCR6. Science 286:525–528
41. Punzi L, Peuravuori H, Jokilammi-Siltanen A et al (2000) Bactericidal/permeability increasing protein and proinflammatory cytokines in synovial fluid of psoriatic arthritis. Clin Exp Rheumatol 18:613–615
42. Bokarewa MI, Jin T, Tarkowski A (2003) Intraarticular release and accumulation of defensins and bactericidal/permeability-increasing protein in patients with rheumatoid arthritis. J Rheumatol 30:1719–1724

Virchows Arch (2009) 454:695–702
DOI 10.1007/s00428-009-0787-x

ORIGINAL ARTICLE

Nuclear thymidylate synthase expression in sporadic colorectal cancer depends on the site of the tumor

Violetta Sulzyc-Bielicka · Pawel Domagala · Ewa Majdanik · Maria Chosia · Dariusz Bielicki · Jozef Kladny · Mariusz Kaczmarczyk · Krzysztof Safranow · Wenancjusz Domagala

Received: 22 January 2009 / Revised: 30 April 2009 / Accepted: 4 May 2009 / Published online: 15 May 2009

Abstract Colorectal carcinoma (CRC) is a heterogeneous disease with specific epidemiological, pathological, molecular, and clinical characteristics that depend on the location of the tumor relative to the splenic flexure. Thymidylate synthase (TS) is a major target of 5-fluorouracil-based chemotherapy for CRC and high expression of this enzyme in tumor cells can influence the effect of therapy. We examined differences in TS protein expression in nuclei of tumor cells between CRCs located proximal and distal to the splenic flexure. Nuclear TS was detected by immunohistochemistry with a TS 106 monoclonal antibody on tissue microarrays constructed from 269 CRCs. The median histological score of nuclear TS expression of all proximal tumors was two times higher (p=0.0003) and in men three times higher (p=0.00023) than that found in distal tumors. In multivariate analysis which included age, sex, Astler–Coller stage, histological grade, and site, only proximal location of the tumor was identified as an independent factor associated with higher TS expression (odds ratio 2.46, 95% confidence interval=1.29–4.70, p=0.0062). These results demonstrate significant differences in nuclear TS expression between proximal and distal cancers and suggest the potential importance of the site of the tumor for proper stratification of patients for chemotherapy.

Keywords Nuclear thymidylate synthase · Tissue microarrays · Colorectal cancer · Tumor site

V. Sulzyc-Bielicka · J. Kladny
Department of Oncological Surgery,
Pomeranian Medical University,
Szczecin, Poland

P. Domagala
Department of Genetics and Pathology,
Pomeranian Medical University,
Szczecin, Poland

E. Majdanik · M. Chosia · W. Domagala (✉)
Department of Pathology, Pomeranian Medical University,
ul. Unii Lubelskiej 1,
71-252 Szczecin, Poland
e-mail: sekrpato@ams.edu.pl

D. Bielicki
Department of Gastroenterology and Internal Medicine,
Pomeranian Medical University,
Szczecin, Poland

M. Kaczmarczyk
Department of Laboratory Diagnostics and Molecular Medicine,
Pomeranian Medical University,
Szczecin, Poland

K. Safranow
Department of Biochemistry and Medical Chemistry,
Pomeranian Medical University,
Szczecin, Poland

Introduction

Although the majority of colorectal carcinomas (CRC) are histologically similar, i.e., they are adenocarcinomas, it has become clear that carcinomas proximal and distal to the colon's splenic flexure represent distinct entities with specific epidemiological, pathological, molecular, and clinical characteristics [1, 2]. Two different genetic pathways are thought to be involved in CRC pathogenesis: microsatellite instability and chromosomal instability, and CRCs with high-frequency microsatellite instability (MSI-H) are characterized by proximal location and relatively good prognosis [3, 4]. Hence, CRC is a heterogeneous disease that may be characterized by a different clinical outcome depending on the location of the tumor.

Thymidylate synthase (TS) catalyzes the reductive methylation of deoxyuridine monophosphate to deoxythymidine monophosphate and this reaction provides a principal precursor for DNA replication and repair. TS is the main target of 5-fluorouracil (5-FU) because 5-fluorodeoxyuridine-5′- monophosphate, a 5-FU metabolite, binds TS and forms a stable ternary complex that prevents DNA synthesis [5]. Thus, the level of expression of TS is a potential maker for predicting response to 5-FU [6]. This is supported by in vitro studies which indicate a relationship between TS levels and response to 5-FU [7]. However, it has not been established whether a cytoplasmic or nuclear TS is relevant and the results of studies correlating cytoplasmic TS expression with responses to 5-FU-based therapy are heterogeneous. High TS levels in tumor cells are associated with poor response to 5-FU- based therapy in advanced CRCs [8–10]. On the other hand, high TS expression may be associated with benefits from such therapy in adjuvant setting [11, 12]. A recent meta-analysis has shown a moderate negative predictive effect of TS overexpression [13].

In the vast majority of immunohistochemical studies in which cytoplasmic staining has been used as an indicator of TS expression (or no information was given whether cytoplasmic or nuclear staining was assessed), no correlation has been found with site of the CRC [14–21]. However, there is strong evidence for the association of the tumor site with survival benefit from 5-FU-based adjuvant chemotherapy in CRC [22]. Since TS may be found either as a ternary complex in the cytoplasm or as free TS in the nucleus [23], we asked whether nuclear TS expression differs between proximal and distal CRCs.

Materials and methods

Patients The study was based on tumor tissue from 269 unselected consecutive patients who met the following criteria: (1) had undergone potentially curative colorectal resection for sporadic CRC (absence of relevant family history at the time of admission to the hospital),(2) had no chemotherapy prior to the operation, (3) invasive adenocarcinoma Astler–Coller B_2 or C without involvement of resection margins was diagnosed by histopathological examination, (4) distant metastases at the time of operation were excluded. Thirty-eight patients with rectal cancer received preoperative radiotherapy and tissues of these cancers were obtained from posttherapeutic resection specimens. Since we did not find a statistically significant difference (p=0.88) in TS expression between this group (2.92±3.69) and the remaining 98 rectal tumors not treated with preoperative radiotherapy (2.68±3.16), the former were also included in the study.

Tissue microarray construction Tumor tissue was fixed in buffered 10% formalin and embedded in paraffin. Sections (4 μm thick) were stained with hematoxylin and eosin for histopathological diagnosis. Regions of tumors in the area of outer invasive margin of cancer with highest mitotic activity were identified and marked on hematoxylin-and-eosin-stained sections. The corresponding areas on the tissue paraffin blocks were cored and transferred to a recipient master block using a Tissue Microarrayer (Beeacher Instruments, Silver Spring, MD, USA). Each core was 0.6 mm wide. The recipient block was cut and sections were transferred to coated slides. One slide was stained with hematoxylin and eosin and a subsequent slide for immunohistochemistry.

Immunohistochemistry The immunohistochemical procedure has been optimized to detect nuclear TS. Slides with TMs were deparaffinized and rehydrated, and endogenous peroxidase activity was blocked. Slides were immersed in pH 9.0 buffer and heat-induced antigen retrieval was performed in a pressure cooker (Pascal, DakoCytomation). Monoclonal TS-106 (Chemicon, Temecula, CA, USA) antibody was used (dilution 1:50, incubation time 30 min) and the TMs were immunostained using the Dako Envision™ kit according to the manufacturer's instructions (Envision™+ peroxidase antimouse polymer labeled with horseradish peroxidase—Dako Co., Carpinteria, CA, USA). The reaction was developed with a diaminobenzidine substrate–chromogen solution and slides were counterstained with hematoxylin. Strong positive staining in stromal macrophages, lymphocytes, and plasma cells served as a built-in positive control. Appropriate positive and negative controls were run.

We optimized the immunohistochemical procedure for detection of nuclear TS by the following. (1) We used TMs. Tumor areas at the advancing outer invasive zone with highest mitotic activity were chosen for TMs and immunohistochemical procedure for all TMs from 269 tumors was performed at the same time under identical conditions. Immunohistochemistry on tissue microarrays minimizes between-batch variations which may be associated with immunohistochemical processing of groups of slides, and a large numbers of specimens can be assessed rapidly. (2) We used well-characterized and widely used TS-106 monoclonal antibody [10, 14, 24, 25]. (3) We improved antigen retrieval step (pressure cooker, buffer pH 9.0). (4) We used the sensitive Envision™+ visualization system. The detection system used is regarded as a critically important variable in immunohistochemical analysis, and detection methods using signal amplification with horseradish-peroxidase-labeled polymer (such as Envision™+) have been shown to be more sensitive than methods without such a layer of amplification [26]. (5) We used a well-defined

and tested scoring system [27, 28]. (6) Finally, we stratified CRC cases as proximal or distal in relation to the splenic flexure.

Scoring Tumor cores were independently assessed by two observers (PD and WD) who were blinded to clinical and pathological data. In cases of disagreement, the result was reached by consensus. Semiquantitative evaluation of immunostained sections was done using a histoscore system [27, 28]. Various scoring systems have been used in the literature to determine the expression status of immunohistochemically assessed proteins. Of the three most frequently applied (i.e., intensity score, pattern score, or both combined), we used intensity and pattern score because it seems to be the most reliable and proved to be useful and reproducible in assessment of immunohistochemical staining [27–29]. Both intensity (0–3) and pattern (1–6) scores were assessed. Each intensity score was multiplied by its corresponding pattern score (1=0–4% of positive tumor cells; 2=5–19%; 3=20–39%; 4=40–59%; 5=60–79%; 6=80–100%) and these grades were added to give the final histoscore (e.g., tumor with weak staining intensity in 70% of tumor cells and very strong staining intensity in 30% would have a final histoscore: $1\times5 + 3\times3=14$) [27, 28]. In order to reach the histoscore, all tumor cells in the core of the tissue microarray were counted.

Statistics Since the distribution of TS histoscore was significantly different from the normal distribution (Shapiro–Wilk test), nonparametric tests were used for the analysis. The association of TS histoscore values with categorical variables was analyzed with Mann–Whitney test. Associations between the presence of high TS histoscore (above the median value) and the site of the tumor were analyzed using the Fisher exact test. Multivariate logistic regression model was used to find the independent factors associated with TS histoscore values. The dependent variable was the presence of TS histoscore above the median calculated for all patients. The independent variables included in the model were: age, male gender, proximal tumor site, Astler–Coller stage C, and histological grade 3. $p<0.05$ was considered statistically significant. STATISTICA version 7.1 (StatSoft Inc., Tulsa, OK, USA) was used for the statistical analysis.

Results

Table 1 lists the clinicopathological details of 269 tumors and patients. The mean age of the patients was 60.9 years, with a range 33.0–83.0 years, and a median of 62.0 years.

Table 1 Clinicopathological characteristics

Feature	*n* (%)
Sex	
Males	150 (55.76%)
Females	119 (44.24%)
Site of CRC	
Proximal	51 (18.96%)
Distal	218 (81.04%)
Histological grade	
G1+G2	154 (57.25%)
G3[a]	115 (42.75%)
Astler–Coller	
B2	132 (49.07%)
C	137 (50.93%)

[a] Including 46 mucinous adenocarcinomas and signet-ring carcinomas

Immunohistochemical nuclear staining with the TS antibody was assessed (Figs. 1 and 2). Strong and moderate nuclear staining was often associated with cytoplasmic staining; however, the latter was not assessed because the immunostaining procedure had been optimized for nuclear but not cytoplasmic staining. The distribution of TS histoscores among the 269 CRCs is shown in Fig. 3. The median nuclear TS histoscore was 2. High TS immunoreactivity (histoscore>2) was found in 45% (121/269) of all cases, in 63% (32/51) of proximal cancers, and in 41% (89/218) of distal tumors ($p=0.0051$). In female CRCs, high TS immunoreactivity was seen in 50% (9/18) of proximal and 43% (43/101) of distal tumors ($p=0.61$) whereas in men it was 70% (23/33) *versus* 39% (46/117; $p=0.0028$), respectively.

There was statistically significant correlation between nuclear TS histoscore and the site of the CRC in all tumors and in tumors in men (Table 2). Univariate analysis revealed statistically significant association of TS nuclear expression with site of CRC in all tumors and in tumors in men (Table 2) but not with sex ($p=0.7$), Astler–Coller stage (mean TS in B2 *versus* C=3.62±4.09 *vs.* 3.11±3.30, $p=0.49$), or grade (mean TS in G1 + G2 *versus* G3=3.12±3.68 *vs.* 3.68±3.75, $p=0.11$). Altogether, median TS expression in proximal tumors was two times higher than that in distal ones ($p=0.0003$). This ratio was increased to three in men ($p=0.00023$). In women, the median TS histoscore in proximal tumors was 1.25 times higher than that in distal ones but the difference did not reach statistical significance, probably as a result of the small sample size (only 18 proximal tumors). The mean TS expression in proximal tumors was 1.8 times higher than that in distal ones in all tumors, 2.0 times higher in tumors in men, and 1.6 times higher in tumors in women (Table 2). Association of high TS expression with site in men remained statistically significant after stratifying for Astler–Coller stage in both the B2 and C subgroups (Table 2).

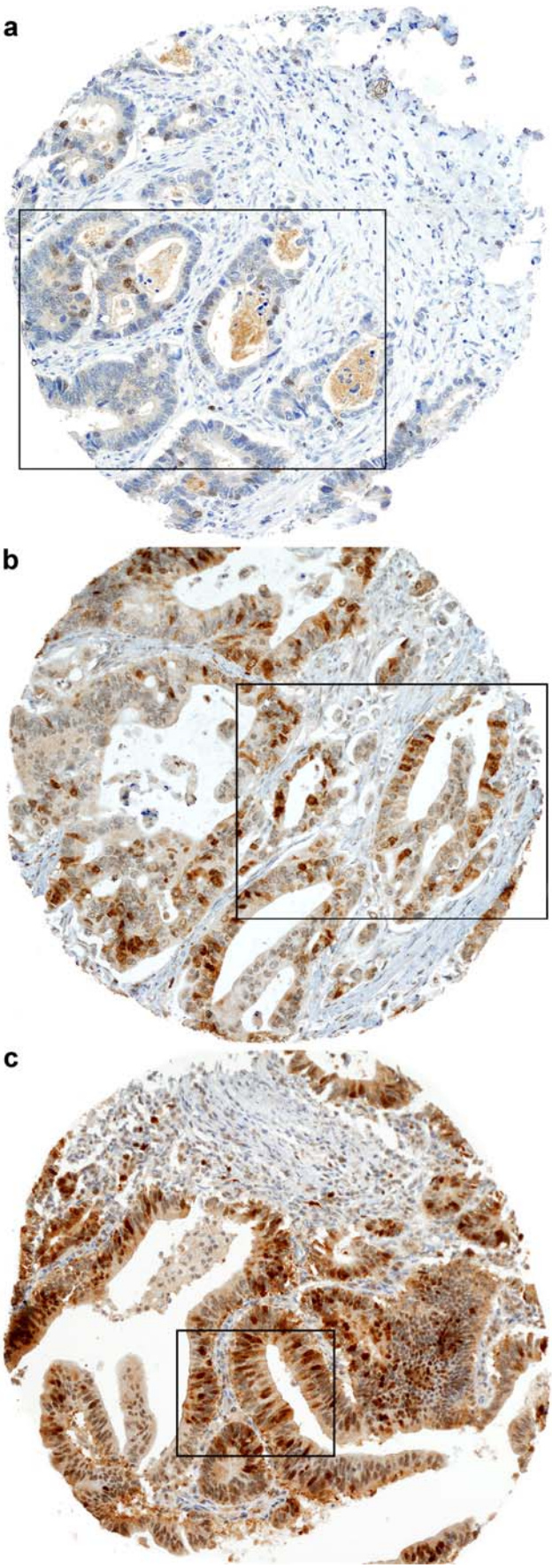

Fig. 1 Expression of TS protein in a representative cores of colorectal cancer. **a** Histoscore=4, distal CRC; **b** histoscore=10, proximal CRC; (*C*) histoscore=15, proximal CRC. Note nuclear stain (*brown*) in cancer cells and a few dispersed TS-positive stromal cells (**c**). Cytoplasmic stain was not counted because the immunostaining was optimized for nuclear but not cytoplasmic staining (see "Materials and methods"; immunohistochemical reaction with TS-106 monoclonal antibody)

When histoscore>*vs*. ≤ median was used as the cutoff level, univariate logistic regression analysis has shown that odds ratio (OR) of histoscore being >2 was 2.44 (95% confidence interval (CI)=1.30–4.59, p=0.0054) for proximal tumors as compared with distal tumors. A multivariate logistic regression analysis adjusted for age, gender, grade, and Astler–Coller stage demonstrated that the CRC site was the only independent parameter significantly associated with TS expression (OR=2.46, 95% CI=1.29–4.70, p=0.0062 Table 3).

Discussion

The level of TS expression in tumor cells in CRC seems to be of obvious clinical significance. However, the question of association of TS expression with proximal or distal site of CRC has not been resolved. In multiple publications using immunohistochemistry and assessment of cytoplasmic TS expression, such an association has not been found [14–21]. Lenz et al. [30] found a significant association of higher TS expression with left-sided tumors but the study was based on only 45 stage II CRCs and did not state whether cytoplasmic or nuclear TS was measured. In contrast, higher TS levels were found in right colon carcinomas as compared with left colon and rectum ones (p<0.05); however, that study was based on pulverized tumor tissue and thus the results (which were based on only 62 tumors) pertain to the TS level in the mixture of tumor cells and surrounding stroma [31]. We report here statistically significant differences of immunohistochemically detected tumoral nuclear TS protein expression between proximal and distal CRCs. The mean expression of TS protein in nuclei of tumor cells of proximal CRCs was 1.8 times higher than that in distal colon cancer (p=0.0003). Wong et al. [10] suggest that the mean TS histoscore may be higher in proximal than distal CRCs, although the difference has not reached statistical significance (p=0.08) probably due to a small sample size (52 cancers). In that report, high TS nuclear expression was correlated with a worse response to 5-FU-based therapy in patients with metastatic cancer. Similarly, a trend was found suggesting an association between TS expression and tumor location (p=0.051), but the small sample size (77 patients) and assessment of "cytoplasmic and nuclear" TS together could

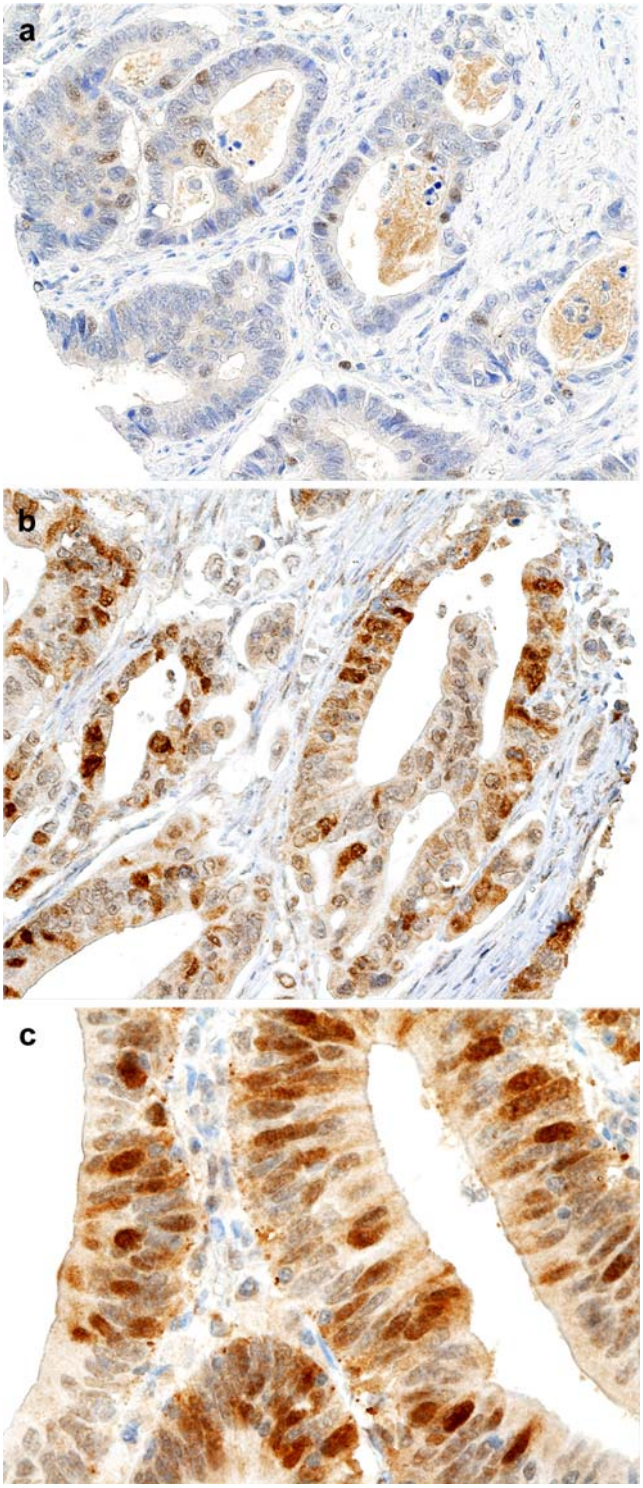

Fig. 2 Marked fragments of cores from Fig. 1a–c at high magnification showing TS-positive (*brown*) nuclei of some cancer cells

be responsible for the lack of a clear correlation [14]. Ricciardiello et al. [25] assessed nuclear TS expression in 192 CRCs and found no site differences. However, for statistical analysis, they combined nuclear and cytoplasmic TS expression. Thus, TS was considered high only if both (nuclear and cytoplasmic) scores were high, and cases with high nuclear TS but low cytoplasmic TS were analyzed as low TS.

In contrast to multiple studies based on analysis of cytoplasmic TS expression (which have not shown signif-

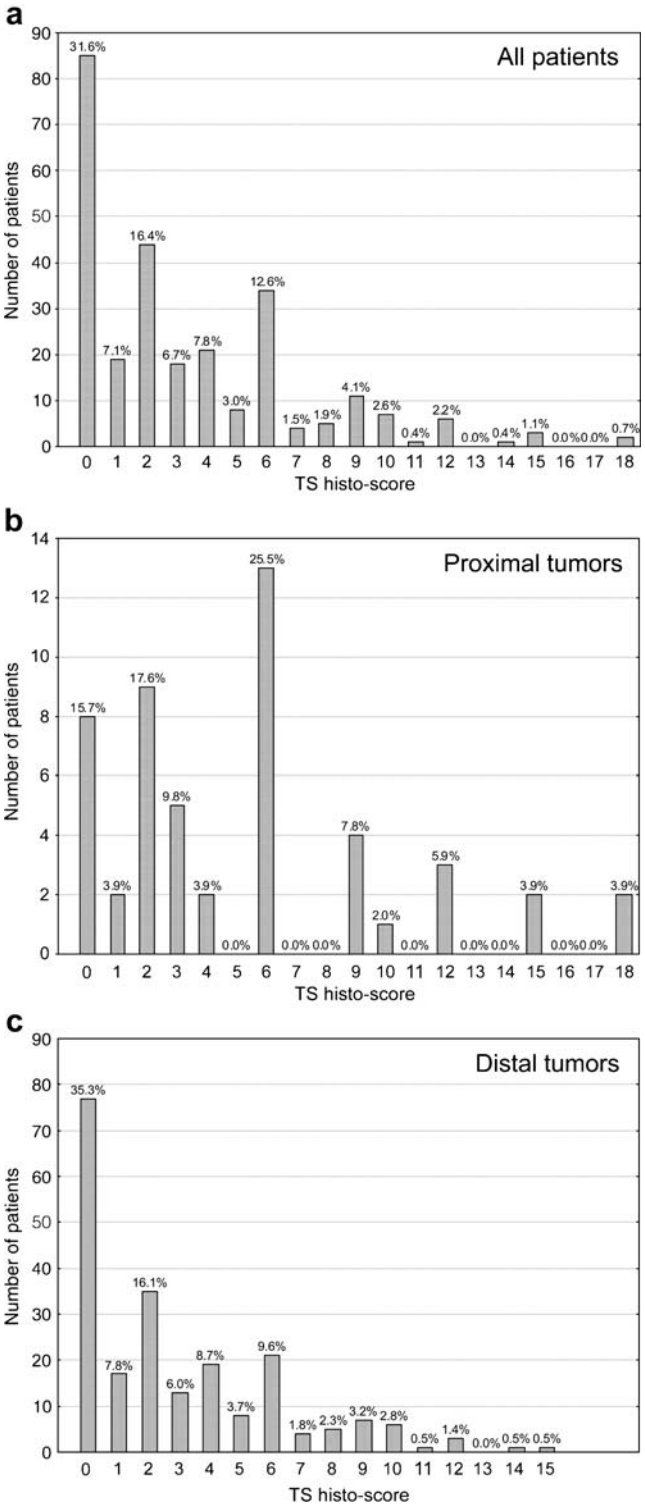

Fig. 3 Histograms showing distribution of TS histoscores among **a** all 269 primary CRCs, **b** 51 proximal, and **c** 218 distal CRCs

Table 2 Histoscore of nuclear TS expression in relation to site of CRC

	Number	Mean±SD	Median	*p*
All	269	3.36±3.71	2.0	0.00030
Proximal	51	5.27±4.73	4.0	
Distal	218	2.91±3.28	2.0	
Men	150	3.35±3.81	2.0	
Proximal	33	5.45±4.56	6.0	0.00023
Distal	117	2.75±3.36	2.0	
Women	119	3.38±3.60	2.0	
Proximal	18	4.94±5.14	2.5	0.25
Distal	101	3.10±3.20	2.0	
Astler–Coller B2 tumors in men	76			
Proximal	17	6.24±5.48	4.0	0.0030
Distal	59	2.78±3.63	1.0	
Astler–Coller C tumors in men	74			
Proximal	16	4.63±3.30	6.0	0.034
Distal	58	2.72±3.09	2.0	

icant association with site of the tumor and reported conflicting results on association of TS expression with other clinicopathological features and prognostic and predictive significance), only a few reports have documented nuclear TS expression, including six dealing with colorectal cancer cell lines or clinical tumor samples [10, 14, 23–25, 32–34]. As early as 1991, Johnston et al. [24] noticed that, in human colon carcinoma cell lines and in biopsy specimens of colorectal carcinoma, TS was "predominantly cytoplasmic with nuclear staining visible in some sections". Samsonoff et al. [32] using immunogold electron microscopy and autoradiography proved that TS was indeed located in the nucleus, particularly in the nucleolar region of H35 rat hepatomas. However, although nuclear immunohistochemical staining with the TS-106 antibody was documented in 1991 [24] and nuclear and nucleolar location were shown in H35 rat hepatoma cells by both immunogold electron microscopy and autoradiography [32], it was not until 2001 [10] that nuclear expression of TS in CRC cell lines and clinical samples was examined further. The biological significance of nuclear TS expression is unclear. In HeLa-55 cells exposed to 5-FUdR, both free TS and the TS ternary complex were seen in the cytoplasm whereas only free TS was found in the nuclear fraction [23]. In normal colonic mucosa, immunohistochemical TS staining was only observed in the nucleus [33]; cytoplasmic TS expression was not seen in normal colonic mucosa or other normal proliferating tissues [14, 33]. TS is present in the nuclei of some colorectal cancer cell lines although the levels of expression vary [23]. Strong overexpression of TS may be sufficient for TS to be present in the nucleus [23].

Table 3 Multivariate logistic regression analysis of associations between clinicopathological parameters and TS histoscore level above median

Variable	OR (95% CI)	*p*
Age	0.99 (0.97–1.01)	0.42
Male Sex	1.06 (0.64–1.77)	0.81
Astler–Coller C	0.68 (0.41–1.14)	0.14
Grade G3	1.29 (0.79–2.17)	0.33
Proximal site[a]	2.46 (1.29–4.70)	0.0062

[a] With regard to splenic flexure

Divergent and inconsistent results of clinicopathological studies of the relationship between TS expression levels and the clinical course of patients treated with 5-FU might be attributed partially to different methods of scoring of immunohistochemical preparations, to some technical differences and small groups of patients, or to different categorization of tumors with regard to site of origin, but they may also be a result of inappropriately assessing the pattern of TS expression by focusing on cytoplasmic rather than nuclear expression.

Our results support the hypothesis [22] that selection of patients for adjuvant chemotherapy should include not only the clinical stage of the disease but also tumor site to better stratify subgroups of patients who may benefit from chemotherapy. There are important physiological differences (blood supply, innervation, embryological origin, expression of differentiation markers such as, e.g., carbohydrate antigens or blood group antigens, epithelial cell apoptosis) between normal proximal and distal colonic mucosa [35, 36]. Several genetic molecular differences between proximal and distal CRCs have also been reported. For example, methylation of the *p16INK4a* is 13 times more frequent in proximal than in distal CRCs and nine times more frequent in CRCs from women than from men [37]. The CpG island methylator phenotype was significantly associated with proximal location of CRCs [38].

Higher frequency of nuclear TS expressing cells in proximal tumors could partially be explained by the known fact that CRCs with MSI-H are characterized by a tendency for right-sided location and poor differentiation [4], hence increased tumor cell proliferation [39]. However, TS expression was similar in MSI-H and stable/low-frequency MSI CRCs [40] so some other factors must be responsible for increased TS expression on the right side. Our data further emphasize biological differences among CRCs which may influence results of 5-FU treatment. Different 5-FU treatment outcomes with regard to site of the tumor and sex of the patient [22] can be explained partially by differences in TS nuclear protein expression in tumor cells. Since the relationship between the 5′ TS genotype and TS expression is not simple, it has been suggested that, for clinical trials incorporating TS status, detection of TS expression in tumors by immunohistochemistry must still remain the benchmark over genotype [41].

In summary, we have shown significant differences in the level of nuclear TS protein expression between proximal and distal CRCs. Our results support the hypothesis that these tumors represent two distinct entities, lend further support to the potential predictive significance of immunohistochemical assessment of nuclear TS level in CRCs [34], and suggest the potential importance of tumor location (relative to the splenic flexure) for proper stratification of patients for chemotherapy. Future studies relating to the use of nuclear TS expression to predict response to 5-FU treatment should take into account differences in TS expression between proximal and distal CRCs. Clearly, further research on immunohistochemical nuclear TS expression in CRC is needed for its application as a treatment strategy.

Acknowledgement This study was supported by a grant (KBN 2P05B 174 28) from the Polish Committee for Scientific Research.

Disclosure/conflict of interest All authors declare that they have no conflict of interest to disclose.

References

1. Azzoni C, Bottarelli L, Campanini N et al (2007) Distinct molecular patterns based on proximal and distal sporadic colorectal cancer: arguments for different mechanisms in the tumorigenesis. Int J Colorectal Dis 22:115–126
2. Gervaz P, Bucher P, Morel P (2004) Two colons-two cancers: paradigm shift and clinical implications. J Surg Oncol 88:261–266
3. Thibodeau SN, Bren G, Schaid D (1993) Microsatellite instability in cancer of the proximal colon. Science 260:816–819
4. S-Ch C, Lin J, Yang S, Wand H-S et al (2006) Relationship between genetic alterations and prognosis in sporadic colorectal cancer. Int J Cancer 118:1721–1727
5. van Triest B, Peters GJ (1999) Thymidylate synthase: a target for combination therapy and determinant of chemotherapeutic response in colorectal cancer. Oncology 57:179–194
6. Allegra C, Sargent D (2003) Molecular diagnostics: assays, tissues, progress, and pitfalls. J Clin Oncol 21:395–396
7. van Triest B, Pinedo HM, van Hensbergen Y et al (1999) Thymidylate synthase level as main predictive parameter for sensitivity to 5-fluorouracil but not for folate-based thymidylate synthase inhibitors in 13 nonselected colon cancer cell lines. Clin Cancer Res 5:643–654
8. Ichikawa W, Uetake H, Shirota Y et al (2003) Combination of dihydropyrimidine dehydrogenase and thymidylate synthase gene expressions in primary tumors as predictive parameters for the efficacy of fluoropyrimidine-based chemotherapy for metastatic colorectal cancer. Clin Cancer Res 9:786–791
9. Etienne MC, Chazal M, Laurent-Puig P et al (2002) Prognostic value of tumoral thymidylate synthase and p53 in metastatic colorectal cancer patients receiving fluorouracil-based chemotherapy: phenotypic and genotypic analyses. J Clin Oncol 20:2832–2843
10. Wong NACS, Brett L, Stewart M et al (2001) Nuclear thymidylate synthase expression, p53 expression and 5FU response in colorectal carcinoma. Br J Cancer 85:1937–1943
11. Kornmann M, Schwabe W, Sander S et al (2003) Thymidylate synthase and dihydropyrimidine dehydrogenase mRNA expression levels: predictors for survival in colorectal cancer receiving adjuvant chemotherapy. Clin Cancer Res 9:4116–4124
12. Edler D, Glimelius B, Hallström M et al (2002) Thymidylate synthase expression in colorectal cancer: a prognostic and predictive marker of benefit from adjuvant fluorouracil based chemotherapy. J Clin Oncol 20:1721–1728
13. Popat S, Matakidou A, Houlston RS (2004) Thymidylate synthase expression and prognosis in colorectal cancer: a systematic review and meta-analysis. J Clin Oncol 22:529–536
14. Fernandes-Contreras M-E, Jimenez de Ayala B, Garcia de Paredes M-L et al (2004) Thymidylate synthase expression pattern is a prognostic factor in patients of colorectal cancer treated with 5-fluorouracil. Inter J Oncol 25:877–885
15. Edler D, Kressner U, Ragnhammar P et al (2000) Immunohistochemically detected thymidylate synthase in colorectal cancer: an independent prognostic factor of survival. Clin Cancer Res 6:488–492
16. Kamoshida S, Matsuoka H, Ishikawa T et al (2004) Immunohistochemical evaluation of thymidylate synthase (TS) and p16INK4a in advanced colorectal cancer: implication of TS expression in FU-based adjuvant chemotherapy. Jpn J Clin Oncol 34:594–601
17. Popat S, Chen Z, Zhao D et al (2006) A prospective, blinded analysis of thymidylate synthase and p53 expression as prognostic markers in the adjuvant treatment of colorectal cancer. Ann Oncol 17:810–817
18. Jensen SA, Vainer B, Sørensen JB (2006) The prognostic significance of thymidylate synthase and dihydropyrimidine dehydrogenase in colorectal cancer of 303 patients adjuvantly treated with 5-fluorouracil. Int J Cancer 120:694–701
19. Broll R, Busch P, Duchrow M et al (2005) Influence of thymidylate synthase and p53 protein expression on clinical outcome in patients with colorectal cancer. Int J Colorectal Dis 20:94–102
20. Tomiak A, Vincent M, Earle CC et al (2001) Thymidylate synthase expression in stage II and III colon cancer. Am J Clin Oncol 24:597–602
21. Ciaparrone M, Quirino M, Schinzari G et al (2006) Predictive role of thymidylate synthase, dihydropyrimidine dehydrogenase and thymidine phosphorylase expression in colorectal cancer patients receiving adjuvant 5-fluorouracil. Oncology 70:366–377
22. Elsaleh H, Joseph D, Grieu F et al (2000) Association of tumor site and sex with survival benefit from adjuvant chemotherapy in colorectal cancer. Lancet 355:1745–1750

23. Bissoon-Haqqani S, Moyana T, Jonker D et al (2006) Nuclear expression of thymidylate synthase in colorectal cancer cell lines and clinical samples. J Histochem Cytochem 54:19–20
24. Johnston PG, Liang C-H, Henry S et al (1991) Production and characterization of monoclonal antibodies that localize human thymidylate synthase in the cytoplasm of human cells and tissue. Cancer Res 51:6668–6676
25. Ricciardiello L, Ceccarelli C, Angiolini G et al (2005) High thymidylate synthase expression in colorectal cancer with microsatellite instability: implications for chemotherapeutic strategies. Clin Cancer Res 11:4234–4240
26. Chung GG, Kielhorn EP, Rimm DL (2002) Subjective differences in outcome are seen as a function of the immunohistochemical method used on a colorectal cancer tissue microarray. Clin Colorectal Cancer 1:237–242
27. Jakob C, Liersch T, Meyer W et al (2005) Immunohistochemical analysis of thymidylate synthase, thymidine phosphorylase, and dihydropyrimidine dehydrogenase in rectal cancer (cUICC II/III). Correlation with histopathologic tumor regression after 5-fluorouracil-based long-term neoadjuvant chemoradiotherapy. Am J Surg Pathol 29:1304–1309
28. Detre S, Saccani Jotti G, Dowsett M (1995) A "quickscore" method for immunohistochemical semiquantitation: validation for oestrogen receptor in breast carcinomas. J Clin Pathol 48:876–878
29. Kirkegaard T, Edwards J, Tovey S et al (2006) Observer variation in immunohistochemical analysis of protein expression, time for a change? Histopathology 48:787–794
30. Lenz HJ, Danenberg KD, Leichman CG et al (1998) p53 and thymidylate synthase expression in untreated stage II colon cancer: associations with recurrence, survival and site. Clin Cancer Res 4:1227–1234
31. Sanguedolce R, Vultaggio G, Sanguedolce F et al (1998) The role of thymidylate synthase levels in the prognosis and the treatment of patients with colorectal cancer. Anticancer Res 18:1515–1520
32. Samsonoff W, Reston J, McKee M et al (1997) Intracellular location of thymidylate synthase and its state of phosphorylation. J Biol Chem 20:13281–13285
33. Santini D, Vincenzi B, Perrone G et al (2004) Thymidylate synthase expression in normal colonic mucosa: a predictive marker of toxicity in colorectal cancer patients receiving 5-fluorouracil-based adjuvant chemotherapy. Oncology 67:135–142
34. Gonen M, Hummer A, Zervoudakis A et al (2003) Thymidylate synthase expression in hepatic tumors is a predictor of survival and progression in patients with resectable metastatic colorectal cancer. J Clin Oncol 21:406–412
35. Bufill JA (1990) Colorectal cancer: evidence for distinct genetic categories based on proximal or distal tumor location. Ann Intern Med 113:779–788
36. Liu LU, Holt PR, Krivosheyev V et al (1999) Human right and left colon differ in epithelial cell apoptosis and in expression of Bak, a pro-apoptotic Bcl-2 homologue. Gut 45:45–50
37. Wiencke JK, Zheng S, Lafuente A et al (1999) Aberrant methylation of p16INK4a in anatomic and gender-specific subtypes of sporadic colorectal cancer. Cancer Epidermiol Biomarkers Prev 8:501–506
38. Rijnsoever M, Elsaleh H, Joseph D et al (2003) CpG island methylator phenotype is an independent predictor of survival benefit from 5-fluorouracil in stage III colorectal cancer. Clin Cancer Res 9:2898–2903
39. Kim GP, Colangelo LH, Wicand HS et al (2007) Prognostic and predictive roles of high-degree microsatellite instability in colon cancer: a National Cancer Institute-National Surgical Adjuvant Breast and Bowel Project Collaborative Study. J Clin Oncol 25:767–772
40. Sinicrope FA, Rego RL, Halling KC et al (2006) Thymidylate synthase expression in colon carcinomas with microsatellite instability. Clin Cancer Res 12:2738–2744
41. Popat S, Wort R, Houlston RS (2005) Relationship between thymidylate synthase (TS) genotype and TS expression: a tissue microarray analysis of colorectal cancers. Int J Surg Pathol 13:127–133

Virchows Arch (2009) 454:703–713
DOI 10.1007/s00428-009-0775-1

ORIGINAL ARTICLE

Extraconal orbital tumors in children—a spectrum

Seethalakshmi Viswanathan · Sophia George · Mukta Ramadwar · Tanuja Shet · Brijesh Arora · Siddhartha Laskar · Sajid Qureshi · Seema Medhi · M. A. Muckaden · P. A. Kurkure · S. V. Kane · S. Banavali

Received: 3 February 2009 / Revised: 22 March 2009 / Accepted: 13 April 2009 / Published online: 7 May 2009

Abstract Orbital masses in children are uncommon but extremely challenging problems for clinicians and pathologists due to their critical location and availability of limited diagnostic material. We analyzed 47 specimens comprising biopsies, excision specimens, and FNAC of extraconal pediatric orbital masses (excluding retinoblastoma) accessioned in the pathology department over 5 years in a tertiary referral cancer center. Immunohistochemistry (IHC—74%) and molecular methods (one case) were done where necessary. The chief presenting symptom was proptosis in 55.3% patients and radiologically 53.8% malignant tumors showed extraorbital extension. A diagnostic algorithm was formulated to assess which cases needed pathology evaluation. Malignant round cell tumors (76.6%), chiefly embryonal rhabdomyosarcoma (51%), benign spindle cell neoplasms, and infectious lesions (tuberculosis, fungal infections), were seen. Of the malignant tumors, those confined to the orbit achieved good treatment response and had an event-free follow-up while those with extraorbital spread had poor outcome. Pediatric orbital masses range from completely treatable infectious lesions, surgically resectable benign neoplasms to aggressive malignancies requiring chemotherapy and radiotherapy. Pathologists play a key role in distinguishing these on small biopsy material and expediating accurate treatment thus saving the vision or life of a patient.

Keywords Orbital masses · Extraconal · Children · Rhabdomyosarcoma pathological evaluation

S. Viswanathan (✉) · S. George · M. Ramadwar · T. Shet · S. V. Kane
Department of Pathology, Tata Memorial Hospital, Parel, Mumbai, 400012, India
e-mail: vishyvidya@hotmail.com

B. Arora · P. A. Kurkure · S. Banavali
Department of Pediatric Oncology, Tata Memorial Hospital, Parel, Mumbai, 400012, India

S. Laskar · M. A. Muckaden
Department of Radiation Oncology, Tata Memorial Hospital, Parel, Mumbai, 400012, India

S. Qureshi
Department of Surgical Oncology, Tata Memorial Hospital, Parel, Mumbai, 400012, India

S. Medhi
Department of Radiodiagnosis, Tata Memorial Hospital, Parel, Mumbai, 400012, India

Introduction

Orbital tumors in children are relatively uncommon and pose a diagnostic challenge to the treating clinician as well as the pathologist [1–7]. The orbit, being a critical site with limited accessibility, is a difficult site to biopsy resulting in limited diagnostic material in the form of tiny biopsies or fine needle aspirates. Most of these tumors grow rapidly and if not promptly treated can cause loss of vision or life [1–4]. These lesions can have varied etiologies ranging from infectious to high-grade malignant lesions. All of these extraocular masses typically manifest with proptosis and imaging differentiation is desirable because the treatments and prognosis vary greatly [7]. This study is based in a tertiary referral center for cancer care in a developing country. It outlines the role of ancillary and imaging techniques in elucidating the nature of these lesions, determines the exact type of lesions are biopsied, and emphasizes the critical role played by the pathologist in evaluating these masses so that patients can receive prompt effective treatment.

Materials and methods

All pediatric orbital tumors (children less than 18 years of age) accessioned in the department of pathology at a tertiary referral cancer center were reviewed over a period of 5 years from 2001 to 2006. A total of 155 cases of pediatric orbital tumors were received during this period, of which 104 retinoblastomas were excluded from the study. A total of 47 lesions (including eight referral cases), which had a predominant extraconal component, were studied in detail. Pathological material received was in the form of incision biopsies, excision specimens, and fine needle aspiration cytology (FNAC) material. The material was subjected to routine histopathology or cytology. Special stains such as Periodic acid Schiff (PAS), Gomori methanamine silver (GMS) for fungal infections, or Ziehl Neelsens (ZN) stain to detect acid fast bacilli for tuberculosis were used where required. Immunohistochemistry (IHC) and molecular diagnostic studies were done to confirm and refine the diagnosis in malignant neoplasms. For the panel of markers we used the DAKO polymer technique and the dilutions of various antibodies were as detailed in Table 1. Details of clinical presentation, treatment, and follow-up were accessioned from patients' charts and hospital records.

Results

Clinical features

The age of the patients ranged from 1 to 18 years (median age—7 years). Twenty-nine (61.7%) patients were boys and 18 (38.3%) were girls. Patients predominantly presented with proptosis (n=26–55.3%) and onset of symptoms was rapid from 1 month to 6 months in 36 of the 47 cases (76.6%). The onset of ocular symptoms was usually acute with the chief presenting symptom being proptosis as seen in 26 cases (Fig. 1a–d). Other symptoms were ocular pain in five cases (20.8%), cranial palsy in five cases (20.8%), loss of vision in two cases (8.3%), and headache and vomiting in six cases (25%) where there was intracranial extension. Three cases presented with nodal enlargement in addition to the ocular symptoms.

A diagnostic algorithm for approach to orbital lesions in the institution is illustrated (Table 2). In a child with an orbital mass with proptosis, benign cystic masses like hemangiomas and dermoids were picked up on radiology and a diagnostic biopsy procedure was avoided. Other investigative techniques like abdominal ultrasound, MIBG, and bone marrow aspirate or biopsy were done to diagnose nonorbital primary tumors such as metastatic neuroblastoma

Table 1 Panel of markers and dilutions of antibodies used (DAKO polymer technique)

Antibody	Monoclonal/polyclonal	Dilution
Vimentin	Monoclonal	1:400
Desmin	Monoclonal	1:200
Myogenin	Monoclonal	1:50
MyoD1	Monoclonal	1:40
Leucocyte common antigen (LCA)	Monoclonal	1:200
CD20	Monoclonal	1:200
CD10	Monoclonal	1:40
MIB1	Monoclonal	1:200
CD30	Monoclonal	1:40
CD99	Monoclonal	1:100
Neuron-specific enolase (NSE)	Monoclonal	1:100
Myeloperoxidase	Polyclonal	1:1,500
CD34	Monoclonal	1:200
Synaptophysin	Polyclonal	1: 100
Chromogranin	Polyclonal	1:400
Cytokeratin (CK)	Monoclonal	1:200
Epithelial membrane antigen (EMA)	Monoclonal	1:200
S100	Polyclonal	1:600
CD1a	Monoclonal	1:50
Smooth muscle actin (SMA)	Monoclonal	1:400
Calponin	Monoclonal	1:50
ALK1	Monoclonal	1:100
Bcl2	Monoclonal	1:50
Glial fibrillary acid protein (GFAP)	Polyclonal	1:1,200

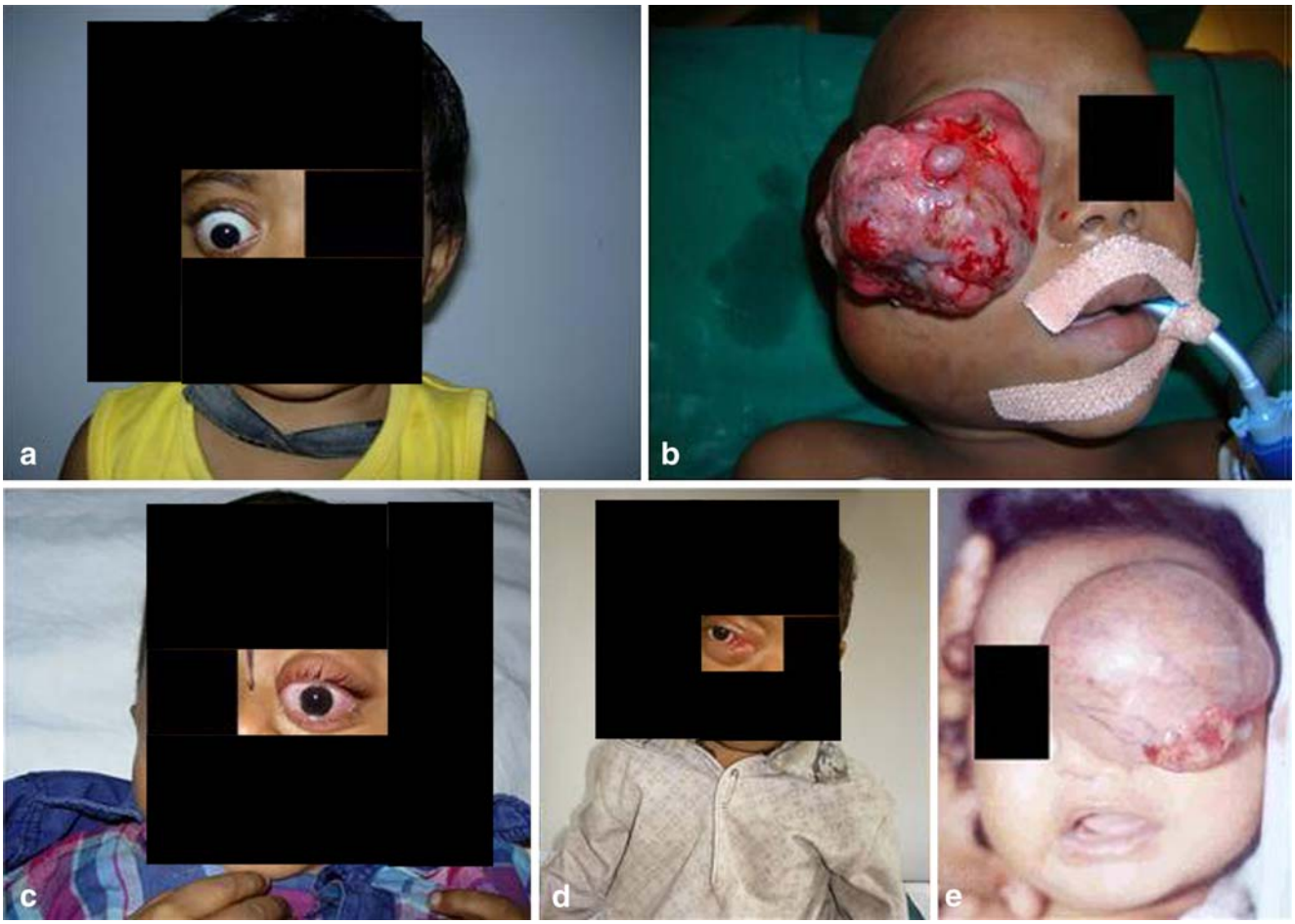

Fig. 1 Clinical presentation of orbital masses. **a** Unilateral proptosis in a case of rhabdomyosarcoma. **b** Recurrent medulloepithelioma of the right orbit with fungation and extraorbital extension. **c** Unilateral proptosis in a case of metastatic neuroblastoma to the orbit. **d** Proptosis, and chemosis of the left orbit, rhabdomyosarcoma. **e** Fungating extraorbital extension in a case of malignant rhabdoid tumor of the left orbit

and hematolymphoid malignancies. For these cases where biopsy of orbital lesions may sometimes be appropriate on a case-by-case basis if there is a clinical suspicion of a second disease process in the orbit. Cases where no diagnosis could be reached by supportive investigations were subjected to a biopsy. Anterior and lateral lesions were more amenable to biopsy than posterior orbital lesions. In an emergency, an FNAC was attempted and with a working diagnosis of a hematolymphoid malignancy or a classical rhabdomyosarcoma treatment was instituted immediately. Posterior lesions, which were not easily amenable to biopsy were also subjected to FNAC. Only rare cases like a pilocytic astriocytoma were not diagnosed by the above algorithm and required an intracranial approach for procurement of tissue for diagnosis (Fig. 2).

Pathology findings

Of the 47 cases, 33 were diagnosed on biopsy, nine on resection specimens, and five on FNAC. Further categorization involved morphological and immunohistochemical evaluation wherever necessary (Table 3). Immunohistochemistry was performed in 35 out of 47 (74%) cases. Round cell tumors constituted 76.6%, spindle cell tumors 8.5%, and miscellaneous lesions were 14.9%. Accurate final diagnosis of individual lesions are detailed in Table 3 and Figs. 3, 4, and 5.

Pediatric orbital masses were subjected to a biopsy if a diagnosis could not be reached by supportive clinical, radiological, and biochemical investigations. By light microscopic examination, infectious lesions such as tuberculosis and fungal infections could be separated from neoplastic lesions. The infectious etiological agents were identified using special stains such as GMS, PAS, and ZN stains. Neoplastic lesions could be further classified into benign spindle cell lesions of fibrohistiocytic origin such as solitary fibrous tumor, fibromatosis, or inflammatory myofibroblastic tumor and separated from malignant round cell tumors which were the commonest tumors seen in this age group. On light microscopy, these lesions needed ancillary investigations such

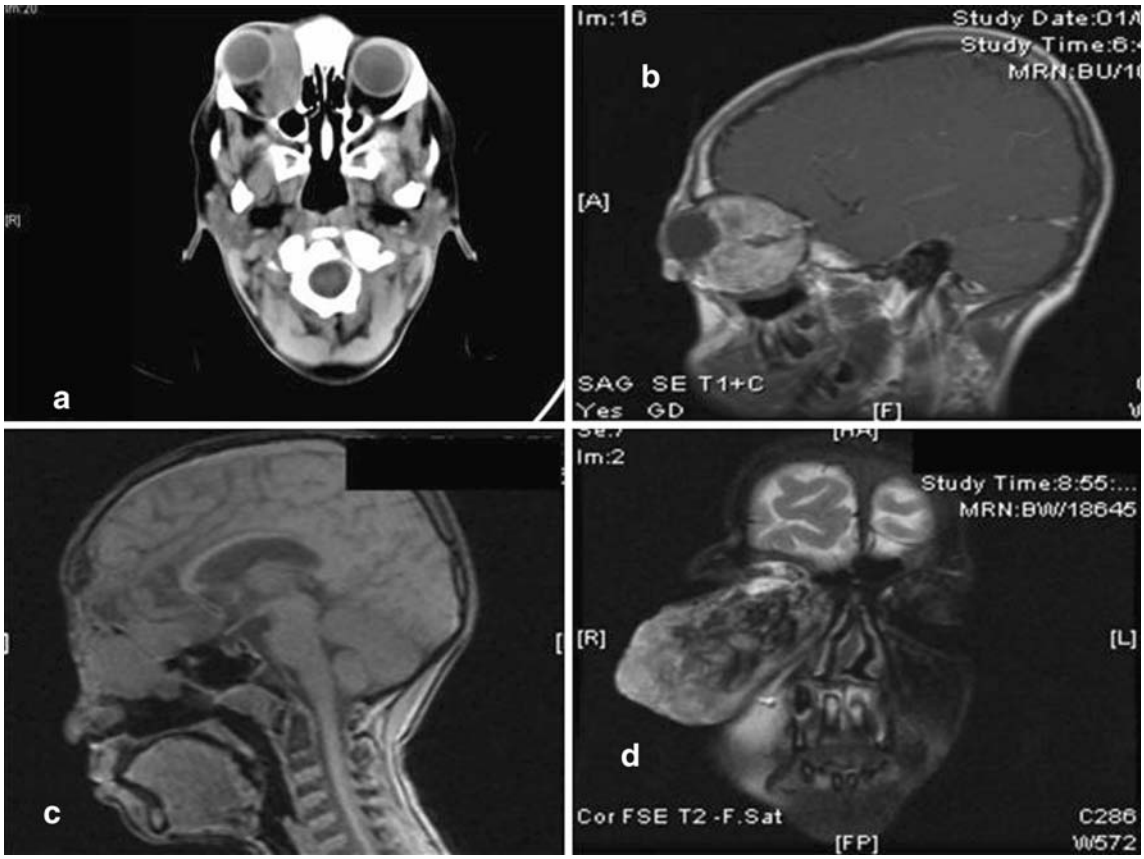

Fig. 2 Radiology of orbital masses. **a** Computerized tomography scan of orbital rhabdomyosarcoma with an extraconal tumor with proptosis. **b** Pilocytic astrocytoma of the optic nerve. **c** Mesenchymal chondrosarcoma of the orbit with intracranial extension. **d** Recurrent meulloepithelioma with extraorbital spread and soft-tissue extension

as a panel of immunohistochemical markers (mentioned in the "Materials and methods" section) to be classified into hematolymphoid malignancies such as granulocytic sarcoma, leukemic infiltrate, and Non-Hodgkins lymphomas which needed to be separated from other round cell tumors such as PNET, rhabdomyosarcoma, metastatic neuroblastoma, malignant rhabdoid tumors, mesenchymal chondrosarcoma, and langerhans cell histiocytosis. Each of these were treated

Table 2 Diagnostic algorithm for approach to orbital tumors

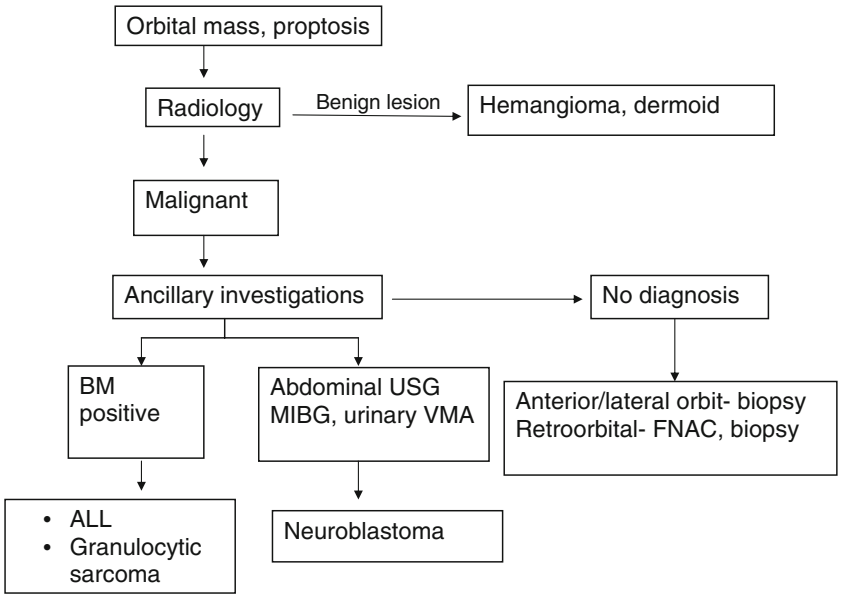

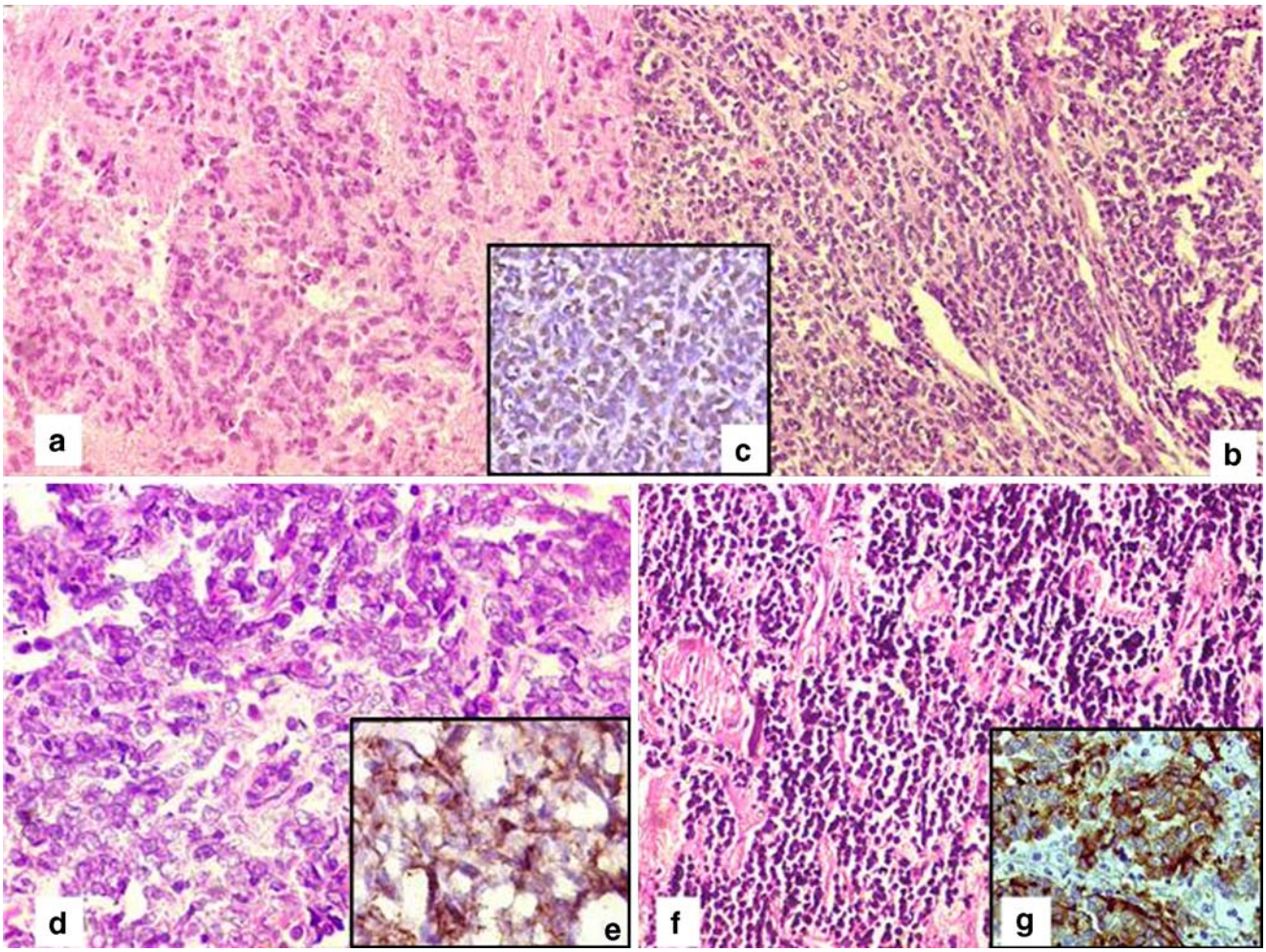

Fig. 3 Histopathology of orbital masses. **a** Embryonal rhabdomyosarcoma (ERMS), (H&E ×100). **b** Alveolar rhabdomyosarcoma (H&E ×100). **c** Desmin positivity in ERMS (ABC ×100). **d** Round cells with scattered eosinophils and myeloid series cells in granulocytic sarcoma, (H&E ×100). **e** Tumor cells positive for myeloperoxidase (ABC ×100). **f** Metastatic undifferentiated neuroblastoma, stroma poor, (H&E ×100). **g** Tumor cells positive for chromogranin (ABC ×100)

with a separate chemotherapy protocol and hence needed to be accurately distinguished and classified. If exact characterization was not possible, RT-PCR was performed on paraffin-embedded material. The panels used were EWS-FLI1, EWS-ERG for Ewings sarcoma and PAX3-FKHR, PAX7-FKHR for confirmation of alveolar rhabdomyosarcoma. The single case of malignant rhabdoid tumor was confirmed by electron microscopy and the intracytoplasmic aggregates of intermediate filaments were demonstrated in addition to typical immunohistochemical findings.

Radiological findings

The CT/MRI findings were reviewed to determine the location and the extent of the disease. These were available in 26 cases (Fig. 2a–d). In 12 (46.2%) cases, the tumors were confined to the orbit, 14 (53.8%) cases showed extraorbital extension, sinonasal extension was seen in eight (ERMS=7, mucormycosis=1) cases, whereas intracranial extension was seen in six cases (ERMS=4, fibromatosis=1, mesenchymal chondrosarcoma=1). Cavernous sinus involvement was seen in two of these cases, both ERMS. Metastasis to cervical lymph nodes at presentation was seen in three cases (ARMS=1, medulloepitheliomas=2)

Follow-up

A complete follow-up was available in 26 cases. Of these, two cases of ERMS died due intracranial extension of the disease. Patients who were disease-free (1–5 years follow-up) were 16 (four benign soft-tissue lesions—spindle cell lesions, two infectious lesions, two granulocytic sarcomas, one LCH, one rhabdoid tumor, and six ERMS confined to the orbit). Local recurrences were seen in five ERMS, one ARMS, and one mesenchymal chondrosarcoma within 6 months of treatment. The single case of fibromatosis

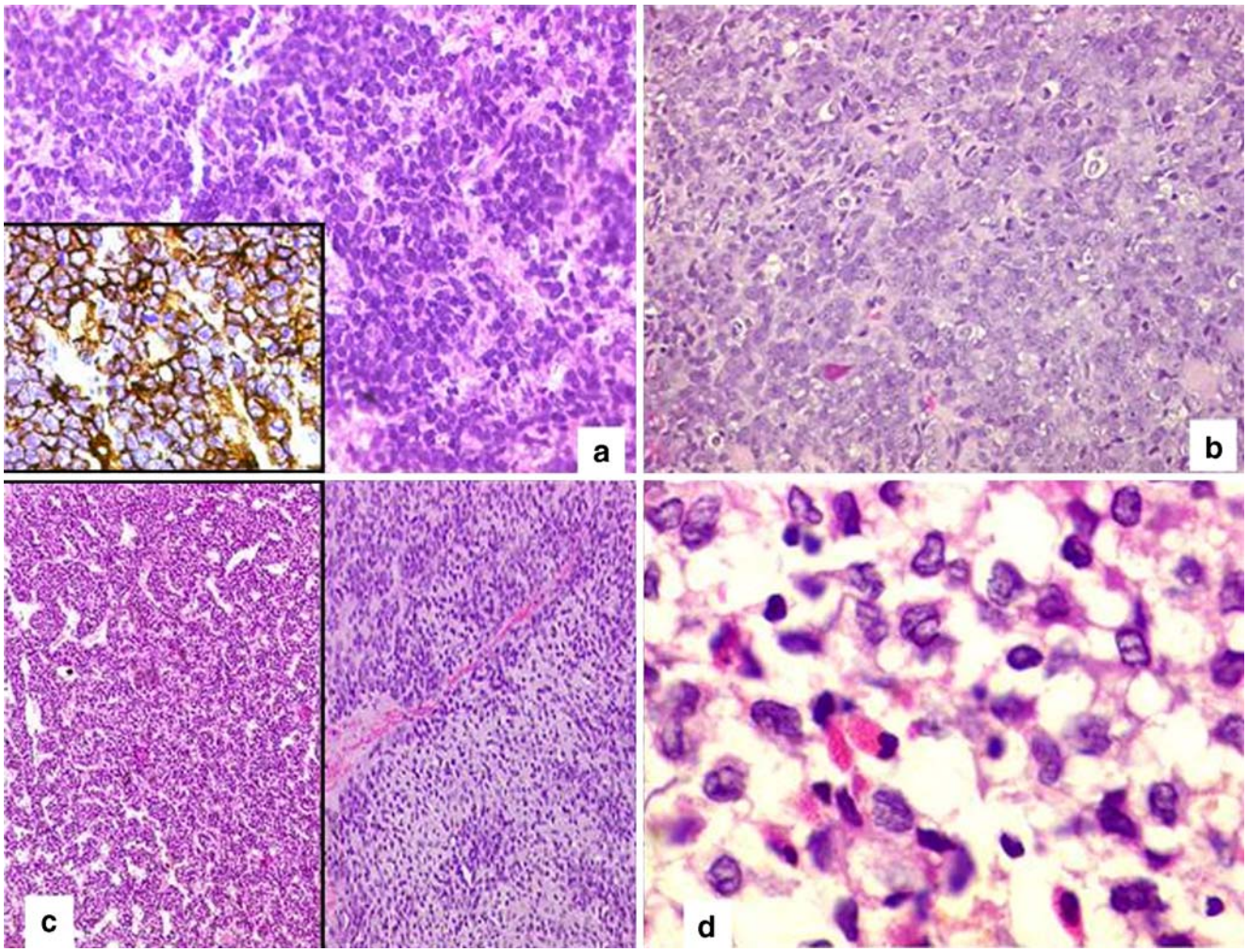

Fig. 4 Histopathology of orbital masses. **a** Burkitt lymphoma involving orbit, (H&E ×100). *Inset* shows the CD 20 positivity (ABC ×400). **b** Malignant rhabdoid tumor (H&E ×100). **c** Mesenchymal chondrosarcoma with hemangiopericytomatous pattern seen to the left and chondroid matrix, to the right. (H&E ×40). **d** Langerhans cell histiocytosis with grooved Langerhans cells and eosinophils in the background, (H&E ×1,000)

recurred after 1 year of surgery and underwent a repeat surgery with subsequent disease-free status on 2 years follow-up. Two local recurrences were seen in one medulloepithelioma in a span of 2 years after initial surgery. No follow-up was available in 13 cases and in eight cases referred from outside.

Discussion

Several studies have reviewed the epidemiology of orbital lesions in the pediatric population. These include a review of 214 orbital tumors from the pathology files of the Armed Forces Institute of Pathology in 1962 [2], 250 biopsied tumors from the Wills Eye Hospital over 20 years by Shields and associates in 1986 [3], and a review of 340 orbital tumors in children over 60 years from Mayo Clinic [1]. All lesions, osseous or non-osseous, appear similar to each other and present with common symptoms though greatly varying in treatments. Knowledge of the pathologic and radiologic features of these tumors is important in guiding clinicians for their effective management [7].

All the major studies across the world including those devoted to pediatric orbital tumors originate from pediatric clinics [1, 3–6]. To the best of our knowledge the present study is the first study outlining the pathologist's point of view of pediatric orbital lesions. In various studies across the world, benign cystic lesions were the commonest lesions seen; ranging from 48% to 52% [1, 3–6]. These are uniformly reported to be developmental cystic lesions such as dermoid cysts followed by benign vascular lesions such as capillary hemangiomas and lymphangiomas [1, 3–6]. In the Indian study by Bajaj et al. [5], again a clinical review, benign cystic lesions (25%) were marginally seen more frequently than rhabdomyosarcoma (24%). Since the present series reports the incidence of lesions as acces-

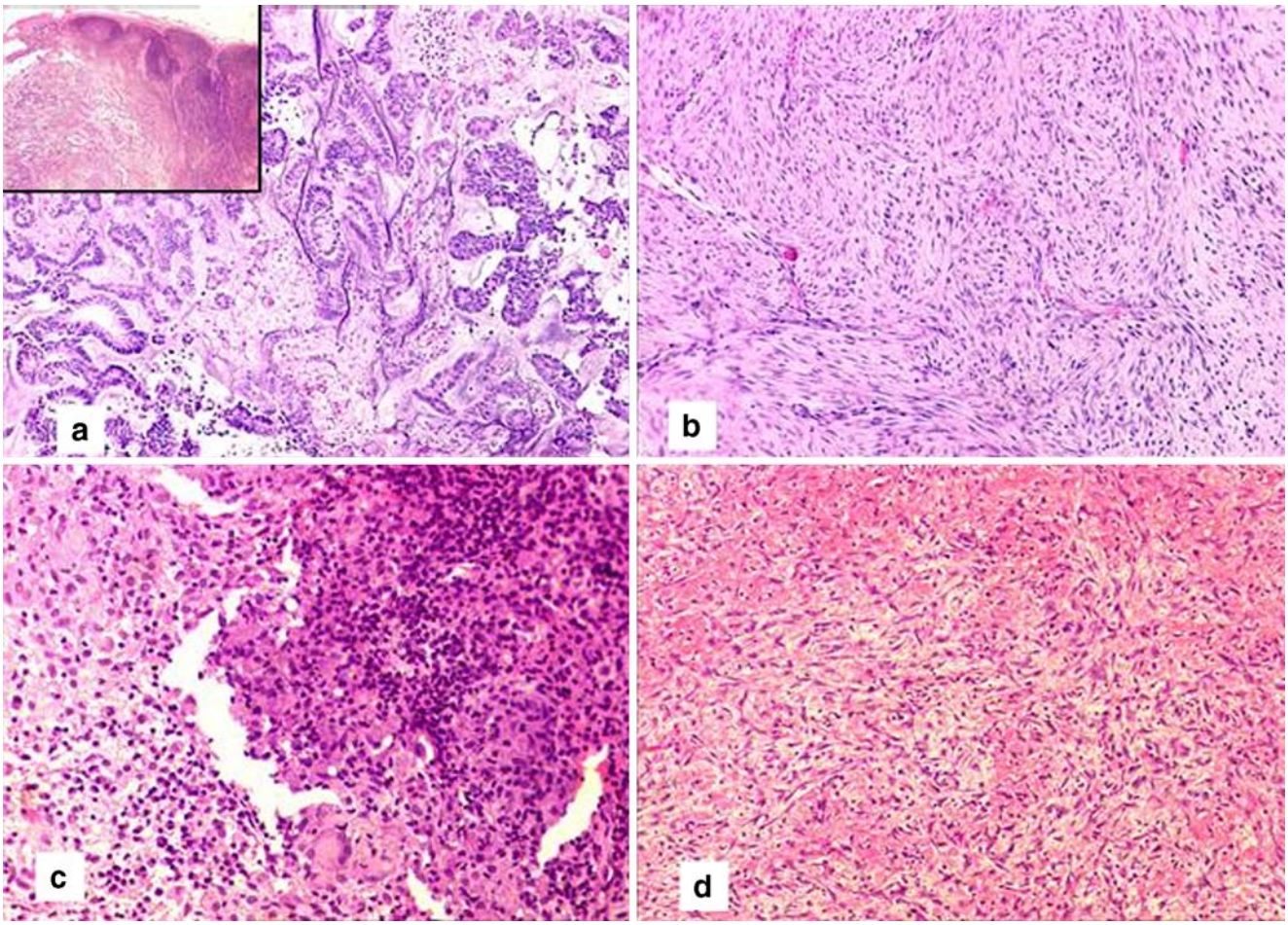

Fig. 5 Histopathology of orbital masses. **a** Recurrent teratoid medulloepithelioma (H&E ×100) with lymph nodal metastasis (*inset*) (H&E ×40). **b** Orbital fibromatosis with collagen producing bland spindle cells (H&E ×100). **c** Caseating granulomatous inflammation of tuberculous etiology (H&E ×100). **d** Inflammatory myofibroblastic tumor comprising spindle cell proliferation with admixed inflammatory infiltrate. (H&E ×100).

sioned in the pathology department of a tertiary referral cancer hospital there is a skew towards malignant lesions and rhabdomyosarcoma in particular which is as high as 51% making it the most common biopsied malignant orbital tumor in a child. All series nevertheless concur with the fact that rhabdomyosarcoma is the commonest malignant tumor seen in the pediatric orbit [1, 3–6]. However the reported incidence is remarkably low ranging from 2.5% to 7% [3, 4, 6] as compared to the previously published Indian study [5] as well as the present study. However, more studies need to be done before concluding that the incidence of this tumor is higher in this part of the world than others. A comparative analysis between part of the Japanese study by Ohtsuka et al. [4] devoted specifically to the study of pediatric orbital tumors, the study in Indian patients by Bajaj et al. [5], and the present study are presented in Table 4. There is a remarkable similarity in the lesions seen except for the lack of infective lesions in the Japanese review which was noted in both the Indian series of patients.

As mentioned earlier though there are many studies evaluating patients as they present in the clinic, there is no study evaluating the pathologist's angle and the diagnostic difficulties encountered in the evaluation of pediatric orbital masses. With advances in medical oncology, common pediatric malignancies having specific treatment protocols are treatable with good long-term survivals, and it becomes imperative for the pathologist to give an accurate specific diagnosis on the limited material available [8].

In our study, we reviewed 155 histopathologically verified cases of orbital masses in children aged 18 years or younger over a period of 5 years. A diagnostic algorithm for approach to orbital lesions is illustrated to delineate the cases accessioned to the pathology service (Table 3). We have not come across any reference for a systematic approach to pediatric orbital lesions outlined above to the best of our knowledge. However, reports in literature also support avoiding a diagnostic biopsy on benign cystic lesions [1, 4] and using supportive radiological and biochemical investigations for tumors arising elsewhere [8].

Table 3 Spectrum of pediatric orbital lesions

Round cell tumors	Positive IHC markers	No.
Rhabdomyosarcoma embryonal subtype (ERMS) = 23; alveolar subtype (ARMS)=1; FNAC—3 cases	Vimentin, desmin, myogenin, MyoD1; confirmed by desmin positivity	24 (51%)
Metastases from neuroblastoma	Chromogranin, synaptophysin, NSE	2 (4.3%)
Primitive neuroectodermal tumor (PNET)	CD99, NSE, FLI1	1 (2.1%)
Malignant rhabdoid tumor	Vimentin, CK, EMA, desmin, Mic2	1 (2.1%)
Round cell tumor (not categorized)	Negative for all IHC and molecular markers	1 (2.1%)
Granulocytic sarcoma	MPO, CD43, CD34, CAE.	4 (8.5%)
Burkitt's lymphoma	LCA, CD20, CD10, Mib1	1 (2.1%)
Langerhans' cell histiocytosis (LCH)	S100, CD1a	1 (2.1%)
Mesenchymal chondrosarcoma	S100, Mic2	1 (2.1%)
Spindle cell tumors		
Fibromatosis	Vimentin	1 (2.1%)
Solitary fibrous tumor	Calponin, CD34, bcl2	1 (2.1%)
Inflammatory myofibroblastic tumor	SMA, calponin, ALK1	3 (6.4%)
Miscellaneous lesions		
Medulloepithelioma		2 (4.3%)
Pilocytic astrocytoma	GFAP	1 (2.1%)
Hemangioma		1 (2.1%)
Inflammatory lesions mucormycosis (n=1), Kochs (n=2)		3 (6.4%)

Radiologically, 14 of our cases had extraorbital spread as patients present in advanced stages due to lack of awareness or treatment facilities. The single remaining case was that of mucormycosis, an opportunistic infection in a treated case of T-ALL involving the orbit and sinonasal region.

As seen in our study the predominant lesions were round cell tumors (34 cases). Of these rhabdomyosarcomas predominated 24 (51%). Among the malignant tumors of the orbit, rhabdomyosarcoma is the most common reported mesenchymal tumor in children, accounting for about 5% of all childhood cancers [7] and the most prevalent

Table 4 Comparative incidences of pediatric orbital lesions between Japanese patients, the previously published Indian study and the present study

Lesion	Ohtsuka et al. (%)	Bajaj et al. (%)	Viswanathan et al. (%)
Medulloepithelioma	4		4.3
Ewing sarcoma	4	3	2.1
Aneurysmal bone cyst	4		0
Benign lymphoid hyperplasia	4		0
Retinoblastoma	7	–	–
Rhabdomyosarcoma	7	24	51
Dermoid cyst	26	10	0
Eosinophilic granuloma	4		2.1
Hematoma	7		0
Hemorrhagic lymphangioma	11	15	0
Capillary hemangioma	11		2.1
Optic nerve glioma	11	17	2.1
Hematolymphoid malignancies	0	2.5	10.6
Mesenchymal chondrosarcoma	0		2.1
Benign spindle cell tumors	0		10.6
Metastatic neuroblastoma	0	17	4.3
Malignant rhabdoid tumor	0		2.1
Infective lesions	0	7.5	4.3

extraocular orbital malignancy in children, although it is only one-tenth as common as retinoblastoma, which is itself a rare tumor [9]. This is similar to the finding in our study. Over one-third (35–40%) of rhabdomyosarcomas arise in the head and neck, and orbital primary tumors account for about 25–35% of head and neck rhabdomyosarcomas and about 10% of all rhabdomyosarcomas [10–12]. The orbit can also be involved secondarily by the spread of tumors originating in the nasopharynx, pterygopalatine fossa, infratemporal fossa, or paranasal sinuses (the so-called parameningeal sites) or as a site of metastasis [11]. Primary orbital rhabdomyosarcoma most often occurs in the first decade of life, with a mean patient age of 6–8 years [9, 10]. Similarly, age range of our patients was 0–14 years with most patients below the age of 10 years. They are always unilateral [10, 13] as seen in all our cases, although Sohaib et al. [14] reported a case of one patient with multicentric disease in one eye. Most tumors are reported to be extraconal (37–87% of cases) [13] as seen in our study. Patients with rhabdomyosarcoma are reported to present with rapidly progressive proptosis or globe displacement and conjunctival or palpebral swelling [10]. The children in our study had similar complaints but additionally presented with loss of vision and ocular palsies.

Of a total of 24 of our cases, 11 patients (45.8%) had extraobital spread with bone erosion into the sinonasal (seven cases—29.2%) and intracranial regions (four cases—16.7%). Of these, two patients had cavernous sinus involvement. This is similar to reports in literature whereby rhabdomyosarcomas grow rapidly and behave aggressively, frequently invading adjacent bones and soft tissues. Bone erosion is reported to be seen in 30–40%, invasion of the paranasal sinuses in 20% of patients and intracranial extension in 3% of patients at presentation [10]. Regional lymph node metastases are reported to be rare except in advanced disease, because the posterior orbit is relatively devoid of lymphatic tissue [10] and likewise this was seen in only one of the 24 (4.2%) of our patients.

On histopathological evaluation, 20 of the 24 rhabdomyosarcomas were of embryonal type while one was of the alveolar type. Three cases were diagnosed on FNAC. All cases showed immunopositivity for desmin (100%), and 21 cases for myoglobin, and myoD1 which is similar to reports in literature [15, 16]. Desmin stain performed on FNAC material precluded performing a formal biopsy in three patients which is rarely reported in literature [17]. Thus diagnostic biopsies were done in 21 patients and three patients were diagnosed on FNAC. Out of the 24 cases, a single case showed the morphology of alveolar RMS. This was confirmed by the presence of PAX3-FKHR translocation.

At primary presentation, 20 of the 24 patients (83.3%) of the children had stage III disease. Seven (29.2%) were operated outside and presented to the hospital with recurrent tumors. One case developed nodal metastasis, a rare event in orbital RMS. This was the case diagnosed as alveolar RMS and proved by presence of PAX3-FKHR translocation. While 22 of 24 cases received RCT-II protocol, two cases were treated with the latest IRS_VAC protocol with complete disease remission to date [9]. Surgery was performed in five cases. Of all patients with RMS treated with multimodal therapy, orbital RMS are reported to have the most favorable outcome [9]. The reported 5-year survival with the latest IRS-IV protocol is 80–90% [15]. Hence early diagnosis on biopsy with the help of IHC can guide initiation of correct therapy.

Granulocytic sarcoma was diagnosed in four of our cases. It is a solid tumor that may occur in children with acute or chronic myelogenous leukemia. These tumors tend to arise in the subperiosteum of the lateral orbital wall, although they usually do not disrupt the bone [18]. If they are bilateral at presentation the diagnosis may be suspected [18]. Leukemic involvement was reported by Ohtsuka et al. as 0.4% of all orbital lesions [4]. However, biopsy diagnosis is difficult in primary orbital involvement with no evidence of systemic leukemia as they mimic other round cell tumors [19]. Our cases presented with primary orbital swelling and proptosis. Peripheral smears and bone marrow aspirates and biopsies showed no evidence of hematolymphoid malignancy. Biopsy diagnosis was confirmed with MPO, CD34, CD43, and CAE positivity [19, 20].

Five cases showed spindle cell proliferations on biopsy. IHC panel of vimentin, SMA, desmin, CD34, and Mic-2 demonstrated these lesions to be fibromatosis, solitary fibrous tumor, and myofibroblastic tumors, respectively. Fibrous proliferations in infancy and childhood share several features. They are locally invasive, tend to recur after surgical resection, and do not metastasize. In contrast to round cell tumors which need chemotherapy, these tumors need to be surgically excised. One-third of these occur in the head and neck [21]. Chung and Enzinger [21] reported five cases with orbital involvement in their series of 61 cases referred to the Armed Forces Institute of Pathology. Infantile fibromatosis (juvenile fibromatosis) is the most common fibrous tumor of infancy. The presentation is usually as a painless swelling of few months duration. Deep lesions of the orbit including fibroblastic and myofibroblastic tumors most commonly manifest with proptosis which was the case in all five patients. The fibromatosis in the 2-year-old child recurred once and necessitated repeated surgery. The other four cases were cured by primary surgery and were disease-free after a follow-up of 3 years.

Metastatic neuroblastoma primarily presented with orbital masses in two patients. Routine ultrasound examina-

tion of the abdomen raised a suspicion of neuroblastoma and subsequently MIBG scans were positive precluding the need for a biopsy diagnosis. The orbit is a common site for bone metastases from neuroblastoma, which cause aggressive periosteal reaction in the orbital roof or lateral wall and bilaterality on imaging evaluation raises their suspicion [16].

Medulloepitheliomas are rare intraconal tumors; however, they are known for their tendency to mimic carcinomas in their growth and spread [22, 23]. If these are very large lesions they present as extraconal tumors and enter into differential diagnosis for these lesions. Two patients in our series had this presentation and in addition had cervical nodal metastasis. One case had two local recurrences over a period of 2 years. This has already been reported by our group [23].

A single case of mesenchymal chondrosarcoma presented with recurrent disease with intracranial extension. He was treated with radical surgery; however, he was lost to follow-up. This tumor has a tendency to involve soft tissues and bones of the jaw and ribs, and is rarely seen in the orbit [24]. However, microscopically a small biopsy can show only the round cell component with the absence of chondroid areas and hence they need to be differentiated from other round cell tumors. This is extremely important therapeutically as the treatment modality is principally surgery and not chemotherapy or radiotherapy which are not efficacious and which is the standard of care for other tumors [24, 25].

The sole case of a PNET, already published, was a rare case involving the maxilla and secondarily infiltrating the orbit. The diagnosis was confirmed by Mic2 and synaptophysin positivity and also by EWS–FLI1 translocation. This case has also been published by our group [26].

Malignant rhabdoid tumors are extremely aggressive lesions associated with high mortality [27]. These lesions were found to comprise 4% of orbital tumors in Japanese children [4]. A single case was seen in an extraconal location in a 6-month child in this study. Biopsy showed cells with a rhabdoid phenotype with vimentin, cytokeratin, desmin, epithelial membrane antigen, and Mic2 positivity. However, contrary to all reported literature, the tumor in this child completely regressed postchemotherapy and the child is disease-free after 6 years of follow-up.

A single case of Langerhans Cell histiocytosis showed the typical morphology with CD 1a positivity in the langerhans cells. The patient was adequately treated and was disease-free on follow-up. Langerhans cell histiocytosis, an idiopathic reticuloendothelial proliferative disorder, tends to involve the bones of the skull, especially the lateral orbital roof; it produces lytic destruction of bone with a sclerotic rim and a large intraorbital soft-tissue mass [16].

Besides these, infectious lesions can involve the orbit to cause mass lesions and loss of vision. These clinically simulate malignancy needing a biopsy and a pathologist can play a very important role in their diagnosis [28]. Two of the cases in this study had proptosis which on radiology was suspicious of malignancy. One of these was a case of ALL with a suspicion of orbital involvement; however, biopsy and culture showed mucormycosis. This patient received antifungal treatment and was disease-free on follow-up. Rhinocerebral mucormycosis is a rare fungal infection of the nasal cavity and sinuses that can spread to the orbits and cranium within days and is a life-threatening clinical emergency [28]. The second case had typical caseating epithelioid granulomas suggestive or tuberculosis and was cured with AKT. If an infectious etiology is suspected histopathology, it needs to be additionally subjected to culture for confirmation of diagnosis especially cases of tuberculosis where AFB may not be detected in the histopathology sections as the overall sensitivity of the procedure is low.

Conclusion

Pediatric orbital masses range from completely treatable infectious lesions, surgically resectable benign neoplasms to aggressive malignancies requiring chemotherapy and radiotherapy. The pathologist needs to distinguish these on small biopsies which are of immense help in separating infectious from neoplastic lesions, characterize neoplastic lesions as surgically treatable or those requiring chemotherapy, and accurately typing small round cell tumors. Ancillary techniques like special stains, IHC, and molecular techniques are extremely useful and in almost all cases an accurate diagnosis can be rendered. The pathologist thus plays a key role in expediating accurate treatment which can be critical in saving the vision or life of a patient.

Conflicts of Interest statement We declare that we have no conflict of interest.
Dr. Seethalakshmi Viswanathan

References

1. Kodsi SR, Shetlar DJ, Campbell RJ et al (1994) A review of 340 orbital tumors in children during a 60-year period. Am J Ophthalmol 117:177–82
2. Porterfield JS (1962) Orbital tumours in children. A report of 214 cases. Int Ophthalmol Clin 2:319
3. Shields JA, Bakewell B, Augsburger JJ et al (1986) Space occupying orbital masses in children: a review of 250 consecutive biopsies. Ophthalmology 93:379–384
4. Ohtsuka K, Hashimoto M, Suzuki Y (2005) A review of 244 orbital tumors in Japanese patients during a 21-year period: origins and locations. Jpn J Ophthalmol 49:49–55

5. Bajaj MS, Pushker N, Chaturvedi A et al (2007) Orbital space-occupying lesions in Indian children. J Pediatr Ophthalmol Strabismus 44:106–111
6. Castillo BV Jr, Kaufman L (2003) Pediatric tumors of the eye and orbit. Pediatr Clin North Am 50:149–172
7. Chung EM, Smirniotopoulos JG, Specht CS et al (2007) From the archives of the AFIP: pediatric orbit tumors and tumor like lesions: nonosseous lesions of the extraocular orbit. Radiographics 27:1777–1799
8. Triche TJ, Hicks J, Sorensen PHB (2005) Diagnostic pathology of pediatric malignancies. In: Pizzo P, Poplack D (eds) Principles & Practice of Pediatric Oncology. Lippincott Williams & Wilkins, Philadelphia, pp 185–232
9. Crist WM, Anderson JR, Meza JL et al (2001) Intergroup Rhabdomyosarcoma Study-IV: results for patients with nonmetastatic disease. J Clin Oncol 19:3091–3102
10. Shields JA, Shields CL, Scartozzi R (2004) Survey of 1264 patients with orbital tumors and simulating lesions: the 2002 Montgomery Lecture, part 1. Ophthalmology 111:997–1008
11. Shields JA, Shields CL (2003) Rhabdomyosarcoma: review for the ophthalmologist. Surv Ophthalmol 48:39–54
12. Maurer HM, Beltangady M, Gehan EA et al (1988) The Intergroup Rhabdomyosarcoma Study-I: a final report. Cancer 61:209–220
13. Conneely MF, Mafee MF (2005) Orbital rhabdomyosarcoma and simulating lesions. Neuroimaging Clin N Am 15:121–136
14. Sohaib SA, Moseley I, Wright JE (1998) Orbital rhabdomyosarcoma: the radiological characteristics. Clin Radiol 53:357–362
15. Shields CL, Shields JA, Honavar SG et al (2001) Primary ophthalmic rhabdomyosarcoma in 33 patients. Trans Am Ophthalmol Soc 99:133–142 discussion 142–143
16. Sebire NJ, Malone M (2003) Myogenin and MyoD1 expression in paediatric rhabdomyosarcomas. J Clin Pathol 56:412–416
17. Meng MV, Grossfeld GD, Sudilovsky D et al (2006) Fine needle aspiration cytology of adult perineal rhabdomyosarcoma: a case report. Acta Cytol 50:88–92
18. Chung EM, Murphey MD, Specht CS et al (2008) From the Archives of the AFIP. Pediatric orbit tumors and tumorlike lesions: osseous lesions of the orbit. Radiographics 28:1193–214
19. Stockl FA, Dolmetsch AM, Saornil MA et al (1997) Jr. Orbital granulocytic sarcoma. Br J Ophthalmol 81:1084–1088
20. Zimmerman LE, Font RL (1975) Ophthalmic manifestations of granulocytic sarcoma (myeloid sarcoma or chloroma). Am J Ophthalmol 80:975–955
21. Chung EB, Enzinger FM (1981) Infantile myofibromatosis. Cancer 48:1807–1818
22. Broughton LW, Zimmerman LE (1978) A clinicopathologic study of 56 cases of intraocular medulloepitheliomas. Am J Ophthalmol 85:407–418
23. Viswanathan S, Mukul D, Qureshi S et al (2008) Orbital medulloepitheliomas—with extensive local invasion and metastasis: a series of three cases with review of literature. Int J Pediatr Otorhinolaryngol 72:971–975
24. Jacobs JL, Merriam JC, Chadburn A et al (1994) Mesenchymal chondrosarcoma of the orbit. Report of three new cases and review of the literature. Cancer 73:399–405
25. Verma-Pradhan S, Sayami G, Sharma MR (2004) Intracranial Mesenchymal chondrosarcoma: case report and review of literature. Nepal J Neuroscience 1:131–134
26. Mohindra P, Zade B, Basu A et al (2008) Primary PNET of maxilla: an unusual presentation. J Pediatr Hematol Oncol 30:474–477
27. Gündüz K, Shields JA, Eagle RC Jr et al (1998) Malignant rhabdoid tumor of the orbit. Arch Ophthalmol 116:243–246
28. Hendrickson RG, Olshaker J, Duckett O (1999) Rhinocerebral mucormycosis: a case of a rare, but deadly disease. J Emerg Med 17:641–645

Virchows Arch (2009) 454:715–716
DOI 10.1007/s00428-009-0773-3

LETTER TO THE EDITOR

Sampling lobular neoplasia of the breast: underestimation despite technical success?

Flora Zagouri · Theodoros N. Sergentanis · Afrodite Nonni · Alexandros Papalabros · George C. Zografos

Received: 28 December 2008 / Revised: 5 April 2009 / Accepted: 10 April 2009 / Published online: 24 May 2009

Keywords Lobular neoplasia · Underestimation · Vacuum-assisted breast biopsy

Dear Editor,

In a recently published article in *Virchows Archiv*, Menon et al. [1] provide interesting insight into the significance of lobular neoplasia (LN) on needle core biopsy of the breast. More specifically, commenting on 25 immediately excised LN cases, nine cases were apparently underestimated (five missed masses, two missed calcifications and two adequately sampled lesions). As a result, the overall underestimation rate is equal to nine of 25 (36%; 95%CI, 18.0–57.5%). However, as the authors noted, after the exclusion of the non-successful procedures, the underestimation rate becomes equal to two of 18 (11.1%; 95%CI, 1.4–34.7%).

In this letter, we comparatively present the experience of our centre, expanding our LN series [2, 3]. Our series is based on stereotactically guided vacuum-assisted breast biopsy performed with 11 Gauge needle; indeed, the setting and needle diameter utilised may exert a significant effect upon the crucial underestimation rates. In our setting, the underestimation rate was equal to 6.1% (two of 33; 95%CI, 0.7–20.2%); interestingly enough, no cases of technical failure occurred. The underestimation rate in our setting was significantly lower than the overall underestimation rate reported by Menon et al. (two of 33 vs. nine of 25; $p=0.006$, Fisher's exact test). The above may be attributed to more accurate targeting of the lesion through the stereotactic guidance, as well as to the greater number of cores excised (24–96 cores, according to the results of a double-blind study [3]). These two factors might effectively reduce the technical failure rate.

On the other hand, our underestimation rate did not significantly differ from the one derived after the exclusion of unsuccessfully performed biopsy procedures (two of 33 vs. two of 18, $p=0.607$, Fisher's exact test). That points to the existence of a lower threshold for underestimation in LN, at which different techniques and settings converge and below which needle-based techniques may not proceed. Given the small sample sizes in the various studies, imposed by the relative rarity of the LN lesion, the exact magnitude of this inherent underestimation threshold may not be accurately estimated. Indeed, this is reflected upon the large confidence intervals presented above. However, it should be noted that the underestimation rate of about 20% for LN followed by surgical excision is a well-known phenomenon, and it is partly due to the fact that LN is clinically silent and to the multicentricity of the lesion itself. To have 6% of underestimation rate is very unusual, and it might be consequent to some selection artefact [4, 5].

F. Zagouri · T. N. Sergentanis · A. Papalabros · G. C. Zografos
Breast Unit, 1st Department of Propaedeutic Surgery,
Hippokratio Hospital, University of Athens,
114 V. Sofias Ave,
Athens 116 27, Greece

A. Nonni
First Department of Pathology, Medical School,
University of Athens,
Athens, Greece

Present Address:
G. C. Zografos (✉)
University of Athens,
101, Vas Sofias Ave, Ampelokipi,
Athens 11521, Greece
e-mail: gzografo@med.uoa.gr

Consequently, the existence of inherent underestimation in LN cases renders the topic of subsequent follow-up or excision extremely interesting. Larger, collaborative and comparative studies seem at present to be needed for the optimal management of LN.

References

1. Menon S, Porter GJ, Evans AJ et al (2008) The significance of lobular neoplasia on needle core biopsy of the breast. Virchows Arch 452:473–479
2. Zografos GC, Zagouri F, Sergentanis TN (2007) Lobular neoplasia in vacuum-assisted breast biopsy: extended protocols and underestimation. AJR Am J Roentgenol 965:324–456
3. Zografos GC, Zagouri F, Sergentanis TN et al (2008) Minimizing underestimation rate of microcalcifications excised via vacuum-assisted breast biopsy: a blind study. Breast Cancer Res Treat 109:397–402
4. Elsheikh TM, Silverman JF (2005) Follow-up surgical excision is indicated when breast core needle biopsies show atypical lobular hyperplasia or lobular carcinoma in situ. A correlative study of 33 patients with review of the literature. Am J Surg Pathol 29:534–543
5. Foschini MP, Righi A, Cucchi MC et al (2006) The impact of large sections and 3D technique on the study of lobular in situ and invasive carcinoma of the breast. Virchows Arch 448:256–261

Virchows Arch (2009) 454:717–718
DOI 10.1007/s00428-009-0785-z

LETTER TO THE EDITOR

Primary thyroid and thyroid-like follicular carcinoma of the kidney versus solitary metastatic carcinoma of the thyroid: a vexing issue

Luigi Insabato · David Ben-Dor · Carlos A. Galliani · Gaetano Lastilla · Michele Bisceglia

Received: 26 April 2009 / Accepted: 29 April 2009 / Published online: 16 May 2009

Keywords Thyroid-like follicular carcinoma · Renal metastasis · Renal tumor · Thyroid carcinoma · Nephroblastoma · Immunohistochemistry

To the Editor

In 2008, Sterlacci et al. [1] reported on a puzzling renal tumor presenting as a solitary mass mimicking thyroid follicular carcinoma (with focal "papillary differentiation"), which was thyroglobulin (TG) and TTF1 immunonegative. Initially interpreted as a metastasis from the thyroid, it was then considered to be primary after the histopathological examination of the excised thyroid failed to show any evidence of malignancy, but the patient subsequently developed a pulmonary metastasis, with identical histomorphology which demonstrated TTF-1 immunoexpression. This year, Amin et al. [2] described six cases of a primary thyroid-like renal follicular carcinoma.

We would like to comment more on this issue

Distinguishing thyroid-like primary carcinoma of the kidney versus thyroid cancer metastatic to the kidney can be problematic. Renal metastasis from thyroid carcinoma occurs rarely. About 20 cases, detected clinically, have been reported so far of both follicular and papillary type ([2, 3] and refs therein), and only five appeared as isolated deposits. The presumptive existence of TG-immunopositive "primary (papillary) thyroid carcinoma of the kidney" was proposed in 1996 by Angel et al. [4], but the report was soon questioned by DK Heffner. While agreeing with Amin et al. that that case has to be considered as metastatic, we would be interested in having subsequent clinical follow-up. Amin et al. described "genuine" primary TG and TTF-1 immunonegative thyroid-like renal follicular carcinoma. They did not accept the case of Sterlacci et al. as similar to their own, implicitly considering it as metastatic (occult) thyroid cancer. It would be of great interest to know whether the lung metastasis in this case was immunoreactive *also* for TG and not just for TTF-1. If TG was positive, this would definitely confirm that it was metastatic.

It is a currently accepted view not to regard as a primary any thyroid-like tumor in the kidney which displays immunopositivity for TG and/or TTF-1. These tumors are

L. Insabato
Department of Pathology, "Federico II" University of Naples, Naples, Italy

D. Ben-Dor
Department of Pathology, The Barzilai Medical Center, Ashkelon, Israel

C. A. Galliani
Department of Pathology, Cook Children's Medical Center, Fort Worth, TX, USA

G. Lastilla
Department of Pathology, Polyclinic Hospital, Bari, Italy

M. Bisceglia
Department of Pathology, IRCCS–"Casa Sollievo della Sofferenza" Hospital, San Giovanni Rotondo, Italy

M. Bisceglia (✉)
Unità Operativa di Anatomia Patologica, IRCCS–"Casa Sollievo della Sofferenza" Hospital, 71013 San Giovanni Rotondo (FG), Italy
e-mail: bismi@libero.it
e-mail: m.bisceglia@operapadrepio.it

considered to be metastatic, the primary being a clinically inapparent tumor in patients in whom clinical investigation was negative for thyroid tumors of both orthotopic and heterotopic sites. Inapparent tumors can be either extremely small (occult) or else may have completely regressed.

A secondary tumor should always be considered in the differential diagnosis of thyroid-like renal neoplasms and any such renal tumor has to be shown to be immunonegative for thyroid markers before being considered as a true primary. The diagnosis should be straightforward in the event of TTF-1 and TG immunopositivity. Clinicopathologic correlation is paramount in cases which are TTF-1 and TG immunonegative.

Notwithstanding, immunoexpression of thyroid differentiation may not be an absolute criterion to exclude a primary renal tumor. In 2008, we described a case of nephroblastoma with papillary thyroid carcinoma-like morphology featuring both diffuse nuclear TTF-1 expression and focal cytoplasmic TG immunopositivity (personal communication, full article in preparation). While in need of further substantiation, that tumor (case 16 in the series of 48 nephroblastomas investigated for TTF-1 expression) [5] let us believe that there is a subset of nephroblastoma displaying papillary thyroid carcinoma-like histology along with TTF-1 and TG immunoexpression.

Conflict of interest All the authors declare they have no conflict of interest.

References

1. Sterlacci W, Verdorfer I, Gabriel M et al (2008) Thyroid follicular carcinoma-like renal tumor: a case report with morphologic, immunophenotypic, cytogenetic, and scintigraphic studies. Virchows Arch 452:91–95
2. Amin MB, Gupta R, Ondrej H et al (2009) Primary thyroid-like follicular carcinoma of the kidney: report of 6 cases of a histologically distinctive adult renal epithelial neoplasm. Am J Surg Pathol 33:393–400
3. Insabato L, Di Vizio D, De Rosa G et al (2003) Renal metastasis from thyroid carcinoma 35 years after detection of the primary tumor. Tumori 89:99–101
4. Angell SK, Pruthi R, Freiha FS (1996) Primary thyroidlike carcinoma of the kidney. Urology 48:632–635. (comment in Urology 1997:50:485–486, by Heffner DK—Letter to the Editor)
5. Bisceglia M, Ragazzi M, Galliani C et al (2009) TTF-1 expression in nephroblastoma. Am J Surg Pathol 33:454–461

Virchows Arch (2009) 454:719
DOI 10.1007/s00428-009-0788-9

LETTER TO THE EDITOR

Difference between RAT and clear cell papillary renal cell carcinoma/clear renal cell carcinoma

Michal Michal · Ondrej Hes · Naoto Kuroda · Dmitry V. Kazakov · Milan Hora

Received: 4 May 2009 / Accepted: 4 May 2009 / Published online: 27 May 2009

We would like to thank Dr. Verine for his interest in our paper on renal angiomyoadenomatous tumors (RAT) [1] and for his letter to the editor [2]. Dr. Verine finds it unfortunate that we did not compare clear cell papillary renal cell carcinoma with RAT. In his view, clear cell papillary renal cell carcinoma shares a lot of similarities with RAT, namely CK7, CA-IX, and CD10 immunohistochemical positivity and presence of clear cell snouts as shown in the paper of Tickoo et al. [3].

We have several cases of clear cell papillary renal cell carcinoma in our files and we must state that this type of carcinoma is so much different from RAT that we did not (and do not) consider it worth listing in the differential diagnosis of RAT. Just for mentioning a few major differences between RAT and clear cell papillary renal cell carcinoma: RAT is not a papillary tumor at all and is not composed of clear cells either. When present in RAT, clear cell areas comprise usually only a focal change. Most of the RAT is usually a basophilic tumor growing as a solid lesion, composed of variously collapsed tubules. Immunohistochemistry does not play any practical role in the diagnosis of RAT as it shares an identical immunohistochemical profile with several entities (it is beyond the scope of this letter to discuss this matter in detail). The immunohistochemistry of RATs was described in our paper [1] only to complete the pathological features of this distinct entity. We further do not see any similarity between the clear snouts of RAT and those illustrated in the paper of Tickoo et al. [3] as suggested by Dr. Verine.

Taking further into account the facts that RAT, in contrast to the cases of Tickoo et al. [3], has a typical angioleiomyomatous stroma, typical capillary vascularity, and lacks the end-stage kidney background, we think that the difference between RAT and clear cell papillary renal cell carcinoma/clear renal cell carcinoma is like that between the day and the night or like that between a rat and a hedgehog.

In closing, we thank again Dr. Verine for his comments.

M. Michal (✉) · O. Hes · D. V. Kazakov
Sikl's Department of Pathology, Medical Faculty Hospital,
Charles University,
Alej Svobody 80,
304 60 Pilsen, Czech Republic
e-mail: michal@medima.cz

N. Kuroda
Department of Diagnostic Pathology,
Kochi Red Cross Hospital,
Kochi, Japan

M. Hora
Department of Urology, Charles University Hospital,
Pilsen, Czech Republic

References

1. Michal M, Hes O, Nemcova J, Sima R, Kuroda N, Bulimbasic S, Franco M, Danis D, Kazakov DV, Ohe C, Hora M (2009) Renal angiomyoadenomatous tumor: morphologic, immunohistochemical and molecular genetic study of a distinct entity. Virchows Archiv 454:89–99
2. Verine J (2009) Renal angiomyoadenomatous tumor: morphologic, immunohistochemical and molecular genetic study of a distinct entity. Virchows Archiv 454:479–480
3. Tickoo SK, de Peralta-Venturina MN, Harik LR, Worcester HD, Salama ME, Young AN, Moch H, Amin MB (2006) Spectrum of epithelial neoplasms in end-stage renal disease: an experience from 66 tumor-bearing kidney with emphasis on histologic patterns distinct from those in sporadic adult renal neoplasia. Am J Surg Pathol 30:141–150

Virchows Arch (2009) 454:721–722
DOI 10.1007/s00428-009-0779-x

ERRATUM

Kidney biopsy findings in heterozygous Fabry disease females with early nephropathy

Carmen Valbuena · Elísio Carvalho · Manuela Bustorff · Mariana Ganhão · Sandra Relvas · Rosete Nogueira · Fátima Carneiro · João Paulo Oliveira

Published online: 30 May 2009

Erratum to: Virchows Arch
DOI 10.1007/s00428-008-0653-2

There was an error in Table 6. The error was limited to the data shown in the table and did not affect any of the statistical analyses presented in the Results and Discussion, which were based on a SPSS file that the authors have double-checked for accuracy. The corrected table is reproduced here.

The authors very much regret their error.

The online version of the original article can be found at http://dx.doi.org/10.1007/s00428-008-0653-2

C. Valbuena · M. Ganhão · S. Relvas · F. Carneiro
Department of Pathology, Hospital São João,
Porto, Portugal

C. Valbuena · F. Carneiro
Department of Pathology, Faculty of Medicine,
University of Porto,
Porto, Portugal

E. Carvalho · M. Bustorff · J. Paulo Oliveira
Department of Nephrology, Hospital São João,
Porto, Portugal

R. Nogueira
Department of Pathology, Centro Hospitalar de Gaia,
Vila Nova de Gaia, Portugal

F. Carneiro
Department of Pathology, Institute of Molecular
Pathology and Immunology (IPATIMUP),
University of Porto,
Porto, Portugal

J. Paulo Oliveira
Department of Genetics, Faculty of Medicine,
University of Porto,
Porto, Portugal

C. Valbuena (✉)
Serviço de Anatomia Patológica, Hospital São João,
Alameda Hernâni Monteiro,
4200-319 Porto, Portugal
e-mail: valbuena@med.up.pt

Table 6 Comparison of the three largest kidney biopsy series reporting pathology findings in females with Fabry disease

	Gubler et al. [10]			Gubler et al. [10]					Present series			
Age at kidney biopsy (years)	8	22	51	30	37	54	55	73	32	42	45	50
CKD stage	0	0	2	?	2	4	5	4	2	1	2	2
Proteinuria	0	0	0	+++	+++	+++	++++	++++	++++	0	++	0
No. of evaluated glomeruli	8	15	25	2	4	17	23	5	12	31	29	17
No. of sclerotic glomeruli	0	0	5	1	2	17	22	3	9	2	7	4
(% of sclerotic glomeruli)	0%	0%	20%	50%	50%	100%	96%	60%	75%	6%	24%	24%
Tubular atrophy/interstitial fibrosis	0	0	+	0	+	++	+++	+	+/++	+	+	+

CKD stages classified according to the clinical practice guidelines of the National Kidney Foundation [33], using reported Creatinine Clearance or available algorithms to estimated GFR (eGFR): "0" — no evidence of kidney disease, "1" — eGFR ≥ 90 ml/min/1.73m2, "2" — eGFR = 89–60 ml/min/1.73m2, "3" — eGFR = 59–30 ml/min/1.73m2, "4" — eGFR = 29–15 ml/min/1.73m2, "5" — eGFR < 15 ml/min/1.73m2.

No. of sclerotic glomeruli is the total number of evaluated glomeruli that showed either segmental or global sclerosis.

Proteinuria was graded as: "0" = no overt proteinuria, "+" = 0.3–0.5 g/day, "++" = 0.5–1.0 g/day, "+++" = 1.0–3.5 g/day, "++++" ≥ 3.5g/day.

Tubular atrophy/interstitial fibrosis graded as: "0" = absent, "+" = mild, "++" = moderate, "+++" = severe.